General Disclaimer

One or more of the Following Statements may affect this Document

- This document has been reproduced from the best copy furnished by the organizational source. It is being released in the interest of making available as much information as possible.

- This document may contain data, which exceeds the sheet parameters. It was furnished in this condition by the organizational source and is the best copy available.

- This document may contain tone-on-tone or color graphs, charts and/or pictures, which have been reproduced in black and white.

- This document is paginated as submitted by the original source.

- Portions of this document are not fully legible due to the historical nature of some of the material. However, it is the best reproduction available from the original submission.

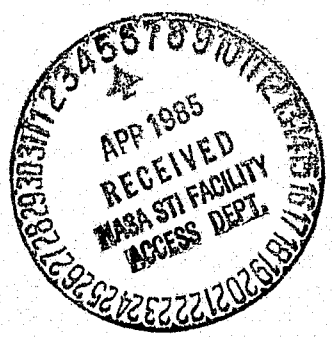
Produced by the NASA Center for Aerospace Information (CASI)

NASA Technical Memorandum 83693

Bibliography of Lewis Research Center Technical Publications Announced in 1983

(NASA-TM-83693) BIBLIOGRAPHY OF LEWIS RESEARCH CENTER TECHNICAL PUBLICATIONS ANNOUNCED IN 1983 (NASA) 345 p
HC A16/MF A01
CSCL 05B
N85-22255
Unclas
G3/82 19483

June 1984



NASA

PREFACE

In 1983, Lewis Research Center's 1061 research authors published 439 technical publications which were announced to and reached the worldwide scientific community. This is the highest number since 1979, and it was accomplished with fewer research authors since the "new hires" had not begun to publish. The 439 papers included 200 symposium/seminar presentations and 53 articles sent directly to journals for publication. This is the highest number of journal article submissions in almost a decade. The number of reports published per person per year has increased slightly. In 1983, Lewis authors published approximately 58 percent of their research contributions in outside publications and the remainder as NASA research reports. Three out of five Lewis authored society presentations and journal articles were addressed to members of the following five technical societies: AIAA, 63 papers; ASME, 46 papers; SAE, 18 papers; ASLE, 12 papers; IEEE, 12 papers.

Many Lewis authors have received awards for their contributions; among them are the following:

The 1983 Lewis Distinguished Paper Awards were presented to Richard Seasholtz and Louis Goldman for their papers entitled "Comparison of Laser Anemometer Measurements and Theory in an Annular Turbine Cascade with Experimental Accuracy Determined by Parameter Estimation" and "Laser Anemometer Using A Fabry-Perot Interferometer for Measuring Mean Velocity and Turbulence Intensity Along the Optical Axis in Turbomachinery" and to Paul Durbin for his paper entitled "Analysis of the Decay of Temperature Fluctuations in Isotropic Turbulence." In 1983 William C. Strack received an award from the Society of Automotive Engineers for "Best Oral Presentation." His paper was entitled "Technology and Benefits of Aircraft Counter Rotation Propellers" by W. C. Strack and G. Knip, Lewis Research Center; A. L. Weisbrich, Hamilton-Standard; J. Godston, Pratt & Whitney; and E. Bradley, Lockheed-Georgia.

In 1983, 315 contractor-authored research reports were produced, the most since 1967. In addition, 23 patent applications were filed and 22 patents were issued.

All the publications in this collection were announced in the 1983 issues of STAR (Scientific and Technical Aerospace Reports) and IAA (International Aerospace Abstracts).

The arrangement of the material is by NASA subject category, as noted in the Contents. The various indexes will help locate specific publications by subject, author, contractor organization, contract number, and report number.

George Mandel
Chief, Technical Information Services Division

TABLE OF CONTENTS

PREFACE i

AERONAUTICS

Includes aeronautics (general); aerodynamics; air transportation and safety; aircraft communications and navigation; aircraft design, testing and performance; aircraft instrumentation; aircraft propulsion and power; aircraft stability and control; and research and support facilities (air).

For related information see also *Astronautics.*

01 AERONAUTICS (GENERAL) 1

02 AERODYNAMICS 2

Includes aerodynamics of bodies, combinations, wings, rotors, and control surfaces; and internal flow in ducts and turbomachinery.

For related information see also *34 Fluid Mechanics and Heat Transfer*

03 AIR TRANSPORTATION AND SAFETY 16

Includes passenger and cargo air transport operations; and aircraft accidents.

For related information see also *16 Space Transportation* and *85 Urban Technology and Transportation.*

04 AIRCRAFT COMMUNICATIONS AND NAVIGATION 17

Includes digital and voice communication with aircraft; air navigation systems (satellite and ground based); and air traffic control.

For related information see also *17 Spacecraft Communications, Command and Tracking* and *32 Communications.*

05 AIRCRAFT DESIGN, TESTING AND PERFORMANCE 17

Includes aircraft simulation technology.

For related information see also *18 Spacecraft Design, Testing and Performance* and *39 Structural Mechanics.*

06 AIRCRAFT INSTRUMENTATION 18

Includes cockpit and cabin display devices; and flight instruments.

For related information see also *19 Spacecraft Instrumentation* and *35 Instrumentation and Photography.*

07 AIRCRAFT PROPULSION AND POWER 19

Includes prime propulsion systems and systems components, e.g., gas turbine engines and compressors; and on-board auxiliary power plants for aircraft.

For related information see also *20 Spacecraft Propulsion and Power, 28 Propellants and Fuels,* and *44 Energy Production and Conversion.*

08 AIRCRAFT STABILITY AND CONTROL 43

Includes aircraft handling qualities; piloting; flight controls; and autopilots.

09 RESEARCH AND SUPPORT FACILITIES (AIR) 43

Includes airports, hangars and runways; aircraft repair and overhaul facilities; wind tunnels; shock tube facilities; and engine test blocks.

For related information see also *14 Ground Support Systems and Facilities (Space).*

ASTRONAUTICS

Includes astronautics (general); astrodynamics; ground support systems and facilities (space); launch vehicles and space vehicles; space transportation; spacecraft communications, command and tracking; spacecraft design, testing and performance; spacecraft instrumentation; and spacecraft propulsion and power.

For related information see also *Aeronautics*

12 ASTRONAUTICS (GENERAL) 44

For extraterrestrial exploration see *91 Lunar and Planetary Exploration.*

13 ASTRODYNAMICS N.A.

Includes powered and free-flight trajectories; and orbit and launching dynamics.

14 GROUND SUPPORT SYSTEMS AND FACILITIES (SPACE) 44

Includes launch complexes, research and production facilities; ground support equipment, e.g., mobile transporters; and simulators.

For related information see also *09 Research and Support Facilities (Air).*

15 LAUNCH VEHICLES AND SPACE VEHICLES 45

Includes boosters; manned orbital laboratories; reusable vehicles; and space stations.

16 SPACE TRANSPORTATION 46

Includes passenger and cargo space transportation, e.g., shuttle operations; and rescue techniques.

For related information see also *03 Air Transportation and Safety* and *85 Urban Technology and Transportation.*

17 SPACECRAFT COMMUNICATION, COMMAND AND TRACKING 47

Includes telemetry; space communications networks; astronavigation; and radio blackout.

For related information see also *04 Aircraft Communications and Navigation* and *32 Communications.*

18 SPACECRAFT DESIGN, TESTING AND PERFORMANCE 48

Includes spacecraft thermal and environmental control; and attitude control.

For life support systems see *54 Man/System Technology and Life Support.* For related information see also *05 Aircraft Design, Testing and Performance* and *39 Structural Mechanics.*

19 SPACECRAFT INSTRUMENTATION N.A.

For related information see also *06 Aircraft Instrumentation* and *35 Instrumentation and Photography.*

20 SPACECRAFT PROPULSION AND POWER 51

Includes main propulsion systems and components, e.g., rocket engines; and spacecraft auxiliary power sources.

For related information see also *07 Aircraft Propulsion and Power, 28 Propellants and Fuels,* and *44 Energy Production and Conversion.*

PRECEDING PAGE BLANK NOT FILMED

CHEMISTRY AND MATERIALS

Includes chemistry and materials (general); composite materials; inorganic and physical chemistry; metallic materials; nonmetallic materials; and propellants and fuels.

23 CHEMISTRY AND MATERIALS (GENERAL) 61
Includes biochemistry and organic chemistry.

24 COMPOSITE MATERIALS 62
Includes laminates.

25 INORGANIC AND PHYSICAL CHEMISTRY 67
Includes chemical analysis, e.g., chromatography; combustion theory; electrochemistry; and photochemistry.
For related information see also *77 Thermodynamics and Statistical Physics.*

26 METALLIC MATERIALS 74
Includes physical, chemical, and mechanical properties of metals, e.g., corrosion; and metallurgy.

27 NONMETALLIC MATERIALS 88
Includes physical, chemical, and mechanical properties of plastics, elastomers, lubricants, polymers, textiles, adhesives, and ceramic materials.

28 PROPELLANTS AND FUELS 98
Includes rocket propellants, igniters, and oxidizers; storage and handling; and aircraft fuels.
For related information see also *07 Aircraft Propulsion and Power, 20 Spacecraft Propulsion and Power,* and *44 Energy Production and Conversion.*

ENGINEERING

Includes engineering (general); communications; electronics and electrical engineering; fluid mechanics and heat transfer; instrumentation and photography; lasers and masers; mechanical engineering; quality assurance and reliability; and structural mechanics.
For related information see also *Physics.*

31 ENGINEERING (GENERAL) 102
Includes vacuum technology; control engineering; display engineering; and cryogenics.

32 COMMUNICATIONS 103
Includes land and global communications; communications theory; and optical communications.
For related information see also *04 Aircraft Communications and Navigation* and *17 Spacecraft Communications, Command and Tracking.*

33 ELECTRONICS AND ELECTRICAL ENGINEERING 110
Includes test equipment and maintainability; components, e.g., tunnel diodes and transistors; microminiaturization; and integrated circuitry.
For related information see also *60 Computer Operations and Hardware* and *76 Solid-State Physics.*

34 FLUID MECHANICS AND HEAT TRANSFER 118
Includes boundary layers; hydrodynamics; fluidics; mass transfer; and ablation cooling.
For related information see also *02 Aerodynamics* and *77 Thermodynamics and Statistical Physics.*

35 INSTRUMENTATION AND PHOTOGRAPHY 133
Includes remote sensors; measuring instruments and gages; detectors; cameras and photographic supplies; and holography.
For aerial photography see *43 Earth Resources.* For related information see also *06 Aircraft Instrumentation* and *19 Spacecraft Instrumentation.*

36 LASERS AND MASERS 135
Includes parametric amplifiers.

37 MECHANICAL ENGINEERING 135
Includes auxiliary systems (non-power); machine elements and processes; and mechanical equipment.

38 QUALITY ASSURANCE AND RELIABILITY 152
Includes product sampling procedures and techniques; and quality control.

39 STRUCTURAL MECHANICS 154
Includes structural element design and weight analysis; fatigue; and thermal stress.
For applications see *05 Aircraft Design, Testing and Performance* and *18 Spacecraft Design, Testing and Performance.*

GEOSCIENCES

Includes geosciences (general); earth resources; energy production and conversion; environment pollution; geophysics; meteorology and climatology; and oceanography.
For related information see also *Space Sciences.*

42 GEOSCIENCES (GENERAL) N.A.

43 EARTH RESOURCES N.A.
Includes remote sensing of earth resources by aircraft and spacecraft; photogrammetry; and aerial photography.
For instrumentation see *35 Instrumentation and Photography.*

44 ENERGY PRODUCTION AND CONVERSION 163
Includes specific energy conversion systems, e.g., fuel cells and batteries; global sources of energy; fossil fuels; geophysical conversion; hydroelectric power; and wind power.
For related information see also *07 Aircraft Propulsion and Power, 20 Spacecraft Propulsion and Power, 28 Propellants and Fuels,* and *85 Urban Technology and Transportation.*

45 ENVIRONMENT POLLUTION 186
Includes air, noise, thermal and water pollution; environment monitoring; and contamination control.

46 GEOPHYSICS 187
Includes aeronomy; upper and lower atmosphere studies; ionospheric and magnetospheric physics; and geomagnetism.
For space radiation see *93 Space Radiation.*

47 METEOROLOGY AND CLIMATOLOGY 187
Includes weather forecasting and modification.

48 OCEANOGRAPHY N.A.
Includes biological, dynamic and physical oceanography; and marine resources.

LIFE SCIENCES

Includes sciences (general); aerospace medicine; behavioral sciences; man/system technology and life support; and planetary biology.

51 LIFE SCIENCES (GENERAL) **N.A.**
Includes genetics.

52 AEROSPACE MEDICINE **188**
Includes physiological factors; biological effects of radiation; and weightlessness.

53 BEHAVIORAL SCIENCES **N.A.**
Includes psychological factors; individual and group behavior; crew training and evaluation; and psychiatric research.

54 MAN/SYSTEM TECHNOLOGY AND LIFE SUPPORT **N.A.**
Includes human engineering; biotechnology; and space suits and protective clothing.

55 PLANETARY BIOLOGY **N.A.**
Includes exobiology; and extraterrestrial life.

MATHEMATICAL AND COMPUTER SCIENCES

Includes mathematical and computer sciences (general); computer operations and hardware; computer programming and software; computer systems; cybernetics; numerical analysis; statistics and probability; systems analysis; and theoretical mathematics.

59 MATHEMATICAL AND COMPUTER SCIENCES (GENERAL) **N.A.**

60 COMPUTER OPERATIONS AND HARDWARE **188**
Includes computer graphics and data processing.
For components see *33 Electronics and Electrical Engineering.*

61 COMPUTER PROGRAMMING AND SOFTWARE **189**
Includes computer programs, routines, and algorithms.

62 COMPUTER SYSTEMS **189**
Includes computer networks.

63 CYBERNETICS **190**
Includes feedback and control theory.
For related information see also *54 Man/System Technology and Life Support.*

64 NUMERICAL ANALYSIS **190**
Includes iteration, difference equations, and numerical approximation.

65 STATISTICS AND PROBABILITY **192**
Includes data sampling and smoothing; Monte Carlo method; and stochastic processes.

66 SYSTEMS ANALYSIS **N.A.**
Includes mathematical modeling; network analysis; and operations research.

67 THEORETICAL MATHEMATICS **N.A.**
Includes topology and number theory.

PHYSICS

Includes physics (general); acoustics; atomic and molecular physics; nuclear and high-energy physics; optics; plasma physics; solid-state physics; and thermodynamics and statistical physics.
For related information see also *Engineering.*

70 PHYSICS (GENERAL) **192**
For geophysics see *46 Geophysics.* For astrophysics see *90 Astrophysics.* For solar physics see *92 Solar Physics.*

71 ACOUSTICS **192**
Includes sound generation, transmission, and attenuation.
For noise pollution see *45 Environment Pollution.*

72 ATOMIC AND MOLECULAR PHYSICS **202**
Includes atomic structure and molecular spectra.

73 NUCLEAR AND HIGH-ENERGY PHYSICS **N.A.**
Includes elementary and nuclear particles; and reactor theory.
For space radiation see *93 Space Radiation.*

74 OPTICS **202**
Includes light phenomena.

75 PLASMA PHYSICS **203**
Includes magnetohydrodynamics and plasma fusion.
For ionospheric plasmas see *46 Geophysics.* For space plasmas see *90 Astrophysics.*

76 SOLID-STATE PHYSICS **204**
Includes superconductivity.
For related information see also *33 Electronics and Electrical Engineering* and *36 Lasers and Masers.*

77 THERMODYNAMICS AND STATISTICAL PHYSICS **207**
Includes quantum mechanics; and Bose and Fermi statistics.
For related information see also *25 Inorganic and Physical Chemistry* and *34 Fluid Mechanics and Heat Transfer.*

SOCIAL SCIENCES

Includes social sciences (general); administration and management; documentation and information science; economics and cost analysis; law and political science; and urban technology and transportation.

80 SOCIAL SCIENCES (GENERAL) **208**
Includes educational matters.

81 ADMINISTRATION AND MANAGEMENT **208**
Includes management planning and research.

82 DOCUMENTATION AND INFORMATION SCIENCE **208**
Includes information storage and retrieval technology; micrography; and library science.
For computer documentation see *61 Computer Programming and Software.*

83 ECONOMICS AND COST ANALYSIS **N.A.**
Includes cost effectiveness studies.

84 LAW AND POLITICAL SCIENCE **N.A.**
Includes space law; international law; international cooperation; and patent policy.

85 URBAN TECHNOLOGY AND TRANSPORTATION **209**
Includes applications of space technology to urban problems; technology transfer; technology assessment; and surface and mass transportation.
For related information see *03 Air Transportation and Safety, 16 Space Transportation,* and *44 Energy Production and Conversion.*

SPACE SCIENCES

Includes space sciences (general); astronomy; astrophysics; lunar and planetary exploration; solar physics; and space radiation.
For related information see also *Geosciences.*

88 SPACE SCIENCES (GENERAL) **N.A.**

89 ASTRONOMY **N.A.**
Includes radio and gamma-ray astronomy; celestial mechanics; and astrometry.

90 ASTROPHYSICS **N.A.**
Includes cosmology; and interstellar and interplanetary gases and dust.

91 LUNAR AND PLANETARY EXPLORATION **N.A.**
Includes planetology; and manned and unmanned flights.
For spacecraft design see *18 Spacecraft Design, Testing and Performance.* For space stations see *15 Launch Vehicles and Space Vehicles.*

92 SOLAR PHYSICS **N.A.**
Includes solar activity, solar flares, solar radiation and sunspots.

93 SPACE RADIATION **N.A.**
Includes cosmic radiation; and inner and outer earth's radiation belts.
For biological effects of radiation see *52 Aerospace Medicine.* For theory see *73 Nuclear and High-Energy Physics.*

GENERAL

99 GENERAL **N.A.**

Note: N.A. means that no abstracts were assigned to this category for this issue.

SUBJECT INDEX **A1**
PERSONAL AUTHOR INDEX **B1**
CORPORATE SOURCE INDEX **C1**
CONTRACT NUMBER INDEX **D1**
REPORT/ACCESSION NUMBER INDEX **E1**

Bibliography of Lewis Research Center Technical Publications Announced in 1983

01

AERONAUTICS (GENERAL)

A83-16582*# National Aeronautics and Space Administration. Lewis Research Center, Cleveland, Ohio.
NASA LEWIS RESEARCH CENTER'S PROGRAM ON ICING RESEARCH
J. J. REINMANN, R. J. SHAW, and W. A. OLSEN, JR. (NASA, Lewis Research Center, Cleveland, OH) American Institute of Aeronautics and Astronautics, Aerospace Sciences Meeting, 21st, Reno, NV, Jan. 10-13, 1983, 10 p. refs
(AIAA PAPER 83-0204)

NASA is again actively involved in aircraft icing research. This paper briefly describes the new research activity in ice protection systems, icing instrumentation, experimental methods, analytical modeling for the above, and in-flight research. The renewed interest in aircraft icing has come about mainly because of the new need for all-weather helicopters and general aviation aircraft. Because of increased fuel costs, tomorrow's commercial transports also will require new types of ice protection systems compatible with the more efficient high by-pass and turboprop engines. And all types of aircraft require better estimates of the aeropenalties caused by ice on unprotected surfaces. (Author)

A83-39941*# General Electric Co., Cincinnati, Ohio.
COMPOSITE ENGINE DUCT FABRICATION
R. D. PRATT, C. L. STOTLER, and A. J. WILSON (General Electric Co., Aircraft Engine Business Group, Cincinnati, OH) U.S. Army Materials and Mechanics Research Center, Conference on Fibrous Composites in Structural Design, 6th, New Orleans, LA, Jan. 24-27, 1983, Paper. 9 p.
(Contract NAS3-21854; N00019-82-C-0077)

The trimonomer polyimide resin reinforced with graphite fibers, PMR15, is lower in weight (by 20 percent) and less expensive than titanium. The duct walls are of solid laminate and are made of woven T300 graphite cloth. The original concept for the duct involved a solid shell of T300/PMR15 made up of seven plies of cloth tapered to eleven plies at each end. The bosses and built-up areas around the cutouts are also of T300/PMR15. The end flages riveted to the shell, however, are of titanium. A buckling test demonstrated the ability of the composite analytical design techniques employed to predict the buckling strength of the composite shell. Engines tests are described, noting that the successful repair of a hole demonstrated an important advantage over titanium. The development work now being done to eliminate the titanium end flanges is described, noting that an all-composite duct is in prospect. The savings estimated with a titanium-flanged composite duct are $16,891,000 (1982 dollars) and $35,504,000 (then-year dollars); the savings possible with an all-composite duct are put at $27,025,000 (1982 dollars) and $56,806,000 (then-year dollars). C.R.

N83-14061*# National Aeronautics and Space Administration. Lewis Research Center, Cleveland, Ohio.
AN ANALYTICAL AND EXPERIMENTAL COMPARISON OF THE FLOW FIELD OF AN ADVANCED SWEPT TURBOPROP
H. E. NEUMANN, L. J. BOBER, J. S. SERAFINI, and L. K. CHANG (Purdue Univ., Lafayette, Ind.) 1983 16 p refs Presented at the 21st Aerospace Sci. Conf., Reno, Nev., 10-13 Jan. 1983; sponsored by AIAA Original contains color illustrations
(NASA-TM-83037; E-1481; NAS 1.15:83037; AIAA-83-0189)
Avail: NTIS HC A02/MF A01 CSCL 01B

An argon ion laser velocimeter with four beams was used to measure the detailed flow-field of an advanced eight blade propeller with 45% of tip sweep in an 8x6 foot supersonic wind tunnel. Data were obtained at a free stream Mach number of 0.8, the design advance ratio of 3.06 and a power coefficient of 1.8. Data are presented for inlet flow, exit flow, flow within the blades and flow slightly outside the blade tips. The data are compared to a lifting line theory. In general, the results of the comparison are considered favorable. R.J.F.

N83-16279*# Toledo Univ., Ohio.
SENSOR FAILURE AND MULTIVARIABLE CONTROL FOR AIRBREATHING PROPULSION SYSTEMS Ph.D. Thesis - Dec. 1979 Final Report
K. BEHBEHANI Mar. 1980 244 p refs
(Contract NSG-3084)
(NASA-CR-159791; NAS 1.26:159791) Avail: NTIS HC A11/MF A01 CSCL 01B

A new sensor/actuator failure analysis technique for turbofan jet engines was developed. Three phases of failure analysis, namely detection, isolation, and accommodation are considered. Failure detection and isolation techniques are developed by utilizing the concept of Generalized Likelihood Ratio (GLR) tests. These techniques are applicable to both time varying and time invariant systems. Three GLR detectors are developed for: (1) hard-over sensor failure; (2) hard-over actuator failure; and (3) brief disturbances in the actuators. The probability distribution of the GLR detectors and the detectability of sensor/actuator failures are established. Failure type is determined by the maximum of the GLR detectors. Failure accommodation is accomplished by extending the Multivariable Nyquest Array (MNA) control design techniques to nonsquare system designs. The performance and effectiveness of the failure analysis technique are studied by applying the technique to a turbofan jet engine, namely the Quiet Clean Short Haul Experimental Engine (QCSEE). Single and multiple sensor/actuator failures in the QCSEE are simulated and analyzed and the effects of model degradation are studied.
Author

N83-17453*# Neilsen Engineering and Research, Inc., Mountain View, Calif.
DEVELOPMENT OF A MULTIPLE-PARAMETER NONLINEAR PERTURBATION PROCEDURE FOR TRANSONIC TURBOMACHINERY FLOWS: PRELIMINARY APPLICATION TO DESIGN/OPTIMIZATION PROBLEMS Final Report
S. S. STAHARA, J. P. ELLIOTT, and J. R. SPREITER Washington NASA Jan. 1983 120 p refs
(Contract NAS3-20836)
(NASA-CR-3657; E-1395; NAS 1.26:3657; NEAR-TR-276) Avail: NTIS HC A06/MF A01 CSCL 01A

An investigation was conducted to continue the development of perturbation procedures and associated computational codes for rapidly determining approximations to nonlinear flow solutions, with the purpose of establishing a method for minimizing computational requirements associated with parametric design studies of transonic flows in turbomachines. The results reported here concern the extension of the previously developed successful method for single parameter perturbations to simultaneous multiple-parameter perturbations, and the preliminary application of the multiple-parameter procedure in combination with an optimization method to blade design/optimization problem. In order to provide as severe a test as possible of the method, attention is focused in particular on transonic flows which are highly supercritical. Flows past both isolated blades and compressor cascades, involving simultaneous changes in both flow and geometric parameters, are considered. Comparisons with the corresponding exact nonlinear solutions display remarkable accuracy and range of validity, in direct correspondence with previous results for single-parameter perturbations. B.W.

N83-22092*# National Aeronautics and Space Administration. Lewis Research Center, Cleveland, Ohio.
NEW TEST TECHNIQUES AND ANALYTICAL PROCEDURES FOR UNDERSTANDING THE BEHAVIOR OF ADVANCED PROPELLERS
G. L. STEFKO, L. J. BOBER, and H. E. NEUMANN 1983 24 p refs Presented at the 1983 Business Aircraft Meeting and Exposition, Wichita, Kans., 12-15 Apr. 1983; sponsored by the Society of Automotive Engineers
(NASA-TM-83360; E-1622; NAS 1.15:83360; SAE-830729) Avail: NTIS HC A02/MF A01 CSCL 01B

Analytical procedures and experimental techniques were developed to improve the capability to design advanced high speed propellers. Some results from the propeller lifting line and lifting surface aerodynamic analysis codes are compared with propeller force data, probe data and laser velocimeter data. In general, the code comparisons with data indicate good qualitative agreement. A rotating propeller force balance demonstrated good accuracy and reduced test time by 50 percent. Results from three propeller flow visualization techniques are shown which illustrate some of the physical phenomena occurring on these propellers. S.L.

N83-24467*# National Aeronautics and Space Administration. Lewis Research Center, Cleveland, Ohio.
EFFICIENT SOLUTION OF THE EULER AND NAVIER-STOKES EQUATIONS WITH A VECTORIZED MULTIPLE-GRID ALGORITHM
R. V. CHIMA and G. M. JOHNSON 1983 31 p refs Proposed for presentation at the 6th Computational Fluid Dyn. Conf., Danvers, Mass., 13-15 Jul. 1983; sponsored by AIAA
(NASA-TM-83376; E-1644; NAS 1.15:83376) Avail: NTIS HC A03/MF A01 CSCL 01A

A multiple-grid algorithm for use in efficiently obtaining steady solutions to the Euler and Navier-Stokes equations is presented. The convergence of the explicit MacCormack algorithm on a fine grid is accelerated by propagating transients from the domain using a sequence of successively coarser grids. Both the fine and coarse grid schemes are readily vectorizable. The combination of multiple-gridding and vectorization results in substantially reduced computational times for the numerical solution of a wide range of flow problems. Results are presented for subsonic, transonic, and supersonic inviscid flows and for subsonic attached and separated laminar viscous flows. Work reduction factors over a scalar, single-grid algorithm range as high as 76.8. M.G.

N83-34885*# National Aeronautics and Space Administration. Lewis Research Center, Cleveland, Ohio.
DESIGN OF A MICROPROCESSOR-BASED CONTROL, INTERFACE AND MONITORING (CIM UNIT FOR TURBINE ENGINE CONTROLS RESEARCH
J. C. DELAAT and J. F. SOEDER Jun. 1983 39 p refs
(NASA-TM-83433; E-1725; NAS 1.15:83433) Avail: NTIS HC A03/MF A01 CSCL 01B

High speed minicomputers were used in the past to implement advanced digital control algorithms for turbine engines. These minicomputers are typically large and expensive. It is desirable for a number of reasons to use microprocessor-based systems for future controls research. They are relatively compact, inexpensive, and are representative of the hardware that would be used for actual engine-mounted controls. The Control, Interface, and Monitoring Unit (CIM) contains a microprocessor-based controls computer, necessary interface hardware and a system to monitor while it is running an engine. It is presently being used to evaluate an advanced turbofan engine control algorithm. Author

N83-34886*# National Aeronautics and Space Administration. Lewis Research Center, Cleveland, Ohio.
THE TREND OF FUTURE GAS TURBINE TECHNOLOGY
M. J. HARTMAN 1983 16 p Presented at the Tokyo Intern. Gas Turbine Congr., Tokyo, 23-28 Oct. 1983; sponsored by GTSJ, AMSE, IMechE, JSME, and VDI
(NASA-TM-83505; E-1844; NAS 1.15:83505) Avail: NTIS HC A02/MF A01 CSCL 01B

Turbomachinery system component research to advance the technology of aviation turbofan and turbojet engines is discussed. Areas of research include compressors, turbines, internal flow analysis, combustion, fuels, materials, structures, bearings, seals, lubrication, dynamics and controls, and instrumentation. A review of the research directions being taken in these areas and the steady advances being made provides a reasonable glimpse at gas turbine technology of the future. Author

02

AERODYNAMICS

Includes aerodynamics of bodies, combinations, wings, rotors, and control surfaces; and internal flow in ducts and turbomachinery.

A83-16455*# National Aeronautics and Space Administration. Lewis Research Center, Cleveland, Ohio.
EXPERIMENTAL EVALUATION OF SHOCKLESS SUPERCRITICAL AIRFOILS IN CASCADE
D. R. BOLDMAN, A. E. BUGGELE, and L. M. SHAW (NASA, Lewis Research Center, Cleveland, OH) American Institute of Aeronautics and Astronautics, Aerospace Sciences Meeting, 21st, Reno, NV, Jan. 10-13, 1983, 11 p. refs
(AIAA PAPER 83-0003)

Surface Mach number distributions, total pressure loss coefficients, and schlieren images of the flow are presented over a range of inlet Mach numbers and air angles. Several different trailing edge geometries were tested. At design conditions a leading edge separation bubble was observed resulting in higher losses than anticipated. The minimum losses were obtained at a negative incidence condition in which the flow was accelerating over most of the supercritical region. Relatively minor differences in losses were measured with the different trailing edge geometries studied. (Author)

A83-16525*# Ohio State Univ., Columbus.
AN ANALYTICAL EVALUATION OF THE ICING PROPERTIES OF SEVERAL LOW AND MEDIUM SPEED AIRFOILS
M. B. BRAGG and G. M. GREGOREK (Ohio State University, Columbus, OH) American Institute of Aeronautics and Astronautics, Aerospace Sciences Meeting, 21st, Reno, NV, Jan. 10-13, 1983, 16 p. refs
(Contract NAG3-28)
(AIAA PAPER 83-0109)

A droplet trajectory computer code is used to analyze the water droplet impingement characteristics of several low and medium speed airfoils. The results are reported in terms of the airfoil maximum impingement efficiency, and limits of impingement. The airfoils are analyzed for angles of attack of -4 to 12 degrees, and modified inertia parameters of 0.01 to 1.0. These data are then used to evaluate the effect of airfoil geometry: leading edge radius, maximum thickness, maximum camber, and angle of attack on airfoil icing characteristics. Airfoils from the NACA four digit series to the new NASA NLF airfoils are considered. The strongest correlations were seen between airfoil leading edge radius and maximum local collection efficiency, thickness and total collection efficiency, and camber and the limits of impingement. (Author)

A83-16614*# Georgia Inst. of Tech., Atlanta.
A VISCOUS-INVISCID INTERACTIVE PROCEDURE FOR ROTATIONAL FLOW IN CASCADES OF TWO-DIMENSIONAL AIRFOILS OF ARBITRARY SHAPE
W. JOHNSTON (Georgia Institute of Technology, Atlanta, GA) and P. SOCKOL (NASA, Lewis Research Center, Viscous Methods Section, Cleveland, OH) American Institute of Aeronautics and Astronautics, Aerospace Sciences Meeting, 21st, Reno, NV, Jan. 10-13, 1983, 14 p. refs
(Contract NSG-3260)
(AIAA PAPER 83-0256)

A viscous-inviscid interactive calculation procedure is developed for application to flow in cascades of two-dimensional airfoils. This procedure has essentially three components. First, a numerical solution of the Euler equations which can accommodate an arbitrarily specified cascade geometry is carried out on a nonorthogonal curvileanear grid mesh that is fitted to the geometry of the cascade. A method of grid generation has been used which relies in part on a succession of conformal mappings. Second, a viscous solution for use in boundary layer and wake regions has been programmed. Finally, an interactive scheme which takes the form of a source-sink distribution along the blade surface and wake centerline is employed. Results have been obtained with this procedure for several cascade flow situations, and some comparisons with experiment are presented. (Author)

A83-16823*# National Aeronautics and Space Administration. Lewis Research Center, Cleveland, Ohio.
NUMERICAL SOLUTION TO THE GLANCING SIDEWALL OBLIQUE SHOCK WAVE/TURBULENT BOUNDARY LAYER INTERACTION IN THREE-DIMENSION
B. H. ANDERSON and T. J. BENSON (NASA, Lewis Research Center, Cleveland, OH) American Institute of Aeronautics and Astronautics, Aerospace Sciences Meeting, 21st, Reno, NV, Jan. 10-13, 1983, 22 p. refs
(AIAA PAPER 83-0136)

A supersonic three-dimensional viscous forward-marching computer design code called PEPSIS is used to obtain a numerical solution of the three-dimensional problem of the interaction of a glancing sidewall oblique shock wave and a turbulent boundary layer. Very good results are obtained for a test case that was run to investigate the use of the wall-function boundary-condition approximation for a highly complex three-dimensional shock-boundary layer interaction. Two additional test cases (coarse mesh and medium mesh) are run to examine the question of near-wall resolution when no-slip boundary conditions are applied. A comparison with experimental data shows that the PEPSIS code gives excellent results in general and is practical for three-dimensional supersonic inlet calculations. F.G.M.

A83-19581*# National Aeronautics and Space Administration. Lewis Research Center, Cleveland, Ohio.
EXPERIMENTAL INVESTIGATION OF A TWO-DIMENSIONAL SHOCK-TURBULENT BOUNDARY LAYER INTERACTION WITH BLEED
W. R. HINGST and F. T. TANJI (NASA, Lewis Research Center, Cleveland, OH) American Institute of Aeronautics and Astronautics, Aerospace Sciences Meeting, 21st, Reno, NV, Jan. 10-13, 1983, 17 p. refs
(AIAA PAPER 83-0135)

The two-dimensional interaction of an oblique shock wave with a turbulent boundary layer that included the effect of bleed was examined experimentally using a shock generator mounted across a supersonic wind tunnel. The studies were performed at Mach numbers 2.5 and 2.0 and unit Reynolds number of approximately 2.0 x 10 to the 7th/meter. The study includes surface oil flow visualization, wall static pressure distributions and boundary layer pitot pressure profiles. In addition, the variation of the local bleed rates were measured. The results show the effect of the bleed on the boundary layer as well as the effect of the flow conditions on the local bleed rate. (Author)

A83-21080*# National Aeronautics and Space Administration. Lewis Research Center, Cleveland, Ohio.
AN ANALYTICAL AND EXPERIMENTAL COMPARISON OF THE FLOW FIELD OF AN ADVANCED SWEPT TURBOPROP
H. E. NEUMANN, L. J. BOBER, J. S. SERAFINI (NASA, Lewis Research Center, Cleveland, OH), and L.-K. CHANG (Purdue University, West Lafayette, IN) American Institute of Aeronautics and Astronautics, Aerospace Sciences Meeting, 21st, Reno, NV, Jan. 10-13, 1983, 15 p. refs
(AIAA PAPER 83-0189)
(Previously announced in STAR as N83-14061)

A83-22129*# Purdue Univ. School of Science at Indianapolis, Ind.
A FINITE ELEMENT FORMULATION FOR STEADY TRANSONIC EULER EQUATIONS
A. ECER and H. U. AKAY (Purdue University, Indianapolis, IN) AIAA Journal, vol. 21, Mar. 1983, p. 343-350. refs
(Contract NSG-3294)
(Previously cited in issue 06, p. 795, Accession no. A82-17759)

A83-22138*# Pennsylvania State Univ., University Park.
BLADE LOADING AND ROTATION EFFECTS ON COMPRESSOR ROTOR WAKE NEAR END WALLS
B. LAKSHMINARAYANA, T. R. GOVINDAN, and B. REYNOLDS (Pennsylvania State University, University Park, PA) AIAA Journal, vol. 21, Mar. 1983, p. 407-414. refs
(Contract NSG-3012)
(Previously cited in issue 08, p. 1179, Accession no. A82-22063)

A83-27478*# Cincinnati Univ., Ohio.
SOLID PARTICLE DYNAMIC BEHAVIOR THROUGH TWISTED BLADE ROWS
A. HAMED (Cincinnati, University, Cincinnati, OH) In: Particulate laden flows in turbomachinery; Proceedings of the Joint Fluids, Plasma, Thermophysics and Heat Transfer Conference, St. Louis, MO, June 7-11, 1982. New York, American Society of Mechanical Engineers, 1982, p. 33-41. refs
(Contract N00014-78-C-0590; NSG-3218)

The particle trajectory calculations provide the essential information which is required for predicting the pattern and intensity of turbomachinery erosion. Consequently, the evaluation of the machine performance deterioration due to erosion is extremely sensitive to the accuracy of the flow field and blade geometry representation in the trajectory computational model. A model is presented that is simple and efficient yet versatile and general to be applicable to axial, radial and mixed flow machines, and to inlets, nozzles, return passages and separators. The results of the computations are presented for the particle trajectories through

a row of twisted vanes in the inlet flow field. The effect of the particle size on their trajectories, blade impacts, and on their redistribution and separation are discussed. (Author)

A83-28833*# National Aeronautics and Space Administration. Lewis Research Center, Cleveland, Ohio.
COMPARISON OF LASER ANEMOMETER MEASUREMENTS AND THEORY IN AN ANNULAR TURBINE CASCADE WITH EXPERIMENTAL ACCURACY DETERMINED BY PARAMETER ESTIMATION
L. J. GOLDMAN and R. G. SEASHOLTZ (NASA, Lewis Research Center, Cleveland, OH) IN: Engineering applications of laser velocimetry; Proceedings of the Symposium, Phoenix, AZ, November 14-19, 1982 . New York, American Society of Mechanical Engineers, 1982, p. 83-92. refs
Previously announced in STAR as N82-28250

A83-28843*# Pennsylvania State Univ., University Park.
INVESTIGATION OF THE TIP CLEARANCE FLOW INSIDE AND AT THE EXIT OF A COMPRESSOR ROTOR PASSAGE. II - TURBULENCE PROPERTIES
A. PANDYA and B. LAKSHMINARAYANA (Pennsylvania State University, University Park, PA) ASME, Transactions, Journal of Engineering for Power (ISSN 0022-0825), vol. 105, Jan. 1983, p. 13-17.
(Contract NSG-3212)
The flow in the tip clearance region of a compressor rotor is highly turbulent due to the strong interaction of the leakage flow with the annulus wall boundary layer. This paper deals with the turbulence properties of the flow in the tip clearance region of a moderately loaded compressor rotor. The experimental results reported in this paper were obtained using a two-sensor hot-wire probe in combination with an ensemble averaging technique. Blade-to-blade distribution of the axial and tangential turbulence intensities at various radial locations and ten axial locations (four inside the blade passage and the remaining six outside the passage) were derived from this data. Isointensity contours in the clearance region at various radial locations were also obtained from the experimental data. A region of very high turbulence intensities was indicated at the half-chord location from these results. The turbulence intensity profiles also indicated that the leakage flow travels toward the midpassage before rolling up. The turbulence is almost isotropic beyond three-quarter chord downstream of the trailing edge. Author

A83-29012*# Lockheed-California Co., Burbank.
ZERO-LENGTH INLETS FOR SUBSONIC V/STOL AIRCRAFT
E. R. GLASGOW, W. E. BECK (Lockheed-California Co., Burbank, CA), and R. R. WOOLLETT (NASA, Lewis Research Center, Cleveland, OH) Journal of Aircraft (ISSN 0021-8669), vol. 20, May 1983, p. 397-403. refs
(Contract NAS3-21461)
Previously cited in issue 19, p. 3257, Accession no. A81-42186

A83-29535*# National Aeronautics and Space Administration. Lewis Research Center, Cleveland, Ohio.
PREDICTION OF HIGH SPEED PROPELLER FLOW FIELDS USING A THREE-DIMENSIONAL EULER ANALYSIS
L. J. BOBER (NASA, Lewis Research Center, Cleveland, OH), D. S. CHAUSSEE, and P. KUTLER (NASA, Ames Research Center, Moffett Field, CA) American Institute of Aeronautics and Astronautics, Aerospace Sciences Conference, 21st, Reno, NV, Jan. 10-13, 1983. 31 p. refs
(AIAA PAPER 83-0188)
Previously announced in STAR as N83-19710

A83-35855*# Pennsylvania State Univ., University Park.
TIP CLEARANCE FLOW IN A COMPRESSOR ROTOR PASSAGE AT DESIGN AND OFF-DESIGN CONDITIONS
B. LAKSHMINARAYANA and A. PANDYA (Pennsylvania State University, University Park, PA) IN: International Symposium on Air Breathing Engines, 6th, Paris, France, June 6-10, 1983, Symposium Papers . New York, American Institute of Aeronautics and Astronautics, 1983, p. 468-478. refs
(Contract NSG-3212)
The flow field in the tip clearance region of a compressor rotor at an off-design condition is reported in this paper. The earlier data at the design condition has also been re-interpreted and correlated with the blade and the flow parameters. The measurements inside the rotor tip region are acquired using a miniature hot wire sensor of 'V' configuration. The instantaneous velocity data is analyzed by the ensemble averaging technique to derive the blade-to-blade velocity field at various axial and radial locations between the rotor tip and the casing. The flow and the blade pressure data at the design condition are compared with the data at the off-design condition (lower blade loading). In addition to a reduction in the leakage velocities, its chordwise variation is also altered substantially at the lower blade loading. Author

A83-36391*# Garrett Turbine Engine Co., Phoenix, Ariz.
THREE-DIMENSIONAL COMPRESSIBLE VISCOUS ANALYSIS OF MIXER NOZZLES
R. K. GOYAL, W. L. BLACKMORE (Garrett Turbine Engine Co., Phoenix, AZ), V. HEAD, and L. POVINELLI (NASA, Lewis Research Center, Cleveland, OH) AIAA, SAE, and ASME, Joint Propulsion Conference, 19th, Seattle, WA, June 27-29, 1983. 13 p. refs
(AIAA PAPER 83-1401)
An analysis-based design procedure for compound-mixer exhaust nozzles is presented and compared to test data. The design approach is based on two numerical solutions to the 3-D viscous compressible Navier-Stokes equations: an equation splitting technique used for the analysis of the core and bypass flow, and a parabolic marching scheme used in the analysis of the mixing duct. The selection of the analytical methods through test data comparisons and their coupling into an integrated design system are discussed. NASA test data is used to demonstrate the validity of the computations from the exhaust system rating station, upstream of the mixer lobe, to the nozzle throat. An estimate is made of the savings in development time and cost utilizing the new procedure. Author

A83-37218*# Tennessee Univ. Space Inst., Tullahoma.
MEASUREMENTS OF COMPRESSIBLE SECONDARY FLOW IN A CIRCULAR S-DUCT
A. VAKILI, J. M. WU, P. LIVER, and M. K. BHAT (Tennessee, University, Tullahoma, TN) American Institute of Aeronautics and Astronautics, Fluid and Plasma Dynamics Conference, 16th, Danvers, MA, July 12-14, 1983. 9 p. refs
(Contract NAG3-233)
(AIAA PAPER 83-1739)
This paper presents the results of an experimental study of secondary flow in a circular cross section 30 deg - 30 deg S-duct with entrance Mach number of 0.6. Local flow velocity vectors have been measured along the length of the duct at six stations. These measurements have been made using a five-port cone probe. Static and total pressure profiles in the transverse planes are obtained from the cone probe measurements. Wall static pressure measurements along three azimuth angles of 0 deg, 90 deg, and 180 deg along the duct are also made. Contour plots presenting the three dimensional velocity field as well as the total- and static-pressure fields are obtained. Surface oil flow visualization technique has been used to provide details of the flow on the S-duct boundaries. The experimental observations have been compared with typical computational results. Author

A83-37957* Lockheed-Georgia Co., Marietta.
INLET DESIGN FOR HIGH-SPEED PROPFANS
B. H. LITTLE, JR. and B. L. HINSON (Lockheed-Georgia Co., Marietta, GA) Society of Automotive Engineers, Aerospace Congress and Exposition, Anaheim, CA, Oct. 25-28, 1982. 15 p. refs
(Contract NAS3-22751)
(SAE PAPER 821359)

A two-part study was performed to design inlets for high-speed propfan installation. The first part was a parametric study to select promising inlet concepts. A wide range of inlet geometries was examined and evaluated - primarily on the basis of cruise thrust and fuel burn performance. Two inlet concepts were than chosen for more detailed design studies - one apropriate to offset engine/gearbox arrangements and the other to in-line arrangements. In the second part of this study, inlet design points were chosen to optimize the net installed thrust, and detailed design of the two inlet configurations was performed. An analytical methodology was developed to account for propfan slipstream effects, transonic flow efects, and three-dimensional geometry effects. Using this methodology, low drag cowls were designed for the two inlets. Author

A83-38652*# Purdue Univ., Lafayette, Ind.
QUASI-THREE-DIMENSIONAL TURBOMACHINERY FLOW CALCULATIONS ON MULTIPLE HUB-TO-SHROUD STREAM SURFACES
H. D. THOMPSON (Purdue University, West Lafayette, IN), K. M. RAGSDELL (Arizona, University, Tucson, AZ), and M. A. ROBINSON American Institute of Aeronautics and Astronautics, Applied Aerodynamics Conference, Danvers, MA, July 13-15, 1983. 15 p. refs
(Contract NSG-3105)
(AIAA PAPER 83-1820)

Results are presented from a quasi-three-dimensional calculation of steady (relative), inviscid, adiabatic, subsonic/shock-free transonic flow on multiple hub-to-shroud stream surfaces through turbomachinery blade rows. The quasi-three-dimensional technique incorporates some three-dimensional effects while retaining much of the simplicity of two-dimensional computational methods. Three typical turbomachinery flowfield calculations are presented including an axial-flow compressor rotor, a turbine stator vane cascade, and a radial-inflow turbine rotor. The calculations were performed using quasi-three-dimensional extensions of existing two-dimensional methods. The current results represent an intermediate step in the complete quasi-three-dimensional solution process. However, the results demonstrate the usefulness of the quasi-three-dimensional technique in complementing and extending the applicability of the two-dimensional methods of turbomachinery flow analysis. Author

A83-38798* Flow Research, Inc., Kent, Wash.
AN EXPERIENCE IN MESH GENERATION FOR THREE-DIMENSIONAL CALCULATION OF POTENTIAL FLOW AROUND A ROTATING PROPELLER
W.-H. JOU (Flow Research Co., Kent, WA) IN: Numerical grid generation; Proceedings of the Symposium on Numerical Generation of Curvilinear Coordinate Systems and Their Use in the Numerical Solution of Partial Differential Equations, Nashville, TN, April 13-16, 1982 . New York and Amsterdam, North-Holland, 1982, p. 547-561. refs
(Contract NAS3-22148)

An attempt is made to develop a three-dimensional, finite volume computational code for highly swept, twisted, small aspect ratio propeller blades with supersonic tip speeds, in a way that accounts for cascade effects, hub-induced flow, and nonlinear transonic effects. Attention is presently given to the generation of a computational mesh for such a complex propeller configuration, with the aim of sharing developmental process experience. The problem treated is unique, in that blade chord, blade length, hub length and blade-to-blade distance represent several characteristic length scales among which there is considerable disparity. An ad hoc mesh-generation scheme is accordingly developed. O.C.

A83-39358*# Scientific Research Associates, Inc., Glastonbury, Conn.
NUMERICAL SOLUTION OF THE NAVIER-STOKES EQUATIONS FOR COMPRESSIBLE TURBULENT TWO/THREE DIMENSIONAL FLOWS IN THE TERMINAL SHOCK REGION OF AN INLET/DIFFUSER
N.-S. LIU, S. J. SHAMROTH, and H. MCDONALD (Scientific Research Associates, Inc., Glastonbury, CT) IN: Computational Fluid Dynamics Conference, 6th, Danvers, MA, July 13-15, 1983, Collection of Technical Papers . New York, American Institute of Aeronautics and Astronautics, 1983, p. 61-71. refs
(Contract NAS3-22747)
(AIAA PAPER 83-1892)

The multidimensional, ensemble-averaged, compressible, time-dependent Navier-Stokes equations in conjunction with mixing length turbulence model and shock capturing technique have been used to study the terminal shock type of flows in various flight regimes occurring in a diffuser/inlet model. The numerical scheme for solving the governing equations is based on a linearized block implicit approach and the following high Reynolds number calculations have been carried out: (1) 2-D, steady, subsonic; (2) 2-D, steady, transonic with normal shock, (3) 2-D, steady, supersonic with terminal shock, (4) 2-D, transient process of shock development and (5) 3-D, steady, transonic with normal shock. The numerical results obtained for the 2-D and 3-D transonic shocked flows have been compared with corresponding experimental data; the calculated wall static pressure distributions agree well with the measured data. The predicted transient responses of the flow to externally applied impulsive disturbance are consistent with results obtained via asymptotic analysis.
Author

A83-39359*# National Aeronautics and Space Administration. Lewis Research Center, Cleveland, Ohio.
EFFICIENT SOLUTION OF THE EULER AND NAVIER-STOKES EQUATIONS WITH A VECTORIZED MULTIPLE-GRID ALGORITHM
R. V. CHIMA and G. M. JOHNSON (NASA, Lewis Research Center, Cleveland, OH) IN: Computational Fluid Dynamics Conference, 6th, Danvers, MA, July 13-15, 1983, Collection of Technical Papers . New York, American Institute of Aeronautics and Astronautics, 1983, p. 72-89. refs
(AIAA PAPER 83-1893)

A multiple-grid algorithm for use in efficiently obtaining steady solutions to the Euler and Navier-Stokes equations is presented. The convergence of the explicit MacCormack algorithm on a fine grid is accelerated by propagating transients from the domain using a sequence of successively coarser grids. Both the fine and coarse grid schemes are readily vectorizable. The combination of multiple-gridding and vectorization results in substantially reduced computational times for the numerical solution of a wide range of flow problems. Results are presented for subsonic, transonic, and supersonic inviscid flows and for subsonic attached and separated laminar viscous flows. Work reduction factors over a scalar, single-grid algorithm range as high as 76.8. Previously announced in STAR as N83-24467 M.G.

A83-39392*# National Aeronautics and Space Administration. Lewis Research Center, Cleveland, Ohio.
MULTIPLE-GRIDDING OF THE EULER EQUATIONS WITH AN IMPLICIT SCHEME
R. M. STUBBS (NASA, Lewis Research Center, Cleveland, OH) IN: Computational Fluid Dynamics Conference, 6th, Danvers, MA, July 13-15, 1983, Collection of Technical Papers . New York, American Institute of Aeronautics and Astronautics, 1983, p. 383-389. refs
(AIAA PAPER 83-1945)

The multiple-grid scheme of Ni (1981) for the solution of the unsteady Euler equations for quasi-one-dimensional transonic flow problems is analyzed according to its ability to accelerate

convergence to a steady state solution, its applicability to an implicit scheme, its accuracy, and its stability limits. This scheme is applied successfully to McCormack's (1981) implicit method of solving quasi-one-dimensional transonic flow problems for CFL numbers significantly greater than unity. It is determined that the second order accuracy of this implicit method is preserved by employing the multiple gridding. However, stability limitations that are flow dependent are introduced into the implicit method by the use of the multiple-grid scheme which will curtail its use under certain flow conditions. A scaling modification for the multiple grid scheme is developed which further improves its performance when used with explicit and artificially-damped implicit methods without any increase in computational work. N.B.

A83-42100*# National Aeronautics and Space Administration. Lewis Research Center, Cleveland, Ohio.
EXPERIMENTAL RESULTS OF A DEFLECTED THRUST V/STOL NOZZLE RESEARCH PROGRAM
P. L. BURSTADT and A. L. JOHNS (NASA, Lewis Research Center, Cleveland, OH) American Institute of Aeronautics and Astronautics, Aerospace Sciences Conference, 21st, Reno, NV, Jan. 10-13, 1983. 25 p. refs
(AIAA PAPER 83-0170)

Four deflected thrust nozzle concepts, designed to operate at the low pressure ratio typical of high bypass-ratio turbofan engines for medium speed (subsonic) V/STOL aircraft, were studied. Maps of overall performance characteristics and exit velocity distributions are used to highlight similarities and differences between the four concepts. Analytically determined secondary flows at the exit of a 90 deg circular pipe bend are compared with the experimental results from the more complex three dimensional geometries. The relative impact of total-pressure losses and secondary flows on nozzle thrust coefficient is addressed by numerical integration of exit velocity measurements. Previously announced in STAR as N83-25657 Author

A83-42562*# Cincinnati Univ., Ohio.
EFFECT OF PARTICLE PRESENCE ON THE INCOMPRESSIBLE INVISCID FLOW THROUGH A TWO DIMENSIONAL COMPRESSOR CASCADE
C. BALAN and W. TABAKOFF (Cincinnati, University, Cincinnati, OH) IN: Annual Mini-Symposium on Aerospace Science and Technology, 9th, Wright-Patterson AFB, OH, March 22, 1983, Proceedings . New York, American Institute of Aeronautics and Astronautics, 1983, p. 13-6-1 to 13-6-5. refs
(Contract NSG-3218; DAAG29-82-K-0029)

A computational model for calculating the flow field, in the presence of solid particles, through a two dimensional compressor cascade is presented. The method treats the particle phase in the Lagrangian system and the fluid phase in the Eulerian system. The equations of momentum of the fluid phase are modified to account for the momentum exchange between the two phases. The resulting modified momentum and continuity equations are reduced to the conventional stream function-vorticity formulation. The analysis yields the change in the blade surface pressure distribution, the total pressure and velocity in the flow field. Based on this, it is possible to predict the decrease in compressor performance under the presence of particles. Author

A83-43446*# National Aeronautics and Space Administration. Lewis Research Center, Cleveland, Ohio.
DESIGN OF SUPERCRITICAL CASCADES WITH HIGH SOLIDITY
J. M. SANZ (NASA, Lewis Research Center, Fluid Mechanics and Acoustics Div., Cleveland, OH) AIAA Journal (ISSN 0001-1452), vol. 21, Sept. 1983, p. 1289-1293. refs

Previously cited in issue 15, p. 2343, Accession no. A82-31931

A83-45508*# National Aeronautics and Space Administration. Lewis Research Center, Cleveland, Ohio.
AERODYNAMIC PERFORMANCE OF A FAN STAGE UTILIZING VARIABLE INLET GUIDE VANES (VIGV'S) FOR THRUST MODULATION
R. R. WOOLLETT (NASA, Lewis Research Center, Cleveland, OH) AIAA, SAE, and ASME, Joint Propulsion Conference, 19th, Seattle, WA, June 27-29, 1983. 16 p. refs
(AIAA PAPER 83-1162)

An experimental research program was conducted in the Lewis Research Center's 9 x 15-foot (2.74 x 4.57 m) low speed wind tunnel to evaluate the aerodynamic performance of an inlet and fan system with variable inlet guide vanes (VIGVs) for use on a subsonic V/STOL aircraft. At high VIGV blade angles (lower weight flow and thrust levels), the fan stage was stalled over a major portion of its radius. In spite of the stall, fan blade stresses only exceeded the limits at the most extreme flow conditions. It was found that inlet flow separation does not necessarily lead to poor inlet performance or adverse fan operating conditions. Generally speaking, separated inlet flow did not adversely affect the fan blade stress levels. There were some cases, however, at high VIGV angles and high inlet angles-of-attack where excessive blade stress levels were encountered. An evaluation term made up of the product of the distortion parameter, K alpha, the weight flow and the fan pressure ratio minus one, was found to correlate quite well with the observed blade stress results. Previously announced in STAR as N83-27957 Author

A83-45509*# National Aeronautics and Space Administration. Lewis Research Center, Cleveland, Ohio.
A SURVEY OF INLET/ENGINE DISTORTION COMPATIBILITY
D. N. BOWDITCH and R. E. COLTRIN (NASA, Lewis Research Center, Cleveland, OH) AIAA, SAE, and ASME, Joint Propulsion Conference, 19th, Seattle, WA, June 27-29, 1983. 21 p. refs
(AIAA PAPER 83-1166)

The history of distortion analysis is traced back to its origin in parallel compressor theory which was initially proposed in the late fifties. The development of this theory is reviewed up to its inclusion in the complex computer codes of today. It is found to be a very useful tool to guide development but not quantitative enough to predict compatibility. Dynamic or instantaneous distortion methodology is also reviewed from its origins in the sixties, to its current application in the eighties. Many of the requirements for interpreting instantaneous distortion are considered and illustrated. Statistical methods for predicting the peak distortion are described, and their limitations and advantages discussed. Finally, some Reynolds number and scaling considerations for inlet testing are considered. It is concluded that the deterministic instantaneous distortion methodology combined with distortion testing of engines with screens will remain the primary method of predicting compatibility for the near future. However, parallel compressor analysis and statistical peak distortion prediction will be important tools employed during the development of inlet/engine compatibility. Previously announced in STAR as N83-27991 Author

A83-45510*# National Aeronautics and Space Administration. Lewis Research Center, Cleveland, Ohio.
ANALYTICAL AND EXPERIMENTAL STUDY OF FLOW THROUGH AN AXIAL TURBINE STAGE WITH A NONUNIFORM INLET RADIAL TEMPERATURE PROFILE
J. R. SCHWAB, R. G. STABE, and W. J. WHITNEY (NASA, Lewis Research Center, Cleveland, OH) AIAA, SAE, and ASME, Joint Propulsion Conference, 19th, Seattle, WA, June 27-29, 1983. 23 p. refs
(AIAA PAPER 83-1175)

Results are presented for a typical nonuniform inlet radial temperature profile through an advanced single-stage axial turbine and compared with the results obtained for a uniform profile. Gas temperature rises of 40 K to 95 K are predicted at the hub and tip corners at the trailing edges of the pressure surfaces in both the stator and rotor due to convection of hot fluid from the mean by the secondary flow. The inlet temperature profile is shown to

be mixed out at the rotor exit survey plane (2.3 axial chords downstream of the rotor trailing edge) in both the analysis and the experiment. The experimental rotor exit angle profile for the nonuniform inlet temperature profile indicates underturning at the tip caused by increased clearance. Severe underturning also occurs at the mean, both with and without the nonuniform inlet temperature profile. The inviscid rotational flow code used in the analysis fails to predict the underturning at the mean, which may be caused by viscous effects. Previously announced in STAR as N83-27958
Author

A83-45516*# National Aeronautics and Space Administration. Lewis Research Center, Cleveland, Ohio.
LOW SPEED PERFORMANCE OF A SUPERSONIC AXISYMMETRIC MIXED COMPRESSION INLET WITH AUXILIARY INLETS
J. F. WASSERBAUER, R. W. CUBBISON, and C. J. TREFNY (NASA, Lewis Research Center, Cleveland, OH) AIAA, SAE, and ASME, Joint Propulsion Conference, 19th, Seattle, WA, June 27-29, 1983. 31 p. refs
(AIAA PAPER 83-1414)

The aerodynamic performance of a representative supersonic cruise inlet was investigated using a fan simulator coupled to the inlet to provide characteristic noise signatures and to pump the inlet flow. Data were obtained at Mach numbers from 0 to 0.2 for the inlet equipped with an auxiliary inlet system that provided 20 to 40 percent of the fan flow. Results show that inlet performance improved when the inlet bleed systems were sealed; when the freestream Mach number was increased; and when the auxiliary inlets were opened. The inlet flow could not be choked by either centerbody translation or by increasing the fan speed when the 40 percent auxiliary inlet was incorporated. Previously announced in STAR as N83-27992
A.R.H.

A83-45577*# Flow Research, Inc., Kent, Wash.
FINITE VOLUME CALCULATION OF THREE-DIMENSIONAL POTENTIAL FLOW AROUND A PROPELLER
W.-H. JOU (Flow Research, Inc., Research and Technology Div., Kent, WA) AIAA Journal (ISSN 0001-1452), vol. 21, Oct. 1983, p. 1360-1364. refs
(Contract NAS3-22148)
Previously cited in issue 15, p. 2344, Accession A82-31933

A83-47022* Pennsylvania State Univ., University Park.
EXPERIMENTAL STUDY OF THE BOUNDARY LAYER ON A TURBOMACHINERY ROTOR BLADE
B. LAKSHMINARAYANA, T. R. GOVINDAN, and C. HAH (Pennsylvania State University, University Park, PA) IN: Three-dimensional turbulent boundary layers; Proceedings of the Symposium, Berlin, West Germany, March 29-April 1, 1982 . Berlin, Springer-Verlag, 1982, p. 165-176. refs
(Contract NSG-3266)

The development of the turbulent boundary layer on a turbomachinery rotor blade is very complex. This paper is concerned with the measurement, analysis, and prediction of the blade boundary layer on a rotor blade. A comprehensive measurement of the blade boundary layer on a fan rotor blade was carried out in the axial flow fan facility at the Applied Research Laboratory. The measurements were taken with a miniature 'x' configuration hot-wire probe. The streamwise and the radial velocity profiles as well as the turbulence intensities at one radius are presented and interpreted.
Author

A83-47891*# Arizona State Univ., Tempe.
HEAT TRANSFER CHARACTERISTICS FOR JET ARRAY IMPINGEMENT WITH INITIAL CROSSFLOW
L. W. FLORSCHUETZ, D. E. METZGER, and C. C. SU (Arizona State University, Tempe, AZ) American Society of Mechanical Engineers, International Gas Turbine Conference and Exhibit, 28th, Phoenix, AZ, Mar. 27-31, 1983. 10 p. refs
(Contract NSG-3075)
(ASME PAPER 83-GT-28)

Two-dimensional arrays of circular air jets impinging on a heat transfer surface parallel to the jet orifice plate are considered. The jet flow, after impingement, is constrained to exit in a single direction along the channel formed by the jet orifice plate and the heat transfer surface. In addition to the crossflow which originates from the jets following impingement, an initial crossflow is present which approaches the array through an upstream extension of the channel. The temperature of the initial crossflow air may differ from the jet air temperature. The configurations considered are intended to model the impingement cooled midchord region of gas turbine airfoils in cases where an initial crossflow is also present. Nusselt numbers and dimensionless adiabatic wall temperatures resolved to one streamwise jet hole spacing were experimentally determined for ratios of the initial crossflow rate to the total jet flow rate ranging from zero to unity. These are presented and discussed relative to the flow and geometric parameters.
Author

A83-47901*# Delaware Univ., Newark.
INLET-FAN FLOW FIELD COMPUTATION
M. D. MATWEY, B. S. SEIDEL (Delaware, University, Newark, DE), and C. A. FARRELL, JR. (NASA, Lewis Research Center, Cleveland, OH) American Society of Mechanical Engineers, International Gas Turbine Conference and Exhibit, 28th, Phoenix, AZ, Mar. 27-31, 1983. 7 p. refs
(Contract NSG-3270; NAG3-121)
(ASME PAPER 83-GT-41)

The flow field of a tilt-nacelle inlet-fan combination used for V/STOL aircraft is studied. Under certain flight conditions the inlet is subjected to high angles of attack and/or yaw. This produces a non-uniform or distorted flow field at the fan-face that can lead to large blade stresses. This paper presents an analytical approach to the coupled inlet-fan problem. The nacelle is modelled by a distribution of source panels and the fan by a distribution of radial vortices. A modified actuator disc with losses and a quasi-steady rotor response is used to derive the boundary condition at the fan-face. An example of the calculation is shown.
Author

A83-47904*# Cornell Univ., Ithaca, N.Y.
A THEORY OF ROTATING STALL OF MULTISTAGE AXIAL COMPRESSORS. I - SMALL DISTURBANCES
F. K. MOORE (Cornell University, Ithaca, NY) American Society of Mechanical Engineers, International Gas Turbine Conference and Exhibit, 28th, Phoenix, AZ, Mar. 27-31, 1983. 8 p. refs
(Contract NAG3-349)
(ASME PAPER 83-GT-44)

An analysis is made of rotating stall in compressors of many stages, finding conditions under which a flow distortion can occur which is steady in a traveling reference frame, even through upstream total and downstream static pressure are constant. In the compressor, a pressure-rise hysteresis is assumed. Flow in entrance and exit ducts yield additional lags. These lags balance to give a formula for stall propagation speed. For small disturbances, it is required that the compressor characteristics be flat in the neighborhood of average flow coefficient. Results are compared with the experiments of Day and Cumpsty. If a compressor lag of about twice that due only to fluid inertia is used, predicted propagation speeds agree almost exactly with experimental values, taking into account changes of number of stages, stagger angle, row spacing, and number of stall zones. The agreement obtained gives encouragement for the extension of the theory to account for large amplitudes.
Author

A83-47905*# Cornell Univ., Ithaca, N.Y.
A THEORY OF ROTATING STALL OF MULTISTAGE AXIAL COMPRESSORS. II - FINITE DISTURBANCES
F. K. MOORE (Cornell University, Ithaca, NY) American Society of Mechanical Engineers, International Gas Turbine Conference and Exhibit, 28th, Phoenix, AZ, Mar. 27-31, 1983. 6 p. refs
(Contract NAG3-349)
(ASME PAPER 83-GT-45)

A small-disturbance theory of rotating stall in axial compressors is extended to finite amplitude, assuming the compressor characteristic is a parabola over the range of the disturbance. An exact solution is found which requires the operating point to be at the minimum or maximum of the parabola. If the characteristic is flat in a deep-stall regime, the previous harmonic solution applies with neither reverse flow or 'unstalling'. If the characteristic is concave upward in deep stall, the disturbance has a skewed shape, steeper at the stall-zone trailing edge as experiment shows. Propagation speed is only slightly affected by this nonlinearity. Near stall inception, negative curvature in combination with multiple stall zones can limit the nonlinear oscillation, in the manner of 'progressive' stall. If, as seems likely, lag at stall inception is negative (opposite to inertia), propagation speed exceeds 1/2 wheel speed, as experiments suggest. Author

A83-47906*# Cornell Univ., Ithaca, N.Y.
A THEORY OF ROTATING STALL OF MULTISTAGE AXIAL COMPRESSORS. III - LIMIT CYCLES
F. K. MOORE (Cornell University, Ithaca, NY) American Society of Mechanical Engineers, International Gas Turbine Conference and Exhibit, 28th, Phoenix, AZ, Mar. 27-31, 1983. 8 p. refs
(Contract NAG3-349)
(ASME PAPER 83-GT-46)

A theory of rotating stall, based on single parameters for blade-passage lag and external-flow lag and a given compressor characteristic yields limit cycles in velocity space. These limit cycles are governed by Lienard's equation with the characteristic playing the role of nonlinear damping function. Cyclic integrals of the solution determine stall propagation speed and the effect of rotating stall on average performance. Solution with various line-segment characteristics and various throttle settings are found and discussed. There is generally a limiting flow coefficient beyond which no solution is possible; this probably represents stall recovery. This recovery point is independent of internal compressor lag, but does depend on external lags and on the height-to-width ratio of the diagram. Tall diagrams and small external lags (inlet and diffusor) favor recovery. Suggestions for future theoretical and experimental research are discussed. Author

A83-47910*# General Motors Corp., Indianapolis, Ind.
MEASUREMENTS OF HEAT TRANSFER DISTRIBUTION OVER THE SURFACES OF HIGHLY LOADED TURBINE NOZZLE GUIDE VANES
D. A. NEALY, M. S. MIHELC, L. D. HYLTON (General Motors Corp., Detroit Diesel Allison Div., Indianapolis, IN), and H. J. GLADDEN (NASA, Lewis Research Center, Cleveland, OH) American Society of Mechanical Engineers, International Gas Turbine Conference and Exhibit, 28th, Phoenix, AZ, Mar. 27-31, 1983. 10 p. refs
(Contract NAS3-22761)
(ASME PAPER 83-GT-53)

The results of an experimental study of aerodynamic (surface velocity) and heat transfer distributions over the surfaces of two different, highly loaded, low-solidity contemporary turbine vane designs are presented. The aerodynamic configurations of the two vanes were carefully selected to emphasize fundamental differences in the character of the solution surface pressure distributions and the consequent effect on surface heat transfer distributions. The experimental measurements were made in moderate-temperature, three-vane cascades under steady-state conditions. The principal independent parameters (Mach number, Reynolds number, turbulence intensity, and wall-to-gas temperature ratio) were varied over ranges consistent with actual engine operation, and the heat matrix was structured to provide an assessment of the independent influence of each parameter. These measurements are intended to serve as verification data for a parallel analytical code development effort. The results of this parallel effort are briefly reviewed, and the principal conclusions to date are summarized. Author

A83-47941*# Cincinnati Univ., Ohio.
EFFECT OF PARTICLE PRESENCE ON THE INCOMPRESSIBLE INVISCID FLOW THROUGH A TWO DIMENSIONAL COMPRESSOR CASCADE
C. BALAN and W. TABAKOFF (Cincinnati, University, Cincinnati, OH) American Society of Mechanical Engineers, International Gas Turbine Conference and Exhibit, 28th, Phoenix, AZ, Mar. 27-31, 1983. 9 p. refs
(Contract NSG-3218; DAAG29-82-K-0029)
(ASME PAPER 83-GT-95)

A computational model is developed for calculating the flow field, in the presence of solid particles, through a two-dimensional compressor cascade. Results show that the effect of solid particles on the flow field contributes to the bending of the streamlines toward the blade suction surface. It is determined that the difference in the pressure coefficient for particulate flow, with 165 micron diameter for the particles, is of the order of 3 percent over the air only flow. The change in the pressure coefficients is shown to be much larger for very small particles. It was found that the total pressure loss associated with the particulate flow is very high for very small particles as compared with large particles. The total pressure loss is also shown to be higher for accelerating flow than for decelerating flow. The total pressure loss is shown to be directly proportional to the particle concentration. It is concluded that significant reductions in performance can occur in a real multistage machine due to the changes in the pressure ratios, particularly if the suspended matter is small particles. N.B.

A83-47957*# Cincinnati Univ., Ohio.
THREE-DIMENSIONAL FLOW MEASUREMENTS IN A TURBINE SCROLL
W. TABAKOFF, B. V. R. VITTAL, and B. WOOD (Cincinnati, University, Cincinnati, OH) American Society of Mechanical Engineers, International Gas Turbine Conference and Exhibit, 28th, Phoenix, AZ, Mar. 27-31, 1983. 7 p. refs
(Contract NAG3-26)
(ASME PAPER 83-GT-128)

A study was conducted to determine experimentally the flow behavior in combined scroll nozzle assembly of a radial inflow turbine. Hot film anemometry technique was used to measure the three-dimensional flow velocity in the scroll. The through-flow and secondary flow velocity components are measured at various points in three scroll sections. Author

A83-47972*# Pennsylvania State Univ., University Park.
WALL BOUNDARY LAYER DEVELOPMENT NEAR THE TIP REGION OF AN IGV OF AN AXIAL FLOW COMPRESSOR
B. LAKSHMINARAYANA and N. SITARAM (Pennsylvania State University, University Park, PA) American Society of Mechanical Engineers, International Gas Turbine Conference and Exhibit, 28th, Phoenix, AZ, Mar. 27-31, 1983. 9 p. refs
(Contract NSG-3032)
(ASME PAPER 83-GT-171)

The annulus wall boundary layer inside the blade passage of the inlet guide vane (IGV) passage of a low-speed axial compressor stage was measured with a miniature five-hole probe. The three-dimensional velocity and pressure fields were measured at various axial and tangential locations. Limiting streamline angles and static pressures were also measured on the casing of the IGV passage. Strong secondary vorticity was developed. The data were analyzed and correlated with the existing velocity profile correlations. The end wall losses were also derived from these data. Author

A83-48012*# United Technologies Corp., East Hartford, Conn.
DEVELOPMENT OF CONTROLLED DIFFUSION AIRFOILS FOR MULTISTAGE COMPRESSOR APPLICATION
D. E. HOBBS and H. D. WEINGOLD (United Technologies Corp., Pratt and Whitney Group, East Hartford, CT) American Society of Mechanical Engineers, International Gas Turbine Conference and Exhibit, 28th, Phoenix, AZ, Mar. 27-31, 1983. 11 p. refs
(Contract N00019-77-C-0546; NAS3-22008)
(ASME PAPER 83-GT-211)

A series of Controlled Diffusion Airfoils has been developed for multistage compressor application. These airfoils are designed analytically to be shock free at transonic Mach number and to avoid suction surface boundary layer separation for a range of inlet conditions necessary for stable compressor operation. They have demonstrated, in cascade testing, higher critical Mach number, higher incidence range, and higher loading capability than standard series airfoils designed for equivalent aerodynamic requirements. These airfoils have been shown, in single and multistage rig testing, to provide high efficiency, high loading capability, and ease of stage matching, leading to reduced development costs and improved surge margin. The Controlled Diffusion Airfoil profile shapes tend to have thicker leading and trailing edges than their standard series counterparts, leading to improved compressor durability. Author

A83-48014*# Cincinnati Univ., Ohio.
A STUDY OF THE SURFACE DETERIORATION DUE TO EROSION
W. TABAKOFF and C. BALAN (Cincinnati, University, Cincinnati, OH) American Society of Mechanical Engineers, International Gas Turbine Conference and Exhibit, 28th, Phoenix, AZ, Mar. 27-31, 1983. 7 p. refs
(Contract NSG-3218)
(ASME PAPER 83-GT-213)

It is pointed out that materials exposed to particle impacts are eroded and subjected to deterioration of their surface quality. In the case of turbomachinery, this surface deterioration can lead to a significant decrease in engine performance. Tabakoff and Balan (1981) have conducted experiments on the erosion related performance changes in two-dimensional airfoil cascades. It was found that the increase in surface roughness associated with erosion is a major factor in the performance decrease of the cascades. Attention is given to experiments which were conducted on 6061 T6 flat plate aluminum specimens. A series of experiments were carried out in an erosion wind tunnel using a collimated beam of particles. In agreement with existing theories and experiments, erosion ripple generation was observed for the angles of attack up to 60 degrees. G.R.

N83-10019*# National Aeronautics and Space Administration. Lewis Research Center, Cleveland, Ohio.
WIND TUNNEL TESTS OF A ZERO LENGTH, SLOTTED-LIP ENGINE AIR INLET FOR A FIXED NACELLE V/STOL AIRCRAFT
R. R. WOOLLETT, W. E. BECK, JR. (Lockheed-California Co., Burbank), and E. R. GLASGOW (Lockheed-California Co., Burbank) Aug. 1982 117 p refs
(NASA-TM-82939; E-1338; NAS 1.15:82939) Avail: NTIS HC A06/MF A01 CSCL 01A

Zero length, slotted lip inlet performance and associated fan blade stresses were determined during model tests using a 20 inch diameter fan simulator in the NASA-LeRC 9 by 15 foot low speed wind tunnel. The model configuration variables consisted of inlet contraction ratio, slot width, circumferential extent of slot fillers, and length of a constant area section between the inlet throat and fan face. The inlet performance was dependent on slot gap width and relatively independent of inlet throat/fan face spacer length and slot flow blockage created by 90 degree slot fillers. Optimum performance was obtained at a slot gap width of 0.36 inch. The zero length, slotted lip inlet satisfied all critical low speed inlet operating requirements for fixed horizontal nacelles subsonic V/STOL aircraft. Author

N83-11058*# National Aeronautics and Space Administration. Lewis Research Center, Cleveland, Ohio.
PERFORMANCE OF A TANDEM-ROTOR/TANDEM-STATOR CONICAL-FLOW COMPRESSOR DESIGNED FOR A PRESSURE RATIO OF 3
J. R. WOOD, A. K. OWEN (Army Aviation Research and Development Command, Cleveland, Ohio), and L. F. SCHUMANN (Army Aviation Research and Development Command, Cleveland, Ohio) Oct. 1982 38 p refs
(NASA-TP-2034; E-369; NAS 1.60:2034; AVRADCOM-TR-81-C-5) Avail: NTIS HC A03/MF A01 CSCL 01A

A conical-flow compressor stage with a large radius change through the rotor was tested at three values of rotor tip clearance. The stage had a tandem rotor and a tandem stator. Peak efficiency at design speed was 0.774 at a pressure ratio of 2.613. The rotor was tested without the stator, and detailed survey data were obtained for each rotor blade row. Overall peak rotor efficiency was 0.871 at a pressure ratio of 2.952. Author

N83-11063*# National Aeronautics and Space Administration. Lewis Research Center, Cleveland, Ohio.
COLD-AIR PERFORMANCE OF COMPRESSOR-DRIVE TURBINE OF DEPARTMENT OF ENERGY UPGRADED AUTOMOBILE GAS TURBINE ENGINE. 2: STAGE PERFORMANCE
R. J. ROELKE and J. E. HAAS Oct. 1982 18 p refs Prepared in cooperation with Army Aviation Research and Development Command, Cleveland
(Contract EC-77-A-31-1011)
(NASA-TM-82818; DOE/NASA/1011-36; NAS 1.15:82818; AVRADCOM-TR-82-C-1) Avail: NTIS HC A02/MF A01 CSCL 10B

The aerodynamic performance of the compressor-drive turbine of the DOE upgraded gas turbine engine was determined in low temperature air. The as-received cast rotor blading had a significantly thicker profile than design and a fairly rough surface finish. Because of these blading imperfections a series of stage tests with modified rotors were made. These included the as-cast rotor, a reduced-roughness rotor, and a rotor with blades thinned to near design. Significant performance changes were measured. Tests were also made to determine the effect of Reynolds number on the turbine performance. Comparisons are made between this turbine and the compressor-drive turbine of the DOE baseline gas turbine engine. Author

N83-11065*# Cincinnati Univ., Ohio. Dept. of Aerospace Engineering and Applied Mechanics.
THREE-DIMENSIONAL FLOW MEASUREMENTS IN A VANELESS RADIAL TURBINE SCROLL
W. TABAKOFF, B. WOOD, and B. V. R. VITTAL Aug. 1982 43 p refs
(Contract NAG3-26)
(NASA-CR-167994; NAS 1.26:167994) Avail: NTIS HC A03/MF A01 CSCL 01A

The flow behavior in a vaneless radial turbine scroll was examined experimentally. The data was obtained using the slant sensor technique of hot film anemometry. This method used the unsymmetric heat transfer characteristics of a constant temperature hot film sensor to detect the flow direction and magnitude. This was achieved by obtaining a velocity vector measurement at three sensor positions with respect to the flow. The true magnitude and direction of the velocity vector was then found using these values and a Newton-Raphson numerical technique. The through flow and secondary flow velocity components are measured at various points in three scroll sections. M.G.

N83-11066*# Purdue Univ., Lafayette, Ind. School of Mechanical Engineering.
A COMPUTER PROGRAM FOR THE CALCULATION OF THE FLOW FIELD INCLUDING BOUNDARY LAYER EFFECTS FOR MIXED-COMPRESSION INLETS AT ANGLE OF ATTACK Final Report
J. VADYAK and J. D. HOFFMAN Oct. 1982 152 p refs
(Contract NSG-3311)
(NASA-CR-168002; NAS 1.26:168002) Avail: NTIS HC A08/MF A01 CSCL 01A

A computer program was developed which is capable of calculating the flow field in the supersonic portion of a mixed compression aircraft inlet operating at angle of attack. The supersonic core flow is computed using a second-order three dimensional method-of-characteristics algorithm. The bow shock and the internal shock train are treated discretely using a three dimensional shock fitting procedure. The boundary layer flows are computed using a second-order implicit finite difference method. The shock wave-boundary layer interaction is computed using an integral formulation. The general structure of the computer program is discussed, and a brief description of each subroutine is given. All program input parameters are defined, and a brief discussion on interpretation of the output is provided. A number of sample cases, complete with data listings, are provided. B.W.

N83-12045*# Cincinnati Univ., Ohio. Dept. of Aerospace Engineering and Applied Mechanics.
THREE DIMENSIONAL FLOW COMPUTATIONS IN A TURBINE SCROLL
A. HAMED and C. A. GHANTOUS Aug. 1982 57 p refs
(Contract NAG3-52)
(NASA-CR-168003; NAS 1.26:168003) Avail: NTIS HC A04/MF A01 CSCL 01A

The compressible three dimensional inviscid flow in the scroll and vaneless nozzle of radial inflow turbines is analyzed. A FORTRAN computer program for the numerical solution of this complex flow field using the finite element method is presented. The program input consists of the mass flow rate and stagnation conditions at the scroll inlet and of the finite element discretization parameters and nodal coordinates. The output includes the pressure, Mach number and velocity magnitude and direction at all the nodal points. S.L.

N83-12047*# Douglas Aircraft Co., Inc., Long Beach, Calif.
CALCULATION OF COMPRESSIBLE FLOW IN AND ABOUT THREE-DIMENSIONAL INLETS WITH AND WITHOUT AUXILIARY INLETS BY A HIGHER-ORDER PANEL METHOD Final Report
J. L. HESS and D. M. FRIEDMAN Oct. 1982 89 p refs
(Contract NAS3-22147)
(NASA-CR-168009; NAS 1.26:168009; MDC-J2548) Avail: NTIS HC A05/MF A01 CSCL 01A

A three dimensional higher order panel method was specialized to the case of inlets with auxiliary inlets. The resulting program has a number of graphical input-output features to make it highly useful to the designer. The various aspects of the program are described instructions for its use are presented. S.L.

N83-13077*# National Aeronautics and Space Administration. Lewis Research Center, Cleveland, Ohio.
A RAPID BLADE-TO-BLADE SOLUTION FOR USE IN TURBOMACHINERY DESIGN
E. R. MCFARLAND 1982 13 p refs Proposed for presentation at the 28th Ann. Intern. Gas Turbine Conf., Phoenix, Ariz., 27-31 Mar. 1983; sponsored by ASME
(NASA-TM-83010; E-1445; NAS 1.15:83010) Avail: NTIS HC A02/MF A01 CSCL 01A

A rapid technique for solving the blade-to-blade turbomachinery flow problem was developed. Approximate governing flow equations, which include the effects of compressibility, radius change, rotation, and variable stream sheet thickness are solved using a panel method. The development and solution of these equations are described. Sample calculations are presented to illustrate the method's capabilities and accuracy. Author

N83-14066*# Neilsen Engineering and Research Co., Palo Alto, Calif.
MEAN-FLOW MEASUREMENTS OF THE FLOW FIELD DIFFUSING BEND Final Report
O. J. MCMILLAN Washington NASA Nov. 1982 166 p refs
(Contract NAS3-22113)
(NASA-CR-3634; NAS 1.26:3624; NEAR-TR-271; NAS 1.26:3634) Avail: NTIS HC A08/MF A01 CSCL 01A

Time-average measurements of the low-speed turbulent flow in a diffusing bend are presented. The experimental geometry consists of parallel top and bottom walls and curved diverging side walls. The turning of the center line of this channel is 40 deg, the area ratio is 1.5 and the ratios of height and center-line length to throat width are 1.5 and 3, respectively. The diffusing bend is preceded and followed by straight constant area sections. The inlet boundary layers on the parallel walls are artificially thickened and occupy about 30% of the channel height; those on the side walls develop naturally and are about half as thick. The free-stream speed at the inlet was approximately 30 m/sec for all the measurements. Inlet boundary layer mean velocity and turbulence intensity profiles are presented, as are data for wall static pressures, and at six cross sections, surveys of the velocity-vector and static-pressure fields. The dominant feature of the flow field is a pair of counter-rotating streamwise vortices formed by the cross-stream pressure gradient in the bend on which an overall deceleration is superimposed. A.R.H.

N83-14068*# San Jose State Univ., Calif. Dept. of Mechanical Engineering.
AN EXPERIMENTAL INVESTIGATION OF INTERNAL AREA RULING FOR TRANSONIC AND SUPERSONIC CHANNEL FLOW Final Scientific Report, 25 Sep. 1981 - 24 Sep. 1982
W. B. ROBERTS, H. L. VANRINTEL, and G. RIZVI 24 Aug. 1982 99 p refs
(Contract NAG3-196)
(NASA-CR-169638; NAS 1.26:169638) Avail: NTIS HC A05/MF A01 CSCL 01A

A simulated transonic rotor channel model was examined experimentally to verify the flow physics of internal area ruling. Pressure measurements were performed in the high speed wind tunnel at transonic speeds with Mach 1.5 and Mach 2 nozzle blocks to get an indication of the approximate shock losses. The results showed a reduction in losses due to internal area ruling with the Mach 1.5 nozzle blocks. The reduction in total loss coefficient was of the order of 17 percent for a high blockage model and 7 percent for a cut-down model. Author

N83-15264*# Lehigh Univ., Bethlehem, Pa. Dept. of Mechanical Engineering and Mechanics.
CRITICAL REVIEW OF THE TRAILING EDGE CONDITION IN STEADY AND UNSTEADY FLOW. BLADE FLUTTER IN COMPRESSORS AND FANS: NUMERICAL SIMULATION OF THE AERODYNAMIC LOADING
S. F. RADWAN, D. O. ROCKWELL, and S. H. JOHNSON Dec. 1982 149 p refs
(Contract NSG-3162)
(NASA-CR-169705; NAS 1.26:169705) Avail: NTIS HC A07/MF A01 CSCL 01A

Existing interpretations of the trailing edge condition, addressing both theoretical and experimental works in steady, as well as unsteady flows are critically reviewed. The work of Kutta and Joukowski on the trailing edge condition in steady flow is reviewed. It is shown that for most practical airfoils and blades (as in the case of most turbomachine blades), this condition is violated due to rounded trailing edges and high frequency effects, the flow dynamics in the trailing edge region being dominated by viscous forces; therefore, any meaningful modelling must include viscous effects. The question of to what extent the trailing edge condition affects acoustic radiation from the edge is raised; it is found that

violation of the trailing edge condition leads to significant sound diffraction at the tailing edge, which is related to the problem of noise generation. Finally, various trailing edge conditions in unsteady flow are discussed, with emphasis on high reduced frequencies. Author

N83-15265*# Ohio State Univ., Columbus. Dept. of Aeronautical and Astronautical Engineering.
WIND TUNNEL EVALUATION OF AIR-FOIL PERFORMANCE USING SIMULATED ICE SHAPES Final Report
M. B. BRAGG, R. J. ZAGULI, and G. M. GREGOREK Nov. 1982 172 p refs
(Contract NAG3-28)
(NASA-CR-167960; NAS 1.26:167960) Avail: NTIS HC A08/MF A01 CSCL 01A

A two-phase wind tunnel test was conducted in the 6 by 9 foot Icing Research Tunnel (IRT) at NASA Lewis Research Center to evaluate the effect of ice on the performance of a full scale general aviation wing. In the first IRT tests, rime and glaze shapes were carefully documented as functions of angle of attack and free stream conditions. Next, simulated ice shapes were constructed for two rime and two glaze shapes and used in the second IRT tunnel entry. The ice shapes and the clean airfoil were tapped to obtain surface pressures and a probe used to measure the wake characteristics. These data were recorded and processed, on-line, with a minicomputer/digital data acquisition system. The effect of both rime and glaze ice on the pressure distribution, Cl, Cd, and Cm are presented. Author

N83-15268*# National Aeronautics and Space Administration. Lewis Research Center, Cleveland, Ohio.
EXPERIMENTAL EVALUATION OF SHOCKLESS SUPERCRITICAL AIRFOILS IN CASCADE
D. R. BOLDMAN, A. E. BUGGELE, and L. M. SHAW 1983 17 p refs Presented at the 21st Aerospace Sci. Conf., Reno, Nevada, 10-13 Jan. 1983; sponsored by the American Inst. of Aeronautics and Astronautics
(NASA-TM-83045; E-1492; NAS 1.15:83045) Avail: NTIS HC A02/MF A01 CSCL 01A

Surface Mach number distributions, total pressure loss coefficients, and schlieren images of the flow are presented over a range of inlet Mach numbers and air angles. Several different trailing edge geometries were tested. At design conditions a leading edge separation bubble was observed resulting in higher losses than anticipated. The minimum losses were obtained at a negative incidence condition in which the flow was accelerating over most of the supercritical region. Relatively minor differences in losses were measured with the different trailing edge geometries studied. Author

N83-16285*# Cincinnati Univ., Ohio. Dept. of Aerospace Engineering and Applied Mechanics.
ENVIRONMENTAL SOLID PARTICLE EFFECTS ON COMPRESSOR CASCADE PERFORMANCE
W. TABAKOFF and C. BALAN Oct. 1982 65 p refs
(Contract NSG-3218)
(NASA-CR-168018; NAS 1.26:168018) Avail: NTIS HC A04/MF A01 CSCL 01A

The effect of suspended solid particles on the performance of the compressor cascade was investigated experimentally in a specially built cascade tunnel, using quartz sand particles. The cascades were made of NACA 65(10)10 airfoils. Three cascades were tested, one accelerating cascade and two diffusing cascades. The theoretical analysis assumes inviscid and incompressible two dimensional flow. The momentum exchange between the fluid and the particle is accounted for by the interphase force terms in the fluid momentum equation. The modified fluid phase momentum equations and the continuity equation are reduced to the conventional stream function vorticity formulation. The method treats the fluid phase in the Eulerian system and the particle phase in Lagrangian system. The experimental results indicate a small increase in the blade surface static pressures, while the theoretical results indicate a small decrease. The theoretical analysis, also predicts the loss in total pressure associated with the particulate flow through the cascade. A.R.H.

N83-16286*# Cincinnati Univ., Ohio. Dept. of Aerospace Engineering and Applied Mechanics.
COMPRESSOR CASCADE PERFORMANCE DETERIORATION CAUSED BY SAND INGESTION
W. TABAKOFF and C. BALAN Nov. 1982 71 p refs
(Contract NSG-3218)
(NASA-CR-168067; NAS 1.26:168067) Avail: NTIS HC A04/MF A01 CSCL 01A

Airfoil cascade erosion and performance deterioration was investigated in a gas particle cascade tunnel. The cascade blades were made of 2024 aluminum alloy and the solid particles used were quartz sand. The results of the experimental measurements are presented to show the change in the blade surface erosion, pressure distribution and the total loss coefficient with erosion. The surface quality of the blades exposed to particulate flows are changing the material surfaces. With time, the surface roughness increases and leads to a decrease in engine performance. It was found that the surface roughness values increase asymptotically to a maximum value with increased erosion. The experimental results indicate that the roughness parameters correlate well against the mass of particles impacting unit area of the surface. Such a correlation is useful in aerodynamics and performance computations in turbomachinery. Author

N83-17502*# Illinois Inst. of Tech., Chicago.
INTERPRETATION OF 2-PROBE TURBULENCE MEASUREMENTS IN AN AXISYMMETRIC CONTRACTION Final Report
C. MARION-MOULIN, J. TAN-ATICHAT, and H. M. NAGIB Jan. 1983 74 p refs
(Contract NSG-3220)
(NASA-CR-169832; NAS 1.26:169832; IIT-FHT-R83-1) Avail: NTIS HC A04/MF A01 CSCL 01A

Simultaneous measurements of the streamwise and radial velocity components at two points, one on and one off the centerline with variable radial separation, were digitally recorded and processed at several stations along a four to one contraction with controlled upstream turbulence conditions. Various statistical quantities are presented including spectra and coherence functions. The integral L sub ux, L sub um, L sub vx, L sub vm were also estimated and their variation along the contraction is examined. Author

N83-17503*# Illinois Inst. of Tech., Chicago.
EXPERIMENTS ON IDENTIFICATION AND CONTROL OF INFLOW DISTURBANCES IN CONTRACTING STREAMS Final Report
A. H. LEE, H. M. NAGIB, J. TAN-ATICHAT, and D. M. WITTWER Dec. 1982 169 p refs
(Contract NSG-3220)
(NASA-CR-169831; NAS 1.26:169831; IIT-FHT-R82-3) Avail: NTIS HC A08/MF A01 CSCL 01A

Vorticity from all surfaces and isolated objects in the vicinity of the fan intake, including the outside surfaces of the fan housing, were identified as the major sources for disturbances leading to blade passing frequency noise. The previously proposed mechanism based on atmospheric turbulence is refuted. Flow visualization and hot wire techniques were used in three different facilities to document the evolution of various types of disturbances, including the details of the mean flow and turbulence characteristics. The results suggest that special attention must be devoted to the design of the inlet and that geometric modeling may not lead to adequate simulation of the in flight characteristics. While honeycomb type flow manipulators appear to be effective in reducing some of the disturbances, higher pressure drop devices that generate adequate turbulence, for mixing of isolated nonuniformities, may be necessary to suppress the remaining disturbances. The results are also applicable to the design of inlets of open return wind tunnels and similar flow facilities. Author

N83-17509*# National Aeronautics and Space Administration. Lewis Research Center, Cleveland, Ohio.
TURBOFAN BLADE STRESSES INDUCED BY THE FLOW DISTORTION OF A VTOL INLET AT HIGH ANGLES OF ATTACK
R. C. WILLIAMS, J. H. DIEDRICH, and R. J. SHAW Jan. 1983 25 p refs
(NASA-TM-82963; E-1380; NAS 1.15:82963) Avail: NTIS HC A02/MF A01 CSCL 01A

A 51-cm-diameter turbofan with a tilt-nacelle VTOL inlet was tested in the Lewis Research Center's 9- by 15-Ft Low Speed Wind Tunnel at velocities up to 72 m/s and angles of attack up to 120 deg. Fan-blade vibratory stress levels were investigated over a full aircraft operating range. These stresses were due to inlet air flow distortion resulting from (1) internal flow separation in the inlet, and (2) ingestion of the exterior nacelle wake. Stress levels are presented, along with an estimated safe operating envelope, based on infinite blade fatigue life. Author

N83-18671*# Flow Simulations, Inc., Sunnyville, Calif.
USER'S MANUAL FOR THREE-DIMENSIONAL ANALYSIS OF PROPELLER FLOW FIELDS Final Report
D. S. CHAUSSEE and P. KUTLER Jan. 1983 129 p refs
(Contract NAS3-22375)
(NASA-CR-167959; NAS 1.26:167959; FSI-80-04) Avail: NTIS HC A07/MF A01 CSCL 01A

A detailed operating manual is presented for the prop-fan computer code (in addition to supporting programs) recently developed by Kutler, Chaussee, Sorenson, and Pulliam while at the NASA'S Ames Research Center. This code solves the inviscid Euler equations using an implicit numerical procedure developed by Beam and Warming of Ames. A description of the underlying theory, numerical techniques, and boundary conditions with equations, formulas, and methods for the mesh generation program (MGP), three dimensional prop-fan flow field program (3DPFP), and data reduction program (DRP) is provided, together with complete operating instructions. In addition, a programmer's manual is also provided to assist the user interested in modifying the codes. Included in the programmer's manual for each program is a description of the input and output variables, flow charts, program listings, sample input and output data, and operating hints.
Author

N83-19710*# National Aeronautics and Space Administration. Lewis Research Center, Cleveland, Ohio.
PREDICTION OF HIGH SPEED PROPELLER FLOW FIELDS USING A THREE-DIMENSIONAL EULER ANALYSIS
L. J. BOBER, D. S. CHAUSSEE (NASA. Ames Research Center), and P. KUTLER (NASA. Ames Research Center) Washington 1983 32 p refs Presented at the 21st Aerospace Sci. Conf., Reno, Nev., 10-13 Jan. 1983; sponsored by AIAA
(NASA-TM-83065; E-1563; NAS 1.15:83065; AIAA-83-0188)
Avail: NTIS HC A03/MF A01 CSCL 01A

To overcome the limitations of classical propeller theory, a computer program, NASPROP-E, was developed which solves for the flow field surrounding a multibladed propeller and axisymmetric nacelle combination using a finite difference method. The governing equations are the three dimensional unsteady Euler equations written in a cylindrical coordinate system. They are marched in time until a steady state solution is obtained. The Euler equations require no special treatment to model the blade work vorticity. The equations are solved using an implicit approximate factorization method. Numerical results are presented which have greatly increased the understanding of high speed propeller flow fields. Numerical results for swirl angle downstream of the propeller and propeller power coefficient are higher than experimental results. The radial variation of coefficient are higher than experimental results. The radial variation of swirl angle, however, is in reasonable agreement with the experimental results. The predicted variation of power coefficient with blade angle agrees very well with data.
S.L.

N83-24470*# National Aeronautics and Space Administration. Lewis Research Center, Cleveland, Ohio.
END-WALL BOUNDARY LAYER MEASUREMENTS IN A TWO-STAGE FAN
C. L. BALL, L. REID, and J. F. SCHMIDT 1983 24 p refs Presented at the Propulsion Energetics Panel 61st A Specialists' Meeting, Copenhagen, 1-3 Jun. 1983; sponsored by AGARD
(NASA-TM-83409; E-1692; NAS 1.15:83409) Avail: NTIS HC A02/MF A01 CSCL 01A

Detailed flow measurements made in the casing boundary layer of a two-stage transonic fan are summarized. These measurements were taken at a station upstream of the fan, between all blade rows, and downstream of the last row. Conventional boundary layer parameters were calculated from the measured data. A classical two dimensional casing boundary layer was measured at the fan inlet and extended inward to approximately 15 percent of span. A highly three dimensional boundary layer was measured at the exit of each blade row and extended inward to approximately 10 percent of span. The steep radial gradient of axial velocity noted at the exit of the rotors was reduced substantially as the flow passed through the stators. This reduced gradient is attributed to flow mixing. The amount of flow mixing was reflected in the radial redistribution of total temperature as the flow passed through the stators. The blockage factors calculated from the measured data show an increase in blockage across the rotors and a decrease across the stators. For this fan the calculated blockages for the second stage were essentially the same as those for the first stage. Author

N83-24474*# Universities Space Research Association, Columbia, Md.
IMPROVED DESIGN OF SUBCRITICAL AND SUPERCRITICAL CASCADES USING COMPLEX CHARACTERISTICS AND BOUNDARY LAYER CORRECTION Final Report
J. M. SANZ May 1983 16 p refs
(Contract NAS3-22531)
(NASA-CR-168166; NAS 1.26:168166) Avail: NTIS HC A02/MF A01 CSCL 01A

The method of complex characteristics and hodograph transformation for the design of shockless airfoils was extended to design supercritical cascades with high solidities and large inlet angles. This capability was achieved by introducing a conformal mapping of the hodograph domain onto an ellipse and expanding the solution in terms of Tchebycheff polynomials. A computer code was developd based on this idea. A number of airfoils designed with the code are presented. Various supercritical and subcritical compressor, turbine and propeller sections are shown. The lag-entrainment method for the calculation of a turbulent boundary layer was incorporated to the inviscid design code. The results of this calculation are shown for the airfoils described. The elliptic conformal transformation developed to map the hodograph domain onto an ellipse can be used to generate a conformal grid in the physical domain of a cascade of airfoils with open trailing edges with a single transformation. A grid generated with this transformation is shown for the Korn airfoil. S.L.

N83-25657*# National Aeronautics and Space Administration. Lewis Research Center, Cleveland, Ohio.
EXPERIMENTAL RESULTS OF A DEFLECTED THRUST V/STOL NOZZLE RESEARCH PROGRAM
P. L. BURSTADT and A. L. JOHNS Mar. 1983 26 p refs Presented at the 21st Aerospace Sci. Conf., Reno, Nev., 10-13 Jan. 1983; sponsored by AIAA Original contains color illustrations
(NASA-TM-83069; E-1539; NAS 1.15:83069) Avail: NTIS HC A03/MF A01 CSCL 01A

Four deflected thrust nozzle concepts, designed to operate at the low pressure ratio typical of high bypass-ratio turbofan engines for medium speed (subsonic) V/STOL aircraft, were studied. Maps of overall performance characteristics and exit velocity distributions are used to highlight similarities and differences between the four concepts. Analytically determined secondary flows at the exit of a 90 deg circular pipe bend are compared with the experimental

results from the more complex three dimensional geometries. The relative impact of total-pressure losses and secondary flows on nozzle thrust coefficient is addressed by numerical integration of exit velocity measurements. Author

N83-25662*# National Aeronautics and Space Administration. Lewis Research Center, Cleveland, Ohio.
NASA LOW-SPEED CENTRIFUGAL COMPRESSOR FOR FUNDAMENTAL RESEARCH
J. R. WOOD, P. W. ADAM, and A. E. BUGGELE 1983 13 p refs Presented at the 19th Joint Propulsion Conf. and Tech. Display, Seattle, 27-29 Jun. 1983; sponsored by AIAA, SAE and ASME
(NASA-TM-83398; E-1675; NAS 1.15:83398) Avail: NTIS HC A02/MF A01 CSCL 01A

A centrifugal compressor facility being built by the NASA Lewis Research Center is described; its purpose is to obtain benchmark experimental data for internal flow code verification and modeling. The facility will be heavily instrumented with standard pressure and temperature probes and have provisions for flow visualization and laser Doppler velocimetry. The facility will accommodate rotational speeds to 2400 rpm and will be rated at pressures to 1.25 atm. The initial compressor stage for testing is geometrically and dynamically representative of modern high-performance stages with the exception of Mach number levels. Design exit tip speed for the initial stage is 500 ft/sec with a pressure ratio of 1.17. The rotor exit backsweep is 55 deg from radial. M.G.

N83-26816*# Pratt and Whitney Aircraft Group, East Hartford, Conn. Commercial Engineering.
MODEL AERODYNAMIC TEST RESULTS FOR A REFINED ACTUATED INLET EJECTOR NOZZLE AT SIMULATED TAKEOFF AND CRUISE CONDITIONS Final Report
D. P. NELSON Jun. 1983 80 p refs
(Contract NAS3-22738)
(NASA-CR-168051; NAS 1.26:168051; PWA-5768-29) Avail: NTIS HC A05/MF A01 CSCL 01A

Wind tunnel model tests were conducted to demonstrate the aerodynamic performance improvements of a refined actuated inlet ejector nozzle. Models of approximately one-tenth scale were configured to simulate nozzle operation at takeoff, subsonic cruise, transonic cruise and supersonic cruise. Variations of model components provided a performance evaluation of ejector inlet and exit area, forebody boattail angle and ejector inlet operation in the open and closed mode. Approximately 700 data points were acquired at Mach numbers of 0, 0.36, 0.9, 1.2, and 2.0 for a wide range of nozzle flow conditions. Results show that relative to two ejector nozzles previously tested performance was improved significantly at takeoff and subsonic cruise performance, a C sub f of 0.982, was atttained equal to the high performance of the previous tests. The established advanced supersonic transport propulsion study performance goals were met or closely approached at takeoff and supersonic cruise. Author

N83-26817*# National Aeronautics and Space Administration. Lewis Research Center, Cleveland, Ohio.
INPUT GENERATOR FOR DENTON 3-DIMENSIONAL TURBOMACHINE-BLADE-ROW ANALYSIS CODE
A. J. GLASSMAN and J. R. WOOD May 1983 22 p refs
(NASA-TM-23324; E-1565; NAS 1.15:23324) Avail: NTIS HC A02/MF A01 CSCL 01A

A users manual is presented for a computer program that prepares the bulk of the input data set required for the Denton three dimensional turbomachine blade row analysis code. The Denton input is generated from a minimum of geometry and flow variable information by using cubic spline curve fitting procedures. The features of the program are discussed. The input is described and special instructions are included to assist in its preparation. Sample input and output are included. A.R.H.

N83-26819*# Pennsylvania State Univ., University Park.
END WALL FLOW CHARACTERISTICS AND OVERALL PERFORMANCE OF AN AXIAL FLOW COMPRESSOR STAGE Final Report
N. SITARAM and B. LAKSHMINARAYANA Washington NASA Feb. 1983 141 p refs
(Contract NSG-3032)
(NASA-CR-3671; NAS 1.26:3671; PSU/TURBO-82-5) Avail: NTIS HC A07/MF A01 CSCL 01A

This review indicates the possible future directions for research on endwall flows in axial flow compressors. Theoretical investigations on the rotor blade endwall flows in axial flow compressors reported here include the secondary flow calculation and the development of the momentum integral equations for the prediction of the annulus wall boundary layer. The equations for secondary vorticity at the rotor exit are solved analytically. The solution includes the effects of rotation and the viscosity. The momentum integral equations derived include the effect of the blade boundary layers. The axial flow compressor facility of the Department of Aerospace Engineering at The Pennsylvania State University, which is used for the experimental investigations of the endwall flows, is described in some detail. The overall performance and other preliminary experimental results are presented. Extensive radial flow surveys are carried out at the design and various off design conditions. These are presented and interpreted in this report. The following experimental investigations of the blade endwall flows are carried out. (1) Rotor blade endwall flows: The following measurements are carried out at four flow coefficients. (a) The rotor blade static pressures at various axial and radial stations (with special emphasis near the blade tips). (b) The hub wall static pressures inside the rotor blade passage at various axial and tangential stations. (2) IGV endwall flows: The following measurements are carried out at the design flow coefficient. (a) The boundary layer profiles at various axial and tangential stations inside the blade passage and at the blade exit. (b) Casing static pressures and limiting streamline angles inside the blade passage. B.W.

N83-27957*# National Aeronautics and Space Administration. Lewis Research Center, Cleveland, Ohio.
AERODYNAMIC PERFORMANCE OF A FAN STAGE UTILIZING VARIABLE INLET GUIDE VANES (VIGVS) FOR THRUST MODULATION
R. R. WOOLLETT 1983 17 p refs Presented at the 19th Joint Propulsion Conf., Seattle, 27-29 Jun. 1983; sponsored by AIAA, SAE and ASME
(NASA-TM-83438; E-1376; NAS 1.15:83438) Avail: NTIS HC A02/MF A01 CSCL 01A

An experimental research program was conducted in the Lewis Research Center's 9x15-foot (2.74x4.57 m) low speed wind tunnel to evaluate the aerodynamic performance of an inlet and fan system with variable inlet guide vanes (VIGVs) for use on a subsonic V/STOL aircraft. At high VIGV blade angles (lower weight flow and thrust levels), the fan stage was stalled over a major portion of its radius. In spite of the stall, fan blade stresses only exceeded the limits at the most extreme flow conditions. It was found that inlet flow separation does not necessarily lead to poor inlet performance or adverse fan operating conditions. Generally speaking, separated inlet flow did not adversely affect the fan blade stress levels. There were some cases, however, at high VIGV angles and high inlet angles-of-attack where excessive blade stress levels were encountered. An evaluation term made up of the product of the distortion parameter, K alpha, the weight flow and the fan pressure ratio minus one, was found to correlate quite well with the observed blade stress results. Author

N83-27958*# National Aeronautics and Space Administration. Lewis Research Center, Cleveland, Ohio.
ANALYTICAL AND EXPERIMENTAL STUDY OF FLOW THROUGH AN AXIAL TURBINE STAGE WITH A NONUNIFORM INLET RADIAL TEMPERATURE PROFILE
J. R. SCHWAB, R. G. STABE, and W. J. WHITNEY 1983 23 p refs Presented at the 19th Joint Propulsion Conf., Seattle, 27-29 Jun. 1983; sponsored by the AIAA, SAE and ASME
(NASA-TM-83431; E-1722; NAS 1.15:83431; AIAA-83-1175)
Avail: NTIS HC A02/MF A01 CSCL 01A

Results are presented for a typical nonuniform inlet radial temperature profile through an advanced single-stage axial turbine and compared with the results obtained for a uniform profile. Gas temperature rises of 40 K to 95 K are predicted at the hub and tip corners at the trailing edges of the pressure surfaces in both the stator and rotor due to convection of hot fluid from the mean by the secondary flow. The inlet temperature profile is shown to be mixed out at the rotor exit survey plane (2.3 axial chords downstream of the rotor trailing edge) in both the analysis and the experiment. The experimental rotor exit angle profile for the nonuniform inlet temperature profile indicates underturning at the tip caused by increased clearance. Severe underturning also occurs at the mean, both with and without the nonuniform inlet temperature profile. The inviscid rotational flow code used in the analysis fails to predict the underturning at the mean, which may be caused by viscous effects. Author

N83-27960*# GMAF, Inc., Freeport, N.Y.
FAST EULER SOLVER FOR STEADY, 1-DIMENSIONAL FLOWS Final Report
G. MORETTI Jun. 1983 39 p refs
(Contract NAS3-22772)
(NASA-CR-3689; NAS 1.26:3689) Avail: NTIS HC A03/MF A01 CSCL 01A

A numerical technique to solve the Euler equations for steady, one dimensional flows is presented. The technique is essentially implicit, but is structured as a sequence of explicit solutions for each Riemann variable separately. Each solution is obtained by integrating in the direction prescribed by the propagation of the Riemann variables. The technique is second-order accurate. It requires very few steps for convergence, and each step requires a minimal number of operations. Therefore, it is three orders of magnitude more efficient than a standard time-dependent technique. The technique works very well for transonic flows and provides shock fitting with errors as small as 0.001. Results are presented for subsonic problems. Errors are evaluated by comparison with exact solutions. Author

N83-29174*# United Technologies Research Center, East Hartford, Conn.
AXIAL COMPRESSOR MIDDLE STAGE SECONDARY FLOW STUDY Final Report
J. H. WAGNER, R. P. DRING, and H. D. JOSLYN Washington NASA Jul. 1983 98 p refs
(Contract NAS3-23157; DA PROJ. 1L1-62209-AH-76)
(NASA-CR-3701; NAS 1.26:3701) Avail: NTIS HC A05/MF A01 CSCL 01A

This report describes an experimental investigation of the secondary flow within and aft of an axial compressor model with thick endwall boundary layers. The objective of the study was to obtain detailed aerodynamic and trace gas concentration traverse data aft of a well documented isolated rotor for the ultimate purpose of improving the design phases of compressor development based on an improved physical understanding of secondary flow. It was determined from the flow visualization, aerodynamic, and trace gas concentration results that the relative unloading of the midspan region of the airfoil inhibitied a fullspan separation at high loading preventing the massive radial displacement of the hub corner stall to the tip. Radial distribution of high and low total pressure fluid influenced the magnitude of the spanwise distribution of loss, such that, there was a general decreases in loss near the hub to the extent that for the least loaded case a negative loss (increase in total pressure) was observed. The ability to determine the spanwise distribution of blockage was demonstrated. Large blockage was present in the endwall regions due to the corner stall and tip leakage with little blockage in the core flow region. Hub blockage was found to increase rapidly with loading. Author

N83-29178*# Hamilton Standard, Windsor Locks, Conn.
SMALL TRANSPORT AIRCRAFT TECHNOLOGY PROPELLER STUDY Final Report
B. M. BLACK, B. MAGLIOZZI, and C. ROHRBACH 11 Apr. 1983 145 p refs
(Contract NAS3-22039)
(NASA-CR-168045; NAS 1.26:168045; HSER-8826) Avail: NTIS HC A07/MF A01 CSCL 01A

A study to define potential benefits of advanced technology propeller for 1985-1990 STAT commuter airplanes was completed. Two baselines, a Convair, 30 passenger, 0.47 Mach number airplane and a Lockheed, 50 passenger, 0.70 Mach number airplane, were selected from NASA-Ames sponsored airframe contracts. Parametric performance, noise level, weight and cost trends for propellers with varying number of blades, activity factor, camber and diameter incorporating blade sweep, tip proplets, advanced composite materials, advanced airfoils, advanced prevision synchrophasing and counter-rotation are presented. The resulting DOC, fuel burned, empty weight and acquisition cost benefits are presented for resizings of the two baseline airplanes. Six-bladed propeller having advanced composite blades, advanced airfoils, tip proplets and advanced prevision synchrophasers provided the maximum DOC improvements for both airplanes. DOC and fuel burned were reduced by 8.3% and 17.0% respectively for the Convair airplane and by 24.9% and 41.2% respectively for the Lockheed airplane. The larger reductions arose from a baseline definition with very heavy fuselage acoustic treatment. An alternate baseline, with a cabin noise 13dB in excess of the objective, was also studied. B.W.

N83-29179*# National Aeronautics and Space Administration. Lewis Research Center, Cleveland, Ohio.
APPLICATIONS OF THE CONTRAVARIANT FORM OF THE NAVIER-STOKES EQUATIONS
T. KATSANIS 1983 11 p refs Presented at the 6th Computational Fluid Dyn. Conf., Danvers, Mass., 13-15 Jul. 1983; sponsored by AIAA
(NASA-TM-83448; E-1749; NAS 1.15:83448) Avail: NTIS HC A02/MF A01 CSCL 01A

The contravariant Navier-Stokes equations in weak conservation form are well suited to certain fluid flow analysis problems. Three dimensional contravariant momentum equations may be used to obtain Navier-Stokes equations in weak conservation form on a nonplanar two dimensional surface with varying streamsheet thickness. Thus a three dimensional flow can be simulated with two dimensional equations to obtain a quasi-three dimensional solution for viscous flow. When the Navier-Stokes equations on the two dimensional nonplanar surface are transformed to a generalized body fitted mesh coordinate system, the resulting equations are similar to the equations for a body fitted mesh coordinate system on the Euclidean plane. Contravariant momentum components are also useful for analyzing compressible, three dimensional viscous flow through an internal duct by parabolic marching. This type of flow is efficiently analyzed by parabolic marching methods, where the streamwise momentum equation is uncoupled from the two crossflow momentum equations. This can be done, even for ducts with a large amount of turning, if the Navier-Stokes equations are written with contravariant components. Author

N83-30392*# National Aeronautics and Space Administration. Lewis Research Center, Cleveland, Ohio.
PERSPECTIVES ON THE MIXING OF A ROW OF JETS WITH A CONFINED CROSSFLOW
J. D. HOLDEMAN 29 Jun. 1983 14 p refs Presented at the 19th Joint Propulsion Conf., Seattle, 27-29 Jun. 1983; sponsored by AIAA, SAE and ASME
(NASA-TM-83457; E-1772; NAS 1.15:83457; AIAA-83-1200)
Avail: NTIS HC A02/MF A01 CSCL 20D

An interactive computer code, written for a microcomputer, is presented which displays 2-D and 3-D oblique plots of the temperature distribution downstream of jets mixing with a confined crossflow, for either single-side or opposed jet injection. Temperature profiles calculated with this routine are presented to show the effects of flow and geometric variables on the mixing. Examples are also shown to illustrate the different perspectives on the mixing available by exercising various view options. In addition, the program is used to calculate profiles for opposed rows of jets with their centerlines in-line, by assuming that the confining effect of an opposite wall is equivalent to that of a plane of symmetry between opposed jets. Author

N83-30393*# National Aeronautics and Space Administration. Lewis Research Center, Cleveland, Ohio.
EXPERIMENTS IN DILUTION JET MIXING
J. D. HOLDEMAN, R. SRINIVASAN (Garrett Turbine Engine Co., Phoenix, Ariz.), and A. BERENFELD (Garrett Turbine Engine Co., Phoenix, Ariz.) 29 Jun. 1983 15 p refs Presented at 19th Joint Propulsion Conf., Seattle, 27-29 Jun. 1983; sponsored by AIAA, SAE and ASME
(NASA-TM-83434; E-1727; NAS 1.15:83434; AIAA-83-1201)
Avail: NTIS HC A02/MF A01 CSCL 20D

Experimental results are given on the mixing of a single row of jets with an isothermal mainstream in a straight duct, to include flow and geometric variations typical of combustion chambers in gas turbine engines. The principal conclusions reached from these experiments were: at constant momentum ratio, variations in density ratio have only a second-order effect on the profiles; a first-order approximation to the mixing of jets with a variable temperature mainstream can be obtained by superimposing the jets-in-an isothermal-crossflow and mainstream profiles; flow area convergence, especially injection-wall convergence, significantly improves the mixing; for opposed rows of jets, with the orifice centerlines in-line, the optimum ratio of orifice spacing to duct height is one half of the optimum value for single side injection at the same momentum ratio; and for opposed rows of jets, with the orifice centerlines staggered, the optimum ratio of orifice spacing to duct height is twice the optimum value for single side injection at the same momentum ratio. R.J.F.

N83-32774*# National Aeronautics and Space Administration. Lewis Research Center, Cleveland, Ohio.
COMPARISON OF TWO- AND THREE-DIMENSIONAL FLOW COMPUTATIONS WITH LASER ANEMOMETER MEASUREMENTS IN A TRANSONIC COMPRESSOR ROTOR
R. V. CHIMA and A. J. STRAZISAR Sep. 1982 21 p refs Presented at ASME 27th Intern. Gas Turbine Conf., London, 18-22 Apr. 1982 Film supplement C-299 available
(NASA-TP-1931; E-1007; NAS 1.60:1931) Avail: NTIS HC A02/MF A01 CSCL 01A

Two and three dimensional inviscid solutions for the flow in a transonic axial compressor rotor at design speed are compared with probe and laser anemometers measurements at near-stall and maximum-flow operating points. Experimental details of the laser anemometer system and computational details of the two dimensional axisymmetric code and three dimensional Euler code are described. Comparisons are made between relative Mach number and flow angle contours, shock location, and shock strength. A procedure for using an efficient axisymmetric code to generate downstream pressure input for computationally expensive Euler codes is discussed. A film supplement shows the calculations of the two operating points with the time-marching Euler code. Author

N83-34908*# National Aeronautics and Space Administration. Lewis Research Center, Cleveland, Ohio.
A SEMI-DIRECT SOLVER FOR COMPRESSIBLE 3-DIMENSIONAL ROTATIONAL FLOW
S. C. CHANG and J. J. ADAMCZYK May 1983 50 p refs
(NASA-TM-83314; E-1556; NAS 1.15:83314) Avail: NTIS HC A03/MF A01 CSCL 01A

An iterative procedure is presented for solving steady inviscid 3-D subsonic rotational flow problems. The procedure combines concepts from classical secondary flow theory with an extension to 3-D of a novel semi-direct Cauchy-Riemann solver. It is developed for generalized coordinates and can be exercised using standard finite difference procedures. The stability criterion of the iterative procedure is discussed along with its ability to capture the evolution of inviscid secondary flow in a turning channel. Author

N83-34909*# National Aeronautics and Space Administration. Lewis Research Center, Cleveland, Ohio.
SEMIDIRECT COMPUTATIONS FOR TRANSONIC FLOW
J. M. SWISSHELM and J. J. ADAMCZYK 1983 15 p refs Presented at the 6th Computational Fluid Dyn. Conf., Danvers, Mass., 13-15 Jul. 1983; sponsored by AIAA
(NASA-TM-83451; E-1765; NAS 1.15:83451) Avail: NTIS HC A02/MF A01 CSCL 01A

A semidirect method, driven by a Poisson solver, was developed for inviscid transonic flow computations. It is an extension of a recently introduced algorithm for solving subsonic rotational flows. Shocks are captured by implementing a form of artificial compressibility. Nonisentropic cases are computed using a shock tracking procedure coupled with the Rankine-Hugoniot relationships. Results are presented for both subsonic and transonic flows. For the test geometry, an unstaggered cascade of 20 percent thick circular arc airfoils at zero angle of attack, shocks are crisply resolved in supercritical situations and the algorithm converges rapidly. In addition, the convergence rate appears to be nearly independent of the entropy and vorticity production at the shock. Author

N83-34911*# Purdue Univ., Lafayette, Ind. Thermal Sciences and Propulsion Center.
THE EFFECT OF INCIDENCE ANGLE ON THE OVERALL THREE-DIMENSIONAL AERODYNAMIC PERFORMANCE OF A CLASSICAL ANNULAR AIRFOIL CASCADE
D. E. BERGSTEN and S. FLEETER Jul. 1983 468 p refs
(Contract NSG-3285)
(NASA-CR-168127; NAS 1.26:168127; ME-TSPC-TR-83-02)
Avail: NTIS HC A20/MF A01 CSCL 01A

To be of quantitative value to the designer and analyst, it is necessary to experimentally verify the flow modeling and the numerics inherent in calculation codes being developed to predict the three dimensional flow through turbomachine blade rows. This experimental verification requires that predicted flow fields be correlated with three dimensional data obtained in experiments which model the fundamental phenomena existing in the flow passages of modern turbomachines. The Purdue Annular Cascade Facility was designed specifically to provide these required three dimensional data. The overall three dimensional aerodynamic performance of an instrumented classical airfoil cascade was determined over a range of incidence angle values. This was accomplished utilizing a fully automated exit flow data acquisition and analysis system. The mean wake data, acquired at two downstream axial locations, were analyzed to determine the effect of incidence angle, the three dimensionality of the cascade exit flow field, and the similarity of the wake profiles. The hub, mean, and tip chordwise airfoil surface static pressure distributions determined at each incidence angle are correlated with predictions from the MERIDL and TSONIC computer codes. Author

N83-35999*# National Aeronautics and Space Administration. Langley Research Center, Hampton, Va.
A NUMERICAL STUDY OF THE STEADY SCALAR CONVECTIVE DIFFUSION EQUATION FOR SMALL VISCOSITY Final Report
M. B. GILES and M. E. ROSE Sep. 1983 30 p refs
(Contract NAS1-17070; NAS1-17130; NAG3-9)
(NASA-CR-172231; ICASE-83-57; NAS 1.26:172231) Avail: NTIS HC A03/MF A01 CSCL 01A

A time-independent convection diffusion equation is studied by means of a compact finite difference scheme and numerical solutions are compared to the analytic inviscid solutions. The correct internal and external boundary layer behavior is observed, due to an inherent feature of the scheme which automatically produces upwind differencing in inviscid regions and the correct viscous behavior in viscous regions. Author

03

AIR TRANSPORTATION AND SAFETY

Includes passenger and cargo air transport operations; and aircraft accidents.

A83-25693*# Tennessee Univ., Knoxville.
'SCALING' ANALYSIS OF THE ICE ACCRETION PROCESS ON AIRCRAFT SURFACES
E. G. KESHOCK, A. H. TABRIZI (Tennessee, University, Knoxville, TN), and J. R. MISSIMER (Environmental Systems Corp., Knoxville, TN) American Society of Mechanical Engineers, Winter Annual Meeting, Phoenix, AZ, Nov. 14-19, 1982, 8 p. refs
(Contract NAG3-90)
(ASME PAPER 82-WA/HT-39)

A comprehensive set of scaling parameters is developed for the ice accretion process by analyzing the energy equations of the dynamic freezing zone and the already frozen ice layer, the continuity equation associated with supercooled liquid droplets entering into and impacting within the dynamic freezing zone, and energy equation of the ice layer. No initial arbitrary judgments are made regarding the relative magnitudes of each of the terms. The method of intrinsic reference variables in employed in order to develop the appropriate scaling parameters and their relative significance in rime icing conditions in an orderly process, rather than utilizing empiricism. The significance of these parameters is examined and the parameters are combined with scaling criteria related to droplet trajectory similitude. N.B.

A83-36042*# Dayton Univ., Ohio.
NUMERICAL SIMULATION OF AIRFOIL ICE ACCRETION
C. D. MACARTHUR (Dayton, University, Dayton, OH) American Institute of Aeronautics and Astronautics, Aerospace Sciences Meeting, 21st, Reno, NV, Jan. 10-13, 1983. 40 p. refs
(Contract NAG3-65)
(AIAA PAPER 83-0112)

A mathematical model of glaze and rime ice accretion on a two-dimensional airfoil is presented. The model employs standard methods for calculating the flow field and cloud droplet trajectories. This data is used as input to a thermodynamic analysis of the ice accretion process which includes liquid runback. The structure of the model allows for dynamic updating of the droplet collection efficiency and heat and mass transfer processes as the accreted ice shape changes. This results in the improved shape prediction over previously described methods. Simulations made with the model are compared to experimental results obtained for a NACA 0012 airfoil in the NASA/Lewis Icing Research Tunnel. The agreement with experiment is found to be generally satisfactory for some cases, but a need for improvements is indicated by others. Suggestions for improvements are made. Author

A83-42099*# National Aeronautics and Space Administration. Lewis Research Center, Cleveland, Ohio.
EXPERIMENTAL COMPARISON OF ICING CLOUD INSTRUMENTS
W. OLSEN (NASA, Lewis Research Center, Cleveland, OH), D. TAKEUCHI (Meteorology Research, Inc., Altadena, CA), and K. ADAMS (USAF, Flight Test Center, Edwards, CA) American Institute of Aeronautics and Astronautics, Aerospace Sciences Conference, 21st, Reno, NV, Jan. 10-13, 1983. 26 p. refs
(AIAA PAPER 83-0026)

Previously announced in STAR as N83-24487

N83-11095*# Lockheed-California Co., Burbank.
ASSESSMENT OF CRASH FIRE HAZARD OF LH SUB 2 FUELED AIRCRAFT Final Report, Aug. 1980 - Sep. 1981
G. D. BREWER, G. WITTLIN, E. F. VERSAW, R. PARMLEY, R. CIMA, and E. G. WALTHER Dec. 1981 199 p refs Sponsored in part by Lockheed Missiles and Space Co., Inc. and The John Muir Inst., Nevada Univ.
(Contract NAS3-2483)
(NASA-CR-165525; NAS 1.26:165525; LR-30060) Avail: NTIS HC A09/MF A01 CSCL 01C

The relative safety of passengers in LH2 - fueled aircraft, as well as the safety of people in areas surrounding a crash scene, has been evaluated in an analytical study. Four representative circumstances were postulated involving a transport aircraft in which varying degrees of severity of damage were sustained. Potential hazard to the passengers and to the surroundings posed by the spilled fuel was evaluated for each circumstance. Corresponding aircraft fueled with liquid methane, Jet A, and JP-4 were also studied in order to make comparisons of the relative safety. The four scenarios which were used to provide a basis for the evaluation included: (1) a small fuel leak internal to the aircraft, (2) a survivable crash in which a significant quantity of fuel is spilled in a radial pattern as a result of impact with a stationary object while taxiing at fairly low speed, (3) a survivable crash in which a significant quantity of fuel is spilled in an axial pattern as a result of impact during landing, and (4) a non-survivable crash in which a massive fuel spill occurs instantaneously. Author

N83-14078*# National Aeronautics and Space Administration. Lewis Research Center, Cleveland, Ohio.
NASA LEWIS RESEARCH CENTER'S PROGRAM ON ICING RESEARCH
J. J. REINMANN, R. J. SHAW, and W. A. OLSEN, JR. 1982 17 p refs Proposed for presentation at the 21st Aerospace Sci. Conf., Reno, Nev., 10-13 Jan. 1983; sponsored by AIAA and presented at the 1st Intern. Workshop on Atmospheric Icing of Struct., Hanover, N.H., 1-3 Jun. 1982; sponsored by EPRI and the Army Cold Regions Research and Engineering Lab.
(NASA-TM-83031; E-1469; NAS 1.15:83031; AIAA-83-0204)
Avail: NTIS HC A02/MF A01 CSCL 01C

The helicopter and general aviation, light transport, and commercial transport aircraft share common icing requirements: highly effective, lightweight, low power consuming deicing systems, and detailed knowledge of the aeropenalties due to ice on aircraft surfaces. To meet current and future needs, NASA has a broadbased icing research program which covers both research and engineering applications, and is well coordinated with the FAA, DOD, universities, industry, and some foreign governments. Research activity in ice protection systems, icing instrumentation, experimental methods, analytical modeling, and in-flight research are described. A.R.H.

N83-23281*# Toledo Univ., Ohio. Dept. of Chemical Engineering.
NUMERICAL SIMULATION OF AN ELECTROTHERMAL DEICER PAD M.S. Thesis. Final Report
J. J. MARANO Mar. 1983 113 p refs
(Contract NAG3-72)
(NASA-CR-168097; NAS 1.26:168097) Avail: NTIS HC A06/MF A01 CSCL 01C

A numerical simulation is developed to investigate the removal of ice from composite aircraft blades by means of electrothermal deicing. The model considers one dimensional, unsteady state heat transfer in the composite blade-ice body. The heat conduction equations are approximated by using the Crank-Nicolson finite difference scheme, and the phase change in the ice layer is handled using the Enthalpy method. To solve the system of equations which result, Gauss-Seidel iteration is used. The simulation computes the temperature profile in the composite blade-ice body, as well as the movement of the ice-water interface, as a function of time. This information can be used to evaluate deicer performance. The simulation can also be used to solve a variety of other heat conduction problems involving composite bodies.
Author

N83-24487*# National Aeronautics and Space Administration. Lewis Research Center, Cleveland, Ohio.
EXPERIMENTAL COMPARISON OF ICING CLOUD INSTRUMENTS
W. OLSEN, D. M. TAKEUCHI (Meteorology Research, Inc.), and K. ADAMS (Air Force Flight Test Center) 1983 27 p refs Presented at the 21st Aerospace Sci. Conf., Reno, Nev., 10-13 Jan. 1983; sponsored by AIAA
(NASA-TM-83340; E-1595; NAS 1.15:83340; AIAA-83-0026)
Avail: NTIS HC A03/MF A01 CSCL 01D

Icing cloud instruments were tested in the spray cloud Icing Research Tunnel (IRT) in order to determine their relative accuracy and their limitations over a broad range of conditions. It was found that the average of the readings from each of the liquid water content (LWC) instruments tested agreed closely with each other and with the IRT calibration; but all have a data scatter (+ or - one standard deviation) of about + or - 20 percent. The effect of this + or - 20 percent uncertainty is probably acceptable in aero-penalty and deicer experiments. Existing laser spectrometers proved to be too inaccurate for LWC measurements. The error due to water runoff was the same for all ice accretion LWC instruments. Any given laser spectrometer proved to be highly repeatable in its indications of volume median drop size (DVM), LWC and drop size distribution. However, there was a significant disagreement between different spectrometers of the same model, even after careful standard calibration and data analysis. The scatter about the mean of the DVM data from five Axial Scattering Spectrometer Probes was + or - 20 percent (+ or - one standard deviation) and the average was 20 percent higher than the old IRT calibration. The + or - 20 percent uncertainty in DVM can cause an unacceptable variation in the drag coefficient of an airfoil with ice; however, the variation in a deicer performance test may be acceptable.
S.L.

N83-32782*# Kansas Univ. Center for Research, Inc., Lawrence. Flight Research Lab.
A METHOD OF PREDICTING FLOW RATES REQUIRED TO ACHIEVE ANTI-ICING PERFORMANCE WITH A POROUS LEADING EDGE ICE PROTECTION SYSTEM Final Report
D. L. KOHLMAN and A. E. ALBRIGHT Aug. 1983 25 p refs Revised
(Contract NAG3-71)
(NASA-CR-168213; NAS 1.26:168213; KU-FRL-464-5-REV-A)
Avail: NTIS HC A02/MF A01 CSCL 01C

An analytical method was developed for predicting minimum flow rates required to provide anti-ice protection with a porous leading edge fluid ice protection system. The predicted flow rates compare with an average error of less than 10 percent to six experimentally determined flow rates from tests in the NASA Icing Research Tunnel on a general aviation wing section.
Author

04

AIRCRAFT COMMUNICATIONS AND NAVIGATION

Includes digital and voice communication with aircraft; air navigation systems (satellite and ground based); and air traffic control.

N83-17461*# National Aeronautics and Space Administration. Lewis Research Center, Cleveland, Ohio.
AIRLINE FLIGHT PLANNING: THE WEATHER CONNECTION
R. STEINBERG *In* DOE Symp. on Com. Aviation Energy Conserv. Strategies p 103-126 Apr. 1981 refs Previously announced as A82-24386
Avail: NTIS HC A17/MF A01 CSCL 01B

Airline flight planning has shown little improvement in accuracy since the introduction of computerized techniques in 1964. This has primarily been, because both the type of weather product utilized by the carriers and the way they have employed it has remained unchanged over the past 15 years. The airlines now have an opportunity to make a significant advance in this area with attendant benefits in fuel savings. Most the technological ingredients are in place, but it will take increased cooperation between government and the private sector if cost effective improvements are to be made on a reasonable time scale. This paper reviews the meteorological basis for the present method of flight planning and analyzes its impact on current flight operations. A new approach is suggested for developing a weather data base, for flight planning, which has the potential of providing a fuel savings of between 2 and 3 percent on long distance flights.
Author

05

AIRCRAFT DESIGN, TESTING AND PERFORMANCE

Includes aircraft simulation technology.

A83-37965* National Aeronautics and Space Administration. Ames Research Center, Moffett Field, Calif.
SUPERSONIC STOVL RESEARCH AIRCRAFT
S. B. WILSON, III, G. H. KIDWELL, JR. (NASA, Ames Research Center, Moffett Field, CA), G. E. TURNEY (NASA, Lewis Research Center, Cleveland, OH), and A. ROGERS (Grumman Aerospace Corp., El Segundo, CA) Society of Automotive Engineers, Aerospace Congress and Exposition, Anaheim, CA, Oct. 25-28, 1982. 18 p. refs
(SAE PAPER 821375)

Two powered-lift concepts, the tandem fan and the longitudinally-arrayed ejector, are integrated with two existing fighter aircraft, the F-14A and F-16A respectively, to indicate the benefits and/or penalties involved with providing STOVL capability to CTOL aircraft. It is shown that properly designed powered-lift aircraft can achieve either comparable or superior mission performance relative to CTOL aircraft.
Author

N83-19738*# Kansas Univ. Center for Research, Inc., Lawrence. Flight Research Lab.
A METHOD OF PREDICTING FLOW RATES REQUIRED TO ACHIEVE ANTI-ICING PERFORMANCE WITH A POROUS LEADING EDGE ICE PROTECTION SYSTEM Final Report
D. L. KOHLMAN Feb. 1983 27 p refs
(Contract NAG3-71)
(NASA-CR-169996; NAS 1.26:169996; KU-FRL-464-5) Avail: NTIS HC A03/MF A01 CSCL 01C

A proposed method of analytically predicting the minimum fluid flow rate required to provide anti-ice protection with a porous leading edge system on a wing under a given set of flight conditions

is presented. Results of the proposed method are compared with the actual results of an icing test of a real wing section in the NASA Lewis Icing Research Tunnel. Author

N83-22188*# Boeing Vertol Co., Philadelphia, Pa.
LARGE ROTORCRAFT TRANSMISSION TECHNOLOGY DEVELOPMENT PROGRAM Final Test Report
J. C. MACK Mar. 1983 106 p
(Contract NAS3-22143)
(NASA-CR-168120; NAS 1.26:168120; D210-11944-1) Avail: NTIS HC A06/MF A01 CSCL 01C

Testing of a U.S. Army XCH-62 HLH aft rotor transmission under NASA Contract NAS 3-22143 was successfully completed. This test establishes the feasibility of large, high power rotorcraft transmissions as well as demonstrating the resolution of deficiencies identified during the HLH advanced technology programs and reported by USAAMRDLTR-77-38. Over 100 hours of testing was conducted. At the 100% design power rating of 10,620 horsepower, the power transferred through a single spiral bevel gear mesh is more than twice that of current helicopter bevel gearing. In the original design of these gears, industry-wide design methods were employed and failures were experienced which identified problem areas unique to gear size. To remedy this technology shortfall, a program was developed to predict gear stresses using finite element analysis for complete and accurate representation of the gear tooth and supporting structure. To validate the finite element methodology gear strain data from the existing U.S. Army HLH aft transmission was acquired, and existing data from smaller gears were made available. Author

N83-29197*# National Aeronautics and Space Administration. Lewis Research Center, Cleveland, Ohio.
PIEZOELECTRIC DEICING DEVICE Patent Application
R. C. FINK and B. A. BANKS, inventors (to NASA) 25 Feb. 1983 10 p
(NASA-CASE-LEW-13773-1; US-PATENT-APPL-SN-469867)
Avail: NTIS HC A02/MF A01 CSCL 01C

A fast voltage pulse is applied to a transducer which comprises a composite of multiple layers of alternately polarized piezoelectric material. These layers are bonded together and positioned over the curved leading edge of an aircraft wing structure. Each layer is relatively thin and metallized on both sides. The strain produced in the transducer causes the composite to push forward resulting in detachment and breakup of ice on the leading edge of the aircraft wing. NASA

N83-30402*# Boeing Commercial Airplane Co., Seattle, Wash.
NACELLE AERODYNAMIC AND INERTIAL LOADS (NAIL) PROJECT Test Report, Oct. 1979 - Nov. 1980
May 1981 352 p refs
(Contract NAS1-15325; NAS3-20632)
(NASA-CR-168712; NAS 1.26:168712) Avail: NTIS HC A16/MF A01 CSCL 01C

The testing was conducted on the Boeing-owned 747 RA001 test bed airplane during the concurrent 767/JT9D-7R4 engine development program. Following a functional check flight conducted from Boeing Field International (BFI) on 3 October 1980, the airplane and test personnel were ferried to Valley Industrial Park (GSG) near Glasgow, Montana, on 7 October 1980. The combined NAL and 7670JT9D-7R4 test flights were conducted at the Glasgow remote test site, and the airplane was returned to Seattle on 26 October 1980. Author

06

AIRCRAFT INSTRUMENTATION

Includes cockpit and cabin display devices; and flight instruments.

A83-16772*# National Aeronautics and Space Administration. Lewis Research Center, Cleveland, Ohio.
FIBEROPTICS TECHNOLOGY AND ITS APPLICATION TO PROPULSION CONTROL SYSTEMS
R. J. BAUMBICK (NASA, Lewis Research Center, Cleveland, OH) American Institute of Aeronautics and Astronautics, Aerospace Sciences Meeting, 21st, Reno, NV, Jan. 10-13, 1983, 7 p. refs (AIAA PAPER 83-0534)

Current work on optical sensors and optically controlled actuators for use in air-breathing engine control systems is reviewed with particular reference to the design and operation of several new fiber-optic devices. These include a tachometer, a rotary position encoder, a Fabry-Perot interferometer and a rare-earth sensor for measuring engine gas temperatures, a high-temperature photoswitch designed for the range -55 to 260 C, and optical cables and connectors. The advantages of optics over conventional wire systems used for sensing and actuator control are briefly discussed. V.L.

N83-14123*# Ideal Research, Inc., Rockville, Md.
DEVELOPMENT AND TEST OF A MICROWAVE ICE ACCRETION MEASUREMENT INSTRUMENT (MIAMI) Final Report
B. MAGENHEIM and J. K. ROCKS Washington NASA Nov. 1982 85 p refs
(Contract NAS3-22765)
(NASA-CR-3598; NAS 1.26:3598; BATT-92880) Avail: NTIS HC A05/MF A01 CSCL 01D

The development of an ice accretion measurement instrument that is a highly sensitive, accurate, rugged and reliable microprocessor controlled device using low level microwave energy for non-instrusive real time measurement and recording of ice growth history, including ice thickness and accretion rate is discussed. Data is displayed and recorded digitally. New experimental data is presented, obtained with the instrument, which demonstrates its ability to measure ice growth on a two-dimensional airfoil. The device is suitable for aircraft icing protection. It may be mounted flush, non-intrusively, on any part of an aircraft skin including rotor blades and engine inlets. R.J.F.

N83-15302*# National Aeronautics and Space Administration. Lewis Research Center, Cleveland, Ohio.
FIBEROPTICS TECHNOLOGY AND ITS APPLICATION TO PROPULSION CONTROL SYSTEMS
R. J. BAUMBICK 1983 12 p refs Presented at the 21st Aerospace Sci. Conf., Reno, Nevada, 10-13 Jan. 1983; sponsored by the American Inst. of Aeronautics and Astronautics
(NASA-TM-83009; E-1444; NAS 1.15:83009) Avail: NTIS HC A02/MF A01 CSCL 01D

Electro-optical systems have many advantages over conventional electrical systems. Among these are optics' insensitivity to electro-magnetic interference, good electrical isolation and the ability to make measurements in highly explosive areas without risk. These advantages promise to help improve the reliability of future aircraft engine control systems which will be entirely electronic digital. To improve the reliability of these systems, especially against lightning strikes, passive, optical, sensors and fiberoptic transmission lines are being considered for use in future engine systems. Also under consideration are actuators which receive their command signals over fiber optic cables. This paper reviews concepts used for optical instrumentation and actuation systems and discusses work being done by NASA Lewis Research Center in this area. Author

N83-18720*# Meteorology Research, Inc., Altadena, Calif.
COMPARISON OF MODERN ICING CLOUD INSTRUMENTS Final Report
D. M. TAKEUCHI, L. J. JAHNSEN, S. M. CALLANDER, and M. C. HUMBERT Jan. 1983 133 p refs
(Contract NAS3-22760; F04611-81-C-0033)
(NASA-CR-168008; NAS 1.26:168008; MRI-82-FR-1862) Avail: NTIS HC A07/MF A01 CSCL 01D

Intercomparison tests with Particle Measuring Systems (PMS) were conducted. Cloud liquid water content (LWC) measurements were also taken with a Johnson and Williams (JW) hot-wire device and an icing rate device (Leigh IDS). Tests include varying cloud LWC (0.5 to 5 au gm), cloud median volume diameter (MVD) (15 to 26 microns), temperature (-29 to 20 C), and air speeds (50 to 285 mph). Comparisons were based upon evaluating probe estimates of cloud LWC and median volume diameter for given tunnel settings. Variations of plus or minus 10% and plus or minus 5% in LWC and MVD, respectively, were determined of spray clouds between test made at given tunnel settings (fixed LWC, MVD, and air speed) indicating cloud conditions were highly reproducible. Although LWC measurements from JW and Leigh devices were consistent with tunnel values, individual probe measurements either consistently over or underestimated tunnel values by factors ranging from about 0.2 to 2. Range amounted to a factor of 6 differences between LWC estimates of probes for given cloud conditions. For given cloud conditions, estimates of cloud MVD between probes were within plus or minus 3 microns and 93% of the test cases. Measurements overestimated tunnel values in the range between 10 to 20 microns. The need for improving currently used calibration procedures was indicated. Establishment of test facility (or facilities) such as an icing tunnel where instruments can be calibrated against known cloud standards would be a logical choice. B.G.

N83-33883*# National Aeronautics and Space Administration. Lewis Research Center, Cleveland, Ohio.
THE NASA HIGH ACCURACY FUEL FLOWMETER (HAFF) DEVELOPMENT PROGRAM
H. F. HOBART 1983 6 p refs Presented at CECON '83, Cleveland, 4-5 Oct. 1983; sponsored by IEEE
(NASA-TM-83484; E-1807; NAS 1.15:83484) Avail: NTIS HC A02/MF A01 CSCL 01D

The high accuracy fuel flowmeter development program is described. A flightworthy meter that measures mass flowrate of aircraft fuels to within + or - 0.25% of reading over a 50:1 range of flow is developed. A study of measurement techniques to achieve this goal yielded three candidates: (1) a dual turbine flowmeter with density and viscosity compensation; (2) an angular momentum flowmeter with a motor-driven, spring-restrained turbine and viscosity shroud; and (3) a vortex precission flowmeter with density and viscosity compensation. An experimental study of each technique was completed and the first two candidates were selected for prototype development. S.L.

07

AIRCRAFT PROPULSION AND POWER

Includes prime propulsion systems and systems components, e.g., gas turbine engines and compressors; and on-board auxiliary power plants for aircraft.

A83-10184*# National Aeronautics and Space Administration. Lewis Research Center, Cleveland, Ohio.
ROTOR WAKE CHARACTERISTICS RELEVANT TO ROTOR-STATOR INTERACTION NOISE GENERATION
L. M. SHAW and J. R. BALOMBIN (NASA, Lewis Research Center, Cleveland, OH) Journal of Aircraft, vol. 19, Nov. 1982, p. 954-962. refs
(Previously cited in issue 01, p. 13, Accession no. A82-10456)

A83-13159*# Pratt and Whitney Aircraft Group, Middletown, Conn.
COMPOSITE FAN EXIT GUIDE VANES FOR HIGH BYPASS RATIO GAS TURBINE ENGINES
S. S. BLECHERMAN and T. N. STANKUNAS (United Technologies Corp., Pratt and Whitney Aircraft Group, Middletown, CT) Journal of Aircraft, vol. 19, Dec. 1982, p. 1032-1037. refs
(Contract NAS3-21037)
(Previously cited in issue 19, p. 3265, Accession no. A81-40839)

A83-15068* Lockheed-Georgia Co., Marietta.
GENERATION OF DESIRED SIGNALS FROM ACOUSTIC DRIVERS
R. RAMAKRISHNAN, M. SALIKUDDIN, and K. K. AHUJA (Lockheed-Georgia Co., Marietta, GA) Journal of Sound and Vibration, vol. 85, Nov. 8, 1982, p. 39-51. Research supported by the Lockheed-Georgia Independent Research Program refs
(Contract NAS3-20797)

A procedure to control transient signal generation is developed for the study of internal noise propagation from aircraft engines. A simple algorithm incorporating transform techniques is used to produce signals of any desired waveform from acoustic drivers. The accurate driver response is then calculated, and from this the limiting frequency characteristics are determined and the undesirable frequencies where the driver response is poor are eliminated from the analysis. A synthesized signal is then produced by convolving the inverse of the response function with the desired signal. Although the shape of the synthesized signal is in general quite awkward, the driver generates the desired signal when the distorted signal is fed into the driver. The results of operating the driver in two environments, in a free field and in a duct, are presented in order to show the impedance matching effect of the driver. In addition, results using a high frequency cut-off value as a parameter is presented in order to demonstrate the extent of the applicability of the synthesis procedure. It is concluded that the desired signals can be generated through the signal synthesis procedure. N.B.

A83-16456*# Purdue Univ., Lafayette, Ind.
AXIAL-COMPRESSOR FLOW DISTORTION WITH WATER INGESTION
T. TSUCHIYA and S. N. B. MURTHY (Purdue University, West Lafayette, IN) American Institute of Aeronautics and Astronautics, Aerospace Sciences Meeting, 21st, Reno, NV, Jan. 10-13, 1983, 9 p. refs
(Contract F33615-78-C-2401; NAG3-63; NAG3-204)
(AIAA PAPER 83-0004)

The objective of the investigation is as follows: to establish relations between the steady state mean flow distortion generated during water ingestion into an axial-flow compressor and (a) characteristic length and time scales pertaining to (1) the centrifugal action and (2) the heat and mass transfer processes and (b) aerodynamic parameters based on blade geometry, aspect ratio and blade loading. Analytical and experimental results are presented for a small compressor to illustrate the extent of the distortion introduced as a function of (1) the operating speed and (2) the mass-based water content in the ingested mixture. Methods of scaling the effects in compressors of different sizes are discussed. (Author)

A83-16572*# Cincinnati Univ., Ohio.
A METHOD OF PREDICTING THE PERFORMANCE DETERIORATION OF A COMPRESSOR CASCADE DUE TO SAND EROSION
C. BALAN and W. TABAKOFF (Cincinnati, University, Cincinnati, OH) American Institute of Aeronautics and Astronautics, Aerospace Sciences Meeting, 21st, Reno, NV, Jan. 10-13, 1983, 13 p. refs
(Contract DAAG29-82-K-0029; NSG-3218)
(AIAA PAPER 83-0178)

Performance deterioration due to sand erosion is a well known phenomena for aircraft engines operating in particulate flow

environments. A method for predicting this performance deterioration is developed and applied to a two dimensional compressor cascade. The locations of the particles impacts are computed by analyzing the trajectories of the individual particles. From this analysis, the material removed, the changes in the airfoil shape, and the roughness development over the surface are estimated as a function of time. The resulting airfoil profiles are analyzed for predicting performance by using an inviscid-viscous interaction technique. The analytical solution is compared with experimental results. (Author)

A83-16663*# National Aeronautics and Space Administration. Lewis Research Center, Cleveland, Ohio.
SMALL GAS TURBINE COMBUSTOR STUDY - COMBUSTOR LINER EVALUATION
C. T. NORGREN and S. M. RIDDLEBAUGH (NASA, Lewis Research Center, Cleveland, OH) American Institute of Aeronautics and Astronautics, Aerospace Sciences Meeting, 21st, Reno, NV, Jan. 10-13, 1983, 12 p. refs
(AIAA PAPER 83-0337)

A reverse flow combustor liner constructed of Lamilloy (a multilaminate transpiration type material) is compared both analytically and experimentally with a conventional splash film-cooled design with the same combustor configuration. Comparison of selected critical combustor panels indicated that it was possible to maintain the liner temperature similar between the two configurations using 50 percent less coolant for the Lamilloy as compared with the reference film-cooled combustor. Additional benefits indicated improvement in outlet temperature distribution and NOx emission level. (Author)

A83-16776*# General Electric Co., Cincinnati, Ohio.
SCALE MODEL PERFORMANCE TEST INVESTIGATION OF MIXED FLOW EXHAUST SYSTEMS FOR AN ENERGY EFFICIENT ENGINE /E3/ PROPULSION SYSTEM
A. P. KUCHAR (General Electric Co., Cincinnati, OH) and R. CHAMBERLIN (NASA, Lewis Research Center, Cleveland, OH) American Institute of Aeronautics and Astronautics, Aerospace Sciences Meeting, 21st, Reno, NV, Jan. 10-13, 1983, 13 p.
(AIAA PAPER 83-0541)

As part of the NASA Energy Efficient Engine program, scale-model performance tests of a mixed flow exhaust system were conducted. The tests were used to evaluate the performance of exhaust system mixers for high-bypass, mixed-flow turbofan engines. The tests indicated that: (1) mixer penetration has the most significant affect on both mixing effectiveness and mixer pressure loss; (2) mixing/tailpipe length improves mixing effectiveness; (3) gap reduction between the mixer and centerbody increases high mixing effectiveness; (4) mixer cross-sectional shape influences mixing effectiveness; (5) lobe number affects mixing degree; and (6) mixer aerodynamic pressure losses are a function of secondary flows inherent to the lobed mixer concept. S.C.S.

A83-19593*# National Aeronautics and Space Administration. Flight Research Center, Edwards, Calif.
FLIGHT EVALUATION OF MODIFICATIONS TO A DIGITAL ELECTRONIC ENGINE CONTROL SYSTEM IN AN F-15 AIRPLANE
F. W. BURCHAM, JR., L. P. MYERS (NASA, Flight Research Center, Edwards, CA), and J. R. ZELLER (NASA, Lewis Research Center, Cleveland, OH) American Institute of Aeronautics and Astronautics, Aerospace Sciences Meeting, 21st, Reno, NV, Jan. 10-13, 1983, 10 p.
(AIAA PAPER 83-0537)

The third phase of a flight evaluation of a digital electronic engine control system in an F-15 has recently been completed. It was found that digital electronic engine control software logic changes and augmentor hardware improvements resulted in significant improvements in engine operation. For intermediate to maximum power throttle transients, an increase in altitude capability of up to 8000 ft was found, and for idle to maximum transients, an increase of up to 4000 ft was found. A nozzle instability noted in earlier flight testing was investigated on a test engine at NASA Lewis Research Center, a digital electronic engine control software logic change was developed and evaluated, and no instability occurred in the Phase 3 flight evaluation. The backup control airstart modification was evaluated, and gave an improvement of airstart capability by reducing the minimum airspeed for successful airstarts by 50 to 75 knots. (Author)

A83-19595*# National Aeronautics and Space Administration. Lewis Research Center, Cleveland, Ohio.
A REMOTE AUGMENTOR LIFT SYSTEM WITH A TURBINE BYPASS ENGINE
L. H. FISHBACH and L. C. FRANCISCUS (NASA, Lewis Research Center, Cleveland, OH) International Council of Aeronautical Sciences, Congress, 13th, and American Institute of Aeronautics and Astronautics Aircraft Systems and Technology Meeting, Seattle, WA, Aug. 22-27, 1982, Paper. 10 p. refs
(Previously announced in STAR as N83-12087)

A83-21079*# National Aeronautics and Space Administration. Lewis Research Center, Cleveland, Ohio.
EFFECT OF BROAD PROPERTIES FUEL ON INJECTOR PERFORMANCE IN A REVERSE FLOW COMBUSTOR
S. M. RIDDLEBAUGH and C. T. NORGREN (NASA, Lewis Research Center, Cleveland, OH) American Institute of Aeronautics and Astronautics, Aerospace Sciences Meeting, 21st, Reno, NV, Jan. 10-13, 1983, 15 p. refs
(AIAA PAPER 83-0154)
(Previously announced in STAR as N83-13101)

A83-22494* National Aeronautics and Space Administration. Lewis Research Center, Cleveland, Ohio.
FIBER OPTICS FOR AIRCRAFT ENGINE/INLET CONTROL
R. J. BAUMBICK (NASA, Lewis Research Center, Cleveland, OH) In: Fiber optics in adverse environments; Proceedings of the Seminar, San Diego, CA, August 25-27, 1981. Bellingham, WA, SPIE - The International Society for Optical Engineering, 1982, p. 148-154. refs
(Previously announced in STAR as N81-31190)

A83-24028*# National Aeronautics and Space Administration. Lewis Research Center, Cleveland, Ohio.
EFFECT OF VARIABLE GUIDE VANES ON THE PERFORMANCE OF A HIGH-BYPASS TURBOFAN ENGINE
G. A. BOBULA (NASA, Lewis Research Center; U.S. Army, Propulsion Laboratory, Cleveland, OH), R. H. SOEDER, and L. A. BURKARDT (NASA, Lewis Research Center, Cleveland, OH) Journal of Aircraft, vol. 20, Apr. 1983, p. 306-311. refs
(Previously cited in issue 19, p. 3265, Accession no. A81-40842)

A83-24038*# Carnegie-Mellon Univ., Pittsburgh, Pa.
FRICTION DAMPING OF FLUTTER IN GAS TURBINE ENGINE AIRFOILS
A. SINHA and J. H. GRIFFIN (Carnegie-Mellon University, Pittsburgh, PA) Journal of Aircraft, vol. 20, Apr. 1983, p. 372-376. refs
(Contract NAG3-231)

This paper investigates the feasibility of using blade-to-ground friction dampers to stabilize flutter in blades. The response of an equivalent one mode model in which the aerodynamic force is represented as negative viscous damping is examined to investigate the following issues: the range of amplitudes over which friction damping can stabilize the response, the maximum negative aerodynamic damping that can be stabilized in such a manner, the effect of simultaneous resonant excitation on these stability limits, and the determination of those damper parameters which will be the best for flutter control. (Author)

A83-24669*# Princeton Univ., N. J.
COMPUTED AND MEASURED TURBULENCE IN AXISYMMETRIC RECIPROCATING ENGINES
F. GRASSO and F. V. BRACCO (Princeton University, Princeton, NJ) AIAA Journal, vol. 21, Apr. 1983, p. 601-607. Research supported by the General Motors Corp., Volkswagenwerk, Fiat S.p.A. and Komatsu, Ltd. refs
(Contract DE-AC04-81AL-16338; NAG3-8)

The turbulent flowfield of a spark-ignition engine affects strongly the combustion characteristics of the engine. The flowfield depends on the design of the combustion chamber and the intake system. The present investigation is concerned with the effect of chamber design, and engine operating conditions on top dead center turbulence prior to ignition. It is shown that many of the trends which were identified in earlier studies can be obtained from a single model. The employed model takes into account a two-dimensional axisymmetric flowfield. Attention is given to governing equations, boundary and initial conditions, a comparison of the computed results with measurements, and the effect of swirl and squish. G.R.

A83-24834* Textron Bell Helicopter, Fort Worth, Tex.
DESIGN OF AN ADVANCED 500-HP HELICOPTER TRANSMISSION
C. E. BRADDOCK (Bell Helicopter Textron, Fort Worth, TX) American Helicopter Society, Specialists Meeting on Rotary Wing Propulsion Systems, Williamsburg, VA, Nov. 16-18, 1982, Preprint. 16 p. refs
(Contract NAS3-21595)

A 500-hp Advanced Technology Demonstrator helicopter transmission was designed by an American aerospace company under a NASA contract. The project was mainly concerned with designing a 500-hp version of the OH-58C 317-hp transmission which would have the capabilities for a long, quiet life at a minimum increase in cost, weight, and space, which usually increase along with power increases. This objective was accomplished by implementing advanced technology which has been developed during the last decade and by making improvements dictated by field experience. The improvements are related to bearings made of cleaner gear steels, spiral bevel gears made of cleaner gear steels, high contact ratio spur gear teeth in the planetary which will reduce noise level and increase gear life, and modifications concerning the sun gear. G.R.

A83-25947*# National Aeronautics and Space Administration. Lewis Research Center, Cleveland, Ohio.
FARFIELD INFLIGHT MEASUREMENTS OF HIGH-SPEED TURBOPROP NOISE
J. R. BALOMBIN and I. J. LOEFFLER (NASA, Lewis Research Center, Cleveland, OH) American Institute of Aeronautics and Astronautics, Aeroacoustics Conference, 8th, Atlanta, GA, Apr. 11-13, 1983, 18 p. refs
(AIAA PAPER 83-0745)

A flight program was carried out to determine the variation of noise level with distance from a model high-speed propeller. Noise measurements were obtained at different distances from a SR-3 propeller mounted on a JetStar aircraft, with the test instrumentation mounted on a Learjet flown in formation. The propeller was operated at 0.8 m flight Mach number, 1.12 helical tip Mach number and at 0.7 flight Mach number, 1.0 helical tip Mach number. The instantaneous pressure from individual blades was observed to rise faster at the 0.8 flight speed, than at the 0.7 M flight speed. The measured levels appeared to decrease in good agreement with a 6 dB/doubling of distance decay, over the measurement range of approximately 16 m to 100 m distance. Further extrapolation, to the distances represented by a community, would suggest that the propagated levels during cruise would not cause a serious community annoyance. (Author)

A83-25957*# National Aeronautics and Space Administration. Lewis Research Center, Cleveland, Ohio.
TONE GENERATION BY ROTOR-DOWNSTREAM STRUT INTERACTION
R. P. WOODWARD and J. R. BALOMBIN (NASA, Lewis Research Center, Cleveland, OH) American Institute of Aeronautics and Astronautics, Aeroacoustics Conference, 8th, Atlanta, GA, Apr. 11-13, 1983, 9 p. refs
(AIAA PAPER 83-0767)

A JT15D fan stage was acoustically tested in the NASA Lewis anechoic chamber as part of the joint Lewis-Langley Research Center investigation of flight simulation techniques and flight effects using the JT15D engine as a common test vehicle. Suspected rotor-downstream support strut interaction was confirmed through the use of simulated support struts which were tested at three axial rotor-strut spacings. Tests were also performed with the struts removed. Inlet boundary layer suction in conjunction with an inflow control device was also explored. The removal of the boundary layer reduced the fan fundamental tone levels suggesting that the mounting and mating of such a device to the nacelle requires careful attention. With the same inflow control device installed good acoustic agreement was shown between the engine on an outdoor test stand and the fan in the anechoic chamber. (Author)

A83-28006*# General Electric Co., Cincinnati, Ohio.
THE INFLUENCE OF INLET DESIGN ON THE AEROACOUSTIC PERFORMANCE OF A JT15D TURBOFAN ENGINE AS MEASURED IN THE NASA-AMES 40 X 80 FOOT WIND TUNNEL
R. G. HOLM (General Electric Co., Aircraft Engine Group, Cincinnati, OH), A. KARCHMER (NASA, Lewis Research Center, Cleveland, OH), C. HORNE, and A. ATENCIO (NASA, Ames Research Center, Moffett Field, CA) American Institute of Aeronautics and Astronautics, Aeroacoustics Conference, 8th, Atlanta, GA, Apr. 11-13, 1983, 58 p. refs
(Contract NAS2-8675)
(AIAA PAPER 83-0681)

The influence of inlet design on the aeroacoustic performance of a JT15D turbofan engine was investigated in the NASA-Ames 40 x 80 ft wind tunnel. Four inlet designs representative of those found in commercial service were evaluated at a forward velocity of 80 kn. The inlet designs considered were selected to evaluate the importance of circumferential static pressure distortion (SPD) for a diffusing sound suppressing inlet and throat Mach number (Mth) for a hardwall inlet on the acoustic characteristics of the JT15D engine. Several speed points were studied simulating the operating conditions spanning approach to take-off. Results demonstrated that the dependency of the forward radiated noise on inlet aerodynamic design parameters was significant (about 5 dB) for the range of SPD (0.1-3.0%) and Mth (0.3-0.6) tested. The performance of the bulk absorber acoustic treatment used in the diffusing sound suppressing inlet is also discussed. (Author)

A83-29024*# General Electric Co., Cincinnati, Ohio.
TURBINE BLADE NONLINEAR STRUCTURAL AND LIFE ANALYSIS
R. L. MCKNIGHT, J. H. LAFLEN (General Electric Co., Aircraft Engine Business Group, Cincinnati, OH), G. R. HALFORD, and A. KAUFMAN (NASA, Lewis Research Center, Structures and Mechanical Technologies Div., Cleveland, OH) Journal of Aircraft (ISSN 0021-8669), vol. 20, May 1983, p. 475-480. refs

Previously cited in issue 17, p. 2687, Accession no. A82-34981

A83-29737*# Pratt and Whitney Aircraft Group, East Hartford, Conn.
STRUCTURAL TAILORING OF ENGINE BLADES (STAEBL)
K. W. BROWN, T. K. PRATT (United Technologies Corp., Pratt and Whitney Aircraft Group, East Hartford, CT), and C. C. CHAMIS (NASA Lewis Research Center, Cleveland, OH) IN: Structures, Structural Dynamics and Materials Conference, 24th, Lake Tahoe, NV, May 2-4, 1983, Collection of Technical Papers. Part 1 . New York, American Institute of Aeronautics and Astronautics, 1983, p. 79-88. refs
(Contract NAS3-22525)
(AIAA 83-0828)

Mathematical optimization is applied to the design of gas turbine fan blades. The automated procedure replaces the current manual process which requires experience and intuition on the part of the designer to achieve successful blade designs. The optimization procedure that is developed utilizes the COPES/CONMIN optimization code. Approximate vibration and stress analyses are used for the optimization process. Analysis recalibrations are achieved through the application of more detailed, refined analysis. Optimizations of a hollow titanium fan blade with composite inlays and of a superhybrid composite blade are demonstrated. Author

A83-32787*# Rensselaer Polytechnic Inst., Troy, N. Y.
STRUCTURAL DYNAMICS STUDIES OF ROTATING BLADED-DISK ASSEMBLIES COUPLED WITH FLEXIBLE SHAFT MOTIONS
R. G. LOEWY (Rensselaer Polytechnic Institute, Troy, NY) and N. KHADER AIAA, ASME, ASCE, and AHS, Structures, Structural Dynamics and Materials Conference, Lake Tahoe, NV, May 2-4, 1983. 10 p. refs
(Contract NAG3-37)
(AIAA PAPER 83-0919)

In order to analyze the dynamic behavior of the first stage compressor/fan of the 'E3' turbofan engine, a classical structural dynamics approach is employed to couple the motions of a flexible bladed disk to a rotating flexible shaft. The analysis accounts for flexible disk displacements which are transverse to the plane of rotation, and radial as well as tangential, and also accounts for rigid disk translations along, and rotations about, axes normal to the undeformed shaft axes. In the case of a wide range of E3 engine shaft flexibilities and speeds, some of the one-diametral node frequencies are shown to be affected by shaft degrees of freedom whose stiffness values are in general range of design practice. Coriolis forces are also found to significantly affect natural frequencies where strong coupling between certain modes is present. O.C.

A83-32791*# Carnegie-Mellon Univ., Pittsburgh, Pa.
EFFECTS OF FRICTION DAMPERS ON AERODYNAMICALLY UNSTABLE ROTOR STAGES
J. H. GRIFFIN (Carnegie-Mellon University, Pittsburgh, PA) and A. SINHA AIAA, ASME, ASCE, and AHS, Structures, Structural Dynamics and Materials Conference, Lake Tahoe, NV, May 2-4, 1983. 12 p. refs
(Contract NAG3-231)
(AIAA PAPER 83-0848)

Attention is given to the physical concepts and mathematical techniques useful in the analysis of the stabilizing effect of friction on aerodynamically unstable rotor stages. Results are presented for three-, four-, and five-bladed disks. In the present multidegree-of-freedom model of an aerodynamically unstable rotor stage, a harmonic steady state solution due to the friction dampers may be either a stability limit, a stable cycle limit, or neither. A criterion is established in the form of an energy function which determines whether the solution is a stabilty limit. In the event that the initial displacement and velocity exeed those associated with the steady state solution corresponding to a stability limit, the reponse becomes unbounded. O.C.

A83-35806*# National Aeronautics and Space Administration. Lewis Research Center, Cleveland, Ohio.
NEW TRENDS IN COMBUSTION RESEARCH FOR GAS TURBINE ENGINES
E. J. MULARZ (NASA, Lewis Research Center, Combustion Fundamentals Section; U.S. Army, Propulsion Laboratory, Cleveland, OH) IN: International Symposium on Air Breathing Engines, 6th, Paris, France, June 6-10, 1983, Symposium Papers . New York, American Institute of Aeronautics and Astronautics, 1983, p. 37-44. Army-supported research. refs

Research on combustion is being conducted to provide improved analytical models of the complex flow and chemical reaction processes which occur in the combustor of gas turbine engines, in order to enable engine manufacturers to reduce the development time of these concepts. The elements of the combustion fundamentals program is briefly discussed with examples of research projects described more fully. Combustion research will continue to emphasize the development of analytical models and the support of these models with fundamental flow experiments to assess the models accuracy and shortcomings. Previously announced in STAR as N83-20947 Author

A83-35856*# Purdue Univ., Lafayette, Ind.
EFFECT OF HUMIDITY ON JET ENGINE AXIAL-FLOW COMPRESSOR PERFORMANCE
C. M. EHRESMAN, S. N. B. MURTHY, and T. TSUCHIYA (Purdue University, West Lafayette, IN) IN: International Symposium on Air Breathing Engines, 6th, Paris, France, June 6-10, 1983, Symposium Papers . New York, American Institute of Aeronautics and Astronautics, 1983, p. 479-486. refs
(Contract NAG3-62; NAG3-204; F33615-78-C-2401)

Two problems related to the ingestion of humid air into jet engine axial compressors have been studied: (1) the changes in the performance of the compressor in the absence of condensation and (2) the changes in the entry conditions to the compressor when condensation occurs. Regarding the first, the extent of changes are predicted and also measured in the case of a six-stage compressor operated with air-methane gas mixture utilizing the similarities in the thermodynamic properties between water vapor and methane. For the condensation process in an inlet, a model is described that takes into account the presence of micro particulates and the flow field changes in the vicinity of the inlet wall. Finally, the effects of humidity on engine performance are discussed in relation to engine trim and control schemes. Author

A83-35883*# Princeton Univ., N. J.
DESIGN OF DRY-FRICTION DAMPERS FOR TURBINE BLADES
W. ANCONA and E. H. DOWELL (Princeton University, Princeton, NJ) IN: International Symposium on Air Breathing Engines, 6th, Paris, France, June 6-10, 1983, Symposium Papers . New York, American Institute of Aeronautics and Astronautics, 1983, p. 708-722. refs
(Contract NAG3-221)

A study is conducted of turbine blade forced response, where the blade has been modeled as a cantilever beam with a generally dry friction damper attached, and where the minimization of blade root strain as the excitation frequency is varied over a given range is the criterion for the evaluation of the effectiveness of the dry friction damper. Attempts are made to determine the location of the damper configuration best satisfying the design criterion, together with the best damping force (assuming that the damper location has been fixed). Results suggest that there need not be an optimal value for the damping force, or an optimal location for the dry friction damper, although there is a range of values which should be avoided. O.C.

A83-36250*# General Motors Corp., Indianapolis, Ind.
ADVANCED PROPFAN ENGINE CHARACTERISTICS AND TECHNOLOGY NEEDS
R. D. ANDERSON, J. C. GILL, and A. S. NOVICK (General Motors Corp., Indianapolis, IN) AIAA, SAE, and ASME, Joint Propulsion Conference, 19th, Seattle, WA, June 27-29, 1983. 9 p.
(Contract NAS3-23046)
(AIAA PAPER 83-1155)

A comparative study is presented for two of the advanced gas turbine engine designs developed in the course of a proprietary research effort for the NASA Advanced Propfan Engine Technology research program. In these engines, a cycle pressure ratio of 32.5:1 and a 2500 F maximum turbine temperature provide fuel efficient operation in the 32,000-ft altitude, Mach 0.72 cruise speed regime stipulated. Both of the engine configurations incorporate three spools, of which the compressors are dual-spool and the power turbines are free. A major design challenge for axial compressors in the 10,000-shp class was the maintenance of adequate blade heights in the later stages. O.C.

A83-36252*# General Electric Co., Cincinnati, Ohio.
THE AERODYNAMIC DESIGN AND PERFORMANCE OF THE GENERAL ELECTRIC/NASA EEE FAN
T. J. SULLIVAN (General Electric Co., Cincinnati, OH) and R. D. HAGER (NASA, Lewis Research Center, Cleveland, OH) AIAA, SAE, and ASME, Joint Propulsion Conference, 19th, Seattle, WA, June 27-29, 1983. 11 p. refs
(AIAA PAPER 83-1160)

The aerodynamic design and test results of the fan and quarter-stage component for the GE/NASA Energy Efficient Engine (EEE) are presented. The fan is a high bypass ratio, single-stage design having 32 part-span shrouded rotor blades, coupled with a unique quarter-stage arrangement that provides additional core-stream pressure ratio and particle separation. The fan produces a bypass pressure ratio of 1.65 at the exit of the low aspect ratio vane/frame and a core-stream pressure ratio of 1.67 at the entrance to the core frame struts. The full-scale fan vehicle was instrumented, assembled and tested as a component in November 1981. Performance mapping was conducted over a range of speeds and bypass ratios using individually-controlled bypass and core-stream discharge valves. The fan bypass and core-stream test data showed excellent results, with the fan exceeding all performance goals at the important engine operating conditions. Author

A83-36263*# National Aeronautics and Space Administration. Lewis Research Center, Cleveland, Ohio.
EFFECTS OF INTERSTAGE DIFFUSER FLOW DISTORTION ON THE PERFORMANCE OF A 15.41-CENTIMETER TIP DIAMETER AXIAL POWER TURBINE
K. L. MCLALLIN, M. G. KOFSKEY (NASA, Lewis Research Center, Cleveland, OH), and K. C. CIVINSKAS (U.S. Army, Propulsion Laboratory, Cleveland, OH) AIAA, SAE, and ASME, Joint Propulsion Conference, 19th, Seattle, WA, June 27-29, 1983. 23 p. refs
(Contract DE-AI01-77CS-51040)
(AIAA PAPER 83-1179)

The performance of a variable-area stator, axial flow power turbine was determined in a cold-air component research rig for two inlet duct configurations. The two ducts were an interstage diffuser duct and an accelerated-flow inlet duct which produced stator inlet boundary layer flow blockages of 11 percent and 3 percent, respectively. Turbine blade total efficiency at design point was measured to be 5.3 percent greater with the accelerated-flow inlet duct installed due to the reduction in inlet blockage. Blade component measurements show that of this performance improvement, 35 percent occurred in the stator and 65 percent occurred in the rotor. Analysis of inlet duct internal flow using an Axisymmetric Diffuser Duct Code (ADD Code) were in substantial agreement with the test data. Author

A83-36314*# United Technologies Corp., East Hartford, Conn.
IMPORTANCE OF INLET BOUNDARY CONDITIONS FOR NUMERICAL SIMULATION OF COMBUSTOR FLOWS
G. J. STURGESS, S. A. SYED, and K. R. MCMANUS (United Technologies Corp., Commercial Engineering Div., East Hartford, CT) AIAA, SAE, and ASME, Joint Propulsion Conference, 19th, Seattle, WA, June 27-29, 1983. 12 p. refs
(Contract NAS3-23524)
(AIAA PAPER 83-1263)

Fluid dynamic computer codes for the mathematical simulation of problems in gas turbine engine combustion systems are required as design and diagnostic tools. To eventually achieve a performance standard with these codes of more than qualitative accuracy it is desirable to use benchmark experiments for validation studies. Typical of the fluid dynamic computer codes being developed for combustor simulations is the TEACH (Teaching Elliptic Axisymmetric Characteristics Heuristically) solution procedure. It is difficult to find suitable experiments which satisfy the present definition of benchmark quality. For the majority of the available experiments there is a lack of information concerning the boundary conditions. A standard TEACH-type numerical technique is applied to a number of test-case experiments. It is found that numerical simulations of gas turbine combustor-relevant flows can be sensitive to the plane at which the calculations start and the spatial distributions of inlet quantities for swirling flows. G.R.

A83-36316*# Detroit Diesel Allison, Indianapolis, Ind.
APPLICATION OF 3D AERODYNAMIC/COMBUSTION MODEL TO COMBUSTOR PRIMARY ZONE STUDY
R. E. SULLIVAN, R. SUTTON, G. MILES, E. YOUNG (General Motors Corp., Detroit Diesel Allison Div., Indianapolis, IN), and D. BRIEHL (NASA, Lewis Research Center, Cleveland, OH) AIAA, SAE, and ASME, Joint Propulsion Conference, 19th, Seattle, WA, June 27-29, 1983. 9 p.
(Contract NAS3-22762)
(AIAA PAPER 83-1265)

A description is provided of the three-dimensional elliptic code for reacting flows used in the combustor design process during the program 'Small Gas Turbine Combustor Primary Zone Study' carried out by a U.S. company. The code, designated MARC-I (multidimensional aerodynamic recirculating combustion-Version I) is an adaptation of the model described by Mongia et al. (1979). The program has the objective to advance the technology of the small reverse-flow annular combustor design through an understanding of primary zone performance factors. The MARC-I code was used for performance predictions of both original designs and later modifications. A test program consisting of both primary zone sampling and overall combustor performance measurements was carried out. It was, therefore, possible to compare the analytical predictions with actual test measurements. G.R.

A83-36323*# Pratt and Whitney Aircraft Group, East Hartford, Conn.
EJECTOR NOZZLE TEST RESULTS AT SIMULATED FLIGHT CONDITIONS FOR AN ADVANCED SUPERSONIC TRANSPORT PROPULSION SYSTEM
D. P. NELSON (United Technologies Corp., Pratt and Whitney Group, East Hartford, CT) and D. L. BRESNAHAN (NASA, Lewis Research Center, Cleveland, OH) AIAA, SAE, and ASME, Joint Propulsion Conference, 19th, Seattle, WA, June 27-29, 1983. 11 p. refs
(AIAA PAPER 83-1287)

Results are presented of wind tunnel tests conducted to verify the performance improvements of a refined ejector nozzle design for advanced supersonic transport propulsion systems. The analysis of results obtained at simulated engine operating conditions is emphasized. Tests were conducted with models of approximately 1/10th scale which were configured to simulate nozzle operation at takeoff, subsonic cruise, transonic cruise, and supersonic cruise. Transonic cruise operation was not a consideration during the nozzle design phase, although an evaluation at this condition was later conducted. Test results, characterized by thrust and flow

coefficients, are given for a range of nozzle pressure ratios, emphasizing the thrust performance at the engine operating conditions predicted for each flight Mach number. The results indicate that nozzle performance goals were met or closely approximated at takeoff and supersonic cruise, while subsonic cruise performance was within 2.3 percent of the goal with further improvement possible. N.B.

A83-36340*# Oklahoma State Univ., Stillwater.
THE PERFORMANCE OF AN ANNULAR VANE SWIRLER
D. G. LILLEY (Oklahoma State University, Stillwater, OK) and G. F. SANDER AIAA, SAE, and ASME, Joint Propulsion Conference, 19th, Seattle, WA, June 27-29, 1983. 14 p. USAF-supported research. refs
(Contract NAS3-74)
(AIAA PAPER 83-1326)

In connection with the desirability of optimizing the design of a gas turbine combustion chamber, there exists a need for a more complete understanding of the fluid dynamics of the flow in such chambers. In order to satisfy this need, experimental and theoretical research is being conducted with the objective to study two-dimensional axisymmetric geometries under low speed, nonreacting, turbulent, swirling flow conditions. The flow enters the test section and proceeds into a larger chamber. Inlet swirl vanes are adjustable to a variety of vane angles. The present investigation concentrates on the time-mean flow characteristics which are generated by the upstream annular swirler. The investigation makes use of a five-hole pitot probe technique. A theoretical analysis of swirl numbers associated with several idealized exit velocity profiles is included, and values of the ratio of maximum swirl velocity to maximum axial velocity at different swirl strengths are given for each case. G.R.

A83-36393*# Tuskegee Inst., Ala.
A COMPREHENSIVE METHOD FOR PRELIMINARY DESIGN OPTIMIZATION OF AXIAL GAS TURBINE STAGES. II - CODE VERIFICATION
R. M. JENKINS (Tuskegee Institute, Tuskegee, AL) AIAA, SAE, and ASME, Joint Propulsion Conference, 19th, Seattle, WA, June 27-29, 1983. 10 p. refs
(Contract NSG-3295)
(AIAA PAPER 83-1403)

The present effort represents an extension of previous work wherein a calculation model for performing rapid pitchline optimization of axial gas turbine geometry, including blade profiles, is developed. The model requires no specification of geometric constraints. Output includes aerodynamic performance (adiabatic efficiency), hub-tip flow-path geometry, blade chords, and estimates of blade shape. Presented herein is a verification of the aerodynamic performance portion of the model, whereby detailed turbine test-rig data, including rig geometry, is input to the model to determine whether tested performance can be predicted. An array of seven (7) NASA single-stage axial gas turbine configurations is investigated, ranging in size from 0.6 kg/s to 63.8 kg/s mass flow and in specific work output from 153 J/g to 558 J/g at design (hot) conditions; stage loading factor ranges from 1.15 to 4.66. Author

A83-37092* Notre Dame Univ., Ind.
NONLINEAR MULTIVARIABLE DESIGN BY TOTAL SYNTHESIS
M. K. SAIN (Notre Dame, University, Notre Dame, IN) and J. L. PECZKOWSKI (Bendix Corp., Energy Controls Div., South Bend, IN) IN: American Control Conference, 1st, Arlington, VA, June 14-16, 1982, Proceedings. Volume 1 . New York, Institute of Electrical and Electronics Engineers, 1982, p. 252-260. refs
(Contract NSG-3048)

The Nominal Design Problem (NDP) is extended to nonlinear cases, and a new case study of robust feedback synthesis for gas turbine control design is presented. The discussion of NDP extends and builds on earlier Total Synthesis Problem theory and ideas. Some mathematical preliminaries are given in which a bijection from a set S onto a set T is considered, with T admitting the structure of an F-vector space. NDP is then discussed for a nonlinear plant, and nonlinear nominal design is defined and characterized. The design of local controllers for a turbojet and the scheduling of these controls into a global control are addressed. C.D.

A83-38001* Avco Lycoming Div., Stratford, Conn.
EXPERIMENTAL EVALUATION OF INLET TURBULENCE, WALL BOUNDARY LAYER, SURFACE FINISH, AND FILLET RADIUS ON SMALL AXIAL TURBINE STATE PERFORMANCE
A. A. KOZAK, W. D. BROCKETT (Avco Corp., Avco Lycoming Div., Stratford, CT), and J. E. HAAS (U.S. Army, Research and Technology Laboratories, Cleveland, OH) Society of Automotive Engineers, Aerospace Congress and Exposition, Anaheim, CA, Oct. 25-28, 1982. 11 p. refs
(Contract NAS3-22109)
(SAE PAPER 821475)

The results of an experimental investigation are presented which establish the effects of surface finish, fillet radius, inlet boundary layer thickness, and free-stream inlet turbulence level on the aerodynamic performance of a small axial flow turbine stator. The principal objective was to help understand why large turbine efficiency is not maintained when a large turbine is scaled to a smaller size and to provide the turbine designer with the performance compromises expected for a small scale design. A comprehensive test matrix was used to gain an understanding of the effects of each variable over the full range of all the other variables. Author

A83-38002*# Pratt and Whitney Aircraft Group, East Hartford, Conn.
DEVELOPMENT AND OPERATING CHARACTERISTICS OF AN ADVANCED TWO-STAGE COMBUSTOR
W. GREENE, S. TANRIKUT (United Technologies Corp., Pratt and Whitney Group, East Hartford, CT), and D. E. SOKOLOWSKI (NASA, Lewis Research Center, Cleveland, OH; United Technologies Corp., Pratt and Whitney Group, East Hartford, CT) Journal of Energy (ISSN 0146-0412), vol. 7, July-Aug. 1983, p. 354-360. refs

Previously cited in issue 06, p. 813, Accession no. A82-17833

A83-39993*# National Aeronautics and Space Administration. Lewis Research Center, Cleveland, Ohio.
THE FEASIBILITY OF WATER INJECTION INTO THE TURBINE COOLANT TO PERMIT GAS TURBINE CONTINGENCY POWER FOR HELICOPTER APPLICATION
G. J. VAN FOSSEN (NASA, Lewis Research Center, Cleveland, OH) ASME, Transactions, Journal of Engineering for Power (ISSN 0022-0825), vol. 105, July 1983, p. 635-642. refs
(ASME PAPER 83-GT-66)

It is pointed out that in certain emergency situations it may be desirable to obtain power from a helicopter engine at levels greater than the maximum rating. Yost (1976) has reported studies concerning methods of power augmentation in the one engine inoperative (OEI) case. It was found that a combination of water/alcohol injection into the inlet and overtemperature/overspeed could provide adequate emergency power. The present investigation is concerned with the results of a feasibility study which analytically investigated the maximum possible level of augmentation with constant gas generator turbine stress rupture life as a constraint. In the proposed scheme, the increased engine output is obtained by turbine overtemperature, however, the temperature of the compressor bleed air used for hot section cooling is lowered by injecting and evaporating water. G.R.

A83-40864*# General Electric Co., Cincinnati, Ohio.
BLADE LOSS TRANSIENT DYNAMIC ANALYSIS OF TURBOMACHINERY
M. J. STALLONE, V. GALLARDO, A. F. STORACE, L. J. BACH, G. BLACK, and E. F. GAFFNEY (General Electric Co, Aircraft Engine Business Group, Cincinnati, OH) AIAA Journal (ISSN 0001-1452), vol. 21, Aug. 1983, p. 1134-1138. refs
(Contract NAS3-22053)
Previously cited in issue 17, p. 2687, Accession no. A82-34982

A83-41040*# National Aeronautics and Space Administration. Lewis Research Center, Cleveland, Ohio.
JT9D PERFORMANCE DETERIORATION RESULTS FROM A SIMULATED AERODYNAMIC LOAD TEST
E. G. STAKOLICH (NASA, Lewis Research Center, Launch Vehicles Div., Cleveland, OH) and W. J. STROMBERG (United Technologies Corp., Pratt and Whitney Aircraft, East Hartford, CT) Journal of Aircraft (ISSN 0021-8669), vol. 20, Aug. 1983, p. 650-658.
Previously cited in issue 19, p. 3268, Accession no. A81-40963

A83-45515*# National Aeronautics and Space Administration. Lewis Research Center, Cleveland, Ohio.
DYNAMIC DISTORTION IN A SHORT S-SHAPED SUBSONIC DIFFUSER WITH FLOW SEPARATION
R. STUMPF, H. E. NEUMANN, and C. C. GIAMATI (NASA, Lewis Research Center, Cleveland, OH) AIAA, SAE, and ASME, Joint Propulsion Conference, 19th, Seattle, WA, June 27-29, 1983. 19 p. refs
(AIAA PAPER 83-1412)
An experimental investigation of the time varying distortion at the diffuser exit of a subsonic HiMAT forebody and inlet was conducted at Mach 0.9 in the Lewis 8 by 6 foot Supersonic Wind Tunnel. A transitory separation was detected within the subsonic diffuser. Vortex generators were installed to eliminate the flow separation. Results from a study of the instantaneous pressure variations at the diffuser exit are presented. The time unsteady total pressures at the diffuser exit are computer interpolated and presented in the form of a movie showing the transitory separation. Limited data showing the instantaneous distortion levels are also presented. Previously announced in STAR as N83-26838 Author

A83-47964*# United Technologies Research Center, East Hartford, Conn.
A VORTEX VENTURI FOR REVERTING ANTIMISTING FUEL PROPERTIES
E. J. SZETELA and J. TEVELDE (United Technologies Research Center, East Hartford, CT) American Society of Mechanical Engineers, International Gas Turbine Conference and Exhibit, 28th, Phoenix, AZ, Mar. 27-31, 1983. 7 p.
(Contract NAS3-22045)
(ASME PAPER 83-GT-137)
The level of degradation of antimisting fuel polymers such as FM-9 which must be accomplished in order to use antimisting fuel in existing engines may require the use of cavitation. The hydrodynamic shear produced by the collapse of vapor bubbles is capable of producing more splitting of polymeric molecules than mechanically-induced shear. A program has been carried out to investigate the possibility of using a cavitating venturi with rotating flow as a fuel reverter. This investigation included the effects of a swirl-inducing twisted tape upstream of the throat, inlet pressure, recovery pressure ratio and a pintle for varying throat area. A correlation of the data was produced, system concepts for using the vortex venturi were investigated and problem areas were delineated. Author

A83-47970*# Lehigh Univ., Bethlehem, Pa.
ANALYSIS OF AN AXIAL COMPRESSOR BLADE VIBRATION BASED ON WAVE REFLECTION THEORY
J. A. OWCZAREK (Lehigh University, Bethlehem, PA) American Society of Mechanical Engineers, International Gas Turbine Conference and Exhibit, 28th, Phoenix, AZ, Mar. 27-31, 1983. 8 p.
(Contract NAG3-135)
(ASME PAPER 83-GT-151)
The paper describes application of the theory of wave reflection in turbomachines to rotor blade vibrations measured in an axial compressor stage. The blade vibrations analyzed could not be predicted using various flutter prediction techniques. The wave reflection theory, first advanced in 1966, is expanded, and more general equations for the rotor blade excitation frequencies are derived. The results of the analysis indicate that all examined rotor blade vibrations can be explained by forced excitations caused by reflecting waves (pressure pulses). Wave reflections between the rotor blades and both the upstream and downstream stator vanes had to be considered. Author

A83-48000*# General Electric Co., Lynn, Mass.
STATUS REPORT - DARPA/NASA CONVERTIBLE TURBOFAN/TURBOSHAFT ENGINE PROGRAM
A. I. BELLIN and A. BROOKS (General Electric Co., Aircraft Engine Business Group, Lynn, MA) American Society of Mechanical Engineers, International Gas Turbine Conference and Exhibit, 28th, Phoenix, AZ, Mar. 27-31, 1983. 6 p.
(Contract NAS3-22752)
(ASME PAPER 83-GT-196)
A development status report is presented for the NASA/Defense Advanced Research Projects Agency convertible turbofan-turboshaft engine, which can power a high speed rotorcraft in vertical flight, as well as in horizontal flight up to speeds of Mach 0.85. The basis for this development program is a modified TF34-GE-400 engine. Program objectives include both the demonstration of dual output mode (jet thrust and shaft horsepower) capability and the development of a control system which will operate the engine in either mode and convert operation between the modes. O.C.

A83-48331*# National Aeronautics and Space Administration. Lewis Research Center, Cleveland, Ohio.
DESIGN CONCEPTS FOR LOW COST COMPOSITE ENGINE FRAMES
C. C. CHAMIS (NASA, Lewis Research Center, Cleveland, OH) American Institute of Aeronautics and Astronautics, Aircraft Design, Systems and Technology Meeting, Fort Worth, TX, Oct. 17-19, 1983. 16 p.
(AIAA PAPER 83-2445)
Design concepts for low-cost, lightweight composite engine frames were applied to the design requirements for the frame of commercial, high-bypass turbine engines. The concepts consist of generic-type components and subcomponents that could be adapted for use in different locations in the engine and to different engine sizes. A variety of materials and manufacturing methods were assessed with a goal of having the lowest number of parts possible at the lowest possible cost. The evaluation of the design concepts resulted in the identification of a hybrid composite frame which would weigh about 70 percent of the state-of-the-art metal frame and cost would be about 60 percent. Author

A83-49581*# TRW, Inc., Redondo Beach, Calif.
THE DEVELOPMENT OF A GENERALIZED ADVANCED PROPELLER ANALYSIS SYSTEM
L. GLATT, J. KOSMATKA, R. SWIGART, E. WONG, D. CRAWFORD (TRW Inc., Space and Technology Group, Redondo Beach, CA), and H. NEUMANN (NASA, Lewis Research Center, Cleveland, OH) American Institute of Aeronautics and Astronautics, Aircraft Design, Systems and Technology Meeting, Fort Worth, TX, Oct. 17-19, 1983. 20 p. refs
(Contract NAS3-22251)
(AIAA PAPER 83-2466)

A Generalized Advanced Propeller Analysis System (GAPAS) is being developed to provide both an optimized design and a performance evaluation capability. The technology areas incorporated in GAPAS include propeller aerodynamic performance, airfoil loading, acoustics, structural analysis and aeroelasticity. The propeller analyses include the most advanced, fully-developed technologies in a modular but unified system. The program will treat multi-bladed propellers having straight or swept blades operating on aircraft at speeds to Mach 0.8 and altitudes to 40,000 feet. The purpose of this paper is twofold. First, it will introduce the GAPAS program to the general industry; and second, since the GAPAS program will be made available for general applications, it is also intended to be a status report on the development stage of the program. Author

N83-10044*# Pratt and Whitney Aircraft Group, East Hartford, Conn. Commercial Products Div.
DEVELOPMENT OF ADVANCED HIGH-TEMPERATURE HEAT FLUX SENSORS
W. H. ATKINSON and R. R. STRANGE Sep. 1982 214 p refs
(Contract NAS3-22133)
(NASA-CR-165618; NAS 1.26:165618; PWA-5723-27) Avail: NTIS HC A10/MF A01 CSCL 21E

Various configurations of high temperature, heat flux sensors were studied to determine their suitability for use in experimental combustor liners of advanced aircraft gas turbine engines. It was determined that embedded thermocouple sensors, laminated sensors, and Gardon gauge sensors, were the most viable candidates. Sensors of all three types were fabricated, calibrated, and endurance tested. All three types of sensors met the fabricability survivability, and accuracy requirements established for their application. Author

N83-10045*# National Aeronautics and Space Administration. Lewis Research Center, Cleveland, Ohio.
FURTHER INDUSTRIAL TESTS OF CERAMIC THERMAL BARRIER COATINGS
C. H. LIEBERT and S. R. LEVINE Sep. 1982 10 p refs
(NASA-TP-2057; E-1184; NAS 1.60:2057) Avail: NTIS HC A02/MF A01 CSCL 21E

The NASA Lewis Research Center made technical assistance arrangements (contracts) with several commercial organizations under which Lewis designed plasma-sprayed thermal-barrier coatings (TBC) for their products. Lewis was then furnished with the test conditions and evaluations of coating usefulness. The coating systems were developed and sprayed at Lewis. All of the systems incorporated a two-layer, ceramic-bond coating concept. Coating thickness and chemical composition were varied to fit three applications: the leading edges of first-stage turbine vanes for an advanced gas turbine engine; the flame impingement surfaces of a combustor transition section; and diesel engine valves and head surfaces. The TBC incorporated yytria-stabilized zirconia, which lowered metal temperatures, protected metal parts, and increased metal part life. In some cases metal burning, melting, and warping were eliminated. Additional benefits were realized from these endeavors: hands-on experience with thermal-barrier coatings was provided to industry; the success of these endeavors encourages these and other organizations to accelerate the implementation of TBC technology. Author

N83-11125*# National Aeronautics and Space Administration. Lewis Research Center, Cleveland, Ohio.
ANALYTICAL AND EXPERIMENTAL INVESTIGATION OF STATOR ENDWALL CONTOURING IN A SMALL AXIAL-FLOW TURBINE. 1: STATOR PERFORMANCE
J. E. HAAS Oct. 1982 26 p refs
(NASA-TP-2023; E-1180; NAS 1.60:2023; AVRADCOM-TR-82-C-4) Avail: NTIS HC A03/MF A01 CSCL 21E

Three stator configurations were studied to determine the effect of stator outer endwall contouring on stator performance. One configuration was a cylindrical stator design. One contoured stator configuration had an S-shaped outer endwall, the other had a conical-convergent outer endwall. The experimental investigation consisted of annular surveys of stator exit total pressure and flow angle for each stator configuration over a range of stator pressure ratio. Radial variations in stator loss and aftermixed flow conditions were obtained when these data were compared with the analytical results to assess the validity of the analysis, good agreement was found. A.R.H.

N83-11126*# National Aeronautics and Space Administration. Lewis Research Center, Cleveland, Ohio.
FILM THICKNESS MEASUREMENT FOR SPIRAL GROOVE AND RAYLEIGH STEP LIFT PAD SELF-ACTING FACE SEALS
E. DIRUSSO Oct. 1982 21 p refs
(NASA-TP-2058; E-1169; NAS 1.60:2058) Avail: NTIS HC A02/MF A01 CSCL 21E

One Rayleigh step lift pad and three spiral groove self-acting face seal configurations were tested to measure film thickness and frictional torque as a function of shaft speed. The seals were tested at a constant face load of 73 N (16.4 lb) with ambient air at room temperature and atmospheric pressure as the fluid medium. The test speed range was from 7000 to 17,000 rpm. The measured film thickness was compared with theoretical data from mathematical models. The mathematical models overpredicted the measured film thickness at the lower speeds of the test speed range and underpredicted the measured film thickness at the higher speeds of the test speed range. Author

N83-11127*# General Electric Co., Cincinnati, Ohio. Aircraft Engine Business Group.
ANALYSIS, DESIGN, FABRICATION AND TESTING OF AN OPTICAL TIP CLEARANCE SENSOR Final Report, Jun. 1979 - Jan. 1981
G. L. POPPEL, D. T. F. MARPLE, and J. D. KINGSLEY May 1981 84 p refs
(Contract NAS3-21843)
(NASA-CR-165265; NAS 1.26:165265; R81AEG215) Avail: NTIS HC A05/MF A01 CSCL 21E

Analyses and the design, fabrication, and testing of an optical tip clearance sensor with intended application in aircraft propulsion control systems are reported. The design of a sensor test rig, evaluation of optical sensor components at elevated temperatures, sensor design principles, sensor test results at room temperature, and estimations of sensor accuracy at temperatures of an aircraft engine environment are discussed. Room temperature testing indicated possible measurement accuracies of less than 12.7 microns (0.5 mils). Ways to improve performance at engine operating temperatures are recommended. The potential of this tip clearance sensor is assessed. Author

N83-11128*# National Aeronautics and Space Administration. Lewis Research Center, Cleveland, Ohio.
ARMY/NASA SMALL TURBOSHAFT ENGINE DIGITAL CONTROLS RESEARCH PROGRAM
J. F. SELLERS and A. N. BAEZ (AVRADCOM Research and Technology Labs., Cleveland, Ohio) 1981 16 p refs Prepared for presentation at the Rotary Wing Propulsion System Specialist Meeting, Williamsburg, Va., 16-18 Nov. 1982; sponsored by the Am. Helicopter Soc.
(NASA-TM-82979; E-1408; NAS 1.15:82979; AVRADCOM-TR-82-C-14; AHS-RWP-7) Avail: NTIS HC A02/MF A01 CSCL 21E

The emphasis of a program to conduct digital controls research for small turboshaft engines is on engine test evaluation of advanced control logic using a flexible microprocessor based digital control system designed specifically for research on advanced control logic. Control software is stored in programmable memory. New control algorithms may be stored in a floppy disk and loaded directly into memory. This feature facilitates comparative evaluation of different advanced control modes. The central processor in the digital control is an Intel 8086 16 bit microprocessor. Control software is programmed in assembly language. Software checkout is accomplished prior to engine test by connecting the digital control to a real time hybrid computer simulation of the engine. The engine currently installed in the facility has a hydromechanical control modified to allow electrohydraulic fuel metering and VG actuation by the digital control. Simulation results are presented which show that the modern control reduces the transient rotor speed droop caused by unanticipated load changes such as cyclic pitch or wind gust transients. A.R.H.

N83-11129*# National Aeronautics and Space Administration. Lewis Research Center, Cleveland, Ohio.
TECHNOLOGY AND BENEFITS OF AIRCRAFT COUNTER ROTATION PROPELLERS
W. C. STRACK, G. KNIP, A. L. WEISBRICH (Hamilton Standard, Windsor Locks, Conn.), J. GODSTON (Pratt and Whitney Aircraft, East Hartford, Conn.), and E. BRADLEY (Lockheed-Georgia Co., Marietta, Ga.) 1981 35 p refs
(NASA-TM-82983; E-1414; NAS 1.15:82983) Avail: NTIS HC A03/MF A01 CSCL 01C

Results are reported of a NASA sponsored analytical investigation into the merits of advanced counter rotation propellers for Mach 0.80 commercial transport application. Propeller and gearbox performance, acoustics, vibration characteristics, weight, cost and maintenance requirements for a variety of design parameters and special features were considered. Fuel savings in the neighborhood of 8 percent relative to single rotation configurations are feasible through swirl recovery and lighter gearboxes. This is the net gain which includes a 5 percent acoustic treatment weight penalty to offset the broader frequency spectrum noise produced by counter rotation blading. Author

N83-11130*# National Aeronautics and Space Administration. Lewis Research Center, Cleveland, Ohio.
EXPERIMENTAL PROGRAM FOR THE EVALUATION OF TURBOFAN/TURBOSHAFT C CONVERSION TECHNOLOGY
J. G. MCARDLE and L. M. WENZEL 1981 25 p refs Prepared for presentation at the Rotary Wing Propulsion System Specialist Meeting, Williamsburg, Va., 16-18 Nov. 1982; sponsored by Am. Helicopter Soc.
(NASA-TM-82988; E-1420; NAS 1.15:82988; AHS-RWP-19) Avail: NTIS HC A02/MF A01 CSCL 21E

A TF34 turbofan engine is being modified to produce shaft power from an output coupling on the fan disk when variable inlet fuide vanes are closed to reduce fan airflow. The engine, called a convertible engine, could be used on advanced rotorcraft such as X-wing, ABC (Advanced Blade Concept), and Folding Tilt Rotor, and on V/STOL craft in which two engines are cross-coupled. The engine will be tested on an outdoor static test stand at NASA Lewis Research Center. Steady-state tests will be made to measure performance in turbofan, turboshaft, and combined power output modes. Transient tests will be made to determine the response to the engine and a new digital engine control system for several types of rapid changes in thrust and shaft loads. The paper describes the engine modifications, the test facility equipment, proposed testing techniques for several types of tests, and typical test results predicted from engine performance computer programs. Author

N83-11138# Advisory Group for Aerospace Research and Development, Neuilly-Sur-Seine (France).
FLUID DYNAMICS PANEL SYMPOSIUM ON AERODYNAMICS OF POWER PLANT INSTALLATION Technical Evaluation Report
W. P. HENDERSON Jun. 1982 15 p Symp. held at Toulouse, 11-14 May 1981 Prepared in cooperation with NASA. Lewis Research Center
(AGARD-AR-173; ISBN-92-835-1436-2; AD-A119357) Avail: NTIS HC A02/MF A01

Powerplant installations involve complex flows, strongly influenced by viscous effects and often with important aerodynamic interactions between the airframe and propulsion system. The introduction of vehicle propulsion concepts, and points of emphasis in aircraft and missile design requirements, provide an expanding range of aerodynamic problems which cal for both experimental and theoretical study. Aerodynamic problems in powerplant installation are surveyed and work which has improved basic understanding or has enhanced prediction and design methods in this field is reviewed. Powerplant installation effects for both combat and transport aircraft are emphasized. S.L.

N83-12087*# National Aeronautics and Space Administration. Lewis Research Center, Cleveland, Ohio.
A REMOTE AUGMENTOR LIFT SYSTEM WITH A TURBINE BYPASS ENGINE
L. H. FISHBACH and L. C. FRANCISCUS 1982 12 p refs Presented at the 13th Cong. of the Intern. Council of Aeronautical Sci. and Aircraft Systems and Technol. Meeting, Seattle, 22-27 Aug. 1982
(NASA-TM-82932; E-1330; NAS 1.15:82932) Avail: NTIS HC A02/MF A01 CSCL 21E

Two supersonic vertical takeoff or landing (VTOL) aircraft engine types, a conventional medium bypass ratio turbofan, and a turbine bypass turbojet were studied. The aircraft assumed was a clipped delta wing with canard configuration. A VTOL deck launched intercept, DLI, mission with Mach 1.6 dash and cruise segments was used as the design mission. Several alternate missions requiring extended subsonic capabilities were analyzed. Comparisons were made between the turbofan (TF) and the turbine bypass turbojet (TBE) engines in airplane types using a Remote Augmented Lift Systems, RALS and a Lift plus Lift Cruise system (L+LC). The figure of merit was takeoff gross weight for the VTOL DLI mission. The results of the study show that the turbine bypass turbojet and the conventional turbofan are competitive engines for both type of aircraft in terms of takeoff gross weight and range. However, the turbine bypass turbojet would be a simpler engine and may result in more attractive life cycle costs and reduced maintenance. The RALS and L+LC airplane types with either TBE or TF engines have approximately the same aircraft takeoff gross weight. Author

N83-12088*# AiResearch Mfg. Co., Phoenix, Ariz.
ADVANCED GAS TURBINE (AGT) POWERTRAIN SYSTEM DEVELOPMENT PROGRAM Monthly Technical Progress Report, 1 Aug. - 31 Aug. 1980
R. A. RACKLEY 26 Sep. 1980 124 p
(Contract DEN3-167)
(NASA-CR-169475; NAS 1.26:169475; AMC-31-3480(11); MTPR-11) Avail: NTIS HC A06/MF A01 CSCL 21E

Gas turbine automobile powertrain research is reported. The compressor, turbine, combustor, regenerator, gearbox, ceramic components/subsystems, bearings, and controls are discussed. N.W.

N83-12089*# Detroit Diesel Allison, Indianapolis, Ind.
COMPONENTS FOR DIGITALLY CONTROLLED AIRCRAFT ENGINES
J. D. MEADOR Aug. 1981 107 p refs
(Contract NAS3-22046)
(NASA-CR-165296; NAS 1.26:165296; EDR-10696) Avail: NTIS HC A06/MF A01 CSCL 21E

Control system components suitable for use in digital electronic control systems are defined. Compressor geometry actuation concepts and fuel handling system concepts suitable for use in large high performance turbofan/turbojet engines are included. Eight conceptual system designs were formulated for the actuation of the compressor geometry. Six conceptual system designs were formulated for the engine fuel handling system. Assessment criteria and weighting factors were established and trade studies performed on their candidate systems to establish the relative merits of the various concepts. Fuel pumping and metering systems for small turboshaft engines were also studied. Seven conceptual designs were formulated, and trade studies performed. A simplified bypassing fuel metering scheme was selected and a preliminary design defined. S.L.

N83-12090*# National Aeronautics and Space Administration. Lewis Research Center, Cleveland, Ohio.
ADVANCED TECHNOLOGIES FOR TURBOMACHINERY SYSTEMS: AN OVERVIEW
M. J. HARTMANN Aug. 1982 78 p refs Presented at the 11th Ann. Turbomachinery Symp., Houston, Tex., 14-16 Dec. 1982
(NASA-TM-82949; E-1302; NAS 1.15:82949) Avail: NTIS HC A05/MF A01 CSCL 21E

Turbomachinery system components and associated technologies are discussed. Specific technologies reviewed include the compressor, turbine, internal flow analysis methods, combustion, fuels, materials, structures, bearings, seals, and lubrication, dynamics and controls, and instrumentation. Analytical procedures as a path to improved performance are discussed. The strong interaction between the various technologies if turbomachinery performance gains are to be realized is reflected. Author

N83-12091*# National Aeronautics and Space Administration. Lewis Research Center, Cleveland, Ohio.
ROTORCRAFT CONVERTIBLE ENGINES FOR THE 1980S
J. D. EISENBERG 1982 28 p refs Presented at the Rotary Wing Propulsion System Specialist Meeting, Williamsburg, Va., 16-18 Nov. 1982
(NASA-TM-83008; E-1443; NAS 1.15:83003) Avail: NTIS HC A03/MF A01 CSCL 21E

Two rotorcraft studies were executed. The goal was to identify attractive techniques for implementing convertible powerplants for the ABC, Folded Tilt Rotor, and X-wing type high speed, high-L/D rotorcraft; to determine the DOC and fuel savings benefits achieved thereby; and to define research required to bring these powerplants into existence by the 1990's. These studies are reviewed herein and the different methods of approach are pointed out as well as the key findings. Fan shaft engines using variable inlet guide vanes or torque converters, and turboprop powerplants appear attractive. Savings in DOC and fuel consumption of over 15 percent are predicted in some cases as a result of convertible engine use rather than using separate engines for the thrust and the shaft functions. Areas of required research are fan performance (including noise), integrated engine/rotorcraft control, torque converters, turbine design, airflow for rotorcraft torque control, bleed for lift flow, and transmissions and clutches. Author

N83-12092*# National Aeronautics and Space Administration. Lewis Research Center, Cleveland, Ohio.
QCSEE UNDER-THE-WING ENGINE-WING-FLAP AERODYNAMIC PROFILE CHARACTERISTICS
H. E. BLOOMER and N. E. SAMANICH Sep. 1982 48 p refs
(NASA-TM-82890; E-1268; NAS 1.15:82890) Avail: NTIS HC A03/MF A01 CSCL 21E

As part of a broad-based NASA program to provide a technology base for future propulsion requirements for powered-lift aircraft, the Quiet, Clean, Short-Haul, Experimental Engine (QCSEE) program was begun by the Lewis Research Center in 1974. The initial buildup of the under-the-wing (UTW) engine was tested by the contractor at his test site. The UTW engine was delivered to Lewis in 1978 for further testing with wing and flap segments simulating an installation on a short-haul transport aircraft. The engine was also tested alone as an aid in identifying the various noise sources and their levels. As part of these tests the aerodynamic profiles at the exhaust nozzle and on the surfaces and in the wake of the wing-flap system were measured. This report documents, in plots and tabular form, the significant results from those tests. The results are presented as tabulations of aerodynamic data for all of the test points and as profiles of pressure, temperature, velocity, and normalized velocity and pressure for selected conditions. One of the main conclusions was that the measured flap surface temperatures were surprisingly low for both approach and takeoff flap settings. Author

N83-12093*# Purdue Univ., Lafayette, Ind. School of Mechanical Engineering.
THE WISGSK: A COMPUTER CODE FOR THE PREDICTION OF A MULTISTAGE AXIAL COMPRESSOR PERFORMANCE WITH WATER INGESTION Final Report
T. TSUCHIYA and S. N. B. MURTHY Washington NASA Nov. 1982 256 p refs
(Contract NAG3-62)
(NASA-CR-3624; NAS 1.26:3624) Avail: NTIS HC A12/MF A01 CSCL 21E

A computer code is presented for the prediction of off-design axial flow compressor performance with water ingestion. Four processes were considered to account for the aero-thermo-mechanical interactions during operation with air-water droplet mixture flow: (1) blade performance change, (2) centrifuging of water droplets, (3) heat and mass transfer process between the gaseous and the liquid phases and (4) droplet size redistribution due to break-up. Stage and compressor performance are obtained by a stage stacking procedure using representative veocity diagrams at a rotor inlet and outlet mean radii. The Code has options for performance estimation with (1) mixtures of gas and (2) gas-water droplet mixtures, and therefore can take into account the humidity present in ambient conditions. A test case illustrates the method of using the Code. The Code follows closely the methodology and architecture of the NASA-STGSTK Code for the estimation of axial-flow compressor performance with air flow. Author

N83-12094*# General Electric Co., Evendale, Ohio. Aircraft Engine Group.
ENERGY EFFICIENT ENGINE. FLIGHT PROPULSION SYSTEM PRELIMINARY ANALYSIS AND DESIGN Report, Jan. 1978 - Nov. 1979
R. P. JOHNSTON Nov. 1979 50 p refs
(Contract NAS3-20643)
(NASA-CR-159859; NAS 1.26:159859; R80AEG396) Avail: NTIS HC A03/MF A01 CSCL 21E

The characteristics of an advanced Flight Propulsion System (FPS) suitable for introduction in the late 1980's to early 1990's, were defined. It was determined that NASA goals for efficiency, environmental considerations, and economics could be met or exceeded with the possible exception of NOx emission. In evaluating the FPS, all aspects were considered including component design, performance, weight, initial cost, maintenance cost, engine-system integration (including nacelle), and aircraft integration considerations. In terms of the NASA goals, the current

FPS installed specific fuel consumption was reduced 14.2% from that of the CF6-50C reference engine. When integrated into an advanced, subsonic, study transport, the FPS produced a fuel-burn savings of 15 to 23% and a direct operating cost reduction of 5 to 12% depending on the mission and study-aircraft characteristics relative to the reference engine. J.M.S.

N83-12163*# National Aeronautics and Space Administration. Lewis Research Center, Cleveland, Ohio.
TURBINE ENGINE MATERIALS DURABILITY RESEARCH
S. R. LEVINE and C. A. STEARNS *In* NASA. Langley Research Center Advan. Mater. Technol. p 313-334 Nov. 1982 refs
Avail: NTIS HC A19/MF A01 CSCL 21E

High temperature environmental attack of dollar intensive turbine components reduces turbine efficiency and can limit life. The mechanisms of alloy and coating attack and the effects of interaction with the environment on mechanical behavior. This base of understanding provides the foundation for developing life prediction methods and identifying strategies for controlling attack. Subjects discussed in detail include oxidation and new developments in thermal barrier coating research. B.W.

N83-13100*# General Electric Co., Cincinnati, Ohio. Aircraft Engine Group.
CF6 JET ENGINE DIAGNOSTICS PROGRAM. HIGH PRESSURE TURBINE ROUNDNESS/CLEARANCE INVESTIGATION
W. D. HOWARD and W. A. FASCHING Jun. 1982 123 p refs
(Contract NAS3-20631)
(NASA-CR-165581; NAS 1.26:165581; R82AEB340) Avail: NTIS HC A06/MF A01 CSCL 21E

The effects of high pressure turbine clearance changes on engine and module performance was evaluated in addition to the measurement of CF6-50C high pressure turbine Stage 1 tip clearance and stator out-of-roundness during steady-state and transient operation. The results indicated a good correlation of the analytical model of round engine clearance response with measured data. The stator out-of-roundness measurements verified that the analytical technique for predicting the distortion effects of mechanical loads is accurate, whereas the technique for calculating the effects of certain circumferential thermal gradients requires some modifications. A potential for improvement in roundness was established in the order of 0.38 mm (0.015 in.), equivalent to 0.86 percent turbine efficiency which translates to a cruise SFC improvement of 0.36 percent. The HP turbine Stage 1 tip clearance performance derivative was established as 0.44 mm (17 mils) per percent of turbine efficiency at take-off power, somewhat smaller, therefore, more sensitive than predicted from previous investigations. M.G.

N83-13101*# National Aeronautics and Space Administration. Lewis Research Center, Cleveland, Ohio.
EFFECT OF BROAD PROPERTIES FUEL ON INJECTOR PERFORMANCE IN A REVERSE FLOW COMBUSTOR
S. M. RADDLEBAUGH and C. T. NORGREN 1983 18 p refs Prepared for presentation at the 21st Aerospace Sci. Conf., Reno, Nev., 10-13 Jan. 1983; sponsored by AIAA
(NASA-TM-83013; E-1448; NAS 1.15:83013; AIAA-83-0154)
Avail: NTIS HC A02/MF A01 CSCL 21E

The effect of fuel type on the performance of various fuel injectors was investigated in a reverse flow combustor. Combustor performance and emissions are documented for simplex pressure atomizing, spill flow, and airblast fuel injectors using a broad properties fuel and compared with performance using Jet A fuel. Test conditions simulated a range of flight conditions including sea level take off, low and high altitude cruise, as well as a parametric evaluation of the effect of increased combustor loading. The baseline simplex injector produced higher emission levels with corresponding lower combustion efficiency with the broad properties fuel. There was little or not loss in performance by the two advanced concept injectors with the broad properties fuel. The airblast injector proved to be especially insensitive to fuel type. S.L.

N83-13103*# General Electric Co., Cincinnati, Ohio. Aircraft Engine Business Group.
CONCEPTUAL DESIGN, EVALUATION AND RESEARCH IDENTIFICATION FOR REMOTE AUGMENTED PROPULSIVE LIFT SYSTEMS (RALS) WITH EJECTORS FOR VTOL AIRCRAFT Final Report
W. S. WILLIS, M. KONARSKI, and M. V. SUTHERLAND May 1982 60 p refs
(Contract NAS3-22042)
(NASA-CR-167906; NAS 1.26:167906; R82AEB315) Avail: NTIS HC A05/MF A01 CSCL 21E

Ejector concepts for use with a remote augmented lift system (RALS) exhaust nozzle were studied. A number of concepts were considered and three were selected as having the greatest promise of providing the desired aircraft and exhaust gas cooling and lift enhancement. A scale model test program is recommended to explore the effects of the more important parameters on ejector performance. M.G.

N83-13104*# Solar Turbines International, San Diego, Calif.
INVESTIGATION OF A LOW NOX FULL-SCALE ANNULAR COMBUSTOR Final Report
Feb. 1982 79 p refs
(Contract NAS3-20616)
(NASA-CR-165518; NAS 1.26:165518; SR82-R-4621-36) Avail: NTIS HC A05/MF A01 CSCL 21E

An atmospheric test program was conducted to evaluate a low NOx annular combustor concept suitable for a supersonic, high-altitude aircraft application. The lean premixed combustor, known as the vortex air blast (VAB) concept, was tested as a 22.0-cm diameter model in the early development phases to arrive at basic design and performance criteria. Final demonstration testing was carried out on a full scale combustor of 0.66-m diameter. Variable geometry dilution ports were incorporated to allow operation of the combustor across the range of conditions between idle (T(in) = 422 K, T(out) = 917 K) and cruise (T(in) = 833 K, T(out) - 1778 K). Test results show that the design could meet the program NOx goal of 1.0 g NO2/kg fuel at a one-atmospheric simulated cruise condition. Author

N83-14126*# National Aeronautics and Space Administration. Lewis Research Center, Cleveland, Ohio.
UNIFORM ENGINE TESTING PROGRAM. PHASE 1: NASA LEWIS RESEARCH CENTER PARTICIPATION
T. BLESIADNY, L. BURKARDT, and W. BRAITHWAITE Oct. 1982 63 p refs
(NASA-TM-82978; E-1407; NAS 1.15:82978) Avail: NTIS HC A04/MF A01 CSCL 21E

Two jet engines were tested under identical conditions in a variety of altitude and ground level facilities as a means to correlating these facilities. Two J57-19W turbojet engines were tested in an altitude test facility. The test results are summarized. S.L.

N83-14127*# National Aeronautics and Space Administration. Lewis Research Center, Cleveland, Ohio.
ANALYTICAL CALCULATION OF A SINGLE JET IN CROSSFLOW AND COMPARISON WITH EXPERIMENT
R. W. CLAUSS 1982 15 p refs Proposed for presentation at the 21th Aerospace Sci. Conf., Reno, Nev., 10-13 1983; sponsored by AIAA
(NASA-TM-83027; E-1462; NAS 1.15:83027) Avail: NTIS HC A02/MF A02 CSCL 21E

A series of calculations of a jet in crossflow using a three-dimensional finite difference model of the Navier-Stokes equations were made on a series of progressively finer grids. With a reasonable number of grid point (40x30x20), calculated jet penetration and mixing characteristics were found to compare favorably with the experimental measurements of Crabb, Durao and Whitelaw. The calculated results were grid dependent (i.e., numerical or false diffusion was present in the result). A finer grid calculation indicated that turbulence model deficiencies may

become more noticeable in the calculated results as the magnitude of numerical diffusion is reduced. Author

N83-14128*# United Technologies Corp., East Hartford, Conn. Commercial Products Div.
ROTOR REDESIGN FOR A HIGHLY LOADED 1800 FT/SEC TIP SPEED FAN. 3: LASER DOPPLER VELOCIMETER REPORT Final Report
W. B. HARVEY, D. E. HOBBS, D. LEE, M. C. WILLIAMS, and K. F. WILLIAMS Apr. 1982 258 p refs
(Contract NAS3-20591)
(NASA-CR-167954; NAS 1.26:167954; PWA-5523-122) Avail: NTIS HC A12/MF A01 CSCL 21E

Laser Doppler velocimeter (LDV) techniques were employed for testing a highly loaded, 550 m/sec (1800 ft/sec) tip speed, test fan stage, the objective to provide detailed mapping of the upstream, intrablade, and downstream flowfields of the rotor. Intrablade LDV measurements of velocity and flow angle were obtained along four streamlines passing through the leading edge at 45%, 69%, 85%, and 95% span measured from hub to tip, at 100% of design speed, peak efficiency; 100% speed, near surge; and 95% speed, peak efficiency. At the design point, most passages appeared to have a strong leading edge shock, which moved forward with increasing strength near surge and at part speeds. The flow behind the shock was of a complex mixed subsonic and supersonic form. The intrablade flowfields were found to be significantly nonperiodic at 100% design speed, peak efficiency. Author

N83-14129*# National Aeronautics and Space Administration. Lewis Research Center, Cleveland, Ohio.
TIP CAP FOR A ROTOR BLADE Patent Application
W. K. KOFFEL (GE, Cincinnati, Ohio), E. N. TULEY (GE, Cincinnati, Ohio), C. H. GAY, JR. (GE, Cincinnati, Ohio), R. E. TROEGER (GE, Cincinnati, Ohio), and A. P. STERMAN, inventors (to NASA) (GE, Cincinnati, Ohio) 20 Mar. 1981 19 p Sponsored by NASA
(NASA-CASE-LEW-13654-1; US-PATENT-APPL-SN-245571)
Avail: NTIS HC A02/MF A01 CSCL 21E

A replaceable tip cap for a rotor blade is disclosed. The tip cap is comprised of a plurality of walls for defining a compartment. The tip cap is attachable to the radially outer end of the rotor blade and may be divided into a plurality of subcompartments. A flow of cooling fluid is introduced through inlet holes in the radially inner wall of the tip cap. The fluid exists through outlet holes in a sidewall. The tip cap design provides for reduced overheating and increased tip cap life as well as increased wear resistance to reduce the rate of engine efficiency loss. NASA

N83-15304*# Pratt and Whitney Aircraft Group, East Hartford, Conn. Energy Efficient Engine Component Development and Integration Program.
ENERGY EFFICIENT HIGH-PRESSURE TURBINE LEAKAGE TECHNOLOGY REPORT
W. B. GARDNER Dec. 1980 82 p refs
(Contract NAS3-20646)
(NASA-CR-165202; NAS 1.26:165202; PWA-5594-106) Avail: NTIS HC A05/MF A01 CSCL 21E

The leakage test program was one of such supporting technology programs structured to provide guidance to the Energy Efficient Engine High Pressure Turbine Component Design Effort. Leakage reduction techniques were identified and evaluated. Test models were used to simulate component leak paths and to evaluate leakage reduction techniques. These models simulated the blade/disk attachment, the vane inner platform attachment, and the vane outer platform attachment combined with the blade outer airseal. Disk blade attachment testing indicated that leakage in this area could be reduced to very low levels by paying careful attention to the tolerances along the contact surface between the blade vibration damper and the blade platform contact surface. The aim of feather seal testing was to achieve a goal for an effective leakage gap of one mil (.001 inch) per inch of feather seal length. Results indicated that effective gaps even below the goal level were achievable by (1) maintaining close tolerances between feather seals and their slots to minimize end gaps and limit seal rotation, (2) avoiding feather seal overlap, and (3) minimizing feather seal intersections. W seals were shown to be effective leakage control devices. Wire rope, in its present state of development, was shown not to be an effective sealing concept for application to the component design. Author

N83-15305*# Pratt and Whitney Aircraft Group, East Hartford, Conn. Commercial Engineering.
JT90 CERAMIC OUTER AIR SEAL SYSTEM REFINEMENT PROGRAM, PHASE 2
L. T. SHIEMBOB Nov. 1982 48 p refs
(Contract NAS3-20630)
(NASA-CR-167962; NAS 1.26:167962; PWA-5515-175) Avail: NTIS HC A03/MF A01 CSCL 21E

The sprayed ceramic gas turbine outer air seal system was tested in two JT9D engines to substantiate the abradability and durability of the seals. Of particular significance was that one of the tests, a 150 hour 1000 cycle endurance program at nominal JT9D operating conditions, was completed with minimal effect on the seals and received Federal Aviation Administration cognizance with respect to potential field service use by the airlines. The other engine test completed 1825 endurance cycles at severe operating conditions and no burn through or other serious defects in the structural integrity of a seal segment was observed. These test results combined with other Pratt and Whitney Aircraft engine tests substantiate the potential of the ceramic outer air seal system to attain the durability goal of 50000 hour engine operating capability. Both engine tests subjected the seals to intentional blade rubs and demonstrated good abradability with volume wear ratios greater than 100, far exceeding the design goal of 10. The improved volume wear ratio will allow the turbine tip clearance to be reduced, thereby resulting in an estimated thrust specific fuel consumption improvement of 0.3 percent. Author

N83-15306*# National Aeronautics and Space Administration. Lewis Research Center, Cleveland, Ohio.
EFFECT OF STEADY-STATE PRESSURE DISTORTION ON INLET FLOW TO A HIGH-BYPASS-RATIO TURBOFAN ENGINE
R. H. SOEDER and G. A. BOBULA Oct. 1982 31 p refs
Prepared in cooperation with Army Aviation Research and Development Command, Cleveland
(NASA-TM-82964; E-1383; NAS 1.15:82964; AVRADCOM-TR-81-C-27) Avail: NTIS HC A03/MF A01 CSCL 21E

Static pressure and total pressure distributions were measured in the inlet duct upstream of the engine inlet and within the fan and compressor of a YTF34 turbofan engine. In addition, the free stream flow angle was measured between the distortion generator and the engine inlet. Distortions were generated using three screen configurations with extents of 90 deg or 180 deg. The screens were mounted on a rotatable screen assembly. Reynolds number index upstream of the distortion device was maintained at 0.5 or 0.2, and engine fan speed corrected to station 2 temperature was maintained at 80 or 90 percent of rated condition (7005 rpm). Flow angle was nearly constant near the distortion device and increased as flow approached the engine inlet. The largest flow angle occurred in the hub region of the engine inlet. Static pressure distortion along the inlet duct increased exponentially as the flow approached the engine. Both static pressure and total pressure distortions were attenuated between engine inlet and compressor exit. Author

N83-15307*# National Aeronautics and Space Administration. Lewis Research Center, Cleveland, Ohio.
FEASIBILITY OF WATER INJECTION INTO THE TURBINE COOLANT TO PERMIT GAS TURBINE CONTINGENCY POWER FOR HELICOPTER APPLICATION
G. J. VANFOSSEN 1983 16 p refs Proposed for presentation at the 28th Ann. Intern. Gas Turbine Conf., Phoenix, Ariz., 27-31 Mar. 1983; sponsored by the American Society of Mechanical Engineers
(NASA-TM-83043; E-1490; NAS 1.15:83043) Avail: NTIS HC A02/MF A01 CSCL 21E

A system which would allow a substantially increased output from a turboshaft engine for brief periods in emergency situations with little or no loss of turbine stress rupture life is proposed and studied analytically. The increased engine output is obtained by overtemperaturing the turbine; however, the temperature of the compressor bleed air used for hot section cooling is lowered by injecting and evaporating water. This decrease in cooling air temperature can offset the effect of increased gas temperature and increased shaft speed and thus keep turbine blade stress rupture life constant. The analysis utilized the NASA-Navy-Engine-Program or NNEP computer code to model the turboshaft engine in both design and off-design modes. This report is concerned with the effect of the proposed method of power augmentation on the engine cycle and turbine components. A simple cycle turboshaft engine with a 16:1 pressure ratio and a 1533 K (2760 R) turbine inlet temperature operating at sea level static conditions was studied to determine the possible power increase and the effect on turbine stress rupture life that could be expected using the proposed emergency cooling scheme. The analysis showed a 54 percent increse in output power can be achieved with no loss in gas generator turbine stress rupture life. A 231 K (415 F) rise in turbine inlet temperature is required for this level of augmentation. The required water flow rate was found to be .0109 kg water per kg of engine air flow. B.W.

N83-15308*# General Electric Co., Cincinnati, Ohio. Aircraft Engine Business Group.
MATERIALS FOR ADVANCED TURBINE ENGINES. VOLUME 1: ADVANCED BLADE TIP SEAL SYSTEM Final Report
J. W. ZELAHY and N. P. FAIRBANKS Jul. 1982 99 p
(Contract NAS3-20074)
(NASA-CR-167851-VOL-1; NAS 1.26:167851-VOL-1; R82AEB403-VOL-1) Avail: NTIS HC A05/MF A01 CSCL 21E

Project 3, the subject of this technical report, was structured toward the successful engine demonstration of an improved-efficiency, long-life, tip-seal system for turbine blades. The advanced tip-seal system was designed to maintain close operating clearances between turbine blade tips and turbine shrouds and, at the same time, be resistant to environmental effects including high-temperature oxidation, hot corrosion, and thermal cycling. The turbine blade tip comprised an environmentally resistant, activated-diffussion-bonded, monocrystal superalloy combined with a thin layer of aluminium oxide abrasive particles entrapped in an electroplated NiCr matrix. The project established the tip design and joint location, characterized the single-crystal tip alloy and abrasive tip treatment, and established the manufacturing and quality-control plans required to fully process the blades. A total of 171 blades were fully manufactured, and 100 were endurance and performance engine-tested. Author

N83-15309*# Michigan Univ., Ann Arbor. Coll. of Engineering.
IGNITION AND COMBUSTION: LOW COMPRESSION RATIO, HIGH OUTPUT DIESEL Final Report, Sep. 1979 - 30 Apr. 1979
Jul. 1981 43 p refs
(Contract NSG-3161)
(NASA-CR-169742; NAS 1.26:169742) Avail: NTIS HC A03/MF A01

The feasibility of converting a spark ignition aircraft engine GTSI0-520 to compression ignition without increasing the peak combustion pressure of 1100 lbs/sq.in. was determined. The final contemplated utilized intake air heating at idle and light load and a compression ratio of about 10:1 with a small amount of fumigation (the addition of about 15% fuel into the combustion air before the cylinder). The engine used was a modification of a Continental-Teledyne gasoline engine cylinder from the GTSI0-520 supercharged aircraft engine. S.L.

N83-16341*# General Electric Co., Cincinnati, Ohio. Aircraft Engine Business Group.
ENERGY EFFICIENT ENGINE: FAN TEST HARDWARE DETAILED DESIGN REPORT
T. J. SULLIVAN Oct. 1980 146 p refs
(Contract NAS3-20643)
(NASA-CR-165148; NAS 1.26:165148; R80AEG417) Avail: NTIS HC A07/MF A01 CSCL 21E

A single stage fan and quarter stage booster were designed for the energy efficient engine. The fan has an inlet radius ratio of 0.342 and a specific flow rate of 208.9 Kg/S sq m (42.8 lbm/sec sq ft). The fan rotor has 32 medium aspect ratio (2.597) titanium blades with a partspan shroud at 55% blade height. The design corrected fan tip speed is 411.5 M/S (1350 ft/sec). The quarter stage island splits the total fan flow with approximately 22% of the flow being supercharged by the quarter stage rotor. The fan bypass ratio is 6.8. The core flow total pressure ratio is 1.67 and the fan bypass pressure ratio is 1.65. The design details of the fan and booster blading, and the fan frame and static structure for the fan configuration are presented. S.L.

N83-16342*# General Electric Co., Cincinnati, Ohio. Aircraft Engine Group.
THE CF6 ENGINE PERFORMANCE IMPROVEMENT Summary Report
W. A. FASCHING Oct. 1982 98 p refs
(Contract NAS3-20629)
(NASA-CR-165612; NAS 1.26:165612; R82AE511) Avail: NTIS HC A05/MF A01 CSCL 21E

As part of the NASA-sponsored Engine Component Improvement (ECI) Program, a feasibility analysis of performance improvement and retention concepts for the CF6-6 and CF6-50 engines was conducted and seven concepts were identified for development and ground testing: new fan, new front mount, high pressure turbine aerodynamic performance improvement, high pressure turbine roundness, high pressure turbine active clearance control, low pressure turbine active clearance control, and short core exhaust nozzle. The development work and ground testing are summarized, and the major test results and an enomic analysis for each concept are presented. Author

N83-16343*# Garrett Turbine Engine Co., Phoenix, Ariz.
A METHOD TO ESTIMATE WEIGHT AND DIMENSIONS OF SMALL AIRCRAFT PROPULSION GAS TURBINE ENGINES: USER'S GUIDE Final Report
P. L. HALE Aug. 1982 136 p refs
(Contract NAS3-23037)
(NASA-CR-168049; NAS 1.26:168049; GARRETT-21-4270-1.1)
Avail: NTIS HC A07/MF A01 CSCL 21E

The weight and major envelope dimensions of small aircraft propulsion gas turbine engines are estimated. The computerized method, called WATE-S (Weight Analysis of Turbine Engines-Small) is a derivative of the WATE-2 computer code. WATE-S determines the weight of each major component in the engine including compressors, burners, turbines, heat exchangers, nozzles, propellers, and accessories. A preliminary design approach is used where the stress levels, maximum pressures and temperatures, material properties, geometry, stage loading, hub/tip radius ratio, and mechanical overspeed are used to determine the component weights and dimensions. The accuracy of the method is generally better than + or - 10 percent as verified by analysis of four small aircraft propulsion gas turbine engines. S.L.

N83-17537*# National Aeronautics and Space Administration. Lewis Research Center, Cleveland, Ohio.
STATUS OF FIBEROPTICS TECHNOLOGY FOR PROPULSION CONTROL SYSTEMS
R. J. BAUMBICK 1982 12 p refs Presented at the Aerospace Congr. and Exposition, Anaheim, Calif., 25-28 Oct. 1982
(NASA-TM-82907; E-1291; NAS 1.15:82907) Avail: NTIS HC A02/MF A01 CSCL 21E

Optical sensors and optically controlled actuators for use in airbreathing engine control systems are discussed. The environmental conditions in which the aircraft will operate require the fiberoptic cables and optical connectors to perform reliably at temperatures over the -55 C to 260 C range. The status of fiberoptics technology for operation in this environment is reviewed. Author

N83-17538*# National Aeronautics and Space Administration. Lewis Research Center, Cleveland, Ohio.
VALIDATION OF A THREE-DIMENSIONAL VISCOUS ANALYSIS OF AXISYMMETRIC SUPERSONIC INLET FLOW FIELDS
T. J. BENSON and B. H. ANDERSON Jan. 1983 17 p refs Presented at the 21st Aerospace Sci. Conf., Reno, Nev., 10-13 Jan. 1983
(NASA-TM-83058; E-1523; NAS 1.15:83058) Avail: NTIS HC A02/MF A01 CSCL 21E

A three-dimensional viscous marching analysis for supersonic inlets was developed. To verify this analysis several benchmark axisymmetric test configurations were studied and are compared to experimental data. Detailed two-dimensional results for shock-boundary layer interactions are presented for flows with and without boundary layer bleed. Three dimensional calculations of a cone at angle of attack and a full inlet at attack are also discussed and evaluated. Results of the calculations demonstrate the code's ability to predict complex flow fields and establish guidelines for future calculations using similar codes. Author

N83-17539*# General Electric Co., Evendale, Ohio. Aircraft Engine Business Group.
SUMMARY REPORT FOR CF6 JET ENGINE DIAGNOSTICS PROGRAM Final Report
W. A. FASCHING and R. STRICKLIN Oct. 1982 44 p refs
(Contract NAG3-20631)
(NASA-CR-165582; NAS 1.26:165582; R81AEG654) Avail: NTIS HC A03/MF A01 CSCL 01E

Cockpit cruise recordings and test cell data in conjunction with hardware inspection results from airline overhaul shops were analyzed to define the extent and magnitude of performance deterioration of the General Electric CF6 high bypass turbofan engines. The magnitude of Short Term deterioration from the Long Term was isolated and the individual damage mechanisms that were the cause for the majority of the performance deterioration were identified. A potential for reduction in compressor clearance and a potential for improvement in turbine roundness, which corresponds to cruise SFC reductions of 0.38 and 0.36 percent, respectively, were identified. Author

N83-17543*# Pratt and Whitney Aircraft Group, East Hartford, Conn. Commercial Products Div.
THE JT8D AND JT9D ENGINE COMPONENT IMPROVEMENT: PERFORMANCE IMPROVEMENT PROGRAM Executive Summary Report
W. O. GAFFIN May 1982 32 p refs
(Contract NAS3-20630)
(NASA-CR-167965; NAS 1.26:167965; PWA-5515-177) Avail: NTIS HC A03/MF A01 CSCL 21E

The NASA sponsored Engine Component Improvement - Performance Improvement Program at Pratt & Whitney Aircraft advanced the state of the art of thermal barrier coatings and ceramic seal systems, demonstrated the practicality of an advanced turbine clearance control system and an advanced fan design in the JT9D engine, and demonstrated the advantages of modern cooling, sealing, and aerodynamic designs in the high pressure turbine and compressor of the JT8D engine. Several of these improvements are already in airline service in JT8D and JT9D engines, and others will enter service soon in advanced models of these engines. In addition, the technology advances are being transferred to completely new engine configurations, the PW2037 engine and the NASA sponsored Energy Efficient Engine. Author

N83-17544*# Pratt and Whitney Aircraft Group, East Hartford, Conn. Commercial Products Div.
THE JT9D JET ENGINE DIAGNOSTICS PROGRAM Executive Summary Report
W. J. OLSSON May 1982 26 p refs
(Contract NAS3-20632)
(NASA-CR-167966; NAS 1.26:167966; PWA-5512-96) Avail: NTIS HC A03/MF A01 CSCL 21E

The various engine deterioration phenomena that affect JT9D performance retention were studied, and approaches to improve performance retention of engines were identified. The program included surveys of historical data, monitoring of in service engines, ground and flight testing of instrumented engines, analysis, and analytical modeling. Performance deterioration is made up of both short and long term modes, both of which are flight cycle related phenomena. Short term deterioration occurs primarily during airplane acceptance testing prior to delivery to the airline. This effect is caused by flight load and power induced clearance closures and engine deflections with resulting rubbing of airfoils and seals. Long term deterioration is caused by erosion of airfoils and gas path seals during ground operation and take off and by cyclic induced thermal distortion of the high pressure turbine airfoils. Studies of possible remedial approaches have shown that performance retention within 1 to 2 percent of initial revenue service performance can be achieved with a proper program of hot section and cold section maintenance. S.L.

N83-17545*# Curtiss-Wright Corp., Wood-Ridge, N.J.
STUDY OF ADVANCED ROTARY COMBUSTION ENGINES FOR COMMUTER AIRCRAFT Final Report
M. BERKOWITZ, C. JONES, and D. MYERS Feb. 1983 58 p refs
(Contract NAS3-22140)
(NASA-CR-165399; NAS 1.26:165399; CW-WR-81-022F) Avail: NTIS HC A04/MF A01 CSCL 21E

Performance, weight, size, and maintenance data for advanced rotary aircraft engines suitable for comparative commuter aircraft system evaluation studies of alternate engine candidates are provided. These are turbocharged, turbocompounded, direct injected, stratified charge rotary engines. Hypothetical engines were defined (an RC4-74 at 895 kW and an RC6-87 at 1490 kW) based on the technologies and design approaches used in the highly advanced engine of a study of advanced general aviation rotary engines. The data covers the size range of shaft power from 597 kW (800 hp) to 1865 kW (2500 hp) and is in the form of drawings, tables, curves and written text. These include data on internal geometry and configuration, installation information, turbocharging and turbocompounding arrangements, design features and technologies, engine cooling, fuels, scaling for weight size BSFC and heat rejection for varying horsepower, engine operating and performance data, and TBO and maintenance requirements. The basic combustion system was developed and demonstrated; however the projected power densities and performance efficiencies require increases in engine internal pressures, thermal loading, and rotative speed. S.L.

N83-17547*# National Aeronautics and Space Administration. Lewis Research Center, Cleveland, Ohio.
AERODYNAMIC EFFECT OF A HONEYCOMB ROTOR TIP SHROUD ON A 50.8-CENTIMETER-TIP-DIAMETER CORE TURBINE
T. P. MOFFITT and W. J. WHITNEY Jan. 1983 19 p refs
(NASA-TP-2112; E-1261; NAS 1.60:2112) Avail: NTIS HC A02/MF A01 CSCL 21E

A 50.8-cm-tip-diameter turbine equipped with a rotor tip shroud of hexagonal cell (or honeycomb) cross section has been tested

in warm air (416 K) for a range of shroud coolant to primary flow rates. Test results were also obtained for the same turbine operated with a solid shroud for comparison. The results showed that the combined effect of the honeycomb shroud and the coolant flow was to cause a reduction of 2.8 points in efficiency at design speed, pressure ratio, and coolant flow rate. With the coolant system inactivated, the honeycomb shroud caused a decrease in efficiency of 2.3 points. These results and those obtained from a small reference turbine indicate that the dominant factor governing honeycomb tip shroud loss is the ratio of honeycomb depth to blade span. The loss results of the two shrouds could be correlated on this basis. The same honeycomb and coolant effects are expected to occur for the hot (2200 K) version of this turbine. Author

N83-18725*# National Aeronautics and Space Administration. Lewis Research Center, Cleveland, Ohio.
SMALL GAS TURBINE COMBUSTOR STUDY: COMBUSTOR LINER EVALUATION
C. T. NORGREN and S. M. RIDDLEBAUGH 1983 20 p refs Presented at 21st Aerospace Sci. Conf., Reno, Nevada, 10-13 Jan. 1983; sponsored by AIAA
(NASA-TM-83028; E-1463; NAS 1.15:83028; AIAA-83-0337) Avail: NTIS HC A02/MF A01 CSCL 21E
For abstract see A83-16663.

N83-18729*# Kansas Univ., Lawrence.
LITERATURE SEARCH OF PUBLICATIONS CONCERNING THE PREDICTION OF DYNAMIC INLET FLOW DISTORTION AND RELATED TOPICS Final Report
W. G. SCHWEIKHHARD and Y. S. CHEN Washington NASA Feb. 1983 141 p refs
(Contract NAG3-11)
(NASA-CR-3673; NAS 1.26:3673) Avail: NTIS HC A07/MF A01 CSCL 21E

Publications prior to March 1981 were surveyed to determine inlet flow dynamic distortion prediction methods and to catalog experimental and analytical information concerning inlet flow dynamic distortion prediction methods and to catalog experimental and analytical information concerning inlet flow dynamics at the engine-inlet interface of conventional aircraft (excluding V/STOL). The sixty-five publications found are briefly summarized and tabulated according to topic and are cross-referenced according to content and nature of the investigation (e.g., predictive, experimental, analytical and types of tests). Three appendices include lists of references, authors, organizations and agencies conducting the studies. Also, selected materials summaries, introductions and conclusions - from the reports are included. Few reports were found covering methods for predicting the probable maximum distortion. The three predictive methods found are those of Melick, Jacox and Motycka. The latter two require extensive high response pressure measurements at the compressor face, while the Melick Technique can function with as few as one or two measurements. Author

N83-19753*# Pratt and Whitney Aircraft Group, East Hartford, Conn. Commercial Products Div.
ENERGY EFFICIENT ENGINE SECTOR COMBUSTOR RIG TEST PROGRAM
D. J. DUBIEL, W. GREENE, C. V. SUNDT, S. TANRIKUT, and M. H. ZEISSER Oct. 1981 160 p refs
(Contract NAS3-20646)
(NASA-CR-167913; NAS 1.26:167913; PWA-5594-180) Avail: NTIS HC A08/MF A01 CSCL 21E

Under the NASA-sponsored Energy Efficient Engine program, Pratt & Whitney Aircraft has successfully completed a comprehensive combustor rig test using a 90-degree sector of an advanced two-stage combustor with a segmented liner. Initial testing utilized a combustor with a conventional louvered liner and demonstrated that the Energy Efficient Engine two-stage combustor configuration is a viable system for controlling exhaust emissions, with the capability to meet all aerothermal performance goals. Goals for both carbon monoxide and unburned hydrocarbons were surpassed and the goal for oxides of nitrogen was closely approached. In another series of tests, an advanced segmented liner configuration with a unique counter-parallel FINWALL cooling system was evaluated at engine sea level takeoff pressure and temperature levels. These tests verified the structural integrity of this liner design. Overall, the results from the program have provided a high level of confidence to proceed with the scheduled Combustor Component Rig Test Program. Author

N83-19754*# National Aeronautics and Space Administration. Lewis Research Center, Cleveland, Ohio.
TONE GENERATION BY ROTOR-DOWNSTREAM STRUT INTERACTION
R. P. WOODWARD and J. R. BALOMBIN 1983 17 p refs Proposed for presentation at the 8th Aeroacoustics Conf., Atlanta, 11-13 Apr. 1983; sponsored by the American Inst. of Aeronautics and Astronautics
(NASA-TM-83330; E-1577; NAS 1.15:83330) Avail: NTIS HC A02/MF A01 CSCL 21E

A JT15D fan stage was acoustically tested in the NASA Lewis anechoic chamber as part of the joint Lewis-Langley Research Center investigation of flight simulation techniques and flight effects using the JT15D engine as a common test vehicle. Suspected rotor-downstream support strut interaction was confirmed through the use of simulated support struts which were tested at three axial rotor-strut spacings. Tests were also performed with the struts removed. Inlet boundary layer suction in conjuction with an inflow control device was also explored. The removal of the boundary layer reduced the fan fundamental tone levels suggesting that the mounting and mating of such a device to the nacelle requires careful attention. With the same inflow control device installed good acoustic agreement was shown between the engine on an outdoor test stand and the fan in the anechoic chamber. Author

N83-20945*# Notre Dame Univ., Ind. Dept. of Electrical Engineering.
ALTERNATIVES FOR JET ENGINE CONTROL Annual Technical Progress Report, 1 Oct. 1981 - 30 Sep. 1982
M. K. SAIN, S. YURKOVICH, J. P. HILL, and T. A. KINGLER 23 Mar. 1983 197 p refs
(Contract NSG-3048)
(NASA-CR-170100; NAS 1.26:170100) Avail: NTIS HC A09/MF A01 CSCL 21E

The development of models of tensor type for a digital simulation of the quiet, clean safe engine (QCSE) gas turbine engine; the extension, to nonlinear multivariate control system design, of the concepts of total synthesis which trace their roots back to certain early investigations under this grant; the role of series descriptions as they relate to questions of scheduling in the control of gas turbine engines; the development of computer-aided design software for tensor modeling calculations; further enhancement of the softwares for linear total synthesis, mentioned above; and calculation of the first known examples using tensors for nonlinear feedback control are discussed. Author

N83-20946*# General Electric Co., Cincinnati, Ohio. Aircraft Engine Business Group.
THE RENE 150 DIRECTIONALLY SOLIDIFIED SUPERALLOY TURBINE BLADES, VOLUME 1 Final Report
G. J. DEBOER Dec. 1981 116 p refs
(Contract NAS3-20074)
(NASA-CR-167992; NAS 1.26:167992; R82AEB540-VOL-1)
Avail: NTIS HC A06/MF A01 CSCL 21E

Turbine blade design and analysis, preliminary Rene 150 system refinement, coating adaptation and evaluation, final Rene 150 system refinement, component-test blade production and evaluation, engine-test blade production, and engine test are discussed. N.W.

N83-20947*# National Aeronautics and Space Administration. Lewis Research Center, Cleveland, Ohio.
NEW TRENDS IN COMBUSTION RESEARCH FOR GAS TURBINE ENGINES
E. J. MULARZ 1983 13 p refs Proposed for presentation at 6th Intern. Symp. on Air Breathing Engines, Paris, 6-11 Jun. 1983; sponsored by the International Society on Air Breathing Engines and the Association Aeronautique et Astronautique de France
(NASA-TM-83338; E-1590; NAS 1.15:83338; AVRADCOM-TR-83-C-1) Avail: NTIS HC A02/MF A01 CSCL 21E

Research on combustion is being conducted to provide improved analytical models of the complex flow and chemical reaction processes which occur in the combustor of gas turbine engines, in order to enable engine manufacturers to reduce the development time of these concepts. The elements of the combustion fundamentals program is briefly discussed with examples of research projects described more fully. Combustion research will continue to emphasize the development of analytical models and the support of these models with fundamental flow experiments to assess the models accuracy and shortcomings. S.L.

N83-20948*# Pennsylvania State Univ., University Park.
THE STRUCTURE OF PARTICLE-LADEN JETS AND NONEVAPORATING SPRAYS Final Report
J. S. SHUEN, A. S. P. SOLOMON, Q. F. ZHANG, and G. M. FAETH Feb. 1983 73 p refs
(Contract NAG3-190)
(NASA-CR-168059; NAS 1.26:168059) Avail: NTIS HC A04/MF A01 CSCL 21E

Mean and fluctuating gas velocities, liquid mass fluxes and drop sizes were in nonevaporating sprays. These results, as well as existing measurements in solid particle-laden jets, were used to evaluate models of these processes. The following models were considered: (1) a locally homogeneous flow (LHF) model, where slip between the phases was neglected; (2) a deterministic separated flow (DSF) model, where slip was considered but effects of particle dispersion by turbulence were ignored; and (3) a stochastic separated flow (SSF) model, where effects of interphase slip and turbulent dispersion were considered using random-walk computations for particle motion. The LHF and DSF models did not provide very satisfactory predictions over the present data base. In contrast, the SSF model performed reasonably well - including conditions in nonevaporating sprays where enhanced dispersion of particles by turbulence caused the spray to spread more rapidly than single-phase jets for comparable conditions. While these results are encouraging, uncertainties in initial conditions limit the reliability of the evaluation. Current work is seeking to eliminate this deficiency. Author

N83-22198*# Westinghouse Research and Development Center, Pittsburgh, Pa.
LABYRINTH SEAL FORCES ON A WHIRLING ROTOR Final Report
D. V. WRIGHT Jan. 1983 111 p refs
(Contract NAS3-10825; DA PROJ. 1L1-62209-AH-76)
(NASA-CR-168016; NAS 1.26:168016) Avail: NTIS HC A06/MF A01 CSCL 21E

An experimental investigation of air labyrinth seal forces on a subsynchronously whirling model rotor is described and test results are given for diverging, converging, and straight two-strip seals. The effects of pressure drop, provide basic experimental data needed in the development of design methods for predicting and preventing self-excited whirl of turbine rotors and other machines having labyrinth seals. The total dynamic seal forces on the whirling model rotor are measured accurately by means of an active damping and stiffness system that is adjusted to obtain neutral whirl stability of the model rotor system. In addition, the whirling pressure pattern in the seal annulus is measured for a few test conditions and the corresponding pressure forces on the rotor are compared with the total measured forces. This comparison shows that either radial and axial pressure gradients in the seal annulus or drag forces on the rotor are significant. Comparisons made between the measured seal forces and theoretical results show that present theory is inadequate. M.G.

N83-22199*# National Aeronautics and Space Administration. Lewis Research Center, Cleveland, Ohio.
NUMERICAL SOLUTION TO THE GLANCING SIDEWALL OBLIQUE SHOCK WAVE/TURBULENT BOUNDARY LAYER INTERACTION IN THREE DIMENSION
B. H. ANDERSON and T. J. BENSON 1983 23 p refs Presented at the 21st Aerospace Sci. Conf., Reno, Nev., 10-13 Jan. 1983; sponsored by AIAA Original document was announced as A83-16823
(NASA-TM-83056; E-1521; NAS 1.15:83056; AIAA-83-0136)
Avail: NTIS HC A02/MF A01 CSCL 21E

A supersonic three-dimensional viscous forward-marching computer design code called PEPSIS is used to obtain a numerical solution of the three-dimensional problem of the interaction of a glancing sidewall oblique shock wave and a turbulent boundary layer. Very good results are obtained for a test case that was run to investigate the use of the wall-function boundary-condition approximation for a highly complex three-dimensional shock-boundary layer interaction. Two additional test cases (coarse mesh and medium mesh) are run to examine the question of near-wall resolution when no-slip boundary conditions are applied. A comparison with experimental data shows that the PEPSIS code gives excellent results in general and is practical for three-dimensional supersonic inlet calculations. F.G.M.

N83-22200*# National Aeronautics and Space Administration. Lewis Research Center, Cleveland, Ohio.
EXPERIMENTAL INVESTIGATION OF A TWO-DIMENSIONAL SHOCK-TURBULENT BOUNDARY LAYER INTERACTION WITH BLEED
W. R. HINST and F. T. TANJI 1983 19 p refs Presented at the 21st Aerospace Sci. Conf., Reno, Nev., 10-13 Jan. 1983; sponsored by AIAA Announced in AIAA as A83-19581
(NASA-TM-83057; E-1522; NAS 1.15:83057; AIAA-83-0135)
Avail: NTIS HC A02/MF A01 CSCL 21E

The two-dimensional interaction of an oblique shock wave with a turbulent boundary layer that included the effect of bleed was examined experimentally using a shock generator mounted across a supersonic wind tunnel The studies were performed at Mach numbers 2.5 and 2.0 and unit Reynolds number of approximately 2.0 x 10 to the 7th/meter. The study includes surface oil flow visualization, wall static pressure distributions and boundary layer pitot pressure profiles. In addition, the variation of the local bleed rates were measured. The results show the effect of the bleed on the boundary layer as well as the effect of the flow conditions on the local bleed rate. Author (IAA)

N83-22204*# General Electric Co., Cincinnati, Ohio. Advanced Engineering and Technology Programs Dept.
ENERGY EFFICIENT ENGINE COMPONENT DEVELOPMENT AND INTEGRATION PROGRAM Semiannual Report, 1 Oct. 1980 - 31 Mar. 1981
30 Jan. 1981 412 p
(Contract NAS3-20643)
(NASA-CR-170089; NAS 1.26:170089; R81AEG316; SAR-6)
Avail: NTIS HC A18/MF A01 CSCL 21E

The technology that will improve the energy efficiency of propulsion systems for subsonic commercial aircraft is investigated. A reduction of 14.4% in cruise installed sfc (0.572 versus 0.668 for the CF6-50C) and a direct operation cost reduction in excess of the 5% goal is projected. Noise and emissions projections are consistent with the established goals. S.L.

N83-22456*# National Aeronautics and Space Administration. Lewis Research Center, Cleveland, Ohio.
AN OVERVIEW OF GENERAL AVIATION PROPULSION RESEARCH PROGRAMS AT NASA LEWIS RESEARCH CENTER
E. A. WILLIS *In its* Aviation Gasolines and Future Alternatives p 149-160 May 1983 Original document was announced as N81-16052
Avail: NTIS HC A08/MF A01 CSCL 21E

The review covers near-term improvements for current-type piston engines, as well as studies and limited corroborative research on several advanced g/a engine concepts, including diesels, small turboprops and both piston and rotary stratified-charge engines. Also described is basic combustion research, cycle modeling and diagnostic instrumentation work that is required to make new engines a reality. T.M.

N83-22457*# National Aeronautics and Space Administration. Lewis Research Center, Cleveland, Ohio.
GENERAL AVIATION TURBINE ENGINE (GATE) OVERVIEW
W. C. STRACK *In its* Aviation Gasolines and Future Alternatives p 161-166 May 1983 refs
Avail: NTIS HC A08/MF A01 CSCL 21E

When all the technology studies were done and the accompanying market analyses were complete, the conclusion was that it is indeed possible to reduce the cost of turbine engines by a factor of 3 using low-cost manufacturing techniques and increased production rates. In the interest of reducing engine cost, some performance was sacrificed. Yet we ended up with about a 20 percent predicted improvement in SFC over current technology turboprops. However, even this level of improvement does not match the low SFC of reciprocating powerplants--particularly those advanced concepts described earlier. The 20 percent better SFC and much lower weight of a turboprop does mean that if such a powerplant were installed in a resized small airplane, one could save between 10 and 30 percent fuel relative to existing recip engines, depending on different mission and airplane combinations. The price of the aircraft would go down about 15 percent in the case of a high powered single, or 25 percent in the case of a normal size twin. The operating costs would decrease about 10 percent in the case of the single, and as much as 35 percent in the case of the twin. Author

N83-23305*# Notre Dame Univ., Ind. Dept. of Electrical Engineering.
ALTERNATIVES FOR JET ENGINE CONTROL Semiannual Status Report, 1 Oct. 1982 - 31 Mar. 1983
M. K. SAIN Apr. 1983 102 p refs
(Contract NSG-3048)
(NASA-CR-170233; NAS 1.26:170233) Avail: NTIS HC A06/MF A01 CSCL 21E

Tensor model order reduction, recursive tensor model identification, input design for tensor model identification, software development for nonlinear feedback control laws based upon tensors, and development of the CATNAP software package for tensor modeling, identification and simulation were studied. The last of these are discussed. Author

N83-23306*# National Aeronautics and Space Administration. Lewis Research Center, Cleveland, Ohio.
DESIGN ANALYSIS OF A SELF-ACTING SPIRAL-GROOVE RING SEAL FOR COUNTER-ROTATING SHAFTS
E. DIRUSSO 1983 12 p refs Presented at the 19th Joint Propulsion Conf. and Tech. Display, Seattle, 27-29 Jun. 1983
(NASA-TM-83346; E-1253; NAS 1.15:83346) Avail: NTIS HC A02/MF A01 CSCL 21E

A self-acting spiral groove inter-shaft ring seal of nominal 16.33 cm (6.43 in.) diameter for sealing fan bleed air between counter rotating shafts in advanced turbofan engines was analyzed. The analysis focused on the lift force characteristics of the spiral grooves. A NASA Lewis developed computer program for predicting the performance of gas lubricated face seals was used to optimize the spiral groove geometry to produce maximum lift force. Load capacity curves (lift force as function of film thickness) were generated for four advanced turbofan engine operating conditions at relative seal speeds ranging from 17,850 to 29,800 rpm, sealed air pressures from 6 to 42 N/sq cm (9 to 60 psi) absolute and temperatures from 95 to 327 C (203 to 620 F). The relative seal sliding speed range was 152 to 255 m/sec (500 to 836 ft/sec). The analysis showed that the spiral grooves are capable of producing sufficient lift force such that the ring seal will operate in a noncontacting mode over the operating range of typical advanced turbofan engines. Author

N83-23309*# National Aeronautics and Space Administration. Lewis Research Center, Cleveland, Ohio.
EFFECT OF FLAMEHOLDER PRESSURE DROP ON EMISSIONS AND PERFORMANCE OF PREMIXED-PREVAPORIZED COMBUSTORS
R. A. DUERR and V. J. LYONS Apr. 1983 22 p refs
(NASA-TP-2131; E-1358; NAS 1.60:2131) Avail: NTIS HC A02/MF A01 CSCL 21E

Parametric tests were conducted to determine the effects of flameholder pressure drop on the emissions and performance of lean premixed-prevaporized combustors. A conical flameholder mounted in a diverging duct was tested with two values of flameholder blockage. Emissions of nitrogen oxides, carbon monoxide, carbon dioxide, and unburned hydrocarbons were measured for combustor entrance conditions of 600 to 800 K air temperature, 0.3 MPa to 0.5 MPa pressure, and 20 m/sec to 35 m/sec reference velocity. Jet A fuel was injected at flow rates corresponding to an equivalence ratio range from 0.8 down to the lean stability limit. Emission results for the high-blockage flameholder were a substantial improvement over the low-blockage emission results. A correlation of combustion efficiency with flameholder pressure drop was developed for pressure drops less than 9 percent. Author

N83-24505*# National Aeronautics and Space Administration. Lewis Research Center, Cleveland, Ohio.
EFFECTS OF INTERSTAGE DIFFUSER FLOW DISTORTION ON THE PERFORMANCE OF A 15.41-CENTIMETER TIP DIAMETER AXIAL POWER TURBINE Final Report
K. L. MCLALLIN, M. G. KOFSKEY, and K. C. CIVINSKAS (Army Research and Technology Labs., Cleveland, Ohio) 1983 22 p refs Proposed for presentation at the 19th Joint Propulsion Conf., Seattle, 27-29 Jun. 1983; sponsored by AIAA, SAE, and ASME
(Contract DE-AI01-77CS-51040)
(NASA-TM-83359; DOE/NASA/51040-46; E-1621; NAS 1.15:83359; AVRADCOM-TR-83-C-2; AIAA-83-1179) Avail: NTIS HC A02/MF A01 CSCL 21E

The performance of a variable-area stator, axial flow power turbine was determined in a cold-air component research rig for two inlet duct configurations. The two ducts were an interstage diffuser duct and an accelerated-flow inlet duct which produced stator inlet boundary layer flow blockages of 11 percent and 3 percent, respectively. Turbine blade total efficiency at design point was measured to be 5.3 percent greater with the accelerated-flow inlet duct installed due to the reduction in inlet blockage. Blade component measurements show that of this performance improvement, 35 percent occurred in the stator and 65 percent occurred in the rotor. Analysis of inlet duct internal flow using an Axisymmetric Diffuser Duct Code (ADD Code) were in substantial agreement with the test data. Author

N83-24506*# National Aeronautics and Space Administration. Lewis Research Center, Cleveland, Ohio.
OPPORTUNITIES FOR RESEARCH IN AEROTHERMODYNAMICS
R. W. GRAHAM 1983 25 p refs Presented at the Meeting of the Thermosci. Affiliates of Stanford Univ., Stanford, Calif., 24 Jan. 1983
(NASA-TM-83348; E-1605; NAS 1.15:83348) Avail: NTIS HC A02/MF A01 CSCL 21E

'Aerothermodynamics' involves the disciplines of chemistry, thermodynamics, fluid mechanics and heat transfer which have

collaborative importance in propulsion systems. There are growing opportunities for the further application of these disciplines to improve the methodology for the design of advanced gas turbines; particularly, the combustor and turbine. Design procedures follow empirical or cut and try guidelines. The tremendous advances in computational analysis and in instrumentation techniques hold promise for research answers to complex physical processes that are currently not well understood. The transfer of basic research understanding to engineering design should result in shorter, less expensive development commitments for engines. The status and anticipated opportunities in research topics relevant to combustors and turbines is reviewed. S.L.

N83-24509*# National Aeronautics and Space Administration. Lewis Research Center, Cleveland, Ohio.
PARTICLE SIZING BY MEASUREMENT OF FORWARD-SCATTERED LIGHT AT TWO ANGLES
D. R. BUCHELE May 1983 25 p refs
(NASA-TP-2156; E-1179; NAS 1.60:2156) Avail: NTIS HC A02/MF A01 CSCL 20F

Fundamental and practical limitations to particle sizing by measurement of forward scattered light are presented. Methods to minimize the limitations are described. Two types of instruments are compared. Author

N83-25711*# National Aeronautics and Space Administration. Lewis Research Center, Cleveland, Ohio.
NASA PROPULSION CONTROLS RESEARCH
F. TEREN 1983 11 p refs Presented at the 6th Intern. Symp. on Air Breathing Engines, Paris, 6-11 Jun. 1983; sponsored by International Society on Air Breathing Engines and Association Aeronautique et Astronautique de France
(NASA-TM-83343; E-1558; NAS 1.15:83343) Avail: NTIS HC A02/MF A01 CSCL 21E

Multivariable control theory is applied to the design of multiple input and output engine controls. Highly-accurate, real-time engine simulations are utilized for control development and checkout. Electro-optical control components are developed for use in electronic control systems having fiber optic data links. Integrated controls are developed for VSTOL and Rotorcraft propulsion systems. Post-stall models of engine systems are developed to aid in understanding and control of post-stall engine behavior. Author

N83-25712*# National Aeronautics and Space Administration. Lewis Research Center, Cleveland, Ohio.
DESIGN ANALYSIS OF A SELF-ACTING SPIRAL-GROOVE RING SEAL FOR COUNTER-ROTATING SHAFTS
E. DIRUSSO May 1983 12 p refs
(NASA-TP-2142; E-1253; NAS 1.60:2142) Avail: NTIS HC A02/MF A01 CSCL 11A

A self-acting spiral groove inter-shaft ring seal of nominal 16.33 cm (6.43 in.) diameter for sealing fan bleed air between counter-rotating hafts in advanced turbofan engines was analyzed. The analysis focused on the lift force characteristics of the spiral grooves. A NASA Lewis developed computer program for predicting the performance of gas lubricated face seals was used to optimize the spiral groove geometry to produce maximum lift force. Load capacity curves (lift force as function of film thickness) were generated for four advanced turbofan engine operating conditions at relative seal speeds ranging from 17,850 to 29,800 rpm, sealed air pressures from 6 to 42 N/sq cm (9 to 60 psi) absolute and temperatures from 95 deg to 327 C (203 deg to 620 F). The relative seal sliding speed range was 152 to 255 m/sec (500 to 836 ft/sec). The analysis showed that the spiral grooves are capable of producing sufficient lift force such that the ring seal will operate in a noncontacting mode over the operating range of typical advanced turbofan engines. Author

N83-26837*# General Applied Science Labs., Inc., Westbury, N. Y.
TESTING OF FELT-CERAMIC MATERIALS FOR COMBUSTOR APPLICATIONS Final Report
R. S. VENKAT and G. ROFFE Apr. 1983 45 p refs Sponsored in part by Army Original doc. contains color illustrations
(Contract NAS3-22775)
(NASA-CR-168103; NAS 1.26:168103; AD-A130069) Avail: NTIS HC A03/MF A01 CSCL 21E

The feasibility of using composite felt ceramic materials as combustor liners was experimentally studied. The material consists of a porous felt pad sandwiched between a layer of ceramic and one of solid metal. Flat, rectangular test panels, which encompassed several design variations of the basic composite material, were tested, two at a time, in a premixed gas turbine combustor as sections of the combustor wall. Tests were conducted at combustor inlet conditions of 0.5 MPa and 533 K with a reference velocity of 25 m/s. The panels were subjected to a hot gas temperature of 2170 K with 1% of the total airflow used to film cool the ceramic surface of the test panel. In general, thin ceramic layers yield low ceramic stress levels with high felt ceramic interface temperatures. On the other hand, thick ceramic layers result in low felt ceramic interface temperatures but high ceramic stress levels. Extensive thermal cycling appears to cause material degradation, but for a limited number of cycles, the survivability of felt ceramic materials, even under extremely severe combustor operating conditions, was conclusively demonstrated. B.W.

N83-26838*# National Aeronautics and Space Administration. Lewis Research Center, Cleveland, Ohio.
DYNAMIC DISTORTION IN A SHORT S-SHAPED SUBSONIC DIFFUSER WITH FLOW SEPARATION
R. STUMPF, H. E. NEUMANN, and C. C. GIAMATI 1983 20 p refs Presented at the 19th Joint Propulsion Conf., Seattle, 27-29 Jun. 1983; sponsored by AIAA, SAE and ASME
(NASA-TM-83412; E-1695; NAS 1.15:83412) Avail: NTIS HC A02/MF A01 CSCL 21E

An experimental investigation of the time varying distortion at the diffuser exit of a subscale HiMAT forebody and inlet was conducted at Mach 0.9 in the Lewis 8 by 6 foot Supersonic Wind Tunnel. A transitory separation was detected within the subsonic diffuser. Vortex generators were installed to eliminate the flow separation. Results from a study of the instantaneous pressure variations at the diffuser exit are presented. The time unsteady total pressures at the diffuser exit are computer interpolated and presented in the form of a movie showing the transitory separation. Limited data showing the instantaneous distortion levels is also presented. Author

N83-26839*# National Aeronautics and Space Administration. Lewis Research Center, Cleveland, Ohio.
THRUST PERFORMANCE OF A VARIABLE-GEOMETRY, DIVERGENT EXHAUST NOZZLE ON A TURBOJET ENGINE AT ALTITUDE
D. M. STRAIGHT and R. R. COLLOM Jun. 1983 39 p refs
(NASA-TP-2171; E-1451; NAS 1.60:2171) Avail: NTIS HC A03/MF A01 CSCL 21E

A variable geometry, low aspect ratio, nonaxisymmetric, two dimensional, convergent-divergent exhaust nozzle was tested at simulated altitude on a turbojet engine to obtain baseline axial, dry thrust performance over wide ranges of operating nozzle pressure ratios, throat areas, and internal expansion area ratios. The thrust data showed good agreement with theory and scale model test results after the data were corrected for seal leakage and coolant losses. Wall static pressure profile data were also obtained and compared with one dimensional theory and scale model data. The pressure data indicate greater three dimensional flow effects in the full scale tests than with models. The leakage and coolant penalties were substantial, and the method to determine them is included. Author

N83-27991*# National Aeronautics and Space Administration. Lewis Research Center, Cleveland, Ohio.
A SURVEY OF INLET/ENGINE DISTORTION COMPATIBILITY
D. N. BOWDITCH and R. E. COLTRIN 1983 22 p refs Presented at the 19th Joint Propulsion Conf., Seattle, 27-29 Jun. 1983; sponsored by AIAA, SAE and ASME
(NASA-TM-83421; E-1711; NAS 1.15:83421) Avail: NTIS HC A02/MF A01 CSCL 21E

The history of distortion analysis is traced back to its origin in parallel compressor theory which was initially proposed in the late fifties. The development of this theory is reviewed up to its inclusion in the complex computer codes of today. It is found to be a very useful tool to guide development but not quantitative enough to predict compatibility. Dynamic or instantaneous distortion methodology is also reviewed from its origins in the sixties, to its current application in the eighties. Many of the requirements for interpreting instantaneous distortion are considered and illustrated. Statistical methods for predicting the peak distortion are described, and their limitations and advantages discussed. Finally, some Reynolds number and scaling considerations for inlet testing are considered. It is concluded that the deterministic instantaneous distortion methodology combined with distortion testing of engines with screens will remain the primary method of predicting compatibility for the near future. However, parallel compressor analysis and statistical peak distortion prediction will be important tools employed during the development of inlet/engine compatibility. Author

N83-27992*# National Aeronautics and Space Administration. Lewis Research Center, Cleveland, Ohio.
LOW SPEED PERFORMANCE OF A SUPERSONIC AXISYMMETRIC MIXED COMPRESSION INLET WITH AUXILIARY INLETS
J. F. WASSERBAUER, R. W. CUBBISON, and C. J. TREFNY 1983 32 p refs Presented at the 19th Joint Propulsion Conf., Seattle, 27-29 Jun. 1983; sponsored by AIAA, SAE and ASME
(NASA-TM-83435; E-1730; NAS 1.15:83435) Avail: NTIS HC A03/MF A01 CSCL 21E

The aerodynamic performance of a representative supersonic cruise inlet was investigated using a fan simulator coupled to the inlet to provide characteristic noise signatures and to pump the inlet flow. Data were obtained at Mach numbers from 0 to 0.2 for the inlet equipped with an auxiliary inlet system that provided 20 to 40 percent of the fan flow. Results show that inlet performance improved when the inlet bleed systems were sealed; when the freestream Mach number was increased; and when the auxiliary inlets were opened. The inlet flow could not be choked by either centerbody translation or by increasing the fan speed when the 40 percent auxiliary inlet was incorporated. A.R.H.

N83-27993*# Pratt and Whitney Aircraft Group, East Hartford, Conn. Commercial Products Div.
JT9D THERMAL BARRIER COATED VANES
K. D. SHEFFLER, R. A. GRAZIANI, and G. C. SINKO Apr. 1982 171 p refs
(Contract NAS3-20630)
(NASA-CR-167964; NAS 1.26:167964; PWA-5515-176) Avail: NTIS HC A08/MF A01 CSCL 21E

The technology of plasma sprayed thermal barrier coatings applied to turbine vane platforms in modern high temperature commercial engines was advanced to the point of demonstrated feasibility for application to commercial aircraft engines. The three thermal barrier coatings refined under this program are zirconia stabilized with twenty-one percent magnesia (21% MSZ), six percent yttria (6% YSZ), and twenty percent yttria (20% YSZ). Improvement in thermal cyclic endurance by a factor of 40 times was demonstrated in rig tests. A cooling system evolved during the program which featured air impingement cooling for the vane platforms rather than film cooling. The impingement cooling system, in combination with the thermal barrier coatings, reduced platform cooling air requirements by 44% relative to the current film cooling system. Improved durability and reduced cooling air requirements were demonstrated in rig and engine endurance tests. Two engine tests were conducted, one of 1000 cycles and the other of 1500 cycles. All three coatings applied to vanes fabricated with the final cooling system configuration completed the final 1500 cycle engine endurance test. Results of this test clearly demonstrated the durability of the 6% YSZ coating which was in very good condition after the test. The 21% MSZ and 20% YSZ coatings had numerous occurrences of significant spalling in the test. Author

N83-27994*# National Aeronautics and Space Administration. Lewis Research Center, Cleveland, Ohio.
ADVANTAGE OF RESONANT POWER CONVERSION IN AEROSPACE APPLICATIONS
I. G. HANSEN May 1983 8 p refs
(NASA-TM-83399; E-1676; NAS 1.15:83399) Avail: NTIS HC A02/MF A01 CSCL 21E

An ultrasonic, sinusoidal aerospace power distribution system is shown to have many advantages over other candidate power systems. These advantages include light weight, ease of fault clearing, versatility in handling many loads including motors, and the capability of production within the limits of present technology. References are cited that demonstrate the state of resonant converter technology and support these conclusions. Author

N83-27995*# National Aeronautics and Space Administration. Lewis Research Center, Cleveland, Ohio.
A VARIABLE-GEOMETRY COMBUSTOR USED TO STUDY PRIMARY AND SECONDARY ZONE STOICHIOMETRY
D. BRIEHL, D. F. SCHULTZ, and R. C. EHLERS 1983 15 p refs Proposed for presentation at the Joint Power Generation Conf., Indianapolis, 25-29 Sep. 1983; sponsored by ASME
(NASA-TM-83372; E-1640; NAS 1.15:83372) Avail: NTIS HC A02/MF A01 CSCL 21E

A combustion program is underway to evaluate fuel quality effects on gas turbine combustors. A rich-lean variable geometry combustor design was chosen to evaluate fuel quality effects over a wide range of primary and secondary zone equivalence ratios at simulated engine operating conditions. The first task of this effort, was to evaluate the performance of the variable geometry combustor. The combustor incorporates three stations of variable geometry to control primary and secondary zone equivalence ratio and overall pressure loss. Geometry changes could be made while a test was in progress through the use of remote control actuators. The primary zone liner was water cooled to eliminate the concern of liner durability. Emissions and performance data were obtained at simulated engine conditions of 80 percent and full power. Inlet air temperature varied from 611 to 665K, inlet total pressure varied from 1.02 to 1.24 MPa, reference velocity was a constant 1400 K. Author

N83-27996*# Detroit Diesel Allison, Indianapolis, Ind.
ROTORCRAFT CONVERTIBLE ENGINE STUDY Final Report, 11 Dec. 1980 - 31 Mar. 1982
J. C. GILL, R. V. EARLE, and H. M. MAR Sep. 1982 114 p refs
(Contract NAS3-22742)
(NASA-CR-168161; NAS 1.26:168161; DDA-EDR-10978) Avail: NTIS HC A06/MF A01 CSCL 21E

The objective of the Rotorcraft Convertible Engine Study was to define future research and technology effort required for commercial development by 1988 of convertible fan/shaft gas turbine engines for unconventional rotorcraft transports. Two rotorcraft and their respective missions were defined: a Fold Tilt Rotor aircraft and an Advancing Blade Concept (ABC) rotorcraft. Sensitivity studies were conducted with these rotorcraft to determine parametrically the influence of propulsion characteristics on aircraft size, mission fuel requirements, and direct operating costs (DOC). The two rotorcraft were flown with conventional propulsion systems (separate lift/cruise engines) and with convertible propulsion systems to determine the benefits to be derived from convertible engines. Trade-off studies were conducted to determine the optimum engine cycle and staging arrangement for a convertible engine. Advanced technology options applicable

to convertible engines were studied. Research and technology programs were identified which would ensure technology readiness for commercial development of convertible engines by 1988.
Author

N83-29208*# National Aeronautics and Space Administration. Lewis Research Center, Cleveland, Ohio.
COMBUSTION FUNDAMENTALS RESEARCH
Washington Mar. 1983 252 p refs Proc. of conf. held in Cleveland, 21-22 Oct. 1982
(NASA-CP-2268; E-1525; NAS 1.55:2268) Avail: NTIS HC A12/MF A01 CSCL 21E

Increased emphasis is placed on fundamental and generic research at Lewis Research Center with less systems development efforts. This is especially true in combustion research, where the study of combustion fundamentals has grown significantly in order to better address the perceived long term technical needs of the aerospace industry. The main thrusts for this combustion fundamentals program area are as follows: analytical models of combustion processes, model verification experiments, fundamental combustion experiments, and advanced numeric techniques.

N83-29211*# Pennsylvania State Univ., University Park. Dept. of Mechanical Engineering.
STRUCTURE OF EVAPORATING AND COMBUSTING SPRAYS: MEASUREMENTS AND PREDICTIONS
J. S. SHUEN, A. S. P. SOLOMON, and G. M. FAETH *In* NASA. Lewis Research Center Combust. Fundamentals Res. p 13-28 Mar. 1983 refs
(Contract NAG3-190)
Avail: NTIS HC A12/MF A01 CSCL 21E

Complete measurements of the structure of nonevaporating, evaporating and combusting sprays for sufficiently well defined boundary conditions to allow evaluation of models of these processes were obtained. The development of rational design methods for aircraft combustion chambers and other devices involving spray combustion were investigated. Three methods for treating the discrete phase are being considered: a locally homogeneous flow (LHF) model, a deterministic separated flow (DSF) model, and a stochastic separated flow (SSF) model. The main properties of these models are summarized. Author

N83-29212*# National Aeronautics and Space Administration. Lewis Research Center, Cleveland, Ohio.
FUEL SPRAY DIAGNOSTICS
F. M. HUMENIK and M. A. BOSQUE *In its* Combust. Fundamentals Res. p 29-38 Mar. 1983 refs
Avail: NTIS HC A12/MF A01 CSCL 21E

Fundamental experimental data base for turbulent flow mixing models is provided and better prediction of the more complex turbulent chemical reacting flows. Analytical application to combustor design is provided and a better fundamental understanding of the combustion process. Author

N83-29219*# National Aeronautics and Space Administration. Lewis Research Center, Cleveland, Ohio.
ANALYTICAL CALCULATION OF A SINGLE JET IN CROSS-FLOW AND COMPARISON WITH EXPERIMENT
R. W. CLAUS *In its* Combust. Fundamentals Res. p 93-100 Mar. 1983 refs
Avail: NTIS HC A12/MF A01 CSCL 21E

A series of progressively finer grid systems to calculate the single jet in cross-flow experimentally measured were employed. The experimental measurements provide a collection of velocities, turbulence intensities, and jet concentration profiles with measurements of the inlet field. The use of a series of progressively finer grid systems allows a differentiation between numerical errors and the hydrodynamic modeling assumptions embodied in the 3D combustor code. E.A.K.

N83-29221*# Detroit Diesel Allison, Indianapolis, Ind.
SMALL GAS TURBINE COMBUSTOR PRIMARY ZONE STUDY
R. E. SULLIVAN and R. D. SUTTON *In* NASA. Lewis Research Center Combust. Fundamentals Res. p 119-130 Mar. 1983
(Contract NAS3-22762)
Avail: NTIS HC A12/MF A01 CSCL 21E

The combustion research program, small gas turbine combustor primary zone study is summarized. The basic elements of a design methodology program to obtain the maximum performance potential of small reverse-flow annular combustors is described. Three preferred combustion design approaches for internal flame stabilization patterns were selected. Design features are incorporated in the combustors to address the performance limiting problem areas associated with smaller annular combustors. Performance is predicted by using a 3-D aerodynamic/chemical kinetic elliptic flow analysis, initially developed by Garrett Corporation for the USARTL. It is shown that the analytical flow field predictive models provide a useful design tool for understanding the combustion performance of a small reverse flow annular combustor. E.A.K.

N83-29234*# Naval Air Propulsion Test Center, Trenton, N.J.
ROTOR FRAGMENT PROTECTION PROGRAM: STATISTICS ON AIRCRAFT GAS TURBINE ENGINE ROTOR FAILURES THAT OCCURRED IN US COMMERCIAL AVIATION DURING 1979 Final Report
R. A. DELUCIA and J. T. SALVINO Oct. 1982 29 p
(Contract NASA ORDER C-41581-B)
(NASA-CR-168163; NAS 1.26:168163; NAPC-PE-80; AD-A130463) Avail: NTIS HC A03/MF A01 CSCL 21E

Statistical information relating to the number of gas turbine engine rotor failures which occurred during 1979 in commercial aviation service use is provided. The predominant failure mode involved blade fragments, 84 percent of which were contained. No uncontained disk failures occurred and although fewer rotor rim and seal failures occurred, 100 percent and 50 percent, respectively, were uncontained. Sixty-eight percent of the 157 rotor failures occurred during the take-off and climb stages of flight.
Author

N83-29235*# National Aeronautics and Space Administration. Lewis Research Center, Cleveland, Ohio.
MULTI-FUEL ROTARY ENGINE FOR GENERAL AVIATION AIRCRAFT
C. JONES (Curtiss-Wright Corp., Woodridge, N.J.), D. R. ELLIS (Cessna Aircraft Co., Wichita, Kans.), and P. R. MENG 1983 47 p refs Presented at the 19th Joint Propulsion Conf., Seattle, 27-29 Jun. 1983; sponsored by AIAA, SAE, and ASME
(NASA-TM-83429; E-1718; NAS 1.15:83429; AIAA-83-1340)
Avail: NTIS HC A03/MF A01 CSCL 21E

Design studies of advanced multifuel general aviation and commuter aircraft rotary stratified charge engines are summarized. Conceptual design studies were performed at two levels of technology, on advanced general aviation engines sized to provide 186/250 shaft kW/hp under cruise conditions at 7620 (25000 m/ft) altitude. A follow on study extended the results to larger (2500 hp max.) engine sizes suitable for applications such as commuter transports and helicopters. The study engine designs were derived from relevant engine development background including both prior and recent engine test results using direct injected unthrottled rotary engine technology. Aircraft studies, using these resultant growth engines, define anticipated system effects of the performance and power density improvements for both single engine and twin engine airplanes. The calculated results indicate superior system performance and 27 to 33 percent fuel economy improvement for the rotary engine airplanes as compared to equivalent airframe concept designs with current baseline engines. The research and technology activities required to attain the projected engine performance levels are also discussed. S.L.

N83-29236*# National Aeronautics and Space Administration. Lewis Research Center, Cleveland, Ohio.
THE NASA BROAD-SPECIFICATION FUELS COMBUSTION TECHNOLOGY PROGRAM: AN ASSESSMENT OF PHASE 1 TEST RESULTS
J. S. FEAR 1983 13 p refs Presented at the Joint Power Generation Conf., Indianapolis, 25-29 Sep. 1983; sponsored by ASME
(NASA-TM-83447; E-1753; NAS 1.15:83447) Avail: NTIS HC A02/MF A01 CSCL 21E

An assessment is made of the results of Phase 1 screening testing of current and advanced combustion system concepts using several broadened-properties fuels. The severity of each of several fuels-properties effects on combustor performance or liner life is discussed, as well as design techniques with the potential to offset these adverse effects. The selection of concepts to be pursued in Phase 2 refinement testing is described. This selection takes into account the relative costs and complexities of the concepts, the current outlook on pollutant emissions control, and practical operational problems. Author

N83-29237*# National Aeronautics and Space Administration. Lewis Research Center, Cleveland, Ohio.
PARAMETRIC STUDY OF FLAME RADIATION CHARACTERISTICS OF A TUBULAR-CAN COMBUSTOR
F. M. HUMENIK, R. W. CLAUS, and G. M. NEELY 1983 13 p refs Proposed for presentation at the Joint Power Generation Conf., Indianapolis, 25-29 Sep. 1983; sponsored by ASME
(NASA-TM-83436; E-1731; NAS 1.15:83436) Avail: NTIS HC A02/MF A01 CSCL 21E

A series of combustor tests were conducted with a tubular-can combustor to study flame radiation characteristics and effects with parametric variations in combustor operating conditions. Two alternate combustor assemblies using a different fuel nozzle were compared. Spectral and total radiation detectors were positioned at three stations along the length of the combustor can. Data were obtained for a range of pressures from 0.34 to 2.07 MPa (50 to 300 psia), inlet temperatures from 533 to 700K (500 to 800 F), for Jet A (13.9 deg hydrogen) and ERBS (12.9% hydrogen) fuels, and with fuel-air ratios nominally from 0.008 to 0.021. Spectral radiation data, total radiant heat flux data, and liner temperature data are presented to illustrate the flame radiation characteristics and effects in the primary, secondary, and tertiary combustion zones. Author

N83-30427*# United Technologies Corp., East Hartford, Conn. Commercial Products Div.
ENERGY EFFICIENT ENGINE LOW-PRESSURE COMPRESSOR COMPONENT TEST HARDWARE DETAILED DESIGN REPORT
C. J. MICHAEL and J. E. HALLE Jun. 1981 80 p refs
(Contract NAS3-20646)
(NASA-CR-165354; NAS 1.26:165354; PWA-5594-157) Avail: NTIS HC A05/MF A01 CSCL 01E

The aerodynamic and mechanical design description of the low pressure compressor component of the Energy Efficient Engine were used. The component was designed to meet the requirements of the Flight Propulsion System while maintaining a low cost approach in providing a low pressure compressor design for the Integrated Core/Low Spool test required in the Energy Efficient Engine Program. The resulting low pressure compressor component design meets or exceeds all design goals with the exception of surge margin. In addition, the expense of hardware fabrication for the Integrated Core/Low Spool test has been minimized through the use of existing minor part hardware. Author

N83-30429*# Pratt and Whitney Aircraft Group, East Hartford, Conn.
ENERGY EFFICIENT ENGINE HIGH-PRESSURE TURBINE SINGLE CRYSTAL VANE AND BLADE FABRICATION TECHNOLOGY REPORT
A. F. GIAMEI, R. W. SALKELD, and C. W. HAYES Jul. 1981 112 p refs
(Contract NAS3-20646)
(NASA-CR-165400; NAS 1.26:165400; PWA-5594-152) Avail: NTIS HC A02/MF A01 CSCL 21E

The objective of the High-Pressure Turbine Fabrication Program was to demonstrate the application and feasibility of Pratt & Whitney Aircraft-developed two-piece, single crystal casting and bonding technology on the turbine blade and vane configurations required for the high-pressure turbine in the Energy Efficient Engine. During the first phase of the program, casting feasibility was demonstrated. Several blade and vane halves were made for the bonding trials, plus solid blades and vanes were successfully cast for materials evaluation tests. Specimens exhibited the required microstructure and chemical composition. Bonding feasibility was demonstrated in the second phase of the effort. Bonding yields of 75 percent for the vane and 30 percent for the blade were achieved, and methods for improving these yield percentages were identified. A bond process was established for PWA 1480 single crystal material which incorporated a transient liquid phase interlayer. Bond properties were substantiated and sensitivities determined. Tooling die materials were identified, and an advanced differential thermal expansion tooling concept was incorporated into the bond process. Author

N83-30430*# National Aeronautics and Space Administration. Lewis Research Center, Cleveland, Ohio. Aircraft Engine Business Group.
ENERGY EFFICIENT ENGINE. CORE ENGINE BEARINGS, DRIVES AND CONFIGURATION: DETAILED DESIGN REPORT
C. L. BROMAN Jun. 1981 61 p refs
(Contract NAS3-20643)
(NASA-CR-165376; NAS 1.26:165376; R81AEG307) Avail: NTIS HC A04/MF A01 CSCL 21E

The detailed design of the forward and aft sumps, the accessory drive system, the lubrication system, and the piping/manifold configuration to be employed in the core engine test of the Energy Efficient Engine is addressed. The design goals for the above components were established based on the requirements of the test cell engine. Author

N83-30431*# National Aeronautics and Space Administration. Lewis Research Center, Cleveland, Ohio.
INCIDENCE LOSS FOR FAN TURBINE ROTOR BLADE IN TWO-DIMENSIONAL CASCADE
J. F. KLINE, T. P. MOFFITT, and R. G. STABE Jul. 1983 11 p refs
(NASA-TP-2188; E-1587; NAS 1.60:2188) Avail: NTIS HC A02/MF A01 CSCL 21E

The effect of incidence angle on the aerodynamic performance of a fan turbine rotor blade was investigated experimentally in a two dimensional cascade. The test covered a range of incidence angles from -15 deg to 10 deg and exit ideal critical velocity ratios from 0.75 to 0.95. The principal measurements were blade-surface static pressures and cross-channel survey of exit total pressure, static pressure, and flow angle. Flow adjacent to surfaces was examined using a visualization technique. The results of the investigation include blade-surface velocity distribution and overall kinetic energy loss coefficients for the incidence angles and exit velocity ratios tested. The measured losses are compared with those from a reference core turbine rotor blade and also with two common analytical methods of predicting incidence loss. Author

N83-30432*# Garrett Turbine Engine Co., Phoenix, Ariz.
SCALED CENTRIFUGAL COMPRESSOR, COLLECTOR AND RUNNING GEAR PROGRAM Final Report
J. G. KENEHAN 31 Mar. 1983 97 p refs
(Contract NAS3-22431)
(NASA-CR-168167; NAS 1.26:168167; GR-21-4269) Avail: NTIS HC A05/MF A01 CSCL 21E

The Scaled Centrifugal Compressor, Collector and Running gear Program was conducted in support of an overall NASA strategy to improve small-compressor performance, durability, and reliability while reducing initial and life-cycle costs. Accordingly, Garrett designed and provided a test rig, gearbox coupling, and facility collector for a new NASA facility, and provided a scaled model of an existing, high-performance impeller for evaluation scaling effects on aerodynamic performance and for obtaining other performance data. Test-rig shafting was designed to operate smoothly throughout a speed range up to 60,000 rpm. Pressurized components were designed to operate at pressures up to 300 psia and at temperatures to 1000 F. Nonrotating components were designed to provide a margin-of-safety of 0.05 or greater; rotating components, for a margin-of-safety based on allowable yield and ultimate strengths. Design activities were supported by complete design analysis, and the finished hardware was subjected to check-runs to confirm proper operation. The test rig will support a wide range of compressor tests and evaluations. Author

N83-31603* National Aeronautics and Space Administration. Lewis Research Center, Cleveland, Ohio.
CONTROL MEANS FOR A GAS TURBINE ENGINE Patent
R. S. BEITLER (General Electric Co., Cincinnati), F. J. SELLERS (General Electric Co., Cincinnati), and G. W. BENNETT, Inventors (to NASA) (General Electric Co., Cincinnati) 6 Jul. 1983 10 p Filed 26 Jun. 1980
(NASA-CASE-LEW-14586-1; US-PATENT-4,338,061; US-PATENT-APPL-SN-163122; US-PATENT-CLASS-415-1; US-PATENT-CLASS-415-47; US-PATENT-CLASS-415-175; US-PATENT-CLASS-415-178) Avail: US Patent and Trademark Office CSCL 21E

A means is provided for developing a signal representative of the actual compressor casing temperature, a second signal representative of compressor inlet gas temperature, and a third signal representative of compressor speed. Another means is provided for receiving the gas temperature and compressor speed signals and developing a schedule output signal which is a representative of a reference casing temperature at which a predetermined compressor blade stabilized clearance is provided. A means is also provided for comparing the actual compressor casing temperature signal and the reference casing temperature signal and developing a clearance control system representative of the difference. The clearance control signal is coupled to a control valve which controls a flow of air to the compressor casing to control the clearance between the compressor blades and the compressor casing. The clearance control signal can be modified to accommodate transient characteristics. Other embodiments are disclosed.
Official Gazette of the U.S. Patent and Trademark Office

N83-32804*# General Electric Co., Evendale, Ohio. Aircraft Engine Business Group.
V/STOL PROPULSION CONTROL ANALYSIS: PHASE 2, TASK 5-9
Nov. 1981 152 p refs
(Contract NAS3-22057)
(NASA-CR-165523; NAS 1.26:165523; R81AEG759) Avail: NTIS HC A08/MF A01 CSCL 21E

Typical V/STOL propulsion control requirements were derived for transition between vertical and horizontal flight using the General Electric RALS (Remote Augmented Lift System) concept. Steady-state operating requirements were defined for a typical Vertical-to-Horizontal transition and for a typical Horizontal-to-Vertical transition. Control mode requirements were established and multi-variable regulators developed for individual operating conditions. Proportional/Integral gain schedules were developed and were incorporated into a transition controller with capabilities for mode switching and manipulated variable reassignment. A non-linear component-level transient model of the engine was developed and utilized to provide a preliminary check-out of the controller logic. An inlet and nozzle effects model was developed for subsequent incorporation into the engine model and an aircraft model was developed for preliminary flight transition simulations. A condition monitoring development plan was developed and preliminary design requirements established. The Phase 1 long-range technology plan was refined and restructured toward the development of a real-time high fidelity transient model of a supersonic V/STOL propulsion system and controller for use in a piloted simulation program at NASA-Ames. Author

N83-32806*# National Aeronautics and Space Administration. Langley Research Center, Hampton, Va.
MODELING INTERFACE MOTION OF COMBUSTION (MINOC). A COMPUTER CODE FOR TWO-DIMENSIONAL, UNSTEADY TURBULENT COMBUSTION
A. F. GHONEIM (California Univ., Berkeley), C. J. MAREK, and A. K. OPPENHEIM (California Univ., Berkeley) Aug. 1983 19 p refs
(Contract NAG3-313)
(NASA-TP-2132; E-1569; NAS 1.60:2132) Avail: NTIS HC A02/MF A01 CSCL 21E

A computer code for calculating the flow field and flame propagation in a turbulent combustion tunnel is described. The model used in the analysis is the random vortex model, which allows the turbulent field to evolve as a fundamental solution to the Navier-Stokes equations without averaging or closure modeling. The program was used to study the flow field in a model combustor, formed by a rearward-facing step in a channel, in terms of the vorticity field, the turbulent shear stresses, the flame contours, and the concentration field. Results for the vorticity field reveal the formation of large-scale eddy structures in the turbulent flow downstream from the step. The concentration field contours indicate that most burning occurred around the outer edges of the large eddies of the shear layer. S.L.

N83-32807*# National Aeronautics and Space Administration. Lewis Research Center, Cleveland, Ohio.
COMPUTER CODE FOR OFF-DESIGN PERFORMANCE ANALYSIS OF RADIAL-INFLOW TURBINES WITH ROTOR BLADE SWEEP
P. L. MEITNER (Army Aviation Research and Development Command, St. Louis, Mo.) and A. J. GLASSMAN Aug. 1983 26 p refs
(NASA-TP-2199; NAS 1.60:2199; AVRADCOM-TR-83-C-4) Avail: NTIS HC A03/MF A01 CSCL 21E

The analysis procedure of an existing computer program was extended to include rotor blade sweep, to model the flow more accurately at the rotor exit, and to provide more detail to the loss model. The modeling changes are described and all analysis equations and procedures are presented. Program input and output are described and are illustrated by an example problem. Results obtained from this program and from a previous program are compared with experimental data. Author

N83-32808*# Oklahoma State Univ., Stillwater.
AXIAL VANE-TYPE SWIRLER PERFORMANCE CHARACTERISTICS M.S. Thesis
G. F. SANDER Jul. 1983 120 p refs
(Contract NAG3-74)
(NASA-CR-172995; NAS 1.26:172995) Avail: NTIS HC A06/MF A01 CSCL 21E

The performance of an axial vane-type swirler was investigated to aid in computer modeling of gas turbine combustor flowfields and in evaluation of turbulence models for swirling confined jet flow. The swirler studied is annular with a hub-to-swirler diameter ratio of 0.25 and ten adjustable vanes of pitch-to-chord ratio 0.68. Measurements of time-mean axial, radial, and tangential velocities were made at the swirler exit plane using a five-hole pitot probe technique with computer data reduction. Nondimensionalized

velocities from both radial and azimuthal traverses are tabulated and plotted for a range of swirl vane angles phi from 0 to 70 degrees. A study was done of idealized exit-plane velocity profiles relating the swirl numbers S and S' to the ratio of maximum swirl and axial velocities for each idealized case, and comparing the idealized swirl numbers with ones calculated from measured profiles. Author

N83-32810*# National Aeronautics and Space Administration. Lewis Research Center, Cleveland, Ohio.
PROPELLER PERFORMANCE AND WEIGHT PREDICTIONS APPENDED TO THE NAVY/NASA ENGINE PROGRAM
R. M. PLENCNER, P. SENTY, and T. J. WICKENHEISER Jul. 1983 41 p refs
(NASA-TM-83458; E-1773; NAS 1.15:83458) Avail: NTIS HC A03/MF A01 CSCL 21E

The Navy/NASA Engine Performance (NNEP) is a general purpose computer program currently employed by government, industry and university personnel to simulate the thermodynamic cycles of turbine engines. NNEP is a modular program which has the ability to evaluate the performance of an arbitrary engine configuration defined by the user. In 1979, a program to calculate engine weight (WATE-2) was developed by Boeing's Military Division under NASA contract. This program uses a preliminary design approach to determine engine weights and dimensions. Because the thermodynamic and configuration information required by the weight code was available in NNEP, the weight code was appended to NNEP. Due to increased emphasis on fuel economy, a renewed interest has developed in propellers. This report describes the modifications developed by NASA to both NNEP and WATE-2 to determine the performance, weight and dimensions of propellers and the corresponding gearbox. The propeller performance model has three options, two of which are based on propeller map interpolation. Propeller and gearbox weights are obtained from empirical equations which may easily be modified by the user. Author

N83-32811*# National Aeronautics and Space Administration. Lewis Research Center, Cleveland, Ohio.
CURRENT AND FUTURE TECHNOLOGY IN RADIAL AND AXIAL GAS TURBINES
H. E. ROHLIK 27 Aug. 1983 45 p refs Presented at Seminar on Fluid Dyn. of Turbomachinery, Ames, Iowa, 18-27 Jul. 1983; sponsored by ASME
(NASA-TM-83414; E-1702; NAS 1.15:83414) Avail: NTIS HC A03/MF A01 CSCL 21E

Design approaches and flow analysis techniques currently employed by aircraft engine manufacturers are assessed. Studies were performed to define the characteristics of aircraft and engines for civil missions of the 1990's and beyond. These studies, coupled with experience in recent years, identified the critical technologies needed to meet long range goals in fuel economy and other operating costs. Study results, recent and current research and development programs, and an estimate of future design and analytic capabilities are discussed. Author

N83-33893*# National Aeronautics and Space Administration. Lewis Research Center, Cleveland, Ohio.
PRELIMINARY TESTS OF AN ADVANCED HIGH-TEMPERATURE COMBUSTION SYSTEM
J. D. WEAR, A. M. TROUT, J. M. SMITH, and R. E. JACOBS Sep. 1983 33 p refs
(NASA-TP-2203; E-1633; NAS 1.60:2203) Avail: NTIS HC A03/MF A01 CSCL 21E

A combustion system has been developed to operate efficiently and with good durability at inlet pressures to 4.05 MPa (40 atm), inlet air temperatures to 900 K, and exhaust gas temperatures to 2480 K. A preliminary investigation of this system was conducted at inlet pressures to 0.94 MPa (9 atm), a nominal inlet air temperature of 560 K, and exhaust gas temperatures to 2135 K. A maximum combustion efficiency of 98.5 percent was attained at a fuel-air ratio of 0.033; the combustion efficiency decreased to about 90 percent as the fuel-air ratio was increased to 0.058. An average liner metal temperature of 915 K, 355 kelvins greater than the nominal inlet air temperature, was reached with an average exhaust gas temperature of 2090 K. The maximum local metal temperature at this condition was about 565 kelvins above the nominal inlet air temperature and decreased to 505 kelvins above with increasing combustor pressure. Tests to determine the isothermal total pressure loss of the combustor showed a liner loss of 1.1 percent and a system loss of 6.5 percent. Author

N83-33894*# Mechanical Technology, Inc., Latham, N. Y.
T55 POWER TURBINE ROTOR MULTIPLANE-MULTISPEED BALANCING STUDY
M. R. MARTIN Feb. 1982 118 p refs
(Contract NAS3-19408)
(NASA-CR-167691; NAS 1.26:167891; MTI-83TR55) Avail: NTIS HC A06/MF A01 CSCL 21E

A rotordynamic analysis of the T55-L-11C engine was used to evaluate the balancing needs of the power turbine and to optimize the balancing procedure. As a result, recommendations were made for implementation of a multiplane-multispeed balancing plan. Precision collars for the attachment of trial weights to a slender rotor were designed enabling demonstration balancing on production hardware. The quality of the balance was then evaluated by installing a high speed balanced power turbine in an engine and running in a test cell at the Corpus Christi Army depot. The engine used had been tested prior to the turbine changeout and showed acceptable overall vibration levels for the engine were significantly reduced, demonstrating the ability of multiplane-multispeed balancing to control engine vibration. Author

N83-34941*# National Aeronautics and Space Administration. Lewis Research Center, Cleveland, Ohio.
EFFECTS OF PERCENTAGE OF BLOCKAGE AND FLAMEHOLDER DOWNSTREAM COUNTERBORES ON LEAN COMBUSTION LIMITS OF PREMIXED, PREVAPORIZED PROPANE-AIR MIXTURE
M. A. B. FERNANDEZ Sep. 1983 11 p refs
(NASA-TP-2227; E-1588; NAS 1.60:2227) Avail: NTIS HC A02/MF A01 CSCL 21E

Lean combustion limits were determined for a premixed prevaporized propane air mixture with flat plate flame stabilizers. Experiments were conducted in a constant area flame tube combustor utilizing flameholders of varying percentages of blockage and downstream counterbores. Combustor inlet air velocity at ambient conditions was varied from 4 to 9 meters per second. Flameholders with a center hole and four half holes surrounding it were tested with 63, 73, and 85 percent blockage and counterbore diameters of 112 and 125 percent of the thru hole diameter, in addition to the no counterbore configuration. Improved stability was obtained by using counterbore flameholders and higher percentages of blockage. Increases in mixture velocity caused the equivalence ratio at blowout to increase in all cases. Author

N83-34942*# National Aeronautics and Space Administration. Lewis Research Center, Cleveland, Ohio.
STUDY OF LH2-FUELED TOPPING CYCLE ENGINE FOR AIRCRAFT PROPULSION
G. E. TURNEY and L. H. FISHBACH 1983 21 p refs Presented at the Aircraft Design Systems and Operations Meeting, Fort Worth, Tex., 17-19 Oct. 1983; sponsored by AIAA and AHS
(NASA-TM-83466; E-1735; NAS 1.15:83466) Avail: NTIS HC A02/MF A01 CSCL 21E

An analytical investigation was made of a topping cycle aircraft engine system which uses a cryogenic fuel. This system consists of a main turboshaft engine which is mechanically coupled (by cross-shafting) to a topping loop which augments the shaft power output of the system. The thermodynamic performance of the topping cycle engine was analyzed and compared with that of a reference (conventional-type) turboshaft engine. For the cycle operating conditions selected, the performance of the topping cycle engine in terms of brake specific fuel consumption (bsfc) was determined to be about 12 percent better than that of the reference

turboshaft engine. Engine weights were estimated for both the topping cycle engine and the reference turboshaft engine. These estimates were based on a common shaft power output for each engine. Results indicate that the weight of the topping cycle engine is comparable to that of the reference turboshaft engine. Author

N83-34943*# National Aeronautics and Space Administration. Lewis Research Center, Cleveland, Ohio.
DETAILED FUEL SPRAY ANALYSIS TECHNIQUES
E. J. MULARZ, M. A. BOSQUE, and F. M. HUMENIK 1983 23 p refs Presented at the 62nd Symp. of the Propulsion and Energetics Panel on Combust. Probl. in Turbine Eng., Cesme, Turkey, 3-6 Oct. 1983; sponsored by AGARD Prepared in cooperation with Army Research and Technology Labs., Cleveland
(NASA-TM-83476; E-1792; NAS 1.15:83476; AVRADCOM-TR-83-C-7) Avail: NTIS HC A02/MF A01 CSCL 21E

Detailed fuel spray analyses are a necessary input to the analytical modeling of the complex mixing and combustion processes which occur in advanced combustor systems. It is anticipated that by controlling fuel-air reaction conditions, combustor temperatures can be better controlled, leading to improved combustion system durability. Thus, a research program is underway to demonstrate the capability to measure liquid droplet size, velocity, and number density throughout a fuel spray and to utilize this measurement technique in laboratory benchmark experiments. The research activities from two contracts and one grant are described with results to data. The experiment to characterize fuel sprays is also described. These experiments and data should be useful for application to and validation of turbulent flow modeling to improve the design systems of future advanced technology engines. Author

N83-34944*# General Electric Co., Lynn, Mass. Aircraft Engine Business Group.
ROTORCRAFT CONVERTIBLE ENGINE STUDY Final Report
D. N. GOLDSTEIN, R. HIRSCHKRON, and C. E. SMITH Aug. 1983 211 p refs
(Contract NAS3-22743)
(NASA-CR-168241; NAS 1.26:168241; R83AEB047) Avail: NTIS HC A10/MF A01 CSCL 21E

Convertible propulsion systems for advanced rotorcraft are evaluated in terms of their impact on aircraft operating economics and fuel consumption. A variety of propulsion system concepts, including separate thrust and power producing engines, convertible fan/shaft engines, and auxiliary propeller configurations are presented. The merits of each are evaluated in two different rotorcraft missions: an intercity, commercial transport of the ABC(TM) type, and an offshore oil ring supply ship of the X-wing type. The variable inlet guide vane fan/shaft converting engine and auxiliary propeller configurations are shown to offer significant advantages over all the other systems evaluated, in terms of both direct operating cost and fuel consumption. S.L.

N83-34945*# National Aeronautics and Space Administration. Lewis Research Center, Cleveland, Ohio.
EFFECTS OF WIND ON TURBOFAN ENGINES IN OUTDOOR STATIC TEST STANDS
J. G. MCARDLE and A. S. MOORE 1983 15 p refs Presented at the 2nd Flight Testing Conf., Las Vegas, Nev., 16-18 Nov. 1983; sponsored by the AIAA, AHS, IES, SETP and SFTE
(NASA-TM-83493; E-1824; NAS 1.15:83493) Avail: NTIS HC A02/MF A01 CSCL 21E

Wind can affect measured thrust and can cause turbofan engine speed to fluctuate during outdoor testing. Techniques used at an outdoor test stand at NASA Lewis Research Center to make testing easier and faster and to improve data repeatability include using an inflow control device (ICD) to make fan speed steadier, taking many raw data samples for better averaging, and correcting thrust for wind direction and speed. Data from engine tests are presented to show that the techniques improve repeatability of thrust and airflow measurements under various wind conditions. Author

N83-34946*# National Aeronautics and Space Administration. Lewis Research Center, Cleveland, Ohio.
USE OF COOLING AIR HEAT EXCHANGERS AS REPLACEMENTS FOR HOT SECTION STRATEGIC MATERIALS
J. W. GAUNTNER 19 Oct. 1983 11 p refs Presented at Aircraft Design Systems and Operations Meeting, 17-19 Oct. 1983; sponsored by AIAA and AHS
(NASA-TM-83494; E-1827; NAS 1.15:83494) Avail: NTIS HC A02/MF A01 CSCL 21E

Because of financial and political constraints, strategic aerospace materials required for the hot section of future engines might be in short supply. As an alternative to these strategic materials, this study examines the use of a cooling air heat exchanger in combination with less advanced hot section materials. Cycle calculations are presented for future turbofan systems with overall pressure ratios to 65, bypass ratios near 13, and combustor exit temperatures to 3260 R. These calculations quantify the effect on TSFC of using a decreased materials technology in a turbofan system. The calculations show that the cooling air heat exchanger enables the feasibility of these engines. Author

N83-34947*# National Aeronautics and Space Administration. Lewis Research Center, Cleveland, Ohio.
SUPERSONIC FAN ENGINES FOR MILITARY AIRCRAFT
L. C. FRANCISCUS 19 Oct. 1983 12 p refs Presented at Aircraft Design Systems and Operations Meeting, Fort Worth, Tex., 17-19 Oct. 1983; sponsored by AIAA and AHS
(NASA-TM-83499; E-1833; NAS 1.15:83499) Avail: NTIS HC A02/MF A01 CSCL 21E

Engine performance and mission studies were performed for turbofan engines with supersonic through-flow fans. A Mach 2.4 CTOL aircraft was used in the study. Two missions were considered: a long range penetrator mission and a long range intercept mission. The supersonic fan engine is compared with an augmented mixed flow turbofan in terms of mission radius for a fixed takeoff gross weight of 75,000 lbm. The mission radius of aircraft powered by supersonic fan engines could be 15 percent longer than aircraft powered with conventional turbofan engines at moderate thrust to gross weight ratios. The climb and acceleration performance of the supersonic fan engines is better than that of the conventional turbofan engines. Author

N83-34948*# National Aeronautics and Space Administration. Lewis Research Center, Cleveland, Ohio.
HIGH-PRESSURE FLAME VISUALIZATION OF AUTOIGNITION AND FLASHBACK PHENOMENA WITH LIQUID-FUEL SPRAY
C. J. MAREK and C. E. BAKER 18 Oct. 1983 18 p refs Presented at Western States Sec. Fall Meeting, 17-18 Oct. 1983; sponsored by the Combustion Inst., Los Angeles
(NASA-TM-83501; E-1840; NAS 1.15:83501) Avail: NTIS HC A02/MF A01 CSCL 21E

A study was undertaken to determine the effect of boundary layers on autoignition and flashback for premixed Jet-A fuel in a unique high-pressure windowed test facility. A plate was placed in the center of the fuel-air stream to establish a boundary layer. Four experimental configurations were tested: a 24.5-cm-long plate with either a pointed leading edge, a rounded edge or an edge with a 0.317-cm step, or the duct without the plate. Experiments at an equivalence ratio ranging from 0.4 to 0.9 were performed at pressures to 2500 kPa (25 atm.) at temperatures of 600, 645, and 700 K and velocities to 115 meters per second. Flame shapes were observed during flashback and autoignition using high speed cinematography. Flashback and autoignition limits were determined. Author

N83-36029* National Aeronautics and Space Administration. Lewis Research Center, Cleveland, Ohio.
APPARATUS FOR IMPROVING THE FUEL EFFICIENCY OF A GAS TURBINE ENGINE Patent
G. A. COFFINBERRY, inventor (to NASA) (GE, Cincinnati) 20 Sep. 1983 7 p Filed 20 Mar. 1980 Supersedes N83-14130 (21 - 05, p 0622) Sponsored by NASA
(NASA-CASE-LEW-13142-1; US-PATENT-4,404,793; US-PATENT-APPL-SN-132364; US-PATENT-CLASS-60-39.07)
Avail: US Patent and Trademark Office CSCL 21E

An energy recovery system is provided for an aircraft gas turbine engine of the type in which some of the pneumatic energy developed by the engine is made available to support systems such as an environmental control system. In one such energy recovery system, some of the pneumatic energy made available to but not utilized by the support system is utilized to heat the engine fuel immediately prior to the consumption of the fuel by the engine. Some of the recovered energy may also be utilized to heat the fuel in the fuel tanks. Provision is made for multiengine applications wherein energy recovered from one engine may be utilized by another one of the engines or systems associated therewith.
Official Gazette of the U.S. Patent and Trademark Office

N83-36031*# National Aeronautics and Space Administration. Lewis Research Center, Cleveland, Ohio.
MULTI-FUEL ROTARY ENGINE FOR GENERAL AVIATION AIRCRAFT
C. JONES (Curtiss-Wright Corp.), D. R. ELLIS (Cessna Aircraft Co.), and P. R. MENG 27 Jun. 1983 86 p refs
(NASA-TM-85428; NAS 1.15:85428) Avail: NTIS HC A05/MF A01 CSCL 21E

Design studies, conducted for NASA, of Advanced Multi-fuel General Aviation and Commuter Aircraft Rotary Stratified Charge Engines are summarized. Conceptual design studies of an advanced engine sized to provide 186/250 shaft KW/HP under cruise conditions at 7620/25,000 m/ft. altitude were performed. Relevant engine development background covering both prior and recent engine test results of the direct injected unthrottled rotary engine technology, including the capability to interchangeably operate on gasoline, diesel fuel, kerosene, or aviation jet fuel, are presented and related to growth predictions. Aircraft studies, using these resultant growth engines, define anticipated system effects of the performance and power density improvements for both single engine and twin engine airplanes. The calculated results indicate superior system performance and 30 to 35% fuel economy improvement for the Rotary-engine airplanes as compared to equivalent airframe concept designs with current baseline engines. The research and technology activities required to attain the projected engine performance levels are also discussed. Author

08

AIRCRAFT STABILITY AND CONTROL

Includes aircraft handling qualities; piloting; flight controls; and autopilots.

N83-30435*# Pratt and Whitney Aircraft Group, East Hartford, Conn. Commercial Products Div.
SUBSONIC-TRANSONIC STALL FLUTTER STUDY Final Report
H. STARDTER Jun. 1979 311 p refs
(Contract NAS3-20606)
(NASA-CR-165256; NAS 1.26:165256; PWA-5517-31) Avail: NTIS HC A14/MF A01 CSCL 01C

The objective of the Subsonic/Transonic Stall Flutter Program was to obtain detailed measurements of both the steady and unsteady flow field surrounding a rotor and the mechanical state of the rotor while it was operating in both steady and flutter modes to provide a basis for future analysis and for development of theories describing the flutter phenomenon. The program revealed that while all blades flutter at the same frequency, they do not flutter at the same amplitude, and their interblade phase angles are not equal. Such a pattern represents the superposition of a number of rotating nodal diameter patterns, each characterized by a different amplitude and different phase indexing, but each rotating at a speed that results in the same flutter frequency as seen in the rotor system. Review of the steady pressure contours indicated that flutter may alter the blade passage pressure distribution. The unsteady pressure amplitude contour maps reveal regions of high unsteady pressure amplitudes near the leading edge, lower amplitudes near the trailing. Author

09

RESEARCH AND SUPPORT FACILITIES (AIR)

Includes airports, hangars and runways; aircraft repair and overhaul facilities; wind tunnels; shock tube facilities; and engine test blocks.

A83-36353*# National Aeronautics and Space Administration. Lewis Research Center, Cleveland, Ohio.
NASA LOW-SPEED CENTRIFUGAL COMPRESSOR FOR FUNDAMENTAL RESEARCH
J. R. WOOD, P. W. ADAM, and A. E. BUGGELE (NASA, Lewis Research Center, Cleveland, OH) AIAA, SAE, and ASME, Joint Propulsion Conference, 19th, Seattle, WA, June 27-29, 1983. 12 p. refs
(AIAA PAPER 83-1351)

A new centrifugal compressor facility being built by the NASA Lewis Research Center is described; its purpose is to obtain 'benchmark' experimental data for internal flow code verification and modeling. The facility will be heavily instrumented with standard pressure and temperature probes and have provisions for flow visualization and laser Doppler velocimetry. The facility will accommodate rotational speeds to 2400 rpm and will be rated at pressures to 1.25 atm. The initial compressor stage for testing is geometrically and dynamically representative of modern high-performance stages with the exception of Mach number levels. Design exit tip speed for the initial stage is 500 ft/sec with a pressure ratio of 1.17. The rotor exit backsweep is 55 deg from radial. The facility is expected to be operational in the first half of 1985. Author

N83-14139*# Shaker Research Corp., Ballston Lake, N. Y.
DIGITAL SYSTEM FOR STRUCTURAL DYNAMICS SIMULATION Final Report
A. I. KRAUTER, L. J. LAGACE, M. K. WOJNAR, and C. GLOR Nov. 1982 125 p
(Contract NAS3-22546)
(NASA-CR-168019; NAS 1.26:168019; MTI-83TR12) Avail: NTIS HC A06/MF A01 CSCL 14B

State-of-the-art digital hardware and software for the simulation of complex structural dynamic interactions, such as those which occur in rotating structures (engine systems). System were incorporated in a designed to use an array of processors in which the computation for each physical subelement or functional subsystem would be assigned to a single specific processor in the simulator. These node processors are microprogrammed bit-slice microcomputers which function autonomously and can communicate with each other and a central control minicomputer over parallel digital lines. Inter-processor nearest neighbor communications busses pass the constants which represent physical constraints and boundary conditions. The node processors are connected to the six nearest neighbor node processors to simulate the actual physical interface of real substructures. Computer generated finite element mesh and force models can be developed with the aid of the central control minicomputer. The control computer also oversees the animation of a graphics

display system, disk-based mass storage along with the individual processing elements. A.R.H.

N83-18763*# National Aeronautics and Space Administration. Lewis Research Center, Cleveland, Ohio.
DEVELOPMENT OF TOUGH, STRONG, IRON-BASE ALLOY FOR CRYOGENIC APPLICATIONS
J. R. STEPHENS *In* NASA. Langley Research Center Cryogenic Wind Tunnel Models p 187-199 Mar. 1983
Avail: NTIS HC A12/MF A01 CSCL 14B

The development of an iron-base alloy that combines the normally divergent properties of high toughness and high strength at cryogenic temperatures is discussed. Specifically, alloy properties were sought which at -196 C would exhibit a fracture toughness of 220 MPa-m(1/2) with a corresponding yield strength of 1.4 GPa (200 ksi). Early work showed that high toughness could be achieved in Fe-12Ni alloys containing reactive metal additions such as Al, Nb, Ti, and V. Further research emphasized strengthening of these tough alloys by thermomechanical processing and the addition of Cu. Results showed that high strength and high toughness could be achieved in a single alloy at temperatures as low as -196 C. An alloy with composition Fe-12Ni-9.5Al-2Cu exhibited a yield strength of 1.65 GPa with a corresponding fracture toughness of 220 MPa-m(1/2) at -196 C. Strengthening due to Cu additions to the Fe-12Ni base alloys results primarily from precipitation of Cu-rich epsilon particles approximately 20 nm in diameter. Strengthening mechanisms are discussed in terms of an elastic modulus hardening model and are supported by transimission electron microscopy examinations of selected test specimens. M.G.

N83-19761*# Connecticut Univ., Storrs. Dept. of Mechanical Engineering.
TURBINE ENDWALL SINGLE CYLINDER PROGRAM Semiannual Status Report, 1 Jul. 1982 - 1 Jan. 1983
L. S. LANGSTON and W. A. ECKERLE 18 Mar. 1983 43 p
(Contract NSG-3238)
(NASA-CR-170008; NAS 1.26:170008) Avail: NTIS HC A03/MF A01 CSCL 14B

Measurements of the flow field in front of a large-scale single cylinder, mounted in a wind tunnel are discussed. Static pressures on the endwall and cylinder surfaces, extensive five-hole probe pressures in front of and around the cylinder, and velocity fluctuations using a hot-wire probe where the flow is steady enough to yield meaningful results are included. Author

N83-24516*# Fairchild Weston Systems, Inc., Sarasota, Fla.
THE DOE/NASA WIND TURBINE DATA ACQUISITION SYSTEM. PART 3: UNATTENDED POWER PERFORMANCE MONITOR
A. HALLEYY, D. HEIDKAMP, H. NEUSTADTER, and R. OLSON Jan. 1983 63 p refs
(Contract DEN3-98)
(NASA-CR-165540; NAS 1.26:165540; FWS-7621) Avail: NTIS HC A04/MF A01 CSCL 14B

Software documentation, operational procedures, and diagnostic instructions for development version of an unattended wind turbine performance monitoring system is provided. Designed to be used for off line intelligent data acquisition in conjunction with the central host computer. S.L.

12

ASTRONAUTICS (GENERAL)

A83-43269* Case Western Reserve Univ., Cleveland, Ohio.
AN EXPERIMENTAL STUDY OF HEAT INDUCED SURFACE-TENSION DRIVEN FLOW
Y. KAMOTANI, S. OSTRACH, and S. LOWRY (Case Western Reserve University, Cleveland, OH) IN: Materials processing in the reduced gravity environment of space; Proceedings of the Annual Meeting, Boston, MA, November 16-18, 1981 . New York and Amsterdam, North-Holland, 1982, p. 161-172. refs
(Contract NAS3-3015)

Laser Doppler anemometry, radiation thermometry, and time-lapse photography have been used to study heat induced surface-tension driven flows in silicone oil and Fluorinert FC-43 in large open containers. For silicone oil, the effect of the surface tension gradient on the velocity field was not apparent enough to be detected. Because of its high viscosity, the oil was insensitive to outside disturbances, and the flow was steady. In the case of FC-43, the fluid was noticeably influenced by outside disturbances, and the flow was unsteady. The work reported here is part of an effort to develop experimental techniques and select test fluids for future space experiments on fluid motion in materials processing. V.L.

14

GROUND SUPPORT SYSTEMS AND FACILITIES (SPACE)

Includes launch complexes, research and production facilities; ground support equipment, e.g., mobile transporters; and simulators.

A83-12478*# Xerox Electro-Optical Systems, Pasadena, Calif.
OPERATIONAL SUMMARY OF AN ELECTRIC PROPULSION LONG TERM TEST FACILITY
G. E. TRUMP, E. L. JAMES (Xerox Electro-Optical Systems, Pasadena, CA), and R. T. BECHTEL (NASA, Marshall Space Flight Center, Huntsville, AL) AIAA, Japan Society for Aeronautical and Space Sciences, and DGLR, International Electric Propulsion Conference, 16th, New Orleans, LA, Nov. 17-19, 1982, AIAA 10 p.
(Contract NAS3-20399)
(AIAA PAPER 82-1903)

An automated test facility capable of simultaneously operating three 2.5 kW, 30-cm mercury ion thrusters and their power processors is described, along with a test program conducted for the documentation of thruster characteristics as a function of time. Facility controls are analog, with full redundancy, so that in the event of malfunction the facility automaticcally activates a backup mode and notifies an operator. Test data are recorded by a central data collection system and processed as daily averages. The facility has operated continuously for a period of 37 months, over which nine mercury ion thrusters and four power processor units accumulated a total of over 14,500 hours of thruster operating time. O.C.

N83-29292*# National Aeronautics and Space Administration. Lewis Research Center, Cleveland, Ohio.
ROLE OF SIMULATION AND EMULATION IN THE DEVELOPMENT OF SHUTTLE-CENTAUR (STS-CENTAUR)
A. L. GORDAN Jul. 1983 22 p
(NASA-TM-83326; E-1568; NAS 1.15:83326) Avail: NTIS HC A02/MF A01 CSCL 22B

To support the task of integrating the Centaur liquid-fueled upper-stage space vehicle into the space shuttle program. A system to simulate and emulate the STS-Centaur avionic flight system and its supporting ground control and checkout equipment was selected and designated the systems integration facility (SIF). Located in San Diego, California, the SIF is composed of integrated simulators that form a composite control system complement to the STS-Centaur airborne and avionic support equipment. An off-line capability to verify the system design of the Centaur airborne support equipment (CASE) and the Centaur avionic flight system is provided as well as a realistic medium for the development and integration of ground checkout and airborne control software programs. Each simulator is composed of prototype hardware, where feasible, to maximize configuration likeness. Where emulated flight or ground hardware is used, it provides physical characteristics (loads, signals, etc.) equivalent to those of the flight hardware. The hardware and software implementation of the SIF are described. A.R.H.

15

LAUNCH VEHICLES AND SPACE VEHICLES

Includes boosters; manned orbital laboratories; reusable vehicles; and space stations.

A83-43773*# National Aeronautics and Space Administration. Lewis Research Center, Cleveland, Ohio.
APPLICATION OF A SPACE STATION TO COMMUNICATIONS SATELLITES
J. R. RAMLER (NASA, Lewis Research Center, Space Communications Div., Cleveland, OH) American Astronautical Society, Goddard Memorial Symposium, 21st, Greenbelt, MD, Mar. 24, 25, 1983. 5 p.
(AAS PAPER 83-197)

The economic benefits of a space station relative to communications satellites are discussed in terms of technology experiments, spacecraft checkout, repair, servicing, and refurbishment (RSR), and mating an OTV with satellites for boost to GEO. The zero gravity, vacuum conditions, and atmosphere free long ranges are environmental features that can be used for testing large, flexible antennas and laser communications devices. Some resistance might be encountered to checkout in LEO due to the substantial success of launches to GEO without LEO checkout. However, new generations of larger, more complex satellites may warrant the presence of a space station to verify performance of new spacecraft. One RSR positive aspect for a space station is as a storage site for propellant, as well as for reusable OTV booster engines. Also, the space station can serve as a base for manned or unmanned repair spacecraft which will travel to GEO to fix malfunctions in geostationary satellites. M.S.K.

N83-12129*# Columbia Univ., New York. Dept. of Electrical Engineering.
NEXT GENERATION COMMUNICATIONS SATELLITES: MULTIPLE ACCESS AND NETWORK STUDIES Final Report
H. E. MEADOWS, M. SCHWARTZ, T. E. STERN, S. GANGULY, B. KRAIMECHE, K. MATSUO, and I. GOPAL Sep. 1982 218 p refs
(Contract NAS3-22464)
(NASA-CR-167903; NAS 1.26:167903) Avail: NTIS HC A10/MF A01 CSCL 22B

Efficient resource allocation and network design for satellite systems serving heterogeneous user populations with large numbers of small direct-to-user Earth stations are discussed. Focus is on TDMA systems involving a high degree of frequency reuse by means of satellite-switched multiple beams (SSMB) with varying degrees of onboard processing. Algorithms for the efficient utilization of the satellite resources were developed. The effect of skewed traffic, overlapping beams and batched arrivals in packet-switched SSMB systems, integration of stream and bursty traffic, and optimal circuit scheduling in SSMB systems: performance bounds and computational complexity are discussed. Author

N83-15330*# National Aeronautics and Space Administration. Lewis Research Center, Cleveland, Ohio.
INFRARED ASTRONOMICAL SATELLITE (IRAS) LAUNCH
1982 55 p
(NASA-TM-85190; E-885-83-01; NAS 1.15:85190) Avail: NTIS HC A04/MF A01 CSCL 22B

The Infrared Astronomical Satellite (IRAS) is scheduled to be launched from the Western Space and Missile Center, Vandenberg Air Force Base at Lompoc, California by a two stage Delta 3910 launch vehicle. The satellite has a design lifetime of 1 year; however, the mission lifetime is expected to be on the order of 7 months. The mission lifetime is determined by the availability of superfluid helium in the cryostat to maintain the infrared detectors at their required 3K operating temperature. The orbital lifetime of the satellite is expected to be at least 3 years before reentry will occur. The first infrared satellite mission is designed to produce an unbiased all sky survey of discrete sources in the form of sky and source catalogs using four broad photometry channels between 8 and 120 micrometers. S.L.

N83-22255*# TRW, Inc., Redondo Beach, Calif. Space and Technology Group.
REQUIREMENTS FOR A MOBILE COMMUNICATIONS SATELLITE SYSTEM. VOLUME 3: LARGE SPACE STRUCTURES MEASUREMENTS STUDY Final Report, 15 Dec. 1981 - 31 Mar. 1983
W. AKLE 31 Mar. 1983 114 p
(Contract NAS3-23257)
(NASA-CR-168105; NAS 1.26:168105) Avail: NTIS HC A06/MF A01 CSCL 22B

This study report defines a set of tests and measurements required to characterize the performance of a Large Space System (LSS), and to scale this data to other LSS satellites. Requirements from the Mobile Communication Satellite (MSAT) configurations derived in the parent study were used. MSAT utilizes a large, mesh deployable antenna, and encompasses a significant range of LSS technology issues in the areas of structural/dynamics, control, and performance predictability. In this study, performance requirements were developed for the antenna. Special emphasis was placed on antenna surface accuracy, and pointing stability. Instrumentation and measurement systems, applicable to LSS, were selected from existing or on-going technology developments. Laser ranging and angulation systems, presently in breadboard status, form the backbone of the measurements. Following this, a set of ground, STS, and GEO-operational were investigated. A third scale (15 meter) antenna system as selected for ground characterization followed by STS flight technology development. This selection ensures analytical scaling from ground-to-orbit, and size scaling. Other benefits are cost and ability to perform reasonable ground

tests. Detail costing of the various tests and measurement systems were derived and are included in the report. Author

N83-26864*# National Aeronautics and Space Administration. Lewis Research Center, Cleveland, Ohio.
LARGE SPACE SYSTEMS AUXILIARY PROPULSION REQUIREMENTS
J. E. MALOY and W. W. SMITH (Boeing Aerospace Co., Seattle, Wash.) *In* NASA. Langley Research Center Large Space Antenna Systems Technol., Pt. 1 p 175-200 May 1983 refs
Avail: NTIS HC A25/MF A01 CSCL 22B

To meet the needs of a variety of civilian and military missions objectives large space systems (LSS) will become a greater percentage of our orbiting hardware. These LSS's will be transported to low Earth orbit (LEO) by the space transportation system (STS Shuttle). Concurrently, for LSS missions to orbit higher than LEO, the predominant mission scenario is that the LSS will be deployed or assembled in LEO and then transferred to a higher orbit. In support of the LSS concepts, the Office of Aeronautics and Space Technology (OAST) has sponsored studies to determine LSS mission propulsion requirements. Since the fall of 1979, the Boeing Aerospace Company, under contract to NASA and Lewis Research Center, has been studying the disturbance forces and torques that will be experienced by LSS, and they have identified some of the associated auxiliary propulsion systems (APS) requirements. This presentation provides an insight into the results of some of the APS studies, focusing primarily on the APS requirements of single Shuttle launchable LSS's. Author

N83-26889*# National Aeronautics and Space Administration. Lewis Research Center, Cleveland, Ohio.
SCANNING BEAM ANTENNA CONCEPTUAL DESIGN FOR 20/30 GHZ SATELLITE SYSTEMS
J. SMETANA, R. SORBELLO (Communications Satellite Corp., Clarksburg, Md.), and W. F. CROSSWELL (Harris Corp., Melbourne, Fla.) *In* NASA. Langley Research Center Large Space Antenna Systems Technol., Pt. 2 p 767-795 May 1983
Avail: NTIS HC A20/MF A01

The configuration described is one of four antenna system configurations developed using a variety of monolithic microwave integrated circuit module arrangements and optical systems. A parametric analysis is expected to produce a data base for the selection of design points for a variety of applications. Soon to be accomplished is the design concept of the active (lens) array, which will take into consideration such factors as, coupling effects, the space-fed power divider network design, input bias and control layout, investigation of thermal distribution, and analysis of module failure (graceful degradation). L.F.M.

N83-26897*# National Aeronautics and Space Administration. Lewis Research Center, Cleveland, Ohio.
NEAR-FIELD MEASUREMENT FACILITY PLANS AT LEWIS RESEARCH CENTER
R. G. SHARP *In* NASA. Langley Research Center Large Space Antenna Systems Technol., Pt. 2 p 899-922 May 1983 refs
Avail: NTIS HC A20/MF A01 CSCL 20N

The direction of future antenna technology will be toward antennas which are large, both physically and electrically, will operate at frequencies up to 60 GHz, and are non-reciprocal and complex, implementing multiple-beam and scanning beam concepts and monolithic semiconductor devices and techniques. The acquisition of accurate antenna performance measurements is a critical part of the advanced antenna research program and represents a substantial antenna measurement technology challenge, considering the special characteristics of future spacecraft communications antennas. Comparison of various antenna testing techniques and their relative advantages and disadvantages shows that the near-field approach is necessary to meet immediate and long-term testing requirements. The LeRC facilities, the 22 ft x 22 ft horizontal antenna boresight planar scanner and the 60 ft x 60 ft vertical antenna boresight plant scanner (with a 60 GHz frequency and D/lamdba = 3000 electrical size capabilities), will meet future program testing requirements. L.F.M.

N83-26903*# National Aeronautics and Space Administration. Marshall Space Flight Center, Huntsville, Ala.
SAFE II: LARGE SYSTEMS SPACE PLASMA EVALUATION EXPERIMENT
M. R. CARRUTH, JR., L. E. YOUNG, C. K. PURVIS, and N. J. STEVENS *In* NASA. Langley Research Center Large Space Antenna Systems Technol., Pt. 2 p 991-1006 May 1983 refs Prepared in cooperation with NASA. Lewis Research Center
Avail: NTIS HC A20/MF A01 CSCL 20I

A shuttle flight experiment, the purpose of which is to obtain space data on the interaction of a high voltage solar array with the ambient space plasma is addressed. This flight experiment is a reflight of the solar array flight experiment, SAFE, except that three active solar array panels, electron release devices and plasma diagnostics are added. This experiment, SAFE 2, evaluates power loss due to parasitic current collected by the solar array, arcing on the solar array and perturbations to the plasma which may increase power loss and disturb plasma and charged particle science acquisition. S.L.

N83-34998*# General Electric Co., Philadelphia, Pa. Valley Forge Space Center.
SPACECRAFT IN SWITCH MATRIX FOR WIDE BAND SERVICE APPLICATONS IN 30/20 GHZ COMMUNICATIONS SATELLITE SYSTEMS Final Report
B. J. CORY 10 Dec. 1982 217 p
(Contract NAS3-22500)
(NASA-CR-168089; NAS 1.26:168089) Avail: NTIS HC A10/MF A01 CSCL 22B

Bandwidth, switching speed, off-state isolation, and reliability over a ten-year mission were factors in determining the optimum available technology for satellite communications switching in 1982. A proof of concept model for a 20 x 20 coupled crossbar switch matrix designed with FET devices for microwave switching and with high speed CMOS LIS for switch crosspoint addressing was fabricated and tested. Results show the design is feasible for application in a multichannel SS-TDMA communications system. Expandibility can readily be achieved with this design. A conceptual design study for a 100 x 100 switch matrix utilizing a coupled crossbar architecture implemented with a monolithic microwave integrated circuits revealed technology needs for high capacity switch matrices. A.R.H.

16

SPACE TRANSPORTATION

Includes passenger and cargo space transportation, e.g., shuttle operations; and rescue techniques.

N83-25766*# Beech Aircraft Corp., Boulder, Colo.
PRELIMINARY DESIGN OF FLIGHT HARDWARE FOR TWO-PHASE FLUID RESEARCH
D. C. HUSTVEDT and R. L. OONK Feb. 1982 209 p refs
(Contract NAS3-23160)
(NASA-CR-168072; NAS 1.26:168072; BAC-ER-15049) Avail: NTIS HC A10/MF A01 CSCL 22A

This study defined the preliminary designs of flight software for the Space Shuttle Orbiter for three two-phase fluid research experiments: (1) liquid reorientation - to study the motion of liquid in tanks subjected to small accelerations; (2) pool boiling - to study low-gravity boiling from horizontal cylinders; and (3) flow boiling - to study low-gravity forced flow boiling heat transfer and flow phenomena in a heated horizontal tube. The study consisted of eight major tasks: reassessment of the existing experiment designs, assessment of the Spacelab facility approach, assessment of the individual carry-on approach, selection of the preferred

approach, preliminary design of flight hardware, safety analysis, preparation of a development plan, estimates of detailed design, fabrication and ground testing costs. The most cost effective design approach for the experiments is individual carry-ons in the Orbiter middeck. The experiments were designed to fit into one or two middeck lockers. Development schedules for the detailed design, fabrication and ground testing ranged from 15 1/2 to 18 months. Minimum costs (in 1981 dollars) ranged from $463K for the liquid reorientation experiment to $998K for the pool boiling experiment. Author

17

SPACECRAFT COMMUNICATION, COMMAND AND TRACKING

Includes telemetry; space communications networks; astronavigation; and radio blackout.

A83-41389* Motorola, Inc., Scottsdale, Ariz.
A NETWORK CONTROL CONCEPT FOR THE 30/20 GHZ COMMUNICATION SYSTEM BASEBAND PROCESSOR
D. J. SABOURIN and R. E. HAY (Motorola, Inc., Government Electronics Group, Scottsdale, AZ) IN: ICC '82 - The digital revolution; International Conference on Communications, Philadelphia, PA, June 13-17, 1982, Conference Record. Volume 3 . New York, Institute of Electrical and Electronics Engineers, 1982, p. 5E.1.1-5E.1.6.
(Contract NAS3-22502)

The architecture and system design for a satellite-switched TDMA communication system employing on-board processing was developed by Motorola for NASA's Lewis Research Center. The system design is based on distributed processing techniques that provide extreme flexibility in the selection of a network control protocol without impacting the satellite or ground terminal hardware. A network control concept that includes system synchronization and allows burst synchronization to occur within the system operational requirement is described. This concept integrates the tracking and control links with the communication links via the baseband processor, resulting in an autonomous system operational approach. Author

A83-41391* Hughes Aircraft Co., Culver City, Calif.
ONBOARD PROCESSING FOR A 30/20 GHZ COMMUNICATIONS SATELLITE
S. REISENFELD (Hughes Aircraft Co., Culver City, CA) IN: ICC '82 - The digital revolution; International Conference on Communications, Philadelphia, PA, June 13-17, 1982, Conference Record. Volume 3 . New York, Institute of Electrical and Electronics Engineers, 1982, p. 5E.3.1-5E.3.4. refs
(Contract NAS3-22340)

A systems configuration for the baseband processor for a TDMA communications satellite utilizing the 30 GHz uplink and 20 GHz downlink bands will be discussed. The baseband processor functions include QPSK burst demodulation, convolutional decoding, data routing, encoding, QPSK modulation, and antenna steering. The performance of the burst demodulator will be examined. Power and weight estimates for the baseband processor will be presented. Author

A83-49855*# National Aeronautics and Space Administration. Lewis Research Center, Cleveland, Ohio.
ADVANCED COMMUNICATIONS SATELLITE SYSTEMS
J. N. SIVO (NASA, Lewis Research Center, Space Communications Div., Cleveland, OH) IEEE Journal on Selected Areas in Communications (ISSN 0733-8716), vol. SAC-1, Sept. 1983, p. 580-588.

There is a rapidly growing demand for satellite circuits, particularly for domestic service within the U.S. NASA's current program is aimed at developing the high risk, advanced satellite communications technologies required to significantly increase the capacity of future satellite communications systems. Attention is given to aspects of traffic distribution and service scenario, problems related to effects of rain attenuation, details regarding system configuration, a 30/20 GHz technology development approach, an experimental flight system, the communications payload for the experimental flight system, a typical experiment flight system coverage, and a typical three axis stabilized flight spacecraft. G.R.

N83-11210*# National Aeronautics and Space Administration. Lewis Research Center, Cleveland, Ohio.
CONCEPT FOR ADVANCED SATELLITE COMMUNICATIONS AND REQUIRED TECHNOLOGIES
J. R. RAMLER and J. A. SALZMAN 1982 12 p refs Presented at 1982 Natl. Telesystems Conf., Galveston, Tex., 7-10 Nov. 1982; sponsored by IEEE
(NASA-TM-82984; E-1415; NAS 1.15:82984) Avail: NTIS HC A02/MF A01 CSCL 17B

The advanced communications technology satellite (ACTS) program of NASA is aimed at the development of high risk technologies that will enable exploiting higher frequency bands and techniques for improving frequency reuse. The technologies under development include multiple beam spacecraft antennas, on-board switching and processing, RF devices and components and advanced Earth stations. The program focus is on the Ka-band (30/20 GHz) as the implementing frequency since it has five times the bandwidth of either the C- or Ku-bands. However, the technology being developed is applicable to other frequency bands as well and will support a wide range of future communications systems required by NASA, other Government agencies and the commercial sector. An overview is presented of an operational 30/20 GHz satellite system that may evolve. How the system addresses service requirements is discussed, and the technology required and being developed is considered. A.R.H.

N83-18835*# Acurex Corp., Mountain View, Calif.
DEVELOPMENT OF A ROTARY INSTRUMENTATION SYSTEM, PHASE 2 Final Report
A. ADLER and W. SKIDMORE Dec. 1982 72 p refs
(Contract NAS3-20796)
(NASA-CR-168013; NAS 1.26:168013; ACUREX-TR-82-02/AD)
Avail: NTIS HC A04/MF A01 CSCL 09F

A rotary instrumentation system which consists of ruggedized miniature telemetry transmitters installed on the rotating shaft of a gas turbine engine to telemeter the outputs of sensors (strain gages, thermocouples, etc.) on rotating engine components was designed. A small prototype system, which demonstrates the capabilities of performing in the intended environment and demonstrates that the system is expandable to handle about 100 data channels was developed. S.L.

N83-20994*# National Aeronautics and Space Administration. Lewis Research Center, Cleveland, Ohio.
A STUDY OF 60 GIGAHERTZ INTERSATELLITE LINK APPLICATIONS
G. ANZIC, D. J. CONNOLLY, E. J. HAUGLAND, H. G. KOSMAHL, and J. S. CHITWOOD 1983 15 p refs Presented at Intern. Conf. on Commun. (ICC 1983), Boston, 19-22 Jun. 1983; sponsored by IEEE
(NASA-TM-83337; E-1467; NAS 1.15:83337) Avail: NTIS HC A02/MF A01 CSCL 09F

Applications of intersatellite links operating at 60 GHz are reviewed. Likely scenarios, ranging from transmission of moderate and high data rates over long distances to low data rates over short distances are examined. A limited parametric tradeoff is performed with system variables such as radiofrequency power, receiver noise temperature, link distance, data rate, and antenna size. Present status is discussed and projections are given for both electron tube and solid state transmitter technologies. Monolithic transmit and receive module technology, already under development at 20 to 30 GHz, is reviewed and its extension to 60 GHz, and possible applicability is discussed. Author

N83-22313*# National Aeronautics and Space Administration. Lewis Research Center, Cleveland, Ohio.
APPLICATION OF MMIC MODULES IN FUTURE MULTIPLE BEAM SATELLITE ANTENNA SYSTEMS
J. SMETANA 1982 14 p refs Presented at the 1982 Antenna Appl. Symp., Monticello, Illinois, 22-24 Sep. 1982; sponsored by Rome Air Development Center and Illinois Univ.
(NASA-TM-83344; E-1598; NAS 1.15:83344) Avail: NTIS HC A02/MF A01 CSCL 17B

Multiple beam antenna systems for advanced communication satellites operating in the 30/20 GHz frequency bands (30 GHz uplink, 20 GHz downlink) were developed. Up to twenty 0.3 deg HPBW fixed spot beams and six 0.3 deg HPBW scanning spot beams will be required. Array-fed dual reflector antenna systems in which monolithic microwave integrated circuit (MMIC) phase shift and amplifier modules are used with each radiating element of the feed array for beam pointing and power gain were developed. The feasibility of distributed power amplification and beam pointing with MMIC modules in the elements of an array and to develop a data base for future development were demonstrated. The technical discussion centers around the potential advantages of "monolithic" antennas for specific applications as compared to systems using high powered TWT's. These include: reduced losses in the beam forming network; advantage of space combining and graceful degradation; dynamic control of beam pointing and illumination contour; and possibilities for cost and weight reduction. B.G.

N83-35004*# National Aeronautics and Space Administration. Lewis Research Center, Cleveland, Ohio.
NASA'S ADVANCED COMMUNICATIONS TECHNOLOGY SATELLITE (ACTS)
R. T. GEDNEY 1983 13 p refs Presented at the Ohmcon Electron. Show and Conv., Detroit, 16 Jun. 1983; sponsored by IEEE, NWPCA, and ERA
(NASA-TM-83416; E-1704; NAS 1.15:83416) Avail: NTIS HC A02/MF A01 CSCL 17B

NASA recently restructured its Space Communications Program to emphasize the development of high risk communication technology useable in multiple frequency bands and to support a wide range of future communication needs. As part of this restructuring, the Advanced Communications Technology Satellite (ACTS) Project will develop and experimentally verify the technology associated with multiple fixed and scanning beam systems which will enable growth in communication satellite capacities and more effective utilization of the radio frequency spectrum. The ACTS requirements and operations as well as the technology significance for future systems are described. Author

18

SPACECRAFT DESIGN, TESTING AND PERFORMANCE

Includes spacecraft thermal and environmental control; and attitude control.

A83-12460*# Hughes Research Labs., Malibu, Calif.
ON-ORBIT PROPULSION REQUIREMENTS AND PERFORMANCE ASSESSMENT OF ION PROPULSION SUBSYSTEMS FOR FUTURE GEO LARGE SATELLITE MISSIONS
F. J. WESSEL (Hughes Research Laboratories, Malibu, CA), M. E. MANTENIEKS, and R. S. DEESPOSTI (NASA, Lewis Research Center, Cleveland, OH) AIAA, Japan Society for Aeronautical and Space Sciences, and DGLR, International Electric Propulsion Conference, 16th, New Orleans, LA, Nov. 17-19, 1982, AIAA 13 p. refs
(Contract NAS3-22447)
(AIAA PAPER 82-1872)

It is pointed out that a large class of future spacecraft, referred to as large space structures (LSS), will require advanced stationkeeping thrust subsystems. The present investigation is concerned with the performance requirements of such advanced stationkeeping thrust subsystems. An analytical model is employed to evaluate the sensitivity of the total stationkeeping thrust-system mass, for geosynchronous spacecraft, to variations in the mission parameters and thrust-system performance, taking into account ion propulsion thrust systems. The model is formulated for geosynchronous missions and considers only the N-S orbit perturbations due to sun-moon forces and the E-W orbit perturbations due to solar pressure, since these are the dominant orbit perturbations of LSS missions. The thrust system is scaled in relation to the performance capabilities of the existing 8- and 30-cm diameter ion-thruster technology and consists of separate N-S and E-W thrusters. G.R.

A83-12475*# TRW, Inc., Redondo Beach, Calif.
OPTIMAL SUN-ALIGNMENT TECHNIQUES OF LARGE SOLAR ARRAYS IN ELECTRIC PROPULSION SPACECRAFT
H. F. MEISSINGER, C. L. DAILEY (TRW, Inc., Space and Technology Group, Redondo Beach, CA), and M. E. VALGORA (NASA, Lewis Research Center, Cleveland, OH) AIAA, Japan Society for Aeronautical and Space Sciences, and DGLR, International Electric Propulsion Conference, 16th, New Orleans, LA, Nov. 17-19, 1982, AIAA 13 p. refs
(Contract NAS3-22661)
(AIAA PAPER 82-1898)

Optimum sun-alignment of large solar arrays in electric propulsion spacecraft operating in earth orbit requires periodic roll motions around the thrust axis, synchronized with the apparent conical motion of the sun line. This oscillation is sustained effectively with the aid of gravity gradient torques while only a small share of the total torque is being contributed by the attitude control system. Tuning the system for resonance requires an appropriate choice of moment-of-inertia characteristics. To minimize atmospheric drag at low orbital altitudes the solar array is oriented parallel, or nearly parallel, to the flight direction. This can increase the thrust-to-drag ratio by as much as an order of magnitude. Coupled with optimal roll orientation, this feathering technique will permit use of electric propulsion effectively at low altitudes in support of space shuttle or space station activities and in spiral ascent missions. (Author)

A83-17488*
POTENTIALS ON LARGE SPACECRAFT IN LEO
M. J. MANDELL, I. KATZ, and D. L. COOKE (IEEE, DOD, NASA, and DOE, Annual Conference on Nuclear and Space Radiation

Effects, 19th, Las Vegas, NV, July 20-22, 1982.) IEEE Transactions on Nuclear Science, vol. NS-29, Dec. 1982, p. 1584-1588. refs
(Contract NAS3-22826)

A system-oriented computer code is used to predict surface charging due to voltages generated within a satellite operating in the typical dense plasma environment of LEO. The use of this code is demonstrated by predicting the expansion of electric fields onto a kapton surface from a pinhole over a biased conductor in a LEO environment. The results are compared to a more-exact solution and experimental data. (Author)

A83-20415*# Systems Science and Software, La Jolla, Calif.
SPACE SHUTTLE ORBITER CHARGING
I. KATZ and D. E. PARKS (Systems, Science and Software, La Jolla, CA) Journal of Spacecraft and Rockets, vol. 20, Jan.-Feb. 1983, p. 22-25. USAF-supported research refs
(Contract NAS3-22536)

(Previously cited in issue 06, p. 822, Accession no. A82-17793)

A83-29791*# General Dynamics/Convair, San Diego, Calif.
STABILITY ANALYSIS OF CENTAUR-IN-SHUTTLE COMPOSITE CORRUGATED ADAPTERS
E. E. SPIER, J. W. EARLEY, P. A. FERNANDEZ (General Dynamics Corp., Convair Div., San Diego, CA), and J. L. FUKANO IN: Structures, Structural Dynamics and Materials Conference, 24th, Lake Tahoe, NV, May 2-4, 1983, Collection of Technical Papers. Part 1 . New York, American Institute of Aeronautics and Astronautics, 1983, p. 600-611. refs
(Contract NAS3-22901)
(AIAA 83-1003)

This paper evaluates analytically the structural integrity of discretely-loaded, graphite-epoxy, corrugated adapters for the Centaur-in-Shuttle, where combined compression and shear are the critical loads involved. With normal build-ups in the thickness at load introduction boundaries, the structural integrity for both compression and shear buckling was little (or not at all) affected by the discrete load introductions. The analytical tool employed was the STAGSC computer code, and both bifurction buckling and nonlinear collapse options were used; the latter option was limited to shear since postbuckling strength in compression for plate-type structures is governed by crippling strengths, which is not attainable by existing computer codes. Author

A83-32782*# Martin Marietta Aerospace, Denver, Colo.
CRYOGENIC FLUID MANAGEMENT EXPERIMENT TRUNNION FATIGUE VERIFICATION
W. J. BAILEY, D. A. FESTER, J. M. TOTH, JR. (Martin Marietta Aerospace, Denver, CO), and H. J. KASPER (NASA, Lewis Research Center, Cleveland, OH) AIAA, ASME, ASCE, and AHS, Structures, Structural Dynamics and Materials Conference, Lake Tahoe, NV, May 2-4, 1983. 9 p.
(Contract NAS3-23245)
(AIAA PAPER 83-0911)

A subcritical liquid hydrogen orbital storage and transfer experiment was designed for flight in the Shuttle cargo bay. The Cryogenic Fluid Management Experiment (CFME) includes a liquid hydrogen tank supported in a vacuum jacket by two fiberglass epoxy trunnion mounts. This composite material was selected for the trunnions since it provides desirable strength, weight and thermal characteristics for supporting cryogenic tankage. An experimental program was conducted to provide material property and fatigue data for S-glass epoxy composite materials at ambient and liquid hydrogen temperatures and to verify structural integrity of the CFME trunnion supports. Author

A83-36306*# Martin Marietta Aerospace, Denver, Colo.
BENEFITS AND COSTS OF LOW THRUST PROPULSION SYSTEMS
R. I. ROBERTSON, L. J. ROSE (Martin Marietta Aerospace, Denver, CO), and J. E. MALOY (NASA, Lewis Research Center, Cleveland, OH) AIAA, SAE, and ASME, Joint Propulsion Conference, 19th, Seattle, WA, June 27-29, 1983. 11 p.
(Contract NAS3-23246)
(AIAA PAPER 83-1248)

The results of costs/benefits analyses of three chemical propulsion systems that are candidates for transferring high density, low volume STS payloads from LEO to GEO are reported. Separate algorithms were developed for benefits and costs of primary propulsion systems (PPS) as functions of the required thrust levels. The life cycle costs of each system were computed based on the developmental, production, and deployment costs. A weighted criteria rating approach was taken for the benefits, with each benefit assigned a value commensurate to its relative worth to the overall system. Support costs were included in the costs modeling. Reference missions from NASA, commercial, and DoD catalog payloads were examined. The program was concluded reliable and flexible for evaluating benefits and costs of launch and orbit transfer for any catalog mission, with the most beneficial PPS being a dedicated low thrust configuration using the RL-10 system. M.S.K.

A83-37591* Alabama Univ., Huntsville.
OBSERVATIONS OF CHARGING DYNAMICS
R. C. OLSEN (Alabama, University, Huntsville, AL) and C. K. PURVIS (NASA, Lewis Research Center, Cleveland, OH) Journal of Geophysical Research (ISSN 0148-0227), vol. 88, July 1, 1983, p. 5657-5667. refs
(Contract NAS8-33982; NSG-3150)

Plasma data from the University of California, San Diego, Auroral Particles experiments on Applied Technology satellites 5 and 6 are used to investigate the dynamics of natural charging events. Both eclipse and daylight charging events are considered, and typical responses are illustrated by data from specific events. Two different physical processes are found to be involved in the charging process. One of these is straightforward: the spacecraft structure potential responds rapidly to changes in the environment, typically changing by hundreds of volts in a few seconds. The other process is more subtle: differential charging and potential barrier formation precede structural charging and determine the time scale; typically, tens of minutes are required for the potential to change by several hundreds of volts. The latter process is found to be predominately responsible for daylight charging on both spacecraft. Author

N83-12136*# IRT Corp., San Diego, Calif.
DEVELOPMENT OF ELECTRICAL TEST PROCEDURES FOR QUALIFICATION OF SPACECRAFT AGAINST EID. VOLUME 1: THE CAN TEST AND OTHER RELEVANT DATA Progress Report, Mar. - Sep. 1981
J. M. WILKENFELD, R. J. R. JUDGE, and B. L. HARLACHER Apr. 1982 152 p refs 2 Vol.
(Contract NAS3-21967)
(NASA-CR-165590; NAS 1.26:165990; IRT-8195-018-VOL-1; NASA-CR-165990) Avail: NTIS HC A08/MF A01 CSCL 22B

A combined experimental and analytical program to develop system electrical test procedures for the qualification of spacecraft against damage produced by space-electron-induced discharges (EID) occurring on spacecraft dielectric outer surfaces is described. The data on the response of a simple satellite model, called CAN, to electron-induced discharges is presented. The experimental results were compared to predicted behavior and to the response of the CAN to electrical injection techniques simulating blowoff and arc discharges. Also included is a review of significant results from other ground tests and the P78-2 program to form a data base from which is specified those test procedures which optimally simulate the response of spacecraft to EID. The electrical and electron spraying test data were evaluated to provide a first-cut determination of the best methods for performance of electrical

excitation qualification tests from the point of view of simulation fidelity. Author

N83-12137*# IRT Corp., San Diego, Calif.
DEVELOPMENT OF ELECTRICAL TEST PROCEDURES FOR QUALIFICATION OF SPACECRAFT AGAINST EID. VOLUME 2: REVIEW AND SPECIFICATION OF TEST PROCEDURES Progress Report, Mar. - Sep. 1981
J. M. WILKENFELD, B. L. HARLACHER, and D. MATHEWS Apr. 1982 118 p refs 2 Vol.
(Contract NAS3-21967)
(NASA-CR-165590; NAS 1.26:165590; IRT-8195-022-1-VOL-2)
Avail: NTIS HC A06/MF A01 CSCL 22B

A combined experimental and analytical program to develop system electrical test procedures for the qualification of spacecraft against damage produced by space-electron-induced discharges (EID) occurring on spacecraft dielectric outer surfaces is described. A review and critical evaluation of possible approaches to qualify spacecraft against space electron-induced discharges (EID) is presented. A variety of possible schemes to simulate EID electromagnetic effects produced in spacecraft was studied. These techniques form the principal element of a provisional, recommended set of test procedures for the EID qualification spacecraft. Significant gaps in our knowledge about EID which impact the final specification of an electrical test to qualify spacecraft against EID are also identified. Author

N83-13154*# National Aeronautics and Space Administration. Lewis Research Center, Cleveland, Ohio.
ADVANCED 30/20 GHZ MULTIPLE-BEAM ANTENNAS FOR COMMUNICATIONS SATELLITES
R. W. MYHRE 1982 21 p refs Presented at the Symp. on Antenna Applications, Monticello, Ill., 22-24 Sep. 1982; sponsored by AFSC and Illinois Univ.
(NASA-TM-82952; E-1365; NAS 1.15:82952) Avail: NTIS HC A02/MF A01 CSCL 22B

Design concepts under development utilize two separate spacecraft antenna systems, one uplink at 30 GHz and the other a downlink at 20 GHz, where each antenna provides multiple fixed and scanning beams. Two contractors completed configuration trade-off studies and breadboarding of critical technology components, and are fabricating and testing proof-of-concept (POC) models to demonstrate the technology feasibility. Technology developments required for the proposed systems are presented, along with each contractor's progress to date. The technology development areas discussed include: (1) offset Cassegrain and shaped reflector systems for narrow beams with low sidelobes and wideangle off-axis scan; (2) diplexed beam-forming networks for dual polarization, low sidelobes, and fixed and scan-beam operation; (3) fast switching networks for scanning beams; and (4) fabrication of precision feed components and large offset reflectors. A.R.H.

N83-18805*# TRW Defense and Space Systems Group, Redondo Beach, Calif. Electromagnetic Environmental Effects.
NUMERICAL SIMULATION OF A CONDUCTING DISK PARTIALLY COVERED BY AN INSULATOR INTERACTING WITH A PLASMA
R. C. CHAKY, J. ENOCH (Kansas Univ., Lawrence), and J. H. NONNAST (Mission Res., Colorado Springs, Colo.) *In* ESA Spacecraft Mater. in a Space Environ. p 253-262 Jul. 1982 refs Sponsored by Kansas Univ.
(Contract NSG-3290)
Avail: NTIS HC A15/MF A01 CSCL 22B

A numerical simulation has been made of the 'pinhole effect' which produces the characteristic 'S-shaped' current-voltage curve. A disk-shaped conducting probe immersed in a plasma is modeled using a particle-in-cell (PIC) code. A probe partially covered by a very thin insulating layer is considered, as well as a probe mounted on an insulating disk. The simulation uses a cylindrical particle mover and allows for a variable number of particles in the system. The simulation space grid uses three different mesh sizes, the coarsest being away from the probe and the finest near the probe, in order to accurately calculate the trajectories of the simulation particles contributing the current to the probe and to the surface charge density on the dielectric. The calculation of the electrostatic potential is done self-consistently using successive over-relaxation (SOR). Backscattering and secondary electron emission are included for the case of positive probe voltage. Author

N83-20996* National Aeronautics and Space Administration. Lewis Research Center, Cleveland, Ohio.
LASER SURFACE FUSION OF PLASMA SPRAYED CERAMIC TURBINE SEALS Patent
D. W. WISANDER and R. C. BILL, inventors (to NASA) 11 Mar. 1981 5 p Filed 11 Mar. 1981 Supersedes N81-22190 (19 - 13, p 1739)
(NASA-CASE-LEW-13269-1; US-PATENT-4,377,371; US-PATENT-APPL-SN-242795; US-PATENT-CLASS-415-174; US-PATENT-CLASS-415-197) Avail: US Patent and Trademark Office CSCL 22B

The thermal shock resistance of a ceramic layer is improved. An improved abradable lining that is deposited on a shroud forming a gas path seal in turbomachinery is emphasized. Improved thermal shock resistance of a shroud is effective through the deliberate introduction of 'benign' cracks. These are microcracks which will not propagate appreciably upon exposure to the thermal shock environment in which a turbine seal must function. Laser surface fusion treatment is used to introduce these microcracks. The ceramic surface is laser scanned to form a continuous dense layer. As this cools and solidifies, shrinkage results in the formation of a very fine crack network. The presence of this deliberately introduced fine crack network precludes the formation of a catastrophic crack during thermal shock exposure.
Official Gazette of the U.S. Patent and Trademark Office

N83-23347*# Pennsylvania State Univ., University Park. Dept. of Physics.
MASS ANALYSIS OF NEUTRAL PARTICLES AND IONS RELEASED DURING ELECTRICAL BREAKDOWNS ON SPACECRAFT SURFACES Semiannual Status Report, 4 Sep. 1982 - 3 Mar. 1983
B. R. F. KENDALL 21 Apr. 1983 18 p refs
(Contract NSG-3301)
(NASA-CR-170299; NAS 1.26:170299; SASR-7) Avail: NTIS HC A02/MF A01 CSCL 22B

A specialized spectrometer was designed and developed to measure the mass and velocity distributions of neutral particles (molecules and molecular clusters) released from metal-backed Teflon and Kapton films. Promising results were obtained with an insulation breakdown initiation system based on a moveable contact touching the insulated surfaces. A variable energy, high voltage pulse is applied to the contact. The resulting surface damage sites can be made similar in size and shape to those produced by a high voltage electron beam system operating at similar discharge energies. The point discharge apparatus was used for final development of several high speed recording systems and for measurements of the composition of the materials given off by the discharge. Results with this apparatus show evolution of large amounts of fluorocarbon fragments from discharge through Teflon FEP, while discharges through Kapton produce mainly very light hydrocarbon fragments at masses below about 80 a.m.u. A.R.H.

N83-35005*# National Aeronautics and Space Administration. Lewis Research Center, Cleveland, Ohio.
THE ROLE OF POTENTIAL BARRIER FORMATION IN SPACECRAFT CHARGING
C. K. PURVIS 1983 17 p refs Presented at the 17th ESLAB Symp., Noordwijk, Netherlands, 13-16 Sep. 1983; sponsored by ESA, ESTEC, and ESLAB
(NASA-TM-83500; E-1837; NAS 1.15:83500) Avail: NTIS HC A02/MF A01 CSCL 22B

The role of potential barrier formation in spacecraft charging at geosynchronous orbit is discussed. The evidence for, and understanding of, spacecraft charging and its hazards to spacecraft

operation in the early 1970's are summarized. Theoretical and experimental advances which have changed the basic understanding of the role of barrier formation in charging phenomenology are described. Potential barriers are found to play a fundamental role in the dynamics of spacecraft charging. The consequences for structural and differential charging and for discharging are described. Author

20

SPACECRAFT PROPULSION AND POWER

Includes main propulsion systems and components, e.g., rocket engines; and spacecraft auxiliary power sources.

A83-12466*# Hughes Research Labs., Malibu, Calif.
ADVANCES IN SERIES RESONANT INVERTER TECHNOLOGY AND ITS EFFECT ON SPACECRAFT EMPLOYING ELECTRIC PROPULSION
R. R. ROBSON (Hughes Research Laboratories, Malibu, CA) AIAA, Japan Society for Aeronautical and Space Sciences, and DGLR, International Electric Propulsion Conference, 16th, New Orleans, LA, Nov. 17-19, 1982, AIAA 5 p. refs
(Contract NAS3-22471; NAS3-23159)
(AIAA PAPER 82-1881)

The efficiency of transistorized Series Resonant Inverters (SRIs), which is higher than that of silicon-controlled rectifier alternatives, reduces spacecraft radiator requirements by 40% and may eliminate the need for heat pipes on 30-cm ion thruster systems. Recently developed 10- and 25-kW inverters have potential applications in gas thrusters, and represent the first spaceborne SRI designs for such power levels. Attention is given to the design and control system approaches employed in these inverter designs to improve efficiency and reduce weight, along with the impact of such improved parameters on electric propulsion systems. O.C.

A83-12479*# Hughes Research Labs., Malibu, Calif.
STATUS OF THE J-SERIES 30-CM MERCURY ION THRUSTER
S. KAMI, C. R. DULGEROFF (Hughes Research Laboratories, Malibu, CA), and R. T. BECHTEL (NASA, Marshall Space Flight Center, Huntsville, AL) AIAA, Japan Society for Aeronautical and Space Sciences, and DGLR, International Electric Propulsion Conference, 16th, New Orleans, LA, Nov. 17-19, 1982, AIAA 6 p. refs
(Contract NAS3-22655)
(AIAA PAPER 82-1904)

This paper describes the status of the 30-cm J-series mercury ion thruster. This thruster was baselined for the Solar Electric Propulsion System (SEPS) vehicle. This thruster is described and several modifications plus suggested modifications are presented. Some of the modifications resulted from tests performed with the thruster. The operational characteristics of eight J-series thrusters are presented. Isolator contamination and flake formation are also discussed. (Author)

A83-12483*# Hughes Research Labs., Malibu, Calif.
A DIRECT-MEASUREMENT TECHNIQUE FOR ESTIMATING DISCHARGE-CHAMBER LIFETIME
J. R. BEATTIE and H. L. GARVIN (Hughes Research Laboratories, Malibu, CA) AIAA, Japan Society for Aeronautical and Space Sciences, and DGLR, International Electric Propulsion Conference, 16th, New Orleans, LA, Nov. 17-19, 1982, AIAA 8 p. refs
(Contract NAS3-18914)
(AIAA PAPER 82-1908)

The use of short-term measurement techniques for predicting the wearout of ion thrusters resulting from sputter-erosion damage is investigated. The laminar-thin-film technique is found to provide high precision erosion-rate data, although the erosion rates are generally substantially higher than those found during long-term erosion tests, so that the results must be interpreted in a relative sense. A technique for obtaining absolute measurements is developed using a masked-substrate arrangement. This new technique provides a means for estimating the lifetimes of critical discharge-chamber components based on direct measurements of sputter-erosion depths obtained during short-duration (approximately 1 hr) tests. Results obtained using the direct-measurement technique are shown to agree with sputter-erosion depths calculated for the plasma conditions of the test. The direct-measurement approach is found to be applicable to both mercury and argon discharge-plasma environments and will be useful for estimating the lifetimes of inert gas and extended performance mercury ion thrusters currently under development. N.B.

A83-12484*# Hughes Research Labs., Malibu, Calif.
ADVANCED-TECHNOLOGY 30-CM-DIAMETER MERCURY ION THRUSTER
J. R. BEATTIE and S. KAMI (Hughes Research Laboratories, Malibu, CA) AIAA, Japan Society for Aeronautical and Space Sciences, and DGLR, International Electric Propulsion Conference, 16th, New Orleans, LA, Nov. 17-19, 1982, AIAA 9 p. refs
(Contract NAS3-21943)
(AIAA PAPER 82-1910)

An advanced-technology mercury ion thruster designed for operation at high thrust and high thrust-to-power ratio is described. The laboratory-model thruster employs a highly efficient discharge-chamber design that uses high-field-strength samarium-cobalt magnets arranged in a ring-cusp configuration. Ion extraction is achieved using an advanced three-grid ion-optics assembly which utilizes flexible mounts for supporting the screen, accel, and decel electrodes. Performance results are presented for operation at beam currents in the range from 1 to 5 A. The baseline specific discharge power is shown to be about 125 eV/ion, and the acceptable range of net-to-total accelerating-voltage ratio is shown to be in the range of 0.2-0.8 for beam currents in the range of 1-5 A. (Author)

A83-12485*# Hughes Research Labs., Malibu, Calif.
SOFTWARE AND SYSTEM LEVEL TESTS OF A TEST FLIGHT MERCURY ION THRUSTER SUBSYSTEM
R. R. ROBSON (Hughes Research Laboratories, Malibu, CA) and C. A. LOW, JR. (NASA, Lewis Research Center, Cleveland, OH) AIAA, Japan Society for Aeronautical and Space Sciences, and DGLR, International Electric Propulsion Conference, 16th, New Orleans, LA, Nov. 17-19, 1982, AIAA 16 p.
(Contract NAS3-21055)
(AIAA PAPER 82-1912)

A U.S. Air Force technology spacecraft flight is scheduled to carry an Ion Auxiliary Propulsion System (IAPS) as part of its experimental payload. This paper presents the results of the successful flight-software qualification and system-level tests which were performed on IAPS. The software tests were performed with an operating engineering model ion thruster and power processing unit, and failure/off-normal recovery modes, operation with and without temperature telemetry from the thruster vaporizers, and with closed-loop control or fixed setpoint operation of the thruster vaporizers. The system-level tests cover a wide range of thermal and operating conditions with the entire system exposed to a simulated space environment. (Author)

A83-12494*# Xerox Electro-Optical Systems, Pasadena, Calif.
INERT GAS TEST OF TWO 12-CM MAGNETOSTATIC THRUSTERS
W. D. RAMSEY (Xerox Electro-Optical Systems, Pasadena, CA) AIAA, Japan Society for Aeronautical and Space Sciences, and DGLR, International Electric Propulsion Conference, 16th, New Orleans, LA, Nov. 17-19, 1982, AIAA 7 p. refs
(Contract NAS3-22876)
(AIAA PAPER 82-1925)

Comparative performance tests were conducted with 12 cm line and ring magnetic cusp thrusters. Shell anode and magnetoelectrostatic containment boundary anode configurations were evaluated with each magnet array. The best performance

was achieved with the 12-cm ring cusp-shell anode configuration. Argon operation of this configuration produced 65-81 percent mass utilization efficiency at 170-208 watts/single-charged-equivalent (SCE) ampere beam. Xenon test results showed 75-95 percent utilization at 162-188 watts/SCE ampere beam. (Author)

A83-12495*# Iowa Univ., Iowa City.
PLASMA CHARACTERISTICS OF A 17 CM DIAMETER LINE-CUSP ION THRUSTER
R. T. CARPENTER, S. A. BOARDSEN, and S. W. DANIELS (Iowa, University, Iowa City, IA) AIAA, Japan Society for Aeronautical and Space Sciences, and DGLR, International Electric Propulsion Conference, 16th, New Orleans, LA, Nov. 17-19, 1982, AIAA 7 p. refs
(Contract NAG3-206)
(AIAA PAPER 82-1926)

A 17 cm line cusp argon ion thruster has been subjected to a variety of tests using collecting probes in an attempt to determine and understand its plasma properties. Plasma density, space potential and electron temperature have been mapped throughout the interior of the device for several sets of operating conditions. Electron and ion losses have been measured in and near the cusps. Correlations between interior plasma properties and external parameters such as discharge current and beam current are made where appropriate and are found to be understandable in terms of basic plasma concepts. However, a simple model, which cannot account for spatial variations of the plasma parameters, is not able to predict the performance of the device. Directions for further work are discussed. (Author)

A83-12496*# Xerox Electro-Optical Systems, Pasadena, Calif.
DEVELOPMENT OF A LARGE INERT GAS ION THRUSTER
G. STEINER (Xerox Electro-Optical Systems, Pasadena, CA) AIAA, Japan Society for Aeronautical and Space Sciences, and DGLR, International Electric Propulsion Conference, 16th, New Orleans, LA, Nov. 17-19, 1982, AIAA 7 p. refs
(Contract NAS3-22444)
(AIAA PAPER 82-1927)

A 30 cm inert gas electrostatic ion thruster has been developed, exhibiting excellent performance. In the development, the effective anode area was reduced by altering the magnetic field geometry to improve plasma containment, consistent with operational stability. The propellant introduction scheme has the effect of 'folding' the discharge chamber without the increased wall loss penalty associated with a longer chamber. These features contribute to a low discharge cost (eV/ion) versus mass utilization characteristic which remains relatively flat even to high mass utilizations. (Author)

A83-12501*# IAP Research, Inc., Dayton, Ohio.
ELECTRIC RAIL GUN PROJECTILE ACCELERATION TO HIGH VELOCITY
D. P. BAUER, T. J. MCCORMICK, and J. P. BARBER (IAP Research, Inc., Dayton, OH) AIAA, Japan Society for Aeronautical and Space Sciences, and DGLR, International Electric Propulsion Conference, 16th, New Orleans, LA, Nov. 17-19, 1982, AIAA 7 p. refs
(Contract NAS3-22819)
(AIAA PAPER 82-1939)

Electric rail accelerators are being investigated for application in electric propulsion systems. Several electric propulsion applications require that the rail accelerator be capable of launching projectiles at velocities above 10 km/s. An experimental program was conducted to develop rail accelerator technology for high velocity projectile launch. Several 6 mm bore, 3 m long rail accelerators were fabricated. Projectiles with a mass of 0.2 g were accelerated by plasmas, carrying currents up to 150 kA. Experimental design and results are described. Results indicate that the accelerator performed as predicted for a fraction of the total projectile acceleration. The disparity between predicted and measured results are discussed. (Author)

A83-12506*# Page (R. J.) Co., Santa Ana, Calif.
THE DESIGN AND TECHNOLOGY DEVELOPMENT FOR A 150 MLB RESISTOJET FOR H2 OR NH3
R. J. PAGE and W. A. STONER (R. J. Page Co., Santa Ana, CA) s,AIAA, Japan Society for Aeronautical and Space Sciences, and DGLR, International Electric Propulsion Conference, 16th, New Orleans, LA, Nov. 17-19, 1982, AIAA 12 p. refs
(Contract NAS3-23337)
(AIAA PAPER 82-1949)

A 150 mlb thrust level hybrid resistojet which may operate on either H2 or NH3 is described whose design technique allows temperature distribution forecasting by means of a microcomputer-implemented mathematical model. The longer computer run times that accompany the exclusive use of BASIC, relative to assembled languages, are offset by the flexibility offered and the reduction of reprogramming and debugging efforts. The integration of a compact first-stage coiled heater with a concentric tubular gas heater offers direct matching of the 28 V terminal of the spacecraft system, while keeping maximum heater wall temperatures to less than 60 K over that of the gas temperature at the throat. Among the novel materials employed are grain-stabilized rhenium for heating elements and high purity aluminas for insulators. O.C.

A83-12508*# Michigan State Univ., East Lansing.
MEASUREMENTS OF ENERGY DISTRIBUTION AND THRUST FOR MICROWAVE PLASMA COUPLING OF ELECTRICAL ENERGY TO HYDROGEN FOR PROPULSION
T. MORIN, R. CHAPMAN, J. FILPUS, M. HAWLEY, R. KERBER, J. ASMUSSEN (Michigan State University, East Lansing, MI), and S. NAKANISHI (NASA, Lewis Research Center, Cleveland, OH) AIAA, Japan Society for Aeronautical and Space Sciences, and DGLR, International Electric Propulsion Conference, 16th, New Orleans, LA, Nov. 17-19, 1982, AIAA 12 p.
(AIAA PAPER 82-1951)

A microwave plasma system for transfer of electrical energy to hydrogen flowing through the system has potential application for coupling energy to a flowing gas in the electrothermal propulsion concept. Experimental systems have been designed and built for determination of the energy inputs and outputs and thrust for the microwave coupling of energy to hydrogen. Results for experiments with pressure in the range 100 microns-6 torr, hydrogen flow rate up to 1000 micronmoles/s, and total absorbed power to 700 w are presented. (Author)

A83-12511*# Hughes Research Labs., Malibu, Calif.
QUALIFICATION TEST RESULTS OF IAPS 8 CM ION THRUSTERS
C. COLLETT (Hughes Research Laboratories, Malibu, CA) and J. L. POWER (NASA, Lewis Research Center, Cleveland, OH) AIAA, Japan Society for Aeronautical and Space Sciences, and DGLR, International Electric Propulsion Conference, 16th, New Orleans, LA, Nov. 17-19, 1982, AIAA 8 p.
(Contract NAS3-21055)
(AIAA PAPER 82-1954)

Two 8-cm-diameter 5-mN mercury ion thrusters with associated beam shields and gimbals have been fabricated and qualification-tested for the Ion Auxiliary Propulsion System (IAPS) flight test. Functional and performance tests of the thrusters, conducted before, during and after exposure to protoflight vibration and thermal vacuum conditions demonstrated no effects of the environmental exposure and little performance dispersion between the thrusters. (Author)

A83-12512*# Hughes Research Labs., Malibu, Calif.
EXTENDED-PERFORMANCE 8-CM ION THRUSTER OPERATION
F. J. WESSEL, W. S. WILLIAMSON, and C. R. DULGEROFF (Hughes Research Laboratories, Malibu, CA) AIAA, Japan Society for Aeronautical and Space Sciences, and DGLR, International Electric Propulsion Conference, 16th, New Orleans, LA, Nov. 17-19, 1982, AIAA 10 p. refs
(Contract NAS3-22447)
(AIAA PAPER 82-1955)

The performance of an 8-cm ion thruster has been extended to 32-mN thrust, 4062-s specific impulse, and 0.033-mN/W thrust-to-power ratio. The design of this thruster is similar to the IAPS (Ion Auxiliary Propulsion System), which has a performance of 5-mN thrust, 3500-s specific impulse, and 0.036-mN/W thrust-to-power ratio. The above level of extended performance has been achieved by increasing the discharge power, ion-beam accelerating voltage, and propellant flowrate, and by modifying the propellant-vapor injection, discharge-chamber magnetic-field strength, high-voltage insulators, and electron baffle. This paper describes results obtained in characterizing the extended-performance operation of both the unmodified thruster (i.e., in an IAPS-like configuration) and the modified thruster. Lifetime-estimating measurements for the modified thruster at extended-performance conditions are also presented. (Author)

A83-13090*# Michigan State Univ., East Lansing.
MICROWAVE PLASMA GENERATION OF HYDROGEN ATOMS FOR ROCKET PROPULSION
R. CHAPMAN, J. FILPUS, T. MORIN, R. SNELLENBERGER, J. ASMUSSEN, M. HAWLEY, and R. KERBER (Michigan State University, East Lansing, MI) Journal of Spacecraft and Rockets, vol. 19, Nov.-Dec. 1982, p. 579-585. refs
(Contract NSG-3299)

(Previously cited in issue 12, p. 1959, Accession no. A81-29533)

A83-13141*# National Aeronautics and Space Administration. Lewis Research Center, Cleveland, Ohio.
FREE RADICAL PROPULSION CONCEPT
C. E. HAWKINS (Northern Kentucky University, Highland Heights, KY) and S. NAKANISHI (NASA, Lewis Research Center, Space Propulsion Div., Cleveland, OH) AIAA Journal, vol. 20, Dec. 1982, p. 1737, 1738.

(Previously cited in issue 14, p. 2320, Accession no. A81-32905)

A83-16925*# National Aeronautics and Space Administration, Washington, D. C.
ELECTRIC PROPULSION RESEARCH AND TECHNOLOGY IN THE UNITED STATES
W. R. HUDSON (NASA, Washington, DC), R. J. VONDRA (USAF, Rocket Propulsion Laboratory, Edwards AFB, CA), T. COCHRAN (NASA, Lewis Research Center, Cleveland, OH), and E. PAWLIK (California Institute of Technology, Jet Propulsion Laboratory, Pasadena, CA) AIAA, Japan Society for Aeronautical and Space Sciences, and DGLR, International Electric Propulsion Conference, 16th, New Orleans, LA, Nov. 17-19, 1982, AIAA 14 p. refs
(AIAA PAPER 82-1867)

Near-, mid-, and long-term technology goals for space electric propulsion systems are reviewed. Technological readiness has been demonstrated for 8 cm, 5 mN, and 30 cm, 30 mN electrostatic thrusters, with major use seen for GEO communications satellites in the near-term, and space station orbit adjustments later. Ion thrusters and/or MPD thrusters are projected to become viable if a space nuclear reactor system is operational in the 1990s, allowing the transport of thousands of kilograms to the outer planets. Basic research is proceeding on the electrothermal propulsion concept to provide resistojet thrusters suitable for a space station by 1986, although the program is hindered by insufficient funding. A flight test for the ion auxiliary propulsion system is detailed, and test results of the solar electric rocket (SERT II) are reported. Particular note is made of the progress on the solar electric propulsion system for the Shuttle and the Nuclear electric propulsion system for thermal-to-electric conversion for mid-1990s applications.
M.S.K.

A83-20423*# Colorado State Univ., Fort Collins.
INERT GAS THRUSTER TECHNOLOGY
H. R. KAUFMAN, R. S. ROBINSON, and D. C. TROCK (Colorado State University, Fort Collins, CO) Journal of Spacecraft and Rockets, vol. 20, Jan.-Feb. 1983, p. 77-83. refs
(Contract NSG-3011)

(Previously cited in issue 12, p. 1961, Accession no. A81-29555)

A83-21078*# National Aeronautics and Space Administration. Lewis Research Center, Cleveland, Ohio.
EXTENDED PERFORMANCE 8-CM MERCURY ION THRUSTER
M. A. MANTENIEKS (NASA, Lewis Research Center, Cleveland, OH) AIAA, Japan Society for Aeronautical and Space Sciences, and DGLR, International Electric Propulsion Conference, 16th, New Orleans, LA, Nov. 17-19, 1982, AIAA 28 p. refs
(AIAA PAPER 82-1913)

(Previously announced in STAR as N83-14157)

A83-21099*# National Aeronautics and Space Administration. Lewis Research Center, Cleveland, Ohio.
SIMPLIFICATION OF POWER ELECTRONICS FOR ION THRUSTER NEUTRALIZERS
R. P. GRUBER (NASA, Lewis Research Center, Cleveland, OH) AIAA, Japan Society for Aeronautical and Space Sciences, and DGLR, International Electric Propulsion Conference, 16th, New Orleans, LA, Nov. 17-19, 1982, AIAA 17 p. refs
(AIAA PAPER 82-1880)

(Previously announced in STAR as N83-12141)

A83-21100*# National Aeronautics and Space Administration. Lewis Research Center, Cleveland, Ohio.
IMPROVED ION CONTAINMENT USING A RING-CUSP ION THRUSTER
J. S. SOVEY (NASA, Lewis Research Center, Cleveland, OH) AIAA, Japan Society for Aeronautical and Space Sciences, and DGLR, International Electric Propulsion Conference, 16th, New Orleans, LA, Nov. 17-19, 1982, AIAA 24 p. refs
(AIAA PAPER 82-1928)

(Previously announced in STAR as N83-13164)

A83-21900*# National Aeronautics and Space Administration. Lewis Research Center, Cleveland, Ohio.
PARALLEL PLATE RADIOFREQUENCY ION THRUSTER
S. NAKANISHI (NASA, Lewis Research Center, Cleveland, OH) AIAA, Japan Society for Aeronautical and Space Sciences, and DGLR, International Electric Propulsion Conference, 16th, New Orleans, LA, Nov. 17-19, 1982, AIAA 11 p. refs
(AIAA PAPER 82-1937)

(Previously announced in STAR as N83-12142)

A83-22075*# National Aeronautics and Space Administration. Lewis Research Center, Cleveland, Ohio.
RAIL ACCELERATOR RESEARCH AT LEWIS RESEARCH CENTER
W. R. KERSLAKE and B. Z. CYBYK (NASA, Lewis Research Center, Cleveland, OH) AIAA, Japan Society for Aeronautical and Space Sciences, and DGLR, International Electric Propulsion Conference, 16th, New Orleans, LA, Nov. 17-19, 1982, AIAA 29 p. refs
(AIAA PAPER 82-1938)

(Previously announced in STAR as N83-12143)

A83-24360*# National Aeronautics and Space Administration. Lewis Research Center, Cleveland, Ohio.
PROPULSION AND FLUID MANAGEMENT - STATION KEEPING WILL EAT ENERGY ON A NEW SCALE
D. A. PETRASH (NASA, Lewis Research Center, Cleveland, OH) Astronautics and Aeronautics, vol. 21, Mar. 1983, p. 64, 65.

An attempt is made to identify technologies that could be brought to a state of minimal development risk in the near term, yet offer the potential for evolutionary growth consistent with future space station propulsion requirements. Prospective auxiliary propulsion propellants will be usable by other systems, thereby offering resupply benefits and a benign rather than corrosive or toxic handling environment. NASA programs are currently underway to develop the storage and supply methods for cryogenic liquids in orbit. The recovery of unused propellants from the Space Shuttle Orbiter and External Tank are being evaluated in order to define Shuttle modifications and performance penalties. Fluid management subsystem requirements and characteristics cannot, however, be fully defined until a firm mission scenario has been established and other space station subsystems are more clearly defined. O.C.

A83-26625*# National Aeronautics and Space Administration. Lewis Research Center, Cleveland, Ohio.
OPERATION OF THE J-SERIES THRUSTER USING INERT GAS
V. K. RAWLIN (NASA, Lewis Research Center, Cleveland, OH) AIAA, Japan Society for Aeronautical and Space Sciences, and DGLR, International Electric Propulsion Conference, 16th, New Orleans, LA, Nov. 17-19, 1982, AIAA 16 p. refs
(AIAA PAPER 82-1929)
(Previously announced in STAR as N83-17587)

A83-27132* TRW Defense and Space Systems Group, Redondo Beach, Calif.
SOLAR ARRAY SWITCHING POWER MANAGEMENT
J. E. CASSINELLI, L. D. SMITH (TRW Defense and Space Systems Group, Redondo Beach, CA), and M. VALGORA (NASA, Lewis Research Center, Cleveland, OH) In: IECEC '82; Proceedings of the Seventeenth Intersociety Energy Conversion Engineering Conference, Los Angeles, CA, August 8-12, 1982. Volume 1. New York, Institute of Electrical and Electronics Engineers, p. 77-82.

Solar array power switching concepts are explored for a 250 kWe manned LEO platform, a 50-250 kWe load for an orbit transfer vehicle (OTV), and an unmanned platform with a 50 kWe load in GEO. A solar array switching power management (SASPM) system is under study to satisfy the switching demands. Direct connections to arrays would be implemented for voltage regulations, power distribution, and the capability of reconfiguring the arrays to meet requirements. Mission characteristics that would require the power sources were explored. The LEO platform was projected to use a concentrator, have no reconfigurability, use 250 NiH2 batteries, supply 80-0 Vdc to an ion drive, and have a 20-30 yr life. Both GEO and OTV arrays were planar, would feature reconfigurability, and supply 800 Vdc to an ion drive. NiH2 batteries would be on the OTV, while the GEO spacecraft would use AgH2 cells. A block diagram of the basic switching configuration is presented.
D.H.K.

A83-27198* TRW, Inc., Redondo Beach, Calif.
DEVELOPMENT OF IMPROVED HYDROGEN RECOMBINATION IN SEALED NICKEL-CADMIUM AEROSPACE CELLS
P. F. RITTERMAN (TRW, Inc., TRW Space and Technology Group, Redondo Beach, CA) In: IECEC '82; Proceedings of the Seventeenth Intersociety Energy Conversion Engineering Conference, Los Angeles, CA, August 8-12, 1982. Volume 2. New York, Institute of Electrical and Electronics Engineers, 1982, p. 739-745.
(Contract NAS3-21253)

The identification and measurement of a hydrogen recombination mechanism in nickel-cadmium cells has made deep reconditioning on a battery basis safe and feasible. Deep reconditioning has been shown to improve performance and increase life of nickel-cadmium batteries in geosynchronous orbit applications. The hydrogen recombination mechanism and data supporting the mechanism are presented. Parameteric cell design experiments are described which have lead to the definition of nickel-cadmium cells capable of high rate overdischarge. Nickel-cadmium cells with optimum hydrogen recombination capability were successfully cycled for 7 seasons in simulation of the geosynchronous orbit regime at 75 percent depth-of-discharge with extensive midseason and end-of-season overdischarge at rates ranging from C/4 to C/20. (Author)

A83-27205*# National Aeronautics and Space Administration. Lewis Research Center, Cleveland, Ohio.
DESIGN OF A 35-KILOWATT BIPOLAR NICKEL-HYDROGEN BATTERY FOR LOW-EARTH-ORBIT APPLICATIONS
R. L. CATALDO and J. J. SMITHRICK (NASA, Lewis Research Center, Cleveland, OH) In: IECEC '82; Proceedings of the Seventeenth Intersociety Energy Conversion Engineering Conference, Los Angeles, CA, August 8-12, 1982. Volume 2. New York, Institute of Electrical and Electronics Engineers, 1982, p. 780-783.
(Previously announced in STAR as N82-24647)

A83-27206* United Technologies Corp., South Windsor, Conn.
ALKALINE REGENERATIVE FUEL CELL ENERGY STORAGE SYSTEM FOR MANNED ORBITAL SATELLITES
R. E. MARTIN, B. GITLOW (United Technologies Corp., South Windsor, CT), and D. W. SHEIBLEY (NASA, Lewis Research Center, Cleveland, OH) In: IECEC '82; Proceedings of the Seventeenth Intersociety Energy Conversion Engineering Conference, Los Angeles, CA, August 8-12, 1982. Volume 2. New York, Institute of Electrical and Electronics Engineers, 1982, p. 790-795. refs
(Contract NAS3-22234)

It is pointed out that the alkaline regenerative fuel cell system represents a highly efficient, lightweight, reliable approach for providing energy storage in an orbiting satellite. In addition to its energy storage function, the system can supply hydrogen and oxygen for attitude control of the satellite and for life support. A summary is presented of the results to date obtained in connection with the NASA-sponsored fuel cell technology advancement program, giving particular attention to the requirements of the alkaline regenerative fuel cell and the low-earth mission. Attention is given to system design guidelines, weight considerations, gold-platinum cathode cell performance, matrix development, the electrolyte reservoir plate, and the cyclical load profile tests.
G.R.

A83-27298* Thermo Electron Corp., Waltham, Mass.
THERMIONIC TECHNOLOGY INFRASTRUCTURE FOR SPACE POWER
F. HUFFMAN, P. REAGAN, G. MISKOLCZY, and O. MERRILL (Thermo Electron Corp., Waltham, MA) In: IECEC '82; Proceedings of the Seventeenth Intersociety Energy Conversion Engineering Conference, Los Angeles, CA, August 8-12, 1982. Volume 4. New York, Institute of Electrical and Electronics Engineers, 1982, p. 1908-1912. refs
(Contract DE-AC02-76ET-11291; DE-AC02-81CS-90215; JPL-955009 ; NAS3-20270)

An assessment is made of the potential effectiveness, designs, and technological difficulties involved in the construction of space nuclear reactors coupled to thermionic energy converters (TEC). The TECs can be positioned either inside or outside of the reactor core. The out-of-core design lowers the reactor shielding requirements, as well as removing the need for mechanically pumped coolant for the reactor. R&D is still needed for the heat pipes for the reactor and the collectors, electrical insulation, and to reduce the potential losses in the interelectrode space. A cylindrical converter for the out-of-core configuration consists of a tungsten emitter heated by a tungsten-lithium heat pipe. The collector is a layer of tungsten oxide deposited on a Nb-1%Zr alloy, and has been tested at emitter temperatures of 1300-1850 K and a collector temperature range of 700-850 K. A design of a

superheated thermionic converter is described, noting that a prototype has been operated at 1730 K for 12,000 hr. M.S.K.

A83-27350*# Michigan State Univ., East Lansing.
PERFORMANCE CHARACTERISTICS OF A MICROWAVE PLASMA DISK ION SOURCE
J. ASMUSSEN, J. ROOT (Michigan State University, East Lansing, MI), and S. NAKANISHI (NASA, Lewis Research Center, Cleveland, OH) AIAA, Japan Society for Aeronautical and Space Sciences, and DGLR, International Electric Propulsion Conference, 16th, New Orleans, LA, Nov. 17-19, 1982, AIAA 21 p. refs
(AIAA PAPER 82-1935)

The development, design, and preliminary performance characteristics of a microwave plasma disk ion source are presented. Several important design concepts indigenous to microwave plasmas have been utilized in the development of this ion source: generation of a resonantly sustained microwave discharge inside a microwave/plasma coupler, probe and length tuning of the microwave/plasma coupler, and minimization of plasma volume. The experimental results for a 2.45 GHz, eight cm ion source excited in the TE(211) and TM(011) modes are described. Results are presented for electromagnetic mode excitation, electron density, coupling efficiency and loaded cavity Q, and I-V characteristics and efficiencies. It is preliminarily shown that a microwave disk-like plasma can be sustained adjacent to the grids with either TE or TM cavity modes at pressures below 2 x 10 to the -4th torr. Over 80% of the power absorbed in the cavity is coupled into the plasma. C.D.

A83-33744*# Tuskegee Inst., Ala.
CHARACTERIZATION OF ADVANCED ELECTRIC PROPULSION SYSTEMS
P. K. RAY (Tuskegee Institute, Tuskegee, AL) Journal of Spacecraft and Rockets (ISSN 0022-4560), vol. 20, May-June 1983, p. 305-309. refs
(Contract NAG3-76)

Previously cited in issue 17, p. 2707, Accession no. A82-35083

A83-36281*# Washington Univ., Seattle.
RADIATION ENERGY RECEIVER FOR LASER AND SOLAR PROPULSION SYSTEMS
D. F. G. RAULT and A. HERTZBERG (Washington, University, Seattle, WA) AIAA, SAE, and ASME, Joint Propulsion Conference, 19th, Seattle, WA, June 27-29, 1983. 9 p. refs
(Contract NAG3-16)
(AIAA PAPER 83-1207)

The concept of remotely heating a rocket propellant with a high intensity radiant energy flux is especially attractive due to its high specific impulse and large payload mass capabilities. In this paper, a radiation receiver-thruster which is especially suited to the particular thermodynamic and spectral characteristics of highly concentrated solar energy is proposed. In this receiver, radiant energy is volumetrically absorbed within a hydrogen gas seeded with alkali metal vapors. The alkali atoms and molecules absorb the radiant flux and, subsequently, transfer their internal excitation to hydrogen molecules through collisional quenching. It is shown that such a radiation receiver would outperform a blackbody cavity type receiver in both efficiency and maximum operating temperatures. A solar rocket equipped with such a receiver-thruster would deliver thrusts of several hundred newtons at a specific impulse of 1000 seconds. Author

A83-36333*# Rockwell International Corp., Canoga Park, Calif.
ADVANCED LOX/H2 ENGINE TECHNOLOGIES FOR FUTURE OTVS
A. MARTINEZ and D. L. FULTON (Rockwell International Corp., Rocketdyne Div., Canoga Park, CA) AIAA, SAE, and ASME, Joint Propulsion Conference, 19th, Seattle, WA, June 27-29, 1983. 15 p.
(Contract NAS3-23172; NAS8-33568)
(AIAA PAPER 83-1312)

It is pointed out that NASA and DOD missions of the near future include, by current estimates, approximately 50 highly energetic missions to geosynchronous orbit. Advanced concepts make use of the Space Shuttle to transport the assembled orbital transfer vehicle (OTV) to low earth orbit (LEO) or to bring components and propellants from which to assemble the OTV in LEO. An advanced expander cycle engine based upon the RS-44 engine design has been planned for ultimate use with advanced space-based OTVs. Its design features complement the characteristics of manned space-based aeroassist vehicles which will provide the most cost-effective means for payload transfer between LEO and GEO orbits. A test-bed program is planned for early demonstration of the advanced expander cycle engine operation. G.R.

A83-36371*# Southwest Research Inst., San Antonio, Tex.
VAPOR FLOW INTO A CAPILLARY PROPELLANT-ACQUISITION DEVICE
F. T. DODGE and E. B. BOWLES (Southwest Research Institute, San Antonio, TX) AIAA, SAE, and ASME, Joint Propulsion Conference, 19th, Seattle, WA, June 27-29, 1983. 10 p. refs
(Contract NAS3-22664)
(AIAA PAPER 83-1380)

An analytical model is described that specifies the conditions needed to cause a flow of vapor through the screens of a start basket. The analytical model is composed of several original submodels that interrelate the evaporation of the liquid in the basket, the bubble-point change of a screen in the presence of wicking, the drying out of a screen through a combination of evaporation and pressure difference, the vapor flow rate across a wet screen as a function of pressure difference, and the effect on wicking of a difference between the static pressure of the liquid reservoir and the vapor surrounding the screen. Most of the interrelations were demonstrated by a series of separate-effects tests, which were also used to determine certain empirical constants. The equations of the model were solved numerically for typical start basket designs. A simplified start basket was constructed and tested to verify these predictions, using both volatile and non-volatile liquids. The test results verified the trends predicted by the model. Author

A83-36384*# Hughes Research Labs., Malibu, Calif.
SIMPLIFIED POWER PROCESSING FOR ION-THRUSTER SUBSYSTEMS
F. J. WESSEL and D. J. HANCOCK (Hughes Research Laboratories, Malibu, CA) AIAA, SAE, and ASME, Joint Propulsion Conference, 19th, Seattle, WA, June 27-29, 1983. 8 p. Research supported by Hughes Aircraft Co. refs
(Contract NAS3-22447)
(AIAA PAPER 83-1394)

A review of the thruster/power-processor-interface requirements for (mercury and inert gas) ion-thrusters, an evaluation of various approaches to simplifying the power-processor circuitry, and the test results of the recently developed 8-cm mercury-ion-thruster simplified power-processor unit (SPPU) are presented. The SPPU demonstrates the feasibility of stable thruster operation using highly simplified power-processing techniques and achieves an approximately tenfold reduction in the electronic parts count when compared to the existing power-processor unit (PPU) used in the Hughes/NASA Lewis Research Center 8-cm-diameter (mercury) Ion Auxiliary Propulsion Subsystem (IAPS). Author

A83-39271*# Hughes Research Labs., Malibu, Calif.
SIMPLIFIED POWER PROCESSING FOR ION-THRUSTER SUBSYSTEMS
F. J. WESSEL and D. J. HANCOCK (Hughes Research Laboratories, Malibu, CA) Joint Army-Navy-NASA-Air Force Interagency Propulsion Committee, Propulsion Meeting, Monterey, CA, Feb. 1983, Paper. 8 p. refs
(Contract NAS3-22447)

Compared to chemical propulsion, ion propulsion offers distinct payload-mass increases for many future low-thrust earth-orbital and deep-space missions. Despite this advantage, the high initial cost and complexity of ion-propulsion subsystems reduce their attractiveness for most present and near-term spacecraft missions. Investigations have, therefore, been conducted with the objective to attempt to simplify the power-processing unit (PPU), which is the single most complex and expensive component in the thruster subsystem. The present investigation is concerned with a program to simplify the design of the PPU employed in a 8-cm mercury-ion-thruster subsystem. In this program a dramatic simplification in the design of the PPU could be achieved, while retaining essential thruster control and subsystem operational flexibility. G.R.

A83-45512*# National Aeronautics and Space Administration. Lewis Research Center, Cleveland, Ohio.
AUXILIARY PROPULSION REQUIREMENTS FOR LARGE SPACE SYSTEMS
J. E. MALOY (NASA, Lewis Research Center, Cleveland, OH), W. W. SMITH, and G. W. MACHLES (Boeing Aerospace Co., Seattle, WA) AIAA, SAE, and ASME, Joint Propulsion Conference, 19th, Seattle, WA, June 27-29, 1983. 23 p.
(AIAA PAPER 83-1217)

An insight into auxiliary propulsion systems (APS) requirements for large space systems (LSS) launchable by a single shuttle is presented. In an effort to scope the APS requirements for LSS, a set of generic LSSs were defined. For each generic LSS class a specific structural configuration, representative of that most likely to serve the needs of the 1980's and 1990's was defined. The environmental disturbance forces and torques which would be acting on each specific structural configuration in LEO and GEO orbits were then determined. Auxiliary propulsion requirements were determined as a function of: generic class specific configuration, size and openness of structure, orbit, angle of orientation, correction frequency, duty cycle, number and location of thrusters and direction of thrusters and APS/LSS interactions. The results of this analysis were used to define the APS characteristics of: (1) number and distribution of thrusters, (2) thruster modulation, (3) thrust level, (4) mission energy requirements, (5) total APS mass component breakdown, and (6) state of the art adequacy/deficiency. Previously announced in STAR as N83-26922 S.L.

A83-45513*# National Aeronautics and Space Administration. Lewis Research Center, Cleveland, Ohio.
ADVANCED PROPULSION CONCEPTS FOR ORBITAL TRANSFER VEHICLES
L. P. COOPER (NASA, Lewis Research Center, Cleveland, OH) AIAA, SAE, and ASME, Joint Propulsion Conference, 19th, Seattle, WA, June 27-29, 1983. 14 p. refs
(AIAA PAPER 83-1243)

Studies of the United States Space Transportation System show that in the mid-to-late 1990s expanded capabilities for Orbital Transfer Vehicles (OTV) will be needed to meet increased payload requirements for transporting materials and possible men to geosynchronous orbit. NASA is conducting a technology program in support of an advanced propulsion system for future OTVs. This program is briefly described with results to date of the first program element, the Conceptual Design and Technology Definition studies. Previously announced in STAR as N83-26924 Author

N83-12141*# National Aeronautics and Space Administration. Lewis Research Center, Cleveland, Ohio.
SIMPLIFICATION OF POWER ELECTRONICS FOR ION THRUSTER NEUTRALIZERS
R. P. GRUBER 1982 18 p refs Presented at the 16th Intern. Electric Propulsion Conf., New Orleans, 17-19 Nov. 1982
(NASA-TM-83004; E-1441; NAS 1.15:83004; AIAA-82-1880)
Avail: NTIS HC A02/MF A01 CSCL 21C

A need exists for less complex and lower cost ion thruster systems. Design approaches and the demonstration of neutralizer power electronics for relaxed neutralizer keeper, tip heater, and vaporizer requirements are discussed. The neutralizer circuitry is operated from a 200 to 400 V bus and demonstrates an order of magnitude reduction in parts count. Furthermore, a new technique is described for regulating tip heater power and automatically switching over to provide keeper power with only four additional components. A new design to control the flow rate of the neutralizer with one integrated circuit is also presented. Author

N83-12142*# National Aeronautics and Space Administration. Lewis Research Center, Cleveland, Ohio.
PARALLEL PLATE RADIOFREQUENCY ION THRUSTER
S. NAKANISHI Oct. 1982 12 p refs Presented at the 16th Intern. Electric Propulsion Conf., New Orleans, 17-19 Nov. 1982
(NASA-TM-83014; E-1432; NAS 1.15:83014) Avail: NTIS HC A02/MF A01 CSCL 21C

An 8-cm-diam. argon ion thruster is described. It is operated by applying 100 to 160 Mhz rf power across a thin plasma volume in a strongly divergent static magnetic field. No cathode or electron emitter is required to sustain a continuous wave plasma discharge over a broad range of propellant gas flow. Preliminary results indicate that a large fraction of the incident power is being reflected by impedance mismatching in the coupling structure. Resonance effects due to plasma thickness, magnetic field strength, and distribution are presented. Typical discharge losses obtained to date are 500 to 600 W per beam ampere at extracted beam currents up to 60 mA. Author

N83-12143*# National Aeronautics and Space Administration. Lewis Research Center, Cleveland, Ohio.
RAIL ACCELERATOR RESEARCH AT LEWIS RESEARCH CENTER
W. R. KERSLAKE and B. Z. CYBYK 1982 30 p refs Presented at the 16th Intern. Electric Propulsion Conf., New Orleans, 17-19 Nov. 1982
(NASA-TM-83015; E-1449; NAS 1.15:83015; AIAA-82-1938)
Avail: NTIS HC A03/MF A01 CSCL 21C

A rail accelerator was chosen for study as an electromagnetic space propulsion device because of its simplicity and existing technology base. The results of a mission feasibility study using a large rail accelerator for direct launch of ton-size payloads from the Earth's surface to space, and the results of initial tests with a small, laboratory rail accelerator are presented. The laboratory rail accelerator has a bore of 3 by 3 mm and has accelerated 60 mg projectiles to velocities of 300 to 1000 m/s. Rail materials of Cu, W, and Mo were tested for efficiency and erosion rate. Author

N83-13164*# National Aeronautics and Space Administration. Lewis Research Center, Cleveland, Ohio.
IMPROVED ION CONTAINMENT USING A RING-CUSP ION THRUSTER
J. S. SOVEY 1982 25 p refs Presented at the 16th Intern. Elec. Propulsion Conf., New Orleans, 17-19 Nov. 1982; sponsored by the AIAA, Japan Society for Aeronautical and Space Sciences and Deutsche Gesselschaft fuer Luftund Raumfahrt
(NASA-TM-82990; E-1422; NAS 1.15:82990) Avail: NTIS HC A02/MF A01 CSCL 21C

A 30-centimeter diameter ring-cusp ion thruster is described which operates at inert gas ion beam currents up to about 7 ampere, with significant improvements in discharge chamber performance over conventional divergent-field thrusters. The thruster has strong boundary ring-cusp magnetic fields, a diverging field on the cathode region, and a nearly field-free volume upstream

of the ion extraction system. Minimum ion beam production costs of 90 to 100 watts per beam ampere (W/A) were obtained for argon, krypton and xenon. Propellant efficiencies in excess of 0.90 were achieved at 100 to 120 W/A for the three inert gases. The ion beam charge-state was documented with a collimating mass spectrometer probe to allow evaluation of overall thruster efficiencies. Author

N83-14157*# National Aeronautics and Space Administration. Lewis Research Center, Cleveland, Ohio.
EXTENDED PERFORMANCE 8-CM MERCURY ION THRUSTER
M. A. MANTENIEKS 1981 30 p refs Presented at the 16th Intern. Elec. Propulsion Conf., New Orleans, 17-19 Nov. 1982; sponsored by AIAA, Japan Soc. for Aeron. and Space Sci., and Deut. Gesselschaft fuer Luft und Raumfahrt
(NASA-TM-83029; E-1464; NAS 1.15:83029; AIAA-82-1913) Avail: NTIS HC A03/MF A1 CSCL 21C

A slightly modified 8-cm Hg ion thruster demonstrated significant increase in performance. Thrust was increased by almost a factor of five over that of the baseline thruster. Thruster operation with various three grid ion optics configurations; thruster performance as a function of accelerator grid open area, cathode baffle, and cathode orifice size; and a life test of 614 hours at a beam current of 250 mA (17.5 mN thrust) are discussed. Highest thruster efficiency was obtained with the smallest open area accelerator grid. The benefits in efficiency from the low neutral loss grids were mitigated, however, by the limitation such grids place on attainable ion beam current densities. The thruster components suffered negligible weight losses during a life test, which indicated that operation of the 8-cm thruster at extended levels of thrust and power is possible with no significant loss of lifetime. Author

N83-14158*# Hughes Research Labs., Malibu, Calif.
ANALYSIS AND DESIGN OF ION THRUSTER FOR LARGE SPACE SYSTEMS Final Report, 21 May 1979 - 21 May 1980
R. L. POESCHEL and S. KAMI Sep. 1980 113 p refs
(Contract NAS3-21936)
(NASA-CR-165140; NAS 1.26:165140) Avail: NTIS HC A06/MF A01 CSCL 21C

Design analyses showed that an ion thruster of approximately 50 cm in diameter will be required to produce a thrust of 0.5 N using xenon or argon as propellants, and operating the thruster at a specific impulse of 3530 sec or 6076 sec respectively. A multipole magnetic confinement discharge chamber was specified. Author

N83-14159*# Xerox Electro-Optical Systems, Pasadena, Calif.
ANALYSIS AND DESIGN OF ION THRUSTERS FOR LARGE SPACE SYSTEMS Final Report, 23 May 1979 - 23 May 1980
E. L. JAMES 31 Jul. 1980 88 p refs
(Contract NAS3-21937)
(NASA-CR-165160; NAS 1.26:165160) Avail: NTIS HC A05/MF A01 CSCL 21C

This study undertakes the analysis and conceptual design of a 0.5 Newton electrostatic ion thruster suitable for use on large space system missions in the next decade. Either argon or xenon gas shall be used as propellant. A 50 cm diameter discharge chamber was selected to meet stipulated performance goals. The discharge plasma is contained at the boundary by a periodic structure of alternating permanent magnets generating a series of line cusps. Anode strips between the magnets collect Maxwellian electrons generated by a central cathode. Ion extraction utilizes either two or three grid optics at the user's choice. An extensive analysis was undertaken to investigate optics behavior in the high power environment of this large thruster. A plasma bridge neutralizer operating on inert gas provides charge neutralizing electrons to complete the design. The resulting conceptual thruster and the necessary power management and control requirements are described. Author

N83-17586*# Hughes Research Labs., Malibu, Calif.
THE 8-CM ION THRUSTER CHARACTERIZATION Final Report, 8 Aug. 1980 - 9 Oct. 1981
F. J. WESSEL and W. S. WILLIAMSON Jan. 1983 52 p refs
(Contract NAS3-22447)
(NASA-CR-167887; NAS 1.26:167887) Avail: NTIS HC A04/MF A01 CSCL 21C

The performance capabilities of the 8 cm diameter mercury ion thruster were increased by modifying the thruster operating parameters and component hardware. The initial performance levels, representative of the Hughes/NASA Lewis Research Center Ion Auxiliary Propulsion Subsystem (IAPS) thruster, were raised from the baseline values of thrust, T = 5 mN, and specific impulse, I sub sp = 2,900s, to thrust, T = 25 mN and specific impulse, I sub sp = 4,300 s. Performance characteristics including estmates of the erosion rates of various component surfaces are presented. Author

N83-17587*# National Aeronautics and Space Administration. Lewis Research Center, Cleveland, Ohio.
OPERATION OF THE J-SERIES THRUSTER USING INERT GAS
V. K. RAWLIN 1982 17 p refs Presented at the 16th Intern. Elec. Propulsion Conf., New Orleans, 17-19 Nov. 1982; sponsored by AIAA, Japan Soc. for Aeronautical and Space Sciences, and DGLR
(NASA-TM-82977; E-1406; NAS 1.15:82977; AIAA-PAPER-82-1929) Avail: NTIS HC A02/MF A01 CSCL 21H

Electron bombardment ion thrusters using inert gases are candidates for large space systems. The J-Series 30 cm diameter thruster, designed for operation up to 3 k-W with mercury, is at a state of technology readiness. The characteristics of operation with xenon, krypton, and argon propellants in a J-Series thruster with that obtained with mercury are compared. The performance of the discharge chamber, ion optics, and neutralizer and the overall efficiency as functions of input power and specific impulse and thruster lifetime were evaluated. As expected, the discharge chamber performance with inert gases decreased with decreasing atomic mass. Aspects of the J-Series thruster design which would require modification to provide operation at high power with insert gases were identified. A.R.H.

N83-21002*# Martin Marietta Aerospace, Denver, Colo.
STUDY FOR ANALYSIS OF BENEFIT VERSUS COST OF LOW THRUST PROPULSION SYSTEM Final Report, Nov. 1982 - Feb. 1983
K. M. HAMLYN, R. I. ROBERTSON, and L. J. ROSE Mar. 1983 154 p refs
(Contract NAS3-23246)
(NASA-CR-168011; NAS 1.26:168011; MCR-82-521) Avail: NTIS HC A08/MF A01 CSCL 21H

The benefits and costs associated with placing large space systems (LSS) in operational orbits were investigated, and a flexible computer model for analyzing these benefits and costs was developed. A mission model for LSS was identified that included both NASA/Commercial and DOD missions. This model included a total of 68 STS launches for the NASA/Commercial missions and 202 launches for the DOD missions. The mission catalog was of sufficient depth to define the structure type, mass and acceleration limits of each LSS. Conceptual primary propulsion stages (PPS) designs for orbital transfer were developed for three low thrust LO2/LH2 engines baselined for the study. The performance characteristics for each of these PPS was compared to the LSS mission catalog to create a mission capture. The costs involved in placing the LSS in their operational orbits were identified. The two primary costs were that of the PPS and of the STS launch. The cost of the LSS was not included as it is not a function of the PPS performance. The basic relationships and algorithms that could be used to describe the costs were established. The benefit criteria for the mission model were also defined. These included mission capture, reliability, technical risk, development time, and growth potential. Rating guidelines were

established for each parameter. For flexibility, each parameter is assigned a weighting factor. S.L.

N83-22318*# National Aeronautics and Space Administration. Lewis Research Center, Cleveland, Ohio.
DESIGN, FABRICATION AND TESTING OF POROUS TUNGSTEN VAPORIZERS FOR MERCURY ION THRUSTERS
R. ZAVESKY, E. KROEGER, and S. KAMI (Hughes Research Labs., Malibu, Calif.) Feb. 1983 62 p refs
(NASA-TM-83063; E-1534; NAS 1.15:83063) Avail: NTIS HC A04/MF A01 CSCL 21C

The dispersions in the characteristics, performance and reliability of vaporizers for early model 30-cm thrusters were investigated. The purpose of the paper is to explore the findings and to discuss the approaches that were taken to reduce the observed dispersion and present the results of a program which validated those approaches. The information that is presented includes porous tungsten materials specifications, a discussion of assembly procedures, and a description of a test program which screens both material and fabrication processes. There are five appendices providing additional detail in the areas of vaporizer contamination, nitrogen flow testing, bubble testing, porosimeter testing, and mercury purity. Four neutralizers, seven cathodes and five main vaporizers were successfully fabricated, tested, and operated on thrusters. Performance data from those devices is presented and indicates extremely repeatable results from using the design and fabrication procedures. Author

N83-24552*# National Aeronautics and Space Administration. Lewis Research Center, Cleveland, Ohio.
DESIGN CONSIDERATIONS FOR LARGE SPACE ELECTRIC POWER SYSTEMS
D. D. RENZ, R. C. FINKE, N. J. STEVENS, J. E. TRINER, and I. G. HANSEN Apr. 1983 23 p refs
(NASA-TM-83064; E-1535; NAS 1.15:83064) Avail: NTIS HC A02/MF A01 CSCL 22B

As power levels of spacecraft rise to the 50 to 100 kW range, it becomes apparent that low voltage (28 V) dc power distribution and management systems will not operate efficiently at these higher power levels. The concept of transforming a solar array voltage at 150 V dc into a 1000 V ac distribution system operating at 20 kHz is examined. The transformation is accomplished with series-resonant inverter by using a rotary transformer to isolate the solar array from the spacecraft. The power can then be distributed in any desired method such as three phase delta to delta. The distribution voltage can be easily transformed to any desired load voltage and operating frequency. The reasons for the voltage limitations on the solar array due to plasma interactions and the many advantages of a high voltage, high frequency at distribution system are discussed. S.L.

N83-25779*# Hughes Research Labs., Malibu, Calif.
ENDURANCE TEST OF A 30-CM-DIAMETER ENGINEERING MODEL ION THRUSTER. TASK 12: INVESTIGATION OF THIN-FILM EROSION MONITORS FOR ION THRUSTERS Final Report, 5 Feb. 1981 - 30 Jun. 1982
J. R. BEATTIE May 1983 41 p refs
(Contract NAS3-18914)
(NASA-CR-168132; NAS 1.26:168132) Avail: NTIS HC A03/MF A01 CSCL 21C

An investigation of short term measurement techniques for predicting the wearout of ion thrusters resulting from sputter erosion damage is described. The previously established laminar thin film techniques to provide high precision erosion rate data. However, the erosion rates obtained using this technique are generally substantially higher than those obtained during long term endurance tests (by virtue of the as deposited nature of the thin films), so that the results must be interpreted in a relative sense. Absolute measurements can be performed using a new masked substrate arrangement which was developed during this study. This new technique provides a means for estimating the lifetimes of critical discharge chamber components based on direct measurements of sputter erosion depths obtained during short duration (10 hour) tests. The method enables the effects on lifetime of thruster design and operating parameters to be inferred without the investment of the time and capital required to conduct long term (1000 hour) endurance tests. Results obtained using the direct measurement technique are shown to agree with sputter erosion depths calculated for the plasma conditions of the test and also with lifetest results. The direct measurement approach is shown to be applicable to both mercury and argon discharge plasma environments and should be useful in estimating the lifetimes of inert gas and extended performance mercury ion thrusters presently under development. Author

N83-26922*# National Aeronautics and Space Administration. Lewis Research Center, Cleveland, Ohio.
AUXILIARY PROPULSION REQUIREMENTS FOR LARGE SPACE SYSTEMS
J. E. MALOY, W. W. SMITH (Boeing Aerospace, Seattle, Wash.), and G. W. MACHLES (Boeing Aerospace, Seattle, Wash.) 1983 23 p refs Presented at the 19th Joint Propulsion Conf. and Tech. Display, Seattle, 27-29 Jun. 1983; sponsored by the AIAA, SAE and ASME
(NASA-TM-83388; E-1666; NAS 1.15:83388; AIAA-83-1217)
Avail: NTIS HC A02/MF A01 CSCL 21H

An insight into auxiliary propulsion systems (APS) requirements for large space systems (LSS) launchable by a single shuttle is presented. In an effort to scope the APS requirements for LSS, a set of generic LSSs were defined. For each generic LSS class a specific structural configuration, representative of that most likely to serve the needs of the 1980's and 1990's was defined. The environmental disturbance forces and torques which would be acting on each specific structural configuration in LEO and GEO orbits were then determined. Auxiliary propulsion requirements were determined as a function of: generic class specific configuration, size and openness of structure, orbit, angle of orientation, correction frequency, duty cycle, number and location of thrusters and direction of thrusters and APS/LSS interactions. The results of this analysis were used to define the APS characteristics of: (1) number and distribution of thrusters, (2) thruster modulation, (3) thrust level, (4) mission energy requirements, (5) total APS mass component breakdown, and (6) state of the art adequacy/deficiency. S.L.

N83-26923*# National Aeronautics and Space Administration. Lewis Research Center, Cleveland, Ohio.
THE PERFORMANCE AND APPLICATION OF HIGH SPEED LONG LIFE LH2 HYBRID BEARINGS FOR REUSABLE ROCKET ENGINE TURBOMACHINERY
N. P. HANNUM and C. E. NIELSON (Rockwell International, Canoga Park, Calif.) 1983 27 p refs Presented at the 19th Joint Propulsion Conf., Seattle, 27-29 Jun. 1983; sponsored by AIAA, SAE and ASME
(NASA-TM-83417; E-1707; NAS 1.15:83417; AIAA-83-1389)
Avail: NTIS HC A03/MF A01 CSCL 21H

Data are presented for two different experimental programs which were conducted to investigate the characteristics of a hybrid (hydrostatic/ball) bearing operating in liquid hydrogen. The same bearing design was used in both programs. Analytical predictions were made of the bearing characteristics and are compared with the experimental results when possible. The first program used a bearing tester to determine the steady state, transient, and cyclic life characteristics of the bearing over a wide range of operating conditions. The second program demonstrated the feasibility of applying hybrid bearings to an actual high speed turbopump by retrofitting and then testing an existing liquid hydrogen turbopump with the bearings. Author

N83-26924*# National Aeronautics and Space Administration. Lewis Research Center, Cleveland, Ohio.
ADVANCED PROPULSION CONCEPTS FOR ORBITAL TRANSFER VEHICLES
L. P. COOPER 1982 15 p refs Prepared for Presentation at the 19th Joint Propulsion Conf., Seattle, Wash., 27-29 Jun. 1983; sponsored by AIAA, SAE, and ASME
(NASA-TM-83419; E-1709; NAS 1.15:83419) Avail: NTIS HC A02/MF A01 CSCL 21H

Studies of the United States Space Transportation System show that in the mid-to-late 1990s expanded capabilities for Orbital Transfer Vehicles (OTV) will be needed to meet increased payload requirements for transporting materials and possible men to geosynchronous orbit. NASA is conducting a technology program in support of an advanced propulsion system for future OTVs. This program is briefly described with results to date of the first program element, the Conceptual Design and Technology Definition studies. Author

N83-28071*# National Aeronautics and Space Administration. Lewis Research Center, Cleveland, Ohio.
A NEW STRATEGY FOR EFFICIENT SOLAR ENERGY CONVERSION: PARALLEL-PROCESSING WITH SURFACE PLASMONS
L. M. ANDERSON 1982 16 p refs Presented at the 17th Intersoc. Energy Conversion Eng. Conf., Los Angeles, 8-13 Aug. 1982; sponsored by IEEE
(NASA-TM-82867; NE-1236; NAS 1.15:82867) Avail: NTIS HC A02/MF A01 CSCL 10A

This paper introduces an advanced concept for direct conversion of sunlight to electricity, which aims at high efficiency by tailoring the conversion process to separate energy bands within the broad solar spectrum. The objective is to obtain a high level of spectrum-splitting without sequential losses or unique materials for each frequency band. In this concept, sunlight excites a spectrum of surface plasma waves which are processed in parallel on the same metal film. The surface plasmons transport energy to an array of metal-barrier-semiconductor diodes, where energy is extracted by inelastic tunneling. Diodes are tuned to different frequency bands by selecting the operating voltage and geometry, but all diodes share the same materials. Author

N83-28072*# TRW Defense and Space Systems Group, Redondo Beach, Calif.
HIGH FREQUENCY PLASMA GENERATORS FOR ION THRUSTERS Interim Report, Sep. 1980 - Nov. 1981
W. F. DIVERGILIO, H. GOEDE, and V. V. FOSNIGHT Nov. 1981 131 p refs
(Contract NAS3-22473)
(NASA-CR-167957; NAS 1.26:167957) Avail: NTIS HC A07/MF A01 CSCL 21C

The results of a one year program to experimentally adapt two new types of high frequency plasma generators to Argon ion thrusters and to analytically study a third high frequency source concept are presented. Conventional 30 cm two grid ion extraction was utilized or proposed for all three sources. The two plasma generating methods selected for experimental study were a radio frequency induction (RFI) source, operating at about 1 MHz, and an electron cyclotron heated (ECH) plasma source operating at about 5 GHz. Both sources utilize multi-linecusp permanent magnet configurations for plasma confinement. The plasma characteristics, plasma loading of the rf antenna, and the rf frequency dependence of source efficiency and antenna circuit efficiency are described for the RFI Multi-cusp source. In a series of tests of this source at Lewis Research Center, minimum discharge losses of 220+/-10 eV/ion were obtained with propellant utilization of .45 at a beam current of 3 amperes. Possible improvement modifications are discussed. Author

N83-30516*# National Aeronautics and Space Administration. Lewis Research Center, Cleveland, Ohio.
POWER GENERATION FROM NUCLEAR REACTORS IN AEROSPACE APPLICATIONS
R. E. ENGLISH 1982 76 p refs Presented at the Symp. on Advanced Compact Reactors, Washington, D.C., 15-17 Nov. 1982; sponsored by NRC
(NASA-TM-83342; E-1597; NAS 1.15:83342) Avail: NTIS HC A05/MF A01 CSCL 18E

Power generation in nuclear powerplants in space is addressed. In particular, the states of technology of the principal competitive concepts for power generation are assessed. The possible impact of power conditioning on power generation is also discussed. For aircraft nuclear propulsion, the suitability of various technologies is cursorily assessed for flight in the Earth's atmosphere; a program path is suggested to ease the conditions of first use of aircraft nuclear propulsion. Author

N83-32842*# Hughes Research Labs., Malibu, Calif.
EVALUATION OF THE USE OF ON-BOARD SPACECRAFT ENERGY STORAGE FOR ELECTRIC PROPULSION MISSIONS
R. L. POESCHEL and F. M. PALMER Aug. 1983 42 p
(Contract NAS3-23258)
(NASA-CR-168209; NAS 1.26:168209) Avail: NTIS HC A03/MF A01 CSCL 21C

On-board spacecraft energy storage represents an under utilized resource for some types of missions that also benefit from using relatively high specific impulse capability of electric propulsion. This resource can provide an appreciable fraction of the power required for operating the electric propulsion subsystem in some missions. The most probable mission requirement for utilization of this energy is that of geostationary satellites which have secondary batteries for operating at high power levels during eclipse. The study summarized in this report selected four examples of missions that could benefit from use of electric propulsion and on-board energy storage. Engineering analyses were performed to evaluate the mass saved and economic benefit expected when electric propulsion and on-board batteries perform some propulsion maneuvers that would conventionally be provided by chemical propulsion. For a given payload mass in geosynchronous orbit, use of electric propulsion in this manner typically provides a 10% reduction in spacecraft mass. Author

N83-32843*# Colorado State Univ., Fort Collins. Dept. of Mechanical Engineering.
ELECTRIC THRUSTER RESEARCH
H. R. KAUFMAN and R. S. ROBINSON Dec. 1982 134 p refs
(Contract NSG-3011)
(NASA-CR-168134; NAS 1.26:168134) Avail: NTIS HC A07/MF A01 CSCL 21C

It has been customary to assume that ions flow nearly equally in all directions from the ion production region within an electron-bombardment discharge chamber. In general, the electron current through a magnetic field can alter the electron density, and hence the ion density, in such a way that ions tend to be directed away from the region bounded by the magnetic field. When this mechanism is understood, it becomes evident that many past discharge chamber designs have operated with a preferentially directed flow of ions. Thermal losses were calculated for an oxide-free hollow cathode. At low electron emissions, the total of the radiation and conduction losses agreed with the total discharge power. At higher emissions, though, the plasma collisions external to the cathode constituted an increasingly greater fraction of the discharge power. Experimental performance of a Hall-current thruster was adversely affected by nonuniformities in the magnetic field, produced by the cathode heating current. The technology of closed-drift thrusters was reviewed. The experimental electron diffusion in the acceleration channel was found to be within about a factor of 3 of the Bohm value for the better thruster designs at most operating conditions. Thruster efficiencies of about 0.5 appear practical for the 1000 to 2000 s range of specific impulse. Lifetime information is limited, but values of several thousands of hours

should be possible with anode layer thrusters operated or = to 2000 s. Author

N83-33942*# TRW, Inc., Redondo Beach, Calif. Space and Technology Group.
ELECTROTHERMAL THRUSTER DIAGNOSTICS. VOLUME 1: EXECUTIVE SUMMARY
S. ZAFRAN and B. JACKSON May 1983 12 p refs 2 Vol.
(Contract NAS3-23265)
(NASA-CR-168174-VOL-1; NAS 1.26:168174-VOL-1; TRW-39152-6011-UE-00-VOL-1) Avail: NTIS HC A02/MF A01 CSCL 21H

A flight-qualified electrothermal thruster demonstrated its adaptability to a variety of propellants. Originally qualified for operation with hydrazine propellant, it was operated with nitrogen, hydrogen, and ammonia propellants, demonstrating 73, 61, and 52 percent overall efficiency with these propellants, respectively, when tested over a wide range of operating conditions. By introducing a preheater to admit hot, rather than cold, propellant inlet gases to the thruster's augmentation heat exchanger, delivered specific impulse closer to theoretical performance limits should be achieved. Author

N83-33943*# TRW, Inc., Redondo Beach, Calif. Space and Technology Group.
ELECTROTHERMAL THRUSTER DIAGNOSTICS. VOLUME 2: TECHNICAL
S. ZAFRAN and B. JACKSON May 1983 57 p refs 2 Vol.
(Contract NAS3-23265)
(NASA-CR-168174-VOL-2; NAS 1.26:168174-VOL-2; TRW-39152-6012-UE-00-VOL-2) Avail: NTIS HC A04/MF A01 CSCL 21H

Test data taken with nitrogen, hydrogen, and ammonia propellants are presented over a wide range of operating conditions at thrust levels up to 225 mN (50 mlb). The design adaptation of a flight-qualified thruster for operation with gaseous propellant inlet is described. Post-test analysis includes evaluation of thruster performance and efficiency, and shows the effects of propellant contamination on an immersed heating element. Author

N83-35013*# Rocketdyne, Canoga Park, Calif.
ADVANCED LOX/H SUB 2 ENGINE TECHNOLOGIES FOR FUTURE OTVS
J. GLASS and A. MARTINEZ *In* APL The 1983 JANNAF Propulsion Meeting, Vol. 1 p 29-40 Feb. 1983
(Contract NAS3-23172; NAS8-33568)
Avail: NTIS HC A15/MF A01 CSCL 21H

The optimization methods and trade studies which were used to define a 1980 state-of-the-art design of orbital transfer vehicles are summarized. The advanced thrust chamber, turbomachinery, and engine power cycle technologies recommended for development and verification during the 1980's are discussed. The state-of-the-art design serves as one of the reference points for evaluation of the advanced technology concepts. A second reference point is provided by the 1960 state-of-the-art RL-10 engine. Advanced heat energy extraction concepts in the combustor and injector are presented that will permit the high chamber pressures expected of the advanced expander cycle engine concept. Advanced turbomachinery concepts are selected that will help utilize efficiently the heat energy extracted in the thrust chamber and aid in uprating chamber pressures to values five times those realized with 1960 to 1980 technologies. The higher chamber pressure benefits are maximized with nozzle concepts that will package within a short retracted length and extend to the very high expansion area ratios required for specific impulse values significantly higher than those now realized by operational systems. Control system component concepts studied will allow utilization of the high turbine drive energy levels in a reliable repeatable manner that will reduce program risk and enhance overall space transportation system mission life cycle cost. R.J.F.

N83-35018*# Hughes Research Labs., Malibu, Calif.
SIMPLIFIED POWER PROCESSING FOR ION-THRUSTER SUBSYSTEMS
F. J. WESSEL and D. J. HANCOCK *In* APL The 1983 JANNAF Propulsion Meeting, Vol. 1 p 77-84 Feb. 1983 refs
(Contract NAS3-22447)
Avail: NTIS HC A15/MF A01 CSCL 21C

A design for a greatly simplified power-processing unit (SPPU) for the 8-cm diameter mercury-ion-thruster subsystem is discussed. This SPPU design will provide a tenfold reduction in parts count, a decrease in system mass and cost, and an increase in system reliability compared to the existing power-processing unit (PPU) used in the Hughes/NASA Lewis Research Center Ion Auxiliary Propulsion Subsystem. The simplifications achieved in this design will greatly increase the attractiveness of ion propulsion in near-term and future spacecraft propulsion applications. A description of a typical ion-thruster subsystem is given. An overview of the thruster/power-processor interface requirements is given. Simplified thruster power processing is discussed. R.J.F.

N83-35053*# National Aeronautics and Space Administration. Lewis Research Center, Cleveland, Ohio.
THE LERC RAIL ACCELERATORS: TEST DESIGNS AND DIAGNOSTIC TECHNIQUES
L. M. ZANA, W. R. KERSLAKE, J. C. STURMAN, S. Y. WANG, and F. F. TERDAN 14 Oct. 1983 21 p refs Presented at 2nd Symp. on Electromagnetic Launch Technol., Cambridge, Mass., 11-14 Oct. 1983; sponsored by IEEE
(NASA-TM-83496; E-1830; NAS 1.15:83496) Avail: NTIS HC A02/MF A01 CSCL 21H

The feasibility of using rail accelerators for various in-space and to-space propulsion applications was investigated. A 1 meter, 24 sq mm bore accelerator was designed with the goal of demonstrating projectile velocities of 15 km/sec using a peak current of 200 kA. A second rail accelerator, 1 meter long with a 156.25 sq mm bore, was designed with clear polycarbonate sidewalls to permit visual observation of the plasma arc. A study of available diagnostic techniques and their application to the rail accelerator is presented. Specific topics of discussion include the use of interferometry and spectroscopy to examine the plasma armature as well as the use of optical sensors to measure rail displacement during acceleration. Standard diagnostics such as current and voltage measurements are also discussed. S.L.

N83-36101*# Rocketdyne, Canoga Park, Calif.
SSME MAIN COMBUSTION CHAMBER LIFE PREDICTION Final Report, Jan. 1982 - May 1983
R. T. COOK, E. E. FRYK, and J. F. NEWELL May 1983 294 p refs
(Contract NAS3-23256)
(NASA-CR-168215; NAS 1.26:168215; RI/RD83-150) Avail: NTIS HC A13/MF A01 CSCL 21H

Typically, low cycle fatigue life is a function of the cyclic strain range, the material properties, and the operating temperature. The reusable life is normally defined by the number of strain cycles that can be accrued before severe material degradation occurs. Reusable life is normally signified by the initiation or propagation of surface cracks. Hot-fire testing of channel wall combustors has shown significant mid-channel wall thinning or deformation during accrued cyclic testing. This phenomenon is termed cyclic-creep and appears to be significantly accelerated at elevated surface temperatures. This failure mode was analytically modelled. The cyclic life of the baseline SSME-MCC based on measured calorimeter heat transfer data, and the life sensitivity of local hot spots caused by injector effects were determined. Four life enhanced designs were assessed. S.L.

23

CHEMISTRY AND MATERIALS (GENERAL)

Includes biochemistry and organic chemistry.

A83-21054* City Coll. of the City Univ. of New York.
EFFECT OF HYDROGEN BONDING ON THE VIBRATIONAL DEPHASING TIME IN GLYCEROL
R. DORSINVILLE, W. M. FRANKLIN, N. OCKMAN, and R. R. ALFANO (City College, New York, NY) Chemical Physics Letters, vol. 92, Oct. 8, 1982, p. 100-102. refs
(Contract NAG3-130)

The vibrational dephasing of the methyl CH2 symmetric stretch mode in glycerol was directly measured over an extended temperature range using picosecond coherent Raman pump and probe spectroscopy. The dephasing time was found to increase dramatically as the temperature of the supercooled liquid was lowered. This observation is attributed to the increased hydrogen bonding with decreasing temperature which hinders the dephasing of the CH2 vibration by reducing molecular motions. (Author)

A83-22269* IIT Research Inst., Chicago, Ill.
IMPROVED UNIFORMITY OF MULTIPHASE CERAMIC-METAL PLASMA-SPRAYED COATS
H. H. NAKAMURA, W. R. LOGAN, Y. HARADA (IIT Research Institute, Chicago, IL), T. P. JACOBSON, and H. E. SLINEY (NASA, Lewis Research Center, Cleveland, OH) Ceramic Engineering and Science Proceedings, vol. 3, Sept.-Oct. 1982, p. 722-736. refs
(Contract NAS3-21979)

Processing-technology development of a multiphase, self-lubricating, plasma-spray powder resulted in greater uniformity and reproducibility of plasma-sprayed coats. The effect of particle-size variation, binder concentration, and reproducible processing parameters are reported. Greater adhesive strengths of coats to substrates were achieved by particle-size variation, use of an intermediate bond coat such as Ni-Cr, or heat treatment. Quantitative analyses of polished, coated specimens are also given. (Author)

N83-13169*# National Aeronautics and Space Administration. Lewis Research Center, Cleveland, Ohio.
MICROHARDNESS STUDIES ON THIN CARBON FILMS GROWN ON P-TYPE, (100) SILICON
J. C. KOLECKI Nov. 1982 11 p refs
(NASA-TM-82980; E-1410; NAS 1.15:82980) Avail: NTIS HC A02/MF A01 CSCL 20L

A program to grow thin carbon films and investigate their physical and electrical properties is described. Characteristics of films grown by rf sputtering and vacuum arc deposition on p type, (100) silicon wafers are presented. Microhardness data were obtained from both the films and the silicon via the Vickers diamond indentation technique. These data show that the films are always harder than the silicon, even when the films are thin (of the order of 1000 A). Vacuum arc films were found to contain black carbon inclusions of the order of a few microns in size, and clusters of inclusions of the order of tens of microns. Transmission electron diffraction showed that the films being studied were amorphous in structure. Author

N83-19812*# Arkansas State Univ., State University.
VAPORIZATION THERMODYNAMICS OF K2S AND K2SO3 Final Report
J. E. BENNET Jun. 1982 65 p refs
(Contract NSG-3249; DE-AI01-77ET-10769)
(NASA-CR-168080; DOE/NASA/3249-1; NAS 1.26:168080)
Avail: NTIS HC A04/MF A01 CSCL 20M

The vaporization reactions, vapor pressures, and thermodynamics of potassium sulfide and potassium sulfite were studied for purposes of providing fundamental data for the seed cycle in magnetohydrodynamic electric power generation. Rate of effusion studies, supported by tube furnace experiments, X-ray powder diffraction, mass spectrometry and appropriate chemical analyses and tests, revealed that potassium sulfite disproportionates at high temperatures to form potassium sulfide and potassium sulfate. Potassium sulfide was observed to vaporize incongruently, the initial vapors beng predominantly potassium atoms, with minor species being S2 and various K-S molecules. The ratio of K/S2 in the vapor is very large initially and decreases steadily with prolonged heating. Several materials were evaluated for purposes of containing K2S/K2SO3 at temperatures or = 800 C: Pt, Mo, W, quartz, machinable glass, BN, high density graphite, pyrolytic coated graphite, and alumina. Of these, only alumina was observed to be chemically inert to both K2S but reacted with K2SO3. The other materials were not suitable for either substance. Thermodynamic calculations based on measured vapor pressures and approximate free energy functions are described. Results from isothermal total mass loss experiments and from thermogravimetric experiments are also included. S.L.

N83-25786*# National Aeronautics and Space Administration. Lewis Research Center, Cleveland, Ohio.
KINETICS OF COPPER ION ABSORPTION BY CROSS-LINKED CALCIUM POLYACRYLATE MEMBRANES
W. H. PHILIPP and C. E. MAY Feb. 1983 11 p refs
(NASA-TM-83052; E-1506; NAS 1.15:83052) Avail: NTIS HC A02/MF A01 CSCL 07C

The absorption of copper ions from aqueous copper acetate solutions by cross-linked calcium acrylate membranes was found to obey parabolic kinetics similar to that found for oxidation of metals that form protective oxide layers. For pure calcium polyacrylate membranes the rate constant was essentially independent of copper acetate concentration and film thickness. For a cross-linked copolymer film of polyvinyl alcohol and calcium polyacrylate, the rate constant was much greater and dependent on the concentration of copper acetate. The proposed mechanism in each case involves the formation of a copper polyacrylate phase on the surface of the membrane. The diffusion of the copper ion through this phase appears to be the rate controlling step for the copolymer film. The diffusion of the calcium ion is apparently the rate controlling step for the calcium polyacrylate. At low pH, the copper polyacrylate phase consists of the normal copper salt; at higher pH, the phase appears to be the basic copper salt.
Author

N83-28077*# Toledo Univ., Ohio. Dept. of Chemistry.
THERMODYNAMICS OF THE POTASSIUM-SULFUR-OXYGEN AND RELATED SYSTEMS Final Report
J. G. EDWARDS May 1983 56 p refs
(Contract NSG-3250)
(NASA-CR-168155; NAS 1.26:168155) Avail: NTIS HC A04/MF A01 CSCL 20M

The chemical reactions which occur when potassium sulfide, K2S, and potassium sulfite, K2SO3, are heated at temperatures where their vapor pressures are significant, were studied and the vapor pressures and the partial pressures of the chemical products were measured. Mass spectrometry of the vapor of potassium sulfide revealed only K(g). X-ray studies of the solid residues from vaporization experiments revealed K2S2(s) and chemical analyses of the same solid residues showed that the residues approached a composition K2Sx with x in the range 3-4. Vapor pressure of K2S was measured by simultaneous Knudsen-effusion and torsion-effusion (SKETE) in crucibles of aluminum oxide and of graphite. In each such experiment, the vapor pressures agreed initially, but then the apparent pressure by Knudsen-effusion increased suddenly and remained much greater than that by torsion-effusion for the remainder of the experiment. Results of third-law analysis of the torsion pressures imply a delta H (298K) of formation of K2S(s) of -364 + or - 12 kJ/mol. Vapor pressures over K2SO3(s) were measured by simultaneous Knudsen and torsion-effusion and by mass spectrometry. The vapor pressures of both K2S2O5(s) and K2SO3(s) were nonreproducible at a given temperature due to the vaporization reactions of the materials being irreversible under conditions in effusion cells. A.R.H.

N83-29311*# National Aeronautics and Space Administration. Lewis Research Center, Cleveland, Ohio.
THE ADSORPTION AND THERMAL DECOMPOSITION OF TRICRESYLPHOSPHATE (TCP) ON IRON AND GOLD
D. R. WHEELER and O. D. FAUT (Wilkes Coll.) 1983 17 p refs Presented at the 5th Symp. on Appl. Surface Analysis, Dayton, Ohio, 8-10 Jun. 1983; sponsored by Dayton Univ.
(NASA-TM-83441; E-1738; NAS 1.15:83441) Avail: NTIS HC A02/MF A01 CSCL 07E

Because tricresyl-phosphate (TCP) is a common antiwear additive in lubricants, there is great interest in its interactions with metal substrates. The TCP was allowed to adsorb on polycrystalline iron and gold at room temperature. X-ray photoelectron spectroscopy (XPS) was used to analyze the adsorbed species. The substrate was then heated in steps to 330 C, and the changes in the adsorbate were analyzed after each step. On both substrates saturation adsorption occurred at about one monolayer, but the sticking coefficient was less on gold than on iron. Comparison of the XPS spectra of TCP on each substrate with the spectrum from condensed TCP indicated nondissociative adsorption on gold, possibly by dipole-induced dipole interaction. On iron, there was apparently additional interaction between the substrate and the tolyl groups on the TCP molecule. TCP began to desorb molecularly from gold as soon as the gold was heated above room temperature. The desorption was complete by 200 C. However, when the iron substrate was heated, TCP did not desorb but decomposed between 150 and 250 C. S.L.

24

COMPOSITE MATERIALS

Includes laminates.

A83-12414* Army Propulsion Lab., Cleveland, Ohio.
FATIGUE BEHAVIOR OF SIC REINFORCED TI/6AL-4V/ AT 650 C
R. T. BHATT (U.S. Army, Propulsion Laboratory, Cleveland, OH) and H. H. GRIMES (NASA, Lewis Research Center, Cleveland, OH) Metallurgical Transactions A - Physical Metallurgy and Materials Science, vol. 13A, Nov. 1982, p. 1933-1938. refs

Axial, low cycle fatigue properties of 25 and 44 fiber vol pct SiC/Ti(6Al-4V) composites, measured at 650 C, were compared with the fatigue properties of unreinforced Ti(6Al-4V) at the same temperature. A prior study of the fatigue behavior of this composite system at room temperature indicated that the SiC fiber reinforcement did not provide the anticipated improvement of fatigue resistance of this alloy. At 650 C, the composite fatigue properties degraded somewhat from those at room temperature. However, these properties degraded more for the unreinforced matrix at 650 C with the result that the composite fatigue strength was two to three times the fatigue strength of the matrix alloy. The reasons for this reversal are discussed in terms of crack initiation at broken fibers and residual matrix stresses. (Author)

A83-12734* Northwestern Univ., Evanston, Ill.
COMPOSITES WITH PERIODIC MICROSTRUCTURE
T. IWAKUMA and S. NEMAT-NASSER (Northwestern University, Evanston, IL) (Symposium on Advances and Trends in Structural and Solid Mechanics, Washington, DC, Oct. 4-7, 1982.) Computers and Structures, vol. 16, no. 1-4, 1983, p. 13-19. refs
(Contract NAG3-134)

For an elastic body containing periodically distributed inhomogeneities, a general procedure is developed for estimating the overall properties of the composite in terms of several infinite series which, for the isotropic matrix (but anisotropic inclusions), depend only on the geometry of the inhomogeneities and hence can be calculated once and for all for each geometry. These infinite series are obtained and tabulated for ellipsoidal inhomogeneities, and the results are used to estimate the overall elastic moduli of composites which contain spherical or ellipsoidal voids or elastic inclusions. (Author)

A83-20447* National Aeronautics and Space Administration. Lewis Research Center, Cleveland, Ohio.
PMR POLYIMIDES - REVIEW AND UPDATE
T. T. SERAFINI, P. DELVIGS, and W. B. ALSTON (NASA, Lewis Research Center; U.S. Army, Research and Technology Laboratories, Cleveland, OH) In: National SAMPE Symposium and Exhibition, 27th, San Diego, CA, May 4-6, 1982, Proceedings. Azusa, CA, Society for the Advancement of Material and Process Engineering, 1982, p. 320-335. refs
(Previously announced in STAR as N82-24342)

A83-23608* United Technologies Research Center, East Hartford, Conn.
BISIMIDE AMINE CURED EPOXY /IME/ RESINS AND COMPOSITES. II - TEN-DEGREE OFF-AXIS TENSILE AND SHEAR PROPERTIES OF CELION 6000/IME COMPOSITES
D. A. SCOLA (United Technologies Research Center, East Hartford, CT) In: Material and process advances '82; Proceedings of the Fourteenth National SAMPE Technical Conference, Atlanta, GA, October 12-14, 1982. Azusa, CA, Society for the Advancement of Material and Process Engineering, 1982, p. 58-69. refs
(Contract NAS3-22521)

Bisimide amines (BIAs), which are presently used as curing agents in a state-of-the-art epoxy resin, are oligomeric and polymeric mixtures. A series of composites consisting of the novel BIA-cured epoxy resin reinforced with Celion 6000 graphite fibers were fabricated and evaluated, and the ten-degree, off-axis uniaxial tensile and shear properties of these composites were determined. The use of the intralaminar shear strain-to-failure was used in the calculation of resin shear strain-to-failure. Study results indicate that several of these novel composite systems exhibit shear strain properties that are superior to those of the control composite system of the present experiments, which employed a sulfone curing agent. O.C.

A83-29886*# National Aeronautics and Space Administration. Lewis Research Center, Cleveland, Ohio.
LOW CYCLE FATIGUE BEHAVIOR OF ALUMINUM/STAINLESS STEEL COMPOSITES
R. B. BHAGAT (NASA, Lewis Research Center, Cleveland, OH; Indian Institute of Technology, Bombay, India) IN: Structures, Structural Dynamics and Materials Conference, 24th, Lake Tahoe, NV, May 2-4, 1983, Collection of Technical Papers. Part 2 . New York, American Institute of Aeronautics and Astronautics, 1983, p. 744-752. refs
(AIAA 83-0806)

Composites consisting of an aluminum matrix reinforced with various volume fractions of stainless steel wire were fabricated by hot die pressing under various conditions of temperature, time, and pressure. The composites were tested in plane bending to complete fracture under cycle loading, and the results were analyzed on a computer to obtain a statistically valid mathematical relationship between the low-cycle fatigue life and the fiber volume fraction of the composite. The fractured surfaces of the composites were examined by scanning electron microscopy to identify the characteristic features of fatigue damage. Fatigue damage mechanisms are proposed and discussed. V.L.

A83-31793* National Aeronautics and Space Administration. Lewis Research Center, Cleveland, Ohio.
DYNAMIC MECHANICAL CHARACTERIZATION OF CURE OF A POLYIMIDE-GRAPHITE FIBER COMPOSITE (PMR 15/CELION 6000)
F. I. HURWITZ (NASA, Lewis Research Center, Cleveland, OH) Polymer Composites (ISSN 0272-8397), vol. 4, April 1983, p. 90-97. refs

Dynamic mechanical studies of thermosetting PMR 15 polyimide/Celion 6000 composites were used to characterize cure behavior. Variation in composite shear modulus with cure time for laminates partially cured under 3.45 MPa pressure was compared

with that of laminates fully cured under pressure to select a partially cured system whose behavior corresponded with that of the pressure-cured composites. An empirical kinetic model was developed that relates relative composite shear moduli to cure time and temperature. This model, coupled with standard statistical techniques, was used in the determination of an overall activation energy, E = 145 kj/mole (35 kcal/mole) and order of reaction, n, for the cure reaction(s). The empirical relationship defining dynamic modulus as a function of time and temperature remained linear well into the glassy region. Changes in dynamic glass-transition temperature and in the breadth of the transition peaks with cure time are discussed. Shear modulus and damping were found to be more sensitive measures of relative extent of cure than Fourier transform infrared spectroscopy. Author

A83-33115* National Aeronautics and Space Administration. Lewis Research Center, Cleveland, Ohio.
ENVIRONMENTAL EFFECTS ON GRAPHITE FIBER REINFORCED PMR-15 POLYIMIDE
T. T. SERAFINI and M. P. HANSON (NASA, Lewis Research Center, Cleveland, OH) IN: Composites for extreme environments . Philadelphia, PA, American Society for Testing and Materials, 1982, p. 5-19. refs

Studies were conducted to establish the effects of thermo-oxidative and hydrothermal exposure on the mechanical properties of T300 graphite fabric reinforced PMR-15 composites. The effects of hydrothermal exposure on the mechanical properties of HTS-2 continuous graphite fiber composites were also investigated. The thermo-oxidative stability characteristics of T300 fabric and T300 fabric/PMR-15 composites were determined. Flexural strengths of specimens were determined. The useful lifetime of T300 fabric/PMR-15 composites in air at 316 C was found to be about 100 hours. The useful lifetimes in air at 228 and 260 C were determined to be 500 and 1000 hours, respectively. Absorbed moisture was found to reduce the elevated temperature properties of both the T300 fabricate and HTS-2 continuous fiber composites. The moisture effect was found to be reversible. Previously announced in STAR as N81-32194 Author

A83-40129* National Aeronautics and Space Administration. Lewis Research Center, Cleveland, Ohio.
HIGH-TEMPERATURE COMPOSITES - STATUS AND FUTURE DIRECTIONS
R. A. SIGNORELLI (NASA, Lewis Research Center, Materials Div., Cleveland, OH) IN: Progress in science and engineering of composites; Proceedings of the Fourth International Conference on Composite Materials, Tokyo, Japan, October 25-28, 1982. Volume 1 . Tokyo/Amsterdam, Japan Society for Composite Materials/North-Holland, 1982, p. 37-48. refs

A summary of research investigations of manufacturing methods, fabrication methods, and testing of high temperature composites for use in gas turbine engines is presented. Ceramic/ceramic, ceramic/metal, and metal/metal composites are considered. Directional solidification of superalloys and eutectic alloys, fiber reinforced metal and ceramic composites, ceramic fibers and whiskers, refractory coatings, metal fiber/metal composites, matrix metal selection, and the preparation of test specimens are discussed. Previously announced in STAR as N82-30336 J.D.

N83-10117* National Aeronautics and Space Administration. Lewis Research Center, Cleveland, Ohio.
ION SPUTTER TEXTURED GRAPHITE Patent
J. S. SOVEY, R. FORMAN, A. N. CURREN, and E. G. WINTUCKY, inventors (to NASA) 15 May 1981 7 p Filed 15 May 1981 Supersedes N81-27198 (19 - 18, p 2448)
(NASA-CASE-LEW-12919-1; US-PATENT-4,349,424; US-PATENT-APPL-SN-264378; US-PATENT-CLASS-204-192E; US-PATENT-CLASS-313-106; US-PATENT-CLASS-313-107; US-PATENT-CLASS-315-5.38) Avail: US Patent and Trademark Office CSCL 11D

A specially textured surface of pyrolytic graphite exhibits extremely low yields of secondary electrons and reduced numbers of reflected primary electrons after impingement of high energy primary electrons. An ion flux having an energy between 500 eV and 1000 eV and a current density between 1.0 mA/sq cm and 6.0 mA/sq cm produces surface roughening or texturing which is in the form of needles or spines. Such textured surfaces are especially useful as anode collector plates in high efficiency electron tube devices.
Official Gazette of the U.S. Patent and Trademark Office

N83-10118*# National Aeronautics and Space Administration. Lewis Research Center, Cleveland, Ohio.
LOWER-CURING-TEMPERATURE PMR POLYIMIDES
P. DELVIGS Oct. 1982 11 p refs Presented at the Natl. Tech. Conf. of the Soc. of Plastics Engr., Bal Harbour, Fla., 25-27 Oct. 1982
(NASA-TM-82958; E-1375; NAS 1.15:82958) Avail: NTIS HC A02/MF A01 CSCL 11G

Partial substitution of a p-aminostyrene end-cap for the monomethyl ester of 5-norbornene-2, 3-dicarboxylic acid lowered the final cure temperature of typical PMR resins from 600 F to 500 F. The weight loss characteristics of neat resins and graphite fiber composites prepared by using the mixed end-cap approach were determined at 600 F. The room temperature and short-time elevated temperature mechanical properties of the composites at 550 F and 600 F were determined. The mechanical property retention characteristics of the composites at 550 F and 600 F are discussed. Author

N83-11231*# National Aeronautics and Space Administration. Lewis Research Center, Cleveland, Ohio.
ACOUSTO-ULTRASONIC CHARACTERIZATION OF FIBER REINFORCED COMPOSITES
A. VARY *In* Army Materials and Mechanics Research Center Proc. of the Critical Rev. p 231-242 May 1982 refs Document previously announced as N81-28458
Avail: NTIS HC A21/MF A01 CSCL 11D

The advantageous aspects of acoustic emission and ultrasonic methodologies are combined in a technique which operates by introducing a repeating series of ultrasonic pulses into a material. The waves introduced simulate the spontaneous stress waves that would arise if the material were put under stress as in the case of acoustic emission measurements. These benign stress waves are detected by an acoustic emission sensor. The physical arrangement of the ultrasonic (input) transducer and acoustic emission (output) sensor is such that the resultant waveform carries an imprint of morphological factors that govern or contribute to material performance. The output waveform is quite complex, but it can be quantitized in terms of a 'stress wave factor'. The stress wave factor, which can be defined in a number of ways, is essentially a relative measure of the efficiency of energy dissipation in a material. If flaws or other material anomalies exist in the volume being examined, their combined effect will appear in the stress wave factor. Author

N83-11247*# Fiber Materials, Inc., Biddeford, Maine.
ALUMINA FIBER STRENGTH IMPROVEMENT Final Report
R. T. PEPPER and D. C. NELSON Sep. 1982 53 p refs (Contract NAS3-22154)
(NASA-CR-167999; NAS 1.26:167999) Avail: NTIS HC A04/MF A01 CSCL 11D

The effective fiber strength of alumina fibers in an aluminum composite was increased to 173,000 psi. A high temperature heat treatment, combined with a glassy carbon surface coating, was used to prevent degradation and improve fiber tensile strength. Attempts to achieve chemical strengthening of the alumina fiber by chromium oxide and boron oxide coatings proved unsuccessful. A major problem encountered on the program was the low and inconsistent strength of the Dupont Fiber FP used for the investigation. Author

N83-12161*# National Aeronautics and Space Administration. Lewis Research Center, Cleveland, Ohio.
RESEARCH ON ULTRA-HIGH-TEMPERATURE MATERIALS, MONOLITHIC CERAMICS, CERAMIC MATRIX COMPOSITES AND CARBON/CARBON COMPOSITES
T. J. MILLER and H. H. GRIMES *In* NASA. Langley Research Center Advan. Mater. Technol. p 275-292 Nov. 1982 refs
Avail: NTIS HC A19/MF A01 CSCL 11D

Research on three classes of materials that show potential for allowing significant increases in operating temperatures in gas turbine engines is discussed. Monolithic ceramics, ceramic matrix composites, and carbon-carbon composites are discussed. Sintering, hot pressing, and densification are discussed. R.J.F.

N83-12175*# National Aeronautics and Space Administration. Lewis Research Center, Cleveland, Ohio.
PMR-15 POLYIMIDE MODIFICATIONS FOR IMPROVED PREPREG TACK
R. D. VANNUCCI 1982 13 p refs Presented at the Natl. Tech. Conf. of the Soc. of Plastic Engr., Bal Harbour, Fla., 25-27 Oct. 1982
(NASA-TM-82951; E-1361; NAS 1.15:82951) Avail: NTIS HC A02/MF A01 CSCL 11D

The use of mixed solvents and of modified monomeric ester reactants was investigated as a means of improving the tack and drape retention characteristics of PMR-15 polyimide prepreg. Methanol, ethanol, 1-propanol and 1-butaol were used to prepare the esters, prepreg solutions, and T-300 graphite fabric and Celion 6000 unidirectional fiber prepregs. The tack retention characteristics of the T-300 fabric prepreg after exposure to simulated use conditions were determined using a simple lap shear test. Drape was qualitatively assessed by visually monitoring the deformability of the prepreg. Thermo-oxidative stability and mechanical properties retention of the Celion 6000 grahite fiber composites were determined as a function of exposure time in air at 600 F.
Author

N83-12176*# National Aeronautics and Space Administration. Lewis Research Center, Cleveland, Ohio.
METHOD AND APPARATUS FOR GRIPPING UNIAXIAL FIBROUS COMPOSITE MATERIALS Patent Application
J. D. WHITTENBERGER and F. I. HURWITZ, inventors (to NASA) 15 Sep. 1982 11 p
(NASA-CASE-LEW-13758-1; US-PATENT-APPL-SN-418139)
Avail: NTIS HC A02/MF A01 CSCL 11D

A strip specimen is cut from a unidirectional strong, brittle fiber composite material, and the surfaces of both ends of the specimen are grit-blasted. The specimen is then placed between metal load transfer members having grit-blasted surfaces. Sufficient compressive stress is applied to the load transfer members to prevent slippage during testing at both elevated temperatures and room temperatures. The need for adhesives, load pads, and other secondary composite processing is eliminated. This gripping system was successful in tensil testing, creep-rupture testing, and fatigue testing uniaxial composite materials at 316 C. NASA

N83-13173*# Purdue Univ., Lafayette, Ind. Composite Materials Lab.
DYNAMIC RESPONSES OF GRAPHITE/EPOXY LAMINATED BEAM TO IMPACT OF ELASTIC SPHERES
C. T. SUN and T. WANG Sep. 1982 59 p refs
(Contract NSG-3185)
(NASA-CR-165461; NAS 1.26:165461; CML-82-4) Avail: NTIS HC A04/MF A01 CSCL 11D

Wave propagation in 90/45/90/-45/90$_2$s and 0/45/0/-45/0$_2$s laminates of a graphite/epoxy composite due to impact of a steel ball was investigated experimentally and also by using a high order beam finite element. Dynamic strain responses at several locations were obtained using strain gages. The finite element program which incorporated statically determined contact laws was employed to calculate the contact force history as well as the target beam dynamic deformation. The comparison of the finite element solutions with the experimental data indicated that the static contact laws for loading and unloading (developed under this grant) are adequate for the dynamic impact analysis. It was found that for the 0/45/0/-45/0$_2$s laminate which has a much larger longitudinal bending rigidity, the use of beam finite elements is not suitable and plate finite element should be used instead.
Author

N83-13178*# IIT Research Inst., Chicago, Ill.
HIGH STRAIN RATE PROPERTIES OF UNDIRECTIONAL COMPOSITES, PART 1 Final Report, 11 Jul. 1977 - 11 Apr. 1981
I. M. DANIEL Nov. 1981 460 p refs
(Contract NAS3-21016)
(NASA-CR-167969; NAS 1.26:167969) Avail: NTIS HC A20/MF A01 CSCL 11D

Experimental methods were developed for testing and characterization of composite materials at strain rates ranging from quasi-static to over 500s-1. Three materials were characterized, two graphite/epoxies and a graphite/S-glass/epoxy. Properties were obtained by testing thin rings 10.16 cm (4 in.) in diameter, 2.54 cm (1 in.) wide, and 6 to 8 plies thick under internal pressure. Unidirectional 0-deg, 90-deg, and 10-deg off-axis rings were tested to obtain longitudinal, transverse, and in-plane shear properties. In the dynamic tests internal pressure was applied explosively through a liquid and the pressure was measured with a calibrated steel ring. Strains in the calibration and specimen rings were recorded with a digital processing oscilloscope. The data were processed and the equation of motion solved numerically by the mini-computer attached to the oscilloscope. Results were obtained and plotted in the form of dynamic stress-strain curves. Longitudinal properties which are governed by the fibers do not vary much with strain rate with only a moderate (up to 20 percent) increase in modulus.
Author

N83-13179*# IIT Research Inst., Chicago, Ill.
HIGH STRAIN RATE PROPERTIES OF OFF-AXIS COMPOSITE LAMINATES, PART 2 Final Report, 11 Jul. 1977 - 11 Apr. 1981
I. M. DANIEL Nov. 1981 172 p refs
(Contract NAS3-21016)
(NASA-CR-167970; NAS 1.26:167970) Avail: NTIS HC A08/MF A01 CSCL 11D

Unidirectional off-axis graphite/epoxy and graphite/S-glass/epoxy laminates were characterized in uniaxial tension at strain rates ranging from quasi-static to over 500s-1. Laminate ring specimens were loaded by internal pressure with the tensile stress at 22.5, 30, and 45 deg with the fiber direction. Results were presented in the form of stress-strain curves to failure. Properties determined included moduli, Poisson's ratios, strength, and ultimate strain. In all three laminates of both materials the modulus and strength increase sharply with strain rate, reaching values roughly 100%, 150%, and 200% higher than corresponding static values for the (22.5 sub 8, (30 sub 8), and 45 sub 8) laminates, respectively. In the case of ultimate strain no definite trends could be established, but the maximum deviation from the average of any value for any strain rate was less than 18%.
Author

N83-13180*# IIT Research Inst., Chicago, Ill.
HIGH STRAIN PROPERTIES OF ANGLE-PLY COMPOSITE LAMINATE, PART 3 Final Report, 11 Jul. 1977 - 11 Apr. 1981
I. M. DANIEL Nov. 1982 383 p refs
(Contract NAS3-21016)
(NASA-CR-167971; NAS 1.26:167971) Avail: NTIS HC A17/MF A01 CSCL 11D

Angle-ply graphite/epoxy and graphite/S-glass/epoxy laminates were characterized in uniaxial tension at strain rates ranging from quasi-static to over 500s-1. Laminate ring specimens and layups were loaded under internal pressure. Results were presented in the form of stress-strain curves to failure. Properties determined included moduli, Poisson's ratios, strength, and ultimate strain. In all seven laminates for the two materials tested the modulus and strength increase with strain rate. The effect of strain rate varies with layup, being lowest for the fiber dominated laminates and

highest for the matrix dominated laminates. Ultimate strains do not show any significant trends with strain rate. In almost all cases the ultimate strain values are within plus or minus 20 percent of the mean value and in half of the cases the deviations from the mean are less than 10 percent. R.J.F.

N83-15362*# National Aeronautics and Space Administration. Lewis Research Center, Cleveland, Ohio.
HYGROTHERMOMECHANICAL EVALUATION OF TRANSVERSE FILAMENT TAPE EPOXY/POLYESTER FIBERGLASS COMPOSITES
R. L. LARK and C. C. CHAMIS 1983 24 p refs Proposed for presentation at the 38th Ann. Conf. of the Society of Plastics Industry (SPI) Reinforced Plastics/Composites Inst., Houston, Tex., 7-11 Feb. 1983
(NASA-TM-83044; E-1491; NAS 1.15:83044) Avail: NTIS HC A02/MF A01 CSCL 11D

The static and cyclic load behavior of transverse filament tape (TFT) fiberglass/epoxy and TFY fiberglass/polyester composites, intended for use in the design of low-cost wind turbine blades, are presented. The data behavior is also evaluated with respect to predicted properties based on an integrated hygrothermomechanical response theory. Experimental TFT composite data were developed by the testing of laminates made by using composite layups typical of those used for the fabrication of TFT fiberglass wind turbine blades. Static properties include tension, compression, and interlaminar shear strengths at ambient conditions and at high humidity/elevated temperature conditions after a 500 hour exposure. Cyclic fatigue data were obtained using similar environmental conditions and a range of cyclic stresses. The environmental (temperature and moisture) and cyclic load effects on composite strength degradation are subsequently compared with the predictions obtained by using the composite life/durability theory. The results obtained show that the predicted hygrothermomechanical environmental effects on TFT composites are in good agreement with measured data for various properties including fatigue at different cyclic stresses. S.L.

N83-15363*# National Aeronautics and Space Administration. Lewis Research Center, Cleveland, Ohio.
DYNAMIC MECHANICAL PROPERTIES OF N-PHENYLNADIMIDE MODIFIED PMR POLYIMIDE COMPOSITES
R. H. PATER 1983 9 p refs Proposed for presentation at the 185th Natl. Meeting of the Am. Chem. Soc., Seattle, 20-25 Mar. 1983
(NASA-TM-83051; E-1505; NAS 1.15:83051) Avail: NTIS HC A02/MF A01 CSCL 11D

The rheological behavior of newly developd Celion 6000/N-phenylnadimide modified PMR polyimide and PMR-15 composites was investigated. The dynamic mechanical properties were correlated with the structure of N-phenylnadimide modified PMR polyimides. The storage modulus (G'), loss modulus (G''), and loss tangent (tan delta) of four composite systems were measured over a temperature range from -150 to 400 C. Three well defined peaks were seen in the regions of 360, 100, and -120 C, corresponding to the alpha, beta, and gamma relaxations, respectively, of the matrix resins. The activation energies of the alpha, beta, and gamma relaxations were estimated to be 232, 60, and 14 kcal/mole, respectively, for PMR-15. Addition of N-phenylnadimide to the PMR-15 composition lowered the glass transition temperature and the activation energies of PMR-15 polyimide. The dynamic mechanical data appear to be consistent with the formation of a copolymer from N-phenylnadimide and a PMR-15 prepolymer. S.L.

N83-15364*# National Aeronautics and Space Administration. Lewis Research Center, Cleveland, Ohio.
PMR POLYIMIDE COMPOSITES FOR AEROSPACE APPLICATIONS
T. T. SERAFINI 1982 22 p refs Presented at the 1st Tech. Conf. on Polyimides, Ellenville, N.Y., 10-12 Nov. 1982; sponsored by the Society of Plastics Engineers, Inc.
(NASA-TM-83047; E-1494; NAS 1.15:83047) Avail: NTIS HC A02/MF A01 CSCL 11D

Fiber reinforced PMR polyimides are finding increased acceptance as engineering materials for high performance structural applications. Prepreg materials based on this novel class of highly processable, high temperature resistant polyimides, are commercially available and the PMR concept was incorporated in several industrial applications. The status of PMR polyimides is reviewed. Emphasis is given to the chemistry, processing, and applications of the first generation PMR polyimides known as PMR-15. S.L.

N83-15365*# National Aeronautics and Space Administration. Lewis Research Center, Cleveland, Ohio.
THE 371 DEG C(700 DEG F) PROPERTIES OF CELION 6000/N-PHENYLNADIMIDE MODIFIED PMR POLYIMIDE COMPOSITES
R. H. PATER 1982 12 p refs Presented at the Natl. Tech. conf. of the Society of Plastics Engineers, Bal Harbour, Fla., 25-27 Oct. 1982
(NASA-TM-83050; E-1504; NAS 1.15:83050) Avail: NTIS HC A02/MF A01 CSCL 11D

The 371 C (700 F) properties of Celion 6000/N-phenylnadimide modified PMR-15 polyimide composites were investigated to determine the feasibility of using these materials at a 371 C (700 F) service temperature. The processing characteristics and physical and mechanical properties of the composite systems are presented. The results of the 371 C (700 F) thermo-oxidation stability study suggest that the composite materials can be considered for short term (at least 100 hours) application at 371 C (700 F). S.L.

N83-16394*# Wyoming Univ., Laramie. Dept. of Mechanical Engineering.
THREE-DIMENSIONAL ELASTOPLASTIC STRESS ANALYSIS OF UNIDIRECTIONAL BORON/ALUMINUM COMPOSITES
J. M. MAHISHI and D. F. ADAMS Oct. 1982 37 p refs (Contract NSG-3217)
(NASA-CR-169796; NAS 1.26:169796; UWME-DR-201-107-1) Avail: NTIS HC A03/MF A01 CSCL 11D

A three dimensional elastoplastic finite element micromechanical model was developed to study the state of stress around a broken fibers in a unidirectional composite. A boron/aluminum composite consisting of 50 percent by volume of fibers in a square array and subjected to an axial loading is taken as a specific example. This loading in the fiber direction is applied in small increments, by prescribing increments of boundary displacement, until the first failure occurs. The effect of reduced material properties of the aluminum matrix material at elevated temperature is also studied. The results are presented in the form of stress contours and stress-strain plots. Author

N83-18853*# Carnegie-Mellon Univ., Pittsburgh, Pa. Dept. of Mechanical Engineering.
RESEARCH PRIORITIES FOR ADVANCED FIBROUS COMPOSITES
K. J. BAUMANN and J. L. SWEDLOW Jul. 1981 209 p refs (Contract NSG-3172)
(NASA-CR-165414; NAS 1.26:165414; SM-79-15A) Avail: NTIS HC A10/MF A01 CSCL 11D

Priorities for research in advanced laminated fibrous composite materials are presented. Supporting evidence is presented in two bodies, including a general literature survey and a survey of aerospace composite hardware and service experience. Both surveys were undertaken during 1977-1979. Specific results and conclusions indicate that a significant portion of contemporary published research diverges from recommended priorites. Author

N83-18854*# Carnegie-Mellon Univ., Pittsburgh, Pa. Dept. of Mechanical Engineering.
RESEARCH PRIORITIES AND HISTORY OF ADVANCED COMPOSITE COMPRESSION TESTING
K. J. BAUMANN Jul. 1981 47 p refs
(Contract NSG-3172)
(NASA-CR-165415; NAS 1.26:165415; SM-79-25B) Avail: NTIS HC A03/MF A01 CSCL 11D

Priorities for standard compression testing research in advanced laminated fibrous composite materials are presented along with a state of the art survey (completed in 1979) including history and commentary on industrial test methods. Historically apparent research priorities and consequent (lack of) progress are supporting evidence for newly derived priorities. Author

N83-19817*# National Aeronautics and Space Administration. Lewis Research Center, Cleveland, Ohio.
SIMPLIFIED COMPOSITE MICROMECHANICS EQUATIONS FOR HYGRAL, THERMAL AND MECHANICAL PROPERTIES
C. C. CHAMIS 1983 20 p refs Presented at the 38th Ann. Conf. of the Society of the Plastics INdustry (SPI) Reinforced Plastics/Composites Inst., Houston, Tex., 7-11 Feb. 1983
(NASA-TM-83320; E-1561; NAS 1.15:83320) Avail: NTIS HC A02/MF A01 CSCL 11D

A unified set of composite micromechanics equations of simple form is summarized and described. This unified set can be used to predict unidirectional composite (ply) geometric, mechanical, thermal and hygral properties using constituent material (fiber/matrix) properties. This unified set also includes approximate equations for predicting (1) moisture absorption; (2) glass transition temperature of wet resins; and (3) hygrothermal degradation effects. Several numerical examples are worked-out to illustrate ease of use and versatility of these equations. These numerical examples also demonstrate the interrelationship of the various factors (geometric to environmental) and help provide insight into composite behavior at the micromechanistic level. Author

N83-22325*# Purdue Univ., Lafayette, Ind. School of Aeronautics and Astronautics.
WAVE PROPAGATION IN GRAPHITE/EPOXY LAMINATES DUE TO IMPACT Interim Report
T. M. TAN and C. T. SUN Dec. 1982 171 p refs
(Contract NSG-3185)
(NASA-CR-168057; NAS 1.26:168057; CML-82-5) Avail: NTIS HC A08/MF A01 CSCL 11D

The low velocity impact response of graphite-epoxy laminates is investigated theoretically and experimentally. A nine-node isoparametric finite element in conjunction with an empirical contact law was used for the theoretical investigation. Flat laminates subjected to pendulum impact were used for the experimental investigation. Theoretical results are in good agreement with strain gage experimental data. The collective results of the investigation indicate that the theoretical procedure describes the impact response of the laminate up to about 150 in/sec. impact velocity. S.L.

N83-22326*# Avco Corp., Lowell, Mass. Specialty Materials Div.
HYBRIDIZED POLYMER MATRIX COMPOSITES Final Report
J. HENSHAW 4 Apr. 1983 70 p
(Contract NAS3-21385)
(NASA-CR-165341; NAS 1.26:165341) Avail: NTIS HC A04/MF A01 CSCL 11D

Methods of improving the fire resistance of graphite epoxy composite laminates were investigated with the objective of reducing the volume of loose graphite fibers disseminated into the airstream as the result of a high intensity aircraft fuel fire. Improvements were sought by modifying the standard graphite epoxy systems without significantly negating their structural effectiveness. The modifications consisted primarily of an addition of a third constituent material such as glass fibers, glass flakes, carbon black in a glassy resin. These additions were designed to encourage coalescense of the graphite fibers and thereby reduce their aerodynamic float characteristics. A total of 38 fire tests were conducted on thin (1.0 mm) and thick (6.0 mm) hybrid panels. Author

N83-24559*# National Aeronautics and Space Administration. Lewis Research Center, Cleveland, Ohio.
DESIGN PROCEDURES FOR FIBER COMPOSITE STRUCTURAL COMPONENTS: RODS, COLUMNS AND BEAM COLUMNS
C. C. CHAMIS 1983 32 p refs Presented at the 38th Ann. Conf. of the Soc. of the Plastics Ind. (SPI) Reinforced Plastics/Composites Inst., Houston, Tex., 7-11 Feb. 1983
(NASA-TM-83321; E-1562; NAS 1.15:83321) Avail: NTIS HC A03/MF A01 CSCL 11D

Step by step procedures are described which are used to design structural components (rods, columns, and beam columns) subjected to steady state mechanical loads and hydrothermal environments. Illustrative examples are presented for structural components designed for static tensile and compressive loads, and fatigue as well as for moisture and temperature effects. Each example is set up as a sample design illustrating the detailed steps that are used to design similar components. Author

N83-25790*# National Aeronautics and Space Administration. Lewis Research Center, Cleveland, Ohio.
EVALUATION OF LOW-COST ALUMINUM COMPOSITES FOR AIRCRAFT ENGINE STRUCTURAL APPLICATIONS
D. L. MCDANIELS and R. A. SIGNORELLI 1983 31 p refs Presented at the 112th Ann. Meeting of the Met. Soc. of the Am. Inst. of Mining, Met. and Petroleum Engineers, Atlanta, 6-10 Mar. 1983
(NASA-TM-83357; E-1618; NAS 1.15:83357) Avail: NTIS HC A03/MF A01 CSCL 11D

Panels of discontinuous SiC composites, with several aluminum matrices, were fabricated and evaluated. Modulus, yield strength and tensile strength results indicated that the properties of composites containing SiC whisker, nodule or particulate reinforcements were similar. The modulus of the composites was controlled by the volume percentage of the SiC reinforcement content, while the strength and ductility were controlled by both the reinforcement content and the matrix alloy. The feasibility of fabricating structural shapes by both wire performs and direct casting was demonstrated for Al2O3/Al composites. The feasibility of fabricating high performance composites into structural shapes by low pressure hot molding was demonstrated for B4C-coated B/Al composites. Author

N83-26928*# Boeing Military Airplane Development, Seattle, Wash. Advanced Airplane Branch.
COMPRESSION AND COMPRESSION FATIGUE TESTING OF COMPOSITE LAMINATES Final Report, 1 Jun. 1981 - 31 Aug. 1982
T. R. PORTER 1982 135 p refs
(Contract NAS3-22812)
(NASA-CR-168023; NAS 1.26:168023; D180-27619-1) Avail: NTIS HC A07/MF A01 CSCL 11D

The effects of moisture and temperature on the fatigue and fracture response of composite laminates under compression loads were investigated. The structural laminates studied were an intermediate stiffness graphite-epoxy composite (a typical angle ply laimna liminate had a typical fan blade laminate). Full and half penetration slits and impact delaminations were the defects examined. Results are presented which show the effects of moisture on the fracture and fatigue strength at room temperature, 394 K (250 F), and 422 K (300 F). Static tests results show the effects of defect size and type on the compression-fracture strength under moisture and thermal environments. The cyclic tests results compare the fatigue lives and residual compression strength under compression only and under tension-compression fatigue loading. A.R.H.

N83-28095*# National Aeronautics and Space Administration. Lewis Research Center, Cleveland, Ohio.
DIAMONDLIKE FLAKE COMPOSITES Patent Application
B. A. BANKS, inventor (to NASA) 17 May 1983 10 p
(NASA-CASE-LEW-13837-1; US-PATENT-APPL-SN-495381)
Avail: NTIS HC A02/MF A01 CSCL 11D

A carbon coating is vacuum arc deposited on a smooth surface of a target which is simultaneously ion beam sputtered. The bombarding ions have sufficient energy to create diamond bombs. Spalling occurs as the carbon deposit thickens. The resulting diamond like carbon flakes are mixed with a binder or matrix material to form a composite material having improved thermal, electrical, mechanical, and tribological properties when used in aerospace structures and components. NASA

25

INORGANIC AND PHYSICAL CHEMISTRY

Includes chemical analysis, e.g., chromatography; combustion theory; electrochemistry; and photochemistry.

A83-10612* Massachusetts Inst. of Tech., Cambridge.
MOLECULAR-ORBITAL MODEL FOR METAL-SAPPHIRE INTERFACIAL STRENGTH
K. H. JOHNSON (MIT, Cambridge, MA) and S. V. PEPPER (NASA, Lewis Research Center, Cleveland, OH) Journal of Applied Physics, vol. 53, Oct. 1982, p. 6634-6637. refs
(Contract NSF DMR-78-24185; NCC3-1)

Self-consistent-field X-Alpha scattered-wave cluster molecular-orbital models have been constructed for transition and noble metals (Fe, Ni, Cu, and Ag) in contact with a sapphire (Al2O3) surface. It is found that a chemical bond is established between the metal d-orbital electrons and the nonbonding 2p-orbital electrons of the oxygen anions on the Al2O3 surface. An increasing number of occupied metal-sapphire antibonding molecular orbitals explains qualitatively the observed decrease of contact shear strength through the series Fe, Ni, Cu, and Ag. (Author)

A83-11491*# Solar Turbines International, San Diego, Calif.
COMBUSTION CHARACTERISTICS OF HYDROGEN-CARBON MONOXIDE BASED GASEOUS FUELS
D. J. WHITE, A. J. KUBASCO, R. T. LECREN (Solar Turbines, Inc., San Diego, CA), and J. J. NOTARDONATO (NASA, Lewis Research Center, Cleveland, OH) IEEE, ASME, and ASCE, Joint Power Generation Conference, Denver, CO, Oct. 17-21, 1982, Paper. 13 p. Research supported by the U.S. Department of Energy
(Contract DEN3-145)

The results of trials with a staged combustor designed to use coal-derived gaseous fuels and reduce the NO(x) emissions from nitrogen-bound fuels to 75 ppm and 37 ppm without bound nitrogen in 15% O2 are reported. The combustor was outfitted with primary zone regenerative cooling, wherein the air cooling the primary zone was passed into the combustor at 900 F and mixed with the fuel. The increase in the primary air inlet temperature eliminated flashback and autoignition, lowered the levels of CO, unburned hydrocarbons, and smoke, and kept combustion efficiencies to the 99% level. The combustor was also equipped with dual fuel injection to test various combinations of liquid/gas fuel mixtures. Low NO(x) emissions were produced burning both Lurgi and Winkler gases, regardless of the inlet pressure and temperature conditions. Evaluation of methanation of medium energy gases is recommended for providing a fuel with low NO(x) characteristics. M.S.K.

A83-11492*# General Motors Corp., Indianapolis, Ind.
MULTIFUEL EVALUATION OF RICH/QUENCH/LEAN COMBUSTOR
A. S. NOVICK, D. L. TROTH (General Motors Corp., Detroit Diesel Allison Div., Indianapolis, IN), and J. NOTARDONATO (NASA, Lewis Research Center, Cleveland, OH) IEEE, ASME, and ASCE, Joint Power Generation Conference, Denver, CO, Oct. 18, 1982, Paper. 9 p. Research supported by the U.S. Department of Energy. refs

Test results on the RQL low NO(x) industrial gas turbine engine are reported. The air-staged combustor comprises an initial rich burning zone, followed by a quench zone, and a lean reaction and dilution zone. The combustor was tested as part of the DoE/NASA program to define the technology for developing a durable, low-emission gas turbine combustor capable of operation with minimally processed petroleum residual, synthetic, or low/mid-heating value gaseous fuels. The properties of three liquid and two gaseous fuels burned in the combustor trials are detailed. The combustor featured air staging, variable geometry, and generative/convective cooling. The lean/rich mixtures could be varied in zones simultaneously or separately while maintaining a specified pressure drop. Low NO(x) and smoke emissions were produced with each fuel burned, while high combustor efficiencies were obtained. M.S.K.

A83-13108* Michigan State Univ., East Lansing.
HIGH-VOLTAGE SPARK ATOMIC EMISSION DETECTOR FOR GAS CHROMATOGRAPHY
C. L. CALKIN, S. M. KOEPLIN, and S. R. CROUCH (Michigan State University, East Lansing, MI) Applied Spectroscopy, vol. 36, no. 4, 1982, p. 369-374. refs
(Contract NAG3-93)

A dc-powered, double-gap, miniature nanosecond spark source for emission spectrochemical analysis of gas chromatographic effluents is described. The spark is formed between two thoriated tungsten electrodes by the discharge of a coaxial capacitor. The spark detector is coupled to the gas chromatograph by a heated transfer line. The gas chromatographic effluent is introduced into the heated spark chamber where atomization and excitation of the effluent occurs upon breakdown of the analytical gap. A microcomputer-controlled data acquisition system allows the implementation of time-resolution techniques to distinguish between the analyte emission and the background continuum produced by the spark discharge. Multiple sparks are computer averaged to improve the signal-to-noise ratio. The application of the spark detector for element-selective detection of metals and nonmetals is reported. (Author)

A83-13488*# Kentucky Univ., Lexington.
BOUNDARY INTEGRAL EQUATION METHOD CALCULATIONS OF SURFACE REGRESSION EFFECTS IN FLAME SPREADING
R. A. ALTENKIRCH, M. REZAYAT, R. EICHHORN, and F. J. RIZZO (Kentucky, University, Lexington, KY) ASME, Transactions, Journal of Heat Transfer, vol. 104, Nov. 1982, p. 734-740. refs
(Contract NSG-3114)

A solid-phase conduction problem that is a modified version of one that has been treated previously in the literature and is applicable to flame spreading over a pyrolyzing fuel is solved using a boundary integral equation (BIE) method. Results are compared to surface temperature measurements that can be found in the literature. In addition, the heat conducted through the solid forward of the flame, the heat transfer responsible for sustaining the flame, is also computed in terms of the Peclet number based on a heated layer depth using the BIE method and approximate methods based on asymptotic expansions. Agreement between computed and experimental results is quite good as is agreement between the BIE and the approximate results. (Author)

A83-15870* Case Western Reserve Univ., Cleveland, Ohio.
EXPERIMENTAL STUDY OF ELECTROCHEMICAL FLUORINATION OF TRICHLOROETHYLENE
C. POLISENA, C. C. LIU (Case Western Reserve University, Cleveland, OH), and R. F. SAVINELL (Akron University, Akron, OH) Electrochemical Society, Journal, vol. 129, Dec. 1982, p. 2720-2724. refs
(Contract NSF CPE-81-20216; NAG3-66)

The electrochemical fluorination of trichloroethylene in anhydrous hydrogen fluoride at 0 C and at constant cell potential was investigated. A microprocessor-aided electrochemical fluorination reactor system that yields highly reproducible results was utilized. The following major two-carbon-chain products were observed: CHCl2-CCl2F, CHCl2-CClF2, CHClF-CCl2F, and CCl2F-CClF2. The first step in the reaction sequence was determined to be fluorine addition to the double bond, followed by replacement of first hydrogen and then chlorine by fluorine. Polymerization reactions yielded higher molecular weight or possible ring-type chlorofluorohydrocarbons. A comparison of the reaction products of electrochemical and chemical fluorinations of trichloroethylene is also discussed. (Author)

A83-16606*# Carnegie-Mellon Univ., Pittsburgh, Pa.
IGNITION OF CONFINED GASEOUS MIXTURES BY HOT SURFACES AND HOT WIRES
J. I. RAMOS (Carnegie-Mellon University, Pittsburgh, PA) American Institute of Aeronautics and Astronautics, Aerospace Sciences Meeting, 21st, Reno, NV, Jan. 10-13, 1983, 9 p. refs
(Contract NAG3-21)
(AIAA PAPER 83-0240)

Ignition times and spatial and temporal variations of temperature and concentration in gaseous mixtures confined between two infinite parallel walls or two infinite cylinders have been obtained by numerical integration of the appropriate conservation equations written in Lagrangian coordinates. Ignition times and ignition energies are presented for the case of an isothermal wall in terms of the initial mixture pressure and equivalence ratio for both one and two-step chemical reaction mechanisms. The numerical results indicate that there is a critical mixture pressure for which the ignition time is minimum. The values of this critical pressure are larger (smaller) than 1 atm for the one- (two-) step reaction mechanism. The critical pressure for the ignition time is not equal to the critical pressure for the ignition energy. The ignition time and energy decrease with the equivalence ratio within a certain range and then remain constant. (Author)

A83-20576* National Aeronautics and Space Administration. Lewis Research Center, Cleveland, Ohio.
CROSS-LINKED POLYVINYL ALCOHOL FILMS AS ALKALINE BATTERY SEPARATORS
D. W. SHEIBLEY, M. A. MANZO, and O. D. GONZALEZ-SANABRIA (NASA, Lewis Research Center, Cleveland, OH) Electrochemical Society, Journal, vol. 130, Feb. 1983, p. 255-259. refs
(Contract NAS3-22223)

Cross-linking methods have been investigated to determine their effect on the performance of polyvinyl alcohol (PVA) films as alkaline battery separators. The following types of cross-linked PVA films are discussed: (1) PVA-dialdehyde blends post-treated with an acid or acid periodate solution (two-step method) and (2) PVA-dialdehyde blends cross-linked during film formation (drying) by using a reagent with both aldehyde and acid functionality (one-step method). Laboratory samples of each cross-linked type of film were prepared and evaluated in standard separator screening tests. Then pilot-plant batches of films were prepared and compared to measure differences due to the cross-linking method. The pilot-plant materials were then tested in nickel oxide-zinc cells to compare the two methods with respect to performance characteristics and cycle life. Cell test results are compared with those from tests with Celgard. (Author)

A83-22738* Northwestern Univ., Evanston, Ill.
IGNITION OF A COMBUSTIBLE HALF SPACE
W. E. OLMSTEAD (Northwestern University, Evanston, IL) SIAM Journal on Applied Mathematics, vol. 43, Feb. 1983, p. 1-15. refs
(Contract DE-AC02-78ER-04650; NAS3-3881; N00014-80-C-0196 ; NSF MCS-80-02759)

A half space of combustible material is subjected to an arbitrary energy flux at the boundary where convection heat loss is also allowed. An asymptotic analysis of the temperature growth reveals two conditions necessary for ignition to occur. Cases of both large and order unity Lewis number are shown to lead to a nonlinear integral equation governing the thermal runaway. Some global and asymptotic properties of the integral equation are obtained. (Author)

A83-25268*# Drexel Univ., Philadelphia, Pa.
DROPLET SIZE EFFECTS ON NO/X/ FORMATION IN A ONE-DIMENSIONAL MONODISPERSE SPRAY COMBUSTION SYSTEM
H. SARV, A. A. NIZAMI, and N. P. CERNANSKY (Drexel University, Philadelphia, PA) American Society of Mechanical Engineers, Joint Power Generation Conference, Denver, CO, Oct. 17-21, 1982, 9 p. refs
(Contract NAG3-1)
(ASME PAPER 82-JPGC-GT-10)

A one-dimensional monodisperse aerosol spray combustion facility is described and experimental results of post flame NO/NO(x) emissions are presented. Four different hydrocarbon fuels were studied: isopropanol, methanol, n-heptane, and n-octane. The results indicate an optimum droplet size in the range of 48-58 microns for minimizing NO/NO(x) production for all of the test fuels. This NO(x) behavior is associated with droplet interactions and the transition from diffusive type of spray burning to that of a prevaporized and premixed case. Decreasing the droplet size results in a trend of increasing droplet interactions, which suppresses temperatures and reduces NO(x). This trend continues until prevaporization effects begin to dominate and the system tends towards the premixed limit. The occurrence of the minimum NO(x) point at different droplet diameters for the different fuels appears to be governed by the extent of prevaporization of the fuel in the spray, and is consistent with theoretical calculations based on each fuel's physical properties. (Author)

A83-25269*# General Electric Co., Cincinnati, Ohio.
NASA CLEAN CATALYTIC COMBUSTOR PROGRAM
E. E. EKSTEDT, T. F. LYON, P. E. SABLA, W. J. DODDS (General Electric Co., Cincinnati, OH), and A. J. SZANISZLO (NASA, Lewis Research Center, Cleveland, OH) American Society of Mechanical Engineers, Joint Power Generation Conference, Denver, CO, Oct. 17-21, 1982, 12 p. refs
(ASME PAPER 82-JPGC-GT-11)

The successful operation of an aircraft gas turbine combustion system incorporating a state-of-the-art catalytic reactor as the main stage, along with a conventional pilot stage for low power operation, is reported to have been achieved with high combustion efficiency at moderate engine pressure ratios. The extremely low nitrogen oxides emission goal set by the program as its goal has also been achieved. It is noted that significant improvements in the operating temperature capability of catalytic reactor materials will be required for the successful application of such devices to the very high pressure ratio, high temperature engines assumed to be the ultimate application of the devices studied. O.C.

A83-25675* National Aeronautics and Space Administration. Lewis Research Center, Cleveland, Ohio.
DIAMOND /111/ STUDIED BY ELECTRON ENERGY LOSS SPECTROSCOPY IN THE CHARACTERISTIC LOSS REGION
S. V. PEPPER (NASA, Lewis Research Center, Cleveland, OH) Surface Science, vol. 123, 1982, 47-60. refs

Unoccupied surface states on diamond (111) annealed at greater than 900 C are studied by electron energy loss spectroscopy with valence band excitation. A feature found at 2.1

eV loss energy is attributed to an excitation from occupied surface states into unoccupied surface states of energy within the bulk band gap. A surface band gap of approximately 1 eV is estimated. This result supports a previous suggestion for unoccupied band gap states based on core level energy loss spectroscopy. Using the valence band excitation energy loss spectrosocpy, it is also suggested that hydrogen is removed from the as-polished diamond surface by a Menzel-Gomer-Redhead mechanism. (Author)

A83-30921* National Aeronautics and Space Administration. Lewis Research Center, Cleveland, Ohio.
DIATOMIC MOLECULES AND METALLIC ADHESION, COHESION, AND CHEMISORPTION - A SINGLE BINDING-ENERGY RELATION
J. FERRANTE (NASA, Lewis Research Center, Cleveland, OH), J. R. SMITH (GM Research Laboratories, Warren, MI; California, University, Santa Barbara, CA), and J. H. ROSE (U.S. Department of Energy, Ames Laboratory, Ames, IA) Physical Review Letters (ISSN 0031-9007), vol. 50, May 2, 1983, p. 1385, 1386. refs
(Contract NSF PHY-77-27084; W-7405-ENG-82)

Potential-energy relations involving a few parameters in simple analytic forms have been found to represent well the energetics of a wide variety of diatomic molecules. However, such two-atom potential functions are not appropriate for metals. It is well known that, in the case of metals, there exist strong volume-dependent forces which can never be expressed as pairwise interactions. The present investigation has the objective to show that, in spite of the observation concerning metals, a single binding-energy relation can be found which accurately describes diatomic molecules as well as adhesion, cohesion, and chemisorption on metals. This universality reveals a commonality between the molecular and metallic bond. G.R.

A83-36062*# California Univ., Berkeley.
NUMERICAL SOLUTION OF THE PROBLEM OF FLAME PROPAGATION BY THE USE OF THE RANDOM ELEMENT METHOD
A. F. GHONIEM and A. K. OPPENHEIM (California, University, Berkeley, CA) American Institute of Aeronautics and Astronautics, Aerospace Sciences Meeting, 21st, Reno, NV, Jan. 10-13, 1983. 11 p. refs
(Contract W-7405-ENG-48; NSF CPE-81-15163; NAG3-131)
(AIAA PAPER 83-0600)

A numerical, grid-free algorithm is presented for one-dimensional reaction-diffusion model of laminar flame propagation in premixed gases. It is based on the random element method we developed for the analysis of diffusional processes. The effect of combustion is taken into account by applying the principle of fractional steps to separate the process of diffusion, modeled by the random walk of computational elements, from the exothermic effects of chemical reaction, monitoring their strength. The validity of the algorithm is demonstrated by application to flame propagation problems for which exact solutions exist. The flame speed evaluated by its use oscillates around the exact value at a relatively small amplitude, while the temperature and species concentration profiles are self-correcting in the convergence to the exact solution. A satisfactory resolution is obtained by the use of quite a small number of computational elements which automatically adjust their distribution of fit sharp gradients. Author

A83-36315*# General Electric Co., Schenectady, N. Y.
PREDICTION OF AN AXISYMMETRIC COMBUSTING FLOW
S. M. CORREA (General Electric Co., Schenectady, NY) AIAA, SAE, and ASME, Joint Propulsion Conference, 19th, Seattle, WA, June 27-29, 1983. 7 p. refs
(Contract NAS3-23525)
(AIAA PAPER 83-1264)

A numerical model for turbulent, recirculating combusting flow is developed and applied to a research combustor. The model is based on the time-averaged Navier-Stokes equations with k-epsilon turbulence closure and the compositional fluctuations at each point are given probabilistically in terms of the mixture fraction. The probability density function is derived from transport equations for its first two moments along with an assumption regarding its shape. The resulting equations are solved using a standard line relaxation algorithm. It is found that the predictions of the model are in good agreement with data from an axisymmetric, bluff-body stabilized research combustor, while the major discrepancies are similar to those found in isothermal flow comparisons. The peculiar features of this flow which contribute to the errors are examined. The agreement between the theory and data deteriorates as the central jet velocity is increased which indicates an enhanced role for unsteady effects. N.B.

A83-37045* Kentucky Univ., Lexington.
CORRELATING DOWNWARD FLAME SPREAD RATES FOR THICK FUEL BEDS
R. A. ALTENKIRCH, R. EICHHORN, and A. R. RIZVI (Kentucky, University, Lexington, KY) Combustion Science and Technology (ISSN 0010-2202), vol. 32, no. 1-4, 1983, p. 49-66. refs
(Contract NSG-3114)

Flame spread rates are presented for polymethylmethacrylate fuel beds as a function of gravitational acceleration and ambient pressure and oxygen concentration. The data are correlated by plotting a dimensionless spread rate that is a measure of the heat transferred forward of the flame, required to sustain the flame, compared to the maximum possible forward heat transfer against a Damkoehler number. The latter parameter indicates the approach of the flame to its maximum temperature, where the maximum possible forward heat transfer occurs, such that the dimensionless spread rate approaches unity at large Damkoehler number. Surface regression effects on the flame spread process are incorporated into the dimensionless spread rate, and the final correlation is independent of bed thickness. Author

A83-39274*# Louisiana State Univ., Baton Rouge.
SOOT FORMATION IN PYROLYSIS OF ACETYLENE, ALLENE AND 1,3-BUTADIENE
M. FRENKLACH, M. B. DURGAPRASAD, R. A. MATULA (Louisiana State University, Baton Rouge, LA), and S. TAKI (Louisiana State University, Baton Rouge, LA; Fukui University, Fukui, Japan) Combustion Institute, Spring Technical Meeting, Pasadena, CA, Apr. 11, 12, 1983, Paper. 48 p. refs
(Contract DE-FG22-80PC-30247; NAS3-23542)

The formation of soot behind reflected shock waves in argon-diluted mixtures of acetylene, allene, and 1,3-butadiene was investigated by monitoring the attenuation of a laser beam in both the visible (632.8 nm) and the infrared (3.39 microns) regions of the spectrum. The experiments utilized temperatures ranging from 1500-3100 K, reflected shock pressures of 0.3-7.0 bar, and total carbon atom concentrations of 2-20 x 10 to the 17th atoms/cu cm. A bell-shaped dependence of soot yield on temperature was observed during the pyrolysis of all three compounds, which was similar to that previously found for toluene. For acetylene, the decrese in total pressure was found to shift the soot bell to higher temperatures with a significant increase in the maximum soot yield. A computer simulation for acetylene pyrolysis suggested that the reactions between C2H3, C4H3, and C4H4 may be those which lead to the formation of aromatic structures. In addition, it was found that soot is formed much faster and in much larger quantities from allene than from 1,3-butadiene. N.B.

A83-42246* National Aeronautics and Space Administration. Lewis Research Center, Cleveland, Ohio.
COMBUSTION SYSTEM PROCESSES LEADING TO CORROSIVE DEPOSITS
C. A. STEARNS, F. J. KOHL (NASA, Lewis Research Center, Cleveland, OH), and D. E. ROSNER (Yale University, New Haven, CT) IN: High temperature corrosion; Proceedings of the International Conference, San Diego, CA, March 2-6, 1981 . 1983, p. 441-450. refs

Degradation of turbine engine hot gas path components by high temperature corrosion can usually be associated with deposits even though other factors may also play a significant role. The origins of the corrosive deposits are traceable to chemical reactions which take place during the combustion process. In the case of

hot corrosion/sulfidation, sodium sulfate was established as the deposited corrosive agent even when none of this salt enters the engine directly. The sodium sulfate is formed during the combustion and deposition processes from compounds of sulfur contained in the fuel as low level impurities and sodium compounds, such as sodium chloride, ingested with intake air. In other turbine and power generation situations, corrosive and/or fouling deposits can result from such metals as potassium, iron, calcium, vanadium, magnesium, anad silicon. Previously announced in STAR as N81-23243 Author

A83-46608* Varian Associates, Palo Alto, Calif.
USE OF COLUMN V ALKYLS IN ORGANOMETALLIC VAPOR PHASE EPITAXY (OMVPE)
M. J. LUDOWISE and C. B. COOPER, III (Varian Associates Corporate Solid State Laboratory, Palo Alto, CA) IN: Semiconductor growth technology; Proceedings of the Meeting, Los Angeles, CA, January 26, 27, 1982. Bellingham, WA, SPIE - The International Society for Optical Engineering (SPIE Proceedings. Volume 323), 1982, p. 117-124. refs
(Contract XP-9-8081-1; DE-AC03-79SF-10610; NAS3-22232)

The use of the column V-trialkyls trimethylarsenic (TMAs) and trimethylantimony (TMSb) for the organometallic vapor phase epitaxy (OM-VPE) of III-V compound semiconductors is reviewed. A general discussion of the interaction chemistry of common Group III and Group V reactants is presented. The practical application of TMSb and TMAs for OM-VPE is demonstrated using the growth of GaSb, GaAs(1-y)Sb(y), Al(x)Ga(1-x)Sb, and Ga(1-x)In(x)As as examples. Author

A83-48156* Massachusetts Inst. of Tech., Cambridge.
TURBULENT FLAME PROPAGATION AND COMBUSTION IN SPARK IGNITION ENGINES
G. P. BERETTA, M. RASHIDI, and J. C. KECK (MIT, Cambridge, MA) Combustion and Flame (ISSN 0010-2180), vol. 52, Oct. 1983, p. 217-245. Research supported by the Massachusetts Institute of Technology. refs
(Contract NSG-3245)

Pressure measurements synchronized with high-speed motion-picture records of flame propagation have been made in a transparent-piston engine. The data show that the initial expansion speed of the flame front is close to that of a laminar flame. As the flame expands, its speed rapidly accelerates to a quasi-steady value comparable with that of the turbulent velocity fluctuations in the unburned gas. During the quasi-steady propagation phase, a significant fraction of the gas behind the visible front is unburned. Final burnout of the charge may be approximated by an exponential decay in time. The data have been analyzed in a model-independent way to obtain a set of empirical equations for calculating mass burning rates in spark-ignition engines. The burning equations contain three parameters: the laminar burning speed, a characteristic speed (uT), and a characteristic length (lT). The laminar burning speed is known from laboratory measurements. Tentative correlations relating uT and lT to engine geometry and operating variables have been derived from the engine data. Author

N83-10134*# National Aeronautics and Space Administration. Lewis Research Center, Cleveland, Ohio.
PORE SIZE ENGINEERING APPLIED TO STARVED ELECTROCHEMICAL CELLS AND BATTERIES
K. M. ABBEY and L. H. THALLER 1982 16 p refs Presented at the 17th Intersoc. Energy Conversion Eng. Conf., Los Angeles 8-13 Aug. 1982; sponsored by IEEE
(NASA-TM-82893; E-1271; NAS 1.15:82893) Avail: NTIS HC A02/MF A01 CSCL 10C

To maximize performance in starved, multiplate cells, the cell design should rely on techniques which widen the volume tolerance characteristics. These involve engineering capillary pressure differences between the components of an electrochemical cell and using these forces to promote redistribution of electrolyte to the desired optimum values. This can be implemented in practice by prescribing pore size distributions for porous back-up plates, reservoirs, and electrodes. In addition, electrolyte volume management can be controlled by incorporating different pore size distributions into the separator. In a nickel/hydrogen cell, the separator must contain pores similar in size to the small pores of both the nickel and hydrogen electrodes in order to maintain an optimum conductive path for the electrolyte. The pore size distributions of all components should overlap in such a way as to prevent drying of the separator and/or flooding of the hydrogen electrode. Author

N83-10135*# National Aeronautics and Space Administration. Lewis Research Center, Cleveland, Ohio.
POLYVINYL ALCOHOL MEMBRANES AS ALKALINE BATTERY SEPARATORS
D. W. SHEIBLEY, O. GONZALEZ-SANABRIA, and M. A. MANZO 1982 23 p refs Presented at the Symp. of Membranes and Ionic and Electron. Conducting Polymers, Cleveland, 17-19 May 1982; sponsored by the Electrochemical Society
(NASA-TM-82961; E-1378; NAS 1.15:82961) Avail: NTIS HC A02/MF A01 CSCL 10C

Polyvinly alcohol (PVA) cross-linked with aldehyde reagents yields membranes that demonstrate properties that make them suitable for use as alkaline battery separators. Film properties can be controlled by the choice of cross-linker, cross-link density and the method of cross-linking. Three methods of cross-linking and their effects on film properties are discussed. Film properties can also be modified by using a copolymer of vinyl alcohol and acrylic acid as the base for the separator and cross-linking it similarly to the PVA. Fillers can be incorporated into the films to further modify film properties. Results of separator screening tests and cell tests for several variations of PBA films are discussed. Author

N83-12181*# National Aeronautics and Space Administration. Lewis Research Center, Cleveland, Ohio.
A SOFTWARE SYSTEM FOR EMISSION SPECTROMETRY
J. V. AUPING and R. G. MEGARGLE (Cleveland State Univ., Ohio) 1981 12 p refs Presented at the 9th Meeting of the Federation of Analytical Chem. and Spectry. Soc., Philadelphia, 19-24 Sep. 1982
(Contract NSG-3308)
(NASA-TM-83001; E-1437; NAS 1.15:83001) Avail: NTIS HC A02/MF A01 CSCL 07D

A computer system was developed for an emission spectrometry facility consisting of a direct current (DC) argon arc spectrograph optically coupled to an inductively coupled plasma multichannel spectrometer. Custom hardware and software were designed to control analytical functions and perform data acquisition. The software system was designed to make operation of the facility simple for routine operation and flexible for research and development. Special software was written to collect data under controlled conditions to characterize and monitor system response. One sequence collects intensity versus time data on all channels and displays the data graphically. These profiles are useful in studying the effects of operating parameters on measurement precision. Another special sequence performs calibration using a spline curve fit procedure. Routines were also written to measure dark currents and signals from a standard tungsten halogen lamp mounted in place of the DC arc. For quality control purposes, histories of these values are kept and monitored for excess scatter or drift. Author

N83-12182*# National Aeronautics and Space Administration. Lewis Research Center, Cleveland, Ohio.
SHOCK TUBE MEASUREMENTS OF GROWTH CONSTANTS IN THE BRANCHED CHAIN FORMALDEHYDE-CARBON MONOXIDE-OXYGEN SYSTEM
T. A. BRABBS and R. S. BROKAW (Baldwin-Wallace Coll.) Sep. 1982 16 p refs
(Contract NAS3-22115)
(NASA-TM-82954; E-1371; NAS 1.15:82954) Avail: NTIS HC A02/MF A01 CSCL 07D

Exponential free radical growth constants were measured for formaldehyde carbon monoxide-oxygen systems by monitoring the growth of oxygen atom concentration as manifested by CO flame band emission. Data were obtained over the temperature range of 1200 to 2000 K. The data were analyzed using a formaldehyde oxidation mechanism involving 12 elementary reaction steps. The computed growth constants are roughly in accord with experimental values, but are much more temperature dependent. The data was also analyzed assuming formaldehyde is rapidly decomposed to carbon monoxide and hydrogen. Growth constants computed for the resulting carbon monoxide hydrogen oxygen mixtures have a temperature dependence similar to experiments; however, for most mixtures, the computed growth constants were larger than experimental values. S.L.

N83-13186* National Aeronautics and Space Administration. Lewis Research Center, Cleveland, Ohio.
POLYVINYL ALCOHOL CROSS-LINKED WITH TWO ALDEHYDES Patent
D. W. SHEIBLEY, L. L. RIEKER, L. C. HSU, and M. A. MANZO, inventors (to NASA) 2 Nov. 1982 6 p Filed 10 Jun. 1981 Supersedes N81-27279 (19 - 18, p 2459)
(NASA-CASE-LEW-13504-1; US-PATENT-4,357,402; US-PATENT-APPL-SN-272234; US-PATENT-CLASS-429-206; US-PATENT-CLASS-264-104; US-PATENT-CLASS-429-253; US-PATENT-CLASS-525-61) Avail: US Patent and Trademark Office CSCL 07D

A film forming polyvinyl alcohol resin is admixed, in aqueous solution, with a dialdehyde crosslinking agent which is capable of crosslinking the polyvinyl alcohol resin and a water soluble acid aldehyde containing a reactive aldehyde group capable of reacting with hydroxyl groups in the polyvinyl alcohol resin and an ionizable acid hydrogen atom. The dialdehyde is present in an amount sufficient to react with from 1 to 20% by weight of the theoretical amount required to react with all of the hydroxyl groups of the polyvinyl alcohol. The amount of acid aldehyde is from 1 to 50% by weight, same basis, and is sufficient to reduce the pH of the aqueous admixture to 5 or less. The admixture is then formed into a desired physical shape, such as by casting a sheet or film, and the shaped material is then heated to simultaneously dry and crosslink the article.
Official Gazette of the U.S. Patent and Trademark Office

N83-14177*# Florida Univ., Gainesville. Ceramics Div.
MECHANISMS OF DEVITRIFICATION OF GRAIN BOUNDARY GLASSY PHASES IN SI3N4 MATERIALS Summary Technical Report
L. L. HENCH 17 Dec. 1982 129 p refs
(Contract NSG-3254)
(NASA-CR-169670; NAS 1.26:169670) Avail: NTIS HC A07/MF A01 CSCL 07D

Changes in the grain boundary (g.b.) phases of Si3N4 are analyzed, the effects of composition and thermal history on devitrification of the g.b. phases are determined, devitrification of the g.b. phases of Si3N are related to mechanical behavior and oxidation sensitivity of the material. The phase relationships that occur within the grain boundaries of Si3N4 containing various densification aids are reviewed. Comparisons of the effects of MgO, Y2O3, CeO2, and Y2O3 + AL2O3 are made in terms of the phase equilibria of the Si3N4 + SiO2 + additive compositional system. Two new equilibrium phase diagrams for the Si3N4-SiO2 and Y2O3 and Si3N4-SiO2-Ce2O3 systems are preented. The effects of Y2O3 vs CeO2 densification aids on the fracture surfaces of Si3N4 are compared. Auger electron spectroscopy shows that both oxides are concentrated within the fracture surface. Scanning electron microscopy shows evidence that Si3N4 with CeO2 formed an intergranular structure of fine grained oxynitride reaction products, as predicted by phase quilibria, whereas the Y2O3 containing sample shows evidence of an intergranular glassy phase. S.L.

N83-15372*# National Aeronautics and Space Administration. Lewis Research Center, Cleveland, Ohio.
DEVELOPMENT AND EVALUATION OF POLYVINYL-ALCOHOL BLEND POLYMER FILMS AS BATTERY SEPARATORS
M. A. MANZO Dec. 1982 25 p refs
(NASA-TM-82981; E-1412; NAS 1.15:82981) Avail: NTIS HC A02/MF A01 CSCL 10C

Several dialdehydes and epoxies were evaluated for their suitability as cross-linkers. Optium concentrations of several cross-linking reagents were determined. A two-step method of cross-linking, which involves treatment of the film in an acid or acid periodate bath, was investigated and dropped in favor of a one-step method in which the acid catalyst, which initiates cross-linking, is added to the PVA - cross-linker solution before casting. The cross-linking was thus achieved during the drying step. This one-step method was much more adaptable to commercial processing. Cross-linked films were characterized as alkaline battery separators. Films were prepared in the lab and tested in cells in order to evaluate the effect of film composition and a number of processing parameters on cell performance. These tests were conducted in order to provide a broader data base from which to select optimum processing parameters. Results of the separator screening tests and the cell tests are discussed.
M.G.

N83-16418*# Texas Univ., Austin. Dept. of Chemistry.
PREPARATION, CHARACTERIZATION, PHYSICAL TESTING AND PERFORMANCE OF FLUROCARBON MEMBRANES AND SEPARATORS Final Report
R. J. LAGOW and E. T. DUMITRU 17 Jan. 1983 19 p refs
(Contract NSG-3190)
(NASA-CR-169756; NAS 1.26:169756) Avail: NTIS HC A02/MF A01 CSCL 07D

The direct fluorination method of converting carefully selected hydrocarbon substrates to fluorinated membranes was successfully applied to produce promising, novel membranes for electrochemical devices. A family of polymer blends was identified which permits wide latitude in the concentration of both crosslinks and carboxyl groups in hydrocarbon membranes. The membranes of paragraph two were successfully fluorinated. Author

N83-17625*# California Univ., Santa Barbara. Quantum Inst.
LASER FLUORESCENCE STUDIES OF THE CHEMICAL INTERACTIONS OF SODIUM SPECIES WITH SULFUR BEARING FUELS Final Report, Mar. 1979 - Dec. 1981
M. STEINBERG and K. SCHOFIELD 25 Jan. 1983 24 p refs
(Contract NSG-3256)
(NASA-CR-169861; NAS 1.26:169861) Avail: NTIS HC A02/MF A01 CSCL 07D

By using a large matrix of fuel rich and fuel lean H2/O2/N2 and fuel rich C2H2/O2/N2 flames, the behavior of sodium and its interactions with sulfur at high temperatures was extensively characterized. OH concentrations were measured for each flame using the previously validated laser induced fluorescence technique. Sodium atomic concentrations were obtained by the saturated laser fluorescence method. Measurements were made in the absence and presence of up to 2% sulfur. In oxygen rich systems sodium is depleted by NaO2 and NaOH formation. The relative amounts of each are controlled by the degree of nonequilibration of the flame radicals and by the temperature. The bond strength of NaO2 was established. For the first time, a complete understanding of the complex behavior of sodium in fuel lean H2/O2 flames has emerged and computer modeling has permitted various rate constants of Na, NaO2 and NaOH reactions to be approximately fixed. S.L.

N83-17626*# California Univ., Santa Barbara. Quantum Inst.
THE DETAILED CHEMISTRY AND THERMODYNAMICS OF SODIUM IN OXYGEN-RICH FLAMES
A. J. HYNES (Oberlin Coll., Ohio), M. STEINBERG, and K. SCHOFIELD 1982 27 p refs Presented at the Fall Meeting of the Western States Sect. of the Combust. Inst., Livermore, Calif., 11-12 Oct. 1982
(Contract NSG-3256; DE-AM03-76SF-00034)
(NASA-CR-169848; NAS 1.26:169848; WSCI-82-45) Avail: NTIS HC A03/MF A01

Measurement of sodium and OH concentrations in ten oxygen-rich H2/O2/N2 flames by respective saturated and low-power laser induced fluorescence techniques have permitted a detailed examination of the pronounced flame chemistry of sodium in such oxygen rich media. Previous interpretations have been shown to be largely incomplete or in error. The flame downstream profiles indicate that the amount of free sodium tracks the decay of H-atom and as the flame radicals decay sodium becomes increasingly bound in a molecular form. A detailed kinetic model indicates that the sodium is distributed between NaOH and NaO2 species. Concentrations of NaO are very small and NaH negligible. The actual distribution is controlled by the state of equilibrium of the flames' basic free radicals. Na, NaO2 and NaOH are all coupled to one another by fast reactions which can rapidly interconvert one to another as flame conditions vary. Above about 2000K, NaOH becomes dominant whereas NaO2 plays an increasingly important contribution at lower temperatures. B.W.

N83-17628*# National Aeronautics and Space Administration. Lewis Research Center, Cleveland, Ohio.
STEAM COOLED RICH-BURN COMBUSTOR LINER Patent Application
D. F. SCHULTZ, inventor (to NASA) 23 Dec. 1982 10 p
(NASA-CASE-LEW-13609-1; US-PATENT-APPL-SN-452465)
Avail: NTIS HC A02/MF A01 CSCL 21B

Stress on the wall of the primary combustor is minimized. Thus, the steam pressure in the inlet manifold is approximately the same as the combustor discharge pressure at the throat, and annular expansion tubes minimize stresses in the jacket. The second combustor accomplishes lean burning of the gases discharged from primary combustor. The combination of the rich burning of heavy fuels followed by lean burning minimizes the NOx in the exhaust gas discharged from combustor. The novelty of the invention appears to lie in cooling a rich burn combustor with spiral streams of saturated steam flowing between the combustor linear and the jacket at a predetermined pressure; the jacket including stress relief means. NASA

N83-18862*# National Aeronautics and Space Administration. Lewis Research Center, Cleveland, Ohio.
ELECTROLYTE MANAGEMENT IN POROUS BATTERY COMPONENTS. STATIC MEASUREMENTS
K. M. ABBEY and D. L. BRITTON 1982 26 p refs Presented at the Autumn Ann. Meeting of the Electrochemical Society, Detroit, 17-22 Oct. 1982
(NASA-TM-83073; E-1545; NAS 1.15:83073) Avail: NTIS HC A03/MF A01 CSCL 07D

The interaction between the porous hydrogen and nickel electrodes and microporous separator with respect to electrolyte management in nickel/hydrogen cells has been investigated. The distribution of electrolyte among the components has been measured and correlated with the pore size distributions, total void volume, and resistance of a variety of electrodes and separators. Calculations are used to show the effects of systematically varying these properties. Author

N83-18863*# National Aeronautics and Space Administration. Lewis Research Center, Cleveland, Ohio.
MECHANISM OF LUBRICATION BY TRICRESYLPHOSPHATE (TCP)
O. D. FAUT and D. R. WHEELER Feb. 1983 13 p refs Presented at the ASLE Lubrication Conf., Washington, D.C., 5-7 Oct. 1982
(NASA-TP-2053; E-1244; NAS 1.60:2053) Avail: NTIS HC A02/MF A01 CSCL 11H

A pin-on-disk tribometer equipped with an induction heater was used to study the coefficient of friction as a function of temperature for tricresylphosphate (TCP) on continuous vacuum melted (CVM) M-50 tool steel when the TCP was present in a liquid reservoir (bulk lubrication), and when it was applied as a liquid layer directly to the disk (limited lubrication). Under limited lubrication conditions, experiments were performed in dry (100 ppm H2O) air, dry (20 ppm H2O) nitrogen, dry nitrogen with the disks heated to 700 C then cooled to room temperature before the TCP was applied and the measurements made (preheated disks), and moist nitrogen using preheated disks. When the coefficient of friction was plotted as a function of the disk temperature, the friction decreased at a characteristic temperature, T sub r whose observed values were 265 C for bulk lubrication conditions in dry air, 225 C for limited lubrication conditions in dry air, and 215 C for limited lubrication conditions in dry nitrogen. No decrease in friction was observed with preheated disks; instead a sharp failure temperature was observed at 218 C, which was taken as the temperature about which the behavior of TCP should be judged, X-ray photoelectron spectroscopy confirmed the presence of phosphate on the surface of the iron pins used in the tribometer under TCP lubrication. Depth profile studies support the idea that a chemical reaction occurs between the TCP and the metal surface at T sub r. S.L.

N83-19824*# Virginia Polytechnic Inst. and State Univ., Blacksburg. Dept. of Mechanical Engineering.
EXPERIMENTAL STUDY OF THE THERMAL-ACOUSTIC EFFICIENCY IN A LONG TURBULENT DIFFUSION-FLAME BURNER Final Report
J. R. MAHAN Feb. 1983 72 p refs
(Contract NAG3-124)
(NASA-CR-170003; NAS 1.26:170003) Avail: NTIS HC A04/MF A01 CSCL 21B

A two-year study of noise production in a long tubular burner is described. The research was motivated by an interest in understanding and eventually reducing core noise in gas turbine engines. The general approach is to employ an acoustic source/propagation model to interpret the sound pressure spectrum in the acoustic far field of the burner in terms of the source spectrum that must have produced it. In the model the sources are assumed to be due uniquely to the unsteady component of combustion heat release; thus only direct combustion-noise is considered. The source spectrum is then the variation with frequency of the thermal-acoustic efficiency, defined as the fraction of combustion heat release which is converted into acoustic energy at a given frequency. The thrust of the research was to study the variation of the source spectrum with the design and operating parameters of the burner. Author

N83-21056*# Case Western Reserve Univ., Cleveland, Ohio. Dept. of Chemical Engineering.
THE ELECTROCHEMICAL FLUORINATION OF POLYMERIC MATERIALS FOR HIGH ENERGY DENSITY AQUEOUS AND NON-AQUEOUS BATTERY AND FUEL CELL SEPARATORS Final Report
C. C. LIU Feb. 1983 103 p refs
(Contract NAG3-66)
(NASA-CR-167961; NAS 1.26:167961) Avail: NTIS HC A06/MF A01 CSCL 07D

A computerized system was established and the electrochemical fluorination of trichloroethylene, polyacrylic acid and polyvinyl alcohol in anhydrous hydrogen fluoride was attempted. Both solid substrates as well as membranes were used. Some difficulties were found in handling and analyzing the solid substrates and

membranes. Further studies are needed in this area. A microprocessor aided electrochemical fluorination system capable of obtaining highly reproducible experimental results was established. Author

N83-24571*# National Aeronautics and Space Administration. Lewis Research Center, Cleveland, Ohio.
PORE SIZE ENGINEERING APPLIED TO THE DESIGN OF SEPARATORS FOR NICKEL-HYDROGEN CELLS AND BATTERIES
K. M. ABBEY and D. L. BRITTON 1983 11 p refs Proposed for presentation at the 18th Intersoc. Energy Conversion Eng. Conf., Orlando, Fla., 21-26 Aug. 1983; sponsored by American Inst. of Chemical Engineers, IEEE, AIAA, American Chemical Society, ANS, ASME, and SAE
(NASA-TM-83386; E-1663; NAS 1.15:83386) Avail: NTIS HC A02/MF A01 CSCL 10C

Pore size engineering in starved alkaline multiplate cells involves adopting techniques to widen the volume tolerance of individual cells. Separators with appropriate pore size distributions and wettability characteristics (capillary pressure considerations) to have wider volume tolerances and an ability to resist dimensional changes in the electrodes were designed. The separators studied for potential use in nickel-hydrogen cells consist of polymeric membranes as well as inorganic microporous mats. In addition to standard measurements, the resistance and distribution of electrolyte as a function of total cell electrolyte content were determined. New composite separators consisting of fibers, particles and/or binders deposited on Zircar cloth were developed in order to engineer the proper capillary pressure characteristics in the separator. These asymmetric separators were prepared from a variety of fibers, particles and binders. Author

N83-24575*# National Aeronautics and Space Administration. Lewis Research Center, Cleveland, Ohio.
EXPERIMENTAL DESIGN OF AN INTERLABORATORY STUDY FOR TRACE METAL ANALYSIS OF LIQUID FLUIDS
L. A. GREENBAUER-SENG May 1983 44 p refs
(NASA-TP-2148; E-1311; NAS 1.60:2148) Avail: NTIS HC A03/MF A01 CSCL 07D

The accurate determination of trace metals and fuels is an important requirement in much of the research into and development of alternative fuels for aerospace applications. Recognizing the detrimental effects of certain metals on fuel performance and fuel systems at the part per million and in some cases part per billion levels requires improved accuracy in determining these low concentration elements. Accurate analyses are also required to ensure interchangeability of analysis results between vendor, researcher, and end use for purposes of quality control. Previous interlaboratory studies have demonstrated the inability of different laboratories to agree on the results of metal analysis, particularly at low concentration levels, yet typically good precisions are reported within a laboratory. An interlaboratory study was designed to gain statistical information about the sources of variation in the reported concentrations. Five participant laboratories were used on a fee basis and were not informed of the purpose of the analyses. The effects of laboratory, analytical technique, concentration level, and ashing additive were studied in four fuel types for 20 elements of interest. The prescribed sample preparation schemes (variations of dry ashing) were used by all of the laboratories. The analytical data were statistically evaluated using a computer program for the analysis of variance technique. S.L.

N83-26936*# Texas Univ., Austin. Dept. of Chemistry.
PREPARATION, CHARACTERIZATION, PHYSICAL TESTING AND PERFORMANCE OF FLUOROCARBON MEMBRANES AND SEPARATORS Final Report
R. J. LAGOW and E. T. DUMITRU Feb. 1982 24 p refs (Contract NSG-3190)
(NASA-CR-167880; NAS 1.26:167880) Avail: NTIS HC A02/MF A01 CSCL 07D

The direct fluorination method of converting carefully selected hydrocarbon substrates to fluorinated membranes was successfully applied to produce promising, novel membranes for electrochemical devices. A family of polymer blends was identified which permits wide latitude in the concentration of both crosslinks and carboxyl groups in hydrocarbon membranes. These membranes were successfully fluorinated and are potentially competitive with commercial membranes in performance, and potentially much cheaper in price. Author

N83-29228*# National Aeronautics and Space Administration. Lewis Research Center, Cleveland, Ohio.
FLAME RADIATION MEASUREMENTS
R. W. CLAUS, F. M. HUMENIK, and G. M. NEELY *In its* Combust. Fundamentals Res. p 199-206 Mar. 1983 refs
Avail: NTIS HC A12/MF A01 CSCL 21B

Spectral and total flame radiation measurements exhibited: (1) that radiant heat flux increases with vision combustor inlet air pressure; (2) the effect of fuel atomization characteristics on radiant heat flux; and (3) that a reduction in fuel hydrogen content produces a significant increase in radiant heat flux primarily at low combustor pressures. Author

N83-29326*# National Aeronautics and Space Administration. Lewis Research Center, Cleveland, Ohio.
AN ELECTROCHEMICAL REBALANCE CELL FOR REDOX SYSTEMS Final Report
J. C. ACEVEDO and D. K. STALNAKER Jun. 1983 15 p refs (Contract DE-AI04-80AL-12726)
(NASA-TM-83363; E-1628; DOE/NASA/12726-20; NAS 1.15:83363) Avail: NTIS HC A02/MF A01 CSCL 10C

An electrochemical rebalance cell for maintaining electrochemical balance, at the system level, of the acidified aqueous iron chloride and chromium chloride reactant solutions in the redox energy storage system was constructed and evaluated. The electrochemical reaction for the cathode is Fe(+3) + e(-) yields Fe(+2), and that for the anode is 1/2H2 yields H(+) + e(-). The iron (carbon felt) electrode and the hydrogen (platinized carbon) electrode are separated by an anion exchange membrane. The performance of the rebalance cell is discussed as well as the assembly of a single rebalance cell and multicell stacks. Various cell configurations were tested and the results are presented and discussed. The rebalance cell was also used to demonstrate its ability, as a preparative tool, for making high purity solutions of soluble reduced metal ionic species. Preparations of titanium, copper, vanadium and chromium ions in acidified solutions were evaluated. Author

N83-30550*# National Aeronautics and Space Administration. Lewis Research Center, Cleveland, Ohio.
ACTIVATION PARAMETERS OF FLOW THROUGH BATTERY SEPARATORS
R. L. BLOKHRA (Himachal Pradesh Univ., Simla, India) May 1983 15 p refs
(NASA-TM-83371; E-1637; NAS 1.15:83371) Avail: NTIS HC A02/MF A01 CSCL 10C

Studies of the hydrodynamic flow of water and 45 percent potassium hydroxide (KOH) solution through a microporous and an ion exchange separator are described. The permeability values are interpreted in terms of a pseudoactivation process. The enthalpy of activation deltaH* and the entropy of activation deltaS* were estimated from Eyring's rate equation. Author

N83-30551*# Pratt and Whitney Aircraft Group, East Hartford, Conn. Commercial Engineering.
BROAD SPECIFICATION FUELS TECHNOLOGY PROGRAM, PHASE 1 Final Report
R. P. LOHMANN and R. A. JEROSZKO 11 Oct. 1982 210 p refs
(Contract NAS3-22392)
(NASA-CR-168180; NAS 1.26:168180; PWA-5719-34) Avail: NTIS HC A10/MF A01 CSCL 21B

An experimental evaluation was conducted to assess the impact of the use of broadened properties fuels on combustor design concepts. Emphasis was placed on establishing the viability of design modifications to current combustor concepts and the use of advanced technology concepts to facilitate operation on Experimental Referee Broad Specification (ERBS) fuel while meeting exhaust emissions and performance specifications and maintaining acceptable durability. Three different combustor concepts, representative of progressively more aggressive technology levels, were evaluated. When operated on ERBS rather than Jet A fuel, a single stage combustor typical of that in the most recent versions of the JT9D-7 engine was found to produce excess carbon monoxide emissions at idle and elevated liner temperatures at high power levels that were projected to reduced liner life by 13 percent. The introduction of improved component technology, such as refined fuel injectors and advanced liner cooling concepts were shown to have the potential of enhancing the fuel flexibility of the single stage combustor. Author

N83-32870*# Spring Arbor Coll., Mich. Dept. of Chemistry.
ANALYSIS OF THE VISIBLE SPECTRA OF CONCENTRATED CHROMIC CHLORIDE SOLUTIONS Thesis. Final Report
W. D. BUNCH May 1983 37 p refs
(Contract NAG3-148)
(NASA-CR-172998; NAS 1.26:172998) Avail: NTIS HC A03/MF A01 CSCL 07D

In the development of the Redox Energy Storage System, the electrical storage efficiency is low due to the complex chemical reaction of the chromium II and III species. Several studies dealing with the processes occurring at the catalyzed carbon electrode during the charging and discharging of the system are described. S.L.

N83-32871*# Spring Arbor Coll., Mich.
THE CHEMICAL BEHAVIOR OF ACIDIFIED CHROMIUM (3) SOLUTIONS B.S. Thesis
D. K. TERMAN May 1981 29 p refs
(Contract NAG3-148)
(NASA-CR-172997; NAS 1.26:172997) Avail: NTIS HC A03/MF A01 CSCL 07D

A unique energy-storage system has been developed at NASA's Lewis Research Center called REDOX. This NASA-REDOX system is an electrochemical storage device that utilized the oxidation and reduction of two fully soluble redox couples for charging and discharging. The redox couples now being investigated are acidified chloride solutions of chromium (Cr(+2)/Cr(+3)) and iron (Fe(+2)/Fe(+3)). B.W.

N83-32872*# Spring Arbor Coll., Mich.
SPECTROPHOTOMETRIC ANALYSIS OF AQUEOUS MIXTURES OF SOME CHROMIUM (III) COMPLEXES Thesis
G. STEVENS May 1983 27 p refs
(Contract NAG3-148)
(NASA-CR-172999; NAS 1.26:172999) Avail: NTIS HC A03/MF A01 CSCL 07D

Several methods of determining the relative concentrations of Cr(H2O)5C1(+2) and Cr(H2O)6(+3) are described. The three methods studied are curved resolving methods, used in evaluating spectrophotometric results, mixture results, used in verifying curve resolving techniques, and chromium analysis. S.L.

26

METALLIC MATERIALS

Includes physical, chemical, and mechanical properties of metals, e.g., corrosion; and metallurgy.

A83-10249* Case Western Reserve Univ., Cleveland, Ohio.
O-18 TRACER STUDIES OF AL2O3 SCALE FORMATION ON NICRAL ALLOYS
K. P. R. REDDY, A. R. COOPER (Case Western Reserve University, Cleveland, OH), and J. L. SMIALEK (NASA, Lewis Research Center, Cleveland, OH) Oxidation of Metals, vol. 17, June 1982, p. 429-449. refs

Diffusion processes in Al2O3 scales formed on NiCrAl + Zr alloys were studied by the proton activation technique employing the O-18 isotope as a tracer. The O-18 profiles identified a zone of oxide penetration beneath the external scale. Both this subscale formation and the outer Al2O3 scale thickness were shown by this technique to increase with Zr content in the alloy. Estimated kp's from scale thicknesses were in agreement with gravimetric measurements for various Zr levels. Alternate exposures in O-16 and O-18 revealed that oxygen inward transport was the primary growth mechanism. A qualitative analysis of these O-18 profiles indicated that the oxygen transport was primarily via short-circuit paths, such as grain boundaries. (Author)

A83-10299* National Aeronautics and Space Administration. Lewis Research Center, Cleveland, Ohio.
A NEW DIFFUSION-INHIBITED OXIDATION-RESISTANT COATING FOR SUPERALLOYS
M. A. GEDWILL, T. K. GLASGOW, and S. R. LEVINE (NASA, Lewis Research Center, Cleveland, OH) (International Conference on Metallurgical Coatings and Process Technology, San Diego, CA, Apr. 5-8, 1982.) Thin Solid Films, vol. 95, 1982, p. 65-72. refs
(Previously announced in STAR as N81-33273)

A83-12650* National Aeronautics and Space Administration. Lewis Research Center, Cleveland, Ohio.
TRIBOLOGICAL PROPERTIES AND X-RAY PHOTOELECTRON SPECTROSCOPY STUDIES OF ION-PLATED GOLD ON NICKEL AND IRON
K. MIYOSHI, T. SPALVINS, and D. H. BUCKLEY (NASA, Lewis Research Center, Cleveland, OH) Thin Solid Films, vol. 96, 1982, p. 9-16. refs
(Previously announced in STAR as N82-22344)

A83-13226* National Aeronautics and Space Administration. Lewis Research Center, Cleveland, Ohio.
CORRELATION OF TENSILE AND SHEAR STRENGTHS OF METALS WITH THEIR FRICTION PROPERTIES
K. MIYOSHI and D. H. BUCKLEY (NASA, Lewis Research Center, Cleveland, OH) American Society of Mechanical Engineers and American Society of Lubrication Engineers, Lubrication Conference, Washington, DC, Oct. 5-7, 1982, ASLE 9 p. refs
(ASLE PREPRINT 82-LC-UB-1)
(Previously announced in STAR as N82-24325)

A83-21071* General Electric Co., Cincinnati, Ohio.
REQUIREMENTS OF CONSTITUTIVE MODELS FOR TWO NICKEL-BASE SUPERALLOYS
J. H. LAFLEN and T. S. COOK (General Electric Co., Aircraft Engine Business Group, Cincinnati, OH) International Conference on Constitutive Laws of Engineering Materials: Theory and Application, University of Arizona, Tucson, AZ, Jan. 1983, Paper. 3 p. refs
(Contract NAS3-22534)

The constitutive behavior of two nickel-base superalloys, Rene '80 and Inconel 718, utilized in gas turbine blade and disk components, respectively, is presented. In turbine blade applications, the high homologous temperatures result in strain-rate

effects dominating behavior. In turbine disks, the temperatures are cooler so that mean stress effects become important. The impact of these two variables on the overall crack initiation lifetime and analysis methodology is discussed. (Author)

A83-22017* National Aeronautics and Space Administration. Lewis Research Center, Cleveland, Ohio.
INFLUENCE OF THERMOMECHANICAL PROCESSING ON ELEVATED TEMPERATURE SLOW PLASTIC FLOW PROPERTIES OF B2 ALUMINIDE FE-39.8AT.% AL
J. D. WHITTENBERGER (NASA, Lewis Research Center, Cleveland, OH) Materials Science and Engineering, vol. 57, Jan. 1983, p. 77-85. refs

A study of the elevated temperature slow plastic flow properties of the B2 aluminide Fe-39.8at.% Al was undertaken. Polycrystalline materials possessing several different microstructures were produced by the hot extrusion of prealloyed powder and, in some cases, postextrusion heat treatments. Compression tests were conducted in air at 1200, 1300 and 1400 K. Such testing revealed that the extrusion temperature affected the active deformation mechanisms where material extruded at 1505 K had a stress exponent about twice that of the intermetallic extruded at 1200 K. Grain size refinement to about 10 microns was found to strengthen the Fe-39.8at.% Al material; unfortunately, the effectiveness of such strengthening is limited to a homologous temperature of about 0.75 for strain rates of commercial interest (less than 10 to the -7th/sec). (Author)

A83-22019* Cincinnati Univ., Ohio.
METALLURGICAL INSTABILITIES DURING THE HIGH TEMPERATURE LOW CYCLE FATIGUE OF NICKEL-BASE SUPERALLOYS
S. D. ANTOLOVICH and N. JAYARAMAN (Cincinnati, University, Cincinnati, OH) Materials Science and Engineering, vol. 57, Jan. 1983, p. L9-L12. refs
(Contract AF-AFOSR-80-0065; NSG-3263)

An investigation is made of the microstructural instabilities that affect the high temperature low cycle fatigue (LCF) life of nickel-base superalloys. Crack initiation processes, provoked by the formation of carbides and the coarsening of the grains of the material at high temperatures are discussed. Experimental results are examined, and it is concluded that LCF behavior can be understood more fully only if details of the material and its dynamic behavior at high temperatures are considered. The effects of high stress, dislocation debris, and increasing environmental damage on the life of the alloy are discussed. M.I.I.

A83-23922* National Aeronautics and Space Administration. Lewis Research Center, Cleveland, Ohio.
INTERRELATION OF MATERIAL · MICROSTRUCTURE, ULTRASONIC FACTORS, AND FRACTURE TOUGHNESS OF A TWO-PHASE TITANIUM ALLOY
A. VARY and D. R. HULL (NASA, Lewis Research Center, Materials Div., Cleveland, OH) Materials Evaluation, vol. 41, Mar. 1983, p. 309-314. refs
(Previously announced in STAR as N82-20551)

A83-27421*# National Aeronautics and Space Administration. Lewis Research Center, Cleveland, Ohio.
THE INITIAL STAGES OF CAVITATION DAMAGE AND EROSION ON COPPER AND BRASS TESTED IN A ROTATING DISK DEVICE
P. VEERABHADRA RAO (NASA, Lewis Research Center, Tribology Branch, Cleveland, OH), N. S. LAKSHMANA RAO, and B. C. SYAMALA RAO (Indian Institute of Science, Bangalore, India) In: Cavitation and Polyphase Flow Forum - 1982; Proceedings of the Third Joint Thermophysics, Fluids, Plasma, and Heat Transfer Conference, St. Louis, MO, June 7-11, 1982. New York, American Society of Mechanical Engineers, 1982, p. 16-19. refs
(Previously announced in STAR as N83-13231)

A83-29726* Dartmouth Coll., Hanover, N.H.
A BRITTLE TO DUCTILE TRANSITION IN NIAL OF A CRITICAL GRAIN SIZE
E. M. SCHULSON and D. R. BARKER (Dartmouth College, Hanover, NH) Scripta Metallurgica (ISSN 0036-9748), vol. 17, April 1983, p. 519-522. Research supported by the Research Corp. refs
(Contract NAG3-13)

Tensile tests have been carried out on the strongly ordered B2 aluminide NiAl at 400 C to investigate the effect of the grain size on the ductility of the material. It is found that the ductility is very low and essentially independent of the grain size for aggregates of grains larger than about 20 microns; for finer-grained aggregates, the ductility increases sharply with decreasing grain size. Thus, NiAl exhibits a critical grain size below which polycrystalline aggregates are ductile in tension. For all grain sizes, fracture occurs in a brittle manner through a combination of intergranular decohesion and transgranular cleavage. V.L.

A83-32624* National Aeronautics and Space Administration. Lewis Research Center, Cleveland, Ohio.
MORPHOLOGY OF DUCTILE METALS ERODED BY A JET OF SPHERICAL PARTICLES IMPINGING AT NORMAL INCIDENCE
P. VEERABHADRA RAO, S. G. YOUNG, and D. H. BUCKLEY (NASA, Lewis Research Center, Cleveland, OH) Wear (ISSN 0043-1648), vol. 85, March 1, 1983, p. 223-237. refs

Scanning electron microscopy and energy-dispersive X-ray spectroscopy are used, together with surface profile measurements, in the present morphological study of the erosion of an aluminum alloy and copper by the normal impact of spherical glass erodent particles. The morphology of the damage pattern is a manifestation of the flow pattern of erodent particles, and yields insight into the mechanisms that may be active at different stages of erosion. The simultaneous appearance of radial cracks and concentric rings is reported, together with wave crests which contain an accumulation of metallic flakes. A preliminary analysis is advanced to explain the formation of the various damage patterns observed. O.C.

A83-36166* Cincinnati Univ., Ohio.
THE EFFECT OF MICROSTRUCTURE ON THE FATIGUE BEHAVIOR OF NI BASE SUPERALLOYS
S. D. ANTOLOVICH (Cincinnati, University, Cincinnati, OH) and N. JAYARAMAN IN: Fatigue: Environment and temperature effects . New York, Plenum Press, 1983, p. 119-144. refs
(Contract AF-AFOSR-80-0065; NSG-3263)

Nickel-base superalloys are used in jet engine components such as disks, turbine blades, and vanes. Improvements in the fatigue behavior will allow the life to be extended or the payloads to be increased. The first part of the present investigation deals primarily with the effects of microstructural variations on the fatigue crack propagation (FCP) behavior of nickel-base alloys, while the second part is concerned with low-cycle fatigue (LCF) behavior of Ni base systems. Waspaloy at low temperature is considered, taking into account material heat treatment and test procedures, a composite plot of Waspaloy FCP data, Paris law fatigue crack propagation constants, monotonic tensile data, and overload FCP test results for Waspaloy. It is found that the FCP and overload behavior of nickel-base alloys may be markedly improved by heat treating. Attention is given to effects of cyclic deformation on microstructure and substructure, environmental damage, and an environmental/deformation model of high temperature LCF. G.R.

A83-37824* National Aeronautics and Space Administration. Lewis Research Center, Cleveland, Ohio.
TRIBOLOGICAL CHARACTERISTICS OF NITROGEN (N+) IMPLANTED IRON
W. R. JONES, JR. and J. FERRANTE (NASA, Lewis Research Center, Cleveland, OH) ASLE Transactions, vol. 26, July 1983, p. 351-359; Discussion, p. 359. refs

The effect of implantation of nitrogen ions (1.5 MeV) on the friction and wear characteristics of pure ion sliding against M-50 steel (unimplanted) was studied in a pin-on-disk sliding friction

apparatus. Test conditions included room temperature (25 C), a dry air atmosphere, a load of 1/2 kg (4.9 N), sliding velocities of 0.043 to 0.078 m/sec (15 to 25 rpm), a pure hydrocarbon lubricant (n-hexadecane), or a U.S.P. mineral oil and nitrogen ion implantation doses of 5x10 to the 15th power and 5x10 to the 17th power ions/sq cm. No differences in wear rates were observed in the low dose experiments. In the high dose experiments, small reductions in initial (40 percent) and steady state (20 percent) wear rates were observed for nitrogen implanted iron riders as compared with unimplanted controls. No differences in average friction coefficients were noted for either dose. Auger electron spectroscopy combined with argon ion bombardment revealed a subsurface Gaussian nitrogen distribution with a maximum concentration of 6 atomic percent at a depth of 0.8 microns. Similar analysis within the wear scar of an implanted rider after 20 microns of wear yielded only background nitrogen concentration. No inward migration of nitrogen ions was observed. Previously announced in STAR as N82-24322 M.G.

A83-41199* National Aeronautics and Space Administration. Lewis Research Center, Cleveland, Ohio.
FATIGUE CRACK INITIATION AND PROPAGATION IN SEVERAL NICKEL-BASE SUPERALLOYS AT 650 C
J. GAYDA and R. V. MINER (NASA, Lewis Research Center, Materials Div., Cleveland, OH) International Journal of Fatigue (ISSN 0142-1123), vol. 5, July 1983, p. 135-143. refs

The modes of crack initiation and propagation of several nickel-base superalloys have been examined after fatigue and creep-fatigue testing at 650 C. In fatigue, crack initiation was transgranular and frequently associated with porosity or inclusions in the higher strength alloys. These defects were usually located at the surface, except for tests at low strain ranges where larger, internal defects often initiated failure. Although fatigue crack initiation was transgranular, in those alloys with grain sizes of less than 15 microns, fatigue crack growth quickly became intergranular. This transition was environmentally assisted and did not occur for subsurface cracks until the crack broke through to the atmosphere. In the creep-fatigue cycle, which included a 900 s tensile dwell, crack initiation and propagation were both intergranular in all alloys. Author

A83-42234* National Aeronautics and Space Administration. Lewis Research Center, Cleveland, Ohio.
CYCLIC OXIDATION OF SUPERALLOYS
C. E. LOWELL, J. L. SMIALEK, and C. A. BARRETT (NASA, Lewis Research Center, Materials Div., Cleveland, OH) IN: High temperature corrosion; Proceedings of the International Conference, San Diego, CA, March 2-6, 1981 . Houston, TX, National Association of Corrosion Engineers, 1983, p. 219-226. refs

The development of mathematical/computer models of cyclic oxidation in high-temperature alloys is described. The acceleration of oxidation attack caused by the spalling of protective oxide scales is discussed. The COREST paralinear model based on empirical data, designed by Barrett and Pressler, is found to be of limited value. Basic research on the spalling process in different alloy systems is reviewed, and the phenomenon is characterized: occurring mainly within the oxide, it is caused by the different thermal expansion coefficients of oxide and metal and is a linear function of the total retained oxide. This information has been used in the development of the discrete oxide-spall model COSP and in its modification by addition of a diffusion-zone-profile model to predict the failure of components (Heckel and Nesbitt, unpublished). The COSP model is shown to produce good predictions of cyclic oxidation under a variety of conditions, using data from simple isothermic tests. T.K.

A83-42238* National Aeronautics and Space Administration. Lewis Research Center, Cleveland, Ohio.
DIFFUSION PROCESSES IN AL2O3 SCALES - VOID GROWTH, GRAIN GROWTH, AND SCALE GROWTH
J. L. SMIALEK (NASA, Lewis Research Center, Materials Div., Cleveland, OH) and R. GIBALA (Case Western Reserve University, Cleveland, OH) IN: High temperature corrosion; Proceedings of the International Conference, San Diego, CA, March 2-6, 1981 . Houston, TX, National Association of Corrosion Engineers, 1983, p. 274-283. refs

The internal microstructure and growth kinetics of Al2O3 scales on Ni-15Cr-13Al (wt percent) are investigated by TEM and analyzed in relation to models of diffusivity. Polished arc-melted specimens were oxidized in 1-atm air at 1100 C for 0.1, 1.0, and 20 hours and ion-thinned for TEM at 100 kV. The frequency distribution of void size and grain size is determined for different oxidation times and scale depths. The kinetics of microvoid growth and of grain and scale growth are plotted and related via simplified models to lattice and grain-boundary oxygen diffusivity, respectively. Good agreement is found between model predictions and data obtained by Oishi and Kingery (1960) on oxygen diffusion in bulk Al2O3. The further implications and limitations of these findings are discssed. T.K.

A83-42241* United Technologies Research Center, East Hartford, Conn.
THE OXIDATION BEHAVIOR OF A MODEL MOLYBDENUM/TUNGSTEN-CONTAINING ALLOY IN AIR ALONE AND IN AIR WITH TRACE LEVELS OF NACL(G)
J. G. SMEGGIL and N. S. BORNSTEIN (United Technologies Research Center, Hartford, CT) IN: High temperature corrosion; Proceedings of the International Conference, San Diego, CA, March 2-6, 1981 . Houston, TX, National Association of Corrosion Engineers, 1983, p. 310-315. refs
(Contract NAS3-22488)

Thermogravimetric, metallographic, and X-ray studies of a model alloy, Ni-(17 a/o)Al-(10 a/o)Mo+W, oxidized in dry air at 600-1200 C and in air with 10 ppm NaCl gas at 900 C, are reported. The alloy was melted under Ar and pretreated in flowing H2 for 24 h at 1300 C. Polished 1.3 x 1.3 x 0.2-cm specimens were washed and degreased prior to oxidation in a quartz tube within a furnace for up to 120 hr. The oxidation activation energy of the alloy is determined to be about 30 kcal/mole. The specimens oxidized at 900 C and hotter exhibited oxidized and nitrided phases covered by complex NiMoO4, NiWO4, and NiAl2O4 scales and a porous, nonprotective outer layer of NiO. The oxidation behavior is found to be determined by the formation and growth of the scale, especially the (Mo,W)O2 component. Al2O3 scale layers were not formed, and further runs with pure O2 or Ar-(20 percent)O2 ruled out an explanation of this phenomenon based on aluminum nitride formation. The oxidation was accelerated by the addition of NaCl gas, a finding attributed to the reaction of NaCl with external locally protective Al2O3 scales and with the internal(Mo, W)O2 layers. T.K.

A83-42252* Pittsburgh Univ., Pa.
LOW TEMPERATURE HOT CORROSION
K. T. CHIANG, F. S. PETTIT, and G. H. MEIER (Pittsburgh, University, Pittsburgh, PA) IN: High temperature corrosion; Proceedings of the International Conference, San Diego, CA, March 2-6, 1981 . Houston, TX, National Association of Corrosion Engineers, 1983, p. 519-530. refs
(Contract DE-AC01-79ET-13547; NSG-3214)

The reaction of Co-Cr, Ni-Cr, Co-Cr-Al, and Ni-Cr-Al alloys with Na2SO4 in the presence of SO3 at temperatures between 700 and 750 C leads to the formation of liquid CoSO4-Na2SO4 or NiSO4-Na2SO4 deposits on the alloy surface. The formation of Cr2O3 and/or Al2O3 below this deposit results in a locally low P(O2) and a higher P(S2) and P(SO2). It is noted that these conditions can prevent protective oxide formation either by sulfide formation in the alloy, which localizes the Cr and/or Al in discrete particles, or by acid fluxing involving a reaction between Al2O3 or Cr2O3 and SO2 to form a salt-soluble species and subsequent

reprecipitation as porous oxides in regions of higher P(O2). These processes may occur simultaneously, although a given alloy generally exhibits features of predominantly one type. Here, the Ni-Cr and Ni-Cr-Al alloys, and to some extent the Co-Cr alloys, exhibit features indicative of the sulfidation mechanism, whereas the morphology for the Co-Cr-Al alloy is more consistent with a predominant acid fluxing mechanism. C.R.

A83-44340* National Aeronautics and Space Administration. Lewis Research Center, Cleveland, Ohio.
EFFECT OF SWAGING ON THE 1000 C COMPRESSIVE SLOW PLASTIC FLOW CHARACTERISTICS OF THE DIRECTIONALLY SOLIDIFIED EUTECTIC ALLOY GAMMA/GAMMA PRIME-ALPHA
J. D. WHITTENBERGER (NASA, Lewis Research Center, Cleveland, OH) and G. WIRTH (Deutsche Forschungs- und Versuchsanstalt fuer Luft- und Raumfahrt, Cologne, West Germany) Journal of Materials Science (ISSN 0022-2461), vol. 18, Sept. 1983, p. 2581-2588. refs

Swaging between 750 and 1050 C has been investigated as a means to introduce work into the directionally solidified eutectic alloy gamma/gamma prime-alpha (Ni-32.3 wt percent Mo-6.3 wt percent Al) and increase the elevated temperature creep strength. The 1000 C slow plastic compressive flow stress-strain rate properties in air of as-grown, annealed, and worked nominally 10 and 25 percent materials have been determined. Swaging did not improve the slow plastic behavior. In fact large reductions tended to degrade the strength and produced a change in the deformation mechanism from uniform flow to one involving intense slip band formation. Comparison of 1000 C tensile and compressive strength-strain rate data reveals that deformation is independent of the stress state. Author

A83-44619* National Aeronautics and Space Administration. Ames Research Center, Moffett Field, Calif.
INTERFACIAL LAYERS IN HIGH-TEMPERATURE-OXIDIZED NICRAL
L. A. LARSON, R. BROWNING, H. POPPA (NASA, Ames Research Center, Moffett Field, CA), and J. SMIALEK (NASA, Lewis Research Center, Cleveland, OH) Journal of Vacuum Science and Technology A (ISSN 0734-2101), vol. 1, Apr.-June 1983, pt. 2, p. 1029-1032. refs
(Contract NCC2-176; NAS2-10987)

The utility of Auger electron spectroscopy combined with ball cratering for depth analysis of oxide and diffusion layers produced in a Ni-14Cr-24Al alloy by oxidation in air at 1180 C for 25 hr is demonstrated. During postoxidation cooling, the oxide layers formed by this alloy spalled profusely. The remaining very thin oxide was primarily Cr2O3 with a trace of Ni. The underlying metal substrate exhibited gamma/gamma-prime and beta phases with a metallic interfacial layer which was similar to the bulk gamma/gamma-prime phase but slightly enriched in Cr and Al. These data are compared to electron microprobe results from a nominally identical alloy. The diffusion layer thickness is modelled with a simple mass balance equation and compared to recent results on the diffusion process in NiCrAl alloys. C.D.

A83-47855* National Aeronautics and Space Administration. Lewis Research Center, Cleveland, Ohio.
GAMMA PRIME SHAPE CHANGES DURING CREEP OF A NICKEL-BASE SUPERALLOY
M. V. NATHAL (NASA, Lewis Research Center, Cleveland, OH) and L. J. EBERT (Case Western Reserve University, Cleveland, OH) Scripta Metallurgica (ISSN 0036-9748), vol. 17, Sept. 1983, p. 1151-1154. refs
(Contract NSG-330)

Changes in the shape of the gamma-prime phase in the single-crystal nickel base alloy NASAIR 100 during tensile and compressive creep have been investigated experimentally by Laue X-ray diffractometry. It is found that under tensile loading, gamma-prime changes from the initial cubic shape to plates perpendicular to the applied stress. This change occurs during primary creep at 1000 C, 148 MPa. Prolonged creep exposures result in a thickening of the gamma-prime plates that is similar to Ostwald ripening often observed in other superalloys during creep. Under compressive loading, two sets of gamma-prime plates parallel to the applied stress are formed. V.L.

A83-48922* Toledo Univ., Ohio.
FRICTION AND WEAR OF IRON AND NICKEL IN SODIUM HYDROXIDE SOLUTIONS
G. P. RENGSTORFF (Toledo, University, Toledo, OH), K. MIYOSHI, and D. H. BUCKLEY (NASA, Lewis Research Center, Cleveland, OH) ASLE Transactions, vol. 26, Oct. 1983, p. 509-515; Discussion, p. 515; Authors' Closure, p. 515, 516. refs

A loaded spherical aluminum oxider rider was made to slide, while in various solutions, on a flat iron or nickel surface reciprocate a distance of 1 cm. Time of experiments was 1 hr during which the rider passed over the center section of the track 540 times. Coeficients of friction were measured throughout the experiments. Wear was measured by scanning the track with a profilometer. Analysis of some of the wear tracks included use of the SEM (scanning electron microscope) and XPS (X-ray photoelectron spectroscopy). Investigated were the effect of various concentrations of NaOH and of water. On iron, increasing NaOH concentration above 0.01 N caused the friction and wear to decrease. This decrease is accompanied by a decrease in surface concentration of ferric oxide (Fe2O3) while more complex iron-oxygen compounds, not clearly identified, also form. At low concentrations of NaOH, such as 0.01 N, where the friction is high, the wear track is badly torn up and the surface is broken. At high concentration, such as 10 N, where the friction is low, the wear track is smooth. The general conclusion is that NaOH forms a protective, low friction film on iron which is destroyed by wear at low concentrations but remains intact at high conentrations of NaOH. Nickel behaves differently than iron in that only a little NaOH gives a low coefficient of friction and a surface which, although roughened in the wear track. remains intact. Previously announced in STAR as N83-10171 Author

N83-10170* National Aeronautics and Space Administration. Lewis Research Center, Cleveland, Ohio.
MECHANICAL BONDING OF METAL METHOD
B. A. BANKS, inventor (to NASA) 26 Nov. 1980 11 p Filed 26 Nov. 1980 Supersedes N81-16329 (19 - 07, p 0899)
(NASA-CASE-LEW-12941-1; US-PATENT-4,349,954; US-PATENT-APPL-SN-210632; US-PATENT-CLASS-29-458; US-PATENT-CLASS-29-521; US-PATENT-CLASS-403-282)
Avail: US Patent and Trademark Office CSCL 11F

A method is disclosed for joining the surfaces of two metal structures in a mechanical bond. The joining process can be performed in either air or vacuum. The metal surfaces of the structures that are to be bonded are exposed to an ion beam together with a target of low sputtering yield material. This material deposits on the surfaces and creates sites of sputter resistance which evolve into peaks of a cone like surface microstructure. The textured metal surfaces are arranged in face to face relationship and compressed together with plastic deformation which mechanically interlocks the cone. A large interface area is produced which minimizes thermal and electrical losses. Also, no electrical power or heat is required during metal joining.
Official Gazette of the U.S. Patent and Trademark Office

N83-10171*# National Aeronautics and Space Administration. Lewis Research Center, Cleveland, Ohio.
FRICTION AND WEAR OF IRON AND NICKEL IN SODIUM HYDROXIDE SOLUTIONS
G. W. P. RENGSTORFF (Toledo Univ., Ohio), K. MIYOSHI, and D. H. BUCKLEY 1982 23 p refs Presented at the Joint Lubrication Conf., Washington D.C., 5-7 Oct. 1982; sponsored by ASME and American Society of Lubrication Engineers
(NASA-TM-82935; E-638; NAS 1.15:82935) Avail: NTIS HC A02/MF A01 CSCL 11F

A loaded spherical aluminum oxider rider was made to slide, while in various solutions, on a flat iron or nickel surface reciprocate a distance of 1 cm. Time of experiments was 1 hr during which

the rider passed over the rider passed over the center section of the track 540 times. Coefficients of friction were measured throughout the experiments. Wear was measured by scanning the track with a profilometer. Analysis of some of the wear tracks included use of the SEM (scanning electron microscrope) and XPS (X-ray photoelectron spectroscopy). Investigated were the effect of various concentractions of NaOH and of water. On iron, increasing NaOH concentration above 0.01 N caused the friction and wear to decrease. This decrease is accompanied by a decrease in surface concentration of ferric oxide (Fe2O3) while more complex iron-oxygen compounds, not clearly identified, also form. At low concentrations of NaOH, such as 0.01 N, where the friction is high, the wear track is badely torn up and the surface is broken. At high concentration, such as 10 N, where the friction is low, the wear track is smooth. The general conclusion is that NaOH forms a protective, low friction film on iron which is destroyed by wear at low concentrations but remains intact at high concentrations of NaOH. Nickel behaves differently than iron in that only a little NaOH gives a low coefficient of friction and a surface which, although roughened in the wear track, remains intact. B.W.

N83-11282*# National Aeronautics and Space Administration. Lewis Research Center, Cleveland, Ohio.
COSAM (CONSERVATION OF STRATEGIC AEROSPACE MATERIALS) PROGRAM OVERVIEW
Washington Oct. 1982 227 p Workshop held at Cleveland, 14-15 Oct. 1982
(NASA-TM-83006; E-1382; NAS 1.15:83006) Avail: NTIS HC A11/MF A01 CSCL 11F

Abstracts and visual materials used to illustrate presentations reviewing progress in the Conservation of Strategic Materials Program (COSAM) are presented.

N83-11283*# National Aeronautics and Space Administration. Lewis Research Center, Cleveland, Ohio.
COSAM PROGRAM OVERVIEW
J. R. STEPHENS *In its* COSAM (Conserv. Of Strategic Aerospace Mater.) Program Overview p 1-11 Oct. 1982
Avail: NTIS HC A11/MF A01 CSCL 11F

The COSAM program for reduction of the use of strategic alloying elements in nickel-based superalloys for gas turbine engines was reviewed. Sources, consumption, and pricing of cobalt, tantalum, columbium, and chromium are surveyed. Research projects in strategic element substitution, advanced processing concepts, and the development of alternate materials (intermetallics and iron-base alloys) are listed and research plans for FY 1983 and FY 1984 summarized. J.D.

N83-11284*# Columbia Univ., New York.
SUPERALLOY COMPOSITION MODELING
J. BAREFOOT, R. JARRETT, J. SANCHEZ, and J. TIEN *In* NASA. Lewis Research Center COSAM (Conserv. Of Strategic Aerospace Mater.) Program Overview p 13-19 Oct. 1982
(Contract NAG3-57)
Avail: NTIS HC A11/MF A01 CSCL 11F

Development of a predictive method for determination of the gamma/gamma prime phase fields, i.e., gamma prime volume fraction as a function of the multicomponent composition, is described. The cluster variation method used for binary alloys in which the precipitated phase is coherent with the matrix phase is extended for application to the multicomponent coherent gamma/gamma prime nickel-based superalloys. It is shown that the cluster variation method can accurately describe the equilibrium (incoherent) gamma/gamma prime phase fields in the binary Ni-Al phase diagram. The gamma/gamma prime phase field for the Ni-Cr-Al ternary phase diagram is computed as a function of temperature. A reasonable fit results between the calculated and the experimental diagrams. The modeling of the six-component Ni-Cr-Al-Co-Mo-Ti base superalloy and the effect of Ni substitution of Co are discussed. J.D.

N83-11286*# Columbia Univ., New York.
ROLE OF COBALT IN NICKEL BASE SUPERALLOYS
R. JARRETT, J. BAREFOOT, J. TIEN, and J. SANCHEZ *In* NASA. Lewis Research Center COSAM (Conserv. Of Strategic Aerospace Mater.) Program Overview p 37-62 Oct. 1982
(Contract NAG3-57)
Avail: NTIS HC A11/MF A01 CSCL 11F

The effect of cobalt or substituting for cobalt on the mechanical properties of nickel-based superalloys is discussed. Waspaloy, UDIMET 700, and NIMONIC 115, which are representative of Ni-Cr-Co-Al-Ti-Mo superalloys having different gamma prime contents which are strengthened by a heavily alloyed matrix, coherent gamma prime precipitates, and carbides at the grain boundaries. Microstructure and in situ and extracted phase STEM micro-analysis were used to evaluate the three alloys. J.D.

N83-11287*# National Aeronautics and Space Administration. Lewis Research Center, Cleveland, Ohio.
EFFECT OF REDUCED COBALT CONTENTS ON HOT ISOSTATICALLY PRESSED POWDER METALLURGY U-700 ALLOYS
F. H. HARF *In its* COSAM (Conserv. Of Strategic Aerospace Mater.) Program Overview p 63-70 Oct. 1982
Avail: NTIS HC A11/MF A01 CSCL 11F

The effect of reducing the cobalt content of prealloyed powders of UDIMET 700 (U-700) alloys to 12.7, 8.6, 4.3, and 0% was examined. The powders were hot isostatically pressed into billets, which were given heat treatments appropriate for turbine disks, namely partial solutioning at temperatures below the gamma prime solvus and four step aging treatments. Chemical analyses, metallographic examinations, and X-ray diffraction measurements were performed on the materials. Minor effects on gamma prime content and on room temperature and 650 C tensile properties were observed. Creep rupture lives at 650 C reached a maximum at the 8.4% concentration, while at 760 C a maximum in life was reached at the 4.3% cobalt level. Minimum creep rates increased with decreasing cobalt content at both test temperatures. Extended exposures at 760 and 815 C resulted in decreased tensile strengths and rupture lives for all alloys. Evidence of sigma phase formation was also found. J.D.

N83-11288*# National Aeronautics and Space Administration. Lewis Research Center, Cleveland, Ohio.
LOW-COBALT SINGLE CRYSTAL RENE 150
C. M. SCHEUERMANN *In its* COSAM (Conserv. Of Strategic Aerospace Mater.) Program Overview p 71-76 Oct. 1982
Avail: NTIS HC A11/MF A01 CSCL 11F

The effects of cobalt content on a single crystal version of the advanced, high gamma prime content turbine airfoil alloy Rene 150 were investigated. Cobalt contents under investigation include 12 wt.% (composition level of Rene 150), 6 wt.%, and 0 wt.%. Preliminary test results are presented and compared with the properties of standard DS Rene 150. DTA results indicate that the liquidus goes through a maximum of about 1435 C near 6 wt.% Co. The solidus remains essentially constant at 1390 C with decreasing Co content. The gamma prime solvus appears to go through a minimum of about 1235 C near 6 wt.% Co content. Preliminary as-cast tensile and stress rupture results are presented along with heat treat schedules and future test plans. Author

N83-11289*# National Aeronautics and Space Administration. Lewis Research Center, Cleveland, Ohio.
THERMAL FATIGUE RESISTANCE OF COBALT-MODIFIED UDIMET 700
P. T. BIZON *In its* COSAM (Conserv. Of Strategic Aerospace Mater.) Program Overview p 77-81 Oct. 1982
Avail: NTIS HC A11/MF A01 CSCL 11F

The determination of comparative thermal fatigue resistances of five cobalt composition modifications of UDIMET 700 from fluidized bed tests is described. Cobalt compositional levels of 0.1, 4.3, 8.6, 12.8, 17.0 percent were being investigated in both the bare and coated (NiCrAlY overlay) conditions. Triplicate tests of each variation including duplicate tests of three control alloys

are under investigation. Fluidized beds were maintained at 550 and 1850 F for the first 5500 cycles at which time the hot bed was increased to 1922 F. Immersion time in each bed is always 3 minutes. Upon the completion of 10,000 cycles, it appears that the 8.6 percent cobalt level gives the best thermal fatigue life. Considerable deformation of the test bars was observed. Author

N83-11290*# National Aeronautics and Space Administration. Lewis Research Center, Cleveland, Ohio.
CREEP-FATIGUE OF LOW COBALT SUPERALLOYS
G. R. HALFORD *In its* COSAM (Conserv. Of Strategic Aerospace Mater.) Program Overview p 83-88 Oct. 1982
Avail: NTIS HC A11/MF A01 CSCL 11F

Testing for the low cycle fatigue and creep fatigue resistance of superalloys containing reduced amounts of cobalt is described. The test matrix employed involves a single high temperature appropriate for each alloy. A single total strain range, again appropriate to each alloy, is used in conducting strain controlled, low cycle, creep fatigue tests. The total strain range is based upon the level of straining that results in about 10,000 cycles to failure in a high frequency (0.5 Hz) continuous strain-cycling fatigue test. No creep is expected to occur in such a test. To bracket the influence of creep on the cyclic strain resistance, strain hold time tests with ore minuto hold periods are introduced. One test per composition is conducted with the hold period in tension only, one in compression only, and one in both tension and compression. The test temperatures, alloys, and their cobalt compositions that are under study are given. J.D.

N83-11291*# National Aeronautics and Space Administration. Lewis Research Center, Cleveland, Ohio.
OXIDATION OF LOW COBALT ALLOYS
C. A. BARRETT *In its* COSAM (Conserv. Of Strategic Aerospace Mater.) Program Overview p 89-94 Oct. 1982
Avail: NTIS HC A11/MF A01 CSCL 11F

Four high temperature alloys: U-700, Mar M-247, Waspaloy and PM/HIP U-700 were modified with various cobalt levels ranging from 0 percent to their nominal commercial levels. The alloys were then tested in cyclic oxidation in static air at temperatures ranging from 1000 to 1150 C at times from 500 to 100 1 hour cycles. Specific weight change with time and X-ray diffraction analyses of the oxidized samples were used to evaluate the alloys. The alloys tend to be either Al_2O_3/aluminate spinel or Cr_2O_3/chromite spinel formers depending on the Cr/Al ratio in the alloy. Waspaloy with a ratio of 15:1 is a strong Cr_2O_3 former while this U-700 with a ratio of 3.33:1 tends to form mostly Cr_2O_3 while Mar M-247 with a ratio of 1.53:1 is a strong Al_2O_3 former. The best cyclic oxidation resistance is associated with the Al_2O_3 formers. The cobalt levels appear to have little effect on the oxidation resistance of the Al_2O_3/aluminate spinel formers while any tendency to form Cr_2O_3 is accelerated with increased cobalt levels and leads to increased oxidation attack. S.L.

N83-11292*# National Aeronautics and Space Administration. Lewis Research Center, Cleveland, Ohio.
HOT CORROSION OF LOW COBALT ALLOYS
C. A. STEARNS *In its* COSAM (Conserv. Of Strategic Aerospace Mater.) Program Overview p 95-106 Oct. 1982
Avail: NTIS HC A11/MF A01 CSCL 11F

The hot corrosion attack susceptibility of various alloys as a function of strategic materials content are investigated. Preliminary results were obtained for two commercial alloys, UDIMET 700 and Mar-M 247, that were modified by varying the cobalt content. For both alloys the cobalt content was reduced in steps to zero. Nickel content was increased accordingly to make up for the reduced cobalt but all other constituents were held constant. Wedge bar test samples were produced by casting. The hot corrosion test consisted of cyclically exposing samples to the high velocity flow of combustion products from an air-fuel burner fueled with jet A-1 and seeded with a sodium chloride aqueous solution. The flow velocity was Mach 0.5 and the sodium level was maintained at 0.5 ppm in terms of fuel plus air. The test cycle consisted of holding the test samples at 900 C for 1 hour followed by 3 minutes in which the sample could cool to room temperature in an ambient temperature air stream. S.L.

N83-11293*# National Aeronautics and Space Administration. Lewis Research Center, Cleveland, Ohio.
INFLUENCE OF COBALT, TANTALUM, AND TUNGSTEN ON THE MICROSTRUCTURE AND MECHANICAL PROPERTIES OF SUPERALLOY SINGLE CRYSTALS
M. V. NATHAL and L. J. EBERT (Case Western Reserve Univ.) *In its* COSAM (Conserv. Of Strategic Aerospace Mater.) Program Overview p 107-116 Oct. 1982
Avail: NTIS HC A11/MF A01 CSCL 11F

The influence of Co, Ta, and W on the microstructure and mechanical properties of nickel base super-alloy single crystals was investigated. A matrix of alloys was based on Mar-M 247 stripped of C, B, Zr, and Hf. The microstructures of the alloys were examined using optical and electron microscopy, phase extraction, X-ray diffraction, and differential thermal analysis. Tensile and creep-rupture tests were performed at 1000 C. An increase in tensile and creep strength resulted when Co was removed from alloys containing high refractory metal contents, but Co effects were negligible for alloys with lower refractory metal levels. In the composition range studied, W was more effective than Ta in increasing the creep resistance. The mechanical properties are discussed in relation to the microstructures of the alloys. S.L.

N83-11297*# National Aeronautics and Space Administration. Lewis Research Center, Cleveland, Ohio.
DUAL ALLOY INTERFACE STABILITY
F. H. HARF *In its* COSAM (Conserv. Of Strategic Aerospace Mater.) Program Overview p 141-152 Oct. 1982
Avail: NTIS HC A11/MF A01 CSCL 11F

Powder metallurgy dual alloy fabrication is applied to combinations of superalloys having a high iron, and low strategic metal content, with standard nickel base superalloys, containing the strategic metals chromium, cobalt, and columbium. The possibility of combining Alloy 901 (12 percent Cr, 36 percent Fe, 0 percent Co, and 0 percent Cb) with turbine disk alloys Rene 95 (13 percent Cr, 8 percent Co, and 4 percent Cb) or low carbon astroloy (L.C.A.; 15 percent Cr, 17 percent Co, and 0 percent Cb) is investigated. Preliminary results for combinations show that a strong interface with rapid diffusion is obtained between alloys and that the standard heat treatments for either alloy may be satisfactory. S.L.

N83-11299*# National Aeronautics and Space Administration. Lewis Research Center, Cleveland, Ohio.
EFFECTS ON STRESS RUPTURE LIFE AND TENSILE STRENGTH OF TIN ADDITIONS TO INCONEL 718
R. L. DRESHFIELD and W. JOHNSON (Special Metals Corp.) *In its* COSAM (Conserv. Of Strategic Aerospace Mater.) Program Overview p 157-160 Oct. 1982
Avail: NTIS HC A11/MF A01 CSCL 11F

Because Inconel 718 represents a major use of columbium and a large potential source of columbium for aerospace alloys could be that of columbium derived from tin slags, the effects of tin additions to Inconel 718 at levels which might be typical of or exceed those anticipated if tin slag derived columbium were used as a melting stock were investigated. Tin was added to 15 pound Inconel 718 heats at levels varying from none added to approximately 10,000 ppm (1 wt%). Limited 1200 F stress rupture testing was performed at stresses from 68,000 to 115,000 psi and a few tensile tests were performed at room temperature, 800 and 1200 F. Additions of tin in excess of 800 ppm were detrimental to ductility and stress rupture life. S.L.

N83-11300*# National Aeronautics and Space Administration. Lewis Research Center, Cleveland, Ohio.
INTERMETALLICS AS ALTERNATIVE MATERIALS
J. D. WHITTENBERGER *In its* COSAM (Conserv. Of Strategic Aerospace Mater.) Program Overview p 163-174 Oct. 1982
Avail: NTIS HC A11/MF A01 CSCL 11F

Aluminum containing intermetallics have B2 cubic crystal structures, exist over a wide range of composition, have large solubilities for third element alloying additions, are capable of both low and high temperature plastic flow, and have very high melting temperatures (approximately 1900 K) except for FeAl. The slow strain rate elevated temperature properties of Fe, Ni, and Co aluminides are investigated. Because of the reported difficulties with traditional melting/casting methods, sound polycrystalling materials are fabricated by hot extrusion of steel canned blended prealloyed powders. These binary aluminides are used to develop base line elevated temperature mechanical properties as well as an understanding of the factors which affect/control the strength and ductility. S.L.

N83-11307*# National Aeronautics and Space Administration. Lewis Research Center, Cleveland, Ohio.
DEVELOPMENT OF FE-MN-AL-X-C ALLOYS
S. R. SCHUON *In its* COSAM (Conserv. of Strategic Aerospace Mater.) Program Overview p 217-223 Oct. 1982
Avail: NTIS HC A11/MF A01 CSCL 11F

Development of a low cost Cr-free, iron-base alloy for aerospace applications involves both element substitution and enhancement of microstructural strengthening. When Mn is substituted for Ni and Al or Si is substituted for Cr, large changes occur in the mechanical and thermal stability of austenite in FeMnAlC alloys. The in situ strength of MC or M2C (M = Ti, V, Hf, Ta, or Mo) in FeMnAlC alloys was determined. The high temperature tensile strength depends more on the distribution of carbides than the carbide composition. Precipitation of a high volume percent-ordered phase was achieved in Fe2OMnlONi6Al6Ti (IC) alloys. As case, these alloys have a homogeneous austenitic structure. After solutioning at 1100 C for 5 hr followed by aging at 600 C for 16 hr, gamma prime or a perovskite carbide is precipitated. Overaging occurs at 900 C where eta is precipitated. J.M.S.

N83-11308*# National Aeronautics and Space Administration. Lewis Research Center, Cleveland, Ohio.
SiC OR B4C-B/LOW STRATEGIC ELEMENT CONTENT COMPOSITE
D. W. PETRASEK *In its* COSAM (Conserv. of Strategic Aerospace Mater.) Program Overview p 225-230 Oct. 1982
Avail: NTIS HC A11/MF A01 CSCL 11F

Advancements in materials technologies are needed to provide the aerospace industry with alternate material options in the event of future strategic metal shortages and to optimize performance of engines. Composite materials are promising candidates for such an application. The potential of SiC and B4C-B filament reinforced low strategic element iron-base alloy content composites or use at 760 to 870 C is considered. A limiting factor towards developing this material for high temperature use has been the reaction between the filament and matrix material during fabrication and service which degrades filament strength. A low temperature fabrication process to limit filament/matrix reaction is being developed which involves the use of hollow cathode sputtering to coat the filaments with iron-base alloys of various compositions. An investigation is being conducted to determine the interfacial reaction effects of SiC and B4C-B filaments with iron-base alloys to develop an understanding of filament/matrix alloy compatibility for 760 to 870 C service. Author

N83-11309*# National Aeronautics and Space Administration. Lewis Research Center, Cleveland, Ohio.
MICROSTRUCTURAL BEHAVIOR OF INTERFACES IN HOT ISOSTATICALLY PRESSED, DUAL ALLOY COMBINATIONS
F. H. HARF Sep. 1981 11 p refs
(NASA-TM-82698; E-981; NAS 1.15:82698) Avail: NTIS HC A02/MF A01 CSCL 11F

Combinations of the nickel-base superalloys MERL 76 and low carbon Astroloy, Rene 95 and low carbon Astroloy, Rene 95 and NASA-TRW-VIA were consolidated from prealloyed powders by hot isostatic pressing. These combinations were exposed to 870 C for 1500 hours, and in a gradient furnance to temperatures up to incipient melting and subjected to microstructural examinations. The only phases found at the interfaces were those which were also present in the component alloys. Author

N83-12154*# National Aeronautics and Space Administration. Lewis Research Center, Cleveland, Ohio.
CONSERVATION OF STRATEGIC METALS
J. R. STEPHENS *In* NASA. Langley Research Center Advan. Mater. Technol. p 141-164 Nov. 1982 refs
Avail: NTIS HC A19/MF A01 CSCL 11F

A long-range program in support of the aerospace industry aimed at reducing the use of strategic materials in gas turbine engines is discussed. The program, which is called COSAM (Conservation of Strategic Aerospace Materials), has three general objectives. The first objective is to contribute basic scientific understanding to the turbine engine technology bank so that our national security is not jeopardized if our strategic material supply lines are disrupted. The second objective is to help reduce the dependence of United States military and civilian gas turbine engines on worldwide supply and price fluctuations in regard to strategic materials. The third objective is, through research, to contribute to the United States position of preeminence in the world gas turbine engine markets by minimizing the acquisition costs and optimizing the performance of gas turbine engines. Three major research thrusts are planned: strategic element substitution; advanced processing concepts; and alternate material identification. Results from research and any required supporting technology will give industry the materials technology options it needs to make tradeoffs in material properties for critical components against the cost and availability impacts related to their strategic metal content. R.J.F.

N83-12214*# AiResearch Casting Co., Torrance, Calif.
CAST FE-BASE CYLINDER/REGENERATOR HOUSING ALLOY Quarterly Technical Narrative Report, 25 Aug. - 30 Nov. 1980
F. LARSON and L. KINDLIMANN 10 Dec. 1980 39 p refs
(Contract DEN3-234)
(NASA-CR-169474; NAS 1.26:169474; ACC-80-17602; QTNR-1)
Avail: NTIS HC A03/MF A01 CSCL 11F

The development of an iron-base alloy that can meet the requirements of automotive Stirling engine cylinders and regenerator housings is described. Alloy requirements are as follows: a cast alloy, stress for 5000-hr rupture life of 200 MPa (29 ksi) at 775 C (1427 F), oxidation/corrosion resistance comparable to that of N-155, compatibility with hydrogen, and an alloy cost less than or equal to that of 19-9DL. The preliminary screening and evaluation of ten alloys are described. J.D.

N83-12215*# IIT Research Inst., Chicago, Ill.
DETERMINATION OF HYDROGEN PERMEABILITY IN UNCOATED AND COATED SUPERALLOYS Interim Report
S. BHATTACHARYYA, E. J. VESELY, JR., and V. L. HILL Jan. 1981 65 p refs
(Contract DEN3-6; DE-A101-77CS-51040)
(NASA-CR-165209; DOE/NASA/0006-1; NAS 1.26:165209; IITRE-M06004-36) Avail: NTIS HC A04/MF A01 CSCL 11F

Hydrogen permeability, diffusivity, and solubility data were obtained for eight wrought and cast high temperature alloys over the range 650 to 815 C. Data were obtained for both uncoated alloys and wrought alloys coated with four commercially available

coatings. Activation energies for permeability, diffusivity and solubility were calculated. Author

N83-13231*# National Aeronautics and Space Administration. Lewis Research Center, Cleveland, Ohio.
INITIAL STAGES OF CAVITATION DAMAGE AND EROSION ON COPPER AND BRASS TESTED IN A ROTATING DISK DEVICE
P. V. RAO, B. C. S. RAO, and N. S. L. RAO (Indian Inst. of Science) 1982 16 p refs Presented at the Cavitation and Polyphase Flow Forum, St. Louis, Mo., 7-11 Jun. 1982
(NASA-TM-82993; E-1424; NAS 1.15:82993) Avail: NTIS HC A02/MF A01 CSCL 11F

In view of the differences in flow and experimental conditions, there has been a continuing debate as to whether or not the ultrasonic method of producing cavitation damage is similar to the damage occurring in cavitating flow systems, namely, venturi and rotating disk devices. In this paper, the progress of cavitation damage during incubation periods on polycrystalline copper and brass tested in a rotating disk device is presented. The results indicate several similarities and differences in the damage mechanism encountered in a rotating disk device (which simulates field rotary devices) and a magnetostriction apparatus. The macroscopic erosion appears similar to that in the vibratory device except for nonuniform erosion and apparent plastic flow during the initial damage phase. Author

N83-13232*# National Aeronautics and Space Administration. Lewis Research Center, Cleveland, Ohio.
EVALUATION OF DOPANTS IN HYDROGEN TO REDUCE HYDROGEN PERMEATION IN CANDIDATE STIRLING ENGINE HEATER HEAD TUBE ALLOYS AT 760 DEG AND 820 DEG
J. A. MISENCIK Oct. 1982 32 p refs
(Contract DE-AI01-77CS-51040)
(NASA-TM-82920; DOE/NASA/51040-41; R-1309; NAS 1.15:82920) Avail: NTIS HC A03/MF A01 CSCL 11F

Alloy tubes filled with hydrogen doped with various amounts of carbon monoxide, carbon dioxide, ethane, ethylene, methane, ammonia, or water were heated in a diesel fuel-fired Stirling engine simulator materials test rig for 100 hours at 21 MPa and 760 or 820 C to determine the effectiveness of the dopants in reducing hydrogen permeation through the hot tube walls. Ultra high purity (UHP) hydrogen was used for comparison. The tube alloys were N-155, A-286, Incoloy 800, Nitronic 40, 19-9DL, 316 stainless steel, Inconel 718, and HS-188. Carbon dioxide and carbon monoxide in the concentration range 0.2 to 5 vol % were most effective in reducing hydrogen permeation through the hot tube walls for all alloys. Ethane, ethylene, methane, ammonia, and water at the concentrations investigated were not effective in reducing the permeation below that achieved with UHP hydrogen. One series of tests were conducted with UHP hydrogen in carburized tubes. Carburization of the tubes prior to exposure reduced permeation to values similar to those for carbon monoxide; however, carbon dioxide was the most effective dopant. Author

N83-13233*# Ohio State Univ., Columbus. Dept. of Industrial and Systems Engineering.
THE ORTHOGONAL IN-SITU MACHINING OF SINGLE AND POLYCRYSTALLINE ALUMINUM AND COPPER, VOLUME 2 Ph.D. Thesis. Final Report
P. H. COHEN May 1982 377 p
(Contract NSG-3164)
(NASA-CR-169528; NAS 1.26:169528; OSURF-760931/710709)
Avail: NTIS HC A17/MF A01 CSCL 11F

Data are presented for aluminum and copper with 20, 30 and 50 deg tools. Data for computed mechanics on the shear plane and rake face are also included. S.L.

N83-14245*# National Aeronautics and Space Administration. Lewis Research Center, Cleveland, Ohio.
INVESTIGATION OF WEAR PHENOMENA BY MICROSCOPY
D. H. BUCKLEY 16 Jul. 1982 43 p refs Presented at Microscopy of the Degradation of Materials (Wear and Erosion), MICRO 1982, Intern. Symp. and Exhibition, London, 12-16 Jul. 1982; sponsored by Royal Microscopial Society
(NASA-TM-82934; E-1239; NAS 1.15:82934) Avail: NTIS HC A03/MF A01 CSCL 11F

The various wear mechanisms involved in the loss of material from metallic and nonmetallic surfaces are discussed. The results presented indicate how various microscopy techniques used in conjunction with other analytical tools can assist in the elucidation of a wear mechanism. Without question, microscopy is the single most important tool for the study of the wear of surfaces, to assess and address inherent mechanisms of the material removal process. Author

N83-14246*# National Aeronautics and Space Administration. Lewis Research Center, Cleveland, Ohio.
STRAINRANGE PARTITIONING: A TOTAL STRAIN RANGE VERSION
G. R. HALFORD and J. F. SALTSMAN 1983 12 p refs Proposed for presentation at the Intern. Conf. on Advan. in Life Prediction, Albany, N.Y., 18-21 Apr. 1983; sponsored by ASME
(NASA-TM-83023; E-1459; NAS 1.15:83023) Avail: NTIS HC A02/MF A01 CSCL 11F

Procedures are presented for expressing the Strainrange Partitioning (SRP) method for creep fatigue life prediction in terms of total strain range. Inelastic and elastic strain-range - life relations are summed to give total strain-range - life relations. The life components due to inelastic strains are dealt with using conventional SRP procedures while the life components due to elastic strains are expressed as families of time-dependent terms for each type of SRP cycle. Cyclic constitutive material behavior plays an important role in establishing the elastic strain-range - life relations as well as the partitioning of the inelastic strains. To apply the approach, however, it is not necessary to have to determine the magnitude of the inelastic strain range. The total strain SRP approach is evaluated and verified using two nickel base superalloys, AF2-1DA and Rene 95. Excellent agreement is demonstrated between observed and predicted cyclic lifetimes with 70 to 80 percent of the predicted lives falling within factors of two of the observed lives. The total strain-range SRP approach should be of considerable practical value to designers who are faced with creep-fatigue problems for which the inelastic strains cannot be calculated with sufficient accuracy to make reliable life predictions by the conventional inelastic strain range SRP approach. Author

N83-15411*# Pittsburgh Univ., Pa. Dept. of Metallurgical and Materials Engineering.
MECHANISM OF HOT CORROSION OF IN-738 Final Report
G. H. MEIER 9 Dec. 1982 20 p refs
(Contract NSG-3214)
(NASA-CR-169706; NAS 1.26:169706) Avail: NTIS HC A02/MF A01 CSCL 11F

The Na2SO4 - induced hot corrosion of IN-738 in the temperature range 900 C to 1000 C is characterized by an initiation stage during which the corrosion rate is slow followed by a propagation stage during which the corrosion rate is markedly accelerated. In the second stage, corrosion is accelerated due essentially to a sulfidation/oxidation mechanism; in the third stage, the rate becomes catastrophic due to acid fluxing induced by an accumulation of refractory metal oxides (particularly MoO3) in the Na2SO4. The sequential stages in the corrosion process are described and a mechanism proposed. The influence of alloy microstructure on the corrosion mechanism is also discussed. A.R.H.

N83-15412*# General Electric Co., Cincinnati, Ohio. Aircraft Engine Business Group.
POWDER METALLURGY RENE 95 ROTATING TURBINE ENGINE PARTS, VOLUME 2 Final Report
L. G. WILBERS and T. K. REDDEN Jan. 1981 30 p refs
(Contract NAS3-20074)
(NASA-CR-165141; NAS 1.26:165141; R80AEG664-VOL-2)
Avail: NTIS HC A03/MF A01 CSCL 11F

A Rene 95 alloy as-HIP high pressure turbine aft shaft in the CF6-50 engine and a HIP plus forged Rene 95 compressor disk in the CFM56 engine were tested. The CF6-50 engine test was conducted for 1000 C cycles and the CFM56 test for 2000 C cycles. Post test evaluation and analysis of the CF6-50 shaft and the CFM56 compressor disk included visual, fluorescent penetrant, and dimensional inspections. No defects or otherwise discrepant conditions were found. These parts were judged to have performed satisfactorily. S.L.

N83-15413*# National Aeronautics and Space Administration. Lewis Research Center, Cleveland, Ohio.
UNIVERSAL APPROACH TO ANALYSIS OF CAVITATION AND LIQUID-IMPINGEMENT EROSION DATA
P. V. RAO and S. G. YOUNG Nov. 1982 39 p refs
(NASA-TP-2061; E-1087; NAS 1.60:2061) Avail: NTIS HC A03/MF A01 CSCL 20D

Cavitation erosion experimental data was analyzed by using normalization and curve-fitting techniques. Data were taken from experiments on several materials tested in both a rotating disk device and a magnetostriction apparatus. Cumulative average volume loss rate and time data were normalized relative to the peak erosion rate and the time to peak erosion rate, respectively. From this process a universal approach was derived that can include data on specific materials from different test devices for liquid impingement and cavitation erosion studies. S.L.

N83-16493*# Kent State Univ., Ohio. Dept. of Physics.
APPLICATIONS OF ION BEAM TECHNOLOGY Final Report
E. GELERINTER and N. SPIELBERG Aug. 1980 40 p refs
(Contract NAS3-21945)
(NASA-CR-169797; NAS 1.26:169797) Avail: NTIS HC A03/MF A01 CSCL 11F

Wire adhesion in steel belted radial tires; carbon fibers and composite; cold welding, brazing, and fabrication; hydrogen production, separation, and storage; membrane use; catalysis; sputtering and texture; and ion beam implantation are discussed. Author

N83-17682*# National Aeronautics and Space Administration. Lewis Research Center, Cleveland, Ohio.
SURFACE PROFILE CHANGES OF SCUFFED BEARING SURFACES
J. L. LAUER (Rensselaer Polytechnic Inst.), S. S. FUNG (Rensselaer Polytechnic Inst.), and W. R. JONES, JR. 1982 15 p refs Presented at the Israel Conf. on Mech. Eng., Haifa, Israel, 13-14 Jul. 1982
(Contract NSG-3170; AF-AFOSR-005-81)
(NASA-TM-83055; E-1402; NAS 1.15:83055) Avail: NTIS HC A02/MF A01 CSCL 11F

A phase locked interference microscope capable of resolving depth differences to 30 A and planar displacements of 6000 A was constructed for the examination of the profiles of bearing surfaces without physical contact. This instrument was used to determine surface chemical reactivity by applying a drop of dilute alcoholic hydrochloric acid and measuring the profile of the solid surface before and after application of this probe. Scuffed bearing surfaces reacted much faster than unscuffed ones, but bearing surfaces which had been previously exposed to lubricants containing an organic chloride reacted much more slowly. In a separate series of experiments, a number of stainless steel plates were heated in a nitrogen atmosphere to different temperatures and their reactivity examined later at room temperature. The change of surface contour as a result of the probe reaction followed an Arrhenius type relation with respect to heat treatment temperature. This result could have implications on the scuffing mechanism. Author

N83-17683*# National Aeronautics and Space Administration. Lewis Research Center, Cleveland, Ohio.
COATING WITH OVERLAY METALLIC-CERMET ALLOY SYSTEMS Patent Application
M. A. GEDWILL, S. R. LEVINE, and T. K. GLASGOW, inventors (to NASA) 7 Jan. 1983 12 p
(NASA-CASE-LEW-13639-2; US-PATENT-APPL-SN-456460)
Avail: NTIS HC A02/MF A01 CSCL 11F

A base layer of an oxide dispersed, metallic alloy (cermet) is arc plasma sprayed onto a substrate, such as a turbine blade, vane, or the like, which is subjected to high temperature use. A top layer of an oxidation, hot corrosion, erosion resistant alloy of nickel, cobalt, or iron is then arc plasma sprayed onto the base layer. A heat treatment is used to improve the bonding. The base layer serves as an inhibitor to interdiffusion between the protective top layer and the substrate. Otherwise, the 10 protective top layer would rapidly interact detrimentally with the substrate and degrade by spalling of the protective oxides formed on the outer surface at elevated temperatures. NASA

N83-19885*# American Society of Metals, Metals Park, Ohio.
BINARY NICKEL ALLOY PHASE DIAGRAMS COMPILATION AND CRITICAL EVALUATION Status Report, Jun. 1982 - Feb. 1983
J. HONTAS 16 Mar. 1982 17 p refs
(Contract NAG3-302)
(NASA-CR-170016; NAS 1.26:170016) Avail: NTIS HC A02/MF A01 CSCL 11F

Equilibrium diagrams general features, intermediate phases, liquidus and solidus, terminal solid solutions, metastable phases, crystallography, and thermodynamics are covered. Author

N83-19886*# National Aeronautics and Space Administration. Lewis Research Center, Cleveland, Ohio.
FRICTION AND WEAR OF SOME FERROUS-BASE METALLIC GLASSES
K. MIYOSHI and D. H. BUCKLEY Washington 1983 24 p refs Proposed for presentation at the Joint Lubrication Conf., Hartford, Conn., 18-20 Oct. 1983; sponsored by American Society of Mechanical Engineers and American Society of Lubrication Engineers
(NASA-TM-83067; E-1502; NAS 1.15:83067) Avail: NTIS HC A02/MF A01 CSCL 11F

Sliding friction experiments, X-ray photoelectron spectroscopy (XPS) analysis, and electron microscopy and diffraction studies were conducted with ferrous base metallic glasses (amorphous alloys) in contact with aluminum oxide at temperatures to 750 C in a vacuum. Sliding friction experiments were also conducted in argon and air atmospheres. The results of the investigation indicate that the coefficient of friction increases with increasing temperature to 350 C in vacuum. The increase in friction is due to an increase in adhesion resulting from surface segregation of boric oxide and/or silicon oxide to the surface of the foil. Above 500 C the coefficient of friction decreased rapidly. The decrease correlates with the segregation of boron nitride to the surface. Contaminants can come from the bulk of the material to the surface upon heating and impart boric oxide and/or silicon oxide at 350 C and boron nitride above 500 C. The segregation of contaminants is responsible for the friction behavior. The amorphous alloys have superior wear resistance to crystalline 304 stainless steel. The relative concentrations of the various constituents at the surfaces of the amorphous alloys are very different from the nominal bulk compositions. Author

N83-19887*# National Aeronautics and Space Administration. Lewis Research Center, Cleveland, Ohio.
BURNER RIG STUDY OF VARIABLES INVOLVED IN HOLE PLUGGING OF AIR COOLED TURBINE ENGINE VANES
D. L. DEADMORE and C. E. LOWELL Feb. 1983 12 p refs
(NASA-TM-83308; E-1547; NAS 1.15:83308) Avail: NTIS HC A02/MF A01 CSCL 21E

The effects of combustion gas composition, flame temperatures, and cooling air mass flow on the plugging of film cooling holes by a Ca-Fe-P-containing deposit were investigated. The testing was performed on film-cooled vanes exposed to the combustion gases of an atmospheric Mach 0.3 burner rig. The extent of plugging was determined by measurement of the open hole area at the conclusion of the tests as well as continuous monitoring of some of the tests using stop-action photography. In general, as the P content increased, plugging rates also increased. The plugging was reduced by increasing flame temperature and cooling air mass flow rates. At times up to approximately 2 hours little plugging was observed. This apparent incubation period was followed by rapid plugging, reaching in several hours a maximum closure whose value depended on the conditions of the test. Author

N83-21110*# National Aeronautics and Space Administration. Lewis Research Center, Cleveland, Ohio.
SLIDING INDUCED CRYSTALLIZATION OF METALLIC GLASS
K. MIYOSHI and D. H. BUCKLEY Mar. 1983 23 p refs
(NASA-TP-2140; E-1278; NAS 1.60:2140) Avail: NTIS HC A02/MF A01 CSCL 11F

Sliding friction and wear experiments, electron microscopy, and diffraction studies were conducted with an Fe67Co18B14Si1 ferrous-base metallic glass in sliding contact with aluminum oxide at room temperature in air. The results indicate that the amorphous alloy can be crystallized during the sliding process. Crystallization of the wear surface causes high friction. Plastic flow occurred on the amorphous alloy with sliding, and the flow film of the alloy transferred to the aluminum oxide surface. Two distinct types of wear debris were observed as a result of sliding: an alloy wear debris, and powdery and whiskery oxide debris. Generation of oxide wear debris particles on an alloy can cause transitions in friction behavior. Author

N83-22387*# National Aeronautics and Space Administration. Lewis Research Center, Cleveland, Ohio.
PROGRESS TOWARD DETERMINING THE POTENTIAL OF ODS ALLOYS FOR GAS TURBINE APPLICATIONS
R. L. DRESHFIELD, G. HOPPIN, III (Garrett Turbine Engine Company, Phoenix, Ariz.), and K. SHEFFLER (Pratt and Whitney Aircraft Company, East Hartford, Conn.) 1983 16 p refs Presented at Frontiers of High Temperature Mater. II, London, 22-25 May 1983; sponsored by the International Nickel Company
(NASA-TM-83332; E-1579; NAS 1.15:83332) Avail: NTIS HC A02/MF A01 CSCL 11F

The Materials for Advanced Turbine Engine (MATE) Program managed by the NASA Lewis Research Center is supporting two projects to evaluate the potential of oxide dispersion strengthened (ODS) alloys for aircraft gas turbine applications. One project involves the evaluation of Incoloy (TM) MA-956 for application as a combustor liner material. An assessment of advanced engine potential will be conducted by means of a test in a P&WA 2037 turbofan engine. The other project involves the evaluation of Inconel (TM) MA 6000 for application as a high pressure turbine blade material and includes a test in a Garrett TFE 731 turbofan engine. Both projects are progressing toward these engine tests in 1984. Author

N83-22389*# IIT Research Inst., Chicago, Ill.
CREEP-RUPTURE BEHAVIOR OF 6 CANDIDATE STIRLING ENGINE IRON-BASE SUPERALLOYS IN HIGH PRESSURE HYDROGEN. VOLUME 1: AIR CREEP-RUPTURE BEHAVIOR Final Report
S. BHATTACHARYYA Dec. 1982 128 p refs
(Contract DEN3-217; DE-AI01-77CS-51040)
(NASA-CR-168071; NAS 1.26:168071; IITRI-M06061-38) Avail: NTIS HC A07/MF A01 CSCL 11F

Four wrought alloys (A-286, IN 800H, N-155, and 19-9DL) and two cast alloys (CRM-6D and XF-818) were tested to determine their creep-rupture behavior. The wrought alloys were used in the form of sheets of 0.89 mm (0.035 in.) average thickness. The cast alloy specimens were investment cast and machined to 6.35 mm (0.250 in.) gage diameter. All specimens were tested to rupture in air at different times up to 3000 h over the temperature range of 650 C to 925 C (1200 F to 1700 F). Rupture life, minimum creep rate, and time to 1% creep strain were statistically analyzed as a function of stress at different temperatures. Temperature-compensated analysis was also performed to obtain the activation energies for rupture life, time to 1% creep strain, and the minimum creep rate. Microstructural and fracture analyses were also performed. Based on statistical analyses, estimates were made for stress levels at different temperatures to obtain 3500 h rupture life and time to 1% creep strain. Test results are to be compared with similar data being obtained for these alloys under 15 MPa (2175 psi) hydrogen. A.R.H.

N83-22390*# National Aeronautics and Space Administration. Lewis Research Center, Cleveland, Ohio.
FRICTIONAL AND MORPHOLOGICAL CHARACTERISTICS OF ION PLATED SOFT, METALLIC FILMS
T. SPALVINS and B. BUZEK 1981 14 p refs Presented at the Intern. Conf. on Metall. Coatings, San Francisco, 6-10 Apr. 1981 Announced in AIAA as A81-38066
(NASA-TM-81723; E-760; NAS 1.15:81723) Avail: NTIS HC A02/MF A01 CSCL 11F

Ion plated metallic films in contrast to films applied by other deposition techniques offer a lower friction coefficient, longer endurance lives and exhibit a gradual increase in friction coefficient after the film has been worn off. The friction coefficients of metallic films are affected by the degree of adherence, thickness and nucleation and growth characteristics during ion plating lead to a fine, continuous crystalline structure, which contributes to a lower friction coefficient. Author (IAA)

N83-23417*# National Aeronautics and Space Administration. Lewis Research Center, Cleveland, Ohio.
THE XPS DEPTH PROFILING AND TRIBOLOGICAL CHARACTERIZATION OF ION-PLATED GOLD ON VARIOUS METALS
K. MIYOSHI, T. SPALVINS, and D. H. BUCKLEY 1983 17 p refs Presented at the Intern. Conf. on Met. Coatings, San Diego, Calif., 18-20 Apr. 1983; sponsored by American Vacuum Society
(NASA-TM-83350; E-1582; NAS 1.15:83350) Avail: NTIS HC A02/MF A01 CSCL 11F

Friction properties were measured with a gold film; the graded interface between gold and nickel substrate; and the nickel substrate. All sliding was conducted against hard silicon carbide pins in two processes. In the adhesive process, friction arises primarily from adhesion between sliding surfaces. In the abrasion process, friction occurs as a result of the hard pin sliding against the film, indenting into it, and plowing a series of grooves. Copper and 440 C stainless steel substrates were also used. Results indicate that the friction related to both adhesion and abrasion is influenced by coating depth. The trends in friction behavior as a function of film depth are, however, just the opposite. The graded interface exhibited the highest adhesion and friction, while the graded interface resulted in the lowest abrasion and friction. The coefficient of friction due to abrasion is inversely related to the hardness. The greater the hardness of the surface, the lower is the abrasion and friction. The microhardness in the graded interface exhibited the highest hardness due to an alloy hardening effect.

Almost no graded interface between the vapor-deposited gold film and the substrates was detected. A.R.H.

N83-23419*# National Aeronautics and Space Administration. Lewis Research Center, Cleveland, Ohio.
X-RAY PHOTOELECTRON SPECTROSCOPY AND FRICTION STUDIES OF NICKEL-ZINC AND MANGANESE-ZINC FERRITES IN CONTACT WITH METALS
K. MIYOSHI and D. H. BUCKLEY Apr. 1983 19 p refs
(NASA-TP-2163; E-1349; NAS 1.60:2163) Avail: NTIS HC A02/MF A01 CSCL 11F

X-ray photoelectron spectroscopy analysis and sliding friction experiments were conducted with hot-pressed, polycrystalline Ni-Zn and Mn-Zn ferrites in sliding contact with various transition metals at room temperature in a vacuum of 30 nPa. The results indicate that the coefficients of friction for Ni-Zn and Mn-Zn ferrites in contact with metals are related to the relative chemical activity in these metals: the more active the metal, the higher is the coefficient of friction. The coefficients of friction for the ferrites correlate with the free energy of formation of the lowest metal oxide. The interfacial bond can be regarded as a chemical bond between the metal atoms and the oxygen anions in the ferrite surfaces. The adsorption of oxygen on clean metal and ferrite surfaces increases the coefficients of friction for the Ni-Zn and Mn-Zn ferrite-metal interfaces. Author

N83-24634*# National Aeronautics and Space Administration. Lewis Research Center, Cleveland, Ohio.
A COMPREHENSIVE ANALYSIS OF CAVITATION AND LIQUID IMPINGEMENT EROSION DATA
P. V. RAO and S. G. YOUNG 1983 18 p refs Proposed for presentation at 2nd Conf. on Cavitation, Edinburg, 6-8 Sep. 1983; Sponsored by Institute of Mechanical Engineers
(NASA-TM-83352; E-1388; NAS 1.15:83352) Avail: NTIS HC A02/MF A01 CSCL 11F

Cavitation-erosion experimental data previously covering several materials tested in a rotating disk device and a magnetostriction apparatus were analyzed using new normalization and curve-fitting techniques. From this process a universal approach is derived which can include data from cavitation and liquid impingement studies for specific materials from different test devices. Author

N83-24635*# National Aeronautics and Space Administration. Lewis Research Center, Cleveland, Ohio.
TRIBOLOGICAL AND MICROSTRUCTURAL CHARACTERISTICS OF ION-NITRIDED STEELS
T. SPALVINS 1983 12 p refs Presented at the Intern. Conf. on Met. Coatings, San Diego, Calif., 18-22 Apr. 1983; sponsored by Am. Vacuum Soc.
(NASA-TM-83368; E-1609; NAS 1.15:83368) Avail: NTIS HC A02/MF A01 CSCL 11F

Three steels AISI 4140, AISI 4340 and AISI 304 stainless steel were ion nitrided in a plasma consisting of a 75:25 mixture of H2:N2, sometimes with a trace of CH4. Their surface topography was characterized by SEM and two distinct compound phases were identified: the gamma and the epsilon. The core-case hardness profiles were also established. The low Cr alloy steels have an extended diffusion zone in contrast to the 304 stainless steels which have a sharp interface. The depth of ion-nitriding is increased as the Cr content is decreased. Friction tests reveal that the gamma surface phase has a lower coefficient of friction than the epsilon phase. The lowest coefficient of friction is achieved when both the rider and the specimen surface are ion nitrided. S.L.

N83-24636*# National Aeronautics and Space Administration. Lewis Research Center, Cleveland, Ohio.
EFFECT OF OXYGEN CONCENTRATION IN ZDP CONTAINING OILS ON SURFACE COMPOSITION AND WEAR
W. A. BRAINARD and J. FERRANTE Apr. 1983 12 p refs
(NASA-TM-83000; E-1436; NAS 1.15:83000) Avail: NTIS HC A02/MF A01 CSCL 11F

A pin-on-disk wear study was performed with the lubricants dibutyl sebacate (DBS) and mineral oil (MO) with and without 1 weight percent zinc-dialkyl-dithiophospatee (ZDP) as an additive. The pin was annealed pure iron and the disk was M-2 tool steel. The selected load and speed guaranteed boundary lubrication. The ambient atmospheric oxygen concentration in an oxygen-nitrogen mixture was varied from 0 percent to 20 percent in order to examine its relationship to ZDP effectiveness. Auger electron spectroscopy combined with argon ion bombardment (depth profiling) was used to determine surface elemental composition on the pin when tested in DBS with and without ZDP. The ambient atmosphere was found to cause large variations in wear rate and surface composition. With MO, ZDP reduced wear under all conditions, but had little advantage over oxides formed at 20 percent oxygen atmosphere. With DBS, ZDP reduced wear at 0 percent oxygen, but gave varied results at other oxygen concentrations. Depth profiling revealed sulfuide formation at 0 percent oxygen and probably sulfates at 20 percent oxygen. The results are significant because varied oxygen concentrations can occur under actual lubricating conditions in practical machinery. Author

N83-24637*# National Aeronautics and Space Administration. Lewis Research Center, Cleveland, Ohio.
TIME EFFECT OF EROSION BY SOLID PARTICLE IMPINGEMENT ON DUCTILE MATERIALS
P. V. RAO and D. H. BUCKLEY Apr. 1983 18 p refs Proposed for presentation at the 6th Intern. Conf. on Erosion by Liquid and Solid Impact, 4-8 Sep. 1983, Cambridge, England; sponsored by Cavendish Lab.
(NASA-TM-83369; E-1592; NAS 1.15:83369) Avail: NTIS HC A02/MF A01 CSCL 11F

Erosion and morphological studies of several metals and alloys eroded by normal impingement jets of spherical glass beads and angular crushed-glass erodent particles were conducted. Erosion morphology (the width, depth, and width-depth ratio of the pit) was studied in order to fully investigate the effect of time on erosion rate. The eroded surfaces were studied with a scanning electron microscope, and surface profiles were measured with a profilometer. A large amount of experimental data reported in the literature was also analyzed in order to understand the effect of variables such as the type of device, the erodent particle size and shape, the impact velocity, and the abrasive charge on erosion-rate-versus-time curves. In the present experiments the pit-width-versus-time or pit-depth-versus-time curves were similar to erosion-versus-time curves for glass-bead impingement. The pit-depth-rate-versus-time curves were similar to erosion-rate-versus-time curves for crushed-glass impingement. Analysis of experimental data with two forms of glass resulted in four types of erosion-rate-versus-time curves: (1) incubation, acceleration, and steady-state periods (type I), (2) incubation, acceleration, deceleration, and steady-state periods (type III), (3) incubation, acceleration, peak rate, and deceleration periods (type IV), and (4) incubation, acceleration, steady-state, and deceleration periods (type V). B.W.

N83-24638*# National Aeronautics and Space Administration. Lewis Research Center, Cleveland, Ohio.
THE EFFECTS OF NI, MO, TI AND SI ON THE MECHANICAL PROPERTIES OF CR FREE MN STEEL (FE-25MN-5AL-2C)
S. R. SCHUON 1982 18 p refs Presented at Fall Meeting of the Met. Soc., St. Louis, 24-28 Oct. 1982; sponsored by American Institute of Mining, Metallurgical and Petroleum Engineers
(NASA-TM-83355; E-1612; NAS 1.15:83355) Avail: NTIS HC A02/MF A01 CSCL 11F

The FeMnAlC alloys may hold potential as Cr-free replacements for high strategic material iron base superalloys, but little is known about their intermediate temperature (650 C to 870 C) mechanical properties. The effects of alloying elements on the mechanical properties of model FeMnAlC alloys were studied. Results showed that modified FeMnAlC alloys had promising short term, intermediate temperature properties but had relatively poor stress rupture lives at 172 MPa and 788 C. Room temperature and 788 C tensile strength of FeMnAlC alloys were better than common cast stainless steels. Changes in room temperature tensile and 788 C tensile strength and ductility, and 788 C stress rupture life were correlated with changes in Ni, Mo, Ti, and Si levels due to alloying effects on interstitial carbon levels and carbide morphology. Fe-25Mn-5Al-2C had a very poor stress rupture life at 172 MPa and 788 C. Addition of carbide-forming elements improved the stress rupture life. Author

N83-24639*# National Aeronautics and Space Administration. Lewis Research Center, Cleveland, Ohio.
IMPROVED NICKEL BASE COATING ALLOY Patent Application
C. A. BARRETT and C. E. LOWELL, inventors (to NASA) 23 Mar. 1983 7 p
(NASA-CASE-LEW-13834-1; US-PATENT-APPL-SN-478131) Avail: NTIS HC A02/MF A01 CSCL 11F

Zirconium is added to a Ni-30 Al (beta) intermetallic alloy in the range of 0.05 w/o to 0.25 w/o. This addition is made during melting or by using metal powders. The addition of zirconium improves the cyclic oxidation resistance of the alloys at temperatures above 1100 C. NASA

N83-24640*# National Aeronautics and Space Administration. Lewis Research Center, Cleveland, Ohio.
NITRIDING OF TITANIUM AND TITANIUM: 8 PERCENT ALUMINUM, 1 PERCENT MOLYBDENUM, 1 PERCENT VANADIUM ALLOY WITH AN ION-BEAM SOURCE
A. GILL (Ben Gurion Univ. of the Negev) Apr. 1983 11 p refs
(NASA-TP-2149; E-1227; NAS 1.60:2149) Avail: NTIS HC A02/MF A01 CSCL 11F

Titanium and Ti-8Al-1Mo-1V alloy were nitrided with an ion-beam source of nitrogen or argon and nitrogen at a total pressure of 2 x 10 to the minus 4th power to 10 x 10 to the minus 4th power torr. The treated surface was characterized by surface profilometry, X-ray diffractometry, Auger electron spectroscopy and microhardness measurements. The tetragonal Ti_2N phase formed in pure titanium and Ti-8Al-1Mo-1V alloy with traces of AlN in the alloy. Two opposite processes competed during the ion-beam-nitriding process: (1) formation of nitrides in the surface layer and (2) sputtering of the nitrided layers by the ion beam. The highest surface hardnesses, about 500 kg/sq mm in titanium and 800 kg/sq mm in Ti-8Al-1Mo-1V, were obtained by ion nitriding with an ion beam of pure nitrogen at 4.2 x 10 to the minus 4th power torr at a beam voltage of 1000 V. Author

N83-24641*# National Aeronautics and Space Administration. Lewis Research Center, Cleveland, Ohio.
MORPHOLOGY OF AN ALUMINUM ALLOY ERODED BY A JET OF ANGULAR PARTICLES IMPINGING AT NORMAL INCIDENCE
P. V. RAO, S. G. YOUNG (NASA. Kennedy Space Center), and D. H. BUCKLEY May 1983 15 p refs
(NASA-TP-2139; E-1166; NAS 1.60:2139) Avail: NTIS HC A02/MF A01 CSCL 11F

The erosion of an aluminum alloy impinged by crushed glass particles at normal incidence was studied. The erosion patterns were analyzed by scanning electron microscopy, energy dispersive X-ray spectroscopy, and surface profilometer measurements. From the analysis of specimens tested at various driving gas pressures and time intervals, four distinct erosion regions were identified. A study of pit morphology and its relationship to cumulative erosion was made. Cutting wear is believed to be the predominant material removal mechanism; some evidence of deformation wear was found during the incubation period. Author

N83-25853*# National Aeronautics and Space Administration. Lewis Research Center, Cleveland, Ohio.
SOLID PARTICLE IMPINGEMENT EROSION CHARACTERISTICS OF CYLINDRICAL SURFACES, PRE-EXISTING HOLES AND SLITS
P. V. RAO and D. H. BUCKLEY 1983 23 p refs Presented at the Cavitation and Multiphase Flow Forum, Houston, Tex., 20-22 Jun. 1983; sponsored by the ASME
(NASA-TM-83322; E-1526; NAS 1.15:83322) Avail: NTIS HC A02/MF A01 CSCL 11F

The erosion characteristics of aluminum cylinders sand-blasted with both spherical and angular erodent particles were studied and compared with results from previously studied flat surfaces. The cylindrical results are discussed with respect to impact conditions. The relationship between erosion rate and pit morphology (width, depth, and width to depth ratio) is established. The aspects of (1) erosion rate versus time curves on cylindrical surfaces; (2) long-term exposures; and (3) erosion rate versus time curves with spherical and angular particles are presented. The erosion morphology and characteristics of aluminum surfaces with pre-existing circular cylindrical and conical holes of different sizes were examined using weight loss measurements, scanning electron microscopy, a profilometer, and a depth gage. The morphological features (radial and concentric rings) are discussed with reference to flat surfaces, and the erosion features with spherical microglass beads. The similarities and differences of erosion and morphological features are highlighted. The erosion versus time curves of various shapes of holes are discussed and are compared with those of a flat surface. The erosion process at slits is considered. A.R.H.

N83-28208*# Case Western Reserve Univ., Cleveland, Ohio. Dept. of Civil Engineering.
SOLUTION OF ELASTIC AND ELASTO-PLASTIC PROBLEMS BY THE METHOD OF LINES Final Report
A. MENDELSON and J. ALAM Apr. 1983 350 p refs (Contract NSG-3251)
(NASA-CR-168125; NAS 1.26:168125) Avail: NTIS HC A15/MF A01 CSCL 11F

The solution of a crack problem by the method of lines, the solution of elasto-plastic problem using the method of lines, and the stress intensity factors and J-integral determination are discussed. Author

N83-29358*# National Aeronautics and Space Administration. Lewis Research Center, Cleveland, Ohio.
REACTIONS OF NACL WITH GASEOUS SO3, SO2, AND O2
W. L. FIELDER, C. A. STEARNS, and F. J. KOHL Washington 1983 19 p refs Presented at the 163d Meeting of the Electrochem. Soc., San Francisco, 9-13 May 1983
(NASA-TM-83423; E-1712; NAS 1.15:83423) Avail: NTIS HC A02/MF A01 CSCL 11F

Hot corrosion of gas turbine engine components involves deposits of Na2SO4 which are produced by reactions between NaCl and oxides of sulfur. For the present investigation, NaCl single crystals were exposed at 100 to 850 C to gaseous mixtures of SO3, SO2, and O2. The products formed during this exposure depend, primarily, on the temperatures. The four product films were: NaCl-SO3; Na2S2O7; Na2SO4; and NaCl-Na2SO4. The kinetics of the reactions were measured. Author

N83-29359*# Southwest Research Inst., San Antonio, Tex.
EVALUATION OF FUEL ADDITIVES FOR REDUCTION OF MATERIAL IMCOMPATIBILITIES IN METHANOL-GASOLINE BLENDS Final Report
C. F. RODRIGUEZ, J. G. BARBEE, W. K. KNUTSON, and J. P. CUELLAR, JR. Mar. 1983 41 p refs
(Contract DEN3-287; DE-AI01-81CS-50006)
(NASA-CR-168061; DOE/NASA/0287-1; NAS 1.26:168061; SWRI-7080) Avail: NTIS HC A03/MF A01 CSCL 11F

Screening tests determined the efficacy of six commercially available additives as modifiers of methanol's corrosivity toward metals and its weakening of tensile properties of nonmetals in automotive fuel systems. From the screening phase, three additives which seemed to protect some of the metals were tested in higher concentrations and binary combinations in search of optimal application conditions. Results indicate that two of the additives have protective properties and combining them increases the protection of the metals corroded by methanol-gasoline blends. Half of the metals in the tests were not corroded. Testing at recommended concentrations and then at higher concentrations and in combinatioins shows that the additives would have no protective or harmful effects on the nonmetals. Two additives emerged as candidates for application to the protection of metals in automotive methanol-gasoline fuel systems. The additives tested were assigned letter codes to protect their proprietary nature.
A.R.H.

N83-29360*# National Aeronautics and Space Administration. Lewis Research Center, Cleveland, Ohio.
CONSIDERATIONS OF TECHNOLOGY TRANSFER BARRIERS IN THE MODIFICATION OF STRATEGIC SUPERALLOYS FOR AIRCRAFT TURBINE ENGINES
J. R. STEPHENS and J. K. TIEN (Columbia Univ., New York) 1983 25 p refs Presented at the 112th Ann. Meeting of the Am. Inst. of Mining, Metall. and Petroleum Engr., Atlanta, 7-10 May 1983
(NASA-TM-83395; E-1672; NAS 1.15:83395) Avail: NTIS HC A02/MF A01 CSCL 11F

A typical innovation-to-commercialization process for the development of a new hot section gas turbine material requires one to two decades with attendant costs in the tens of millions of dollars. This transfer process is examined to determine the potential rate-controlling steps for introduction of future low strategic metal content alloys or processes. Case studies are used to highlight the barriers to commercialization as well as to identify the means by which these barriers can be surmounted. The opportunities for continuing joint government-university-industry partnerships in planning and conducting strategic materials R&D programs are also discussed. Author

N83-31795* National Aeronautics and Space Administration. Lewis Research Center, Cleveland, Ohio.
SILICON-SLURRY/ALUMINIDE COATING Patent
D. L. DEADMORE and S. G. YOUNG, inventors (to NASA) 15 Feb. 1983 6 p Filed 14 Aug. 1981
(NASA-CASE-LEW-13343; US-PATENT-4,374,183; US-PATENT-APPL-SN-293418; US-PATENT-CLASS-428-641; US-PATENT-CLASS-428-650; US-PATENT-CLASS-428-680; US-PATENT-CLASS-428-450; US-PATENT-CLASS-428-469; US-PATENT-CLASS-427-318; US-PATENT-CLASS-427-419.2) Avail: US Patent and Trademark Office CSCL 11F

A low cost coating protects metallic base system substrates from high temperatures, high gas velocity ovidation, thermal fatigue and hot corrosion and is particularly useful fo protecting vanes and blades in aircraft and land based gas turbine engines. A lacquer slurry comprising cellulose nitrate containing high purity silicon powder is sprayed onto the superalloy substrates. The silicon layer is then aluminized to complete the coating. The Si-Al coating is less costly to produce than advanced aluminides and protects the substrates from oxidation and thermal fatigue for a much longer period of time than the conventional aluminide coatings. While more expensive Pt-Al coatings and physical vapor deposited MCrAlY coatings may last longer or provide equal protection on certain substrates, the Si-Al coating exceeded the performance of both types of coatings on certain superalloys in high gas velocity oxidation and thermal fatigue and increased the resistance of certain superalloys to hot corrosion.
Official Gazette of the U.S. Patent and Trademark Office

N83-32908*# National Aeronautics and Space Administration. Lewis Research Center, Cleveland, Ohio.
TIME DEPENDENCE OF SOLID-PARTICLE IMPINGEMENT EROSION OF AN ALUMINUM ALLOY
P. VEERABHADRARAO and D. H. BUCKLEY Aug. 1983 24 p refs Presented at 6th Intern. Conf. on Erosion by Liquid and Solid Impact, Cambridge, England, 4-8 Sep. 1983
(NASA-TP-2169; E-1381; NAS 1.60:2169) Avail: NTIS HC A02/MF A01 CSCL 11F

Erosion studies were conducted on 6061-T6511 aluminum alloy by using jet impingement of glass beads and crushed glass particles to investigate the influence of exposure time on volume loss rate at different pressures. The results indicate a direct relationship between erosion-versus-time curves and pitmorphology (width, depth, and width-depth ratio)-versus-time curves for both glass forms. Extensive erosion data from the literature were analyzed to find the variations of erosion-rate-versus-time curves with respect to the type of device, the size and shape of erodent particles, the abrasive charge, the impact velocity, etc. Analysis of the experimental data, obtained with two forms of glass, resulted in three types of erosion-rate-versus-time curves: (1) curves with incubation, acceleration, and steadystate periods (type 1); (2) curves with incubation, acceleration, decleration, and steady-state periods (type 3); and (3) curves with incubation, acceleration, peak rate, and deceleration periods (type 4). The type 4 curve is a less frequently seen curve and was not reported in the literature. Analysis of extensive literature data generally indicated three types of erosion-rate-versus-time curves. Two types (types 1 and 3) were observed in the present study; the third type involves incubation (and deposition), acceleration, and steady-state periods (type 2). Examination of the extensive literature data indicated that it is absolutely necessary to consider the corresponding stages or periods of erosion in correlating and characterizing erosion resistance of a wide spectrum of ductile materials. S.L.

N83-34014*# National Aeronautics and Space Administration. Lewis Research Center, Cleveland, Ohio.
IMPROVED THERMAL BARRIER COATING SYSTEM Patent Application
S. STECKRA, inventor (to NASA) 16 Aug. 1983 12 p
(NASA-CASE-LEW-13324-2; US-PATENT-APPL-SN-523297)
Avail: NTIS HC A02/MF A01 CSCL 11F

A high temperature oxidation resistant thermal barrier coating system for a nickel, cobalt, or iron base alloy substrate is described.

An inner metal bond coating contacts the substrate, and a thermal barrier coating covers the bond coating. NiCrAlR, FeCrAlR, and CoCrAlR alloys were satisfactory as bond coating compositions where R = Y or Yb. These alloys contain, by weight, 24.9 to 36.7% chromium, 5.4 to 18.5% aluminum, and 0.05 to 1.55% yttrium or 0.05 to 0.53% ytterbium. The coatings containing ytterbium are preferred over those containing yttrium. An outer thermal barrier coating of partially stabilized zirconium oxide (zirconia) which is between 6% and 8%, by weight, of yttrium oxide (yttria) covers the bond coating. Partial stabilization provides a material with superior durability. NASA

N83-34015*# National Aeronautics and Space Administration. Lewis Research Center, Cleveland, Ohio.
PRELIMINARY RESULTS OF THE COMPARISON OF THE ELECTROCHEMICAL BEHAVIOR OF A THIOETHER AND BIPHENYL
W. MORALES and W. R. JONES Jul. 1983 18 p refs
(NASA-TM-83450; E-1555; NAS 1.15:83450) Avail: NTIS HC A02/MF A01 CSCL 11F

An electrochemical cell was constructed to explore the feasibility of using electrochemical techniques to simulate the tribochemistry of various substances. The electrochemical cell was used to study and compare the behavior of a thioether 1,3-bis(phenylthio) benzene and biphenyl. It is found that under controlled conditions biphenyl undergoes a reversible reduction to a radical anion whereas the thioether undergoes an irreversible reduction yielding several products. The results are discussed in relationship to boundary lubrication. E.A.K.

N83-34016*# National Aeronautics and Space Administration. Lewis Research Center, Cleveland, Ohio.
EFFECT OF THE AMOUNT OF NA2SO4 ON THE HIGH TEMPERATURE CORROSION OF UDIMET-700
A. K. MISRA and F. J. KOHL 1983 19 p refs Presented at the Ann. Meeting of the Electrochemical Society, San Francisco, 8-13 May 1983
(NASA-TM-83459; E-1774; NAS 1.15:83459) Avail: NTIS HC A02/MF A01 CSCL 11F

The corrosion of Udimet-700, coated with different doses of Na2SO4, was studied in an isothermal thermogravimetric test in the temperature range 900 to 950 C. The weight gain curve is characterized by five distinct stages: an initial period of linear corrosion; an induction period; a period of accelerated corrosion; a period of decelerating corrosion; and a period of parabolic oxidation. The time required for the failure of the alloy increases with an increase in the amount of Na2SO4, reaches a peak and then decreases with further increase in the amount of Na2SO4. For low and intermediate doses (0.3 to 2.0 mg/sq cm), the catastrophic failure of the material occurs by the formation of Na2MoO4 and interaction of the liquid Na2MoO4 with the alloy. For heavy doses, the degradation of the material is due to the formation of large amounts of sulfides. Author

N83-34019*# National Aeronautics and Space Administration. Lewis Research Center, Cleveland, Ohio.
FRICTION AND HARDNESS OF GOLD FILMS DEPOSITED BY ION PLATING AND EVAPORATION
K. MIYOSHI, T. SPALVINS, and D. H. BUCKLEY Aug. 1983 10 p refs
(NASA-TP-2207; E-1528; NAS 1.60:2207) Avail: NTIS HC A02/MF A01 CSCL 11F

Sliding friction experiments were conducted with ion-plated and vapor-deposited gold films on various substrates in contact with a 0.025-mm-radius spherical silicon carbide rider in mineral oil. Hardness measurements were also made to examine the hardness depth profile of the coated gold on the substrate. The results indicate that the hardness is influenced by the depth of the gold coating from the surface. The hardness increases with an increase in the depth. The hardness is also related to the composition gradient in the graded interface between the gold coating and the substrate. The graded interface exhibited the highest hardness resulting from an alloy hardening effect. The coefficient of friction is inversely related to the hardness, namely, the load carrying capacity of the surface. The greater the hardness that the metal surface possesses, the lower is the coefficient of friction. The graded interface exhibited the lowest coefficient of friction. Author

N83-35101*# IIT Research Inst., Chicago, Ill.
DETERMINATION OF HYDROGEN PERMEABILITY IN COMMERCIAL AND MODIFIED SUPERALLOYS
S. BHATTACHARYYA and W. PETERMAN May 1983 91 p refs
(Contract DEN3-6; DE-A101-77CS-51040)
(NASA-CR-168195; DOE/NASA/0006-2; NAS 1.26:168195; IITRI-M06004-67) Avail: NTIS HC A05/MF A01 CSCL 11F

The results of hydrogen permeability measurements on several iron- and cobalt-base alloys as well as on two long-ranged ordered alloys over the range of 705 to 870 C (1300 to 1600 F) are summarized. The test alloys included wrought alloys N-155, IN 800, A-286, 19-9DL, and 19-9DL modifications with aluminum, niobium, and misch metal. In addition, XF-818, CRM-6D, SA-F11, and HS-31 were evaluated. Two wrought long-range ordered alloys, Ni3Al and (Fe,Ni)3(V,Al) were also evaluated. All tests were conducted at 20.7 MPa pressure in either pure and/or 1% CO2-doped H2 for test periods as long as 133 h. Detailed analyses were conducted to determine the relative permeability rankings of these alloys and the effect of doping, exit surface oxidation, specimen design variations, and test duration on permeability coefficient, and permeation activation energies were determined. The two long-range ordered alloys had the lowest permeability coefficients in pure H2 when compared with the eight commercial alloys and their modifications. With CO2 doping, significant decrease in permeability was observed in commercial alloys--no doped tests were conducted with the long-range ordered alloys. Author

N83-35102*# National Aeronautics and Space Administration. Lewis Research Center, Cleveland, Ohio.
UNDERSTANDING THE ROLES OF THE STRATEGIC ELEMENT COBALT IN NICKEL BASE SUPERALLOYS
J. R. STEPHENS and R. L. DRESHFIELD 1983 25 p refs Presented at the Mater. Substitution and Recycling Meeting, Vimeiro, Portugal, 10-14 Oct. 1983; sponsored by AGARD
(NASA-TM-83475; E-1790; NAS 1.15:83475) Avail: NTIS HC A02/MF A01 CSCL 11F

The United States imports over 90% of its cobalt, chromium, columbium, and tantalum, all key elements in high temperature nickel base superalloys for aircraft gas turbine disks and airfoils. Research progress in understanding the roles of cobalt and some possible substitutes effects on microstructure, mechanical properties, and environmental resistance of turbine alloys is discussed. Author

N83-35103*# National Aeronautics and Space Administration. Lewis Research Center, Cleveland, Ohio.
THE THERMAL FATIGUE RESISTANCE OF H-13 DIE STEEL FOR ALUMINUM DIE CASTING DIES
7 Aug. 1982 22 p refs Presented at Let's Do It Ourselves: In Sci. and Technol., Baltimore, 2-7 Aug. 1982, sponsored by National Technical Association
(NASA-TM-83331; E-1578; NAS 1.15:83331) Avail: NTIS HC A02/MF A01 CSCL 11F

The effects of welding, five selected surface coatings, and stress relieving on the thermal fatigue resistance of H-13 Die Steel for aluminum die casting dies were studied using eleven thermal fatigue specimens. Stress relieving was conducted after each 5,000 cycle interval at 1050 F for three hours. Four thermal fatigue specimens were welded with H-13 or maraging steel welding rods at ambient and elevated temperatures and subsequently, subjected to different post-weld heat tretments. Crack patterns were examined at 5,000, 10,000, and 15,000 cycles. The thermal fatigue resistance is expressed by two crack parameters which are the average maximum crack and the average cracked area. The results indicate that a significant improvement in thermal fatigue resistance over

the control was obtained from the stress-relieving treatment. Small improvements were obtained from the H-13 welded specimens and from a salt bath nitrogen and carbon-surface treatment. The other surface treatments and welded specimens either did not affect or had a detrimental influence on the thermal fatigue properties of the H-13 die steel. A.R.H.

N83-35104*# National Aeronautics and Space Administration. Lewis Research Center, Cleveland, Ohio.
REACTION OF COBALT IN SO2 ATMOSPHERIC AT ELEVATED TEMPERATURES
N. S. JACOBSON and W. L. WORRELL (Pennsylvania Univ.) 14 Oct. 1983 18 p refs Presented at the Fall Meeting of the Electrochem. Soc., Washington, D.C., 9-14 Oct. 1983
(Contract NSF DMR-99-23647)
(NASA-TM-83485; E-1809; NAS 1.15:83485) Avail: NTIS HC A02/MF A01 CSCL 11F

The reaction rate of cobalt in SO2 argon environments was measured at 650 C, 700 C, 750 C and 800 C. Product scales consist primarily of an interconnected sulfide phase in an oxide matrix. At 700 C to 800 C a thin sulfide layer adjacent to the metal is also observed. At all temperatures, the rapid diffusion of cobalt outward through the interconnected sulfide appears to be important. At 650 C, the reaction rate slows dramatically after five minutes due to a change in the distribution of these sulfides. At 700 C and 750 C the reaction is primarily diffusion controlled values of diffusivity of cobalt (CoS) calculated from this work show favorable agreement with values of diffusivity of cobalt (CoS) calculated from previous sulfidation work. At 800 C, a surface step becomes rate limiting. Author

27

NONMETALLIC MATERIALS

Includes physical, chemical, and mechanical properties of plastics, elastomers, lubricants, polymers, textiles, adhesives, and ceramic materials.

A83-10300* National Aeronautics and Space Administration. Lewis Research Center, Cleveland, Ohio.
PERFORMANCE OF LASER-GLAZED ZIRCONIA THERMAL BARRIER COATINGS IN CYCLIC OXIDATION AND CORROSION BURNER RIG TESTS
I. ZAPLATYNSKY (NASA, Lewis Research Center, Cleveland, OH) (International Conference on Metallurgical Coatings and Process Technology, San Diego, CA, Apr. 5-8, 1982.) Thin Solid Films, vol. 95, 1982, p. 275-284. refs
(Previously announced in STAR as N82-22346)

A83-11486*# United Technologies Research Center, East Hartford, Conn.
SYNTHESIS AND CHARACTERIZATION OF BISIMIDE AMINES AND BISIMIDE AMINE-CURED EPOXY RESINS
D. A. SCOLA (United Technologies Research Center, East Hartford, CT) Society of Plastics Engineers, National Technical Conference, Miami, FL, Oct. 25-27, 1982, Paper. 9 p. refs
(Contract NAS3-22521)

A study has been conducted with the objective of developing tough, moisture resistant, high char yield epoxy resins using novel bisimide amine (BIA) hardeners as curing agents with MY-720, a commercial state-of-the-art epoxy resin system. BIA cured epoxies are shown to have lower moisture absorption than MY-720 and other state-of-the-art epoxy resins; the tensile strengths and strain-to-failures of several of the bisimide epoxy resins (IME's) are higher than those of the state-of-the-art epoxies. Most IME's have compression properties equivalent to those of state-of-the-art epoxies. Two resin systems, IME-10 and IME-12-3, have better overall properties than other resin systems investigated. V.L.

A83-12651* National Aeronautics and Space Administration. Lewis Research Center, Cleveland, Ohio.
SPUTTERED SILICON NITRIDE COATINGS FOR WEAR PROTECTION
A. GRILL (NASA, Lewis Research Center, Cleveland, OH; Negev, University, Beersheba, Israel) and P. R. ARON (NASA, Lewis Research Center, Cleveland, OH) Thin Solid Films, vol. 96, 1982, p. 25-30. refs
(Previously announced in STAR as N82-20314)

A83-12652* National Aeronautics and Space Administration. Lewis Research Center, Cleveland, Ohio.
MORPHOLOGICAL AND FRICTIONAL BEHAVIOR OF SPUTTERED MOS2 FILMS
T. SPALVINS (NASA, Lewis Research Center, Cleveland, OH) Thin Solid Films, vol. 96, 1982, p. 17-24. refs
(Previously announced in STAR as N82-22387)

A83-12653* National Aeronautics and Space Administration. Lewis Research Center, Cleveland, Ohio.
SOME PROPERTIES OF R.F.-SPUTTERED HAFNIUM NITRIDE COATINGS
P. R. ARON (NASA, Lewis Research Center, Cleveland, OH) and A. GRILL (NASA, Lewis Research Center, Cleveland, OH; Negev, University, Beersheba, Israel) Thin Solid Films, vol. 96, 1982, p. 87-91. refs
(Previously announced in STAR as N82-21331)

A83-18052* National Aeronautics and Space Administration. Lewis Research Center, Cleveland, Ohio.
THERMODYNAMICS OF SILICON NITRIDATION - EFFECT OF HYDROGEN
N. J. SHAW and F. J. ZELEZNIK (NASA, Lewis Research Center, Cleveland, OH) American Ceramic Society, Journal, vol. 65, Nov. 1982, p. C-180, C-181. refs
(ACS PAPER 33-B-80P)

Equilibrium compositions for the nitridization of Si were calculated to detect the effectiveness of H2 in removal of the oxide film and in increasing the concentration of SiO and reducing the proportions of O2. Gibbs free energy for the formation of SIN2O was computed above 1685 K, and at lower temperatures. The thermodynamic properties of SiN2O2 were then considered from 1000-3000 K, taking into account the known thermodynamic data for 39 molecular combinations of the Si, Ni, and O. The gases formed were assumed ideal mixtures with pure phase condensed species. The mole fractions were obtained for a system of SiO2 with each Si particle covered with a thin layer of SiO2 before nitridation, and a system in which the nitriding atmosphere had access to the Si. The presence of H2 was determined to enhance the removal of NiO2 in the first system, decrease the partial pressure of O2, increase the partial pressures of SiO, Si, H2O, NH3, and SiH4, while its effects were negligible in the Si system. M.S.K.

A83-22258* Florida Univ., Gainesville.
EFFECT OF Y2O3 AND AL2O3 ON THE OXIDATION RESISTANCE OF SI3N4
L. L. HENCH, P. N. VAIDYANATHAN (Florida, University, Gainesville, FL), and S. DUTTA (NASA, Lewis Research Center, Cleveland, OH) Ceramic Engineering and Science Proceedings, vol. 3, Sept.-Oct. 1982, p. 587-595. refs
(Contract NSG-3254)

Oxidation of cold-pressed and sintered Si3N4 containing 15 wt% Y2O3 and 2, 4, 6, and 8% Al2O3 is observed at temperatures as low as 1000 C with IR reflection spectroscopy. Concentrations of Al2O3 in excess of 4% greatly retard the rate of oxidation and alter the mechanism of surface attack by promoting formation of a glassy layer on the surface containing mixed oxynitride bonds. The glassy layer retards heterogeneous attack and reduces the effect of an oxidation transition temperature between 1000 and 1100 C for these materials. (Author)

A83-22270* National Aeronautics and Space Administration. Lewis Research Center, Cleveland, Ohio.
EFFECTS OF ARC CURRENT ON THE LIFE IN BURNER-RIG THERMAL CYCLING OF PLASMA-SPRAYED ZRO2-O3
R. C. HENDRICKS and G. MCDONALD (NASA, Lewis Research Center, Cleveland, OH) Ceramic Engineering and Science Proceedings, vol. 3, Sept.-Oct. 1982, p. 737-743. refs
(Previously announced in STAR as N82-17453)

A83-22271* National Aeronautics and Space Administration. Lewis Research Center, Cleveland, Ohio.
USE OF FIBER-LIKE MATERIALS TO AUGMENT CYCLE LIFE OF THICK, THERMOPROTECTIVE-SEAL COATINGS
R. C. HENDRICKS and G. MCDONALD (NASA, Lewis Research Center, Cleveland, OH) Ceramic Engineering and Science Proceedings, vol. 3, Sept.-Oct. 1982, p. 744-749. refs
(Previously announced in STAR as N82-32633)

A83-22272* National Aeronautics and Space Administration. Lewis Research Center, Cleveland, Ohio.
SOME INELASTIC EFFECTS OF THERMAL CYCLING ON ZRO2-Y2O3 MATERIALS
R. C. HENDRICKS, G. MCDONALD, and R. C. BILL (NASA, Lewis Research Center, Cleveland, OH) Ceramic Engineering and Science Proceedings, vol. 3, Sept.-Oct. 1982, p. 750-757. refs
An analysis has been developed which relates the effects of inelastic behavior of Y2O3 stabilized ZrO2 (YSZ) materials. The results show these materials to be sensitive to small changes in temperature and are supported by measurements of inelastic behavior in disk and bar specimens at temperatures as low as 1010 C (1850 F). At higher thermomechanical loads, the test specimens can deform to strains greater than 1 percent and for bar specimens, with sufficient strength, to remain bonded to the metallic substrate. (Author)

A83-22273* IIT Research Inst., Chicago, Ill.
CREEP OF PLASMA-SPRAYED-ZRO2 THERMAL-BARRIER COATINGS
R. F. FIRESTONE, W. R. LOGAN, J. W. ADAMS (IIT Research Institute, Chicago, IL), and R. C. BILL, JR. (NASA, Lewis Research Center, Cleveland, OH) Ceramic Engineering and Science Proceedings, vol. 3, Sept.-Oct. 1982, p. 758-771.
Specimens of plasma-sprayed-zirconia thermal-barrier coatings with three different porosities and different initial particle sizes were deformed in compression at initial loads of 6900, 13,800, and 24,100 kPa (1000, 2000, and 3500 psi) and temperatures of 1100, 1250, and 1400 C. The coatings were stabilized with lime, MgO, and two different concentrations of Y2O3. Creep began as soon as the load was applied and continued at a constantly decreasing rate until the load was removed. Temperature and stabilization had a pronounced effect on creep rate while the stress, particle size, and porosity had a lesser effect. Creep deformation was due to cracking and particle sliding. (Author)

A83-27422*# National Aeronautics and Space Administration. Lewis Research Center, Cleveland, Ohio.
DYNAMICS AND MECHANISM OF CAVITATION EROSION ON PERSPEX AND EPOXY RESIN TESTED IN A ROTATING DISK DEVICE
P. VEERABHADRA RAO (NASA, Lewis Research Center, Tribology Branch, Cleveland, OH), N. S. LAKSHMANA RAO, and B. C. SYAMALA RAO (Indian Institute of Science, Bangalore, India) In: Cavitation and Polyphase Flow Forum - 1982; Proceedings of the Third Joint Thermophysics, Fluids, Plasma, and Heat Transfer Conference, St. Louis, MO, June 7-11, 1982. New York, American Society of Mechanical Engineers, 1982, p. 20-23. refs
(Previously announced in STAR as N83-11329)

A83-29397* National Aeronautics and Space Administration. Lewis Research Center, Cleveland, Ohio.
TRIBOLOGICAL PROPERTIES OF SINTERED POLYCRYSTALLINE AND SINGLE-CRYSTAL SILICON CARBIDE
K. MIYOSHI, D. H. BUCKLEY (NASA, Lewis Research Center, Cleveland, OH), and M. SRINIVASAN (Carborundum Resistant Materials Co., Niagara Falls, NY) American Ceramic Society Bulletin (ISSN 0002-7812), vol. 62, April 1983, p. 494-500. refs
Previously announced in STAR as N82-24343

A83-29734*# National Aeronautics and Space Administration. Lewis Research Center, Cleveland, Ohio.
RESIN SELECTION CRITERIA FOR TOUGH COMPOSITE STRUCTURES
C. C. CHAMIS (NASA, Lewis Research Center, Cleveland, OH) and G. T. SMITH IN: Structures, Structural Dynamics and Materials Conference, 24th, Lake Tahoe, NV, May 2-4, 1983, Collection of Technical Papers. Part 1 . New York, American Institute of Aeronautics and Astronautics, 1983, p. 45-60. refs
(AIAA 83-0801)
Resin selection criteria are derived using a structured methodology consisting of an upward integrated mechanistic theory and its inverse (top-down structured theory). These criteria are expressed in a 'criteria selection space' which can be used to identify resin bulk properties for improved composite 'toughness'. The resin selection criteria correlate with a variety of experimental data including laminate strength, elevated temperature effects and impact resistance. Author

A83-36973* National Aeronautics and Space Administration. Lewis Research Center, Cleveland, Ohio.
XPS, AES AND FRICTION STUDIES OF SINGLE-CRYSTAL SILICON CARBIDE
K. MIYOSHI and D. H. BUCKLEY (NASA, Lewis Research Center, Cleveland, OH) Applications of Surface Science (ISSN 0378-5963), vol. 10, 1982, p. 357-376. refs
The surface chemistry and friction behavior of a single crystal silicon carbide surface parallel to the 0001 plane in sliding contact with iron at various temperatures to 1500 C in a vacuum of 3 x 10 nPa are investigated using X-ray photoelectron and Auger electron spectroscopy. Results show that graphite and carbide-type carbon are seen primarily on the silicon carbide surface in addition to silicon at temperatures to 800 C by both types of spectroscopy. The coefficients of friction for iron sliding against a silicon carbide surface parallel to the 0001 plane surface are found to be high at temperatures up to 800 C, with the silicon and carbide-type carbon at maximum intensity in the X-ray photoelectron spectroscopy at 800 C. The concentration of the graphite increases rapidly on the surface as the temperature is increased above 800 C, while the concentrations of the carbide-type carbon and silicon decrease rapidly and this presence of graphite is accompanied by a significant decrease in friction. Preheating the surfaces to 1500 C also gives dramatically lower coefficients of friction when reheating in the sliding temperature range of from room temperature to 1200 C, with this reduction in friction due to the graphite layer on the silicon carbide surface. N.B.

A83-40923* National Aeronautics and Space Administration. Lewis Research Center, Cleveland, Ohio.
LOWER-CURING-TEMPERATURE PMR POLYIMIDES
P. DELVIGS (NASA, Lewis Research Center, Cleveland, OH) Polymer Composites (ISSN 0272-8397), vol. 4, July 1983, p. 150-153. refs
Partial substitution of a p-aminostyrene end-cap for the monomethyl ester of 5-norbornene-2, 3-dicarboxylic acid lowered the final cure temperature of typical PMR resins from 600 F to 500 F. The weight loss characteristics of neat resins and graphite fiber composites prepared by using the mixed end-cap approach were determined at 600 F. The room temperature and short-time elevated temperature mechanical properties of the composites at 550 F and 600 F were determined. The mechanical property retention characteristics of the composites at 550 F and 600 F

are discussed. Previously announced in STAR as N83-10118
Author

A83-40924* United Technologies Research Center, East Hartford, Conn.
SYNTHESIS AND CHARACTERIZATION OF BISIMIDE AMINES AND BISIMIDE AMINE-CURED EPOXY RESINS
D. A. SCOLA (United Technologies Research Center, East Hartford, CT) Polymer Composites (ISSN 0272-8397), vol. 4, July 1983, p. 154-161. refs
(Contract NAS3-22521)

An attempt is made to develop tough, moisture resistant, high char yield epoxy resins by means of novel bisimide amine (BIA) hardener curing agents and a state-of-the-art epoxy resin system. The BIAs are isolated as mixtures containing monomer, oligomer, and polymeric species, and then characterized by elemental analysis and high pressure liquid chromatography. The bisimide amine-cured epoxies (IMEs) were characterized with respect to moisture absorption, thermal properties, and physical and mechanical properties, as well as in the role of matrices in Celion 6000/IME composites. The relative toughness characteristics of each IME formulation was measured by the 10 deg off-axis tensile test, measuring the uniaxial tensile strength, shear strength, and shear-strain-to-failure of the composite systems. O.C.

A83-41851* National Aeronautics and Space Administration. Lewis Research Center, Cleveland, Ohio.
CAVITATION EROSION CHARACTERISTICS OF POLY(METHYL METHACRYLATE) IN A ROTATING DISK DEVICE
P. VEERABHADRA RAO (NASA, Lewis Research Center, Cleveland, OH), N. S. L. RAO, and B. C. S. RAO (Indian Institute of Science, Bangalore, India) (Cavitation and Polyphase Flow Forum, St. Louis, MO, June 7-11, 1982) Wear (ISSN 0043-1648), vol. 86, 1983, p. 119-131. refs

The cavitation erosion behavior including the initiation, dynamics and mechanism of damage process on perspex and epoxy resin specimens tested in a rotating disk device were discussed with respect to exposure time. The inception of erosion always took place at the location nearest to the center of rotation of the disk. Subsequently, as exposure time increased, erosion initiated at other locations as well. Light optical photographs and scanning electron micrographs clearly indicate that most of the material loss appears to occur form the networks of cracks due to their interaction and pits indicate particle debris. The optical degradation (loss of transmittance) on perspex was observed to be more on the rear side than on the front side. Previously announced in STAR as N83-11329 . Author

A83-42261* National Aeronautics and Space Administration. Lewis Research Center, Cleveland, Ohio. .
IMPROVED PERFORMANCE THERMAL BARRIER COATINGS
S. R. LEVINE, R. A. MILLER, and S. STECURA (NASA, Lewis Research Center, Cleveland, OH) IN: High temperature corrosion; Proceedings of the International Conference, San Diego, CA, March 2-6, 1981 . Houston, TX, National Association of Corrosion Engineers, 1983, p. 621-627. refs
(Contract DE-AI01-77ET-13111; DE-AI01-77ET-10350)

Thermal barrier coatings offer an attractive approach to improving the durability and efficiency of the hot section of heat engines. The coatings typically consist of an inner alloy bond coating about 0.01 cm thick resistant to oxidation and hot corrosion and an outer ceramic layer, usually a stabilized zirconia, 0.01-0.05 cm thick. Here, the materials, thermomechanical stress, and hot corrosion problems associated with thermal barrier coatings are reviewed along with the capabilities and limitations of current technology. The coatings discussed include ZrO2-Y2O3/NiCrAlY, ZrO2-Y2O3/NiCoCrAlY, ZrO2-MgO/NiCoCrAlY, CaO-SiO2/Co-Cr-Al-Y, and CaO-SiO2/NiCrAlY systems. It is emphasized that the performance of thermal barrier coatings is governed by many complex and interrelated factors, so that optimization of these coatings always involves certain tradeoffs. V.L.

A83-48261* Ford Motor Co., Dearborn, Mich.
THE EFFECT OF SILICON PARTICLE SIZE ON THE NITRIDING BEHAVIOUR OF REACTION BONDED SI3N4 COMPACTS
J. A. MANGELS (Ford Motor Co., Ceramic Materials Dept., Dearborn, MI) IN: Progress in nitrogen ceramics; Proceedings of the Second Advanced Study Institute, Brighton, England, July 27-August 7, 1981 . Boston, MA and The Hague, Martinus Nijhoff Publishers, 1983, p. 135-139; Discussion, p. 139, 140. Research supported by the U.S. Department of Energy. refs
(Contract DEN3-20)

A83-48270* Ford Motor Co., Dearborn, Mich.
SINTERING OF REACTION BONDED SILICON NITRIDE
J. A. MANGELS (Ford Motor Co., Ceramic Materials Dept., Dearborn, MI) IN: Progress in nitrogen ceramics; Proceedings of the Second Advanced Study Institute, Brighton, England, July 27-August 7, 1981 . Boston, MA and The Hague, Martinus Nijhoff Publishers, 1983, p. 231-236; Discussion, p. 236. Research supported by the U.S. Department of Energy. refs
(Contract DEN3-167)

A process to produce sintered reaction-bonded Si3N4 (SRBSN) articles has been developed. This process consists of the addition of an appropriate sintering aid to reaction-bonded Si3N4 followed by sintering between 1780 and 2000 C, using an over pressure of nitrogen. The principal advantage of this process is the low sintering shrinkages of 5 to 10 percent. The properties and microstructure of two SRBSN systems sintered with MgO and Y2O3 additives are described and were found to be comparable to corresponding hot-pressed Si3N4 systems. Examples of applications of both systems are illustrated, demonstrating near net shape fabrication capability of the process. Author

A83-48303* GTE Labs., Inc., Waltham, Mass.
SINTERING, PROPERTIES AND FABRICATION OF SI3N4 + Y2O3 BASED CERAMICS
C. L. QUACKENBUSH, J. T. SMITH, J. T. NEIL, and K. W. FRENCH (GTE Laboratories, Inc., Waltham, MA) IN: Progress in nitrogen ceramics; Proceedings of the Second Advanced Study Institute, Brighton, England, July 27-August 7, 1981 . Boston, MA and the Hague, Martinus Nijhoff Publishers, 1983, p. 669-682; Discussion, p. 682. Research supported by the U.S. Department of Energy. refs
(Contract DEN3-17)

Pure silicon nitride shows a remarkable resistance to sintering without the use of densification additives. The present investigation is concerned with results which show the effect of chemical content on sinterability, taking into account the composition, raw material impurities, and processing contaminants. Aspects of sintering are discussed along with strength characteristics, and oxidation relations. Attention is given to phase field I and II materials, phase field III and IV materials, tungsten carbide and oxidation at 600 C, and studies involving shape fabrication by injection molding. It was found that in sintering Si3N4 + Y2O3 an increase in the amount of Y2O3 and, in particular, the addition of Al2O3 enhances the fluidity of the liquid phase. G.R.

N83-10194*# National Aeronautics and Space Administration. Lewis Research Center, Cleveland, Ohio.
PLASMA DEPOSITION AND SURFACE MODIFICATION TECHNIQUES FOR WEAR RESISTANCE
T. SPALVINS 1982 19 p refs Presented at the Joint Lubrication Conf., Washington, D.C., 5-7 Oct. 1982; sponsored by ASME and American Society of Lubrication Engineers
(NASA-TM-82972; E-1399; NAS 1.15:82972) Avail: NTIS HC A02/MF A01 CSCL 20I

The ion-assisted or plasma coating technology is discussed as it applies to the deposition of hard, wear resistant refractory compound films. Of the many sputtering and ion plating modes and configurations the reactive magnetron sputtering and the reactive triode ion plating techniques are the preferred ones to deposit wear resistant coatings for tribological applications. Both of these techniques incorporate additional means to enhance the ionization efficiency and chemical reaction to precision tailor

desirable tribological characteristics. Interrelationships between film formation, structure, and ribological properties are strictly controlled by the deposition parameters and the substrate condition. The enhanced ionization contributes to the excellent adherence and coherence, reduced internal stresses and improved structural growth to form dense, cohesive, equiaxed grain structure for improved wear resistance and control. Author

N83-11328*# Georgia Inst. of Tech., Atlanta. School of Mechanical Engineering.
SURFACE TEMPERATURES AND GLASSY STATE INVESTIGATIONS IN TRIBOLOGY, PART 5 Final Report
S. BAIR and W. O. WINER Washington NASA Oct. 1982 64 p refs
(Contract NSG-3106)
(NASA-CR-3632; NAS 1.26:3632) Avail: NTIS HC A04/MF A01 CSCL 11B

Preliminary measurements of high shear rate viscosity at near atmospheric but variable pressure suggest the importance of low normal stress and cavitation or fluid fracture in the type of stress field existing in elastohydrodynam ic inlets and classical hydrodynamic configurations. An experimental basis is given for three regimes of traction in concentrated contacts: a thin film regime characterized by high traction and determined by lambda ratio, a thick film regime characterized by low traction and determined by the speed parameter, and the elastohydrodynamic regime for which traction is controlled by limiting shear stress. Traction measurements were performed with various liquids, two solid lubricants, and a grease. Film thickness and traction measurements of polymer blends and base oils are compared.
A.R.H.

N83-11329*# National Aeronautics and Space Administration. Lewis Research Center, Cleveland, Ohio.
DYNAMICS AND MECHANISM OF CAVITATION EROSION ON PERSPEX AND EPOXY RESINS TESTED IN A ROTATING DISK DEVICE
P. V. RAO, N. S. L. RAO (Indian Inst. of Science, Bangalore), and B. C. S. RAO (Indian Inst. of Science, Bangalore) 1982 14 p refs Presented at the Cavitation and Polyphase Flow Forum, St. Louis, 7-11 Jun. 1982; sponsored by ASME
(NASA-TM-82962; E-1379; NAS 1.15:82962) Avail: NTIS HC A02/MF A01 CSCL 11G

The cavitation erosion behavior including the initiation, dynamics and mechanism of damage process on perspex and epoxy resin specimens tested in a rotating disk device were discussed with respect to exposure time. The inception of erosion always took place at the location nearest to the center of rotation of the disk. Subsequently, as exposure time increased, erosion initiated at other locations as well. Light optical photographs and scanning electron micrographs clearly indicate that most of the material loss appears to occur form the networks of cracks due to their interaction and pits indicate particle debris. The optical degradation (loss of transmittance) on perspex was observed to be more on the rear side than on the front side. Author

N83-12151*# National Aeronautics and Space Administration. Lewis Research Center, Cleveland, Ohio.
POLYMER MATRIX COMPOSITES RESEARCH AT NASA LEWIS RESEARCH CENTER
T. T. SERAFINI *In* NASA. Langley Research Center Advan. Mater. Technol. p 65-90 Nov. 1982 refs
Avail: NTIS HC A19/MF A01 CSCL 11I

The in situ polymerization of monomer reactants (PMR) approach was demonstrated to be a powerful approach for solving many of the processing difficulties associated with the use of high temperature resistant polymers as matrix resins in high performance composites. The PMR-15 polyimide provides the best overall balance of processing characteristics and elevated temperature properties. The excellent properties and commercial availability of composite materials based on PMR-15 led to their acceptance as viable engineering materials. The PMR-15 composites are used to produce a variety of high quality structural components. S.L.

N83-13257*# National Aeronautics and Space Administration. Lewis Research Center, Cleveland, Ohio.
POLYIMIDES: TRIBOLOGICAL PROPERTIES AND THEIR USE AS LUBRICANTS
R. L. FUSARO 1982 31 p refs Presented at the 1st Tech. Conf. on Polyimides, Ellenville, N.Y., 10-12 Nov. 1982; sponsored by the Society of Plastics Engineers, Inc.
(NASA-TM-82959; E-1376; NAS 1.15:82959) Avail: NTIS HC A03/MF A01 CSCL 11I

Friction, wear, and wear mechanisms of several different polyimide films, solid bodies, composites, and bonded solid lubricant films are compared and discussed. In addition, the effect of such parameters as temperatures, type of atmosphere, contact stress, and specimen configuration are investigated. A friction and wear transition occurs in some polyimides at elevated temperatures and this transition is related to molecular relaxations that occur in polyimides. Friction and wear data from an accelerated test (pin-on-disk) are compared to similar data from an end use test device (plain spherical bearing), and to other polymers investigated in a similar geometry. Author

N83-13258*# National Aeronautics and Space Administration. Lewis Research Center, Cleveland, Ohio.
CHEMICAL APPROACH FOR CONTROLLING NADAMIDE CURE TEMPERATURE AND RATE Patent Application
R. W. LAUVER, inventor (to NASA) 3 Aug. 1982 22 p
(NASA-CASE-LEW-13770-1; US-PATENT-APPL-SN-404809)
Avail: NTIS HC A02/MF A01 CSCL 11I

Polyimide resins suitable for use as composite matrix materials are formed by copolymerization of maleic and norbornenyl endcapped monomers and oligomers. The copolymers can be cured at temperatures under about 300 C by controlling the available concentration of the maleic-capped reactant. This control can be achieved by adding sufficient amounts of said maleic reactant, or by chemical modification of either copolymer, so as to either increase Diels-Alder retrogression of the norbornenyl capped reactant and/or holding initiation and polymerization to a rate compatible with the availability of the maleic-capped reactant. Author

N83-14269*# National Aeronautics and Space Administration. Lewis Research Center, Cleveland, Ohio.
EFFECT OF SLIDING SPEED AND CONTACT STRESS ON TRIBOLOGICAL PROPERTIES OF ULTRA-HIGH-MOLECULAR-WEIGHT POLYETHYLENE
R. L. FUSARO Nov. 1982 22 p refs
(NASA-TP-2059; E-1060; NAS 1.60:2059) Avail: NTIS HC A02/MF A01 CSCL 11G

A pin on disk apparatus was used to investigate the effect of sliding speed on the friction, wear, and transfer film characteristics of hemispherically tipped AISI 440C high temperature (HT) stainless steel riders sliding against ultrahigh molecular weight polyethylene (UHMWPE) disks. The surface morphology of the wear track was studied to determine possible wear mechanisms. Geometry effects were determined by comparing the results to those of others who used different specimen configurations. The results indicate that sliding speed, sliding distance, contact stress, and specimen geometry can all markedly influence the tribological properties of UHMWPE. S.L.

N83-14270*# National Aeronautics and Space Administration. Lewis Research Center, Cleveland, Ohio.
USE OF HIGH PRESSURE LIQUID CHROMATOGRAPHY IN THE STUDY OF LIQUID LUBRICANT OXIDATION
W. MORALES 1982 20 p refs Presented at the Joint Lubrication Conf., Washington, D.C., 5-7 Oct. 1982; sponsored by ASME and Am. Soc. of Lubrication Engr.
(NASA-TM-83033; E-1409; NAS 1.15:83033) Avail: NTIS HC A02/MF A01 CSCL 11H

The general principles of classical liquid chromatography and high-pressure liquid chromatography (HPLC) are reviewed, and their advantages and disadvantages are compared. Several chromatographic techniques are reviewed, and the analysis of a C-ether liquid lubricant by each technique is illustrated. An analysis by size exclusion chromatography of an ester lubricant, which had been degraded using a micro-oxidation apparatus, is illustrated to show how HPLC can be used in the study of high-temperature lubricant degradation. Author

N83-14271*# National Aeronautics and Space Administration. Lewis Research Center, Cleveland, Ohio.
FUNDAMENTAL ASPECTS OF POLYIMIDE DRY FILM AND COMPOSITE LUBRICATION: A REVIEW
R. L. FUSARO 1982 42 p refs Presented at the Joint Lubrication Conf., Washington, D.C., 5-7 Oct. 1982; sponsored by ASME and American Society of Lubrication Engineers
(NASA-TM-82968; E-1317; NAS 1.15:82968) Avail: NTIS HC A03/MF A01 CSCL 11H

The tribological properties of polyimide dry films and composites are reviewed. Friction coefficients, wear rates, transfer film characteristics, wear surface morphology, and possible wear mechanisms of several different polyimide films, polyimide-bonded solid lubricants, polyimide solid bodies, and polyimide composites are discussed. Such parameters as temperature, type of atmosphere, load, contact stress, and specimen configuration are investigated. Data from an accelerated test device (Pin-on-Disk) are compared to similar data obtained from an end use application test device (plain spherical bearing). S.L.

N83-15466*# National Aeronautics and Space Administration. Lewis Research Center, Cleveland, Ohio.
INFRARED EMISSION SPECTROPHOTOMETRIC STUDY OF THE CHANGES PRODUCED BY TIN COATING OF METAL SURFACES IN AN OPERATING EHD CONTACT
L. E. KELLER, J. L. LAUER, and W. R. JONES, JR. 1982 19 p refs Presented at the Joint Lubrication Conf., Washington, D.C., 5-7 Oct. 1982; sponsored by the Am. Soc. of Lubrication Engr. and ASME Sponsored by Army Research Office Prepared in cooperation with Rensselaer Polytechnic Inst.
(Contract NSG-3170; AF-AFOSR-3473-78)
(NASA-TM-82989; E-1398; NAS 1.15:82989) Avail: NTIS HC A02/MF A01 CSCL 20K

Infrared emission spectra and related measurements were obtained from an operating ball/plate elastohydrodynamic (EHD) sliding contact under a variety of operating conditions. In order to be able to compare the effect of the ball surface, some of the balls were coated with a thin layer of titanium nitride (TiN) by vapor deposition. Polyphenyl ether (5P4E) was used as lubricant and 1 percent of 1,1,2-trichloroethane (TCE) as a surface-probing additive. TiN is chemically inert and its thermal conductivity is lower than that of steel. Therefore, the overall temperatures with TiN coated balls were higher. Nevertheless, no scuffing was observed with the coated balls under conditions giving rise to scuffing with the uncoated balls. Tractions were lower with the TiN coated balls and always when TCE was added to the 5P4E. These findings were found to be inversely related to the degree of polarization of the spectral emission bands. The intensity and the dichrosim of these bands were related to shear rates and inlet conditions of the EHD contact. S.L.

N83-15467*# Westinghouse Electric Corp., Pittsburgh, Pa. Research and Development Center.
ADVANCED CERAMIC COATING DEVELOPMENT FOR INDUSTRIAL/UTILITY GAS TURBINE APPLICATIONS Final Report
C. A. ANDERSSON, S. K. LAU, R. J. BRATTON, S. Y. LEE, K. L. RIEKE, J. ALLEN, and K. E. MUNSON Feb. 1982 154 p refs (Contract DEN3-110; DE-AI01-77ET-13111)
(NASA-CR-165619; NAS 1.26:165619) Avail: NTIS HC A08/MF A01 CSCL 11B

The effects of ceramic coatings on the lifetimes of metal turbine components and on the performance of a utility turbine, as well as of the turbine operational cycle on the ceramic coatings were determined. When operating the turbine under conditions of constant cooling flow, the first row blades run 55K cooler, and as a result, have 10 times the creep rupture life, 10 times the low cycle fatigue life and twice the corrosion life with only slight decreases in both specific power and efficiency. When operating the turbine at constant metal temperature and reduced cooling flow, both specific power and efficiency increases, with no change in component lifetime. The most severe thermal transient of the turbine causes the coating bond stresses to approach 60% of the bond strengths. Ceramic coating failures was studied. Analytic models based on fracture mechanics theories, combined with measured properties quantitatively assessed both single and multiple thermal cycle failures which allowed the prediction of coating lifetime. Qualitative models for corrosion failures are also presented. E.A.K.

N83-15468*# National Aeronautics and Space Administration. Lewis Research Center, Cleveland, Ohio.
A COMMENTARY ON SOLID LUBRICANTS AND WEAR RESISTANT SOLIDS FOR USE IN EXTREME ENVIRONMENTS
H. E. SLINEY 1982 17 p refs Presented at the Joint Lubrication Conf., Washington, D.C., 4-6 Oct. 1982; sponsored by ASME and Am. Soc. of Lubrication Engr.
(NASA-TM-83042; E-1486; NAS 1.15:83042) Avail: NTIS HC A02/MF A01 CSCL 11H

The need for high temperature tribological coatings and self-lubricating materials in advanced technology is discussed. A qualitative model for the mechanism of solid lubrication is proposed. The model is based upon microscopic observations of the dynamics of third-body solids in lubricated contacts. In this model, the rheology of plastic flow is suggested as a more general criterion for predicting the lubricating potential of a solid material than, for example, a specific crystal structure. Some examples of layer-lattice and nonlayer-lattice solids that lubricate by virtue of their extreme plasticity, film coherence, and adhesion to the lubricated metal are described. Circumstantial evidence for the model is presented for low shear-strength solids at room temperature and for solids such as calcium fluoride that become lubricative only when their brittle-to-ductile transition temperature is exceeded. Some materials considerations in the selection of hard-coat materials for wear control are also presented. M.G.

N83-16527*# Rensselaer Polytechnic Inst., Troy, N. Y. Dept. of Mechanical Engineering.
DETERMINATION OF PHYSICAL AND CHEMICAL STATES OF LUBRICANTS IN CONCENTRATED CONTACTS, PART 3 Final Report
J. L. LAUER and L. E. KELLER Washington NASA Feb. 1983 111 p refs
(Contract NSG-3170)
(NASA-CR-3658; NAS 1.26:3658) Avail: NTIS HC A06/MF A01 CSCL 11H

Solid and liquid thin films were analyzed by infrared emission Fourier microspectrophotometry. The apparatus used is a commercial absorption instrument modified to an emission instrument, comprising a rotating polarizing device, a miniature blackbody temperature reference adjustable in temperature and radiant flux and a microscope lens with a high numerical aperture in the entrance system for increased sensitivity and resolution. Studies of lubricant behavior in a simulated ball bearing showed

C-2

the alignment of the fluid molecules in the Hertzian area. Polyphenyl ether plus 1% 1,1,2-trichloroethane (TCE) required lower shear rates for the same degree of alignment than without TCE. The experiment was run with 440 C stainless steel balls coated with TiN, a chemically inert material. In both cases, the alignment was strongly influenced by the presence of TCE. The results showed (1) the dependence of alignment of fluid molecules on flow and not on adsorption at metallic surfaces, (2) phase separation between lubricant and additive under high pressure which results in two phase flow and (3) reduction in traction of torque transmitting (traction) fluids. Author

N83-16528*# National Aeronautics and Space Administration. Lewis Research Center, Cleveland, Ohio.
ANALYSIS OF A MIL-L-27502 LUBRICANT FROM A GAS-TURBINE ENGINE TEST BY SIZE-EXCLUSION CHROMATOGRAPHY
W. R. JONES, JR. and W. MORALES Jan. 1983 15 p refs
(NASA-TP-2063; E-1075; NAS 1.60:2063) Avail: NTIS HC A02/MF A01 CSCL 11H

Size exclusion chromatography was used to determine the chemical degradation of MIL-L-27502 oil samples from a gas turbine engine test run at a bulk oil temperature of 216 C. Results revealed a progressive loss of primary ester and additive depletion and the formation of higher molecular weight products with time. The high molecular weight products absorbed strongly in the ultraviolet indicating the presence of chromophoric groups. S.L.

N83-17714*# National Aeronautics and Space Administration. Lewis Research Center, Cleveland, Ohio.
METHOD OF FABRICATING AN ABRADABLE GAS PATH SEAL Patent Application
D. W. WISANDER and R. C. BILL, inventors (to NASA) 30 Sep. 1982 9 p
(NASA-CASE-LEW-13269-2; US-PATENT-APPL-SN-431448)
Avail: NTIS HC A02/MF A01 CSCL 11B

This invention is directed to improving the thermal shock resistance of a ceramic layer. The invention is particularly directed to an improved abradable lining that is deposited on a shroud forming a gas-path seal in turbomachinery. Improved thermal shock resistance of a shroud is effected through the deliberate introduction of 'benign' cracks. These are microcracks which will not propagate appreciably upon exposure to the thermal shock environment in which a turbine seal must function. Laser surface fusion treatment is used to introduce these microcracks. The ceramic surface is laser scanned to form a continuous dense layer. As this layer cools and solidifies, shrinkage results in the formation of a very fine crack network. The presence of this deliberately introduced fine crack network precludes the formation of a catastrophic crack during thermal shock exposure. NASA

N83-17715*# National Aeronautics and Space Administration. Lewis Research Center, Cleveland, Ohio.
IMPROVED HIGH TEMPERATURE RESISTANT POLYIMIDES Patent Application
R. H. PATER, inventor (to NASA) 13 Oct. 1982 21 p
(NASA-CASE-LEW-13864-1; US-PATENT-APPL-SN-434087)
Avail: NTIS HC A02/MF A01 CSCL 11G

The invention relates to improved polyimide resins which are noted for their high thermal and oxidative stability, high strength at elevated temperatures and which exhibit many other outstanding physical and chemical properties, especially useful in high temperature applications. The polyimides are prepared by the reaction, with application of heat of a mixture of monomers comprising (a) a dialkyl or tetraalkyl ester of an aromatic tetracarboxylic acid; (b) an aromatic diamine; (c) a monoalkyl or dialkyl ester of a dicarboxylic acid; and (d) a N-arylnadimide such as N-phenylnadimide. Polyimides of monomers (a), (b) and (c) are known. The novelty of the invention resides in the discovery that the inclusion of N-arylnadimide as a reactant provides an improved flow, superior elevated temperature thermo-oxidative stability and better tack and drape characteristics. NASA

N83-18909*# United Technologies Corp., East Hartford, Conn.
IMIDE MODIFIED EPOXY MATRIX RESINS Final Report
D. A. SCOLA 27 Feb. 1982 106 p refs
(Contract NAS3-22521)
(NASA-CR-167942; NAS 1.26:167942; R82-915366-13) Avail: NTIS HC A06/MF A01 CSCL 11G

Results of a program designed to develop tough imide modified epoxy (IME) resins cured by bisimide amine (BIA) hardeners are presented. State of the art epoxy resin, MY720, was used. Three aromatic bisimide amines and one aromatic aliphatic BIA were evaluated. BIA's derived from 6F anhydride (3,3 prime 4,4 prime-(hexafluoro isopropyl idene) bis (phthalic anhydride) and diamines, 3,3 prime-diam nodiphenyl sulfone (3,3 prime-DDS), 4,4 prime-diamino diphenyl sulfone (4,4 prime-DDS), 1.12-dodecane diamine (1,12-DDA) were used. BIA's were abbreviated 6F-3,3 prime-DDS, 6F-4,4 prime-DDS, 6F-3,3 prime-DDS-4,4 prime DDS, and 6F-3,3 prime-DDS-1,12-DDA corresponding to 6F anhydride and diamines mentioned. Epoxy resin and BIA's (MY720/6F-3,3 prime-DDS, MY720/6F-3,3 prime-DDS-4,4 prime-DDS, MY720/6F-3,3 prime-DDS-1,12-DDA and a 50:50 mixture of a BIA and parent diamine, MY720/6F-3,3 prime-DDS/3,3 prime-DDS, MY720/6F-3,3 prime-DDS-4,4 prime-DDS/3,3 prime-DDS, MY720/6F-3,3 prime-DDS-1,12-DDA/3,3 prime-DDS were studied to determine effect of structure and composition. Effect of the addition of two commercial epoxies, glyamine 200 and glyamine 100 on the properties of several formulations was evaluated. Bisimide amine cured epoxies were designated IME's (imide modified epoxy). Physical, thermal and mechanical properties of these resins were determined. Moisture absorption in boiling water exhibited by several of the IME's was considerably lower than the state of the art epoxies (from 3.2% for the control and state of the art to 2.0 wt% moisture absorption). Char yields are increased from 20% for control and state of the art epoxies to 40% for IME resins. Relative toughness characteristics of IME resins were measured by 10 deg off axis tensile tests of Celion 6000/IME composites. Results show that IME's containing 6F-3,3 prime-DDS or 6F-3,3 prime-DDS-1,12-DDA improved the 'toughness' characteristics of composites by about 35% (tensile strength), about 35% (intralaminar shear strength), and about 78% (shear strain to failure) relative to the control composite. B.G.

N83-19901*# National Aeronautics and Space Administration. Lewis Research Center, Cleveland, Ohio.
SURFACE CHEMISTRY, FRICTION AND WEAR OF NI-ZN AND MN-ZN FERRITES IN CONTACT WITH METALS
K. MIYOSHI and D. H. BUCKLEY 1982 20 p refs Presented at the 7th Ann. Conf. on Composites and Advan. Ceram. Mater., Cocoa Beach, Fla., 16-20 Jan. 1983; sponsored by American Ceramic Society
(NASA-TM-83068; E-1503; NAS 1.15:83068) Avail: NTIS HC A02/MF A01 CSCL 11B

X-ray photoelectron and Auger electron spectroscopy analysis were used in sliding friction experiments. These experiments were conducted with hot-pressed polycrystalline Ni-Zn and Mn-Zn ferrites, and single-crystal Mn-Zn ferrite in contact with various transition metals at room temperature in both vacuum and argon. The results indicate that Ni2O3 and Fe3O4 were present on the Ni-Zn ferrite surface in addition to the nominal bulk constituents, while MnO2 and Fe3O4 were present on the Mn-Zn ferrite surface in addition to the nominal bulk constituents. The coefficients of friction for the ferrites in contact with metals were related to the relative chemical activity of these metals. The more active the metal, the higher is the coefficient of friction. The coefficients of friction for the ferrites were correlated with the free energy of formation of the lowest metal oxide. The interfacial bond can be regarded as a chemical bond between the metal atoms and the oxygen anions in the ferrite surfaces. The adsorption of oxygen on clean metal and ferrite does strengthen the metal-ferrite contact and increase the friction. The ferrites exhibit local cracking and fracture with sliding under adhesive conditions. All the metals transferred to he surfaces of the ferrites in sliding. Author

N83-19902*# National Aeronautics and Space Administration. Lewis Research Center, Cleveland, Ohio.
SPECIMEN SIZE AND GEOMETRY EFFECTS ON FRACTURE TOUGHNESS OF AL2O3 MEASURED WITH SHORT ROD AND SHORT BAR CHEVRON-NOTCH SPECIMENS
J. L. SHANNON, JR. and D. G. MUNZ (Karlsruhe Univ.) 1983 14 p refs Proposed for presentation at the Symp. on Chevron-Notched Specimens: Testing and Stress Anal., Louisville, Ky., 21 Apr. 1983; sponsored by American Society for Testing and Materials
(NASA-TM-83319; E-1560; NAS 1.15:83319) Avail: NTIS HC A02/MF A01 CSCL 07C

Plane strain fracture toughness measurements were made on Al2O3 using short rod and short bar chevron notch specimens previously calibrated by the authors for their dimensionless stress intensity factor coefficients. The measured toughness varied systematically with variations in specimen size, proportions, and chevron notch angle apparently due to their influence on the amount of crack extension to maximum load (the measurement point). The toughness variations are explained in terms of a suspected rising R curve for the material tested, along with a discussion of an unavoidable imprecision in the calculation of K sub Ic for materials with rising R curves when tested with chevron notch specimens. Author

N83-22422*# IIT Research Inst., Chicago, Ill.
PLASMA-SPRAYED SELF-LUBRICATING COATINGS Final Report, 21 May 1979 - 3 Mar. 1982
H. H. NAKAMURA, W. R. LOGAN, and Y. HARADA Washington May 1982 131 p refs
(Contract NAS3-21979)
(NASA-CR-3680; NAS 1.26:3680; IITRI-M06051-33) Avail: NTIS HC A07/MF A01 CSCL 11H

One of the most important criterion for acceptable commercial application of a multiple phase composition is uniformity and reproducibility. This means that the performance characteristics of the coat - e.g., its lubricating properties, bond strength to the substrate, and thermal properties - can be readily predicted to give a desired performance. The improvement of uniformity and reproducibility of the coats, the oxidation behavior at three temperature ranges, the effect of bond coat and the effect of preheat treatment as measured by adhesive strength tests, coating examination procedures, and physical property measurements were studied. The following modifications improved the uniformity and reproducibility: (1) changes and closer control in the particle size range of the raw materials used, (2) increasing the binder content from 3.2% to 4.1% (dried weight), and (3) analytical processing procedures using step by step checking to assure consistency. S.L.

N83-22423*# National Aeronautics and Space Administration. Lewis Research Center, Cleveland, Ohio.
POLYIMIDES FORMULATED FROM A PARTIALLY FLUORINATED DIAMINE FOR AEROSPACE TRIBOLOGICAL APPLICATIONS
R. L. FUSARO 1983 28 p refs Presented at the Ann. Meeting of the Am. Soc. of Lubrication Engr., Houston, Tex., 25-28 Apr. 1983
(NASA-TM-83339; E-1593; NAS 1.15:83339) Avail: NTIS HC A03/MF A01 CSCL 11H

Preliminary tribological studies on polyimides formulated from the diamine 2,2-bis 4-(4-aminophenoxy)phenyl hexafluorapane (4-BDAF) indicate that polyimides formulated from this diamine have excellent potential for high temperature tribological applications. The dianhydrides used to make the polyimides were pyromellitic (PMDA) and benzophenonetetracarboxylic acid (BTDA). Friction and wear studies at 25 and 200 C indicate that polyimides formulated using 50 mole percent of the PMDA dianhydride and 50 mole percent of the BTDA dianhydride perform better than polyimides formulated solely with the BTDA dianhydride. Graphite fiber reinforced polyimide composites were formulated with the polyimide made from the BTDA dianhydride, both graphitic and non-graphitic fibers were evaluated. Graphitic fibers produced better tribological results, since thin, flowing, 'layer-like' transfer films were produced which did not build-up with long sliding durations. Non-graphitic fibers did not produce this type of transfer. M.G.

N83-24695*# National Aeronautics and Space Administration. Lewis Research Center, Cleveland, Ohio.
SOLID SPHERICAL GLASS PARTICLE IMPINGEMENT STUDIES OF PLASTIC MATERIALS
P. V. RAO (National Academy of Sciences - National Research Council, Washington, D.C.), S. G. YOUNG, and D. H. BUCKLEY 1983 19 p refs
(NASA-TP-2161; E-1122; NAS 1.60:2161) Avail: NTIS HC A02/MF A01 CSCL 11I

Erosion experiments on polymethyl methacrylate (PMMA), polycarbonate, and polytetrafluoroethylene (PTFE) were conducted with spherical glass beads impacting at normal incidence. Optical and scanning electron microscopic studies and surface profile measurements were made on specimens at predetermined test intervals. During the initial stage of damage to PMMA and polycarbonate, material expands or builds up above the original surface. However, this buildup disappears as testing progresses. Little or no buildup was observed on PTFE. PTFE is observed to be the most resistant material to erosion and PMMA the least. At low impact pressures, material removal mechanisms are believed to be similar to those for metallic materials. However, at higher pressures, surface melting is indicated at the center of impact. Deformation and fatigue appear to play major roles in the material removal process with possible melting or softening. Author

N83-25882*# National Aeronautics and Space Administration. Lewis Research Center, Cleveland, Ohio.
FRICTION, WEAR, TRANSFER AND WEAR SURFACE MORPHOLOGY OF ULTRA-HIGH-MOLECULAR-WEIGHT POLYETHYLENE
R. L. FUSARO 1983 30 p refs Presented at the Joint Lubrication Conf., Hartford, 18-20 Oct. 1983; sponsored by the American Society of Lubrication Engineers and the ASME
(NASA-TM-83364; E-1629; NAS 1.15:83364) Avail: NTIS HC A03/MF A01 CSCL 11G

Tribological studies at 25 C in a 50-percent-relative-humidity air atmosphere were conducted using hemispherically tipped 440 C HT (high temperature) stainless steel pins sliding against ultra-high-molecular-weight polyethylene (UHMWPE) disks. The results indicate that sliding speed, sliding distance, contact stress and specimen geometry can markedly affect friction, UHMWPE wear, UHMWPE transfer and the type of wear mechanisms that occur. Adhesion appears to be the predominant wear mechanism; but after long sliding distances at slow speeds, heavy ridges of transfer result which can induce fatigue-like wear on the UHMWPE disk wear track. In one instance, abrasive wear to the metallic pin was observed. This was caused by a hard particle embedded in the UHMWPE disk wear track. Author

N83-25883*# National Aeronautics and Space Administration. Lewis Research Center, Cleveland, Ohio.
SPHERICAL MICRO-GLASS PARTICLE IMPINGEMENT STUDIES OF THERMOPLASTIC MATERIALS AT NORMAL INCIDENCE
P. V. RAO and D. H. BUCKLEY 1983 26 p refs Presented at the Joint Lubrication Conf., Hartford, 18-20 Oct. 1983; sponsored by the ASME and the American Society of Lubrication Engineers
(NASA-TM-83410; E-1591; NAS 1.15:83410) Avail: NTIS HC A03/MF A01 CSCL 11G

Light optical and scanning electron microscope studies were conducted to characterize the erosion resistance of polymethyl methacrylate (PMMA), polycarbonate (PC), polytetrafluoroethylene (PTFE) and ultra-high-molecular-weight-polyethylene (UHMWPE). Erosion was caused by a jet of spherical micro-glass beads at normal impact. During the initial stages of damage, the surfaces of these materials were studied using a profilometer. Material buildup above the original surface was observed on PC and PMMA. As erosion progressed, this buildup disappeared as the pit became deeper. Little or no buildup was observed on PTFE and on

UHMWPE. UHMWPE and PTFE are the most resistant materials and PMMA the least. Favorable properties for high erosion resistance seem to be high values of ultimate elongation, and strain energy and a low value of the modulus of elasticity. Erosion-rate-versus-time curves of PC and PTFE exhibit incubation, acceleration and steady state periods. A continuously increasing erosion rate period was observed however for PMMA instead of a steady state period. At early stages of damage and at low impact pressure material removal mechanisms appear to be similar to those for metallic materials. Author

N83-27016*# National Aeronautics and Space Administration. Lewis Research Center, Cleveland, Ohio.
CORRELATION OF COMPRESSIVE STRESS WITH SPALLING OF PLASMA SPRAYED CERAMIC MATERIALS
R. L. MULLEN (Case Western Reserve Univ.), G. MCDONALD, R. C. HENDRICKS (Rensselaer Polytechnic Inst.), and M. M. HOFLE 1983 18 p refs Presented at the 7th Ann. Conf. on Ceram. and Advan. Mater., Cocoa Beach, Fla., 16-23 Jan. 1983; sponsored by American Ceramic Society
(NASA-TM-83406; E-1684; NAS 1.15:83406) Avail: NTIS HC A02/MF A01 CSCL 11G

Ceramics on metal substrates for potential use as high temperature seals or other applications are exposed to forces originating from differences in thermal expansion between the ceramic and the metal substrate. This report develops a relationship between the difference in expansion of the ceramic and the substrate, defines conditions under which shear between the ceramic and the substrate occurs, and those under which bending forces are produced in the ceramic. The off-axis effect of compression forces resulting from high temperature plastic flow of the ceramic producing buckling of the ceramic is developed. Shear is associated with the edge or boundary stresses on the component while bending is associated with the distortion of an interior region. Both modes are significant in predicting life of the ceramic. Author

N83-27019*# National Aeronautics and Space Administration. Lewis Research Center, Cleveland, Ohio.
PROCESSING OF FUSED SILICIDE COATINGS FOR CARBON-BASED MATERIALS
J. L. SMIALEK 1982 39 p refs Presented at the Ceramic-Metal Systems Div. Conf. of the Am. Ceramic Soc. Meeting, Cocoa Beach, Fla., 19-24 Jan. 1983
(NASA-TM-83362; E-1624; NAS 1.15:83362) Avail: NTIS HC A03/MF A01 CSCL 11C

The processing and oxidation resistance of fused Al-Si and Ni-Si slurry coatings on ATJ graphite was studied. Ni-Si coatings in the 70 to 90 percent Si range were successfully processed to melt, wet, and bond to the graphite. The molten coatings also infiltrated the porosity in graphite and reacted with it to form SiC in the coating. Cyclic oxidation at 1200 C showed that these coatings were not totally protective because of local attack of the substrate, due to the extreme thinness of the coatings in combination with coating cracks. S.L.

N83-27020*# National Aeronautics and Space Administration. Lewis Research Center, Cleveland, Ohio.
RF SPUTTERED SILICON AND HAFNIUM NITRIDES: PROPERTIES AND ADHESION TO 440C STAINLESS STEEL
A. GRILL (Ben Gurion Univ. of the Negev, Beer Sheva, Israel) and P. R. ARON 1982 11 p refs Presented at the Intern. Conf. on Met. Coatings, San Diego, Calif. 18-22 Apr. 1983; sponsored by Am. Vacuum Soc.
(NASA-TM-83400; E-1677; NAS 1.15:83400) Avail: NTIS HC A02/MF A01 CSCL 11G

Silicon nitride and hafnium nitride coatings were deposited by reactive RF sputtering on oxidized and unoxidized 440C stainless steel substrates. Sputtering was done in mixtures of argon and nitrogen gases from pressed powder silicon nitride and from hafnium metal targets. Depositions were at two background pressures, 8 and 20 mtorr, and at two different fractions (f) of nitrogen in argon, 0.25 and 0.60, for hafnium nitride and at f = 0.25 for silicon nitride. The coatings and the interface between the coating and substrates were investigated by X-ray diffractometry, scanning electron microscopy, energy dispersive X-ray analysis and Auger electron spectroscopy. A Knoop microhardness of 1650 + or - 100 kg/sq mm was measured for hafnium nitride and 3900 + or - 500 kg/sq mm for silicon nitride. The friction coefficients between a 440C rider and the coatings were measured under lubricated conditions. Scratch test results demonstrate that the adhesion of hafnium nitride to both oxidized and unoxidized 440C is superior to that of silicon nitride. Oxidized 440C is found to have increased adhesion, to both nitrides, over that of unoxidized 440C. Author

N83-27021*# Georgia Inst. of Tech., Atlanta. School of Mechanical Engineering.
NASA INTERDISCIPLINARY COLLABORATION IN TRIBOLOGY. A REVIEW OF OXIDATIONAL WEAR Final Report
T. F. J. QUINN Washington NASA Jun. 1983 113 p refs (Contract NCC3-14)
(NASA-CR-3686; E-1573; NAS 1.26:3686) Avail: NTIS HC A06/MF A01 CSCL 11F

An in-depth review of oxidational wear of metals is presented. Special emphasis is given to a description of the concept of oxidational wear and the formulation of an Oxidational Wear Theory. The parallelism between the formation of an oxide film for dry contact conditions and the formation of other surface films for a lubricated contact is discussed. The description of oxidational wear is prefaced with a unification of wear modes into two major classes of mild and severe wear including both lubricated and dry contacts. Oxidational wear of metals is a class of mild wear where protective oxide films are formed at real areas of contact and during the time of contact at temperataure T sub c. When the oxide reaches a critical thickness, frequently in the range of 1 to 3 microns, the oxide breaks up and eventually appears as a wear particle. These oxides are preferentially formed on plateaux which alternately carry the load as they reach their critical thickness and are removed. If the system is operated at elevated temperatures, thick oxides can form both out of contact and between the plateaux. Temperature is important in determining the structure of the oxide film present. Spinel oxide (Fe3O4) which forms above 300 C is more protective than the lower temperature rhombohedral (alpha-Fe2O3) oxide which is abrasive. An Oxidational Wear Theory is derived using a modified Archard wear law expressed in terms of activation energy (Qp) and Arrhenius constant (Ap). S.L.

N83-27022*# National Aeronautics and Space Administration. Lewis Research Center, Cleveland, Ohio.
THERMAL-BARRIER COATINGS FOR UTILITY GAS TURBINES Final Report
S. R. LEVINE and R. A. MILLER Sep. 1982 66 p refs Sponsored by EPRI
(Contract EPRI PROJ. 1039)
(NASA-TM-85349; NAS 1.15:85349; DE83-900154; EPRI-AP-2618) Avail: NTIS HC A04/MF A01 CSCL 11B

The potential of thermal barrier coatings for use in utility gas turbines was assessed. Pressurized passage and ambient pressure doped fuel burner rig tests revealed that thermal barrier coatings are not resistant to dirty combustion environments. However, present thermal barrier coatings, such as duplex partially stabilized zirconia and duplex Ca2SiO4 have ample resistance to the thermo-mechanical stress and temperature levels anticipated for heavy duty gas turbines firing clean fuel as revealed by clean fuel pressurized passage and ambient pressure burner rig tests. Thus, it is appropriate to evaluate such coatings on blades, vanes and combustors in the field. However, such field tests should be backed up with adequate effort in the areas of coating application technology and design analysis so that the field tests yield unequivocal results. M.G.

N83-28243*# National Aeronautics and Space Administration. Lewis Research Center, Cleveland, Ohio.
WEAR PARTICLE ANALYSIS USING THE FERROGRAPH
W. R. JONES, JR. 1983 23 p refs Presented at the Joint Meeting of the Fluid Power Soc. and the Am. Soc. of Lubrication Engr., Detroit, 26 Apr. 1983
(NASA-TM-83422; E-1648; NAS 1.15:83422) Avail: NTIS HC A02/MF A01 CSCL 11H

The use of the Ferrograph in analyzing wear particles from a variety of different sources is reported. Examples of wear particles from gas turbine engines, bearing tests, friction and wear tests, hydraulic systems, and human joints are illustrated. In addition, the separation of bacteria and human cells is described. Author

N83-29388* National Aeronautics and Space Administration. Lewis Research Center, Cleveland, Ohio.
METHOD OF FORMING OXIDE COATINGS Patent
G. E. MCDONALD, inventor (to NASA) 12 Jul. 1983 3 p Filed 10 Jun. 1981 Supersedes N81-27616 (19 - 18, p 2509)
(NASA-CASE-LEW-13132-1; US-PATENT-4,392,920; US-PATENT-APPL-SN-272152; US-PATENT-CLASS-204-37R; US-PATENT-CLASS-204-35N; US-PATENT-CLASS-204-56R)
Avail: US Patent and Trademark Office CSCL 11D

This invention is concerned with an improved plating process for covering a substrate with a black metal oxide film. The invention is particularly directed to making a heating panel for a solar collector. A compound is electrodeposited from an aqueous solution containing cobalt metal salts onto a metal substrate. This compound is converted during plating into a black, highly absorbing oxide coating which contains hydrated oxides. This is achieved by the inclusion of an oxidizing agent in the plating bath. The inclusion of an oxidizing agent in the plating bath is contrary to standard electroplating practice. The hydrated oxides are converted to oxides by treatment in a hot bath, such as boiling water. An oxidizing agent may be added to the hot liquid treating bath.
Official Gazette of the U.S. Patent and Trademark Office

N83-29392*# National Aeronautics and Space Administration. Lewis Research Center, Cleveland, Ohio.
LOW TEMPERATURE CROSS LINKING POLYIMIDES Patent Application
T. T. SERAFINI and P. DELVIGS, inventors (to NASA) 30 Jun. 1982 14 p
(NASA-CASE-LEW-12876-2; US-PATENT-APPL-SN-393583)
Avail: NTIS HC A02/MF A01 CSCL 11I

A polyimide is formed by cross linking a prepolymer formed by reacting a polyfunctional ester, a polyfunctional amine, and an end-capping unit. By providing an end-capping unit, the prepolymer is curable at a relatively low temperature of about 175 to 245 C.
NASA

N83-29393*# IIT Research Inst., Chicago, Ill.
CREEP OF PLASMA SPRAYED ZIRCONIA Final Report
R. F. FIRESTONE, W. R. LOGAN, and J. W. ADAMS Nov. 1982 61 p refs
(Contract NAS3-20828; NAS3-22127)
(NASA-CR-167868; NAS 1.26:167868; IITRI-M06071-20) Avail: NTIS HC A04/MF A01 CSCL 11B

Specimens of plasma-sprayed zirconia thermal barrier coatings with three different porosities and different initial particle sizes were deformed in compression at initial loads of 1000, 2000, and 3500 psi and temperatures of 1100 C, 1250 C, and 1400 C. The coatings were stabilized with lime, magnesia, and two different concentrations of yttria. Creep began as soon as the load was applied and continued at a constantly decreasing rate until the load was removed. Temperature and stabilization had a pronounced effect on creep rate. The creep rate for 20% Y2O3-80% ZrO2 was 1/3 to 1/2 that of 8% Y2O3-92% ZrO2. Both magnesia and calcia stabilized ZrO2 crept at a rate 5 to 10 times that of the 20% Y2O3 material. A near proportionality between creep rate and applied stress was observed. The rate controlling process appeared to be thermally activated, with an activation energy of approximately 100 cal/gm mole K. Creep deformation was due to cracking and particle sliding. Author

N83-30651*# National Aeronautics and Space Administration. Lewis Research Center, Cleveland, Ohio.
CHEMICAL APPROACH FOR CONTROLLING NADAMIDE CURE TEMPERATURE AND RATE Patent Application
R. W. LAUVER, inventor (to NASA) 22 Jul. 1983 19 p
(NASA-CASE-LEW-13770-2; US-PATENT-APPL-SN-516217)
Avail: NTIS HC A02/MF A01 CSCL 11G

Polyimide resins suitable for use as composite matrix materials are formed by copolymerization of maleic and norbornenyl endcapped monomers and oligomers. The copolymers can be cured at temperatures under about 300 C by controlling the available concentration of the maleic end-capped reactant. This control can be achieved by adding sufficient amounts of said maleic reactant, or by chemical modification of either copolymer, so as to either increase Diels-Alder retrogression of the norbornenyl capped reactant and/or holding initiation and polymerization to a rate compatible with the availability of the maleic-capped reactant. NASA

N83-30660*# National Aeronautics and Space Administration. Lewis Research Center, Cleveland, Ohio.
USE OF HIGH L.E.T. RADIATION TO IMPROVE ADHESION OF METALS TO POLYTETRAFLUOROETHYLENE
D. R. WHEELER and S. V. PEPPER 1982 15 p refs Presented at the 5th Biennial Carl S. Marvel Symp. on Polymer Surface Anal., Tucson, Ariz., 14-15 Mar. 1983; sponsored by the Am. Chem. Soc.
(NASA-TM-83413; E-1701; NAS 1.15:83413) Avail: NTIS HC A02/MF A01 CSCL 11B

MgK alpha X-rays (1254 eV) and 2 keV electrons irradiate the surface of polytetrafluoro ethylene (PTFE). The damage is confined to a few tenths of a micron below the surface, and the doses exceed 10 to the eight power rad. X-ray Photoelectron Spectroscopy (XPS) of the irradiated surfaces and mass spectroscopy of the gaseous products of irradiation indicate that the damaged layer is crosslinked or branched PTFE. After either type of irradiation, the surface has enhanced affinity for metals and a lower contact angle with hexadecane. Tape pull tests show that evaporated Ni and Au films adhere better to the irradiated surface. XPS shows the Ni interacts chemically with PTFE forming NiF2 and possibly NiC. However, the gold adhesion and contact angle results indicate that the interaction is, at least in part, chemically nonspecific. Decreased contact angles on FEP Teflon crystallized against gold were attributed to either the presence of a polar oxygen layer or increased physical forces due to greater density. In the case of irradiated PTFE, no oxygen on the surface was observed. The crosslinked structure might, however, have a greater density, thus accounting for the observed increase in adhesion and wettability. Author

N83-30662*# Ford Motor Co., Dearborn, Mich. Research Staff.
EVALUATION OF CERAMICS FOR STATOR APPLICATIONS: GAS TURBINE ENGINES INTERIM REPORT. STATOR FABRICATION AND EVALUATION Final Report
N. ARNON and W. TRELA Mar. 1983 67 p refs
(Contract DEN3-0019)
(NASA-CR-168140; DOE/NASA/0019-83/1; NAS 1.26:168140)
Avail: NTIS HC A04/MF A01 CSCL 11B

The objective was to assess current ceramic materials, fabrication processes, reliability prediction, and stator durability when subjected to simulated automotive gas turbine engine operating conditions. Ceramic one-piece stators were fabricated of two materials, silicon nitride and silicon carbide, using two near-net-shape processes, slip casting and injection molding. Non-destructive evaluation tests were conducted on all stators identifying irregularities which could contribute to failures under durability testing. Development of the test rig and automatic control system for repeatably controlling air flow rate and temperature over a highly transient durability duty cycle is discussed. Durability results are presented for repeated thermal cycle testing of the

ceramic one-piece stators. Two duty cycles were used, encompassing the temperature ranges of 704 to 1204 C (1300 to 2200 F) and 871 to 1371 C (1600 to 2500 F). Tests were conducted on 28 stators, accumulating 135,551 cycles in 2441 hours of hot testing. Cyclic durability for the ceramic one-piece stator was demonstrated to be in excess of 500 hours, accumulating over 28,850 thermal cycles. Ceramic interface forces were found to be the significant factor in limiting stator life rather than the scatter in material strength properties or the variation in component defects encountered. R.J.F.

N83-31855* National Aeronautics and Space Administration. Lewis Research Center, Cleveland, Ohio.
THERMAL BARRIER COATING SYSTEM HAVING IMPROVED ADHESION Patent
R. C. BILL and J. S. SOVEY, inventors (to NASA) 15 Jun. 1982 3 p Filed 28 Jan. 1981 Supersedes N81-24265 (19 - 15, p 2038)
(NASA-CASE-LEW-1335901; US-PATENT-4,335,190; US-PATENT-APPL-SN-229233; US-PATENT-CLASS-428-623; US-PATENT-CLASS-428-633; US-PATENT-CLASS-428-678; US-PATENT-CLASS-427-34; US-PATENT-CLASS-427-405; US-PATENT-CLASS-427-219.2; US-PATENT-CLASS-427-423)
Avail: US Patent and Trademark Office CSCL 11A

The adherence between a ceramic thermal barrier coating and a metal bond coating is improved by ion sputtering a ceramic film on the bond cost. A ceramic thermal barrier coating is then plasma-sprayed onto this primer film. This improves the integrity and strength of the interface between the plasma-sprayed ceramic layer and metallic bond coat which insures stronger adherence between the metal and the ceramic.
Official Gazette of the U.S. Patent and Trademark Office

N83-32943*# National Aeronautics and Space Administration. Lewis Research Center, Cleveland, Ohio.
TRIBOLOGICAL MEASUREMENTS ON A CHARNLEY-TYPE ARTIFICIAL HIP JOINT
W. R. JONES, JR. Jul. 1983 30 p refs
(NASA-TM-83440; E-1501; NAS 1.15:83440) Avail: NTIS HC A03/MF A01 CSCL 11D

A total hip simulator was used to determine the friction and wear properties of Charnley-type (316L stainless steel balls and sterile ultrahigh molecular weight polyethylene cups) hip prostheses. Three different sets of specimens were tested to 395,000, 101,500 and 233,000 walking cycles, respectively. All tests were run unlubricated, at ambient conditions (22 to 26 C, 30 to 50 percent relative humidity), at 30 walking cycles per minute, under a dynamic load simulating walking. Polyethylene cup wear rates ranged from 1.4 to 39 ten billions cu m which corresponds to dimensional losses of 4.0 to 11 microns per year. Although these wear rates are lower than those obtained from other hip simulators and from in vivo X-ray measurements, they are comparable when taking run-in and plastic deformation into account. Maximum tangential friction forces ranged from 93 to 129 N under variable load (267 to 3090 N range) and from 93 to 143 N under a static load of 3090 N. A portion of one test 250,000 walking cycles) run under dry air (1 percent relative humidity) yielded a wear rate almost 6 times greater than that obtained under wet air (70 percent relative humidity) conditions. Author

N83-34045*# Cincinnati Univ., Ohio. Solid State Electronics Lab.
RESEARCH INTO THE USE OF PYROLYTIC OXIDES AND POLYMERS FOR THE FABRICATION OF THIN FILM HIGH ENERGY CAPACITORS Final Report
J. H. NEVIN Jun. 1983 134 p
(Contract NSG-3024)
(NASA-CR-173012; NAS 1.26:173012) Avail: NTIS HC A07/MF A01 CSCL 11G

Construction, capacitance and dissipation factor, and electrode materials for single layer capacitors are discussed. Basic construction, phosphosilicate glass, ten layer capacitors, twenty layer capacitors, stress measurements, buffered oxide layers, and 30 layer capacitors are also discussed. Spin-on phosphosilicate glass is addressed. Polymers as dielectric materials are also considered. Author

N83-34048*# National Aeronautics and Space Administration. Lewis Research Center, Cleveland, Ohio.
SEARCH FOR SELECTIVE ION DIFFUSION THROUGH MEMBRANES
C. E. MAY and W. H. PHILIPP Jun. 1983 13 p refs
(NASA-TM-83426; E-1715; NAS 1.15:83426) Avail: NTIS HC A02/MF A01 CSCL 07D

The diffusion rates of several ions through some membranes developed as battery separators were measured. The ions investigated were Li(+), Rb(+), Cl(-), and So4. The members were crosslinked polyvinyl alcohol, crosslinked polyacrylic acid, a copolymer of the two, crosslinked calcium polyacrylate, cellulose, and several microporous polyphenylene oxide based films. No true specificity for diffusion of any of these ions was found for any of the membranes. But the calcium polyacrylate membrane was found to exhibit ion exchange with the diffusing ions giving rise to the leaching of the calcium ion and low reproducibility. These findings contrast earlier work where the calcium polyacrylate membrane did show specificity to the diffusion of the copper ion. In general, Fick's law appeared to be obeyed. Except for the microporous membranes, the coefficients for ion diffusion through the membranes were comparable with their values in water. For the microporous membranes, the values found for the coefficients were much less, due to the tortuosity of the micropores. Author

N83-34049*# National Aeronautics and Space Administration. Lewis Research Center, Cleveland, Ohio.
THE EFFECTS OF METALS AND INHIBITORS ON THERMAL OXIDATIVE DEGRADATION REACTIONS OF UNBRANCHED PERFLUOROALKYLETHERS
W. R. JONES, JR., K. J. L. PACIOREK (Ultrasystems, Inc., Irvine, Calif.), D. H. L. HARRIS (Ultrasystems, Inc., Irvine, Calif.), M. E. SMYTHE (Ultrasystems, Inc., Irvine, Calif.), and R. H. KRATZER (Ultrasystems, Inc., Irvine, Calif.) Jul. 1983 20 p refs Presented at the 6th Winter Symp. on Fluorine Chem., Daytona Beach, Fla., 6-11 Feb. 1983; sponsored by American Chemical Society
(NASA-TM-83464; E-1729; NAS 1.15:83464) Avail: NTIS HC A02/MF A01 CSCL 11G

Thermal oxidative degradation studies were performed on unbranched perfluoroalkylethers at 288 C in oxygen. Metals and alloys studied included Ti, Al, and Ti (4 Al, 4 Mn). The mechanism of degradation was by chain scission. Ti and Al promoted less degradation than Ti (4 Al, 4 Mn). The two inhibitors investigated (a perfluorophenyl phosphine and a phosphatriazine) reduced degradation rates by several orders of magnitude. Both inhibitors were effective for the same duration (75 to 100 hours). The phosphatriazine appeared to provide more surface protection. Author

N83-35142*# National Aeronautics and Space Administration. Lewis Research Center, Cleveland, Ohio.
ION EXCHANGE SELECTIVITY FOR CROSS-LINKED POLYACRYLIC ACID
C. E. MAY and W. H. PHILIPP Sep. 1983 14 p refs
(NASA-TM-83427; E-1717; NAS 1.15:83427) Avail: NTIS HC A02/MF A01 CSCL 07D

The ion separation factors for 21 common metal ions with cross-linked polyacrylic acid were determined as a function of pH and the percent of the cross-linked polyacrylic acid neutralized. The calcium ion was used as a reference. At a pH of 5 the decreasing order of affinity of the ions for the cross-linked polyacrylic acid was found to be: Hg++, Fe+++, Pb++, Cr+++, Cu++, Cd++, Al+++, Ag+, Zn++, Ni++, Mn++, Co++, Ca++, Sr++, Ba++, Mg++, K+, Rb+, Cs+, Na+, and Li+. Members of a chemical family exhibited similar selectivities. The Hg++ ion appeared to be about a million times more strongly bound than the alkali metal ions. The relative binding of most of the metal ions varied with pH; the very tightly and very weakly bound ions showed the largest variations with pH. The

calcium ion-hydrogen ion equilibrium was perturbed very little by the presence of the other ions. The separation factors and selectivity coefficients are discussed in terms of equilibrium and thermodynamic significance. Author

N83-35143*# National Aeronautics and Space Administration. Lewis Research Center, Cleveland, Ohio.
A REVIEW OF LIQUID LUBRICANT THERMAL/OXIDATIVE DEGRADATION
W. R. JONES, JR. Aug. 1983 60 p refs Presented at the Intern. Conf. on Tribology in the 80's, Cleveland, 18-22 Apr. 1983
(NASA-TM-83465; E-1559-5; NAS 1.15:83465) Avail: NTIS HC A04/MF A01 CSCL 11H

The fundamental processes occurring during the thermal and oxidative degradation of hydrocarbons are reviewed. Particular emphasis is given to various classes of liquid lubricants such as mineral oils, esters, polyphenyl ethers, C-ethers, and fluorinated polyethers. Experimental techniques for determining thermal and oxidative stabilities of lubricants are discussed. The role of inhibitors and catalysis is also covered. Author

N83-35144*# National Aeronautics and Space Administration. Lewis Research Center, Cleveland, Ohio.
HIGH-PRESSURE LIQUID CHROMATOGRAPHY: A BRIEF INTRODUCTION AND ITS APPLICATION IN ANALYZING THE DEGRADATION OF A C-ETHER (THIO-ETHER) LIQUID LUBRICANT
Sep. 1983 25 p refs
(NASA-TM-83474; E-1769; NAS 1.15:83474) Avail: NTIS HC A02/MF A01 CSCL 11H

The general principles of classical liquid chromatography and high pressure liquid chromatography (HPLC) are reviewed, and their advantages and disadvantages are compared. Several chromatographic techniques are reviewed, and the analytical separation of a C-ether liquid lubricant by each technique is illustrated. A practical application of HPLC is then demonstrated by analyzing a degraded C-ether liquid lubricant from full scale, high temperature bearing tests. Author

28

PROPELLANTS AND FUELS

Includes rocket propellants, igniters, and oxidizers; storage and handling; and aircraft fuels.

A83-11050*# Southwest Research Inst., San Antonio, Tex.
TESTS OF BLENDING AND CORRELATION OF DISTILLATE FUEL PROPERTIES
J. ERWIN and J. N. BOWDEN (Southwest Research Institute, San Antonio, TX) American Institute of Chemical Engineers, Summer National Meeting, Cleveland, OH, Aug. 29-Sept. 1, 1982, Paper. 38 p.
(Contract NAS3-22783)

The development of a fuel test matrix, results from tests of several blends of distillate aircraft fuels, and the use of correlations in formulation determination during a NASA-sponsored program to identify new aircraft fuels are described. The program was initiated in order to characterize fuel blends which are appropriate for different types of combustors in use and under development. The fuels were required to feature a specified range of properties. Attention is given to fuel volatility, hydrogen content, aromatic content, freezing point, kinematic viscosity, and naphthalene content. Paraffinic and naphtenic base stocks were employed, using alkyl benzene, naphthene benzenes, and naphthalenes to adjust the blend properties. Categories for the test fuels comprised source-controlled and composition controlled fuels. Test results and compositions of various fuels are provided. M.S.K.

A83-11482*# Utah Univ., Salt Lake City.
A CARBON-13 AND PROTON NUCLEAR MAGNETIC RESONANCE STUDY OF SOME EXPERIMENTAL REFEREE BROADENED-SPECIFICATION /ERBS/ TURBINE FUELS
D. K. DALLING and R. J. PUGMIRE (Utah, University, Salt Lake City, UT) American Institute of Chemical Engineers, Summer National Meeting, Cleveland, OH, Aug. 29-Sept. 1, 1982, Paper. 20 p. refs
(Contract NAG3-27)

Preliminary results of a nuclear magnetic resonance (NMR) spectroscopy study of alternative jet fuels are presented. A referee broadened-specification (ERBS) aviation turbine fuel, a mixture of 65 percent traditional kerosene with 35 percent hydrotreated catalytic gas oil (HCGO) containing 12.8 percent hydrogen, and fuels of lower hydrogen content created by blending the latter with a mixture of HCGO and xylene bottoms were studied. The various samples were examined by carbon-13 and proton NMR at high field strength, and the resulting spectra are shown. In the proton spectrum of the 12.8 percent hydrogen fuel, no prominent single species is seen while for the blending stock, many individual lines are apparent. The ERBS fuels were fractionated by high-performance liquid chromatography and the resulting fractions analyzed by NMR. The species found are identified. C.D.

A83-39270*# Aerojet Tactical Systems, Sacramento, Calif.
PROCESS AND QUALITY VERIFICATION CONTROLS FOR SOLID PROPELLANT MANUFACTURING
C. J. ROGERS (Aerojet Tactical Systems Co., Sacramento, CA) International Conference on Propellants and Explosives, Karlsruhe, West Germany, June 29-July 1, 1983, Paper. 13 p.
(Contract NAS3-6284)

It is pointed out that in-process tests to verify quality and detect discrepant propellant which could compromise motor performance are essential elements of the solid composite propellant manufacturing process. The successful performance of the 260SL-1 and 260SL-2 motors aptly verified the controls used for manufacturing the propellant. The present investigation is concerned with the selected control parameters, and their relationships to composition and final propellant properties. Control performance is evaluated by comparison with processing data experienced in the manufacture of the propellant for the 260SL-1 motor. It is found that the in-process quality verification controls utilized in the propellant manufacturing process for the 260-in. diameter motor contributed significantly to the confidence of successful and predictable motor performance. G.R.

N83-10207*# Midwest Research Inst., Kansas City, Mo.
EVALUATION OF METHODS FOR RAPID DETERMINATION OF FREEZING POINT OF AVIATION FUELS Final Report
B. MATHIPRAKASAM Sep. 1982 105 p refs
(Contract NAS3-22543)
(NASA-CR-167981; NAS 1.26:167981; MRI-7014-G) Avail: NTIS HC A06/MF A01 CSCL 21D

Methods for identification of the more promising concepts for the development of a portable instrument to rapidly determine the freezing point of aviation fuels are described. The evaluation process consisted of: (1) collection of information on techniques previously used for the determination of the freezing point, (2) screening and selection of these techniques for further evaluation of their suitability in a portable unit for rapid measurement, and (3) an extensive experimental evaluation of the selected techniques and a final selection of the most promising technique. Test apparatuses employing differential thermal analysis and the change in optical transparency during phase change were evaluated and tested. A technique similar to differential thermal analysis using no reference fuel was investigated. In this method, the freezing point was obtained by digitizing the data and locating the point of inflection. Results obtained using this technique compare well with those obtained elsewhere using different techniques. A conceptual design of a portable instrument incorporating this technique is presented. J.D.

N83-10208*# National Aeronautics and Space Administration. Lewis Research Center, Cleveland, Ohio.
LITERATURE SURVEY OF PROPERTIES OF SYNFUELS DERIVED FROM COAL Final Report
F. FLORES Aug. 1982 187 p refs Presented at ASTM Symp. on alternate fuels and future fuels specifications for stationary gas turbine applications, Phoenix, Ariz., 9-10 Dec. 1981
(Contract DE-AI01-77ET-10350)
(NASA-TM-82739; E-1052; DOE/NASA/10350-30; NAS 1.15:82739) Avail: NTIS HC A09/MF A01 CSCL 21D

A literature survey of the properties of synfuels for ground-based turbine applications is presented. The four major concepts for converting coal into liquid fuels (solvent extraction, catalytic liquefaction, pyrolysis, and indirect liquefaction), and the most important concepts for coal gasification (fixed bed, fluidized bed, entrained flow, and underground gasification) are described. Upgrading processes for coal derived liquid fuels are also described. Data presented for liquid fuels derived from various processes, including H-coal, synthoil, solvent refined coal, COED, donor solvent, zinc chloride hydrocracking, co-steam, and flash pyrolysis. Typical composition, and property data is also presented for low and medium-BTU gases derived from the various coal gasification processes. M.G.

N83-11340*# National Aeronautics and Space Administration. Lewis Research Center, Cleveland, Ohio.
RECENT TRENDS IN AVIATION TURBINE FUEL PROPERTIES
R. FRIEDMAN Oct. 1982 33 p refs
(NASA-TP-2056; E-1127; NAS 1.60:2056) Avail: NTIS HC A03/MF A01 CSCL 21D

Plots and tables, compiled from Department of Energy (and predecessor agency) inspection reports from 1969 to 1980, present ranges, averages, extremes, and trends for most of the 22 properties of Jet A aviation turbine fuel. In recent years, average values of aromatics content, mercaptan sulfur content, distillation temperature of 10 percent recovered, smoke point, and freezing point show small but recognizable trends toward their specification limits. About 80 percent of the fuel samples had at least one property near specification, defined as within a standard band about the specification limit. By far the most common near-specification properties were aromatics content, smoke point, and freezing point. Author

N83-12250*# Pennsylvania State Univ., University Park. Center for Air Environment Studies.
PERFORMANCE AND EMISSIONS CHARACTERISTICS OF AQUEOUS ALCOHOL FUMES IN A DI DIESEL ENGINE Final Report
J. B. HEISEY and S. S. LESTZ Aug. 1981 141 p refs
(Contract DE-AI01-81CS-50006; NAG3-91)
(NASA-CR-167917; DOE/NASA/0091-2; NAS 1.26:167917; CAES-590-81) Avail: NTIS HC A07/MF A01 CSCL 21D

A single cylinder DI Diesel engine was fumigated with ethanol and methanol in amounts up to 55% of the total fuel energy. The effects of aqueous alcohol fumigation on engine thermal efficiency, combustion intensity and gaseous exhaust emissions were determined. Assessment of changes in the biological activity of raw particulate and its soluble organic fraction were also made using the Salmonella typhimurium test. Alcohol fumigation improved thermal efficiency slightly at moderate and heavy loads, but increased ignition delay at all operating conditions. Carbon monoxide and unburned hydrocarbon emission generally increased with alcohol fumigation and showed no dependence on alcohol type or quality. Oxide of nitrogen emission showed a strong dependence on alcohol quality; relative emission levels decreased with increasing water content of the fumigant. Particulate mass loading rates were lower for ethanol fueled conditions. However, the biological activity of both the raw particulate and its soluble organic fraction was enhanced by ethanol fumigation at most operating conditions. S.L.

N83-13272*# Pennsylvania State Univ., University Park. Center for Air Environment Studies.
FUMIGATION OF ALCOHOL IN A LIGHT DUTY AUTOMOTIVE DIESEL ENGINE Final Report
E. M. H. BROUKHIYAN and S. S. LESTZ Aug. 1981 121 p refs
(Contract NAG3-91; DE-AI01-81CS-50006)
(NASA-CR-167915; DOE/NASA/0091-1; NAS 1.26:167915; CAES-600-81) Avail: NTIS HC A06/MF A01 CSCL 21D

A light-duty automotive Diesel engine was fumigated with methanol in amounts up to 35% and 50% of the total fuel energy respectively in order to determine the effect of alcohol fumigation on engine performance at various operating conditons. Engine fuel efficiency, emissions, smoke, and the occurrence of severe knock were the parameters used to evaluate performance. Raw exhaust particulate and its soluble organic extract were screened for biological activity using the Ames Salmonella typhimurium assay. Results are given for a test matrix made up of twelve steady-state operating conditions. For all conditions except the 1/4 rack (light load) condition, modest thermal efficiency gains were noted upon ethanol fumigation. Methanol showed the same increase at 3/4 and full rack (high load) conditions. However, engine roughness or the occurrence of severe knock limited the maximum amount of alcohol that could be fumigated. Brake specific nitrogen oxide concentrations were found to decrease for all ethanol conditions tested. Oxides of nitrogen emissions, on a volume basis, decreased for all alcohol conditions tested. Based on the limited particulate data analyzed, it appears that ethanol fumigation, like methanol fumigation, while lowering the mass of particulated emitted, does enhance the biological activity of that particulate. Author

N83-13273*# National Aeronautics and Space Administration. Lewis Research Center, Cleveland, Ohio.
VACUUM SPUTTERED AND ION-PLATED COATINGS FOR WEAR AND CORROSION PROTECTION
T. SPALVINS 1982 17 p refs Presented at the 1982 Ann. Meeting of the Am. Inst. of Chem. Eng., Los Angeles, 14-19 Nov. 1982
(NASA-TM-83007; E-1411; NAS 1.15:83007) Avail: NTIS HC A02/MF A01 CSCL 21D

The plasma or ion-assisted coating techniques such as sputtering and ion plating are discussed in view of wear and corrosion protection. The basic processes and the unique features of the technique are discussed in regard to the synthesis and development of high reliability wear and corrosion resistant films. The ions of the plasma which transfer energy, momentum, and charge to the substrate and the growing films can be beneficially used. As a result, coating adherence and cohesion is improved. Favorable morphological growth such as high density and porosity-free films can be developed, and residual stresses can be reduced. Author

N83-15483*# National Aeronautics and Space Administration. Lewis Research Center, Cleveland, Ohio.
EVALUATION OF ULTRAVIOLET SPECTROPHOTOMETRY FOR SIMULTANEOUS ANALYSIS OF ALKYLBENZENES, ALKYLNAPHTHALENES,
ENES AND TOTAL AROMATICS IN MID-DISTILLATE FUELS
W. S. KIM and G. T. SENG Nov. 1982 47 p refs
(NASA-TM-83032; E-1470; NAS 1.15:83032) Avail: NTIS HC A03/MF A01 CSCL 21D

A rapid ultraviolet spectrophotometric method for the simultaneous determination of aromatics in middistillate fuels was developed and evaluated. In this method, alkylbenzenes, alkylnaphthalenes, alkylanthracenes/phenanthracenes and total aromatics were determined from ultraviolet spectra of the fuels. The accuracy and precision were determined using simulated standard fuels with known compositions. The total aromatics fraction accuracy was 5% for a Jet A type fuel and 0.6% for a broadened properties jet turbine type fuel. Precision, expressed as relative standard deviations, ranged from 2.9% for the alkylanthracenes/phenanthrenes to 15.3% for the alkylbenzenes. The accuracy, however, was less for actual fuel samples when

compared to the results obtained by a mass spectrometric method. In addition, the ASTM D-1840 method for naphthalenes by ultraviolet spectroscopy was evaluated. S.L.

N83-16545*# National Aeronautics and Space Administration. Lewis Research Center, Cleveland, Ohio.
MODELING OF SPACE VEHICLE PROPELLANT MIXING
J. C. AYDELOTT Jan. 1983 27 p refs
(NASA-TP-2107; E-1275; NAS 1.60:2107) Avail: NTIS HC A03/MF A01 CSCL 21I

An experimental program was conducted to examine the liquid flow patterns that result from the axial-jet mixing of ethanol in 10-cm-diameter spherical and cylindrical containers under zero-, reduced-, and normal-gravity conditions. Dimensionless parameters were developed that characterized the observed liquid flow patterns and the bulk-liquid mixing phenomena. The correlations developed, were used to analyze a typical liquid hydrogen tank and internal thermodynamic vent system for a shuttle-compatible space tug similar to current orbit transfer vehicle concepts. A.R.H.

N83-17728*# United Technologies Research Center, East Hartford, Conn.
EXPERIMENTAL STUDY OF THE THERMAL STABILITY OF HYDROCARBON FUELS
P. J. MARTENEY, M. B. COLKET, and A. VRANOS Dec. 1982 70 p refs
(Contract NAS3-22511)
(NASA-CR-168027; NAS 1.26:168027; R82-955319-20) Avail: NTIS HC A04/MF A01 CSCL 21D

The thermal stability of two hydrocarbon fuels (premium diesel and regular diesel) was determined in a flow reactor under conditions representing operation of an aircraft gas turbine engine. Temperature was varied from 300 to 750 F (422 to 672 K) for fuel flows of 2.84 to 56.8 liters/hr (corresponding to 6.84 x 0.00010 to 1.63 x 0.010 kg/sec for regular diesel fuel and 6.55 x 0.00010 to 1.37 x 0.010 kg/sec for premium diesel fuel); test times varied between 1 and 8 hr. The rate of deposition was obtained through measurement of weight gained by metal discs fixed along the channel wall. The rate of deposit formation is best correlated by an Arrhenius expression. The sample discs in the flow reactor were varied among stainless steel, aluminum and brass; fuels were doped with quinoline, indole, and benzoyl perioxide to yield nitrogen or oxygen concentrations of approximately 1000 ppm. The most substantial change in rate was an increase in deposits for brass discs; other disc materials or the additives caused only small perturbations. Tests were also conducted in a static reactor at temperatures of 300 to 800 F for times of 30 min to 2 1/2 hr. Much smaller deposition was found, indicating the importance of fluid transport in the mechanism. Author

N83-18924*# Colorado School of Mines, Golden. Dept. of Chemistry and Geochemistry.
STUDIES OF THE MECHANISMS OF TURBINE FUEL INSTABILITY Final Report
S. R. DANIEL Jan. 1983 88 p refs
(Contract NSG-3122)
(NASA-CR-167963; NAS 1.26:167963) Avail: NTIS HC A05/MF A01 CSCL 21D

The formation of insoluble deposits in a Jet A, a Diesel, and a model fuel (1/10 v/v tetralin/dodecane) was studied. Experiments were conducted using glass containers at 394 K with an air/fuel ratio of 14/1. The effects of addition of ppm levels of various compounds on deposit formation were evaluated. Nitrogen heterocycles were shown to produce a basicity dependent acceleration of deposition. Thiols and thiophene were shown to increase deposition while sulfides and disulfides act as inhibitors. Copper metal and its salts also promote deposition. Results of various instrumental analyses of deposits and development of a high performance liquid chromatographic method for monitoring deposit precursors are discussed. Author

N83-19920*# National Aeronautics and Space Administration. Lewis Research Center, Cleveland, Ohio.
HIGH PERFORMANCE LIQUID CHROMATOGRAPHIC HYDROCARBON GROUP-TYPE ANALYSES OF MID-DISTILLATES EMPLOYING FUEL-DERIVED FRACTIONS AS STANDARDS
G. T. SENG and D. A. OTTERSON Mar. 1983 19 p refs
(NASA-TM-83072; E-1544; NAS 1.15:83072) Avail: NTIS HC A02/MF A01 CSCL 21D

Two high performance liquid chromatographic (HPLC) methods have been developed for the determination of saturates, olefins and aromatics in petroleum and shale derived mid-distillate fuels. In one method the fuel to be analyzed is reacted with sulfuric acid, to remove a substantial portion of the aromatics, which provides a reacted fuel fraction for use in group type quantitation. The second involves the removal of a substantial portion of the saturates fraction from the HPLC system to permit the determination of olefin concentrations as low as 0.3 volume percent, and to improve the accuracy and precision of olefins determinations. Each method was evaluated using model compound mixtures and real fuel samples. Author

N83-19921*# National Aeronautics and Space Administration. Lewis Research Center, Cleveland, Ohio.
FUELS RESEARCH STUDIES AT NASA LEWIS
A. C. ANTOINE 1982 19 p refs Presented at the 54th Ann. Conv. of the National Technical Association, Inc., Baltimore, 2-7 Aug. 1982
(NASA-TM-83003; E-1439; NAS 1.15:83003) Avail: NTIS HC A02/MF A01 CSCL 21D

Fuels research studies carried out in a variety of areas related to aviation propulsion, ground transportation, and stationary power generation systems are discussed. The major efforts are directed to studies on fuels for jet aircraft. These studies involve fuels preparation, fuels analysis, and fuel quality evaluations. The scope and direction of research activities in these areas is discussed, descriptions of Lewis capabilities and facilities given, and results of recent research efforts reported. Author

N83-22442*# National Aeronautics and Space Administration. Lewis Research Center, Cleveland, Ohio.
AVIATION GASOLINES AND FUTURE ALTERNATIVES
D. J. PATTERSON, ed. Washington May 1983 164 p refs Workshop held in Cleveland, Ohio, 3-5 Feb. 1981
(NASA-CP-2267; E-1260; NAS 1.55:2267) Avail: NTIS HC A08/MF A01 CSCL 21D

General aviation industry needs and directions, fuel supply/demand issues, and general aviation technology prospects are discussed.

N83-22444*# National Aeronautics and Space Administration. Lewis Research Center, Cleveland, Ohio.
AVIATION ENERGY AND THE FUTURE OF THE RECREATIONAL USE OF SPORT AND GENERAL AVIATION AIRCRAFT
P. POBEREZNY (Experimental Aircraft Association) and H. ZEISLOFT (Experimental Aircraft Association) *In its* Aviation Gasolines and Future Alternatives p 9-14 May 1983
Avail: NTIS HC A08/MF A01 CSCL 21D

The activities of the Experimental Aviation Association (EAA) are summarized. N.W.

N83-22445*# National Aeronautics and Space Administration. Lewis Research Center, Cleveland, Ohio.
INDUSTRY'S ASSESSMENT OF THE NUMBER OF AIRPLANES IN THE GENERAL AVIATION FLEET ALONG WITH THEIR HOURS FLOWN AND FUEL CONSUMPTION DATA POWERED BY WHAT TYPE OF ENGINES, WHEN AND FOR WHAT REASONS, THROUGH THE YEAR 2000
T. J. SMITH (Mooney Aircraft) *In its* Aviation Gasolines and Future Alternatives p 15-32 May 1983
Avail: NTIS HC A08/MF A01 CSCL 21D

The future of general aviation, its fuels, and the piston powered fleet of aircraft up to the year 2000, and beyond are considered. Author

N83-22449*# National Aeronautics and Space Administration. Lewis Research Center, Cleveland, Ohio.
FUEL SUPPLY AND DISTRIBUTION. FIXED BASE OPERATION
L. C. BURIAN (National Air Transportation Association) *In its* Aviation Gasolines and Future Alternatives p 63-67 May 1983
Avail: NTIS HC A08/MF A01 CSCL 21D

Aviation gasoline versus other products, a changing marketplace, the Airline Deregulation Act of 1978, aviation fuel credit card purchases, strategic locations, storage, co-mingling of fuel, and transportation to/from central storage are discussed. Author

N83-23464*# General Electric Co., Lynn, Mass. Aircraft Engine Business Group.
ANALYTICAL FUEL PROPERTY EFFECTS, SMALL COMBUSTORS, PHASE 1 Final Report
J. D. COHEN Apr. 1983 32 p
(Contract NAS3-22829)
(NASA-CR-168138; NAS 1.26:168138; R82AEB078) Avail: NTIS HC A03/MF A01 CSCL 21D

The effects of nonstandard aviation fuels on a typical small gas turbine combustor was analyzed. The T700/CT7 engine family was chosen as being representative of the class of aircraft power plants desired. Fuel properties, as specified by NASA, are characterized by low hydrogen content and high aromatics levels. Higher than normal smoke output and flame radiation intensity for the current T700 combustor which serves as a baseline were anticipated. It is, therefore, predicted that out of specification smoke visibility and higher than normal shell temperatures will exist when using NASA ERBS fuels with a consequence of severe reduction in cyclic life. Three new designs are proposed to compensate for the deficiencies expected with the existing design. They have emerged as the best of the eight originally proposed redesigns or combinations thereof. After the five choices that were originally made by NASA on the basis of competing performance factors, General Electric narrowed the field to the three proposed. Author

N83-23465*# SRI International Corp., Menlo Park, Calif.
OXIDATION AND FORMATION OF DEPOSIT PRECURSORS IN HYDROCARBON FUELS Final Report
F. R. MAYO, B. LAN, D. B. COTTS, S. E. BUTTRILL, JR., and G. A. ST.JOHN Mar. 1983 32 p refs
(Contract NAS3-22510)
(NASA-CR-168121; NAS 1.26:168121; SRI-2115) Avail: NTIS HC A03/MF A01 CSCL 21D

The oxidation of two jet turbine fuels and some pure hydrocarbons was studied at 130 C with and without the presence of small amounts of N-methyl pyrrole (NMP) or indene. Tendency to form solid-deposit precursors was studied by measuring soluble gum formation as well as dimer and trimer formation using field ionization mass spectrometry. Pure n-dodecane oxidized fastest and gave the smallest amount of procursors. An unstable fuel oil oxidized much slower but formed large amounts of precursors. Stable Jet A fuel oxidized slowest and gave little precursors. Indene either retarded or accelerated the oxidation of n-dodecane, depending on its concentration, but always caused more gum formation. The NMP greatly retarded n-dodecane oxidation but accelerated Jet A oxidation and greatly increased the latter's gum formation. In general, the additive reacted faster and formed most of the gum. Results are interpreted in terms of classical cooxidation theory. The effect of oxygen pressure on gum formation is also reported. Author

N83-28255*# National Aeronautics and Space Administration. Lewis Research Center, Cleveland, Ohio.
RESEARCH ON AVIATION FUEL INSTABILITY
C. E. BAKER, D. A. BITTKER, S. M. COHEN, and G. T. SENG 1983 20 p refs Proposed for presentation at the AGARD Propulsion and Energetics Panel Symp. on Combust. Probl. in Turbine Eng., Cesme, Turkey, 3-7 Oct. 1983
(NASA-TM-83420; E-1710; NAS 1.15:83420) Avail: NTIS HC A02/MF A01 CSCL 21D

The underlying causes of fuel thermal degradation are discussed. Topics covered include: nature of fuel instability and its temperature dependence, methods of measuring the instability, chemical mechanisms involved in deposit formation, and instrumental methods for characterizing fuel deposits. Finally, some preliminary thoughts on design approaches for minimizing the effects of lowered thermal stability are briefly discussed. Author

N83-29214*# National Aeronautics and Space Administration. Lewis Research Center, Cleveland, Ohio.
FUEL VAPORIZATION EFFECTS
M. A. BOSQUE *In its* Combust. Fundamentals Res. p 49-54 Mar. 1983
Avail: NTIS HC A12/MF A01 CSCL 21D

A study of the effects of fuel-air preparation characteristics on combustor performance and emissions at temperature and pressure ranges representative of actual gas turbine combustors is discussed. The effect of flameholding devices on the vaporization process and NOx formation is discussed. Flameholder blockage and geometry are some of the elements that affect the recirculation zone characteristics and subsequently alter combustion stability, emissions and performance. A water cooled combustor is used as the test rig. Preheated air and Jet A fuel are mixed at the entrance of the apparatus. A vaporization probe is used to determine percentage of vaporization and a gas sample probe to determine concentration of emissions in the exhaust gases. The experimental design is presented and experimental expected results are discussed. R.J.F.

N83-31886*# Aerojet Liquid Rocket Co., Sacramento, Calif.
LOX/HYDROCARBON FUEL CARBON FORMATION AND MIXING DATA ANALYSIS
J. FANG Nov. 1983 184 p refs
(Contract NAS3-22823)
(NASA-CR-168066; NAS 1.26:168066) Avail: NTIS HC A09/MF A01 CSCL 21H

By applying the Priem-Heidmann Generalized-Length vaporization correlation, the computer model developed by the present study predicts the spatial variation of propellant vaporization rate using the injector cold flow results to define the streamtubes. The calculations show that the overall and local propellant vaporization rate and mixture ratio change drastically as the injection element type or the injector operating condition is changed. These results are compared with the regions of carbon formation observed in the photographic combustion testing. The correlation shows that the fuel vaporization rate and the local mixture ratio produced by the injector element have first order effects on the degree of carbon formation. Author

N83-35159*# United Technologies Research Center, East Hartford, Conn.
DEPOSIT FORMATION IN HYDROCARBON ROCKET FUELS: EXECUTIVE SUMMARY Summary Report, Apr. 1980 - May 1981
R. ROBACK, E. J. SZETELA, and L. J. SPADACCINI Cleveland NASA. Lewis Research Center Sep. 1981 23 p refs
(Contract NAS3-22277)
(NASA-CR-165492; NAS 1.26:165492; P81-915216-2) Avail: NTIS HC A02/MF A01 CSCL 21I

An experimental program was conducted to study deposit formation in hydrocarbon fuels under flow conditions that exist in high-pressure, rocket engine cooling systems. A high pressure fuel coking test apparatus was designed and developed and was used to evaluate thermal decomposition (coking) limits and carbon deposition rates in heated copper tubes for two hydrocarbon rocket fuels, RP-1 and commercial-grade propane. Tests were also conducted using JP-7 and chemically-pure propane as being representative of more refined cuts of the baseline fuels. A parametric evaluation of fuel thermal stability was performed at pressures of 136 atm to 340 atm, bulk fuel velocities in the range 6 to 30 m/sec, and tube wall temperatures in the range 422 to 811K. In addition, the effect of the inside wall material on deposit formation was evaluated in selected tests which were conducted using nickel-plated tubes. The results of the tests indicated that substantial deposit formation occurs with RP-1 fuel at wall temperatures between 600 and 800K, with peak deposit formation occurring near 700K. No improvements were obtained when de-oxygenated JP-7 fuel was substituted for RP-1. The carbon deposition rates for the propane fuels were generally higher than those obtained for either of the kerosene fuels at any given wall temperature. There appeared to be little difference between commercial-grade and chemically-pure propane with regard to type and quantity of deposit. The results of tests conducted with RP-1 indicated that the rate of deposit formation increased slightly with pressure over the range 136 atm to 340 atm. Finally, plating the inside wall of the tubes with nickel was found to significantly reduce carbon deposition rates for RP-1 fuel. Author

N83-35160*# National Aeronautics and Space Administration. Lewis Research Center, Cleveland, Ohio.
EFFECT OF DEOXYGENATION AND PRESTRESSING ON HYDROCARBON FUEL THERMAL STABILITY
D. A. BITTKER Aug. 1983 19 p refs
(NASA-TM-83456; E-1771; NAS 1.15:83456) Avail: NTIS HC A02/MF A01 CSCL 21D

A jet fuel thermal oxidation tester was used to study the effect of deoxygenation and deoxygenated prestressing on deposit formation when hydrocarbon fuels are thermally stressed. Four pure hydrocarbons (n-decane, cyclohexane, benzene and 1-hexene) and two mixtures (10 percent tetralin in n-dodecane and commercial Jet A) were used at temperatures of 250 C to 400 C. Deoxygenation decreased deposit formation for cycloheaxane but increased it for benzene. Deoxygenation decreased deposit formation for the two fuel mixtures at 250 C but had no effect at 350 C. Deoxygenated prestressing either increased or decreased deposit formation depending on the fuel used and the temperature. Author

31

ENGINEERING (GENERAL)

Includes vacuum technology; control engineering; display engineering; and cryogenics.

A83-11487*# Martin Marietta Aerospace, Denver, Colo.
LONG TERM STORAGE OF CRYOGENS IN SPACE
D. A. FESTER and R. N. EBERHARDT (Martin Marietta Aerospace, Denver, CO) International Symposium on Space Technology and Science, 13th, Tokyo, Japan, June 27-July 3, 1982, Paper. 9 p.
(Contract NAS3-22264; NAS3-21591)

Experimental design procedures leading to the configuration of a space-based cryogenic fluids test system are reported. Large quantities of cryogenic fluids are expected to be required in space for cooling systems, chemical and electrical OTVs, and resupply tankers. The design was guided by the necessity for representative storage and supply systems to be compatible with the Shuttle. Consideration was given to liquid hydrogen, oxygen, methane, and argon containers and concommitant fluid dynamics, thermal, and structural analyses. A 5% initial ullage was included for the liquids, except for methane, which was calculated at 8.9%. The Ar, CH4, and O2 tanks were set at 12.5 cu m, while the H2 tank was 37.4 cu m. The orbital experiment is required to provide actual thermal stabilization lags in a zero-g environment. Details of the Cryogenic Fluid Management Facility test module for flight on board the Shuttle are presented. M.S.K.

N83-12259*# Colorado State Univ., Fort Collins. Dept. of Physics.
INDUSTRIAL ION SOURCE TECHNOLOGY Annual Report
H. R. KAUFMAN and R. S. ROBINSON Dec. 1979 67 p refs
(Contract NSG-3086)
(NASA-CR-159877; NAS 1.26:159877) Avail: NTIS HC A04/MF A01 CSCL 13H

In reactive ion etching of Si, varying amounts of O2 were added to the CF4 background. The experimental results indicated an etch rate less than that for Ar up to an O2 partial pressure of about .00006 Torr. Above this O2 pressure, the etch rate with CF4 exceeded that with Ar alone. For comparison the random arrival rate of O2 was approximately equal to the ion arrival rate at a partial pressure of about .00002 Torr. There were also ion source and ion pressure gauge maintenance problems as a result of the use of CF4. Large scale (4 sq cm) texturing of Si was accomplished using both Cu and stainless steel seed. The most effective seeding method for this texturing was to surround the sample with large inclined planes. Designing, fabricating, and testing a 200 sq cm rectangular beam ion source was emphasized. The design current density was 6 mA/sq cm with 500 eV argon ions, although power supply limitations permitted operation to only 2 mA/sq cm. The use of multiple rectangular beam ion sources for continuous processing of wider areas than would be possible with a single source was also studied. In all cases investigated, the most uniform coverage was obtained with 0 to 2 cm beam overlay. The maximum departure from uniform processing at optimum beam overlap was found to be +15%. S.L.

N83-17745*# National Aeronautics and Space Administration. Lewis Research Center, Cleveland, Ohio.
MULTICOLOR PRINTING PLATE JOINING Patent Application
W. J. WATERS, inventor (to NASA) 28 Sep. 1982 12 p
(NASA-CASE-LEW-13598-1; US-PATENT-APPL-SN-425203)
Avail: NTIS HC A02/MF A01 CSCL 13H

An upper plate having ink flow channels and a lower plate having a multicolored 5 pattern are joined without clogging any ink flow paths. A pattern having different colored parts and apertures is formed in a lower plate. Ink flow channels each having respective ink input ports are formed in an upper plate. The ink flow channels are coated with solder mask and the bottom of the

upper plate is then coated with solder. The upper and lower plates are pressed together at from 2 to 5 psi and heated to a temperature of from 295 F to 750 F or enough to melt the solder. After the plates have cooled and the pressure is released, the solder mask is removed from the interior passageways by means of a liquid solvent. NASA

N83-35177* National Aeronautics and Space Administration. Lewis Research Center, Cleveland, Ohio.
COVERING SOLID, FILM COOLED SURFACES WITH A DUPLEX THERMAL BARRIER COATING Patent
C. H. LIEBERT, inventor (to NASA) 6 Sep. 1983 4 p Filed 7 Dec. 1981 Supersedes N82-25463 (20 - 16, p 2232)
(NASA-CASE-LEW-13450-1; US-PATENT-4,402,992; US-PATENT-APPL-SN-328760; US-PATENT-CLASS-427-34; US-PATENT-CLASS-427-243; US-PATENT-CLASS-427-247; US-PATENT-CLASS-427-423) Avail: US Patent and Trademark Office CSCL 13H

Thermal barrier coating systems were applied to hardware having passageways in the walls connecting apertures in the surface to a gas supply for film cooling. An inert gas, such as argon, is discharged through the apertures during the application of the thermal barrier coating system by plasma spraying. This flow of inert gas reduces both blocking of the holes and base metal oxidation during the coating operation.
Official Gazette of the U.S. Patent and Trademark Office

32

COMMUNICATIONS

Includes land and global communications; communications theory; and optical communications.

A83-11485*# Hughes Aircraft Co., El Segundo, Calif.
A MULTIPLE BEAM ANTENNA CONCEPT FOR A 30/20 GHZ SATELLITE COMMUNICATIONS SYSTEM
B. J. FORMAN, H. H. OHTA, and L. M. BRONSTEIN (Hughes Aircraft Co., Space and Communications Group, El Segundo, CA) Institute of Electrical and Electronics Engineers and American Physical Society, International Symposium, University of New Mexico, Albuquerque, NM, May 24-28, 1982, Paper. 4 p.
(Contract NAS3-22340)

Design and operational performance features of a NASA planned 30/30 GHz flight experiment communications system multiple-beam antenna (MBA) are described. The MBA is a shared aperture offset Cassegrain type with a main reflector diameter of 3 m and physically separated transmit and receive feeds. A planar frequency selective surface is employed which is transmissive to the receive signals and reflective to the transmit signals. Trade-offs and constraints in the MBA feed design are explored, noting the higher feed loss and complexity due to choosing variable power dividers for the beam forming network. Doublet beam coverage of the east coast of the continental U.S. is shown to be possible with a triangular lattice array of feed horns with aperture diameters and element spacings of two wavelengths. The doublet configuration requires ten times the components as a singlet array. M.S.K.

A83-19686* Cleveland State Univ., Ohio.
EXPERIMENTAL RESULTS FOR THE INTERFERENCE BETWEEN FM TELEVISION SIGNALS
P. P. GROUMPOS (Cleveland State University, Cleveland, OH) and G. D. VERNON (RCA, Consumer Electronics Div., Indianapolis, IN) In: NTC '81; National Telecommunications Conference, New Orleans, LA, November 29-December 3, 1981, Record. Volume 1. New York, Institute of Electrical and Electronics Engineers, Inc., 1981, p. A10.6.1-A10.6.5. refs
(Contract NAG3-156)

Experimental results based on subjective evaluation of picture quality of FM television systems are presented. Curves indicating the variation in protection ratio with impairment grade are provided. Such an analysis would be useful to the broadcasting satellite system designer. The experimental procedures and test conditions followed are briefly summarized. The need for a theoretical planning method is briefly discussed. (Author)

A83-19688*# National Aeronautics and Space Administration. Lewis Research Center, Cleveland, Ohio.
30/20 GHZ EXPERIMENTAL COMMUNICATIONS SATELLITE SYSTEM
J. N. SIVO (NASA, Lewis Research Center, Cleveland, OH) In: NTC '81; National Telecommunications Conference, New Orleans, LA, November 29-December 3, 1981, Record. Volume 1. New York, Institute of Electrical and Electronics Engineers, Inc., 1981, p. B5.2.1-B5.2.5.
(Previously announced in STAR as N81-30172)

A83-19698* Missouri Univ., Rolla.
ADJACENT CHANNEL INTERFERENCE DEGRADATION WITH MINIMUM SHIFT KEYED MODULATION
R. E. ZIEMER (Missouri-Rolla, University, Rolla, MO) In: NTC '81; National Telecommunications Conference, New Orleans, LA, November 29-December 3, 1981, Record. Volume 1. New York, Institute of Electrical and Electronics Engineers, Inc., 1981, p. B7.5.1-B7.5.5. refs
(Contract NAS3-22501)

Computer simulation results for degradation in signal-to-noise ratio for various values of bit error probability are given for minimum shift-keyed-type signaling in the presence of adjacent channel interference. A serial modulator structure which utilizes spectral shaping is characterized in terms of envelope deviation and bandwidth efficiency. This serial generation technique is convenient for implementation at high data rates and results in signal spectra with lower sidelobe levels than conventional minimum shift-keyed modulation at the expense of moderate envelope deviation. Because of the lower sidelobe levels, the resulting spectra allow denser channel packing than does ideal MSK. (Author)

A83-19732* Toledo Univ., Ohio.
A NEW ARCHITECTURE FOR ADAPTIVE TRANSFORM COMPRESSION OF NTSC COMPOSITE VIDEO SIGNAL
C. EKAMBARAM and S. C. KWATRA (Toledo, University, Toledo, OH) In: NTC '81; National Telecommunications Conference, New Orleans, LA, November 29-December 3, 1981, Record. Volume 2. New York, Institute of Electrical and Electronics Engineers, Inc., 1981, p. C9.6.1-C9.6.5. refs
(Contract NAG3-42)

In orthogonal transform coding of NTSC video signal, the data is processed in blocks. Processing a block of data that is maximally correlated leads to larger compression. This paper describes a new architecture for arranging the pixels in a block that yields higher correlation than the adjacent pixel blocks. The data is processed using adaptive, intrafield, discrete cosine transform, variable bit allocation coding. In subjective tests, the picture quality was good for an average of about 2 bits/pel for intrafield processing. (Author)

A83-19762* Western Union Telegraph Co., New York.
FUTURE SATELLITE SYSTEMS - MARKET DEMAND ASSESSMENT
P. S. REINER (Western Union Telegraph Co., New York, NY) In: NTC '81; National Telecommunications Conference, New Orleans, LA, November 29-December 3, 1981, Record. Volume 3. New York, Institute of Electrical and Electronics Engineers, Inc., 1981, p. E7.4.1-E7.4.6.
(Contract NAS3-834505)

During 1979-80, a market study was performed regarding the future total demand for communications services, and satellite transmission service at the 4/6 GHz, 12/14 GHz, and 20/30 GHz frequencies. Included in the study were a variety of communications traffic characteristics as well as projections of the cost of C and Ku band satellite systems through the year 2000. In connection with the considered study, a total of 15 major study tasks and subtasks were undertaken and were all interrelated in various ways. The telecommunications service forecasts were concerned with a total of 21 data services, 5 voice services, and 5 video services. The traffic volumes within the U.S. for the three basic services were projected for three time periods. It is found that the fixed frequency allocation for domestic satellites combined with potential interference from adjacent satellites means a near term lack of orbital positions above the U.S. G.R.

A83-19776* General Electric Co., Philadelphia, Pa.
A HIGH CAPACITY SATELLITE SWITCHED TDMA MICROWAVE SWITCH MATRIX
B. J. CORY and M. BERKOWITZ (GE Valley Forge Space Center, Philadelphia, PA) In: NTC '81; National Telecommunications Conference, New Orleans, LA, November 29-December 3, 1981, Record. Volume 3. New York, Institute of Electrical and Electronics Engineers, Inc., 1981, p. F7.6.1-F7.6.5.
(Contract NAS3-22500)

A description is given of the conceptual design of a high-capacity satellite switched-time division multiple access (SS-TDMA) microwave switch matrix fabricated with GaAs monolithic microwave integrated circuits (MMICs), including integration of both microwave and control logic circuits into the monolithic design. The technology required for a 30/20 GHz communications system includes an on-board SS-TDMA switch matrix. A conceptual design study that has been completed for a wideband, high-capacity (typically 100 x 100) channel switch matrix using technology anticipated for 1987 is described, noting that the study resulted in a switch matrix design concept using a coupled crossbar architecture implemented with MMIC. The design involves basic building block MMIC, permitting flexible growth and efficient wraparound redundancy to increase reliability. C.R.

A83-21072*# Solar Energy Technology, Inc., Bedford, Mass.
TECHNIQUES FOR LOW SIDELOBE, HIGH EFFICIENCY OFFSET DUAL REFLECTOR ANTENNAS
C. J. SLETTEN (Solar Energy Technology, Inc., Bedford, MA) Antenna Applications Symposium, Monticello, IL, Sept. 23-25, 1981, Paper. 8 p.
(Contract NAS3-22343)

Antennas with very low sidelobe levels and high aperture efficiencies are employed in satellite communications for both ground and satellite borne systems to reduce microwave interference due to traffic congestion to and from the geostationary satellite orbit. Multiple beam antennas with sidelobes 30 to 40 dB below main beam peaks are required with aperture efficiencies approaching 80%. In the present investigation techniques are presented which make it possible to obtain multibeam patterns with the required characteristics. The considered limited scanned antennas have applications to military and commercial radars as well as to space communications. It is pointed out that offset dual reflector antennas designed according to Japanese tilt criteria offer attractive solutions because optimum aperture distributions can be realized without aperture blocking. Attention is given to ideal aperture distributions, corrugated conical horn design, and subreflector design. G.R.

A83-41336* General Electric Co., Schenectady, N. Y.
PACKET COMMUNICATION SYSTEM FOR A MULTI-BEAM BEAM SWITCHED SATELLITE REPEATER
S. K. BOSE (General Electric Co., Schenectady, NY) IN: ICC '82 - The digital revolution; International Conference on Communications, Philadelphia, PA, June 13-17, 1982, Conference Record. Volume 1 . New York, Institute of Electrical and Electronics Engineers, 1982, p. 1E.4.1-1E.4.7. refs
(Contract NAS3-22500)

This paper presents the design of a packet-switched communication system using a multi-beam, beam switched satellite repeater. The protocol provides a combination of random access via Slotted ALOHA techniques and demand assigned access using collision requests. This allows efficient bandwidth usage and low average delays. Minimization of earth station cost was a major objective. This was achieved by transferring the bulk of the system complexity to the satellite repeater and the (ground) network controller. This centrally controlled protocol would allow greater system stability and would permit system reconfiguration in response to changes in traffic intensity. Sufficient signalling is also incorporated to allow both rate diversity to combat fading and timing corrections to account for satellite drift. Author

A83-41363* Columbia Univ., New York.
COMPARISON OF CHANNEL ASSIGNMENT TECHNIQUES FOR HYBRID SWITCHING
M. SCHWARTZ and B. KRAIMECHE (Columbia University, New York, NY) IN: ICC '82 - The digital revolution; International Conference on Communications, Philadelphia, PA, June 13-17, 1982, Conference Record. Volume 1 . New York, Institute of Electrical and Electronics Engineers, 1982, p. 2F.3.1-2F.3.5. refs
(Contract NAS3-22464)

The performance of four circuit-switched channel assignment strategies for use in a hybrid switch accommodating multiple users is analyzed and compared. Each scheme is associated with a fixed frame movable boundary TDM channel that multiplexes circuit-switched (CS) and packet-switched (PS) traffic. The performance measures used are blocking probability for the circuit-switched traffic and time delay for the packet-switched traffic. Author

A83-41367* TRW, Inc., Redondo Beach, Calif.
ADVANCED 30/20 GHZ MULTIPLE BEAM ANTENNA FOR FUTURE COMMUNICATIONS SATELLITES
C. C. CHEN (TRW, Inc., Space Communications Div., Redondo Beach, CA) and R. W. MYHRE (NASA, Lewis Research Center, Cleveland, OH) IN: ICC '82 - The digital revolution; International Conference on Communications, Philadelphia, PA, June 13-17, 1982, Conference Record. Volume 2 . New York, Institute of Electrical and Electronics Engineers, 1982, p. 3A.2.1-3A.2.6.

A multiple offset reflector system is being used to provide multiple fixed and scanning beams at 30 GHz by means of a polarization grid diplexer to separate two orthogonally polarized feed assemblies. Each feed assembly consists of multiple fixed and scanning beam feeds. The technology developments required for successful operation of this proposed system are presented. These technologies include: (1) an offset Cassegrain system for low sidelobe wide angle scan beams; (2) a diplexed beam forming network for overlapping low sidelobe beams; (3) a fast switching network for scanning beams; and (4) fabrication of precision feed components and large offset reflectors. Author

A83-41417*# National Aeronautics and Space Administration. Lewis Research Center, Cleveland, Ohio.
SATELLITE-AIDED LAND MOBILE COMMUNICATIONS SYSTEM IMPLEMENTATION CONSIDERATIONS
B. E. LEROY (NASA, Lewis Research Center, Cleveland, OH) IN: ICC '82 - The digital revolution; International Conference on Communications, Philadelphia, PA, June 13-17, 1982, Conference Record. Volume 3 . New York, Institute of Electrical and Electronics Engineers, 1982, p. 7H.3.1-7H.3.5. refs

It was proposed that a satellite-based land mobile radio system could effectively extend the terrestrial cellular mobile system into

rural and remote areas. The market, technical and economic feasibility for such a system is studied. Some of the aspects of implementing an operational mobile-satellite system are discussed. In particular, two key factors in implementation are examined: (1) bandwidth requirements; and (2) frequency sharing. Bandwidth requirements are derived based on the satellite antenna requirements, modulation characteristics and numbers of subscribers. Design trade-offs for the satellite system and potential implementation scenarios are identified. Frequency sharing is examined from a power flux density and modulation viewpoint. Previously announced in STAR as N82-25290 B.W.

N83-10322*# National Aeronautics and Space Administration. Lewis Research Center, Cleveland, Ohio.
MULTI-STAGE DEPRESSED COLLECTORS (MDC) FOR EFFICIENCY IMPROVEMENTS OF UHF BROADCAST KLYSTRONS
H. G. KOSMAHL 1982 9 p Presented at the 32d Natl. Broadcasting Symp., Washington, D.C., 16-17 Sep. 1982; sponsored by IEEE
(NASA-TM-82970; E-1391; NAS 1.15:82970) Avail: NTIS HC A02/MF A01 CSCL 17B

The consumed primary power is reduced and the efficiency of traveling wave tubes is raised through the use of depressed collectors which passively convert potential energy into electric energy. Efficiency was kept with constant within a 3 dB range while the output power varied by 10 dB. Aspects to be considered in transferring this technology to UHF klystrons are the electron energy spectrum of the klystron and the magnitude of the injection angle required. A.R.H.

N83-10329*# City Coll. of the City Univ. of New York. Communications Systems Lab.
MODULATION TECHNIQUES
D. L. SCHILLING 1982 47 p refs
(Contract NAG3-299)
(NASA-CR-169460; NAS 1.26:169460; TR-1) Avail: NTIS HC A03/MF A01 CSCL 17B

Bandwidth efficient digital modulation techniques, proposed for use on and/or applied to satellite channels, are reviewed. In a survey of recent works on digital modulation techniques, the performance of several schemes operating in various environments are compared. Topics covered include: (1) quadrature phase shift keying; (2) offset - QPSK and MSK; (3) combined modulation and coding; and (4) spectrally efficient modulation techniques. A.R.H.

N83-14365*# National Aeronautics and Space Administration. Lewis Research Center, Cleveland, Ohio.
ENVIRONMENTALLY INDUCED DISCHARGES ON SATELLITES
N. J. STEVENS *In* ESA 2nd ESTEC Spacecraft Electromag. Compatibility Seminar p 161-172 Jul. 1982 refs
Avail: NTIS HC A10/MF A01

A discharge process whose trigger conditions are a negative exposed metallic surface surrounded by a less negative dielectric, and a large voltage gradient at a dielectric/metal interface is proposed. Analysis of SCATHA data for a discharge substantiates the postulation. Surface discharges cause a small transient charge transfer to space which results in voltage transients. A method of computing these transients, based on the charge lost through the capacitance to space and a fraction of charge stored in the dielectric at the discharge source was developed. It gives an estimate of the discharge transients at the discharge site, which is used as input for coupling code analysis of structure/system response. The transient computations were applied to a three-axis stabilized, geosynchronous satellite for both sunlight and eclipse charging. The energy of the transient pulses are about 1 mJ for sunlight discharge and 8 mJ for eclipse. Changing of selected coatings on the satellite would relieve the stress. Author (ESA)

N83-15543*# Motorola, Inc., Scottsdale, Ariz. Government Electronics Group.
SATELLITE SWITCHED FDMA ADVANCED COMMUNICATION TECHNOLOGY SATELLITE PROGRAM Final Report, Nov. 1981 - Dec. 1982
S. ATWOOD, G. H. HIGTON, K. WOOD, A. KLINE, A. FURIGA, M. RAUSCH, and Y. JAN Dec. 1982 308 p
(Contract NAS3-22895)
(NASA-CR-168034; NAS 1.26:168034; PJ050) Avail: NTIS HC A14/MF A01 CSCL 17B

The satellite switched frequency division multiple access system provided a detailed system architecture that supports a point to point communication system for long haul voice, video and data traffic between small Earth terminals at Ka band frequencies at 30/20 GHz. A detailed system design is presented for the space segment, small terminal/trunking segment at network control segment for domestic traffic model A or B, each totaling 3.8 Gb/s of small terminal traffic and 6.2 Gb/s trunk traffic. The small terminal traffic (3.8 Gb/s) is emphasized, for the satellite router portion of the system design, which is a composite of thousands of Earth stations with digital traffic ranging from a single 32 Kb/s CVSD voice channel to thousands of channels containing voice, video and data with a data rate as high as 33 Mb/s. The system design concept presented, effectively optimizes a unique frequency and channelization plan for both traffic models A and B with minimum reorganization of the satellite payload transponder subsystem hardware design. The unique zoning concept allows multiple beam antennas while maximizing multiple carrier frequency reuse. Detailed hardware design estimates for an FDMA router (part of the satellite transponder subsystem) indicate a weight and dc power budget of 353 lbs, 195 watts for traffic model A and 498 lbs, 244 watts for traffic model B. S.L.

N83-16600*# Virginia Univ., Charlottesville. Communication Systems Lab.
AN IMPROVED ALGORITHM FOR EVALUATING TRELLIS PHASE CODES
M. G. MULLIGAN and S. G. WILSON 16 Sep. 1982 18 p refs
(Contract NAG3-141)
(NASA-CR-169354; NAS 1.26:169354; UVA/528200/EE82/104)
Avail: NTIS HC A02/MF A01 CSCL 20N

A method is described for evaluating the minimum distance parameters of trellis phase codes, including CPFSK, partial response FM, and more importantly, coded CPM (continuous phase modulation) schemes. The algorithm provides dramatically faster execution times and lesser memory requirements than previous algorithms. Results of sample calculations and timing comparisons are included. Author

N83-17769*# General Electric Co., Philadelphia, Pa. Space Systems Div.
CUSTOMER PREMISE SERVICE STUDY FOR 30/20 GHZ SATELLITE SYSTEM Final Report
R. T. MILTON, D. P. ROSS, A. R. HARCAR, P. FREEDENBERG (M/A COM, Inc.), and D. SCHOEN (M/A COM, Inc.) Jan. 1983 594 p refs
(Contract NAS3-22890)
(NASA-CR-167986; NAS 1.26:167986; GE-83SDS4206) Avail: NTIS HC A25/MF A01 CSCL 17B

Satellite systems in which the space segment operates in the 30/20 GHz frequency band are defined and compared as to their potential for providing various types of communications services to customer premises and the economic and technical feasibility of doing so. Technical tasks performed include: market postulation, definition of the ground segment, definition of the space segment, definition of the integrated satellite system, service costs for satellite systems, sensitivity analysis, and critical technology. Based on an analysis of market data, a sufficiently large market for services is projected so as to make the system economically viable. A large market, and hence a high capacity satellite system, is found to be necessary to minimize service costs, i.e., economy of scale is found to hold. The wide bandwidth expected to be available

in the 30/20 GHz band, along with frequency reuse which further increases the effective system bandwidth, makes possible the high capacity system. Extensive ground networking is required in most systems to both connect users into the system and to interconnect Earth stations to provide spatial diversity. Earth station spatial diversity is found to be a cost effective means of compensating the large fading encountered in the 30/20 GHz operating band. S.L.

N83-21207*# Communications Satellite Corp., Clarksburg, Md.
PLANNING ASSISTANCE FOR THE NASA 30/20 GHZ PROGRAM. NETWORK CONTROL ARCHITECTURE STUDY. Final Report, Mar. 1981 - Mar. 1983
T. INUKAI, B. BONNELYCKE, and S. STRICKLAND Mar. 1982 240 p refs
(Contract NAS3-22905)
(NASA-CR-168058; NAS 1.26:168058; REPT-110-5) Avail: NTIS HC A11/MF A01 CSCL 17B

Network Control Architecture for a 30/20 GHz flight experiment system operating in the Time Division Multiple Access (TDMA) was studied. Architecture development, identification of processing functions, and performance requirements for the Master Control Station (MCS), diversity trunking stations, and Customer Premises Service (CPS) stations are covered. Preliminary hardware and software processing requirements as well as budgetary cost estimates for the network control system are given. For the trunking system control, areas covered include on board SS-TDMA switch organization, frame structure, acquisition and synchronization, channel assignment, fade detection and adaptive power control, on board oscillator control, and terrestrial network timing. For the CPS control, they include on board processing and adaptive forward error correction control. Author

N83-21218*# Deutsche Forschungs- und Versuchsanstalt fuer Luft- und Raumfahrt, Berlin (West Germany). Abteilung Turbulenzforschung.
EXCITED WAVES IN SHEAR LAYERS
D. W. BECHERT Apr. 1982 151 p refs
(Contract NAG3-1981; DFG-BE-889/1-1)
(DFVLR-FB-82-23) Avail: NTIS HC A08/MF A01

The generation of instability waves in free shear layers is investigated. The model assumes an infinitesimally thin shear layer shed from a semi-infinite plate which is exposed to sound excitation. The acoustical shear layer excitation by a source further away from the plate edge in the downstream direction is very weak while upstream from the plate edge the excitation is relatively efficient. A special solution is given for the source at the plate edge. The theory is then extended to two streams on both sides of the shear layer having different velocities and densities. Furthermore, the excitation of a shear layer in a channel is calculated. A reference quantity is found for the magnitude of the excited instability waves. For a comparison with measurements, numerical computations of the velocity field outside the shear layer were carried out. M.G.

N83-22493*# City Coll. of the City Univ. of New York. Communications Systems Lab.
COMPUTER SIMULATOR FOR A MOBILE TELEPHONE SYSTEM Progress Report, 21 Apr. 1982 - 25 Jan. 1983
D. L. SCHILLING and C. ZIEGLER 12 Apr. 1983 97 p refs
(Contract NAG3-277)
(NASA-CR-170181; NAS 1.26:170181) Avail: NTIS HC A05/MF A01 CSCL 17B

A software simulator was developed to help in the design of the LMSS. The simulator is used to study the characteristics and implementation requirements of the LMSS' configuration. S.L.

N83-22494*# Ohio State Univ., Columbus. Dept. of Electrical Engineering.
ENGINEERING CALCULATIONS FOR COMMUNICATIONS SYSTEMS PLANNING Summary Report, 20 Jan. 1981 - 15 Jul. 1982
C. A. LEVIS, C. H. MARTIN, C. W. WANG, and D. GONSALVEZ Mar. 1982 70 p refs
(Contract NAG3-159)
(NASA-CR-170182; NAS 1.26:170182; ESL-713533-2; SR-1)
Avail: NTIS HC A04/MF A01 CSCL 17B

The single entry interference problem is treated for frequency sharing between the broadcasting satellite and intersatellite services near 23 GHz. It is recommended that very long (more than 120 longitude difference) intersatellite hops be relegated to the unshared portion of the band. When this is done, it is found that suitable orbit assignments can be determined easily with the aid of a set of universal curves. An attempt to develop synthesis procedures for optimally assigning frequencies and orbital slots for the broadcasting satellite service in region 2 was initiated. Several discrete programming and continuous optimization techniques are discussed. S.L.

N83-22495*# Harris Corp., Melbourne, Fla. Government Electronic Systems Div.
PHASED ARRAY-FED ANTENNA CONFIGURATION STUDY: TECHNOLOGY ASSESSMENT
W. F. CROSWELL, D. E. BALL, and R. C. TAYLOR Apr. 1983 141 p refs
(Contract NAS3-23252)
(NASA-CR-168078; NAS 1.26:168078) Avail: NTIS HC A07/MF A01 CSCL 20N

Spacecraft array fed reflector antenna systems were assessed for particular application to a multiple fixed spot beam/multiple scanning spot beam system. Reflector optics systems are reviewed in addition to an investigation of the feasibility of the use of monolithic microwave integrated circuit power amplifiers and phase shifters in each element of the array feed. S.L.

N83-23497*# TRW, Inc., Redondo Beach, Calif.
REQUIREMENTS FOR A MOBILE COMMUNICATIONS SATELLITE SYSTEM. VOLUME 1: EXECUTIVE SUMMARY Final Report, 15 Dec. 1981 - 31 Mar. 1983
11 Apr. 1983 50 p refs 2 Vol.
(Contract NAS3-23257)
(NASA-CR-168128; NAS 1.26:168128) Avail: NTIS HC A03/MF A01 CSCL 17B

Three types of satellite-aided mobile communications are considered for users in areas not served by (terrestrial) cellular radio systems. In System 1, mobile units are provided a direct satellite link to a gateway station, which serves as the interface to the terrestrial toll network. In System 2, a terrestrial radio link similar to those in cellular systems connects the mobile unit to a translator station; each translator relays the traffic from mobile units in its vicinity, via satellite, to the regional gateway. It is not feasible for System 2 to provide ubiquitous coverage. Therefore, System 3 is introduced, in which the small percentage of users not within range of a translator are provided a direct satellite link as in System 1. While System 2 can operate with leased satellite capacity, Systems 1 and 3 require a dedicated satellite. A major portion of this study is concerned with the design of a satellite for System 1. A weight limit of 10,000 lbs, corresponding to the projected 1990 STS capability, is imposed on the design. Frequency re-use of the allocated spectrum, through multiple satellite beams, is employed to generate the specified system capacity. Both offset-fed and center-fed reflectors are considered. For an assumed 10-MHz allocation and a population of 350,000 subscribers, a two-satellite system is required. The reflector diameters corresponding to offset-fed and center-fed geometries are 46 m and 62 m, respectively. Thus, large-space-structure technology is inherent to the implementation of System 1. In addition to establishing the technical requirements for the three types of satellite systems, the monthly service charge needed to provide a

specified return on invested capital is computed. A net present value analysis is used for this purpose. Author

N83-23498*# TRW, Inc., Redondo Beach, Calif.
REQUIREMENTS FOR A MOBILE COMMUNICATIONS SATELLITE SYSTEM. VOLUME 2: TECHNICAL REPORT Final Report, 15 Dec. 1981 - 31 Mar. 1983
M. HORSTEIN 11 Apr. 1983 382 p refs 2 Vol.
(Contract NAS3-23257)
(NASA-CR-168129; NAS 1.26:168129) Avail: NTIS HC A17/MF A01 CSCL 17B

Three types of satellite aided mobile communications are considered for users in areas not served by (terrestrial) cellular radio systems. In system 1, mobile units are provided a direct satellite link to a gateway station, which serves as the interface to the terrestrial toll network. In system 2, a terrestrial radio link similar to those in cellular systems connects the mobile unit to a translator station; each translator relays the traffic from mobile units in its vicinity, via satellite, to the regional gateway. It is not feasible for system 2 to provide obiquitous coverage. Therefore, system 3 is introduced, in which the small percentage of users not within range of a translator are provided a direct satellite link as in system 1. Author

N83-27086*# Harris Corp., Melbourne, Fla. Government Electronic Systems Div.
PHASED ARRAY-FED ANTENNA CONFIGURATION STUDY Final Report
W. F. CROSSWELL, D. E. BALL, and R. C. TAYLOR Apr. 1983 163 p refs
(Contract NAS3-23252)
(NASA-CR-168077; NAS 1.26:168077) Avail: NTIS HC A08/MF A01 CSCL 20N

The scope of this contract entails a configuration study for a phased array fed transmit antenna operating in the frequency band of 17.7 to 20.2 GHz. This initial contract provides a basis for understanding the design limitations and advantages of advanced phased array and cluster feeds (both utilizing intergral MMIC modules) illuminating folded reflector optics (both near field and focused types). Design parametric analyses are performed utilizing as constraints the objective secondary performance requirements of the Advanced Communications Technology Satellite (Table 1.0). The output of the study provides design information which serves as a data base for future active phased array fed antenna studies such as detailed designs required to support the development of a ground tested breadboard. In general, this study is significant because it provides the antenna community with an understanding of the basic principles which govern near field phased scanned feed effects on secondary reflector system performance. Although several articles have been written on analysis procedures and results for these systems, the authors of this report have observed phenomenon of near field antenna systems not previously documented. Because the physical justification for the exhibited performance is provided herein, the findings of this study add a new dimension to the available knowledge of the subject matter. Author

N83-28295*# National Aeronautics and Space Administration. Lewis Research Center, Cleveland, Ohio.
SPACE POWER TUBES - VERY MUCH ALIVE
H. G. KOSMAHL 1983 13 p Presented at CECON '83, Cleveland, 4-6 Oct. 1983; sponsored by the Inst. of Electrical and Electronics Engineers, Inc. and at the IEEE 1982 Intern. Electron Devices Meeting, San Franciso, 13-15 Dec. 1982
(NASA-TM-83425; E-1714; NAS 1.15:83425) Avail: NTIS HC A02/MF A01 CSCL 17B

The application of the traveling wave tubes (TWT), the backbone of all civilian and military space communication programs, to past, present and future satellites is discussed. Performance characteristics and the trends and challenges in the future are reviewed. Finally, a comparison with Solid State devices, as derived from fundamental laws, is made and limitations discussed. Author

N83-28297*# Ecosystems International, Inc., Gambrills, Md.
NON-URBAN MOBILE RADIO MARKET DEMAND FORECAST Final Report
P. A. CASTRUCCIO and J. COOPER 25 Jun. 1982 112 p
(Contract NAS3-23244)
(NASA-CR-168065; NAS 1.26:168065) Avail: NTIS HC A07/MF A01 CSCL 17B

A national nonmetropolitan land mobile traffic model for 1990-2000 addresses user classes, density classes, traffic mix statistics, distance distribution, geographic distribution, price elasticity, and service quality elasticity. Traffic demands for business, special industrial, and police were determined on the basis of surveys in 73 randomly selected nonurban counties. The selected services represent 69% of total demand. The results were extrapolated to all services in the non-SMSA areas of the contiguous United States. Radiotelephone services were considered separately. Total non-SMSA mobile radio demand (one way) estimates are given. General functional requirements include: hand portability, privacy, reduction of blind spots, two way data transmission, position location, slow scan imagery. S.L.

N83-29492*# Ford Aerospace and Communications Corp., Palo Alto, Calif. Western Development Labs. Div.
SPACECRAFT IF SWITCH MATRIX FOR WIDEBAND SERVICE APPLICATIONS IN 30/20 GHZ COMMUNICATIONS SATELLITE SYSTEMS: PROOF-OF-CONCEPT MODEL, EXECUTIVE SUMMARY Final Report
P. T. HO, E. COBAN, and J. PELOSE 1 Jul. 1983 337 p
(Contract NAS3-22501)
(NASA-CR-168175; NAS 1.26:168175) Avail: NTIS HC A15/MF A01 CSCL 17B

The design and development of a unique coupler crossbar 20 x 20 microwave switch matrix are described. The test results of the proof of concept model that meets the requirements for a high speed satellite switched, time division multiple access (SS-TDMA) system are presented. Author

N83-29493*# National Aeronautics and Space Administration. Lewis Research Center, Cleveland, Ohio.
CAPABILITIES, LIMITATIONS, AND USE OF BC SAT-R2 CONFERENCE SOFTWARE
E. F. MILLER 1983 9 p Presented at the BC SAT-R2 Seminar, Lima, 18-22 Apr. 1983; sponsored by the International Frequency Registration Board (IFRB)
(NASA-TM-83383; E-1656; NAS 1.15:83383) Avail: NTIS HC A02/MF A01 CSCL 09B

The computer software developed for the BC SAT-R2 Conference has certain capabilities and limitations which are described. Capabilities of each major program element are addressed with respect to providing the required functions for planning and output reporting. Limitations arise from the inability to exactly represent certain systems that may be examined. Expected use of the software package during the Conference is outlined. Author

N83-30832*# National Aeronautics and Space Administration. Lewis Research Center, Cleveland, Ohio.
METHOD FOR TERMINAL POSITION DETERMINATION IN EARTH TERMINAL-TO-SATELLITE BURST ACQUISITION AND SYNCHRONIZATION Patent Application
R. E. HAY and D. J. SABOURIN, inventors (to NASA) 11 Jun. 1982 24 p
(NASA-CASE-LEW-13893-1; US-PATENT-APPL-SN-387622)
Avail: NTIS HC A02/MF A01 CSCL 17B

A method is presented for determining positions of Earth stations in a satellite switched time-division multiple access communication system having a means for measuring transmission delays. The position of the Earth terminal is triangulated using transmission delay data obtained from message alignment at three or more positions in a satellite's orbit for which coordinates are known. NASA

N83-31925*# American Telephone and Telegraph Co., New York.
CUSTOMER PREMISES SERVICES MARKET DEMAND ASSESSMENT 1980 - 2000. VOLUME 1: EXECUTIVE SUMMARY
R. B. GAMBLE, L. SAPORTA (Data Industries Corp.), and G. A. HEIDENRICH May 1983 33 p
(Contract NAS3-22893)
(NASA-CR-168150; NAS 1.26:168150) Avail: NTIS HC A03/MF A01 CSCL 17B

Estimates of market demand for domestic civilian telecommunications services for the years 1980 to 2000 are provided. Overall demand, demand or satellite services, demand for satellite delivered Customer Premises Service (CPS), and demand for 30/20 GHz Customer Premises Services are covered. Emphasis is placed on the CPS market and demand is segmented by market, by service, by user class and by geographic region. Prices for competing services are discussed and the distribution of traffic with respect to distance is estimated. A nationwide traffic distribution model for CPS in terms of demand for CPS traffic and earth stations for each of the major SMSAs in the United States are provided. Author

N83-31926*# International Telephone and Telegraph Corp., Secaucus, N.J.
CUSTOMER PREMISES SERVICES MARKET DEMAND ASSESSMENT 1980 - 2000: VOLUME 2 Final Report
R. B. GAMBLE, L. SAPORTA (Data Industries Corp.), and G. A. HEIDENRICH (INPUT) May 1983 362 p refs 2 Vol.
(Contract NAS3-22893)
(NASA-CR-168151; NAS 1.26:168151) Avail: NTIS HC A16/MF A01 CSCL 17B

Potential customer premises service (CPS), telecommunication services, potential CPS user classes, a primary research survey, comparative economics, market demand forcasts, distance distribution of traffic, segmentation of market demand, and a nationwide traffic distribution model are discussed. Author

N83-33010*# Western Union Telegraph Co., McLean, Va.
PLANNING ASSISTANCE FOR THE 30/20 GHZ PROGRAM, VOLUME 1 Final Report
G. AL-KINANI, M. FRANKFORT, D. KAUSHAL, R. MARKHAM, C. SIPERKO, and M. WALL Sep. 1981 272 p refs 3 Vol.
(Contract NAS3-22461)
(NASA-CR-165484-VOL-1; NAS 1.26:165484-VOL-1; WUT-3413-10-VOL-1) Avail: NTIS HC A12/MF A01 CSCL 20N

Functional requirements for the 30/20 GHz communication system, planning assistance for the 30/20 GHz program, and a review of specified conceptual designs and recommendations are provided. N.W.

N83-33011*# Western Union Telegraph Co., McLean, Va.
PLANNING ASSISTANCE FOR THE 30/20 GHZ PROGRAM, VOLUME 2 Final Report
G. AL-KINANI, M. FRANKFORT, D. KAUSHAL, R. MARKHAM, C. SIPERKO, and M. WALL Sep. 1981 191 p 3 Vol.
(Contract NAS3-22461)
(NASA-CR-165484-VOL-2; NAS 1.26:165484-VOL-2; WUT-3413-10-VOL-2) Avail: NTIS HC A09/MF A01 CSCL 20N

In the baseline concept development the communications payload on Flight 1 was specified to consist of on-board trunking and emergency communications systems (ECS). On Flight 2 the communications payloads consisted of trunking and CPS on-board systems, the CPS capability replacing the Flight 1 ECS. No restriction was placed on the launch vehicle size. Constraints placed on multiple concept development effort were that launch vehicle size for Concept 1 was restricted to SUSS-D and for Concept 2 a SUSS-A. The design concept development was based on satisfying the baseline requirements set forth in the SOW for a single demonstration flight system. Key constraints on contractors were cost and launch vehicle size. Five major areas of new technology development were reviewed: (1) 30 GHz low noise receivers; (2) 20 GHz Power Amplifiers; (3) SS-TDMA switch; (4) Baseband Processor; (5) Multibeam Antennas. Author

N83-33012*# Western Union Telegraph Co., McLean, Va.
PLANNING ASSISTANCE FOR THE 30/20 GHZ PROGRAM, VOLUME 3 Final Report
G. AL-KINANI, M. FRANKFORT, D. KAUSHAL, R. MARKHAM, C. SIPERKO, and M. WALL Sep. 1981 63 p 3 Vol.
(Contract NAS3-22461)
(NASA-CR-165484; NAS.1:26165484-VOL-3; WUT-3413-10-VOL-3) Avail: NTIS HC A04/MF A01 CSCL 20N

The three basic experiment categories and consolidated experiments proposed by members of the Carrier Working Group are defined by category and by carrier. The three experiment categories are: (1) Possible Service (PS); (2) Possible Service and Technology (PSAT); and (3) Possible Technology (PT). Under Task 9 Western Union provided review, recommendations and critique of the NASA generated Statement of Work (SOW) defining the technical requirements governing design, launch and operation of the 30/20 GHz experimental systems. Author

N83-34113*# Western Union Telegraph Co., McLean, Va. Government Systems Div.
SATELLITE PROVIDED FIXED COMMUNICATION SERVICES: A FORECAST OF POTENTIAL DOMESTIC DEMAND THROUGH THE YEAR 2000. VOLUME 1: EXECUTIVE SUMMARY Final Report
D. KRATOCHVIL, J. BOWYER, C. BHUSHAN, K. STEINNAGEL, D. KAUSHAL, and G. AL-KINANI Aug. 1983 41 p refs 3 Vol.
(Contract NAS3-22894)
(NASA-CR-168145; NAS 1.26:168145) Avail: NTIS HC A03/MF A01 CSCL 17B

Telecommunications service demand, net addressable forecast, capacity requirements, and satellite system market development are considered. Author

N83-34114*# Western Union Telegraph Co., McLean, Va. Government Services Div.
SATELLITE PROVIDED FIXED COMMUNICATIONS SERVICES: A FORECAST OF POTENTIAL DOMESTIC DEMAND THROUGH THE YEAR 2000: VOLUME 2: MAIN TEST Final Report
D. KRATOCHVIL, J. BOWYER, and C. BHUSHAN Aug. 1983 208 p refs 3 Vol.
(Contract NAS3-22894)
(NASA-CR-168146; NAS 1.26:168146) Avail: NTIS HC A10/MF A01 CSCL 17B

Potential satellite-provided fixed communications services, baseline forecasts, net long haul forecasts, cost analysis, net addressable forecasts, capacity requirements, and satellite system market development are considered. Author

N83-34115*# Western Union Telegraph Co., McLean, Va. Government Systems Div.
SATELLITE FIXED COMMUNICATIONS SERVICE: A FORECAST OF POTENTIAL DOMESTIC DEMAND THROUGH THE YEAR 2000. VOLUME 3: APPENDICES Final Report
D. KRATOCHVIL, J. BOWYER, and C. BHUSHAN 14 Sep. 1983 417 p refs 3 Vol.
(Contract NAS3-22894)
(NASA-CR-168147; NAS 1.26:168147) Avail: NTIS HC A18/MF A01 CSCL 17B

Voice applications, data applications, video applications, impacted baseline forecasts, market distribution model, net long haul forecasts, trunking earth station definition and costs, trunking space segment cost, trunking entrance/exit links, trunking network costs and crossover distances with terrestrial tariffs, net addressable forecasts, capacity requirements, improving spectrum utilization, satellite system market development, and the 30/20 net accessible market are considered. Author

N83-34116*# Western Union Telegraph Co., McLean, Va. Government Systems Div.
SATELLITE PROVIDED CUSTOMER PREMISES SERVICES: A FORECAST OF POTENTIAL DOMESTIC DEMAND THROUGH THE YEAR 2000. VOLUME: EXECUTIVE SUMMARY Final Report
D. KRATOCHVIL, J. BOWYER, C. BHUSHAN, K. STEINNAGEL, D. KAUSHAL, and G. AL-KINANI Aug. 1983 46 p refs 3 Vol.
(Contract NAS3-23255)
(NASA-CR-168142; NAS 1.26:168142) Avail: NTIS HC A03/MF A01 CSCL 17B

Development of a forecast of the total domestic telecommunications demand, identification of that portion of the telecommunications demand suitable for transmission by satellite systems, identification of that portion of the satellite market addressable by CPS systems, identification of that portion of the satellite market addressable by Ka-band CPS system, and postulation of a Ka-band CPS network on a nationwide and local level were achieved. The approach employed included the use of a variety of forecasting models, a parametric cost model, a market distribution model and a network optimization model. Forecasts were developed for: 1980, 1990, 2000; voice, data and video services; terrestrial and satellite delivery modes; and C, Ku and Ka-bands. Author

N83-34117*# Western Union Telegraph Co., McLean, Va. Government Systems Div.
SATELLITE PROVIDED CUSTOMER PREMISE SERVICES: A FORECAST OF POTENTIAL DOMESTIC DEMAND THROUGH THE YEAR 2000. VOLUME 2: TECHNICAL REPORT Final Report
Aug. 1983 315 p refs 3 Vol.
(Contract NAS3-23255)
(NASA-CR-168143; NAS 1.26:168143) Avail: NTIS HC A13/MF A01 CSCL 17B

The potential United States domestic telecommunications demand for satellite provided customer premises voice, data and video services through the year 2000 were forecast, so that this information on service demand would be available to aid in NASA program planning. To accomplish this overall purpose the following objectives were achieved: development of a forecast of the total domestic telecommunicatons demand, identification of that portion of the telecommunications demand suitable for transmission by satellite systems, identification of that portion of the satellite market addressable by Computer premises services systems, identification of that portion of the satellite market addressabble by Ka-band CPS system, and postulation of a Ka-band CPS network on a nationwide and local level. The approach employed included the use of a variety of forecasting models, a market distribution model and a network optimization model. Forecasts were developed for; 1980, 1990, and 2000; voice, data and video services; terrestrial and satellite delivery modes; and C, Ku and Ka-bands. Author

N83-34118*# Western Union Telegraph Co., McLean, Va. Governmet Systems Div.
SATELLITE PROVIDED CUSTOMER PREMISE SERVICES: A FORECAST OF POTENTIAL DOMESTIC DEMAND THROUGH THE YEAR 2000. VOLUME 3: APPENDICES Final Report
D. KRATOCHVIL, J. BOWYER, C. BRUSHAN, K. STEINNAGEL, D. KAUSHAL, and G. AL-KINANI Aug. 1983 675 p refs 3 Vol.
(Contract NAS3-23255)
(NASA-CR-168144; NAS 1.26:168144) Avail: NTIS HC A99/MF A01 CSCL 17B

Voice applications, data applications, video applications, impacted baseline forecasts, market distribution, potential CPS (customers premises services) user classes, net long haul forecasts, CPS cost analysis, overall satellite forecast, CPS satellite market, Ka-band CPS satellite forecast, nationwide traffic distribution model, and intra-urban topology are discussed. Author

N83-34119*# General Electric Co., Schenectady, N. Y. Corporate Research and Development.
MOBILE RADIO ALTERNATIVE SYSTEMS STUDY, EXECUTIVE SUMMARY Final Report
R. E. ANDERSON, N. CROMWELL, and H. L. LESTER Jun. 1983 41 p
(Contract NAS3-23244)
(NASA-CR-168207; NAS 1.26:168207; REPT-83SRD038) Avail: NTIS HC A03/MF A01 CSCL 17B

Present day mobile communication technologies, systems and equipment are described from background in evaluating the concepts generated in the study. Average propagation ranges are calculated for terrestrial installations in each of seven physiographic areas of the contiguous states to determine the number of installations that would be required for nationwide coverage. Four system concepts are defined and analyzed to determine how well terrestrial systems can fulfill the requirements at acceptable costs. Author

N83-34120*# National Aeronautics and Space Administration. Lewis Research Center, Cleveland, Ohio.
A COMPARISON OF FREQUENCY DOMAIN MULTIPLE ACCESS (FDMA) AND TIME DOMAIN MULTIPLE ACCESS (TDMA) APPROACHES TO SATELLITE SERVICE FOR LOW DATA RATE EARTH STATIONS
G. STEVENS Jun. 1983 54 p refs
(NASA-TM-83430; E-1721; NAS 1.15:83430) Avail: NTIS HC A04/MF A01 CSCL 17B

A technological and economic assessment is made of providing low data rate service to small earth stations by satellite at Ka-band. Various Frequency Domain Multiple Access (FDMA) and Time Domain Multiple Access (TDMA) scenarios are examined and compared on the basis of cost to the end user. Very small stations (1 to 2 meters in diameter) are found not to be viable alternatives to available terrestrial services. However, medium size (3 to 5 meters) earth stations appear to be very competitive if a minimum throughput of about 1.5 Mbs is maintained. This constrains the use of such terminals to large users and shared use by smaller users. No advantage was found to the use of FDMA. TDMA had a slight advantage from a total system viewpoint and a very significant advantage in the space segment (about 1/3 the required payload weight for an equivalent capacity). Author

N83-36299*# Virginia Univ., Charlottesville. Dept. of Electrical Engineering.
ADVANCED DIGITAL MODULATION: COMMUNICATION TECHNIQUES AND MONOLITHIC GAAS TECHNOLOGY
S. G. WILSON, J. D. OLIVER, JR., R. C. KOT, and C. R. RICHARDS Jul. 1983 94 p refs
(Contract NAG3-316)
(NASA-CR-174452; NAS 1.26:174452; UVA/528219/EE84/101)
Avail: NTIS HC A05/MF A01 CSCL 17B

Communications theory and practice are merged with state-of-the-art technology in IC fabrication, especially monolithic GaAs technology, to examine the general feasibility of a number of advanced technology digital transmission systems. Satellite-channel models with (1) superior throughput, perhaps 2 Gbps; (2) attractive weight and cost; and (3) high RF power and spectrum efficiency are discussed. Transmission techniques possessing reasonably simple architectures capable of monolithic fabrication at high speeds were surveyed. This included a review of amplitude/phase shift keying (APSK) techniques and the continuous-phase-modulation (CPM) methods, of which MSK represents the simplest case. N.W.

N83-36300*# Virginia Univ., Charlottesville. Communication Systems Lab.
FOUR-DIMENSIONAL MODULATION AND CODING: AN ALTERNATE TO FREQUENCY-REUSE Final Report
S. G. WILSON and H. A. SLEEPER Sep. 1983 60 p refs
(Contract NAG3-141)
(NASA-CR-174453; NAS 1.26:174453; UVA/528200/EE83/107)
Avail: NTIS HC A04/MF A01 CSCL 20N

Four dimensional modulation as a means of improving communication efficiency on the band-limited Gaussian channel, with the four dimensions of signal space constituted by phase orthogonal carriers (cos omega sub c t and sin omega sub c t) simultaneously on space orthogonal electromagnetic waves are discussed. 'Frequency reuse' techniques use such polarization orthogonality to reuse the same frequency slot, but the modulation is not treated as four dimensional, rather a product of two-d modulations, e.g. QPSK. It is well known that, higher dimensionality signalling affords possible improvements in the power bandwidth sense. Four-D modulations based upon subsets of lattice-packings in four-D, which afford simplification of encoding and decoding are described. Sets of up to 1024 signals are constructed in four-D, providing a (Nyquist) spectral efficiency of up to 10 bps/Hz. Energy gains over the reuse technique are in the one to three dB range t equal bandwidth. S.L.

33

ELECTRONICS AND ELECTRICAL ENGINEERING

Includes test equipment and maintainability; components, e.g., tunnel diodes and transistors; microminiaturization; and integrated circuitry.

A83-11002* Virginia Polytechnic Inst. and State Univ., Blacksburg.
INVESTIGATIONS OF STABILITY AND DYNAMIC PERFORMANCES OF SWITCHING REGULATORS EMPLOYING CURRENT-INJECTED CONTROL
F. C. LEE and R. A. CARTER (Virginia Polytechnic Institute and State University, Blacksburg, VA) In: PESC '81; Power Electronics Specialists Conference, Boulder, CO, June 29-July 3, 1981, Record. New York, Institute of Electrical and Electronics Engineers, Inc., 1981, p. 3-16. refs
(Contract NAS3-21051)

The stability and dynamic performances of a buck/boost regulator employing a current-injected control are examined. Small-signal models for the power state, the multi-loop error processor and the duty-cycle pulse-modulator are developed. The error-processor model which incorporates the current-injected loop, the dc loop and the compensation network permits evaluation of the effects of each individual control loop and their combined efforts toward shaping the performance characteristics of the closed-loop system. Comparisons are made between this modeling approach and earlier approaches. Some important yet subtle dissimilarities are discussed. This model predicts the constant-frequency 50 percent duty-cycle instability which is inherent to the current-injected control. (Author)

A83-11011* Duke Univ., Durham, N. C.
PARAMETRIC STUDY OF MINIMUM REACTOR MASS IN ENERGY-STORAGE DC-TO-DC CONVERTERS
R. C. WONG, H. A. OWEN, JR., and T. G. WILSON (Duke University, Durham, NC) In: PESC '81; Power Electronics Specialists Conference, Boulder, CO, June 29-July 3, 1981, Record. New York, Institute of Electrical and Electronics Engineers, Inc., 1981, p. 99-111. refs
(Contract NSG-3157)

Closed-form analytical solutions for the design equations of a minimum-mass reactor for a two-winding voltage-or-current step-up converter are derived. A quantitative relationship between the three parameters - minimum total reactor mass, maximum output power, and switching frequency - is extracted from these analytical solutions. The validity of the closed-form solution is verified by a numerical minimization procedure. A computer-aided design procedure using commercially available toroidal cores and magnet wires is also used to examine how the results from practical designs follow the predictions of the analytical solutions. (Author)

A83-11016* Virginia Polytechnic Inst. and State Univ., Blacksburg.
NONLINEAR PROGRAM BASED OPTIMIZATION OF BOOST AND BUCK-BOOST CONVERTER DESIGNS
S. RAHMAN and F. C. LEE (Virginia Polytechnic Institute and State University, Blacksburg, VA) In: PESC '81; Power Electronics Specialists Conference, Boulder, CO, June 29-July 3, 1981, Record. New York, Institute of Electrical and Electronics Engineers, Inc., 1981, p. 180-191. refs
(Contract NAS3-21051)

The facility of an Augmented Lagrangian (ALAG) multiplier based nonlinear programming technique is demonstrated for minimum-weight design optimizations of boost and buck-boost power converters. Certain important features of ALAG are presented in the framework of a comprehensive design example for buck-boost power converter design optimization. The study provides refreshing design insight of power converters and presents such information as weight and loss profiles of various semiconductor components and magnetics as a function of the switching frequency. (Author)

A83-11484*# General Electric Co., Philadelphia, Pa.
DEVELOPMENT OF A MICROWAVE 20 X 20 SWITCH MATRIX FOR 30/20 GHZ SS-TDMA APPLICATION
B. J. CORY, M. BERKOWITZ, R. WALLIS, A. SCHIAVONE, D. SHIEH, and J. CAMPBELL (General Electric Co., Valley Forge Space Center, Philadelphia, PA) Institute of Electrical and Electronics Engineers, National Telecommunication Conference, Galveston, TX, Nov. 7-10, 1982, Paper. 5 p.
(Contract NAS3-22500)

The design and fabrication of a 3-8 GHz, 20 x 20 Satellite Switched-Time Division Multiple Access IF switch matrix applicable to a 30/20 GHz communications satellite are described. An assessment of switch architecture in 1980 concluded that the GaAs FET-based coupled crossbar switch matrix, incorporating high speed CMOS LSI logic for switch crosspoint addressing, would be the optimum technology available for communications satellite switching by 1982. This assessment was based on such factors as switching speed, bandwidth, off-state isolation, and reliability, over a 10-year mission life. A proof-of-concept model's construction and testing are presented. O.C.

A83-11488*# General Electric Co., Schenectady, N. Y.
TRANSISTORIZED PWM INVERTER-INDUCTION MOTOR DRIVE SYSTEM
S. C. PEAK and A. B. PLUNKETT (General Electric Co., Schenectady, NY) Institute of Electrical and Electronics Engineers, Annual Meeting, San Francisco, CA, Oct. 4-8, 1982, Paper. 7 p. Research supported by the U.S. Department of Energy refs
(Contract DEN3-59)

This paper describes the development of a transistorized PWM inverter-induction motor traction drive system. A vehicle performance analysis was performed to establish the vehicle tractive effort-speed requirements. These requirements were then converted into a set of inverter and motor specifications. The inverter was a transistorized three-phase bridge using General Electric power Darlington transistors. The description of the design and development of this inverter is the principal object of this paper. The high-speed induction motor is a design which is optimized for use with an inverter power source. The primary feedback control is a torque angle control with voltage and torque outer loop controls. A current-controlled PWM technique is used to control the motor voltage. The drive has a constant torque output with PWM operation to base motor speed and a constant horsepower output with square wave operation to maximum speed.

The drive system was dynamometer tested and the results are presented. (Author)

A83-11489*# TRW, Inc., Redondo Beach, Calif.
A 1 WATT GAAS POWER AMPLIFIER FOR THE NASA 30/20 GHZ COMMUNICATION SYSTEM
J. GOEL, G. ORANSKY, S. YUAN, P. OSULLIVAN, and J. BURCH (TRW, Inc., Advanced Microwave Technology Dept., Redondo Beach, CA) Institute of Electrical and Electronics Engineers, International Microwave Symposium, Dallas, TX, June 15-17, 1982, Paper. 12 p. refs
(Contract NAS3-22503)

A multistage GaAs FET power amplifier, employing cascaded balanced stages using state-of-the-art 1/4, 1/2, and 1 watt devices, has been developed. A linear gain of 30 dB with 1.25 watts output has been achieved over a 17.7 to 19.4 GHz frequency band. The development and performance of the amplifier and its components are discussed. (Author)

A83-11494*# Virginia Polytechnic Inst. and State Univ., Blacksburg.
A NOVEL INPUT FILTER COMPENSATION SCHEME FOR SWITCHING REGULATORS
S. S. KELKAR and F. C. LEE (Virginia Polytechnic Institute and State University, Blacksburg, VA) Institute of Electrical and Electronics Engineers, Power Electronics Specialists Conference, Cambridge, MA, June 14-17, 1982, Paper. 12 p. refs
(Contract NAG3-81)

A novel input-filter compensation scheme is proposed which uses feedforward loops to cancel the effects of peaking of the output impedance of the input filter, such that the converter is immune from performance degradation due to loop gain reduction. The scheme makes it possible to concurrently implement a high-performance converter and an effective input filter design with minimum weight and loss. A buck regulator with continuous current conduction is used as an example, and an analysis followed by a design procedure for the feedforward loops is presented. V.L.

A83-11495*# Virginia Polytechnic Inst. and State Univ., Blacksburg.
AN IMPROVED SWITCHING CONVERTER MODEL USING DISCRETE AND AVERAGE TECHNIQUES
D. J. SHORTT and F. C. LEE (Virginia Polytechnic Institute and State University, Blacksburg, VA) Institute of Electrical and Electronics Engineers, Power Electronics Specialists Conference, Boston, MA, June 14-17, 1982, Paper. 14 p. refs
(Contract NSG-3274)

The nonlinear modeling and analysis of dc-dc converters has been done by averaging and discrete-sampling techniques. The averaging technique is simple, but inaccurate as the modulation frequencies approach the theoretical limit of one-half the switching frequency. The discrete technique is accurate even at high frequencies, but is very complex and cumbersome. An improved model is developed by combining the aforementioned techniques. This new model is easy to implement in circuit and state variable forms and is accurate to the theoretical limit. (Author)

A83-16095* Nebraska Univ., Lincoln.
METALLIC CONDUCTIVITY AND AIR STABILITY IN COPPER CHLORIDE INTERCALATED CARBON FIBERS
H. OSHIMA, J. A. WOOLLAM (Nebraska, University, Lincoln, NE), and A. YAVROUIAN (California Institute of Technology, Jet Propulsion Laboratory, Pasadena, CA) Journal of Applied Physics, vol. 53, Dec. 1982, p. 9220-9223. refs
(Contract NAG3-95)

Carbon-copper chloride intercalation compounds have been obtained by using variously graphitized carbon fibers as host materials. The resultant conductors are air stable, thermally stable to 450 K, have electrical resistivities as low as 12.9 microohm cm at room temperature, and have metallic conductivity temperature dependencies. These intercalated fibers have tensile strengths of 160000 psi, and Young's moduli of 25 x 10 to the 6th psi. For aerospace use, 1/(resistivity x density) is a figure of merit. On this basis, a reduction in resistivity by a factor of two will make this conductor competitive with copper. (Author)

A83-19032* Virginia Polytechnic Inst. and State Univ., Blacksburg.
COMPUTER SIMULATIONS OF OPTIMUM BOOST AND BUCK-BOOST CONVERTERS
S. RAHMAN (Virginia Polytechnic Institute and State University, Blacksburg, VA) IEEE Transactions on Aerospace and Electronic Systems, vol. AES-18, Sept. 1982, p. 598-608. refs
(Contract NAS3-21051)

The development of mathematicl models suitable for minimum weight boost and buck-boost converter designs are presented. The facility of an augumented Lagrangian (ALAG) multiplier-based nonlinear programming technique is demonstrated for minimum weight design optimizations of boost and buck-boost power converters. ALAG-based computer simulation results for those two minimum weight designs are discussed. Certain important features of ALAG are presented in the framework of a comprehensive design example for boost and buck-boost power converter design optimization. The study provides refreshing design insight of power converters and presents such information as weight annd loss profiles of various semiconductor components and magnetics as a function of the switching frequency. (Author)

A83-19754* Motorola, Inc., Scottsdale, Ariz.
A LOW-POWER, HIGH-THROUGHPUT MAXIMUM-LIKELIHOOD CONVOLUTIONAL DECODER CHIP FOR NASA'S 30/20 GHZ PROGRAM
R. D. MCCALLISTER and J. J. CRAWFORD (Motorola, Inc., Government Electronics Div., Scottsdale, AZ) In: NTC '81; National Telecommunications Conference, New Orleans, LA, November 29-December 3, 1981, Record. Volume 3. New York, Institute of Electrical and Electronics Engineers, Inc., 1981, p. E1.1.1-E1.1.5.
(Contract NAS3-22502)

It is pointed out that the NASA 30/20 GHz program will place in geosynchronous orbit a technically advanced communication satellite which can process time-division multiple access (TDMA) information bursts with a data throughput in excess of 4 GBPS. To guarantee acceptable data quality during periods of signal attenuation it will be necessary to provide a significant forward error correction (FEC) capability. Convolutional decoding (utilizing the maximum-likelihood techniques) was identified as the most attractive FEC strategy. Design trade-offs regarding a maximum-likelihood convolutional decoder (MCD) in a single-chip CMOS implementation are discussed. G.R.

A83-19789* Motorola, Inc., Scottsdale, Ariz.
ADVANCES IN SERIAL MSK MODEMS
C. R. RYAN (Motorola, Inc., Governmental Electronics Div., Scottsdale, AZ) In: NTC '81; National Telecommunications Conference, New Orleans, LA, November 29-December 3, 1981, Record. Volume 4. New York, Institute of Electrical and Electronics Engineers, Inc., 1981, p. G3.6.1-G3.6.5. refs
(Contract NAS3-22502)

Lumped element as well as distributed element networks are used in the Serial MSK (SMSK) modems, for 20-1000 Mbps data rate range applications, whose design and performance characteristics are described. It is noted that the use of baseband conversion filters for the modulator yields good performance in many applications, with typical matched filter designs (structurally simple to implement) causing less than 0.5 dB bit error rate performance degradation. The SMSK modem technique begins with the use of a biphased shift-keyed modulator, and then employs passive filters to obtain the MSK signal. O.C.

A83-24035*# National Aeronautics and Space Administration. Lewis Research Center, Cleveland, Ohio.
MODERN MULTISTAGE DEPRESSED COLLECTORS - A REVIEW
H. G. KOSMAHL (NASA, Lewis Research Center, Cleveland, OH) IEEE Proceedings, vol. 70, Nov. 1982, p. 1325-1334. refs

The design and performance of the Lewis Research Center (LeRC) electrostatic collector and the associated passive permanent magnetic beam reconditioning (refocusing) are discussed and compared with numerous experimental results on wide- and narrow-band TWT and two klystron cases. Universal designs for efficient collectors for TV klystrons are presented. Collectors other than those based on the symmetric LeRC concept are reviewed only briefly, either because they have not been treated analytically or because only sporadic or incomplete experimental evaluation results are available. It is concluded that significant, a priori predictable performance improvements for TWTs have been demonstrated and that a substantial reduction in the dc power input to TV klystron transmitters could be effected by using well-designed multistage depressed collectors. C.R.

A83-28160* National Aeronautics and Space Administration. Lewis Research Center, Cleveland, Ohio.
TUBES IN SPACE - VERY MUCH ALIVE
H. G. KOSMAHL (NASA, Lewis Research Center, Microwave Amplifier Section, Cleveland, OH) Microwaves & RF, vol. 22, Mar. 1983, p. 107-109.

Some advantages of TWTs over SSDs are discussed. Wideband TWTs have been developed which can produce 20 W of RF power at 20 GHz with 40 percent efficiency, a figure three or four times that available from SSDs such as FETs. The basic performance of TWTs exceeds that of SSDs for any given bandwidth and frequency. SSDs are transit time limited, and their performance deteriorates fundamentally as the reciprocal of the square of the operating frequency. Power limits for SSDs have been reached or are quickly being approached. Free electron devices such as tubes have an efficiency advantage because electrons in the vacuum travel faster than bulk charges in SSDs. Combined SSD devices are prone to burnout and incur penalties due to the need to dissipate heat. TWTs have a 6.7:1 advantage in radiator area ratio. Recent progress in TWT technology has produced a tenfold increase in CW output power, doubled to quadrupled the efficiency, and pushed frequency ranges into the tetrahertz region, orders of magnitude beyond the SSD cutoff. C.D.

A83-33133* Virginia Polytechnic Inst. and State Univ., Blacksburg.
A NOVEL FEEDFORWARD COMPENSATION CANCELING INPUT FILTER-REGULATOR INTERACTION
S. S. KELKAR and F. C. LEE (Virginia Polytechnic Institute and State University, Blacksburg, VA) IEEE Transactions on Aerospace and Electronic Systems (ISSN 0018-9251), vol. AES-19, March 1983, p. 258-268. refs
(Contract NAG3-81)

The interaction between the input and the control loop of switching regulators often results in deterimental effects, such as loop instability, degradation of transient response, and audiosusceptibility, etc. The concept of pole-zero cancelation is employed to mitigate some of these detrimental effects and is implemented using a novel feedforward loop, in addition to existing feedback loops of a buck regulator. Experimental results are presented which show excellent correlation with theory. Author

A83-33846* Texas Instruments, Inc., Dallas.
HIGH-PERFORMANCE K-BAND GAAS POWER FIELD-EFFECT TRANSISTORS PREPARED BY MOLECULAR BEAM EPITAXY
P. SAUNIER and H. D. SHIH (Texas Instruments Central Research Laboratories, Dallas, TX) Applied Physics Letters (ISSN 0003-6951), vol. 42, June 1, 1983, p. 966-968. refs
(Contract NAS3-22886)

The maturity of the molecular beam epitaxy (MBE) technique for preparing device quality GaAs material for microwave applications is demonstrated by the excellent performance characteristics of K-band GaAs power field-effect transistors (FETs) fabricated on the MBE wafers. An output power of 710 mW with 4.5-dB gain and 17.7 percent power-added efficiency was achieved at 21 GHz with a 1.26-mm gate width pi-gate device. A similar device with a 0.56-mm gate width produced an output power of 320 mW with 5.0-dB gain and 26.6 percent power-added efficiency at 21 GHz. These are the best results yet reported to date for GaAs power FETs operated in the K-band frequency range. Author

A83-36479* Texas Instruments, Inc., Dallas.
GAAS INTEGRATED DIGITAL-TO-ANALOGUE CONVERTOR FOR CONTROL OF POWER DUAL-GATE FETS
P. SAUNIER, B. KIM, and W. R. FRENSLEY (Texas Instruments, Inc., Dallas, TX) Electronics Letters (ISSN 0013-5194), vol. 19, March 3, 1983, p. 162, 163.
(Contract NAS3-22886)

The design, fabrication and performance of a TTL compatible 4-bit GaAs integrated digital-to-analog convertor with an output voltage between -2.8 V and +2.8 V are reported. This circuit has been especially designed to control the gain of power dual-gate FETs by applying a voltage on the capacitively terminated second gate. Author

A83-38216* Beers Associates, Inc., Reston, Va.
THERMAL DIELECTRIC BREAKDOWN WITH CYLINDRICAL ELECTRODES
B. L. BEERS (Beers Associates, Reston, VA) and J. J. ODWYER (New York, State University, Oswego, NY) Journal of Applied Physics (ISSN 0021-8979), vol. 54, July 1983, p. 4083-4086.
(Contract NAS3-22530)

Solutions to the equations of thermal breakdown are computed for cylindrial electrodes with different boundary conditions. The development of the electric field and the temperature distributions are followed as functions of time, consequent on the application of a constant interelectrode voltage. The implications for possible breakdown by modes other than thermal are briefly discussed. Author

A83-39272*# Rockwell International Corp., Thousand Oaks, Calif.
A TWO-STAGE MONOLITHIC BUFFER AMPLIFIER FOR 20 GHZ SATELLITE COMMUNICATION
W. C. PETERSEN and A. K. GUPTA (Rockwell International Microelectronics Research and Development Center, Thousand Oaks, CA) Institute of Electrical and Electronics Engineers, Microwave and Millimeter-Wave Monolithic Circuits Symposium, Boston, MA, May 31, 1983, Paper. 3 p.
(Contract NAS3-23247)

Design, fabrication, and test results of a two-stage GaAs monolithic buffer amplifier for 20 GHz satellite communication are described in this paper. A gain of 13 + or - 0.75 dB from 17.7 to 20.2 GHz was obtained from the 1.5 x 1.5 millimeter chip, which includes all necessary bias and dc blocking circuitry. Author

A83-39273*# Michigan Univ., Ann Arbor.
IMAGE-OPTIMIZED, FREQUENCY-SCALABLE MIXERS FOR MILLIMETER-WAVE APPLICATIONS
D. F. PETERSON (Michigan, University, Ann Arbor, MI) and D. H. STEINBRECHER (Steinbrecher Corp., Woburn, MA) Institute of Electrical and Electronics Engineers, International Microwave Symposium, Boston, MA, June 1-3, 1983, Paper. 4 p.
(Contract NAS3-22493)

A unique IF measurement procedure for evaluating mixer performance and identifying optimum circuit boundary conditions is presented. The technique is applied to a scalable mm-wave single-sideband (image-sum enhanced) mixer design which provides 3.5 to 5 dB typical conversion loss from conventional, packaged devices. Author

A83-41152* Toledo Univ., Ohio.
TRANSFORMER INDUCED INSTABILITY OF THE SERIES RESONANT CONVERTER
R. J. KING (Toledo, University, Toledo, OH) and T. A. STUART IEEE Transactions on Aerospace and Electronic Systems (ISSN 0018-9251), vol. 19, May 1983, p. 474-482. refs
(Contract NSG-3281)

It is shown that the common series resonant power converter is subject to a low frequency oscillation that can lead to the loss of cyclic stability. This oscillation is caused by a low frequency resonant circuit formed by the normal L and C components in series with the magnetizing inductance of the output transformer. Three methods for eliminating this oscillation are presented and analyzed. One of these methods requires a change in the circuit topology during the resonance cycle. This requires a new set of steady state equations which are derived and presented in a normalized form. Experimental results are included which demonstrate the nature of the low frequency oscillation before cyclic stability is lost. Author

A83-41369* Ford Aerospace and Communications Corp., Palo Alto, Calif.
20 X 20 IF SWITCH MATRIX FOR SS-TDMA SYSTEMS
P. T. HO, J. H. WISNIEWSKI, J. R. PELOSE, N. CHIANG, E. COBAN, E. BALDERRAMA, and J. LEGG (Ford Aerospace and Communications Corp., Western Development Laboratories Div., Palo Alto, CA) IN: ICC '82 - The digital revolution; International Conference on Communications, Philadelphia, PA, June 13-17, 1982, Conference Record. Volume 2 . New York, Institute of Electrical and Electronics Engineers, 1982, p. 3A.4.1-3A.4.5. refs
(Contract NAS3-22501)

Satellite-switched TDMA, an effective means for the increasing of communication satellite channel capacity and the improvement of system flexibility, requires that the spacecraft carry an IF switch matrix in order to provide interconnectivity among multiple beam antennas. Attention is presently given to the development of a 20 x 20 IF switch matrix for the NASA 30/20 GHz communications satellite which will provide a 2.5 GHz bandwidth at C-band frequencies with a switching speed of 10 nsec. Switch matrix architecture, switching device characteristic, and distribution control unit design practices are discussed, together with switch matrix reliability. O.C.

A83-44970* Texas Instruments, Inc., Dallas.
EQUIVALENT-CIRCUIT CONSIDERATION OF DUAL-GATE MESFETS AT HIGH FREQUENCY
B. KIM (Texas Instruments, Inc., Central Research Laboratories, Dallas, TX) Electronics Letters (ISSN 0013-5194), vol. 19, Aug. 18, 1983, p. 705, 706. refs
(Contract NAS3-22886)

The simplified high-frequency equivalent circuit of a dual-gate FET is described. It is shown that the input impedance is similar to that of a single-gate FET but the output resistance and capacitance (parallel equivalent circuit) are higher. The output resistance and the transconductance decrease as frequency increases. The unilateral gain of a dual-gate FET rolls off 12 dB/octave. Author

N83-10348*# AiResearch Mfg. Co., Torrance, Calif.
A LIGHTWEIGHT ELECTRONICALLY COMMUTATED DC MOTOR FOR ELECTRIC PASSENGER VEHICLES Final Report
E. F. ECHOLDS and P. S. WALLA 1 Sep. 1982 96 p refs
(Contract DEN3-64; DE-AI01-77CS-51044)
(NASA-CR-165601; NAS 1.26:165601; AMC-81-18266) Avail: NTIS HC A05/MF A01 CSCL 09A

A functional model breadboard converter and a rare-earth-cobalt, permanent magnet motor; as well as an engineering model converter and PM motor suitable for vehicle installations were developed and tested. The converter and motor achieved an 88% peak efficiency, a maximum output of 26 kW at 26,000 rpm, and a continuous rating of 15 kW. The system also generated power to the source during braking, with a demonstrated peak power available at the converter terminals of approximately 26 kW at 88% efficiency. Major conclusions include: (1) the SAE J227a(D) driving cycle efficiency for the converter/motor is 86% to 88% when energy available for recovery at the converter terminals is included; (2) the converter initial cost is approximately five times that of the permanent magnet motor, but can be reduced by means of LSI logic and integrated liquid cooled semiconductor packages; and (3) an electronically commutated motor with a liquid cooled converter will operate reliably without service or maintenance for the life of a passenger vehicle. A.R.H.

N83-10349*# General Electric Co., Schenectady, N. Y. Power Electronics Lab.
IMPROVED TRANSISTORIZED AC MOTOR CONTROLLER FOR BATTERY POWERED URBAN ELECTRIC PASSENGER VEHICLES Final Report
S. C. PEAK Sep. 1982 242 p refs
(Contract DEN3-59; DE-AI01-77CS-51044)
(NASA-CR-167978; DOE/NASA/0059-82/1; NAS 1.26:167978; SRD-81-088) Avail: NTIS HC A11/MF A01 CSCL 09C

An ac motor controller for an induction motor electric vehicle drive system was designed, fabricated, tested, evaluated, and cost analyzed. A vehicle performance analysis was done to establish the vehicle tractive effort-speed requirements. These requirements were then converted into a set of ac motor and ac controller requirements. The power inverter is a three-phase bridge using power Darlington transistors. The induction motor was optimized for use with an inverter power source. The drive system has a constant torque output to base motor speed and a constant horsepower output to maximum speed. A gear shifting transmission is not required. The ac controller was scaled from the base 20 hp (41 hp peak) at 108 volts dec to an expanded horsepower and battery voltage range. Motor reversal was accomplished by electronic reversal of the inverter phase sequence. The ac controller can also be used as a boost chopper battery charger. The drive system was tested on a dynamometer and results are presented. The current-controlled pulse width modulation control scheme yielded improved motor current waveforms. The ac controller favors a higher system voltage. A.R.H.

N83-11446*# National Aeronautics and Space Administration. Lewis Research Center, Cleveland, Ohio.
ADVANCES IN CORE LOSS CALCULATIONS FOR MAGNETIC MATERIALS
J. E. TRINER 1982 33 p refs Presented at the Fall Meeting of the Am. Ceram. Soc., Cambridge, Mass., 12-15 Sep. 1982
(NASA-TM-82947; E-1353; NAS 1.15:82947) Avail: NTIS HC A03/MF A01 CSCL 09C

A new analytical technique which predicts the basic magnetic properties under various operating conditions encountered in state-of-the-art dc-ac/dc converters is discussed. Using a new flux-controlled core excitation circuit, magnetic core characteristics were developed for constant values of ramp flux (square wave voltage excitation) and frequency. From this empirical data, a mathematical loss characteristics equation is developed to analytically predict the specific core loss of several magnetic materials under various waveform excitation conditions. In addition, these characteristics show the circuit designer for the first time the direct functional relatonships between induction level and specific core loss as a function of the two key dc-dc converter operating parameters of input voltage and duty cycle. R.J.F.

N83-11447*# National Aeronautics and Space Administration. Lewis Research Center, Cleveland, Ohio.
SPACE TUBES: A MAJOR CHALLENGE
H. KOSMAHL 1982 12 p Proposed for presentation at the Intern. Electron Devices Meeting, San Francisco, 13-15 Dec. 1982; sponsored by IEEE
(NASA-TM-82971; E-1397; NAS 1.15:82971) Avail: NTIS HC A02/MF A01 CSCL 09C

The application of the TWT - the backbone of all civilian and military space communication programs - to past, present and

future satellites is discussed. Performance characteristics and the trends and challenges in the future are reviewed. Finally, a comparison with Solid States devices, as derived from fundamental laws, is made and limitations discussed. Author

N83-12329*# Dayton Univ., Ohio. School of Engineering.
TESTING OF THE PERMANENT MAGNET MATERIAL MN-AL-C FOR POTENTIAL USE IN PROPULSION MOTORS FOR ELECTRIC VEHICLES
Z. A. ABDELNOUR, H. F. MILDRUM, and K. J. STRNAT 12 Nov. 1980 107 p refs
(Contract DEN3-189)
(NASA-CR-169481; NAS 1.26:169481) Avail: NTIS HC A06/MF A01 CSCL 09C

The development of Mn-Al-C permanent magnets is reviewed. The general properties of the material are discussed and put into perspective relative to alnicos and ferrites. The commercial material now available is described by the manufacturer's data. The traction motor designer's demands of a permanent magnet for potential use in electric vehicle drives are reviewed. From this, a list of the needed specific information is extracted. A plan for experimental work is made which would generate this information, or verify data supplied by the producer. The results of these measurements are presented in the form of tables and graphs. The tests determined magnetic design data and some mechanical strength properties. Easy axis hysteresis and demagnetization curves, recoil loops and other minor loop fields were measured over a temperature range from -50 C to +150 C. Hysteresis loops were also measured for three orthogonal directions (the easy and 2 hard axes of magnetization). S.L.

N83-12330*# Varian Associates, Palo Alto, Calif. Microwave Tube Div.
DESIGN CONCEPTS FOR A HIGH-IMPEDANCE NARROW-BAND 42 GHZ POWER TWT USING A FUNDAMENTAL/FORWARD LADDER-BASED CIRCUIT Final Report
A. KARP Aug. 1980 79 p refs
(Contract NAS3-21930)
(NASA-CR-165282; NAS 1.26:165282; JO-19128) Avail: NTIS HC A05/MF A01 CSCL 09A

A low-cost, narrowband, millimeter wave space communications TWT design was studied. Cold test interaction structure scale models were investigated and analyses were undertaken to predict the electrical and thermal response of the hypothetical 200 W TWT at 42 GHz and 21 kV beam voltage. An intentionally narrow instantaneous bandwidth (1%, with the possibility of electronic tuning of the center frequency over several percent) was sought with a highly dispersive, high impedance 'forward wave' interaction structure based on a ladder (for economy in fabrication) and nonspace harmonic interaction, for a high gain rate and a short, economically focused tube. The 'TunneLadder' interaction structure devised combines ladder properties with accommodation for a pencil beam. Except for the impedance and bandwidth, there is much in common with the millimeter wave helix TWTs which provided the ideal of diamond support rods. The benefits of these are enhanced in the TunneLadder case because of spatial separation of beam interception and RF current heating. S.L.

N83-13359*# Pittsburgh Univ., Pa.
LOSSES IN CHOPPER-CONTROLLED DC SERIES MOTORS Final Report
H. B. HAMILTON Apr. 1982 127 p refs
(Contract NSG-3163; DE-AI01-77CS-51044)
(NASA-CR-167845; DOE/NASA/3163-1; NAS 1.26:167845)
Avail: NTIS HC A07/MF A01 CSCL 09C

Motors for electric vehicle (EV) applications must have different features than dc motors designed for industrial applications. The EV motor application is characterized by the following requirements: (1) the need for highest possible efficiency from light load to overload, for maximum EV range, (2) large short time overload capability (The ratio of peak to average power varies from 5/1 in heavy city traffic to 3/1 in suburban driving situations) and (3) operation from power supply voltage levels of 84 to 144 volts (probably 120 volts maximum). A test facility utilizing a dc generator as a substitute for a battery pack was designed and utilized. Criteria for the design of such a facility are presented. Two motors, differing in design detail, commercially available for EV use were tested. Losses measured are discussed, as are waves forms and their harmonic content, the measurements of resistance and inductance, EV motor/chopper application criteria, and motor design considerations. S.L.

N83-14397*# National Aeronautics and Space Administration. Lewis Research Center, Cleveland, Ohio.
HIGH SPEED COMPUTERIZED DATA ACQUISITION OF PHOTOVOLTAIC V-I CHARACTERISTICS Final Report
R. DELOMBARD and R. C. CULL Nov. 1982 23 p
(Contract DE-AI01-79ET-20485)
(NASA-TM-82967; E-1387; NAS 1.15:82967;
DOE/NASA/20485-12) Avail: NTIS HC A02/MF A01 CSCL 09C

The voltage current (5-1) characteristics of the photovoltaic array were studied under actual environmental conditions. A method of data acquisition was devised that uses a capacitor charge technique to obtain the 5-1 characteristic and a computerized data system to display, record and process the data. The capacitor charge technique uses an array shorting transistor and a capacitor bank to sweep the array operating voltage and current from short circuit to open circuit in a specified time (approximately 125 ms). The computerized data system is synchronized with this transition and repetitively samples the array voltage and current during the transition and records the ambient conditions. This data is then normalized by the computer to standard conditions (100 mW/sq cm, 28 C) and is available in tabular and graphic form for both the voltage current and voltage power characteristics. The capacitor charge technique is described. S.L.

N83-14398*# Virginia Polytechnic Inst. and State Univ., Blacksburg. Dept. of Electrical Engineering.
AN IMPROVED SWITCHING CONVERTER MODEL Ph.D. Thesis. Final Report
D. J. SHORTT Nov. 1982 286 p refs
(Contract NSG-3274)
(NASA-CR-169669; NAS 1.26:169669) Avail: NTIS HC A13/MF A01 CSCL 09C

The nonlinear modeling and analysis of dc-dc converters in the continuous mode and discontinuous mode was done by averaging and discrete sampling techniques. A model was developed by combining these two techniques. This model, the discrete average model, accurately predicts the envelope of the output voltage and is easy to implement in circuit and state variable forms. The proposed model is shown to be dependent on the type of duty cycle control. The proper selection of the power stage model, between average and discrete average, is largely a function of the error processor in the feedback loop. The accuracy of the measurement data taken by a conventional technique is affected by the conditions at which the data is collected. S.L.

N83-14399*# National Aeronautics and Space Administration. Lewis Research Center, Cleveland, Ohio.
DESIGN OF A MULTISTAGE DEPRESSED COLLECTOR FOR THE F-16 RADAR DUAL MODE TRANSMITTER TUBE
J. A. DAYTON, JR. Nov. 1982 18 p refs
(NASA-TM-82982; E-1413; NAS 1.15:82982) Avail: NTIS HC A02/MF A01 CSCL 09C

The design of a multistage depressed collector (MDC) for use with the F-16 radar dual mode transmitter tube is described. The methods employed and the rationale on which the design is based are presented. E.A.K.

N83-16628*# General Electric Co., Schenectady, N. Y. Power Electronics Lab.

ADVANCED AC PERMANENT MAGNET AXIAL FLUX DISC MOTOR FOR ELECTRIC PASSENGER VEHICLE Final Report

G. B. KLIMAN Oct. 1982 227 p refs

(Contract DEN3-76; DE-AI01-77CS-51044)

(NASA-CR-167975; DOE/NASA/0076-82/1; NAS 1.26:167975; SRD-81-097) Avail: NTIS HC A11/MF A01 CSCL 09C

An ac permanent magnet axial flux disc motor was developed to operate with a thyristor load commutated inverter as part of an electric vehicle drive system. The motor was required to deliver 29.8 kW (40 hp) peak and 10.4 kW (14 hp) average with a maximum speed of 11,000 rpm. It was also required to run at leading power factor to commutate the inverter. Three motors were built.

Author

N83-16630*# General Electric Co., Philadelphia, Pa. Space Div.

DESIGN STUDY OF A HIGH POWER ROTARY TRANSFORMER

S. M. WEINBERGER Jul. 1982 59 p refs

(Contract NAS3-23155)

(NASA-CR-168012; NAS 1.26:168012; GE-82SDS4222) Avail: NTIS HC A04/MF A01 CSCL 09C

A design study was made on a rotary transformer for transferring electrical power across a rotating spacecraft interface. The analysis was performed for a 100 KW, 20 KHz unit having a "pancake" geometry. The rotary transformer had a radial (vertical) gap and consisted of 4-25 KW modules. It was assumed that the power conditioning comprised of a Schwarz resonant circuit with a 20 KHz switching frequency. The rotary transformer, mechanical and structural design, heat rejection system and drive mechanism which provide a complete power transfer device were examined. The rotary transformer losses, efficiency, weight and size were compared with an axial (axial symmetric) gap transformer having the same performance requirements and input characteristics which was designed as part of a previous program. The "pancake" geometry results in a heavier rotary transformer primarily because of inefficient use of the core material. It is shown that the radial gap rotary transformer is a feasible approach for the transfer of electrical power across a rotating interface and can be implemented using presently available technology. Author

N83-17802*# National Aeronautics and Space Administration. Lewis Research Center, Cleveland, Ohio.

DIELECTRIC BASED SUBMILLIMETER BACKWARD WAVE OSCILLATOR CIRCUIT Patent Application

H. G. KOSMAHL, inventor (to NASA) 13 Oct. 1982 9 p

(NASA-CASE-LEW-13736-1; US-PATENT-APPL-SN-434084)

Avail: NTIS HC A02/MF A01 CSCL 09C

A ladder circuit especially useful in backward wave oscillators operating in the 500 GHz to 2000 GHz range has a waveguide with transversely orientated slabs which contact an upper wall of the waveguide. The edges of the slabs adjacent to the physical center of waveguide curved segments and stubs of electrically conductive, nonmagnetic material. The ends of slabs include metal layers at opposite ends to provide a conductive leakage path. A ridge bar is attached to the inside of the bottom wall of the waveguide and includes a concave upper surface which partially straddles the electron beam. The novelty of the invention lies in the ladder structure compared of thin, vapor deposited rungs supported on the edge of diamond slabs; each rung having a curved segment which straddles the electron beam together with a ridge bar which also straddles the electron beam. NASA

N83-18997*# SRI International Corp., Menlo Park, Calif. Engineering Sciences Lab.

DEVELOPMENT PROGRAM ON A SPINDT COLD-CATHODE ELECTRON GUN Final Report

C. A. SPINDT Nov. 1982 51 p refs

(Contract NAS3-22469; SRI PROJ 2590)

(NASA-CR-168055; NAS 1.26:168055) Avail: NTIS HC A04/MF A01 CSCL 09A

A thin film field emission cathode (TFFEC) array and a cold cathode electron gun based on the emitter were developed. A microwave tube gun that uses the thin film field emission cathode as an electron source is produced. State-of-the-art cathodes were fabricated and tested. The tip-packing density of the arrays were increased thereby increasing the cathode's current density capability. The TFFEC is based on the well known field emission effect and was conceived to exploit the advantages of that phenomenon while minimizing the difficulties associated with conventional field emission structures, e.g. limited life and high voltage requirements. Field emission follows the Fowler-Nordheim equation. S.L

N83-21028*# Duke Univ., Durham, N. C. Dept. of Electrical Engineering.

HIGH-FREQUENCY HIGH-VOLTAGE HIGH-POWER DC-TO-DC CONVERTERS

T. G. WILSON, H. A. OWEN, and P. M. WILSON *In* ESA 4th ESTEC Spacecraft Power-Conditioning Seminar p 167-173 Sep. 1982 refs Presented at US-Japan Cooperative Sci. Sem. on Anal. and Design in Power Electron. 1981, Kobe, Japan, Nov. 1981

(Contract NSG-3157)

Avail: NTIS HC A09/MF A01

A simple analysis of the current and voltage waveshapes associated with the power transistor and the power diode in an example current-or-voltage step-up (buck-boost) converter is presented. The purpose of the analysis is to provide an overview of the problems and design trade-offs which must be addressed as high-power high-voltage converters are operated at switching frequencies in the range of 100 kHz and beyond. Although the analysis focuses on the current-or-voltage step-up converter as the vehicle for discussion, the basic principles presented are applicable to other converter topologies as well. Author

N83-21236*# Westinghouse Electric Corp., Lima, Ohio. Electrical Systems Div.

KILOVOLT DC SOLID STATE REMOTE POWER CONTROLLER DEVELOPMENT Final Report

J. T. MITCHELL Oct. 1982 169 p

(Contract NAS3-22646)

(NASA-CR-168041; NAS 1.26:168041; WES/DL-82-07E) Avail: NTIS HC A08/MF A01 CSCL 09C

The experience gained in developing and applying solid state power controller (SSPC) technology at high voltage dc (HVDC) potentials and power levels of up to 25 kilowatts is summarized. The HVDC switching devices, power switching concepts, drive circuits, and very fast acting overcurrent protection circuits were analyzed. A 25A bipolar breadboard with Darlington connected switching transistor was built. Fault testing at 900 volts was included. A bipolar transistor packaged breadboard design was developed. Power MOSFET remote power controller (RPC) was designed. Author

N83-24764*# National Aeronautics and Space Administration. Lewis Research Center, Cleveland, Ohio.

ADVANCED ELECTRICAL POWER SYSTEM TECHNOLOGY FOR THE ALL ELECTRIC AIRCRAFT

R. C. FINKE and G. R. SUNDBERG 1983 15 p refs Presented at the 35th Ann. Natl. Aerospace and Electron. Conf. (NAECON '83), Dayton, Ohio, 17-19 May 1983

(NASA-TM-83390; E-1667; NAS 1.15:83390) Avail: NTIS HC A02/MF A01 CSCL 09C

The application of advanced electric power system technology to an all electric airplane results in an estimated reduction of the

total takeoff gross weight of over 23,000 pounds for a large airplane. This will result in a 5 to 10 percent reduction in direct operating costs (DOC). Critical to this savings is the basic electrical power system component technology. These advanced electrical power components will provide a solid foundation for the materials, devices, circuits, and subsystems needed to satisfy the unique requirements of advanced all electric aircraft power systems. The program for the development of advanced electrical power component technology is described. The program is divided into five generic areas: semiconductor devices (transistors, thyristors, and diodes); conductors (materials and transmission lines); dielectrics; magnetic devices; and load management devices. Examples of progress in each of the five areas are discussed. Bipolar power transistors up to 1000 V at 100 A with a gain of 10 and a 0.5 microsec rise and fall time are presented. A class of semiconductor devices with a possibility of switching up to 100 kV is described. Solid state power controllers for load management at 120 to 1000 V and power levels to 25 kW were developed along with a 25 kW, 20 kHz transformer weighing only 3.2 kg. S.L.

N83-25982*# National Aeronautics and Space Administration. Lewis Research Center, Cleveland, Ohio.
NEW PROPULSION COMPONENTS FOR ELECTRIC VEHICLES
R. R. SECUNDE 1982 19 p refs Presented at the 18th Intersoc. Energy Conversion Engr. Conf., Orlando, Fla., 21-26 Aug. 1983
(Contract DE-AI01-77CS-51044)
(NASA-TM-83404; E-1682; NAS 1.15:83404; DOE/NASA/51044-31) Avail: NTIS HC A02/MF A01 CSCL 09C

Improved component technology is described. This includes electronically commutated permanent magnet motors of both drum and disk configurations, an unconventional brush commutated motor, ac induction motors, various controllers, transmissions and complete systems. One or more of these approaches to electric vehicle propulsion may eventually dispslace presently used controllers and brush commutated dc motors. S.L.

N83-25983*# National Aeronautics and Space Administration. Lewis Research Center, Cleveland, Ohio.
INELASTIC TUNNEL DIODES Patent Application
L. M. ANDERSON, inventor (to NASA) 19 Apr. 1983 13 p
(NASA-CASE-LEW-13833-1; US-PATENT-APPL-SN-486471)
Avail: NTIS HC A02/MF A01 CSCL 09A

Power is extracted from plasmons, photons, or other guided electromagnetic waves at infrared to mid-ultraviolet frequencies by inelastic tunneling in metal-insulator-semiconductor-metal diodes. Inealstic tunneling produces power by absorbing plasmons to pump electrons to higher potential. Specifically, an electron from a semiconductor layer absorbs a plasmon and simultaneously tunnels across an insulator into a metal layer which is at higher potential. The diode voltage determines the fraction of energy extracted from the plasmons; any excess is lost to heat. NASA

N83-25984*# National Aeronautics and Space Administration. Lewis Research Center, Cleveland, Ohio.
A LINEARIZED TRAVELING WAVE AMPLIFIER WITH HARD LIMITER CHARACTERISTICS Patent Application
H. G. KOSMAHL, inventor (to NASA) 9 May 1983 13 p
(NASA-CASE-LEW-13981-1; US-PATENT-APPL-SN-492522)
Avail: NTIS HC A02/MF A01 CSCL 09A

A traveling wave tube with increased linearity to avoid intermodulation of signals being amplified is described. A traveling electromagnetic wave and an electron beam interact to effect amplification of a radio frequency signal. L.F.M.

N83-25985*# National Aeronautics and Space Administration. Lewis Research Center, Cleveland, Ohio.
EXPERIMENTAL VERIFICATION OF THE MULTISTAGE DEPRESSED COLLECTOR DESIGN PROCEDURE FOR A HIGH-PERVEANCE, HELIX-TYPE, TRAVELING-WAVE TUBE
J. A. DAYTON, JR., H. G. KOSMAHL, and P. RAMINS May 1983 24 p refs
(NASA-TP-2162; E-1362; NAS 1.60:2162) Avail: NTIS HC A02/MF A01 CSCL 09A

The validity of a computational procedure for the design of multistage depressed collectors (MDC's) is demonstrated for a traveling wave tube (TWT) with a perveance of .00000123. The MDC is used with spent-beam refocusing to improve substantially the efficiency of the TWT. Reports on this subject have verified, under a variety of operating conditions, the MDC design procedure for TWT's with lower perveance. The design procedure is based on two computer programs that create a mathematical model of the electric and magnetic fields of the TWT refocuser MDC system and its electron beam. The two principal outputs of the analysis are a description of the radiofrequency (RF) performance of the TWT and the trajectories of representatives groups of charges from the input of the TWT to their points of interception on the MDC electrodes. S.L.

N83-27127*# Maxwell Labs., Inc., San Diego, Calif.
HIGH FREQUENCY, HIGH POWER CAPACITOR DEVELOPMENT Final Report
C. W. WHITE and P. S. HOFFMAN 10 Mar. 1983 89 p
(Contract NAS3-22668)
(NASA-CR-168035; NAS 1.26:168035; MLR-1430) Avail: NTIS HC A05/MF A01 CSCL 09A

A program to develop a special high energy density, high power transfer capacitor to operate at frequency of 40 kHz, 600 V rms at 125 A rms plus 600 V dc bias for space operation. The program included material evaluation and selection, a capacitor design was prepared, a thermal analysis performed on the design. Fifty capacitors were manufactured for testing at 10 kHz and 40 kHz for 50 hours at Industrial Electric Heating Co. of Columbus, Ohio. The vacuum endurance test used on environmental chamber and temperature plate furnished by Maxwell. The capacitors were energized with a special power conditioning apparatus developed by Industrial Electric Heating Co. Temperature conditions of the capacitors were monitored by IEHCo test equipment. Successful completion of the vacuum endurance test series confirmed achievement of the main goal of producing a capacitor or reliable operation at high frequency in an environment normally not hospitable to electrical and electronic components. The capacitor developed compared to a typical commercial capacitor at the 40 kHz level represents a decrease in size and weight by a factor of seven. Author

N83-29596*# Thermal Technology Labs., Buffalo, N. Y.
DESIGN AND DEVELOPMENT OF MULTI-KW POWER ELECTRONIC TRANSFORMERS Final Report
J. P. WELSH Feb. 1983 20 p refs
(Contract NAS3-21948)
(NASA-CR-168082; NAS 1.26:168082; TTL-83-1) Avail: NTIS HC A02/MF A01 CSCL 09C

A technology for conduction cooled transformers having low internal thermal resistance was developed. To demonstrate this technology a lightweight 25-KVA, 20 kHz, high efficiency, high frequency power transformer was designed and fabricated. The weight of the transformer was 6.95 pounds, the efficiency was 99.2% and the maximum temperature rise in the windings was 43C. S.L.

N83-29597*# National Aeronautics and Space Administration. Lewis Research Center, Cleveland, Ohio.
DESIGN OF A HIGH-SPEED DIGITAL PROCESSING ELEMENT FOR PARALLEL SIMULATION
E. J. MILNER and D. S. CWYNAR Jun. 1983 24 p refs
(NASA-TM-83373; E-1641; NAS 1.15:83373) Avail: NTIS HC A02/MF A01 CSCL 09C

A prototype of a custom designed computer to be used as a processing element in a multiprocessor based jet engine simulator is described. The purpose of the custom design was to give the computer the speed and versatility required to simulate a jet engine in real time. Real time simulations are needed for closed loop testing of digital electronic engine controls. The prototype computer has a microcycle time of 133 nanoseconds. This speed was achieved by: prefetching the next instruction while the current one is executing, transporting data using high speed data busses, and using state of the art components such as a very large scale integration (VLSI) multiplier. Included are discussions of processing element requirements, design philosophy, the architecture of the custom designed processing element, the comprehensive instruction set, the diagnostic support software, and the development status of the custom design. Author

N83-30914*# Westinghouse Electric Corp., Pittsburgh, Pa.
ADVANCED AXIAL FIELD D.C. MOTOR DEVELOPMENT FOR ELECTRIC PASSENGER VEHICLE Final Report
W. J. JONES Dec. 1982 125 p
(Contract DEN3-75; DE-AI01-77CS-51044)
(NASA-CR-167985; DOE/NASA/0075-82/1; NAS 1.26:167985; REPT-83-8J22-EVMOT-R1) Avail: NTIS HC A06/MF A01 CSCL 13F

A wound-field axial-flux dc motor was developed for an electric vehicle drive system. The motor is essentially an axial-flux version of the classical Gramme-ring winding motor, but the active conductors are recessed into slots cut into the two opposite faces of the laminated tape-wound core ring. Three motors were built and tested in the program. The second (functional) model was a six-pole machine which weighed 88.5 kg. It developed 16.9 km (33.0 hp), and a max speed of 4800 rpm. Full load efficiency was 92% and predicted SAE D-cycle efficiency was 88%. The last engineering) model was a 4-pole machine with compoles, allowing a weight reduction to 45 kg (100 lbs.) while addressing some manufacturability problems. The engineering model was rated at 13.2 kw (17.6 hp) at 3000 rpm, with a peak power of 19.8 km (26.4 hp) and a max speed of 7200 rpm. Initial test results on this motor showed poor commutation and efficiency; the program was terminated without resolution of these problems. Author

N83-30915*# Levi (Enrico), Inc., Forest Hills, N.Y.
PRELIMINARY ASSESSMENT OF THE TRADEOFFS BETWEEN THE ELECTRIC MOTOR AND THE TRANSMISSION IN ELECTRIC VEHICLES Final Report
E. LEVI May 1983 63 p refs
(Contract DE-AI01-77CS-51044; NASA ORDER C-41981-D)
(NASA-CR-168199; DOE/NASA/1981-1; NAS 1.26:168199)
Avail: NTIS HC A04/MF A01 CSCL 13F

The efficiency, weight, and cost of various propulsion system for 4-passenger electric vehicles are compared. These systems comprise the electric motor and the required speed reducing transmission to obtain the appropriate speed at the wheel. Three types of motors, dc synchronous, and squirrel-cage were considered at 6000 ycm and 24 000 rpm for a peak power of 40 kW. Two types of gearing selected were a single speed differential and a differential with a differential with a 4-speed gearbox. Only components that were readily realizable within present state-of-the-art were considered. Author

N83-31952* National Aeronautics and Space Administration. Lewis Research Center, Cleveland, Ohio.
GYROTRON TRANSMITTING TUBE Patent
H. G. KOSMAHL, inventor (to NASA) 26 Jul. 1983 4 p Filed 24 Dec. 1980 Supersedes N81-16384 (19 - 07 p 0907)
(NASA-CASE-LEW-13429-1; US-PATENT-4,395,656; US-PATENT-APPL-SN-220212; US-PATENT-CLASS-315-4; US-PATENT-CLASS-315-3; US-PATENT-CLASS-315-5; US-PATENT-CLASS-315-5.35; US-PATENT-CLASS-315-5.38)
Avail: US Patent and Trademark Office CSCL 09A

An RF transmitting tube for the 20 GHz to 500 GHz range comprises a gyrotron and a multistage depressed collector. A winding provides a magnetic field which acts on spent, spinning or orbiting electrons changing their motion to substantially forward linear motion in a downstream direction. The spent electrons then pass through a focusser into the collector. Nearly all of the electrons injected into the collector will remain within an imaginary envelope as they travel forward toward the end collector plate. The apertures in the collector plates are at least as large in diameter as the envelope at any particular axial position.
Official Gazette of the U.S. Patent and Trademark Office

N83-34192*# National Aeronautics and Space Administration. Lewis Research Center, Cleveland, Ohio.
A MATHEMATICAL MODEL FOR THE DOUBLY FED WOUND ROTOR GENERATOR
F. J. BRADY 1983 8 p refs Presented at the Power Eng. Soc. Conf., Los Angeles, 17-22 Jul. 1983; sponsored by IEEE
(Contract DE-AI01-76ET-20320)
(NASA-TM-83454; E-1008-1; DOE/NASA/20320-48; NAS 1.15:83454) Avail: NTIS HC A02/MF A01 CSCL 09C

A mathematical analysis of a doubly-fed wound rotor machine used as a constant frequency generator is presented. The purpose of this analysis is to derive a consistent set of circuit equations which produce constant stator frequency and constant stator voltage. Starting with instantaneous circuit equations, the necessary rotor voltages and currents are derived. The model, thus obtained, is assumed to be valid, since the resulting relationships between mechanical power and active volt-amperes agrees with the results of others. In addition, the model allows for a new interpretation of the power flow in the doubly-fed generator. M.G.

N83-35261*# National Aeronautics and Space Administration. Lewis Research Center, Cleveland, Ohio.
TEST METHODS AND RESULTS OF THE 10-CELL BIPOLAR NI-H2 BATTERY
R. CATALDO *In* NASA. Goddard Space Flight Center The 1982 Goddard Space Flight Center Battery Workshop p 496-500 Aug. 1983
Avail: NTIS HC A23/MF A01 CSCL 10C

Characterization tests were carried out at three charge levels and four discharge levels. The 'c' or capacity of the battery is designated at 6.5 ampere-hours. The recharge ampere-hours was the same for all test conditions, 6.5 A-H, regardless of the discharge capacity removed for any particular discharge rate. Less capacity can be removed at higher discharge rates to the same termination voltage, which was 0.50 volts for the weakest (lowest voltage) cell. The general trend of efficiencies increases as the charge rate increases as noted in results of the table included in the handout package. The data also indicate the efficiency increases as the discharge rate decreases. This is true; however, efficiencies at the discharge rates of c and 2c are penalized because these cycles received more overcharge than necessary. Author

N83-36358*# City Coll. of the City Univ. of New York. Communications Systems Lab.
VLSI TECHNOLOGY AND APPLICATIONS Final Report, 25 Jun. 1982 - 24 Jun. 1983
D. L. SCHILLING 1983 90 p refs
(Contract NAG3-299)
(NASA-CR-174451; NAS 1.26:174451) Avail: NTIS HC A05/MF A01 CSCL 09C

Metal oxide semiconductor and GaAs devices are discussed. Digital and analog circuits are described. Applications to communications circuits are presented. Author

N83-36359*# EIC, Inc., Newton, Mass.
MODERATE TEMPERATURE RECHARGEABLE SODIUM BATTERIES Final Report, Oct. 1978 - Jan. 1983
K. M. ABRAHAM, M. W. RUPICH, L. PITTS, and J. E. ELLIOTT Jul. 1983 120 p refs
(Contract NAS3-21726)
(NASA-CR-168220; NAS 1.26:168220) Avail: NTIS HC A06/MF A01 CSCL 10C

Cells utilizing the organic electrolyte, NaI in triglyme, operated at approx. 130 C with Na(+) - intercalating cathodes. However, their rate and stability were inadequate. NaAlCl4 was found to be a highly useful electrolyte for cell operation at 165-190 C. Na(+) intercalating chalcogenides reacted with NaAlCl4 during cycling to form stable phases. Thus, VS2 became essentially VS2Cl, with reversible capacity of approx 2.8 e(-)/V, and a mid-discharge voltage of approx 2.5V and 100 deep discharge cycles were readily achieved. A positive electrode consisting of VCl3 and S plus NaAlCl4 was subjected to deep-discharge cycles 300 times and it demonstrated identity with the in-situ-formed BSxCly cathode. NiS2 and NiS which are not Na(+)-intercalating structures formed highly reversible electrodes in NaAlCl4. The indicated discharge mechanism implies a theoretical capacity 4e(-)/Ni for NiS2 and 2e(-)/Ni for NiS. The mid-discharge potentials are, respectively, 2.4V and 2.1V. A Na/NiS2 cell cycling at a C/5 rate has exceeded 500 deep discharge cycles with 2.5e(-)/Ni average utilization. A 4 A-hr nominal capacity prototype Na/NiS2 cell was tested at 190 C. It was voluntarily terminated after 80 cycles. Further development, particularly of cathode structure and hardware should produce a battery capable of at least 50-W-hr/lb and more than 1000 cycles. Author

34

FLUID MECHANICS AND HEAT TRANSFER

Includes boundary layers; hydrodynamics; fluidics; mass transfer; and ablation cooling.

A83-10650*# Yale Univ., New Haven, Conn.
SMALL PARTICLE TRANSPORT ACROSS TURBULENT NONISOTHERMAL BOUNDARY LAYERS
D. E. ROSNER and J. FERNANDEZ DE LA MORA (Yale University, New Haven, CT) ASME, Transactions, Journal of Engineering for Power, vol. 104, Oct. 1982, p. 885-892; Discussion, p. 892-894; Author's Closure, p. 894. refs
(Contract F49620-76-C-0020; NAG3-201)

The interaction between turbulent diffusion, Brownian diffusion, and particle thermophoresis in the limit of vanishing particle inertial effects is quantitatively modeled for applications in gas turbines. The model is initiated with consideration of the particle phase mass conservation equation for a two-dimensional boundary layer, including the thermophoretic flux term directed toward the cold wall. A formalism of a turbulent flow near a flat plate in a heat transfer problem is adopted, and variable property effects are neglected. Attention is given to the limit of very large Schmidt numbers and the particle concentration depletion outside of the Brownian sublayer. It is concluded that, in the parameter range of interest, thermophoresis augments the high Schmidt number mass-transfer coefficient by a factor equal to the product of the outer sink and the thermophoretic suction. M.S.K.

A83-12795*# Iowa Univ., Iowa City.
FINITE ANALYTIC NUMERICAL SOLUTION OF AXISYMMETRIC NAVIER-STOKES AND ENERGY EQUATIONS
C.-J. CHEN and Y.-H. YOON (Iowa Institute of Hydraulic Research, Iowa City, IA) American Institute of Aeronautics and Astronautics and American Society of Mechanical Engineers, Joint Thermophysics, Fluids, Plasma and Heat Transfer Conference, 3rd, St. Louis, MO, June 7-11, 1982, ASME 12 p.
(Contract DE-AC02-79ER-10515; NSG-3305)
(ASME PAPER 82-HT-42)

Convective heat transfer for steady state laminar flow in axisymmetric coordinates is considered. Numerical solutions for flow pattern and temperature distribution are obtained by the finite analytic numerical method applied to the Navier-Stokes equations expressed in terms of vorticity and stream function, and the energy equation. The finite analytic numerical method differs from other numerical methods in that it utilizes a local analytic solution in an element of the problem to construct the total numerical solution. Finite analytic solutions of vorticity, stream function, temperature and heat transfer coefficients for flow with Reynolds number of 5.0, 100.0, 1000.0, and 2000.0, and Prandtl number of 0.1, 1.0, and 10.0 with uniform grid sizes are reported for axisymmetric pipe with sudden expansion and contraction. The wall temperature is considered to be isothermal and differs from the inlet temperature. It is shown that the finite analytic solution is stable, converges rapidly, and simulates the convection of fluid flow accurately since the local analytic solution is capable of simulating automatically the influence of skewed convection through the element boundary on the interior nodal values thereby minimizing the false numerical diffusion. (Author)

A83-13133*# Ohio State Univ., Columbus.
A SIMILARITY ANALYSIS OF THE DROPLET TRAJECTORY EQUATION
M. B. BRAGG (Ohio State University, Columbus, OH) AIAA Journal, vol. 20, Dec. 1982, p. 1681-1686. refs
(Contract NAG3-28)

A procedure is established to reduce the number of similarity parameters in the trajectory equation for particles in a moving fluid. This is accomplished by the use of an approximate sphere drag law to derive a new trajectory scaling parameter. The modified inertia parameter proposed by Langmuir specifically for the aircraft icing problem is analyzed and for the first time a closed-form solution is obtained. Both experimental and analytical results are presented to verify this new trajectory scaling parameter. (Author)

A83-13487*# National Aeronautics and Space Administration. Lewis Research Center, Cleveland, Ohio.
DETERMINATION OF BOUNDARY SHAPE OF COOLED POROUS REGION
A. SNYDER and R. SIEGEL (NASA, Lewis Research Center, Cleveland, OH) ASME, Transactions, Journal of Heat Transfer, vol. 104, Nov. 1982, p. 722-727. refs

The shape of a cooled porous wall section is found that will provide a uniform surface temperature, as dictated by material limitations, when the surface is subjected to spatially nonuniform heating. In the analysis, local temperatures and pressures in the porous material are expressed in terms of a potential function. From the imposed thermal conditions, this potential function is governed by the dual constraints of both its value and its normal derivative being specified along the heated surface. The unknown shape of this surface is obtained by meeting these dual conditions. The analytical method uses a generalized conformal mapping procedure that includes a curved boundary. The coolant flow can be compressible or incompressible, and its viscosity can depend on temperature. (Author)

A83-16141*# Pennsylvania State Univ., University Park.
DEVELOPMENT OF SECONDARY FLOW AND VORTICITY IN CURVED DUCTS, CASCADES, AND ROTORS, INCLUDING EFFECTS OF VISCOSITY AND ROTATION
M. POUAGARE and B. LAKSHMINARAYANA (Pennsylvania State University, University Park, PA) ASME, Transactions, Journal of Fluids Engineering, vol. 104, Dec. 1982, p. 505-512. refs
(Contract NSG-3212)

This paper is concerned with the numerical solution of the secondary vorticity equations in curved ducts, cascades, and rotors. The classical approach of splitting the flow into primary and secondary flow fields is employed and extended to include effects of viscosity, rotation, and density stratification. All elliptical effects are neglected and the Crank-Nicolson method is used to solve the secondary vorticity equation. The secondary flow field is obtained by solving a Poisson equation using a successive over-relaxation method. The results are compared with theoretical and experimental data from stationary ducts, compressor and turbine cascades. The agreement is good for most of the cases. (Author)

A83-16498*# Pennsylvania State Univ., University Park.
PREDICTIONS OF THE STRUCTURE OF TURBULENT, PARTICLE-LADEN, ROUND JETS
J.-S. SHUEN, L.-D. CHEN, and G. M. FAETH (Pennsylvania State University, University Park, PA) American Institute of Aeronautics and Astronautics, Aerospace Sciences Meeting, 21st, Reno, NV, Jan. 10-13, 1983, 11 p. refs
(Contract NAG3-190)
(AIAA PAPER 83-0066)

Models of gas and particle motion in turbulent, particle-laden, round jets were evaluated using existing measurements of flow structure. Three models were considered: (1) a locally homogeneous flow model, where velocities and turbulent mixing properties of both phases were assumed to be equal; (2) a deterministic separated flow model, where interphase slip was considered but effects of turbulent dispersion were ignored; and (3) a stochastic separated flow model where effects of interphase slip and turbulent dispersion were considered using random sampling techniques. In all three cases, mean and turbulent properties of the continuous phase were found with a well-calibrated k-epsilon model. The locally homogeneous flow and deterministic separated flow models over- and underestimated particle spread and flow development rates, respectively. The stochastic separated flow model, however, yielded satisfactory predictions of flow structure - except at high particle loadings. Uncertainties in initial conditions for the measurements and possible effects of turbulence modulation by the particles are proposed as the reason for these errors. (Author)

A83-16558*# Pennsylvania State Univ., University Park.
MEASUREMENTS AND PREDICTIONS FOR NONEVAPORATING SPRAYS IN A QUIESCENT ENVIRONMENT
A. S. P. SOLOMON, J.-S. SHUEN, G. M. FAETH (Pennsylvania State University, University Park, PA), and Q.-F. ZHANG American Institute of Aeronautics and Astronautics, Aerospace Sciences Meeting, 21st, Reno, NV, Jan. 10-13, 1983, 10 p. refs
(Contract NAG3-190)
(AIAA PAPER 83-0151)

Yule et al. (1982) have conducted a study of vaporizing sprays with the aid of laser techniques. The present investigation has the objective to supplement the measurements performed by Yule et al., by considering the limiting case of a spray in a stagnant environment. Mean and fluctuating velocities of the continuous phase are measured by means of laser Doppler anemometry (LDA) techniques, while Fraunhofer diffraction and slide impaction methods are employed to determine drop sizes. Liquid fluxes in the spray are found by making use of an isokinetic sampling probe. The obtained data are used as a basis for the evaluation of three models of the process, including a locally homogeneous flow (LHF) model, a deterministic separated flow (DSF) model, and a stochastic separated flow (SSF) model. It is found that the LHF and DSF models do not provide very satisfactory predictions for the test sprays, while the SSF model does provide reasonably good predictions of the observed structure. G.R.

A83-16645*# Oklahoma State Univ., Stillwater.
FIVE-HOLE PITOT PROBE TIME-MEAN VELOCITY MEASUREMENTS IN CONFINED SWIRLING FLOWS
H. K. YOON and D. G. LILLEY (Oklahoma State University, Stillwater, OK) American Institute of Aeronautics and Astronautics, Aerospace Sciences Meeting, 21st, Reno, NV, Jan. 10-13, 1983, 12 p. refs
(Contract NAG3-74)
(AIAA PAPER 83-0315)

Nonswirling and swirling nonreacting flows in an axisymmetric test section with an expansion ratio D/d = 2, which may be equipped with contraction nozzles of area ratios 2 and 4, are investigated. The effects of a number of geometric parameters on the flow-field are investigated, among them side-wall expansion angles of 90 and 45 deg, swirl vane angles of 0, 38, 45, 60 and 70 deg, and contraction nozzle locations L/D = 1 and 2 (if present). Data are acquired by means of a five-hole pitot probe enabling three time-mean velocity components in the axial, radial, and azimuthal directions to be measured. The velocities are extensively plotted and artistic impressions of recirculation zones are set forth. The presence of a swirler is found to shorten the corner recirculation zone and to generate a central recirculation zone followed by a precessing vortex core. A gradual inlet expansion has the effect of encouraging the flow to remain close to the sidewall and shortening the extent of the corner recirculation zone in all cases investigated. C.R.

A83-16646*# Oklahoma State Univ., Stillwater.
CONFINED SWIRLING FLOW PREDICTIONS
M. T. ABUJELALA and D. G. LILLEY (Oklahoma State University, Stillwater, OK) American Institute of Aeronautics and Astronautics, Aerospace Sciences Meeting, 21st, Reno, NV, Jan. 10-13, 1983, 12 p. refs
(Contract NAG3-74)
(AIAA PAPER 83-0316)

The validity of flowfield predictions resulting from the choice of inlet velocity profiles is assessed. Results demonstrate that realistic predictions are forthcoming only from the inclusion of realistic axial, radial and swirl velocity profiles as inlet conditions. Predictions are then exhibited for a range of swirl strengths phi = 0, 38, 45, 60 and 70 degrees using measured inlet axial, radial and swirl velocity profiles in each case. Downstream nozzle effects (two blockage size at two axial locations) are included. The ensuing flowfields are characterized via velocity profiles and streamline patterns, and illustrate the large-scale effects of inlet swirl and outlet nozzles on flowfields. (Author)

A83-16737*# California Univ., Berkeley.
AERODYNAMIC FEATURES OF TURBULENT FLAMES
A. K. OPPENHEIM and A. F. GHONIEM (California, University, Berkeley, CA) American Institute of Aeronautics and Astronautics, Aerospace Sciences Meeting, 21st, Reno, NV, Jan. 10-13, 1983, 11 p. refs
(Contract W-7405-ENG-48; NSF CPE-81-15163; NAG3-131)
(AIAA PAPER 83-0470)

The paper provides an interpretation for a variety of turbulent flame phenomena relating them to the aerodynamic properties of the flow field. This includes the classical notion of the breakdown of laminar flames propagation in ducts, the characteristic features of turbulent flame-fronts recorded by schlieren photography, as well as flame instabilities leading to flashback occurring in a combustion chamber behind a bluff-body flame holder. The rudimentary nature of turbulent flame propagation is shown to be associated with (1) vortex motion of a large-scale turbulent eddy, combined with (2) self-advancement of the flame at the appropriate normal burning speed and (3) the concomitant action of distributed sources of specific volume. The results furnish an insight into the macroscopic properties of the mechanism of turbulent flame propagation, rationalizing in particular its capability to sustain high flow velocities at relatively low normal burning speeds. (Author)

A83-16786*# Cincinnati Univ., Ohio.
MULTI-GRID SOLUTION OF NEUMANN PRESSURE PROBLEM FOR VISCOUS FLOWS USING PRIMITIVE VARIABLES
U. GHIA, K. N. GHIA, and R. RAMAMURTI (Cincinnati, University, Cincinnati, OH) American Institute of Aeronautics and Astronautics, Aerospace Sciences Meeting, 21st, Reno, NV, Jan. 10-13, 1983, 12 p. refs
(Contract AF-AFOSR-80-0160; NSG-3267)
(AIAA PAPER 83-0557)

The multi-grid (MG) technique has been advanced for use with the Neumann boundary-value problem in clustered curvilinear orthogonal coordinates. This comprises an important step in the analysis of viscous flows using the velocity-pressure formulation of the Navier-Stokes equations. With successive over-relaxation (SOR) as the smoothing operator and with suitably formulated restriction and coarse-grid-correction operators, a 4-grid procedure enhances the efficiency of fine-grid solutions of the Neumann problem by a factor of 3 to 5, depending on the problem parameters. Thy influence of the smoothing operator is also examined by employing the alternating-direction implicit and the strongly implicit techniques instead of SOR. (Author)

A83-16787*# Pennsylvania State Univ., University Park.
A TURBULENCE MODEL FOR THREE DIMENSIONAL TURBULENT SHEAR FLOWS OVER CURVED ROTATING BODIES
J. M. GALMES and B. LAKSHMINARAYANA (Pennsylvania State University, University Park, PA) American Institute of Aeronautics and Astronautics, Aerospace Sciences Meeting, 21st, Reno, NV, Jan. 10-13, 1983, 13 p. refs
(Contract NSG-3266)
(AIAA PAPER 83-0559)

There exists currently considerable interest in the development of numerical procedures for solving the equations governing three-dimensional fluid flows. In particular, improved calculations of viscous flows on rotating bodies such a turbomachinery rotors are of great importance. The present investigation is mainly concerned with the analysis of the effect of rotation on the dissipation rate equation and the Reynolds stress equations. Attention is given to governing equations and modelling, algebraic Reynolds stress equations, a procedure for implementing the turbulence closure scheme, results for a model representative of centrifugal turbomachinery, and results for axial turbomachinery. The proposed turbulence model is valid for three-dimensional, rotating, and curved flows. The model has all the essential physics of turbulence, mean flow, rotation, and the curvature. G.R.

A83-19022* California Inst. of Tech., Pasadena.
THREE-DIMENSIONAL STABILITY OF VORTEX ARRAYS
A. C. ROBINSON and P. G. SAFFMAN (California Institute of Technology, Pasadena, CA) Journal of Fluid Mechanics, vol. 125, Dec. 1982, p. 411-427. Research supported by the U.S. Department of Energy refs
(Contract NAG3-179)

The stability to three-dimensional disturbances of three classical steady vortex configurations in an incompressible inviscid fluid is studied in the limit of small vortex cross-sectional area and long axial disturbance wavelength. The configurations examined are the single infinite vortex row, the Karman vortex street of staggered vortices and the symmetric vortex street. It is shown that the single row is most unstable to a two-dimensional disturbance, while the Karman vortex street is most unstable to a three-dimensional disturbance over a significant range of street spacing ratios. The symmetric vortex street is found to be most unstable to three-dimensional or two-dimensional symmetric disturbances depending on the spacing ratio of the street. Short remarks are made concerning the relevance of the calculations to the observed instabilities in free shear layer, wake and boundary-layer type flows. (Author)

A83-22381* Illinois Inst. of Tech., Chicago.
RAPID DISTORTION OF SMALL-SCALE TURBULENCE BY AN AXISYMMETRIC CONTRACTION
L. S. HULTGREN and S.-C. CHEN (Illinois Institute of Technology, Chicago, IL) Physics of Fluids, vol. 26, Feb. 1983, p. 409-415. refs
(Contract NSG-3220)

The rapid distortion of small-scale turbulence by an axisymmetric internal contracting flow has been investigated. The analysis is an example of the modern version of rapid distortion theory in that the effects of vortex bending and tilting are included. On the axis of symmetry, the classical results are recovered. The longitudinal and lateral velocity components are suppressed and amplified, respectively, with increasing contraction ratio. These effects are enhanced with increasing radial position. The numerical calculations also show that the correlation between the streamwise and radial velocity components increases monotonically with respect to both the radial location and the contraction ratio. The longitudinal and lateral one-dimensional spectra show a shift towards higher and lower wavenumbers, respectively, as the contraction ratio increases. Here, these effects become less pronounced for larger radii. These results also show that the downstream longitudinal integral length scale based on the streamwise velocity as well as the one based on the transverse velocity increase with the radial coordinate. (Author)

A83-24410* National Aeronautics and Space Administration. Lewis Research Center, Cleveland, Ohio.
THE EVOLUTION OF TOLLMIEN-SCHLICHTING WAVES NEAR A LEADING EDGE
M. E. GOLDSTEIN (NASA, Lewis Research Center, Cleveland, OH) Journal of Fluid Mechanics, vol. 127, Feb. 1983, p. 59-81. refs

The method of matched asymptotic expansions is used to study the generation of Tollmien-Schlichting waves by free-stream disturbances incident on a flat-plate boundary layer. Near the leading edge, the motion is governed by the unsteady boundary-layer equation, while farther downstream it is governed (to lowest order) by the Orr-Sommerfeld equation with slowly varying coefficients. It is shown that there is an overlap domain where the Tollmien-Schlichting wave solutions to the Orr-Sommerfeld equation and appropriate asymptotic solutions of the unsteady boundary-layer equation match, in the matched-asymptotic-expansion sense. The analysis explains how long-wavelength free-stream disturbances can generate Tollmien-Schlichting waves of much shorter wavelength. It also leads to a set of scaling laws for the asymptotic structure of the unsteady boundary layer. (Author)

A83-24668*# Texas A&M Univ., College Station.
MEAN FLOWFIELDS IN AXISYMMETRIC COMBUSTOR GEOMETRIES WITH SWIRL
D. L. RHODE (Texas A & M University, College Station, TX), D. G. LILLEY (Oklahoma State University, Stillwater, OK), and D. K. MCLAUGHLIN (Dynamics Technology, Inc., Torrance, CA) AIAA Journal, vol. 21, Apr. 1983, p. 593-600. refs
(Contract NAG3-74)
(Previously cited in issue 06, p. 860, Accession no. A82-17824)

A83-27137* Washington Univ., Seattle.
DIRECT CONTACT DROPLET HEAT EXCHANGERS FOR THERMAL MANAGEMENT IN SPACE
A. P. BRUCKNER and A. HERTZBERG (Washington, University, Seattle, WA) In: IECEC '82; Proceedings of the Seventeenth Intersociety Energy Conversion Engineering Conference, Los Angeles, CA, August 8-12, 1982. Volume 1. New York, Institute of Electrical and Electronics Engineers, 1982, p. 107-112. refs
(Contract NAG3-16)

A liquid droplet heat exchanger for space applications is described which transfers heat between a gas and a liquid metal dispersed into droplets. The ability of the droplet heat exchanger to transfer heat between two media in direct contact over a wide

temperature range circumvents many of the material limitations of conventional tube-type heat exchangers and does away with complicated plumbing systems and their tendency toward single point failure. Droplet heat exchangers offer large surface to volume ratios in a compact geometry, very low gas pressure drop, and high effectiveness. The application of the droplet heat exchanger in a high temperature Brayton cycle is discussed to illustrate its performance and operational characteristics. (Author)

A83-27412*# Oklahoma State Univ., Stillwater.
A BASIC CODE FOR THE PREDICTION OF TRANSIENT THREE-DIMENSIONAL TURBULENT FLOWFIELDS
A. A. BUSNAINA and D. G. LILLEY (Oklahoma State University, Stillwater, OK) In: Three dimensional turbulent shear flows; Proceedings of the Joint Fluids, Plasma, Thermophysics and Heat Transfer Conference, St. Louis, MO, June 7-11, 1982. New York, American Society of Mechanical Engineers, 1982, p. 33-40. USAF-supported research. refs
(Contract NAG3-74)

A primitive pressure-velocity finite difference code has been developed to predict transient three-dimensional turbulent flow. The code is a simplified yet effective prediction procedure for use by persons with little experience in computational fluid dynamics, and into which user-oriented complexities can easily be added. The method is based on the transient two-dimensional Los Alamos SOLA prediction technique for laminar flows. Turbulence is simulated by means of a two-equation turbulence model; species diffusion and buoyancy are also included. Two applications of the code are presented to local destratification near the release structure of a reservoir and to the deflection of a jet entering normally into a uniform cross-flow. Predicted results exhibit good agreement with experimental data, showing that a useful characterization of fully three-dimensional flows is now available. (Author)

A83-27481*# Yale Univ., New Haven, Conn.
CORRELATION AND PREDICTION OF THERMOPHORETIC AND INERTIAL EFFECTS ON PARTICLE DEPOSITION FROM NON-ISOTHERMAL TURBULENT BOUNDARY LAYERS
D. E. ROSNER and J. FERNANDEZ DE LA MORA (Yale University, New Haven, CT) In: Particulate laden flows in turbomachinery; Proceedings of the Joint Fluids, Plasma, Thermophysics and Heat Transfer Conference, St. Louis, MO, June 7-11, 1982. New York, American Society of Mechanical Engineers, 1982, p. 85-94. refs
(Contract F49620-76-C-0020; NSG-3107)

The problem of small particle deposition which can cause hot stage corrosion and/or fouling in combustion turbines operating on fuels containing ash or inorganic salts is investigated. Two boundary layer transport phenomena are shown to assume importance in these cases: particle thermophoresis (migration down a temperature gradient) and particle inertia. Thermophoretic and eddy transport across turbulent boundary layers without and with particle inertia effects are quantitatively analyzed. The effects of streamwise blade curvature on particle transport across turbulent boundary layers are determined. It is shown that these phenomena destroy the analogy between mass and heat transfer or mass and momentum transfer. Also studied are the effects on particle deposition of distributed or localized wall blowing, surface roughness, and mainstream turbulence. N.B.

A83-28104* Pennsylvania State Univ., University Park.
EVALUATION OF A STOCHASTIC MODEL OF PARTICLE DISPERSION IN A TURBULENT ROUND JET
J.-S. SHUEN, L.-D. CHEN, and G. M. FAETH (Pennsylvania State University, University Park, PA) AIChE Journal, vol. 29, Jan. 1983, p. 167-170. refs
(Contract NAG3-190)

A stochastic model of particle dispersion by turbulence, proposed by Gosman and Ioannides (1981), is evaluated. The method employs a k-epsilon model to estimate turbulence properties. Dispersion is determined by computing particle motion, with random sampling to obtain instantaneous flow properties for a statistically significant number of particle trajectories. The stochastic model yields good results particularly when eddy lifetimes are evaluated. The method allows the effects of large relative velocities between the particles and the flow, drag properties at Reynolds numbers greater than the Stokes flow regime, and the variations of local turbulence properties to be readily handled, at least for boundary layer flows. C.D.

A83-30109* California Univ., Irvine.
A TWO-EQUATION TURBULENCE MODEL FOR TWO-PHASE FLOWS
S. E. ELGHOBASHI and T. W. ABOU-ARAB (California, University, Irvine, CA) Physics of Fluids (ISSN 0031-9171), vol. 26, April 1983, p. 931-938. refs
(Contract DE-FG22-80PC-30303; NAG3-176)

A two-equation turbulence model has been developed for predicting two-phase flows. The two equations describe the conservation of turbulence kinetic energy and dissipation rate of that energy for the carrier fluid in a two-phase flow. They have been derived rigorously from the momentum equations of the carrier fluid. Closure of the time-mean equations is achieved by modeling the turbulent correlations up to third order. The new model eliminates the need to simulate in an ad hoc manner the effects of the dispersed phase on turbulence structure. Preliminary testing indicates that the model is successful in predicting the main features of a round gaseous jet laden with uniform-size solid particles. Author

A83-32701*# Tennessee Univ., Knoxville.
MEASUREMENT OF THERMOACOUSTIC CONVECTION HEAT TRANSFER PHENOMENON
M. PARANG (Tennessee, University, Knoxville, TN) and A. SALAH-EDDINE American Institute of Aeronautics and Astronautics, Thermophysics Conference, 18th, Montreal, Canada, June 1-3, 1983. 5 p. refs
(Contract NAG3-239)
(AIAA PAPER 83-1422)

In this paper the results of an experimental investigation of thermoacoustic convection (TAC) heat transfer phenomenon in both zero-gravity and gravity environment are presented and compared with pure conduction heat transfer. The numerical solutions of the governing equations obtained by others for TAC heat transfer phenomenon are also discussed. The experimental results show that for rapid heating rate at a boundary, the contribution of TAC heat transfer to a gas could be significantly (one order of magnitude) higher than heat transfer rate from pure conduction. The results also show significantly reduced transient time in heat transfer processes involving thermoacoustic convective heat transfer mode in both space and gravity environment. Author

A83-32989*# Akron Univ., Ohio.
PSEUDO-UPDATED CONSTRAINED SOLUTION ALGORITHM FOR NONLINEAR HEAT CONDUCTION
S. TOVICHAKCHAIKUL and J. PADOVAN (Akron, University, Akron, OH) AIAA Journal (ISSN 0001-1452), vol. 21, June 1983, p. 902-908. refs
(Contract NAG3-54; NAG3-265)

This paper develops efficiency and stability improvements in the incremental successive substitution (ISS) procedure commonly used to generate the solution to nonlinear heat conduction problems. This is achieved by employing the pseudo-update scheme of Broyden, Fletcher, Goldfarb and Shanno in conjunction with the constrained version of the ISS. The resulting algorithm retains the formulational simplicity associated with ISS schemes while incorporating the enhanced convergence properties of slope driven procedures as well as the stability of constrained approaches. To illustrate the enhanced operating characteristics of the new scheme, the results of several benchmark comparisons are presented. Author

A83-35346* National Aeronautics and Space Administration. Lewis Research Center, Cleveland, Ohio.
THE EVOLUTION OF TOLLMIEN-SCHLICHTING WAVES NEAR A LEADING EDGE. II - NUMERICAL DETERMINATION OF AMPLITUDES
M. E. GOLDSTEIN, P. M. SOCKOL, and J. SANZ (NASA, Lewis Research Center, Cleveland, OH) Journal of Fluid Mechanics (ISSN 0022-1120), vol. 129, April 1983, p. 443-453. refs

In the first part of this investigation, Goldstein (1983) has shown that the amplitude of the spatially growing Tollmien-Schlichting wave generated by a time-harmonic free-stream disturbance is related to the coefficient multiplying the lowest-order asymptotic eigensolution of the unsteady boundary-layer equation. In the present study, a numerical solution of the unsteady boundary-layer equation is used to relate the amplitude of the asymptotic eigensolution, and consequently of the Tollmien-Schlichting wave, to that of the imposed free-stream disturbance for the special case of a uniformly pulsating stream. It is pointed out that the ideas of this study can be extended to other, more complex bodies and free-stream oscillations. G.R.

A83-36082*# National Aeronautics and Space Administration. Lewis Research Center, Cleveland, Ohio.
MODE PROPAGATION IN NONUNIFORM CIRCULAR DUCTS WITH POTENTIAL FLOW
Y. C. CHO (NASA, Lewis Research Center, Cleveland, OH) and K. U. INGARD (MIT, Cambridge, MA) AIAA Journal (ISSN 0001-1452), vol. 21, July 1983, p. 970-977. refs

Previously cited in issue 07, p. 969, Accession no. A82-20290

A83-36276*# National Aeronautics and Space Administration. Lewis Research Center, Cleveland, Ohio.
PERSPECTIVES ON THE MIXING OF A ROW OF JETS WITH A CONFINED CROSSFLOW
J. D. HOLDEMAN (NASA, Lewis Research Center, Cleveland, OH) AIAA, SAE, and ASME, Joint Propulsion Conference, 19th, Seattle, WA, June 27-29, 1983. 13 p. refs
(AIAA PAPER 83-1200)

An interactive computer code, written for a microcomputer, is presented which displays 2-D and 3-D oblique plots of the temperature distribution downstream of jets mixing with a confined crossflow, for either single-side or opposed jet injection. Temperature profiles calculated with this routine are presented to show the effects of flow and geometric variables on the mixing. Examples are shown to illustrate the different perspectives on the mixing available by exercising various view options. In addition, the program is used to calculate profiles for opposed rows of jets with their centerlines in-line, by assuming that the confining effect of an opposite wall is equivalent to that of a plane of symmetry between opposed jets. Author

A83-36277*# National Aeronautics and Space Administration. Lewis Research Center, Cleveland, Ohio.
EXPERIMENTS IN DILUTION JET MIXING
J. D. HOLDEMAN (NASA, Lewis Research Center, Cleveland, OH), R. SRINIVASAN, and A. BERENFELD (Garrett Turbine Engine Co., Phoenix, AZ) AIAA, SAE, and ASME, Joint Propulsion Conference, 19th, Seattle, WA, June 27-29, 1983. 14 p. refs
(AIAA PAPER 83-1201)

Experimental results are presented on the mixing of a single row of jets with an isothermal mainstream in a straight duct, with flow and geometric variations typical of combustion chambers in gas turbine engines included. It is found that at a constant momentum ratio, variations in the density ratio have only a second-order effect on the profiles. A first-order approximation to the mixing of jets with a variable temperature mainstream can, it is found, be obtained by superimposing the jets-in-an-isothermal-crossflow and mainstream profiles. Another finding is that the flow area convergence, especially injection-wall convergence, significantly improves the mixing. For opposed rows of jets with the orifice cone centerlines in-line, the optimum ratio of orifice spacing to duct height is determined to be 1/2 of the optimum value for single injection at the same momentum ratio. For opposed rows of jets with the orifice centerlines staggered, the optimum ratio of orifice spacing to duct height is found to be twice the optimum value for single side injection at the same momentum ratio. C.R.

A83-36278*# Oklahoma State Univ., Stillwater.
SINGLE-WIRE SWIRL FLOW TURBULENCE MEASUREMENTS
D. G. LILLEY (Oklahoma State University, Stillwater, OK) and T. W. JACKSON AIAA, SAE, and ASME, Joint Propulsion Conference, 19th, Seattle, WA, June 27-29, 1983. 13 p. USAF-supported research. refs
(Contract NAG3-74)
(AIAA PAPER 83-1202)

A six-orientation, single wire hot wire technique is used to investigate nonswirling and swirling nonreacting flow in an axisymmetric test section with expansion ratio (test section/inlet nozzle diameter) = 2, which may be equipped with a strong contraction nozzle of area ratio 4 at a contraction nozzle downstream distance/test section diameter value = 2. The flowfield contains corner and central recirculation zones typical of gas turbine and ramjet combustion chambers. Swirl may be imparted to the incoming flow by means of a variable angle vane swirler. The effect of swirl on time mean velocities and complete Reynolds stress tensor is investigated, and extensive results are given for swirl vane angles of zero (swirler removed), 38, 45, 60 and 70 deg. The data are being used to aid in the evolution of turbulence models for these complex flow situations. A directional sensitivity analysis is included, which determines the relative accuracy of the measurement technique to approach velocity orientation. Author

A83-38796* United Technologies Research Center, East Hartford, Conn.
SOLUTION OF VISCOUS INTERNAL FLOWS ON CURVILINEAR GRIDS GENERATED BY THE SCHWARZ-CHRISTOFFEL TRANSFORMATION
O. L. ANDERSON, G. B. HANKINS, D. E. EDWARDS (United Technologies Research Center, East Hartford, CT), and R. T. DAVIS (Cincinnati, University, Cincinnati, OH) IN: Numerical grid generation; Proceedings of the Symposium on Numerical Generation of Curvilinear Coordinate Systems and Their Use in the Numerical Solution of Partial Differential Equations, Nashville, TN, April 13-16, 1982 . New York and Amsterdam, North-Holland, 1982, p. 507-524. refs
(Contract DEN3-235)

The combination of an orthogonal, curvilinear coordinate generation procedure with a stable forward marching viscous flow solution technique is presently employed in the solution of flow fields for arbitrary, axisymmetric ducts. Coordinate generation is accomplished by means of both potential lines and plane potential flow streamlines. Since the coordinate streamlines approximate actual ones, the equations of motion for viscous compressible flow can be parabolized in order to solve for both the boundary layer and the core flow in a single streamwise pass. The method's versatility is demonstrated by two examples of viscous compressible swirling flow through complex radial gas turbine passages. O.C.

A83-39367*# National Aeronautics and Space Administration. Lewis Research Center, Cleveland, Ohio.
A SEMI-DIRECT SOLVER FOR COMPRESSIBLE THREE-DIMENSIONAL ROTATIONAL FLOW
S.-C. CHANG and J. J. ADAMCZYK (NASA, Lewis Research Center, Cleveland, OH) IN: Computational Fluid Dynamics Conference, 6th, Danvers, MA, July 13-15, 1983, Collection of Technical Papers . New York, American Institute of Aeronautics and Astronautics, 1983, p. 163-182. refs
(AIAA PAPER 83-1909)

An iterative procedure is presented for solving steady inviscid 3-D subsonic rotational flow problems. The procedure combines concepts from classical secondary flow theory with an extension to 3-D of a novel semi-direct Cauchy-Riemann solver. It is developed for generalized coordinates and can be exercised using standard finite difference procedures. The stability criterion of the

iterative procedure is discussed along with its ability to capture the evolution of inviscid secondary flow in a turning channel.
Author

A83-39389*# GMAF, Inc., Freeport, N.Y.
A FAST EULER SOLVER FOR STEADY FLOWS
G. MORETTI (GMAF, Inc., Freeport, NY) IN: Computational Fluid Dynamics Conference, 6th, Danvers, MA, July 13-15, 1983, Collection of Technical Papers . New York, American Institute of Aeronautics and Astronautics, 1983, p. 357-362.
(Contract NAS3-22772)
(AIAA PAPER 83-1940)

A numerical technique to solve the Euler equations for steady, two-dimensional flows is presented. The technique extends to two-dimensional problems a formulation which was found to be extremely efficient for one-dimensional flows. Generalized Riemann variables are defined along two families of orthogonal coordinates, and integrated separately, sweeping back and forth alternatively along coordinate lines. The technique is second-order accurate and converges very rapidly. In addition, each step requires a minimal number of operations. Preliminary results for subsonic and transonic shockless flows are presented and discussed. Author

A83-42532*# Cincinnati Univ., Ohio.
STUDY OF ASYMPTOTIC INCOMPRESSIBLE FLOW IN CURVED DUCTS USING A MULTI-GRID TECHNIQUE
K. N. GHIA, U. GHIA, and C. T. SHIN (Cincinnati, University, Cincinnati, OH) IN: Annual Mini-Symposium on Aerospace Science and Technology, 9th, Wright-Patterson AFB, OH, March 22, 1983, Proceedings . New York, American Institute of Aeronautics and Astronautics, 1983, p. 1-9-1 to 1-9-6. refs
(Contract AF-AFOSR-80-0160; NSG-3267)

Asymptotic flows inside curved ducts of rectangular as well as polar cross sections have been analyzed using the Navier-Stokes equations in terms of the axial velocity and vorticity and the cross-flow stream function. Numerical solutions of the three second-order coupled elliptic partial differential equations governing this flow have been obtained using the multi-grid-SI scheme, to determine fine-grid results for configurations with strong secondary flow. Author

A83-42703* Iowa Univ., Iowa City.
FINITE ANALYTIC NUMERICAL SOLUTION OF HEAT TRANSFER AND FLOW PAST A SQUARE CHANNEL CAVITY
C.-J. CHEN and K. OBASIH (Iowa, University, Iowa City, IA) IN: Heat transfer 1982; Proceedings of the Seventh International Conference, Munich, West Germany, September 6-10, 1982. Volume 3 . Washington, DC, Hemisphere Publishing Corp., 1982, p. 27-32. refs
(Contract NSG-3305; DE-AC02-79ER-10515A000)

A numerical solution of flow and heat transfer characteristics is obtained by the finite analytic method for a two dimensional laminar channel flow over a two-dimensional square cavity. The finite analytic method utilizes the local analytic solution in a small element of the problem region to form the algebraic equation relating an interior nodal value with its surrounding nodal values. Stable and rapidly converged solutions were obtained for Reynolds numbers ranging to 1000 and Prandtl number to 10. Streamfunction, vorticity and temperature profiles are solved. Local and mean Nusselt number are given. It is found that the separation streamlines between the cavity and channel flow are concave into the cavity at low Reynolds number and convex at high Reynolds number (Re greater than 100) and for square cavity the mean Nusselt number may be approximately correlated with Peclet number as Nu(m) = 0.365 Pe exp 0.2. Author

A83-42711* Cleveland State Univ., Ohio.
EFFECTS OF FREE STREAM TURBULENCE INTENSITY AND INTEGRAL LENGTH SCALE ON HEAT TRANSFER FROM A CIRCULAR CYLINDER IN CROSSFLOW
R. S. R. GORLA and N. NEMETH (Cleveland State University, Cleveland, OH) IN: Heat transfer 1982; Proceedings of the Seventh International Conference, Munich, West Germany, September 6-10, 1982. Volume 3 . Washington, DC, Hemisphere Publishing Corp., 1982, p. 153-158. refs
(Contract NCC3-3)

A model has been proposed for the momentum eddy diffusivity induced by free stream turbulence intensity and integral length scale. The eddy diffusivity model is applied to a cylinder situated in a uniform crossflow in the presence of free stream turbulence. Numerical solution of the governing momentum and energy equations with the proposed eddy diffusivity model yielded results for the skin friction coefficient and the Nusselt number. The numerical predictions of the present work are compared with experimental data and the agreement between the two is seen to be very good. Author

A83-42733* Minnesota Univ., Minneapolis.
CONVEX CURVATURE EFFECTS ON THE HEATED TURBULENT BOUNDARY LAYER
T. W. SIMON (Minnesota, University, Minneapolis, MN) and R. J. MOFFAT (Stanford University, Stanford, CA) IN: Heat transfer 1982; Proceedings of the Seventh International Conference, Munich, West Germany, September 6-10, 1982. Volume 3 . Washington, DC, Hemisphere Publishing Corp., 1982, p. 295-300. refs
(Contract NSG-3124; NAG3-3)

A convexly curved and isothermally heated wall with a 45-cm radius of curvature is subjected to turbulent boundary layer flow measurements in order to determine wall heat transfer rates and mean velocity and temperature profiles. Significant curvature effects are noted, with Stanton number and skin friction coefficient reductions of 35-40 percent by comparison with flat plate values for the same momentum or enthalpy thickness Reynolds numbers. Profiles of mean velocity and temperature show a more rapid growth of the wake regions, and a shortening of the log-linear region, as a result of curvature. Turbulent Prandtl numbers deduced from the mean temperature profiles under the assumption of a wall thermal law were found to be increased by 40-50 percent by this strong convex curvature. O.C.

A83-42743* New Jersey Inst. of Tech., Newark.
HEAT TRANSFER AND FLOW CHARACTERISTICS OF JETS IMPINGING ON A CONCAVE HEMISPHERICAL PLATE
P. HRYCAK (New Jersey Institute of Technology, Newark, NJ) IN: Heat transfer 1982; Proceedings of the Seventh International Conference, Munich, West Germany, September 6-10, 1982. Volume 3 . Washington, DC, Hemisphere Publishing Corp., 1982, p. 357-362. refs
(Contract NAS3-11175)

The present study is concerned with an experimental investigation of the flow characteristics and heat transfer from turbulent air jets impinging normally on a concave hemispherical plate (CHP). It is found that the incompressible, turbulent jets impinging on a CHP are in many respects similar to the jets impinging on a flat plate. The observed differences are due to effects of curvature and to a slightly higher turbulence level inside of the CHP. Attention is given to the experimental apparatus, aspects of inner boundary layer development, the maximum velocity decay in a wall jet, the derivation of a maximum velocity decay formula, the influence of curvature on stagnation point heat transfer, and heat transfer calculations for a concave hemispherical plate. G.R.

A83-42762* National Aeronautics and Space Administration. Lewis Research Center, Cleveland, Ohio.
THE DRYOUT REGION IN FRICTIONALLY HEATED SLIDING CONTACTS
R. C. HENDRICKS (NASA, Lewis Research Center, Cleveland, OH), J. BRAUN (NASA, Lewis Research Center, Cleveland; Akron, University, Akron, OH), V. ARP, and P. J. GIARRATANO (NASA, Lewis Research Center, Cleveland, OH; National Bureau of Standards, Boulder, CO) IN: Heat transfer 1982; Proceedings of the Seventh International Conference, Munich, West Germany, September 6-10, 1982. Volume 4 . Washington, DC, Hemisphere Publishing Corp., 1982, p. 137-142. refs

Some conditions under which boiling and two-phase flow can occur in or near a wet sliding contact are determined and illustrated. The experimental apparatus consisted of a tool pressed against an instrumented slider plate and motion picture sequences at 4000 frames/sec. The temperature and photographic data demonstated surface conditions of boiling, dry, trapped gas evolution (solutions), and volatility of fluid mixture components. The theoretical modeling and analysi are in reasonable agreement with experimental data. Previously announced in STAR as N82-28574 Author

A83-43012* Tennessee Technological Univ., Cookeville.
ACOUSTIC VELOCITIES OF TWO-PHASE MIXTURES OF CRYOGENIC FLUIDS
E. I. GRIGGS (Tennessee Technological University, Cookeville, TN), E. R. F. WINTER (Muenchen, Technische Universitaet, Munich, West Germany), R. J. SCHOENHALS (Purdue University, West Lafayette, IN), and R. C. HENDRICKS (NASA, Lewis Research Center, Cleveland, OH) IN: Heat transfer 1982; Proceedings of the Seventh International Conference, Munich, West Germany, September 6-10, 1982. Volume 5. Washington, DC, Hemisphere Publishing Corp., 1982, p. 225-230. refs
(Contract NAS8-20222)

Calculated values of the acoustic velocity are presented for single-component and two-component, two-phase mixtures. Three different analytic models were employed. For purposes of comparison, all three models were used in making acoustic-velocity calculations for single-component, equivalent bubbly two-phase mixtures (with insoluble gas) of oxygen and helium and hydrogen and helium. In all cases the results are shown graphically so that the effects of variation in quality or void fraction, temperature and pressure are illustrated. Author

A83-43019* Rensselaer Polytechnic Inst., Troy, N. Y.
SPANWISE MASS TRANSFER VARIATIONS ON A CYLINDER IN 'NOMINALLY' UNIFORM CROSSFLOW
R. E. MAYLE and M. MARZIALE (Rensselaer Polytechnic Institute, Troy, NY) IN: Heat transfer 1982; Proceedings of the Seventh International Conference, Munich, West Germany, September 6-10, 1982. Volume 6 . Washington, DC, Hemisphere Publishing Corp., 1982, p. 135-140. refs
(Contract NSG-3262)

Mass transfer experiments on a circular cylinder in a 'nominally' uniform crossflow are described. Experiments were conducted at the tunnel's turbulence level and with a woven-wire turbulence screen. In both cases spanwise and circumferential mass transfer measurements were made. Without the turbulence screen, the results were found to be spanwise independent and agreed quite well with both theory and the result of others. In addition to the mass transfer measurements, spanwise traverse measurements of the mean velocity and turbulence quantities in the incident flow were made and showed that the screen produced a small-amplitude spanwise periodic perturbation in the incident flow. Although this perturbation was only one quarter of a percent in the mean velocity and buried in the stream's turbulence, disproportionately large spanwise variations of 15 percent were found in the mass transfer rate. Author

A83-43235* National Aeronautics and Space Administration. Lewis Research Center, Cleveland, Ohio.
EXPERIMENTS ON FLOW THROUGH ONE TO FOUR INLETS OF THE ORIFICE AND BORDA TYPE
R. C. HENDRICKS and T. T. STETZ (NASA, Lewis Research Center, Cleveland, OH) IN: Advances in cryogenic engineering. Volume 27 - Proceedings of the Cryogenic Engineering Conference, San Diego, CA, August 11-14, 1981 . New York, Plenum Press, 1982, p. 817-828. refs

Choked flow rate and pressure profile data were taken on sequential axially aligned inlets of the orifice and Borda type. The configuration consisted of from two to four inlets spaced at two nominal separation distances of 0.7 and 30 diameters. At the nominal 30 diameter spacing, the reduced flow rate follows a simple empirical relation based on the reduced flow rate for a single inlet. At the nominal 0.7 diameter spacing, fluid jetting was prevalent at low temperatures and flow rates were the same as for a single inlet. Previously announced in STAR as N81-30391 Author

A83-43361*# National Aeronautics and Space Administration. Lewis Research Center, Cleveland, Ohio.
ANALYSIS OF COOLANT ENTRANCE BOUNDARY SHAPE OF POROUS REGION TO CONTROL COOLING ALONG EXIT BOUNDARY
R. SIEGEL and A. SNYDER (NASA, Lewis Research Center, Cleveland, OH) ASME, Transactions, Journal of Heat Transfer (ISSN 0022-1481), vol. 105, Aug. 1983, p. 513-518. refs

A cooled porous region has a plane surface exposed to a specified spatially varying heat flux. The coolant leaves the region through this surface, and it is desired to control the flow distribution to maintain a specified uniform surface temperature. This is accomplished by having the coolant entrance surface shaped to provide in the region the necessary variation of path length and, hence, flow resistance. The surface shape at the coolant entrance is found by solving a Cauchy boundary value problem. An exact solution is obtained that will deal with a wide variety of heating distributions for both two- and three-dimensional shapes. Author

A83-45511*# National Aeronautics and Space Administration. Lewis Research Center, Cleveland, Ohio.
AERODYNAMIC-WAVE BREAK-UP OF LIQUID SHEETS IN SWIRLING AIRFLOWS AND COMBUSTOR MODULES
R. INGEBO (NASA, Lewis Research Center, Cleveland, OH) AIAA, SAE, and ASME, Joint Propulsion Conference, 19th, Seattle, WA, June 27-29, 1983. 11 p. refs
(AIAA PAPER 83-1204)

Experimental mean drop diameter data were obtained for the atomization of liquid sheets injected axially downstream in high velocity swirling and nonswirling airflow. Conventional simplex pressure atomizing fuel nozzles and splash type fuel injectors were studied under simulated combustor inlet airflow conditions. A general empirical expression relating reciprocal mean drop diameter to airstream mass velocity was obtained and is presented. The finest degree of atomization, i.e., the highest value of the coefficient C, was obtained with swirl can combustor modules (C = 15) as compared with pressure atomizing nozzles (C = 12). Previously announced in STAR as N83-23545 A.R.H.

A83-46445* Rutgers Univ., New Brunswick, N. J.
UNSTEADY TURBULENT SHEAR FLOW IN SHOCK TUBE DISCONTINUITIES
J. A. JOHNSON, III, R. RAMAIAH, and I. LIN (Rutgers University, New Brunswick, NJ) IN: Unsteady turbulent shear flows; Proceedings of the Symposium, Toulouse, France, May 5-8, 1981 . Berlin, Springer-Verlag, 1981, p. 305-315. refs
(Contract NSG-3280)

A pressure-ruptured shock tube and an arc driven shock tube, have been used to study the evolution of turbulent fluctuations at contact surfaces with N2O4-2NO2 mixtures and at ionizing shock fronts in argon. The study has focused on point density diagnostics derived from crossed light beam correlations and electric probes. Turbulent bursts are found for which dynamical and spectral

analyses suggest a particle-like evolution of fluctuation segments with a unique and characteristic frequency, independent of flow history and overall flow conditions. Author

A83-46718* California Inst. of Tech., Pasadena.
VORTICES, STABILITY, AND TURBULENCE
P. G. SAFFMAN (California Institute of Technology, Pasadena, CA) New York Academy of Sciences, Annals (ISSN 0077-8923), 1983, p. 12-24. Research supported by the U.S. Department of Energy and U.S. Navy. refs
(Contract NAG3-179)

The transition process between laminar flow to turbulent flow is discussed in terms of a third state of fluid motion, vortical motion that is approximately periodic in space and/or time and displays symmetrical properties. The possibility that the transition from laminar to turbulent flow is accompanied by intermediate vortical states, with turbulence being an instability of the vortical states, is examined, with consideration given to the hypothesis that the turbulent state retains a memory of the vortex structures. Solutions are sought for the Navier-Stokes equations for a viscous liquid in a channel. Instances of inviscid vortical states and the presence of a three-dimensional instability are studied, demonstrating that transition phenomena can be explained qualitatively in terms of vortical state characteristics. M.S.K.

A83-47899*# United Technologies Corp., East Hartford, Conn.
STATISTICAL CHARACTERISTICS OF VELOCITY, CONCENTRATION, MASS TRANSPORT, AND MOMENTUM TRANSPORT FOR COAXIAL JET MIXING IN A CONFINED DUCT
B. V. JOHNSON (United Technologies Research Center, East Hartford, CT) and J. C. BENNETT (Connecticut, University, Storrs, CT) American Society of Mechanical Engineers, International Gas Turbine Conference and Exhibit, 28th, Phoenix, AZ, Mar. 27-31, 1983. 7 p. refs
(Contract NAS3-22771)
(ASME PAPER 83-GT-39)

An experimental study of mixing downstream of coaxial jets discharging into an expanded circular duct was conducted to obtain data for the evaluation and improvement of turbulent transport models currently used for combustor flow modeling. A combination of turbulent momentum transport rate and two velocity component data was obtained from simultaneous measurements with a two-color LV system. A combination of turbulent mass transport rate, concentration and velocity data was obtained from simultaneous measurements with laser velocimeter (LV) and laser induced fluorescence (LIF) systems. These measurements were used to obtain mean, second central moment, skewness and kurtosis values for three velocity components and the concentration. These measurements showed the existence of countergradient turbulent axial mass transport where the annular jet fluid was accelerating the inner jet fluid. Results from the study are related to the assumptions employed in the current mass and momentum turbulent transport models. Author

A83-47933*# Stanford Univ., Calif.
A MIXING-LENGTH MODEL FOR THE PREDICTION OF CONVEX CURVATURE EFFECTS ON TURBULENT BOUNDARY LAYERS
E. W. ADAMS and J. P. JOHNSTON (Stanford University, Stanford, CA) American Society of Mechanical Engineers, International Gas Turbine Conference and Exhibit, 28th, Phoenix, AZ, Mar. 27-31, 1983. 7 p. Research supported by the Stanford University. refs
(Contract NAG3-3)
(ASME PAPER 83-GT-80)

A mixing-length model is developed for the prediction of turbulent boundary layers with convex streamwise curvature. For large layer thickness ratio, delta/R greater than 0.05, the model scales mixing length on the wall radius of curvature, R. For small delta/R, ordinary flat wall modeling is used for the mixing-length profile with curvature corrections, following the recommendations of Eide and Johnston (1976). Effects of streamwise change of curvature are considered; a strong lag from equilibrium is required when R increases downstream. Fifteen separate data sets were compared, including both hydrodynamic and heat transfer results. Six of these computations are presented and compared to experiment. Author

A83-48678*# National Aeronautics and Space Administration. Lewis Research Center, Cleveland, Ohio.
STUDIES OF FLOWS THROUGH N-SEQUENTIAL ORIFICES
R. C. HENDRICKS and T. T. STETZ (NASA, Lewis Research Center, Cleveland, OH) ASME, Transactions, Journal of Fluids Engineering (ISSN 0098-2202), vol. 105, Sept. 1983, p. 297-302. refs
(ASME PAPER 83-FE-22)

Critical mass flux and axial pressure profile data for fluid nitrogen are presented for N = 20, 15, 10, and 7 N-sequential-orifice-inlet configurations uniformly spaced at 15.5 cm. These data correlate well over a wide range in reduced temperature and reduced pressure, and are in general agreement with previous studies of one to four inlets. Experimental and theoretical agreement is good for liquid and gas critical mass flux, but inconclusive in the near thermodynamic critical regions. Author

A83-49472* Houston Univ., Tex.
THE 'WHISTLER-NOZZLE' PHENOMENON
A. K. M. F. HUSSAIN and M. A. Z. HASAN (Houston, University, Houston, TX) Journal of Fluid Mechanics (ISSN 0022-1120), vol. 134, Sept. 1983, p. 431-458. refs
(Contract NAG3-198)

The whistler nozzle is a simple device which can induce jet self-excitations of controllable amplitudes and frequencies and appears highly promising for many applications involving turbulent transport, combustion and aerodynamic noise. The characteristics of this curious phenomenon are documented for different values of the controlling parameters and attempts to explain the phenomenon. It is shown that the whistler excitation results from the coupling of two independent resonance mechanisms: shear-layer tone resulting from the impingement of the pipe-exit shear layer on the collar lip, and organ-pipe resonance of the pipe-nozzle. The crucial role of the shear-layer tone in driving the organ-pipe resonance is proven by reproducing the event in pipe-ring and pipe-hole configurations in the absence of the collar. It is also shown that this phenomenon is the strongest when the self-excitation frequency matches the preferred mode of the jet. Previously announced in STAR as N83-20706 Author

N83-10389*# National Aeronautics and Space Administration. Lewis Research Center, Cleveland, Ohio.
IMPLICIT MARCHING SOLUTION OF COMPRESSIBLE VISCOUS SUBSONIC FLOW IN PLANAR AND AXISYMMETRIC DUCTS Ph.D. Thesis
C. E. TOWNE and J. D. HOFFMAN (Purdue Univ., West Lafayette, Ind.) Sep. 1982 222 p refs
(NASA-TM-82876; E-1251; NAS 1.15:82876) Avail: NTIS HC A10/MF A01 CSCL 20D

A new streamwise marching procedure was developed and coded for compressible viscous subsonic flow in planar or axisymmetric ducts with or without centerbodies. The continuity, streamwise momentum, cross-flow momentum, and energy equations are written in generalized orthogonal curvilinear coordinates. To allow the use of a marching procedure, second derivatives in the streamwise momentum equation are written as the sum of a known two dimensional imposed pressure field and an unknown one dimensional viscous correction. For turbulent flow, the Reynolds stress and heat flux terms are modeled using two-layer eddy viscosity turbulence models. Author

N83-12353*# United Technologies Research Center, East Hartford, Conn.

ANALYTICAL MODELING OF OPERATING CHARACTERISTICS OF PREMIXING-PREVAPORIZING FUEL-AIR MIXING PASSAGES. VOLUME 1: ANALYSIS AND RESULTS Final Report

O. L. ANDERSON, L. M. CHIAPPETTA, D. E. EDWARDS, and J. B. MCVEY 1982 145 p refs 2 Vol.
(Contract NAS3-21269)
(NASA-CR-167990-VOL-1; NAS 1.26.167990-VOL-1; R82-915362-40-VOL-1) Avail: NTIS HC A07/MF A01 CSCL 20D

A model for predicting the distribution of liquid fuel droplets and fuel vapor in premixing-prevaporizing fuel-air mixing passages of the direct injection type is reported. This model consists of three computer programs; a calculation of the two dimensional or axisymmetric air flow field neglecting the effects of fuel; a calculation of the three dimensional fuel droplet trajectories and evaporation rates in a known, moving air flow; a calculation of fuel vapor diffusing into a moving three dimensional air flow with source terms dependent on the droplet evaporation rates. The fuel droplets are treated as individual particle classes each satisfying Newton's law, a heat transfer, and a mass transfer equation. This fuel droplet model treats multicomponent fuels and incorporates the physics required for the treatment of elastic droplet collisions, droplet shattering, droplet coalescence and droplet wall interactions. The vapor diffusion calculation treats three dimensional, gas phase, turbulent diffusion processes. The analysis includes a model for the autoignition of the fuel air mixture based upon the rate of formation of an important intermediate chemical species during the preignition period. S.L.

N83-12354*# United Technologies Research Center, East Hartford, Conn.

ANALYTICAL MODELING OF OPERATING CHARACTERISTICS OF PREMIXING-PREVAPORIZING FUEL-AIR MIXING PASSAGES. VOLUME 2: USER'S MANUAL

O. L. ANDERSON, L. M. CHIAPPETTA, D. E. EDWARDS, and J. B. MCVEY Feb. 1982 158 p refs 2 Vol.
(Contract NAS3-21269)
(NASA-CR-167990-VOL-2; NAS 1.26:167990-VOL-2; R82-915362-40-VOL-2) Avail: NTIS HC A08/MF A01 CSCL 20D

A user's manual describing the operation of three computer codes (ADD code, PTRAK code, and VAPDIF code) is presented. The general features of the computer codes, the input/output formats, run streams, and sample input cases are described. S.L.

N83-12357*# National Aeronautics and Space Administration. Lewis Research Center, Cleveland, Ohio.

TURBULENT SOLUTION OF THE NAVIER-STOKES EQUATIONS FOR AN INHOMOGENOUS DEVELOPING SHEAR LAYER

R. G. DEISSLER 1982 14 p refs Presented at the Am. Phys. Soc. Meeting on Fluid Dynamics, New Brunswick, N.J., 21-23 Nov. 1982
(NASA-TM-82969; E-1339; NAS 1.15:82969) Avail: NTIS HC A02/MF A01 CSCL 20D

To study the nonlinear physics of inhomogeneous turbulent shear flow, the unaveraged Navier-Stokes equations are solved numerically. For initial conditions a three-dimensional cosine velocity fluctuation and a mean-velocity profile with a step are used. Although the initial conditions are nonrandom. The flow soon becomes turbulent. Concentrated turbulent energy develops near the plane where the mean velocity gradient is initially infinite. The terms in the one-point correlation equation for turbulent energy, including those for the diffusion and production of turbulence, are calculated, the diffusion terms tend to make the turbulence more homogeneous. Author

N83-12358*# National Aeronautics and Space Administration. Lewis Research Center, Cleveland, Ohio.

NUMERICAL SIMULATION OF THE FLOW AND FUEL-AIR MIXING IN AN AXISYMMETRIC PISTON-CYLINDER ARRANGEMENT

T. I. P. SHIH, G. E. SMITH (Michigan Univ, Ann Arbor), and G. S. SPRINGER (Michigan Univ., Ann Arbor) 1982 25 p refs
(NASA-TM-83011; E-1446; NAS 1.15:83011) Avail: NTIS HC A02/MF A01 CSCL 20D

The implicit factored method of Beam and Warming was employed to describe the flow and the fuel-air mixing in an axisymmetric piston-cylinder configuration during the intake and compression strokes. The governing equations were established on the basis of laminar flow. The increased mixing due to turbulence was simulated by appropriately chosen effective transport properties. Calculations were performed for single-component gases and for two-component gases and for two-component gas mixtures. The flow field was calculated as functions of time and position for different geometries, piston speeds, intake-charge-to-residual-gas-pressure ratios, and species mass fractions of the intake charge. Results are presented in graphical form which show the formation, growth, and break-up of those vortices which form during the intake stroke and the mixing of fuel and air throughout the intake and compression strokes. It is shown that at bore-to-stroke ratio of less than unity, the vortices may break-up during the intake stroke. It is also shown that vortices which do not break-up during the intake stroke coalesce during the compression stroke. The results generated were compared to existing numerical solutions and to available experimental data. Author

N83-12359*# National Aeronautics and Space Administration. Lewis Research Center, Cleveland, Ohio.

COMPUTER PROGRAM FOR A FOUR-CYLINDER-STIRLING-ENGINE CONTROLS SIMULATION Final Report

C. J. DANIELS and C. F. LORENZO Jun. 1982 83 p refs
(Contract DE-AI01-77CS-51040)
(NASA-TM-82774; E-1103; DOE/NASA/51040-37; NAS 1.15:82774) Avail: NTIS HC A05/MF A01 CSCL 09B

A four cylinder Stirling engine, transient engine simulation computer program is presented. The program is intended for controls analysis. The associated engine model was simplified to shorten computer calculation time. The model includes engine mechanical drive dynamics and vehicle load effects. The computer program also includes subroutines that allow: (1) acceleration of the engine by addition of hydrogen to the system, and (2) braking of the engine by short circuiting of the working spaces. Subroutines to calculate degraded engine performance (e.g., due to piston ring and piston rod leakage) are provided. Input data required to run the program are described and flow charts are provided. The program is modular to allow easy modification of individual routines. Examples of steady state and transient results are presented. S.L.

N83-12360*# National Aeronautics and Space Administration. Lewis Research Center, Cleveland, Ohio.

FILM-COOLING EFFECTIVENESS WITH DEVELOPING COOLANT FLOW THROUGH STRAIGHT AND CURVED TUBULAR PASSAGES

S. S. PAPELL, C. R. WANG, and R. W. GRAHAM Nov. 1982 21 p refs
(NASA-TP-2062; E-1206; NAS 1.60:2062) Avail: NTIS HC A02/MF A01 CSCL 20D

The data were obtained with an apparatus designed to determine the influence of tubular coolant passage curvature on film-cooling performance while simulating the developing flow entrance conditions more representative of cooled turbine blade. Data comparisons were made between straight and curved single tubular passages embedded in the wall and discharging at 30 deg angle in line with the tunnel flow. The results showed an influence of curvature on film-cooling effectiveness that was inversely proportional to the blowing rate. At the lowest blowing

rate of 0.18, curvature increased the effectiveness of film cooling by 35 percent; but at a blowing rate of 0.76, the improvement was only 10 percent. In addition, the increase in film-cooling area coverage ranged from 100 percent down to 25 percent over the same blowing rates. A data trend reversal at a blowing rate of 1.5 showed the straight tubular passage's film-cooling effectiveness to be 20 percent greater than that of the curved passage with about 80 percent more area coverage. An analysis of turbulence intensity detain the mixing layer in terms of the position of the mixing interface relative to the wall supported the concept that passage curvature tends to reduce the diffusion of the coolant jet into the main stream at blowing rates below about. Explanations for the film-cooling performance of both test sections were made in terms differences in turbulences structure and in secondary flow patterns within the coolant jets as influenced by flow passage geometry. Author

N83-13387*# Colorado State Univ., Fort Collins. Fluid Mechanics and Wind Engineering Program.

TURBULENCE EFFECT ON CROSSFLOW AROUND A CIRCULAR CYLINDER AT SUBCRITICAL REYNOLDS NUMBERS Final Report

W. Z. SADEH and D. B. SAHARON Washington NASA Nov. 1982 153 p refs

(Contract NSG-3127)

(NASA-CR-3622; NAS 1.26:3622; CER-81-82-WZS-DBS51)

Avail: NTIS HC A08/MF A01 CSCL 20D

An investigation of the effect of freestream turbulence on the flow around a smooth circular cylinder at subcritical Reynolds numbers from 5.2 x 10 to the 4th power to 2.09 x 10 to the 5th power was conducted. Measurements show that the interaction of incident turbulence with the initial laminar boundary layer: (1) modifies the characteristics of the mean surface pressure distribution; (2) induces an aft shift in the separation point ranging from 5 to 50 beyond the laminar separation angle of 80 degrees; and, (3) reduces the mean drag coefficient to values between 97 and 46% of its nearly constant laminar counterpart. The extent of these changes depends on the particular Reynolds number background turbulence combination. These results demonstrate that a boundary-layer flow similar to that found in critical, supercritical and/or transcritical flow regimes is induced by turbulence at subcritical Reynolds numbers and, hence, the effect of turbulence is equivalent to an effective increase in the Reynolds number. The change in the nature and properties of the boundary layer in the subcritical regime, consequent upon the penetration of turbulence into it, is in agreement with the model proposed by the vorticity-amplification theory. Author

N83-13392*# National Aeronautics and Space Administration. Lewis Research Center, Cleveland, Ohio.

COMPARISON OF PREDICTED AND EXPERIMENTAL EXTERNAL HEAT TRANSFER AROUND A FILM COOLED CYLINDER IN CROSSFLOW

F. S. STEPKA and R. E. GAUGLER 1983 14 p refs To be presented at the 28th Ann. Intern. Gas Turbine Conf., Phoenix, 27-31 Mar. 1983; sponsored by ASME

(NASA-TM-83017; E-1452; NAS 1.15:83017) Avail: NTIS HC A02/MF A01 CSCL 20D

Calculations were made of the film cooling provided by rows of holes around the circumference of a cylinder in crossflow and the results were compared to experimental data. The calculations and experimental data were for conditions that simulate most of those that are typical of air cooled turbine vane leading edges. Injection was from a single and multiple rows of holes located at different angular locations from the stagnation line. The holes in the rows were angled normal to the flow direction and at a 25 degree angle to the cylinder wall. The calculations and experimental data were for several constant values of blowing ratios for all rows and for different blowing ratios for each row, representing a simulation of a common coolant plenum supply to multiple rows of holes. The calculations were made using a finite difference boundary layer code, STAN5. Contrary to initial expectations that injection would trip the boundary layer flow into the turbulent regime, the results indicated that the high free stream acceleration apparently kept the flow laminar for holes in the first 45 degrees past stagnation. The trend in Stanton number reduction due to coolant injection was predicted with generally good agreement at the lower blowing rates, but for multile rows of holes, agreement was poor beyond the first row. Author

N83-14431*# National Aeronautics and Space Administration. Lewis Research Center, Cleveland, Ohio.

LENGTH TO DIAMETER RATIO AND ROW NUMBER EFFECTS IN SHORT PIN FIN HEAT TRANSFER

B. A. BRIGHAM and G. J. VANFOSSEN 1982 10 p refs Proposed for presentation at the 28th Ann. Intern. Gas Turbine Conf., Phoenix, Ariz., 27-31 Mar. 1983; sponsored by ASME

(NASA-TM-83005; E-1442; NAS 1.15:83005) Avail: NTIS HC A02/MF A01 CSCL 20D

The relative effects of pin length to diameter ratio and of pin row geometry on the heat transfer from pin fins, was determined. Array averaged heat transfer coefficients on pin and endwall surfaces were measured for two configurations of staggered arrays of short pin fins (length to diameter ratio of 4). One configuration contained eight streamwise rows of pins, while the other contained only four rows. Results showed that both the 8-row and the 4-row configurations for an L sub p/D of 4, exhibit higher heat transfer than in similar tests on shorter pin fns (L sub p/D of 1/2 and 2). It was also found that for this L sub p/D ratio, the array averaged heat transfer was slightly higher with eight rows of staggered pins than with only four rows. J.D.

N83-14432*# National Aeronautics and Space Administration. Lewis Research Center, Cleveland, Ohio.

MEASURED AND CALCULATED WALL TEMPERATURES ON AIR-COOLED TURBINE VANES WITH BOUNDARY LAYER TRANSITION

C. H. LIEBERT, R. E. GAUGLER, and H. J. GLADDEN 1982 12 p refs Proposed for presentation at the 28th Ann. Intern. Gas Turbine Conf., Phoenix, Ariz., 27-31 Mar. 1983; sponsored by ASME

(NASA-TM-83030; E-1466; NAS 1.15:83030) Avail: NTIS HC A02/MF A01 CSCL 20D

Convection cooled turbine vane metal wall temperatures experimentally obtained in a hot cascade for one vane design were compared with wall temperatures calculated with TACT1 and STAN5 computer codes which incorporated various models for predicting laminar-to-turbulent boundary layer transition. Favorable comparisons on both vane surface were obtained at high Reynolds number with only one of these transition models. When other models were used, temperature differences between calculated and experimental data obtained at the high Reynolds number were as much as 14 percent in the separation bubble region of the pressure surface. On the suction surface and at lower Reynolds number, predictions and data unsatisfactorily differed by as much as 22 percent. Temperature differences of this magnitude can represent orders of magnitude error in blade life prediction.

Author

N83-14434*# Dynamics Technology, Inc., Torrance, Calif.

TURBULENCE MEASUREMENTS IN A SWIRLING CONFINED JET FLOWFIELD USING A TRIPLE HOT-WIRE PROBE

S. I. JANJUA and D. K. MCLAUGHLIN 27 Dec. 1982 63 p refs Prepared for Oklahoma State Univ. Sponsored in part by Air Force Wright Aeronautical Labs.

(Contract NAG3-74)

(NASA-CR-169668; NAS 1.26:169668; DT-8178-02) Avail: NTIS HC A04/MF A01 CSCL 20D

An axisymmetric swirling confined jet flowfield, similar to that encountered in gas turbine combustors was investigated using a triple hot-wire probe. The raw data from the three sensors were digitized using ADC's and stored on a Tektronix 4051 computer. The data were further reduced on the computer to obtain time-series for the three instantaneous velocity components in the flowfield. The time-mean velocities and the turbulence quantities were deduced. Qualification experiments were performed and

where possible results compared with independent measurements. The major qualification experiments involved measurements performed in a non-swirling flow compared with conventional X-wire measurements. In the swirling flowfield, advantages of the triple wire technique over the previously used multi-position single hot-wire method are noted. The measurements obtained provide a data base with which the predictions of turbulence models in a recirculating swirling flowfield can be evaluated. A.R.H.

N83-14435*# National Aeronautics and Space Administration. Lewis Research Center, Cleveland, Ohio.
COMPARISON OF VISUALIZED TURBINE ENDWALL SECONDARY FLOWS AND MEASURED HEAT TRANSFER PATTERNS
R. E. GAUGLER and L. M. RUSSELL 1983 14 p refs Proposed for presentation at the 28th Ann. Intern. Gas Turbine Conf., Phoenix, Ariz., 27-31 Mar. 1983; sponsored by ASME
(NASA-TM-83016; E-1450; NAS 1.15:83016) Avail: NTIS HC A02/MF A01 CSCL 20D

Various flow visualization techniques were used to define the secondary flows near the endwall in a large heat transfer data. A comparison of the visualized flow patterns and the measured Stanton number distribution was made for cases where the inlet Reynolds number and exit Mach number were matched. Flows were visualized by using neutrally buoyant helium-filled soap bubbles, by using smoke from oil soaked cigars, and by a few techniques using permanent marker pen ink dots and synthetic wintergreen oil. Details of the horseshoe vortex and secondary flows can be directly compared with heat transfer distribution. Near the cascade entrance there is an obvious correlation between the two sets of data, but well into the passage the effect of secondary flow is not as obvious. M.G.

N83-15590*# Garrett Turbine Engine Co., Phoenix, Ariz.
DILUTION JET MIXING PROGRAM, PHASE 1
R. SRINIVASAN, A. BERENFELD, and H. C. MONGIA Nov. 1982 236 p refs
(Contract NAS3-22110)
(NASA-CR-168031; NAS 1.26:168031; GARRETT-21-4302)
Avail: NTIS HC A11/MF A01 CSCL 20D

The effect of jet to mainstream density ratio, flow area convergence as encounted in transition sections, and nonuniform mainstream profile upstream of dilution orifices on the mixing of a row of jets with a confined cross flow was quantified. It is found that: (1) jet spreading rate in transverse direction is increased with increasing J, H/D and with decreasing S/D; (2) the density ratio has only a second order effect on the jet mixing characteristics for a constant momentum ratio; (3) the temperature distributions in the jet mixing region are strongly influenced by the undisturbed mainstream profile; (4) flow area convergence enhances mixing in radial and transverse directions. An asymmetric convergent duct with flat wall injection has the same jet mixing characteristics as a symmetric convergent duct. An asymmetric convergent duct with slant wall injection has a faster jet spreading rate in the transverse direction. E.A.K.

N83-15592*# Arizona State Univ., Tempe. Dept. of Mechanical and Aerospace Engineering.
JET ARRAY IMPINGEMENT FLOW DISTRIBUTIONS AND HEAT TRANSFER CHARACTERISTICS. EFFECTS OF INITIAL CROSSFLOW AND NONUNIFORM ARRAY GEOMETRY Final Report
L. W. FLORSCHUETZ, D. E. METZGER, C. C. SU, Y. ISODA, and H. H. TSENG Washington NASA Nov. 1982 178 p
(Contract NSG-3075)
(NASA-CR-3630; NAS 1.26:3630; ERC-R-82038) Avail: NTIS HC A09/MF A01 CSCL 20D

Two-dimensional arrays of circular air jets impinging on a heat transfer surface parallel to the jet orifice plate are considered. The jet flow, after impingement, is constrained to exit in a single direction along the channel formed by the jet orifice plate and the heat transfer surface. The configurations considered are intended to model those of interest in current and contemplated gas turbine airfoil midchord cooling applications. The effects of an initial crossflow which approaches the array through an upstream extension of the channel are considered. Flow distributions as well as heat transfer coefficients and adiabatic wall temperatures resolved to one streamwise hole spacing were measured as a function of the initial crossflow rate and temperature relative to the jet flow rate and temperature. Both Nusselt number profiles and dimensionless adiabatic wall temperature (effectiveness) profiles are presented and discussed. Special test results which show a significant reduction of jet orifice discharge coefficients owing to the effect of a confined crossflow are also presented, along with a flow distribution model which incorporates those effects. A nonuniform array flow distribution model is developed and validated. M.G.

N83-16678*# Pennsylvania State Univ., University Park. Turbomachinery Lab.
END WALL FLOWS IN ROTORS AND STATORS OF A SINGLE STAGE COMPRESSOR Semiannual Progress Report
T. R. GOVINDAN, K. N. S. MURTHY, and B. LAKSHMINARAYANA Jan. 1983 25 p refs
(Contract NSG-3212)
(NASA-CR-169800; NAS 1.26:169800; PSU/TURBO-83-2) Avail: NTIS HC A02/MF A01 CSCL 20D

A computer code for solving the parabolized Navier-Stokes equations for internal flows was developed. Oscillations that develop in the calculation procedure are discussed. The measurements made in the hub and annulus wall boundary layers are summarized. The flow in the hub wall boundary layer, starting ahead of the inlet guide vanes to the inlet of the rotor is traced. S.L.

N83-16679*# Pennsylvania State Univ., University Park. Turbomachinery Lab.
THREE DIMENSIONAL FLOW FIELD INSIDE COMPRESSOR ROTOR, INCLUDING BLADE BOUNDARY LAYERS Semiannual Progress Report
M. POUAGARE, B. LAKSHMINARAYANA, and J. M. GALMES Jan. 1983 52 p refs
(Contract NSG-3266)
(NASA-CR-169788; NAS 1.26:169788; PSU/TURBO-83-1) Avail: NTIS HC A04/MF A01 CSCL 20A

The space marching code was modified in order to be able to predict the flow field inside a rotor passage, including the blade and hub wall boundary layers. The basic changes incorporated are modifications of the equations so that the code can handle three dimensional configurations with changes in the radial direction (for example changes in stagger angle, blade camber and thickness), extensions and modifications in order to implement a physically realistic turbulence model such as a k sigma model and an algebraic Reynolds stress model. S.L.

N83-17833*# National Aeronautics and Space Administration. Lewis Research Center, Cleveland, Ohio.
EXPERIMENTAL INVESTIGATION OF THE VAPOROUS/GASEOUS CAVITY CHARACTERISTICS OF AN ECCENTRIC JOURNAL BEARING
M. J. BRAUN and R. C. HENDRICKS Oct. 1982 15 p refs Presented at the Joint Lubrication Conf., Washington, 4-6 Oct. 1982 Previously announced as A83-13230
(NASA-TM-82996; E-1429; NAS 1.15:82996) Avail: NTIS HC A02/MF A01 CSCL 20D

For abstract see A83-13230

N83-17834*# National Aeronautics and Space Administration. Lewis Research Center, Cleveland, Ohio.
FINITE ELEMENT FORMULATION FOR TRANSIENT HEAT TREAT PROBLEMS
R. L. MULLEN (Case Western Reserve Univ.) and R. C. HENDRICKS 1983 9 p refs Proposed for presentation at the Thermal Eng. Joint Conf., Honolulu, Hawaii, 20-24 Mar. 1983; sponsored by ASME and the Japan Society of Mechanical Engineers
(NASA-TM-83070; E-1520; NAS 1.15:83070) Avail: NTIS HC A02/MF A01 CSCL 20D

The macrothermomechanical behavior of materials subjected to rapid thermal or mechanical loading such as occurs in most heat treatments is described. The equations are developed for Lagrangian, Eulerian, and intermediary kinematic descriptions and are independent of the constitutive laws and the equation of state; they can be solved numerically for a specified material and boundary conditions. The coupled transport effects between dissipation and energy are included. The conventional linearized stability approach indicates the numerical procedure to be stable, with certain restriction on the time step size. S.L.

N83-19016*# National Aeronautics and Space Administration. Lewis Research Center, Cleveland, Ohio.
SURFACE ROUGHNESS EFFECTS IN HYDRODYNAMIC LUBRICATION: THE FLOW FACTOR METHOD
J. H. TRIPP 1982 17 p refs Presented at the Joint Lubrication Conf., Washington, D.C., 4-6 Oct. 1982; sponsored by ASME and the American Society of Lubrication Engineers Previously announced in IAA as A83-13523
(NASA-TM-83024; E-1460; NAS 1.15:83024) Avail: NTIS HC A02/MF A01 CSCL 20D

For abstract see A83-13523.

N83-19020*# National Aeronautics and Space Administration. Lewis Research Center, Cleveland, Ohio.
STUDIES OF FLOWS THROUGH N-SEQUENTIAL ORIFICES
R. C. HENDRICKS 1983 16 p refs Proposed for presentation at the Spring Meeting of the Fluids Eng. Appl. Mech. and Bioeng. Div. of the ASME, Houston, Tex., 20-22 Jun. 1983
(NASA-TM-83313; E-1554; NAS 1.15:83313) Avail: NTIS HC A02/MF A01 CSCL 20D

Critical mass flux and axial pressure profile data for fluid nitrogen are presented for N = 20, 15, 10, and 7 N-sequential orifice inlet configurations uniformly spaced at 15.5 cm. These data correlate well over a wide range in reduced temperature (0.7 T sub r,o ambient) and reduced pressure (to P sub r = 2) and are in general agreement with studies of one to four inlets and labyrinth seal gas data for 33 tooth equivalent sequential inlets. Experimental and theoretical agreement is good for liquid and gas critical mass flux. A.L.

N83-20029*# National Aeronautics and Space Administration. Lewis Research Center, Cleveland, Ohio.
THERMOMECHANICAL LOADING OF MULTILAYERED CYLINDRICAL GEOMETRIES IN THERMAL CYCLING FROM 300 TO 1300 K
R. C. HENDRICKS, G. MCDONALD, R. L. MULLEN (Case Western Reserve Univ.), M. J. BRAUN (Akron Univ.), B. T. CHUNG (Akron Univ.), and J. PADOVAN (Akron Univ.) 1983 28 p refs Presented at the Thermal Eng. Joint Conf., Honolulu, Hawaii, 20-24 Mar. 1983; sponsored by the ASME and the Japan Society of Mechanical Engineers
(NASA-TM-83312; E-1518; NAS 1.15:83312) Avail: NTIS HC A03/MF A01 CSCL 20D

The principal of multiple material layering is well known as an effective method of reducing heat transfer; however, thermal gradients can impose significant loads and lead to delamination and subsequent component failure. An analysis is developed and experimental data are discussed for the thermomechanical effects of multilayered materials on a heat sink substrate of cylindrical geometry subject to thermal cycling. The geometry is heated in cross-flow by a high-velocity flame and cooled in crossflow by ambient-temperature air from a critical flow orifice. Each layer of material possesses a threshold beyond which small changes in temperature or mechanical loading greatly influence the life in thermal cycling of the layered materials. Comparisons are made between the thermomechanical loads predicted by various numerical codes for the linear case and by a simplified analytic model. Author

N83-22542*# National Aeronautics and Space Administration. Lewis Research Center, Cleveland, Ohio.
ANALOGY BETWEEN FLUID CAVITATION AND FRACTURE MECHANICS
R. C. HENDRICKS, R. L. MULLEN (Case Western Reserve Univ.), and M. J. BRAUN (Akron Univ., Ohio) 1983 26 p refs Presented at the Thermal Eng. Joint Conf., Honolulu, Hawaii, 20-24 Mar. 1983; sponsored by ASME and Japan Society of Mechanical Engineers
(NASA-TM-83071; E-1519; NAS 1.15:83071) Avail: NTIS HC A03/MF A01 CSCL 20D

When the stresses imposed on a fluid are sufficiently large, rupture or cavitation can occur. Such conditions can exist in many two-phase flow applications, such as the choked flows, which can occur in seals and bearings. Nonspherical bubbles with large aspect ratios have been observed in fluids under rapid acceleration and high shear fields. These bubbles are geometrically similar to fracture surface patterns (Griffith crack model) existing in solids. Analogies between crack growth in solid and fluid cavitation are proposed and supported by analysis and observation (photographs). Healing phenomena (void condensation), well accepted in fluid mechanics, have been observed in some polymers and hypothesized in solid mechanics. By drawing on the strengths of the theories of solid mechanics and cavitation, a more complete unified theory can be developed. Author

N83-22546*# National Aeronautics and Space Administration. Lewis Research Center, Cleveland, Ohio.
STOCHASTIC DIFFERENTIAL EQUATIONS AND TURBULENT DISPERSION
P. A. DURBIN Apr. 1983 72 p refs
(NASA-RP-1103; E-1425; NAS 1.61:1103) Avail: NTIS HC A04/MF A01 CSCL 20D

Aspects of the theory of continuous stochastic processes that seem to contribute to an understanding of turbulent dispersion are introduced and the theory and philosophy of modelling turbulent transport is emphasized. Examples of eddy diffusion examined include shear dispersion, the surface layer, and channel flow. Modeling dispersion with finite-time scale is considered including the Langevin model for homogeneous turbulence, dispersion in nonhomogeneous turbulence, and the asymptotic behavior of the Langevin model for nonhomogeneous turbulence. A.R.H.

N83-22550*# Pennsylvania State Univ., University Park. Dept. of Mechanical Engineering.
THE STRUCTURE OF EVAPORATING AND COMBUSTING SPRAYS: MEASUREMENTS AND PREDICTIONS Semiannual Status Report, 1 Sep. 1981 - 28 Feb. 1982
J. S. SHUEN, A. S. P. SOLOMON, and G. M. FAETH Mar. 1982 43 p refs
(Contract NAG3-190)
(NASA-CR-170176; NAS 1.26:170176) Avail: NTIS HC A03/MF A01 CSCL 20D

An apparatus was constructed to provide measurements in open sprays with no zones of recirculation, in order to provide well-defined conditions for use in evaluating spray models. Measurements were completed in a gas jet, in order to test experimental methods, and are currently in progress for nonevaporating sprays. A locally homogeneous flow (LHF) model where interphase transport rates are assumed to be infinitely fast; a separated flow (SF) model which allows for finite interphase transport rates but neglects effects of turbulent fluctuations on drop motion; and a stochastic SF model which considers effects of turbulent fluctuations on drop motion were evaluated using existing data on particle-laden jets. The LHF model generally

overestimates rates of particle dispersion while the SF model underestimates dispersion rates. The stochastic SF flow yield satisfactory predictions except at high particle mass loadings where effects of turbulence modulation may have caused the model to overestimate turbulence levels. A.R.H.

N83-23544*# National Aeronautics and Space Administration. Lewis Research Center, Cleveland, Ohio.
GENERATION OF TOLLMIEN-SCHLICHTING WAVES BY FREE-STREAM DISTURBANCES AT LOW MACH NUMBERS
M. E. GOLDSTEIN Mar. 1983 76 p
(NASA-TM-83026; E-1480; NAS 1.15:83026) Avail: NTIS HC A05/MF A01 CSCL 20D

The method of matched asymptotic expansions is used to study the generation of Tollmien-Schlichting waves by free stream disturbances incident on a flat plate boundary layer. Near the leading edge, the motion is governed by the unsteady boundary layer equation, while farther downstream it is governed (to lowest order) by the Orr-Sommerfeld equation with slowly varying coefficients. It is shown that there is an overlap domain where the Tollmien-Schlichting wave solutions to the Orr-Sommerfeld equation and an appropriate asymptotic solution of the unsteady boundary layer equation match, in the matched asymptotic expansion sense. The analysis leads to a set of scaling laws for the asymptotic structure of the unsteady boundary layer. Author

N83-23545*# National Aeronautics and Space Administration. Lewis Research Center, Cleveland, Ohio.
AERODYNAMIC-WAVE BREAK-UP OF LIQUID SHEETS IN SWIRLING AIRFLOWS AND COMBUSTOR MODULES
R. INGEBO 1983 16 p refs Presented at the 19th Joint Propulsion Conf. and Tech. Display, Seattle, 27-29 Jun. 1983; sponsored by AIAA, SAE, and ASME
(NASA-TM-83353; E-1610; NAS 1.15:83353) Avail: NTIS HC A02/MF A01 CSCL 20D

Experimental mean drop diameter data were obtained for the atomization of liquid sheets injected axially downstream in high velocity swirling and nonswirling airflow. Conventional simplex pressure atomizing fuel nozzles and splash type fuel injectors were studied under simulated combustor inlet airflow conditions. A general empirical expression relating recirprocal mean drop diameter to airstream mass velocity was obtained and is presented. The finest degree of atomization, i.e., the highest value of the coefficient C, was obtained with swirl can combustor modules (C = 15) as compared with pressure atomizing nozzles (C = 12). A.R.H.

N83-24795*# Pennsylvania State Univ., University Park. Dept. of Mechanical Engineering.
THE STRUCTURE OF EVAPORATING AND COMBUSTING SPRAYS: MEASUREMENTS AND PREDICTIONS Semiannual Status Report, 1 Sep. 1982 - 28 Feb. 1983
J. S. SHUEN, A. S. P. SOLOMON, and F. M. FAETH Mar. 1983 37 p refs
(Contract NAG3-190)
(NASA-CR-170312; NAS 1.26:170312) Avail: NTIS HC A02/MF A01 CSCL 20D

The structure of particle-laden jets and nonevaporating and evaporating sprays was measured in order to evaluate models of these processes. Three models are being evaluated: (1) a locally homogeneous flow model, where slip between the phases is neglected and the flow is assumed to be in local thermodynamic equilibrium; (2) a deterministic separated flow model, where slip and finite interphase transport rates are considered but effects of particle/drop dispersion by turbulence and effects of turbulence on interphase transport rates are ignored; and (3) a stochastic separated flow model, where effects of interphase slip, turbulent dispersion and turbulent fluctuations are considered using random sampling for turbulence properties in conjunction with random-walk computations for particle motion. All three models use a k-e-g turbulence model. All testing and data reduction are completed for the particle laden jets. Mean and fluctuating velocities of the continuous phase and mean mixture fraction were measured in the evaporating sprays. A.R.H.

N83-24798*# National Aeronautics and Space Administration. Lewis Research Center, Cleveland, Ohio.
A REFRIGERATED DYNAMIC SEAL
R. C. HENDRICKS 1983 10 p refs Proposed for presentation at Cryogenic Engr. Conf./Intern Cryogenic Mater. Conf., Colorado Springs, 15-19 Aug. 1983
(NASA-TM-83378; E-1649; NAS 1.15:83378) Avail: NTIS HC A02/MF A01 CSCL 11A

A new sealing concept is proposed where the fluid to be sealed flows through a refrigerated housing or constriction, is frozen to the housing during the transient phase, and under steady state conditions provides a dynamic seal with essentially 'zero' leakage. Author

N83-24799*# National Aeronautics and Space Administration. Lewis Research Center, Cleveland, Ohio.
THE EFFECT OF ANNEALING ON THE CREEP OF PLASMA SPRAYED CERAMICS
R. C. HENDRICKS, G. MCDONALD, and R. L. MULLEN (Case Western Reserve Univ.) 1983 18 p refs Presented at 7th Ann. Conf. on Ceramics and Advanced Mater., Cocoa Beach, Fla., 16-23 Jan. 1983; sponsored by American Ceramic Society
(NASA-TM-83396; E-1673; NAS 1.15:83396) Avail: NTIS HC A02/MF A01 CSCL 20D

The creep of plasma sprayed ZrO2-8Y2O3 was measured at temperatues from 98 to 1250 C (180 to 220 F), and compared to creep of identical samples after annealing at temperatures from 98 to 1316 C (1800 to 2400 F). Loads and temperatures which produced significant creep of as sprayed ceramics produced no creep after annealing. Author

N83-24800*# National Bureau of Standards, Boulder, Colo. Thermophysical Properties Div.
TRANSPORT PROPERTIES OF OXYGEN
H. M. RODER Apr. 1983 86 p refs
(Contract NASA ORDER C-32369-C)
(NASA-RP-1102; NAS 1.61:1102; NBSIR-82-1672) Avail: NTIS HC A05/MF A01 CSCL 20D

Tables of viscosity, thermal conductivity, and thermal diffusivity of oxygen as a function of temperature and pressure from the triple point to 320 K and at pressures to 100 MPa are presented. Auxiliary tables in engineering units are also given. Viscosity and thermal conductivity are calculated from published correlations. Density and specific heat at constant pressure, required to calculate thermal diffusivity, are obtained from an equation of state. The Prandtl number can be obtained quite easily from the values tabulated. S.L.

N83-26017*# National Aeronautics and Space Administration. Lewis Research Center, Cleveland, Ohio.
A 4-CYLINDER STIRLING ENGINE COMPUTER PROGRAM WITH DYNAMIC ENERGY EQUATIONS Final Report
C. J. DANIELE and C. F. LORENZO May 1983 65 p refs
(Contract DE-AI01-77CS-51040)
(NASA-TM-83053; E-1348; NAS 1.15:83053; DOE/NASA/52040-44) Avail: NTIS HC A04/MF A01 CSCL 10B

A computer program for simulating the steady state and transient performance of a four cylinder Stirling engine is presented. The thermodynamic model includes both continuity and energy equations and linear momentum terms (flow resistance). Each working space between the pistons is broken into seven control volumes. Drive dynamics and vehicle load effects are included. The model contains 70 state variables. Also included in the model are piston rod seal leakage effects. The computer program includes a model of a hydrogen supply system, from which hydrogen may be added to the system to accelerate the engine. Flow charts are provided. Author

N83-27144* National Aeronautics and Space Administration. Lewis Research Center, Cleveland, Ohio.
CURVED FILM COOLING ADMISSION TUBE Patent
R. W. GRAHAM and S. S. PAPELL, inventors (to NASA) 27 Oct. 1980 6 p Filed 27 Oct. 1980 Supersedes N81-12363 (19 - 03, p 0343)
(NASA-CASE-LEW-13174-1; US-PATENT-4,384,823; US-PATENT-APPL-SN-200634; US-PATENT-CLASS-416-1; US-PATENT-CLASS-415-115; US-PATENT-CLASS-416-97R)
Avail: US Patent and Trademark Office CSCL 20D

Effective film cooling to protect a wall surface from a hot fluid which impinges on or flows along the surface is provided. A film of cooling fluid having increased area is provided by changing the direction of a stream of cooling fluid through an angle of from 135 deg. to 165 deg. before injecting it through the wall into the hot flowing gas. The 1, cooling fluid is injected from an orifice through a wall into a hot flowing gas at an angle to form a cooling fluid film. Cooling fluid is supplied to the orifice from a cooling fluid source via a turbulence control passageway having a curved portion between two straight portions. The angle through which the direction of the cooling fluid is turned results in less mixing of the cooling fluid with the hot gas, thereby substantially increasing the length of the film in a downstream direction.

Official Gazette of the U.S. Patent and Trademark Office

N83-28376*# Detroit Diesel Allison, Indianapolis, Ind.
ANALYTICAL AND EXPERIMENTAL EVALUATION OF THE HEAT TRANSFER DISTRIBUTION OVER THE SURFACES OF TURBINE VANES Final Report
L. D. HYLTON, M. S. MIHELC, E. R. TURNER, D. A. NEALY, and R. E. YORK May 1983 228 p refs
(Contract NAS3-22761)
(NASA-CR-168015; NAS 1.26:168015; EDR-11209) Avail: NTIS HC A11/MF A01 CSCL 20D

Three airfoil data sets were selected for use in evaluating currently available analytical models for predicting airfoil surface heat transfer distributions in a 2-D flow field. Two additional airfoils, representative of highly loaded, low solidity airfoils currently being designed, were selected for cascade testing at simulated engine conditions. Some 2-D analytical methods were examned and a version of the STAN5 boundary layer code was chosen for modification. The final form of the method utilized a time dependent, transonic inviscid cascade code coupled to a modified version of the STAN5 boundary layer code featuring zero order turbulence modeling. The boundary layer code is structured to accommodate a full spectrum of empirical correlations addressing the coupled influences of pressure gradient, airfoil curvature, and free-stream turbulence on airfoil surface heat transfer distribution and boundary layer transitional behavior. Comparison of pedictions made with the model to the data base indicates a significant improvement in predictive capability. A.R.H.

N83-28380*# National Aeronautics and Space Administration. Lewis Research Center, Cleveland, Ohio.
RESIDUAL STRESS IN PLASMA SPRAYED CERAMIC TURBINE TIP AND GAS PATH SEAL SPECIMENS
R. C. HENDRICKS, G. MCDONALD, and R. L. MULLEN (Case Western Reserve Univ.) 1983 15 p refs Presented at the 7th Ann. Conf. on Ceramics and Advan. Mater., Cocoa Beach, Fla., 16-23 Jan. 1983; sponsored by the American Ceramic Society
(NASA-TM-83418; E-1706; NAS 1.15:83418) Avail: NTIS HC A02/MF A01 CSCL 20D

The residual stresses in a ceramic sheet material used for turbine blade tip gas path seals, were estimated. These stresses result from the plasma spraying process which leaves the surface of the sheet in tension. To determine the properties of plasma sprayed ZrO2-Y2O3 sheet material, its load deflection characteristics were measured. Estimates of the mechanical properties for sheet materials were found to differ from those reported for plasma sprayed bulk materials. Author

N83-29216*# National Aeronautics and Space Administration. Lewis Research Center, Cleveland, Ohio.
DILUTION ZONE MIXING
J. D. HOLDEMAN *In its* Combust. Fundamentals Res. p 65-76 Mar. 1983 refs
Avail: NTIS HC A12/MF A01 CSCL 20D

Studies to characterize dilution zone mixing; experiments on the effects of free-stream turbulence on a jet in crossflow; and the development of an interactive computer code for the analysis of the mixing of jets with a confined crossflow are reviewed.

R.J.F.

N83-29625* National Aeronautics and Space Administration. Lewis Research Center, Cleveland, Ohio.
MAGNETIC HEAT PUMPING Patent
G. V. BROWN, inventor (to NASA) 12 Jul. 1983 9 p Filed 19 Feb. 1981 Supersedes N82-24449 (20 - 15, p 2082)
(NASA-CASE-LEW-12508-3; US-PATENT-4,392,356; US-PATENT-APPL-SN-235868; US-PATENT-CLASS-62-3) Avail: US Patent and Trademark Office CSCL 20D

The method employs ferromagnetic or ferromagnetic elements, preferably of rare-earth based material, for example gadolinium, and preferably employs a regenerator. The steps comprise controlling the temperature and applied magnetic field of the element to cause the state of the element as represented on a temperature-magnetic entropy diagram repeatedly to traverse a loop. The loop may have a first portion of concurrent substantially isothermal or constant temperature and increasing applied magnetic field, a second portion of lowering temperature and constant applied magnetic field, a third portion of isothermal and decreasing applied magnetic field, and a fourth portion of increasing temperature and constant applied magnetic field. Other loops may be four sided, with, for example, two isotherms and two adiabats (constant entropy portions.

Official Gazette of the U.S. Patent and Trademark Office

N83-30957*# National Aeronautics and Space Administration. Lewis Research Center, Cleveland, Ohio.
AIR MODULATION APPARATUS Patent Application
D. T. LENAHAN, R. J. CORSMEIER, and A. P. STERMAN, inventors (to NASA) 25 Feb. 1981 18 p
(NASA-CASE-LEW-13524-1; US-PATENT-APPL-SN-238257)
Avail: NTIS HC A02/MF A01 CSCL 20D

An air modulation apparatus, such as for use in modulating cooling air to the turbine section of a gas turbine engine includes a valve means disposed around an annular conduit, such as a nozzle, in the engine cooling air circuit. The valve means, when in a closed position, blocks a portion of the conduit, and thus reduces the amount and increases the velocity of cooling air flowing through the nozzle. The apparatus also includes actuation means, which can operate in response to predetermined engine conditions, for enabling opening and closing of the valve. NASA

N83-30959*# Pratt and Whitney Aircraft Group, East Hartford, Conn.
AEROTHERMAL MODELING PROGRAM, PHASE 1 Final Report, Jul. 1982 - May 1983
G. J. STURGESS Jul. 1983 190 p refs
(Contract NAS3-23524)
(NASA-CR-168202; NAS 1.26:168202; PWA-5907-19) Avail: NTIS HC A09/MF A01 CSCL 20D

The physical modeling embodied in the computational fluid dynamics codes is discussed. The objectives were to identify shortcomings in the models and to provide a program plan to improve the quantitative accuracy. The physical models studied were for: turbulent mass and momentum transport, heat release, liquid fuel spray, and gaseous radiation. The approach adopted was to test the models against appropriate benchmark-quality test cases from experiments in the literature for the constituent flows that together make up the combustor real flow. Author

N83-30960*# Purdue Univ., Lafayette, Ind. Thermal Sciences and Propulsion Center.
STAGNATION REGION GAS FILM COOLING: EFFECTS OF DIMENSIONLESS COOLANT TEMPERATURE Final Report
M. A. BONNICE and M. R. LECUYER Jul. 1983 192 p refs
(Contract NSG-3071)
(NASA-CR-168197; NAS 1.26:168197) Avail: NTIS HC A09/MF A01 CSCL 20D

An experimental investigation was conducted to mode the film cooling performance for a turbine vane leading edge using the stagnation region of a cylinder in cross flow. Experiments were conducted with a single row of spanwise angled (25 deg) coolant holes for a range of the coolant blowing ratio and dimensionless coolant temperature with free stream-to-wall temperature ratio approximately 1.7 and Re sub D = 90000. the cylindrical test surface was instrumented with miniature heat flux gages and wall thermocouples to determine the percentage reduction in the Stanton number as a function of the distance downstream from injection (x/d sub 0) and the location between adjacent holes (z/S). Data from local heat flux measurements are presented for injection from a single row located at 5 deg, 22.9 deg, 40.8 deg, from stagnation using a hole spacing ratio of S/d = 5. The film coolant was injected with T sub c T sub w with a dimensionless coolant temperature in the range 1.18 or equal to theta sub c or equal to 1.56. The data for local Stanton Number Reduction (SNR) showed a significant increase in SNR as theta sub c was increased above 1.0. Author

N83-33103*# National Aeronautics and Space Administration. Lewis Research Center, Cleveland, Ohio.
A COMPARISON OF FLOW RATES AND PRESSURE PROFILES FOR N-SEQUENTIAL INLETS AND THREE RELATED SEAL CONFIGURATIONS
R. C. HENDRICKS 19 Aug. 1983 15 p refs Cryogen. Mater. Conf., Colorado Springs, Cryogen. Mater. Conf., Colarado Springs, Colo., 15-19 Aug. 1983; sponsored by Cryogenics Engineering Conference/International Cryogenic Materials Conference and Dept. of Commerce and National Bureau of Standards
(NASA-TM-83442; E-1741; NAS 1.15:83442) Avail: NTIS HC A02/MF A01 CSCL 20D

Experimental and analytical results are presented for choked flows of fluid nitrogen over a range of reduced inlet stagnation temperatures (from 0.67 to ambient) and reduced inlet stagnation pressures to 2. Flow rate and pressure profile comparisons are made between N aligned sequential orifice inlets, a 33-tooth labyrinth seal, a 3-step seal, a cylindrical seals and the classic venturi. Seal effectiveness appears strongly dependent on upstream losses and geometry configuration. Author

N83-33105*# City Coll. of the City Univ. of New York. Dept. of Chemical Engineering.
NUMERICAL ANALYSIS OF TURBULENT COAXIAL FLOW WITH INTERNAL HEAT GENERATION
A. LIN and H. WEINSTEIN Jan. 1981 88 p refs
(Contract NSG-3174)
(NASA-CR-172633; NAS 1.26:172633) Avail: NTIS HC A05/MF A01 CSCL 20D

A computational method with which to obtain a physical understanding of the turbulent field of two coaxial jets entering an axisymmetric chamber is developed. Even the laminar field of this flow is quite complicated. This is due to the many different domains which exist in the field especially in the entrance region. Physically, three regions may be identified: the wall region, the initial region near the axis of symmetry and the mixing region. Advancing downstream, these regions change relative size with the ratio of the two jets' mass fluxes as the main parameter. The turbulent field of these flows is much more complicated due to the difference in the effective transport coefficients and turbulence level from region to region. However, being aware beforehand of the complications and the different regions of this field, the appropriate turbulence model and numerical scheme can be adjusted to treat the problem. S.L.

N83-34230*# Scientific Research Associates, Inc., Glastonbury, Conn.
NUMERICAL SOLUTIONS OF NAVIER-STOKES EQUATIONS FOR COMPRESSIBLE TURBULENT TWO/THREE DIMENSIONAL FLOWS IN TERMINAL SHOCK REGION OF AN INLET/DIFFUSER Final Report
N. S. LIU, S. J. SHAMROTH, and H. MCDONALD Washington NASA Aug. 1983 106 p refs
(Contract NAS3-22747)
(NASA-CR-3723; NAS 1.26:3723) Avail: NTIS HC A06/MF A01 CSCL 20D

The multidimensional ensemble averaged compressible time dependent Navier Stokes equations in conjunction with mixing length turbulence model and shock capturing technique were used to study the terminal shock type of flows in various flight regimes occurring in a diffuser/inlet model. The numerical scheme for solving the governing equations is based on a linearized block implicit approach and the following high Reynolds number calculations were carried out: (1) 2 D, steady, subsonic; (2) 2 D, steady, transonic with normal shock; (3) 2 D, steady, supersonic with terminal shock; (4) 2 D, transient process of shock development and (5) 3 D, steady, transonic with normal shock. The numerical results obtained for the 2 D and 3 D transonic shocked flows were compared with corresponding experimental data; the calculated wall static pressure distributions agree well with the measured data. S.L.

N83-34232*# National Aeronautics and Space Administration. Lewis Research Center, Cleveland, Ohio.
THREE-DIMENSIONAL TURBULENT-MIXING-LENGTH MODELING FOR DISCRETE-HOLE COOLANT INJECTION INTO A CROSSFLOW
C. R. WANG and S. S. PAPELL Sep. 1983 16 p refs
(NASA-TP-2200; E-1497; NAS 1.60:2200) Avail: NTIS HC A02/MF A01 CSCL 20D

Three dimensional mixing length models of a flow field immediately downstream of coolant injection through a discrete circular hole at a 30 deg angle into a crossflow were derived from the measurements of turbulence intensity. To verify their effectiveness, the models were used to estimate the anisotropic turbulent effects in a simplified theoretical and numerical analysis to compute the velocity and temperature fields. With small coolant injection mass flow rate and constant surface temperature, numerical results of the local crossflow streamwise velocity component and surface heat transfer rate are conistent with the velocity measurement and the surface film cooling effectiveness distributions reported in previous studies. Author

N83-35316*# Oklahoma State Univ., Stillwater.
TURBULENCE MEASUREMENTS IN A COMPLEX PLOWFIELD USING A CROSSED HOT-WIRE M.S. Thesis
B. E. MCKILLOP Jul. 1983 132 p refs
(Contract NAG3-74)
(NASA-CR-173080; NAS 1.26:173080) Avail: NTIS HC A07/MF A01 CSCL 20D

Turbulence was quantified in complex axisymmetric, nonreacting, nonswirling flowfields using a crossed hot-wire anemometer. Mean velocity, turbulence intensities, turbulent viscosity, and Reynolds tree were measured in round free jet and confined jet flowfields. The confined jet, a model of an axisymmetric can combustor, had an expansion ratio D/d=2, an expansion angle of 90 deg, and an axial location increments of 0.5 diameters. The confined jet was studied with and without a contraction nozzle. Free jet measurements validated the experimental technique and data reduction. Results show good agreement with those of previous research. Measurements in the confined jet indicate that the cross hot-wire used cannot handle axial flow reversal and the experimental technique is inadequate for measuring time-mean radial velocity. Other quantities show a high level of comparability. A.R.H.

N83-35318*# National Aeronautics and Space Administration. Lewis Research Center, Cleveland, Ohio.
VORTEX MOTION IN AXISYMMETRIC PISTON-CYLINDER CONFIGURATIONS
T. I. P. SHIH, G. E. SMITH, and O. S. SPRINGER Sep. 1982 22 p refs Backup document for AIAA Synoptic scheduled for publication in AIAA Journal in Mar. 1984 Prepared in cooperation with Michigan Univ., Ann Arbor and Florida Univ., Gainesville (NASA-TM-85404; NAS 1.15:85404; LOG-J13452) Avail: NTIS HC A02/MF A01 CSCL 20D

By using the Beam and Warming implicit-factored method of solution of the Navier-Stokes equations, velocities were calculated inside axisymmetric piston cylinder configurations during the intake and compression strokes. Results are presented in graphical form which show the formation, growth and breakup of those vortices which form during the intake stroke by the jet issuing from the valve. It is shown that at bore-to-stroke ratio of less than unity, the vortices may breakup during the intake stroke. It is also shown that vortices which do not breakup during the intake stroke coalesce during the compression stroke. S.L.

35

INSTRUMENTATION AND PHOTOGRAPHY

Includes remote sensors; measuring instruments and gages; detectors; cameras and photographic supplies; and holography.

A83-14172* California Univ., La Jolla.
MODIFIED GAUGE FOR TIME-RESOLVED SKIN-FRICTION MEASUREMENTS
C. O. AJAGU, P. A. LIBBY (California, University, La Jolla, CA), and J. C. LARUE (California University, Irvine, CA) Review of Scientific Instruments, vol. 53, Dec. 1982, p. 1920-1926. refs
(Contract NSG-3219)

A new gauge for skin-friction measurements in turbulent flows involving a wire close to the surface and a second, flush-mounted film which serves as a constant temperature guard heater is described and evaluated. It is shown that a laminar calibration of the gauge applies to measurements in turbulent flow and that the frequency response of the gauge is appropriate for time-resolved data in such a flow. Initial results from a turbulent channel flow are presented. (Author)

A83-19016* Connecticut Univ., Storrs.
A NEW SURFACE-STREAMLINE FLOW-VISUALIZATION TECHNIQUE
L. S. LANGSTON and M. T. BOYLE (Connecticut, University, Storrs, CT) Journal of Fluid Mechanics, vol. 125, Dec. 1982, p. 53-57. refs
(Contract NSG-3238)

This paper describes a new surface-streamline flow-visualization technique that is suitable for use in low-speed wind tunnels or other low-speed gas flows. The technique provides a permanent record of ink traces that show surface-streamline direction and shape. The visualization of the endwall surface flow of the horseshoe-vortex system formed around the base of a cylinder by a separating turbulent boundary layer is used as an example. The results of the new technique are compared with those obtained from a conventional flow-visualization technique. Good agreement was found between the two, with the new technique appearing to give more-accurate surface streamlines. (Author)

A83-22336* Kansas Univ., Lawrence.
NUMERICAL SIMULATION OF A DISK-SHAPED ELECTRON ACCELERATING ELECTROSTATIC PROBE
J. H. NONNAST and J. ENOCH (Kansas, University, Lawrence, KS) Journal of Applied Physics, vol. 54, Feb. 1983, p. 621-631. refs
(Contract NSG-3290)

This paper presents a method utilizing the numerical plasma simulation particle-in-cell technique for studying electron accelerating probe characteristics. A probe configuration other than the commonly used plane, cylindrical, or spherical case will be studied; the probe configuration used is that of a disk. Cylindrical geometry is used in the simulation model. One of the advantages of a numerical simulation is the ease with which the details of the system can be examined. Therefore, in addition to the current-voltage characteristics of the static probe, other results are presented such as the time evolution of the plasma properties and studies of the sheath region surrounding the probe. (Author)

A83-23596* Carnegie-Mellon Univ., Pittsburgh, Pa.
ELECTRO-OPTICAL PROCESSOR FOR OPTIMAL CONTROL
D. CASASENT, C. NEUMAN, and M. CARLOTTO (Carnegie-Mellon University, Pittsburgh, PA) In: Control and communication technology in laser systems; Proceedings of the Twenty-fifth Annual International Technical Symposium, San Diego, CA, August 25, 26, 1981. Bellingham, WA, SPIE - The International Society for Optical Engineering, 1981, p. 176-183. refs
(Contract NAG3-5)

An iterative optical processor has been developed for applications in the optimal control of advanced sensor systems. The processor is designed for the realization of the Richardson algorithm on bipolar data, using as input a linear array of LEDs. The usefulness of the processor has been demonstrated by the solution of the linear quadratic regulator problem for the optimal control signals of the F100 turbofan engine. In this case study, the algebraic Riccati equation matrix was solved by the use of a modified Kleinman algorithm along with the Richardson algorithm applied to a system of linear algebraic equations. Preliminary experimental results demonstrate the gradual convergence of the processor. A.L.W.

A83-28834*# National Aeronautics and Space Administration. Lewis Research Center, Cleveland, Ohio.
LASER ANEMOMETER USING A FABRY-PEROT INTERFEROMETER FOR MEASURING MEAN VELOCITY AND TURBULENCE INTENSITY ALONG THE OPTICAL AXIS IN TURBOMACHINERY
R. G. SEASHOLTZ and L. J. GOLDMAN (NASA, Lewis Research Center, Cleveland, OH) IN: Engineering applications of laser velocimetry; Proceedings of the Symposium, Phoenix, AZ, November 14-19, 1982 . New York, American Society of Mechanical Engineers, 1982, p. 93-101. refs

Previously announced in STAR as N82-28605

A83-45962* Stanford Univ., Calif.
LASER-INDUCED FLUORESCENCE TECHNIQUE FOR VELOCITY FIELD MEASUREMENTS IN SUBSONIC GAS FLOWS
B. HILLER, J. C. MCDANIEL, E. C. REA, JR., and R. K. HANSON (Stanford University, Stanford, CA) Optics Letters (ISSN 0146-9592), vol. 8, Sept. 1983, p. 474-476. refs
(Contract F49620-83-K-0004; NAG3-285)

A nonintrusive optical technique is reported for multiple-point velocity measurements in subsonic flows. The technique is based on the detection of fluorescence from a Doppler-shifted absorption line of seeded iodine molecules excited at a laser frequency fixed in the wing of the line. Counterpropagating laser sheets are used to illuminate the flow, in the present case a nitrogen round jet, thereby eliminating the need for an unshifted reference signal. The fluorescence is detected simultaneously at 10,000 points in a plane of the flow using a 100 x 100 element photodiode-array camera. The velocity at each point is computed from four successive camera frames, each recorded with a different beam

direction. The measured mean velocities between 5 and 50 m/sec agree well with data from the literature. Author

A83-48120* Case Western Reserve Univ., Cleveland, Ohio.
PARTICLE-SAMPLING STATISTICS IN LASER ANEMOMETERS SAMPLE-AND-HOLD SYSTEMS AND SATURABLE SYSTEMS
R. V. EDWARDS (Case Western Reserve University, Cleveland, OH) and A. S. JENSEN (Forsogsanlaeg Riso, Roskilde, Denmark) Journal of Fluid Mechanics (ISSN 0022-1120), vol. 133, Aug. 1983, p. 397-411. refs
(Contract NSF CPE-80-17868; NAG3-2)

The effect of the data-processing system on the particle statistics obtained with laser anemometry of flows containing suspended particles is examined. Attention is given to the sample and hold processor, a pseudo-analog device which retains the last measurement until a new measurement is made, followed by time-averaging of the data. The second system considered features a dead time, i.e., a saturable system with a significant reset time with storage in a data buffer. It is noted that the saturable system operates independent of the particle arrival rate. The probabilities of a particle arrival in a given time period are calculated for both processing systems. It is shown that the system outputs are dependent on the mean particle flow rate, the flow correlation time, and the flow statistics, indicating that the particle density affects both systems. The results are significant for instances of good correlation between the particle density and velocity, such as occurs near the edge of a jet. M.S.K.

A83-48604* Northwestern Univ., Evanston, Ill.
AN EXTENSOMETER FOR AXIAL STRAIN MEASUREMENT AT HIGH TEMPERATURE
J. SCHMIDT (Northwestern University, Evanston, IL), K. MOTOIE, and M. SAKANE Mechanics of Materials (ISSN 0167-6636), vol. 2, Aug. 1983, p. 179-182. refs
(Contract NAG3-134)

Most existing strain measuring instruments, important for the investigation of the mechanical behavior of metals at high temperature, have temperature, strain range, and size limitations. In this short note the authors give the design and construction of an extensometer with sufficient dynamic range and good stability over long periods of time, for measuring the longitudinal strain of plane specimens from 0.001 to 0.1 at temperatures up to 800 C. Author

N83-15601*# Auburn Univ., Ala. Dept. of Mechanical Engineering.
MANUAL FOR EXTENDING THE LASER SPECKLEGRAM TECHNIQUE TO STRAIN ANALYSIS OF ROTATING COMPONENTS Final Report
L. C. CHIEN, J. L. TURNER, J. WEATHERS, and W. F. SWINSON Nov. 1982 79 p refs
(Contract NAG3-103)
(NASA-CR-167932; NAS 1.26:167932) Avail: NTIS HC A05/MF A01 CSCL 14B

The theory, techniques, and equipment necessary for extending laser speckle techniques to analyze stresses in rotating blades are described. Details for setting up the equipment, for timing the events, for data recording, and for data analysis are discussed. Finite element techniques are investigated for analysis of speckle data. Advantages and limitations of the finite element analysis for the speckle data are discussed. The finite element program is listed. M.G.

N83-15602*# National Aeronautics and Space Administration. Lewis Research Center, Cleveland, Ohio.
EXPERIMENTAL FEASIBILITY STUDY OF A THERMOELECTRIC HEAT FLUX GAGE
G. J. VANFOSSEN and I. LOPEZ 1983 10 p refs Proposed for presentation at the Thermal Eng. Joint Conf., Honolulu, Hawaii, 20-24 Mar. 1983; sponsored by the American Society of Mechanical Engineers and the Japan Society of Mechanical Engineers Prepared in cooperation with Army Aviation Research and Development Command, Cleveland
(NASA-TM-83048; E-1498; NAS 1.15:83048; AVRADCOM-TR-82-C-17) Avail: NTIS HC A02/MF A01 CSCL 14B

An experiment was conducted to determine the feasibility of using a commercially available thermoelectric device as a heat flux gage at near ambient conditions. In certain research applications, the thermoelectric heat flux gage can provide a relatively simple means to model a warm fluid cold wall convection environment. The experiment showed that heat flux through the gage could be correlated within 2.5 percent with a simple algebraic equation which considered the thermoelectric current through the device and the hot and cold side temperatures. Author

N83-21314*# General Electric Co., Wilmington, Mass. Aircraft Instruments Dept.
HIGH ACCURACY FUEL FLOWMETER, PHASE 1 Final Report
C. MAYER, L. ROSE, A. CHAN, B. CHIN, and W. GREGORY Mar. 1983 156 p refs
(Contract NAS3-22139)
(NASA-CR-167893; NAS 1.26:167893) Avail: NTIS HC A08/MF A01 CSCL 14B

Technology related to aircraft fuel mass - flowmeters was reviewed to determine what flowmeter types could provide 0.25%-of-point accuracy over a 50 to one range in flowrates. Three types were selected and were further analyzed to determine what problem areas prevented them from meeting the high accuracy requirement, and what the further development needs were for each. A dual-turbine volumetric flowmeter with densi-viscometer and microprocessor compensation was selected for its relative simplicity and fast response time. An angular momentum type with a motor-driven, spring-restrained turbine and viscosity shroud was selected for its direct mass-flow output. This concept also employed a turbine for fast response and a microcomputer for accurate viscosity compensation. The third concept employed a vortex precession volumetric flowmeter and was selected for its unobtrusive design. Like the turbine flowmeter, it uses a densi-viscometer and microprocessor for density correction and accurate viscosity compensation. Author

N83-24829*# National Aeronautics and Space Administration. Lewis Research Center, Cleveland, Ohio.
ANALYSIS OF STRAIN GAGE RELIABILITY IN F-100 JET ENGINE TESTING AT NASA LEWIS RESEARCH CENTER
R. HOLANDA Mar. 1983 12 p refs
(NASA-TM-83325; NAS 1.15:83325) Avail: NTIS HC A03/MF A01 CSCL 14B

A reliability analysis was performed on 64 strain gage systems mounted on the 3 rotor stages of the fan of a YF-100 engine. The strain gages were used in a 65 hour fan flutter research program which included about 5 hours of blade flutter. The analysis was part of a reliability improvement program. Eighty-four percent of the strain gages survived the test and performed satisfactorily. A post test analysis determined most failure causes. Five failures were caused by open circuits, three failed gages showed elevated circuit resistance, and one gage circuit was grounded. One failure was undetermined. Author

N83-33126*# National Aeronautics and Space Administration Lewis Research Center, Cleveland, Ohio.
RAINBOW SCHLIEREN
W. L. HOWES May 1983 21 p refs Original contains color illustrations
(NASA-TP-2166; E-1173; NAS 1.60:2166) Avail: NTIS HC A02/MF A01 CSCL 14B

The rainbow schlieren is an apparatus in which the usual schlieren knife edge cutoff is replaced by a radial rainbow filter with a transparent center and an opaque surround. With this apparatus most refractive index nonuniformities in the test section appear varicolored whereas uniformities appear white. The rainbow schlieren is simple, easy to use, and relatively inexpensive and gives much greater detail regarding nonuniformities than does the ordinary schlieren. Moreover, the rainbow schlieren permits quantitative evaluation of certain refractive index distributions, including those involving turbulence, by simple calculations. S.L.

N83-35338* National Aeronautics and Space Administration. Lewis Research Center, Cleveland, Ohio.
JOINING LEAD WIRES TO THIN PLATINUM ALLOY FILMS
J. S. PRZYBYSZEWSKI (United Technologies Corp., East Hartford, Conn.) and R. G. CLAING, inventors (to NASA) (United Technologies Corp., East Hartford, Conn.) 6 Sep. 1983 8 p Filed 4 Dec. 1980 Supersedes N83-19949 (21 - 10, p 1496)
(NASA-CASE-LEW-13934-1; US-PATENT-4,402,447; US-PATENT-APPL-SN-212949; US-PATENT-CLASS-228-103; US-PATENT-CLASS-228-193; US-PATENT-CLASS-228-263.18; US-PATENT-CLASS-415-118) Avail: US Patent and Trademark Office CSCL 14B

A two step process of joining a lead wire to .000002 m thick platinum alloy film which rests upon an equally thin alumina insulating layer which is adhered to a metal substrate is described. Typically the platinum alloy film forms part of a thermocouple for measuring the surface temperature of a gas turbine airfoil. In the first step the lead wire is deformed 30 to 60% at room temperature while the characteristic one million ohm resistance of the alumina insulating layer is monitored for degradation. In the second step the cold pressed assembly is heated at 865 to 1025 C for 4 to 75 hr in air. During the heating step any degradation of insulating layer resistance may be reversed, provided the resistance was not decreased below 100 ohm in the cold pressing.
Official Gazette of the U.S. Patent and Trademark Office

36

LASERS AND MASERS

Includes parametric amplifiers.

A83-31133* KMS Fusion, Inc., Ann Arbor, Mich.
GAIN-ENHANCED FREE-ELECTRON LASER WITH AN ELECTROMAGNETIC PUMP FIELD
H. R. HIDDLESTON, S. B. SEGALL, and G. C. CATELLA (KMS Fusion, Inc., Ann Arbor, MI) IN: Free-electron generators of coherent radiation - /Volume 9/ . Reading, MA, Addison-Wesley Publishing Co., 1982, p. 849-865. refs
(Contract N00014-80-C-0614; NAS3-22659)

The feasibility of enhancing the gain for the free electron laser (FEL) with an electromagnetic (EM) pump field has been considered. The enhancement is provided by reacceleration of the electrons in the interaction region by means of a static, axial electric field. A FEL utilizing a low energy electron beam and a wiggler magnet with a periodicity on the order of 1 cm would produce far infared (FIR) radiation with wavelengths on the order of a few hundred microns. The use of the FIR radiation as the pump field in a two-stage FEL is envisioned to obtain visible radiation with a low energy electron beam. A summary is provided regarding the theory and equations of motion for the EM-pumped FEL. The derived relations are applied to the second stage of such a two-stage FEL. The obtained equations have been incorporated into a computer code which has been used to calculate laser gain and energy conversion efficiency. G.R.

A83-31141* KMS Fusion, Inc., Ann Arbor, Mich.
THE APPLICATION OF FREE-ELECTRON LASERS TO THE TRANSMISSION OF ENERGY IN SPACE
S. B. SEGALL, H. R. HIDDLESTON, and G. C. CATELLA (KMS Fusion, Inc., Ann Arbor, MI) IN: Free-electron generators of coherent radiation - /Volume 9/ . Reading, MA, Addison-Wesley Publishing Co., 1982, p. 1013-1046. refs
(Contract NAS3-22659)
Previously announced in STAR as N82-25499

37

MECHANICAL ENGINEERING

Includes auxiliary systems (non-power); machine elements and processes; and mechanical equipment.

A83-13228* National Aeronautics and Space Administration. Lewis Research Center, Cleveland, Ohio.
ON THE MECHANISM OF LUBRICATION BY TRICRESYLPHOSPHATE /TCP/ - THE COEFFICIENT OF FRICTION AS A FUNCTION OF TEMPERATURE FOR TCP ON M-50 STEEL
O. D. FAUT and D. R. WHEELER (NASA, Lewis Research Center, Cleveland, OH) American Society of Mechanical Engineers and American Society of Lubrication Engineers, Lubrication Conference, Washington, DC, Oct. 5-7, 1982, ASLE 6 p. refs
(ASLE PREPRINT 82-LC-4C-1)

A83-13229* Rensselaer Polytechnic Inst., Troy, N. Y.
INFRARED EMISSION SPECTROPHOTOMETRIC STUDY OF THE CHANGES PRODUCED BY TIN COATING OF METAL SURFACES IN AN OPERATING EHD CONTACT
L. E. KELLER, J. L. LAUER (Rensselaer Polytechnic Institute, Troy, NY), and W. R. JONES, JR. (NASA, Lewis Research Center, Cleveland, OH) American Society of Mechanical Engineers and American Society of Lubrication Engineers, Lubrication Conference, Washington, DC, Oct. 5-7, 1982, ASLE 8 p. refs
(Contract NSG-3180; AF-AFOSR-78-3473; DAAG29-79-C-0204)
(ASLE PREPRINT 82-LC-3C-3)

Infrared emission spectra and related measurements were obtained from an operating ball/plate EHD sliding contact under a variety of operating conditions. In order to be able to compare the effect of the ball surface, some of the steel balls were coated with a thin layer of titanium nitride (TiN) by vapor deposition. Polyphenyl ether (5P4E) was used as the lubricant and 1 percent of 1,1,2-trichloroethane TCE) as an additive with a high affinity for steel but a low affinity for TiN. TiN is chemically inert, but its thermal conductivity is lower than that of steel. Therefore, the overall temperatures with TiN-coated balls were higher. Nevertheless, no scuffng was observed with the coated balls under conditions giving rise to scuffing with the uncoated balls. Tractions were lower with the TiN-coated balls and with the steel balls when TCE was added to the 5P4E. These findings were found to be inversely related to the degree of polarization of the spectral emission bands. The intensity and the dichroism of these bands were related to shear rates and inlet conditions of the EHD contact. (Author)

A83-13230* Akron Univ., Ohio.
AN EXPERIMENTAL INVESTIGATION OF THE VAPOROUS/GASEOUS CAVITY CHARACTERISTICS OF AN ECCENTRIC JOURNAL BEARING
M. J. BRAUN (Akron, University, Akron, OH) and R. C. HENDRICKS (NASA, Lewis Research Center, Cleveland, OH) American Society of Mechanical Engineers and American Society of Lubrication Engineers, Lubrication Conference, Washington, DC, Oct. 5-7, 1982, ASLE 13 p. refs
(ASLE PREPRINT 82-LC-3A-1)

This paper describes the experimental pressure and temperature results obtained when rotating a shaft in an eccentric lucite casing at velocities ranging from 209 to 628 rad/s (2000 to 6000 rpm). The results are presented in terms of three-dimensional plots and contour maps. Photographic evidence is presented to illustrate how the downstream and upstream regions of the cavity develop and evolve into the well-known finger patterns. A comparison between pressure and temperature profiles in air-saturated oil and carbon dioxide-saturated oil is presented; the origin and nature of the gases contained in the cavity are discussed. Three analytical models (Swift-Stieber, separation, Floberg) predicting the formation of the cavitation zone are presented and evaluated in light of the experimental results. A motion-picture supplement depicting these results is available upon request. (Author)

A83-13237* Rensselaer Polytechnic Inst., Troy, N. Y.
MICROSCOPIC CONTOUR CHANGES OF TRIBOLOGICAL SURFACES BY CHEMICAL AND MECHANICAL ACTION
J. L. LAUER and S. S. FUNG (Rensselaer Polytechnic Institute, Troy, NY) American Society of Mechanical Engineers and American Society of Lubrication Engineers, Lubrication Conference, Washington, DC, Oct. 5-7, 1982, ASLE 7 p. refs
(Contract AF-AFOSR-81-0005; NSG-3180)
(ASLE PREPRINT 82-LC-3B-3)

An electronic optical laser interferometer capable of resolving depth differences of as low as 30 A and planar displacements of 6000 A was constructed for the examination of surface profiles of bearing surfaces without physical contact. This instrument was used to determine topological chemical reactivity by applying a drop of dilute alcoholic hydrochloric acid and measuring the profile of the solid surface before and after application of this probe. It was found that scuffed bearing surfaces reacted much faster than virgin ones but that bearing surfaces exposed to lubricants containing an organic chloride reacted much more slowly. In a separate series of experiments, a number of stainless steel plates were heated in a nitrogen atmosphere to different temperatures and their reactivity examined later at ambient temperature. The change of surface contour as a result of the probe reaction was found to follow an Arrhenius-type relation with respect to heat treatment temperature. This result could have implications on the scuffing mechanism. (Author)

A83-13509*# National Aeronautics and Space Administration. Lewis Research Center, Cleveland, Ohio.
HIGH-SPEED MOTION PICTURE CAMERA EXPERIMENTS OF CAVITATION IN DYNAMICALLY LOADED JOURNAL BEARINGS
B. O. JACOBSON and B. J. HAMROCK (NASA, Lewis Research Center, Cleveland, OH) American Society of Mechanical Engineers and American Society of Lubrication Engineers, Lubrication Conference, Washington, DC, Oct. 5-7, 1982, ASME 7 p. Research supported by the Hogskolan i Lulea, National Research Council, and NASA. refs
(ASME PAPER 82-LUB-18)
(Previously announced in STAR as N82-20543)

A83-13516*# Toledo Univ., Ohio.
INVESTIGATION OF THE EFFECTS OF INITIAL FLUID FILM PROFILE ON PUMPING RING OPERATION
P. J. SMITH and T. G. KEITH, JR. (Toledo, University, Toledo, OH) American Society of Mechanical Engineers and American Society of Lubrication Engineers, Lubrication Conference, Washington, DC, Oct. 5-7, 1982, ASME 6 p. refs
(Contract NSG-3156)
(ASME PAPER 82-LUB-35)

The effect of the initial fluid film profile on the pumping capacity of a pumping ring shaft seal has been investigated numerically. Linear, concave, convex and compound film shapes were considered. It was found that initial film shape has a pronounced effect on both the amount of fluid pumped and on the character of the flow pattern and pressure distribution within the film. (Author)

A83-13521*# Texas A&M Univ., College Station.
FINITE-LENGTH SOLUTIONS FOR ROTODYNAMIC COEFFICIENTS OF TURBULENT ANNULAR SEALS
D. W. CHILDS (Texas A & M University, College Station, TX) American Society of Mechanical Engineers and American Society of Lubrication Engineers, Lubrication Conference, Washington, DC, Oct. 5-7, 1982, ASME 8 p. refs
(Contract NAS8-33716; NAG3-181)
(ASME PAPER 82-LUB-42)

A finite-length solution procedure is developed for perturbation equations which are based on Hirs' (1973) turbulent lubrication model. The equations apply to small motions about a centered position and include the influence of swirl and changes in Reynolds number due to perturbations in clearances. Numerical results are presented for a range of L/D ratios, with and without swirl. For zero swirl, changes in the L/D ratios show results which are similar to those obtained by Black and Jenssen (1970), but when L/D = 1, differences of about 15 percent appear. The results including swirl give physically insupportable results at small L/D ratios, such as a negative cross-coupled stiffness coefficient at L/D = 0.2. This result demonstrates that the complete Hirs turbulence model is not suitable for short seals with significant swirling flow. C.D.

A83-16749*# National Aeronautics and Space Administration. Lewis Research Center, Cleveland, Ohio.
NUMERICAL STUDIES OF THE FORMATION AND DESTRUCTION OF VORTICES IN A MOTORED FOUR-STROKE PISTON-CYLINDER CONFIGURATION
H. J. SCHOCK, D. J. SOSOKA (NASA, Lewis Research Center, Cleveland, OH), and J. I. RAMOS (Carnegie-Mellon University, Pittsburgh, PA) American Institute of Aeronautics and Astronautics, Aerospace Sciences Meeting, 21st, Reno, NV, Jan. 10-13, 1983, 17 p. refs
(AIAA PAPER 83-0497)

A finite-difference procedure which solves the conservation equations of mass, momentum, and energy is used to investigate the effects of the compression ratio, engine speed, bore-to-stroke ratio, and air intake flow angle on the turbulent flow field within an axisymmetric piston-cylinder configuration. It is shown that in a four-stroke piston-cylinder configuration, the intake stroke is characterized by the formation of a piston vortex. The piston vortex is stretched during the intake stroke, and the head vortex has an almost constant diameter. For a 0-deg air intake flow angle, both vortices disappear by the end of the compression stroke; for an air intake flow angle of 45 deg, the flow field within the cylinder shows three elongated vortices which persist into the compression stroke and then break up and merge. It is also shown that larger bore-to-stroke ratios give rise to lower turbulent levels than smaller bore-to-stroke ratios and that the turbulent intensity is almost independent of the rpm. V.L.

A83-17259* National Aeronautics and Space Administration. Lewis Research Center, Cleveland, Ohio.
REVIEW OF FACTORS THAT INFLUENCE FRETTING WEAR
R. C. BILL (NASA, Lewis Research Center, Cleveland, OH) In: Materials evaluation under fretting conditions; Proceedings of the Symposium, Warminster, PA, June 3, 1981. Philadelphia, PA, American Society for Testing and Materials, 1982, p. 165-182. refs

An assessment is made of presently obtained as well as published results in order to characterize the effects of contact conditions, environmental conditions, and material properties and behavior on fretting wear. The importance of material properties is discussed on the basis of interaction with other factors during fretting. While the isolated effect of contact load, fretting amplitude, temperature and atmosphere have been well explored, especially for the case mild steel, a deficiency is noted in studies of the effects of contact geometry and relative humidity, as well as the interaction of various fretting parameters. O.C.

A83-22319* National Aeronautics and Space Administration. Lewis Research Center, Cleveland, Ohio.
ADVANCES IN HIGH-SPEED ROLLING-ELEMENT BEARINGS
E. V. ZARETSKY (NASA, Lewis Research Center, Cleveland, OH) (Israel Conference on Mechanical Engineering, 16th, Haifa, Israel, July 13, 14, 1982.) Israel Journal of Technology, vol. 20, no. 1-2, 1982, p. 3-16. refs

The research program begun by NASA in 1959 in order to investigate the projected temperature and speed requirements of large bore ball and roller bearings was expanded in the 1970s to include tapered roller and small bore bearings. In the course of the program, bearing speeds as high as 3 million DN and 2.4 million DN, respectively, were achieved for ball and tapered roller bearings with fatigue lives exceeding those common in commercial aircraft. The computer analysis of rolling element bearings operation have yielded reasonably accurate performance predictions for speeds up to 3 million DN. It was found that under-race bearing lubrication improved operational performance over that achieved with conventional jet lubrication methods at high bearing speeds. O.C.

A83-22322* Toledo Univ., Ohio.
THERMOELASTOHYDRODYNAMIC ANALYSIS OF AN OIL PUMPING RING SEAL
P. J. SMITH and T. G. KEITH, JR. (Toledo, University, Toledo, OH) (Israel Conference on Mechanical Engineering, 16th, Haifa, Israel, July 13, 14, 1982.) Israel Journal of Technology, vol. 20, no. 1-2, 1982, p. 49-59. refs
(Contract NSG-3156)

The selection and evaluation of the numerical methods used in the thermoelastohydrodynamic analysis of an oil pumping ring seal are described, and the results from test problems used to demonstrate the validity of the implementing computer program are presented. A sampling of predicted pumping ring performance values is compared with existing experimental data. Agreement between prediction and test performance is obtained, yielding detailed information concerning fluid and solid parameters. O.C.

A83-25270*# Acurex Corp., Mountain View, Calif.
CATALYST DURABILITY EVALUATION FOR ADVANCED GAS TURBINE ENGINES
G. C. SNOW and S. L. PESSAGNO (Acurex Corp., Energy and Environmental Div., Mountain View, CA) American Society of Mechanical Engineers, Joint Power Generation Conference, Denver, CO, Oct. 17-21, 1982. 7 p. Research supported by the Acurex Corp.; U.S. Environmental Protection Agency refs
(Contract EPA-68-02-3122; DEN3-83)
(ASME PAPER 82-JPGC-GT-21)

Catalytic combustion has demonstrated the ability to provide low NO(x) emissions while maintaining high combustion efficiency. Recently, under joint NASA Lewis, EPA, and Acurex sponsorship, a catalytic reactor was tested for 1000 hours to demonstrate durability in combustion environments representative of advanced automotive gas turbine engines. At a 740K air preheat temperature and a propane fuel/air ratio of 0.028 by mass, the adiabatic flame temperature was held at about 1700K. The graded cell monolithic reactor measured 5 cm in diameter by 10.2 cm in length and was operated at a reference velocity of 13.4 m/s at 1 atmosphere pressure. Measured NO(x) levels remained below 5 ppm while unburned hydrocarbon concentrations registered near zero and carbon monoxide levels were nominally below 20 ppm. The durability test included several parametric turndown studies and ended with a series of on/off cycling tests to further characterize reactor performance. (Author)

A83-27288* Rasor Associates, Inc., Sunnyvale, Calif.
IMPROVED STIRLING ENGINE PERFORMANCE USING JET IMPINGEMENT
D. C. JOHNSON, E. J. BRITT (Rasor Associates, Inc., Sunnyvale, CA), and L. G. THIEME (NASA, Lewis Research Center, Cleveland, OH) In: IECEC '82; Proceedings of the Seventeenth Intersociety Energy Conversion Engineering Conference, Los Angeles, CA, August 8-12, 1982. Volume 4. New York, Institute of Electrical and Electronics Engineers, 1982, p. 1845-1849. Research supported by the U.S. Department of Energy refs
(Contract DEN3-177)

Of the many factors influencing the performance of a Stirling engine, that of transferring the combustion gas heat into the working fluid is crucial. By utilizing the high heat transfer rates obtainable with a jet impingement heat transfer system, it is possible to reduce the flame temperature required for engine operation. Also, the required amount of heater tube surface area may be reduced, resulting in a decrease in the engine nonswept volume and a related increase in engine efficiency. A jet impingement heat transfer system was designed by Rasor Associates, Inc., and tested in the GPU-3 Stirling engine at the NASA Lewis Research Center. For a small penalty in pumping power (less than 0.5% of engine output) the jet impingement heat transfer system provided a higher combustion-gas-side heat transfer coefficient and a smoothing of heater temperature profiles resulting in lower combustion system temperatures and a 5 to 8% increase in engine power output and efficiency. (Author)

A83-33515* Ford Motor Co., Dearborn, Mich.
INJECTION MOLDING CERAMICS TO HIGH GREEN DENSITIES
J. A. MANGELS and R. M. WILLIAMS (Ford Motor Co., Dearborn, MI) American Ceramic Society, Bulletin (ISSN 0002-7812), vol. 62, May 1983, p. 601-606. Research sponsored by the U.S. Department of Energy. refs
(Contract DEN3-20)

The injection molding behavior of a concentrated suspension of Si powder in wax was studied. It was found that the injection molding behavior was a function of the processing techniques used to generate the powder. Dry ball-milled powders had the best molding behavior, while air classified and impact-milled powders demonstrated poorer injection moldability. The relative viscosity of these molding batches was studied as a function of powder properties: distribution shape, surface area, packing density, and particle morphology. The experimental behavior, in all cases, followed existing theories. The relative viscosity of an injection molding composition composed of dry ball-milled powders could be expressed using Farris' relation. Author

A83-36239*# National Aeronautics and Space Administration. Lewis Research Center, Cleveland, Ohio.
DESIGN ANALYSIS OF A SELF-ACTING SPIRAL-GROOVE RING SEAL FOR COUNTER-ROTATING SHAFTS
EL DI RUSSO (NASA, Lewis Research Center, Cleveland, OH) AIAA, SAE, and ASME, Joint Propulsion Conference, 19th, Seattle, WA, June 27-29, 1983. 8 p.
(AIAA PAPER 83-1134)

A self-acting spiral groove inter-shaft ring seal of nominal 16.33 cm (6.43 in.) diameter for sealing fan bleed air between counter rotating shafts in advanced turbofan engines was analyzed. The analysis focused on the lift force characteristics of the spiral grooves. A NASA Lewis developed computer program for predicting

the performance of gas lubricated face seals was used to optimize the spiral groove geometry to produce maximum lift force. Load capacity curves (lift force as function of film thickness) were generated for four advanced turbofan engine operating conditions at relative seal speeds ranging from 17,850 to 29,800 rpm, sealed air pressures from 6 to 42 N/sq cm (9 to 60 Psi) absolute and temperatures from 95 to 327 C (203 to 620 F). The relative seal sliding speed range was 152 to 255 m/sec (500 to 836 ft/sec). The analysis showed that the spiral grooves are capable of producing sufficient lift force such that the ring seal will operate in a noncontacting mode over the operating range of typical advanced turbofan engines. Previously announced in STAR as N83-23306 Author

A83-36379*# National Aeronautics and Space Administration. Lewis Research Center, Cleveland, Ohio.
THE PERFORMANCE AND APPLICATION OF HIGH SPEED LONG LIFE LH2 HYBRID BEARINGS FOR REUSABLE ROCKET ENGINE TURBOMACHINERY
N. P. HANNUM (NASA, Lewis Research Center, Cleveland, OH) and C. E. NIELSON (Rockwell International Corp., Rocketdyne Div., Canoga Park, CA) AIAA, SAE, and ASME, Joint Propulsion Conference, 19th, Seattle, WA, June 27-29, 1983. 26 p. refs
(AIAA PAPER 83-1389)

Data are presented for two different experimental programs which were conducted to investigate the characteristics of a hybrid (hydrostatic/ball) bearing operating in liquid hydrogen. The same bearing design was used in both programs. Analytical predictions were made of the bearing characteristics and are compared with the experimental results when possible. The first program used a bearing tester to determine the steady state, transient, and cyclic life characteristics of the bearing over a wide range of operating conditions. The second program demonstrated the feasibility of applying hybrid bearings to an actual high speed turbopump by retrofitting and then testing an existing liquid hydrogen turbopump with the bearings. Author

A83-37822* National Aeronautics and Space Administration. Lewis Research Center, Cleveland, Ohio.
PLASTIC DEFORMATION AND WEAR PROCESS AT A SURFACE DURING UNLUBRICATED SLIDING
T. YAMAMOTO (NASA, Lewis Research Center, Cleveland, OH; Tokyo University of Agriculture and Technology, Tokyo, Japan) and D. H. BUCKLEY (NASA, Lewis Research Center, Cleveland, OH) ASLE Transactions, vol. 26, July 1983, p. 277-286; Discussion, p. 286, 287. refs

The plastic deformation and wear of a 304 stainless steel surface sliding against an aluminum oxide rider with a spherical surface (the radius of curvature: 1.3 cm) were observed by using scanning electron and optical microscopes. Experiments were conducted in a vacuum of one million Pa and in an environment of fifty thousandth Pa of chlorine gas at 25 C. The load was 500 grams and the sliding velocity was 0.5 centimeter per second. The deformed surface layer which accumulates and develops successively is left behind the rider, and step shaped proturbances are developed even after single pass sliding under both environmental conditions. A fully developed surface layer is gradually torn off leaving a characteristic pattern. The mechanism for tearing away of the surface layer from the contact area and sliding track contour is explained assuming the simplified process of material removal based on the adhesion theory for the wear of materials. Previously announced in STAR as N82-32735 S.L.

A83-37823* Illinois Univ., Urbana.
THE INFLUENCE OF SURFACE DENTS AND GROOVES ON TRACTION IN SLIDING EHD POINT CONTACTS
C. CUSANO (Illinois, University, Urbana, IL) and L. D. WEDEVEN (NASA, Lewis Research Center, Cleveland, OH) ASLE Transactions, vol. 26, July 1983, p. 306-310. refs

Changes in traction, caused by dents and grooves on a highly polished ball, are investigated as these defects approach and go through sliding elastohydrodynamic point contacts. The contacts are formed with the ball loading against a transparent disk. The ball and thus the topographical features are held stationary at various locations in the vicinity and within the contact while the disk is rotating. These topographical features can cause substantial changes in the traction when compared to traction obtained with smooth surfaces. Previously announced in STAR as N82-32734 S.L.

A83-39944*# National Aeronautics and Space Administration. Lewis Research Center, Cleveland, Ohio.
HIGH-SPEED MOTION PICTURE CAMERA EXPERIMENTS OF CAVITATION IN DYNAMICALLY LOADED JOURNAL BEARINGS
B. J. HAMROCK (NASA, Lewis Research Center, Cleveland, OH) and B. O. JACOBSON ASME, Transactions, Journal of Lubrication Technology (ISSN 0022-2305), vol. 105, July 1983, p. 446-452. Research supported by the Hogskolan i Lulea, U.S. National Research Council, and NASA. refs
(ASME PAPER 82-LUB-18)

A high-speed camera was used to investigate cavitation in dynamically loaded journal bearings. The length-diameter ratio of the bearing, the speeds of the shaft and bearing, the surface material of the shaft, and the static and dynamic eccentricity of the bearing were varied. The results reveal not only the appearance of gas cavitation, but also the development of previously unsuspected vapor cavitation. It was found that gas cavitation increases with time until, after many hundreds of pressure cycles, there is a constant amount of gas kept in the cavitation zone of the bearing. The gas can have pressures of many times the atmospheric pressure. Vapor cavitation bubbles, on the other hand, collapse at pressures lower than the atmospheric pressure and cannot be transported through a high-pressure zone, nor does the amount of vapor cavitation in a bearing increase with time. Analysis is given to support the experimental findings for both gas and vapor cavitation. Previously announced in STAR as N82-20543 J.D.H.

A83-43339* Mechanical Technology, Inc., Latham, N. Y.
ANALYSIS OF SPIRAL-GROOVE FACE SEALS FOR LIQUID OXYGEN
W. SHAPIRO, J. WALOWIT, and H. F. JONES (Mechanical Technology, Inc., Latham, NY) American Society of Lubrication Engineers, Annual Meeting, 38th, Houston, TX, Apr. 24-28, 1983. 11 p. refs
(Contract NAS3-23260)
(ASLE PREPRINT 83-AM-4B-2)

Analyses and predicted performance of a 50-mm diameter, spiral-groove face seal to seal liquid oxygen at 5.17 MPa pressure, and operating at surface speeds of 183 m/s are described. The pressure-balanced spiral-groove concept is introduced that circulates spiral-groove flow independent of leakage flow. Independent flow paths preclude overheating from vaporization and consequent flow blockage. The analysis accounts for fluid turbulence and inertia, thermoelastic distortions, and dynamic response. An operating-range map was developed as a function of speed and pressure. The fluid-film analysis is summarized in the Appendix. Author

A83-48023*# Detroit Diesel Allison, Indianapolis, Ind.
COMPONENT QUALIFICATION AND INITIAL BUILD OF THE AGT 100 ADVANCED AUTOMOTIVE GAS TURBINE
R. A. JOHNSON (General Motors Corp., Detroit Diesel Allison Div., Indianapolis, IN) American Society of Mechanical Engineers, International Gas Turbine Conference and Exhibit, 28th, Phoenix, AZ, Mar. 27-31, 1983. 9 p. Research supported by the U.S. Department of Energy. refs
(Contract DEN3-168)
(ASME PAPER 83-GT-225)

In advance of initial dynamometer testing of the AGT 100 engine, all prime components and subsystems were bench/rig tested. Included were compressor, combustor, turbines, regenerator, ceramic components, and electronic control system. Results are briefly reviewed. Initial engine buildup was completed and rolled-out for test cell installation in July 1982. Shakedown

testing included motoring and sequential firing of the combustor's three fuel nozzles. Author

A83-48025*# Mechanical Technology, Inc., Latham, N. Y.
POWER TURBINE DYNAMICS - AN EVALUATION OF A SHEAR-MOUNTED ELASTOMERIC DAMPER
E. S. ZORZI, J. WALTON (Mechanical Technology, Inc., Latham, NY), and R. CUNNINGHAM (NASA, Lewis Research Center, Cleveland, OH) American Society of Mechanical Engineers, International Gas Turbine Conference and Exhibit, 28th, Phoenix, AZ, Mar. 27-31, 1983. 6 p. refs
(Contract NAS3-21623; NAS3-20609)
(ASME PAPER 83-GT-228)

As an alternative to the more conventional squeeze-film bearing damper designs, a Viton-70 shear-mounted, elastomeric damper was built and tested in a T-55 power turbine high-speed balancing rig. This application demonstrated, for the first time, the feasibility of using elastomers as the primary rotor damping source in production turbine engine hardware. The shear-mounted damper design was selected because of its compatibility with actual gas turbine engine radial space constraints, its accommodation of both the radial and axial thrust loads present in gas turbine engines, and its capability of controlled axial preload. Test results showed that the Viton-70 elastomeric damper operated successfully and provided excellent control of both synchronous and nonsynchronous vibrations through all phases of testing to the maximum rotor speed of 1676 rad/s (16,000 rpm). Excellent correlation between the predicted and experienced critical speeds, mode shapes, and log decrements for the power turbine rotor and elastomer damper assembly was also achieved. Author

A83-48030*#
PROGRESS IN NET SHAPE FABRICATION OF ALPHA SIC TURBINE COMPONENTS
R. S. STORM and R. G. NAUM (Carborundum Resistant Materials Co., Niagara Falls, NY) American Society of Mechanical Engineers, International Gas Turbine Conference and Exhibit, 28th, Phoenix, AZ, Mar. 27-31, 1983. 6 p. Research supported by the U.S. Department of Energy.
(Contract DEN3-17; DEN3-168; DEN3-167)
(ASME PAPER 83-GT-238)

The development status of component technology in an automotive gas turbine Ceramic Applications in Turbine Engines program is discussed, with attention to such materials and processes having a low cost, net shape fabrication potential as sintered alpha-SiC that has been fashioned by means of injection molding, slip casting, and isostatic pressing. The gas turbine elements produced include a gasifier turbine rotor, a turbine wheel, a connecting duct, a combustor baffle, and a transition duct. O.C.

N83-10425*# National Aeronautics and Space Administration. Lewis Research Center, Cleveland, Ohio.
LIFE AND RELIABILITY MODELS FOR HELICOPTER TRANSMISSIONS
M. SAVAGE (Akron Univ., Ohio), R. J. KNORR (Akron Univ., Ohio), and J. J. COY 1982 14 p refs Proposed for presentation at the Rotary Wing Propulsion System Specialist Meeting, Williamsburg, Va., 16-18 Nov. 1982; sponsored by the American Helicopter Society Prepared in cooperation with Army Aviation Research and Development Command, Cleveland
(NASA-TM-82976; E-1405; NAS 1.15:82976; AHS-RWP-16; AVRADCOM-TR-82-C-15) Avail: NTIS HC A02/MF A01 CSCL 01C

Computer models of life and reliability are presented for planetary gear trains with a fixed ring gear, input applied to the sun gear, and output taken from the planet arm. For this transmission the input and output shafts are co-axial and the input and output torques are assumed to be coaxial with these shafts. Thrust and side loading are neglected. The reliability model is based on the Weibull distributions of the individual reliabilities of the in transmission components. The system model is also a Weibull distribution. The load versus life model for the system is a power relationship as the models for the individual components. The load-life exponent and basic dynamic capacity are developed as functions of the components capacities. The models are used to compare three and four planet, 150 kW (200 hp), 5:1 reduction transmissions with 1500 rpm input speed to illustrate their use. A.R.H.

N83-11495*# Bolt, Beranek, and Newman, Inc., Cambridge, Mass.
THE TRANSFER FUNCTION METHOD FOR GEAR SYSTEM DYNAMICS APPLIED TO CONVENTIONAL AND MINIMUM EXCITATION GEARING DESIGNS Final Report
W. D. MARK Washington NASA Oct. 1982 111 p refs
(Contract NAS3-21978)
(NASA-CR-3626; NAS 1.26:3626; BBN-4712) Avail: NTIS HC A06/MF A01 CSCL 13I

A transfer function method for predicting the dynamic responses of gear systems with more than one gear mesh is developed and applied to the NASA Lewis four-square gear fatigue test apparatus. Methods for computing bearing-support force spectra and temporal histories of the total force transmitted by a gear mesh, the force transmitted by a single pair of teeth, and the maximum root stress in a single tooth are developed. Dynamic effects arising from other gear meshes in the system are included. A profile modification design method to minimize the vibration excitation arising from a pair of meshing gears is reviewed and extended. Families of tooth loading functions required for such designs are developed and examined for potential excitation of individual tooth vibrations. The profile modification design method is applied to a pair of test gears. Author

N83-11496*# National Aeronautics and Space Administration. Lewis Research Center, Cleveland, Ohio.
PLASTIC DEFORMATION AT SURFACE DURING UNLUBRICATED SLIDING
T. YAMAMOTO (Tokyo Univ.) and D. H. BUCKLEY Oct. 1982 20 p refs
(NASA-TP-2036; E-1036; NAS 1.60:2036) Avail: NTIS HC A02/MF A01 CSCL 20K

The plastic deformation and wear of 304 stainless-steel surface slid against an aluminum oxide rider were observed by using a scanning electron microscope and an optical microscope. Experiments were conducted in a vacuum of 0.000001 Pa and in an environment of 0.0005 Pa chlorine gas at 25 C. The load was 500 grams and the sliding velocity was 0.5 centimeter per second. The deformed surface layer which accumulates and develops successively is left behind the rider, and step-shaped protuberances are developed even after single pass sliding under both environmental conditions. A fully developed surface layer is gradually torn off leaving a characteristic pattern. These observations result from both adhesion and an adhesive wear mechanism. Author

N83-11497*# Detroit Diesel Allison, Indianapolis, Ind.
ADVANCED GAS TURBINE (AGT) POWERTRAIN SYSTEM Semiannual Technical Summary Report
H. E. HELMS, J. KAUFELD, and R. KORDES Jul. 1981 111 p refs
(Contract DEN3-168)
(NASA-CR-165346; NAS 1.26:165346; EDR-10578; SATSR-2)
Avail: NTIS HC A06/MF A01 CSCL 21E

A 74.5 kW(100 hp) advanced automotive gas turbine engine is described. A design iteration to improve the weight and production cost associated with the original concept is discussed. Major rig tests included 15 hours of compressor testing to 80% design speed and the results are presented. Approximately 150 hours of cold flow testing showed duct loss to be less than the design goal. Combustor test results are presented for initial checkout tests. Turbine design and rig fabrication is discussed. From a materials study of six methods to fabricate rotors, two have been selected for further effort. A discussion of all six methods is given. S.L.

N83-11498*# National Aeronautics and Space Administration. Lewis Research Center, Cleveland, Ohio.
TRIBOLOGICAL PROPERTIES OF AMORPHOUS ALLOYS AND THE ROLE OF SURFACES IN ABRASIVE WEAR OF MATERIALS
K. MIYOSHI and D. H. BUCKLEY 1982 26 p refs Presented at the TMS-AIME Fall Meeting, St. Louis, 24-28 Oct. 1982
(NASA-TM-82973; E-1359; NAS 1.15:82973) Avail: NTIS HC A03/MF A01 CSCL 11G

The research approach undertaken by the authors relative to the subject, and examples of results from the authors are reviewed. The studies include programs in adhesion, friction, and various wear mechanisms (adhesive and abrasive wear). The materials which have been studied include such ceramic and metallic materials as silicon carbide, ferrites, diamond, and amorphous alloys.

N83-12167*# National Aeronautics and Space Administration. Lewis Research Center, Cleveland, Ohio.
TRIBOLOGY
D. H. BUCKLEY *In* NASA. Langley Research Center Advan. Mater. Technol. p 391-410 Nov. 1982 refs
Avail: NTIS HC A19/MF A01 CSCL 20K

The adhesion, friction, and wear properties of materials are reviewed and some of the factors influencing these properties are discussed. The forms of lubrication and types of lubricants will also be discussed. B.W.

N83-12431*# Detroit Diesel Allison, Indianapolis, Ind.
ADVANCED GAS TURBINE (AGT) POWERTRAIN SYSTEM DEVELOPMENT FOR AUTOMOTIVE APPLICATIONS Semiannual Report, 1 Oct. 1979 - 30 Jun. 1980
May 1981 285 p refs
(Contract DEN3-168)
(NASA-CR-165178; DOE/NASA/0168-80/1; NAS 1.26:165178; DDA-EDR-10327; SAR-1) Avail: NTIS HC A13/MF A01 CSCL 21E

Preliminary layouts were made for the exhaust system, air induction system, and battery installation. Points of interference were identified and resolved by altering either the vehicle or engine designs. An engine general arrangement evolved to meet the vehicle engine compartment constraints while minimizing the duct pressure losses and the heat rejection. A power transfer system (between gasifier and power turbines) was developed to maintain nearly constant temperatures throughout the entire range of engine operation. An advanced four speed automatic transmission was selected to be used with the engine. Performance calculations show improvements in component efficiencies and an increase in fuel economy. A single stage centrifugal compressor design was completed and released for procurement. Gasifier turbine, power turbine, combustor, generator, secondary systems, materials, controls, and transmission development are reported. Author

N83-12432*# National Aeronautics and Space Administration. Lewis Research Center, Cleveland, Ohio.
ELASTOHYDRODYNAMIC LUBRICATION THEORY
B. J. HAMROCK and D. DOWSON (Leeds Univ.) Oct. 1982 56 p refs
(NASA-TM-81695; E-209; NAS 1.15:81695) Avail: NTIS HC A04/MF A01 CSCL 11H

The isothermal elastohydrodynamic lubrication (EHL) of a point contact was analyzed numerically by simultaneously solving the elasticity and Reynolds equations. In the elasticity analysis the contact zone was divided into equal rectangular areas, and it was assumed that a uniform pressure was applied over each area. In the numerical analysis of the Reynolds equation, a phi analysis (where phi is equal to the pressure times the film thickness to the 3/2 power) was used to help the relaxation process. The EHL point contact analysis is applicable for the entire range of elliptical parameters and is valid for any combination of rolling and sliding within the contact. Author

N83-12433*# National Aeronautics and Space Administration. Lewis Research Center, Cleveland, Ohio.
FERROGRAPHIC AND SPECTROMETER OIL ANALYSIS FROM A FAILED GAS TURBINE ENGINE
W. R. JONES, JR. 1982 15 p refs Presented at the Intern. Conf. on Advan. in Ferrography, Swansee, UK, 22-24 Sep. 1982
(NASA-TM-82956; E-1267; NAS 1.15:82956) Avail: NTIS HC A02/MF A01 CSCL 14D

An experimental gas turbine engine was destroyed as a result of the combustion of its titanium components. It was concluded that a severe surge may have caused interference between rotating and stationary compressor that either directly or indirectly ignited the titanium components. Several engine oil samples (before and after the failure) were analyzed with a Ferrograph, a plasma, an atomic absorption, and an emission spectrometer to see if this information would aid in the engine failure diagnosis. The analyses indicated that a lubrication system failure was not a causative factor in the engine failure. Neither an abnormal wear mechanism nor a high level of wear debris was detected in the engine oil sample taken just prior to the test in which the failure occurred. However, low concentrations (0.2 to 0.5 ppm) of titanium were evident in this sample and samples taken earlier. After the failure, higher titanium concentrations (2 ppm) were detected in oil samples taken from different engine locations. Ferrographic analysis indicated that most of the titanium was contained in spherical metallic debris after the failure. The oil analyses eliminated a lubrication system bearing or shaft seal failure as the cause of the engine failure. Author

N83-13457*# National Aeronautics and Space Administration. Lewis Research Center, Cleveland, Ohio.
ROLLING-ELEMENT FATIGUE LIFE WITH TRACTION FLUIDS AND AUTOMATIC TRANSMISSION FLUID IN A HIGH-SPEED ROLLING-CONTACT RIG
R. J. PARKER, A. H. NAHM (General Electric Co., Cincinnati), and S. H. LOEWENTHAL Nov. 1982 16 p refs
(Contract NAS3-20832)
(NASA-TP-2050; E-1091; NAS 1.60:2050) Avail: NTIS HC A02/MF A01 CSCL 13I

Rolling-element fatigue tests were run in standard and high-speed rolling-contact rigs at bar speeds from 5000 to 50,000 rpm to determine the effects of speed and lubricant film parameter on rolling-element fatigue life. AISI 52100 test bars were tested at a maximum Hertz stress of 4.83 GPa (700,000 psi) with three traction fluids and an automatic transmission fluid. Rolling-element fatigue life increased with speed, with the greatest increases occurring from 10,000 to 50,000 rpm. The life data tended to follow published life-versus-lubricant-film-parameter data up to a film parameter of approximately 3. Author

N83-13458*# National Aeronautics and Space Administration. Lewis Research Center, Cleveland, Ohio.
THEORETICAL RESULTS FOR FULLY FLOODED, ELLIPTICAL HYDRODYNAMIC CONTACTS
B. J. HAMROCK and D. DOWSON (Leeds Univ., Engl.) Oct. 1982 84 p refs Repr. from Ball Bearing Lubrication, Sep. 1981
(NASA-TM-81696; E-209; NAS 1.15:81696) Avail: NTIS HC A05/MF A01 CSCL 13I

The influence of the ellipticity parameter and the dimensionless speed, load, and materials parameters on minimum film thickness was investigated. The ellipticity parameter was varied from 1 (a ball-on-plate configuration) to 8 (a configuration approaching a line contact). The dimensionless speed parameter was varied over a range of nearly two orders of magnitude. Conditions corresponding to the use of solid materials of bronze, steel, and silicon nitride and lubricants of praffinic and naphthenic mineral oils were considered in obtaining the exponent in the dimensionless materials parameter. Thirty-four different cases were used in obtaining the minimum film thickness formula H min = 3.63U to the 0.68 power G to the 0.49 power W to the -0.073 power 1-e to the 0.68K power). A simplified expression for the ellipticity parameter was found where k = 1.03 (r(y)/r(x)) to the 0.64 power.

Contour plots were also shown which indicate in detail the pressure spike and two side lobes in which the minimum film thickness occurs. These theoretical solutions of film thickness have all the essential features of the previously reported experimental observations based upon optical interferometry. Author

N83-14494*# Massachusetts Inst. of Tech., Cambridge. National Magnet Lab.
MAGNETOHYDRODYNAMICS (MHD) ENGINEERING TEST FACILITY (ETF) 200 MWE POWER PLANT. CONCEPTUAL DESIGN ENGINEERING REPORT (CDER) SUPPLEMENT. MAGNET SYSTEM SPECIAL INVESTIGATIONS Final Report
Sep. 1981 86 p
(Contract NAG3-100; DE-AI01-77ET-10769)
(NASA-CR-165509; DOE/NASA/0100-1; NAS 1.26:165509; NAS-E-1) Avail: NTIS HC A05/MF A01 CSCL 10A

The results of magnet system special investigations listed below are summarized: 4 Tesla Magnet Alternate Design Study; 6 Tesla Magnet Manufacturability Study. The conceptual design for a 4 Tesla superconducting magnet system for use with an alternate (supersonic) ETF power train is described, and estimated schedule and cost are identified. The magnet design is scaled from the ETF 6 T Tesla design. Results of a manufacturability study and a revised schedule and cost estimate for the ETF 6 T magnet are reported. Both investigations are extensions of the conceptual design of a 6 T magnet system performed earlier as a part of the overall MED-ETF conceptual design described in Conceptual Design Engineering Report (CDER) Vol. V, System Design Description (SDD) 503 dated September, 1981, DOE/NASA/0224-1; NASA CR-165/52. Author

N83-15512*# National Aeronautics and Space Administration. Lewis Research Center, Cleveland, Ohio.
LUBRICATION OF 35-MILLIMETER-BORE BALL BEARINGS OF SEVERAL DESIGNS AT SPEEDS TO 2.5 MILLION DN
H. R. SIGNER (Industrial Tectonics, Inc.) and F. T. SCHULLER *In* AGARD Probl. in Bearings and Lubrication 15 p Aug. 1982 refs
(Contract NAS3-19779)
Avail: NTIS HC A20/MF A01 CSCL 13I

Parametric tests were conducted with 35mm bore, angular contact ball bearings with either a single or double-outer-land-guided cage. The bearings were either lubricated by oil jets or employed inner ring lubrication. Outer ring cooling was added in selected tests. Test conditions were a radial load of 222 N (50 lb) and/or a thrust load of 667 N (150 lb), shaft speeds to 72,000 rpm, and an oil inlet temperature of 394 K (250 F). Lubricant flow to the bearing ranged rom 300 to 1900 cc/min (0.08 to 0.50 gal/min). All bearings were successfully run at speeds to 2.5 million DN. Increasing the lubricant flow decreased bearing ring temperatures but increased bearing power loss. The power loss and race temperatures of a jet lubricated bearing with double-outer-land-guided cage were always higher than those of the single-land-guided-design at similar test conditions. The lowest bearing operating temperatures were achieved when inner ring lubrication and outer ring cooling were combined. Cage slip of a double-outer-land-guided cage was approximately twice that of a single-outer-land-guided cage. Author

N83-15514*# National Aeronautics and Space Administration. Lewis Research Center, Cleveland, Ohio.
ELASTOHYDRODYNAMIC LUBRICATION OF ELLIPTICAL CONTACTS
B. J. HAMROCK *In* AGARD Probl. in Bearings and Lubrication 14 p Aug. 1982 refs Presented at the 1st Symp. INTERTRIBO, Stvbske Pleso Czechoslovakia, 27-29 Apr. 1981
Avail: NTIS HC A20/MF A01

Fully flooded, elastohydrodynamically lubricated, elliptical contacts are discussed. The relevant equations used in the elastohydrodynamic lubrication (EHL) of elliptical contacts are briefly described. Film thickness equations are developed for materials of high elastic modulus, such as metal, and for materials of low elastic modulus, such as rubber. In addition to the film thickness equations that are developed, plots of pressure and film thickness are presented. A theoretical study of the influence of lubricant starvation on film thickness and pressure in hard and soft elliptical elastohydrodynamic contacts is presented. From the results for both hard and soft EHL contacts a simple and important dimensionless inlet boundary distance is specified. It is also found that the film thickness for a starved condition can be written in dimensionless terms as a function of the inlet distance parameter and the film thickness for a fully flooded condition. contour plots of pressure and film thickness in and around the contact are shown for fully flooded and starved conditions. The theoretical findings are compared directly with results obtained experimentally. Author

N83-15520*# Missouri Univ., Rolla. Dept. of Mechanical and Aerospace Engineering.
A DETAILED TREATMENT OF TWO-DIMENSIONAL, STARVED LUBRICATION IN THE VICINITY OF TWO COUNTER-ROTATING CYLINDERS
R. A. MEDROW and L. R. SHIPERS *In* AGARD Probl. in Bearings and Lubrication 10 p Aug. 1982
(Contract NSG-3113)
Avail: NTIS HC A20/MF A01 CSCL 13I

The problem of starved lubrication in the inlet region for the case of line contact between two nondeforming, equal radii cylinders rotating in opposite directions with equal surface speeds is considered. The lubricant is assumed to be a constant density, isoviscous, Newtonian fluid. The usual approach, which involves the use of Reynolds equation everywhere, is not followed. Instead, the situation is restricted to one in which the lubricant enters the contact region in thin films which adhere to the cylinders. Using Reynolds equation only at the line of centers and a suitable thin film approximation far from that point, the intervening region is treated as a general creeping flow region. Solutions, incorporating complete free surface boundary conditions, are obtained numerically. The hitherto unobtained results due to this approach include the existence of a unique free surface location for a fixed set of operating conditions. Author

N83-15522*# National Aeronautics and Space Administration. Lewis Research Center, Cleveland, Ohio.
GEOMETRY AND STARVATION EFFECTS IN HYDRODYNAMIC LUBRICATION
D. BREWE (AVRADCOM) and B. J. HAMROCK *In* AGARD Probl. in Bearings and Lubrication 12 p Aug. 1982 refs
Avail: NTIS HC A20/MF A01

Numerical methods were used to detemine the effects of lubricant starvation on the minimum film thickness under conditions of a hydrodynamic point contact. Starvation was effected by varying the fluid inlet level. The Reynolds boundary conditions were applied at the cavitation boundary and zero pressure was stipulated at the meniscus or inlet boundary. A minimum film thickness equation as a function of both the ratio of dimensionless load to dimensionless speed and inlet supply level was determined. By comparing the film generated under the starved inlet condition with the film generated from the fully flooded inlet, an expression for the film reduction factor was obtained. Based on this factor a starvation threshold was defined as well as a critically starved inlet. The changes in the inlet pressure buildup due to changing the available lubricant supply are presented in the form of three dimensional isometric plots and also in the form of contour plots. Author

N83-15523*# National Aeronautics and Space Administration. Lewis Research Center, Cleveland, Ohio.
LUBRICANT EFFECTS ON EFFICIENCY OF A HELICOPTER TRANSMISSION
A. M. MITCHELL and J. J. COY (AVRADCOM) *In* AGARD Probl. in Bearings and Lubrication 14 p Aug. 1982 refs
Avail: NTIS HC A20/MF A01 CSCL 11H

Efficiency tests were conducted using eleven different lubricants in the NASA Lewis Research Center's 500 hp torque regenerative helicopter transmission test stand. The test transmission was the

OH58A helicopter main transmission. The mechanical power input to the test transmission was 224 kW (300 hp) at 6060 rpm. Tests were run at oil-in temperatures of 355 K (180 F) and 372 K (210 F). The efficiency was calculated from a heat balance on the water running through an oil-to-water heat exchanger while the transmission was heavily insulated. The following results were obtained: (1) Among the eleven different lubricants, the efficiency ranged from 98.3 to 98.8 percent, which is a 50 percent variation relative to the losses associated with the maximum efficiency measured; (2) For a given lubricant, the efficiency increased as temperature increased and thus a viscosity decreased. There were two exceptions which could not be explained on the basis of available data; (3) Between lubricants, efficiency was not correlated with viscosity. There were relatively large variations in efficiency with the different lubricants whose viscosity generally fell in the 5 to 7 centistoke range; and (4) The lubricants had no significant effect on the vibration signature of the transmission. Author

N83-15530*# National Aeronautics and Space Administration. Lewis Research Center, Cleveland, Ohio.
EXPERIMENTAL AND ANALYTICAL DETERMINATION OF GEAR TOOTH TEMPERATURES WITH OIL JET LUBRICATION
D. P. TOWNSEND and L. S. AKIN (Western Gear Corp.) *In* AGARD Probl. in Bearings and Lubrication 14 p Aug. 1982 refs Presented at the ASME 3rd Intern. Power Transmission and Gearing Conf., San Francisco, 18-22 Aug. 1980
Avail: NTIS HC A20/MF A01

Gear tooth average and instantaneous surface temperatures were measured with a fast response infrared radiometric microscope, while operating at arious speeds, loads and oil jet pressures. Increased oil jet pressure had a significant effect on both average and peak surface temperatures at all test conditions, increasing the speed at constant load and increasing the load at constant speed causes a significant rise in average and peak surface temperatures of gear teeth. A gear tooth temperature analysis was conducted by a finite element method combined with a calculated heat input and oil jet impingment depth with estimated heat transfer coefficients based on the experimental data. It is concluded that oil jet pressures required for adequate cooling at high load and speed conditions must be high enough to get full penetration depth of the teeth. E.A.K.

N83-15627*# Detroit Diesel Allison, Indianapolis, Ind.
ADVANCED GAS TURBINE (AGT) POWER-TRAIN SYSTEM DEVELOPMENT Semiannual Report, 1 Jul. - 31 Dec. 1981
H. E. HELMS, R. A. JOHNSON, and R. K. GIBSON Feb. 1982 65 p refs Sponsored in cooperation with DOE
(Contract DEN3-168)
(NASA-CR-167875; DOE/NASA/0168-82/4, DDA-EDR-10977; NAS 1.26:167875; SAR-4) Avail: NTIS HC A04/MF A01 CSCL 13I

Technical work on the design and component testing of a 74.5 kW (100 hp) advanced automotive gas turbine is described. Selected component ceramic component design, and procurement were tested. Compressor tests of a modified rotor showed high speed performance improvement over previous rotor designs; efficiency improved by 2.5%, corrected flow by 4.6%, and pressure ratio by 11.6% at 100% speed. The aerodynamic design is completed for both the gasifier and power turbines. Ceramic (silicon carbide) gasifier rotors were spin tested to failure. Improving strengths is indicated by burst speeds and the group of five rotors failed at speeds between 104% and 116% of engine rated speed. The emission results from combustor testing showed NOx levels to be nearly one order of magnitude lower than with previous designs. A one piece ceramic exhaust duct/regenerator seal platform is designed with acceptable low stress levels. E.A.K.

N83-15629*# National Aeronautics and Space Administration. Lewis Research Center, Cleveland, Ohio.
ROTORDYNAMIC INSTABILITY PROBLEMS IN HIGH-PERFORMANCE TURBOMACHINERY
Washington Dec. 1982 460 p refs Workshop held in College Station, Tex., 10-12 May 1982; sponsored by Texas A and M Univ. and the Army Research Office
(NASA-CP-2250; E-1287; NAS 1.55:2250) Avail: NTIS HC A20/MF A01 CSCL 13I

Rotor dynamic instability problems in high performance turbomachinery are reviewed. Mechanical instability mechanisms are discussed. Seal forces and working fluid forces in turbomachinery are discussed. Control of rotor instability is also investigated.

N83-15650*# Virginia Univ., Charlottesville. Dept. of Mechanical and Aerospace Engineering.
AERODYNAMIC STIFFNESS OF AN UNBOUND ECCENTRIC WHIRLING CENTRIFUGAL IMPELLER WITH AN INFINITE NUMBER OF BLADES
P. E. ALLAIRE, L. A. BRANAGAN (Pacific Gas and Electric Co., San Ramon, Calif.), and J. A. KOCUR *In* NASA. Lewis Research Center Rotordyn. Instability Probl. in High-Performance Turbomachinery p 323-343 Dec. 1982 refs
(Contract NAG3-180)
Avail: NTIS HC A20/MF A01 CSCL 13I

An unbounded eccentric centrifugal impeller with an infinite number of log spiral blades undergoing synchronous whirling in an incompressible fluid is considered. The forces acting on it due to coriolis forces, centripetal forces, changes in linear momentum, changes in pressure due to rotating and changes in pressure due to changes in linear momentum are evaluated. Author

N83-15659*# Crane Packing Co., Morton Grove, Ill.
ENERGY EFFICIENT FACE SEAL
J. SEHNAL, J. SEDY, I. ETSION, and A. ZOBENS 11 Feb. 1982 113 p refs
(Contract NAS3-22128)
(NASA-CR-165591; NAS 1.26:165591) Avail: NTIS HC A06/MF A01 CSCL 11A

Torque, face temperature, leakage, and wear of a flat face seal were compared with three coned face seals at pressures up to 2758 kPa and speeds up to 8000 rpm. Axial movement of the mating seal parts was recorded by a digital data acquisition system. The coning of the tungsten carbide primary ring ranged from .51 micro-m to 5.6 micro-m. The torque of the coned face seal balanced to 76.3% was an average 42% lower, the leakage eleven times higher, than that of the standard flat face seal. The reduction of the balance of the coned face seal to 51.3% resulted by decreasing the torque by an additional 44% and increasing leakage 12 to 230 times, depending on the seal shaft speed. No measurable wear was observed on the face of the coned seals. E.A.K.

N83-16758*# National Aeronautics and Space Administration. Lewis Research Center, Cleveland, Ohio.
ROLLING-ELEMENT FATIGUE LIFE OF AMS 5900 BALLS
R. J. PARKER Jan. 1983 13 p refs
(NASA-TP-2080; E-1190; NAS 1.60:2080) Avail: NTIS HC A02/MF A01 CSCL 13I

The rolling-element fatigue life of AMS 5900 12.7-mm (1/2-in.) dia was determined in five-ball fatigue testers. The 10% life with the warm headed AMS 5900 balls was equivalent to that of AMS 5749 and over eight times that of AISI M-50. The AMS balls fabricated by cold heading had small surface cracks which initiated fatigue spalls where these cracks were crossed by running tracks. The cold-headed AMS 5900 balls had a 10% fatigue life an order of magnitude less than that of the warm headed balls even when failures on the cold headed balls at visible surface cracks were omitted. Author

N83-16759*# National Aeronautics and Space Administration. Lewis Research Center, Cleveland, Ohio.

ELASTOHYDRODYNAMIC LUBRICATION OF RECTANGULAR CONTACTS

B. J. HAMROCK and B. O. JACOBSON (Lulea Univ.) Jan. 1983 30 p refs

(NASA-TP-2111; E-1277; NAS 1.60:2111) Avail: NTIS HC A03/MF A01 CSCL 11H

An isothermal elastohydrodynamically lubricated rectangular contact was evaluated numerically. This required the simultaneous solution of the elasticity and Reynolds equations. In the elasticity analysis the contact zone was divided into equal rectangular areas, and it was assumed that a uniform pressure was applied over each area. The elastohydrodynamic lubrication theory thus developed was used to investigate the influence of the dimensionless speed, load, and materials parameters on minimum film thickness. Ten cases were used in obtaining the minimum film thickness formula. Plots are shown that indicate the details of the pressure distribution, film shape, and flow. The characteristic pressure spike is clearly in evidence as is the parallel film shape through the central portion of the contact, with a minimum film thickness occurring near the outlet of the contact. S.L.

N83-17880*# General Electric Co., Cincinnati, Ohio. Aircraft Engine Business Group.

BEARING FATIGUE INVESTIGATION 3 Final Report

A. H. NAHM, E. N. BAMBERGER, and H. R. SIGNER (Industrial Tectonics, Inc., Compton, Calif.) May 1982 83 p refs (Contract NAS3-15337)

(NASA-CR-168029; NAS 1.26:168029; GE-R82AEB304) Avail: NTIS HC A05/MF A01 CSCL 13I

The operating characteristics of large diameter rolling-element bearings in the ultra high speed regimes expected in advanced turbine engines for high performance aircraft were investigated. A high temperature lubricant, DuPont Krytox 143 AC, was evaluated at bearing speeds to 3 million DN. Compared to the results of earlier, similar tests using a MIL-L-23699 (Type II) lubricant, bearings lubricated with the high density Krytox fluid showed significantly higher power requirements. Additionally, short bearing lives were observed when this fluid was used with AISI M50 bearings in an air atmosphere. The primary mode of failure was corrosion initiated surface distress (fatigue) on the raceways. The potential of a case-carburized bearing to sustain a combination of high-tangential and hertzian stresses without experiencing race fracture was also investigated. Limited full scale bearing tests of a 120 mm bore ball bearing at a speed of 25,000 rpm (3 million DN) indicated that a carburized material could sustain spalling fatigue without subsequent propagation to fracture. Planned life tests of the carburized material had to be aborted, however, because of apparent processing-induced material defects. J.M.S.

N83-17883*# National Aeronautics and Space Administration. Lewis Research Center, Cleveland, Ohio.

MULTIPLE PLATE HYDROSTATIC VISCOUS DAMPER Patent Application

L. P. LUDWIG, inventor (to NASA) 10 Jan. 1983 9 p

(NASA-CASE-LEW-13445-2; US-PATENT-APPL-SN-456929) Avail: NTIS HC A02/MF A01 CSCL 13I

The damping radial motion of a rotating shaft is addressed. The damper comprises a series of spaced plates extending in a radial direction. A hydraulic piston is utilized to place a load in these plates. Each annular plate is provided with a suitable hydrostatic bearing geometry on at least one of its faces. This structure provides a high degree of dampening in a rotor case system of turbomachinery in general. The damper is particularly useful in gas turbine engines. NASA

N83-19092*# National Aeronautics and Space Administration. Lewis Research Center, Cleveland, Ohio.

INTO MESH LUBRICATION OF SPUR GEARS WITH ARBITRARY OFFSET OIL JET. 1: FOR JET VELOCITY LESS THAN OR EQUAL TO GEAR VELOCITY

L. S. AKIN (California State Univ., Long Beach) and D. P. TOWNSEND 1982 22 p refs Presented at Winter Ann. Meeting of the Am. Soc. of Mech. Engr., Phoenix, Ariz., 15-19 Nov. 1982

(NASA-TM-83040; E-1389; NAS 1.15:83040) Avail: NTIS HC A02/MF A01 CSCL 13I

An analysis was conducted for into mesh oil jet lubrication with an arbitrary offset and inclination angle from the pitch point for the case where the oil jet velocity is equal to or less than pitch line velocity. The analysis includes the case for the oil jet offset from the pitch point in the direction of the pinion and where the oil jet is inclined to intersect the common pitch point. Equations were developed for the minimum oil jet velocity required to impinge on the pinion or gear and the optimum oil jet velocity to obtain the maximum impingement depth. Author

N83-19093*# National Aeronautics and Space Administration. Lewis Research Center, Cleveland, Ohio.

INTO MESH LUBRICATION OF SPUR GEARS WITH ARBITRARY OFFSET OIL JET. 2: FOR JET VELOCITIES EQUAL TO OR GREATER THAN GREAT VELOCITY

L. S. AKIN (California State Univ., Long Beach) and D. P. TOWNSEND 1982 23 p refs Presented at Winter Ann. Meeting of the Am. Soc. of Mech. Engr., Phoenix, Ariz., 15-19 Nov. 1982

(NASA-TM-83041; E-1390; NAS 1.15:83041) Avail: NTIS HC A02/MF A01 CSCL 13I

An analysis was conducted for into mesh oil jet lubrication with an arbitrary offset and inclination angle from the pitch point for the case where the oil jet velocity is equal to or greater than gear pitch line velocity. Equations were developed for minimum and maximum oil jet impingement depth. The analysis also included the minimum oil jet velocity required to impinge on the gear or pinion and the optimum oil jet velocity required to obtain the best lubrication condition of maximum impingement depth and gear cooling. It was shown that the optimum oil jet velocity for best lubrication and cooling is when the oil jet velocity equals the gear pitch line velocity. When the oil jet velocity is slightly greater than the pitch line velocity the loaded side of the driven gear and the unloaded side of the pinion receive the best lubrication and cooling with slightly less impingement depth. As the jet velocity becomes much greater than the pitch line velocity the impingement depth is considerably reduced and may completely miss the pinion. Author

N83-20115*# National Aeronautics and Space Administration. Lewis Research Center, Cleveland, Ohio.

CORROSION OF SIMULATED BEARING COMPONENTS OF THREE BEARING STEELS IN THE PRESENCE OF CHLORIDE-CONTAMINATED LUBRICANT

R. J. PARKER, E. N. BAMBERGER (GE Co., Cincinnati), and A. H. NAHM (GE Co., Cincinnati) Washington 1983 20 p refs Proposed for presentation at the Ann. Meeting of the Am. Soc. of Lubrication Engr., Cincinnati, 24-28 Apr. 1983

(NASA-TM-82955; E-1370; NAS 1.15:82955) Avail: NTIS HC A02/MF A01 CSCL 11F

Corrosion tests were run with AISI 52100, AISI M-50 and AMS 5794 under conditions that simulate the crevice corrosion found in aircraft ball and roller bearings rejected at overhaul for corrosion. Test specimens were fabricated that simulated the contacts of balls or rollers and the raceways. Corrosion cells were assembled in the presence of a lubricant contaminated with water and chloride ions. The cell was then thermally cycled between 339 K (150 F) and 276 K (37 F). The corrosion observed after 14 cycles was that of crevice and pitting corrosion typically found in aircraft bearings. AMS 5749 showed a very slight amount of corrosion. No appreciable differences were noted between AISI 52100 and AISI M-50, but both showed much greater corrosion than AMS

5749. The corrosion pits observed in AISI M-50 appeared to be fewer in number but generally deeper and larger than in AISI 52100. S.L.

N83-20116*# National Aeronautics and Space Administration. Lewis Research Center, Cleveland, Ohio.
TRACTION BEHAVIOR OF TWO TRACTION LUBRICANTS
S. H. LOEWENTHAL and D. A. ROHN 1983 21 p refs Proposed for presentation at the Ann. Meeting of the Am. Soc. of Lubrication Engr., Houston, 24-29 Apr. 1983
(NASA-TM-83311; E-1507; NAS 1.15:83311) Avail: NTIS HC A02/MF A01 CSCL 11H

In the analysis of rolling-sliding concentrated contacts, such as gears, bearings and traction drives, the traction characteristics of the lubricant are of prime importance. The elastic shear modulus and limiting shear stress properties of the lubricant dictate the traction/slip characteristics and power loss associated with an EHD contact undergoing slip and/or spin. These properties can be deducted directly from the initial slope m and maximum traction coefficient micron of an experimental traction curve. In this investigation, correlation equations are presented to predict m and micron for two modern traction fluids based on the regression analysis of 334 separate traction disk machine experiments. The effects of contact pressure, temperature, surface velocity, ellipticity ratio are examined. Problems in deducing lubricant shear moduli from disk machine tests are discussed. Author

N83-20117*# National Aeronautics and Space Administration. Lewis Research Center, Cleveland, Ohio.
PRECISION OPTICAL ANGULAR POSITION MARKER SYSTEM FOR ROTATING MACHINERY
J. P. BARRANGER Feb. 1983 12 p refs
(NASA-TM-83062; E-1533; NAS 1.15:83062) Avail: NTIS HC A02/MF A01 CSCL 13I

An optical system is described which generates one or more markers of the angular shaft position of rotating machinery. The system consists of a light source, an optical cable, a machinery mounted lens assembly, a light detector, and a signal conditioner. Light reflected by targets on the rotor is converted to a digital output signal. The system is highly immune to extreme environments of vibration and temperature and achieved a 0.002 percent precision under operational test conditions. Author

N83-20118*# National Aeronautics and Space Administration. Lewis Research Center, Cleveland, Ohio.
ASSESSMENT OF LUBRICATED CONTACTS: MECHANISMS OF SCUFFING AND SCORING
A. DYSON (Wychwood, Birkenhead Merseyside, England) and L. D. WEDEVEN Feb. 1983 18 p refs
(NASA-TM-83074; E-1478; NAS 1.15:83074) Avail: NTIS HC A02/MF A01 CSCL 11H

Scoring and scuffing are defined as two distinct but related forms of failure of hardened ferrous components lubricated by liquids. Experimental observations of these phenomena are described, and criteria for scoring and scuffing are discussed. The mechanisms proposed by various authors to explain these observations are enumerated. The view presented here is that, under conditions yet to be defined, scoring is a gradual breakdown of the lubrication of interacting asperities, such lubrication being boundary or microelastohydrodynamic in nature, or a mixture of the two. The final scuffing stage represents a breakdown of the main elastohydrodynamic system, but this may be triggered by the deterioration in surface topography as a result of scoring. An extension of published theoretical treatment of elastohydrodynamic breakdown is proposed, and a critical experiment to assess the importance of edge effects in band contacts is suggested. The practical implications of the proposed mechanism are reviewed, and recommendations for further work are made. A possible thermal instability mechanism for the breakdown of boundary lubrication is outlined. Author

N83-20119*# National Aeronautics and Space Administration. Lewis Research Center, Cleveland, Ohio.
ADVANCED POWER TRANSMISSION TECHNOLOGY
G. K. FISCHER, ed. Jan. 1983 541 p refs Proc. of symp. held in Cleveland, Ohio, 9-11 Jun. 1981 Sponsored in cooperation with Army Aviation Research and Development Command
(NASA-CP-2210; E-817; NAS 1.55:2210; AVRADCOM-TR-82-C-16) Avail: NTIS HC A23/MF A01 CSCL 13I

Technology overviews, advanced transmission concepts, rolling-element bearing technology, traction drive technology, spiral bevel gear technology, and spur gear technology are discussed.

N83-20120*# National Aeronautics and Space Administration. Lewis Research Center, Cleveland, Ohio.
NASA HELICOPTER TRANSMISSION SYSTEM TECHNOLOGY PROGRAM
E. V. ZARETSKY *In its* Advanced Power Transmission Technol. p 15-34 Jan. 1983 refs
Avail: NTIS HC A23/MF A01 CSCL 01C

The purpose of the NASA Helicopter Transmission System Technology Program is to improve specific mechanical components and the technology for combining these into advanced drive systems to make helicopters more viable and cost competitive for commerical applications. The history, goals, and elements of the program are discussed. Author

N83-20121*# National Aeronautics and Space Administration. Lewis Research Center, Cleveland, Ohio.
PRESENT TECHNOLOGY OF ROLLING-ELEMENT BEARINGS
R. J. PARKER *In its* Advanced Power Transmission Technol. p 35-47 Jan. 1983 refs
Avail: NTIS HC A23/MF A01 CSCL 13I

The present technology of rolling-element bearings, the barriers and limits which currently exist, and some of the future requirements that will demand further advancements are identified. Author

N83-20123*# National Aeronautics and Space Administration. Lewis Research Center, Cleveland, Ohio.
A HISTORICAL PERSPECTIVE OF TRACTION DRIVES AND RELATED TECHNOLOGY
S. H. LOEWENTHAL *In its* Advanced Power Transmission Technol. p 79-108 Jan. 1983 refs
Avail: NTIS HC A23/MF A01 CSCL 13I

The evolution of traction-drive technology, in a limited sense, is traced from its early development to the efforts underway today. Author

N83-20124*# United Technologies Corp., Stratford, Conn. Aircraft Div.
AN OVERVIEW OF ADVANCEMENTS IN HELICOPTER TRANSMISSION DESIGN
J. H. MANCINI *In* NASA. Lewis Research Center Advanced Power Transmission Technol. p 109-122 Jan. 1983
(Contract NAS3-17859; DAAJ02-76-C-0044)
Avail: NTIS HC A23/MF A01 CSCL 01C

Development of a high temperature operating helicopter gearbox is discussed. Author

N83-20125*# Bell Helicopter Co., Fort Worth, Tex.
DESIGN OF AN ADVANCED 500-HP HELICOPTER TRANSMISSION
C. E. BRADDOCK and R. A. BATTLES *In* NASA. Lewis Research Center Advanced Power Transmission Technol. p 123-140 Jan. 1983 refs
(Contract NAS3-21595)
Avail: NTIS HC A23/MF A01 CSCL 01C

High contact ratio spar gears planetary, spiral besel gears, bearings, investment-cast planet carrier, and investment cast stainless-steel housings are discussed. Author

N83-20127*# Transmission Technology Co., Inc., Fairfield, N. J.
DESIGN STUDY OF SELF-ALINING BEARINGLESS PLANETARY (SABP) GEAR
D. J. FOLENTA *In* NASA. Lewis Research Center Advanced Power Transmission Technol. p 151-160 Jan. 1983 refs
(Contract NAS3-21604)
Avail: NTIS HC A23/MF A01 CSCL 13I

The feasibility of using the self alining, bearingless planetary (SABP) transmission in an uprated version of the OH-58 helicopter was evaluated, specific performance comparisons of this new transmission with contemporary helicopter transmission systems and with the uprated version of the OH-58 power transmission were made. Author

N83-20128*# Transmission Research, Inc., Cleveland, Ohio.
HYBRID GEARED TRACTION TRANSMISSIONS
A. L. NASVYTIS and G. WHITE *In* NASA. Lewis Research Center Advanced Power Transmission Technol. p 161-172 Jan. 1983 refs
(Contract NAS3-20812; NAS3-22108; NAS3-22120)
Avail: NTIS HC A23/MF A01 CSCL 13I

The basic configuration of geared traction drives, geometric and structural factors to be considered in their construction, and current work on hybrid helicopter transmissions rated at 500 and 3000 hp are discussed. Author

N83-20131*# National Aeronautics and Space Administration. Lewis Research Center, Cleveland, Ohio.
PREDICTED AND EXPERIMENTAL PERFORMANCE OF LARGE-BORE HIGH-SPEED BALL AND ROLLER BEARINGS
H. H. COE *In its* Advanced Power Transmission Technol. p 203-220 Jan. 1983 refs
Avail: NTIS HC A23/MF A01 CSCL 13I

The values of inner and outer race temperature, cage speed, and heat transferred to the lubricant or bearing power loss, calculated using the computer programs Shaberth and Cybean, with the corresponding experimental data for the large bore ball and roller bearings were compared. After the development of computer program, it is important that values calculated using such program are compared with actual bearing performance data to assess the programs predictive capability. Several comprehensive computer programs currently in use are capable of predicting rolling bearing operating and performance characteristics. These programs accept input data of bearing internal geometry, bearing material and lubricant properties, and bearing operating conditions. The programs solve several sets of equations that characterize rolling element bearings. The output produced typically consists of rolling element loads and Hertz stresses, operating contact angles, component speed, heat generation, local temperatures, bearing fatigue life, and power loss. Two of these programs, Shaberth and Cybean were developed. E.A.K.

N83-20132*# National Aeronautics and Space Administration. Lewis Research Center, Cleveland, Ohio.
LUBRICATION OF 35-MILLIMETER-BORE BALL BEARINGS OF SEVERAL DESIGNS TO 2.5 MILLION DN
F. T. SCHULLER *In its* Advanced Power Transmission Technol. p 221-238 Jan. 1983 refs
Avail: NTIS HC A23/MF A01 CSCL 13I

Parametric tests were conducted with 35mm bore, angular contact ball bearings with either a single or double outer and guided cage. The bearings were either lubricated by oil jets or employed inner ring lubrication. Outer ring cooling was added in selected tests. Lubricant flow to the bearing ranged from 300 to 1900 cc/min. All bearings were successfully run at speeds to 2.5 million DN. Increasing the lubricant flow decreased bearing ring temperatures but increased bearing power lines. The power loss and race temperatures of a jet lubricated with double outer land guided cage were always higher than those of the single land guided design at similar test conditions. The lowest bearing operating temperatures were achieved when inner ring lubrication and outer ring cooling were combined. It is found that cage slip of a double outer land guided cage is approximately twice that of a single outer land guided cage E.A.K.

N83-20133*# SKF Industries, Inc., Philadelphia, Pa.
HIGH SPEED SPHERICAL ROLLER-BEARING ANALYSIS AND COMPARISON WITH EXPERIMENTAL PERFORMANCE
R. J. KLECKNER and G. DYBA *In* NASA. Lewis Research Center Advanced Power Transmission Technol. p 239-252 Jan. 1983 refs
(Contract NAS3-20824)
Avail: NTIS HC A23/MF A01 CSCL 13I

The capabilities of a spherical roller bearing analysis/design tool, Spherbean (spherical bearing analysis) are described. Capabilities of the analysis are demonstrated and verified by comparison with experimental data. A practical design problem is presented where the computer program is used to improve a particular bearing's performance. E.A.K.

N83-20134*# National Aeronautics and Space Administration. Lewis Research Center, Cleveland, Ohio.
LARGE-BORE TAPERED-ROLLER BEARING PERFORMANCE AND ENDURANCE TO 2.4 MILLION DN
R. J. PARKER *In its* Advanced Power Transmission Technol. p 253-270 Jan. 1983 refs
Avail: NTIS HC A23/MF A01 CSCL 13I

The operating characteristics and experimental life estimates for 120.65 mm bore tapered roller bearings of two designs under combined radial and thrust loads were determined. A modified standard bearing design was tested at speeds up to 15,000 rpm. A computer optimized, high speed design was tested at speeds up to 20,000 rpm. Both designs were tested at a combined load of 26,700 N (6000 lb) radial load and and 53,400 N (12,000 lb) thrust load. Advanced helicopter transmissions which require the higher-speed capability of tapered-roller bearings also require higher temperature capability (ref. 2). Thus, materials with temperature capabilities higher than the conventional carburizing steels are required. EAK

N83-20135*# National Aeronautics and Space Administration. Lewis Research Center, Cleveland, Ohio.
EVALUATION OF A HIGH PERFORMANCE, FIXED-RATIO, TRACTION DRIVE
S. H. LOEWENTHAL, N. E. ANDERSON (Army Research and Technology Labs.), and D. A. ROHN *In its* Advanced Power Transmission Technol. p 271-284 Jan. 1983 refs Submitted for publication
Avail: NTIS HC A23/MF A01 CSCL 13I

A test program was initiated to evaluate the key operational and performance factors associated with the Nasvytis multiroller concept. Two sets of Nasvytis drives, each of slightly geometry, were parametrically tested on a back to back test stand. Initial results from these tests are reported. One of these units was later retrofitted to the power turbine of an automotive gas turbine engine and dynamometer tested. E.A.K.

N83-20136*# Transmission Research, Inc., Cleveland, Ohio.
TRACTION CALCULATIONS AND DESIGN DATA FOR TWO TRACTION FLUIDS
J. L. TEVAARWERK (Applied Tribology, Ltd.) *In* NASA. Lewis Research Center Advanced Power Transmission Technol. p 285-298 Jan. 1983 refs
(Contract DEN3-35)
Avail: NTIS HC A23/MF A01 CSCL 13I

The rheological properties of the fluid under these certain conditions which precludes the use of most of the conventional instruments for steady state measurement were studied. The only suitable type of instrument is a disk machine where most of the conditions are the same of similar to those in traction drives. From the resulting traction tests, certain models are inferred. To the designer of traction drives, the traction behavior of the fluid under the severe conditions is of utmost importance because of the direct influence that it has on the efficiency, size, and life of a given drive. E.A.K.

N83-20137*# National Aeronautics and Space Administration, Lewis Research Center, Cleveland, Ohio.
SIZING CRITERIAL FOR TRACTION DRIVES
D. A. ROHN, S. H. LOEWENTHAL, and J. J. COY (Army Research and Technology Labs.) *In its* Advanced Power Transmission Technol. p 299-316 Jan. 1983 refs
Avail: NTIS HC A23/MF A01 CSCL 13I

A simplified traction drive fatigue analysis which was derived from the Lundberg-Palmgren theory is measured and the effects of rotational speed, multiplicity of contacts, and variation in the available traction coefficient on traction drive system life, size, and power capacity was investigated. Simplified equations are provided for determining the 90% survival life rating of steel traction drive contacts of arbitrary geometry. References to life modifying factors for material, lubrication, and traction will be made. E.A.K.

N83-20138*# Cincinnati Univ., Ohio.
A BASIS FOR THE ANALYSIS OF SURFACE GEOMETRY OF SPIRAL BEVEL GEARS
R. L. HUSTON and J. J. COY (Army Research and Technology Labs.) *In* NASA. Lewis Research Center Advanced Power Transmisssion Technol. p 317-334 Jan. 1983 refs
(Contract NSG-3188)
Avail: NTIS HC A23/MF A01 CSCL 13I

Geomtrical procedures helpful in the fundamental studies of the surface geometry of spiral bevel gears are summarized. These procedures are based upon: (1) fundamental gear geometry and kinematics as exposited by Buckingham, et al; (2) formulas developed from differential geometry; and (3) geometrical concepts developed in recent papers and reports on spiral bevel gear surface geometry. Procedures which characterize the geometry so that the surface parametric equations, the principal radii of curvature, and the meshing kinematics are systematically determined are emphasized. Initially, the focus in on theoretical, logarithmic spiral bevel gears as defined by Buckingham. The gears, however, are difficult to fabricate and are sometimes considered to be too straight. Circular-cut spiral bevel gears are an alternative to this. Surface characteristics of crown circular cut gears are analyzed. E.A.K.

N83-20139*# National Aeronautics and Space Administration. Lewis Research Center, Cleveland, Ohio.
SPIRAL-BEVEL GEOMETRY AND GEAR TRAIN PRECISION
F. L. LITVIN (Illinois Univ.) and J. J. COY *In its* Advanced Power Transmission Technol. p 335-344 Jan. 1983 refs
Avail: NTIS HC A23/MF A01 CSCL 13I

A new aproach to the solution of determination of surface principal curvatures and directions is proposed. Direct relationships between the principal curvatures and directions of the tool surface and those of the principal curvatures and directions of generated gear surface are obtained. The principal curvatures and directions of geartooth surface are obtained without using the complicated equations of these surfaces. A general theory of the train kinematical errors exerted by manufacturing and assembly errors is discussed. Two methods for the determination of the train kinematical errors can be worked out: (1) with aid of a computer, and (2) with a approximate method. Results from noise and vibration measurement conducted on a helicopter transmission are used to illustrate the principals contained in the theory of kinematic errors. E.A.K.

N83-20141*# National Aeronautics and Space Administration. Lewis Research Center, Cleveland, Ohio.
COMPARISON OF SPUR GEAR EFFICIENCY PREDICTION METHODS
N. E. ANDERSON (Army Research and Technology Labs.) and S. H. LOEWENTHAL *In its* Advanced Power Transmission Technol. p 365-382 Jan. 1983 refs
Avail: NTIS HC A23/MF A01 CSCL 13I

The predictions of five spur-gear efficiency calculation methods were compared with three sets of test data using different gear geometries. The data and the analysis methods were limited to jet lubricated, ground, spur gears. The data covered a range in pitch line velocity to 1 to 20 m/sec (200 to 4000 ft/min) and K-load factor range of 17 to 1600. S.L.

N83-20142*# Hamilton Standard Div., United Aircraft Corp., Windsor Locks, Conn.
COMPLIANCE AND STRESS SENSITIVITY OF SPUR GEAR TEETH
R. W. CORNELL *In* NASA. Lewis Research Center Advanced Power Transmission Technol. p 383-402 Jan. 1983 refs Submitted for publication
(Contract NAS3-22138)
Avail: NTIS HC A23/MF A01 CSCL 13I

The magnitude and variation of tooth pair compliance with load position affects the dynamics and loading significantly, and the tooth root stressing per load varies significantly with load position. Therefore, the recently developed time history, interactive, closed form solution for the dynamic tooth loads for both low and high contact ratio spur gears was expanded to include improved and simplified methods for calculating the compliance and stress sensitivity for three involute tooth forms as a function of load position. The compliance analysis has an improved fillet/foundation. The stress sensitivity analysis is a modified version of the Heywood method but with an improvement in the magnitude and location of the peak stress in the fillet. These improved compliance and stress sensitivity analyses are presented along with their evaluation using test, finite element, and analytic transformation results, which showed good agreement. S.L.

N83-20143*# Cleveland State Univ., Ohio. Coll of Engineering.
A METHOD FOR STATIC AND DYNAMIC LOAD ANALYSIS OF STANDARD AND MODIFIED SPUR GEARS
R. KASUBA *In* NASA. Lewis Research Center Advanced Power Transmission Technol. p 403-420 Jan. 1983 refs Sponsored in part by the Army Aviation Research and Technology Labs.
(Contract NAS3-18547)
Avail: NTIS HC A23/MF A01 CSCL 13I

The mesh stiffness and dynamic load characteristics for several cases of the Normal Contract Ratio and High Contact ratio gearing. The considered contact ratios were grouped in the general range of 1.7,2.0, and 2.3. The HCR gearing is defined by contact ratios equal to or greater than 2.0. The HCR gearing is represented by a group of small pressure angle, fine pitch, and long addendum gearing. S.L.

N83-20144*# National Aeronautics and Space Administration. Lewis Research Center, Cleveland, Ohio.
AN UPDATE ON THE LIFE ANALYSIS OF SPUR GEARS
J. J. COY (Army Research and Technology Labs.), D. P. TOWNSEND, and E. V. ZARETSKY *In its* Advanced Power Transmission Technol. p 421-434 Jan. 1983 refs
Avail: NTIS HC A23/MF A01 CSCL 13I

An analytical method for predicting surface fatigue life of gears was presented. General statistical methods were outlined, showing the application of the general methods to a simple gear mesh. Experimentally determined values for constants in the life equation were given. Comparison of the life theory with test results and AGMA standards was made. Gear geometry pertinent to life calculations was reviewed. S.L.

N83-20145*# National Aeronautics and Space Administration. Lewis Research Center, Cleveland, Ohio.
THE OPTIMAL DESIGN OF STANDARD GEARSETS
M. SAVAGE (Akron Univ.), J. J. COY (Army Research and Technology Labs.), and D. P. TOWNSEND *In its* Advanced Power Transmission Technol. p 435-460 Jan. 1983 refs
(Contract NAG3-55)
Avail: NTIS HC A23/MF A01 CSCL 13I

A design procedure for sizing standard involute spur gearsets is presented. The procedure is applied to find the optimal design for two examples - an external gear mesh with a ratio of 5:1 and an internal gear mesh with a ratio of 5:1. In the procedure, the gear mesh is designed to minimize the center distance for a given gear ratio, pressure angle, pinion torque, and allowable tooth

strengths. From the methodology presented, a design space may be formulated for either external gear contact or for internal contact. The design space includes kinematics considerations of involute interference, tip fouling, and contact ratio. Also included are design constraints based on bending fatigue in the pinion fillet and Hertzian contact pressure in the full load region and at the gear tip where scoring is possible. This design space is two dimensional, giving the gear mesh center distance as a function of diametral pitch and the number of pinion teeth. The constraint equations were identified for kinematic interference, fillet bending fatigue, pitting fatigue, and scoring pressure, which define the optimal design space for a given gear design. The locus of equal size optimum designs was identified as the straight line through the origin which has the least slope in the design region. S.L.

N83-20146*# National Aeronautics and Space Administration. Lewis Research Center, Cleveland, Ohio.
STUDY OF LUBRICANT JET FLOW PHENOMENA IN SPUR GEARS: OUT OF MESH CONDITION
D. P. TOWNSEND and L. S. AKIN (Western Gear Corp.) *In its* Advanced Power Transmission Technol. p 461-476 Jan. 1983 refs Submitted for publication
Avail: NTIS HC A23/MF A01 CSCL 13I

The penetration depth onto the tooth flank of a jet of oil at different velocities pointed at the pitch line on the outgoing side of mesh was determined. The analysis determines the impingement depth for both the gear and the pinion. It includes the cases for speed increasers and decreasers as well as for one to one gear ratio. In some cases the jet will strike the loaded side of the teeth, and in others it will strike the unloaded side of the teeth. In nearly all cases the top land will be cooled regardless of the penetration depth, and postimpingement oil spray will usually provide adequate amounts of oil for lubrication but is marginal or inadequate for cooling. S.L.

N83-20147*# National Aeronautics and Space Administration. Lewis Research Center, Cleveland, Ohio.
GEAR LUBRICATION AND COOLING EXPERIMENT AND ANALYSIS
D. P. TOWNSEND and L. S. AKIN (Western Gear Corp.) *In its* Advanced Power Transmission Technol. p 477-490 Jan. 1983 refs Submitted for publication
Avail: NTIS HC A23/MF A01 CSCL 13I

A gear tooth temperature analysis was performed using a finite element method combined with a calculated heat input, a calculated oil jet impingement depth, and estimated heat transfer coefficients for the different parts of the gear tooth that are oil cooled and air cooled. Experimental measurements of gear tooth average surface temperature and gear tooth instantaneous surface temperature were made with a fast response, infrared, radiometric microscope. Increasing oil pressure has a significant effect on both average surface temperature and peak surface temperature at loads above 1895 N/cm(1083 lb/in) and speeds of 10,000 and 7500 rpm. Both increasing speed (from 5000 to 10,000 rpm) at constant speed cause a significant rise in the average surface temperature and in the instantaneous peak surface temperatures on the gear teeth. The oil jet pressure required to provide the best cooling for gears is the pressure required to obtain full gear tooth impingement. Calculated results for gear tooth temperatures were close to experimental results for various oil jet impingement depths for identical operating conditions. S.L.

N83-20148*# Hamilton Standard Div., United Aircraft Corp., Windsor Locks, Conn.
DYNAMIC TOOTH LOADS AND STRESSING FOR HIGH CONTACT RATIO SPUR GEARS
R. W. CORNELL and W. W. WESTERVELT *In* NASA. Lewis Research Center Advanced Power Transmission Technol. p 491-502 Jan. 1983 refs Submitted for publication
(Contract NAS3-17859)
Avail: NTIS HC A23/MF A01 CSCL 13I

An analysis and computer program were developed for calculating the dynamic gear tooth loading and root stressing for high contact ratio gearing (HCRG) as well as LCRG. The analysis includes the effects of the variable tooth stiffness during the mesh, tooth profile modification, and gear errors. The calculation of the tooth root stressing caused by the dynamic gear tooth loads is based on a modified Heywood gear tooth stress analysis, which appears more universally applicable to both LCRG and HCRG. The computer program is presently being expanded to calculate the tooth contact stressing and PV values. Sample application of the gear program to equivalent LCRG (1.566 contact ratio) and HCRG (2.40 contact ratio) revealed the following: (1) the operating conditions and dynamic characteristics of the gear system an affect the gear tooth loading and root stressing, and therefore, life significantly; (2) the length of the profile modification affect the tooth loading and root stressing significantly, the amount depending on the applied load, speed, and contact ratio; and (3) the effect of variable tooth stiffness is small, shifting and increasing the response peaks slightly from those for constant tooth stiffness. S.L.

N83-20150*# National Aeronautics and Space Administration. Lewis Research Center, Cleveland, Ohio.
EVALUATION OF HIGH-CONTACT-RATIO SPUR GEARS WITH PROFILE MODIFICATION
D. P. TOWNSEND, B. B. BABER (Midwest Research Inst.), and A. NAGY (Midwest Research Inst.) *In its* Advanced Power Transmission Technol. p 519-531 Jan. 1983 refs
(Contract NAS3-20026)
Avail: NTIS HC A23/MF A01 CSCL 13I

Scoring tests, surface fatigue tests, and single-tooth bending fatigue tests were conducted with four sets of spur gears of standard design and three sets of spur gears of the new tooth form (NTF) design. Scoring tests were conducted in a gear test rig at a speed of 10,000 rpm using a synthetic polyester C5, C6, C7 substituted pentaerythritol oil. Surface fatigue tests were conducted in the same rig at a speed of 10,000 rpm and Hertz stresses of 173 x 10 to the 7th power and 143 x 10 to the 7th power Pa (250,000 and 214,000 psi). Single tooth bending fatigue tests were conducted on both the standard and NTF gears at an initial load that produced a 10.35 x 10 to the eight power Pa (150,000-psi) bending stress. The gears were load cycled to failure or for 3 x 10 to the 5th power cycles, whichever occurred first. The load was increased after test until failure occurred at 3 x 10 to the 6th power cycles or less. Both the standard and NTF gears scored at a gear bulk temperature of approximately 409 K (277 F). At this temperature the load on the NTF gears was 22 percent less than the load on the standard gears. The scoring failure was a function of gear bulk temperature, where for a given lubricant the temperature is a function of gear design, operating load, and speed. S.L.

N83-20159*# National Aeronautics and Space Administration. Lewis Research Center, Cleveland, Ohio.
LUBRICATION BACKGROUND
B. J. HAMROCK and D. DOWSON (Leeds Univ.) Sep. 1981 70 p refs Submitted for publication
(NASA-TM-81692; E-209; NAS 1.15:81692) Avail: NTIS HC A04/MF A01 CSCL 13I

Surface topography, including the various physical methods of measuring surfaces, and the various lubrication regimes (hydrodynamic, elastohydrodynamic, boundary, and mixed) are discussed. The historical development of elastohydrodynamic lubrication is outlined. The major accomplishments in four periods, the pre-1950's, the 1950's, the 1960's, and the 1970's are presented. Author

N83-23606*# National Aeronautics and Space Administration. Lewis Research Center, Cleveland, Ohio.
CAVITATION PITTING AND EROSION OF AL 6061-T6 IN MINERAL OIL AND WATER
B. C. S. RAO (Concordia Univ., Montreal) and D. H. BUCKLEY 1983 7 p refs Presented at the Cavitation and Polyphase Flow Forum, Houston, Tex., 20-22 Jun. 1983; sponsored by ASME
(NASA-TM-83345; E-1516; NAS 1.15:83345) Avail: NTIS HC A02/MF A01 CSCL 11F

The authors are currently carrying out a study of the cavitation erosion of different bearing metals and alloys in mineral oils were studied. The variations of weight loss, the pit diameter and depth due to cavitation erosion on Al 6061-T6 in mineral oil and water are presented. S.L.

N83-24855*# National Aeronautics and Space Administration. Lewis Research Center, Cleveland, Ohio.
OPTIMUM PARALLEL STEP-SECTOR BEARING LUBRICATED WITH AN INCOMPRESSIBLE FLUID
B. J. HAMROCK Apr. 1983 7 p refs
(NASA-TM-83356; E-1616; NAS 1.15:83356) Avail: NTIS HC A02/MF A01 CSCL 11H

The dimensionless parameters normally associated with a step sector thrust bearing are the film thickness ratio, the dimensionless step location, the number of sectors, the radius ratio, and the angular extent of the lubrication feed groove. The optimum number of sectors and the parallel step configuration for a step sector thrust bearing while considering load capacity or stiffness and assuming an incompressible fluid are presented. Author

N83-24856*# National Aeronautics and Space Administration. Lewis Research Center, Cleveland, Ohio.
CAVITATION EROSION OF COPPER, BRASS, ALUMINUM AND TITANIUM ALLOYS IN MINERAL OIL
B. C. S. RAO (National Academy Science - National Research Council, Washington, D.C.) and D. H. BUCKLEY 1983 12 p refs Proposed for presentation at 6th Intern. Conf. on Erosion by Liquid and Solid Impact, 4-8 Sep. 1983; sponsored by Cavendish Lab., Cambridge, England
(NASA-TM-83402; E-1614; NAS 1.15:83402) Avail: NTIS HC A02/MF A01 CSCL 11F

The variations of the mean depth of penetration, the mean depth rate of penetration, MDRP, the pit diameter 2a and depth h due to cavitation attack on Al 6061-T6, Cu, brass of composition Cu-35Zn-3Pb and Ti-5A1-2.5Sn are presented. The experiments are conducted in a mineral oil of viscosity 110 CS using a magnetostrictive oscillator of 20 kHz frequency. Based on MDRP on the materials, it is found that Ti-5Al-2.5Sn exhibits cavitation erosion resistance which is two orders of magnitude higher than the other three materials. The values of h/a are the largest for copper and decreased with brass, titanium, and aluminum. Scanning electron microscope studies show that extensive slip and cross slip occurred on the surface prior to pitting and erosion. Twinning is also observed on copper and brass. Author

N83-24857*# Michigan Univ., Ann Arbor.
CLASSIFICATION OF JOURNAL SURFACES USING SURFACE TOPOGRAPHY PARAMETERS AND SOFTWARE METHODS TO COMPENSATE FOR STYLUS GEOMETRY Interim Report
C. J. LI, W. R. DEVRIES, and K. C. LUDEMA Apr. 1983 54 p refs
(Contract NCC3-11; DE-AI01-80CS-50194)
(NASA-CR-168153; DOE/NASA/0011-1; NAS 1.26:168153)
Avail: NTIS HC A04/MF A01 CSCL 09B

Measurements made with a stylus surface tracer which provides a digitized representation of a surface profile are discussed. Parameters are defined to characterize the height (e.g., RMS roughness, skewness, and kurtosis) and length (e.g., autocorrelation) of the surface topography. These are applied to the characterization of crank shaft journals which were manufactured by different grinding and lopping procedures known to give significant differences in crank shaft bearing life. It was found that three parameters (RMS roughness, skewness, and kurtosis) are necessary to adequately distinguish the character of these surfaces. Every surface specimen has a set of values for these three parameters. They can be regarded as a set coordinate in a space constituted by three characteristics axes. The various journal surfaces can be classified along with the determination of a proper wavelength cutoff (0.25 mm) by using a method of separated subspace. The finite radius of the stylus used for profile tracing gives an inherent measurement error as it passes over the fine structure of the surface. A mathematical model is derived to compensate for this error. S.L.

N83-24858*# National Aeronautics and Space Administration. Lewis Research Center, Cleveland, Ohio.
NASA TRANSMISSION RESEARCH AND ITS PROBABLE EFFECTS ON HELICOPTER TRANSMISSION DESIGN
E. V. ZARETSKY, J. J. COY (Army Research and Technology Labs., Cleveland, Ohio), and D. P. TOWNSEND 1983 20 p refs Presented at the 39th Ann. Forum of the Am. Helicopter Soc., St. Louis, 9-11 May 1983
(NASA-TM-83389; E-1601; NAS 1.15:83389; AVRADCOM-TR-83-C-3) Avail: NTIS HC A02/MF A01 CSCL 01C

Transmissions studied for application to helicopters in addition to the more conventional geared transmissions include hybrid (traction/gear), bearingless planetary, and split torque transmissions. Research is being performed to establish the validity of analysis and computer codes developed to predict the performance, efficiency, life, and reliability of these transmissions. Results of this research should provide the transmission designer with analytical tools to design for minimum weight and noise with maximum life and efficiency. In addition, the advantages and limitations of drive systems as well as the more conventional systems will be defined. S.L.

N83-24862*# National Aeronautics and Space Administration. Lewis Research Center, Cleveland, Ohio.
REGRESSION ANALYSIS OF TRACTION CHARACTERISTICS OF TRACTION FLUIDS
S. H. LOEWENTHAL and D. A. ROHN May 1983 17 p refs
(NASA-TP-2154; E-1300; NAS 1.60:2154) Avail: NTIS HC A02/MF A01 CSCL 11H

Traction data for Santotrac 50 and TDF-88 over a wide range of operating conditions were analyzed. An eight term correlation equation to predict the maximum traction coefficient and a six term correlation equation to predict the initial slope of the traction curve were developed. The slope correlation was corrected for size effect considering the compliance of the disks. The effects of different operating conditions on the traction performance of each traction fluid were studied. Both fluids exhibited a loss in traction with increases in spin, but the losses with the TDF-88 fluid were not as severe as those with Santotrac 50. Overall, both fluids exhibited similar performance, showing an increase in traction with contact pressure up to about 2.0 GPa, and a reduction in traction with higher surface speeds up to about 100 m/sec. The apparent stiffness of the traction contact, that is, film disk combination, increases with contact pressure and decreases with speed. A.R.H.

N83-26079*# National Aeronautics and Space Administration. Lewis Research Center, Cleveland, Ohio.
PIVOTING AND SLIP IN AN ANGULAR CONTACT BEARING
E. KINGSBURY 1983 14 p refs Presented at the Joint Lubrication Conf., Hartford, 18-20 Oct. 1983; sponsored by the ASME and American Society of Lubrication Engineers
(NASA-TM-83408; E-1570; NAS 1.15:83408) Avail: NTIS HC A02/MF A01 CSCL 13I

Pivoting slips are calculated for the ball-race and ball-ball contacts in a retainerless bearing. The calculation is kinematic, ignoring all inertial loadings. Pure spin and uniform precession of the balls are considered. Pivoting slip magnitudes are compared with several other kinds of slip which were previously reported in an R4 size bearing. Author

N83-27213*# Rocketdyne, Canoga Park, Calif.
HYBRID HYDROSTATIC/BALL BEARINGS IN HIGH-SPEED TURBOMACHINERY Final Report, 29 Aug. 1980 - 15 Dec. 1982
C. E. NIELSON Jan. 1983 381 p refs
(Contract NAS3-22480)
(NASA-CR-168124; NAS 126:168124; RI/RD83-104; NAS 1.26:168124) Avail: NTIS HC A17/MF A01 CSCL 13I

A high speed, high pressure liquid hydrogen turbopump was designed, fabricated, and tested under a previous contract. This design was then modified to incorporate hybrid hydrostatic/ball bearings on both the pump end and turbine end to replace the original conventional ball bearing packages. The design, analysis, turbopump modification, assembly, and testing of the turbopump with hybrid bearings is presented here. Initial design considerations and rotordynamic performance analysis was made to define expected turbopump operating characteristics and are reported. The results of testing the turbopump to speeds of 9215 rad/s (88,000 rpm) using a wide range of hydrostatic bearing supply pressures are presented. The hydrostatic bearing test data and the rotordynamic behavior of the turbopump was closely analyzed and are included in the report. The testing of hybrid hydrostatic/ball bearings on a turbopump to the high speed requirements has indicated the configuration concept is feasible. The program has presented a great deal of information on the technology requirements of integrating the hybrid bearing into high speed turbopump designs for improved bearing life. Author

N83-27214*# National Aeronautics and Space Administration. Lewis Research Center, Cleveland, Ohio.
ROLLING-ELEMENT BEARINGS
B. J. HAMROCK and W. J. ANDERSON (Bearings and Lubrication, North Olmsted, Ohio) Jun. 1983 61 p refs Submitted for publication
(NASA-RP-1105; E-1440; NAS 1.61:1105) Avail: NTIS HC A04/MF A01 CSCL 13I

Rolling element bearings are a precision, yet simple, machine element of great utility. A brief history of rolling element bearings is reviewed and the type of rolling element bearings, their geometry and kinematics, as well as the materials they are made from and the manufacturing processes they involve are described. Unloaded and unlubricated rolling element bearings, loaded but unlubricated rolling element bearings and loaded and lubricated rolling element bearings are considered. The recognition and understanding of elastohydrodynamic lubrication covered, represents one of the major development in rolling element bearings. S.L.

N83-28448*# General Motors Corp., Indianapolis, Ind.
SMALL GAS TURBINE COMBUSTOR PRIMARY ZONE STUDY Final Report, Sep. 1980 - Dec. 1982
R. E. SULLIVAN, E. R. YOUNG, G. A. MILES, and J. R. WILLIAMS Mar. 1983 208 p refs
(Contract NAS3-22762; DA PROJ. 1L1-62209-AH-76)
(NASA-CR-168122; NAS 1.26:168122; DDA-EDR-11170) Avail: NTIS HC A10/MF A01 CSCL 21E

A development process is described which consists of design, fabrication, and preliminary test evaluations of three approaches to internal aerodynamic primary zone flow patterns: (1) conventional double vortex swirl stabilization; (2) reverse flow swirl stabilization; and (3) large single vortex flow system. Each concept incorporates special design features aimed at extending the performance capability of the small engine combustor. Since inherent geometry of these combustors result in small combustion zone height and high surface area to volume ratio, design features focus on internal aerodynamics, fuel placement, and advanced cooling. The combustors are evaluated on a full scale annular combustor rig. A correlation of the primary zone performance with the overall performance is accomplished using three intrusion type gas sampling probes located at the exit of the primary zone section. Empirical and numerical methods are used for designing and predicting the performance of the three combustor concepts and their subsequent modifications. The calibration of analytical procedures with actual test results permits an updating of the analytical design techniques applicable to small reverse flow annular combustors. A.R.H.

N83-28449*# National Aeronautics and Space Administration. Lewis Research Center, Cleveland, Ohio.
FILM THICKNESS FOR DIFFERENT REGIMES OF FLUID-FILM LUBRICATION
B. J. HAMROCK and D. DOWSON (Leeds Univ.) May 1983 55 p refs
(NASA-TM-81700; E-209; NAS 1.15:81700) Avail: NTIS HC A04/MF A01 CSCL 11H

Mathematical formulas are presented which express the dimensionless minimum film thickness for the four lubrication regimes found in elliptical contacts: isoviscous-rigid regime; piezoviscous-rigid regime; isoviscous-elastic regime; and piezoviscous-elastic regime. The relative importance of pressure on elastic distortion and lubricant viscosity is the factor that distinguishes these regimes for a given conjunction geometry. In addition, these equations were used to develop maps of the lubrication regimes by plotting film thickness contours on a log-log grid of the dimensionless viscosity and elasticity parameters for three values of the ellipticity parameter. These results present a complete theoretical film thickness parameter solution for elliptical contancts in the four lubrication regimes. The results are particularly useful in initial investigations of many practical lubrication problems involving elliptical conjunctions. A.R.H.

N83-28450*# National Aeronautics and Space Administration. Lewis Research Center, Cleveland, Ohio.
FULLY PLASMA-SPRAYED COMPLIANT BACKED CERAMIC TURBINE SEAL Patent Application
R. C. BILL and D. W. WISANDER, inventors (to NASA) 1 Jun. 1983 8 p
(NASA-CASE-LEW-13268-3; US-PATENT-APPL-SN-500045)
Avail: NTIS HC A02/MF A01 CSCL 11A

This invention is concerned with a seal having a high temperature abradable lining material encircling the tips of turbine blades in turbomachinery. The invention is particularly directed to maintaining the minimum operating clearance between the blade tips and the lining of a high pressure turbine. A low temperature easily decomposable material, such as a polymer, in powder form is blended with a high temperature oxidation resistant metal powder. The two materials are simultaneously deposited on a substrate formed by the turbine casing. Alternately, the polymer powder may be added to the metal powder during plasma spraying. A bond coating is then applied to the metal-polymer composite. A ceramic layer forming a shroud is deposited on the bond coating. The polymer additive mixed with the metal is then completely volatilized to provide a porous layer between the ceramic layer and the substrate. NASA

N83-28452*# Cleveland State Univ., Ohio.
DYNAMIC EFFECTS OF INTERNAL SPUR GEAR DRIVES Ph.D. Thesis - Jun. 1982 Final Report
A. PINTZ, R. KASUBA, J. L. FRATER, and R. AUGUST Washington NASA Jun. 1983 286 p refs
(Contract NAG3-186)
(NASA-CR-3692; NAS 1.26:3692) Avail: NTIS HC A13/MF A01 CSCL 13I

Static analysis, dynamic analysis, and computer programs are discussed. Spur gear formulae and involute profile development and deflection are also discussed. Author

N83-28453*# National Aeronautics and Space Administration. Lewis Research Center, Cleveland, Ohio.
ELASTOHYDRODYNAMIC CONTACTS. EFFECTS OF DENTS AND GROOVES ON TRACTION AND LOCAL FILM THICKNESS
L. D. WEDEVEN and C. CUSANO (Illinois Univ., Urbana) Jun. 1983 19 p refs
(NASA-TP-2175; E-1333; NAS 1.60:2175) Avail: NTIS HC A02/MF A01 CSCL 11H

Traction and film thickness were simultaneously measured under sliding elastohydrodynamic (EHD) conditions. The influence of surface topography was investigated by using simulated surfaces produced by depressing dents and grooves in highly polished steel balls. Significant changes in traction occurred depending on the orientation of the surface defects and their location with respect to the contact region. The results can be explained in terms of changes in overall film thickness and redistribution of pressure within the contact region due to micro-EHD effects. It can be concluded that the traction capability of mechanical components operating in thin film lubrication can be enhanced particularly by surface topographical orientation perpendicular to the surface motion. Associated with the higher traction are increases in local shear stress and normal stress as well as an increase in temperature at asperity sites. It is postulated that the local surface topography can become involved in run in or failure initiation even without actual asperity contact. Author

N83-28454*# National Aeronautics and Space Administration. Lewis Research Center, Cleveland, Ohio.
NON-NEWTONIAN FLUID MODEL INCORPORATED INTO ELASTOHYDRODYNAMIC LUBRICATION OF RECTANGULAR CONTACTS
B. O. JACOBSON (Lulea Univ., Sweden) and B. J. HAMROCK 1983 36 p refs Proposed for presentation at the Joint Lubrication Conf., Hartford, Conn., 18-20 Oct. 1983; sponsored by the AMSE and the American Society of Lubrication Engineers
(NASA-TM-83318; E-1396; NAS 1.15:83318) Avail: NTIS HC A03/MF A01 CSCL 11H

A procedure is outlined for the numerical solution of the complete elastohydrodynamic lubrication of rectangular contacts incorporating a non-Newtonian fluid model. The approach uses a Newtonian model as long as the shear stress is less than a limiting shear stress. If the shear stress exceeds the limiting value, the shear stress is set equal to the limiting value. The numerical solution requires the coupled solution of the pressure, film shape, and fluid rheology equations from the inlet to the outlet. Isothermal and no-side-leakage assumptions were imposed in the analysis. The influence of dimensionless speed, load, materials, and sliding velocity and limiting-shear-strength proportionality constant on dimensionless minimum film thickness was investigated. Fourteen cases were used in obtaining the minimum-film-thickness equation for an elastohydrodynamically lubricated rectangular contact incorporating a non-Newtonian fluid model. Computer plots are also presented that indicate in detail pressure distribution, film shape, shear stress at the surfaces, and flow throughout the conjunction. Author

N83-28455*# National Aeronautics and Space Administration. Lewis Research Center, Cleveland, Ohio.
ADVANCES IN TRACTION DRIVE TECHNOLOGY
S. H. LOEWENTHAL, N. E. ANDERSON, and D. A. ROHN 1983 21 p refs Proposed for presentation at the Intern. Off-Highway Meeting and Exposition, Milwaukee, 12-15 Sep. 1983; sponsored by SAE Prepared in cooperation with Army Aviation Research and Development Command, Cleveland
(NASA-TM-83397; E-1674; NAS 1.15:83397; AVRADCOM-TR-83-C-5) Avail: NTIS HC A02/MF A01 CSCL 13I

Traction drives are traced from early uses as main transmissions in automobiles at the turn of the century to modern, high-powered traction drives capable of transmitting hundreds of horsepower. Recent advances in technology are described which enable today's traction drive to be a serious candidate for off-highway vehicles and helicopter applications. Improvements in materials, traction fluids, design techniques, power loss and life prediction methods will be highlighted. Performance characteristics of the Nasvytis fixed-ratio drive are given. Promising future drive applications, such as helicopter main transmissions and servo-control positioning mechanisms are also addressed. Author

N83-29709*# National Aeronautics and Space Administration. Lewis Research Center, Cleveland, Ohio.
VIBRATION IN PLANETARY GEAR SYSTEMS WITH UNEQUAL PLANET STIFFNESSES
J. L. FRATER, R. AUGUST, and F. B. OSWALD 1982 16 p refs Proposed for presentation at the 8th Appl. Mech. Conf., St. Louis, 19-21 Sep. 1983; sponsored by Oklahoma State Univ. Prepared in cooperation with Cleveland State Univ., Ohio
(NASA-TM-83428; E-1716; NAS 1.15:83428) Avail: NTIS HC A02/MF A01 CSCL 13I

An algorithm suitable for a minicomputer was developed for finding the natural frequencies and mode shapes of a planetary gear system which has unequal stiffnesses between the Sun/planet and planet/ring gear meshes. Mode shapes are represented in the form of graphical computer output that illustrates the lateral and rotational motion of the three coaxial gears and the planet gears. This procedure permits the analysis of gear trains utilizing nonuniform mesh conditions and user specified masses, stiffnesses, and boundary conditions. Numerical integration of the equations of motion for planetary gear systems indicates that this algorithm offers an efficient means of predicting operating speeds which may result in high dynamic tooth loads. Author

N83-29710*# National Aeronautics and Space Administration. Lewis Research Center, Cleveland, Ohio.
THEORETICAL RESULTS FOR STARVED ELLIPTICAL CONTACTS
B. J. HAMROCK and D. DOWSON (Leeds Univ., England) May 1983 63 p refs Submitted for publication
(NASA-TM-81697; E-209; NAS 1.15:81697) Avail: NTIS HC A04/MF A01 CSCL 11H

Eighteen cases were used in the theoretical study of the influence of lubricant starvation on film thickness and pressure in elliptical elastohydrodynamic conjunctions. From the results a simple and important critical dimensionless inlet boundary distance at which lubricant starvation becomes significant was specified. This inlet boundary distance defines whether a fully flooded or a starved condition exists in the contact. Furthermore, it was found that the film thickness for a starved condition is written in dimensionless terms as a function of the inlet distance parameter and the film thickness for a fully flooded condition. Contour plots of pressure and film thickness in and around the contact are shown for fully flooded and starved conditions. Author

N83-29711*# National Aeronautics and Space Administration. Lewis Research Center, Cleveland, Ohio.
EXPERIMENTAL INVESTIGATIONS OF ELASTOHYDRODYNAMIC LUBRICATION
B. J. HAMROCK and D. DOWSON (Leeds Univ., England) May 1983 102 p refs Repr. from Ball Bearing Lubrication, Sep. 1981
(NASA-TM-81698; E-209; NAS 1.15:81698) Avail: NTIS HC A06/MF A01 CSCL 11H

Various experimental studies of elastohydrodynamic lubrication have been reviewed. The various types of machines used in these investigations, such as the disc, two and four ball, crossed-cylinders, and crossed-axes rolling disc machine, are described. The measurement of the most important parameters, such as film shape, film thickness, pressure, temperature, and traction, is considered. Determination of the film thickness is generally the most important of these effects since it dictates the extent to which the asperities on opposing surfaces can come into contact and thus has a direct bearing on wear and fatigue failure of the contacting surfaces. Several different techniques for measuring film thickness have been described, including electrical resistance, capacitance, X-ray, optical interferometry, laser beam

diffraction, strain gage, and spring dynamometer methods. An attempt has been made to describe the basic concepts and limitations of each of these techniques. These various methods have been used by individual researchers, but there is no universally acceptable technique for measuring elastohydrodynamic film thickness. Capacitance methods have provided most of the reliable data for nominal line or rectangular conjunctions, but optical interferometry has proved to be the most effective procedure for elliptical contacts. Optical interferometry has the great advantage that it reveals not only the film thickness, but also details of the film shape over the complete area of the conjunction. Author

N83-29712*# National Aeronautics and Space Administration. Lewis Research Center, Cleveland, Ohio.
ELASTOHYDRODYNAMICS OF ELLIPTICAL CONTACTS FOR MATERIALS OF LOW ELASTIC MODULUS
B. J. HAMROCK and D. DOWSON (Leeds Univ.) May 1983 65 p refs Repr. from Ball Bearing Lubrication, chapter 11, Sep. 1981
(NASA-TM-81699; E-209; NAS 1.15:81699) Avail: NTIS HC A04/MF A01 CSCL 11H

The influence of the ellipticity parameter k and the dimensionless speed U, load W, and materials G parameters on minimum film thickness for materials of low elastic modulus was investigated. The ellipticity parameter was varied from 1 (a ball-on-plane configuration) to 12 (a configuration approaching a line contact); U and W were each varied by one order of magnitude. Seventeen cases were used to generate the minimum- and central-film-thickness relations. The influence of lubricant starvation on minimum film thickness in starved elliptical, elastohydrodynamic configurations was also investigated for materials of low elastic modulus. Lubricant starvation was studied simply by moving the inlet boundary closer to the center of the conjunction in the numerical solutions. Contour plots of pressure and film thickness in and around the contact were presented for both fully flooded and starved lubrication conditions. It is evident from these figures that the inlet pressure contours become less circular and closer to the edge of the Hertzian contact zone and that the film thickness decreases substantially as the serverity of starvation increases. The results presented reveal the essential features of both fully flooded and starved, elliptical, elastohydrodynamic conjunctions for materials of low elastic modulus. Author

N83-29713*# National Aeronautics and Space Administration. Lewis Research Center, Cleveland, Ohio.
APPLICATIONS OF FILM THICKNESS EQUATIONS
B. J. HAMROCK and D. DOWSON (Leeds Univ.) May 1983 108 p refs Repr. from Ball Bearing Lubrication, chapter 13, Sep. 1981
(NASA-TM-81701; E-209; NAS 1.15:81701) Avail: NTIS HC A06/MF A01 CSCL 11H

A number of applications of elastohydrodynamic film thickness expressions were considered. The motion of a steel ball over steel surfaces presenting varying degrees of conformity was examined. The equation for minimum film thickness in elliptical conjunctions under elastohydrodynamic conditions was applied to roller and ball bearings. An involute gear was also introduced, it was again found that the elliptical conjunction expression yielded a conservative estimate of the minimum film thickness. Continuously variable-speed drives like the Perbury gear, which present truly elliptical elastohydrodynamic conjunctions, are favored increasingly in mobile and static machinery. A representative elastohydrodynamic condition for this class of machinery is considered for power transmission equipment. The possibility of elastohydrodynamic films of water or oil forming between locomotive wheels and rails is examined. The important subject of traction on the railways is attracting considerable attention in various countries at the present time. The final example of a synovial joint introduced the equation developed for isoviscous-elastic regimes of lubrication. Author

N83-32070*# Rockwell International Corp., Canoga Park, Calif. Rocketdyne Div.
HIGH SPEED CRYOGENIC SELF-ACTING, SHAFT SEALS FOR LIQUID ROCKET TURBOPUMPS Final Report, Jun. 1972 - Sep. 1983
R. E. BURCHAM Jun. 1983 287 p refs
(Contract NAS3-20807)
(NASA-CR-168194; NAS 1.26:168194; RI/RD83-163) Avail: NTIS HC A13/MF A01 CSCL 11A

Three self acting lift pad liquid oxygen face seals and two self acting gaseous helium circumferential seals for high speed liquid oxygen turbopump were evaluated. The development of a technology for reliable, 10 hour life, multiple start seals for use in high speed liquid oxygen turbopumps is discussed. E.A.K.

N83-33166*# National Aeronautics and Space Administration. Lewis Research Center, Cleveland, Ohio.
EFFECT OF CARBIDE DISTRIBUTION ON ROLLING-ELEMENT FATIGUE LIFE OF AMS 5749
R. J. PARKER and E. N. BAMBERGER (GE, Cincinnati) Aug. 1983 14 p refs
(NASA-TP-2189; E-1243; NAS 1.60:2189) Avail: NTIS HC A02/MF A01 CSCL 13I

Endurance tests with ball bearings made of corrosion resistant bearing steel which resulted in fatigue lives much lower than were predicted are discussed. Metallurgical analysis revealed an undesirable carbide distribution in the races. It was shown in accelerated fatigue tests in the RC rig that large, banded carbides can reduce rolling element fatigue life by a factor of approximately four. The early spalling failures on the bearing raceways are attributed to the large carbide size and banded distribution. E.A.K.

N83-33167*# Cincinnati Univ., Ohio. Dept. of Mechanical and Industrial Engineering.
GEOMETRICAL ANALYSIS OF CIRCULAR-CUT SPIRAL BEVEL GEARS Final Report
R. L. HUSTON Aug. 1983 59 p refs
(Contract NSG-3188)
(NASA-CR-168226; NAS 1.26:168226) Avail: NTIS HC A04/MF A01 CSCL 13I

Geometrical studies of circular cut spiral bevel gears are reported. Tooth profile changes heel to toe are studied in the transverse plane. Pressure angle changes are determined. The radiuses of curvature of the tooth surfaces generated by various cutter profiles are also determined. The consequences of cutter profile changes are explored. Crown gears are emphasized and the implications for conical gears are discussed. E.A.K.

N83-33168*# Santa Clara Univ., Calif.
AN ANALYTICAL INVESTIGATION OF NO SUB X CONTROL TECHNIQUES FOR METHANOL FUELED SPARK IGNITION ENGINES
L. H. BROWNING and L. A. ARGENBRIGHT 1983 8 p refs
(Contract NAG3-143)
(NASA-CR-172847; NAS 1.26:172847) Avail: NTIS HC A02/MF A01 CSCL 13I

A thermokinetic SI engine simulation was used to study the effects of simple nitrogen oxide control techniques on performance and emissions of a methanol fueled engine. As part of this simulation, a ring crevice storage model was formulated to predict UBF emissions. The study included spark retard, two methods of compression ratio increase and EGR. The study concludes that use of EGR in high turbulence, high compression engines will both maximize power and thermal efficiency while minimizing harmful exhaust pollutants. Author

N83-34325*# National Aeronautics and Space Administration. Lewis Research Center, Cleveland, Ohio.
COMPARATIVE EVALUATION OF THREE SHAFT SEALS PROPOSED FOR HIGH PERFORMANCE TURBOMACHINERY
R. C. HENDRICKS 1982 13 p refs Presented at the Joint Lubrication Conf., Washington, D.C., 4-6 Oct. 1982; sponsored by ASME and American Society of Lubrication Engineers
(NASA-TM-83021; E-1457; NAS 1.15:83021) Avail: NTIS HC A02/MF A01 CSCL 11A

Experimental pressure profiles and leak rate characteristics for three shaft seal prototype model configurations proposed for the space shuttle turbopump were assessed in the concentric and fully eccentric, to point of rub, positions without the effects of rotation. The parallel-cylindrical configuration has moderate to good stiffness with a higher leak rate. It represents a simple concept, but for practical reasons and possible increases in stability, all such seals should be conical-convergent. The three-stepdown-sequential, parallel-cylindrical seal is converging and represents good to possible high stiffness when fluid separation occurs, with a significant decrease in leak rate. Such seals can be very effective. The three-stepdown-sequential labyrinth seal of 33-teeth (i.e., 12-11-10 teeth from inlet to exit) provides excellent leak control but usually has very poor stiffness, depending on cavity design. The seal is complex and not recommended for dynamic control. M.G.

N83-34326*# National Aeronautics and Space Administration. Lewis Research Center, Cleveland, Ohio.
THERMAL ELASTOHYDRODYNAMIC LUBRICATION OF LINE CONTACTS
M. K. GHOSH (Banaras Hindu Univ.) and B. J. HAMROCK Jun. 1983 30 p refs
(NASA-TM-83424; E-1617; NAS 1.15:83424) Avail: NTIS HC A03/MF A01 CSCL 11H

A numerical solution to the problem of thermal elastohydrodynamic lubrication of line contacts was obtained by using a finite difference formulation. The solution procedure consists of simultaneous solution of the thermal Reynolds equation, the elasticity equation, and the energy equation subject to appropriate boundary conditions. Pressure distribution, film shape, and temperature distribution were obtained for fully flooded conjunctions, a paraffinic lubricant, and various dimensionless speed parameters while the dimensionless load and materials parameters were held constant. Reduction in the minimum film thickness due to thermal effects (as a ratio of thermal to isothermal minimum film thickness) is given by a simple formula as a function of the thermal loading parameter Q: $H(min)/H(min,I) = 10/10+Q(0.4)$. Plots of pressure distribution, film shape, temperature distribution, and flow are shown for some representative cases. M.G.

N83-34327*# National Aeronautics and Space Administration. Lewis Research Center, Cleveland, Ohio.
APPLICATION OF MODERN SURFACE ANALYTICAL TOOLS IN THE INVESTIGATION OF SURFACE DETERIORATION PROCESSES
D. H. BUCKLEY 1983 24 p refs Proposed for presentation at SURTEC - KONGRESS 83, Berlin, West Germany, 24-27 Oct. 1983
(NASA-TM-83452; E-1766; NAS 1.15:83452) Avail: NTIS HC A02/MF A01 CSCL 20K

Surface profilometry and scanning electron microscopy were utilized to study changes in the surface of polymers when eroded. The X-ray photoelectron spectroscopy (XPS) and depth profile analysis indicate the corrosion of metal and ceramic surfaces and reveal the diffusion of certain species into the surface to produce a change in mechanical properties. Ion implantation, nitriding and plating and their effects on the surface are characterized. Auger spectroscopy analysis identified morphological properties of coatings applied to surfaces by sputter deposition. M.G.

N83-35400*# National Aeronautics and Space Administration. Lewis Research Center, Cleveland, Ohio.
CAVITATION PITTING AND EROSION OF ALUMINUM 6061-T6 IN MINERAL OIL WATER
B. C. S. RAO (Indian Inst. of Science) and D. H. BUCKLEY Aug. 1983 9 p refs Presented at ASME Cavitation and Polyphase Flow Forum, Houston, Tex., 20-22 Jun. 1983
(NASA-TP-2146; E-1516; NAS 1.60:2146) Avail: NTIS HC A02/MF A01 CSCL 11F

Cavitation erosion studies of aluminum 6061-T6 in mineral oil and in ordinary tap water are presented. The maximum erosion rate (MDPR, or mean depth of penetration rate) in mineral oil was about four times that in water. The MDPR in mineral oil decreased continuously with time, but the MDPR in water remained approximately constant. The cavitation pits in mineral oil were of smaller diameter and depth than the pits in water. Treating the pits as spherical segments, we computed the radius r of the sphere. The logarithm of h/a, where h is the pit depth and 2a is the top width of the pit, was linear when plotted against the logarithm of $2r/h - 1$. Author

38

QUALITY ASSURANCE AND RELIABILITY

Includes product sampling procedures and techniques; and quality control.

A83-22265* Carborundum Co., Niagara Falls, N. Y.
COMPARISON OF NDE TECHNIQUES FOR SINTERED-SIC COMPONENTS
M. SRINIVASAN, D. LAWLER (Carborundum Co., Niagara Falls, NY), L. J. INGLEHART, R. L. THOMAS (Wayne State University, Detroit, MI), and D. YUHAS (Sonoscan, Inc., Bensenville, IL) Ceramic Engineering and Science Proceedings, vol. 3, Sept.-Oct. 1982, p. 654-679. Research supported by the U.S. Department of Energy
(Contract DEN3-168; DEN3-167)

High frequency, bulk-wave ultrasonics detected defects in manufactured SiC components. In addition, gas-turbine blades and vanes were examined by scanning laser acoustic microscopy (SLAM). Comparative results obtained on simple shapes such as disks and bars by microfocus X-ray radiography, ultrasonics, scanning photoacoustic spectroscopy, and SLAM are discussed. (Author)

A83-25571* Ohio State Univ., Columbus.
MECHANICS ASPECTS OF NDE BY SOUND AND ULTRASOUND
L. S. FU (Ohio State University, Columbus, OH) Applied Mechanics Reviews, vol. 35, Aug. 1982, p. 1047-1057. refs
(Contract NSG-3269)

Nondestructive evaluation (NDE) is considered as a means to detect the energy release mechanism of defects and the interaction of microstructures within materials with sound waves and/or ultrasonic waves. Ultrasonic inspection involves the frequency range 20 kHz-1 GHz with amplitudes depending on the sensitivity of the test instrumentation. Pulse echo systems are most frequently used in NDE. Information is extracted from the signals through measurements of the signal velocity, attenuation, the acoustic emission when stress is applied, and calculation of the acoustoelastic coefficients. Fracture properties, tensile and shear strengths, the interlaminar shear strength, the cohesive strength, yield and impact strengths, the hardness, and the residual stress can be assayed by ultrasonic methods. Finally, attention is given to analytical treatment of the derived data, with mention given to transition matrix, integral equation, and eigenstrain approaches. M.S.K.

A83-39620*# National Aeronautics and Space Administration. Lewis Research Center, Cleveland, Ohio.
METAL HONEYCOMB TO POROUS WIREFORM SUBSTRATE DIFFUSION BOND EVALUATION
A. VARY, P. E. MOORHEAD, and D. R. HULL (NASA, Lewis Research Center, Nondestructive Evaluation Section, Cleveland, OH) Materials Evaluation (ISSN 0025-5327), vol. 41, July 1983, p. 942-945. refs

Two nondestructive techniques were used to evaluate diffusion bond quality between a metal fail honeycomb and porous wireform substrate. The two techniques, cryographics and acousto-ultrasonics, are complementary in revealing variations of bond integrity and quality in shroud segments from an experimental aircraft turbine engine. Previously announced in STAR as N82-18612 Author

N83-11506*# Ohio State Univ., Columbus. Dept. of Engineering Mechanics.
PHENOMENOLOGICAL AND MECHANICS ASPECTS OF NONDESTRUCTIVE EVALUATION AND CHARACTERIZATION BY SOUND AND ULTRASOUND OF MATERIAL AND FRACTURE PROPERTIES Final Report
L. S. W. FU Washington NASA Oct. 1982 32 p refs
(Contract NSG-3269)
(NASA-CR-3623; NAS 1.26:3623) Avail: NTIS HC A03/MF A01 CSCL 14D

Developments in fracture mechanics and elastic wave theory enhance the understanding of many physical phenomena in a mathematical context. Available literature in the material, and fracture characterization by NDT, and the related mathematical methods in mechanics that provide fundamental underlying principles for its interpretation and evaluation are reviewed. Information on the energy release mechanism of defects and the interaction of microstructures within the material is basic in the formulation of the mechanics problems that supply guidance for nondestructive evaluation (NDE). A.R.H.

N83-11507*# Ohio State Univ., Columbus. Dept. of Engineering Mechanics.
FUNDAMENTAL ASPECTS IN QUANTITATIVE ULTRASONIC DETERMINATION OF FRACTURE TOUGHNESS: THE SCATTERING OF A SINGLE ELLIPSOIDAL INHOMOGENEITY Final Report
L. S. W. FU Washington NASA Oct. 1981 37 p refs
(Contract NSG-3269)
(NASA-CR-3625; NAS 1.26:3625) Avail: NTIS HC A03/MF A01 CSCL 14D

The scattering of a single ellipsoidal inhomogeneity is studied via an eigenstrain approach. The displacement field is given in terms of volume integrals that involve eigenstrains that are related to mismatch in mass density and that in elastic moduli. The governing equations for these unknown eigenstrains are derived. Agreement with other approaches for the scattering problem is shown. The formulation is general and both the inhomogeneity and the host medium can be anisotrophic. The axisymmetric scattering of an ellipsoidal inhomogeneity in a linear elastic isotropic medium is given as an example. The angular and frequency dependence of the scattered displacement field, the differential and total cross sections are formally given in series expansions for the case of uniformly distributed eigenstrains. Author

N83-16773*# Ohio State Univ., Columbus. Dept. of Engineering Mechanics.
THE TRANSMISSION OR SCATTERING OF ELASTIC WAVES BY AN INHOMOGENEITY OF SIMPLE GEOMETRY: A COMPARISON OF THEORIES Final Report
Y. C. SHEU and L. S. FU Washington NASA Jan. 1983 91 p refs
(Contract NSG-3269)
(NASA-CR-3659; E-1394; NAS 1.26:3659; RF-TECH-104) Avail: NTIS HC A05/MF A01 CSCL 20N

The extended method of equivalent inclusions is applied to study the specific wave problems: (1) the transmission of elastic waves in an infinite medium containing a layer of inhomogeneity, and (2) the scattering of elastic waves in an infinite medium containing a perfect spherical inhomogeneity. Eigenstrains are expanded as a geometric series and a method of integration based on the inhomogeneous Helmholtz operator is adopted. This study compares results, obtained by using limited number of terms in the eigenstrain expansion, with exact solutions for the layer problem and that for a perfect sphere. S.L.

N83-21373*# Massachusetts Inst. of Tech., Cambridge. Dept. of Mechanical Engineering.
EFFECTS OF SPECIMEN RESONANCES ON ACOUSTIC-ULTRASONIC TESTING Final Report
J. H. WILLIAMS, JR., E. B. KAHN, and S. S. LEE Washington NASA Mar. 1983 36 p refs
(Contract NSG-3210)
(NASA-CR-3679; NAS 1.26:3679) Avail: NTIS HC A03/MF A01 CSCL 14D

The effects of specimen resonances on acoustic ultrasonic (AU) nondestructive testing were investigated. Selected resonant frequencies and the corresponding normal mode nodal patterns of the aluminum block are measured up to 75.64 kHz. Prominent peaks in the pencil lead fracture and sphere impact spectra from the two transducer locations corresponded exactly to resonant frequencies of the block. It is established that the resonant frequencies of the block dominated the spectral content of the output signal. The spectral content of the output signals is further influenced by the transducer location relative to the resonant frequency nodal lines. Implications of the results are discussed in relation to AU parameters and measurements. E.A.K.

N83-23620*# National Aeronautics and Space Administration. Lewis Research Center, Cleveland, Ohio.
ULTRASONIC RANKING OF TOUGHNESS OF TUNGSTEN CARBIDE
A. VARY and D. R. HULL Apr. 1983 11 p refs Presented at the 14th Symp. on Nondestructive Evaluation, San Antonio, Tex., 19-21 Apr. 1983
(NASA-TM-83358; E-1619; NAS 1.15:83358) Avail: NTIS HC A02/MF A01 CSCL 14D

The feasibility of using ultrasonic attenuation measurements to rank tungsten carbide alloys according to their fracture toughness was demonstrated. Six samples of cobalt-cemented tungsten carbide (WC-Co) were examined. These varied in cobalt content from approximately 2 to 16 weight percent. The toughness generally increased with increasing cobalt content. Toughness was first determined by the Palmqvist and short rod fracture toughness tests. Subsequently, ultrasonic attenuation measurements were correlated with both these mechanical test methods. It is shown that there is a strong increase in ultrasonic attenuation corresponding to increased toughness of the WC-Co alloys. A correlation between attenuation and toughness exists for a wide range of ultrasonic frequencies. However, the best correlation for the WC-Co alloys occurs when the attenuation coefficient measured in the vicinity of 100 megahertz is compared with toughness as determined by the Palmqvist technique. Author

N83-27248*# Virginia Polytechnic Inst. and State Univ., Blacksburg. Dept. of Engineering Science and Mechanics.
A STUDY OF THE STRESS WAVE FACTOR TECHNIQUE FOR THE CHARACTERIZATION OF COMPOSITE MATERIALS Final Report
E. G. HENNEKE, II, J. C. DUKE, JR., W. W. STINCHCOMB, A. GOVADA, and A. LEMASCON Washington Feb. 1983 74 p refs
(Contract NSG-3172)
(NASA-CR-3670; NAS 1.26:3670) Avail: NTIS HC A04/MF A01 CSCL 14D

A testing program was undertaken to provide an independent investigation and evaluation of the stress wave factor for characterizing the mechanical behavior of composite laminates. Some of the data which was obtained after performing a very large number of tests to determine the reproducibility of the SWF

measurement is presented. It was determined that, with some optimizing of experimental parameters, the SWF value can be reproduced to within + or - 10%. Results are also given which show that, after careful calibration procedures, the lowest SWF value along the length of a specimen will correlate very closely to the site of final failure when the specimen is loaded in tension. Finally, using a moire interferometry technique, it was found that local regions having the highest in plane strains under tensile loading also had the lowest SWF values. S.L.

N83-28466*# Massachusetts Inst. of Tech., Cambridge. Dept. of Mechanical Engineering.
ULTRASONIC ATTENUATION OF A VOID-CONTAINING MEDIUM FOR VERY LONG WAVELENGTHS Final Report
J. H. WILLIAMS, JR., S. S. LEE, and H. YUECE NASA Washington Jun. 1983 22 p refs
(Contract NSG-3210)
(NASA-CR-3693; NAS 1.26:3693) Avail: NTIS HC A02/MF A01 CSCL 14D

Ultrasonic longitudinal through-thickness attenuation in an isotropic medium due to scattering by randomly distributed voids is considered analytically. The attenuation is evaluated on the assumption of no interaction between voids. The scattered power is assumed to be entirely lost, thus accounting for the ultrasonic attenuation. The scattered power due to the presence of a void is described in terms of the scattering cross section of the void. An exact solution exists for the scattering cross section of a spherical void. An approximate solution for the scattering cross section of an ellipsoidal void is developed based on the so-called Born approximation commonly used in quantum mechanics This approximate solution is valid for k sub p a sub i 1, where k sub p is the wave number of the incident longitudinal wave and a sub i is the largest dimension of the void. It is found that the shape of the void has negligible effect on the scattering cross section and that only the volume of the void is important. Thus, it is noted that in cases where k sup p a sub i 1, the exact scattering cross section of a spherical void having the same volume as an arbitrarily shaped void can be used for evaluating ultrasonic attenuation. M.G.

N83-33180*# Cleveland State Univ., Ohio. Coll. of Engineering.
THE EFFECT OF STRESS ON ULTRASONIC PULSES IN FIBER REINFORCED COMPOSITES Final Report
J. H. HEMANN and G. Y. BAAKLINI Washington NASA Aug. 1983 80 p refs
(Contract NAG3-106)
(NASA-CR-3724; NAS 1.26:3724) Avail: NTIS HC A05/MF A01 CSCL 20K

An acoustical-ultrasonic technique was used to demonstrate relationships existing between changes in attenuation of stress waves and tensile stress for an eight ply 0 degree graphite-epoxy fiber reinforced composite. All tests were conducted in the linear range of the material for which no mechanical or macroscopic damage was evident. Changes in attenuation were measured as a function of tensile stress in the frequency domain and in the time domain. Stress wave propagation in these specimens was dispersive, i.e., the wave speed depends on frequency. Wave speeds varied from 267 400 cm/sec to 680 000 cm/sec as the frequency of the signal was varied from 150 kHz to 1.9 MHz which strongly suggests that flexural/lamb wave modes of propagation exist. The magnitude of the attenuation changes depended strongly on tensile stress. It was further observed that the wave speeds increased slightly for all tested frequencies as the stress was increased. Author

N83-33182*# Pratt and Whitney Aircraft Group, East Hartford, Conn.
SENSOR FAILURE DETECTION FOR JET ENGINES Final Report
E. C. BEATTIE, R. F. LAPRAD, M. M. AKHTER (Systems Control Technology), and S. M. ROCK (Systems Control Technology) May 1983 152 p refs
(Contract NAS3-23282)
(NASA-CR-168190; NAS 1.26:168190; PWA-5891-18) Avail: NTIS HC A08/MF A01 CSCL 14D

Revisions to the advanced sensor failure detection, isolation, and accommodation (DIA) algorithm, developed under the sensor failure detection system program were studied to eliminate the steady state errors due to estimation filter biases. Three algorithm revisions were formulated and one revision for detailed evaluation was chosen. The selected version modifies the DIA algorithm to feedback the actual sensor outputs to the integral portion of the control for the nofailure case. In case of a failure, the estimates of the failed sensor output is fed back to the integral portion. The estimator outputs are fed back to the linear regulator portion of the control all the time. The revised algorithm is evaluated and compared to the baseline algorithm developed previously. E.A.K.

39

STRUCTURAL MECHANICS

Includes structural element design and weight analysis; fatigue; and thermal stress.

A83-10283* Northwestern Univ., Evanston, Ill.
ON COMPOSITES WITH PERIODIC STRUCTURE
S. NEMAT-NASSER, T. IWAKUMA, and M. HEJAZI (Northwestern University, Evanston, IL) Mechanics of Materials, vol. 1, Sept. 1982, p. 239-267. refs
(Contract DAAG29-79-C-0168; NAG3-134)

The overall moduli of a composite with an isotropic elastic matrix containing periodically distributed (anisotropic) inclusions or voids, can be expressed in terms of several infinite series which only depend on the geometry of the inclusions or voids, and hence can be computed once and for all for given geometries. For solids with periodic structures these infinite series play exactly the same role as does Eshelby's tensor for a single inclusion or void in an unbounded elastic medium. For spherical and circular-cylindrical geometries, the required infinite series are calculated and the results are tabulated. These are then used to estimate the overall elastic moduli when either the overall strains or the overall stresses are prescribed, obtaining the same results. These results are compared with other estimates and with experimental data. It is found that the model of composites with periodic structure yields estimates in excellent agreement with the experimental observations. (Author)

A83-10900*# National Aeronautics and Space Administration. Lewis Research Center, Cleveland, Ohio.
TENSILE BUCKLING OF ADVANCED TURBOPROPS
C. C. CHAMIS and R. A. AIELLO (NASA, Lewis Research Center, Cleveland, OH) AIAA, ASME, ASCE, and AHS, Structures, Structural Dynamics and Materials Conference, 23rd New Orleans, LA, May 10-12, 1982, AIAA 23 p. refs
(AIAA PAPER 82-0776)
(Previously announced in STAR as N82-31708)

A83-12048* Lehigh Univ., Bethlehem, Pa.
MOVING CRACKS IN LAYERED COMPOSITES
G. C. SIH (Lehigh University, Bethlehem, PA) and E. P. CHEN (Sandia National Laboratory, Albuquerque, NM) International Journal of Engineering Science, vol. 20, no. 11, 1982, p. 1181-1192. refs
(Contract NSG-3179)

A three-layered composite with a crack spreading in the center layer has been analytically examined to evaluate the effect of material nonhomogeneity on a constant velocity crack. Two different loading characteristics are considered. In the first case, crack motion is maintained by uniform tensile stresses. In the other, crack deformation is caused by anti-plane shear stresses. Galilean transformation and Fourier sine and cosine transforms are used to determine dynamic crack tip stress fields. Standard Fredholm integral equations yield the dynamic stress intensity factors. The results show that the intensity of local dynamic stresses increases or decreases with crack length to layer thickness as a function of the relative magnitudes of the adjoining layer's material properties. Crack speed tends to increase the effect of material nonhomogeneity. S.C.S.

A83-12514* Illinois Univ., Urbana.
EXTENDING THE LASER-SPECKLEGRAM TECHNIQUE TO STRAIN ANALYSIS OF ROTATING COMPONENTS
C. H. CHIEN (Illinois, University, Urbana, IL), J. L. TURNER, W. F. SWINSON (Auburn University, Auburn, AL), and W. F. RANSON (South Carolina, University, Columbia, SC) (Society for Experimental Stress Analysis, Spring Meeting, Dearborn, MI, May 30-June 4, 1981.) Experimental Mechanics, vol. 22, Nov. 1982, p. 434-440. refs
(Contract NAG3-103)

A technique involving sandwich-speckle interferometry has been investigated for application in making strain measurements on rotating structures. The technique has proven to be effective in relaxing stringent timing requirements for recording laser photographs and provides extended ranges of displacement measurement. Application of the technique to an experimental rotating specimen has demonstrated the potential of the method for making accurate strain measurements. (Author)

A83-12739* Massachusetts Inst. of Tech., Cambridge.
A NEW FORMULATION OF HYBRID/MIXED FINITE ELEMENT
T. H. H. PIAN, D. KANG (MIT, Cambridge, MA), and D.-P. CHEN (Symposium on Advances and Trends in Structural and Solid Mechanics, Washington, DC, Oct. 4-7, 1982.) Computers and Structures, vol. 16, no. 1-4, 1983, p. 81-87. refs
(Contract NAG3-33)

A new formulation of finite element method is accomplished by the Hellinger-Reissner principle for which the stress equilibrium conditions are not introduced initially but are brought-in through the use of additional internal displacement parameters. The method can lead to the same result as the assumed stress hybrid model. However, it is more general and more flexible. The use of natural coordinates for stress assumptions leads to elements which are less sensitive to the choice of reference coordinates. Numerical solutions by 3-D solid element indicate that more efficient elements can be constructed by assumed stresses which only partially satisfy the equilibrium conditions. (Author)

A83-12746* Akron Univ., Ohio.
ON THE SOLUTION OF ELASTIC-PLASTIC STATIC AND DYNAMIC POSTBUCKLING COLLAPSE OF GENERAL STRUCTURE
J. PADOVAN and S. TOVICHAKCHAIKUL (Akron, University, Akron, OH) (Symposium on Advances and Trends in Structural and Solid Mechanics, Washington, DC, Oct. 4-7, 1982.) Computers and Structures, vol. 16, no. 1-4, 1983, p. 199-205. refs
(Contract NAG3-54)

Many investigations have considered structural collapse from strictly the transient point of view. While such an approach is ideally correct, certain difficulties have to be overcome in its implementation. The present investigation is concerned with the development of self-adaptive algorithms which make it possible to conduct the analysis of both static elastic and elastic-plastic postbuckling, as well as static loading to the onset of buckling followed by subsequent dynamic postbuckling. The approach employed to solve the static portion of loading is to extend the constrained Incremental Newton-Raphson (INR) algorithm by incorporating elastic-plastic constitutive characterizations. Large deformation moderate strain theory is adopted to establish the overall strategy. Attention is given to governing field equations, aspects of algorithmic development, and numerical experiments conducted to illustrate the efficiency and stability of the developed schemes. G.R.

A83-12764* Pratt and Whitney Aircraft Group, East Hartford, Conn.
NONLINEAR STRUCTURAL AND LIFE ANALYSES OF A COMBUSTOR LINER
V. MORENO, G. J. MEYERS (United Technologies Corp., Pratt and Whitney Group, East Hartford, CT), A. KAUFMAN, and G. R. HALFORD (NASA, Lewis Research Center, Cleveland, OH) (Symposium on Advances and Trends in Structural and Solid Mechanics, Washington, DC, Oct. 4-7, 1982.) Computers and Structures, vol. 16, no. 1-4, 1983, p. 509-515. refs
(Previously announced in STAR as N82-24501)

A83-14710* Massachusetts Inst. of Tech., Cambridge.
ALTERNATIVE WAYS FOR FORMULATION OF HYBRID STRESS ELEMENTS
T. H. H. PIAN (MIT, Cambridge, MA) and D.-P. CHEN International Journal for Numerical Methods in Engineering, vol. 18, Nov. 1982, p. 1679-1684. refs
(Contract NAG3-33)

An element stiffness matrix can be derived by the conventional potential energy principle and, indirectly, also by generalized variational principles, such as the Hu-Washizu principle and the Hellinger-Reissner principle. The present investigation has the objective to show an approach which is concerned with the formulation of incompatible elements for solid continuum and for plate bending problems by the Hellinger-Reissner principle. It is found that the resulting scheme is equivalent to that considered by Tong (1982) for the construction of hybrid stress elements. In Tong's scheme the inversion of a large flexibility matrix can be avoided. It is concluded that the introduction of additional internal displacement modes in mixed finite element formulations by the Hellinger-Reissner principle and the Hu-Washizu principle can lead to element stiffness matrices which are equivalent to the assumed stress hybrid method. G.R.

A83-15060* Northwestern Univ., Evanston, Ill.
GROWTH AND STABILITY OF INTERACTING SURFACE FLAWS OF ARBITRARY SHAPE
Y. MURAKAMI and S. NEMAT-NASSER (Northwestern University, Evanston, IL) Engineering Fracture Mechanics, vol. 17, no. 3, 1983, p. 193-210. refs
(Contract NSF CME-80-06265; NAG3-134)

Growth regimes of interacting surface flaws of arbitrary shape are analyzed with the aid of the body force method, and the stability of the process is assessed on the basis of the variation of the load during the growth. It is shown that irregularly shaped flaws are often associated with very high stress intensity factors locally, which tend to change as the flaws grow into more regular shapes. Several examples of various flaw shapes are worked out for illustration, and it is shown that a simple formula seems to provide an accurate estimate of the maximum stress intensity factor for surface flaws of various shapes, which are not very slender. The formula involves the overall maximum tension, as well as the area of the projection of the flaw on the plane normal to the maximum tension. (Author)

A83-18383* Rensselaer Polytechnic Inst., Troy, N. Y.
NATURAL FREQUENCY OF ROTATING BEAMS USING NON-ROTATING MODES
R. G. LOEWY (Rensselaer Polytechnic Institute, Troy, NY) and N. KHADER American Helicopter Society, Journal, vol. 27, Apr. 1982, p. 75-78. refs
(Contract NAG3-37)

A Lagrangian approach is formulated for predicting the rotating natural frequencies of a beam from the nonrotating modes and frequencies. Using the first two nonrotating mode shapes in one case and the first four such modes in the other case the frequencies of the rotating modes are calculated for a short tapered beam and a typical helicopter blade, respectively. In each case the beam is represented by lumped parameters. The number of mass points representing the beam and the accuracy of the calculated slopes of the nonrotating mode shapes at those points are both shown to affect the accuracy of the resulting frequencies, but the number of stations is shown to be more important. (Author)

A83-27431*# Virginia Polytechnic Inst. and State Univ., Blacksburg.
GEOMETRICALLY NONLINEAR ANALYSIS OF LAYERED COMPOSITE SHELLS
W. C. CHAO and J. N. REDDY (Virginia Polytechnic Institute and State University, Blacksburg, VA) In: 1982 advances in aerospace structures and materials; Proceedings of the Winter Annual Meeting, Phoenix, AZ, November 14-19, 1982. New York, American Society of Mechanical Engineers, 1982, p. 25-28. refs
(Contract N00014-78-C-0647; NAG3-208)

Two kinds of finite-element analyses are developed for the geometrically nonlinear study of the large deformations in laminated composite structures, especially shells. The first kind of finite-element analysis utilizes the general incremental variational formulation as well as the total Lagrangian description of motion, and a three-dimensional degenerate element is adopted. The second kind of analysis employs a formulation based on deformable shell theory, and the plate-bending element is used. Numerical results for bending are presented for five plate and shell structures of isotropic as well as orthotropic composition, including an isotropic cylindrical panel with uniform loading and a laminated cylindrical panel with uniform loading. The results obtained using these analyses are found to be in good agreement with those available in the literature. N.B.

A83-27432*# Virginia Polytechnic Inst. and State Univ., Blacksburg.
THREE-DIMENSIONAL FINITE-ELEMENT ANALYSIS OF LAYERED COMPOSITE PLATES
N. S. PUTCHA and J. N. REDDY (Virginia Polytechnic Institute and State University, Blacksburg, VA) In: 1982 advances in aerospace structures and materials; Proceedings of the Winter Annual Meeting, Phoenix, AZ, November 14-19, 1982. New York, American Society of Mechanical Engineers, 1982, p. 29-35. refs
(Contract N00014-78-C-0647; NAG3-208)

Results are presented for an investigation of the three-dimensional, geometrically nonlinear, finite-element analysis of the bending of laminated anisotropic composite plates. The individual laminae are treated as homogeneous, transversely isotropic, and linearly elastic. A fully three-dimensional isoparametric finite element with eight modes (i.e., linear element) and 24 degrees of freedom (three displacement components per node) is used. The numerical results obtained using this linear analysis are compared with the exact solutions given in Pagano (1969, 1970). It is found that the results of the linear analysis converge to the exact solution as the mesh is refined. N.B.

A83-29798*# Texas A&M Univ., College Station.
AN UNCOUPLED VISCOPLASTIC CONSTITUTIVE MODEL FOR METALS AT ELEVATED TEMPERATURE
W. E. HAISLER and J. CRONENWORTH (Texas A & M University, College Station, TX) IN: Structures, Structural Dynamics and Materials Conference, 24th, Lake Tahoe, NV, May 2-4, 1983, Collection of Technical Papers. Part 1 . New York, American Institute of Aeronautics and Astronautics, 1983, p. 664-673. refs
(Contract NAG3-31)
(AIAA 83-1016)

An uncoupled constitutive model for predicting the transient response of thermal and rate dependent, inelastic material behavior is presented. The uncoupled model assumes that there is a temperature below which the total strain consists essentially of elastic and rate insensitive inelastic strains only. Above this temperature, the rate dependent inelastic strain (creep) dominates. The rate insensitive inelastic strain component is modeled in an incremental form with a yield function, flow rule and hardening law. Revisions to the hardening rule permit the model to predict temperature-dependent kinematic-isotropic hardening behavior, cyclic saturation, asymmetric stress-strain response upon stress reversal, and variable Bauschinger effect. The rate dependent inelastic strain component is modeled using a rate equation in terms of back stress, drag stress and exponent n as functions of temperature and strain. A sequence of hysteresis loops and relaxation tests are utilized to define the rate dependent inelastic strain rate. Evaluation of the model is performed by comparison with experiments involving various thermal and mechanical load histories on 5086 aluminum alloy, 304 stainless steel and Hastelloy-X. Author

A83-29822*# National Aeronautics and Space Administration. Lewis Research Center, Cleveland, Ohio.
THE COUPLED AEROELASTIC RESPONSE OF TURBOMACHINERY BLADING TO AERODYNAMIC EXCITATIONS
D. HOYNIAK (NASA, Lewis Research Center, Cleveland, OH; Purdue University, West Lafayette, IN) and S. FLEETER (Purdue University, West Lafayette, IN) IN: Structures, Structural Dynamics and Materials Conference, 24th, Lake Tahoe, NV, May 2-4, 1983, Collection of Technical Papers. Part 2 . New York, American Institute of Aeronautics and Astronautics, 1983, p. 137-148. refs
(AIAA 83-0844)

An energy balance technique is developed to predict the coupled bending-torsion mode aerodynamically forced response of an airfoil. In this technique, the energy input to the airfoil system per cycle of oscillation is generated by gust forces and moments and, under certain conditions, the self-induced aerodynamic forces and moments. The energy dissipation per cycle is associated with the structural damping, the static moment term for coupled motions, and under certain conditions, the self-induced aerodynamic forces and moments. The effects of the various aerodynamic parameters on the coupled forced response are then considered.In particular, the effects of the inlet Mach number, the interblade phase angle, the level of structural damping, and the cascade geometry on the coupled bending-torsion aerodynamically forced response of a flat plate airfoil cascade are demonstrated. Author

A83-29823*# Massachusetts Inst. of Tech., Cambridge.
FLUTTER AND FORCED RESPONSE OF MISTUNED ROTORS USING STANDING WAVE ANALYSIS
J. DUGUNDJI and D. J. BUNDAS (MIT, Cambridge, MA) IN: Structures, Structural Dynamics and Materials Conference, 24th, Lake Tahoe, NV, May 2-4, 1983, Collection of Technical Papers. Part 2 . New York, American Institute of Aeronautics and Astronautics, 1983, p. 149-159. refs
(Contract NAG3-214)
(AIAA 83-0845)

A standing wave approach is applied to the analysis of the flutter and forced response of tuned and mistuned rotors. The traditional traveling wave cascade airforces are recast into standing wave arbitrary motion form using Pade approximants, and the resulting equations of motion are written in the matrix form.

Applications for vibration modes, flutter, and forced response are discussed. It is noted that the standing wave methods may prove to be more versatile for dealing with certain applications, such as coupling flutter with forced response and dynamic shaft problems, transient impulses on the rotor, low-order engine excitation, bearing motions, and mistuning effects in rotors. V.L.

A83-29824*# Textron Bell Aerospace Co., Buffalo, N. Y.
FLUTTER ANALYSIS OF ADVANCED TURBOPROPELLERS
V. ELCHURI and G. C. C. SMITH (Bell Aerospace Textron, Buffalo, NY) IN: Structures, Structural Dynamics and Materials Conference, 24th, Lake Tahoe, NV, May 2-4, 1983, Collection of Technical Papers. Part 2 . New York, American Institute of Aeronautics and Astronautics, 1983, p. 160-165. refs
(Contract NAS3-22533)
(AIAA 83-0846)

The two-dimensional subsonic cascade unsteady aerodynamic theory of Jones and Rao (1975) has been modified to account for the variable sweep angles of the blades of advanced turbopropellers. The aerodynamics and the structural modal properties have been formally integrated to determine the generalized aerodynamic coefficients matrix for the blade modes. Modal flutter analysis has been conducted for two SR-5 five- and ten-blade propellers, and analytical results have been found to be in very good agreement with wind tunnel test data. V.L.

A83-32987*# Massachusetts Inst. of Tech., Cambridge.
SOME ANALYSIS METHODS FOR ROTATING SYSTEMS WITH PERIODIC COEFFICIENTS
J. DUGUNDJI (MIT, Cambridge, MA) and J. H. WENDELL AIAA Journal (ISSN 0001-1452), vol. 21, June 1983, p. 890-897. refs
(Contract NSG-3303)

Two of the more common procedures for analyzing the stability and forced response of equations with periodic coefficients are reviewed: the use of Floquet methods, and the use of multiblade coordinate and harmonic balance methods. The analysis procedures of these periodic coefficient systems are compared with those of the more familiar constant coefficient systems. Previously announced in STAR as N82-23702 Author

A83-36958* Ohio State Univ., Columbus.
VIBRATIONS OF CANTILEVERED CIRCULAR CYLINDRICAL SHELLS SHALLOW VERSUS DEEP SHELL THEORY
J. K. LEE, A. W. LEISSA, and A. J. WANG (Ohio State University, Columbus, OH) International Journal of Mechanical Sciences (ISSN 0020-7403), vol. 25, no. 5, 1983, p. 361-383. refs
(Contract NAG3-36)

Free vibrations of cantilevered circular cylindrical shells having rectangular planforms are studied in this paper by means of the Ritz method. The deep shell theory of Novozhilov and Goldenveizer is used and compared with the usual shallow shell theory for a wide range of shell parameters. A thorough convergence study is presented along with comparisons to previously published finite element solutions and experimental results. Accurately computed frequency parameters and mode shapes for various shell configurations are presented. The present paper appears to be the first comprehensive study presenting rigorous comparisons between the two shell theories in dealing with free vibrations of cantilevered cylindrical shells. Author

A83-37388*# Ohio State Univ., Columbus.
THE DETERMINATION OF THE ELASTODYNAMIC FIELDS OF AN ELLIPSOIDAL INHOMOGENEITY
L. S. FU (Ohio State University, Columbus, OH) and T. MURA (Northwestern University, Evanston, IL) ASME, Transactions, Journal of Applied Mechanics (ISSN 0021-8936), vol. 50, June 1983, p. 390-396. refs
(Contract NSG-3269)
(ASME PAPER 83-APM-19)

The determination of the elastodynamic fields of an ellipsoidal inhomogeneity is studied in detail via the eigenstrain approach. A complete formulation and a treatment of both types of eigenstrains for equivalence between the inhomogeneity problem and the inclusion problem are given. This approach is shown to be mathematically identical to other approaches such as the direct volume integral formulation. Expanding the eigenstrains and applied strains in the polynomial form in the position vector and satisfying the equivalence conditions at every point, the governing simultaneous algebraic equations for the unknown coefficients in the eigenstrain expansion are derived. The elastodynamic field outside an ellipsoidal inhomogeneity in a linear elastic isotropic medium is given as an example. The angular and frequency dependence of the induced displacement field, as well as the differential and total cross sections are formally given in series expansion form for the case of uniformly distributed eigenstrains. C.D.

A83-37729* Ohio State Univ., Columbus.
ON THE THREE-DIMENSIONAL VIBRATIONS OF THE CANTILEVERED RECTANGULAR PARALLELEPIPED
A. LEISSA (Ohio State University, Columbus, OH) and Z.-D. ZHANG Acoustical Society of America, Journal (ISSN 0001-4966), vol. 73, June 1983, p. 2013-2021. refs
(Contract NAG3-36)

A solution is presented for the three-dimensional problem of determining the free vibration frequencies and mode shapes for a rectangular parallelepiped which is completely fixed on one face and free on the other five faces. This problem apparently is previously unsolved in the published literature. The Ritz method is used, with displacements assumed in the form of algebraic polynomials. Convergence is studied. Numerical results are given for the first five frequencies of each of the four symmetry classes of vibration, for five thick parallelepiped configurations, including the cube. Contour plots are exhibited for the modal displacements of the cube. The effects of varying Poisson's ratio are also observed. Author

A83-38528* Northwestern Univ., Evanston, Ill.
DYNAMIC FIELDS NEAR A CRACK TIP GROWING IN AN ELASTIC-PERFECTLY-PLASTIC SOLID
S. NEMAT-NASSER (Northwestern University, Evanston, IL) and Y. C. GAO Mechanics of Materials (ISSN 0167-6636), vol. 2, April 1983, p. 47-60. refs
(Contract NAG3-134)

A full asymptotic solution is presented for the fields in the neighborhood of the tip of a steadily advancing crack in an incompressible elastic-perfectly-plastic solid. There are four findings for mode I crack growth in the plane strain condition. The first is that the entire crack tip in steady crack growth is surrounded by a plastic region and that no elastic unloading is predicted by the complete dynamic asymptotic solution. The second is that, in contrast to the quasi-static solution, the dynamic solution yields strain fields with a logarithmic singularity everywhere near the crack tip. The third is that whereas the stress field varies throughout the entire crack tip neighborhood, it does not exhibit behavior that can be approximated by a constant field followed by an essentially centered-fan field and then by another constant field, especially for small crack growth speeds. The fourth finding is that there are two shock fronts emanating from the crack tip across which certain stress and strain components undergo jump discontinuities. After reviewing the mode III steady-state crack growth, it is concluded that ductile fracture criteria for nonstationary cracks must be based on solutions that include the inertia effects and that for this purpose quasi-static solutions may be inadequate. C.R.

A83-39557* Ohio State Univ., Columbus.
VIBRATIONS OF CANTILEVERED DOUBLY-CURVED SHALLOW SHELLS
A. W. LEISSA, J. K. LEE, and A. J. WANG (Ohio State University, Columbus, OH) International Journal of Solids and Structures (ISSN 0020-7683), vol. 19, no. 5, 1983, p. 411-424. refs
(Contract NAG3-36)

Vibrational characteristics are determined for a previously unsolved class of problems, that of doubly-curved shallow shells having rectangular planforms, clamped along one edge and free

on the other three. The solution procedure uses the Ritz method with algebraic polynomial trial functions. Convergence studies are made, and accurate frequencies and contour plots of mode shapes are presented for various curvature ratios, including spherical, circular cylindrical and hyperbolic paraboloidal shells. Particular emphasis is given to the effect of adding spanwise curvature to shells having chordwise curvature; numerous published references already exist for the case of zero spanwise curvature. The effects of changing aspect ratio, thickness ratio and Poisson's ratio are also studied. Author

A83-44050* Purdue Univ., Lafayette, Ind.
WAVE PROPAGATION IN A GRAPHITE/EPOXY LAMINATE
C. T. SUN and T. M. TAN (Purdue University, West Lafayette, IN) IN: Engineering science and mechanics; Proceedings of the International Symposium, Tainan, Republic of China, December 29-31, 1981. Part 2 . San Diego, American Astronautical Society, 1983, p. 1290-1307. refs
(Contract NSG-3185)

Harmonic wave and wave front propagations in a graphite/epoxy laminate are investigated using a plate theory that includes transverse shear deformation. Transient waves produced by impact of a steel ball are studied experimentally and by using finite elements. The statically measured law of contact between the steel ball and the laminate is used in the finite element program to compute the dynamic contact force. It is found that use of this contact law in conjunction with the finite element modeling of the laminate yields excellent agreement with the experimental results. Author

A83-47978*# Ohio State Univ., Columbus.
VIBRATIONS OF BLADES WITH VARIABLE THICKNESS AND CURVATURE BY SHELL THEORY
J. K. LEE, A. W. LEISSA, and A. J. WANG (Ohio State University, Columbus, OH) American Society of Mechanical Engineers, International Gas Turbine Conference and Exhibit, 28th, Phoenix, AZ, Mar. 27-31, 1983. 6 p. refs
(Contract NAG3-36)
(ASME PAPER 83-GT-152)

A procedure for analyzing the vibrations of rotating turbomachinery blades has been previously developed. This procedure is based upon shallow shell theory, and utilizes the Ritz method to determine frequencies and mode shapes. However, it has been limited heretofore to blades of uniform thickness, uniform curvature, and/or twist and rectangular planform. The present work shows how the procedure may be generalized to eliminate the aforementioned restrictions. Nonrectangular planforms are dealt with by a suitable coordinate transformation. This, as well as variable thickness, curvature and twist, require using numerical integration. The procedure is demonstrated on four examples of cantilevered blades for which theoretical and experimental data have been previously published: (1) flat plate with spanwise taper, (2) flat plate with chordwise taper, (3) twisted plate with chordwise taper, and (4) cylindrical shell with chordwise taper. Author

A83-49437* Akron Univ., Ohio.
FINITE ELEMENT ANALYSIS OF STEADILY MOVING CONTACT FIELDS
J. PADOVAN, S. TOVICHAKCHAIKUL (Akron, University, Akron, OH), and I. ZEID (North Eastern University, Boston, MA) Computers and Structures (ISSN 0045-7949), vol. 18, no. 2, 1984, p. 191-200. refs
(Contract NAG3-54)

By introducing a moving updated Lagrangian observer, this paper develops traveling finite elements with the capacity to handle the global response resulting from steadily moving contact fields. The generality of the results is such that large deformation kinematics and kinetics as well as the full compliment of inertial fields can be handled. To streamline the handling of nonlinear behavior, an elliptically constrained solution algorithm is also developed. Employing this algorithm, the results of several numerical benchmarking studies are presented which illustrate the capacity of the moving updated Lagrangian formulation as well as the potential effects of nonlinearity. Author

N83-11514*# National Aeronautics and Space Administration. Lewis Research Center, Cleveland, Ohio.
BENDING-TORSION FLUTTER OF A HIGHLY SWEPT ADVANCED TURBOPROP
O. MEHMED, K. R. V. KAZA, J. F. LUBOMSKI, and R. E. KIELB 1981 24 p refs Prepared for presentation at the 1982 Aerospace Congr. and Exposition, Anaheim, Calif., 25-28 Oct., 1982; sponsored by the Soc. of Automotive Engr.
(NASA-TM-82975; E-1404; NAS 1.15:82975) Avail: NTIS HC A02/MF A01 CSCL 20K

Experimental and analytical results are presented for a bending-torsion flutter phenomena encountered during wind-tunnel testing of a ten-bladed, advanced, high-speed propeller (turboprop) model with thin airfoil sections, high blade sweep, low aspect ratio, high solidity and transonic tip speeds. Flutter occurred at free-stream Mach numbers of 0.6 and greater and when the relative tip Mach number (based on vector sum of axial and tangential velocities) reached a value of about one. The experiment also included two- and five-blade configurations. The data indicate that aerodynamic cascade effects have a strong destabilizing influence on the flutter boundary. The data was correlated with analytical results which include aerodynamic cascade effects and good agreement was found. Author

N83-12449*# National Aeronautics and Space Administration. Lewis Research Center, Cleveland, Ohio.
MATERIALS CONSTITUTIVE MODELS FOR NONLINEAR ANALYSIS OF THERMALLY CYCLED STRUCTURES
A. KAUFMAN and L. E. HUNT (Arizona Univ., Tucson) Oct. 1982 26 p refs
(Contract NAG3-45)
(NASA-TP-2055; E-1125; NAS 1.60:2055) Avail: NTIS HC A03/MF A01 CSCL 20K

Effects of inelastic materials models on computed stress-strain solutions for thermally loaded structures were studied by performing nonlinear (elastoplastic creep) and elastic structural analyses on a prismatic, double edge wedge specimen of IN 100 alloy that was subjected to thermal cycling in fluidized beds. Four incremental plasticity creep models (isotropic, kinematic, combined isotropic kinematic, and combined plus transient creep) were exercised for the problem by using the MARC nonlinear, finite element computer program. Maximum total strain ranges computed from the elastic and nonlinear analyses agreed within 5 percent. Mean cyclic stresses, inelastic strain ranges, and inelastic work were significantly affected by the choice of inelastic constitutive model. The computing time per cycle for the nonlinear analyses was more than five times that required for the elastic analysis. S.L.

N83-12451*# General Electric Co., Cincinnati, Ohio. Aircraft Engine Business Group.
BENCHMARK NOTCH TEST FOR LIFE PREDICTION
P. A. DOMAS, W. N. SHARPE, M. WARD, and J. F. YAU Oct. 1982 212 p refs Prepared in cooperation with Louisiana State Univ., Baton Rouge
(Contract NAS3-22522)
(NASA-CR-165571; NAS 1.26:165571; R82AEB358) Avail: NTIS HC A10/MF A01 CSCL 20L

The laser interferometric Strain Displacement Gage (ISDG) was used to measure local strains in notched Inconel 718 test bars subjected to six different load histories at 649 C (1200 F) and including effects of tensile and compressive hold periods. The measurements were compared to simplified Neuber notch analysis predictions of notch root stress and strain. The actual strains incurred at the root of a discontinuity in cyclically loaded test samples subjected to inelastic deformation at high temperature where creep deformations readily occur were determined. The steady state cyclic, stress-strain response at the root of the discontinuity was analyzed. Flat, double notched uniaxially loaded fatigue specimens manufactured from the nickel base, superalloy Inconel 718 were used. The ISDG was used to obtain cycle by

cycle recordings of notch root strain during continuous and hold time cycling at 649 C. Comparisons to Neuber and finite element model analyses were made. The results obtained provide a benchmark data set in high technology design where notch fatigue life is the predominant component service life limitation. S.L.

N83-12460*# National Aeronautics and Space Administration. Lewis Research Center, Cleveland, Ohio.
LARGE DISPLACEMENTS AND STABILITY ANALYSIS OF NONLINEAR PROPELLER STRUCTURES
R. A. AIELLO and C. C. CHAMIS *In* Georgia Univ. 10th NASTRAN User's Colloq. p 112-132 Nov. 1982
Avail: NTIS HC A12/MF A01 CSCL 20K

The use of linear rigid formats in COSMIC NASTRAN without DMAP procedures for the analysis of nonlinear propeller structures is described. Approaches for updating geometry and applying follower forces for incremental loading are demonstrated. The COSMIC NASTRAN rigid formats and other independent finite element programs are compared. The comparisons include results from the four approaches for updating the geometry using RIGID FORMAT 1, RIGID FORMATS 4 and 13, MARC and MSC/NASTRAN. It is shown that user friendly updating approaches can be used to predict the large displacements and instability of these nonlinear structures. The approaches are easily implemented by the user and predict conservative results. E.A.K.

N83-14523*# National Aeronautics and Space Administration. Lewis Research Center, Cleveland, Ohio.
MEASUREMENTS OF SELF-EXCITED ROTOR-BLADE VIBRATIONS USING OPTICAL DISPACEMENTS
A. P. KURKOV 1982 13 p refs Proposed for presentation at the 28th Ann. Intern. Gas Turbine Conf., Phoenix, Ariz., 27-31 Mar. 1983
(NASA-TM-82953; E-1368; NAS 1.15:82953) Avail: NTIS HC A02/MF A01 CSCL 20K

The characteristics of optical displacement spectra and their role of monitoring rotor blade vibrations are discussed. During the operation of a turbofan engine at part speed, near stall, and elevated inlet pressure and temperature, several vibratory instabilities were excited simultaneously on the first fan rotor. The torsional and bending contributions to the main flutter mode were resolved by using casing-mounted optical displacement sensors. Other instabilities in the blade deflection spectra were identified. E.A.K.

N83-15672*# National Aeronautics and Space Administration. Lewis Research Center, Cleveland, Ohio.
EFFECTS OF STRUCTURAL COUPLING ON MISTUNED CASCADE FLUTTER AND RESPONSE
R. E. KIELB and K. R. V. KAZA (Toledo Univ.) 1983 17 p refs Proposed for presentation at the 28th Ann. Intern. Gas Turbine Conf., Phoenix, Ariz., 27-31 Mar. 1983; sponsored by ASME
(NASA-TM-83049; E-1500; NAS 1.15:83049) Avail: NTIS HC A02/MF A01 CSCL 20K

The effects of structural coupling on mistuned cascade flutter and response are analytically investigated using an extended typical section model. This model includes both structural and aerodynamic coupling between the blades. The model assumes that the structurally coupled system natural modes were determined and are represented in the form of N bending and N torsional uncoupled modes for each blade, where N is the number of blades and, hence, is only valid for blade dominated motion. The aerodynamic loads are calculated by using two dimensional unsteady cascade theories in the subsonic and supersonic flow regimes. The results show that the addition of structural coupling can affect both the aeroelastic stability and frequency. The stability is significantly affected only when the system is mistuned. The resonant frequencies can be significantly changed by structural coupling in both tuned and mistuned systems, however, the peak response is significantly affected only in the latter. S.L.

N83-19121*# Michigan State Univ., East Lansing.
EXPERIMENTAL VERIFICATION OF THE NEUBER RELATION AT ROOM AND ELEVATED TEMPERATURES M.S. Thesis
L. J. LUCAS 1982 100 p refs
(Contract NAG3-51)
(NASA-CR-167967; NAS 1.26:167967) Avail: NTIS HC A05/MF A01 CSCL 20K

The accuracy of the Neuber equation at room temperature and 1,200 F as experimentally determined under cyclic load conditions with hold times. All strains were measured with an interferometric technique at both the local and remote regions of notched specimens. At room temperature, strains were obtained for the initial response at one load level and for cyclically stable conditions at four load levels. Stresses in notched members were simulated by subjecting smooth specimens to he same strains as were recorded on the notched specimen. Local stress-strain response was then predicted with excellent accuracy by subjecting a smooth specimen to limits established by the Neuber equation. Data at 1,200 F were obtained with the same experimental techniques but only in the cyclically stable conditions. The Neuber prediction at this temperature gave relatively accurate results in terms of predicting stress and strain points. S.L.

N83-19246*# National Aeronautics and Space Administration. Lewis Research Center, Cleveland, Ohio.
STRUCTURAL FATIGUE TEST RESULTS FOR LARGE WIND TURBINE BLADE SECTIONS
J. R. FADDOUL and T. L. SULLIVAN *In its* Large Horizontal-Axis Wind Turbines p 303-328 1982 refs
Avail: NTIS HC A99/MF A01 CSCL 20K

In order to provide quantitative information on the operating life capabilities of wind turbine rotor blade concepts for root-end load transfer, a series of cantilever beam fatigue tests was conducted. Fatigue tests were conducted on a laminated wood blade with bonded steel studs, a low cost steel spar (utility pole) with a welded flange, a utility pole with additional root-end thickness provided by a swaged collar, fiberglass spars with both bonded and nonbonded fittings, and, finally, an aluminum blade with a bolted steel fitting (Lockheed Mod-0 blade). Photographs, data, and conclusions for each of these tests are presented. In addition, the aluminum blade test results are compared to field failure information; these results provide evidence that the cantilever beam type of fatigue test is a satisfactory method for obtaining qualitative data on blade life expectancy and for identifying structurally underdesigned areas (hot spots). M.G.

N83-20284*# National Aeronautics and Space Administration. Lewis Research Center, Cleveland, Ohio.
VARIABLE FORCE, EDDY-CURRENT OR MAGNETIC DAMPER Patent Application
R. E. CUNNINGHAM, inventor (to NASA) 3 Feb. 1983 11 p
(NASA-CASE-LEW-13717-1; US-PATENT-APPL-SN-463456)
Avail: NTIS HC A02/MF A01 CSCL 20K

Variable damping for resonant vibrations which may occur at different rotational speeds in the range of rpms in which a rotating machine is operated is provided. A variable force damper includes a rotating mass carried on a shaft which is supported by a bearing in a resilient cage. The cage is attached to a support plate whose rim extends into an annular groove in a housing. Variable damping is effected by tabs of electrically conducting, nonmagnetic material which extend radially from the cage. The tabs at an index position lie between the pole faces of respective C shaped magnets. The magnets are attached by cantilever spring members to the housing. By rotating the support plate about the axis of the shaft, the tabs may be rotated through an angle 0 of about 40 deg away from the index or 0 deg position. At the 40 deg position minimum damping is obtained. NASA

N83-21390*# Pratt and Whitney Aircraft Group, East Hartford, Conn. Commercial Engineering.
DEVELOPMENT OF A SIMPLIFIED ANALYTICAL METHOD FOR REPRESENTING MATERIAL CYCLIC RESPONSE
V. MORENO Jan. 1983 91 p refs
(Contract NAS3-22821)
(NASA-CR-168100; NAS 1.26:168100; PWA-5843-13) Avail: NTIS HC A05/MF A01 CSCL 20K

Development of a simplified method for estimating structural inelastic stress and strain response to cyclic thermal loading is presented. The method assumes that high temperature structural response is the sum of time independent plastic and time dependent elastic/creep components. The local structural stress and strain response predicted by linear elastic analysis is modified by the simplified method to predict the inelastic response. The results with simulations by a nonlinear finite element analysis and used time independent plasticity and unified time dependent material model are compared. E.A.K.

N83-23629*# National Aeronautics and Space Administration. Lewis Research Center, Cleveland, Ohio. Dept. of Aerospace Mechanics.
A TOTAL LIFE PREDICTION MODEL FOR STRESS CONCENTRATION SITES Semiannual Engineering Technical Report, 1 Sep. 1982 - 31 Mar. 1983
G. A. HARTMAN and D. S. DAWICKE 11 Apr. 1983 35 p refs
(Contract NAG3-246)
(NASA-CR-170290; NAS 1.26:170290; UDR-TR-83-57; SATR-2) Avail: NTIS HC A03/MF A01 CSCL 20K

Fatigue crack growth tests were performed on center crack panels and radial crack hole samples. The data were reduced and correlated with the elastic parameter-K taking into account finite width and corner crack corrections. The anomalous behavior normally associated with short cracks was not observed. Total life estimates for notches were made by coupling an initiation life estimate with a propagation life estimate. E.A.K.

N83-23631*# National Aeronautics and Space Administration. Lewis Research Center, Cleveland, Ohio.
ARRAY STRUCTURE DESIGN HANDBOOK FOR STAND ALONE PHOTOVOLTAIC APPLICATIONS
R. C. DIDELOT Oct. 1980 243 p refs
(Contract DE-AI01-79ET-20485)
(NASA-TM-82629; E-882; NAS 1.15:82629; DOE/NASA/20485-2) Avail: NTIS HC A11/MF A01 CSCL 20K

This handbook will permit the user to design a low-cost structure for a variety of photovoltaic system applications under 10 kW. Any presently commercially available photovoltaic modules may be used. Design alternatives are provided for different generic structure types, structural materials, and electric interfaces. The use of a hand-held calculator is sufficient to perform the necessary calculations for the array designs. Author

N83-24874*# National Aeronautics and Space Administration. Lewis Research Center, Cleveland, Ohio.
STRESS INTENSITY AND DISPLACEMENT COEFFICIENTS FOR RADIALLY CRACKED RING SEGMENTS SUBJECT TO THREE-POINT BENDING
B. GROSS and J. E. SRAWLEY Mar. 1983 19 p refs
(NASA-TM-83059; E-1524; NAS 1.15:83059) Avail: NTIS HC A02/MF A01 CSCL 20K

The boudary collocation method was used to generate Mode 1 stress intensity and crack mouth displacement coefficients for internally and externally radially cracked ring segments (arc bend specimens) subjected to three point radial loading. Numerical results were obtained for ring segment outer to inner radius ratios (R sub o/ R sub i) ranging from 1.10 to 2.50 and crack length to width ratios (a/W) ranging from 0.1 to 0.8. Stress intensity and crack mouth displacement coefficients were found to depend on the ratios R sub o/R sub i and a/W as well as the included angle between the directions of the reaction forces. S.L.

N83-24875*# National Aeronautics and Space Administration. Lewis Research Center, Cleveland, Ohio.
VAPOR CAVITATION IN DYNAMICALLY LOADED JOURNAL BEARINGS
B. O. JACOBSON (Lulea Univ.) and B. J. HAMROCK 1983 14 p refs Proposed for presentation at the 2d Intern. Conf. on Cavitation, Edinburgh, 5-8 Sep. 1983
(NASA-TM-83366; E-1401; NAS 1.15:83366) Avail: NTIS HC A02/MF A01 CSCL 20K

High speed motion camera experiments were performed on dynamically loaded journal bearings. The length to diameter ratio of the bearing, the speed of the roller and the tube, the surface material of the roller, and the static and dynamic eccentricity of the bearing were varied. One hundred and thirty-four cases were filmed. The occurrence of vapor cavitation was clearly evident in the films and figures presented. Vapor cavitation was found to occur when the tensile stress applied to the oil exceeded the tensile strength of the oil or the binding of the oil to the surface. The physical situation in which vapor cavitation occurs is during the squeezing and sliding motion within a bearing. Besides being able to accurately capture the vapor cavitation on film, an analysis of the formation and collapse of the cavitation bubbles and characteristics of the bubble content are presented. S.L.

N83-27256*# Case Western Reserve Univ., Cleveland, Ohio.
CRACK LAYER MORPHOLOGY AND TOUGHNESS CHARACTERIZATION IN STEELS Final Report
A. CHUDNOVSKY and M. BESSENDORF May 1983 41 p refs
(Contract NAG3-223)
(NASA-CR-168154; NAS 1.26:168154) Avail: NTIS HC A03/MF A01 CSCL 20K

Both the macro studies of crack layer propagation are presented. The crack extension resistance parameter R sub 1 based on the morphological study of microdefects is introduced. Experimental study of the history dependent nature of G sub c supports the representation of G sub c as a product of specific enthalpy of damage (material constant) and R sub 1. The latter accounts for the history dependence. The observation of nonmonotonic crack growth under monotonic changes of J as well as statistical features of the critical energy release rate (variance of G sub c) indicate the validity of the proposed damage characterization. S.L.

N83-28493*# National Aeronautics and Space Administration. Lewis Research Center, Cleveland, Ohio.
CONSTITUTIVE RELATIONSHIPS FOR ANISOTROPIC HIGH-TEMPERATURE ALLOYS
D. N. ROBINSON 1982 22 p refs Prepared for Presentation at the Intern. Post-Conf. Seminar on Inelastic Analysis and Life Prediction, Chicago, 29-30 Aug. 1983; sponsored by Commission of European Communities and Argonne Natl. Lab., Chicago
(NASA-TM-83437; E-1733; NAS 1.15:83437) Avail: NTIS HC A02/MF A01 CSCL 20K

A constitutive theory is presented for representing the anisotropic viscoplastic behavior of high temperature alloys that posses directional properties resulting from controlled grain growth or solidification. The theory is an extension of a viscoplastic model that was applied in structural analyses involving isotropic metals. Anisotropy is introduced through the definition of a vector field that identifies a preferential (solidification) direction at each material point. Following the development of a full multiaxial theory, application is made to homogeneously stressed elements in pure shear and to a uniaxially stressed rectangular block in plane stress with the stress direction oriented at an arbitrary angle with the material direction. It is shown that an additional material parameter introduced to characterize the degree of anisotropy can be determined on the basis of simple creep tests. S.L.

N83-29731*# Arizona Univ., Tucson. Dept. of Aerospace and Mechanical Engineering.
STATISTICAL SUMMARIES OF FATIGUE DATA FOR DESIGN PURPOSES Final Report
P. H. WIRSCHING Washington, D.C. NASA Jul. 1983 63 p refs
(Contract NAG3-41)
(NASA-CR-3697; NAS 1.26:3697) Avail: NTIS HC A04/MF A01 CSCL 20K

Two methods are discussed for constructing a design curve on the safe side of fatigue data. Both the tolerance interval and equivalent prediction interval (EPI) concepts provide such a curve while accounting for both the distribution of the estimators in small samples and the data scatter. The EPI is also useful as a mechanism for providing necessary statistics on S-N data for a full reliability analysis which includes uncertainty in all fatigue design factors. Examples of statistical analyses of the general strain life relationship are presented. The tolerance limit and EPI techniques for defining a design curve are demonstrated. Examples usng WASPALOY B and RQC-100 data demonstrate that a reliability model could be constructed by considering the fatigue strength and fatigue ductility coefficients as two independent random variables. A technique given for establishing the fatigue strength for high cycle lives relies on an extrapolation technique and also accounts for 'runners.' A reliability model or design value can be specified. Author

N83-29734*# Arizona Univ., Tucson. Dept. of Aerospace and Mechanical Engineering.
APPLICATION OF ADVANCED RELIABILITY METHODS TO LOCAL STRAIN FATIGUE ANALYSIS Final Report
T. T. WU and P. H. WIRSCHING Washington Jul 1983 52 p refs
(Contract NAG3-41)
(NASA-CR-168198; NAS 1.26:168198) Avail: NTIS HC A04/MF A01 CSCL 20K

When design factors are considered as random variables and the failure condition cannot be expressed by a closed form algebraic inequality, computations of risk (or probability of failure) might become extremely difficult or very inefficient. This study suggests using a simple, and easily constructed, second degree polynomial to approximate the complicated limit state in the neighborhood of the design point; a computer analysis relates the design variables at selected points. Then a fast probability integration technique (i.e., the Rackwitz-Fiessler algorithm) can be used to estimate risk. The capability of the proposed method is demonstrated in an example of a low cycle fatigue problem for which a computer analysis is required to perform local strain analysis to relate the design variables. A comparison of the performance of this method is made with a far more costly Monte Carlo solution. Agreement of the proposed method with Monte Carlo is considered to be good. Author

N83-33217*# National Aeronautics and Space Administration. Lewis Research Center, Cleveland, Ohio.
TEMPERATURE DISTRIBUTION IN AN AIRCRAFT TIRE AT LOW GROUND SPEEDS
J. L. MCCARTY and J. A. TANNER Aug. 1983 36 p refs
(NASA-TP-2195; L-15605; NAS 1.60:2195) Avail: NTIS HC A03/MF A01 CSCL 20K

An experimental study was conducted to define temperature profiles of 22 x 5.5, type 7, bias ply aircraft tires subjected to freely rolling, yawed rolling, and light braking conditions. Temperatures along the inner wall of freely rolling tires were greater than those near the outer surface. The effect of increasing tire deflection was to increase the temperature within the shoulder and sidewall areas of the tire carcass. The effect of cornering and braking was to increase the treat temperature. For taxi operations at fixed yaw angles, temperature profiles were not symmetric. Increasing the ground speed produced only moderate increases in tread temperature, whereas temperatures in the carcass shoulder and sidewall were essentially unaffected. Author

N83-33219*# Virginia Polytechnic Inst. and State Univ., Blacksburg. Dept. of Engineering Science and Mechanics.
GEOMETRICALLY NONLINEAR ANALYSIS OF LAYERED COMPOSITE PLATES AND SHELLS Interim Report
W. C. CHAO and J. N. REDDY Feb. 1983 117 p refs
(Contract NAG3-208)
(NASA-CR-168182; NAS 1.26:168182; VPI-E-83.10) Avail: NTIS HC A06/MF A01 CSCL 20K

A degenerated three dimensional finite element, based on the incremental total Lagrangian formulation of a three dimensional layered anisotropic medium was developed. Its use in the geometrically nonlinear, static and dynamic, analysis of layered composite plates and shells is demonstrated. A two dimenisonal finite element based on the Sanders shell theory with the von Karman (nonlinear) strains was developed. It is shown that the deflections obtained by the 2D shell element deviate from those obtained by the more accurate 3D element for deep shells. The 3D degenerated element can be used to model general shells that are not necessarily doubly curved. The 3D degenerated element is computationally more demanding than the 2D shell theory element for a given problem. It is found that the 3D element is an efficient element for the analysis of layered composite plates and shells undergoing large displacements and transient motion. E.A.K.

N83-34349*# National Aeronautics and Space Administration. Lewis Research Center, Cleveland, Ohio.
RELATION OF CYCLIC LOADING PATTERN TO MICROSTRUCTURAL FRACTURE IN CREEP FATIGUE
S. S. MANSON (Case Western Reserve Univ.), G. R. HALFORD, and R. E. OLDRIEVE 1983 44 p refs Proposed for presentation at Fatigue 84 The 2nd Intern. Conf. on Fatigue and Fatigue Thresholds, Birmingham, England, 3-7 Sep. 1984
(NASA-TM-83473; E-1787; NAS 1.15:83473) Avail: NTIS HC A03/MF A01 CSCL 20K

Creep-fatigue-environment interaction is discussed using the 'strainrange partitioning' (SRP) framework as a basis. The four generic SRP strainrange types are studied with a view of revealing differences in micromechanisms of deformation and fatigue degradation. Each combines in a different manner the degradation associated with slip-plane sliding, grain-boundary sliding, migration, cavitation, void development and environmental interaction; hence the approch is useful in delineating the relative importance of these mechanisms in the different loadings. Micromechanistic results are shown for a number of materials, including 316 SS, wrought heat resistant alloys, several nickel-base superalloys, and a tantalum base alloy, T-111. Although there is a commonality of basic behavior, the differences are useful in delineation several important principles of interpretation. Some quantitative results are presented for 316 SS, involving crack initiation and early crack growth, as well as the interaction of low-cycle fatigue with high-cycle fatigue. M.G.

N83-34351*# National Aeronautics and Space Administration. Lewis Research Center, Cleveland, Ohio.
NONLINEAR CONSTITUTIVE RELATIONS FOR HIGH TEMPERATURE APPLICATIONS
Mar. 1983 360 p refs Symp. held in Akron, Ohio, 19-20 May 1982; sponsored by Akron Univ.
(NASA-CP-2271; E-1541; NAS 1.55:2271) Avail: NTIS HC A16/MF A01 CSCL 20K

The topics of discussion addressed were material behavior, design analysis, deformation kinetics, metallurgical characterization, mechanical subelement models, stress analysis, fracture mechanics, viscoplasticity, and thermal loading.

N83-34353*# National Aeronautics and Space Administration. Lewis Research Center, Cleveland, Ohio.
TENSILE AND COMPRESSIVE CONSTITUTIVE RESPONSE OF 316 STAINLESS STEEL AT ELEVATED TEMPERATURES
S. S. MANSON, U. MURALIDHARAN, and G. R. HALFORD *In its* Nonlinear Constitutive Relations for High Temp. Appl. p 13-42 Mar. 1983 refs Prepared in cooperation with Case Western Reserve Univ.
(Contract NAG3-46)
Avail: NTIS HC A16/MF A01 CSCL 20K

Creep rate in compression is lower by factors of 2 to 10 than in tension if the microstructure of the two specimens is the same and are tested at equal temperatures and equal but opposite stresses. Such behavior is characteristic for monotonic creep and conditions involving cyclic creep. In the latter case creep rate in both tension and compression progressively increases from cycle to cycle, rendering questionable the possibility of expressing a time stabilized constitutive relationship. The difference in creep rates in tension and compression is considerably reduced if the tension specimen is first subjected to cycles of tensile creep (reversed by compressive plasticity), while the compression specimen is first subjected to cycles of compressive creep (reversed by tensile plasticity). In both cases, the test temperature is the same and the stresses are equal and opposite. Such reduction is a reflection of differences in microstructure of the specimens resulting from different prior mechanical history. Author

N83-34355*# Michigan State Univ., East Lansing.
EXPERIMENTAL VERIFICATION OF THE NUMBER RELATION AT ROOM AND ELEVATED TEMPERATURES
L. J. LUCAS and J. F. MARTIN *In* NASA. Lewis Research Center Nonlinear Constitutive Relations for High Temp. Appl. p 47-68 Mar. 1983 refs
(Contract NAG3-51)
Avail: NTIS HC A16/MF A01 CSCL 20K

The accuracy of the Neuber equation for predicting notch root stress-strain behavior at room temperature and at 650 C was experimentally investigated. Strains on notched specimens were measured with a non-contacting, interferometric technique and stresses were simulated with smooth specimens. Predictions of notch root stress-strain response were made from the Neuber Equation and smooth specimen behavior. Neuber predictions gave very accurate results at room temperature. However, the predicted interaction of creep and stress relaxation differed from experimentally measured behavior at 650 C. Author

N83-34357*# National Aeronautics and Space Administration. Lewis Research Center, Cleveland, Ohio.
EVALUATION OF INELASTIC CONSTITUTIVE MODELS FOR NONLINEAR STRUCTURAL ANALYSIS
A. KAUFMAN *In its* Nonlinear Constitutive Relations for High Temp. Appl. p 89-106 Mar. 1983 refs
Avail: NTIS HC A16/MF A01 CSCL 20K

The influence of inelastic material models on computed stress-strain states, and therefore predicted lives, was studied for thermomechanically loaded structures. Nonlinear structural analyses were performed on a fatigue specimen which was subjected to thermal cycling in fluidized beds and on a mechanically load cycled benchmark notch specimen. Four incremental plasticity creep models (isotropic, kinematic, combined isotropic-kinematic, combined plus transient creep) were exercised. Of the plasticity models, kinematic hardening gave results most consistent with experimental observations. Life predictions using the computed strain histories at the critical location with a Strainrange Partitioning approach considerably overpredicted the crack initiation life of the thermal fatigue specimen. Author

N83-34359*# Northwestern Univ., Evanston, Ill.
MICROMECHANICALLY BASED CONSTITUTIVE RELATIONS FOR POLYCRYSTALLINE SOLIDS
S. NEMAT-NASSER and T. IWAKUMA *In* NASA. Lewis Research Center Nonlinear Constitutive Relations for High Temp. Appl. p 113-136 Mar. 1983 refs
(Contract NAG3-134)
Avail: NTIS HC A16/MF A01 CSCL 20K

A basic method to estimate the overall mechanical response of solids which contain periodically distributed defects is presented. The method estimates the shape and growth pattern of voids periodically distributed over the grain boundaries in a viscous matrix. The relaxed moduli are obtained for a polycrytalline solid that undergoes relaxation by grain boundary sliding which accounts for the interaction effects. The overall inelastic nonlinear response at elevated temperatures in terms of a model which considers nonlinear power law creep within the grains, and linear viscous flow in the grain boundaries is discussed. E.A.K.

N83-34369*# Massachusetts Inst. of Tech., Cambridge.
TIME-INDEPENDENT ANISOTROPIC PLASTIC BEHAVIOR BY MECHANICAL SUBELEMENT MODELS
T. H. H. PIAN *In* NASA. Lewis Research Center Nonlinear Constitutive Relations for High Temp. Appl. p 283-300 Mar. 1983 refs
(Contract NAG3-33)
Avail: NTIS HC A16/MF A01 CSCL 20K

The paper describes a procedure for modelling the anisotropic elastic-plastic behavior of metals in plane stress state by the mechanical sub-layer model. In this model the stress-strain curves along the longitudinal and transverse directions are represented by short smooth segments which are considered as piecewise linear for simplicity. The model is incorporated in a finite element analysis program which is based on the assumed stress hybrid element and the iscoplasticity-theory. Author

N83-34370*# Akron Univ., Ohio.
CONSTRAINED SELF-ADAPTIVE SOLUTIONS PROCEDURES FOR STRUCTURE SUBJECT TO HIGH TEMPERATURE ELASTIC-PLASTIC CREEP EFFECTS
J. PADOVAN and S. TOVICHAKCHAIKUL *In* NASA. Lewis Research Center Nonlinear Constitutive Relations for High Temp. Appl. p 301-304 Mar. 1983 refs
(Contract NAG3-54)
Avail: NTIS HC A16/MF A01 CSCL 20K

This paper will develop a new solution strategy which can handle elastic-plastic-creep problems in an inherently stable manner. This is achieved by introducing a new constrained time stepping algorithm which will enable the solution of creep initiated pre/postbuckling behavior where indefinite tangent stiffnesses are encountered. Due to the generality of the scheme, both monotone and cyclic loading histories can be handled. The presentation will give a thorough overview of current solution schemes and their short comings, the development of constrained time stepping algorithms as well as illustrate the results of several numerical experiments which benchmark the new procedure. B.W.

N83-34371*# Georgia Inst. of Tech., Atlanta.
STRESS AND FRACTURE ANALYSES UNDER ELASTIC-PLASTIC CREEP CONDITIONS: SOME BASIC DEVELOPMENTS AND COMPUTATIONAL APPROACHES
K. W. REED, R. B. STONESIFER, and S. N. ATLURI *In* NASA. Lewis Research Center Nonlinear Constitutive Relations for High Temp. Appl. p 305-366 Mar. 1983 refs
(Contract NAG3-38)
Avail: NTIS HC A16/MF A01 CSCL 20K

A new hybrid-stress finite element algorith, suitable for analyses of large quasi-static deformations of inelastic solids, is presented. Principal variables in the formulation are the nominal stress-rate and spin. A such, a consistent reformulation of the constitutive equation is necessary, and is discussed. The finite element equations give rise to an initial value problem. Time integration has been accomplished by Euler and Runge-Kutta schemes and

the superior accuracy of the higher order schemes is noted. In the course of integration of stress in time, it has been demonstrated that classical schemes such as Euler's and Runge-Kutta may lead to strong frame-dependence. As a remedy, modified integration schemes are proposed and the potential of the new schemes for suppressing frame dependence of numerically integrated stress is demonstrated. The topic of the development of valid creep fracture criteria is also addressed. B.W.

N83-34372*# National Aeronautics and Space Administration. Lewis Research Center, Cleveland, Ohio.
SIMPLIFIED METHOD FOR NONLINEAR STRUCTURAL ANALYSIS
A. KAUFMAN Sep. 1983 15 p refs
(NASA-TP-2208; E-1646; NAS 1.60:2208) Avail: NTIS HC A02/MF A01 CSCL 20K

A simplified inelastic analysis computer program was developed for predicting the stress-strain history of a thermomechanically cycled structure from an elastic solution. The program uses an iterative and incremental procedure to estimate the plastic strains from the material stress-strain properties and a simulated plasticity hardening model. The simplified method was exercised on a number of problems involving uniaxial and multiaxial loading, isothermal and nonisothermal conditions, and different materials and plasticity models. Good agreement was found between these analytical results and nonlinear finite element solutions for these problems. The simplified analysis program used less than 1 percent of the CPU time required for a nonlinear finite element analysis. Author

N83-34373*# National Aeronautics and Space Administration. Lewis Research Center, Cleveland, Ohio.
A SOLUTION PROCEDURE FOR BEHAVIOR OF THICK PLATES ON A NONLINEAR FOUNDATION AND POSTBUCKLING BEHAVIOR OF LONG PLATES
M. STEIN and P. A. STEIN Sep. 1978 40 p refs
(Contract NCC1-15)
(NASA-TP-2174; L-15587; NAS 1.60:2174) Avail: NTIS HC A03/MF A01 CSCL 20K

Approximate solutions for three nonlinear orthotropic plate problems are presented: (1) a thick plate attached to a pad having nonlinear material properties which, in turn, is attached to a substructure which is then deformed; (2) a long plate loaded in inplane longitudinal compression beyond its buckling load; and (3) a long plate loaded in inplane shear beyond its buckling load. For all three problems, the two dimensional plate equations are reduced to one dimensional equations in the y-direction by using a one dimensional trigonometric approximation in the x-direction. Each problem uses different trigonometric terms. Solutions are obtained using an existing algorithm for simultaneous, first order, nonlinear, ordinary differential equations subject to two point boundary conditions. Ordinary differential equations are derived to determine the variable coefficients of the trigonometric terms. E.A.K.

N83-35412*# National Aeronautics and Space Administration. Lewis Research Center, Cleveland, Ohio.
THE STRUCTURAL RESPONSE OF A RAIL ACCELERATOR
S. Y. WANG 1983 15 p refs Presented at the 2nd Symp. on Electromagnetic Launch Technol., Boston, 1-14 Oct. 1983; sponsored by IEEE
(NASA-TM-83491; E-1820; NAS 1.15:83491) Avail: NTIS HC A02/MF A01 CSCL 20G

The transient response of a 0.4 by 0.6 cm rectangular bore rail accelerator was analyzed by a three dimensional finite element code. The copper rail deflected to a peak value of 0.08 mm in compression and then oscillated at an amplitude of 0.02 mm. Simultaneously the insulating side wall of glass fabric base, epoxy resin laminate (G-10) was compressed to a peak value of 0.13 mm and rebounded to a steady state in extension. Projectile pinch or blowby due to the rail extension or compression, respectively, can be identified by examining the time history of the rail displacement. The effect of blowby was most significant at the side wall characterized by mm size displacement in compression. Dynamic stress calculations indicate that the G-10 supporting material behind the rail is subjected to over 21 MPa at which the G-10 could fail if the laminate was not carefully oriented. Results for a polycarbonate resin (Lexan) side wall show much larger displacements and stresses than for G-10. The tradeoff between the transparency of Lexan and the mechanical strength of G-10 for sidewall material is obvious. Displacement calculations from the modal method are smaller than the results from the direct integration method by almost an order of magnitude, because the high frequency effect is neglected. E.A.K.

N83-35413*# National Aeronautics and Space Administration. Lewis Research Center, Cleveland, Ohio.
ANALYSIS OF AN EXTERNALLY RADIALLY CRACKED RING SEGMENT SUBJECT TO THREE-POINT RADIAL LOADING
B. GROSS, J. E. SRAWLWY, and J. L. SHANNON, JR. 1983 12 p refs Presented at 16th Symp. on Fracture Mech., Columbus, Ohio, 15-17 Aug. 1983; sponsored by Battelle Columbus Labs. and ASTM
(NASA-TM-83482; E-1804; NAS 1.15:83482) Avail: NTIS HC A02/MF A01 CSCL 20K

The boundary collocation method was used to generate Mode 1 stress intensity and crack mouth opening displacement coefficients for externally radially cracked ring segments subjected to three point radial loading. Numerical results were obtained for ring segment outer-to-inner radius ratios (R sub o/R sub i) ranging from 1.10 to 2.50 and crack length to segment width ratios (a/W) ranging from 0.1 to 0.8. Stress intensity and crack mouth displacement coefficients were found to depend on the ratios R sub o/R sub i and a/W as well as the included angle between the directions of the reaction forces. Author

44

ENERGY PRODUCTION AND CONVERSION

Includes specific energy conversion systems, e.g., fuel cells and batteries; global sources of energy; fossil fuels; geophysical conversion; hydroelectric power; and wind power.

A83-13696* National Aeronautics and Space Administration. Lewis Research Center, Cleveland, Ohio.
A REVIEW OF RESONANCE RESPONSE IN LARGE, HORIZONTAL-AXIS WIND TURBINES
T. L. SULLIVAN (NASA, Lewis Research Center, Cleveland, OH) Solar Energy, vol. 29, no. 5, 1982, p. 377-383. refs
(Previously announced in STAR as N82-23711)

A83-13923* Case Western Reserve Univ., Cleveland, Ohio.
PLANAR MULTIJUNCTION HIGH VOLTAGE SOLAR CELL CHIP
G. J. VALCO, V. J. KAPOOR (Case Western Reserve University, Cleveland, OH), and J. C. EVANS, JR. (NASA, Lewis Research Center, Cleveland, OH) Journal of Applied Physics, vol. 53, Nov. 1982, p. 7566-7571. NASA-supported research. refs

A new innovative planar multijunction solar cell chip for concentrated sunlight applications is proposed. The chip consists of many voltage-generating regions, called unit cells, which are connected in series within a single silicon wafer, thereby providing a high open-circuit voltage at multiple sun illumination levels. The unit cells are fabricated on 75 micron thick p-type single crystal silicon substrate. Each chip consists of 1.42 x 9.63 mm n(+)/p collecting junctions on the back of the wafer, while the illuminated front surface area is divided into 0.3 micron deep n(+) regions. The fabrication sequence includes standard degreasing and cleaning procedures, double-sided alignment photomasking, introduction of boron and phosphorus impurities, and photolithography. The open circuit voltage of the chip increased rapidly with illumination up to about 4 AM1 suns, and then began to saturate at the sum of the individual unit cell voltages of 3.5

above 4 AM1 suns. A short circuit density per unit cell of 300 mA/sq cm at 20 AM1 suns was observed. C.D.

A83-24721* General Electric Co., Schenectady, N. Y.
CONTROL DESIGN FOR A WIND TURBINE-GENERATOR USING OUTPUT FEEDBACK
S. H. JAVID, A. MURDOCH, and J. R. WINKELMAN (General Electric Co., Schenectady, NY) In: Conference on Decision and Control, 20th, and Symposium on Adaptive Processes, San Diego, CA, December 16-18, 1981, Proceedings. Volume 1. New York, Institute of Electrical and Electronics Engineers, 1981, p. 451-457. Research supported by the U.S. Department of Energy refs
(Contract DEN3-153)

The modeling and approach to control design for a large horizontal axis wind turbine (WT) generator are presented. The control design is based on a suboptimal output regulator which allows coordinated control of WT blade pitch angle and field voltage for the purposes of regulating electrical power and terminal voltage. Results of detailed non-linear simulation tests of this controller are shown. (Author)

A83-25271*# National Aeronautics and Space Administration. Lewis Research Center, Cleveland, Ohio.
CATALYTIC COMBUSTION WITH STEAM INJECTION
D. N. ANDERSON and R. R. TACINA (NASA, Lewis Research Center, Cleveland, OH) American Society of Mechanical Engineers, Joint Power Generation Conference, Denver, CO, Oct. 17-21, 1982, 9 p. refs
(ASME PAPER 82-JPGC-GT-23)
(Previously announced in STAR as N83-15805)

A83-27138* Washington Univ., Seattle.
RADIATIVE ENERGY RECEIVER FOR HIGH PERFORMANCE ENERGY CONVERSION CYCLES
D. RAULT and A. HERTZBERG (Washington, University, Seattle, WA) In: IECEC '82; Proceedings of the Seventeenth Intersociety Energy Conversion Engineering Conference, Los Angeles, CA, August 8-12, 1982. Volume 1. New York, Institute of Electrical and Electronics Engineers, p. 113-118.
(Contract NAG3-16)

An analysis of gas dynamic processes pertinent to the functioning of earth-based and space-based solar electric power plants is presented, with attention given to potassium vapor as the working fluid. A device is described which features focused photon absorption by a nontransparent flowing gas. The feed flow is effected around the outside walls of a cavity receiver to raise efficiencies by trapping reemitted energy. A theoretical study of the interaction of a photon flux with a coaxial particle flux was performed, with the receiver flow treated as a Graetz flow. The critical parameters were defined, including a figure of merit as the gas enthalpy increase to absorbable energy ratio. A small-scale laboratory model was tested in comparison with the theoretically obtained values. Less than 15% of the absorbed energy was lost through dissipation while an 80% conversion efficiency was attained. D.H.K.

A83-27140*# National Aeronautics and Space Administration. Lewis Research Center, Cleveland, Ohio.
A NEW STRATEGY FOR EFFICIENT SOLAR ENERGY CONVERSION - PARALLEL-PROCESSING WITH SURFACE PLASMONS
L. M. ANDERSON (NASA, Lewis Research Center, Cleveland, OH) In: IECEC '82; Proceedings of the Seventeenth Intersociety Energy Conversion Engineering Conference, Los Angeles, CA, August 8-12, 1982. Volume 1. New York, Institute of Electrical and Electronics Engineers, 1982, p. 125-130. refs
(Previously announced in STAR as N82-29354)

A83-27177*# National Aeronautics and Space Administration. Lewis Research Center, Cleveland, Ohio.
DESIGN FLEXIBILITY OF REDOX FLOW SYSTEMS
N. H. HAGEDORN and L. H. THALLER (NASA, Lewis Research Center, Cleveland, OH) In: IECEC '82; Proceedings of the Seventeenth Intersociety Energy Conversion Engineering Conference, Los Angeles, CA, August 8-12, 1982. Volume 2. New York, Institute of Electrical and Electronics Engineers, 1982, p. 600-609. refs
(Previously announced in STAR as N82-31459)

A83-27183*# National Aeronautics and Space Administration. Lewis Research Center, Cleveland, Ohio.
RESULTS OF CHOPPER-CONTROLLED DISCHARGE LIFE CYCLING STUDIES ON LEAD-ACID BATTERIES
J. G. EWASHINKA and S. M. SIDIK (NASA, Lewis Research Center, Cleveland, OH) In: IECEC '82; Proceedings of the Seventeenth Intersociety Energy Conversion Engineering Conference, Los Angeles, CA, August 8-12, 1982. Volume 2. New York, Institute of Electrical and Electronics Engineers, 1982, p. 648-652. refs
(previously announced in STAR as N82-30700)

A83-27201*# National Aeronautics and Space Administration. Lewis Research Center, Cleveland, Ohio.
PORE SIZE ENGINEERING APPLIED TO STARVED ELECTROCHEMICAL CELLS AND BATTERIES
K. M. ABBEY and L. H. THALLER (NASA, Lewis Research Center, Cleveland, OH) In: IECEC '82; Proceedings of the Seventeenth Intersociety Energy Conversion Engineering Conference, Los Angeles, CA, August 8-12, 1982. Volume 2. New York, Institute of Electrical and Electronics Engineers, 1982, p. 757-764. refs
(Previously announced in STAR as N83-10134)

A83-27236* Cleveland State Univ., Ohio.
PERFORMANCE DEGRADATION AND CLEANING OF PHOTOVOLTAIC ARRAYS
T. J. SHESKIN, G. C. CHANG (Cleveland State University, Cleveland, OH), R. C. CULL, and W. D. KNAPP (NASA, Lewis Research Center, Cleveland, OH) In: IECEC '82; Proceedings of the Seventeenth Intersociety Energy Conversion Engineering Conference, Los Angeles, CA, August 8-12, 1982. Volume 3. New York, Institute of Electrical and Electronics Engineers, 1982, p. 1504-1510. refs

NASA tests results from an 18 mo program of cleaning silicone-encapsulated and glass fronted solar cell panels in urban and desert environments to examine the effects of cleaning on module performance are reported. The panels were cleaned on weekly, monthly, quarterly, or semi-annual basis, while other panels of the same construction were not cleaned and served as controls. Commercially-available detergents and city water were employed for the tests, and the measurements were maintained of the modules' continuing short-circuit current output. The decay of the output was determined by least square regression analyses. Performance degradation was noticeably less in glass covered, rather than silicone-encapsulated modules which decayed faster in urban than in desert environments. Lower frequency cleanings are recommended where labor costs are high. M.S.K.

A83-27260* Varian Associates, Palo Alto, Calif.
SINGLE AND MULTIJUNCTION SPACE SOLAR CELLS GROWN BY ORGANOMETALLIC VAPOR PHASE EPITAXY /OM-VPE/
P. G. BORDEN, R. A. LARUE, M. J. LUDOWISE, and P. E. GREGORY (Varian Associates, Palo Alto, CA) In: IECEC '82; Proceedings of the Seventeenth Intersociety Energy Conversion Engineering Conference, Los Angeles, CA, August 8-12, 1982. Volume 3. New York, Institute of Electrical and Electronics Engineers, 1982, p. 1640-1643.
(Contract NAS3-22232; XP-9-8081-1)

A83-29897* General Electric Co., Schenectady, N. Y.
CONTROL DESIGN AND PERFORMANCE ANALYSIS OF A 6 MW WIND TURBINE-GENERATOR
A. MURDOCH, J. R. WINKELMAN, S. H. JAVID (General Electric Co., Schenectady, NY), and R. S. BARTON (General Electric Co., Valley Forge, PA) (Institute of Electrical and Electronics Engineers, Summer Meeting, San Francisco, CA, July 18-23, 1982) IEEE Transactions on Power Apparatus and Systems (ISSN 0018-9510), vol. PAS-102, May 1983, p. 1340-1347. refs
(Contract DEN3-153)

This paper discusses an approach to the modeling and performance for the preliminary design phase of a large (6.2 MW) horizontal axis wind turbine generator (WTG). Two control philosophies are presented, both of which are based on linearized models of the WT mechanical and electrical systems. The control designs are compared by showing the performance through detailed non-linear time simulation. The disturbances considered are wind gusts, and electrical faults near the WT terminals. Author

A83-32627* National Aeronautics and Space Administration. Lewis Research Center, Cleveland, Ohio.
EXPECTED CYCLE LIFE VS. DEPTH OF DISCHARGE RELATIONSHIPS OF WELL-BEHAVED SINGLE CELLS AND CELL STRINGS
L. H. THALLER (NASA, Lewis Research Center, Cleveland, OH) Electrochemical Society, Journal (ISSN 0013-4651), vol. 130, May 1983, p. 986-990.

The present investigation is concerned with the factors which might influence the cycle life vs. depth of discharge relationship, taking into account the rate of loss of cell capacity, the amount of excess capacity built into the cells, and the penalty in capacity loss resulting from the use of deep depths of discharge. 'First principles' are used to develop a cell life model for somewhat arbitrary conditions. This model is then used to estimate the cycle life vs. depth of discharge relationships for 'well behaved' cells. The stochastic variations associated with groupings of single cells are then introduced to the battery pack cycle life model. The term 'well behaved' cell is used to describe a single cell which does not suffer any abrupt failure mode during the course of its operation. It gradually loses capacity for any number of the usual reasons at a rate which is the product of the fractional depth of discharge and a factor which is characteristic of the cell under consideration. G.R.

A83-36410* Westinghouse Electric Corp., Pittsburgh, Pa.
MEASURED EFFECT OF WIND GENERATION ON THE FUEL CONSUMPTION OF AN ISOLATED DIESEL POWER SYSTEM
P. H. STILLER, G. W. SCOTT (Westinghouse Electric Corp., Pittsburgh, PA), and R. K. SHALTENS (NASA, Lewis Research Center, Cleveland, OH) (Institute of Electrical and Electronics Engineers, Winter Meeting, New York, NY, Jan. 30-Feb. 4, 1983) IEEE Transactions on Power Apparatus and Systems (ISSN 0018-9510), vol. PAS-102, June 1983, p. 1788-1792. Research supported by the U.S. Department of Energy.
(Contract DEN3-275)

The Block Island Power Company (BIPCO), on Block Island, Rhode Island, operates an isolated electric power system consisting of diesel generation and an experimental wind turbine. The 150-kW wind turbine, designated MOD-OA by the U.S. Department of Energy is typically operated in parallel with two diesel generators to serve an average winter load of 350 kW. Wind generation serves up to 60 percent of the system demand depending on wind speed and total system load. Results of diesel fuel consumption measurements are given for the diesel units operated in parallel with the wind turbine and again without the wind turbine. The fuel consumption data are used to calculate the amount of fuel displaced by wind energy. Results indicate that the wind turbine displaced 25,700 lbs. of the diesel fuel during the test period, representing a calculated reduction in fuel consumption of 6.7 percent while generating 11 percent of the total electric energy. The amount of displaced fuel depends on operating conditions and system load. It is also shown that diesel engine throttle activity resulting from wind gusts which rapidly change the wind turbine output do not significantly influence fuel consumption. Author

A83-37790* Communications Satellite Corp., Clarksburg, Md.
LIMITATIONS ON SOLAR CELL OPEN-CIRCUIT VOLTAGE AND EFFICIENCY
A. MEULENBERG, JR. and R. A. ARNDT (COMSAT Laboratories, Clarksburg, MD) COMSAT Technical Review, vol. 13, Spring 1983, p. 57-70. Research sponsored by the Communications Satellite Corp. refs
(Contract NAS3-21227)

Techniques used to determine the open-circuit voltage of solar cells are analyzed. It is noted that the computational procedures for determining the output characteristics of a solar cell depend on a thorough understanding of the behavior of individual components. However, amorphous materials and combination solar cells exhibit increasingly complex behaviors and theoretical analyses therefore are continually more dependent on experimental data for verification. Formulations are defined for the base region and for diffusion length measurement. Experimental results are cited to show that, for low resistivity, planar surface cells, the dark current from the emitter is the dominant factor limiting increases in the Voc, which can be enhanced by improving the efficiency of the doping levels and profile to minimize the effects of bandgap narrowing, junction recombination current, and diffusion length of the emitter region. M.S.K.

A83-44673* Westinghouse Electric Corp., Philadelphia, Pa.
WIND TURBINE GENERATOR INTERACTION WITH DIESEL GENERATORS ON AN ISOLATED POWER SYSTEM
G. W. SCOTT, V. F. WILREKER (Westinghouse Electric Corp., Pittsburgh, PA), and R. K. SHALTENS (NASA, Lewis Research Center, Cleveland, OH) Institute of Electrical and Electronics Engineers, Summer Meeting, Los Angeles, CA, July 17-22, 1983, Paper. 5 p. Research sponsored by the U.S. Department of Energy. refs
(Contract DEN3-275)

The results of a dynamic interaction investigation to characterize any disturbances caused by interfacing the Mod 0A wind turbine (150 kW configuration) with the Block Island utility diesel generator grid are reported. The tests were run when only two diesel generators were on line, and attention was given to power, frequency, and voltage time profiles. The interconnected system was examined in the start-up and synchronization phase, normal shutdown and cut-out of the wind turbine, during fixed pitch generation, and during variable pitch operation. Governors were installed on the diesel generators to accommodate the presence of wind-derived electricity. The blade pitch control was set to maintain power at 150 kW or below. Power and voltage transients were insignificant during start-up and shutdown, and frequency aberrations were within the range caused by load fluctuations. It is concluded that wind turbine generation can be successfully implemented by an isolated utility, even with a significant penetration to the total grid output. M.S.K.

N83-10494* National Aeronautics and Space Administration. Lewis Research Center, Cleveland, Ohio.
METHOD FOR DEPOSITING AN OXIDE COATING Patent
G. E. MCDONALD, inventor (to NASA) 21 Sep. 1982 7 p Filed 23 Mar. 1981 Supersedes N81-24230 (19 - 15, p 2033)
(NASA-CASE-LEW-13131-1; US-PATENT-4,350,574; US-PATENT-APPL-SN-246772; US-PATENT-CLASS-204-56R)
Avail: US Patent and Trademark Office CSCL 10A

A metal oxide coating is plated onto a metal substrate at the cathode from an acid solution which contains an oxidizing agent. The process is particularly useful for producing solar panels. Conventional plating at the cathode avoids the presence of oxidizing agents. Coatings made in accordance with the invention are stable both at high temperatures and while under the influence of high photon flux in the visible range.
Official Gazette of the U.S. Patent and Trademark Office

N83-10502*# TRW, Inc., Redondo Beach, Calif.
DEEP DISCHARGE RECONDITIONING AND SHORTED STORAGE OF BATTERIES Final Report
P. F. RITTERMAN May 1982 72 p refs
(Contract NAS3-21253)
(NASA-CR-167953; NAS 1.26:167953) Avail: NTIS HC A04/MF A01 CSCL 10C

The identification and measurement of hydrogen recombination in sealed nickel-cadium cells makes deep reconditioning on a battery basis safe and feasible. Deep reconditioning improves performance and increases life of nickel-cadium batteries in geosynchronous orbit applications. The hydrogen mechanism and supporting data are presented. Parameter cell design experiments are described which led to the definition of nickel-cadium cells capable of high rate overdischarge without detriment to specific energy. Nickel-cadium calls of identical optimum design were successfully cycled for 7 seasons in simulation of geosynchronous orbit at 75 percent depth-of-discharge with extensive midseason and end-of-season overdischarge at rates varying from C/20 to C/4. Destrucive physical analysis and cyclin data indicated no deterioration or the development of dangerous pressures as a result of the cycling with overdischarge. Author

N83-10554*# National Aeronautics and Space Administration. Lewis Research Center, Cleveland, Ohio.
THE EFFECT OF TA2O5 ON THE INTERACTION BETWEEN SILICON AND ITS CONTACT METALLIZATION
V. G. WEIZER 1982 10 p refs Presented at the 16th Photovoltaic Specialists Conf., San Diego, Calif., 23 Sep. 1982; sponsored by IEEE
(NASA-TM-82948; E-1354; NAS 1.15:82948) Avail: NTIS HC A02/MF A01 CSCL 10A

Evidence is presented showing that the presence of the commonly used antireflection coating material, Ta2O5, on the free surface of contact metallization can either suppress or enhance, depending on the system, the interaction that takes place at elevated temperatures between the metallization and the underlying silicon. The Ta2O5 layer is shown to suppress both the generation and the annihilation of vacancies at the metal free surface which are necessary to support metal-silicon interactions. It is also shown that the mechanical condition of the free metal surface has a significant effect on the passivating ability of the Ta2O5 layer. Author

N83-10555*# National Aeronautics and Space Administration. Lewis Research Center, Cleveland, Ohio.
EVALUATION OF ELECTRODE SHAPE AND NONDESTRUCTIVE EVALUATION METHOD FOR WELDED SOLAR CELL INTERCONNECTS
C. R. BARAONA, S. J. KLIMA, T. J. MOORE, W. E. FREY, and A. F. FORESTIERI Sep. 1982 14 p refs Presented at 16th Photovoltaic Specialists Conf., San Diego, Calif., 27-30 Sep. 1982; sponsored by IEEE
(NASA-TM-82966; E-1386; NAS 1.15:82966) Avail: NTIS HC A02/MF A01 CSCL 10A

Resistance welds of solar cell interconnect tabs were evaluated. Both copper-silver and silver-silver welds were made with various heat inputs and weld durations. Parallel gap and annular gap weld electrode designs were used. The welds were analyzed by light microscope, electron microprobe and scanning laser acoustic microscope. These analyses showed the size and shape of the weld, the relationship between the acoustic micrographs, the visible electrode footprint, and the effect of electrode misalignment. The effect of weld heat input on weld microstructure was also shown. Author

N83-10556*# National Aeronautics and Space Administration. Lewis Research Center, Cleveland, Ohio.
COMBUSTION OF COAL GAS FUELS IN A STAGED COMBUSTOR
T. J. ROSFJORD, J. B. MCVEY, R. A. SEDERQUIST, and D. F. SCHULTZ 1982 14 p refs Presented at the Joint Power Conf., Denver, 17-21 Oct. 1982 Prepared in cooperation with United Technologies Research Center, East Hartford, Conn. and United Technologies Corp., South Windsor, Conn.
(Contract DEN3-149; DE-AI01-77ET-13111)
(NASA-TM-82987; DOE/NASA/13111-12; E-1419; NAS 1.15:82987) Avail: NTIS HC A02/MF A01 CSCL 10B

Gaseous fuels produced from coal resources generally have heating values much lower than natural gas; the low heating value could result in unstable or inefficient combustion. Coal gas fuels may contain ammonia which if oxidized in an uncontrolled manner could result in unacceptable nitrogen oxide exhaust emission levels. Previous investigations indicate that staged, rich lean combustion represents a desirable approach to achieve stable, efficient, low nitrogen oxide emission operation for coal-derived liquid fuels contaning up to 0.8-wt pct nitrgoen. An experimental program was conducted to determine whether this fuel tolerance can be extended to include coal-derived gaseous fuels. The results of tests with three nitrogen-free fuels having heating values of 100, 250, and 350 Btu/scf and a 250 Btu/scf heating value doped to contain 0.7 pct ammonia are presented. Author

N83-10557*# National Aeronautics and Space Administration. Lewis Research Center, Cleveland, Ohio.
EVALUATION OF ADVANCED COMBUSTION CONCEPTS FOR DRY NO SUB X SUPPRESSION WITH COAL-DERIVED, GASEOUS FUELS
K. W. BEEBE (GE, Schenectady, N.Y.), R. A. SYMONDS (GE, Schenectady, N.Y.), and J. J. NOTARDONATO 1982 15 p refs Presented at the Joint Power Conf., Denver, 17-21 Oct. 1982
(Contract DE-AI01-77ET-13111)
(NASA-TM-82985; DOE/NASA/13111-11; E-1417; NAS 1.15:82985) Avail: NTIS HC A02/MF A01 CSCL 10B

The emissions performance of a rich lean combustor (developed for liquid fuels) was determined for combustion of simulated coal gases ranging in heating value from 167 to 244 Btu/scf (7.0 to 10.3 MJ/NCM). The 244 Btu/scf gas is typical of the product gas from an oxygen blown gasifier, while the 167 Btu/scf gas is similar to that from an air blown gasifier. NOx performance of the rich lean combustor did not meet program goals with the 244 Btu/scf gas because of high thermal NOx, similar to levels expected from conventional lean burning combustors. The NOx emissions are attributed to inadequate fuel air mixing in the rich stage resulting from the design of the large central fuel nozzle delivering 71% of the total gas flow. NOx yield from ammonia injected into the fuel gas decreased rapidly with increasing ammonia level, and is projected to be less than 10% at NH3 levels of 0.5% or higher. NOx generation from NH3 is significant at ammonia concentrations significantly less than 0.5%. These levels may occur depending on fuel gas cleanup system design. CO emissions, combustion efficiency, smoke and other operational performance parameters were satisfactory. A test was completed with a catalytic combustor concept with petroleum distillate fuel. Reactor stage NOx emissions were low (1.4g NOx/kg fuel). CO emissions and combustion efficiency were satisfactory. Airflow split instabilities occurred which eventually led to test termination. S.L.

N83-10558*# National Aeronautics and Space Administration. Lewis Research Center, Cleveland, Ohio.
EXPECTED CYCLE LIFE VERSUS DEPTH OF DISCHARGE RELATIONSHIPS OF WELL BEHAVED SINGLE CELLS AND CELL STRINGS
L. H. THALLER 1982 17 p refs Presented at the 162d Meeting of the Electrochem. Soc., Detroit, 17-22 Oct. 1982
(NASA-TM-82957; E-1372; NAS 1.15:82957) Avail: NTIS HC A02/MF A01 CSCL 10C

The factors that might influence the cycle life vs. depth of discharge relationship are examined. This is done first at the single cell level using a progressively more complex cell life model. This is then extended to multicell battery strings where the stochastic aspects associated with groupings of cells are introduced. These relationships are important when considering the weight, cost, and life of battery packs. The results of this theoretical study are compared with a recent review of actual cell cycling data. The factors examined are the rate of capacity loss, the amount of excess capacity built into the cells, and the penalty in capacity loss resulting from the use of deep depths of discharge. This study suggests that the relationship between cycle life and depth of discharge is not one that can be varied of significantly improved by cell research. The relationship appears to be determined by certain more or less fixed cell parameters. Among multicell strings, the standard deviation, as expected, plays an important role in determining overall battery life. Author

N83-10559*# National Aeronautics and Space Administration. Lewis Research Center, Cleveland, Ohio.
MULTIFUEL EVALUATION OF RICH/QUENCH/LEAN COMBUSTOR
J. J. NOTARDONATO, A. S. NOVICK (Detroit Diesel Allison), and D. L. TROTH (Detroit Diesel Allison) 1982 12 p refs Presented at the Joint Power Conf., Denver, 17-21 October 1982
(Contract DE-AI01-77ET-13111)
(NASA-TM-82986; E-1418; DOE/NASA/13111-10; NAS 1.15:82986) Avail: NTIS HC A02/MF A01 CSCL 21B

The fuel flexible combustor technology was developed for application to the Model 570-K industrial gas turbine engine. The technology, to achieve emission goals, emphasizes dry NOx reduction methods. Due to the high levels of fuel-bound nitrogen (FBN), control of NOx can be effected through a staged combustor with a rich initial combustion zone. A rich/quench/lean variable geometry combustor utilizes the technology presented to achieve low NOx from alternate fuels containing FBN. The results focus on emissions and durability for multifuel operation. S.L.

N83-10560*# National Aeronautics and Space Administration. Lewis Research Center, Cleveland, Ohio.
COMBUSTION CHARACTERISTICS OF HYDROGEN. CARBON MONOXIDE BASED GASEOUS FUELS
J. J. NOTARDONATO, D. J. WHITE (Solar Turbines Inc.), A. J. KUBASCO (Solar Turbines Inc.), and R. T. LECREN (Solar Turbines Inc.) 21 Oct. 1981 16 p refs Presented at the Joint Power Conf., Denver, 17-21 Oct. 1982
(Contract DE-AI01-77ET-13111)
(NASA-TM-82998; E-1434; NAS 1.15:82998; DOE/NASA/13111-13) Avail: NTIS HC A02/MF A01 CSCL 21D

An experimental rig program was conducted with the objective of evaluating the combuston performance of a family of fuel gases based on a mixture of hydrogen and carbon monoxide. These gases, in addition to being members of a family, were also representative of those secondary fuels that could be produced from coal by various gasification schemes. In particular, simulated Winkler, Lurgi, and Blue-water low and medium energy content gases were used as fuels in the experimental combustor rig. The combustor used was originally designed as a low NOx rich-lean system for burning liquid fuels with high bound nitrogen levels. When used with the above gaseous fuels this combustor was operated in a lean-lean mode with ultra long residence times. The Blue-water gas was also operated in a rich-lean mode. The results of these tests indicate the possibility of the existence of an 'optimum' gas turbine hydrogen - carbon monoxide based secondary fuel. Such a fuel would exhibit NOx and high efficiency over the entire engine operating range. It would also have sufficient stability range to allow normal light-off and engine acceleration. Solar Turbines Incorporated would like to emphasize that the results presented here have been obtained with experimental rig combustors. The technologies generated could, however, be utilized in future commercial gas turbines. B.W.

N83-10561*# Joint Center for Graduate Study, Richland, Wash.
CONCEPTUAL DESIGN AND COST ANALYSIS OF HYDRAULIC OUTPUT UNIT FOR 15 KW FREE-PISTON STIRLING ENGINE Final Report
M. A. WHITE Aug. 1982 139 p refs Prepared in cooperation with Flow Industries Inc., Kent, Wash.
(Contract DEN3-212)
(NASA-CR-165543; DOE/NASA/0212-1; NAS 1.26:165543)
Avail: NTIS HC A07/MF A01 CSCL 10B

A long-life hydraulic converter with unique features was conceptually designed to interface with a specified 15 kW(e) free-piston Stirling engine in a solar thermal dish application. Hydraulic fluid at 34.5 MPa (5000 psi) is produced to drive a conventional hydraulic motor and rotary alternator. Efficiency of the low-maintenance converter design was calculated at 93.5% for a counterbalanced version and 97.0% without the counterbalance feature. If the converter were coupled to a Stirling engine with design parameters more typcial of high-technology Stirling engines, counterbalanced converter efficiency could be increased to 99.6%. Dynamic computer simulation studies were conducted to evaluate performance and system sensitivities. Production costs of the complete Stirling hydraulic/electric power system were evaluated at $6506 which compared with $8746 for an alternative Stirling engine/linear alternator system. Author

N83-10568*# Mechanical Technology, Inc., Latham, N. Y.
A CONCEPTUAL STUDY OF THE POTENTIAL FOR AUTOMOTIVE-DERIVED AND FREE-PISTON STIRLING ENGINES IN 30- TO 400-KILOWATT STATIONARY POWER APPLICATIONS Final Report
A. VATSKY, H. S. CHEN, and J. DINEEN May 1982 118 p refs
(Contract NAS3-21291)
(NASA-CR-165274; NAS 1.26:165274; MTI-82TR38) Avail: NTIS HC A06/MF A01 CSCL 10B

The technical feasibility of applying automotive-derived kinematic and free-piston Stirling engine concepts for stationary applications was explored. Automotive-derived engines offer cost advantages by providing a mature and developd engine technology base with downrating and parts commonality options for specific applications. Two engine sizes (30 and 400 kW), two Stirling engine configurations (kinematic and free-piston), and two output systems (crankshaft and hydraulic pump) were studied. The study includes the influences of using either hydrogen or helium as the working gas. The first kinematic configuration selects an existing Stirling engine design from an automotive application and adapts it to stationary requirements. A 50,000-hour life requirement was established by downrating the engine to 40 kW and reducing auxiliary loads. Efficiency improvements were gained by selective material and geometric variations and peak brake efficiency of 36.8 percent using helium gas was achieved. The second design was a four-cylinder, 400 kW engine, utilizing a new output drive system known as the z-crank, which provides lower friction losses and variable stroke power control. Three different material and working gas combinations were considered. Brake efficiency levels varied from 40.5 percent to 45.6 percent. A 37.5 kW single-cycle, free-piston hydraulic output design was generated by scaling one cylinder of the original automotive engine and mating it to a counterbalanced reciprocal hydraulic pump. Metallic diaphragms were utilized to transmit power. Author

N83-11579*# Kaman Aerospace Corp., Bloomfield, Conn.
DESIGN AND FABRICATION OF COMPOSITE BLADES FOR THE MOD-1 WIND TURBINE GENERATOR Final Report
W. R. BATESOLE and C. T. GUNSALLUS Nov. 1981 106 p refs
(Contract DEN3-131; DE-AI01-76ET-2030)
(NASA-CR-167987; DOE/NASA/0131-1; NAS 1.26:167987; RR-1685) Avail: NTIS HC A06/MF A01 CSCL 10B

The design, tooling, fabrication, quality control, and testing phases carried out to date, as well as testing still planned are described. Differences from the 150 foot blade which were introduced for cost and manufacturing improvement purposes are discussed as well as the lightning protection system installed in the blades. Actual costs and manhours expended for Blade No. 2 are provided as a base, along with a projection of costs for the blade in production. A.R.H.

N83-12524*# Westinghouse Electric Corp., Pittsburgh, Pa. Advanced Energy Systems Div.
CELL MODULE AND FUEL CONDITIONER DEVELOPMENT Quarterly Report, Jul. - Sep. 1981
J. M. FERET Oct. 1981 33 p
(Contract DEN3-161; DE-AI01-80ET-17088)
(NASA-CR-165462-A; DOE/NASA/0161-9A; NAS 1.26:165462-A; XAL-72760-AL; QR-8) Avail: NTIS HC A03/MF A01 CSCL 10A

A phosphoric acid fuel cell (PAFC) stack design having a 10 kW power rating for operation at higher than atmospheric pressure based on the existing Mark II design configuration is described. Functional analysis, trade studies and thermodynamic cycle analysis for requirements definition and system operating parameter selection purposes were performed. Fuel cell materials and components, and performance testing and evaluation of the repeating electrode components were characterized. The state of the art manufacturing technology for all fuel cell components and the fabrication of short stacks of various sites were established. A 10 kW PAFC stack design for higher pressure operation utilizing the top down systems engineering aproach was developed. S.L.

N83-13579* National Aeronautics and Space Administration. Lewis Research Center, Cleveland, Ohio.
SOLAR CELL HAVING IMPROVED BACK SURFACE REFLECTOR Patent
A. T. CHAI, inventor (to NASA) 19 Oct. 1982 5 p Filed 11 Mar. 1981
(NASA-CASE-LEW-13620-1; US-PATENT-4,335,196; US-PATENT-APPL-SN-242796; US-PATENT-CLASS-136-259; US-PATENT-CLASS-29-572; US-PATENT-CLASS-136-256; US-PATENT-CLASS-357-30; US-PATENT-CLASS-427-88; US-PATENT-CLASS-427-89; US-PATENT-CLASS-427-90; US-PATENT-CLASS-427-91) Avail: US Patent and Trademark Office CSCL 10A

The operating temperature is reduced and the output of a solar cell is increased by using a solar cell which carries electrodes in a grid finger pattern on its back surface. These electrodes are sintered at the proper temperature to provide good ohmic contact. After sintering, a reflective material is deposited on the back surface by vacuum evaporation. Thus, the application of the back surface reflector is separate from the back contact formation. Back surface reflectors formed in conjunction with separate grid finger configuration back contacts are more effective than those formed by full back metallization of the reflector material.

Official Gazette of the U.S. Patent and Trademark Office

N83-13585*# ••023151e of the U.S. Patent and Trademark Office a solar cell is increased by using a solar cell which carries electrodes in a g
MARKET ASSESSMENT OF PHOTOVOLTAIC POWER SYSTEMS FOR AGRICULTURAL APPLICATIONS WORLDWIDE Final Report
A. CABRAAL, D. DELASANTA, J. ROSEN, J. NOLFI (ARD, Inc.), and R. ULMER (ARD, Inc.) Nov. 1981 89 p refs
(Contract DEN3-180; DE-AI01-79ET-20485)
(NASA-CR-165541; DOE/NASA/0180-6; NAS 1.26:165541)
Avail: NTIS HC A05/MF A01 CSCL 10B

Agricultural sector PV market assessments conducted in the Phillippines, Nigeria, Mexico, Morocco, and Colombia are extrapolated worldwide. The types of applications evaluated are those requiring less than 15 kW of power and operate in a stand alone mode. The major conclusions were as follows: PV will be competitive in applications requiring 2 to 3 kW of power prior to 1983; by 1986 PV system competitiveness will extend to applications requiring 4 to 6 kW of power, due to capital constraints, the private sector market may be restricted to applications requiring less than about 2 kW of power; the ultimate purchase of larger systems will be governments, either through direct purchase or loans from development banks. Though fragmented, a significant agriculture sector market for PV exists; however, the market for PV in telecommunications, signalling, rural services, and TV will be larger. Major market related factors influencing the potential for U.S. PV Sales are: lack of awareness; high first costs; shortage of long term capital; competition from German, French and Japanese companies who have government support; and low fuel prices in capital surplus countries. Strategies that may aid in overcoming some of these problems are: setting up of a trade association aimed at overcoming problems due to lack of awareness, innovative financing schemes such as lease arrangements, and designing products to match current user needs as opposed to attempting to change consumer behavior. Author

N83-13588*# General Electric Co., Schenectady, N. Y.
EVALUATION OF CATALYTIC COMBUSTION OF ACTUAL COAL-DERIVED GAS Final Report
J. C. BLANTON and R. A. SHISLER Feb. 1982 54 p refs
(Contract NAS3-22818; DE-AI01-77ET-10350)
(NASA-CR-167842; DOE/NASA/2818-1; NAS 1.26:167842; SRD-82-023) Avail: NTIS HC A04/MF A01 CSCL 21B

The combustion characteristics of a Pt-Pl catalytic reactor burning coal-derived, low-Btu gas were investigated. A large matrix of test conditions was explored involving variations in fuel/air inlet temperature and velocity, reactor pressure, and combustor exit temperature. Other data recorded included fuel gas composition, reactor temperatures, and exhaust emissions. Operating experience with the reactor was satisfactory. Combustion efficiencies were quite high (over 95 percent) over most of the operating range. Emissions of NOx were quite high (up to 500 ppm V and greater), owing to the high ammonia content of the fuel gas. Author

N83-13589*# National Aeronautics and Space Administration. Lewis Research Center, Cleveland, Ohio.
METHODS OF REDUCING ENERGY CONSUMPTION OF THE OXIDANT SUPPLY SYSTEM FOR MHD/STEAM POWER PLANTS
A. J. JUHASZ 1983 15 p Proposed for presentation at the 21st Aerospace Sci. Meeting, Reno, Nev., 10-13 Jan. 1983; sponsored by AIAA
(Contract DE-AI01-77ET-10769)
(NASA-TM-83025; DOE/NASA/10769-28; E-1461; NAS 1.15:83025) Avail: NTIS HC A02/MF A01 CSCL 10B

An in-depth study was conducted to identify possible improvements to the oxidant supply system for combined cycle MHD power plants which would lead to higher thermal efficiency and reduction in the cost of electricity, COE. Results showed that the oxidant system energy consumption could be minimized when the process was designed to deliver a product O2 concentration of 70 mole percent. The study also led to the development of a new air separation process, referred to as liquid pumping and

internal compression. MHD system performance calculations show that the new process would permit an increase in plant thermal efficiency of 0.6 percent while allowing more favorable tradeoffs between magnetic energy and oxidant system capacity requirements. Author

N83-14667*# Case Western Reserve Univ., Cleveland, Ohio.
ELECTROMAGNETIC STUDIES OF REDOX SYSTEMS FOR ENERGY STORAGE Annual Report, Dec. 1981 - Nov. 1982
C. D. WU, D. SCHERSON, and E. YEAGER Nov. 1981 69 p refs
(Contract NAG3-219)
(NASA-CR-169593; NAS 1.26:169593; REPT-2) Avail: NTIS HC A04/MF A01 CSCL 10C

Both chromium and iron couples were studied on various electrode surfaces in acidic perchlorate solution by using rotating ring-disk techniques. It was found that chloride which forms inner sphere coordination complexes with the redox species enhances the electrode kinetics dramatically. The effects of lead underpotential deposition and surface alloy formation on the kinetics of the chromium couple on gold were studied using both linear sweep voltammetry and potential step techniques. The lad underpotential deposition was found to slow down the kinetics of the reduction of the Cr species on gold surfaces although increase the hydrogen overvoltage. The effect on the chromium kinetics can be explained in terms of principally a double layer effect. The underpotential deposition lead species with its positive charge results in a decrease in the concentration of the Cr species at the electrode surface. Similar phenomena were also observed with bismuth underpotential deposition on gold for the iron couple. R.J.F.

N83-14683*# National Aeronautics and Space Administration. Lewis Research Center, Cleveland, Ohio.
THE NASA REDOX STORAGE SYSTEM DEVELOPMENT PROJECT, 1980
Dec. 1982 73 p refs
(Contract DE-AI04-80AL-12726)
(NASA-TM-82940; E-1340; DOE/NASA/12726-18; NAS 1.15:82940) Avail: NTIS HC A04/MF A01 CSCL 10C

The technical accomplishments pertaining to the development of Redox systems and related technology are outlined in terms of the task elements: prototype systems development, application analyses, and supporting technology. Prototype systems development provides for a major procurement to develop an industrial capability to take the current NASA Lewis technology and go on to the design, development, and commercialization of iron-chromium Redox storage systems. Application analyses provides for the definition of application concepts and technology requirements, specific definition studies, and the identification of market sectors and their penetration potential. Supporting technology includes both in house and contractual efforts that encompass implementation of technology improvements in membranes, electrodes, reactant processing, and system design. The status of all elements is discussed. J.M.S.

N83-14688*# National Aeronautics and Space Administration. Lewis Research Center, Cleveland, Ohio.
THE EFFECT OF YAW ON HORIZONTAL AXIS WIND TURBINE LOADING AND PERFORMANCE
J. C. GLASGOW, R. D. CORRIGAN, and D. R. MILLER 1980 22 p refs Presented at the fifth Biennial Wind Energy Conf. and Workshop, Washington, D.C., 5-7 Oct. 1980; sponsored by DOE
(Contract DE-AI07-76ET-20320)
(NASA-TM-82778; E-1108; DOE/NASA/20320-35; NAS 1.15:82778) Avail: NTIS HC A02/MF A01 CSCL 10A

The Mod-0 100 kW experimental wind turbine was tested to determine the effects of yaw on rotor power, blade loads and teeter response. The wind turbine was operated for extended periods at yaw angles up to 49 deg to define average or mean response to yaw. It was determined that the effect of yaw on rotor power can be approximated by the cube of the velocity normal to the rotor disc as long as the yaw angle is less than 30 deg. Blade bending loads were relatively unaffected by yaw, but teeter angle increased with wind speed as the magnitude of the yaw angle exceeded 30 deg, indicating a potential for teeter stop impacts at large yaw angles. No other adverse effects due to yaw were noted during the tests. S.L.

N83-14689*# National Aeronautics and Space Administration. Lewis Research Center, Cleveland, Ohio.
MEASURED PERFORMANCE OF A TIP-CONTROLLED, TEETERED ROTOR WITH AN NACA 64 SUB 3-618 TIP AIRFOIL
R. D. CORRIGAN, J. C. GLASGOW, and P. J. SIROCKY 1982 16 p refs Presented at the Wind and Solar Energy Conf., Kansas City, Mo., 5-7 Apr. 1982
(Contract DE-AI01-76ET-20320)
(NASA-TM-82870; DOE/NASA/20320-40; E-1240; NAS 1.15:82870) Avail: NTIS HC A02/MF A01 CSCL 10A

Tests were conducted on the Mod-O 100 kW Wind Turbine to determine the performance of a tip-controlled rotor having an NACA 64 sub-618 airfoil over the moveable outboard 30% of the blade, while operating at nominal rotor speeds of 21 and 31 rpm. Tests were conducted at two rotor speeds to assess the performance improvement which could be realized with 2-speed operation. Test data are compared with analytical predictions and concluding remarks are presented. The results indicate a clear performance improvement for the 2-speed operation. Author

N83-14690*# National Aeronautics and Space Administration. Lewis Research Center, Cleveland, Ohio.
DOE/NASA LEWIS LARGE WIND TURBINE PROGRAM
R. L. THOMAS 1982 15 p refs Presented at the Natl. Rural Elec. Coop. Assoc. and DOE Rural Elec. Wind Energy Workshop, Boulder, Colo., 1-3 Jun. 1982
(Contract DE-AI01-76ET-20320)
(NASA-TM-82991; DOE/NASA/20320-42; E-1423; NAS 1.15:82991) Avail: NTIS HC A02/MF A01 CSCL 10A

An overview of the large wind turbine activities managed by NASA is given. These activities include resuls from the first and second generation field machines (Mod-0A, -1, and -2), the status of the Department of Interior WTS-4 machine for which NASA is responsible for technical management, and the design phase of the third generation wind turbines (Mod-5). R.J.F.

N83-14691*# National Aeronautics and Space Administration. Lewis Research Center, Cleveland, Ohio.
ASSESSMENT OF ALTERNATIVE POWER SOURCES FOR MOBILE MINING MACHINERY
J. E. CAIRELLI, W. A. TOMAZIC, D. G. EVANS, and J. L. KLANN Dec. 1981 109 p refs
(NASA-TM-82695; E-978; NAS 1.15:82695) Avail: NTIS HC A06/MF A01 CSCL 08I

Alternative mobile power sources for mining applications were assessed. A wide variety of heat engines and energy systems was examined as potential alternatives to presently used power systems. The present mobile power systems are electrical trailing cable, electrical battery, and diesel - with diesel being largely limited in the United States to noncoal mines. Each candidate power source was evaluated for the following requirements: (1) ability to achieve the duty cycle; (2) ability to meet Government regulations; (3) availability (production readiness); (4) market availability; and (5) packaging capability. Screening reduced the list of candidates to the following power sources: diesel, stirling, gas turbine, rankine (steam), advanced electric (batteries), mechanical energy storage (flywheel), and use of hydrogen evolved from metal hydrides. This list of candidates is divided into two classes of alternative power sources for mining applications, heat engines and energy storage systems. E.A.K.

N83-14692* National Aeronautics and Space Administration. Lewis Research Center, Cleveland, Ohio.
HEAT TRANSPARENT HIGH INTENSITY HIGH EFFICIENCY SOLAR CELL Patent
J. C. EVANS, JR., inventor (to NASA) 15 May 1981 7 p Filed 15 May 1981 Supersedes N81-27598 (19 - 18, p 2506)
(NASA-CASE-LEW-12892-1; US-PATENT-4,360,701; US-PATENT-APPL-SN-264380; US-PATENT-CLASS-136-259; US-PATENT-CLASS-136-255; US-PATENT-CLASS-136-256)
Avail: US Patent and Trademark Office CSCL 10A

An improved solar cell design is described. A surface of each solar cell has a plurality of grooves. Each groove has a vertical face and a slanted face that is covered by a reflecting metal. Light rays are reflected from the slanted face through the vertical face where they traverse a photovoltaic junction. As the light rays travel to the slanted face of an adjacent groove, they again traverse the junction. The underside of the reflecting coating directs the light rays toward the opposite surface of solar cell as they traverse the junction again. When the light rays travel through the solar cell and reach the saw toothed grooves on the under side, the process of reflection and repeatedly traversing the junction again takes place. The light rays ultimately emerge from the solar cell. These solar cells are particularly useful at very high levels of insolation because the infrared or heat radiation passes through the cells without being appreciably absorbed to heat the cell.
Official Gazette of the U.S. Patent and Trademark Office

N83-14699*# National Aeronautics and Space Administration. Lewis Research Center, Cleveland, Ohio.
LARGE AREA LOW-COST SPACE SOLAR CELL DEVELOPMENT
C. R. BARONA and J. L. CIONI (NASA, Johnson Space Center) *In* ESA Photovoltaic Generators in Space p 23-26 Jun. 1982 refs
Avail: NTIS HC A15/MF A01 CSCL 10A

A development program to produce 5.9 x 5.9 cm space quality silicon solar cells with a cost goal of 30 $/W is described. Cell types investigated include wraparound dielectric, mechanical wraparound and conventional contact configurations with combinations of 2 or 10 ohm/cm resistivity, back surface reflectors and/or fields, and diffused or ion implanted junctions. A single step process to cut cell and cover glass simultaneously is being developed. Results for cell and array tests are given. Large solar arrays that might use cells of this type are discussed.
Author (ESA)

N83-14705*# National Aeronautics and Space Administration. Lewis Research Center, Cleveland, Ohio.
ON THE CAUSE OF THE FLAT-SPOT PHENOMENON OBSERVED IN SILICON SOLAR CELLS AT LOW TEMPERATURES AND LOW INTENSITIES
V. G. WEIZER, J. D. BRODER, H. W. BRANDHORST, JR., and A. F. FORESTIERI *In* ESA Photovoltaic Generators in Space p 65-70 Jun. 1982 refs
Avail: NTIS HC A15/MF A01 CSCL 10A

A model that explains the flat-spot power loss phenomenon is presented. Evidence suggests that the effect is due to localized metallurgical interactions between the silicon substrate and the contact metallization. These reactions are shown to result in localized regions in which the P-N junction is destroyed and replaced with a metal semiconductor-like interface. The effects of thermal treatment, crystallographic orientation, junction depth, and metallization are shown along with a method of preventing the effect through the suppression of vacancy formation at the free surface of the contact metallization. Data indicating the effectiveness of a TiN diffusion barrier in preventing the effect are also given. Author (ESA)

N83-14708*# National Aeronautics and Space Administration. Lewis Research Center, Cleveland, Ohio.
EFFECTS OF PROCESSING AND DOPANT ON RADIATION DAMAGE REMOVAL IN SILICON SOLAR CELLS
I. WEINBERG, H. W. BRANDHORST, JR., C. K. SWARTZ, and S. MEHTA *In* ESA Photovoltaic Generators in Space p 89-93 Jun. 1982 refs
Avail: NTIS HC A15/MF A01

Gallium and boron doped silicon solar cells, processed by ion implantation followed by either laser or furnace anneal were irradiated by 1 MeV electrons and their postirradiation recovery by thermal annealing was determined. During the postirradiation anneal, gallium doped cells prepared by both processes recovered more rapidly and exhibited none of the severe reverse annealing observed for similarly processed 2 ohm-cm boron doped cells. Ion implanted furnace annealed 0.1 ohm-cm boron doped cells exhibited the lowest post-irradiation annealing temperatures after irradiation. The drastically lowered recovery temperature is attributed to the reduced oxygen and carbon content of the 0.1 ohm-cm cells. Analysis based on defect properties and annealing kinetics indicates that further reduction in annealing temperature is attainable with further reduction in the silicon's carbon and/or divacancy content after irradiation. Author (ESA)

N83-14732*# National Aeronautics and Space Administration. Lewis Research Center, Cleveland, Ohio.
DETERMINATION OF OPTIMUM SUNLIGHT CONCENTRATION LEVEL IN SPACE FOR 3-5 CASCADE SOLAR CELLS
H. B. CURTIS *In* ESA Photovoltaic Generators in Space p 265-270 Jun. 1982 refs
Avail: NTIS HC A15/MF A01

Current-voltage curves were calculated for each cell in a cascade structure using a solar cell diode equation and superposition. Terms for the light generated current, diffusion current, space charge recombination current and series and shunt resistance are included. Individual current voltage curves are added in series with ohmic resistance losses for the cell interconnects to obtain the cascade cell performance. Temperature was varied with concentration, using several models, and ranged from 55 C at one Sun to between 80 and 200 C at 100 Suns. A variety of series resistance and internal resistances were used. Coefficients of the diffusion and recombination terms are strongly temperature dependent. The study indicates that maximum efficiency (30%) occurs in the 50 to 100X Sun concentration range, provided series resistance is below 0.015 ohm-sq cm and cell temperature is 80 C at 100 Suns. Author (ESA)

N83-15805*# National Aeronautics and Space Administration. Lewis Research Center, Cleveland, Ohio.
CATALYTIC COMBUSTION WITH STEAM INJECTION
D. N. ANDERSON and R. R. TACINA 1982 15 p refs Presented at the Joint Power Generation Conf., Denver, 17-21 Oct. 1982; sponsored by ASME
(NASA-TM-82923; E-1315; NAS 1.15:82923) Avail: NTIS HC A02/MF A01 CSCL 10B

The effects of steam injection on (1) catalytic combustion performance, and (2) the tendency of residual fuel to burn in the premixing duct upstream of the catalytic reactor were determined. A petroleum residual, no. 2 diesel, and a blend of middle and heavy distillate coal derived fuels were tested. Fuel and steam were injected together into the preheated airflow entering a 12 cm diameter catalytic combustion test section. The inlet air velocity and pressure were constant at 10 m/s and 600 kPa, respectively. Steam flow rates were varied from 24 percent to 52 percent of the air flow rate. The resulting steam air mixture temperatures varied from 630 to 740 K. Combustion temperatures were in the range of 1200 to 1400 K. The steam had little effect on combustion efficiency or emissions. It was concluded that the steam acts as a diluent which has no adverse effect on catalytic combustion performance for no. 2 diesel and coal derived liquid fuels. Tests with the residual fuel showed that upstream burning could be eliminated with steam injection rates greater than 30 percent of

the air flow rate, but inlet mixture temperatures were too low to permit stable catalytic combustion of this fuel. S.L.

N83-15806*# National Aeronautics and Space Administration. Lewis Research Center, Cleveland, Ohio.
SPACE PHOTOVOLTAIC RESEARCH AND TECHNOLOGY 1982: HIGH EFFICIENCY, RADIATION DAMAGE, AND BLANKET TECHNOLOGY
Washington 1982 263 p refs Conf. held in Cleveland, 20-22 Apr. 1982
(NASA-CP-2256; E-1303; NAS 1.55:2256) Avail: NTIS HC A12/MF A01 CSCL 10A
Space solar cell reseach and development issues are addressed.

N83-15812*# Nebraska Univ., Lincoln. Dept. of Electrical Engineering.
DIFFUSION LENGTH MEASUREMENTS IN SOLAR CELLS: AN ANALYSIS AND COMPARISON OF TECHNIQUES
J. A. WOOLLAM (Universal Energy Systems), A. A. KHAN, R. J. SOUKUP, and A. M. HERMANN (Midwest Research Inst.) *In* NASA. Lewis Research Center Space Photovoltaic Res. and Technol. 1982: High Efficiency, Radiation Damage, and Blanket Technol. p 45-56 1982 refs
(Contract NAG3-120)
Avail: NTIS HC A12/MF A01 CSCL 10A
A brief review of the major techniques for measuring minority carrier diffusion lengths in solar cells is given. Emphasis is placed on comparing limits of applicability for each method, especially as applied to silicon cells or to gallium arsenide cells, including the effects of radiation damage. Author

N83-15813*# Varian Associates, Palo Alto, Calif
PROGRESS TOWARD CASCADE CELLS MADE BY OM-VPE
P. G. BORDEN, R. A. LARUE, and M. J. LUDOWISE *In* NASA. Lewis Research Center Space Photovoltaic Res. and Technol. 1982: High Efficiency, Radiation Damage, and Blanket Technol. p 57-65 1982 refs Sponsored in part by DOE
(Contract NAS3-22232)
Avail: NTIS HC A12/MF A01 CSCL 10A
Organometallic Vapor Phase Epitaxy (COM-VPE) was used to make a sophisticated monolithic cascade cell, with a peak AMO efficiency of 16.6%, not corrected for 14% grid coverage. The cell has 9 epitaxial layers. The top cell is 1.35 microns thick with a 0.1 micron thich emitter. Both cells are heteroface n-p structures. The cascade cell uses metal interconnects. Details of growth and processing are described. Author

N83-15814*# National Aeronautics and Space Administration. Lewis Research Center, Cleveland, Ohio.
DETERMINATION OF OPTIMUM SUNLIGHT CONCENTRATION LEVEL IN SPACE FOR 3-5 CASCADE SOLAR CELLS
H. B. CURTIS *In its* Space Photovoltaic Res. and Technol. 1982: High Efficiency, Radiation Damage, and Blanket Technol. p 69-78 1982 refs Previously announced as 82N-32853
Avail: NTIS HC A12/MF A01 CSCL 10A
The optimum range of concentration levels in space for III-V cascade cells was calculated using a realistic solar cell diode equation. Temperature was varied with concentration using several models and ranged from 55 C at 1 sun to between 80 and 200 C at 100 suns. A variety of series resistance and internal resistances were used. Coefficients of the diffusion and recombination terms are strongly temperature dependent. The study indicates that the maximum efficiency of 30 percent occurs in the 50 to 100 sun concentration range provided series resistance is below 0.015 ohm-sq cm and cell temperature is about 80 C at 100 suns.
Author

N83-15815*# National Aeronautics and Space Administration. Lewis Research Center, Cleveland, Ohio.
SOLAR ENERGY CONVERSION USING SURFACE PLASMONS FOR BROADBAND ENERGY TRANSPORT
L. M. ANDERSON *In its* Space Photovoltaic Res. and Technol. 1982: High Efficiency, Radiation Damage, and Blanket Technol. p 79-87 1982 refs
Avail: NTIS HC A12/MF A01 CSCL 10A
A new strategy for efficient solar energy conversion based on parallel processing with surface plasmons is introduced. The approach is unique in identifying: (1) a broadband carrier with suitable range for energy transport, and (2) a technique to extract more energy from the more energetic photons, without sequential losses or unique materials for each frequency band. The aim is to overcome the fundamental losses associated with the broad solar spectrum and to achieve a higher level of spectrum splitting than has been possible in semiconductor systems. Author

N83-15818*# Rensselaer Polytechnic Inst., Troy, N. Y.
DIFFUSED P+-N SOLAR CELLS IN BULK GAAS
J. M. BORREGO and S. K. GHANDHI *In* NASA. Lewis Research Center Space Photovoltaic Res. and Technol. 1982: High Efficiency, Radiation Damage, and Blanket Technol. p 105-108 1982 refs
(Contract NAG3-188)
Avail: NTIS HC A12/MF A01 CSCL 10A
Recently melt grown GaAs, made by liquid encapsulation techniques, has become available. This material is of sufficiently good quality to allow the fabrication of solar cells by direct diffusion. Results obtained with p(+)/n junction solar cells made by zinc diffusion are described. The quality of bulk GaAs for this application is evaluated. Author

N83-15819*# Rockwell International Corp., Thousand Oaks, Calif. Microelectronics Research and Development Center.
ADVANCES IN LARGE-DIAMETER LIQUID ENCAPSULATED CZOCHRALSKI GAAS
R. T. CHEN, D. E. HOLMES, and C. G. KIRKPATRICK *In* NASA. Lewis Research Center Space Photovoltaic Res. and Technol. 1982: High Efficiency, Radiation Damage, and Blanket Technol. p 109-122 1982 refs
(Contract NAS3-22224; NAS3-22235)
Avail: NTIS HC A12/MF A01 CSCL 10A
The purity, crystalline perfection, and electrical properties of n- and p-type GaAs crystals grown by the liquid encapsulated Czochralski (LEC) technique are evaluated. The determination of the dislocation density, incidence of twinning, microstructure, background purity, mobility, and minority carrier diffusion length is included. The properties of the LEC GaAs crystals are generally comparable to, if not superior to those of small-diameter GaAs material grown by conventional bulk growth techniques. As a result, LEC GaAs is suitable for application to minority carrier devices requiring high-quality and large-area substrates. Author

N83-15820*# Hughes Research Labs., Malibu, Calif.
GAAS SOLAR CELLS FOR CONCENTRATOR SYSTEMS IN SPACE
R. Y. LOO, R. C. KNECHTLI, and G. S. KAMATH *In* NASA. Lewis Research Center Space Photovoltaic Res. and Technol. 1982: High Efficiency, Radiation Damage, and Blanket Technol. p 123-130 1983 refs
(Contract NAS3-22227)
Avail: NTIS HC A12/MF A01 CSCL 10A
Cells for operation in space up to more than 100 suns were made, and an AMO efficiency of 21% at 100 suns with these cells was obtained. The increased efficiency resulted not only from the higher open circuit voltage associated with the higher light intensity (higher short circuit current); it also benefitted from the increase in fill factor caused by the lower relative contribution of the generation recombination current to the forward bias current when the cell's operating current density is increased. The experimental cells exhibited an AMO efficiency close to 16% at 200 C. The prospect of exploiting this capability for the continuous

annealing of radiation damage or for high temperature missions (e.g., near Sun missions) remains therefore open. Space systems with concentration ratios on the order of 100 suns are presently under development. The tradeoff between increased concentration ratio and increased loss due to the cell's series resistance remains attractive even for space applications at a solar concentrator ratio of 100 suns. In the design of contact configuration with low enough series resistance for such solar concentration ratios, the shallow junction depth needed for good radiation hardness and the thin AlGaAs layer thickness needed to avoid excessive optical absorption losses have to be retained. Author

N83-15821*# National Aeronautics and Space Administration. Lewis Research Center, Cleveland, Ohio.
THE EFFECT OF DIFFERENT SOLAR SIMULATORS ON THE MEASUREMENT OF SHORT-CIRCUIT CURRENT TEMPERATURE COEFFICIENTS
H. B. CURTIS and R. E. HART, JR. *In its* Space Photovoltaic Res. and Technol. 1982: High Efficiency, Radiation Damage, and Blanket Technol. p 131-136 1982 refs
Avail: NTIS HC A12/MF A01 CSCL 10A

Gallium arsenide solar cells are considered for several high temperature missions in space. Both near-Sun and concentrator missions could involve cell temperatures on the order of 200 C. Performance measurements of cells at elevated temperatures are usually made using simulated sunlight and a matched reference cell. Due to the change in bandgap with increasing temperature at portions of the spectrum where considerable simulated irradiance is present, there are significant differences in measured short circuit current at elevated temperatures among different simulators. To illustrate this, both experimental and theoretical data are presented for gallium arsenide cells. Author

N83-15825*# Lincoln Lab., Mass. Inst. of Tech., Lexington.
MICRODISTRIBUTION OF OXYGEN IN SILICON AND ITS EFFECTS ON ELECTRONIC PROPERTIES
H. C. GATOS, B. Y. MAO, K. NAUKA, and J. LAGOWSKI *In* NASA. Lewis Research Center Space Photovoltaic Res. and Technol. 1982: High Efficiency, Radiation Damage, and Blanket Technol. p 163-169 1982 refs
(Contract NSG-3017)
Avail: NTIS HC A12/MF A01 CSCL 10A

The effects of interstitial oxygen on the electrical characteristics of Czochralski-grown silicon crystals were investigated for the first time on a microscale. It was found that the generation of thermal donors is not a direct function of the oxygen concentration. It was further found that the minority carrier life-time decreases with increasing oxygen concentration, on a microscale in as-grown crystals. It was thus shown, again for the first time, that oxygen in as grown crystals is not electronically inert as generally believed. Preannealing at 1200 C commonly employed in device fabrication, was found to suppress the donor generation at 450 C and to decrease the deep level concentrations. Author

N83-15826*# National Aeronautics and Space Administration. Lewis Research Center, Cleveland, Ohio.
RADIATION DAMAGE AND ANNEALING IN LARGE AREA N+/P/P+ GAAS SHALLOW HOMOJUNCTION SOLAR CELLS
D. J. FLOOD, D. J. BRINKER, C. K. SWARTZ, R. E. HART, JR., and J. C. C. FAN (MIT, Lincoln Lab., Lexington) *In its* Space Photovoltaic Res. and Technol. 1982: High Efficiency, Radiation Damage, and Blanket Technol. p 179-184 1982 refs
Avail: NTIS HC A12/MF A01 CSCL 10A

Annealing of radiation damage was observed for the first time in VPE-grown, 2- by 2-cm, n+/p/p+ GaAs shallow homojunction solar cells. Electrical performance of several cells was determined as a function of 1-MeV electron fluence in the range of 10 to the 13th power to 10 to the 15th power e-/sq cm and as a function of thermal annealing time at various temperatures. Degradation of normalized power output after a fluence of 10 to the 15th power 1-MeV electrons/sq cm ranged from a low of 24 to 31 percent of initial maximum power. Normalized short circuit current degradation was limited to the range from 10 to 19 percent of preirradiated values. Thermal annealing was carried out in a flowing nitrogen gas ambient, with annealing temperatures spanning the range from 125 to 200 C. Substantial recovery of short circuit current was observed at temperatures as low as 175 C. In one case improvement by as much as 10 percent of the postirradiated value was observed. The key features of these cells are their extremely thin emitter layers (approxmately 0.05 micrometers) the absence of any Al sub xGd sub 1-x As passivating window layer, and their fabrication by vapor phase epitaxy. Author

N83-15833*# National Aeronautics and Space Administration. Lewis Research Center, Cleveland, Ohio.
MICROSTRUCTURAL ANALYSIS OF SOLAR CELL WELDS
T. J. MOORE, G. K WATSON, and C. R. BARAONA *In its* Space Photovoltaic Res. and Technol. 1982: High Efficiency, Radiation Damage, and Blanket Technol. p 237-249 1982 refs
Avail: NTIS HC A12/MF A01 CSCL 10A

Parallel-gap resistance welding of silicon solar cells with copper interconnects results in complex microstructural variations that depend on the welding variables. At relatively low heat input solid-state welds are produced. At medium heat the Ag-Cu eutectic forms resulting in a braze joint. High heat produces a fusion weld with complete melting of the silver layer on the silicon solar cell. If the silicon is also melted, cracking occurs in the silicon cell below the weld nugget. These determinations were made using light microscopy, microprobe, and scanning electron microscopy analyses. Author

N83-15834*# National Aeronautics and Space Administration. Lewis Research Center, Cleveland, Ohio.
EVALUATION OF SOLAR CELL WELDS BY SCANNING ACOUSTIC MICROSCOPY
S. J. KLIMA, W. E. FREY, and C. R. BARAONA *In its* Space Photovoltaic Res. and Technol. 1982: High Efficiency, Radiation Damage, and Blanket Technol. p 251-258 1982 refs
Avail: NTIS HC A12/MF A01 CSCL 10A

Scanning laser acoustic microscopy was used to nondestructively evaluate solar cell interconnect bonds made by resistance welding. Both copper-silver and silver-silver welds were analyzed. The bonds were produced either by a conventional parallel-gap welding technique using rectangular electrodes or new annular gap design with a circular electrode cross section. With the scanning laser acoustic microscope, it was possible to produce a real time television image which reveales the weld configuration as it relates to electrode geometry. The effect of electrode misalinement with the surface of the cell was also determined. A preliminary metallographic analysis was performed on selected welds to establish the relationship between actual size and shape of the weld area and the information available from acoustic micrographs. Author

N83-15837*# National Aeronautics and Space Administration. Lewis Research Center, Cleveland, Ohio.
RADIATION DAMAGE
I. WEINBERG *In its* Space Photovoltaic Res. and Technol. 1982: High Efficiency, Radiation Damage, and Blanket Technol. p 267-268 1982
Avail: NTIS HC A12/MF A01 CSCL 10A

The radiation damage workshop considered a variety of topics among which were the need for equivalent electron fluences in gallium arsenide, the possibility of 15 percent end-of-life efficiencies for silicon, increasing radiation resistance in gallium arsenide, annealing of radiation damage and the need for radiation damage studies in cascade cells. The workshop members agreed that a high priority should be assigned to obtaining equivalent electron fluences for gallium arsenide cells. It was suggested that 1 MeV would be a reasonable electron energy for this purpose. Special care should be given to proton irradiations particularly for energies below 1 MeV. In addition, omnidirectional rather than normal incidence protons should be used. It was also agreed that there was a need for obtaining damage coefficients in gallium arsenide. In silicon, there is a requirement for additional flight data, especially

in proton dominated orbits. These data are needed to further check the accuracy of the 1 MeV equivalence fluences. L.F.M.

N83-15839*# Engelhard Industries, Inc., Edison, N.J.
DEVELOP AND TEST FUEL CELL POWERED ON-SITE INTEGRATED TOTAL ENERGY SYSTEM Quarterly Report
A. KAUFMAN and G. K. JOHNSON 3 Nov. 1982 47 p
(Contract DEN3-241; DE-AI01-80ET-17088)
(NASA-CR-168020; NAS 1.26:168020; QR-5) Avail: NTIS HC A03/MF A01 CSCL 10A

Satisfactory performance is reported for the first 12-cell sub-stack of the 5 kW rebuild using improved ABA reactant distribution plates. Construction and test results are described for the first full-sized single-cell test (0.33 m x 0.56 m). Test duration was 450 hours. Plans are outlined for construction and testing of two methanol reformer units based on commercially-available shell-and-tube heat exchangers. A 5 kW-equivalent precursor and a 50 kW-equivalent prototype will be built. Supporting design and single-tube experimental data are presented. Stack support efforts are summarized on corrosion currents of graphite materials and acid-management of single-cell test facilities. Comparative properties are summarized for the two methanol/steam reforming catalysts evauated under Task V (now completed); T2107RS and C70-2RS. Author

N83-15840*# National Aeronautics and Space Administration. Lewis Research Center, Cleveland, Ohio.
THE WORLDWIDE MARKET FOR PHOTOVOLTAICS IN THE RURAL SECTOR
W. A. BRAINARD 1982 15 p refs Presented at 16th Photovoltaic Specialists Conf., San Diego, Calif., 27-30 Sep. 1982; sponsored by IEEE
(Contract DE-AI01-79ET-20485)
(NASA-TM-83035; E-1473; DOE/NASA/20485-13; NAS 1.15:83035) Avail: NTIS HC A02/MF A01 CSCL 10A

The worldwide market for stand-alone photovoltaic power systems in three specific segments of the rural sector were determined. The worldwide market for photovoltaic power systems for village power, cottage industry, and agricultural applications were addressed. The objectives of these studies were to: The market potential for small stand-alone photovoltaic power system in specific application areas was assessed. Technical, social and institutional barriers to PV utilization were identified. Funding sources available to potential users was also identified and marketing strategies appropriate for each sector were recommended to PV product manufacturers. The studies were prepared on the basis of data gathered from domestic sources and from field trips to representative countries. Both country-specific and sector-specific results are discussed, and broadly applicable barriers pertinent to international marketing of PV products are presented. S.L.

N83-15847*# National Aeronautics and Space Administration. Lewis Research Center, Cleveland, Ohio.
NASA LEWIS RESEARCH CENTER COMBUSTION MHD EXPERIMENT
J. M. SMITH *In* R and D Associates Proc. of the AFOSR Spec. Conf. on Prime-Power for High Energy Space Systems, Vol. 1 10 p 1982 refs
Avail: NTIS HC A99/MF A01 CSCL 10B

The MHD power generation experiments were conducted in a high field strength cryomagnet which was adapted from an existing facility. In its original construction, it consisted of 12 high purity aluminum coils pool cooled in a bath of liquid neon. In this configuration, a peak field of 15 tesla was produced. For the present experiments, the center four coils were removed and a 23 cm diameter transverse warm bore tube was inserted to allow the placement of the MHD experiment between the remaining eight coils. In this configuration, a peak field of 6 tesla should be obtainable. The time duration of the experiment is limited by the neon supply which allows on the order of 1 minute of total operating time followed by an 18-hour reliquefaction period. As a result, the experiments are run in a pulsed mode. The run duration for the data presented here was 5 sec. The magnetic field profile along the MHD duct is shown. Since the working fluid is in essence superheated steam, it is easily water quenched at the exit of the diffuser and the components are designed vacuum tight so that the exhaust pipe and demister an be pumped down to simulate the vacuum of outer space. Author

N83-15865*# National Aeronautics and Space Administration. Lewis Research Center, Cleveland, Ohio.
DIRECT CONVERSION OF INFRARED RADIANT ENERGY FOR SPACE POWER APPLICATIONS Final Report
R. C. FINKE *In* R and D Associates Proc. of the AFOSR Spec. Conf. on Prime-Power for High Energy Space Systems, Vol. 2 22 p 1982
Avail: NTIS HC A99/MF A01

A proposed technology to convert the earth radiant energy (infrared albedo) for spacecraft power is presented. The resultant system would eliminate energy storage requirements and simplify the spacecraft design. The design and performance of a infrared rectenna is discussed. M.G.

N83-15866*# Rice Univ., Houston, Tex. Dept. of Space Physics and Astronomy.
THE PHOTOTRON: A LIGHT TO RF ENERGY CONVERSION DEVICE Final Report
J. W. FREEMAN and S. SIMONS *In* R and D Associates Proc. of the AFOSR Spec. Conf. on Prime-Power for High Energy Space Systems, Vol. 2 17 p 1982 refs
(Contract NAG3-29)
Avail: NTIS HC A99/MF A01

The phototron, a photoelectric device that converts light to radio frequency energy, is described. It is a vacuum tube, free electron, device that is mechanically similar to a reflex klystron with the hot filament cathode replaced by a large area photocathode. The device can operate either with an external voltage source used to accelerate the photoelectrons or with zero bias voltage; in which case the photokinetic energy of the electrons sustains the R.F. oscillations in the tuned R.F. circuit. One basic design of the phototron was tested. Frequencies as high as about 1 GHz and an overall efficiency of about 1% in the biased mode were obtained. In the unbiased mode, the frequencies of operation and efficiences are considerably lower. Success with test model suggests that considerable improvements are possible through design refinements. One such design refinement is the reduction of the length of the electron flight path. M.G.

N83-15869# National Aeronautics and Space Administration. Lewis Research Center, Cleveland, Ohio.
OVERVIEW OF HIGH-TEMPERATURE MATERIALS FOR HIGH-ENERGY SPACE POWER SYSTEMS Final Report
N. T. SAUNDERS *In* R and D Associates Proc. of the AFOSR Spec. Conf. on Prime-Power for High Energy Space Systems, Vol. 2 39 p 1982
Avail: NTIS HC A99/MF A01 CSCL 10B

The current state of technology and some of the more pressing research needs and challenges associated with the possible use of high temperature materials in future high energy space power systems are discussed. Particularly, emphasis is on the need to improve and quantify the fundamental understanding of the effects of the following: (1) fast neutron radiation on the properties and behavior of nuclear reactor fuels and claddings; and (2) long term, high temperature, space (vacuum) exposure on the properties of refractory metals considered for use as structural materials in various power conversion systems. M.G.

N83-15880*# National Aeronautics and Space Administration. Lewis Research Center, Cleveland, Ohio.
GROWTH OF DIAMONDLIKE FILMS FOR POWER APPLICATIONS Final Report
B. A. BANKS *In* R and D Associates Proc. of the AFOSR Spec. Conf. on Prime-Power for High Energy Space Systems, Vol. 2 33 p 1982 refs
Avail: NTIS HC A99/MF A01

Diamond has a high thermal conductivity (approximately 5 times that of copper) and is an ideal heat sink material for high power semiconductor devices as well as being of interest as a semiconductor material. Numerous vacuum deposition processes are being evaluated by NASA-LeRC which have demonstrated the capability to deposit carbon films having some of the properties of diamond. Current activities include investigation of high deposition rate vacuum processes suitable for synthesis of diamondlike carbon films. The results of recent film characterization tests are reported. Author

N83-15911*# National Aeronautics and Space Administration. Lewis Research Center, Cleveland, Ohio.
THE NASA LEWIS LARGE WIND TURBINE PROGRAM
R. L. THOMAS and D. H. BALDWIN *In* Midwest Res. Inst. Fifth Bien. Wind Energy Conf. and Workshop (WW5) p 39-58 1981 refs
Avail: NTIS HC A23/MF A01 CSCL 10A

The large wind turbine program activities are reviewed. These activities include results from the first and second generation field machines (Mod-OA, 1, and 2), the design phase of the third generation wind turbine (Mod-5) and the advanced technology projects. The status of the WTS-4 machine is also presented. S.L.

N83-15916*# National Aeronautics and Space Administration. Lewis Research Center, Cleveland, Ohio.
OPERATING EXPERIENCE WITH THE 200 KW MOD-OA WIND TURBINE GENERATORS
A. G. BIRCHENOUGH, A. L. SAUNDERS, T. W. NYLAND, and R. K. SHALTENS *In* Midwest Res. Inst. Fifth Bien. Wind Energy Conf. and Workshop (WW5) p 107-118 1981 refs
Avail: NTIS HC A23/MF A01 CSCL 10A

The machine configuration and its advantages and disadvantages, particularly as it affects reliability are discussed. The machine performance, both availability and power output characteristics are described. The Mod-OA operational experience is documented. The characteristics of the wind energy generated, the machine performance, and the subsystem strengths and weaknesses are discussed. An assessment of the project success in fulfilling its goals and objectives is also presented. S.L.

N83-16857*# National Aeronautics and Space Administration. Lewis Research Center, Cleveland, Ohio.
CONSTRUCTION OF LOW-COST, MOD-OA WOOD COMPOSITE WIND TURBINE BLADES
R. F. LARK 1983 17 p refs Proposed for presentation at the 28th Natl. SAMPLE Symp. and Exposition, Anaheim, Calif., 12-14, 1983
(Contract DE-AI01-76ET-20320)
(NASA-TM-83046; E-1493; DOE/NASA/20320-43; NAS 1.15:83046) Avail: NTIS HC A02/MF A01 CSCL 10A

Two sixty-foot, low-cost, wood composite blades for service on 200 kW Mod-OA wind turbines were constructed. The blades were constructed of epoxy resin-bonded Douglas fir veneers for the leading edge sections, and paper honeycombcored, birch plywood faced panels for the afterbody sections. The blades were joined to the wind turbine hub by epoxy resin-bonded steel load take-off studs embedded into the root end of the blades. The blades were installed on the 200 kW Mod-OA wind turbine facility at Kahuku, Hawaii, The blades completed nearly 8,000 hours of operation over an 18 month period at an average power of 150 kW prior to replacement with another set of wood composite blades. The blades were replaced because of a corrosion failure of the steel shank on one stud. Inspections showed that the wood composite structure remained in excellent condition. Author

N83-16859*# Westinghouse Electric Corp., Pittsburgh, Pa. Advanced Systems Div.
THE MOD-OA 200 KILOWATT WIND TURBINE GENERATOR DESIGN AND ANALYSIS REPORT Final Report
T. S. ANDERSEN, C. A. BODENSCHATZ, A. G. EGGERS, P. S. HUGHES, R. F. LAMPE, M. H. LIPNER, and J. R. SCHORNHORST Aug. 1980 68 p refs
(Contract DEN3-163; DE-AI01-76ET-20370)
(NASA-CR-165127; DOE/NASA/0163-1; NAS 1.26:165127; AESD-TME-3051) Avail: NTIS HC A04/MF A01 CSCL 10A

The project requirements, approach, system description, design requirements, design, analysis, system tests, installation safety considerations, failure modes and effects analysis, data acquisition, and initial performance for the MOD-OA 200 kw wind turbine generator are discussed. The components, the rotor, driven train, nacelle equipment, yaw drive mechanism and brake, tower, foundation, electrical system, and control systems are presented. The rotor includes the blades, hub and pitch change mechanism. The drive train includes the low speed shaft, speed increaser, high speed shaft, and rotor brake. The electrical system includes the generator, switchgear, transformer, and utility connection. The control systems are the blade pitch, yaw, and generator control, and the safety system. Manual, automatic, and remote control and Dynamic loads and fatigue are analyzed. E.A.K.

N83-18022*# National Aeronautics and Space Administration. Lewis Research Center, Cleveland, Ohio.
EVALUATION OF PRODUCTION VERSION OF THE NASA IMPROVED INORGANIC-ORGANIC SEPARATOR
D. SHEIBLEY Jan. 1983 28 p refs
(NASA-TM-83018; E-1453; NAS 1.15:83018) Avail: NTIS HC A03/MF A01 CSCL 10A

The technology of an inorganic-organic (I/O) separator, which demonstrated improved flexibility, reduced cost, production feasibility and improved cycle life was developed. Substrates to replace asbestos and waterbased separator coatings to replace the solvent based coatings were investigated. An improved fuel cell grade asbestos sheet was developed and a large scale production capability for the solvent based I/O separator was demonstrated. A cellulose based substrate and a nonwoven polypropylene fiber substrate were evaluated as replacements for the asbestos. Both the cellulose and polypropylene substrates were coated with solvent based and water based coatings to produce a modified I/O separator. The solvent based coatings were modified to produce aqueous separator coatings with acceptable separator properties. A single ply fuel cell grade asbestos with a binder (BTA) was produced. It has shown to be an acceptable substrate for the solvent and water based separator coatings, an acceptable absorber for alkaline cells, and an acceptable matrix for alkaline fuel cells. The original solvent based separator (K19W1), using asbestos as a substrate, was prepared. S.L.

N83-19226*# Budd Co., Fort Washington, Pa.
DESIGN AND EVALUATION OF LOW-COST STAINLESS STEEL FIBERGLASS FOAM BLADES FOR LARGE WIND DRIVEN GENERATING SYSTEMS Final Report
W. S. EGGERT Oct. 1982 57 p refs
(Contract DEN3-129; DE-AI01-79ET-20320)
(NASA-CR-165491; DOE/NASA/0129-1; NAS 1.26:165491)
Avail: NTIS HC A04/MF A01 CSCL 10A

A low cost wind turbine blade based on a stainless steel fiberglass foam Budd blade design concept, was evaluated for its principle characteristics, low cost features, and its advantages and disadvantages. A blade structure was designed and construction methods and materials were selected. A complete blade tooling concepts, various technical and economic analysis, and evaluations of the blade design were performed. A comprehensive fatigue test program is conducted to provide data to verify the design stress allowables. E.A.K.

N83-19228*# STD Research Corp., Arcadia, Calif.
ANALYTICAL INVESTIGATION OF CRITICAL MHD PHENOMENA Final Annual Report, Sep. 1980 - Sep. 1981
Sep. 1981 37 p refs
(Contract DEN3-202; DE-AI01-77ET-10769)
(NASA-CR-168079; NAS 1.26:168079; DOE/NASA/0202-1; STDR-82-15) Avail: NTIS HC A03/MF A01 CSCL 10A

Development and analysis of schemes for suppression of the startup overvoltage transient in the AEDC High Performance Demonstration Experiment (HPDE), analysis of performance enhancement due to electrode voltage drop reduction by use of pyrolytic graphites in the HPDE, prediction of optimal loading schemes for the HPDE, prediction of PHDE performance with a diagonal electrical connection, and predictions of the likelihood and effects of axial current leakage between adjacent electrodes in the HPDE are reviewed. Simulations of tests at the AEDC/HPDE with STD Research Corporation multidimensional and time dependent computer codes provided additional validation for the computer codes and shed light on physical mechanisms which govern performance and durability of MHD power generators. The magnetoaerothermal effect was predicted by STD Research Corporation to have a significant effect on the HPDE/MHD generator performance at high interaction. Author

N83-19231*# National Aeronautics and Space Administration. Lewis Research Center, Cleveland, Ohio.
LARGE HORIZONTAL-AXIS WIND TURBINES
R. W. THRESHER, ed. (Oregon State Univ., Corvallis) 1982 823 p refs Workshop held in Cleveland, 28-30 Jul. 1981 Sponsored in part by DOE
(NASA-CP-2230; NAS 1.55:2230; CONF-810752; SERI/CP-635-1273) Avail: NTIS HC A99/MF A01 CSCL 10A

The proceedings of a workshop held in Cleveland, July 28-30, 1981 are described. The workshop emphasized recent experience in building and testing large propeller-type wind turbines, expanding upon the proceedings of three previous DOE/NASA workshops at which design and analysis topics were considered. A total of 41 papers were presented on the following subjects: current and advanced large wind turbine systems, rotor blade design and manufacture, electric utility activities, research and supporting technology, meteorological characteristics for design and operation, and wind resources assessments for siting.

N83-19232*# National Aeronautics and Space Administration. Lewis Research Center, Cleveland, Ohio.
THE RESPONSE OF A 38M HORIZONTAL AXIS TEETERED ROTOR TO YAW
J. C. GLASGOW, H. G. PFANNER, and E. J. WESTERKAMP *In its* Large Horizontal-Axis Wind Turbines p 53-67 1982 refs
Avail: NTIS HC A99/MF A01 CSCL 10A

Recent tests on the 38m Mod-0 100 kW horizontal axis experimental wind turbine yielded quantative data on the teeter response of a rotor to yaw. The test results indicate that yaw rates as high as 5 deg/s could be used in emergency situations to unload and slow a rotor for intermediate sized (500 kW) wind turbines. The results also show that teeter response is sensitive to the direction of yaw, and that teeter response to yaw is reduced as either the rotor speed or the blade lock number is increased. Author

N83-19233*# National Aeronautics and Space Administration. Lewis Research Center, Cleveland, Ohio.
FIXED PITCH ROTOR PERFORMANCE OF LARGE HORIZONTAL AXIS WIND TURBINES
L. A. VITERNA and R. D. CORRIGAN *In its* Large Horizontal-Axis Wind Turbines p 69-85 1982 refs
Avail: NTIS HC A99/MF A01 CSCL 10A

Experimental fixed pitch wind turbine performance data is presented for both the DOE/NASA Mod-0 and the Danish Gedser wind turbines. Furthermore, a method for calculating the output power from large fixed pitch wind turbines is presented. Modifications to classical blade element momentum theory are given that improve correlation with measured data. Improvement is particularly evident in high winds (low tip speed ratios) where aerodynamic stall occurs as the blade experiences high angles of attack. Author

N83-19234*# National Aeronautics and Space Administration. Lewis Research Center, Cleveland, Ohio.
STALL INDUCED INSTABILITY OF A TEETERED ROTOR
J. C. GLASGOW and R. D. CORRIGAN *In its* Large Horizontal-Axis Wind Turbines p 87-100 1982 refs
Avail: NTIS HC A99/MF A01 CSCL 10A

Recent tests on the 38m Mod-0 horizontal experimental wind turbine yielded quantitative information on stall induced instability of a teetered rotor. Tests were conducted on rotor blades with NACA 230 series and NACA 643-618 airfoils at low rotor speeds to produce high angles of attack at relatively low wind speeds and power levels. The behavior of the rotor shows good agreement with predicted rotor response based on blade angle of attack calculations and airfoil section properties. The untwisted blades with the 64 series airfoil sections had a slower rate of onset of rotor instability when compared with the twisted 230 series blades, but high teeter angles and teeter stop impacts were experienced with both rotors as wind speeds increased to produce high angles of attack on the outboard portion of the blade. The relative importance of blade twist and airfoil section stall characteristics on the rate of onset of rotor unstability with increasing wind speed was not established however. Blade pitch was shown to be effective in eliminating rotor instability at the expense of some loss in rotor performance near rated wind speed. Author

N83-19235*# National Aeronautics and Space Administration. Lewis Research Center, Cleveland, Ohio.
FREE YAW PERFORMANCE OF THE MOD-0 LARGE HORIZONTAL AXIS 100 KW WIND TURBINE
R. D. CORRIGAN and L. A. VITERNA *In its* Large Horizontal-Axis Wind Turbines p 103-122 1982 refs
Avail: NTIS HC A99/MF A01 CSCL 10A

The NASA Mod-0 Large Horizontal Axis 100 kW Wind Turbine was operated in free yaw with an unconed teetered, downwind rotor mounted on a nacelle having 8-1/2 deg tilt. Two series of tests were run, the first series with 19 meter twisted aluminum blades and the second series with 19 meter untwisted steel spar blades with tip control. Rotor speed were nominally 20, 26 and 31 rpm. It was found the nacelle stabilized in free yaw at a yaw angle of between -55 deg to -45 deg was relatively independent of wind speed and was well damped to short term variations in wind direction. Power output of the wind turbine in free yaw, aligned at a large yaw angle, was considerably less than that if the wind turbine were aligned with the wind. For the Mod-0 wind turbine at 26 rpm, the MOSTAB computer code calculations of the free yaw alignment angle and power output compare reasonably well with experimental data. MOSTAB calculations indicate that elimination of tilt and adding coning will improve wind turbine alignment with the wind and that wind shear has a slight detrimental effect on the free yaw alignment angle. Author

N83-19244*# Budd Co., Philadelphia, Pa. Technical Center.
DESIGN AND EVALUATION OF LOW COST BLADES FOR LARGE WIND DRIVEN GENERATING SYSTEMS
W. S. EGGERT *In* NASA. Lewis Research Center Large Horizontal-Axis Wind Turbines p 267-284 1982
(Contract DEN3-129)
Avail: NTIS HC A99/MF A01 CSCL 10A

The development and evaluation of a low cost blade concept based on the NASA-Lewis specifications is discussed. A blade structure was designed and construction methods and materials were selected. Complete blade tooling concepts, various technical and economic analysis, and evaluations of the blade design were performed. A comprehensive fatigue test program was conducted to provide data and to verify the design. A test specimen of the spar assembly, including the root end attachment, was fabricated. This is a full-scale specimen of the root end configuration, 20 ft long. A blade design for the Mod '0' system was completed. M.G.

N83-19255*# National Aeronautics and Space Administration. Lewis Research Center, Cleveland, Ohio.
PERFORMANCE AND LOAD DATA FROM MOD-0A AND MOD-1 WIND TURBINE GENERATORS
D. A. SPERA and D. C. JANETZKE *In its* Large Horizontal-Axis Wind Turbines p 447-468 1982 refs
Avail: NTIS HC A99/MF A01 CSCL 10A

Experimental data, together with supporting analysis, are presented on the power conversion performance and blade loading of large, horizontal-axis wind turbines tested at electric utility sites in the U.S. Four turbine rotor configurations, from 28 to 61 meters in diameter, and data from five test sites are included. Performance data are presented in the form of graphs of power and system efficiency versus free-stream wind speed. Deviations from theoretical performance are analyzed statistically. Power conversion efficiency averaged 0.34 for all tests combined, compared with 0.31 predicted. Round blade tips appeared to improve performance significantly. Cyclic blade loads were normalized to develop load factors which can be used in the design of rotors with rigid hubs. Author

N83-19256*# National Aeronautics and Space Administration. Lewis Research Center, Cleveland, Ohio.
OPERATING EXPERIENCE WITH FOUR 200 KW MOD-0A WIND TURBINE GENERATORS
A. G. BIRCHENOUGH, A. L. SAUNDERS, T. W. NYLAND, and R. K. SHALTENS *In its* Large Horizontal-Axis Wind Turbines p 469-487 1982 refs
Avail: NTIS HC A99/MF A01 CSCL 10A

The windpowered generator, Mod-0A, and its advantages and disadvantages, particularly as it affects reliability, are discussed. The machine performance with regard to power availability and power output is discussed. R.J.F.

N83-19257*# National Aeronautics and Space Administration. Lewis Research Center, Cleveland, Ohio.
EXPERIENCE AND ASSESSMENT OF THE DOE/NASA MOD-1 2000 KW WIND TURBINE GENERATOR AT BOONE, NORTH CAROLINA
J. L. COLLINS, R. K. SHALTENS, R. H. POOR, and R. S. BARTON *In its* Large Horizontal-Axis Wind Turbines p 491-571 1982 refs Prepared in cooperation with General Electric Co.
Avail: NTIS HC A99/MF A01 CSCL 10B

The Mod 1 program objectives are defined. The Mod 1 wind turbine is described. In addition to the steel blade operated on the wind turbine, a composite blade was designed and manufactured. During the early phase of the manufacturing cycle of Mod 1A configuration was designed that identified concepts such as partial span control, a soft tower, and upwind teetered rotors that were incorporated in second and third generation industry designs. The Mod 1 electrical system performed as designed, with voltage flicker characteristics within acceptable utility limits. R.J.F.

N83-19262*# National Aeronautics and Space Administration. Lewis Research Center, Cleveland, Ohio.
MOD-2 WIND TURBINE PROJECT ASSESSMENT AND CLUSTER TEST PLANS
L. H. GORDON *In its* Large Horizontal-Axis Wind Turbines p 653-673 1982 refs
Avail: NTIS HC A99/MF A01 CSCL 10A

An assessment of the Mod-2 Wind Turbine project is presented based on initial goals and present results. Specifically, the Mod-2 background, project flow, and a chronology of events/results leading to Mod-2 acceptance is presented. After checkout/acceptance of the three operating turbines, NASA/LeRC will continue management of a two year test program performed at the DOE Goodnoe Hills test site. This test program is expected to yield data necessary for the continued development and optimization of wind energy systems. These test activities, the implementation of, and the results to date are also presented. Author

N83-19273*# EIC, Inc., Newton, Mass.
DEVELOPMENT OF A HIGH CAPACITY TOROIDAL NI/CD CELL Final Report
G. L. HOLLECK, J. S. FOOS, J. W. AVERY, and V. FEIMAN Jul. 1981 114 p refs
(Contract NAS3-21274)
(NASA-CR-169945; NAS 1.26:169945) Avail: NTIS HC A06/MF A01 CSCL 10C

A nickel cadmium battery design which can offer better thermal management, higher energy density and much lower cost than the state-of-the-art is emphasized. A toroidal Ni/Cd cell concept is described. It was critically reviewed and used to develop two cell designs for practical implementation. One is a double swaged and the other a swaged welded configuration. S.L.

N83-20359*# Charles River Associates, Inc., Boston, Mass.
STUDY TO ESTABLISH COST PREDICTIONS FOR THE PRODUCTION OF REDOX CHEMICALS Final Report
P. R. AMMANN, M. LORETH, and W. W. HARVEY Jul. 1982 61 p refs
(Contract DEN3-251; DE-AI04-80AL-12726)
(NASA-CR-167882; DOE/NASA/0251-1; NAS 1.26:167882)
Avail: NTIS HC A04/MF A01 CSCL 10A

The chromium and iron chloride chemicals are significant first costs for NASA Redox energy storage systems. This study was performed to determine the lowest cost at which chromium and iron chlorides could be obtained for a complex of redox energy storage systems. In addition, since the solutions gradually become intermixed during the course of operation of Redox units, it was an objective to evaluate schemes for regeneration of the operating solutions. Three processes were evaluated for the production of chromium and iron chlorides. As a basis for the preliminary plant design and economic evaluation, it was assumed that the plant would produce about 25,000 tons of contained chromium as $CrCl_3$ and an equivalent molar quantity of $FeCl_2$. Preliminary plant designs, including materials and energy balances and sizing of major equipment, were prepared, and capital and operating costs were estimated. Author

N83-20361*# National Aeronautics and Space Administration. Lewis Research Center, Cleveland, Ohio.
CRITICAL RESEARCH AND ADVANCED TECHNOLOGY (CRT) SUPPORT PROJECT Summary Report
E. R. FURMAN, D. N. ANDERSON, P. E. HODGE, C. E. LOWELL, J. J. NAINIGER, and D. F. SCHULTZ Feb. 1983 58 p refs
(Contract DE-AI01-77ET-10350)
(NASA-TM-83019; E-1455; DOE/NASA/10350-35; NAS 1.15:83019) Avail: NTIS HC A04/MF A01 CSCL 10A

A critical technology base for utility and industrial gas turbines by planning the use of coal-derived fuels was studied. Development tasks were included in the following areas: (1) Combustion - investigate the combustion of coal-derived fuels and methods to minimize the conversion of fuel-bound nitrogen to NOx; (2) materials - understand and minimize hot corrosion; (3) system studies - integrate and focus the technological efforts. A literature survey of coal-derived fuels was completed and a NOx emissions model was developed. Flametube tests of a two-stage (rich-lean) combustor defined optimum equivalence ratios for minimizing NOx emissions. Sector combustor tests demonstrated variable air control to optimize equivalence ratios over a wide load range and steam cooling of the primary zone liner. The catalytic combustion of coal-derived fuels was demonstrated. The combustion of coal-derived gases is very promising. A hot-corrosion life prediction model was formulated and verified with laboratory testing of doped fuels. Fuel additives to control sulfur corrosion were studied. The intermittent application of barium proved effective. Advanced thermal barrier coatings were developed and tested. Coating failure modes were identified and new material formulations and fabrication parameters were specified. System studies in support of the thermal barrier coating development were accomplished. Author

N83-20362*# Delaware Univ., Newark. Dept. of Electrical Engineering.
DESIGN RULES FOR A 100X MAXIMUM EFFICIENCY GAAS CONCENTRATOR SOLAR CELL FOR SPACE APPLICATIONS Final Report
A. N. BARNETT 22 Mar. 1983 15 p refs
(Contract NAG3-321)
(NASA-CR-170005; NAS 1.26:170005) Avail: NTIS HC A02/MF A01 CSCL 10A

The preference of N on P as the preferred structure rather than the common P on N structure, the design of an improved transparency top contact based on the separation of the grid and bus bars, and the identification of gallium phosphide as an improved window layer, replacing the (GaAl) are investigated. Author

N83-20374*# National Aeronautics and Space Administration. Lewis Research Center, Cleveland, Ohio.
SCREEN PRINTED INTERDIGITATED BACK CONTACT SOLAR CELL Patent Application
C. R. BARAONA, G. A. MAZARIS, and A. T. CHAI, inventors (to NASA) 10 Feb. 1983 8 p
(NASA-CASE-LEW-13414-1; US-PATENT-APPL-SN-465364)
Avail: NTIS HC A02/MF A01 CSCL 10A

Interdigitated back contact solar cells were made by screen printing dopant materials onto the back surface of a semiconductor substrate in a pair of interdigitated patterns. These dopant materials were then diffused into the substrate to form junctions having configurations corresponding to these patterns. Contacts having configurations which match the patterns were then applied over the junctions. NASA

N83-21508*# Massachusetts Inst. of Tech., Cambridge.
STABILITY ANALYSIS OF FLEXIBLE WIND TURBINE BLADES USING FINITE ELEMENT METHOD Final Report
A. KAMOULAKOS Aug. 1982 156 p refs
(Contract NSG-3303; DE-AI01-76ET-20320)
(NASA-CR-168107; DOE/NASA/3303-2; NAS 1.26:168107; MIT-ARSL-TR-197-3) Avail: NTIS HC A08/MF A01 CSCL 10A

Static vibration and flutter analysis of a straight elastic axis blade was performed based on a finite element method solution. The total potential energy functional was formulated according to linear beam theory. The inertia and aerodynamic loads were formulated according to the blade absolute acceleration and absolute velocity vectors. In vibration analysis, the direction of motion of the blade during the first out-of-lane and first in-plane modes was examined; numerical results involve NASA/DOE Mod-0, McCauley propeller, north wind turbine and flat plate behavior. In flutter analysis, comparison cases were examined involving several references. Vibration analysis of a nonstraight elastic axis blade based on a finite element method solution was performed in a similar manner with the straight elastic axis blade, since it was recognized that a curved blade can be approximated by an assembly of a sufficient number of straight blade elements at different inclinations with respect to common system of axes. Numerical results involve comparison between the behavior of a straight and a curved cantilever beam during the lowest two in-plane and out-of-plane modes. Author

N83-21509*# Massachusetts Inst. of Tech., Cambridge. Aeroelastic and Structures Research Lab.
SIMPLIFIED AEROELASTIC MODELING OF HORIZONTAL AXIS WIND TURBINES Final Report
J. H. WENDELL Sep. 1982 231 p refs
(Contract NSG-3303; DE-AI01-76ET-20320)
(NASA-CR-168109; DOE/NASA/3303-3; NAS 1.26:168109; MIT-ASRL-TR-197-4) Avail: NTIS HC A11/MF A01 CSCL 10A

Certain aspects of the aeroelastic modeling and behavior of the horizontal axis wind turbine (HAWT) are examined. Two simple three degree of freedom models are described in this report, and tools are developed which allow other simple models to be derived. The first simple model developed is an equivalent hinge model to study the flap-lag-torsion aeroelastic stability of an isolated rotor blade. The model includes nonlinear effects, preconing, and noncoincident elastic axis, center of gravity, and aerodynamic center. A stability study is presented which examines the influence of key parameters on aeroelastic stability. Next, two general tools are developed to study the aeroelastic stability and response of a teetering rotor coupled to a flexible tower. The first of these tools is an aeroelastic model of a two-bladed rotor on a general flexible support. The second general tool is a harmonic balance solution method for the resulting second order system with periodic coefficients. The second simple model developed is a rotor-tower model which serves to demonstrate the general tools. This model includes nacelle yawing, nacelle pitching, and rotor teetering. Transient response time histories are calculated and compared to a similar model in the literature. Agreement between the two is very good, especially considering how few harmonics are used. Finally, a stability study is presented which examines the effects of support stiffness and damping, inflow angle, and preconing. Author

N83-22739*# Foster-Miller Associates, Inc., Waltham, Mass.
DESIGN OF HYDRAULIC OUTPUT STIRLING ENGINE Final Report
W. M. TOSCANO, A. C. HARVEY, and K. LEE Jan. 1983 130 p refs
(Contract NAS3-22239)
(NASA-CR-167976; NAS 1.26:167976) Avail: NTIS HC A07/MF A01 CSCL 10B

A hydraulic output system for the RE-1000 free piston stirling engine (FPSE) was designed. The hydraulic output system can be readily integrated with the existing hot section of RE-1000 FPSE. The system has two simply supported diaphragms which separate the engine gas from the hydraulic fluid, a dynamic balance mechanism, and a novel, null center band hydraulic pump. The diaphragms are designed to endure more than 10 billion cycles, and to withstand the differential pressure load as high as 14 MPa. The projected thermodynamic performance of the hydraulic output version of RE-1000 FPSE is 1.87 kW at 29/7 percent brake efficiency. S.L.

N83-22740*# Massachusetts Inst. of Tech., Cambridge. Aeroelastic and Structures Research Lab.
SOME EXPERIMENTS ON YAW STABILITY OF WIND TURBINES WITH VARIOUS CONING ANGLES Final Report
D. BUNDAS and J. DUGUNDJI Jul. 1981 31 p refs
(Contract NSG-3303; DE-AI01-76ET-20320)
(NASA-CR-168108; DOE/NASA/3303-1; NAS 1.26:168108; MIT-ASRL-TR-197-2) Avail: NTIS HC A03/MF A01 CSCL 10B

A horizontal axis wind turbine was constructed to study the effect of coning angle on the yawing moments produced. Coning angles of 0 deg, +10 deg and -10 deg were studied in the upwind and downwind cases. Moment and rotational frequency of the blades at each yaw angle setting were taken. It was found that as the coning angle increased from -10 deg to +10 deg in either the upwind or downwind case the stability decreased. The downwind case was slightly more stable for all coning angles than was the upwind case. It is found that all the previous cases were stable for high rotation speeds, but at lower rotation speeds, they were all unstable and could not self start unless held in the wind. E.A.K.

N83-22746*# IIT Research Inst., Chicago, Ill.
FATIGUE TESTING OF LOW-COST FIBERGLASS COMPOSITE WIND TURBINE BLADE MATERIALS Final Report
K. E. HOFER and L. C. BENNETT Nov. 1981 89 p refs
(Contract DEN3-182; DE-AI01-79ET-20320)
(NASA-CR-165566; DOE/NASA/0182-1; NAS 1.26:165566; IITRI-M06066-22) Avail: NTIS HC A05/MF A01 CSCL 10B

The static and fatigue behavior of transverse filament tape (TFT) fiberglass/epoxy and TFT/polyester composites was established by the testing of specimens cut from panels fabricated by a filament winding process used for the construction of large experimental wind turbine blades. Author

N83-22747*# Massachusetts Inst. of Tech., Cambridge. Aeroelastic and Structures Research Lab.
DEVELOPMENT OF METHODOLOGY FOR HORIZONTAL AXIS WIND TURBINE DYNAMIC ANALYSIS Final Summary Report
J. DUGUNDJI Sep. 1982 11 p refs
(Contract NSG-3303; DE-AI01-76ET-20320)
(NASA-CR-168110; DOE/NASA/3303-4; NAS 1.26:168110; MIT-ASRL-TR-197-5) Avail: NTIS HC A02/MF A01 CSCL 10B

Horizontal axis wind turbine dynamics were studied. The following findings are summarized: (1) review of the MOSTAS computer programs for dynamic analysis of horizontal axis wind turbines; (2) review of various analysis methods for rotating systems with periodic coefficients; (3) review of structural dynamics analysis tools for large wind turbine; (4) experiments for yaw characteristics of a rotating rotor; (5) development of a finite element model for rotors; (6) development of simple models for aeroelastics; and (7) development of simple models for stability and response of wind turbines on flexible towers. E.A.K.

N83-22748*# Gilbert (Glen A.) and Associates, Inc., Reading, Pa.
PARAMETRIC ANALYSIS OF CLOSED CYCLE MAGNETOHYDRODYNAMIC (MHD) POWER PLANTS Final Report
W. OWENS, R. BERG, R. MURTHY, and J. PATTEN Sep. 1981 284 p refs
(Contract DEN3-136; DE-AI01-77ET-10769)
(NASA-CR-165472; DOE/NASA/0136-1; NAS 1.26:165472)
Avail: NTIS HC A13/MF A01 CSCL 10B

A parametric analysis of closed cycle MHD power plants was performed which studied the technical feasibility, associated capital cost, and cost of electricity for the direct combustion of coal or coal derived fuel. Three reference plants, differing primarily in the method of coal conversion utilized, were defined. Reference Plant 1 used direct coal fired combustion while Reference Plants 2 and 3 employed on site integrated gasifiers. Reference Plant 2 used a pressurized gasifier while Reference Plant 3 used a "state of the art' atmospheric gasifier. Thirty plant configurations were considered by using parametric variations from the Reference Plants. Parametric variations include the type of coal (Montana Rosebud or Illinois No. 6), clean up systems (hot or cold gas clean up), on or two stage atmospheric or pressurized direct fired coal combustors, and six different gasifier systems. Plant sizes ranged from 100 to 1000 MWe. Overall plant performance was calculated using two methodologies. In one task, the channel performance was assumed and the MHD topping cycle efficiencies were based on the assumed values. A second task involved rigorous calculations of channel performance (enthalpy extraction, isentropic efficiency and generator output) that verified the original (task one) assumptions. Closed cycle MHD capital costs were estimated for the task one plants; task two cost estimates were made for the channel and magnet only. S.L.

N83-22749*# National Aeronautics and Space Administration. Lewis Research Center, Cleveland, Ohio.
TESTS OF AN ALTERNATING CURRENT PROPULSION SUBSYSTEM FOR ELECTRIC VEHICLES ON A ROAD LOAD SIMULATOR Final Report
F. J. STENGER Dec. 1982 42 p refs
(Contract DE-AI01-77CS-51044)
(NASA-TM-83036; E-1479; DOE/NASA/51044-29; NAS 1.15:83036) Avail: NTIS HC A03/MF A01 CSCL 13F

The test results of a breadboard version of an ac electric-vehicle propulsion subsystem are presented. The breadboard was installed in the NASA Lewis Research Center Road Load Simulator facility and tested under steady-state and transient conditions. Steady-state tests were run to characterize the system and component efficiencies over the complete speed-torque range within the capability of the propulsion subsystem in the motoring mode of operation. Transient tests were performed to determine the energy consumption of the breadboard over the acceleration and cruise portions of SAE J227 and driving schedules B, C, and D. Tests in the regenerative mode were limited to the low-gear-speed range of the two speed transaxle used in the subsystem. The maximum steady-state subsystem efficiency observed for the breadboard was 81.5 percent in the high-gear-speed range in the motoring mode, and 76 percent in the regenerative braking mode (low gear). The subsystem energy efficiency during the transient tests ranged from 49.2 percent for schedule B to 68.4 percent for Schedule D. M.G.

N83-22750*# Gulf Research and Development Co., Pittsburgh, Pa. Chemicals and Minerals Div.
FUEL QUALITY-PROCESSING STUDY. VOLUME 1: OVERVIEW AND RESULTS Final Report
G. E. JONES, JR. May 1982 66 p 4 Vol.
(Contract DEN3-175; DE-AJ01-77ET-13111)
(NASA-CR-165326-VOL-1; DOE/NASA/DEN-175-1-VOL-1; NAS 1.26:165326-VOL-1; GR/DC-625RN209-VOL-1) Avail: NTIS HC A04/MF A01 CSCL 10B

The methods whereby the intermediate results were obtained are outlined, and the evaluation of the feasible paths from liquid fossil fuel sources to generated electricity is presented. The segments from which these paths were built are the results from the fuel upgrading schemes, on-site treatments, and exhaust gas treatments detailed in the subsequent volumes. The salient cost and quality parameters are included. Author

N83-22751*# Gulf Research and Development Co., Pittsburgh, Pa. Chemicals and Minerals Div.
FUEL QUALITY-PROCESSING STUDY. VOLUME 2: LITERATURE SURVEY Final Report
G. E. JONES, JR., R. AMERO, B. MURTHY, and M. CUTRONE Oct. 1981 147 p refs 4 Vol.
(Contract DEN3-175; DE-AJ01-77ET-13111)
(NASA-CR-165326-VOL-2; DOE/NASA/DEN-175-1-VOL-2; NAS 1.26:165326-VOL-2; GR/DC-625RL137-VOL-2) Avail: NTIS HC A07/MF A01 CSCL 10B

The validity of initial assumptions about raw materials choices and relevant upgrading processing options was confirmed. The literature survey also served to define the on-site (at the turbine location) options for fuel treatment and exhaust gas treatment. The literature survey also contains a substantial compilation of specification and physical property information about liquid fuel products relevant to industrial gas turbines. Author

N83-22754*# Gulf Research and Development Co., Pittsburgh, Pa. Chemical and Minerals Div.
FUEL QUALITY/PROCESSING STUDY. VOLUME 3: FUEL UPGRADING STUDIES Final Report
G. E. JONES, JR., P. BRUGGINK, and C. SINNETT Oct. 1981 195 p refs
(Contract DEN3-175; DE-AI01-71ET-13111)
(NASA-CR-165326-VOL-3; DOE/NASA/DEN-175-1-VOL-3; NAS 1.26:165326-VOL-3; GRDC-625-RL-153-VOL-3) Avail: NTIS HC A09/MF A01 CSCL 10B

The methods used to calculate the refinery selling prices for the turbine fuels of low quality are described. Detailed descriptions and economics of the upgrading schemes are included. These descriptions include flow diagrams showing the interconnection between processes and the stream flows involved. Each scheme is in a complete, integrated, stand alone facility. Except for the purchase of electricity and water, each scheme provides its own fuel and manufactures, when appropriate, its own hydrogen. S.L.

N83-22755*# Gulf Research and Development Co., Pittsburgh, Pa. Chemicals and Materials Div.
FUEL QUALITY/PROCESSING STUDY. VOLUME 4: ON SITE PROCESSING STUDIES Final Report
G. E. JONES, JR., M. CUTRONE, H. DOERING, and J. HICKEY Oct. 1981 104 p refs
(Contract DEN3-175; DE-AI01-77ET-13111)
(NASA-CR-165326-VOL-4; DOE/NASA/DEN-175-1-VOL-4; NAS 1.26:165326-VOL-4; GRDC-625-RL-154-VOL-4) Avail: NTIS HC A06/MF A01 CSCL 10B

Fuel treated at the turbine and the turbine exhaust gas processed at the turbine site are studied. Fuel treatments protect the turbine from contaminants or impurities either in the upgrading fuel as produced or picked up by the fuel during normal transportation. Exhaust gas treatments provide for the reduction of NOx and SOx to environmentally acceptable levels. The impact of fuel quality upon turbine maintenance and deterioration is considered. On site costs include not only the fuel treatment costs as such, but also incremental costs incurred by the turbine operator if a turbine fuel of low quality is not acceptably upgraded. S.L.

N83-22756*# TRW Space Technology Labs., Redondo Beach, Calif.
STUDY OF SOLAR ARRAY SWITCHING POWER MANAGEMENT TECHNOLOGY FOR SPACE POWER SYSTEM Final Report
J. E. CASSINELLI Sep. 1982 240 p refs
(Contract NAS3-22656)
(NASA-CR-167890; NAS 1.26:167890; TRW-3724) Avail: NTIS HC A11/MF A01 CSCL 10A

This report documents work performed on the Solar Array Switching Power Management Study. Mission characteristics for three missions were defined to the depth necessary to determine their power management requirements. Solar array switching concepts which could satisfy the mission requirements were identified. The switching concepts were compared with a conventional buck regulator system for cost, weight and volume, reliability, efficiency and thermal control. Solar array switching provided significant advantages in all areas of comparison for the reviewed missions. E.A.K.

N83-23704*# Technical Report Services, Rocky River, Ohio.
DESIGN AND EVALUATION OF LOW-COST LAMINATED WOOD COMPOSITE BLADES FOR INTERMEDIATE SIZE WIND TURBINES: BLADE DESIGN, FABRICATION CONCEPT, AND COST ANALYSIS Interim Report
S. LIEBLEIN, M. GAUGEON, G. THOMAS, and M. ZUECK Nov. 1982 120 p refs
(Contract DEN3-101; DE-AI01-76ET-20320)
(NASA-CR-165463; DOE/NASA/0101-1; NAS 1.26:165463; TRS-107) Avail: NTIS HC A06/MF A01 CSCL 10B

As part of a program to reduce wind turbine costs, an evaluation was conducted of a laminated wood composite blade for the Mod-OA 200 kW wind turbine. The effort included the design and fabrication concept for the blade, together with cost and load analyses. The blade structure is composed of laminated Douglas fir veneers for the primary spar and nose sections, and honeycomb cored plywood panels for the trailing edges sections. The attachment of the wood blade to the rotor hub was through load takeoff studs bonded into the blade root. Tests were conducted on specimens of the key structural components to verify the feasibility of the concept. It is concluded that the proposed wood composite blade design and fabrication concept is suitable for Mod-OA size turbines (125-ft diameter rotor) at a cost that is very competitive with other methods of manufacture. S.L.

N83-23708*# Giner, Inc., Waltham, Mass.
OPTIMIZATION AND FABRICATION OF POROUS CARBON ELECTRODES FOR FE/CR REDOX FLOW CELLS Final Report
V. JALAN, B. MORRISEAU, and L. SWETTE Jul. 1982 157 p refs
(Contract DEN3-198; DE-AI04-80AL-12726)
(NASA-CR-167921; NAS 1.26:167921; DOE/NASA/0198-1)
Avail: NTIS HC A08/MF A01 CSCL 10C

Negative electrode development for the NASA chromous/ferric Redox battery is reported. The effects of substrate material, gold/lead catalyst composition and loading, and catalyzation procedures on the performance of the chromium electrode were investigated. Three alternative catalyst systems were also examined, and 1/3 square foot size electrodes were fabricated and delivered to NASA at the conclusion of the program. Author

N83-23709*# National Aeronautics and Space Administration. Lewis Research Center, Cleveland, Ohio.
ANALYSIS OF THE ECONOMICS OF PHOTOVOLTAIC-DIESEL-BATTERY ENERGY SYSTEMS FOR REMOTE APPLICATIONS
W. A. BRAINARD 1983 9 p refs Presented at the Ann. Meeting of the American Solar Energy Soc., Minneapolis, 1-3 Jun. 1983
(Contract DE-AI01-79ET-20485)
(NASA-TM-83377; DOE/NASA/20485-14; E-1645; NAS 1.15:83377) Avail: NTIS HC A02/MF A01 CSCL 10C

Computer simulations were conducted to analyze the performance and operating cost of a photovoltaic energy source combined with a diesel generator system and battery storage. The simulations were based on the load demand profiles used for the design of an all photovoltaic energy system installed in the remote Papago Indian Village of Schuchuli, Arizona. Twenty year simulations were run using solar insolation data from Phoenix SOLMET tapes. Total energy produced, energy consumed, operation and maintenance costs were calculated. The life cycle and levelized energy costs were determined for a variety of system configurations (i.e., varying amounts of photovoltaic array and battery storage). Author

N83-23710*# National Aeronautics and Space Administration. Lewis Research Center, Cleveland, Ohio.
STRUCTURAL QUALIFICATION TESTING AND OPERATIONAL LOADING ON A FIBERGLASS ROTOR BLADE FOR THE MOD-OA WIND TURBINE Final Report
T. L. SULLIVAN Mar. 1983 26 p refs
(Contract DE-AI01-76ET-20320)
(NASA-TM-83309; NASA/DOE/20320-44; E-1548; NAS 1.15:83309) Avail: NTIS HC A03/MF A01 CSCL 10A

Fatigue tests were performed on full- and half-scale root end sections, first to qualify the root retention design, and second to induce failure. Test methodology and results are presented. Two operational blades were proof tested to design limit load to ascertain buckling resistance. Measurements of natural frequency, damping ratio, and deflection under load made on the operational blades are documented. The tests showed that all structural design requirements were met or exceeded. Blade loads measured during 3000 hr of field operation were close to those expected. The measured loads validated the loads used in the fatigue tests and gave high confidence in the ability of the blades to achieve design life. Author

N83-25026*# California Univ., Berkeley. Electronics Research Lab.
COHERENT CONVERSION OF THE SUNLIGHT SPECTRUM Final Report, 28 Jul. 1980 - 30 Apr. 1982
T. K. GUSTAFSON 1982 147 p refs
(Contract NAG3-88)
(NASA-CR-170185; NAS 1.26:170185) Avail: NTIS HC A07/MF A01 CSCL 10A

Efforts related to the utilization of tunneling junctions for the conversion of radiative power to electrical power are reported. The theoretical foundations for these particular devices is presented

along with a discussion of many of the practical problems associated with the implementation of such devices. Author

N83-25036*# National Aeronautics and Space Administration. Lewis Research Center, Cleveland, Ohio.
TESTING AND PERFORMANCE CHARACTERISTICS OF A 1-KW FREE PISTON STIRLING ENGINE
J. SCHREIBER Apr. 1983 48 p refs
(NASA-TM-82999; E-1435; NAS 1.15:82999) Avail: NTIS HC A03/MF A01 CSCL 10B

A 1 kW single cylinder free piston Stirling engine, configured as a research engine, was tested with helium working gas. The engine features a posted displacer and dashpot load. The test results show the engine power output and efficiency to be lower than those observed during acceptance tests by the manufacturer. Engine tests results are presented for operation at the two heater head temperatures and with two regenerator porosities, along with flow test results for the heat exchangers. Author

N83-25037*# National Aeronautics and Space Administration. Lewis Research Center, Cleveland, Ohio.
IGCC PERFORMANCE COMPARISON FOR VARIATIONS IN GASIFIER TYPE AND GAS TURBINE FIRING TEMPERATURE
R. J. STOCHL and J. J. NAINIGER Jan. 1983 40 p refs
(NASA-TM-83310; E-1549; NAS 1.15:83310) Avail: NTIS HC A03/MF A01 CSCL 10B

Performance estimates were made for a series of integrated coal gasification combined cycle (IGCC) power systems using three generic types of coal gasification subsystems. The objectives of this study were (1) to provide a self consistent comparison of IGCC systems using different types of gasifiers and different oxidants and (2) to use this framework of cases to evaluate the effect of a gas turbine firing temperature and cooling approach an overall system efficiency. The basic IGCC systems considered included both air and oxygen blown versions of a fluidized bed gasifier, represented by the Westinghouse design, and an entrained bed gasifier, represented by the Texaco design. Also considered were systems using an oxygen blown, fixed bed gasifier, represented by the British Gas Corporation (BGC) slagging gasifier. All of these gasifiers were integrated with a combined cycle using a gas turbine firing temperature of 1700 K (2600 F) and a compressor pressure ratio of 16:1. Steam turbine throttle conditions were chosen to be 16.6 MPa/811 K (2400 psia/1000 F) with a single reheat to 810 K (1000 F). Some of these cases were modified to allow the evaluation of the effect of gas turbine firing temperature. Turbine firing temperatures from state of the art 1365 K (2000 F) to an advanced technology 1920 K (3000 F) were analyzed. A turbine cooling technology that maintains metal temperatures below acceptable limits was assumed for each level of firing temperature. System performance comparisons were made using three advanced turbine cooling technologies for the 1920 K (3000 F) firing temperature. The results indicate that the IGCC using the BGC gasifier had the highest net system efficiency (42.1 percent) of the five gasification cases considered. B.W.

N83-25038*# National Aeronautics and Space Administration. Lewis Research Center, Cleveland, Ohio.
CYCLE LIFE TEST AND FAILURE MODEL OF NICKEL-HYDROGEN CELLS
J. J. SMITHRICK 1983 16 p refs Proposed for presentation at the 18th Intersoc. Energy Conversion Eng. Conf., 21-26 Aug. 1983: sponsored by American Inst. of Chemical Engineers, IEEE, AIAA, American Chemical Society, ANS, ASME, and SAE
(NASA-TM-83375; E-1643; NAS 1.15:83375) Avail: NTIS HC A02/MF A01 CSCL 10C

Six ampere hour individual pressure vessel nickel hydrogen cells were charge/discharge cycled to failure. Failure as used here is defined to occur when the end of discharge voltage degraded to 0.9 volts. They were cycled under a low earth orbit cycle regime to a deep depth of discharge (80 percent of rated ampere hour capacity). Both cell designs were fabricated by the same manufacturer and represent current state of the art. A failure model was advanced which suggests both cell designs have inadequate volume tolerance characteristics. The limited existing data base at a deep depth of discharge (DOD) was expanded. Two cells of each design were cycled. One COMSAT cell failed at cycle 1712 and the other failed at cycle 1875. For the Air Force/Hughes cells, one cell failed at cycle 2250 and the other failed at cycle 2638. All cells, of both designs, failed due to low end of discharge voltage (0.9 volts). No cell failed due to electrical shorts. After cell failure, three different reconditioning tests (deep discharge, physical reorientation, and open circuit voltage stand) were conducted on all cells of each design. A fourth reconditioning test (electrolyte addition) was conducted on one cell of each design. In addition post cycle cell teardown and failure analysis were performed on the one cell of each design which did not have electrolyte added after failure. Author

N83-25041*# National Aeronautics and Space Administration. Lewis Research Center, Cleveland, Ohio.
DOE AND AID STAND-ALONE PHOTOVOLTAIC ACTIVITIES
W. J. BIFANO and A. F. RATAJCZAK 1983 9 p refs Presented at the Ann. Meeting of the Am. Solar Energy Soc., Minneapolis, 1-3 Jun. 1983
(Contract DE-AI01-79ET-20485)
(NASA-TM-83374; E-1642; NAS 1.15:83374; DOE/NASA/20485-15) Avail: NTIS HC A02/MF A01 CSCL 10A

The NASA Lewis Research Center (LeRC) is managing stand-alone photovoltaic (PV) system activities sponsored by the U.S. Department of Energy (DOE) and the U.S. Agency for International Development (AID). The DOE project includes village PV power demonstration projects in Gabon (four sites) and the Marshall Islands, PV-powered medical refrigerators in six countries, PV system microprocessor control development activities and PV-hybrid system assessments. The AID project includes a large village system in Tunisia, a water pumping/grain grinding project in Upper Volta, five medical clinics in four countries, PV-powered remote earth station application. These PV activities and summarizes significant findings to data are reviewed. Author

N83-25042*# National Aeronautics and Space Administration. Lewis Research Center, Cleveland, Ohio.
SINGLE CELL PERFORMANCE STUDIES ON THE FE/CR REDOX ENERGY STORAGE SYSTEM USING MIXED REACTANT SOLUTIONS AT ELEVATED TEMPERATURE
R. F. GAHN, N. H. HAGEDORN, and J. S. LING 1983 9 p refs Proposed for presentation at 18th Intersoc. Energy Conversion Engr. Conf., Orlando, Fla., 21-26 Aug. 1983
(Contract DE-AI04-80AL-12726)
(NASA-TM-83385; DOE/NASA/12726-21; E-1662; NAS 1.15:83385) Avail: NTIS HC A02/MF A01 CSCL 10C

Experimental studies in a 14.5 sq cm single cell system using mixed reactant solutions at 65 C are described. Systems were tested under isothermal conditions i.e., reactants and the cell were at the same temperature. Charging and discharging performance were evaluted by measuring watt-hour and coulombic efficiencies, voltage-current relationships, hydrogen evolution and membrane resistivity. Watt-hour efficiencies ranged from 86% at 43 ma/sq cm to 75% at 129 ma/sq cm with corresponding coulombic efficiencies of 92% and 97%, respectively. Hydrogen evolution was less than 1% of the charge coulombic capacity during charge-discharge cycling. Bismuth and bismuth-lead catalyzed chromium electrodes maintained reversible performance and low hydrogen evolution under normal and adverse cycling conditions. Reblending of the anode and cathode solutions was successfully demonstrated to compensate for osmotic volume changes. Improved performance was obtained with mixed reactant systems in comparison to the unmixed reactant systems. Author

N83-25043*# Cleveland State Univ., Ohio.
A STUDY OF DYNAMIC ENERGY EQUATIONS FOR STIRLING CYCLE ANALYSIS Final Report
V. H. LARSON Apr. 1983 44 p refs
(Contract NSG-3257)
(NASA-CR-168152; NAS 1.26:168152) Avail: NTIS HC A03/MF A01 CSCL 10B

An analytical and computer study of the dynamic energy equations that describe the physical phenomena that occurs in a Stirling cycle engine. The basic problem is set up in terms of a set o hyperbolic partial differential equations. The characteristic lines are determined. The equations are then transformed to ordinary differential equations that are valid along characteristic lines. Computer programs to solve the differential equations and to plot pertinent factors are described. Author

N83-25109*# National Aeronautics and Space Administration. Lewis Research Center, Cleveland, Ohio.
SOLAR CELL MEASUREMENTS
H. B. CURTIS *In* Midwest Research Inst. Com. Photovoltaics Meas. Workshop Proc. p 227-233 1981
Avail: NTIS HC A13/MF A01 CSCL 10A

The measurement of the electrical performance characteristics of individual solar cells is discussed. One of the reasons is determination of the output power, measurement of the effect of various degradation mechanisms, and separation of cells by current and voltage for eventual use in series and parallel combinations. Major problem areas in making accurate performance measurements are the determination of the irradiance level during measurement, the measurement and control of cell junction temperature, and the contacting of the separate current and potential leads to the cell under test. Solar cells respond to only part of the solar spectrum, irradiance measurement made with blackbody detectors lead to spectral mismatch errors. The use of reference cells with a spectral response similar to that of the test cell reduces this error. Reference cells are calibrated at standard atmospheric conditions with all cells calibrated at the same conditions. E.A.K.

N83-25112*# Communications Satellite Corp., Clarksburg, Md.
DEVELOPMENTS TOWARD AN 18% EFFICIENT SILICON SOLAR CELL Final Report
A. MEULENBERG, JR. Apr. 1983 142 p refs
(Contract NAS3-22217)
(NASA-CR-168141; NAS 1.26:168141) Avail: NTIS HC A07/MF A01 CSCL 10A

Limitations to increased open-circuit voltage were identified and experimentally verified for 0.1 ohm-cm solar cells with heavily doped emitters. After major reduction in the dark current contribution from the metal-silicon interface of the grid contacts, the surface recombination velocity of the oxide-silicon interface of shallow junction solar cells is the limiting factor. In deep junction solar cells, where the junction field does not aid surface collection, the emitter bulk is the limiting factor. Singly-diffused, shallow junction cells have been fabricated with open circuit voltages in excess of 645 mV. Double-diffusion shallow and deep junctions cells have displayed voltages above 650 mV. MIS solar cells formed on 0.1 ohm-cm substrates have exibited the lowest dark currents produced in the course of the contract work. Author

N83-26251*# National Aeronautics and Space Administration. Lewis Research Center, Cleveland, Ohio.
AUTOIGNITION IN A PREMIXING-PREVAPORIZING FUEL DUCT USING 3 DIFFERENT FUEL INJECTION SYSTEMS AT INLET AIR TEMPERATURES TO 1250 K Final Report
R. R. TACINA May 1983 15 p refs
(Contract DE-AI01-77CS-51040)
(NASA-TM-82938; E-1334; NAS 1.15:82938; DOE/NASA/51040-45) Avail: NTIS HC A02/MF A01 CSCL 21B

Conditions were determined in a continuous-flow, premixing-prevaporizing duct at which autoignition occurred. Test conditions were representative of an advanced, regenerative-cycle, automotive gas turbine. The test conditions inlet air temperatures from 600 to 1250 K (a vitiated preheater was used), pressures from 170 to 600 kPa, air velocities of 10 to 30 m/sec, equivalence ratios from 0.3 to 1.0, mixing lengths from 10 to 60 cm, and residence times of 2 to 100 ms. The fuel was diesel number 2. The duct was insulated and had an inside diameter of 12 cm. Three different fuel injection systems were used: One was a single simplex pressure atomizer, and the other two were multiple-source injectors. The data obtained with the simplex and one of the multiple-source injectors agreed satisfactorily with the references and correlated with an Arrenhius expression. The data obtained with the other multiple source injector, which used multiple cones to improve the fuel-air distribution, did not correlate well with residence time. Author

N83-26252*# National Aeronautics and Space Administration. Lewis Research Center, Cleveland, Ohio.
NASA REDOX STORAGE SYSTEM DEVELOPMENT PROJECT Annual Report
Apr. 1983 45 p refs
(Contract DE-AI04-80AL-12726)
(NASA-TM-83087; E-1546; NAS 1.15:83087; DOE/NASA/12726-19) Avail: NTIS HC A03/MF A05 CSCL 10C

The operating temperature was raised from 25 C to 65 C, which enhanced the kinetics of the chromium electrode charging reactions. The design of the auxiliary electrochemical cell, which is used to keep both reactants at the same state of charge, was modified, leading to better and more stable performance. Preliminary testing has shown that the four tank mode of operation improves energy efficiency as much as 5 percentage points over the conventional two tank mode. Another variation in operating mode, the use of mixed reactants, potentially offers several very attractive advantages. Preliminary reactant cost studies lend further weight to the feasibility of the mixed reactant concept. Electrode studies show that reproducibility of performance is very dependent on the pyrolysis temperature at which the carbon/graphite felt substrate is formed. Membrane development work continued to concentrate on cost reduction and the enhancement of resistivity and selectivity. Author

N83-26253*# National Aeronautics and Space Administration. Lewis Research Center, Cleveland, Ohio.
TEST RESULTS OF A TEN CELL BIPOLAR NICKEL-HYDROGEN BATTERY
R. L. CATALDO 1983 11 p refs Presented at the 18th Intersoc. Energy Conversion Eng. Conf., Orlando, Fla., 21-26 Aug. 1983; sponsored by AIChE, IEEE, AIAA, ACS, ANS, ASME AND SAE
(NASA-TM-83384; E-1657; NAS 1.15:83384) Avail: NTIS HC A02/MF A01 CSCL 10C

A ten cell bipolar nickel hydrogen 6.5 ampere-hour battery demonstrated over 2000 low Earth orbit cycles at an 80 percent depth-of-discharge. Charge/discharge cyclic ampere-hour and watt-hour efficiencies of 88 and 76 percent, respectively, observed. Peak power capability was determined at 1.1 kW. A 10C discharge rate yields 83 percent of the nominal stark capacity to the 1.0 volt cut off in just under 6 minutes. Author

N83-26258*# National Aeronautics and Space Administration. Lewis Research Center, Cleveland, Ohio.
SOLAR ENERGY CONVERTER USING SURFACE PLASMA WAVES Patent Application
L. M. ANDERSON, inventor (to NASA) 19 Apr. 1983 14 p
(NASA-CASE-LEW-10827-1; US-PATENT-APPL-SN-486470)
Avail: NTIS HC A02/MF A01 CSCL 10A

Sunlight is dispersed over a diffraction grating formed on the surface of a conducting film on a substrate. The angular dispersion controls the effective grating period so that a marching spectrum of surface plasmons is excited for parallel processing on the conducting film. The resulting surface plasmons carry energy to an array of inelastic tunnel diodes. This solar energy converter does not require different materials for each frequency band, and

sunlight is directly converted to electricity in an efficient manner by extracting more energy from the more energetic photons.
NASA

N83-26259*# Avco-Everett Research Lab., Mass.
PARAMETRIC STUDY OF POTENTIAL EARLY COMMERCIAL MHD POWER PLANTS. TASK 3: PARAMETER VARIATION OF PLANT SIZE Final Report
F. A. HALS Sep. 1981 221 p refs
(Contract DEN3-51; DE-AI01-77ET-710769)
(NASA-CR-165445; DOE/NASA/0051-3; NAS 1.26:165445)
Avail: NTIS HC A10/MF A01 CSCL 10B

Plants with a nominal output of 200 and 500 MWe and conforming to the same design configuration as the Task II plant were investigated. This information is intended to permit an assessment of the competitiveness of first generation MHD/steam plants with conventional steam plants over the range of 200 to 1000 MWe. The results show that net plant efficiency of the MHD plant is significantly higher than a conventional steam plant of corresponding size. The cost of electricity is also less for the MHD plant over the entire plant size range. As expected, the cost differential is higher for the larger plant and decreases with plant size. Even at the 200 MWe capacity, however, the differential in COE between the MHD plant and the conventional plant is sufficient attractive to warrant serious consideration. Escalating fuel costs will enhance the competitive position of MHD plants because they can utilize the fuel more efficiently than conventional steam plants. S.L.

N83-27344* National Aeronautics and Space Administration. Lewis Research Center, Cleveland, Ohio.
ZIRCONIUM CARBIDE AS AN ELECTROCATALYST FOR THE CHROMOUS-CHROMIC REDOX COUPLE Patent
R. F. GAHN, M. A. REID, and C. Y. YANG, inventors (to NASA) 22 May 1981 8 p Filed 22 May 1981 Supersedes N81-26203 (19 - 18, p 2506)
(NASA-CASE-LEW-13246-1; US-PATENT-4,382,116; US-PATENT-APPL-SN-266255; US-PATENT-CLASS-429-34; US-PATENT-CLASS-429-40; US-PATENT-CLASS-429-105; US-PATENT-CLASS-429-107; US-PATENT-CLASS-429-109)
Avail: US Patent and Trademark Office CSCL 10C

Zirconium carbide is used as a catalyst in a REDOX cell for the oxidation of chromous ions to chromic ions and for the reduction of chromic ions to chromous ions. The zirconium carbide is coated on an inert electronically conductive electrode which is present in the anode fluid of the cell.
Official Gazette, U.S. Patent and Trademark Office

N83-27345*# Engelhard Industries, Inc., Edison, N.J.
DEVELOP AND TEST FUEL CELL POWERED ON-SITE INTEGRATED TOTAL ENERGY SYSTEMS. PHASE 3: FULL-SCALE POWER PLANT DEVELOPMENT Quarterly Report, May - Jul. 1982
20 Apr. 1983 26 p
(Contract DEN3-241; DE-AI01-80ET-17088)
(NASA-CR-168021; DOE/NASA/0241-6; NAS 1.26:168021; QR-6)
Avail: NTIS HC A03/MF A01 CSCL 10A

Satisfactory performance is reported for the first three 12-cell sub-stacks of the 5 kW stack rebuild. Early general conclusions are presented from an economic study. Results are reported on a successful 700-hour test of a 3-cell stack in the full-sized configuration (0.33m x 0.56m). Construction of a 5 kW equivalent methanol/steam reformer based on a commercial shell-and-tube heat exchanger was completed. Several test runs are summarized. Preliminary conclusions are presented on the technical and economic aspects of fuel cell/HVAC interaction. Physical data are presented on several dense graphite materials which are candidates for gas-distribution plates. Performance of a new cathode catalyst is reported. Author

N83-27346*# National Aeronautics and Space Administration. Lewis Research Center, Cleveland, Ohio.
TEST RESULTS AND DESCRIPTION OF A 1-KW FREE-PISTON STIRLING ENGINE WITH A DASHPOT LOAD
J. SCHREIBER 1983 22 p refs Presented at 18th Intersoc. Energy Conversion Engr. Conf., Orlando, Fla., 21-26 Aug. 1983
(Contract DE-AI05-82OR-1055)
(NASA-TM-83407; DOE/NASA/1005-1; E-1688; NAS 1.15:83407)
Avail: NTIS HC A02/MF A01 CSCL 10B

A 1 kW (1.33 hp) single cylinder free piston Stirling engine was installed in the test facilities at the Lewis laboratory. The engine was designed specifically for research of the dynamics of its operation. A more complete description of the engine and its instrumentation is provided in a prior NASA paper TM-82999 by J. G. Schreiber. Initial tests at Lewis showed the power level and efficiency of the engine to be below design level. Tests were performed to help determine the specific problems in the engine causing the below design level performance. Modifications to engine hardware and to the facility where performed in an effort to bring the power output and efficiency to their design values. As finally configured the engine generated more than 1250 watts of output power at an engine efficiency greater than 32 percent. This report presents the tests performed to help determine the specific problems, the results if the problem was eliminated, the fix performed to the hardware, and the test results after the engine was tested. In cases where the fix did not cause the anticipated effects, a possible explanation is given. Author

N83-27347*# National Aeronautics and Space Administration. Lewis Research Center, Cleveland, Ohio.
FABRICATION OF LOW-COST MOD-OA WOOD COMPOSITE WIND TURBINE BLADES Final Report
R. F. LARK, M. GOUGEON (Gougeon Brothers, Inc., Bay City, Mich.), G. THOMAS (Gougeon Brothers, Inc., Bay City, Mich.), and M. ZUTECK (Gougeon Brothers, Inc., Bay City, Mich.) Feb. 1983 70 p refs
(Contract DE-AI01-79ET-20320)
(NASA-TM-83323; E-1564; DOE/NASA/20320-45; NAS 1.15:83323) Avail: NTIS HC A04/MF A01 CSCL 10A

The wood composite blades were fabricated by using epoxy resin-bonded laminates of Douglas fir veneers for the leading edge spar sections and honeycomb-cored birch plywood panels for the blade trailing edge or afterbody sections. The blade was joined to the wind turbine hub assembly by epoxy resin-bonded steel load take-off studs. The wood composite blades were installed in the Mod-OA wind turbine test facility at Kahuku, Hawaii. The wood composite blades have successfully completed high power (average of 150 kW) operations for an eighteen month period (nearly 8,000 hr) before replacement with another set of wood composite blades. The original set of blades was taken out of service because of the failure of the shank on one stud. An inspection of the blades at NASA-Lewis showed that the shank failure was caused by a high stress concentration at a corrosion pit on the shank fillet radius which resulted in fatigue stresses in excess of the endurance limit. Author

N83-27351*# Naval Weapons Support Center, Crane, Ind. Weapons Quality Engineering Center.
EVALUATION PROGRAM FOR SECONDARY SPACECRAFT CELLS. CYCLE LIFE TEST Annual Report
J. D. HARKNESS 22 Feb. 1982 298 p
(Contract NASA ORDER C-13105-D)
(NASA-CR-172679; NAS 1.26:172679; WQEC/C-82-23; AR-18)
Avail: NTIS HC A13/MF A01 CSCL 10C

Evaluation of secondary spacecraft cells was begun according to the program outline. The cycle life test of the evaluation program of secondary spacecraft cells, through 15 December 1981 is covered. Author

N83-27352*# Naval Weapons Support Center, Crane, Ind. Weapons Quality Engineering Center.
EVALUATION PROGRAM FOR SECONDARY SPACECRAFT CELLS. CYCLE LIFE TEST Annual report
J. D. HARKNESS 1983 300 p
(Contract NASA ORDER C-13105-D)
(NASA-CR-172680; NAS 1.26:172680; WQEC/C-83-1; AR-19)
Avail: NTIS HC A13/MF A01 CSCL 10C

Evaluation of secondary spacecraft was begun. The cycle life test of the evaluation program of secondary spacecraft cells, through 15 December 1982 is covered. Author

N83-28580*# Faucett (Jack) Associates, Inc., Chevy Chase, Md.
ENERGY AND PRECIOUS FUELS REQUIREMENTS OF FUEL ALCOHOL PRODUCTION. VOLUME 4: APPENDICES G AND H, METHANOL FROM COAL Final Report
H. WEINBLATT, G. BACK, and T. S. REDDY (Battelle Columbus Labs., Ohio) Dec. 1982 68 p refs
(Contract DEN3-292; DE-AI01-81CS-50006)
(NASA-CR-168093; DOE/NASA/0292-1; NAS 1.26:168093; JACKFAU-82-299-VOL-4) Avail: NTIS HC A04/MF A01 CSCL 10A

Coal mine location, mining technology, energy consumption in mining, coal transport, and potential availability of coal are discussed. Methanol from coal is also discussed. Author

N83-28581*# Faucett (Jack) Associates, Inc., Chevy Chase, Md.
ENERGY AND PRECIOUS FUELS REQUIREMENTS OF FUEL ALCOHOL PRODUCTION, VOLUME 1 Final Report
H. WEINBLATT, M. F. LAWRENCE, and D. JENKINS Dec. 1982 87 p refs Prepared in cooperation with Battelle Columbus Labs. 3 Vol.
(Contract DEN3-292; DE-AI01-81CS-50006)
(NASA-CR-168090; DOE/NASA/0292-1; NAS 1.26:168090; JACKFAU-82-299-VOL-1) Avail: NTIS HC 05/MF A01 CSCL 10A

Ethanol from grain, methanol from cellulose, and methanol from coal are considered. Author

N83-28582*# Faucett (Jack) Associates, Inc., Chevy Chase, Md.
ENERGY AND PRECIOUS FUELS REQUIREMENTS OF FUEL ALCOHOL PRODUCTION. VOLUME 2, APPENDICES A AND B: ETHANOL FROM GRAIN Final Report
H. WEINBLATT, T. S. REDDY (Battelle Columbus Labs.), and A. TURHOLLOW, JR. (Iowa State Univ.) Dec. 1982 78 p refs 3 Vol.
(Contract DEN3-292; DE-AI01-81CS-50006)
(NASA-CR-168091; DOE/NASA/0292-1; NAS 1.26:168091; JACKFAU-82-299-VOL-2) Avail: NTIS HC A05/MF A01 CSCL 10A

Energy currently used in grain production, the effect of ethanol production on agricultural energy consumption, energy credits for ethanol by-products, and land availability and the potential for obtaining ethanol from grain are discussed. Dry milling, wet milling, sensitivity analysis, potential for reduced energy consumption are also discussed. Author

N83-28583*# Faucett (Jack) Associates, Inc., Chevy Chase, Md.
ENERGY AND PRECIOUS FUELS REQUIREMENTS OF FUEL ALCOHOL PRODUCTION. VOLUME 3, APPENDICES C TO F: METHANOL FROM CELLULOSE Final Report
R. MARGULIS, G. BACK, K. ST.JOHN, and T. S. REDDY Dec. 1982 119 p refs Prepared in cooperation with Battelle Columbus Labs. 3 Vol.
(Contract DEN3-292; DE-AI01-81CS-50006)
(NASA-CR-168092; DOE/NASA/0292-1; NAS 1.26:168092; JACKFAU-82-299-VOL-3) Avail: NTIS HC A06/MF A01 CSCL 10A

Forest residues, silvicultural biomass farms, agricultural residues, and methanol from cellulosic feedstocks are discussed. Author

N83-29804*# National Aeronautics and Space Administration. Lewis Research Center, Cleveland, Ohio.
HIGH THERMAL POWER DENSITY HEAT TRANSFER APPARATUS PROVIDING ELECTRICAL ISOLATION AT HIGH TEMPERATURE USING HEAT PIPES Patent Application
J. F. MORRIS, inventor (to NASA) 24 Jun. 1983 10 p
(NASA-CASE-LEW-12950-2; US-PATENT-APPL-SN-507626)
Avail: NTIS HC A02/MF A01 CSCL 10A

This invention is directed to transferring heat from an extremely high temperature source to an electrically isolated lower temperature receiver. The invention is particularly concerned with supplying thermal power to a thermionic converter from a nuclear reactor with electric isolation. Heat from a high temperature heat pipe is transferred through a vacuum or a gap filled with electrically nonconducting gas to a cooler heat pipe. The heat pipe is used to cool the nuclear reactor while the heat pipe is connected thermally and electrically to a thermionic converter. If the receiver requires greater thermal power density, geometries are used with larger heat pipe areas for transmitting and receiving energy than the area for conducting the heat to the thermionic converter. In this way the heat pipe capability for increasing thermal power densities compensates for the comparatively low thermal power densities through the electrically nonconducting gap between the two heat pipes. NASA

N83-29805*# National Aeronautics and Space Administration. Lewis Research Center, Cleveland, Ohio.
POLYVINYL ALCOHOL BATTERY SEPARATOR CONTAINING INERT FILLER Patent Application
D. W. SHEIBLEY, L. C. HSU, and M. A. MANZO, inventors (to NASA) 3 Feb. 1983 13 p
(NASA-CASE-LEW-13556-2; US-PATENT-APPL-SN-463440)
Avail: NTIS HC A02/MF A01 CSCL 10C

A cross-linked polyvinyl alcohol battery separator is described. A particulate filler, inert to the alkaline electrolyte of an alkaline battery, is incorporated in the separator in an amount of 1 to 20% by weight, based on the weight of the polyvinyl alcohol, and is dispersed throughout the product. Incorporation of the filler enhances performance and increases cycle life of alkaline batteries when compared with batteries containing a similar separator not containing filler. Suitable fillers include titanates, silicates, zirconates, aluminates, wood flour, lignin, and titania. Particle size is not greater than about 50 microns. NASA

N83-29810*# National Aeronautics and Space Administration. Lewis Research Center, Cleveland, Ohio.
NASA REDOX PROJECT STATUS SUMMARY
N. H. HAGEDORN Apr. 1983 13 p Presented at the 5th Battery and Electrochem. Contractors' Conf., Arlington, Va., 7-9 Dec. 1982; sponsored by DOE
(Contract DE-AI04-80AL-12726)
(NASA-TM-83401; E-1679; DOE/NASA/12726-22; NAS 1.15:83401) Avail: NTIS HC A02/MF A01 CSCL 10C

This report is a summary of the results of the Redox Project effort during Cy 1982. It was presented at the Fifth U.S. Department of Energy Battery and Electrochemical Contractors Conference, Arlington, Va., Dec. 7-9, 1982. The major development during 1982

was the shift from Redox system operation at 25 C with unmixed reactants to operation at 65 C with mixed reactants. This change has made possible a two- or three-fold increase in operating current density, to about 65 mA/sq cm, and an increase in reactant utilization from 40% to about 90%. Both of these improvements will lead to significant system cost reductions. Contract studies have indicated that Redox reactant costs also will be moderate. A new catalyst for the chromuim electrode offers all the advantages of the conventional gold-lead catalyst while being easier to apply and more forgiving in use. Author

N83-29811*# National Aeronautics and Space Administration. Lewis Research Center, Cleveland, Ohio.
COMPARISON OF ROAD LOAD SIMULATOR TEST RESULTS WITH TRACK TESTS ON ELECTRIC VEHICLE PROPULSION SYSTEM Final Report
M. O. DUSTIN Jun. 1983 18 p refs
(Contract DE-AI01-77CS-51044)
(NASA-TM-83393; E-170; DOE/NASA/51044-30; NAS 1.15:83393) Avail: NTIS HC A02/MF A01 CSCL 13F

A special-purpose dynamometer, the road load simulator (RLS), is being used at NASA's Lewis Research Center to test and evaluate electric vehicle propulsion systems developed under DOE's Electric and Hybrid Vehicle Program. To improve correlation between system tests on the RLS and track tests, similar tests were conducted on the same propulsion system on the RLS and on a test track. These tests are compared in this report. Battery current to maintain a constant vehicle speed with a fixed throttle was used for the comparison. Scatter in the data was greater in the track test results. This is attributable to variations in tire rolling resistance and wind effects in the track data. It also appeared that the RLS road load, determined by coastdown tests on the track, was lower than that of the vehicle on the track. These differences may be due to differences in tire temperature.
Author

N83-29812*# Boeing Engineering and Construction Co., Seattle, Wash.
MOD-2 WIND TURBINE SYSTEM DEVELOPMENT. VOLUME 1: EXECUTIVE SUMMARY Final Report
Sep. 1982 37 p
(Contract DEN3-2; DE-AI01-82ET-20305)
(NASA-CR-168006; DOE/NASA/0002-1; NAS 1.26:168006)
Avail: NTIS HC A03/MF A01 CSCL 10B

The development of the MOD-2 wind turbine through acceptance testing and initial operational evaluation is documented. Pitch control hydraulic system, yaw control system, drive train, electrical power station, control system, operations and maintenance experience, and availability are discussed. Author

N83-29813*# National Aeronautics and Space Administration. Lewis Research Center, Cleveland, Ohio.
RESULTS OF FREE YAW TESTS OF THE MOD-0 100 KILOWATT WIND TURBINE
J. C. GLASGOW and R. D. CORRIGAN 1983 20 p refs Presented at the 6th Biennial Wind Energy Conf. and Workshop, Minneapolis, 1-3 Jun. 1983
(Contract DE-AI01-76ET-20320)
(NASA-TM-83432; DOE/NASA/20320-46; E-1724; NAS 1.15:83432) Avail: NTIS HC A02/MF A01 CSCL 10A

Tests were conducted on the Mod-0 100 kW experimental wind turbine to provide data on yaw alignment characteristics of a large horizontal axis wind turbine with its yaw restraint removed (i.e., in free yaw). The wind turbine consisted of a downwind horizontal axis rotor mounted on a tubular tower. Three rotor configurations were tested. Each rotor was teetered, coned 3 deg and tip-controlled. Two of the rotors had pitch-flap coupling or Delta-3, and one rotor had none. The two rotors with Delta-3 differed in the airfoil used in the tip sections. Test results indicate the rotor without pitch-flap coupling did not align closer than 25 deg with the wind, and pitch-flap coupling improved the wind turbine's alignment with the wind. Yaw damping was shown to have a favorable effect on free yaw characteristics. The change in the tip airfoil section was shown to affect the free yaw alignment also. The rotors with Delta-3 were shown to be capable of responding to wind shifts and exhibited stable operating properties. Author

N83-31107*# National Aeronautics and Space Administration. Lewis Research Center, Cleveland, Ohio.
DOE LARGE HORIZONTAL AXIS WIND TURBINE DEVELOPMENT AT NASA LEWIS RESEARCH CENTER
B. S. LINSCOTT 1982 16 p refs Presented at the Wind/Solar Energy Conf., Kansas City, Mo., 25-26 Apr. 1983
(NASA-TM-83444; E-1744; DOE/NASA/20320-47; NAS 1.15:83444) Avail: NTIS HC A02/MF A01 CSCL 10A

Large wind turbine activities managed by NASA Lewis are reviewed. These activities include results from the first and second generation field machines (Mod-OA, -1, and -2), the status of the Department of Interior WTS-4 machine for which NASA is responsible for technical management, and the design phase of the third generation wind turbines (Mod-5). Author

N83-32175* National Aeronautics and Space Administration. Lewis Research Center, Cleveland, Ohio.
THERMIONIC ENERGY CONVERTERS Patent
J. F. MORRIS, inventor (to NASA) 8 Dec. 1983 6 p Filed 19 Feb. 1981 Supersedes N81-19561 (19 - 10, p 1368)
(NASA-CASE-LEW-12443-1; US-PATENT-4,373,142; US-PATENT-APPL-SN-235797; US-PATENT-CLASS-310-306)
Avail: US Patent and Trademark Office CSCL 10A

The efficiency of thermionic energy converters is improved by internal distribution of tiny sorted cesium diodes driven by the thermal gradient between the primary emitter and the collector. The tiny, sorted diode distribution comprises protrusions of the emitter material from the main emitter face which contact the main collector face thermally but not electrically. The main collector ends of the protrusions are separated from the main collector by a thin layer of insulation, such as aluminum oxide. The shorted tiny diode distribution augments cesium ionization through internal thermal effects only within the main diode. No electrical inputs are required. This ionization enhancement by the distribution of the tiny shorted diodes not only reduces the plasma voltage drop but also increases the power output and efficiency of the overall thermionic energy converter.
Official Gazette of the U.S. Patent and Trademark Office

N83-32176* National Aeronautics and Space Administration. Lewis Research Center, Cleveland, Ohio.
ADVANCED INORGANIC SEPARATORS FOR ALKALINE BATTERIES AND METHOD OF MAKING THE SAME Patent
D. W. SHEIBLEY, inventor (to NASA) 1 Feb. 1983 5 p Filed 22 Dec. 1981
(NASA-CASE-LEW-13171-2; US-PATENT-4,371,596; US-PATENT-APPL-SN-333537; US-PATENT-CLASS-429-144; US-PATENT-CLASS-429-251; US-PATENT-CLASS-429-254; US-PATENT-CLASS-29-623.5) Avail: US Patent and Trademark Office CSCL 10C

A flexible, porous battery separator includes a coating applied to a porous, flexible substrate. The coating comprises: (1) a thermoplastic rubber-based resin which is insoluble and unreactive in the alkaline electrolyte, (2) a polar organic plasticizer which is reactive with the alkaline electrolyte to produce a reaction product which contains a hydroxyl group and/or a carboxylic acid group, and (3) a mixture of polar particulate filler materials which are unreactive with the electrode. The mixture comprises at least one first filler material having a surface area of greater than 25 sq meters/gram, at last one second filler material having a surface area of 10 to 25 sq meters/gram. The volume of the mixture of filler materials is less than 45% of the total volume of the fillers and the binder. The filler surface area per gram of binder is about 20 to 60 sq meters/gram, and the amount of plasticizer is sufficient to coat each filler particle.
Official Gazette of the U.S. Patent and Trademark Office

N83-32177* National Aeronautics and Space Administration. Lewis Research Center, Cleveland, Ohio.
HIGH VOLTAGE V-GROOVE SOLAR CELL Patent
J. C. EVANS, JR., A. T. CHAI, and C. P. GORADIA, inventors (to NASA) 15 Mar. 1983 6 p Filed 18 Mar. 1982 Supersedes N82-24717 (20 - 15, p 2122)
(NASA-CASE-LEW-13401-2; US-PATENT-4,376,872; US-PATENT-APPL-SN-359388; US-PATENT-CLASS-136-249; US-PATENT-CLASS-357-30) Avail: US Patent and Trademark Office CSCL 10A

A high voltage multijunction solar cell comprises a number of discrete voltage generating regions, or unit cells, which are formed in a single semiconductor wafer and are connected together so that the voltages of the individual cells are additive. The unit cells comprise doped regions of opposite conductivity types separated by a gap. The method includes forming V-shaped grooves in the wafer and orienting the wafer so that ions of one conductivity type can be implanted in one face of the groove while the other face is shielded. A metallization layer is applied and selectively etched away to provide connections between the unit cells.
Official Gazette of the U.S. Patent and Trademark Office

N83-33320*# Hughes Aircraft Co., Long Beach, Calif. Support Systems.
MODULAR PHOTOVOLTAIC STAND-ALONE SYSTEMS: PHASE 1 Final Report
G. J. NAFF and N. A. MARSHALL Feb. 1983 298 p
(Contract DEN3-207; DE-AI01-79ET-20485)
(NASA-CR-168075; DOE/NASA/0207-1; NAS 1.26:168075; HAC-F107-500) Avail: NTIS HC A13/MF A01 CSCL 10A

A family of modular stand-alone power systems that covered the range in power level from 1 kw to 14 kw was developed. Products within this family were required to be easily adaptable to different environments and applications, and were to be both reliable and cost effective. Additionally, true commonality in hardware was to be exploited, and unnecessary recurrence of design and development costs were to be minimized; thus improving hardware availability. Assurance of compatibility with large production runs, was also an underlying program goal. A secondary objective was to compile, evaluate, and determine the economic and technical status of available, and potentially available, technology options associated with the balance of systems (BOS) for stand-along photovoltaic (PV) power systems. The secondary objective not only directly supported the primary but additionally contributed to the definition and implementation of the BOS cost reduction plan. Author

N83-33343*# Boeing Engineering and Construction Co., Seattle, Wash.
MOD-2 WIND TURBINE SYSTEM DEVELOPMENT. VOLUME 2: DETAILED REPORT Final Report
Sep. 1982 194 p refs
(Contract DEN3-2; DE-AI01-82ET-20305)
(NASA-CR-168007; DOE/NASA/0002-2; NAS 1.26:168007)
Avail: NTIS HC A09/MF A01 CSCL 10A

Progress in the design, fabrication, and testing of a wind turbine system is reported. The development of the MOD-2 wind turbine through acceptance testing and initial operational evaluation is documented. The MOD-2 project intends to develop early commercialization of wind energy. The first wind turbine farm (three MOD-2 units) are now being operated at the Bonneville Power Administration site near Goldendale, Washington. E.A.K.

N83-34450*# Michigan Univ., Ann Arbor.
PRACTICAL ASPECTS OF PHOTOVOLTAIC TECHNOLOGY, APPLICATIONS, AND COST
L. ROSENBLUM Dec. 1982 249 p
(Contract NAG3-185)
(NASA-CR-168025; NAS 1.26:168025) Avail: NTIS HC A11/MF A01 CSCL 10A

Background, understanding, and computational tools needed to master the practical aspects of photovoltaic (PV) technology, application, and cost are presented. Stand alone silicon solar cell, flat plate systems in the range of 1 to 25 kWH/day output are discussed. Topics covered include: operation and performance of each of the major system components, safety, installation, operation and maintenance, and electrical loads. Application experience and trends are presented. Indices of electrical service performance are reliability, availability, and voltage control are discussed, and the known service performance of central station electric grid, diesel generator, and PV stand alone systems are compared. The PV system sizing methods are reviewed and compared, and a procedure for rapid sizing is described and illustrated by the use of several sample cases. The rapid sizing procedure yields an array and battery size that corresponds to a minimum cost system for a given load requirement, insolation condition, and desired level of service performance. The PV system capital cost and levelized energy cost are derived as functions of service performance and insolation. E.A.K.

N83-34451*# Power Technologies, Inc., Schenectady, N. Y.
CONTROL OF LARGE WIND TURBINE GENERATORS CONNECTED TO UTILITY NETWORKS Final Report
E. N. HINRICHSEN May 1983 91 p refs
(Contract DEN3-252; DE-AI01-76ET-20320)
(NASA-CR-168200; DOE/NASA/0252-1; NAS 1.26:168200; R19-83) Avail: NTIS HC A05/MF A01 CSCL 10B

This is an investigation of the control requirements for variable pitch wind turbine generators connected to electric power systems. The requirements include operation in very small as well as very large power systems. Control systems are developed for wind turbines with synchronous, induction, and doubly fed generators. Simulation results are presented. It is shown how wind turbines and power system controls can be integrated. A clear distinction is made between fast control of turbine torque, which is a peculiarity of wind turbines, and slow control of electric power, which is a traditional power system requirement. Author

N83-34453*# National Aeronautics and Space Administration. Lewis Research Center, Cleveland, Ohio.
SUMMARY OF SYNFUEL CHARACTERIZATION AND COMBUSTION STUDIES Final Report
D. F. SCHULTZ Aug. 1983 57 p refs
(Contract DE-AI01-77ET-13111)
(NASA-TM-83066; DOE/NASA/13111-15; E-1537; NAS 1.15:83066) Avail: NTIS HC A04/MF A01 CSCL 21B

Combustion component research studies aimed at evolving environmentally acceptable approaches for burning coal derived fuels for ground power applications were performed at the NASA Lewis Research Center under a program titled the "Critical Research and Support Technology Program" (CRT). The work was funded by the Department of Energy and was performed in four tasks. This report summarizes these tasks which have all been previously reported. In addition some previously unreported data from Task 4 is also presented. The first, Task 1 consisted of a literature survey aimed at determining the properties of synthetic fuels. This was followed by a computer modeling effort, Task 2, to predict the exhaust emissions resulting from burning coal liquids by various combustion techniques such as lean and rich-lean combustion. The computer predictions were then compared to the results of a flame tube rig, Task 3, in which the fuel properties were varied to simulate coal liquids. Two actual SRC 2 coal liquids were tested in this flame tube task. Author

N83-34454*# General Dynamics Corp., St. Louis, Mo. Convair Div.
ANALYSIS OF THE REFLECTIVE MULTIBANDGAP SOLAR CELL CONCEPT
T. G. STERN Jul. 1983 42 p refs
(Contract NAS3-22252)
(NASA-CR-168186; NAS 1.26:168186; GDC-SP-83-041) Avail: NTIS HC A03/MF A01 CSCL 10A

A new and unique approach to improving photovoltaic conversion efficiency, the reflective multiband gap solar cell concept, was examined. This concept uses back surface reflectors and light trapping with several physically separated cells of different

bandgaps to make more effective use of energy from different portions of the solar spectrum. Preliminary tests performed under General Dynamics Independent Research and Development (IRAD) funding have demonstrated the capability for achieving in excess of 20% conversion efficiency with aluminum gallium arsenide and silicon. This study analyzed the ultimate potential for high conversion efficiency with 2, 3, 4, and 5 different bandgap materials, determined the appropriate bandgaps needed to achieve this optimized efficiency, and identified potential problems or constraints. The analysis indicated that an improvement in efficiency of better than 40% could be attained in this multibandgap approach, compared to a single bandgap converter under the same assumptions. Increased absorption loss on the back surface reflector was found to incur a minimal penalty on efficiency for two and three bandgap systems. Current models for bulk absorption losses in 3-5 materials were found to be inadequate for explaining laboratory observed transmission losses. Recommendations included the continued development of high bandgap back surface reflector cells and basic research on semiconductor absorption mechanisms. Author

N83-35496*# National Aeronautics and Space Administration. Lewis Research Center, Cleveland, Ohio.
STEADY-STATE AND DYNAMIC EVALUATION OF THE ELECTRIC PROPULSION SYSTEM TEST BED VEHICLE ON A ROAD LOAD SIMULATOR Final Report
M. O. DUSTIN Aug. 1983 22 p refs
(Contract DE-AI01-77CS-51044)
(NASA-TM-83445; DOE/NASA/51044-32; E-1745; NAS 1.15:83445) Avail: NTIS HC A02/MF A01 CSCL 13F

The propulsion system of the Lewis Research Center's electric propulsion system test bed vehicle was tested on the road load simulator under the DOE Electric and Hybrid Vehicle Program. This propulsion system, consisting of a series-wound dc motor controlled by an infinitely variable SCR chopper and an 84-V battery pack, is typical of those used in electric vehicles made in 1976. Steady-state tests were conducted over a wide range of differential output torques and vehicle speeds. Efficiencies of all of the components were determined. Effects of temperature and voltage variations on the motor and the effect of voltage changes on the controller were examined. Energy consumption and energy efficiency for the system were determined over the B and C driving schedules of the SAE J227a test procedure. Author

N83-35497*# Hughes Aircraft Co., Long Beach, Calif. Support Systems Div.
PHOTOVOLTAIC STAND-ALONE MODULAR SYSTEMS, PHASE 2 Final Report
G. J. NAFF and N. A. MARSHALL Jul. 1983 105 p
(Contract DEN3-207; DE-AI01-79ET-20485)
(NASA-CR-168230; NAS 1.26:168230; HAC-E8179) Avail: NTIS HC A06/MF A01 CSCL 10A

The final hardware and system qualification phase of a two part stand-alone photovoltaic (PV) system development is covered. The final design incorporated modular, power blocks capable of expanding incrementally from 320 watts to twenty kilowatts (PK). The basic power unit (PU) was nominally rated 1.28 kWp. The controls units, power collection buses and main lugs, electrical protection subsystems, power switching, and load management circuits are housed in a common control enclosure. Photo-voltaic modules are electrically connected in a horizontal daisy-chain method via Amp Solarlok plugs mating with compatible connectors installed on the back side of each photovoltaic module. A pair of channel rails accommodate the mounting of the modules into a frameless panel support structure. Foundations are of a unique planter (tub-like) configuration to allow for world-wide deployment without restriction as to types of soil. One battery string capable of supplying approximately 240 ampere hours nominal of carryover power is specified for each basic power unit. Load prioritization and shedding circuits are included to protect critical loads and selectively shed and defer lower priority or noncritical power demands. The baseline system, operating at approximately 2 1/2 PUs (3.2 kW pk.) was installed and deployed. Qualification was successfully complete in March 1983; since that time, the demonstration system has logged approximately 3000 hours of continuous operation under load without major incident. Author

N83-35498*# National Aeronautics and Space Administration. Lewis Research Center, Cleveland, Ohio.
NICKEL-HYDROGEN COMPONENT DEVELOPMENT
J. A. CHARLESTON 1983 12 p refs Presented at Natl. Tech. Assoc. Conv., Kissimee, Fla., 25-30 Jul. 1983
(NASA-TM-83487; E-1811; NAS 1.15:83487) Avail: NTIS HC A02/MF A01 CSCL 10A

Light weight energy storage systems for future space missions are investigated. One of the systems being studied is the nickel hydrogen battery. This battery is designed to achieve longer life, improve performance, and higher energy densities for space applications. The nickel hydrogen component development is discussed. Test data from polarization measurements of the hydrogen electrode component is presented. S.L.

N83-36549*# National Aeronautics and Space Administration. Lewis Research Center, Cleveland, Ohio.
ANALYSIS OF POTENTIAL BENEFITS OF INTEGRATED-GASIFIER COMBINED CYCLES FOR A UTILITY SYSTEM
Y. K. CHOO Oct. 1983 21 p
(NASA-TP-2172; E-1465; NAS 1.60:2172) Avail: NTIS HC A02/MF A01 CSCL 10B

Potential benefits of integrated gasifier combined cycle (IGCC) units were evaluated for a reference utility system by comparing long range expansion plans using IGCC units and gas turbine peakers with a plan using only state of the art steam turbine units and gas turbine peakers. Also evaluated was the importance of the benefits of individual IGCC unit characteristics, particularly unit efficiency, unit equivalent forced outage rate, and unit size. A range of IGCC units was analyzed, including cases achievable with state of the art gas turbines and cases assuming advanced gas turbine technology. All utility system expansion plans that used IGCC units showed substantial savings compared with the base expansion plan using the steam turbine units. Author

45

ENVIRONMENT POLLUTION

Includes air, noise, thermal and water pollution; environment monitoring; and contamination control.

A83-11493*# Westinghouse Electric Corp., Concordville, Pa.
NOX RESULTS FROM TWO COMBUSTORS TESTED ON MEDIUM BTU COAL GAS
T. P. SHERLOCK, D. E. CARL, G. VERMES (Westinghouse Electric Corp., Concordville, PA), J. SCHWAB (Westinghouse Electric Corp., Pittsburgh, PA), and J. J. NOTARDONATO (NASA, Lewis Research Center, Cleveland, OH) IEEE, ASME, and ASCE, Joint Power Generation Conference, Denver, CO, Oct. 17-21, 1982, Paper. 9 p.

The results of tests of two combustor configurations using coal gas from a 25 ton/day fluidized bed coal gasifier are reported. The trials were run with a ceramic-lined, staged rich/lean burner and an integral, all metal multiannular swirl burner (MASB) using a range of temperatures and pressures representative of industrial turbine inlet conditions. A lean mixture was examined at 104, 197, and 254 Btu/Scf, yielding NO(x) emissions of 5, 20, and 70 ppmv, respectively. The MASB was employed only with a gas rated at 220-270 Btu/Scf, producing 80 ppmv NO(x) at rated engine conditions. The results are concluded to be transferrable to current machines. Further tests on the effects of gas composition, the scaling of combustors to utility size, and the development of improved wall cooling techniques and variable geometry are indicated. M.S.K.

N83-11556*# National Aeronautics and Space Administration. Lewis Research Center, Cleveland, Ohio.
AIRCRAFT SAMPLING OF THE SULFATE LAYER NEAR THE TROPOPAUSE FOLLOWING THE ERUPTION OF MOUNT ST. HELENS
E. A. LEZBERG, D. A. OTTERSON, W. K. ROBERTS, and L. C. PAPATHAKOS *In* NASA. Langley Research Center Atmospheric Effects and Potential Climatic Impact of the 1980 Eruptions of Mt. St. Helens p 251-259 Oct. 1982 refs Originally announced as 82A-37450
Avail: NTIS HC A13/MF A01 CSCL 13B

Twenty filter sampling flights of the NASA Lewis F-106 aircraft were conducted in the Great Lakes region between June 4 and August 8, 1980, following the major eruption of Mount St. Helens, Washington on May 18. The IPC-1478 filters were exposed over an altitude range spanning the local tropopause. Quarter sections were analyzed for sulfate and nitrate by ion chromatography and selected samples were analyzed for chloride by selective ion electrode. Trace elements were searched by X-ray fluorescence analysis. A filter sample taken above the tropopause on June 5 indicated a sulfate level of 50 times the baseline measurements. Subsequent measurements over a period of 2 months showed an initial dropoff and formation of a persistent layer of sulfate above the tropopause with a concentration of 10 to 18 times previously measured background-levels. Concentrations of nitrate above the tropopause exhibited considerable variability and some enhancement compared with previously measured concentration levels. It is suggested that the source of the nitrate may also be volcanic as evidenced by its temporal relationship to the sulfate concentration changes. Based on the null results of X-ray fluorescence measurements, there is no evidence of ash particle concentrations greater than 3.4 microns g/cubic m persisting in the layer above the tropopause after the second transit of the cloud. E.A.K.

N83-13643*# National Aeronautics and Space Administration. Lewis Research Center, Cleveland, Ohio.
WATER VAPOR MEASUREMENT SYSTEM IN GLOBAL ATMOSPHERIC SAMPLING PROGRAM, APPENDIX
D. R. ENGLUND and T. J. DUDZINSKI Nov. 1982 18 p refs (NASA-TP-2051; E-1167; NAS 1.60:2051) Avail: NTIS HC A02/MF A01 CSCL 13B

The water vapor measurement system used in the NASA Global Atmospheric Sampling Program (GASP) is described. The system used a modified version of a commercially available dew/frostpoint hygrometer with a thermoelectrically cooled mirror sensor. The modifications extended the range of the hygrometer to enable air sample measurements with frostpoint temperatures down to -80 C at altitudes of 6 to 13 km. Other modifications were made to permit automatic, unattended operation in an aircraft environment. This report described the hygrometer, its integration with the GASP system, its calibration, and operational aspects including measurement errors. The estimated uncertainty of the dew/frostpoint measurements was + or - 1.7 Celsius. Author

46

GEOPHYSICS

Includes aeronomy; upper and lower atmosphere studies; ionospheric and magnetospheric physics; and geomagnetism.

N83-21677*# Science Applications, Inc., Dayton, Ohio.
ATMOSPHERIC RADIATION MODEL FOR WATER SURFACES
Final Technical Report, 4 Mar. 1981 - 15 Jul. 1982
R. E. TURNER, D. W. GASKILL, and J. R. LIERZER May 1982 67 p refs
(Contract NAS3-22495)
(NASA-CR-167873; NAS 1.26:167873; SAI-82-002-AA) Avail: NTIS HC A04/MF A01 CSCL 04A

An atmospheric correction model was extended to account for various atmospheric radiation components in remotely sensed data. Components such as the atmospheric path radiance which results from singly scattered sky radiation specularly reflected by the water surface are considered. A component which is referred to as the virtual Sun path radiance, i.e. the singly scattered path radiance which results from the solar radiation which is specularly reflected by the water surface is also considered. These atmospheric radiation components are coded into a computer program for the analysis of multispectral remote sensor data over the Great Lakes of the United States. The user must know certain parameters, such as the visibility or spectral optical thickness of the atmosphere and the geometry of the sensor with respect to the Sun and the target elements under investigation. Author

47

METEOROLOGY AND CLIMATOLOGY

Includes weather forecasting and modification.

A83-16526*# Tennessee Univ., Tullahoma.
INFLUENCE OF MULTIDROPLET SIZE DISTRIBUTION ON ICING COLLECTION EFFICIENCY
H.-P. CHANG, K. R. KIMBLE (Tennessee, University, Tullahoma, TN), W. FROST (FWG Associates, Inc.; Tennessee, University, Tullahoma, TN), and R. J. SHAW (NASA, Lewis Research Center, Cleveland, OH) American Institute of Aeronautics and Astronautics, Aerospace Sciences Meeting, 21st, Reno, NV, Jan. 10-13, 1983, 6 p. refs .
(AIAA PAPER 83-0110)

Calculation of collection efficiencies of two-dimensional airfoils for a monodispersed droplet icing cloud and a multidispersed droplet is carried out. Comparison is made with the experimental results reported in the NACA Technical Note series. The results of the study show considerably improved agreement with experiment when multidroplet size distributions are employed. The study then investigates the effect of collection efficiency on airborne particle droplet size sampling instruments. The biased effect introduced due to sampling from different collection volumes is predicted. (Author)

A83-38733* Control Data Corp., Minneapolis, Minn.
CLOUD ENCOUNTER STATISTICS IN THE 28.5-43.5 KFT ALTITUDE REGION FROM FOUR YEARS OF GASP OBSERVATIONS
W. H. JASPERSON, G. D. NASTROM (Control Data Corp., Minneapolis, MN), R. E. DAVIS (NASA, Langley Research Center, Hampton, VA), and J. D. HOLDEMAN (NASA, Lewis Research Center, Cleveland, OH) IN: Conference on Aerospace and

Aeronautical Meteorology, 9th, Omaha, NE, June 6-9, 1983, Preprints . Boston, MA, American Meteorological Society, 1983, p. 159-164. refs

The results of an analysis of cloud encounter measurements taken at aircraft flight altitudes as part of the Global Atmospheric Sampling Program are summarized. The results can be used in estimating the probability of cloud encounter and in assessing the economic feasibility of laminar flow control aircraft along particular routes. The data presented clearly show the tropical circulation and its seasonal migration; characteristics of the mid-latitude regime, such as the large-scale traveling cyclones in the winter and increased convective activity in the summer, can be isolated in the data. The cloud encounter statistics are shown to be consistent with the mid-latitude cyclone model. A model for TIC (time-in-clouds), a cloud encounter statistic, is presented for several common airline routes. V.L.

N83-24048*# Control Data Corp., Minneapolis, Minn.
FLIGHT SUMMARIES AND TEMPERATURE CLIMATOLOGY AT AIRLINER CRUISE ALTITUDES FROM GASP (GLOBAL ATMOSPHERIC SAMPLING PROGRAM) DATA Final Report
G. D. NASTROM and W. H. JASPERSON Mar. 1983 369 p refs
(Contract NAS3-21249)
(NASA-CR-168106; NAS 1.26:168106) Avail: NTIS HC A16/MF A01 CSCL 04B

Temperature data obtained by the Global Atmospheric Sampling Program (GASP) during the period March 1975 to July 1979 are compiled to form flight summaries of static air temperature and a geographic temperature climatology. The flight summaries include the height and location of the coldest observed temperature and the mean flight level, temperature and the standard deviation of temperature for each flight as well as for flight segments. These summaries are ordered by route and month. The temperature climatology was computed for all statistically independent temperture data for each flight. The grid used consists of 5 deg latitude, 30 deg longitude and 2000 feet vertical resolution from FL270 to FL430 for each month of the year. The number of statistically independent observations, their mean, standard deviation and the empirical 98, 50, 16, 2 and .3 probability percentiles are presented. Author

N83-27542*# State Univ. of New York, Albany. Atmosphere Sciences Research Center.
AIRCRAFT MEASUREMENTS OF TRACE GASES AND PARTICLES NEAR THE TROPOPAUSE Final Report
P. FALCONER, R. PRATT, A. DETWILER, C. S. CHEN, A. HOGAN, S. BERNARD, K. KREBSCHULL, and W. WINTERS NASA Washington Jun. 1983 148 p refs
(Contract NSG-3138)
(NASA-CR-3691; NAS 1.26:3691) Avail: NTIS HC A07/MF A01 CSCL 04B

Research activities which were performed using atmospheric constituent data obtained by the NASA Global Atmospheric Sampling Program are described. The characteristics of the particle size spectrum in various meteorological settings from a special collection of GASP data are surveyed. The relationship between humidity and cloud particles is analyzed. Climatological and case studies of tropical ozone distributions measured on a large number of flights are reported. Particle counter calibrations are discussed as well as the comparison of GASP particle data in the upper troposphere with other measurements at lower altitudes over the Pacific Ocean. J.M.S.

52

AEROSPACE MEDICINE

Includes physiological factors; biological effects of radiation; and weightlessness.

N83-20539*# National Aeronautics and Space Administration. Lewis Research Center, Cleveland, Ohio.
ION BEAM SPUTTER ETCHED VENTRICULAR CATHETER FOR HYDROCEPHALUS SHUNT Patent Application
B. A. BANKS, inventor (to NASA) 24 Nov. 1982 13 p
(NASA-CASE-LEW-13107-2; US-PATENT-APPL-SN-444124)
Avail: NTIS HC A02/MF A01 CSCL 06B

An improved cerebrospinal fluid shunt in the form of a ventricular catheter for controlling the condition of hydrocephalus by relieving the excessive cerebrospinal fluid pressure is described. Method for fabricating the catheter and shunting the cerebral fluid from the cerebral ventricles to other areas of the body was improved. The obstruction of cerebrospinal fluid flow pathways or its inadequate absorption via the arachnoid villi into the venus blood of the brain results in hydrocephalus. Surgical correction involves pressure controlled shunting of the cerebrospinal fluid. The shunt will fail to function if the inlet ventricular catheter apertures become blocked. Shunt flow failure also occurs if 15 the ventricle collapses due to improper valve function causing over drainage. The ventricular catheter comprises a multiplicity of inlet microtubules. NASA

N83-21785* National Aeronautics and Space Administration. Lewis Research Center, Cleveland, Ohio.
ION BEAM SPUTTER-ETCHED VENTRICULAR CATHETER FOR HYDROCEPHALUS SHUNT Patent
B. A. BANKS, inventor (to NASA) 10 Jun. 1983 7 p Filed 10 Jun. 1981 Supersedes N81-27786 (19 - 18, p 2531)
(NASA-CASE-LEW-13107-1; US-PATENT-4,377,169; US-PATENT-APPL-SN-272407; US-PATENT-CLASS-604-8; US-PATENT-CLASS-604-280) Avail: US Patent and Trademark Office CSCL 06C

A cerebrospinal fluid shunt in the form of a ventricular catheter for controlling the condition of hydrocephalus by relieving the excessive cerebrospinal fluid pressure is described. A method for fabrication of the catheter and shunting the cerebral fluid from the cerebral ventricles to other areas of the body is also considered. Shunt flow failure occurs if the ventricle collapse due to improper valve function causing overdrainage. The ventricular catheter comprises a multiplicity of inlet microtubules. Each microtubule has both a large openings at its inlet end and a multiplicity of microscopic openings along its lateral surfaces.
Official Gazette, U.S. Patent and Trademark Office

60

COMPUTER OPERATIONS AND HARDWARE

Includes computer graphics and data processing.

A83-16588* Carnegie-Mellon Univ., Pittsburgh, Pa.
FREQUENCY-MULTIPLEXED AND PIPELINED ITERATIVE OPTICAL SYSTOLIC ARRAY PROCESSORS
D. CASASENT, J. JACKSON, and C. NEUMAN (Carnegie-Mellon University, Pittsburgh, PA) Applied Optics, vol. 22, Jan. 1, 1983, p. 115-124. Research supported by Unicorn Systems, Inc refs
(Contract AF-AFOSR-79-0091; NAG3-5)

Optical matrix processors using acoustooptic transducers are described, with emphasis on new systolic array architectures using frequency multiplexing in addition to space and time multiplexing. A Kalman filtering application is considered in a case study from

which the operations required on such a system can be defined. This also serves as a new and powerful application for iterative optical processors. The importance of pipelining the data flow and the ordering of the operations performed in a specific application of such a system are also noted. Several examples of how to effectively achieve this are included. A new technique for handling bipolar data on such architectures is also described. (Author)

A83-36752* Carnegie-Mellon Univ., Pittsburgh, Pa.
TRIANGULAR SYSTEM SOLUTIONS ON AN OPTICAL SYSTOLIC PROCESSOR
A. GHOSH and D. CASASENT (Carnegie-Mellon University, Pittsburgh, PA) Applied Optics (ISSN 0003-6935), vol. 22, June 15, 1983, p. 1795, 1796. refs
(Contract NAG3-5)

It is noted that the simplified system of equations presented by Casasent and Ghosh (1983) can also be solved optically. One realization of this is described, with attention given to data flow and speed for the case of a lower triangular system of equations. The solution of an upper triangular system of equations can be handled in analogous fashion. The problem requires a matrix-vector processor. Only one carrier frequency input to the acoustooptic cell and only one output detector are used. To multiply a matrix by a vector in this system, the time-multiplexed vector elements are fed into the acoustooptic cell. C.R.

A83-38793* Columbia Univ., New York.
AUTOMATIC ALGEBRAIC COORDINATE GENERATION
P. R. EISEMAN (Columbia University, New York, NY) IN: Numerical grid generation; Proceedings of the Symposium on Numerical Generation of Curvilinear Coordinate Systems and Their Use in the Numerical Solution of Partial Differential Equations, Nashville, TN, April 13-16, 1982 . New York and Amsterdam, North-Holland, 1982, p. 447-463. refs
(Contract NAS3-22117; NCC1-59)

A computer software system has been developed to automatically generate two-dimensional coordinates from algebraic transformations. For topologically complex regions, a smooth assembly of the transformations can be used to automatically produce a composite mesh where a general gridded format is retained. The algebraic mesh generation system consists of a collection of operator subroutines which are applied to an established data structure and which automatically perform the necessary parts of mesh construction from a sequence of multisurface transformations. The system operators are discussed, taking into account the data base, the order of application, direct surface generators, geometric surface operators, surface generators from existing surfaces, transverse operators, mesh operators, assembly operators, and data visualization operators. Attention is given to applications related to airfoils. G.R.

A83-43629* Carnegie-Mellon Univ., Pittsburgh, Pa.
LU AND CHOLESKY DECOMPOSITION ON AN OPTICAL SYSTOLIC ARRAY PROCESSOR
D. CASASENT and A. GHOSH (Carnegie-Mellon University, Pittsburgh, PA) Optics Communications (ISSN 0030-4018), vol. 46, July 15, 1983, p. 270-273. refs
(Contract AF-AFOSR-79-0091D; NAG3-5)

Direct solutions of matrix-vector equations on an optical systolic array processor are considered. The solutions are discussed and a parallel algorithm for LU matrix decomposition that is very attractive for an optical realization is formulated. It is noted that when direct techniques are used, it is preferable to realize the matrix decomposition on an optical system and to utilize a digital processor for the solution of the simplified resultant matrix-vector problem. One method of realizing LU matrix decomposition on a new frequency-multiplexed optical systolic array matrix-matrix processor is described. A simple method for extending the process of LU decomposition to Cholesky decomposition on the optical processor is discussed. C.D.

A83-46834* Carnegie-Mellon Univ., Pittsburgh, Pa.
OPTICAL SYSTOLIC ARRAY PROCESSOR USING RESIDUE ARITHMETIC
J. JACKSON and D. CASASENT (Carnegie-Mellon University, Pittsburgh, PA) Applied Optics (ISSN 0003-6935), vol. 22, Sept. 15, 1983, p. 2817-2821. Research supported by the Unicorn Systems, Inc. refs
(Contract NAG3-5)

The use of residue arithmetic to increase the accuracy and reduce the dynamic range requirements of optical matrix-vector processors is evaluated. It is determined that matrix-vector operations and iterative algorithms can be performed totally in residue notation. A new parallel residue quantizer circuit is developed which significantly improves the performance of the systolic array feedback processor. Results are presented of a computer simulation of this system used to solve a set of three simultaneous equations. N.B.

61

COMPUTER PROGRAMMING AND SOFTWARE

Includes computer programs, routines, and algorithms.

N83-19496*# National Aeronautics and Space Administration. Lewis Research Center, Cleveland, Ohio.
BASIC DATA MANIPULATION AND DISPLAY SYSTEM (BDMADS)
J. R. SZUCH Feb. 1983 61 p refs
(NASA-TM-83328; E-1575; NAS 1.15:83328) Avail: NTIS HC A04/MF A01 CSCL 09B

BDMADS, a BASIC Data Manipulation and Display System, is a collection of software programs that run on an Apple II Plus personal computer. BDMADS provides a user-friendly environment for the engineer in which to perform scientific data processing. The computer programs and their use are described. Jet engine performance calculations are used to illustrate the use of BDMADS. Source listings of the BDMADS programs are provided and should permit users to customize the programs for their particular applications. Author

62

COMPUTER SYSTEMS

Includes computer networks.

N83-28921*# National Aeronautics and Space Administration. Lewis Research Center, Cleveland, Ohio.
PARALLEL, ASYNCHRONOUS EXECUTIVE (PAX): SYSTEM CONCEPTS, FACILITIES, AND ARCHITECTURE
W. H. JONES Jun. 1983 60 p refs
(NASA-TP-2179; E-1584; NAS 1.60:2179) Avail: NTIS HC A04/MF A01 CSCL 09B

The Parallel, Asynchronous Executive (PAX) is a software operating system simulation that allows many computers to work on a single problem at the same time. PAX is currently implemented on a UNIVAC 1100/42 computer system. Independent UNIVAC runstreams are used to simulate independent computers. Data are shared among independent UNIVAC runstreams through shared mass-storage files. PAX has achieved the following: (1) applied several computing processes simultaneously to a single, logically unified problem; (2) resolved most parallel processor conflicts by careful work assignment; (3) resolved by means of worker requests to PAX all conflicts not resolved by work assignment; (4) provided fault isolation and recovery mechanisms to meet the problems of an actual parallel, asynchronous processing machine. Additionally,

C-3

one real-life problem has been constructed for the PAX environment. This is CASPER, a collection of aerodynamic and structural dynamic problem simulation routines. CASPER is not discussed in this report except to provide examples of parallel-processing techniques. Author

63

CYBERNETICS

Includes feedback and control theory.

A83-37093* Notre Dame Univ., Ind.
CONTROLLER SCHEDULING - A POSSIBLE ALGEBRAIC VIEWPOINT
M. SAIN and S. YURKOVICH (Notre Dame, University, Notre Dame, IN) IN: American Control Conference, 1st, Arlington, VA, June 14-16, 1982, Proceedings. Volume 1 . New York, Institute of Electrical and Electronics Engineers, 1982, p. 261-269. refs
(Contract NSG-3048)

In the applications, one common way to design a control system for a nonlinear plant is to localize its behavior along lines of operation specified by the plant manufacturer, to develop linear multi-variable controls for these localizations, and to schedule those controls with key plant variables which vary smoothly along operating lines. An important part of practical design lore, the art of controller scheduling has received little modern attention from the conceptual point of view. This paper describes four basic types of scheduling questions and outlines some of the theoretical issues associated with them. Schedules are considered in terms of state equations; however, some relations with the input/output description are discussed, together with an analysis of the effects on the overall configuration of approximations made to the individual subsystems. Author

64

NUMERICAL ANALYSIS

Includes iteration, difference equations, and numerical approximation.

A83-10273* Akron Univ., Ohio.
FORMAL CONVERGENCE CHARACTERISTICS OF ELLIPTICALLY CONSTRAINED INCREMENTAL NEWTON-RAPHSON ALGORITHMS
J. PADOVAN (Akron, University, Akron, OH) and T. ARECHAGA International Journal of Engineering Science, vol. 20, no. 10, 1982, p. 1077-1097. refs
(Contract NAG3-54)

Various aspects of the convergence, uniqueness, and existence properties associated with solutions generated via the elliptically constrained incremental Newton-Raphson (ECINR) algorithm are analyzed. Several theorems are developed, and the formal behavior of the elliptically constrained scheme developed by Padovan (1981) is discussed in detail. Consideration is given to globai and local rates of convergence, to the determination of the occurrence of safety zones wherein the algorithm yields inherently convergent results, to formal limitations on the class of functions which the scheme can be applied to solve, and to single and multidimensional formalisms on existence uniqueness and convergence. Special attention is given to functions whose Jacobian matrix exhibit positive, negative, semi and indefinite properties. Several significant advantages of ECINR over the classical INR are mentioned. C.D.

A83-29631* Columbia Univ., New York.
COORDINATE GENERATION WITH PRECISE CONTROLS OVER MESH PROPERTIES
P. R. EISEMAN (Columbia University, New York, NY) Journal of Computational Physics (ISSN 0021-9991), vol. 47, Sept. 1982, p. 331-351. refs
(Contract F49620-79-C-0132; NAS1-15810; NAS3-22117)

Powerful local controls have been developed for mesh generation with the class of multisurface coordinate transformations. The controls come from local piecewise linear interpolants, and the resulting coordinates have continuous first derivatives. At the boundaries, the mesh controls provide the capability of joining distinct coordinate systems together with continuous derivatives. Away from boundaries, a local region can be given a particular mesh form to model internal objects or to simplify a problem. Applications of the controls are illustrated with a sequence of two-dimensional examples. For simplicity, each is generated about a NACA0012 airfoil which is of unit length and with leading edge pointed in a negative x-direction. C.D.

A83-29632* Columbia Univ., New York.
HIGH LEVEL CONTINUITY FOR COORDINATE GENERATION WITH PRECISE CONTROLS
P. R. EISEMAN (Columbia University, New York, NY) Journal of Computational Physics (ISSN 0021-9991), vol. 47, Sept. 1982, p. 352-374.
(Contract F49620-79-C-0132; NAS1-15810; NAS3-22117)

Coordinate generation techniques with precise local controls have been derived and analyzed for continuity requirements up to both the first and second derivatives, and have been projected to higher level continuity requirements from the established pattern. The desired local control precision was obtained when a family of coordinate surfaces could be uniformly distributed without a consequent creation of flat spots on the coordinate curves transverse to the family. Relative to the uniform distribution, the family could be redistributed from an a priori distribution function or from a solution adaptive approach, both without distortion from the underlying transformation which may be independently chosen to fit a nontrivial geometry and topology. C.D.

N83-12930*# National Aeronautics and Space Administration. Lewis Research Center, Cleveland, Ohio.
CONVERGENCE ACCELERATION OF VISCOUS FLOW COMPUTATIONS
G. M. JOHNSON Oct. 1982 30 p refs
(NASA-TM-83039; E-1484; NAS 1.15:83039) Avail: NTIS HC A03/MF A01 CSCL 12A

A multiple-grid convergence acceleration technique introduced for application to the solution of the Euler equations by means of Lax-Wendroff algorithms is extended to treat compressible viscous flow. Computational results are presented for the solution of the thin-layer version of the Navier-Stokes equations using the explicit MacCormack algorithm, accelerated by a convective coarse-grid scheme. Extensions and generalizations are mentioned. M.G.

N83-21847*# National Aeronautics and Space Administration. Lewis Research Center, Cleveland, Ohio.
MULTIPLE-GRID CONVERGENCE ACCELERATION OF VISCOUS AND INVISCID FLOW COMPUTATIONS
G. M. JOHNSON 1983 28 p refs Presented at the Intern. Multigrid Conf., Copper Mountain, Colo., 6-8 Apr. 1983; sponsored in part by Air Force
(NASA-TM-83361; E-1623; NAS 1.15:83361) Avail: NTIS HC A03/MF A01 CSCL 12A

A multiple-grid algorithm for use in efficiently obtaining steady solution to the Euler and Navier-Stokes equations is presented. The convergence of a simple, explicit fine-grid solution procedure is accelerated on a sequence of successively coarser grids by a coarse-grid information propagation method which rapidly eliminates transients from the computational domain. This use of multiple-gridding to increase the convergence rate results in substantially reduced work requirements for the numerical solution of a wide range of flow problems. Computational results are

presented for subsonic and transonic inviscid flows and for laminar and turbulent, attached and separated, subsonic viscous flows. Work reduction factors as large as eight, in comparison to the basic fine-grid algorithm, were obtained. Possibilities for further performance improvement are discussed. M.G.

N83-23087# Iowa Univ., Iowa City. Inst. of Hydraulic Research.
THE FINITE ANALYTIC METHOD, VOLUME 3 Final Report
C. J. CHEN, M. Z. SHEIKHOLESLAMI, B. KHALIGHI, and K. SINGH Aug. 1981 391 p refs 5 Vol.
(Contract NSG-3305)
(NASA-CR-170186; NAS 1.26:10186; IIHR-232-III-VOL-3) Avail: NTIS HC A17/MF A01 CSCL 12A

The finite analytic (FA) method is applied to the numerical solution of two-point boundary value problems of ordinary differential equation. Convergence, stability, and accuracy of the method are examined and a comparison of the finite analytic solution with solutions obtained from the finite difference method is given for several numerical examples. In addition, the FA method is used to solve the two-dimensional Poisson and Laplace equations. Finally a general 9-point finite analytic formula is developed for the Navier-Stokes equation in a finite element. The Navier-Stokes equations are formulated using the primitive variables. An iterative scheme which solves the continuity equation, Poisson pressure equation and the momentum equations for the three primitive variables is devised. The FA numerical solution is first obtained for stagnation point flow and a comparison with the exact solution is made. Then the formula is used to obtain the numerical solution for a flat plate-wake combined problem and also for a square driven cavity flow. The results are obtained for Reynolds numbers 100, 400, and 800. M.G.

N83-23088# Iowa Univ., Iowa City. Inst. of Hydraulic Research.
THE FINITE ANALYTIC METHOD, VOLUME 4 Final Report
C. J. CHEN and H. C. CHEN Aug. 1982 424 p refs 5 Vol.
(Contract NSG-3305)
(NASA-CR-170187; NAS 1.26:170187; IIHR-232-IV-VOL-4) Avail: NTIS HC A18/MF A01 CSCL 12A

Unsteady 1D, 2D, and 3D incompressible Navier-Stokes equations are numerically analyzed by a numerical scheme called the finite analytic method. The basic idea of the finite analytic method is the incorporation of a local analytic solution in the numerical solution of linear and nonlinear partial differential equations. The local analytic solutions for unsteady 1D, 2D and 3D convective transport equations are obtained from locally linearized governing equations by specifying suitable initial and boundary conditions for each local element. When the local analytic solution is evaluated at a given nodal point, it gives an analytic algebraic relationship between a nodal value in a local element to its neighboring nodal points. The solution of the problem is then achieved by solving the system of algebraic equations. Depending on the boundary and initial functions chosen to represent the boundary and initial conditions for each local element, a number of local analytic solutions are derived. The results show that the boundary approximation based on the combination of exponential and linear function is the best one since the boundary function thus constructed is the natural solution of the governing equation. The finite analytic coefficients thus obtained are shown to be relatively simple and do give the correct asymptotic behavior for both diffusion and convection dominated cases. M.G.

N83-23089# Iowa Univ., Iowa City. Inst. of Hydraulic Research.
THE FINITE ANALYTIC METHOD, VOLUME 5 Final Report
C. J. CHEN, K. S. HO, and W. S. CHENG Oct. 1982 438 p refs 5 Vol.
(Contract NSG-3305)
(NASA-CR-170188; NAS 1.26:170188; IIHR-232-V-VOL-5) Avail: NTIS HC A19/MF A01 CSCL 12A

In order to solve practical engineering problems, a finite analytic (FA) method capable of solving flow and heat transfer problems involving complex geometries is developed. The boundary-fitted coordinate transformation is incorporated into the FA method. The FA method is employed to solve several flow and heat transfer problems. The problem of convective heat transfer in a cavity is studied with the Reynolds number ranging from 100 to 2,000 and the Peclet number ranging from 10 to 20,000 by using an equal size grid in the physical plane. The separation of channel flow is examined at different Reynolds numbers over the range 25 to 229 with both equal and unequal size grids in the physical plane. For problems with complex geometries, flow past an airfoil and convective heat transfer in tube bundles, both are solved with the FA method for the boundary-fitted coordinate system. The FA results are compared with the experimental data, the theoretical calculation, and predictions by other numerical schemes. In additioin, the FA numerical solution for two dimensional incompressible flows over an arbitrary body shape is discussed. M.G.

N83-30113*# National Aeronautics and Space Administration. Lewis Research Center, Cleveland, Ohio.
FLUX-BASED ACCELERATION OF THE EULER EQUATIONS
G. M. JOHNSON 1983 9 p refs Presented at the 6th Computational Fluid Dyn. Conf., Danvers, Mass., 13-15 Jul. 1983; sponsored by AIAA
(NASA-TM-83453; E-1767; NAS 1.15:83453) Avail: NTIS HC A02/MF A01 CSCL 12A

A new coarse grid acceleration scheme for the Euler equations is presented. This flux based scheme eliminates the need, exhibited by previous accelerators, for computing flux vector Jacobian matrices. The method is derived and implemented in a two dimensional flow algorithm. Numerical results are presented for both subcritical and shocked, supercritical flow. These results demonstrate that the flux based accelerator is more efficient than its Jacobian based counterpart. Generalization to three dimensions is immediate. Construction of flux based accelerators for the Navier-Stokes equations is also discussed. Author

N83-31390*# National Aeronautics and Space Administration. Lewis Research Center, Cleveland, Ohio.
CONVERGENCE AND STABILITY PROPERTIES OF MINIMAL POLYNOMIAL AND REDUCED RANK EXTRAPOLATION ALGORITHMS
A. SIDI (Technion - Israel Inst. of Tech., Haifa) Jul. 1983 27 p refs
(NASA-TM-83443; E-1659; NAS 1.15:83443) Avail: NTIS HC A03/MF A01 CSCL 12A

The minimal polynomial and reduced rank extrapolation algorithms are two acceleration of convergence methods for sequences of vectors. In a recent survey these methods were tested and compared with the scalar, vector, topological epsilon algorithms, and were observed to be more efficient than the latter. It was also observed that the two methods have similar convergence properties. The convergence and stability properties of these methods are analyzed and the performance of the acceleration methods when applied to a class of vector sequences that includes those sequences obtained from systems of linear equations by using matrix iterative methods is discussed. M.G.

N83-34656*# Virginia Polytechnic Inst. and State Univ., Blacksburg. Dept. of Mechanical Engineering.
THEORETICAL INVESTIGATION OF THE FORCE AND DYNAMICALLY COUPLED TORSIONAL-AXIAL-LATERAL DYNAMIC RESPONSE OF EARED ROTORS Annual Status Report
J. W. DAVID and L. D. MITCHELL 1982 33 p
(Contract NSG-3239)
(NASA-CR-173013; NAS 1.26:173013) Avail: NTIS HC A03/MF A01 CSCL 12A

Difficulties in solution methodology to be used to deal with the potentially higher nonlinear rotor equations when dynamic coupling is included. A solution methodology is selected to solve the nonlinear differential equations. The selected method was verified to give good results even at large nonlinearity levels. The transfer matrix methodology is extended to the solution of nonlinear problems. Author

65

STATISTICS AND PROBABILITY

Includes data sampling and smoothing; Monte Carlo method; and stochastic processes.

N83-21872*# National Aeronautics and Space Administration. Lewis Research Center, Cleveland, Ohio.
COMPUTER PROGRAM TO MINIMIZE PREDICTION ERROR IN MODELS FROM EXPERIMENTS WITH 16 HYPERCUBE POINTS AND 0 TO 6 CENTER POINTS
A. G. HOLMS Nov. 1982 64 p refs
(NASA-TM-82995; E-1428; NAS 1.15:82995) Avail: NTIS HC A04/MF A01 CSCL 12A

A previous report described a backward deletion procedure of model selection that was optimized for minimum prediction error and which used a multiparameter combination of the F - distribution and an order statistics distribution of Cochran's. A computer program is described that applies the previously optimized procedure to real data. The use of the program is illustrated by examples. Author

70

PHYSICS (GENERAL)

A83-15697*# Texas Univ., Austin.
SOLUTION TO THE BACKWARD-KOLMOGOROV EQUATION FOR A NONSTATIONARY OSCILLATION PROBLEM
G. P. SOLOMOS and P.-T. D. SPANOS (Texas, University, Austin, TX) ASME, Transactions, Journal of Applied Mechanics, vol. 49, Dec. 1982, p. 923-925. refs
(Contract NSF PFR-80-06569; NAG3-210)

The transition probability density function of a Markovian approximation of the response amplitude of an oscillator under nonstationary excitation is determined in an analytical form. A solution is presented for the associated backward-Kolmogorov equation by transforming the equation into a form amenable to solution by the method of the separation of variables. This procedure results in a boundary value problem which is then solved by using an infinite series of Laguerre polynomials. It is found that the infinite series solution is equivalent to a closed-form solution involving a Bessel function. N.B.

A83-29528* Ohio State Univ., Columbus.
VOLUME INTEGRALS OF ELLIPSOIDS ASSOCIATED WITH THE INHOMOGENEOUS HELMHOLTZ EQUATION
L. S. FU (Ohio State University, Columbus, OH) and T. MURA (Northwestern University, Evanston, IL) Wave Motion (ISSN 0165-2125), vol. 4, 1982, p. 141-149. refs
(Contract NSG-3269; DAAG29-81-K-0090)

Problems of wave phenomena in the fields of acoustics, electromagnetics and elasticity are often reduced to an integration of the inhomogeneous Helmholtz equation. Results are presented for volume integrals associated with the inhomogeneous Helmholtz equation, for an ellipsoidal region. By using appropriate Taylor series expansions and the multinomial theorem, these volume integrals are obtained in series form for regions r greater than r-prime and r less than r-prime, where r and r-prime are the distances from the origin to the point of observation and the source. Derivatives of these integrals are easily evaluated. When the wavenumber approaches zero the results reduce directly to the potentials of ellipsoids of variable densities. Author

A83-37947* Arizona Univ., Tucson.
SURFACE-POLARITONLIKE WAVES GUIDED BY THIN, LOSSY METAL FILMS
G. I. STEGEMAN, J. J. BURKE (Arizona, University, Tucson, AZ), and D. G. HALL (Rochester, University, Rochester, NY) Optics Letters (ISSN 0146-9592), vol. 8, July 1983, p. 383-385. refs
(Contract DAAG29-82-K-0018; NAG3-392)

Surface-plasmon polaritons guided by thin, lossy metallic films bounded by dissimilar dielectric media are investigated. New solutions to the dispersion relation are found, representing waves that are leaky (radiative) in one of the dielectrics. The new waves are interpreted in terms of the coupling of a damped surface plasmon at one interface with continuum modes at the other. Their excitation by end-fire coupling techniques is suggested. Author

71

ACOUSTICS

Includes sound generation, transmission, and attenuation.

A83-10183*# Boeing Co., Seattle, Wash.
TESTS OF A THERMAL ACOUSTIC SHIELD WITH A SUPERSONIC JET
N. PICKUP, R. A. MANGIAROTTY, and J. V. OKEEFE (Boeing Co., Seattle, WA) Journal of Aircraft, vol. 19, Nov. 1982, p. 940-946. refs
(Contract NAS3-22137)
(Previously cited in issue 24, p. 4244, Accession no. A81-48623)

A83-13135*# Georgia Inst. of Tech., Atlanta.
AN ITERATIVE METHOD FOR PREDICTING TURBOFAN INLET ACOUSTICS
S. J. HOROWITZ, R. K. SIGMAN, and B. T. ZINN (Georgia Institute of Technology, Atlanta, GA) AIAA Journal, vol. 20, Dec. 1982, p. 1693-1699. refs
(Contract NSG-3036)
(Previously cited in issue 24, p. 4248, Accession no. A81-49736)

A83-13136*# Lockheed Missiles and Space Co., Palo Alto, Calif.
NOISE AND FLOW STRUCTURE OF A TONE-EXCITED JET
K. K. AHUJA, J. LEPICOVSKY, and R. H. BURRIN (Lockheed-Georgia Co., Marietta, GA) AIAA Journal, vol. 20, Dec. 1982, p. 1700-1706. Research supported by the Lockheed-Georgia Co. refs
(Contract NAS3-21987)
(Previously cited in issue 24, p. 4245, Accession no. A81-48640)

A83-15317*# National Aeronautics and Space Administration. Lewis Research Center, Cleveland, Ohio.
WIND TUNNEL MEASUREMENTS OF BLADE/VANE RATIO AND SPACING EFFECTS ON FAN NOISE
R. P. WOODWARD and F. W. GLASER (NASA, Lewis Research Center, Cleveland, OH) Journal of Aircraft, vol. 20, Jan. 1983, p. 58-65. refs
(Previously cited in issue 24, p. 4128, Accession no. A81-48628)

A83-16319* National Aeronautics and Space Administration. Lewis Research Center, Cleveland, Ohio.
PRESSURE TRANSFER FUNCTION OF A JT15D NOZZLE DUE TO ACOUSTIC AND CONVECTED ENTROPY FLUCTUATIONS
J. H. MILES and E. A. KREJSA (NASA, Lewis Research Center, Cleveland, OH) Acoustical Society of America, Journal, vol. 72, Dec. 1982, p. 2008-2019. refs
(Previously announced in STAR as N82-22951)

A83-19809*# National Aeronautics and Space Administration. Lewis Research Center, Cleveland, Ohio.
ACOUSTICS IN VARIABLE AREA DUCT - FINITE ELEMENT AND FINITE DIFFERENCE COMPARISONS TO EXPERIMENT
K. J. BAUMEISTER (NASA, Lewis Research Center, Cleveland, OH), W. EVERSMAN (Missouri Rolla, University, Rolla, MO), J. W. WHITE (Tennessee, University, Knoxville, TN), and R. J. ASTLEY American Institute of Aeronautics and Astronautics, Aeroacoustics Conference, 7th, Palo Alto, CA, Oct. 5-7, 1981, AIAA 81-2016.) AIAA Journal, vol. 21, Feb. 1983, p. 193-199. refs
(Previously cited in issue 24, p. 4243, Accession no. A81-48622)

A83-22128*# National Aeronautics and Space Administration. Lewis Research Center, Cleveland, Ohio.
CONVENTIONAL PROFILE COAXIAL JET NOISE PREDICTION
J. R. STONE, D. E. GROESBECK, and C. L. ZOLA (NASA, Lewis Research Center, Cleveland, OH) AIAA Journal, vol. 21, Mar. 1983, p. 336-342. refs
(Previously cited in issue 24, p. 4249, Accession no. A81-49743) [1] 12, p.

A83-25904*# National Aeronautics and Space Administration. Lewis Research Center, Cleveland, Ohio.
TRANSIENT DIFFERENCE SOLUTIONS OF THE INHOMOGENEOUS WAVE EQUATION - SIMULATION OF THE GREEN'S FUNCTION
K. J. BAUMEISTER (NASA, Lewis Research Center, Cleveland, OH) American Institute of Aeronatuics and Astronautics, Aeroacoustics Conference, 8th, Atlanta, GA, Apr. 11-13, 1983, 11 p. refs
(AIAA PAPER 83-0667)
A time-dependent finite difference formulation to the inhomogeneous wave equation is derived for plane wave propagation with harmonic noise sources. The difference equation and boundary conditions are developed along with the techniques to simulate the Dirac delta function associated with a concentrated noise source. Example calculations are presented for the Green's function and distributed noise sources. For the example considered, the desired Fourier transformed acoustic pressures are determined from the transient pressures by use of a ramping function and an integration technique, both of which eliminates the nonharmonic pressure associated with the initial transient. (Author)

A83-25907*# Missouri Univ., Rolla.
FINITE DIFFERENCE SOLUTIONS TO SHOCKED ACOUSTIC WAVES
N. J. WALKINGTON and W. EVERSMAN (Missouri-Rolla, University, Rolla, MO) American Institute of Aeronautics and Astronautics, Aeroacoustics Conference, 8th, Atlanta, GA, Apr. 11-13, 1983, 11 p. refs
(Contract NAG3-178)
(AIAA PAPER 83-0671)
The MacCormack, Lambda and split flux finite differencing schemes are used to solve a one dimensional acoustics problem. Two duct configurations were considered, a uniform duct and a converging-diverging nozzle. Asymptotic solutions for these two ducts are compared with the numerical solutions. When the acoustic amplitude and frequency are sufficiently high the acoustic signal shocks. This condition leads to a deterioration of the numerical solutions since viscous terms may be required if the shock is to be resolved. A continuous uniform duct solution is considered to demonstrate how the viscous terms modify the solution. These results are then compared with a shocked solution with and without viscous terms. Generally it is found that the most accurate solutions are those obtained using the minimum possible viscosity coefficients. All of the schemes considered give results accurate enough for acoustic power calculations with no one scheme performing significantly better than the others. (Author)

A83-25923*# Florida State Univ., Tallahassee.
ON THE SHOCK CELL STRUCTURE AND NOISE OF SUPERSONIC JETS
C. K. W. TAM (Florida State University, Tallahassee, FL) and J. A. JACKSON American Institute of Aeronautics and Astronautics, Aeroacoustics Conference, 8th, Atlanta, GA, Apr. 11-13, 1983, 7 p. refs
(Contract NAG3-182)
(AIAA PAPER 83-0703)
A linear solution modeling the shock cell structure of an axisymmetric supersonic jet operated at off-design conditions is developed by the method of multiple-scales. The model solution takes into account the gradual spatial change of the mean flow in the downstream direction. Turbulence in the mixing layer of the jet has the tendency of smoothing out the sharp velocity and density gradients induced by the shocks. To simulate this effect, eddy viscosity terms are incorporated in the model. It is known that the interaction between the quasi-periodic shock cells and the downstream propagating large turbulence structures in the mixing layer of the jet is responsible for the generation of broadband shock associated noise. Experimentally, the dominant part of this noise has been found to originate from the part of the jet near the end of the potential core. Calculated shock cell spacing at the end of the jet core according to the present model is used to estimate the peak frequencies of the shock associated noise for a range of observation angles. Very favorable agreement with experimental measurements is found. (Author)

A83-25924*# North Carolina State Univ., Raleigh.
AN EXPERIMENTAL STUDY OF SUPERSONIC JET SHOCK-ASSOCIATED NOISE
R. T. NAGEL and A. G. PAPATHANSIOU (North Carolina State University, Raleigh, NC) American Institute of Aeronautics and Astronautics, Aeroacoustics Conference, 8th, Atlanta, GA, Apr. 11-13, 1983, 8 p. refs
(Contract NAG3-189)
(AIAA PAPER 83-0708)
A new method of screech tone reduction in underexpanded supersonic jets is utilized to determine if the amplitude of screech is related to the level of shock-associated broadband noise. Acoustic measurements show that as the screech tone is reduced, the broadband shock-associated noise may be increased by up to 4dB at some locations. Several experiments were conducted with disturbances put into the flow upstream of the final contraction. Results from these tests support the concept of linkage between the broadband shock noise and screech tones. Some interesting preliminary results were obtained with a disturbance of the flow at several locations downstream of the nozzle. These results are also discussed. (Author)

A83-25926*# Georgia Inst. of Tech., Atlanta.
A THEORETICAL INVESTIGATION OF THE SOUND RADIATION FIELDS ASSOCIATED WITH A BELLMOUTH INLET
W. L. MEYER and B. T. ZINN (Georgia Institute of Technology, Atlanta, GA) American Institute of Aeronautics and Astronautics, Aeroacoustics Conference, 8th, Atlanta, GA, Apr. 11-13, 1983, 6 p. refs
(Contract NAG3-67)
(AIAA PAPER 83-0710)
Analytical results are obtained by numerical integration of a cylindrically symmetric integral representation of the external solutions of the Helmholtz equation. The accuracy of this method is checked by comparisons of computed results with 'exact' solutions generated by the point source method. In all cases, the average error for the amplitude and phase of the points calculated in the field is found to be less than ten percent. Theoretical studies which model experiments run for the NASA Langely Bellmouth

inlet configuration are presented and comparisons are made with the experimental results. In all cases very good agreement is obtained between the experimental and theoretically calculated values. (Author)

A83-25929*# Lockheed-Georgia Co., Marietta.
SOUND RADIATION FROM ANNULAR DUCTS/NOZZLES USING MODAL DECOMPOSITION OF IN-DUCT ACOUSTIC POWER
M. SALIKUDDIN (Lockheed-Georgia Co., Marietta, GA) American Institute of Aeronautics and Astronautics, Aeroacoustics Conference, 8th, Atlanta, GA, Apr. 11-13, 1983, 12 p. refs
(Contract NAS3-20797)
(AIAA PAPER 83-0714)

Using a refined acoustic impulse technique, an experimental program was carried out to determine the proper procedure for measuring the acoustic power for both incident and reflected sound fields for annular ducts with and without nozzles at various flow conditions. Several radial and azimuthal pressure measurements were made, and using these complex pressure data, the modal content of the pressure field was determined. A mathematical approach for the modal decomposition of annular duct acoustic power was developed. The acoustic power due to each individual mode and also their total sum were derived. The acoustic characteristics of annular duct-nozzle systems were studied at various flow conditions. The results derived from the experiments include the termination reflection coefficient, the normalized transmission coefficients, the power transfer functions and the power imbalance. (Author)

A83-26450*# National Aeronautics and Space Administration. Lewis Research Center, Cleveland, Ohio.
COMPARISON OF MEASURED AND PREDICTED FLIGHT EFFECTS ON HIGH-BYPASS COAXIAL JET EXHAUST NOISE
J. R. STONE (NASA, Lewis Research Center, Cleveland, OH) American Institute of Aeronautics and Astronautics, Aeroacoustics Conference, 8th, Atlanta, GA, Apr. 11-13, 1983, 19 p. refs
(AIAA PAPER 83-0749)

A recently developed semi-empirical model for predicting the noise generated by conventional-velocity-profile coaxial jets is compared with full-scale flight data and model-scale simulated flight data for high-bypass nozzles. The prediction model has been shown to agree with small-scale static data for primary jet velocities from 215 to 795 m/s for a wide range of area, temperature and velocity ratios between streams. However, there were insufficient model nozzle, simulated flight data available at that time to permit validation of the flight effects prediction. The comparisons presented in this paper demonstrate that the prediction method is also valid in flight. (Author)

A83-26917*# Georgia Inst. of Tech., Atlanta.
OPTIMIZATION OF ACOUSTIC LINERS BY THE HYBRID FINITE ELEMENT-INTEGRAL APPROACH
R. K. SIGMAN, S. J. HOROWITZ, and B. T. ZINN (Georgia Institute of Technology, Atlanta, GA) American Institute of Aeronautics and Astronautics, Aeroacoustics Conference, 8th, Atlanta, GA, Apr. 11-13, 1983, 8 p. refs
(Contract NSG-3036)
(AIAA PAPER 83-0670)

An iterative solution technique for predicting the sound field radiated from a turbofan inlet is used to predict the optimum inlet acoustic liner. The analytical approach divides the sound field into two regions: the sound field within and near the inlet which is computed using the finite element method and the radiation field beyond the inlet which is calculated using an integral solution technique. A continuous solution is obtained by matching the finite element and integral solutions at the interface between the two regions. Using a trial and error scheme, this analytical procedure is used to calculate the impedance value of the duct liner which will produce a minimum sound pressure level in the far field. Several examples of straight and non-uniform ducts with and without flow are presented. (Author)

A83-28011*# Syracuse Univ., N. Y.
COAXIAL SUPERSONIC JET-FLOWS, SHOCK STRUCTURE AND RELATED PROBLEMS WITH NOISE-SUPPRESSION ASSESSMENT AND PREDICTION
D. S. DOSANJH (Syracuse University, Syracuse, NY) and R. S. MCAFEE, JR. American Institute of Aeronautics and Astronautics, Aeroacoustics Conference, 8th, Atlanta, GA, Apr. 11-13, 1983, 42 p. refs
(Contract NAG3-202)
(AIAA PAPER 83-0707)

It is now reasonably well established that the intense noise radiated by a single turbulent, heated, under or overexpanded round jet of high specific thrust can be significantly reduced if instead, 'equivalent' multinozzle coaxial supersonic jet flows of the same total thrust and mass flow rate were to be operated in the inverted pressure mode. A summary of some of the relevant observations on the coaxial supersonic jet flows and their shock structure is presented. Attention is given to the scope of the optical studies, the development of shock structure, the effects of exit stagger, coaxial supersonic jet flows with inner nozzle overexpanded, the role of the lip thickness, the role of the exit area ratios, cold/heated coaxial supersonic jet flows, acoustic observations, the conventional pressure mode of operation, comparative noise reduction assessment, and problems and prospects of noise prediction. G.R.

A83-28016*# Douglas Aircraft Co., Inc., Long Beach, Calif.
SOUND PROPAGATION IN SEGMENTED EXHAUST DUCTS - THEORETICAL PREDICTIONS AND COMPARISON WITH MEASUREMENTS
M. C. JOSHI, R. E. KRAFT (Douglas Aircraft Co., Long Beach, CA), G. H. FISKE (General Electric Co., Schenectady, NY), A. A. SYED, and R. E. MOTSINGER (General Electric Co., Evendale, OH) American Institute of Aeronautics and Astronautics, Aeroacoustics Conference, 8th, Atlanta, GA, Apr. 11-13, 1983, 12 p. refs
(Contract NAS3-22766)
(AIAA PAPER 83-0734)

Suppressions due to acoustic treatment in the annular exhaust duct of a model fan have been theoretically predicted and compared with measurements. The predictions are based on the modal analysis of sound propagation in a straight annular flow duct with segmented treatment. Measured values of the mode distribution of the fan noise source (fan-stator interaction source only) and the acoustic impedance of the treatment in the duct were used as input to the prediction program. The predicted suppressions (under the assumption of uniform flow in the duct) compared well with the measured in-duct suppression for all test conditions. The measurements were made in an anechoic chamber and the interaction modes generated in the fan spanned a cut-off ratio range from nearly one to seven. (Author)

A83-28021*# National Aeronautics and Space Administration. Lewis Research Center, Cleveland, Ohio.
APPLICATION OF 3-SIGNAL COHERENCE TO CORE NOISE TRANSMISSION
E. A. KREJSA (NASA, Lewis Research Center, Cleveland, OH) American Institute of Aeronautics and Astronautics, Aeroacoustics Conference, 8th, Atlanta, GA, Apr. 11-13, 1983, 16 p. refs
(AIAA PAPER 83-0759)

A method for determining transfer functions across turbofan engine components and from the engine to the far-field is developed. The method is based on the 3-signal coherence technique used previously to obtain far-field core noise levels. This method eliminates the bias error in transfer function measurements due to contamination of measured pressures by nonpropagating pressure fluctuations. Measured transfer functions from the engine to the far-field, across the tailpipe, and across the turbine are presented for three turbofan engines. (Author)

A83-28022*# Arizona Univ., Tucson.
INCIDENCE ANGLE EFFECTS ON CONVECTED GUST AIRFOIL NOISE
E. J. KERSCHEN and M. R. MYERS (Arizona, University, Tucson, AZ) American Institute of Aeronautics and Astronautics, Aeroacoustics Conference, 8th, Atlanta, GA, Apr. 11-13, 1983, 11 p. Research supported by the General Electric Independent Research and Development Program refs
(Contract NAG3-357)
(AIAA PAPER 83-0765)

An analysis is developed which predicts the influence of airfoil mean loading on noise generation due to convected gusts. The theory is based on a linearization of the exact inviscid equations about a nonuniform compressible mean flow and the solution is developed using singular perturbation techniques. The case of a flat plate airfoil, at incidence angle alpha, interacting with three-dimensional disturbances is analyzed. It is found that in the vicinity of the airfoil leading and trailing edges, local regions are present which scale on the disturbance wavelength, with the noise generation concentrated in these regions. Away from the airfoil edges, the mean flow variation is found to be slow compared to the disturbance wavelength and no significant noise generation occurs. The mean flow variation near the leading edge generates additional noise by distorting the convected gust. The cumulative effect of the airfoil mean loading in the trailing edge region produces a 0(1) phase shift between the disturbances on the upper and lower surfaces of the airfoil. A corresponding 0(1) decrease, compared to the alpha = 0 case, is found in the noise generated at the trailing edge. N.B.

A83-28023*# Arizona Univ., Tucson.
NOISE GENERATION BY A FINITE SPAN SWEPT AIRFOIL
E. J. KERSCHEN and E. ENVIA (Arizona, University, Tucson, AZ) American Institute of Aeronautics and Astronautics, Aeroacoustics Conference, 8th, Atlanta, GA, Apr. 11-13, 1983, 9 p. refs
(Contract NAG3-357)
(AIAA PAPER 83-0768)

An analysis is developed for the noise generated by a convected gust interacting with a single swept airfoil. The airfoil spans a channel with infinite parallel walls which contains a uniform subsonic mean flow. High frequency gusts, for which the noise generation is concentrated at the airfoil leading edge, are considered. The solution utilizes the Wiener-Hopf technique applied to the equations in nonorthogonal coordinates. Closed form expressions for the farfield acoustic pressure are obtained. The convected gust is assumed to be a plane wave, i.e., the lowest order spanwise mode. Because of the swept leading edge, this convected gust generates acoustic modes of all orders. At high frequencies and low Mach numbers, moderate sweep angles produce substantial noise reductions. The residual acoustic energy is carried mainly by the higher modes. The airfoil sweep also modulates the basic high frequency farfield directivity, producing lobed patterns. The angular modulation of the directivity patterns is most pronounced for the lower order modes. (Author)

A83-28024*# Hersh Acoustical Engineering, Chatsworth, Calif.
EFFECT OF FLOW ON THE ACOUSTIC PERFORMANCE OF EXTENDED REACTION LINED DUCTS
A. S. HERSH (Hersh Acoustical Engineering, Inc., Chatsworth, CA) and B. WALKER American Institute of Aeronautics and Astronautics, Aeroacoustics Conference, 8th, Atlanta, GA, Apr. 11-13, 1983, 40 p. refs
(Contract NAS3-21975)
(AIAA PAPER 83-0778)

A model is developed for the effects of uniform and boundary-layer mean flow on the attenuation and propagation of harmonically excited sound waves in an extended reaction lined cylindrical duct. A duct geometry consisting of an annular outer region of bulk material surrounding an inner cylinder of air is utilized. A numerical solution is obtained for the coupled wave equations governing the motion of the sound in both the inner and annular regions. It is found that the numerically predicted attenuation and propagations constants are in excellent agreement with measured values using Kevlar as the liner material for plane-wave mode (O,O) excitation over a wide range of mean flows and sound frequency. The boundary-layer effects are determined to be unimportant, at least for plane-wave sound. In addition, numerical studies indicate small differences between the use of either the radial velocity or the radial displacement boundary conditions. N.B.

A83-28848* Minnesota Univ., Minneapolis.
PROPAGATION OF SOUND IN HIGHLY POROUS OPEN-CELL ELASTIC FOAMS
R. F. LAMBERT (Minnesota, University, Minneapolis, MN) Acoustical Society of America, Journal (ISSN 0001-4966), vol. 73, April 1983, p. 1131-1138. refs
(Contract NSF MEA-80-11362; NAG3-161)

This work presents both theoretical predictions and experimental measurements of attenuation and progressive phase constants of sound in open-cell, highly porous, elastic polyurethane foams. The foams are available commercially in graded pore sizes for which information about the static flow resistance, thermal time constant, volume porosity, dynamic structure factor, and speed of sound is known. The analysis is specialized to highly porous foams which can be efficient sound absorbers at audio frequencies. Negligible effect of internal wave coupling on attenuation and phase shift for the frequency range 16-6000 Hz was predicted and no experimentally significant effects were observed in the bulk samples studied. The agreement between predictions and measurements in bulk materials is excellent. The analysis is applicable to both the regular and compressed elastic open-cell foams. Author

A83-28849* Minnesota Univ., Minneapolis.
SURFACE ACOUSTIC ADMITTANCE OF HIGHLY POROUS OPEN-CELL, ELASTIC FOAMS
R. F. LAMBERT (Minnesota, University, Minneapolis, MN) Acoustical Society of America, Journal (ISSN 0001-4966), vol. 73, April 1983, p. 1139-1146. refs
(Contract NAG3-161)

This work presents a comprehensive study of the surface acoustic admittance properties of graded sizes of open-cell foams that are highly porous and elastic. The intrinsic admittance as well as properties of samples of finite depth were predicted and then measured for sound at normal incidence over a frequency range extending from about 35-3500 Hz. The agreement between theory and experiment for a range of mean pore size and volume porosity is excellent. The implications of fibrous structure on the admittance of open-cell foams is quite evident from the results. Author

A83-29235* California Univ., Los Angeles.
THE VELOCITY PERTURBATIONS ABOVE THE ORIFICE OF AN ACOUSTICALLY EXCITED CAVITY IN GRAZING FLOW
A. F. CHARWAT and B. E. WALKER (California, University, Los Angeles, CA) Journal of Fluid Mechanics (ISSN 0022-1120), vol. 128, March 1983, p. 413-426. refs
(Contract NSG-3236)

Detailed measurements of the time-dependent velocities induced inside and outside the opening of an acoustically excited, two-dimensional Helmholtz resonator imbedded in a grazing flow are presented. The remarkably clear structure of the perturbation field which evokes a pulsating source and a coherently pulsating vortex-image pair is described. Author

A83-33485*# National Aeronautics and Space Administration. Lewis Research Center, Cleveland, Ohio.
SOUND DIFFRACTION AT WALL IMPEDANCE DISCONTINUITIES IN A CIRCULAR CYLINDER - INVESTIGATED USING WIENER-HOPF TECHNIQUE
Y.-C. CHO (NASA, Lewis Research Center, Cleveland, OH) American Institute of Aeronautics and Astronautics, Aeroacoustics Conference, 8th, Atlanta, GA, Apr. 11-13, 1983. 26 p. refs
(AIAA PAPER 83-0730)

The results of ground observations as well as high resolution rocket electric field and particle observations during a breakup

event of an intense magnetospheric substorm over northern Scandinavia are discussed. In particular, the characteristics of the substorm-associated electric field, ionospheric currents, and power dissipation during a time period about 15 minutes after substorm onset are addressed. A comparison of the observations with those of a pre-breakup event earlier in the day (Marklund et al., 1982) showed that the ionospheric substorm-related electric field could be split up into two parts: (1) an ambient LT-dependent field, probably of magnetospheric origin; and (2) a small-scale electric field associated with the bright auroral structures, which is superimposed on the LT-dependent field. The consequences for the location of the ionospheric currents and the Joule energy dissipation relative to the auroral forms are discussed. Previously announced in STAR as N83-23117 C.D.

A83-33486*# National Aeronautics and Space Administration. Lewis Research Center, Cleveland, Ohio.
ACOUSTIC MODAL ANALYSIS OF A FULL-SCALE ANNULAR COMBUSTOR
A. M. KARCHMER (NASA, Lewis Research Center, Cleveland, OH) American Institute of Aeronautics and Astronautics, Aeroacoustics Conference, 8th, Atlanta, GA, Apr. 11-13, 1983. 17 p. refs
(AIAA PAPER 83-0760)

An acoustic modal decomposition of the measured pressure field in a full scale annular combustor installed in a ducted test rig is described. The modal analysis, utilizing a least squares optimization routine, is facilitated by the assumption of randomly occurring pressure disturbances which generate equal amplitude clockwise and counter-clockwise pressure waves, and the assumption of statistical independence between modes. These assumptions are fully justified by the measured cross spectral phases between the various measurement points. The resultant modal decomposition indicates that higher order modes compose the dominant portion of the combustor pressure spectrum in the range of frequencies of interest in core noise studies. A second major finding is that, over the frequency range of interest, each individual mode which is present exists in virtual isolation over significant portions of the spectrum. Finally, a comparison between the present results and a limited amount of data obtained in an operating turbofan engine with the same combustor is made. The comparison is sufficiently favorable to warrant the conclusion that the structure of the combustor pressure field is preserved between the component facility and the engine. Previously announced in STAR as N83-21896 Author

A83-33487*# National Aeronautics and Space Administration. Lewis Research Center, Cleveland, Ohio.
CROSS SPECTRA BETWEEN TEMPERATURE AND PRESSURE IN A CONSTANT AREA DUCT DOWNSTREAM OF A COMBUSTOR
J. H. MILES, C. A. WASSERBAUER, and E. A. KREJSA (NASA, Lewis Research Center, Cleveland, OH) American Institute of Aeronautics and Astronautics, Aeroacoustics Conference, 8th, Atlanta, GA, Apr. 11-13, 1983. 27 p. refs
(AIAA PAPER 83-0762)

The feasibility of measuring pressure temperature cross spectra and coherence and temperature-temperature cross spectra and coherence at spatially separated points along with pressure and temperature auto-spectra in a combustion rig was investigated. The measurements were made near the inlet and exit of a 6.44 m long duct attached to a J-47 combustor. The fuel used was Jet A. The cross spectra and coherence measurements show the pressure and temperature fluctuations correlate best at low frequencies. At the inlet the phenomena controlling the phase relationship between pressure and temperature could not be identified. However, at the duct exit the phase angle of the pressure is related to the phase angle of the temperature by the convected flow time delay. Previously announced in STAR as N83-23116 M.G.

A83-45517*# National Aeronautics and Space Administration. Lewis Research Center, Cleveland, Ohio.
LOW FLIGHT SPEED ACOUSTIC RESULTS FOR A SUPERSONIC INLET WITH AUXILIARY INLET DOORS
R. P. WOODWARD, F. W. GLASER, and J. G. LUCAS (NASA, Lewis Research Center, Cleveland, OH) AIAA, SAE, and ASME, Joint Propulsion Conference, 19th, Seattle, WA, June 27-29, 1983. 46 p. refs
(AIAA PAPER 83-1415)

A model supersonic inlet with auxiliary inlet doors and boundary layer bleeds was acoustically tested in simulated low speed flight up to Mach 0.2 in the NASA Lewis 9 x 15 Anechoic Wind Tunnel and statically in the NASA Lewis Anechoic Chamber. A JT8D refan model was used as the noise source. Data were also taken for a CTOL inlet and for an annular inlet with simulated centerbody support struts. Inlet operation with open auxiliary doors increased the blade passage tone by about 10 dB relative to the closed door configuration although noise radiation was primarily through the main inlet rather than the doors. Numerous strong spikes in the noise spectra were associated with the bleed system, and were strongly affected by the centerbody location. The supgrsonic inlet appeared to suppress multiple pure tone (MPT) generation at the fan source. Inlet length and the presence of support struts were shown not to cause this MPT suppression. Previously announced in STAR as N83-27794 Author

N83-10885*# National Aeronautics and Space Administration. Lewis Research Center, Cleveland, Ohio.
UTILIZING NUMERICAL TECHNIQUES IN TURBOFAN INLET ACOUSTIC SUPPRESSOR DESIGN
K. J. BAUMEISTER 1982 23 p refs Presented at the 19th Ann. Meeting of the Soc. of Eng. Sci., Rolla, Mo., 27-29 Oct. 1982
(NASA-TM-82994; E-1427; NAS 1.15:82994) Avail: NTIS HC A02/MF A01 CSCL 20A

Numerical theories in conjunction with previously published analytical results are used to augment current analytical theories in the acoustic design of a turbofan inlet nacelle. In particular, a finite element-integral theory is used to study the effect of the inlet lip radius on the far field radiation pattern and to determine the optimum impedance in an actual engine environment. For some single mode JT15D data, the numerical theory and experiment are found to be in a good agreement. Author

N83-11840*# National Aeronautics and Space Administration. Lewis Research Center, Cleveland, Ohio.
NOISE OF THE 10-BLADED, 40 DEG SWEPT SR-6 PROPELLER IN A WIND TUNNEL
J. H. DITTMAR, G. L. STEFKO, and R. J. JERACKI Sep. 1982 46 p refs
(NASA-TM-82950; E-1357; NAS 1.15:82950) Avail: NTIS HC A03/MF A01 CSCL 20A

The noise generated by supersonic helical-tip-speed propellers is a likely cabin environment problem for future airplanes powered by these propellers. Three propeller models with different tip sweeps. SR-1M, SR-2, and SR-3, designed for 244 m/sec (800 ft/sec) tip speed at a flight Mach number of 0.8 were previously tested in the NASA Lewis 8- by 6-Foot Wind Tunnel. In order to investigated another design point condition, the SR-6 propeller was designed for 213 m-sec (700 ft/sec) tip speed at a flight Mach number of 0.8. The noise data from this propeller are reported herein. Curves of blade passing frequency noise versus tip Mach number (at constant advance ratio) showed that the SR-6 propeller behaved similarly to the SR-1M propeller. The noise of the SR-6 propeller at its design condition, helical tip Mach number of 1.07, is approximately 3 dB quieter than the SR-2 propeller at its higher design helical tip Mach number of 1.15, but about 2.5 dB noisier than SR-3 at its design condition. The helical tip Mach number shift of the steep noise rise followed the same progression as the blade sweep angle for all of the propellers. When operated at the SR-3 design point, the SR-6 propeller was approximately 1.5 dB quieter than SR-2 and 4 dB noisier than SR-3. Author

N83-12966*# National Aeronautics and Space Administration. Lewis Research Center, Cleveland, Ohio.
CORRELATION OF CORE NOISE OBTAINED BY THREE SIGNAL COHERENCE TECHNIQUES
U. VONGLAHN and E. A. KREJSA 1982 22 p refs Presented at the 104th Meeting of the Acoustical Soc. of Am., Orlando, Fla., 9-12 Nov. 1982
(NASA-TM-83012; E-1447; NAS 1.15:83012) Avail: NTIS HC A02/MF A01 CSCL 20A

The prediction of frequency content and noise levels of turbofan engine core noise is reexamined as a result of recent test data and a new diagnostic technique. The diagnostic technique, utilizing a three-signal coherence method, is used to obtain core noise spectra for several engines. Similarities and differences of the spectra are discussed. Finally, the three-signal coherence data are correlated, leading to an improved core noise prediction procedure. B.W.

N83-12967*# Texas Univ., Austin. Dept. of Mechanical Engineering.
HIGH-INTENSITY SOUND IN AIR SATURATED FIBROUS BULK POROUS MATERIALS Final Report, 1 Sep. 1978 - 31 Aug. 1981
H. L. KUNTZ, II 3 Sep. 1982 255 p refs
(Contract NSG-3198)
(NASA-CR-167979; NAS 1.26:167979; ARL-TR-82-54) Avail: NTIS HC A12/MF A01 CSCL 20A

The interaction high-intensity sound with bulk porous materials in porous materials including Kevlar 29 is reported. The nonlinear behavior of the materials was described by dc flow resistivity tests. Then acoustic propagation and reflection were measured and small signal broadband measurements of phase speed and attenuation were carried out. High-intensity tests were made with 1, 2, and 3 kHz tone bursts to measure harmonic generation and extra attenuation of the fundamental. Small signal standing wave tests measured impedence between 0.1 and 3.5 kHz. High level tests with single cycle tone bursts at 1 to 4 kHz show that impedance increases with intensity. A theoretical analysis is presented for high-porosity, rigid-frame, isothermal materials. One dimensional equations of motion are derived and solved by perturbation. The experiments show that there is excess attenuation of the fundamental component and in some cases a close approach to saturation. A separate theoretical model, developed to explain the excess attenuation, yields predictions that are in good agreement with the measurements. Impedance and attenuation at high intensities are modeled. A.R.H.

N83-12968*# Lockheed-Georgia Co., Marietta.
TONE-EXCITED JET: THEORY AND EXPERIMENTS Final Report
K. K. AHUJA, J. LEPICOVSKY, C. K. W. TAM (Florida State Univ., Tallahassee), P. J. MORRIS (Pennsylvania State Univ.), and R. H. BURRIN Washington NASA Nov. 1982 244 p refs
(Contract NAS3-21987)
(NASA-CR-3538; NAS 1.26:3538; LG82ER0031) Avail: NTIS HC A11/MF A01 CSCL 20A

A detailed study to understand the phenomenon of broadband jet-noise amplification produced by upstream discrete-tone sound excitation has been carried out. This has been achieved by simultaneous acquisition of the acoustic, mean velocity, turbulence intensities, and instability-wave pressure data. A 5.08 cm diameter jet has been tested for this purpose under static and also flight-simulation conditions. An open-jet wind tunnel has been used to simulate the flight effects. Limited data on heated jets have also been obtained. To improve the physical understanding of the flow modifications brought about by the upstream discrete-tone excitation, ensemble-averaged schlieren photographs of the jets have also been taken. Parallel to the experimental study, a mathematical model of the processes that lead to broadband-noise amplification by upstream tones has been developed. Excitation of large-scale turbulence by upstream tones is first calculated. A model to predict the changes in small-scale turbulence is then developed. By numerically integrating the resultant set of equations, the enhanced small-scale turbulence distribution in a jet under various excitation conditions is obtained. The resulting changes in small-scale turbulence have been attributed to broadband amplification of jet noise. Excellent agreement has been found between the theory and the experiments. It has also shown that the relative velocity effects are the same for the excited and the unexcited jets. Author

N83-13936*# Georgia Inst. of Tech., Atlanta. School of Aerospace Engineering.
PREDICTION OF SOUND RADIATION FROM DIFFERENT PRACTICAL JET ENGINE INLETS Final Technical Report, 2 Jun. 1980 - 31 Jul. 1982
W. L. MEYER and B. T. ZINN 31 Jul. 1982 365 p refs
(Contract NAG3-67)
(NASA-CR-169533; NAS 1.26:169533) Avail: NTIS HC A16/MF A01 CSCL 20A

Computer codes which were based upon a special integral representation of the external solutions of the Helmholtz equation were upgraded so that they would yield accurate results for the acoustic radiation patterns in the field surrounding an axisymmetric body for nondimensional wave numbers, based on duct radius, of up to twenty. The accuracy of these computer programs was checked by the use of the point source method for the generation of exact solutions and then by comparison with the results of other experimental and theoretical studies. These computer codes were used in a parametric study of the dependence of the radiated sound field on input modal distribution, wave number, and inlet lip shape. The results of this study show that: (1) as the wave number (i.e., cut off ratio) is increased for a given input modal distribution that the acoustic radiation peak moves towards the inlet centerline and becomes more compact (i.e., narrows); (2) as the input mode number is increased for a given cut off ratio the acoustic radiation peak moves away from the inlet centerline and becomes more compact. S.L.

N83-13939*# National Aeronautics and Space Administration. Lewis Research Center, Cleveland, Ohio.
RECENT RESULTS ABOUT FAN NOISE: ITS GENERATION, RADIATION AND SUPPRESSION
C. E. FEILER 1982 37 p refs Presented at the 19th Ann. Meeting of the Soc. of Eng. Sci., Rolla, Mo., 27-29 Oct. 1982
(NASA-TM-83002; E-1438; NAS 1.15:83002) Avail: NTIS HC A03/MF A01 CSCL 20A

Fan noise including its generation, radiation characteristics, and suppression by acoustic treatment is studied. In fan noise generation, results from engine and fan experiments, using inflow control measures to suppress noise sources related to inflow distortion and turbulence, are described. The suppression of sources related to inflow allows the experiments to focus on the fan or engine internal sources. Some of the experiments incorporated pressure sensors on the fan blades to sample the flow disturbances encountered by the blades. From these data some inferences can be drawn about the origins of the disturbances. Also, hot wire measurements of a fan rotor wake field are presented and related to the fan's noise signature. The radiation and the suppression of fan noise are dependent on the acoustic modes generated by the fan. Fan noise suppression and radiation is described by relating these phenomena to the mode cutoff ratio parameter. In addition to its utility in acoustic treatment design and performance prediction, cutoff ratio was useful in developing a simple description of the radiation pattern for broadband fan noise. Some of the findings using the cutoff ratio parameter are presented. S.L.

N83-15041*# Bolt, Beranek, and Newman, Inc., Cambridge, Mass.
TURBOFAN NOISE GENERATION. VOLUME 1: ANALYSIS
C. S. VENTRES, M. A. THEOBALD, and W. D. MARK Jul. 1982 123 p refs
(Contract NAS3-21252)
(NASA-CR-167951; NAS 1.26:167951; REPT-4770) Avail: NTIS HC A06/MF A01 CSCL 20A

Computer programs were developed which calculate the in-duct acoustic modes excited by a fan/stator stae operating at subsonic tip speed. Three noise source mechanisms are included: (1) sound generated by the rotor blades interacting with turbulence ingested into, or generated within, the inlet duct; (2) sound generated by the stator vanes interacting with the turbulent wakes of the rotors blades; and (3) sound generated by the stator vanes interacting with the mean velocity deficit wakes of the rotor blades. The fan/stator stage is modeled as an ensemble of blades and vanes of zero camber and thickness enclosed within an infinite hard-walled annular duct. Turbulence drawn into or generated within the inlet duct is modeled as nonhomogeneous and anisotropic random fluid motion, superimposed upon a uniform axial mean flow, and convected with that flow. Equations for the duct mode amplitudes, or expected values of the amplitudes, are derived. A.R.H.

N83-16152*# National Aeronautics and Space Administration. Lewis Research Center, Cleveland, Ohio.
EXPERIMENTS ON HIGH BYPASS INTERNAL MIXER NOZZLE JET NOISE
J. H. GOODYKOONTZ Dec. 1982 23 p refs
(NASA-TM-83020; E-1456; NAS 1.15:83020) Avail: NTIS HC A02/MF A01 CSCL 20A

Model scale jet noise data are presented for a variety of internal lobed mixer nozzle configurations for take off power settings in a static environment. The results are presented for a 17.5 cm diameter fan nozzle to show the effect on noise levels caused by changes in geometric shape of the internal, or core flow, nozzle. The geometric variables include the lobe discharge angle, the number of lobes, spacing between the center plug and lobe valley, lobe side wall shape and axial contour of the lobes. An annular plug core flow nozzle was also tested and is used as a baseline for comparative purposes. Comparison of data from the internal lobed configurations showed that for comparative effect, in terms of the effect on full scale perceived noise levels, was caused by a change in the lobe discharge angle. The results showed that increasing the discharge angle caused an increase as large as 7 dB in sound pressure levels in the high frequency portion of the spectra. Changes in the other geometric variables cause negligible effects. Author

N83-16153*# National Aeronautics and Space Administration. Lewis Research Center, Cleveland, Ohio.
ANALYSIS OF COMBUSTION SPECTRA CONTAINING ORGAN PIPE TONE BY CEPSTRAL TECHNIQUES
J. H. MILES and C. A. WASSERBAUER 1982 29 p refs Presented at the 104th Meeting of the Acoustical Soc. of Am., Orlando, Fla., 8-12 Nov. 1982
(NASA-TM-83034; E-1472; NAS 1.15:83034) Avail: NTIS HC A03/MF A01 CSCL 20A

Signal reinforcements and cancellations due to standing waves may distort constant bandwidth combustion spectra. Cepstral techniques previously applied to the ground reflection echo problem are used to obtain smooth broadband data and information on combustion noise propagation. Internal fluctuating pressure measurements made using a J47 combustor attached to a 6.44 m long duct are analyzed. Measurements made with Jet A and hydrogen fuels are compared. The acoustic power levels inferred from the measurements are presented for a range of low heat release rate operating conditions near atmospheric pressure. For these cases, the variation with operating condition of the overall acoustic broadband power level for both hydrogen and Jet A fuels is consistent with previous results showing it was proportional to the square of the heat release rate. However, the overall acoustic broadband power level generally is greater for hydrogen than for Jet A. S.L.

N83-17242*# Garrett Turbine Engine Co., Phoenix, Ariz.
COMPUTER PROGRAM TO PREDICT NOISE OF GENERAL AVIATION AIRCRAFT: USER'S GUIDE Final Report
J. A. MITCHELL, C. K. BARTON, L. S. KISNER, and C. A. LYON Sep. 1982 281 p refs
(Contract NAS3-23037)
(NASA-CR-168050; NAS 1.26:168050; GARRETT-21-4270-2)
Avail: NTIS HC A13/MF A01 CSCL 20A

Program NOISE predicts General Aviation Aircraft far-field noise levels at FAA FAR Part 36 certification conditions. It will also predict near-field and cabin noise levels for turboprop aircraft and static engine component far-field noise levels. Author

N83-18405*# National Aeronautics and Space Administration. Lewis Research Center, Cleveland, Ohio.
AIRCRAFT TURBOFAN NOISE
J. F. GROENEWEG and E. J. RICE 1983 17 p refs Presented at the 28th Ann. Intern. Gas Turbine Conf., Phoenix, Ariz., 27-31 Mar. 1983
(NASA-TM-83317; E-1510; NAS 1.15:83317) Avail: NTIS HC A02/MF A01 CSCL 20A

Turbofan noise generation and suppression in aircraft engines are reviewed. The chain of physical processes which connect unsteady flow interactions with fan blades to far field noise is addressed. Mechanism identification and description, duct propagation, radiation and acoustic suppression are discussed. The experimental technique of fan inflow static tests are discussed. Rotor blade surface pressure and wake velocity measurements aid in the determination of the types and strengths of the generation mechanisms. Approaches to predicting or measuring acoustic mode content, optimizing treatment impedance to maximize attenuation, translating impedance into porous wall structure and interpreting far field directivity patterns are illustrated by comparisons of analytical and experimental results. The interdependence of source and acoustic treatment design to minimize far field noise is emphasized. Area requiring further research are discussed and the relevance of aircraft turbofan results to quieting other turbomachinery installations is addressed. S.L.

N83-18408*# General Electric Co., Cincinnati, Ohio. Aircraft Engine Business Group.
FREE-JET ACOUSTIC INVESTIGATION OF HIGH-RADIUS-RATIO COANNULAR PLUG NOZZLES. COMPREHENSIVE DATA REPORT, VOLUME 1
P. R. KNOTT, B. A. JANARDAN, R. K. MAJJIGI, P. K. SHUTIANI, and P. G. VOGT Jan. 1981 859 p refs
(Contract NAS3-20619)
(NASA-CR-168086-VOL-1; NAS 1.26:168086-VOL-1; R81AEG212-VOL-1) Avail: NTIS HC A99/MF A01 CSCL 20A

Six coannular plug nozzle configurations having inverted velocity and temperature profiles, and a baseline convergent conical nozzle were tested for simulated flight acoustic evaluation in General Electric's Anechoic Free-Jet Acoustic Facility. The nozzles were tested over a range of test conditions that are typical of a Variable Cycle Engine for application to advanced high speed aircraft. The outer stream radius ratio for most of the condigurations was 0.853, and the inner-stream-outer-stream area ratio was tested in the range of 0.54. Other variables investigated were the influence of bypass struts, a simple noncontoured convergent-divergent outer stream nozzle for forward quadrant shock noise control, and the effects of varying outer stream radius and inner-stream-to-outer-stream velocity ratios on the flight noise signatures of the nozzles. It was found that in simulated flight, the high-radius-ratio coannular plug nozzles maintain their jet noise and shock noise reduction features previously observed in static testing. The presence of nozzle bypass structs will not significantly effect the acoustic noise reduction features of a General Electric-type nozzle design. A unique coannular plug nozzle flight acoustic spectral prediction method was identified and found to predict the measured results quite well. Special laser velocimeter

and acoustic measurements were performed which have given new insight into the jet and shock noise reduction mechanisms of coannular plug nozzles with regard to identifying further beneficial research efforts. Author

N83-18409*# General Electric Co., Cincinnati, Ohio.
FREE-JET ACOUSTIC INVESTIGATION OF HIGH-RADIUS-RATIO COANNULAR PLUG NOZZLES. COMPREHENSIVE DATA REPORT, VOLUME 2
P. G. VOGT, P. K. BHUTIANI, and P. R. KNOTT Jan. 1981 782 p refs
(Contract NAS3-20619)
(NASA-CR-168086-VOL-2; NAS 1.26:169086-VOL-2; R81AEG212-VOL-2) Avail: NTIS HC A99/MF A01 CSCL 20A

Laser velocimeter data, collected as part of an acoustic investigation of coannular plug nozzles, is provided. The type of traverse, position, and histogram number is given along with the mean and turbulent velocity data. The velocites are normalized with respect to the outer flow velocity and the 'mixed' velocity. N.W.

N83-19575*# Pratt and Whitney Aircraft Group, East Hartford, Conn. Commercial Engineering.
INVESTIGATION OF CONTINUOUSLY TRAVERSING MICROPHONE SYSTEM FOR MODE MEASUREMENT Final Report
D. E. CICON, T. G. SOFRIN, and D. C. MATHEWS Nov. 1982 135 p refs
(Contract NAS3-23168)
(NASA-CR-168040; NAS 1.26:168040; PWA-5846-26) Avail: NTIS HC A07/MF A01 CSCL 20A

The continuously Traversing Microphone System consists of a data acquisition and processing method for obtaining the modal coefficients of the discrete, coherent acoustic field in a fan inlet duct. The system would be used in fan rigs or full scale engine installations where present measurement methods, because of the excessive number of microphones and long test times required, are not feasible. The purpose of the investigation reported here was to develop a method for defining modal structure by means of a continuously traversing microphone system and to perform an evaluation of the method, based upon analytical studies and computer simulated tests. A variety of system parameters were examined, and the effects of deviations from ideal were explored. Effects of traverse speed, digitizing rate, run time, roundoff error, calibration errors, and random noise background level were determined. For constant fan operating speed, the sensitivity of the method to normal errors and deviations was determined to be acceptable. Good recovery of mode coefficients was attainable. Fluctuating fan speed conditions received special attention, and it was concluded that by employing suitable time delay procedures, satisfactory information on mode coefficients can be obtained under realistic conditions. A plan for further development involving fan rig tests was prepared. Author

N83-20706*# Houston Univ., Tex. Aerodynamics and Turbulence Lab.
THE WHISTLER NOZZLE PHENOMENON
A. K. M. F. HUSSAIN and M. A. Z. HASAN Oct. 1982 36 p refs
(Contract NAG3-198)
(NASA-CR-170015; NAS 1.26:170015; FM-15) Avail: NTIS HC A03/MF A01 CSCL 20A

The whistler nozzle is a simple device which can induce jet self-excitations of controllable amplitudes and frequencies and appears highly promising for many applications involving turbulent transport, combustion and aerodynamic noise. The characteristics of this curious phenomenon are documented for different values of the controlling parameters and attempts to explain the phenomenon. It is shown that the whistler excitation results from the coupling of two independent resonance mechanisms: shear-layer tone resulting from the impingement of the pipe-exit shear layer on the collar lip, and organ-pipe resonance of the pipe-nozzle. The crucial role of the shear-layer tone in driving the organ-pipe resonance is proven by reproducing the event in pipe-ring and pipe-hole configurations in the absence of the collar. It is also shown that this phenomenon is the strongest when the self-excitation frequency matches the preferred mode of the jet. Author

N83-20708*# Lockheed-Georgia Co., Marietta.
REFINEMENT AND APPLICATION OF ACOUSTIC IMPULSE TECHNIQUE TO STUDY NOZZLE TRANSMISSION CHARACTERISTICS Final Report
M. SALIKUDDIN, W. H. BROWN, R. RAMAKRISHNAN, and H. K. TANNA Washington NASA Feb. 1983 406 p refs
(Contract NAS3-20797)
(NASA-CR-3656; NAS 1.26:3656; LG82ER0115) Avail: NTIS HC A18/MF A01 CSCL 20A

An improved acoustic impulse technique was developed and was used to study the transmission characteristics of duct/nozzle systems. To accomplish the above objective, various problems associated with the existing spark-discharge impulse technique were first studied. These included (1) the nonlinear behavior of high intensity pulses, (2) the contamination of the signal with flow noise, (3) low signal-to-noise ratio at high exhaust velocities, and (4) the inability to control or shape the signal generated by the source, specially when multiple spark points were used as the source. The first step to resolve these problems was the replacement of the spark-discharge source with electroacoustic driver(s). These included (1) synthesizing on acoustic impulse with acoustic driver(s) to control and shape the output signal, (2) time domain signal averaging to remove flow noise from the contaminated signal, (3) signal editing to remove unwanted portions of the time history, (4) spectral averaging, and (5) numerical smoothing. The acoustic power measurement technique was improved by taking multiple induct measurements and by a modal decomposition process to account for the contribution of higher order modes in the power computation. The improved acoustic impulse technique was then validated by comparing the results derived by an impedance tube method. The mechanism of acoustic power loss, that occurs when sound is transmitted through nozzle terminations, was investigated. Finally, the refined impulse technique was applied to obtain more accurate results for the acoustic transmission characteristics of a conical nozzle and a multi-lobe multi-tube supressor nozzle. Author

N83-21895*# National Aeronautics and Space Administration. Lewis Research Center, Cleveland, Ohio.
FARFIELD INFLIGHT MEASUREMENT OF HIGH-SPEED TURBOPROP NOISE
J. R. BALOMBIN and I. J. LOEFFLER 1982 19 p refs Presented at the AIAA 8th Aeroacoustics Conf., Atlanta, 11-13 Apr. 1983
(NASA-TM-83327; E-1574; NAS 1.15:83327; AIAA-83-9745)
Avail: NTIS HC A02/MF A01 CSCL 20A

A flight program was carried out to determine the variation of noise level with distance from a model high speed propeller. Noise measurements were obtained at different distances from a SR-3 propeller mounted on a JetStar aircraft, with the test instrumentation mounted on a Lear jet flown in formation. The propeller was operated at 0.8 flight Mach number, 1.12 helical tip Mach number and at 0.7 flight Mach number, 1.0 helical tip Mach number. The instantaneous pressure from individual blades was observed to rise faster at the 0.8 M flight speed, than at the 0.7 M flight speed. The measured levels appeared to decrease in good agreement with a 6 dB/doubling of distance decay, over the measurement range of approximately 16 m to 100 m distance. Further extrapolation, to the distances represented by a community, would suggest that the propagated levels during cruise would not cause a serious community annoyance. Author

N83-21896*# National Aeronautics and Space Administration. Lewis Research Center, Cleveland, Ohio.
ACOUSTIC MODAL ANALYSIS OF A FULL-SCALE ANNULAR COMBUSTOR
A. M. KARCHMER 1982 18 p refs Presented at the AIAA 8th Aeroacoustics Conf., Atlanta, 11-13 Apr. 1983
(NASA-TM-83334; E-1581; NAS 1.15:83334; AIAA-83-0760)
Avail: NTIS HC A02/MF A01 CSCL 20A

An acoustic modal decomposition of the measured pressure field in a full scale annular combustor installed in a ducted test rig is described. The modal analysis, utilizing a least squares optimization routine, is facilitated by the assumption of randomly occurring pressure disturbances which generate equal amplitude clockwise and counter-clockwise pressure waves, and the assumption of statistical independence between modes. These assumptions are fully justified by the measured cross spectral phases between the various measurement points. The resultant modal decomposition indicates that higher order modes compose the dominant portion of the combustor pressure spectrum in the range of frequencies of interest in core noise studies. A second major finding is that, over the frequency range of interest, each individual mode which is present exists in virtual isolation over significant portions of the spectrum. Finally, a comparison between the present results and a limited amount of data obtained in an operating turbofan engine with the same combustor is made. The comparison is sufficiently favorable to warrant the conclusion that the structure of the combustor pressure field is preserved between the component facility and the engine. Author

N83-21897*# National Aeronautics and Space Administration. Lewis Research Center, Cleveland, Ohio.
TRANSIENT DIFFERENCE SOLUTIONS OF THE INHOMOGENEOUS WAVE EQUATION: SIMULATION OF THE GREEN'S FUNCTION
K. J. BAUMEISTE 1983 13 p refs Presented at 8th Aeroacoust. Conf., Atlanta, 11-13 Apr. 1983; sponsored by AIAA
(NASA-TM-83336; E-1586; NAS 1.15:83336) Avail: NTIS HC A02/MF A01 CSCL 20A

A time-dependent finite difference formulation to the inhomogeneous wave equation is derived for plane wave propagation with harmonic noise sources. The difference equation and boundary conditions are developed along with the techniques to simulate the Dirac delta function associated with a concentrated noise source. Example calculations are presented for the Green's function and distributed noise sources. For the example considered, the desired Fourier transformed acoustic pressures are determined from the transient pressures by use of a ramping function and an integration technique, both of which eliminates the nonharmonic pressure associated with the initial transient. Author

N83-23112*# National Aeronautics and Space Administration. Lewis Research Center, Cleveland, Ohio.
NOISE OF THE 10-BLADED 60 DEG SWEPT SR-5 PROPELLER IN A WIND TUNNEL
J. H. DITTMAR, G. L. STEFKO, and R. J. JERACKI Feb. 1983 12 p refs
(NASA-TM-83054; E-1508; NAS 1.15:83054) Avail: NTIS HC A02/MF A01 CSCL 20A

Noise generated by supersonic helical tip speed propellers is a possible cabin environment problem for future airplanes powered by these propellers. Noise characteristics of one of these propellers, designated SR-5, are presented. A matrix of tests was conducted to provide as much acoustic information as possible. During aerodynamic testing it was discovered that the propeller had an aeroelastic instability which prevented testing the propeller at its design advance ratio of 4.08 at axial Mach numbers over 0.7. Plots of the variation of the maximum blade passage tone with helical tip Mach number indicate that, at higher helical tip Mach numbers, the propeller operated on sharply increasing portion of the noise curve; therefore, extrapolations to the design condition would not be accurate. A possible extrapolation indicated that SR-5 at its design point should be quieter than SR-3 at its design point. Directivity plots at the higher helical tip Mach numbers indicate a lobed directivity pattern as was observed previously on the SR-3 propeller. M.G.

N83-23114*# National Aeronautics and Space Administration. Lewis Research Center, Cleveland, Ohio.
APPLICATION OF 3-SIGNAL COHERENCE TO CORE NOISE TRANSMISSION
E. A. KREJSA 1983 17 p refs Presented at the 8th Aeroacoustics Conf., Atlanta, 11-13 Apr. 1983; sponsored by AIAA
(NASA-TM-83333; E-1580; NAS 1.15:83333; AIAA-83-0759)
Avail: NTIS HC A02/MF A01 CSCL 20A

A method for determining transfer functions across turbofan engine components and from the engine to the far-field is developed. The method is based on the three-signal coherence technique used previously to obtain far-field core noise levels. This method eliminates the bias error in transfer function measurements due to contamination of measured pressures by nonpropagating pressure fluctuations. Measured transfer functions from the engine to the far-field, across the tailpipe, and across the turbine are presented for three turbofan engines. M.G.

N83-23115*# National Aeronautics and Space Administration. Lewis Research Center, Cleveland, Ohio.
COMPARISON OF MEASURED AND PREDICTED FLIGHT EFFECTS ON HIGH-BYPASS COAXIAL JET EXHAUST NOISE
J. R. STONE 1983 20 p refs Presented at the 8th Aeroacoustics Conf., Atlanta, 11-13 Apr. 1983; sponsored by AIAA
(NASA-TM-83347; E-1604; NAS 1.15:83347; AIAA-83-0749)
Avail: NTIS HC A02/MF A01 CSCL 20A

A semi-empirical model for predicting the noise generated by conventional-velocity profile coaxial jets is compared with full scale flight data and model scale simulated flight data for high bypass nozzles. The prediction model was shown to agree with small scale static data for primary jet velocities from 215 to 795 m/s for a wide range of area, temperature, and velocity ratios between streams. However, there were insufficient model nozzle, simulated flight data available at that time to permit validation of the flight effects prediction. The comparisons presented demonstrate that the prediction method is also valid in flight. M.G.

N83-23116*# National Aeronautics and Space Administration. Lewis Research Center, Cleveland, Ohio.
CROSS SPECTRA BETWEEN TEMPERATURE AND PRESSURE IN A CONSTANT AREA DUCT DOWNSTREAM OF A COMBUSTOR
J. H. MILES, C. A. WASSERBAUER, and E. A. KREJSA 1983 28 p refs Presented at the 8th Aeroacoustics Conf., Atlanta, 11-13 Apr. 1983; sponsored by AIAA
(NASA-TM-83351; E-1608; NAS 1.15:83351; AIAA-83-0762)
Avail: NTIS HC A03/MF A01 CSCL 20A

The feasibility of measuring pressure temperature cross spectra and coherence and temperature-temperature cross spectra and coherence at spatially separated points along with pressure and temperature auto-spectra in a combustion rig was investigated. The measurements were made near the inlet and exit of a 6.44 m long duct attached to a J-47 combustor. The fuel used was Jet A. The cross spectra and coherence measurements show the pressure and temperature fluctuations correlate best at low frequencies. At the inlet the phenomena controlling the phase relationship between pressure and temperature could not be identified. However, at the duct exit the phase angle of the pressure is related to the phase angle of the temperature by the convected flow time delay. M.G.

N83-23117*# National Aeronautics and Space Administration. Lewis Research Center, Cleveland, Ohio.
SOUND DIFFRACTION AT WALL IMPEDANCE DISCONTINUITIES IN A CIRCULAR CYLINDER, INVESTIGATED USING WIENER-HOPF TECHNIQUE
Y. C. CHO 1983 27 p refs Presented at the 8th Aeroacoustics Conf., Atlanta, 11-13 Apr. 1983; sponsored by AIAA
(NASA-TM-83365; E-1631; NAS 1.15:83365; AIAA-83-0730)
Avail: NTIS HC A03/MF A01 CSCL 20A

Rigorous solutions are presented for sound diffraction in a circular cylinder with axial discontinuities of the wall admittance (or impedance). Analytical expressions are derived for the reflection and the transmission copefficients for duct modes. The results are discussed quantitatively in the limits of small admittance shifts (delta) and of low frequencies (ka). One of the results is the low frequency behavior of the reflection coefficient R(o) sub 00 of the fundamental mode. For the mode of a hardwall duct reflected from the junction with a softwall duct, (R(o) sub oo yields - (1-square root of (ka) square root of (2/i delta)); this result is in contrast to the frequency dependence of the reflection from the open end of a hardwall duct, for which R(o) sub oo yields - 1-(ka) squared/2 . M.G.

N83-24287*# National Aeronautics and Space Administration. Lewis Research Center, Cleveland, Ohio.
A PRELIMINARY COMPARISON BETWEEN THE SR-6 PROPELLER NOISE IN FLIGHT AND IN A WIND TUNNEL
J. H. DITTMAR, P. L. LASAGNA, and K. G. MACKALL 1983 18 p refs Presented at the 105th Meeting of the Acoustical Soc. of Am., Cincinnati, 9-13 May 1983
(NASA-TM-83341; E-1596; NAS 1.15:83341) Avail: NTIS HC A02/MF A01 CSCL 20A

High speed turboprops offer an attractive candidate for aircraft because of their high propulsive efficiency. However, one of the possible problems associated with these propellers is their high noise level at cruise condition that may create a cabin environment problem. Models of these propellers were tested for acoustics in the 8 by 6-foot wind tunnel and on the Jet Star airplane. Comparisons between the airplane and wind tunnel data for the SR-6 propeller are shown. The comparison of maximum blade passing tone variation with helical tip Mach number between the tunnel and flight data was good when corrected to the same test conditions. Directivity comparisons also showed fairly good agreement. These good comparisons indicate that the wind tunnel is a viable location for measuring the blade passage tone noise of these propellers. S.L.

N83-25499*# National Aeronautics and Space Administration. Lewis Research Center, Cleveland, Ohio.
ACOUSTICAL MODAL ANALYSIS OF THE PRESSURE FIELD IN THE TAILPIPE OF A TURBOFAN ENGINE
E. A. KREJSA and A. M. KARCHMER 13 May 1983 32 p refs Presented at 105th Meeting of the Acoust. Soc. of Am., Cincinnati, 9-13 May 1983
(NASA-TM-83387; E-1665; NAS 1.15:83387) Avail: NTIS HC A03/MF A01 CSCL 20A

The results of a modal analysis of the pressure field in the tailpipe of a turbofan engine are presented. Modal amplitudes, at the tailpipe inlet and exit, are presented, as a function of frequency, for several operating conditions. The modal amplitudes were obtained using an optimization routine to obtain a best fit between measured cross spectra and an analytical expression for the cross spectra between pressures at circumferentially spaced locations. The measured pressure field was decomposed into a set of five modal amplitudes corresponding to the (0,0), (1,0), (2,0), (3,0), and (4,0) modes. The analysis was limited to frequencies below 1500 Hz where higher order modes are cutoff. The results of the analysis showed that at low frequencies, up to the cuton frequency of the (1,0) mode, the (0,0) mode (plane wave) dominated the pressure field. The frequency range from the cuton of the (1,0) mode to the cuton of the (2,0) mode was dominated by the (1,0) mode. The (2,0) mode dominated from its cuton frequency to the upper limit of the analysis, i.e., 1500 Hz. The contribution of modes other than the dominant mode was usually small. S.L.

N83-26643*# National Aeronautics and Space Administration. Lewis Research Center, Cleveland, Ohio.
A COMPACT INFLOW CONTROL DEVICE FOR SIMULATING FLIGHT FAN NOISE
L. HOMYAK, J. G. MCARDLE, and L. J. HEIDELBERG 1983 11 p refs Presented at the 8th Aeroacoustics Conf., Atlanta, 11-13 Apr. 1983; sponsored by AIAA Previously announced in IAA as A83-28005
(NASA-TM-83349; E-1606; NAS 1.15:83349; AIAA-83-0680)
Avail: NTIS HC A02/MF A01 CSCL 20A

Inflow control device (ICD's) of various shapes and sizes have been used to simulate inflight fan tone noise during ground static tests. A small, simple inexpensive ICD design was optimized from previous design and fabrication techniques. This compact two-fan-diameter ICD exhibits satisfactory acoustic performance characteristics without causing noise attenuation or redirection. In addition, it generates no important new noise sources. Design and construction details of the compact ICD are discussed and acoustic performance test results are presented. Author (IAA)

N83-27793*# National Aeronautics and Space Administration. Lewis Research Center, Cleveland, Ohio.
JT150 1/2-SCALE NOZZLE JET NOISE EXPERIMENT AND COMPARISON WITH PREDICTION
D. E. GROESBECK and C. A. WASSERBAUER May 1983 26 p refs
(NASA-TM-83370; E-1636; NAS 1.15:83370) Avail: NTIS HC A03/MF A01 CSCL 20A

As part of a program to study flight effects on the exhaust noise of a full scale JT15D engine, static half scale model jet noise experiments were conducted. Acoustic data were recorded for microphone angles of 45 deg to 155 deg with jet conditions for the model scale nozzle corresponding closely to those at 55, 73 and 97 percent of corrected rated speed for the full scale engine. These data are useful for determining the relative importance of jet and core noise in the static full scale engine test data and will in turn allow for a proper evaluation of flight effects on the exhaust noise results. The model scale data are also compared with the coaxial jet noise prediction. Above 1000 Hz, the prediction is nominally 0 to 3 dB higher than the data. The arithmetic mean of the differences between the experimental OASPL and the predicted OASPL for all angles for each run ranged from 0 to -3.2 dB. The standard deviation of all the OASPL differences is 2.2 dB. The discrepancies are greatest at low primary jet velocities and appear to be due to inadequacy in the variable jet density exponent incorporated in the prediction procedure. S.L.

N83-27794*# National Aeronautics and Space Administration. Lewis Research Center, Cleveland, Ohio.
LOW FLIGHT SPEED ACOUSTIC RESULTS FOR A SUPERSONIC INLET WITH AUXILIARY INLET DOORS
R. P. WOODWARD, F. W. GLASER, and J. G. LUCAS 1982 47 p refs Presented at the 19th Joint Propulsion Conf., Seattle, Wash., 27-29 Jun. 1983; sponsored by AIAA, SAE, and ASME
(NASA-TM-83411; E-1694; NAS 1.15:83411) Avail: NTIS HC A03/MF A01 CSCL 20A

A model supersonic inlet with auxiliary inlet doors and bounday layer bleeds was acoustically tested in simulated low speed flight up to Mach 0.2 in the NASA Lewis 9x15 Anechoic Wind Tunnel and statically in the NASA Lewis Anechoic Chamber. A JT8D refan model was used as the noise source. Data were also taken for a CTOL inlet and for an annular inlet with simulated centerbody support struts. Inlet operation with open auxiliary doors increased the blade passage tone by about 10 dB relative to the closed door configuration although noise radiation was primarily through the main inlet rather than the doors. Numerous strong spikes in the noise spectra were associated with the bleed system, and were strongly affected by the centerbody location. The supersonic inlet appeared to suppress multiple pure tone (MPT) generation

at the fan source. Inlet length and the presence of support struts were shown not to cause this MPT suppression. Author

N83-30168*# National Aeronautics and Space Administration. Lewis Research Center, Cleveland, Ohio.
TURBULENCE SPECTRA IN THE NOISE SOURCE REGIONS OF THE FLOW AROUND COMPLEX SURFACES
W. A. OLSEN and D. R. BOLDMAN Jun. 1983 14 p refs
(NASA-TM-83392; E-1669; NAS 1.15:83392) Avail: NTIS HC A02/MF A01 CSCL 20A

The complex turbulent flow around three complex surfaces was measured in detail with a hot wire. The measured data include extensive spatial surveys of the mean velocity and turbulence intensity and measurements of the turbulence spectra and scale length at many locations. The publication of the turbulence data is completed by reporting a summary of the turbulence spectra that were measured within the noise source locations of the flow. The results suggest some useful simplifications in modeling the very complex turbulent flow around complex surfaces for aeroacoustic predictive models. The turbulence spectra also show that noise data from scale models of moderate size can be accurately scaled up to full size. Author

N83-33683*# Virginia Polytechnic Inst. and State Univ., Blacksburg. Dept. of Mechanical Engineering.
EXPERIMENTAL STUDY OF THE THERMAL-ACOUSTIC EFFICIENCY IN A LONG TURBULENT DIFFUSION-FLAME BURNER Final Report
J. R. MAHAN Washington NASA Aug. 1983 74 p refs
(Contract NAG3-124)
(NASA-CR-3725; NAS 1.26:3725) Avail: NTIS HC A04/MF A01 CSCL 20A

An acoustic source/propagation model is used to interpret measured noise spectra from a long turbulent burner. The acoustic model is based on the perturbation solution of the equations describing the unsteady one-dimensional flow of an inviscid ideal gas with a distributed heat source. The model assumes that the measured noise spectra are due uniquely to the unsteady component of combustion heat release. The model was applied to a long cylindrical hydrogen burner operating over a range of power levels between 4.5 kW and 22.3 kW. Acoustic impedances at the inlet to the burner and at the exit of the tube downstream of the burner were measured and are used as boundary conditions for the model. These measured impedances are also presented. Author

72

ATOMIC AND MOLECULAR PHYSICS

Includes atomic structure and molecular spectra.

N83-21903*# National Aeronautics and Space Administration. Lewis Research Center, Cleveland, Ohio.
RING-CUSP ION THRUSTER WITH SHELL ANODE Patent Application
J. S. SOVEY, V. K. RAWLIN, and R. F. ROMAN, inventors (to NASA) 9 Mar. 1983 12 p
(NASA-CASE-LEW-13881-1; US-PATENT-APPL-SN-473498)
Avail: NTIS HC A02/MF A01 CSCL 20H

An ion thruster for low specific impulse operation in the 1500 sec to 6000 sec range has a multicusp boundary field provided by high strength magnets on an iron anode shell which lengthens the paths of electrons from a hollow cathode assembly. A downstream anode pole piece in the form of an iron ring supports a ring of magnets to provide a more uniform beam profile. A cylindrical cathode magnet can be moved selectively in an axial direction along a feed tube to produce the desired magnetic field at the cathode tip. NASA

N83-35787*# SRI International Corp., Menlo Park, Calif.
SPINDT COLD CATHODE ELECTRON GUN DEVELOPMENT PROGRAM Final Report, Jan. 1982 - Apr. 1983
C. A. SPINDT May 1983 95 p refs
(Contract NAS3-23261; SRI PROJ. 4032)
(NASA-CR-168212; NAS 1.26:168212) Avail: NTIS HC A05/MF A01 CSCL 20H

A thin film field emission cathode array and an electron gun based on this emitter array are summarized. Fabricating state of the art cathodes for testing at NASA and NRL, advancing the fabrication technology, developing wedge shaped emitters, and performing emission tests are covered. An anistropic dry etching process (reactive ion beam etching) developed that leads to increasing the packing density of the emitter tips to about 5 x 10 to the 6th power/square cm. Tests with small arrays of emitter tips having about 10 tips has demonstrated current densities of over 100 A/sq cm. Several times using cathodes having a packing density of 1.25 x 10 to the 6th power tips/sq cm. Indications are that the higher packing density achievable with the dry etch process may extend this capability to the 500 A/sq cm range and beyond. The wedge emitter geometry was developed and shown to produce emission. This geometry can (in principle) extend the current density capability of the cathodes beyond the 500 A/sq cm level. An emission microscope was built and tested for use with the cathodes. Author

74

OPTICS

Includes light phenomena.

A83-40733* Arizona Univ., Tucson.
LONG-RANGE SURFACE PLASMONS IN ELECTRODE STRUCTURES
G. I. STEGEMAN and J. J. BURKE (Arizona, University, Tucson, AZ) Applied Physics Letters (ISSN 0003-6951), vol. 43, Aug. 1, 1983, p. 221-223. refs
(Contract NAG3-392)

Surface polaritons guided by symmetric double metal film structures are analyzed, with particular attention given to the attenuation of the two long-range modes that occur. It is found that long-range surface plasmon polariton modes do exist for double electrode structures over a limited range of material parameters. Guided by thin metal electrodes, surface plasmon polaritons can achieve millimeter plus propagation distances in the near infrared. It is pointed out that if the slab is electrooptic, then very low voltages will be needed to manipulate the waves. The fact that long-range modes exist simultaneously with junction tunnel plasmons may be of use in providing directional radiation from light-emitting junctions or the inverse process of light to electrical energy conversion. C.R.

A83-42206* Arizona Univ., Tucson.
LONG RANGE SURFACE PLASMONS IN BIREFRINGENT MEDIA
G. I. STEGEMAN (Arizona, University, Tucson, AZ) Applied Optics (ISSN 0003-6935), vol. 22, Aug. 1, 1983, p. 2243-2245. refs
(Contract NSF ECS-81-17483; NAG3-392)

The propagation properties of surface plasmon polaritons guided by thin metal films bounded by birefringent media are investigated. For the very thin (less than or equal to 150 A) films required to produce long propagation distances, the effects of birefringence on the dispersion relations are found to be minimal. A small effect of the birefringence on the mode attenuation is found. C.R.

N83-13979*# National Aeronautics and Space Administration. Lewis Research Center, Cleveland, Ohio.
LARGE-APERTURE INTERFEROMETER USING LOCAL REFERENCE BEAM
W. L. HOWES Nov. 1982 20 p refs
(NASA-TP-2060; E-1153; NAS 1.60:2060) Avail: NTIS HC A02/MF A01 CSCL 20F

A large-aperture interferometer was devised by adding a local-reference-beam-generating optical system to a schlieren system. Two versions of the interferometer are demonstrated, one employing 12.7 cm (5 in.) diameter schlieren optics, the other employing 30.48 cm (12 in.) diameter parabolic mirrors in an off-axis system. In the latter configuration a cylindrical lens is introduced near the light source to correct for astigmatism. A zone plate is a satisfactory decollimating element in the reference-beam arm of the interferometer. Attempts to increase the flux and uniformity of irradiance in the reference beam by using a diffuser are discussed. R.J.F.

N83-15861*# National Aeronautics and Space Administration. Lewis Research Center, Cleveland, Ohio.
A PROPOSED OPTICAL PUMPING SYSTEM REQUIRING NO ELECTRIC POWER Final Report
B. R. PHILLIPS *In* R and D Associates Proc. of the AFOSR Spec. Conf. on Prime-Power for High Energy Space Systems, Vol. 2 11 p 1982
Avail: NTIS HC A99/MF A01 CSCL 20F

A method for optically pumping a fluid without electrical power is described. The method is based on utilizing the radiation from a metal oxidant combustion reaction that is contained within a transparent tube that is immersed in the medium to be pumped. The reaction initiation and maintenance occurs by gas dynamically induced resonance within the transparent cavity. All that is required is a supply of high pressure oxidant and metallic powder. Materials that were successfully evaluated to date include aluminum, steel, magnesium, and titanium. M.G.

N83-19596* National Aeronautics and Space Administration. Lewis Research Center, Cleveland, Ohio.
HEAT PIPES CONTAINING ALKALI METAL WORKING FLUID Patent
J. F. MORRIS, inventor (to NASA) 16 Mar. 1981 4 p Filed 16 Mar. 1981 Supersedes N81-22310 (19 - 13, p 1756)
(NASA-CASE-LEW-12253-1; US-PATENT-4,372,377; US-PATENT-APPL-SN-243682; US-PATENT-CLASS-165-104.26; US-PATENT-CLASS-165-134R; US-PATENT-CLASS-29-157.3H)
Avail: US Patent and Trademark Office CSCL 20F

A technique for improving high temperature evaporation-condensation heat-transfer devices which have important and unique advantage in terrestrial and space energy processing is described. The device is in the form of a heat pipe comprising a sealed container or envelope which contains a capillary wick. The temperature of one end of the heat pipe is raised by the input of heat from an external heat source which is extremely hot and corrosive. A working fluid of a corrosive alkali metal, such as lithium, sodium, or potassium transfers this heat to a heat receiver remote from the heat source. The container and wick are fabricated from a superalloy containing a small percentage of a corrosion inhibiting or gettering element. Lanthanum, scandium, yttrium, thorium, and hafnium are utilized as the alloying metal.
Official Gazette of the U.S. Patent and Trademark Office

75

PLASMA PHYSICS

Includes magnetohydrodynamics and plasma fusion.

A83-10665*# National Aeronautics and Space Administration. Lewis Research Center, Cleveland, Ohio.
END REGION EFFECTS UPON THE PERFORMANCE OF A MAGNETOHYDRODYNAMIC CHANNEL
S. Y. WANG and J. M. SMITH (NASA, Lewis Research Center, Cleveland, OH) Journal of Energy, vol. 6, Nov.-Dec. 1982, p. 438, 439.
(Previously cited in issue 06, p. 945, Accession no. A82-17889)

A83-14398*# Colorado State Univ., Fort Collins.
ION FLOW EXPERIMENTS IN A MULTIPOLE DISCHARGE CHAMBER
H. R. KAUFMAN, R. S. ROBINSON, and L. E. FRISA (Colorado State University, Fort Collins, CO) AIAA, Japan Society for Aeronautical and Space Sciences, and DGLR, International Electric Propulsion Conference, 16th, New Orleans, LA, Nov. 17-19, 1982, AIAA 9 p. refs
(Contract NSG-3011)
(AIAA PAPER 82-1930)

It has been customary to assume that ions flow nearly equally in all directions from the ion production region within an electron-bombardment discharge chamber. Ion flow measurements in a multipole discharge chamber have shown that this assumption is not true. In general, the electron current through a magnetic field can alter the electron density, and hence the ion density, in such a way that ions tend to be directed away from the region bounded by the magnetic field. When this mechanism is understood, it becomes evident that many past discharge chamber designs have operated with a preferentially directed flow of ions. (Author)

A83-16691*# Texas Univ., Arlington.
TRANSIENT FLOW ANALYSIS OF THE AEDC/HPDE MHD GENERATOR
D. R. WILSON, Y. M. LEE (Texas, University, Arlington, TX), and C. S. STEWART (General Dynamics Corp., Fort Worth, TX) American Institute of Aeronautics and Astronautics, Aerospace Sciences Meeting, 21st, Reno, NV, Jan. 10-13, 1983, 10 p. refs
(Contract NSG-3255)
(AIAA PAPER 83-0395)

A hybrid Lax-Wendroff/Method of Characteristics computer code has been developed for numerical simulation of flow transients associated with the operation of MHD generator facilities. The code employs the shock-fitting method, with an Eulerian formulation of the basic conservation equations and explicit tracking of shock waves. Pressure, temperature, and velocity are used as primary integration variables to simplify interfacing of the code with real-gas thermodynamic and transport property tables. Application of the code to the simulation of selected transients for the AEDC/HPDE MHD generator produced results that are in good agreement with experimental observations. (Author)

A83-16735*# National Aeronautics and Space Administration. Lewis Research Center, Cleveland, Ohio.
METHODS OF REDUCING ENERGY CONSUMPTION OF THE OXIDANT SUPPLY SYSTEM FOR MHD/STEAM POWER PLANTS
A. J. JUHASZ (NASA, Lewis Research Center, Cleveland, OH) American Institute of Aeronautics and Astronautics, Aerospace Sciences Meeting, 21st, Reno, NV, Jan. 10-13, 1983, 10 p. refs
(AIAA PAPER 83-0468)

An in-depth study was conducted to identify possible improvements to the oxidant supply system for combined cycle MHD power plants which would lead to higher thermal efficiency and reduction in the cost of electricity, COE. Results showed that

the oxidant system energy consumption could be minimized when the process was designed to deliver a product O2 concentration of 70 mole percent. The study also led to the development of a new air separation process, referred to as 'liquid pumping and internal compression'. MHD system performance calculations show that the new process would permit an increase in plant thermal efficiency of 0.6 percent while allowing more favorable tradeoffs between magnetic energy and oxidant system capacity requirements. (Author)

A83-23134*# Avco-Everett Research Lab., Mass.
MHD CHANNEL PERFORMANCE FOR POTENTIAL EARLY COMMERCIAL MHD POWER PLANTS
D. W. SWALLOM (Avco Everett Research Laboratory, Inc., Everett, MA) (Intersociety Energy Conversion Engineering Conference, 16th, Atlanta, GA, Aug. 9-14, 1981). Journal of Energy, vol. 7, Mar.-Apr. 1983, p. 141-146. refs
(Contract DEN3-51)
(Previously cited in issue 07, p. 1124, Accession no. A82-20750)

A83-46271* Arizona Univ., Tucson.
EFFECTS OF GAPS ON LONG RANGE SURFACE PLASMON POLARITONS
G. I. STEGEMAN and J. J. BURKE (Arizona, University, Tucson, AZ) Journal of Applied Physics (ISSN 0021-8979), vol. 54, Sept. 1983, p. 4841-4843. refs
(Contract NAG3-392)
Fukui et al. (1979) and Stegeman et al. (1982) have shown theoretically that surface plasmon polaritons can be guided over long distances by thin metal films bounded by identical dielectric media. In principle, the possibility arises for the propagation of highly localized fields. In order to obtain long propagation distances, most of the energy will have to be carried outside the metal. THis makess it necessary to operate near the mode cutoff condition. In the present investigation, it is shown that very small air gaps between the metal and dielectric surfaces will cause the mode to become radiative, and, therefore, no longer bounded to the metal film. Calculations show that gaps of dimension 100 A and less can cause severe problems in geometries relying on long range surface plasmon polaritons. High refractive index liquids placed in the gaps should alleviate these problems. G.R.

N83-31474*# Colorado State Univ., Fort Collins. Dept. of Physics.
CURRENT COLLECTION FROM THE SPACE PLASMA THROUGH DEFECTS IN HIGH VOLTAGE SOLAR ARRAY INSULATION Ph.D. Thesis. Final Report
R. P. STILLWELL Jan. 1983 103 p refs
(Contract NSG-3196)
(NASA-CR-168148; NAS 1.26:168148) Avail: NTIS HC A06/MF A01 CSCL 20I
For spacecraft operation in the near Earth environment, solar cell arrays constitute the major source of reliable long term power. Optimization of mass and power efficiency results in a general requirement for high voltage solar arrays. The space plasma environment, though, can result in large currents being collected by exposed solar cells. The solution of a protective covering of transparent insulation is not a complete solution, inasmuch as defects in the insulation result in anomalously large currents being collected through the defects. Tests simulating the electron collection from small defects in an insulation have shown that there are two major collection modes. The first mode involves current enhancement by means of a surface phenomenon involving the surrounding insulator. In the second mode the current collection is enhanced by vaporization and ionization of the insulators materials, in addition to the surface enhancement of the first mode. A model for the electron collection is the surface enhanced collection mode was developed. The model relates the secondary electron emission yield to the electron collection. It correctly predicts the qualitative effects of hole size, sample temperature and roughening of sample surface. The theory was also shown to predict electron collection within a factor of two for the polymers teflon and polyimide. Author

76

SOLID-STATE PHYSICS

Includes superconductivity.

A83-11812* Nebraska Univ., Lincoln.
ELLIPSOMETRIC STUDY OF SILICON NITRIDE ON GALLIUM ARSENIDE
S. A. ALTEROVITZ, G. H. BU-ABBUD, J. A. WOOLLAM (Nebraska, University, Lincoln, NE), D. LIU (NASA, Lewis Research Center, Cleveland, OH), Y. CHUNG (Universal Energy Systems, Dayton, OH), and D. LANGER (USAF, Avionics Laboratory, Wright-Patterson AFB, OH) Applied Physics Communications, vol. 1, no. 2, 1981-1982, p. 163-177. USAF-supported research refs
(Contract NAG3-154)
A method for optimizing the sensitivity of ellipsometric measurements for thin dielectric films on semiconductors is described in simple physical terms. The technique is demonstrated for the case of sputtered silicon nitride films on gallium arsenide. (Author)

A83-13784* Rockwell International Corp., Thousand Oaks, Calif.
LIQUID ENCAPSULATED CZOCHRALSKI GROWTH OF LOW DISLOCATION GAAS
C. G. KIRKPATRICK, R. T. CHEN, and D. E. HOLMES (Rockwell International Microelectronics Research and Development Center, Thousand Oaks, CA) In: Integrated optics and millimeter and microwave integrated circuits; Proceedings of the Conference, Huntsville, AL, November 16-19, 1981. Bellingham, WA, SPIE - The International Society for Optical Engineering, 1982, p. 234-242. refs
(Contract NAS3-22224)
The availability of high-quality, large-diameter GaAs substrates is key to the successful development and production of high-speed GaAs devices and high-efficiency GaAs solar cells. The liquid encapsulated Czochralski (LEC) technique has provided a means for producing large-diameter GaAs. Progress in improving the LEC growth process which has resulted in 3-inch GaAs crystals with exceptionally low dislocation densities and reduced propensity for twinning is reported. Undoped, semi-insulating GaAs ingots were grown in a Melbourn high-pressure LEC system. The effects of seed perfection, seed necking, cone angle, melt stoichiometry, ambient pressure, thickness of the B2O3 encapsulating layer, and diameter control on the dislocation density were investigated. The material was characterized by preferential etching and X-ray topography. It is shown that 3-inch diameter substrates can be produced with dislocation densities as low as 6000 per sq cm through proper selection and control of growth parameters. Also, the incidence of twinning can be reduced significantly by growing from slightly As-rich melts. (Author)

A83-17226* National Aeronautics and Space Administration. Lewis Research Center, Cleveland, Ohio.
DIPOLE-FIELD SUMS AND LORENTZ FACTORS FOR ORTHORHOMBIC LATTICES, AND IMPLICATIONS FOR POLARIZABLE MOLECULES
C. K. PURVIS (NASA, Lewis Research Center, Cleveland, OH) and P. L. TAYLOR (Case Western Reserve University, Cleveland, OH) Physical Review B - Solid State, 3rd Series, vol. 26, Oct. 15, 1982, p. 4547-4563. refs
(Contract DAAG29-78-G-0064)
A method for computing the Lorentz tensor components in single crystals via rapidly convergent sums of Bessels functions is developed using the relationship between dipole-field sums and the tensor components. The Lorentz factors for simple, body-centered, and base-centered orthorhombic lattices are

computed using this method, and the derivative Lorentz factors for simple orthorhombic lattices are also determined. Both the Lorentz factors and their derivatives are shown to be very sensitive to a lattice structure. The equivalent of the Clausius-Mossotti relation for general orthorhombic lattices is derived using the Lorentz-factor formalism, and the permanent molecular dipole moment is related to crystal polarization for the case of a ferroelectric of polarizable point dipoles. It is concluded that the polarization enhancement due to self-polarization familiar from classical theory may actually be a reduction in consequences of negative Lorentz factors in one or two lattice directions for noncubic crystals. N.B.

A83-17227* National Aeronautics and Space Administration. Lewis Research Center, Cleveland, Ohio.
PIEZOELECTRIC AND PYROELECTRIC COEFFICIENTS FOR FERROELECTRIC CRYSTALS WITH POLARIZABLE MOLECULES
C. K. PURVIS (NASA, Lewis Research Center, Cleveland, OH) and P. L. TAYLOR (Case Western Reserve University, Cleveland, OH) Physical Review B - Solid State, 3rd Series, vol. 26, Oct. 15, 1982, p. 4564-4570. refs
(Contract DAAG29-78-G-0064)

Expressions for piezoelectric and pyroelectric coefficients for a crystal of polarizable point dipoles are derived. The effect of crystal structure on the local electric field acting to polarize the molecules is included via the Lorentz-factor formalism. The derived expressions for the piezo- and pyroelectric coefficients are found to contain terms dependent on derivatives of the Lorentz factors. These terms reflect the changing of molecular dipole moments in response to the changing local electric field in the strained crystal. Inclusion of this effect results in predictions of coefficients substantially different from those obtained using the Lorentz field approximation. (Author)

A83-19989* Rockwell International Corp., Thousand Oaks, Calif.
RESIDUAL DOUBLE ACCEPTORS IN BULK GAAS
K. R. ELLIOTT (Rockwell International Microelectronics Research and Development Center, Thousand Oaks, CA) Applied Physics Letters, vol. 42, Feb. 1, 1983, p. 274-276. refs
(Contract NAS3-22235; NAS3-22224)

By using infrared absorption, photoluminescence, and Hall measurements we have observed an additional level associated with a residual acceptor in liquid encapsulated Czochralski GaAs. These results indicate that the defect is a double acceptor with levels 78 and 200 meV above the valence band. (Author)

A83-22756* Rockwell International Corp., Thousand Oaks, Calif.
EL2 DISTRIBUTIONS IN DOPED AND UNDOPED LIQUID ENCAPSULATED CZOCHRALSKI GAAS
D. E. HOLMES, R. T. CHEN, and J. YANG (Rockwell International Microelectronics Research and Development Center, Thousand Oaks, CA) Applied Physics Letters, vol. 42, Mar. 1, 1983, p. 419-421. refs
(Contract NAS3-22224; NAS3-22235)

The longitudinal and radial distributions of EL2 in undoped semi-insulating and intentionally doped n-type GaAs crystals grown by the liquid encapsulated Czochralski technique are compared. Longitudinal profiles in undoped crystals are controlled by changes in melt stoichiometry as the crystal is pulled from the melt. EL2 profiles along crystals doped above about 1 x 10 to the 17th/cu cm, on the other hand, are controlled primarily by the carrier concentration as a result of the suppression of EL2 by free electrons. Radial EL2 profiles are typically W shaped and M shaped in undoped and doped (above threshold) crystals, respectively. The origin of these radial profiles is discussed in terms of residual stress, melt stoichiometry, and the suppresion of EL2 by electrons. The results are also discussed in the light of the antisite model for EL2. (Author)

A83-22767* National Aeronautics and Space Administration. Lewis Research Center, Cleveland, Ohio.
PRODUCTION OF LARGE-AREA SINGLE-CRYSTAL WAFERS OF CUBIC SIC FOR SEMICONDUCTOR DEVICES
S. NISHINO, J. A. POWELL, and H. A. WILL (NASA, Lewis Research Center, Cleveland, OH) Applied Physics Letters, vol. 42, Mar. 1, 1983, p. 460-462. refs

A reproducible process is described for growing a thick single-crystal layer of cubic SiC on a single-crystal Si wafer by chemical vapor deposition. A buffer layer, grown in situ, is used between the cubic SiC and the Si substrate to minimize the effect of lattice mismatch. Layers of up to 34 microns thick and several sq cm in area have been grown. Wafers are obtained by chemically removing the Si substrates from the grown layers. Excellent electron channeling patterns produced by these wafers indicate very good crystal quality. Preliminary electrical measurements have yielded electron mobilities up to 380 sq cm/Vs. (Author)

A83-28448* Nebraska Univ., Lincoln.
MINORITY CARRIER DIFFUSION LENGTH MEASUREMENTS - A REVIEW AND COMPARISON OF TECHNIQUES
A. A. KHAN, J. A. WOOLLAM (Nebraska, University, Lincoln, NE), and A. M. HERMANN (Solar Energy Research Institute, Golden, CO) Applied Physics Communications, vol. 2, no. 1-2, 1982, p. 17-56. refs
(Contract EG-77-C-01-4042; NAG3-120)

A review of the major techniques for measuring minority carrier diffusion lengths in solar cells is given. Limits of applicability are indicated for each method, as relevant to indirect bandgap materials such as silicon, and direct bandgap materials like gallium arsenide. A discussion and bibliography is presented for the following techniques: uniform generation, electron beam induced current, Schottky barrier (and other steady-state) photocurrent, surface photovoltage, transient decay, and luminescence. (Author)

A83-29531* National Aeronautics and Space Administration. Lewis Research Center, Cleveland, Ohio.
PIEZOELECTRICITY AND PYROELECTRICITY IN POLYVINYLIDENE FLUORIDE - INFLUENCE OF THE LATTICE STRUCTURE
C. K. PURVIS (NASA, Lewis Research Center, Cleveland, OH) and P. L. TAYLOR (Case Western Reserve University, Cleveland, OH) Journal of Applied Physics (ISSN 0021-8979), vol. 54, Feb. 1983, p. 1021-1028. NSF-Army-supported research. refs

Piezoelectric and pyroelectric responses of beta-phase (Phase I) polyvinylidene fluoride are predicted for a model system of polarizable point dipoles. The model incorporates the influence of the orthorhombic crystal structure by including the dependence of the internal electric field on the lattice parameters. Strong anisotropy in the piezoelectric response under uniaxial stress is predicted as a consequence of the orthorhombic lattice structure. Predictions are found to be in reasonable agreement with room-temperature experimental data. Author

A83-33920* Nebraska Univ., Lincoln.
INTERFACIAL ELECTRICAL PROPERTIES OF ION-BEAM SPUTTER DEPOSITED AMORPHOUS CARBON ON SILICON
A. A. KHAN, J. A. WOOLLAM (Nebraska, University, Lincoln, NE), Y. CHUNG (Universal Energy Systems, Inc., Dayton, OH), and B. BANKS (NASA, Lewis Resarch Center, Cleveland, OH) IEEE Electron Device Letters (ISSN 0193-8576), vol. EDL-4, May 1983, p. 146-149. Research supported by the University of Nebraska. refs
(Contract NAG3-95)

Amorphous, 'diamond-like' carbon films have been deposited on Si substrates, using ion-beam sputtering. The interfacial properties are studied using capacitance and conductance measurements. Data are analyzed using existing theories for interfacial electrical properties. The density of electronic states at the interface, along with corresponding time constants are determined. Author

A83-37618* Nebraska Univ., Lincoln.
AN ENHANCED SENSITIVITY NULL ELLIPSOMETRY TECHNIQUE FOR STUDYING FILMS ON SUBSTRATES - APPLICATION TO SILICON NITRIDE ON GALLIUM ARSENIDE
S. A. ALTEROVITZ, G. H. BU-ABBUD, J. A. WOOLLAM (Nebraska, University, Lincoln, NE), and D. C. LIU (NASA, Lewis Research Center, Cleveland, OH) Journal of Applied Physics (ISSN 0021-8979), vol. 54, March 1983, p. 1559-1569. refs
(Contract NAG3-154; F33601-81-MJ869)

N83-10962*# National Aeronautics and Space Administration. Lewis Research Center, Cleveland, Ohio.
RADIATION DAMAGE IN FRONT AND BACK ILLUMINATED HIGH RESISTIVITY SILICON SOLAR CELLS
I. WEINBERG, C. P. GORADIA, C. K. SWARTZ, and H. W. BRANDHORST, JR. 1982 12 p refs Presented at 16th Photovoltaic Specialists Conf., San Diego, Calif., 27-30 1982; sponsored by IEEE
(NASA-TM-82965; E-1384; NAS 1.15:82965) Avail: NTIS HC A02/MF A01 CSCL 10A

Radiation induced degradation, in front and back illuminated 84 and 1250 ohm-cm n+pp+ silicon solar cells, was determined and cell performance interpreted using calculated optically injected charge distributions and cell voltage components. The 84 ohm-cm cell degraded less when illuminated from the front or n+ side compared to that when illuminated from the back or p+ side. On the other hand, the 1250 ohm-cm cell degraded less when back illuminated. It is concluded that, in addition to the usual mechanisms leading to decreased collection efficiencies, loss of conductivity modulation is a major cause of radiation damage in high resistivity silicon solar cells. These results suggest that radiation damage to high resistivity n+pp+ cells can be decreased by increasing cell collection efficiency and illuminating the cells from the p+ side.
Author

N83-13009*# Case Western Reserve Univ., Cleveland, Ohio.
ORIENTATION DEPENDENCE OF THE STRESS RUPTURE PROPERTIES OF NICKEL-BASE SUPERALLOY SINGLE CRYSTALS Contractor Report, Jun. 1979 - Jun. 1981
R. A. MACKAY May 1981 97 p refs
(Contract NSG-3246)
(NASA-CR-165394; NAS 1.26:165394) Avail: NTIS HC A05/MF A01 CSCL 20L

The influence of orientation of the stress rupture behavior of Mar-M247 single crystals was studied. Stress rupture tests were performed at 724 MPa and 774 C where the effect of anisotropy is prominent. The mechanical behavior of the single crystals was rationalized on the basis of the Schmid factors for the operative slip systems and the lattice rotations which the crystals underwent during deformation. The stress rupture lives were found to be greatly influenced by the lattice rotations required to produce intersecting slip, because steady-state creep does not begin until after the onset of intersecting slip. Crystals which required large rotations to become oriented for intersecting slip exhibited a large primary creep strain, a large effective stress level at the onset of steady-state creep, and consequently a short stress rupture life. A unified analysis was attained for the stress rupture behavior of the Mar-M247 single crystals tested in this study at 774 C and that of the Mar-M200 single crystals tested in a prior study at 760 C. In this analysis, the standard 001-011-111 stereographic triangle was divided into several regions of crystallographic orientation which were rank ordered according to stress rupture life for this temperature regime. This plot indicates that those crystals having orientations within about 25 deg of the 001 exhibited significantly longer lives when their orientations were closer to the 001-011 boundary of the stereographic triangle than to the 001-111 boundary.
B.W.

N83-15877# National Aeronautics and Space Administration. Lewis Research Center, Cleveland, Ohio.
DEEP IMPURITY TRAPPING CONCEPTS FOR POWER SEMICONDUCTOR DEVICES Final Report
G. R. SUNDBERG *In* R and D Associates Proc. of the AFOSR Spec. Conf. on Prime-Power for High Energy Space Systems, Vol. 2 39 p 1982 refs
Avail: NTIS HC A99/MF A01 CSCL 20L

High voltage semiconductor switches using deep impurity doped silicon now appear feasible for high voltage (1-100 kV), high power (10 Kw) switching and protection functions for future space power applications. Recent discoveries have demonstrated several practical ways of gating deep impurity doped silicon devices in planar configurations and of electrically controlling their characteristics, leading to a vast array of possible circuit applications. A new family of semiconductor switching devices and transducers are possible based on this technology. New deep impurity devices could be simpler than conventional p-n junction devices and yet use the same basic materials and processing techniques. In addition, multiple functions may be possible on a single device as well as increased ratings.
Author

N83-16234*# Beers Associates, Inc., Reston, Va.
CONTINUED DEVELOPMENT OF A DETAILED MODEL OF ARC DISCHARGE DYNAMICS Contract Report, Aug. 1980 - Mar. 1982
B. L. BEERS, V. W. PINE, and S. T. IVES 14 Dec. 1982 156 p refs
(Contract NAS3-22530)
(NASA-CR-167977; NAS 1.26:167977; BEERS-1-82-16-23) Avail: NTIS HC A08/MF A01 CSCL 20L

Using a previously developed set of codes (SEMC, CASCAD, ACORN), a parametric study was performed to quantify the parameters which describe the development of a single electron indicated avalanche into a negative tip streamer. The electron distribution function in Teflon is presented for values of the electric field in the range of four-hundred million volts/meter to four billon volts/meter. A formulation of the scattering parameters is developed which shows that the transport can be represented by three independent variables. The distribution of ionization sites is used to indicate an avalanche. The self consistent evolution of the avalanche is computed over the parameter range of scattering set.
Author

N83-19622*# Rockwell International Corp., Thousand Oaks, Calif.
HIGH PURITY, LOW DISLOCATION GAAS SINGLE CRYSTALS Final Report, 29 Dec. 1980 - 29 Sep. 1981
R. T. CHEN, D. E. HOLMES, and C. G. KIRKPATRICK Feb. 1983 113 p refs Sponsored in part by Army Electronics Research and Development Command
(Contract NAS3-22224)
(NASA-CR-168098; NAS 1.26:16809; MRDC41054.59FR) Avail: NTIS HC A06/MF A01 CSCL 20B

Liquid encapsulated Czochralski crystal growth techniques for producing undoped, high resistivity, low dislocation material suitable for device applications is described. Technique development resulted in reduction of dislocation densities in 3 inch GaAs crystals. Control over the melt stoichiometry was determined to be of critical importance for the reduction of twinning and polycrystallinity during growth.
S.L.

N83-21987*# RCA Labs., Princeton, N. J.
ADVANCED 3-V SEMICONDUCTOR TECHNOLOGY ASSESSMENT Final Report, 20 Jul. 1981 - 19 Jul. 1982
M. NOWOGRODZKI Feb. 1983 235 p refs 2 Vol.
(Contract NAS3-22884)
(NASA-CR-168101; NAS 1.26:168101; RCA-PRRL-82-CR-18)
Avail: NTIS HC A11/MF A01 CSCL 20L

Components required for extensions of currently planned space communications systems are discussed for large antennas, crosslink systems, single sideband systems, Aerostat systems, and digital signal processing. Systems using advanced modulation

concepts and new concepts in communications satellites are included. The current status and trends in materials technology are examined with emphasis on bulk growth of semi-insulating GaAs and InP, epitaxial growth, and ion implantation. Microwave solid state discrete active devices, multigigabit rate GaAs digital integrated circuits, microwave integrated circuits, and the exploratory development of GaInAs devices, heterojunction devices, and quasi-ballistic devices is considered. Competing technologies such as RF power generation, filter structures, and microwave circuit fabrication are discussed. The fundamental limits of semiconductor devices and problems in implementation are explored. A.R.H.

N83-21988*# RCA Labs., Princeton, N. J.
ADVANCED 3-V SEMICONDUCTOR TECHNOLOGY ASSESSMENT Executive Summary Final Report
M. NOWOGRODZKI Feb. 1983 9 p 2 Vol.
(Contract NAS3-22884)
(NASA-CR-168102; NAS 1.26:168102; RCA-PRRL-82-CR-18)
Avail: NTIS HC A02/MF A01 CSCL 20L

Against a background of an extensive survey of the present state of the art in the field of III-V semiconductors for operation at microwave frequencies (or gigabit rate speeds), likely requirements of future space communications systems are identified, competing technologies and physical device limitations are discussed, and difficulties in implementing emerging technologies are projected. On the basis of these analyses, specific research and development programs required for the development of future systems components are recommended. Author

N83-27877*# Rockwell International Corp., Thousand Oaks, Calif. Microelectronics Research and Development Center.
GROWTH AND CHARACTERIZATION OF CZOCHRALSKI-GROWN N AND P-TYPE GAAS FOR SPACE SOLAR CELL SUBSTRATES Final Report, 29 May 1981 - 28 May 1982
R. T. CHEN Jun. 1983 51 p refs
(Contract NAS3-22235)
(NASA-CR-168099; NAS 1.26:168099; MRDC41092.35FR) Avail: NTIS HC A04/MF A01 CSCL 20L

Progress in LEC (liquid encapsulated Czochralski) crystal growth techniques for producing high-quality, 3-inch-diameter, n- and p-type GaAs crystals suitable for solar cell applications is described. The LEC crystals with low dislocation densities and background impurities, high electrical mobilities, good dopant uniformity, and long diffusion lengths were reproducibly grown through control of the material synthesis, growth and doping conditions. The capability for producing these large-area, high-quality substrates should positively impact the manufacturability of highly efficiency, low cost, radiation-hard GaAs solar cells. Author

N83-34796* National Aeronautics and Space Administration. Lewis Research Center, Cleveland, Ohio.
PIEZOELECTRIC COMPOSITE MATERIALS Patent
L. J. KIRALY, inventor (to NASA) 23 Aug. 1983 4 p Filed 12 Jul. 1982 Supersedes N82-31450 (20 - 22, p 3102)
(NASA-CASE-LEW-12582-1; US-PATENT-4,400,642; US-PATENT-APPL-SN-397281; US-PATENT-CLASS-310-332; US-PATENT-CLASS-310-800; US-PATENT-CLASS-428-294; US-PATENT-CLASS-428-421; US-PATENT-CLASS-428-422)
Avail: US Patent and Trademark Office CSCL 20L

A laminated structural devices has the ability to change shape, position and resonant frequency without using discrete motive components. The laminate may be a combination of layers of a piezoelectrically active, nonconductive matrix material. A power source selectively places various levels of charge in electrically conductive filaments imbedded in the respective layers to produce various configurations in a predetermined manner. The layers may be electrically conductive having imbedded piezoelectrically active filaments. A combination of layers of electrically conductive material may be laminated to layers of piezoelectrically active material.
Official Gazette of the U.S. Patent and Trademark Office

77

THERMODYNAMICS AND STATISTICAL PHYSICS

Includes quantum mechanics; and Bose and Fermi statistics.

A83-12094*# National Bureau of Standards, Boulder, Colo.
THE THERMAL CONDUCTIVITY OF OXYGEN
H. M. RODER (National Bureau of Standards, Thermophysical Properties Div., Boulder, CO) Journal of Research, vol. 87, July-Aug. 1982, p. 279-310. refs
(Contract NASA ORDER C-32369-C)

The paper presents new experimental measurements of the thermal conductivity of oxygen for thirteen isotherms at temperatures from 78 to 310 K with pressures to 70 MPa and densities from 0 to 40 mol/L. The measurements were made with a transient hot wire apparatus and they cover a wide range of physical states including the dilute gas, the moderately dense gas, the near critical region, the compressed liquid states, and the vapor at temperatures below the critical temperature. The thermal conductivity surface is represented with an equation that is based in part on an existing correlation of the dilute gas. The date are compared with the experimental measurements of others through the new correlation. The new measurements show that the critical enhancement extends to quite high temperatures, about 300 K. The precision (2 sigma) of the oxygen of the oxygen measurements is between 0.5 and 0.8 percent for wire temperature transients of 4 to 5 K, while the accuracy is estimated to be 1.5 percent. (Author)

A83-27272* Cleveland State Univ., Ohio.
COMPUTATION TECHNIQUES AND COMPUTER PROGRAMS TO ANALYZE STIRLING CYCLE ENGINES USING CHARACTERISTIC DYNAMIC ENERGY EQUATIONS
V. H. LARSON (Cleveland State University, Cleveland, OH) In: IECEC '82; Proceedings of the Seventeenth Intersociety Energy Conversion Engineering Conference, Los Angeles, CA, August 8-12, 1982. Volume 4. New York, Institute of Electrical and Electronics Engineers, 1982, p. 1710-1715. refs
(Contract NSG-3257)

The basic equations that are used to describe the physical phenomena in a Stirling cycle engine are the general energy equations and equations for the conservation of mass and conversion of momentum. These equations, together with the equation of state, an analytical expression for the gas velocity, and an equation for mesh temperature are used in this computer study of Stirling cycle characteristics. The partial differential equations describing the physical phenomena that occurs in a Stirling cycle engine are of the hyperbolic type. The hyperbolic equations have real characteristic lines. By utilizing appropriate points along these curved lines the partial differential equations can be reduced to ordinary differential equations. These equations are solved numerically using a fourth-fifth order Runge-Kutta integration technique. (Author)

N83-20808*# National Aeronautics and Space Administration. Lewis Research Center, Cleveland, Ohio.
A SEARCH FOR EQUILIBRIUM STATES
F. J. ZELEZNIK Nov. 1982 13 p refs Presented at Calphad 11, Argonne, Ill., 16-20 May 1982
(NASA-TM-82898; E-1281; NAS 1.15:82898) Avail: NTIS HC A02/MF A01 CSCL 20M

An efficient search algorithm is described for the location of equilibrium states in a search set of states which differ from one another only by the choice of pure phases. The algorithm has three important characteristics: (1) it ignores states which have little prospect for being an improved approximation to the true equilibrium state; (2) it avoids states which lead to singular iteration equations; (3) it furnishes a search history which can provide clues to alternative search paths. Author

N83-23188*# National Aeronautics and Space Administration. Lewis Research Center, Cleveland, Ohio.
A CLASS OF NONIDEAL SOLUTIONS. 2: APPLICATION TO EXPERIMENTAL DATA
F. J. ZELEZNIK and L. F. DONOVAN Apr. 1983 55 p refs
(NASA-TP-1930; E-020; NAS 1.60:1930) Avail: NTIS HC A04/MF A01 CSCL 20M

Functions for the representation of the thermodynamic properties of nonideal solutions were applied to the experimental data for several highly nonideal solutions. The test solutions were selected to cover both electrolyte behavior. The results imply that the functions are fully capable of representing the experimental data within their accuracy over the whole composition range and demonstrate that many nonideal solutions can be regarded as members of the defined class of nonideal solutions. Author

N83-23189*# National Aeronautics and Space Administration. Lewis Research Center, Cleveland, Ohio.
A CLASS OF NONIDEAL SOLUTIONS. 1: DEFINITION AND PROPERTIES
F. J. ZELEZNIK Apr. 1983 43 p refs
(NASA-TP-1929; E-021; NAS 1.60:1929) Avail: NTIS HC A03/MF A01 CSCL 20M

A class of nonideal solutions is defined by constructing a function to represent the composition dependence of thermodynamic properties for members of the class, and some properties of these solutions are studied. The constructed function has several useful features: (1) its parameters occur linearly; (2) it contains a logarithmic singularity in the dilute solution region and contains ideal solutions and regular solutions as special cases; and (3) it is applicable to N-ary systems and reduces to M-ary systems (M or = N) in a form-invariant manner. Author

80

SOCIAL SCIENCES (GENERAL)

Includes educational matters.

N83-10970*# Akron Univ., Ohio. Dept. of Civil Engineering.
NASA LERC/AKRON UNIVERSITY GRADUATE COOPERATIVE FELLOWSHIP PROGRAM AND GRADUATE STUDENT RESEARCHERS PROGRAM Interim Report
D. G. FERTIS and A. L. SIMON Oct. 1981 95 p refs
(Contract NAG3-50; NGT-36-001-800; NGT-36-001-801)
(NASA-CR-167943; NAS 1.26:167943; NAUFP-202-1) Avail: NTIS HC A05/MF A01 CSCL 05I

The requisite methodology to solve linear and nonlinear problems associated with the static and dynamic analysis of rotating machinery, their static and dynamic behavior, and the interaction between the rotating and nonrotating parts of an engine is developed. Linear and nonlinear structural engine problems are investigated by developing solution strategies and interactive computational methods whereby the man and computer can communicate directly in making analysis decisions. Representative examples include modifying structural models, changing material, parameters, selecting analysis options and coupling with interactive graphical display for pre- and postprocessing capability. S.L.

81

ADMINISTRATION AND MANAGEMENT

Includes management planning and research.

N83-30297*# United Technologies Corp., South Windsor, Conn. Power Systems Div.
TASK 4 COMPLETION REPORT FOR 40 KILOWATT GRID CONNECTED MODIFICATION CONTRACT Final Report
J. H. VOGT Jun. 1983 40 p
(Contract DEN3-210; DE-AI21-80ET-17088)
(NASA-CR-167950; DOE/NASA/0219-1; NAS 1.26:167950; FCR-4294) Avail: NTIS HC A03/MF A01 CSCL 05A

Startup, operation in grid connect mode, shutdown from grid connects, operation in isolated mode, shutdown from isolated mode, steady state operation, mode transfers, and voltage disconnects are addressed. Author

82

DOCUMENTATION AND INFORMATION SCIENCE

Includes information storage and retrieval technology; micrography; and library science.

N83-15169*# National Aeronautics and Space Administration. Lewis Research Center, Cleveland, Ohio.
RESEARCH AND TECHNOLOGY, LEWIS RESEARCH CENTER Annual Report, 1982
1982 47 p refs
(NASA-TM-83038; NAS 1.15:83038) Avail: NTIS HC A03/MF A01 CSCL 05B

Aeronautics, space, and terrestrial energy research is covered. Energy conversion processes and systems for propulsion in the atmosphere, in space, and on the ground are reviewed. Electric energy generation and storage for both terrestrial and space applications and materials and structures for such systems are also reviewed. N.W.

N83-29124*# National Aeronautics and Space Administration. Lewis Research Center, Cleveland, Ohio.
BIBLIOGRAPHY OF LEWIS RESEARCH CENTER TECHNICAL PUBLICATIONS ANNOUNCED IN 1982
Apr. 1983 372 p
(NASA-TM-83335; E-1585; NAS 1.15:83335) Avail: NTIS HC A16/MF A01 CSCL 05B

The technical reporting that resulted from the scientific and engineering work performed and managed by the Lewis Research Center in 1982 is described. All the publications were announced in the 1982 issues of STAR (Scientific and Technical Aerospace Reports) and/or IAA (International Aerospace Abstracts). Included are research reports, journal articles, conference presentations, patents and patent applications, and theses. Author

85

URBAN TECHNOLOGY AND TRANSPORTATION

Includes applications of space technology to urban problems; technology transfer; technology assessment; and surface and mass transportation.

A83-31087* National Aeronautics and Space Administration. Lewis Research Center, Cleveland, Ohio.
A SUMMARY OF EHV PROPULSION TECHNOLOGY
H. J. SCHWARTZ (NASA, Lewis Research Center, Cleveland, OH) IEEE Transactions on Vehicular Technology (ISSN 0018-9545), vol. VT-32, Feb. 1983, p. 3-6.

While the battery used by an electric vehicle is the primary determinant of range, and to a lesser extent of performance, the design of the vehicle's propulsion system establishes its performance level and is the greatest contributor to its purchase price. Propulsion system weight, efficiency and cost are related to the specific combination of components used. Attention is given to the development status of the U.S. Department of Energy's Electric and Hybrid Vehicle Program, through which propulsion component and system design improvements have been made which promise weight savings of 35-50 percent, efficiency gains of 25 percent, and lower costs, when compared to the state of the art at the program's inception. O.C.

N83-10991*# Mechanical Technology, Inc., Latham, N. Y.
AUTOMOTIVE STIRLING ENGINE MOD 1 DESIGN REVIEW, VOLUME 2 Final Report
Aug. 1982 573 p
(Contract DEN3-32; DE-AI01-77CS-51040)
(NASA-CR-167936; DOE/NASA/0032-17-VOL-2; NAS 1.26:167936; REPT-80ASE142DR1-VOL-2) Avail: NTIS HC A04/MF A01 CSCL 13F

The auxiliaries and the control system for the ASE MOD I: (1) provide the required fuel and air flows for a well controlled combustion process, generating heat to the Stirling cycle; (2) provide a driver acceptable method for controlling the power output of the engine; (3) provide adequate lubrication and cooling water circulation; (4) generate the electric energy required for engine and vehicle operation; (5) provide a driver acceptable method for starting, stopping and monitoring the engine; and (6) provide a guard system, that protects the engine at component or system malfunction. The control principles and the way the different components and sub-systems interact are described as well as the different auxiliaries, the air fuel system, the power control systems and the electronics. The arrangement and location of auxiliaries and other major components are also examined.
A.R.H.

N83-13038*# Garrett Turbine Engine Co., Phoenix, Ariz.
ADVANCED GAS TURBINE (AGT) POWERTRAIN SYSTEM DEVELOPMENT FOR AUTOMOTIVE APPLICATIONS Semiannual Progress Report, Jul. - Dec. 1980
Jul. 1981 151 p refs
(Contract DEN3-167)
(NASA-CR-165329; DOE/NASA/0167-81/2; NAS 1.26:165329; GTEC-31-3725(2); SAPR-2) Avail: NTIS HC A08/MF A01 CSCL 13F

An automotive gas turbine powertrain system which, when installed in a 1985 production vehicle (3000 pounds inertia weight), is being developed with a CFDC fuel economy of 42.8 miles per gallon based on Environmental Protection Agency (EPA) test procedures and diesel No. 2 fuel. The AGT-powered vehicle shall give substantially the same overall vehicle driveability and performance as a comparable 1985 production vehicle powered by a conventional spark ignition powertrain system (baseline system). Gaseous emissions and particulate levels less than: NOx = 0.4 gm/mile, HC = 0.41 gm/mile, and CO = 3.4 gm/mile, and a total particulate of 0.2 gm/mile, using the same fuel as used for fuel economy measurements is expected, along with the ability to use a variety of alternate fuels. S.L.

N83-15176*# Mechanical Technology, Inc., Latham, N. Y. Stirling Engine Systems Div.
AUTOMOTIVE STIRLING ENGINE DEVELOPMENT PROGRAM Semiannual Technical Progress Report, 1 Jul. - 31 Dec. 1981
W. ERNST, S. PILLER, A. RICHEY, M. SIMETKOSKY, and M. ANTONELLI, ed. Sep. 1982 84 p refs
(Contract DEN3-32; EC-77-A-31-10040)
(NASA-CR-167907; NAS 1.26:167907; DOE/NASA-0032-15; REPT-82ASE248SA1) Avail: NTIS HC A05/MF A01 CSCL 13F

Activities performed on Mod I engine testing and test results, progress in manufacturing, assembling and testing of a Mod I engine in the United States, P40 Stirling engine dynamometer and multifuels testing, analog/digital controls system testing, Stirling reference engine manufacturing and reduced size studies, components and subsystems, and computer code development are summarized. Author

N83-15177*# Mechanical Technology, Inc., Latham, N. Y. Stirling Engine Systems Div.
AUTOMOTIVE STIRLING ENGINE DEVELOPMENT PROGRAM Semiannual Technical Progress Report, 1 Jan. - 30 Jun. 1982
N. NIGHTINGALE, W. ERNST, A. RICHEY, M. SIMETKOSKY, and M. ANTONELLI, ed. ' Oct. 1982 65 p refs
(Contract DEN3-32; EC-77-A-31-10040)
(NASA-CR-168060; NAS 1.26:168060; DOE/NASA-0032-15; REPT-82ASE278SA2) Avail: NTIS HC A04/MF A01 CSCL 13F

Activities performed on Mod I engine testing and test results; the manufacture, assembly, and test of a Mod I engine in the United States; design initiation of the Mod I-A engine system; transient performance testing; Stirling reference engine manufacturing and reduced size studies; components and subsystems; and the study and test of low cost alloys are summarized. Author

N83-16257*# Gould, Inc., Rolling Meadows, Ill.
IMPROVED SCR AC MOTOR CONTROLLER FOR BATTERY POWERED URBAN ELECTRIC VEHICLES Final Report
T. S. LATOS Dec. 1982 319 p refs
(Contract DEN3-60; DE-AI01-77CS-51044)
(NASA-CR-167919; DOE/NASA/0060-82/1; NAS 1.26:167919; REPT-815-008) Avail: NTIS HC A14/MF A01 CSCL 13F

An improved ac motor controller, which when coupled to a standard ac induction motor and a dc propulsion battery would provide a complete electric vehicle power train with the exception of the mechanical transmission and drive wheels was designed. In such a system, the motor controller converts the dc electrical power available at the battery terminals to ac electrical power for the induction motor in response to the drivers commands. The performance requirements of a hypothetical electric vehicle with an upper weight bound of 1590 kg (3500 lb) were used to determine the power rating of the controller. Vehicle acceleration capability, top speed, and gradeability requisites were contained in the Society of Automotive Engineers (SAE) Schedule 227a(d) driving cycle. The important capabilities contained in this driving cycle are a vehicle acceleration requirement of 0 to 72.4 kmph (0 to 45 mph) in 28 seconds a top speed of 88.5 kmph (55 mph), and the ability to negotiate a 10% grade at 48 kmph (30 mph). A 10% grade is defined as one foot of vertical rise per 10 feet of horizontal distance. S.L.

N83-17423*# National Aeronautics and Space Administration. Lewis Research Center, Cleveland, Ohio.
COMPUTER PROGRAM FOR STIRLING ENGINE PERFORMANCE CALCULATIONS Final Report
R. C. TEW, JR. Jan. 1983 100 p refs
(Contract DE-AI01-77CS-51040)
(NASA-TM-82960; DOE/NASA/51040-42; E-1377; NAS 1.15:82960) Avail: NTIS HC A05/MF A01 CSCL 10B

The thermodynamic characteristics of the Stirling engine were analyzed and modeled on a computer to support its development as a possible alternative to the automobile spark ignition engine. The computer model is documented. The documentation includes a user's manual, symbols list, a test case, comparison of model predictions with test results, and a description of the analytical equations used in the model. S.L.

N83-17424*# Garrett Turbine Engine Co., Phoenix, Ariz. Engineering Staff.
ADVANCED GAS TURBINE (AGT) POWERTRAIN SYSTEM DEVELOPMENT FOR AUTOMOTIVE APPLICATIONS Semiannual Progress Report, Jul. - Dec. 1981
Jul. 1982 79 p refs Sponsored in part by DOE
(Contract DEN3-167)
(NASA-CR-167983; DOE/NASA/0167-82/4; NAS 1.26:167983; GARRETT-31-3725(4); SAPR-4) Avail: NTIS HC A05/MF A01 CSCL 13F

A gas turbine powertrain for automobiles with reduced fuel consumption and reduced environmental impact is investigated. The automotive gas turbine, when installed in an automobile (3000 pounds inertia weight), provides a CFDC fuel economy of 42.8 miles per gallon based on EPA test procedures and diesel No. 2 fuel. The AGT powered vehicle substantially gives the same overall vehicle driveability and performance as a comparable production vehicle powered by a conventional spark ignition powertrain system. The emissions are less than federal standards, and a variety of fuels can be used. S.L.

N83-19651*# National Aeronautics and Space Administration. Lewis Research Center, Cleveland, Ohio.
IMPLEMENTATION OF R & QA PRACTICES IN RESEARCH AND DEVELOPMENT PROGRAMS
H. BANKAITIS 14 Mar. 1983 18 p refs Proposed for presentation at 37th Ann. Quality Congr., Boston, 24-26 May, 1983; sponsored by Am. Soc. for Quality Control
(Contract DE-AI01-77CS-51040)
(NASA-TM-82997; DOE/NASA/51040-42; E-1430; NAS 1.15:82997) Avail: NTIS HC A02/MF A01 CSCL 05A

DOE has established a number of broad programs aimed at reducing fuel consumption. Several programs address the R&D of ground transportation propulsion alternatives to the conventional spark-ignition engine. NASA Lewis is responsible for managing the effort between the Government and industry teams involving American and foreign companies. Thus, existing NASA SR&QA procedure were modified/adapted to these R&D programs and implemented to assure that the test hardware design intent was met, the hardware was not hazardous to personnel, it would demonstrate reliable operation, and it would help establish the future R&D quality assurance and maintainability requirements. This successful low-cost approach might be applicable to other similar projects. Author

N83-20829*# Detroit Diesel Allison, Indianapolis, Ind.
SUPPORT AND POWER PLANT DOCUMENTATION FOR THE GAS TURBINE POWERED BUS DEMONSTRATION PROGRAM Final Report, Jan. 1980 - Sep. 1981
D. N. NIGRO, R. G. STEWART, and S. A. APPLE Mar. 1982 194 p refs
(Contract DEN3-187; EC-77-A-31-1044)
(NASA-CR-165527; DOE/NASA/0187-82/1; NAS 1.26:165527; DDA-EDR-10885) Avail: NTIS HC A09/MF A01 CSCL 13F

The operational experience obtained for the GT404-4 gas turbine engines in the intercity and intracity Bus Demonstration Programs is described for the period January 1980 through September 1981. Support for the engines and automatic transmissions involved in this program provided engineering and field service, spare parts and tools, training, and factory overhauls. the Greyhound (intercity) coaches accumulated 183,054 mi (294,595 km) and 5154 hr of total operation. The Baltimore Transit (intracity) coaches accumulated 40,567 mi (65,285 km) and 1840 hr of total operation. In service, the turbine powered Greyhound and Transit coaches achieved approximately 25% and 40% lower fuel mileage, respectively, than did the production diesel powered coaches. The gas turbine engine will require the advanced ceramic development currently being sponsored by the DOE and NASA to achieve fuel economy equivalent not only to that of today's diesel engines but also to the projected fuel economy of the advanced diesel engines of the 1990s. Sufficient experience was not achieved with the coaches prior to the start of service to identify and eliminate many of the problems associated with the startup of new equipment. Because of these problems, the mean miles between incident were unacceptably low. The future gas turbine system should be developed sufficiently to establish satisfactory durability prior to evaluation in revenue service. Commercialization of the gas turbine bus engine remains a viable goal for the future. Author

N83-22029*# Little (Arthur D.), Inc., Cambridge, Mass.
STIRLING ENGINE APPLICATION STUDY Final Report
W. P. TEAGAN and D. CUNNINGHAM Mar. 1983 261 p refs
(Contract DEN3-254; DE-AI01-77CS-51040)
(NASA-CR-168087; DOE/NASA/0254-1; NAS 1.26:168087)
Avail: NTIS HC A12/MF A01 CSCL 10B

A range of potential applications for Stirling engines in the power range from 0.5 to 5000 hp is surveyed. Over one hundred such engine applications are grouped into a small number of classes (10), with the application in each class having a high degree of commonality in technical performance and cost requirements. A review of conventional engines (usually spark ignition or Diesel) was then undertaken to determine the degree to which commercial engine practice now serves the needs of the application classes and to detemine the nature of the competition faced by a new engine system. In each application class the Stirling engine was compared to the conventional engines, assuming that objectives of ongoing Stirling engine development programs are met. This ranking process indicated that Stirling engines showed potential for use in all application classes except very light duty applications (lawn mowers, etc.). However, this potential is contingent on demonstrating much greater operating life and reliability than has been demonstrated to date by developmental Stirling engine systems. This implies that future program initiatives in developing Stirling engine systems should give more emphasis to life and reliability issues than has been the case in ongoing programs. Author

N83-24431*# National Aeronautics and Space Administration. Lewis Research Center, Cleveland, Ohio.
CHARACTERIZATION OF A HIGH-PRESSURE DIESEL FUEL INJECTION SYSTEM AS A CONTROL TECHNOLOGY OPTION TO IMPROVE ENGINE PERFORMANCE AND REDUCE EXHAUST EMISSIONS Final Report
J. J. MCFADDEN, R. A. DEZELICK, and R. R. BARROWS Mar. 1983 37 p refs
(Contract DE-AI01-80CS-50194)
(NASA-TM-83329; NAS 1.15:83329; DOE/NASA/50194-37)
Avail: NTIS HC A03/MF A01 CSCL 13F

Test results from a high pressure electronically controlled fuel injection system are compared with a commercial mechanical injection system on a single cylinder, diesel test engine using an inlet boost pressure of 2.6:1. The electronic fuel injection system achieved high pressure by means of a fluid intensifier with peak injection pressures of 47 to 69 MPa. Reduced exhaust emissions were demonstrated with an increasing rate of injection followed by a fast cutoff of injection. The reduction in emissions is more responsive to the rate of injection and injection timing than to high peak injection pressure. Author

N83-24432*# South Coast Technology, Inc., Ann Arbor, Mich.
ADVANCED HYBRID VEHICLE PROPULSION SYSTEM STUDY Final Report
R. SCHWARZ May 1982 330 p refs
(Contract DEN3-93; DE-AI01-77CS-51044)
(NASA-CR-159773; NAS 1.26:159773; DOE/NASA/0093-1)
Avail: NTIS HC A15/MF A01 CSCL 13F

Results are presented of a study of an advanced heat engine/electric automotive hybrid propulsion system. The system uses a rotary stratified charge engine and ac motor/controller in a parallel hybrid configuration. The three tasks of the study were (1) parametric studies involving five different vehicle types, (2) design trade-off studies to determine the influence of various vehicle and propulsion system paramaters on system performance fuel economy and cost, and (3) a conceptual design establishing feasibility at the selected approach. Energy consumption for the selected system was .034 1/km (61.3 mpg) for the heat engine and .221 kWh/km (.356 kWh/mi) for the electric power system over a modified J227 a schedule D driving cycle. Life cycle costs were 7.13 cents/km (11.5 cents/mi) at $2/gal gasoline and 7 cents/kWh electricity for 160,000 km (100,000 mi) life. Author

N83-25625*# National Aeronautics and Space Administration. Lewis Research Center, Cleveland, Ohio.
FREE-PISTON STIRLING HYDRAULIC ENGINE AND DRIVE SYSTEM FOR AUTOMOBILES
D. G. BEREMAND, J. G. SLABY, R. C. NUSSLE, and D. MIAO Nov. 1982 28 p refs Presented at Automotive Technol. Develop. Contractor Coordination Meeting, Dearborn, Mich., 25-28 Oct. 1982
(NASA-TM-82992; E-1421; NAS 1.15:82992) Avail: NTIS HC A03/MF A01 CSCL 13F

The calculated fuel economy for an automotive free piston Stirling hydraulic engine and drive system using a pneumatic accumulator with the fuel economy of both a conventional 1980 spark ignition engine in an X body class vehicle and the estimated fuel economy of a 1984 spark ignition vehicle system are compared. The results show that the free piston Stirling hydraulic system with a two speed transmission has a combined fuel economy nearly twice that of the 1980 spark ignition engine - 21.5 versus 10.9 km/liter (50.7 versus 25.6 mpg) under comparable conditions. The fuel economy improvement over the 1984 spark ignition engine was 81 percent. The fuel economy sensitivity of the Stirling hydraulic system to system weight, number of transmission shifts, accumulator pressure ratio and maximum pressure, auxiliary power requirements, braking energy recovery, and varying vehicle performance requirements are considered. An important finding is that a multispeed transmission is not required. The penalty for a single speed versus a two speed transmission is about a 12 percent drop in combined fuel economy to 19.0 km/liter (44.7 mpg). This is still a 60 percent improvement in combined fuel economy over the projected 1984 spark ignition vehicle. S.L.

N83-26757*# United Technologies Corp., East Hartford, Conn.
USER'S MANUAL FOR AXISYMMETRIC DIFFUSER DUCT (ADD) CODE. VOLUME 1: GENERAL ADD CODE DESCRIPTION Final Report
O. L. ANDERSON, G. B. HANKINS, JR., and D. E. EDWARDS Feb. 1982 90 p 3 Vol.
(Contract DEN3-235; DE-AI01-77CS-51040)
(NASA-CR-165598-VOL-1; DOE/NASA/0235-2-VOL-1; NAS 1.26:165598-VOL-1; UTRC81-65-VOL-1) Avail: NTIS HC A05/MF A01 CSCL 09B

This User's Manual contains a complete description of the computer codes known as the AXISYMMETRIC DIFFUSER DUCT code or ADD code. It includes a list of references which describe the formulation of the ADD code and comparisons of calculation with experimental flows. The input/output and general use of the code is described in the first volume. The second volume contains a detailed description of the code including the global structure of the code, list of FORTRAN variables, and descriptions of the subroutines. The third volume contains a detailed description of the CODUCT code which generates coordinate systems for arbitrary axisymmetric ducts. DOE

N83-26758*# United Technologies Corp., East Hartford, Conn.
USER'S MANUAL FOR AXISYMMETRIC DIFFUSER DUCT (ADD) CODE. VOLUME 2: DETAILED ADD CODE DESCRIPTION Final Report
O. L. ANDERSON, G. B. HANKINS, JR., and D. E. EDWARDS Feb. 1982 271 p refs 3 Vol.
(Contract DEN3-235; DE-AI01-77CS-51040)
(NASA-CR-165598-VOL-2; DOE/NASA/0235-2-VOL-2; NAS 1.26:165598-VOL-2; UTRC81-65-VOL-2) Avail: NTIS HC A12/MF A01 CSCL 09B

The global structure of the code, list of FORTRAN variables, and descriptions of the subroutines for the axisymmetric diffuse duct program are presented. A.R.H.

N83-26759*# United Technologies Corp., East Hartford, Conn.
USER'S MANUAL FOR AXISYMMETRIC DIFFUSER DUCT (ADD) CODE. VOLUME 3: ADD CODE COORDINATE GENERATOR Final Report
O. L. ANDERSON, G. B. HANKINS, JR., and D. E. EDWARDS Feb. 1982 90 p refs 3 Vol.
(Contract DEN3-235; DE-AI01-77CS-51040)
(NASA-CR-165598-VOL-3; DOE/NASA/0235-2-VOL-3; NAS 1.26:165598-VOL-3; UTRC81-65-VOL-3) Avail: NTIS HC A05/MF A01 CSCL 09B

This User's Manual contains a complete description of the computer codes known as the Axisymmetric Diffuser Duct (ADD) code. It includes a list of references which describe the formulation of the ADD code and comparisons of calculation with experimental flows. The input/output and general use of the code is described in the first volume. The second volume contains a detailed description of the code including the global structure of the code, list of FORTRAN variables, and descriptions of the subroutines. The third volume contains a detailed description of the CODUCT code which generates coordinate systems for arbitrary axisymmetric ducts. Author

N83-26762*# Mechanical Technology, Inc., Latham, N. Y.
AUTOMOTIVE STIRLING ENGINE DEVELOPMENT PROGRAM Quarterly Technical Report, 4 Oct. - 31 Dec. 1981
T. A. DERIKART, ed. Sep. 1981 88 p refs
(Contract DEN3-32; EC-77-A-31-10040)
(NASA-CR-165263; DOE/NASA/0032-81/11; NAS 1.26:165263; MTI-81ASE185QT11) Avail: NTIS HC A05/MF A01 CSCL 13F

The automotive Stirling engine development program is reviewed. Reference engine, component and subsystem development, engine testing, and computer models are summarized. Author

N83-26763*# Garrett Turbine Engine Co., Phoenix, Ariz.
ADVANCED GAS TURBINE (AGT) POWERTRAIN SYSTEM DEVELOPMENT FOR AUTOMOTIVE APPLICATIONS Semiannual Progress Report, Jan. - Jun. 1982
Dec. 1982 76 p refs
(Contract DEN3-167)
(NASA-CR-168104; NAS 1.26:168104; GTEC-31-3725(5); SAPR-5) Avail: NTIS HC A05/MF A01 CSCL 13F

Topics covered include the AGT 101 engine test; compressor design modification; cold air turbine testing; Mod 1 alloy turbine rotor fabrication; combustion aspects; regenerator development; and thermal screening tests for ceramic materials. The foil gas bearings, rotor dynamics, and AGT controls and accessories are also considered. A.R.H.

N83-27924*# National Aeronautics and Space Administration. Lewis Research Center, Cleveland, Ohio.
DOE/NASA AUTOMOTIVE STIRLING ENGINE PROJECT OVERVIEW '83
D. G. BEREMAND 1982 17 p refs Presented at the 18th Intersoc. Energy Conversion Eng. Conf., Orlando, Fla., 21-26 Aug. 1983
(Contract DE-AI01-77CS-51040)
(NASA-TM-83405; E-1683; NAS 1.15:83405; DOE/NASA/51040-48) Avail: NTIS HC A02/MF A01 CSCL 13F

An overview of the DOE/NASA Automotive Stirling Engine Project is presented. The background and objectives of the project are reviewed. Project activities are described and technical progress and status are presented and assessed. Prospects for achieving the objective 30% fuel economy improvement are considered good. The key remaining technology issues are primarily related to life, reliability and cost, such as piston rod seals, and low cost heat exchanges. Author

N83-27925*# Mechanical Technology, Inc., Latham, N. Y. Stirling Engine Systems Div.
AUTOMOTIVE STIRLING ENGINE DEVELOPMENT PROGRAM Semiannual Technical Progress Report, 1 Jul. - 31 Dec. 1982
N. NIGHTINGALE, W. ERNST, A. RICHEY, M. SIMETKOSKY, G. SMITH, and M. ANTONELLI, ed. Jan. 1983 61 p
(Contract DEN3-32; EC-77-A-31-10040)
(NASA-CR-168074; NAS 1.26:168074; REPT-83-ASE-308-SA-3; SATR-3) Avail: NTIS HC A04/MF A01 CSCL 13F

Mod I engine testing and test results, the test of a Mod I engine in the United States, Mod I engine characterization and analysis, Mod I Transient Test Bed fuel economy, Mod I-A engine performance are discussed. Stirling engine reference engine manufacturing and reduced size studies, components and subsystems, and the study and test of low-cost casting alloys are also covered. The overall program philosophy is outlined, and data and results are presented. J.M.S.

N83-27926*# Booz-Allen and Hamilton, Inc., Bethesda, Md. Transportation Consulting Div.
DEMONSTRATION AND EVALUATION OF GAS TURBINE TRANSIT BUSES Final Report, Jan. 1978 - Jun. 1981
Jun. 1983 78 p
(Contract DEN3-142; EC-77-A-31-1044)
(NASA-CR-165528; DOE/NASA/0142-83/1; NAS 1.26:165528; GT-83-001) Avail: NTIS HC A05/MF A01 CSCL 13F

The Gas Turbine Transit Bus Demonstration Program was designed to demonstrate and evaluate the operation of gas turbine engines in transit coaches in revenue service compared with diesel powered coaches. The main objective of the program was to accelerate development and commercialization of automotive gas turbines. The benefits from the installation of this engine in a transit coach were expected to be reduced weight, cleaner exhaust emissions, lower noise levels, reduced engine vibration and maintenance requirements, improved reliability and vehicle performance, greater engine braking capability, and superior cold weather starting. Four RTS-II advanced design transit coaches were converted to gas turbine power using engines and transmissions. Development, acceptance, performance and systems tests were performed on the coaches prior to the revenue service demonstration. Author

N83-30328*# Martini Engineering, Richland, Wash.
STIRLING ENGINE DESIGN MANUAL, 2ND EDITION
W. R. MARTINI Jan. 1983 412 p refs
(Contract NSG-3194; DE-AI01-77CS-51040)
(NASA-CR-168088; DOE/NASA/3194-1; NAS 1.26:168088)
Avail: NTIS HC A18/MF A01 CSCL 13F

This manual is intended to serve as an introduction to Stirling cycle heat engines, as a key to the available literature on Stirling engines and to identify nonproprietary Stirling engine design methodologies. Two different fully described Stirling engines are discussed. Engine design methods are categorized as first order, second order, and third order with increased order number indicating increased complexity. FORTRAN programs are listed for both an isothermal second order design program and an adiabatic second order design program. Third order methods are explained and enumerated. In this second edition of the manual the references are updated. A revised personal and corporate author index is given and an expanded directory lists over 80 individuals and companies active in Stirling engines. Author

N83-32687*# AiResearch Mfg. Co., Torrance, Calif.
ADVANCED SINGLE PERMANENT MAGNET AXIPOLAR IRONLESS STATOR AC MOTOR FOR ELECTRIC PASSENGER VEHICLES Final Report
E. D. BEAUCHAMP, J. R. HADFIELD, and K. L. WUERTZ 8 Aug. 1983 226 p refs
(Contract DEN3-77; DE-AI01-77CS-51044)
(NASA-CR-167974; DOE/NASA/0077-81/1; NAS 1.26:167974; AIRESEARCH-82-19211) Avail: NTIS HC A11/MF A01 CSCL 13F

A program was conducted to design and develop an advanced-concept motor specifically created for propulsion of electric vehicles with increased range, reduced energy consumption, and reduced life-cycle costs in comparison with conventional systems. The motor developed is a brushless, dc, rare-earth cobalt, permanent magnet, axial air gap inductor machine that uses an ironless stator. Air cooling is inherent provided by the centrifugal-fan action of the rotor poles. An extensive design phase was conducted, which included analysis of the system performance versus the SAE J227a(D) driving cycle. A proof-of-principle model was developed and tested, and a functional model was developed and tested. Full generator-level testing was conducted on the functional model, recording electromagnetic, thermal, aerodynamic, and acoustic noise data. The machine demonstrated 20.3 kW output at 1466 rad/s and 160 dc. The novel ironless stator demonstated the capability to continuously operate at peak current. The projected system performance based on the use of a transistor inverter is 23.6 kW output power at 1466 rad/s and 83.3 percent efficiency. Design areas of concern regarding electric vehicle applications include the inherently high windage loss and rotor inertia. Author

N83-33800*# Garrett Turbine Engine Co., Phoenix, Ariz.
ADVANCED GAS TURBINE (AGT) POWERTRAIN SYSTEM DEVELOPMENT FOR AUTOMOTIVE APPLICATIONS Semiannual Progress Report, Jan. - Jun. 1981
Dec. 1981 87 p refs Prepared for DOE, Washington, D.C.
(Contract DEN3-167)
(NASA-CR-167901; DOE/NASA/0167-81/3; NAS 1.26::167901; GARRETT-31-3725(3); SAPR-3) Avail: NTIS HC A05/MF A01 CSCL 13F

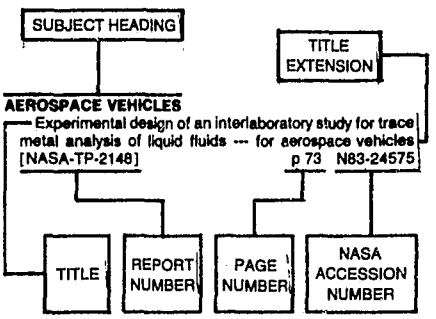
Compressor development, turbine, combustion, regenerator system, gearbox/transmission, ceramic material and component development, foil gas bearings, bearings and seals, rotor dynamics development, and controls and accessories are discussed. Author

N83-37028*# General Motors Corp., Indianapolis, Ind.
CERAMIC APPLICATIONS IN TURBINE ENGINES Progress Report, 1 Jul. - 31 Dec. 1980
J. A. BYRD, M. A. JANOVICZ, and S. R. THRASHER Sep. 1981 165 p
(Contract DEN3-17)
(NASA-CR-165494; DOE/NASA/0017-3; NAS 1.26:165494; DDA-EDR-10672) Avail: NTIS HC A08/MF A01 CSCL 21E

Development testing activities on the 1900 F-configuration ceramic parts were completed, 2070 F-configuration ceramic component rig and engine testing was initiated, and the conceptual design for the 2265 F-configuration engine was identified. Fabrication of the 2070 F-configuration ceramic parts continued, along with burner rig development testing of the 2070 F-configuration metal combustor in preparation for 1132 C (2070 F) qualification test conditions. Shakedown testing of the hot engine simulator (HES) rig was also completed in preparation for testing

of a spin rig-qualified ceramic-bladed rotor assembly at 1132 C (2070 F) test conditions. Concurrently, ceramics from new sources and alternate materials continued to be evaluated, and fabrication of 2070 F-configuration ceramic component from these new sources continued. Cold spin testing of the criatical 2070 F-configuration blade continued in the spin test rig to qualify a set of ceramic blades at 117% engine speed for the gasifier turbine rotor. Rig testing of the ceramic-bladed gasifier turbine rotor assembly at 108% engine speed was also performed, which resulted in the failure of one blade. The new three-piece hot seal with the nickel oxide/calcium fluoride wearface composition was qualified in the regenerator rig and introduced to engine operation wiwth marginal success. N.W.

Typical Subject Index Listing



The subject heading is a key to the subject content of the document. The title is used to provide a description of the subject matter. When the title is insufficiently descriptive of the document content, the title extension is added, separated from the title by three hyphens. The (NASA or AIAA) accession number and the page number are included in each entry to assist the user in locating the abstract in the abstract section. If applicable, a report number is also included as an aid in identifying the document. Under any one subject heading, the accession numbers are arranged in sequence with the AIAA accession numbers appearing first.

A

ABRASION
Materials for advanced turbine engines. Volume 1: Advanced blade tip seal system
[NASA-CR-167851-VOL-1] p 31 N83-15308

ABSORBERS (MATERIALS)
Propagation of sound in highly porous open-cell elastic foams p 195 A83-28848

ABSORPTIVITY
High-intensity sound in air saturated fibrous bulk porous materials
[NASA-CR-167979] p 197 N83-12967

AC GENERATORS
Improved SCR ac motor controller for battery powered urban electric vehicles
[NASA-CR-167919] p 209 N83-16257

ACCEPTOR MATERIALS
Residual double acceptors in bulk GaAs p 205 A83-19989

ACCUMULATORS
Multi-stage Depressed Collectors (MDC) for efficiency improvements of UHF broadcast klystrons
[NASA-TM-82970] p 105 N83-10322
Experimental verification of the multistage depressed collector design procedure for a high-perveance, helix-type, traveling-wave tube --- in communications satellites
[NASA-TP-2162] p 116 N83-25985

ACCURACY
Strainrange partitioning: A total strain range version
[NASA-TM-83023] p 81 N83-14246
Requirements for a mobile communications satellite system. Volume 3: Large space structures measurements study
[NASA-CR-166105] p 45 N83-22255

ACEE PROGRAM
Scale model performance test investigation of mixed flow exhaust systems for an energy efficient engine /E3/ propulsion system
[AIAA PAPER 83-0541] p 20 A83-16776

ACETYLENE
Soot formation in pyrolysis of acetylene, allene and 1,3-butadiene p 69 A83-39274

ACOUSTIC ATTENUATION
Effect of flow on the acoustic performance of extended reaction lined ducts
[AIAA PAPER 83-0778] p 195 A83-28024
Propagation of sound in highly porous open-cell elastic foams p 195 A83-28848
Sound diffraction at wall impedance discontinuities in a circular cylinder - Investigated using Wiener-Hopf technique
[AIAA PAPER 83-0730] p 195 A83-33485
Sound diffraction at wall impedance discontinuities in a circular cylinder, investigated using Wiener-Hopf technique
[NASA-TM-83365] p 201 N83-23117
Ultrasonic attenuation of a void-containing medium for very long wavelengths
[NASA-CR-3693] p 154 N83-28466

ACOUSTIC DUCTS
Acoustics in variable area duct - Finite element and finite difference comparisons to experiment p 193 A83-19809
Sound radiation from annular ducts/nozzles using modal decomposition of in-duct acoustic power
[AIAA PAPER 83-0714] p 194 A83-25929
Effect of flow on the acoustic performance of extended reaction lined ducts
[AIAA PAPER 83-0778] p 195 A83-28024
Turbofan noise generation. Volume 1: Analysis
[NASA-CR-167951] p 198 N83-15041
Refinement and application of acoustic impulse technique to study nozzle transmission characteristics
[NASA-CR-3656] p 199 N83-20708

ACOUSTIC EMISSION
Generation of desired signals from acoustic drivers --- for aircraft engine internal noise propagation experiment p 19 A83-15068
Acousto-ultrasonic characterization of fiber reinforced composites p 63 N83-11231
Fundamental aspects in quantitative ultrasonic determination of fracture toughness: The scattering of a single ellipsoidal inhomogeneity
[NASA-CR-3625] p 153 N83-11507
Effects of specimen resonances on acoustic-ultrasonic testing
[NASA-CR-3679] p 153 N83-21373

ACOUSTIC EXCITATION
Noise and flow structure of a tone-excited jet p 192 A83-13136
Tone generation by rotor-downstream strut interaction
[AIAA PAPER 83-0767] p 21 A83-25957
The velocity perturbations above the orifice of an acoustically excited cavity in grazing flow p 195 A83-29235
Excited waves in shear layers
[DFVLR-FB-82-23] p 106 N83-21218

ACOUSTIC IMPEDANCE
Surface acoustic admittance of highly porous open-cell, elastic foams p 195 A83-28849
The velocity perturbations above the orifice of an acoustically excited cavity in grazing flow p 195 A83-29235
Sound diffraction at wall impedance discontinuities in a circular cylinder - Investigated using Wiener-Hopf technique
[AIAA PAPER 83-0730] p 195 A83-33485
Utilizing numerical techniques in turbofan inlet acoustic suppressor design
[NASA-TM-82994] p 196 N83-10885
High-intensity sound in air saturated fibrous bulk porous materials
[NASA-CR-167979] p 197 N83-12967
Sound diffraction at wall impedance discontinuities in a circular cylinder, investigated using Wiener-Hopf technique
[NASA-TM-83365] p 201 N83-23117

ACOUSTIC INSTABILITY
Excited waves in shear layers
[DFVLR-FB-82-23] p 106 N83-21218

ACOUSTIC MEASUREMENT
Wind tunnel measurements of blade/vane ratio and spacing effects on fan noise p 192 A83-15317
Sound radiation from annular ducts/nozzles using modal decomposition of in-duct acoustic power
[AIAA PAPER 83-0714] p 194 A83-25929
Phenomenological and mechanics aspects of nondestructive evaluation and characterization by sound and ultrasound of material and fracture properties
[NASA-CR-3623] p 153 N83-11506
Investigation of continuously traversing microphone system for mode measurement
[NASA-CR-168040] p 199 N83-19575
Experimental study of the thermal-acoustic efficiency in a long turbulent diffusion-flame burner
[NASA-CR-170003] p 72 N83-19824
Refinement and application of acoustic impulse technique to study nozzle transmission characteristics
[NASA-CR-3656] p 199 N83-20708
Experimental study of the thermal-acoustic efficiency in a long turbulent diffusion-flame burner
[NASA-CR-3725] p 202 N83-33683

ACOUSTIC MICROSCOPES
Comparison of NDE techniques for sintered-SiC components p 152 A83-22265
Evaluation of electrode shape and nondestructive evaluation method for welded solar cell interconnects
[NASA-TM-82966] p 166 N83-10555

ACOUSTIC NOZZLES
Sound radiation from annular ducts/nozzles using modal decomposition of in-duct acoustic power
[AIAA PAPER 83-0714] p 194 A83-25929

ACOUSTIC PROPAGATION
Pressure transfer function of a JT15D nozzle due to acoustic and convected entropy fluctuations p 193 A83-16319
Finite difference solutions to shocked acoustic waves
[AIAA PAPER 83-0671] p 193 A83-25907
Transient difference solutions of the inhomogeneous wave equation: Simulation of the Green's function
[NASA-TM-83336] p 200 N83-21897

ACOUSTIC PROPERTIES
Free-jet acoustic investigation of high-radius-ratio coannular plug nozzles. Comprehensive data report, volume 1
[NASA-CR-168086-VOL-1] p 198 N83-18408
A compact inflow control device for simulating flight fan noise
[NASA-TM-83349] p 201 N83-26643

ACOUSTIC RETROFITTING
Optimization of acoustic liners by the hybrid finite element-integral approach
[AIAA PAPER 83-0670] p 194 A83-26917

ACOUSTIC SCATTERING
Ultrasonic attenuation of a void-containing medium for very long wavelengths
[NASA-CR-3693] p 154 N83-28466

ACOUSTIC VELOCITY
Acoustic velocities of two-phase mixtures of cryogenic fluids p 124 A83-43012

ACOUSTICS
Effects of specimen resonances on acoustic-ultrasonic testing
[NASA-CR-3679] p 153 N83-21373

ACOUSTO-OPTICS
Frequency-multiplexed and pipelined iterative optical systolic array processors p 188 A83-18588
Triangular system solutions on an optical systolic processor p 189 A83-36752
LU and Cholesky decomposition on an optical systolic array processor p 189 A83-43629

ACRYLIC RESINS
Ion exchange selectivity for cross-linked polyacrylic acid
[NASA-TM-83427] p 97 N83-35142

ACTIVATION ANALYSIS
O-18 tracer studies of Al2O3 scale formation on NiCrAl alloys p 74 A83-10249
ACTIVATION ENERGY
Dynamic mechanical properties of n-phenylnadimide modified PMR polyimide composites
[NASA-TM-83051] p 65 N83-15363
ACTUATORS
Fiber optics for aircraft engine/inlet control p 20 A83-22494
Fiberoptics technology and its application to propulsion control systems
[NASA-TM-83009] p 18 N83-15302
Sensor failure and multivariable control for airbreathing propulsion systems
[NASA-CR-159791] p 1 N83-16279
ADAPTERS
Stability analysis of Centaur-in-Shuttle composite corrugated adapters
[AIAA 83-1003] p 49 A83-29791
ADDITIVES
PMR-15 polyimide modifications for improved prepreg tack
[NASA-TM-82951] p 64 N83-12175
Evaluation of dopants in hydrogen to reduce hydrogen permeation in candidate Stirling engine heater head tube alloys at 760 deg and 820 deg
[NASA-TM-82920] p 81 N83-13232
Improved high temperature resistant polyimides
[NASA-CASE-LEW-13864-1] p 93 N83-17715
Developments toward an 18% efficient silicon solar cell
[NASA-CR-168141] p 181 N83-25112
The adsorption and thermal decomposition of tricresylphosphate (TCP) on iron and gold
[NASA-TM-83441] p 62 N83-29311
Evaluation of fuel additives for reduction of material imcompatibilities in methanol-gasoline blends
[NASA-CR-168061] p 86 N83-29359
ADHESION
Tribological properties of amorphous alloys and the role of surfaces in abrasive wear of materials
[NASA-TM-82973] p 140 N83-11498
Tribology p 140 N83-12167
ADHESIVE BONDING
Diatomic molecules and metallic adhesion, cohesion, and chemisorption - A single binding-energy relation p 69 A83-30921
Use of high L.E.T. radiation to improve adhesion of metals to polytetrafluoroethylene
[NASA-TM-83413] p 96 N83-30660
Thermal barrier coating system having improved adhesion
[NASA-CASE-LEW-13359-1] p 97 N83-31855
ADIABATIC CONDITIONS
Stirling engine design manual, 2nd edition
[NASA-CR-168088] p 212 N83-30328
ADSORPTION
The adsorption and thermal decomposition of tricresylphosphate (TCP) on iron and gold
[NASA-TM-83441] p 62 N83-29311
AEROACOUSTICS
Tests of a thermal acoustic shield with a supersonic jet p 192 A83-10183
Noise and flow structure of a tone-excited jet p 192 A83-13136
Generation of desired signals from acoustic drivers — for aircraft engine internal noise propagation experiment p 19 A83-15068
An experimental study of supersonic jet shock-associated noise
[AIAA PAPER 83-0708] p 193 A83-25924
Tone generation by rotor-downstream strut interaction
[AIAA PAPER 83-0767] p 21 A83-25957
The influence of inlet design on the aeroacoustic performance of a JT15D turbofan engine as measured in the NASA-Ames 40 x 80 foot wind tunnel
[AIAA PAPER 83-0681] p 21 A83-26006
Incidence angle effects on convected gust airfoil noise
[AIAA PAPER 83-0765] p 195 A83-26022
Noise generation by a finite span swept airfoil
[AIAA PAPER 83-0768] p 195 A83-26023
Effect of flow on the acoustic performance of extended reaction lined ducts
[AIAA PAPER 83-0778] p 195 A83-26024
The velocity perturbations above the orifice of an acoustically excited cavity in grazing flow p 195 A83-29235
Low speed performance of a supersonic axisymmetric mixed compression inlet with auxiliary inlets
[AIAA PAPER 83-1414] p 7 A83-45516
Correlation of core noise obtained by three signal coherence techniques
[NASA-TM-83012] p 197 N83-12966
Excited waves in shear layers
[DFVLR-FB-82-23] p 106 N83-21218
Low speed performance of a supersonic axisymmetric mixed compression inlet with auxiliary inlets — Lewis 9x15-ft anechoic wind tunnel tests
[NASA-TM-83435] p 37 N83-27992
Turbulence spectra in the noise source regions of the flow around complex surfaces
[NASA-TM-83392] p 202 N83-30168
Experimental study of the thermal-acoustic efficiency in a long turbulent diffusion-flame burner
[NASA-CR-3725] p 202 N83-33683
AERODYNAMIC CHARACTERISTICS
Aerodynamic features of turbulent flames
[AIAA PAPER 83-0470] p 119 A83-16737
Comparison of laser anemometer measurements and theory in an annular turbine cascade with experimental accuracy determined by parameter estimation p 4 A83-28833
The aerodynamic design and performance of the General Electric/NASA EEE fan — Energy Efficient Engine
[AIAA PAPER 83-1160] p 23 A83-36252
Application of 3D aerodynamic/combustion model to combustor primary zone study
[AIAA PAPER 83-1265] p 23 A83-36316
Experimental evaluation of inlet turbulence, wall boundary layer, surface finish, and fillet radius on small axial turbine state performance
[SAE PAPER 821475] p 24 A83-38001
Finite volume calculation of three-dimensional potential flow around a propeller p 7 A83-45577
Measurements of heat transfer distribution over the surfaces of highly loaded turbine nozzle guide vanes
[ASME PAPER 83-GT-53] p 8 A83-47910
Cold-air performance of compressor-drive turbine of Department of Energy upgraded automobile gas turbine engine. 2: Stage performance
[NASA-TM-82818] p 9 N83-11063
QCSEE under-the-wing engine-wing-flap aerodynamic profile characteristics
[NASA-TM-82890] p 28 N83-12092
Measured performance of a tip-controlled, teetered rotor with an NACA 64 sub 3-618 tip airfoil
[NASA-TM-82870] p 169 N83-14689
Wind tunnel evaluation of air-foil performance using simulated ice shapes
[NASA-CR-167960] p 11 N83-15265
Aerodynamic stiffness of an unbound eccentric whirling centrifugal impeller with an infinite number of blades p 142 N83-15650
Energy efficient engine: Fan test hardware detailed design report
[NASA-CR-165148] p 31 N83-16341
The JT8D and JT9D engine component improvement: Performance improvement program
[NASA-CR-167965] p 32 N83-17543
Aerodynamic effect of a honeycomb rotor tip shroud on a 50.8-centimeter-tip-diameter core turbine
[NASA-TP-2112] p 32 N83-17547
Fixed pitch rotor performance of large horizontal axis wind turbines p 175 N83-19233
Stall induced instability of a teetered rotor p 175 N83-19234
Free yaw performance of the Mod-0 large horizontal axis 100 kW wind turbine p 175 N83-19235
AERODYNAMIC CONFIGURATIONS
The JT8D and JT9D engine component improvement: Performance improvement program
[NASA-CR-167965] p 32 N83-17543
AERODYNAMIC FORCES
The coupled aeroelastic response of turbomachinery blading to aerodynamic excitations
[AIAA 83-0844] p 156 A83-29822
AERODYNAMIC HEAT TRANSFER
Measurements of heat transfer distribution over the surfaces of highly loaded turbine nozzle guide vanes
[ASME PAPER 83-GT-53] p 8 A83-47910
AERODYNAMIC LOADS
Blade loading and rotation effects on compressor rotor wake near end walls p 3 A83-22138
JT9D performance deterioration results from a simulated aerodynamic load test p 25 A83-41040
Effects of structural coupling on mistuned cascade flutter and response
[NASA-TM-83049] p 159 N83-15672
Nacelle Aerodynamic and Inertial Loads (NAIL) project
[NASA-CR-168712] p 18 N83-30402
AERODYNAMIC NOISE
Tests of a thermal acoustic shield with a supersonic jet p 192 A83-10183
Noise and flow structure of a tone-excited jet p 192 A83-13136
Conventional profile coaxial jet noise prediction p 193 A83-22128
On the shock cell structure and noise of supersonic jets
[AIAA PAPER 83-0703] p 193 A83-25923
Low flight speed acoustic results for a supersonic inlet with auxiliary inlet doors
[AIAA PAPER 83-1415] p 196 A83-45517
Noise of the 10-bladed 60 deg swept SR-5 propeller in a wind tunnel
[NASA-TM-83054] p 200 N83-20112
Low flight speed acoustic results for a supersonic inlet with auxiliary inlet doors
[NASA-TM-83411] p 201 N83-27794
AERODYNAMIC STABILITY
Effects of friction dampers on aerodynamically unstable rotor stages
[AIAA PAPER 83-0848] p 22 A83-32791
Measurements of self-excited rotor-blade vibrations using optical dispacements
[NASA-TM-82953] p 158 N83-14523
Some experiments on Yaw stability of wind turbines with various coning angles
[NASA-CR-168108] p 177 N83-22740
AERODYNAMIC STALLING
Subsonic-transonic stall flutter study
[NASA-CR-165256] p 43 N83-30435
AEROELASTICITY
Friction damping of flutter in gas turbine engine airfoils p 20 A83-24038
The coupled aeroelastic response of turbomachinery blading to aerodynamic excitations
[AIAA 83-0844] p 156 A83-29822
Flutter and forced response of mistuned rotors using standing wave analysis
[AIAA 83-0845] p 156 A83-29823
Measurements of self-excited rotor-blade vibrations using optical dispacements
[NASA-TM-82953] p 159 N83-14523
Effects of structural coupling on mistuned cascade flutter and response
[NASA-TM-83049] p 159 N83-15672
Simplified aeroelastic modeling of horizontal axis wind turbines
[NASA-CR-168109] p 177 N83-21509
AEROSPACE ENGINEERING
COSAM (Conservation Of Strategic Aerospace Materials) program overview
[NASA-TM-83006] p 78 N83-11282
Advantage of resonant power conversion in aerospace applications
[NASA-TM-83399] p 37 N83-27994
AEROSPACE ENVIRONMENTS
The application of free-electron lasers to the transmission of energy in space p 135 A83-31141
On the cause of the flat-spot phenomenon observed in silicon solar cells at low temperatures and low intensities p 170 N83-14705
Design and development of multi-kW power electronic transformers — for long duration space applications
[NASA-CR-168082] p 116 N83-29596
AEROSPACE INDUSTRY
Advantage of resonant power conversion in aerospace applications
[NASA-TM-83399] p 37 N83-27994
Combustion Fundamentals Research
[NASA-CP-2268] p 38 N83-29208
Considerations of technology transfer barriers in the modification of strategic superalloys for aircraft turbine engines
[NASA-TM-83395] p 86 N83-29360
AEROSPACE SYSTEMS
Development of improved hydrogen recombination in sealed nickel-cadmium aerospace cells p 54 A83-27198
AEROSPACE TECHNOLOGY TRANSFER
Considerations of technology transfer barriers in the modification of strategic superalloys for aircraft turbine engines
[NASA-TM-83395] p 86 N83-29360
AEROSPACE VEHICLES
Experimental design of an interlaboratory study for trace metal analysis of liquid fluids — for aerospace vehicles
[NASA-TP-2148] p 73 N83-24575
AEROTHERMODYNAMICS
Axial-compressor flow distortion with water ingestion
[AIAA PAPER 83-0004] p 19 A83-16456
Advanced Gas Turbine (AGT) powertrain system development for automotive applications
[NASA-CR-167983] p 210 N83-17424
Opportunities for research in aerothermodynamics
[NASA-TM-83348] p 35 N83-24506
Aerothermal modeling program, phase 1
[NASA-CR-168202] p 131 N83-30959
AFTERBODIES
Fluid Dynamics Panel Symposium on Aerodynamics of Power Plant Installation
[AGARD-AR-173] p 27 N83-11138

AGRICULTURE
Market assessment of photovoltaic power systems for agricultural applications worldwide
[NASA-CR-165541] p 168 N83-13585
The worldwide market for photovoltaics in the rural sector
[NASA-TM-83035] p 173 N83-15840
Energy and precious fuels requirements of fuel alcohol production. Volume 2, appendices A and B: Ethanol from grain
[NASA-CR-168091] p 183 N83-28582
AIR
The oxidation behavior of a model molybdenum/tungsten-containing alloy in air alone and in air with trace levels of NaCl(g) p 76 A83-42241
AIR BREATHING ENGINES
Status of fiberoptics technology for propulsion control systems
[NASA-TM-82907] p 32 N83-17537
NASA propulsion controls research
[NASA-TM-83343] p 36 N83-25711
AIR COOLING
Heat transfer characteristics for jet array impingement with initial crossflow
[ASME PAPER 83-GT-28] p 7 A83-47891
Comparison of predicted and experimental external heat transfer around a film cooled cylinder in crossflow
[NASA-TM-83017] p 127 N83-13392
Tip cap for a rotor blade
[NASA-CASE-LEW-13654-1] p 30 N83-14129
Air modulation apparatus --- cooling gas turbine engines
[NASA-CASE-LEW-13524-1] p 131 N83-30957
Use of cooling air heat exchangers as replacements for hot section strategic materials
[NASA-TM-83494] p 42 N83-34946
AIR FLOW
Aerodynamic-wave break-up of liquid sheets in swirling airflows and combustor modules
[AIAA PAPER 83-1204] p 124 A83-45511
Experimental program for the evaluation of turbofan/turboshaft c conversion technology
[NASA-TM-82988] p 27 N83-11130
Aerodynamic-wave break-up of liquid sheets in swirling airflows and combustor modules
[NASA-TM-83353] p 130 N83-23545
Preliminary tests of an advanced high-temperature combustion system
[NASA-TP-2203] p 41 N83-33893
AIR INTAKES
Numerical studies of the formation and destruction of vortices in a motored four-stroke piston-cylinder configuration
[AIAA PAPER 83-0497] p 136 A83-16749
Low flight speed acoustic results for a supersonic inlet with auxiliary inlet doors
[AIAA PAPER 83-1415] p 196 A83-45517
Low flight speed acoustic results for a supersonic inlet with auxiliary inlet doors
[NASA-TM-83411] p 201 N83-27794
Control means for a gas turbine engine
[NASA-CASE-LEW-14586-1] p 40 N83-31603
AIR JETS
The structure of particle-laden jets and nonevaporating sprays
[NASA-CR-168059] p 34 N83-20948
Analytical calculation of a single jet in cross-flow and comparison with experiment p 38 N83-29219
AIR LOCKS
JT90 ceramic outer air seal system refinement program, phase 2
[NASA-CR-167962] p 30 N83-15305
AIRBORNE/SPACEBORNE COMPUTERS
Software and system level tests of a test flight mercury ion thruster subsystem
[AIAA PAPER 82-1912] p 51 A83-12485
Flight evaluation of modifications to a digital electronic engine control system in an F-15 airplane
[AIAA PAPER 83-0537] p 20 A83-19593
AIRCRAFT COMPARTMENTS
A preliminary comparison between the SR-6 propeller noise in flight and in a wind tunnel
[NASA-TM-83341] p 201 N83-24287
AIRCRAFT CONFIGURATIONS
Rotorcraft convertible engine study
[NASA-CR-168161] p 37 N83-27996
Energy efficient engine. Core engine bearings, drives and configuration: Detailed design report
[NASA-CR-165376] p 39 N83-30430
AIRCRAFT CONSTRUCTION MATERIALS
Fatigue crack initiation and propagation in several nickel-base superalloys at 650 C p 76 A83-41199
Effects on stress rupture life and tensile strength of tin additions to Inconel 718 p 79 N83-11299
Polymer matrix composites research at NASA Lewis Research Center p 91 N83-12151
PMR polyimide composites for aerospace applications
[NASA-TM-83047] p 65 N83-15364
Research priorities for advanced fibrous composites
[NASA-CR-165414] p 65 N83-18853
Hybridized polymer matrix composites
[NASA-CR-165341] p 66 N83-22326
AIRCRAFT DESIGN
Supersonic STOVL research aircraft
[SAE PAPER 821375] p 17 A83-37965
The development of a generalized advanced propeller analysis system
[AIAA PAPER 83-2466] p 26 A83-49581
Aviation energy and the future of the recreational use of sport and general aviation aircraft
p 100 N83-22444
Improved design of subcritical and supercritical cascades using complex characteristics and boundary layer correction
[NASA-CR-168166] p 12 N83-24474
AIRCRAFT ENGINES
Generation of desired signals from acoustic drivers --- for aircraft engine internal noise propagation experiment
p 19 A83-15068
A method of predicting the performance deterioration of a compressor cascade due to sand erosion
[AIAA PAPER 83-0178] p 19 A83-16572
Advances in high-speed rolling-element bearings --- for aircraft engine and transmission application
p 137 A83-22319
Fiber optics for aircraft engine/inlet control
p 20 A83-22494
Effect of variable guide vanes on the performance of a high-bypass turbofan engine p 20 A83-24028
NASA clean catalytic combustor program
[ASME PAPER 82-JPGC-GT-11] p 68 A83-25269
The influence of inlet design on the aeroacoustic performance of a JT15D turbofan engine as measured in the NASA-Ames 40 x 80 foot wind tunnel
[AIAA PAPER 83-0681] p 21 A83-28006
Effect of humidity on jet engine axial-flow compressor performance p 22 A83-35856
Inlet design for high-speed propfans
[SAE PAPER 821359] p 5 A83-37957
Supersonic STOVL research aircraft
[SAE PAPER 821375] p 17 A83-37965
Blade loss transient dynamic analysis of turbomachinery p 25 A83-40864
JT9D performance deterioration results from a simulated aerodynamic load test p 25 A83-41040
Dynamic distortion in a short s-shaped subsonic diffuser with flow separation --- Lewis 8 by 6 foot Supersonic Wind Tunnel
[AIAA PAPER 83-1412] p 25 A83-45515
Design concepts for low cost composite engine frames
[AIAA PAPER 83-2445] p 25 A83-48331
NASA LeRC/Akron University Graduate Cooperative Fellowship Program and Graduate Student Researchers Program
[NASA-CR-167943] p 208 N83-10970
Analysis, design, fabrication and testing of an optical tip clearance sensor --- turbocompressor blade tips
[NASA-CR-165265] p 26 N83-11127
Fluid Dynamics Panel Symposium on Aerodynamics of Power Plant Installation
[AGARD-AR-173] p 27 N83-11138
Components for digitally controlled aircraft engines
[NASA-CR-165296] p 28 N83-12089
Energy efficient engine. Flight propulsion system preliminary analysis and design
[NASA-CR-159859] p 28 N83-12094
Polymer matrix composites research at NASA Lewis Research Center p 91 N83-12151
Materials for advanced turbine engines. Volume 1: Advanced blade tip seal system
[NASA-CR-167851-VOL-1] p 31 N83-15308
Ignition and combustion: Low compression ratio, high output diesel
[NASA-CR-169742] p 31 N83-15309
Energy efficient engine: Fan test hardware detailed design report
[NASA-CR-165148] p 31 N83-16341
A method to estimate weight and dimensions of small aircraft propulsion gas turbine engines: User's guide
[NASA-CR-168049] p 31 N83-16343
The JT9D Jet Engine Diagnostics Program
[NASA-CR-167966] p 32 N83-17544
Study of advanced rotary combustion engines for commuter aircraft
[NASA-CR-165399] p 32 N83-17545
Bearing fatigue investigation 3
[NASA-CR-168029] p 143 N83-17880
Aircraft turbofan noise
[NASA-TM-83317] p 198 N83-18405
Energy efficient engine sector combustor rig test program
[NASA-CR-167913] p 33 N83-19753
Energy efficient engine component development and integration program
[NASA-CR-170089] p 34 N83-22204
An overview of general aviation propulsion research programs at NASA Lewis Research Center
p 35 N83-22456
General Aviation Turbine Engine (GATE) overview
p 35 N83-22457
Application of 3-signal coherence to core noise transmission
[NASA-TM-83333] p 200 N83-23114
Opportunities for research in aerothermodynamics
[NASA-TM-83348] p 35 N83-24506
Advanced electrical power system technology for the all electric aircraft
[NASA-TM-83390] p 115 N83-24764
Dynamic distortion in a short s-shaped subsonic diffuser with flow separation --- Lewis 8 by 6 foot Supersonic Wind Tunnel
[NASA-TM-83412] p 36 N83-26838
JT90 thermal barrier coated vanes
[NASA-CR-167964] p 37 N83-27993
Multi-fuel rotary engine for general aviation aircraft
[NASA-TM-83429] p 38 N83-29235
Considerations of technology transfer barriers in the modification of strategic superalloys for aircraft turbine engines
[NASA-TM-83395] p 86 N83-29360
Energy efficient engine. Core engine bearings, drives and configuration: Detailed design report
[NASA-CR-165376] p 39 N83-30430
Current and future technology in radial and axial gas turbines
[NASA-TM-83414] p 41 N83-32811
Study of LH2-fueled topping cycle engine for aircraft propulsion
[NASA-TM-83466] p 41 N83-34942
Supersonic fan engines for military aircraft
[NASA-TM-83499] p 42 N83-34947
Multi-fuel rotary engine for general aviation aircraft
[NASA-TM-85428] p 43 N83-36031
AIRCRAFT FUELS
Tests of blending and correlation of distillate fuel properties p 98 A83-11050
Effect of broad properties fuel on injector performance in a reverse flow combustor
[AIAA PAPER 83-0154] p 20 A83-21079
A vortex venturi for reverting antimisting fuel properties
[ASME PAPER 83-GT-137] p 25 A83-47964
Evaluation of methods for rapid determination of freezing point of aviation fuels
[NASA-CR-167981] p 98 N83-10207
Effect of broad properties fuel on injector performance in a reverse flow combustor
[NASA-TM-83013] p 29 N83-13101
Experimental study of the thermal stability of hydrocarbon fuels
[NASA-CR-168027] p 100 N83-17728
High accuracy fuel flowmeter, phase 1
[NASA-CR-167893] p 134 N83-21314
Aviation Gasolines and Future Alternatives
[NASA-CP-2267] p 100 N83-22442
Industry's assessment of the number of airplanes in the general aviation fleet along with their hours flown and fuel consumption data powered by what type of engines, when and for what reasons, through the year 2000
p 101 N83-22445
Fuel supply and distribution. Fixed base operation
p 101 N83-22449
Flight summaries and temperature climatology at airliner cruise altitudes from GASP (Global Atmospheric Sampling Program) data
[NASA-CR-168106] p 188 N83-24048
Research on aviation fuel instability
[NASA-TM-83420] p 101 N83-28255
The NASA High Accuracy Fuel Flowmeter (HAFF) development program
[NASA-CR-83484] p 19 N83-33883
AIRCRAFT HAZARDS
A similarity analysis of the droplet trajectory equation
p 118 A83-13133
NASA Lewis Research Center's program on icing research
[AIAA PAPER 83-0204] p 1 A83-16582
Assessment of crash fire hazard of LH sub 2 fueled aircraft
[NASA-CR-165525] p 16 N83-11095
AIRCRAFT NOISE
Farfield inflight measurements of high-speed turboprop noise
[AIAA PAPER 83-0745] p 21 A83-25947

Application of 3-signal coherence to core noise transmission
[AIAA PAPER 83-0759] p 194 A83-28021
Correlation of core noise obtained by three signal coherence techniques
[NASA-TM-83012] p 197 N83-12966
Aircraft turbofan noise
[NASA-TM-83317] p 198 N83-18405
Farfield inflight measurement of high-speed turboprop noise
[NASA-TM-83327] p 199 N83-21895
A preliminary comparison between the SR-6 propeller noise in flight and in a wind tunnel
[NASA-TM-83341] p 201 N83-24287

AIRCRAFT PARTS
Design of an advanced 500-HP helicopter transmission p 21 A83-24834
Tribology p 140 N83-12167

AIRCRAFT PERFORMANCE
The CF6 engine performance improvement
[NASA-CR-165612] p 31 N83-16342
The JT9D Jet Engine Diagnostics Program
[NASA-CR-167966] p 32 N83-17544
BASIC Data Manipulation And Display System (BDMADS)
[NASA-TM-83328] p 189 N83-19496

AIRCRAFT STRUCTURES
'Scaling' analysis of the ice accretion process on aircraft surfaces
[ASME PAPER 82-WA/HT-39] p 16 A83-25693
Evaluation of low-cost aluminum composites for aircraft engine structural applications
[NASA-TM-83357] p 66 N83-25790

AIRCRAFT TIRES
Temperature distribution in an aircraft tire at low ground speeds
[NASA-TP-2195] p 161 N83-33217

AIRFOIL PROFILES
Influence of multidroplet size distribution on icing collection efficiency
[AIAA PAPER 83-0110] p 187 A83-16526
A viscous-inviscid interactive procedure for rotational flow in cascades of two-dimensional airfoils of arbitrary shape
[AIAA PAPER 83-0256] p 3 A83-16614
The coupled aeroelastic response of turbomachinery blading to aerodynamic excitations
[AIAA 83-0844] p 156 A83-29822

AIRFOILS
An analytical evaluation of the icing properties of several low and medium speed airfoils
[AIAA PAPER 83-0109] p 3 A83-16525
Incidence angle effects on convected gust airfoil noise
[AIAA PAPER 83-0765] p 195 A83-28022
Coordinate generation with precise controls over mesh properties p 190 A83-29631
Numerical simulation of airfoil ice accretion
[AIAA PAPER 83-0112] p 16 A83-36042
Development of controlled diffusion airfoils for multistage compressor application
[ASME PAPER 83-GT-211] p 9 A83-48012
Development and test of a Microwave Ice Accretion Measurement Instrument (MIAMI)
[NASA-CR-3596] p 18 N83-14123
Measured performance of a tip-controlled, teetered rotor with an NACA 64 sub 3-618 tip airfoil
[NASA-TM-82870] p 169 N83-14689
Experimental evaluation of shockless supercritical airfoils in cascade
[NASA-TM-83045] p 11 N83-15268
Environmental solid particle effects on compressor cascade performance
[NASA-CR-168018] p 11 N83-16285
Design and evaluation of low cost blades for large wind driven generating systems p 175 N83-19244
Structural fatigue test results for large wind turbine blade sections p 159 N83-19246
Numerical simulation of an electrothermal deicer pad
[NASA-CR-168097] p 17 N83-23281
Improved design of subcritical and supercritical cascades using complex characteristics and boundary layer correction
[NASA-CR-168166] p 12 N83-24474
Axial compressor middle stage secondary flow study
[NASA-CR-3701] p 14 N83-29174
Small transport aircraft technology propeller study
[NASA-CR-168045] p 14 N83-29178
The effect of incidence angle on the overall three-dimensional aerodynamic performance of a classical annular airfoil cascade
[NASA-CR-168127] p 15 N83-34911

AIRFRAMES
Small transport aircraft technology propeller study
[NASA-CR-168045] p 14 N83-29178

AIRLINE OPERATIONS
Cloud encounter statistics in the 28.5-43.5 KFT altitude region from four years of GASP observations p 186 A83-38733
Airline flight planning: The weather connection p 17 N83-17461

AIRSPEED
Comparison of modern icing cloud instruments
[NASA-CR-168008] p 19 N83-18720

ALCOHOLS
Fumigation of alcohol in a light duty automotive diesel engine
[NASA-CR-167915] p 99 N83-13272

ALDEHYDES
Polyvinyl alcohol cross-linked with two aldehydes
[NASA-CASE-LEW-13504-1] p 71 N83-13188

ALGEBRA
Controller scheduling - A possible algebraic viewpoint p 190 A83-37093
Automatic algebraic coordinate generation p 189 A83-38793

ALGORITHMS
Pseudo-updated constrained solution algorithm for nonlinear heat conduction p 121 A83-32989
Efficient solution of the Euler and Navier-Stokes equations with a vectorized multiple-grid algorithm
[AIAA PAPER 83-1893] p 5 A83-39359
An improved algorithm for evaluating trellis phase codes
[NASA-CR-169354] p 105 N83-16600
Efficient solution of the Euler and Navier-Stokes equations with a vectorized multiple-grid algorithm
[NASA-TM-83376] p 2 N83-24467
Vibration in planetary gear systems with unequal planet stiffnesses
[NASA-TM-83428] p 150 N83-29709
Flux-based acceleration of the Euler equations
[NASA-TM-83453] p 191 N83-30113
Convergence and stability properties of minimal polynomial and reduced rank extrapolation algorithms
[NASA-TM-83443] p 191 N83-31390
Constrained self-adaptive solutions procedures for structure subject to high temperature elastic-plastic creep effects p 162 N83-34370
Stress and fracture analyses under elastic-plastic creep conditions: Some basic developments and computational approaches p 162 N83-34371

ALKALI METALS
Heat pipes containing alkali metal working fluid
[NASA-CASE-LEW-12253-1] p 203 N83-19596

ALKALINE BATTERIES
Cross-linked polyvinyl alcohol films as alkaline battery separators p 68 A83-20576
Alkaline regenerative fuel cell energy storage system for manned orbital satellites p 54 A83-27206
Polyvinyl alcohol membranes as alkaline battery separators
[NASA-TM-82961] p 70 N83-10135
Pore size engineering applied to the design of separators for nickel-hydrogen cells and batteries
[NASA-TM-83386] p 73 N83-24571
Polyvinyl alcohol battery separator containing inert filler
[NASA-CASE-LEW-13556-2] p 183 N83-29805
Advanced inorganic separators for alkaline batteries and method of making the same
[NASA-CASE-LEW-13171-2] p 184 N83-32176

ALKENES
High performance liquid chromatographic hydrocarbon group-type analyses of mid-distillates employing fuel-derived fractions as standards
[NASA-TM-83072] p 100 N83-19920

ALKYL COMPOUNDS
Use of column V alkyls in organometallic vapor phase epitaxy (OMVPE) p 70 A83-46608

ALLOYS
Materials for advanced turbine engines. Volume 1: Advanced blade tip seal system
[NASA-CR-167851-VOL-1] p 31 N83-15308
Time effect of erosion by solid particle impingement on ductile materials
[NASA-TM-83369] p 84 N83-24637
The effects of Ni, Mo, Ti and Si on the mechanical properties of Cr free Mn steel (Fe-25Mn-5Al-2C)
[NASA-TM-83355] p 85 N83-24638

ALTERNATING CURRENT
Improved transistorized AC motor controller for battery powered urban electric passenger vehicles
[NASA-CR-167978] p 113 N83-10349
Design considerations for large space electric power systems
[NASA-TM-83064] p 58 N83-24552

ALTITUDE TESTS
Uniform engine testing program. Phase 1: NASA Lewis Research Center participation
[NASA-TM-82978] p 29 N83-14126

ALUMINUM
Low cycle fatigue behavior of aluminum/stainless steel composites
[AIAA 83-0806] p 62 A83-29886
The orthogonal in-situ machining of single and polycrystalline aluminum and copper, volume 2
[NASA-CR-169528] p 81 N83-13233
Three-dimensional elastoplastic stress analysis of unidirectional boron/aluminum composites
[NASA-CR-169796] p 65 N83-16394
Cavitation pitting and erosion of aluminum 6061-T6 in mineral oil water
[NASA-TP-2146] p 152 N83-35400

ALUMINUM ALLOYS
Influence of thermomechanical processing on elevated temperature slow plastic flow properties of B2 aluminide Fe-39.8at.% Al p 75 A83-22017
A brittle to ductile transition in NiAl of a critical grain size p 75 A83-29726
Morphology of ductile metals eroded by a jet of spherical particles impinging at normal incidence p 75 A83-32624
Intermetallics as alternative materials p 80 N83-11300
Testing of the permanent magnet material Mn-Al-C for potential use in propulsion motors for electric vehicles
[NASA-CR-169481] p 114 N83-12329
Cavitation pitting and erosion of Al 6061-T6 in mineral oil and water
[NASA-TM-83345] p 148 N83-23606
Morphology of an aluminum alloy eroded by a jet of angular particles impinging at normal incidence
[NASA-TP-2139] p 85 N83-24641
Cavitation erosion of copper, brass, aluminum and titanium alloys in mineral oil
[NASA-TM-83402] p 148 N83-24856
Evaluation of low-cost aluminum composites for aircraft engine structural applications
[NASA-TM-83357] p 66 N83-25790
Time dependence of solid-particle impingement erosion of an aluminum alloy
[NASA-TP-2169] p 86 N83-32908

ALUMINUM COATINGS
Silicon-slurry/aluminide coating — protecting gas turbine engine vanes and blades
[NASA-CASE-LEW-13343] p 86 N83-31795

ALUMINUM OXIDES
O-18 tracer studies of Al2O3 scale formation on NiCrAl alloys p 74 A83-10249
Effect of Y2O3 and Al2O3 on the oxidation resistance of Si3N4 p 88 A83-22258
Plastic deformation and wear process at a surface during unlubricated sliding p 138 A83-37822
Diffusion processes in Al2O3 scales - Void growth, grain growth, and scale growth p 76 A83-42238
Friction and wear of iron and nickel in sodium hydroxide solutions p 77 A83-48922
Friction and wear of iron and nickel in sodium hydroxide solutions
[NASA-TM-82935] p 77 N83-10171
Alumina fiber strength improvement
[NASA-CR-167999] p 63 N83-11247
Oxidation of low cobalt alloys p 79 N83-11291
Plastic deformation at surface during unlubricated sliding
[NASA-TP-2036] p 139 N83-11496
Specimen size and geometry effects on fracture toughness of Al2O3 measured with short rod and short bar chevron-notch specimens
[NASA-TM-83319] p 94 N83-19902

AMINES
Synthesis and characterization of bisimide amines and bisimide amine-cured epoxy resins p 88 A83-11486
Synthesis and characterization of bisimide amines and bisimide amine-cured epoxy resins p 90 A83-40924
Imide modified epoxy matrix resins
[NASA-CR-167942] p 93 N83-18909

AMMONIA
Electrothermal thruster diagnostics. Volume 2: Technical
[NASA-CR-168174-VOL-2] p 60 N83-33943

AMORPHOUS MATERIALS
Interfacial electrical properties of ion-beam sputter deposited amorphous carbon on silicon p 205 A83-33920
Sliding induced crystallization of metallic glass
[NASA-TP-2140] p 83 N83-21110

AMPLIFICATION
Tone-excited jet: Theory and experiments
[NASA-CR-3538] p 197 N83-12968

AMPLIFIER DESIGN
A two-stage monolithic buffer amplifier for 20 GHz satellite communication p 112 A83-39272

Design concepts for a high-impedance narrow-band 42 GHz power TWT using a fundamental/forward ladder-based circuit
[NASA-CR-165282] p 114 N83-12330

AMPLIFIERS
Space tubes: A major challenge
[NASA-TM-82971] p 113 N83-11447

ANALOG CIRCUITS
VLSI technology and applications
[NASA-CR-174451] p 118 N83-36358

ANALYSIS (MATHEMATICS)
A detailed treatment of two-dimensional, starved lubrication in the vicinity of two counter-rotating cylinders
p 141 N83-15520
Geometry and starvation effects in hydrodynamic lubrication p 141 N83-15522

ANECHOIC CHAMBERS
Wind tunnel measurements of blade/vane ratio and spacing effects on fan noise p 192 A83-15317

ANGLE OF ATTACK
An analytical evaluation of the icing properties of several low and medium speed airfoils
[AIAA PAPER 83-0109] p 3 A83-16525
A computer program for the calculation of the flow field including boundary layer effects for mixed-compression inlets at angle of attack
[NASA-CR-168002] p 10 N83-11066

ANGLES (GEOMETRY)
Some experiments on Yaw stability of wind turbines with various coning angles
[NASA-CR-168108] p 177 N83-22740
The effect of incidence angle on the overall three-dimensional aerodynamic performance of a classical annular airfoil cascade
[NASA-CR-168127] p 15 N83-34911

ANGULAR VELOCITY
Pivoting and slip in an angular contact bearing
[NASA-TM-83408] p 148 N83-26079

ANISOTROPIC MEDIA
Constitutive relationships for anisotropic high-temperature alloys
[NASA-TM-83437] p 160 N83-28493

ANISOTROPIC PLATES
Three-dimensional finite-element analysis of layered composite plates p 156 A83-27432

ANISOTROPY
Time-independent anisotropic plastic behavior by mechanical subelement models p 162 N83-34369

ANNEALING
Microdistribution of oxygen in silicon and its effects on electronic properties p 172 N83-15825
Radiation damage and annealing in large area n+/p/p+ GaAs shallow homojunction solar cells p 172 N83-15826
Radiation damage p 172 N83-15837
The effect of annealing on the creep of plasma sprayed ceramics
[NASA-TM-83396] p 130 N83-24799

ANNULAR DUCTS
Sound radiation from annular ducts/nozzles using modal decomposition of in-duct acoustic power
[AIAA PAPER 83-0714] p 194 A83-25929
Sound propagation in segmented exhaust ducts - Theoretical predictions and comparison with measurements
[AIAA PAPER 83-0734] p 194 A83-28016

ANNULAR FLOW
End wall flows in rotors and stators of a single stage compressor
[NASA-CR-169800] p 128 N83-16678
The effect of incidence angle on the overall three-dimensional aerodynamic performance of a classical annular airfoil cascade
[NASA-CR-168127] p 15 N83-34911

ANNULAR NOZZLES
Free-jet acoustic investigation of high-radius-ratio coannular plug nozzles. Comprehensive data report, volume 1
[NASA-CR-168086-VOL-1] p 198 N83-18408
Model aerodynamic test results for a refined actuated inlet ejector nozzle at simulated takeoff and cruise conditions
[NASA-CR-168051] p 13 N83-26818

ANNULI
Investigation of a low NOx full-scale annular combustor
[NASA-CR-165518] p 29 N83-13104

ANODES
Ion sputter textured graphite — anode collector plates in electron tube devices
[NASA-CASE-LEW-12919-1] p 63 N83-10117
Ring-cusp ion thruster with shell anode
[NASA-CASE-LEW-13881-1] p 202 N83-21903

ANTENNA ARRAYS
Auxiliary propulsion requirements for large space systems
[AIAA PAPER 83-1217] p 56 A83-45512
Application of MMIC modules in future multiple beam satellite antenna systems
[NASA-TM-83344] p 48 N83-22313
Phased array-fed antenna configuration study: Technology assessment
[NASA-CR-168078] p 106 N83-22495
Auxiliary propulsion requirements for large space systems
[NASA-TM-83388] p 58 N83-26922

ANTENNA COMPONENTS
Scanning beam antenna conceptual design for 20/30 GHz satellite systems p 46 N83-26889

ANTENNA DESIGN
A multiple beam antenna concept for a 30/20 GHz satellite communications system p 103 A83-11485
Techniques for low sidelobe, high efficiency offset dual reflector antennas p 104 A83-21072
Advanced 30/20 GHz multiple beam antenna for future communications satellites p 104 A83-41367
Advanced 30/20 GHz multiple-beam antennas for communications satellites
[NASA-TM-82952] p 50 N83-13154
Scanning beam antenna conceptual design for 20/30 GHz satellite systems p 46 N83-26889

ANTENNA FEEDS
Phased array-fed antenna configuration study: Technology assessment
[NASA-CR-168078] p 106 N83-22495

ANTENNA RADIATION PATTERNS
Techniques for low sidelobe, high efficiency offset dual reflector antennas p 104 A83-21072
Near-field measurement facility plans at Lewis Research Center p 46 N83-26897

ANTENNAS
Requirements for a mobile communications satellite system. Volume 3: Large space structures measurements study
[NASA-CR-168105] p 45 N83-22255

ANTHRACENE
Evaluation of ultraviolet spectrophotometry for simultaneous analysis of alkylbenzenes, alkylnaphthalenes, alkylanthracenes/phenanthrenes and total aromatics in mid-distillate fuels
[NASA-TM-83032] p 78 N83-15483

ANTICING ADDITIVES
A method of predicting flow rates required to achieve anti-icing performance with a porous leading edge ice protection system
[NASA-CR-168213] p 17 N83-32782

ANTIMISTING FUELS
A vortex venturi for reverting antimisting fuel properties
[ASME PAPER 83-GT-137] p 25 A83-47964

ANTIREFLECTION COATINGS
The effect of Ta2O5 on the interaction between silicon and its contact metallization
[NASA-TM-82948] p 166 N83-10554

AQUEOUS SOLUTIONS
Performance and emissions characteristics of aqueous alcohol fumes in a DI diesel engine
[NASA-CR-167917] p 99 N83-12250
An electrochemical rebalance cell for Redox systems
[NASA-TM-83363] p 73 N83-29326

ARC DISCHARGES
Continued development of a detailed model of arc discharge dynamics
[NASA-CR-167977] p 206 N83-16234

ARCHITECTURE (COMPUTERS)
Frequency-multiplexed and pipelined iterative optical systolic array processors p 188 A83-18588
A new architecture for adaptive transform compression of NTSC composite video signal p 103 A83-19732
Optical systolic array processor using residue arithmetic p 189 A83-46834
Planning assistance for the NASA 30/20 GHz program. Network control architecture study.
[NASA-CR-168058] p 106 N83-21207
Parallel, Asynchronous Executive (PAX): System concepts, facilities, and architecture
[NASA-TP-2179] p 189 N83-28921

ARGON
Analysis and design of ion thrusters for large space systems
[NASA-CR-165160] p 57 N83-14159
Nitriding of titanium and titanium: 8 percent aluminum, 1 percent molybdenum, 1 percent vanadium alloy with an ion-beam source
[NASA-TP-2149] p 85 N83-24640
High frequency plasma generators for ion thrusters
[NASA-CR-167957] p 59 N83-28072

ARITHMETIC
Optical systolic array processor using residue arithmetic p 189 A83-46834

ARRAYS
Jet array impingement flow distributions and heat transfer characteristics. Effects of initial crossflow and nonuniform array geometry — gas turbine engine component cooling
[NASA-CR-3630] p 128 N83-15592

ARTIFICIAL SATELLITES
Potentials on large spacecraft in LEO p 49 A83-17489

ASYMMETRY
Numerical simulation of the flow and fuel-air mixing in an axisymmetric piston-cylinder arrangement
[NASA-TM-83011] p 126 N83-12358

ASYMPTOTIC METHODS
The evolution of Tollmien-Schlichting waves near a leading edge. II - Numerical determination of amplitudes p 122 A83-35346

ASYMPTOTIC SERIES
The evolution of Tollmien-Schlichting waves near a leading edge p 120 A83-24410

ATMOSPHERIC ATTENUATION
Advanced communications satellite systems p 47 A83-49855

ATMOSPHERIC CIRCULATION
Cloud encounter statistics in the 28.5-43.5 KFT altitude region from four years of GASP observations p 188 A83-38733

ATMOSPHERIC COMPOSITION
Aircraft measurements of trace gases and particles near the tropopause
[NASA-CR-3691] p 188 N83-27542

ATMOSPHERIC EFFECTS
Effect of humidity on jet engine axial-flow compressor performance p 22 A83-35856
Aircraft sampling of the sulfate layer near the tropopause following the eruption of Mount St. Helens p 187 N83-11556

ATMOSPHERIC PRESSURE
The detailed chemistry and thermodynamics of sodium in oxygen-rich flames
[NASA-CR-169848] p 72 N83-17626

ATMOSPHERIC RADIATION
Atmospheric radiation model for water surfaces
[NASA-CR-167873] p 187 N83-21677

ATMOSPHERIC TEMPERATURE
Flight summaries and temperature climatology at airliner cruise altitudes from GASP (Global Atmospheric Sampling Program) data
[NASA-CR-168106] p 188 N83-24048

ATOMIZING
Aerodynamic-wave break-up of liquid sheets in swirling airflows and combustor modules
[AIAA PAPER 83-1204] p 124 A83-45511
Aerodynamic-wave break-up of liquid sheets in swirling airflows and combustor modules
[NASA-TM-83353] p 130 N83-23545

ATTACK AIRCRAFT
Fluid Dynamics Panel Symposium on Aerodynamics of Power Plant Installation
[AGARD-AR-173] p 27 N83-11138

AUGER SPECTROSCOPY
Application of modern surface analytical tools in the investigation of surface deterioration processes
[NASA-TM-83452] p 152 N83-34327

AUSTENITE
Development of Fe-Mn-Al-X-C alloys p 80 N83-11307

AUTOMATIC FLIGHT CONTROL
Software and system level tests of a test flight mercury ion thruster subsystem
[AIAA PAPER 82-1912] p 51 A83-12485

AUTOMATIC TEST EQUIPMENT
Operational summary of an electric propulsion long term test facility
[AIAA PAPER 82-1903] p 44 A83-12478

AUTOMOBILE ENGINES
Catalyst durability evaluation for advanced gas turbine engines
[ASME PAPER 82-JPGC-GT-21] p 137 A83-25270
Component qualification and initial build of the AGT 100 advanced automotive gas turbine
[ASME PAPER 83-GT-225] p 138 A83-48023
Progress in net shape fabrication of alpha SiC turbine components
[ASME PAPER 83-GT-238] p 139 A83-48030
Automotive Stirling Engine Mod 1 Design Review, volume 2
[NASA-CR-167936] p 209 N83-10991
Cold-air performance of compressor-drive turbine of Department of Energy upgraded automobile gas turbine engine. 2: Stage performance
[NASA-TM-82818] p 9 N83-11063

Advanced Gas Turbine (AGT) powertrain system
[NASA-CR-165346] p 139 N83-11497
Advanced Gas Turbine (AGT) powertrain system development program — automobile engines
[NASA-CR-169475] p 27 N83-12068
Advanced Gas Turbine (AGT) powertrain system development for automotive applications
[NASA-CR-165178] p 140 N83-12431
Advanced Gas Turbine (AGT) powertrain system development for automotive applications
[NASA-CR-165329] p 209 N83-13038
Losses in chopper-controlled DC series motors
[NASA-CR-167845] p 114 N83-13359
Automotive Stirling engine development program
[NASA-CR-167907] p 209 N83-15176
Automotive Stirling engine development program
[NASA-CR-168060] p 209 N83-15177
Computer program for Stirling engine performance calculations
[NASA-TM-82960] p 210 N83-17423
Advanced Gas Turbine (AGT) powertrain system development for automotive applications
[NASA-CR-167963] p 210 N83-17424
Advanced hybrid vehicle propulsion system study
[NASA-CR-159773] p 211 N83-24432
Free-piston Stirling hydraulic engine and drive system for automobiles
[NASA-TM-82992] p 211 N83-25625
Automotive Stirling engine development program
[NASA-CR-165263] p 211 N83-26762
Advanced Gas Turbine (AGT) powertrain system development for automotive applications
[NASA-CR-168104] p 211 N83-26763
DOE/NASA Automotive Stirling Engine Project overview '83
[NASA-TM-83405] p 212 N83-27924
Automotive Stirling Engine Development Program
[NASA-CR-168074] p 212 N83-27925
An analytical investigation of NO sub x control techniques for methanol fueled spark ignition engines
[NASA-CR-172647] p 151 N83-33168

AUTOMOBILE FUELS
Evaluation of fuel additives for reduction of material incompatibilities in methanol-gasoline blends
[NASA-CR-168061] p 86 N83-29359

AUXILIARY PROPULSION
Qualification test results of IAPS 8 cm ion thrusters
[AIAA PAPER 82-1954] p 52 A83-12511
Auxiliary propulsion requirements for large space systems
[AIAA PAPER 83-1217] p 56 A83-45512
The 8-CM ion thruster characterization — mercury ion engine
[NASA-CR-167887] p 57 N83-17586
Auxiliary propulsion requirements for large space systems
[NASA-TM-83388] p 58 N83-26922

AVALANCHES
Continued development of a detailed model of arc discharge dynamics
[NASA-CR-167977] p 206 N83-16234

AVIONICS
Fiberoptics technology and its application to propulsion control systems
[AIAA PAPER 83-0534] p 18 A83-16772
Flight evaluation of modifications to a digital electronic engine control system in an F-15 airplane
[AIAA PAPER 83-0537] p 20 A83-19593

AXES OF ROTATION
Simplified aeroelastic modeling of horizontal axis wind turbines
[NASA-CR-168109] p 177 N83-21509
Some experiments on Yaw stability of wind turbines with various coning angles
[NASA-CR-168108] p 177 N83-22740
DOE large horizontal axis wind turbine development at NASA Lewis Research Center
[NASA-TM-83444] p 184 N83-31107

AXIAL FLOW
The WISGSK: A computer code for the prediction of a multistage axial compressor performance with water ingestion
[NASA-CR-3624] p 28 N83-12093
End wall flow characteristics and overall performance of an axial flow compressor stage
[NASA-CR-3671] p 13 N83-26819
Advanced axial field D.C. motor development for electric passenger vehicle
[NASA-CR-167965] p 117 N83-30914

AXIAL FLOW TURBINES
Effects of interstage diffuser flow distortion on the performance of a 15.41-centimeter tip diameter axial power turbine
[AIAA PAPER 83-1179] p 23 A83-36263
A comprehensive method for preliminary design optimization of axial gas turbine stages. II - Code verification
[AIAA PAPER 83-1403] p 24 A83-36393
Experimental evaluation of inlet turbulence, wall boundary layer, surface finish, and fillet radius on small axial turbine state performance
[SAE PAPER 821475] p 24 A83-38001
Analytical and experimental study of flow through an axial turbine stage with a nonuniform inlet radial temperature profile
[AIAA PAPER 83-1175] p 6 A83-45510
Wall boundary layer development near the tip region of an IGV of an axial flow compressor
[ASME PAPER 83-GT-171] p 8 A83-47972
Analytical and experimental investigation of stator endwall contouring in a small axial-flow turbine. 1: Stator performance
[NASA-TP-2023] p 26 N83-11125
Effects of interstage diffuser flow distortion on the performance of a 15.41-centimeter tip diameter axial power turbine
[NASA-TM-83359] p 35 N83-24505
Analytical and experimental study of flow through an axial turbine stage with a nonuniform inlet radial temperature profile
[NASA-TM-83431] p 14 N83-27958
Current and future technology in radial and axial gas turbines
[NASA-TM-83414] p 41 N83-32811

AXIAL STRAIN
An extensometer for axial strain measurement at high temperature p 134 A83-48604
High strain rate properties of off-axis composite laminates, part 2
[NASA-CR-167970] p 64 N83-13179
High strain properties of angle-ply composite laminate, part 3
[NASA-CR-167971] p 64 N83-13180

AXIAL STRESS
Three-dimensional elastoplastic stress analysis of unidirectional boron/aluminum composites
[NASA-CR-169796] p 65 N83-16394

AXISYMMETRIC BODIES
Low speed performance of a supersonic axisymmetric mixed compression inlet with auxiliary inlets
[AIAA PAPER 83-1414] p 7 A83-45516
Low speed performance of a supersonic axisymmetric mixed compression inlet with auxiliary inlets — Lewis 9x15-ft anechoic wind tunnel tests
[NASA-TM-83435] p 37 N83-27992

AXISYMMETRIC FLOW
Finite analytic numerical solution of axisymmetric Navier-Stokes and energy equations
[ASME PAPER 82-HT-42] p 118 A83-12795
Rapid distortion of small-scale turbulence by an axisymmetric contraction p 120 A83-22381
Mean flowfields in axisymmetric combustor geometries with swirl p 120 A83-24668
On the shock cell structure and noise of supersonic jets
[AIAA PAPER 83-0703] p 193 A83-25923
Prediction of an axisymmetric combusting flow
[AIAA PAPER 83-1264] p 69 A83-36315
Interpretation of 2-probe turbulence measurements in an axisymmetric contraction
[NASA-CR-169832] p 11 N83-17502
Validation of a three-dimensional viscous analysis of axisymmetric supersonic inlet flow fields
[NASA-TM-83058] p 32 N83-17538
User's manual for Axisymmetric Diffuser Duct (ADD) code. Volume 2: Detailed ADD code description
[NASA-CR-165598-VOL-2] p 211 N83-26758
User's manual for Axisymmetric Diffuser Duct (ADD) code. Volume 3: ADD code coordinate generator
[NASA-CR-165598-VOL-3] p 211 N83-26759
Vortex motion in axisymmetric piston-cylinder configurations
[NASA-TM-85404] p 133 N83-35318

B

BACKSCATTERING
Numerical simulation of a conducting disk partially covered by an insulator interacting with a plasma p 50 N83-18805

BACKWARD WAVES
Dielectric based submillimeter backward wave oscillator circuit
[NASA-CASE-LEW-13736-1] p 115 N83-17802

BALANCING
T55 power turbine rotor multiplane-multispeed balancing study
[NASA-CR-167891] p 41 N83-33894

BALL BEARINGS
Advances in high-speed rolling-element bearings — for aircraft engine and transmission application p 137 A83-22319
The performance and application of high speed long life LH2 hybrid bearings for reusable rocket engine turbomachinery
[AIAA PAPER 83-1389] p 138 A83-36379
Theoretical results for fully flooded, elliptical hydrodynamic contacts
[NASA-TM-81696] p 140 N83-13456
Lubrication of 35-millimeter-bore ball bearings of several designs at speeds to 2.5 million DN p 141 N83-15512
Rolling-element fatigue life of AMS 5900 balls
[NASA-TP-2060] p 142 N83-16758
Surface profile changes of scuffed bearing surfaces — before and after acid treatment
[NASA-TM-83055] p 82 N83-17682
Predicted and experimental performance of large-bore high-speed ball and roller bearings p 145 N83-20131
Lubrication of 35-millimeter-bore ball bearings of several designs to 2.5 million DN p 145 N83-20132
High speed spherical roller-bearing analysis and comparison with experimental performance p 145 N83-20133
Pivoting and slip in an angular contact bearing
[NASA-TM-83406] p 148 N83-26079
Hybrid hydrostatic/ball bearings in high-speed turbomachinery
[NASA-CR-168124] p 149 N83-27213
Theoretical results for starved elliptical contacts
[NASA-TM-81697] p 150 N83-29710

BARS
Specimen size and geometry effects on fracture toughness of Al2O3 measured with short rod and short bar chevron-notch specimens
[NASA-TM-83319] p 94 N83-19902

BASIC (PROGRAMMING LANGUAGE)
BASIC Data Manipulation And Display System (BDMADS)
[NASA-TM-83328] p 189 N83-19496

BATTERY CHARGERS
Deep discharge reconditioning and shorted storage of batteries — nickel cadmium batteries
[NASA-CR-167953] p 166 N83-10502

BEADS
Solid spherical glass particle impingement studies of plastic materials
[NASA-TP-2161] p 94 N83-24695
Spherical micro-glass particle impingement studies of thermoplastic materials at normal incidence
[NASA-TM-83410] p 94 N83-25883
Time dependence of solid-particle impingement erosion of an aluminum alloy
[NASA-TP-2159] p 86 N83-32908

BEAM CURRENTS
Improved ion containment using a ring-cusp ion thruster
[AIAA PAPER 82-1928] p 53 A83-21100
Operation of the J-series thruster using inert gas
[AIAA PAPER 82-1929] p 54 A83-26625
Improved ion containment using a ring-cusp ion thruster
[NASA-TM-82990] p 56 N83-13164
Operation of the J-series thruster using inert gas
[NASA-TM-82977] p 57 N83-17587

BEAM SWITCHING
Packet communication system for a multi-beam beam switched satellite repeater p 104 A83-41336

BEAMS (RADIATION)
Stability analysis of flexible wind turbine blades using finite element method
[NASA-CR-168107] p 177 N83-21508

BEARING ALLOYS
Effect of carbide distribution on rolling-element fatigue life of AMS 5749
[NASA-TP-2189] p 151 N83-33166

BEARINGLESS ROTORS
Design study of Self-Aligning Bearingless Planetary (SABP) gear p 145 N83-20127

BEARINGS
Microscopic contour changes of tribological surfaces by chemical and mechanical action
[ASLE PREPRINT 82-LC-3B-3] p 136 A83-13237
Rolling-element fatigue life with traction fluids and automatic transmission fluid in a high-speed rolling-contact rig
[NASA-TP-2050] p 140 N83-13457
Corrosion of simulated bearing components of three bearing steels in the presence of chloride-contaminated lubricant
[NASA-TM-82955] p 143 N83-20115
Variable force, eddy-current or magnetic damper
[NASA-CASE-LEW-13717-1] p 159 N83-20284

Cavitation pitting and erosion of Al 6061-T6 in mineral oil and water
[NASA-TM-83345] p 148 N83-23606
Wear particle analysis using the ferrograph
[NASA-TM-83422] p 96 N83-28243
The trend of future gas turbine technology
[NASA-TM-83505] p 2 N83-34886

BENDING
Stress intensity and displacement coefficients for radially cracked ring segments subject to three-point bending
[NASA-TM-83059] p 160 N83-24874

BENDING FATIGUE
Evaluation of high-contact-ratio spur gears with profile modification p 147 N83-20150

BENDING THEORY
Alternative ways for formulation of hybrid stress elements p 155 A83-14710
Three-dimensional finite-element analysis of layered composite plates p 156 A83-27432

BENZENE
Evaluation of ultraviolet spectrophotometry for simultaneous analysis of alkylbenzenes, alkylnaphthalenes, alkylanthracenes/phenanthrenes and total aromatics in mid-distillate fuels
[NASA-TM-83032] p 99 N83-15483

BIBLIOGRAPHIES
Bibliography of Lewis Research Center technical publications announced in 1982
[NASA-TM-83335] p 208 N83-29124

BINARY SYSTEMS (MATERIALS)
Binary nickel alloy phase diagrams compilation and critical evaluation
[NASA-CR-170016] p 82 N83-19885

BIPOLARITY
Test results of a ten cell bipolar nickel-hydrogen battery
[NASA-TM-83384] p 181 N83-26253
Test methods and results of the 10-cell bipolar Ni-H2 battery p 117 N83-35261

BIREFRINGENCE
Long range surface plasmons in birefringent media p 202 A83-42206

BIT ERROR RATE
Adjacent channel interference degradation with minimum shift keyed modulation p 103 A83-19698

BLADE SLAP NOISE
Noise generation by a finite span swept airfoil
[AIAA PAPER 83-0768] p 195 A83-28023

BLADE TIPS
Turbine blade nonlinear structural and life analysis p 21 A83-29024
Tip clearance flow in a compressor rotor passage at design and off-design conditions p 4 A83-35855
Analysis, design, fabrication and testing of an optical tip clearance sensor — turbocompressor blade tips
[NASA-CR-165265] p 26 N83-11127
CF6 jet engine diagnostics program. High pressure turbine roundness/clearance investigation
[NASA-CR-165581] p 29 N83-13100
Tip cap for a rotor blade
[NASA-CASE-LEW-13654-1] p 30 N83-14129
Measured performance of a tip-controlled, teetered rotor with an NACA 64 sub 3-618 tip airfoil
[NASA-TM-82870] p 169 N83-14689
Materials for advanced turbine engines. Volume 1: Advanced blade tip seal system
[NASA-CR-167851-VOL-1] p 31 N83-15308
Aerodynamic effect of a honeycomb rotor tip shroud on a 50.8-centimeter-tip-diameter core turbine
[NASA-TP-2112] p 32 N83-17547
Residual stress in plasma sprayed ceramic turbine tip and gas path seal specimens
[NASA-TM-83418] p 131 N83-28380
Fully plasma-sprayed compliant backed ceramic turbine seal
[NASA-CASE-LEW-13268-3] p 149 N83-28450

BOEING 747 AIRCRAFT
Nacelle Aerodynamic and Inertial Loads (NAIL) project
[NASA-CR-168712] p 18 N83-30402

BOILING
The dryout region in frictionally heated sliding contacts p 124 A83-42762
Analogy between fluid cavitation and fracture mechanics
[NASA-TM-83071] p 129 N83-22542
Preliminary design of flight hardware for two-phase fluid research
[NASA-CR-168072] p 46 N83-25766

BONDING
Plasma-sprayed self-lubricating coatings
[NASA-CR-3680] p 94 N83-22422
Energy efficient engine high-pressure turbine single crystal vane and blade fabrication technology report
[NASA-CR-165400] p 39 N83-30429

BORON
Three-dimensional elastoplastic stress analysis of unidirectional boron/aluminum composites
[NASA-CR-169796] p 65 N83-16394

BOUNDARY INTEGRAL METHOD
Boundary integral equation method calculations of surface regression effects in flame spreading p 67 A83-13488

BOUNDARY LAYER FLOW
Effect of flow on the acoustic performance of extended reaction lined ducts
[AIAA PAPER 83-0778] p 195 A83-28024
Experimental evaluation of inlet turbulence, wall boundary layer, surface finish, and fillet radius on small axial turbine state performance
[SAE PAPER 821475] p 24 A83-38001
Convex curvature effects on the heated turbulent boundary layer p 123 A83-42733
Wall boundary layer development near the tip region of an IGV of an axial flow compressor
[ASME PAPER 83-GT-171] p 8 A83-47972
End wall flows in rotors and stators of a single stage compressor
[NASA-CR-169800] p 128 N83-16678
Three dimensional flow field inside compressor rotor, including blade boundary layers
[NASA-CR-169788] p 128 N83-16679
Analytical and experimental evaluation of the heat transfer distribution over the surfaces of turbine vanes
[NASA-CR-168015] p 131 N83-28376

BOUNDARY LAYER TRANSITION
The evolution of Tollmien-Schlichting waves near a leading edge p 120 A83-24410
Measured and calculated wall temperatures on air-cooled turbine vanes with boundary layer transition
[NASA-TM-83030] p 127 N83-14432
Generation of Tollmien-Schlichting waves by free-stream disturbances at low Mach numbers
[NASA-TM-83026] p 130 N83-23544

BOUNDARY LAYERS
A computer program for the calculation of the flow field including boundary layer effects for mixed-compression inlets at angle of attack
[NASA-CR-168002] p 10 N83-11066
Farfield inflight measurement of high-speed turboprop noise
[NASA-TM-83327] p 199 N83-21895
End-wall boundary layer measurements in a two-stage fan
[NASA-TM-83409] p 12 N83-24470
End wall flow characteristics and overall performance of an axial flow compressor stage
[NASA-CR-3671] p 13 N83-26819
Axial compressor middle stage secondary flow study
[NASA-CR-3701] p 14 N83-29174

BOUNDARY LUBRICATION
On the mechanism of lubrication by tricresylphosphate /TCP/ - The coefficient of friction as a function of temperature for TCP on M-50 steel
[ASLE PREPRINT 82-LC-4C-1] p 135 A83-13228
Finite-length solutions for rotodynamic coefficients of turbulent annular seals
[ASME PAPER 82-LUB-42] p 136 A83-13521
Lubrication background
[NASA-TM-81692] p 147 N83-20159
Theoretical results for starved elliptical contacts
[NASA-TM-81697] p 150 N83-29710
Preliminary results of the comparison of the electrochemical behavior of a thioether and biphenyl
[NASA-TM-83450] p 87 N83-34015
Thermal elastohydrodynamic lubrication of line contacts
[NASA-TM-83424] p 152 N83-34326

BOUNDARY VALUE PROBLEMS
Coordinate generation with precise controls over mesh properties p 190 A83-29631
Importance of inlet boundary conditions for numerical simulation of combustor flows
[AIAA PAPER 83-1263] p 23 A83-36314
The finite analytic method, volume 3
[NASA-CR-170186] p 191 N83-23087

BRAIN
Ion beam sputter etched ventricular catheter for hydrocephalus shunt
[NASA-CASE-LEW-13107-2] p 188 N83-20539

BRAYTON CYCLE
Direct contact droplet heat exchangers for thermal management in space p 120 A83-27137
Power generation from nuclear reactors in aerospace applications
[NASA-TM-83342] p 59 N83-30516

BRAZING
Applications of ion beam technology
[NASA-CR-169797] p 82 N83-16493

BROADBAND
Tone-excited jet: Theory and experiments
[NASA-CR-3538] p 197 N83-12968
Solar energy conversion using surface plasmons for broadband energy transport p 171 N83-15815

BROADCASTING
Multi-stage Depressed Collectors (MDC) for efficiency improvements of UHF broadcast klystrons
[NASA-TM-82970] p 105 N83-10322
Engineering calculations for communications systems planning
[NASA-CR-170182] p 106 N83-22494
Capabilities, limitations, and use of BC SAT-R2 conference software
[NASA-TM-83383] p 107 N83-29493

BUBBLES
Vapor cavitation in dynamically loaded journal bearings
[NASA-TM-83366] p 160 N83-24875

BUCKLING
Tensile buckling of advanced turboprops
[AIAA PAPER 82-0776] p 154 A83-10900
On the solution of elastic-plastic static and dynamic postbuckling collapse of general structure p 155 A83-12746
Structural qualification testing and operational loading on a fiberglass rotor blade for the Mod-OA wind turbine
[NASA-TM-83309] p 179 N83-23710
The effect of annealing on the creep of plasma sprayed ceramics
[NASA-TM-83396] p 130 N83-24799
A solution procedure for behavior of thick plates on a nonlinear foundation and postbuckling behavior of long plates
[NASA-TP-2174] p 163 N83-34373

BURNERS
Experimental study of the thermal-acoustic efficiency in a long turbulent diffusion-flame burner
[NASA-CR-3725] p 202 N83-33683

BUTADIENE
Soot formation in pyrolysis of acetylene, allene and 1,3-butadiene p 69 A83-39274

BYPASS RATIO
Composite fan exit guide vanes for high bypass ratio gas turbine engines p 19 A83-13159
Experimental results of a deflected thrust V/STOL nozzle research program
[AIAA PAPER 83-0170] p 6 A83-42100
Effect of steady-state pressure distortion on inlet flow to a high-bypass-ratio turbofan engine
[NASA-TM-82964] p 30 N83-15306
Experimental results of a deflected thrust V/STOL nozzle research program
[NASA-TM-83069] p 12 N83-25657

BYPASSES
Ion beam sputter etched ventricular catheter for hydrocephalus shunt
[NASA-CASE-LEW-13107-2] p 188 N83-20539

C

C BAND
20 x 20 IF switch matrix for SS-TDMA systems p 113 A83-41369

C-140 AIRCRAFT
Farfield inflight measurements of high-speed turboprop noise
[AIAA PAPER 83-0745] p 21 A83-25647

CANTILEVER BEAMS
Natural frequency of rotating beams using non-rotating modes p 156 A83-18383
Design of dry-friction dampers for turbine blades p 22 A83-35883

CANTILEVER MEMBERS
Vibrations of cantilevered circular cylindrical shells Shallow versus deep shell theory p 157 A83-36958
On the three-dimensional vibrations of the cantilevered rectangular parallelepiped p 157 A83-37729
Vibrations of cantilevered doubly-curved shallow shells p 157 A83-39557

CAPACITORS
High frequency, high power capacitor development
[NASA-CR-168035] p 116 N83-27127
Research into the use of pyrolytic oxides and polymers for the fabrication of thin film high energy capacitors
[NASA-CR-173012] p 97 N83-34045

CAPACITY
Expected cycle life versus depth of discharge relationships of well behaved single cells and cell strings
[NASA-TM-82957] p 167 N83-10558

CAPILLARY FLOW
Vapor flow into a capillary propellant-acquisition device
[AIAA PAPER 83-1380] p 55 A83-36371

CARBIDES
Effect of carbide distribution on rolling-element fatigue life of AMS 5749
[NASA-TP-2189] p 151 N83-33166
CARBON
Interfacial electrical properties of ion-beam sputter deposited amorphous carbon on silicon
p 205 A83-33920
Testing of the permanent magnet material Mn-Al-C for potential use in propulsion motors for electric vehicles
[NASA-CR-169481] p 114 N83-12329
Microhardness studies on thin carbon films grown on P-type, (100) silicon
[NASA-TM-82980] p 61 N83-13169
Diamondlike flake composites --- for use in aerospace structures and components
[NASA-CASE-LEW-13837-1] p 67 N83-28095
CARBON DIOXIDE
Evaluation of dopants in hydrogen to reduce hydrogen permeation in candidate Stirling engine heater head tube alloys at 760 deg and 820 deg
[NASA-TM-82920] p 81 N83-13232
CARBON DIOXIDE REMOVAL
Methods of reducing energy consumption of the oxidant supply system for MHD/steam power plants
[NASA-TM-83025] p 168 N83-13589
CARBON FIBERS
Metallic conductivity and air stability in copper chloride intercalated carbon fibers p 111 A83-16095
Lower-curing-temperature PMR polyimides
p 89 A83-40923
Lower-curing-temperature PMR polyimides
[NASA-TM-82958] p 63 N83-10118
Applications of ion beam technology
[NASA-CR-169797] p 82 N83-16493
CARBON MONOXIDE
Combustion characteristics of hydrogen-carbon monoxide based gaseous fuels p 67 A83-11491
Combustion characteristics of hydrogen. Carbon monoxide based gaseous fuels
[NASA-TM-82998] p 167 N83-10560
Shock tube measurements of growth constants in the branched chain formaldehyde-carbon monoxide-oxygen system
[NASA-TM-82954] p 71 N83-12182
CARBON 13
A carbon-13 and proton nuclear magnetic resonance study of some experimental referee broadened-specification /ERBS/ turbine fuels
p 98 A83-11482
CARBON-CARBON COMPOSITES
Research on ultra-high-temperature materials, monolithic ceramics, ceramic matrix composites and carbon/carbon composites p 64 N83-12161
CARRIER TRANSPORT (SOLID STATE)
Minority carrier diffusion length measurements - A review and comparison of techniques p 205 A83-28448
CASCADE CONTROL
Determination of optimum sunlight concentration level in space for 3-5 cascade solar cells p 171 N83-15814
CASCADE FLOW
Development of secondary flow and vorticity in curved ducts, cascades, and rotors, including effects of viscosity and rotation p 119 A83-16141
Experimental evaluation of shockless supercritical airfoils in cascade
[AIAA PAPER 83-0003] p 2 A83-16455
A viscous-inviscid interactive procedure for rotational flow in cascades of two-dimensional airfoils of arbitrary shape
[AIAA PAPER 83-0256] p 3 A83-16614
Comparison of laser anemometer measurements and theory in an annular turbine cascade with experimental accuracy determined by parameter estimation
p 4 A83-28833
Effect of particle presence on the incompressible inviscid flow through a two dimensional compressor cascade
p 6 A83-42562
Design of supercritical cascades with high solidity
p 6 A83-43446
Effect of particle presence on the incompressible inviscid flow through a two dimensional compressor cascade
[ASME PAPER 83-GT-95] p 8 A83-47941
A rapid blade-to-blade solution for use in turbomachinery design
[NASA-TM-83010] p 10 N83-13077
Comparison of visualized turbine endwall secondary flows and measured heat transfer patterns
[NASA-TM-83016] p 128 N83-14435
Experimental evaluation of shockless supercritical airfoils in cascade
[NASA-TM-83045] p 11 N83-15268
Effects of structural coupling on mistuned cascade flutter and response
[NASA-TM-83049] p 159 N83-15672
Environmental solid particle effects on compressor cascade performance
[NASA-CR-168018] p 11 N83-16285
Improved design of subcritical and supercritical cascades using complex characteristics and boundary layer correction
[NASA-CR-168166] p 12 N83-24474
The effect of incidence angle on the overall three-dimensional aerodynamic performance of a classical annular airfoil cascade
[NASA-CR-168127] p 15 N83-34911
CASSEGRAIN ANTENNAS
A multiple beam antenna concept for a 30/20 GHz satellite communications system p 103 A83-11485
Advanced 30/20 GHz multiple-beam antennas for communications satellites
[NASA-TM-82952] p 50 N83-13154
CASTING
Energy efficient engine high-pressure turbine single crystal vane and blade fabrication technology report
[NASA-CR-165400] p 39 N83-30429
CATALYSIS
NASA clean catalytic combustor program
[ASME PAPER 82-JPGC-GT-11] p 68 A83-25269
Evaluation of catalytic combustion of actual coal-derived gas
[NASA-CR-167842] p 168 N83-13588
Applications of ion beam technology
[NASA-CR-169797] p 82 N83-16493
CATALYSTS
Develop and test fuel cell powered on-site integrated total energy systems. Phase 3: Full-scale power plant development
[NASA-CR-168021] p 182 N83-27345
NASA Redox Project status summary
[NASA-TM-83401] p 183 N83-29810
The chemical behavior of acidified chromium (3) solutions
[NASA-CR-172997] p 74 N83-32871
CATALYTIC ACTIVITY
Catalyst durability evaluation for advanced gas turbine engines
[ASME PAPER 82-JPGC-GT-21] p 137 A83-25270
Catalytic combustion with steam injection
[ASME PAPER 82-JPGC-GT-23] p 164 A83-25271
Catalytic combustion with steam injection
[NASA-TM-82923] p 170 N83-15805
Critical research and advanced technology (CRT) support project
[NASA-TM-83019] p 176 N83-20361
Analysis of the visible spectra of concentrated chromic chloride solutions
[NASA-CR-172998] p 74 N83-32870
CATHETERIZATION
Ion beam sputter etched ventricular catheter for hydrocephalus shunt
[NASA-CASE-LEW-13107-2] p 186 N83-20539
Ion beam sputter-etched ventricular catheter for hydrocephalus shunt
[NASA-CASE-LEW-13107-1] p 188 N83-21785
CATHODES
Development program on a Spindt cold-cathode electron gun
[NASA-CR-168055] p 115 N83-18997
Moderate temperature rechargeable sodium batteries
[NASA-CR-168220] p 118 N83-36359
CAVITATION CORROSION
Dynamics and mechanism of cavitation erosion on perspex and epoxy resin tested in a rotating disk device
p 89 A83-27422
Cavitation erosion characteristics of poly(methyl methacrylate) in a rotating disk device
p 90 A83-41851
Dynamics and mechanism of cavitation erosion on perspex and epoxy resins tested in a rotating disk device
[NASA-TM-82962] p 91 N83-11329
Universal approach to analysis of cavitation and liquid-impingement erosion data
[NASA-TP-2061] p 82 N83-15413
Cavitation pitting and erosion of Al 6061-T6 in mineral oil and water
[NASA-TM-83345] p 148 N83-23606
A comprehensive analysis of cavitation and liquid impingement erosion data
[NASA-TM-83352] p 84 N83-24634
Cavitation erosion of copper, brass, aluminum and titanium alloys in mineral oil
[NASA-TM-83402] p 148 N83-24856
Cavitation pitting and erosion of aluminum 6061-T6 in mineral oil water
[NASA-TP-2146] p 152 N83-35400
CAVITATION FLOW
High-speed motion picture camera experiments of cavitation in dynamically loaded journal bearings
[ASME PAPER 82-LUB-18] p 136 A83-13509
The initial stages of cavitation damage and erosion on copper and brass tested in a rotating disk device
p 75 A83-27421
High-speed motion picture camera experiments of cavitation in dynamically loaded journal bearings
[ASME PAPER 82-LUB-18] p 138 A83-39944
Initial stages of cavitation damage and erosion on copper and brass tested in a rotating disk device
[NASA-TM-82993] p 81 N83-13231
Analogy between fluid cavitation and fracture mechanics
[NASA-TM-83071] p 129 N83-22542
Vapor cavitation in dynamically loaded journal bearings
[NASA-TM-83366] p 160 N83-24875
CAVITIES
Predicted and experimental performance of large-bore high-speed ball and roller bearings p 145 N83-20131
Lubrication of 35-millimeter-bore ball bearings of several designs to 2.5 million DN p 145 N83-20132
Large-bore tapered-roller bearing performance and endurance to 2.4 million DN p 145 N83-20134
CAVITY RESONATORS
A proposed optical pumping system requiring no electric power p 203 N83-15861
CELLULOSE
Evaluation of production version of the NASA improved inorganic-organic separator
[NASA-TM-83018] p 174 N83-18022
Energy and precious fuels requirements of fuel alcohol production, volume 1
[NASA-CR-168090] p 183 N83-28581
Energy and precious fuels requirements of fuel alcohol production. Volume 3, appendices C to F: Methanol from cellulose
[NASA-CR-168092] p 183 N83-28583
CENTAUR LAUNCH VEHICLE
Stability analysis of Centaur-in-Shuttle composite corrugated adapters
[AIAA 83-1003] p 49 A83-29791
Role of simulation and emulation in the development of Shuttle-Centaur (STS-Centaur)
[NASA-TM-83326] p 45 N83-29292
CENTRIFUGAL COMPRESSORS
NASA low-speed centrifugal compressor for fundamental research
[AIAA PAPER 83-1351] p 43 A83-36353
NASA low-speed centrifugal compressor for fundamental research
[NASA-TM-83398] p 13 N83-25662
Scaled centrifugal compressor, collector and running gear program
[NASA-CR-168167] p 40 N83-30432
CERAMIC BONDING
The effect of silicon particle size on the nitriding behaviour of reaction bonded Si3N4 compacts
p 90 A83-48261
The effect of annealing on the creep of plasma sprayed ceramics
[NASA-TM-83396] p 130 N83-24799
CERAMIC COATINGS
Infrared emission spectrophotometric study of the changes produced by TiN coating of metal surfaces in an operating EHD contact
[ASLE PREPRINT 82-LC-3C-3] p 135 A83-13229
Improved uniformity of multiphase ceramic-metal plasma-sprayed coats p 61 A83-22269
Use of fiber-like materials to augment cycle life of thick, thermoprotective-seal coatings --- for gas turbine engine components p 89 A83-22271
Some inelastic effects of thermal cycling on ZrO2-Y2O3 materials p 89 A83-22272
Creep of plasma-sprayed-ZrO2 thermal-barrier coatings p 89 A83-22273
High-temperature composites - Status and future directions p 63 A83-40129
Improved performance thermal barrier coatings
p 90 A83-42261
JT9D ceramic outer air seal system refinement program, phase 2
[NASA-CR-167962] p 30 N83-15305
Advanced ceramic coating development for industrial/utility gas turbine applications
[NASA-CR-165619] p 92 N83-15467
Laser surface fusion of plasma sprayed ceramic turbine seals
[NASA-CASE-LEW-13269-1] p 50 N83-20996
Thermal-barrier coatings for utility gas turbines
[NASA-TM-85349] p 95 N83-27022
Creep of plasma sprayed zirconia
[NASA-CR-167868] p 96 N83-29393
Thermal barrier coating system having improved adhesion
[NASA-CASE-LEW-1335901] p 97 N83-31855

CERAMICS
Comparison of NDE techniques for sintered-SiC components p 152 A83-22265
Tribological properties of sintered polycrystalline and single-crystal silicon carbide p 89 A83-29397
Injection molding ceramics to high green densities p 137 A83-33515
High-temperature composites - Status and future directions p 63 A83-40129
Progress in net shape fabrication of alpha SiC turbine components
[ASME PAPER 83-GT-238] p 139 A83-48030
Sintering of reaction bonded silicon nitride p 90 A83-48270
Sintering, properties and fabrication of Si3N4 + Y2O3 based ceramics p 90 A83-48303
Further industrial tests of ceramic thermal barrier coatings
[NASA-TP-2057] p 26 N83-10045
Research on ultra-high-temperature materials, monolithic ceramics, ceramic matrix composites and carbon/carbon composites p 64 N83-12161
Turbine engine materials durability research p 29 N83-12163
Advanced Gas Turbine (AGT) power-train system development
[NASA-CR-167875] p 142 N83-15627
Advanced Gas Turbine (AGT) powertrain system development for automotive applications
[NASA-CR-167983] p 210 N83-17424
Advanced Gas Turbine (AGT) powertrain system development for automotive applications
[NASA-CR-168104] p 211 N83-26763
Testing of felt-ceramic materials for combustor applications
[NASA-CR-168103] p 36 N83-26837
Correlation of compressive stress with spalling of plasma sprayed ceramic materials
[NASA-TM-83406] p 95 N83-27016
Residual stress in plasma sprayed ceramic turbine tip and gas path seal specimens
[NASA-TM-83418] p 131 N83-28380
Evaluation of ceramics for stator applications: Gas turbine engines interim report. Stator fabrication and evaluation
[NASA-CR-168140] p 96 N83-30662
Ceramic applications in turbine engines
[NASA-CR-165494] p 212 N83-37028
CEREBROSPINAL FLUID
Ion beam sputter etched ventricular catheter for hydrocephalus shunt
[NASA-CASE-LEW-13107-2] p 188 N83-20539
Ion beam sputter-etched ventricular catheter for hydrocephalus shunt
[NASA-CASE-LEW-13107-1] p 188 N83-21785
CERMETS
A new diffusion-inhibited oxidation-resistant coating for superalloys p 74 A83-10299
Fatigue behavior of SiC reinforced Ti/6Al-4V/ at 650 C p 62 A83-12414
Coating with overlay metallic-cermet alloy systems
[NASA-CASE-LEW-13639-2] p 82 N83-17683
CESIUM DIODES
Thermionic energy converters
[NASA-CASE-LEW-12443-1] p 184 N83-32175
CHANNEL CAPACITY
Advances in Serial MSK modems p 111 A83-19789
20 x 20 IF switch matrix for SS-TDMA systems p 113 A83-41369
CHANNEL FLOW
Aerodynamic features of turbulent flames
[AIAA PAPER 83-0470] p 119 A83-16737
Finite analytic numerical solution of heat transfer and flow past a square channel cavity p 123 A83-42703
Three-dimensional flow measurements in a vaneless radial turbine scroll
[NASA-CR-167994] p 9 N83-11065
An experimental investigation of internal area ruling for transonic and supersonic channel flow
[NASA-CR-169638] p 10 N83-14068
CHANNELS (DATA TRANSMISSION)
Adjacent channel interference degradation with minimum shift keyed modulation p 103 A83-19690
CHEMICAL ANALYSIS
High performance liquid chromatographic hydrocarbon group-type analyses of mid-distillates employing fuel-derived fractions as standards
[NASA-TM-83072] p 100 N83-19920
CHEMICAL BONDS
A review of liquid lubricant thermal/oxidative degradation
[NASA-TM-83465] p 98 N83-35143
CHEMICAL COMPOSITION
Tests of blending and correlation of distillate fuel properties p 98 A83-11050
Some properties of r.f.-sputtered hafnium nitride coatings p 88 A83-12653
Superalloy composition modeling p 78 N83-11284
Role of cobalt in nickel base superalloys p 78 N83-11286
Effect of reduced cobalt contents on hot isostatically pressed powder metallurgy U-700 alloys p 78 N83-11287
Low-cobalt single crystal Rene 150 p 78 N83-11288
Thermal fatigue resistance of cobalt-modified UDIMET 700 p 78 N83-11289
Creep-fatigue of low cobalt superalloys p 79 N83-11290
Low temperature cross linking polyimides
[NASA-CASE-LEW-12876-2] p 96 N83-29392
The chemical behavior of acidified chromium (3) solutions
[NASA-CR-172997] p 74 N83-32871
CHEMICAL EQUILIBRIUM
Thermodynamics of silicon nitridation - Effect of hydrogen
[ACS PAPER 33-B-80P] p 88 A83-18052
An electrochemical rebalance cell for Redox systems
[NASA-TM-83363] p 73 N83-29326
Spectrophotometric analysis of aqueous mixtures of some chromium (III) complexes
[NASA-CR-172999] p 74 N83-32872
CHEMICAL PROPERTIES
Recent trends in aviation turbine fuel properties
[NASA-TP-2056] p 99 N83-11340
Surface chemistry, friction and wear of Ni-Zn and Mn-Zn ferrites in contact with metals
[NASA-TM-83068] p 93 N83-19901
CHEMICAL PROPULSION
Study for analysis of benefit versus cost of low thrust propulsion system
[NASA-CR-168011] p 57 N83-21002
The performance and application of high speed long life LH2 hybrid bearings for reusable rocket engine turbomachinery
[NASA-TM-83417] p 58 N83-26923
CHEMICAL REACTIONS
New trends in combustion research for gas turbine engines p 22 A83-35806
Mechanism of lubrication by tricresylphosphate (TCP)
[NASA-TP-2053] p 72 N83-18863
New trends in combustion research for gas turbine engines
[NASA-TM-83338] p 34 N83-20947
Thermodynamics of the potassium-sulfur-oxygen and related systems
[NASA-CR-168155] p 61 N83-28077
Combustion Fundamentals Research
[NASA-CP-2268] p 38 N83-29208
Reactions of NaCl with gaseous SO3, SO2, and O2
[NASA-TM-83423] p 86 N83-29358
Chemical approach for controlling nadamide cure temperature and rate
[NASA-CASE-LEW-13770-2] p 96 N83-30651
CHEMISORPTION
Diatomic molecules and metallic adhesion, cohesion, and chemisorption - A single binding-energy relation p 69 A83-30921
CHIPS (ELECTRONICS)
Planar multijunction high voltage solar cell chip p 163 A83-13923
A low-power, high-throughput maximum-likelihood convolutional decoder chip for NASA's 30/20 GHz program p 111 A83-19754
CHLORIDES
Corrosion of simulated bearing components of three bearing steels in the presence of chloride-contaminated lubricant
[NASA-TM-82955] p 143 N83-20115
Study to establish cost predictions for the production of Redox chemicals
[NASA-CR-167882] p 176 N83-20359
CHLOROETHYLENE
Experimental study of electrochemical fluorination of trichloroethylene p 68 A83-15870
CHOKES (FUEL SYSTEMS)
Studies of flows through N-sequential orifices
[NASA-TM-83313] p 129 N83-19020
CHOKES (RESTRICTIONS)
Experiments on flow through one to four inlets of the orifice and Borda type p 124 A83-43235
CHROMATOGRAPHY
Aircraft sampling of the sulfate layer near the tropopause following the eruption of Mount St. Helens p 187 N83-11556
CHROMIUM
COSAM (Conservation Of Strategic Aerospace Materials) program overview
[NASA-TM-83006] p 78 N83-11282
COSAM program overview p 78 N83-11283
Conservation of strategic metals p 80 N83-12154
Study to establish cost predictions for the production of Redox chemicals
[NASA-CR-167882] p 176 N83-20359
CHROMIUM ALLOYS
Dual alloy interface stability p 79 N83-11297
CHROMIUM COMPOUNDS
An electrochemical rebalance cell for Redox systems
[NASA-TM-83363] p 73 N83-29326
Analysis of the visible spectra of concentrated chromic chloride solutions
[NASA-CR-172998] p 74 N83-32870
Spectrophotometric analysis of aqueous mixtures of some chromium (III) complexes
[NASA-CR-172999] p 74 N83-32872
CHROMIUM OXIDES
Oxidation of low cobalt alloys p 79 N83-11291
CIRCUITS
Dielectric based submillimeter backward wave oscillator circuit
[NASA-CASE-LEW-13736-1] p 115 N83-17802
CIRCULAR CYLINDERS
Sound diffraction at wall impedance discontinuities in a circular cylinder - Investigated using Wiener-Hopf technique
[AIAA PAPER 83-0730] p 195 A83-33485
Mode propagation in nonuniform circular ducts with potential flow p 122 A83-36082
Effects of free stream turbulence intensity and integral length scale on heat transfer from a circular cylinder in crossflow p 123 A83-42711
Spanwise mass transfer variations on a cylinder in 'nominally' uniform crossflow p 124 A83-43019
Turbulence effect on crossflow around a circular cylinder at subcritical Reynolds numbers
[NASA-CR-3622] p 127 N83-13387
Sound diffraction at wall impedance discontinuities in a circular cylinder, investigated using Wiener-Hopf technique
[NASA-TM-83365] p 201 N83-23117
Solid particle impingement erosion characteristics of cylindrical surfaces, pre-existing holes and slits
[NASA-TM-83322] p 85 N83-25853
CIRCULAR SHELLS
Vibrations of cantilevered circular cylindrical shells Shallow versus deep shell theory p 157 A83-36958
CIVIL AVIATION
Airline flight planning: The weather connection p 17 N83-17461
Aviation Gasolines and Future Alternatives
[NASA-CP-2267] p 100 N83-22442
Aviation energy and the future of the recreational use of sport and general aviation aircraft p 100 N83-22444
An overview of general aviation propulsion research programs at NASA Lewis Research Center p 35 N83-22456
CLEANING
Performance degradation and cleaning of photovoltaic arrays p 164 A83-27236
CLEARANCES
Film thickness measurement for spiral groove and Rayleigh step lift pad self-acting face seals
[NASA-TP-2058] p 26 N83-11126
Analysis, design, fabrication and testing of an optical tip clearance sensor --- turbocompressor blade tips
[NASA-CR-165265] p 26 N83-11127
CF6 jet engine diagnostics program. High pressure turbine roundness/clearance investigation
[NASA-CR-165581] p 29 N83-13100
Materials for advanced turbine engines. Volume 1: Advanced blade tip seal system
[NASA-CR-167851-VOL-1] p 31 N83-15308
The JT8D and JT9D engine component improvement: Performance improvement program
[NASA-CR-167965] p 32 N83-17543
Fully plasma-sprayed compliant backed ceramic turbine seal
[NASA-CASE-LEW-13268-3] p 149 N83-28450
Control means for a gas turbine engine
[NASA-CASE-LEW-14586-1] p 40 N83-31603
CLIMATOLOGY
Flight summaries and temperature climatology at airliner cruise altitudes from GASP (Global Atmospheric Sampling Program) data
[NASA-CR-168106] p 188 N83-24048
CLOSED CYCLES
Parametric analysis of closed cycle magnetohydrodynamic (MHD) power plants
[NASA-CR-165472] p 178 N83-22748
CLOUD COVER
Cloud encounter statistics in the 28.5-43.5 KFT altitude region from four years of GASP observations p 188 A83-38733

CLOUD GLACIATION
Influence of multidroplet size distribution on icing collection efficiency
[AIAA PAPER 83-0110] p 187 A83-16526
Comparison of modern icing cloud instruments
[NASA-CR-168008] p 19 N83-18720
CLOUD PHYSICS
Comparison of modern icing cloud instruments
[NASA-CR-168008] p 19 N83-18720
CLOUDS
Experimental comparison of icing cloud instruments
[AIAA PAPER 83-0026] p 16 A83-42099
Experimental comparison of icing cloud instruments
[NASA-TM-83340] p 17 N83-24487
CLUSTER ANALYSIS
Superalloy composition modeling p 78 N83-11284
CMOS
A low-power, high-throughput maximum-likelihood convolutional decoder chip for NASA's 30/20 GHz program p 111 A83-19754
COAL DERIVED GASES
Combustion characteristics of hydrogen-carbon monoxide based gaseous fuels p 67 A83-11491
Literature survey of properties of synfuels derived from coal
[NASA-TM-82739] p 99 N83-10208
Combustion of coal gas fuels in a staged combustor
[NASA-TM-82987] p 166 N83-10556
Evaluation of advanced combustion concepts for dry NO sub x suppression with coal-derived, gaseous fuels
[NASA-TM-82985] p 166 N83-10557
Evaluation of catalytic combustion of actual coal-derived gas
[NASA-CR-167842] p 168 N83-13588
Critical research and advanced technology (CRT) support project
[NASA-TM-83019] p 176 N83-20351
COAL DERIVED LIQUIDS
Literature survey of properties of synfuels derived from coal
[NASA-TM-82739] p 99 N83-10208
Studies of the mechanisms of turbine fuel instability
[NASA-CR-167963] p 100 N83-18924
COAL GASIFICATION
NOx results from two combustors tested on medium BTU coal gas p 186 A83-11493
Literature survey of properties of synfuels derived from coal
[NASA-TM-82739] p 99 N83-10208
IGCC performance comparison for variations in gasifier type and gas turbine firing temperature
[NASA-TM-83310] p 180 N83-25037
Analysis of potential benefits of integrated-gasifier combined cycles for a utility system
[NASA-TP-2172] p 186 N83-36549
COAL LIQUEFACTION
Literature survey of properties of synfuels derived from coal
[NASA-TM-82739] p 99 N83-10208
Energy and precious fuels requirements of fuel alcohol production. Volume 4: Appendices G and H, methanol from coal
[NASA-CR-168093] p 183 N83-28580
Energy and precious fuels requirements of fuel alcohol production, volume 1
[NASA-CR-168090] p 183 N83-28581
COAL UTILIZATION
Parametric analysis of closed cycle magnetohydrodynamic (MHD) power plants
[NASA-CR-165472] p 178 N83-22748
COATING
Vacuum sputtered and ion-plated coatings for wear and corrosion protection
[NASA-TM-83007] p 99 N83-13273
COATINGS
Infrared emission spectrophotometric study of the changes produced by TiN coating of metal surfaces in an operating EHD contact
[NASA-TM-82989] p 92 N83-15466
Evaluation of production version of the NASA improved inorganic-organic separator
[NASA-TM-83018] p 174 N83-18022
The Rene 150 directionally solidified superalloy turbine blades, volume 1
[NASA-CR-167992] p 33 N83-20946
RF sputtered silicon and hafnium nitrides: Properties and adhesion to 440C stainless steel
[NASA-TM-83400] p 95 N83-27020
JT9D thermal barrier coated vanes
[NASA-CR-167964] p 37 N83-27993
Advanced inorganic separators for alkaline batteries and method of making the same
[NASA-CASE-LEW-13171-2] p 184 N83-32176
COAXIAL FLOW
Conventional profile coaxial jet noise prediction p 193 A83-22128
Coaxial supersonic jet-flows, shock structure and related problems with noise-suppression assessment and prediction
[AIAA PAPER 83-0707] p 194 A83-28011
Comparison of measured and predicted flight effects on high-bypass coaxial jet exhaust noise
[NASA-TM-83347] p 200 N83-23115
Numerical analysis of turbulent coaxial flow with internal heat generation
[NASA-CR-172633] p 132 N83-33105
COAXIAL NOZZLES
Comparison of measured and predicted flight effects on high-bypass coaxial jet exhaust noise
[AIAA PAPER 83-0749] p 194 A83-26450
Statistical characteristics of velocity, concentration, mass transport, and momentum transport for coaxial jet mixing in a confined duct
[ASME PAPER 83-GT-39] p 125 A83-47899
COBALT
COSAM (Conservation Of Strategic Aerospace Materials) program overview
[NASA-TM-83006] p 78 N83-11282
COSAM program overview p 78 N83-11283
Role of cobalt in nickel base superalloys p 78 N83-11286
Effect of reduced cobalt contents on hot isostatically pressed powder metallurgy U-700 alloys p 78 N83-11287
Low-cobalt single crystal Rene 150 p 78 N83-11288
Thermal fatigue resistance of cobalt-modified UDIMET 700 p 78 N83-11289
Creep-fatigue of low cobalt superalloys p 79 N83-11290
Conservation of strategic metals p 80 N83-12154
Understanding the roles of the strategic element cobalt in nickel base superalloys
[NASA-TM-83475] p 87 N83-35102
Reaction of cobalt in SO2 atmospheric at elevated temperatures
[NASA-TM-83485] p 88 N83-35104
COBALT ALLOYS
Oxidation of low cobalt alloys p 79 N83-11291
Hot corrosion of low cobalt alloys p 79 N83-11292
Influence of cobalt, tantalum, and tungsten on the microstructure and mechanical properties of superalloy single crystals p 79 N83-11293
Dual alloy interface stability p 79 N83-11297
Intermetallics as alternative materials p 80 N83-11300
COEFFICIENT OF FRICTION
On the mechanism of lubrication by tricresylphosphate /TCP/ - The coefficient of friction as a function of temperature for TCP on M-50 steel
[ASLE PREPRINT 82-LC-4C-1] p 135 A83-13228
Tribological properties of sintered polycrystalline and single-crystal silicon carbide p 89 A83-29397
Mechanism of lubrication by tricresylphosphate (TCP)
[NASA-TP-2053] p 72 N83-18863
Comparison of spur gear efficiency prediction methods p 146 N83-20141
Frictional and morphological characteristics of ion plated soft, metallic films
[NASA-TM-81723] p 83 N83-22390
Tribological and microstructural characteristics of ion-nitrided steels
[NASA-TM-83368] p 84 N83-24635
COGENERATION
Measured effect of wind generation on the fuel consumption of an isolated diesel power system p 165 A83-36410
COHERENCE
Correlation of core noise obtained by three signal coherence techniques
[NASA-TM-83012] p 197 N83-12966
COHERENT LIGHT
Coherent conversion of the sunlight spectrum
[NASA-CR-170185] p 179 N83-25026
COHESION
Diatomic molecules and metallic adhesion, cohesion, and chemisorption - A single binding-energy relation p 69 A83-30921
COLD CATHODES
Spindt cold cathode electron gun development program
[NASA-CR-168212] p 202 N83-35787
COLD PLASMAS
Potentials on large spacecraft in LEO p 49 A83-17489
COLD WELDING
Applications of ion beam technology
[NASA-CR-169797] p 82 N83-16493
COLLECTION
Influence of multidroplet size distribution on icing collection efficiency
[AIAA PAPER 83-0110] p 187 A83-16526
COMBINED CYCLE POWER GENERATION
IGCC performance comparison for variations in gasifier type and gas turbine firing temperature
[NASA-TM-83310] p 180 N83-25037
Analysis of potential benefits of integrated-gasifier combined cycles for a utility system
[NASA-TP-2172] p 186 N83-36549
COMBINED STRESS
Stability analysis of Centaur-in-Shuttle composite corrugated adapters
[AIAA 83-1003] p 49 A83-29791
COMBUSTIBLE FLOW
Measurements and predictions for nonevaporating sprays in a quiescent environment
[AIAA PAPER 83-0151] p 119 A83-16558
Importance of inlet boundary conditions for numerical simulation of combustor flows
[AIAA PAPER 83-1263] p 23 A83-36314
Prediction of an axisymmetric combusting flow
[AIAA PAPER 83-1264] p 69 A83-36315
Correlating downward flame spread rates for thick fuel beds p 69 A83-37045
The structure of evaporating and combusting sprays: Measurements and predictions
[NASA-CR-170312] p 130 N83-24795
Modeling Interface Motion Of Combustion (MINOC). A computer code for two-dimensional, unsteady turbulent combustion
[NASA-TP-2132] p 40 N83-32806
COMBUSTION
Burner rig study of variables involved in hole plugging of air cooled turbine engine vanes
[NASA-TM-83308] p 83 N83-19887
Experimental study of the thermal-acoustic efficiency in a long turbulent diffusion-flame burner
[NASA-CR-3725] p 202 N83-33683
Preliminary tests of an advanced high-temperature combustion system
[NASA-TP-2203] p 41 N83-33893
Effects of percentage of blockage and flameholder downstream counterbores on lean combustion limits of premixed, prevaporized propane-air mixture
[NASA-TP-2227] p 41 N83-34941
COMBUSTION CHAMBERS
Combustion characteristics of hydrogen-carbon monoxide based gaseous fuels p 67 A83-11491
Multifuel evaluation of rich/quench/lean combustor p 67 A83-11492
NOx results from two combustors tested on medium BTU coal gas p 186 A83-11493
Nonlinear structural and life analyses of a combustor liner p 155 A83-12764
Small gas turbine combustor study - Combustor liner evaluation
[AIAA PAPER 83-0337] p 20 A83-16663
Effect of broad properties fuel on injector performance in a reverse flow combustor
[AIAA PAPER 83-0154] p 20 A83-21079
Mean flowfields in axisymmetric combustor geometries with swirl p 120 A83-24668
NASA clean catalytic combustor program
[ASME PAPER 82-JPGC-GT-11] p 68 A83-25269
Catalyst durability evaluation for advanced gas turbine engines
[ASME PAPER 82-JPGC-GT-21] p 137 A83-25270
Acoustic modal analysis of a full-scale annular combustor
[AIAA PAPER 83-0760] p 196 A83-33486
Cross spectra between temperature and pressure in a constant area duct downstream of a combustor
[AIAA PAPER 83-0762] p 196 A83-33487
New trends in combustion research for gas turbine engines p 22 A83-35806
Experiments in dilution jet mixing
[AIAA PAPER 83-1201] p 122 A83-36277
Application of 3D aerodynamic/combustion model to combustor primary zone study
[AIAA PAPER 83-1265] p 23 A83-36316
The performance of an annular vane swirler --- to aid in modeling gas turbine combustor flowfields and swirling confined flow turbulence
[AIAA PAPER 83-1326] p 24 A83-36340
Development and operating characteristics of an advanced two-stage combustor p 24 A83-38022
Aerodynamic-wave break-up of liquid sheets in swirling airflows and combustor modules
[AIAA PAPER 83-1204] p 124 A83-45511
Development of advanced high-temperature heat flux sensors
[NASA-CR-165618] p 26 N83-10044
Multifuel evaluation of rich/quench/lean combustor
[NASA-TM-82986] p 167 N83-10559
Combustion characteristics of hydrogen. Carbon monoxide based gaseous fuels
[NASA-TM-82998] p 167 N83-10560

Effect of broad properties fuel on injector performance in a reverse flow combustor
[NASA-TM-83013] p 29 N83-13101
Investigation of a low NOx full-scale annular combustor
[NASA-CR-165518] p 29 N83-13104
Advanced Gas Turbine (AGT) power-train system development
[NASA-CR-167875] p 142 N83-15627
Steam cooled rich-burn combustor liner
[NASA-CASE-LEW-13609-1] p 72 N83-17628
Small gas turbine combustor study: Combustor liner evaluation
[NASA-TM-83028] p 33 N83-18725
Experimental verification of the Neuber relation at room and elevated temperatures --- to predict stress-strain behavior in notched specimens of hastelloy x
[NASA-CR-167967] p 159 N83-19121
Energy efficient engine sector combustor rig test program
[NASA-CR-167913] p 33 N83-19753
New trends in combustion research for gas turbine engines
[NASA-TM-83338] p 34 N83-20947
Acoustic modal analysis of a full-scale annular combustor
[NASA-TM-83334] p 200 N83-21896
Cross spectra between temperature and pressure in a constant area duct downstream of a combustor
[NASA-TM-83351] p 200 N83-23116
Analytical fuel property effects, small combustors, phase 1
[NASA-CR-168138] p 101 N83-23464
Aerodynamic-wave break-up of liquid sheets in swirling airflows and combustor modules
[NASA-TM-83353] p 130 N83-23545
Testing of felt-ceramic materials for combustor applications
[NASA-CR-168103] p 36 N83-26837
A variable-geometry combustor used to study primary and secondary zone stoichiometry
[NASA-TM-83372] p 37 N83-27995
Small gas turbine combustor primary zone study
[NASA-CR-168122] p 149 N83-28448
Analytical calculation of a single jet in cross-flow and comparison with experiment p 38 N83-29219
Small gas turbine combustor primary zone study p 38 N83-29221
Flame radiation measurements p 73 N83-29228
Parametric study of flame radiation characteristics of a tubular-can combustor
[NASA-TM-83436] p 39 N83-29237
Broad specification fuels technology program, phase 1
[NASA-CR-168180] p 74 N83-30551
Axial vane-type swirler performance characteristics
[NASA-CR-172995] p 40 N83-32808
Preliminary tests of an advanced high-temperature combustion system
[NASA-TP-2203] p 41 N83-33893
Effects of percentage of blockage and flameholder downstream counterbores on lean combustion limits of premixed, prevaporized propane-air mixture
[NASA-TP-2227] p 41 N83-34941
Detailed fuel spray analysis techniques
[NASA-TM-83476] p 42 N83-34943
Turbulence measurements in a complex plowfield using a crossed hot-wire
[NASA-CR-173080] p 132 N83-35316
SSME main combustion chamber life prediction
[NASA-CR-168215] p 60 N83-36101

COMBUSTION CONTROL
Small gas turbine combustor primary zone study p 38 N83-29221

COMBUSTION EFFICIENCY
Computed and measured turbulence in axisymmetric reciprocating engines p 21 A83-24669
Catalyst durability evaluation for advanced gas turbine engines
[ASME PAPER 82-JPGC-GT-21] p 137 A83-25270
Development and operating characteristics of an advanced two-stage combustor p 24 A83-36022
Combustion of coal gas fuels in a staged combustor
[NASA-TM-82967] p 166 N83-10556
Effect of flameholder pressure drop on emissions and performance of premixed-prevaporized combustors
[NASA-TP-2131] p 35 N83-23309
Analytical fuel property effects, small combustors, phase 1
[NASA-CR-168138] p 101 N83-23464

COMBUSTION PHYSICS
Ignition of confined gaseous mixtures by hot surfaces and hot wires
[AIAA PAPER 83-0240] p 68 A83-16606
Ignition of a combustible half space p 68 A83-22738
Turbulent flame propagation and combustion in spark ignition engines p 70 A83-48156
Evaluation of catalytic combustion of actual coal-derived gas
[NASA-CR-167842] p 168 N83-13588
NASA Lewis Research Center combustion MHD experiment p 173 N83-15847
An overview of general aviation propulsion research programs at NASA Lewis Research Center p 35 N83-22456
Combustion Fundamentals Research
[NASA-CP-2268] p 38 N83-29208
The NASA broad-specification fuels combustion technology program: An assessment of phase 1 test results
[NASA-TM-83447] p 39 N83-29236
Parametric study of flame radiation characteristics of a tubular-can combustor
[NASA-TM-83436] p 39 N83-29237
Summary of synfuel characterization and combustion studies
[NASA-TM-83066] p 185 N83-34453
Detailed fuel spray analysis techniques
[NASA-TM-83476] p 42 N83-34943

COMBUSTION PRODUCTS
Combustion characteristics of hydrogen-carbon monoxide based gaseous fuels p 67 A83-11491
NOx results from two combustors tested on medium BTU coal gas p 186 A83-11493
Soot formation in pyrolysis of acetylene, allene and 1,3-butadiene p 69 A83-39274
Combustion system processes leading to corrosive deposits p 69 A83-42246

COMMERCIAL AIRCRAFT
Advances in high-speed rolling-element bearings --- for aircraft engine and transmission application p 137 A83-22319
Energy efficient engine component development and integration program
[NASA-CR-170089] p 34 N83-22204

COMMUNICATION EQUIPMENT
Advanced 3-V semiconductor technology assessment
[NASA-CR-168101] p 206 N83-21987
Advanced 3-V semiconductor technology assessment --- space communications
[NASA-CR-168102] p 207 N83-21988

COMMUNICATION NETWORKS
Concept for advanced satellite communications and required technologies
[NASA-TM-82984] p 47 N83-11210
Next generation communications satellites: multiple access and network studies
[NASA-CR-167903] p 45 N83-12129
Customer premise service study for 30/20 GHz satellite system
[NASA-CR-167986] p 105 N83-17769
A study of 60 Gigahertz intersatellite link applications
[NASA-TM-83337] p 47 N83-20994
Requirements for a mobile communications satellite system. Volume 1: Executive summary
[NASA-CR-168128] p 106 N83-23497
Planning assistance for the 30/20 GHz program, volume 1
[NASA-CR-165484-VOL-1] p 108 N83-33010
Satellite provided customer premises services: A forecast of potential domestic demand through the year 2000. Volume: Executive summary
[NASA-CR-168142] p 109 N83-34116

COMMUNICATION SATELLITES
Development of a microwave 20 x 20 switch matrix for 30/20 GHz SS-TDMA application p 110 A83-11484
A multiple beam antenna concept for a 30/20 GHz satellite communications system p 103 A83-11485
A 1 watt GaAs power amplifier for the NASA 30/20 GHz communication system p 111 A83-11489
30/20 GHz experimental communications satellite system p 103 A83-19688
Future satellite systems - Market demand assessment p 104 A83-19762
A high capacity satellite switched TDMA microwave switch matrix p 104 A83-19775
Packet communication system for a multi-beam beam switched satellite repeater p 104 A83-41336
Advanced 30/20 GHz multiple beam antenna for future communications satellites p 104 A83-41367
20 x 20 IF switch matrix for SS-TDMA systems p 113 A83-41369
A network control concept for the 30/20 GHz communication system baseband processor p 47 A83-41389
Onboard processing for a 30/20 GHz communications satellite p 47 A83-41391
Application of a space station to communications satellites
[AAS PAPER 83-197] p 45 A83-43773
Advanced communications satellite systems p 47 A83-49855
Space tubes: A major challenge
[NASA-TM-82971] p 113 N83-11447
Next generation communications satellites: multiple access and network studies
[NASA-CR-167903] p 45 N83-12129
Advanced 30/20 GHz multiple-beam antennas for communications satellites
[NASA-TM-82952] p 50 N83-13154
Requirements for a mobile communications satellite system. Volume 3: Large space structures measurements study
[NASA-CR-168105] p 45 N83-22255
Application of MMIC modules in future multiple beam satellite antenna systems
[NASA-TM-83344] p 48 N83-22313
Experimental verification of the multistage depressed collector design procedure for a high-perveance, helix-type, traveling-wave tube --- in communications satellites
[NASA-TP-2162] p 116 N83-25985
Planning assistance for the 30/20 GHz program, volume 1
[NASA-CR-165484-VOL-1] p 108 N83-33010
Planning assistance for the 30/20 GHz program, volume 2
[NASA-CR-165484-VOL-2] p 108 N83-33011
Planning assistance for the 30/20 GHz program, volume 3
[NASA-CR-165484] p 108 N83-33012
Satellite provided fixed communication services: A forecast of potential domestic demand through the year 2000. Volume 1: Executive summary
[NASA-CR-168145] p 108 N83-34113
Satellite provided fixed communications services: A forecast of potential domestic demand through the year 2000: Volume 2: Main test
[NASA-CR-168146] p 108 N83-34114
Satellite fixed communications service: A forecast of potential domestic demand through the year 2000. Volume 3: Appendices
[NASA-CR-168147] p 108 N83-34115
Satellite provided customer premises services: A forecast of potential domestic demand through the year 2000. Volume: Executive summary
[NASA-CR-168142] p 109 N83-34116
Satellite provided customer premise services: A forecast of potential domestic demand through the year 2000. Volume 3: Appendices
[NASA-CR-168144] p 109 N83-34118
A comparison of Frequency Domain Multiple Access (FDMA) and Time Domain Multiple Access (TDMA) approaches to satellite service for low data rate Earth stations
[NASA-TM-83430] p 109 N83-34120
Spacecraft in switch matrix for wide band service applicatons in 30/20 GHz communications satellite systems
[NASA-CR-168089] p 46 N83-34998
NASA's Advanced Communications Technology Satellite (ACTS)
[NASA-TM-83416] p 48 N83-35004
Four-dimensional modulation and coding: An alternate to frequency-reuse
[NASA-CR-174453] p 110 N83-36300

COMMUTATION
A lightweight electronically commutated dc motor for electric passenger vehicles
[NASA-CR-165601] p 113 N83-10348
New propulsion components for electric vehicles
[NASA-TM-83404] p 116 N83-25982

COMPARISON
Preliminary assessment of the tradeoffs between the electric motor and the transmission in electric vehicles
[NASA-CR-168199] p 117 N83-30915

COMPATIBILITY
Aerodynamic performance of a fan stage utilizing variable inlet guide vanes (VIGV's) for thrust modulation --- subsonic V/STOL aircraft
[AIAA PAPER 83-1162] p 6 A83-45508
A survey of inlet/engine distortion compatibility
[AIAA PAPER 83-1166] p 6 A83-45509
Aerodynamic performance of a fan stage utilizing Variable Inlet Guide Vanes (VIGVs) for thrust modulation --- subsonic V/STOL aircraft
[NASA-TM-83438] p 13 N83-27957
A survey of inlet/engine distortion compatibility
[NASA-TM-83421] p 37 N83-27991
Evaluation of fuel additives for reduction of material imcompatibilities in methanol-gasoline blends
[NASA-CR-168061] p 86 N83-29359

COMPENSATION
A novel feedforward compensation canceling input filter-regulator interaction p 112 A83-33133

COMPLEX COMPOUNDS
Analysis of the visible spectra of concentrated chromic chloride solutions
[NASA-CR-172998] p 74 N83-32870
Spectrophotometric analysis of aqueous mixtures of some chromium (III) complexes
[NASA-CR-172999] p 74 N83-32872
COMPOSITE MATERIALS
On composites with periodic structure
p 154 A83-10283
Composites with periodic microstructure
p 62 A83-12734
Composite fan exit guide vanes for high bypass ratio gas turbine engines p 19 A83-13159
Applications of ion beam technology
[NASA-CR-169797] p 82 N83-16493
Fatigue testing of low-cost fiberglass composite wind turbine blade materials
[NASA-CR-165566] p 177 N83-22746
Design and evaluation of low-cost laminated wood composite blades for intermediate size wind turbines: Blade design, fabrication concept, and cost analysis
[NASA-CR-165463] p 179 N83-23704
Piezoelectric composite materials
[NASA-CASE-LEW-12582-1] p 207 N83-34796
COMPOSITE STRUCTURES
Geometrically nonlinear analysis of layered composite shells p 156 A83-27431
Three-dimensional finite-element analysis of layered composite plates p 156 A83-27432
Design concepts for low cost composite engine frames
[AIAA PAPER 83-2445] p 25 A83-48331
Design and fabrication of composite blades for the Mod-1 wind turbine generator
[NASA-CR-167987] p 168 N83-11579
Design and evaluation of low cost blades for large wind driven generating systems p 175 N83-19244
Design procedures for fiber composite structural components: Rods, columns and beam columns
[NASA-TM-83321] p 66 N83-24559
Evaluation of low-cost aluminum composites for aircraft engine structural applications
[NASA-TM-83357] p 66 N83-25790
COMPRESSIBILITY
Tensile and compressive constitutive response of 316 stainless steel at elevated temperatures
p 162 N83-34353
COMPRESSIBLE FLOW
Three-dimensional compressible viscous analysis of mixer nozzles
[AIAA PAPER 83-1401] p 4 A83-36391
Measurements of compressible secondary flow in a circular S-duct
[AIAA PAPER 83-1739] p 4 A83-37218
Numerical solution of the Navier-Stokes equations for compressible turbulent two/three dimensional flows in the terminal shock region of an inlet/diffuser
[AIAA PAPER 83-1892] p 5 A83-39358
A semi-direct solver for compressible three-dimensional rotational flow
[AIAA PAPER 83-1909] p 122 A83-39367
Implicit marching solution of compressible viscous subsonic flow in planar and axisymmetric ducts
[NASA-TM-82876] p 125 N83-10389
Three dimensional flow computations in a turbine scroll
[NASA-CR-168003] p 10 N83-12045
Calculation of compressible flow in and about three-dimensional inlets with and without auxiliary inlets by a higher-order panel method
[NASA-CR-168009] p 10 N83-12047
Convergence acceleration of viscous flow computations
[NASA-TM-83039] p 190 N83-12930
Numerical solutions of Navier-Stokes equations for compressible turbulent two/three dimensional flows in terminal shock region of an inlet/diffuser
[NASA-CR-3723] p 132 N83-34230
A semi-direct solver for compressible 3-dimensional rotational flow
[NASA-TM-83314] p 15 N83-34908
COMPRESSION LOADS
Benchmark notch test for life prediction
[NASA-CR-165571] p 158 N83-12451
Ignition and combustion: Low compression ratio, high output diesel
[NASA-CR-169742] p 31 N83-15309
Design procedures for fiber composite structural components: Rods, columns and beam columns
[NASA-TM-83321] p 66 N83-24559
Optimum parallel step-sector bearing lubricated with an incompressible fluid
[NASA-TM-83356] p 148 N83-24855
Vortex motion in axisymmetric piston-cylinder configurations
[NASA-TM-85404] p 133 N83-35318
COMPRESSION RATIO
Numerical studies of the formation and destruction of vortices in a motored four-stroke piston-cylinder configuration
[AIAA PAPER 83-0497] p 136 A83-16749
COMPRESSION TESTS
Research priorities and history of advanced composite compression testing
[NASA-CR-165415] p 66 N83-18854
Compression and compression fatigue testing of composite laminates
[NASA-CR-168023] p 66 N83-26928
COMPRESSOR BLADES
Experimental evaluation of shockless supercritical airfoils in cascade
[AIAA PAPER 83-0003] p 2 A83-16455
A method of predicting the performance deterioration of a compressor cascade due to sand erosion
[AIAA PAPER 83-0178] p 19 A83-16572
Effect of particle presence on the incompressible inviscid flow through a two dimensional compressor cascade
[ASME PAPER 83-GT-95] p 8 A83-47941
Analysis of an axial compressor blade vibration based on wave reflection theory
[ASME PAPER 83-GT-151] p 25 A83-47970
Analysis, design, fabrication and testing of an optical tip clearance sensor --- turbocompressor blade tips
[NASA-CR-165265] p 26 N83-11127
Energy efficient engine low-pressure compressor component test hardware detailed design report
[NASA-CR-165354] p 39 N83-30427
Subsonic-transonic stall flutter study
[NASA-CR-165256] p 43 N83-30435
Control means for a gas turbine engine
[NASA-CASE-LEW-14586-1] p 40 N83-31603
COMPRESSOR EFFICIENCY
Effect of humidity on jet engine axial-flow compressor performance p 22 A83-35856
Effect of particle presence on the incompressible inviscid flow through a two dimensional compressor cascade
p 6 A83-42562
COMPRESSOR ROTORS
Investigation of the tip clearance flow inside and at the exit of a compressor rotor passage. II - Turbulence properties p 4 A83-28843
Tip clearance flow in a compressor rotor passage at design and off-design conditions p 4 A83-35855
Powder metallurgy Rene 95 rotating turbine engine parts, volume 2
[NASA-CR-165141] p 82 N83-15412
End wall flows in rotors and stators of a single stage compressor
[NASA-CR-169800] p 128 N83-16678
Three dimensional flow field inside compressor rotor, including blade boundary layers
[NASA-CR-169788] p 128 N83-16679
Energy efficient engine low-pressure compressor component test hardware detailed design report
[NASA-CR-165354] p 39 N83-30427
Comparison of two- and three-dimensional flow computations with laser anemometer measurements in a transonic compressor rotor
[NASA-TP-1931] p 15 N83-32774
COMPRESSORS
Performance of a tandem-rotor/tandem-stator conical-flow compressor designed for a pressure ratio of 3
[NASA-TP-2034] p 9 N83-11058
Advanced technologies for turbomachinery systems: An overview
[NASA-TM-82949] p 28 N83-12090
Effect of steady-state pressure distortion on inlet flow to a high-bypass-ratio turbofan engine
[NASA-TM-82964] p 30 N83-15306
Environmental solid particle effects on compressor cascade performance
[NASA-CR-168018] p 11 N83-16285
Compressor cascade performance deterioration caused by sand ingestion
[NASA-CR-168067] p 11 N83-16286
Summary report for CF6 jet engine diagnostics program
[NASA-CR-165582] p 32 N83-17539
Literature search of publications concerning the prediction of dynamic inlet flow distortion and related topics
[NASA-CR-3673] p 33 N83-18729
Advanced Gas Turbine (AGT) powertrain system development for automotive applications
[NASA-CR-167901] p 212 N83-33800
The trend of future gas turbine technology
[NASA-TM-83505] p 2 N83-34886
COMPUTATION
Multiple-grid convergence acceleration of viscous and inviscid flow computations
[NASA-TM-83361] p 190 N83-21847
Convergence and stability properties of minimal polynomial and reduced rank extrapolation algorithms
[NASA-TM-83443] p 191 N83-31390
COMPUTATIONAL FLUID DYNAMICS
Finite analytic numerical solution of axisymmetric Navier-Stokes and energy equations
[ASME PAPER 82-HT-42] p 118 A83-12795
Development of secondary flow and vorticity in curved ducts, cascades, and rotors, including effects of viscosity and rotation p 119 A83-16141
A method of predicting the performance deterioration of a compressor cascade due to sand erosion
[AIAA PAPER 83-0178] p 19 A83-16572
A viscous-inviscid interactive procedure for rotational flow in cascades of two-dimensional airfoils of arbitrary shape
[AIAA PAPER 83-0256] p 3 A83-16614
Confined swirling flow predictions
[AIAA PAPER 83-0316] p 119 A83-16646
Transient flow analysis of the AEDC/HPDE MHD generator
[AIAA PAPER 83-0395] p 203 A83-16691
Multi-grid solution of Neumann pressure problem for viscous flows using primitive variables
[AIAA PAPER 83-0557] p 120 A83-16786
Numerical solution to the glancing sidewall oblique shock wave/turbulent boundary layer interaction in three-dimension
[AIAA PAPER 83-0136] p 3 A83-16823
A finite element formulation for steady transonic Euler equations p 3 A83-22129
Computed and measured turbulence in axisymmetric reciprocating engines p 21 A83-24669
A basic code for the prediction of transient three-dimensional turbulent flowfields
p 121 A83-27412
Solid particle dynamic behavior through twisted blade rows p 3 A83-27478
A two-equation turbulence model for two-phase flows
p 121 A83-30109
The evolution of Tollmien-Schlichting waves near a leading edge. II - Numerical determination of amplitudes
p 122 A83-35346
Mode propagation in nonuniform circular ducts with potential flow p 122 A83-36082
Importance of inlet boundary conditions for numerical simulation of combustor flows
[AIAA PAPER 83-1263] p 23 A83-36314
Prediction of an axisymmetric combusting flow
[AIAA PAPER 83-1264] p 69 A83-36315
Three-dimensional compressible viscous analysis of mixer nozzles
[AIAA PAPER 83-1401] p 4 A83-36391
Quasi-three-dimensional turbomachinery flow calculations on multiple hub-to-shroud stream surfaces
[AIAA PAPER 83-1620] p 5 A83-38652
Solution of viscous internal flows on curvilinear grids generated by the Schwarz-Christoffel transformation
p 122 A83-38796
An experience in mesh generation for three-dimensional calculation of potential flow around a rotating propeller
p 5 A83-38798
Numerical solution of the Navier-Stokes equations for compressible turbulent two/three dimensional flows in the terminal shock region of an inlet/diffuser
[AIAA PAPER 83-1892] p 5 A83-39358
Efficient solution of the Euler and Navier-Stokes equations with a vectorized multiple-grid algorithm
[AIAA PAPER 83-1893] p 5 A83-39359
A semi-direct solver for compressible three-dimensional rotational flow
[AIAA PAPER 83-1909] p 122 A83-39367
A fast Euler solver for steady flows
[AIAA PAPER 83-1940] p 123 A83-39389
Multiple-gridding of the Euler equations with an implicit scheme
[AIAA PAPER 83-1945] p 5 A83-39392
Study of asymptotic incompressible flow in curved ducts using a multi-grid technique p 123 A83-42532
Finite analytic numerical solution of heat transfer and flow past a square channel cavity p 123 A83-42703
Design of supercritical cascades with high solidity
p 6 A83-43446
Finite volume calculation of three-dimensional potential flow around a propeller p 7 A83-45577
Inlet-fan flow field computation
[ASME PAPER 83-GT-41] p 7 A83-47901
A theory of rotating stall of multistage axial compressors. II - Finite disturbances
[ASME PAPER 83-GT-45] p 8 A83-47905

Effect of particle presence on the incompressible inviscid flow through a two dimensional compressor cascade [ASME PAPER 83-GT-95] p 8 A83-47941
Convergence acceleration of viscous flow computations [NASA-TM-83039] p 190 N83-12930
A rapid blade-to-blade solution for use in turbomachinery design [NASA-TM-83010] p 10 N83-13077
Surface roughness effects in hydrodynamic lubrication: The flow factor method [NASA-TM-83024] p 129 N83-19016
Numerical solution to the glancing sidewall oblique shock wave/turbulent boundary layer interaction in three dimension [NASA-TM-83056] p 34 N83-22199
The finite analytic method, volume 3 [NASA-CR-170186] p 191 N83-23087
The finite analytic method, volume 4 [NASA-CR-170187] p 191 N83-23088
The finite analytic method, volume 5 [NASA-CR-170188] p 191 N83-23089
Efficient solution of the Euler and Navier-Stokes equations with a vectorized multiple-grid algorithm [NASA-TM-83376] p 2 N83-24467
A 4-cylinder Stirling engine computer program with dynamic energy equations [NASA-TM-83053] p 130 N83-26017
User's manual for Axisymmetric Diffuser Duct (ADD) code. Volume 2: Detailed ADD code description [NASA-CR-165598-VOL-2] p 211 N83-26758
Applications of the contravariant form of the Navier-Stokes equations [NASA-TM-83448] p 14 N83-29179
Semidirect computations for transonic flow [NASA-TM-83451] p 15 N83-34909

COMPUTATIONAL GRIDS

Automatic algebraic coordinate generation p 189 A83-36793
Efficient solution of the Euler and Navier-Stokes equations with a vectorized multiple-grid algorithm [AIAA PAPER 83-1893] p 5 A83-39359
A fast Euler solver for steady flows [AIAA PAPER 83-1940] p 123 A83-39389
Multiple-gridding of the Euler equations with an implicit scheme [AIAA PAPER 83-1945] p 5 A83-39392
Study of asymptotic incompressible flow in curved ducts using a multi-grid technique p 123 A83-42532
Multiple-grid convergence acceleration of viscous and inviscid flow computations [NASA-TM-83361] p 190 N83-21847
Efficient solution of the Euler and Navier-Stokes equations with a vectorized multiple-grid algorithm [NASA-TM-83376] p 2 N83-24467

COMPUTER AIDED DESIGN

Parametric study of minimum reactor mass in energy-storage dc-to-dc converters p 110 A83-11011
Nonlinear program based optimization of boost and buck-boost converter designs p 110 A83-11016
The design and technology development for A 150 mlb resistojet for H2 or NH3 [AIAA PAPER 82-1949] p 52 A83-12506
Computer simulations of optimum boost and buck-boost converters p 111 A83-19032
Computation techniques and computer programs to analyze Stirling cycle engines using characteristic dynamic energy equations p 207 A83-27272
Structural tailoring of engine blades (STAEBL) [AIAA 83-0828] p 22 A83-29737
The development of a generalized advanced propeller analysis system [AIAA PAPER 83-2466] p 26 A83-49581
A rapid blade-to-blade solution for use in turbomachinery design [NASA-TM-83010] p 10 N83-13077
Improved design of subcritical and supercritical cascades using complex characteristics and boundary layer correction [NASA-CR-168166] p 12 N83-24474
Small gas turbine combustor primary zone study [NASA-CR-168122] p 149 N83-28448
Vibration in planetary gear systems with unequal planet stiffnesses [NASA-TM-83428] p 150 N83-29709
Stirling engine design manual, 2nd edition [NASA-CR-168088] p 212 N83-30328

COMPUTER DESIGN

Design of a high-speed digital processing element for parallel simulation [NASA-TM-83373] p 117 N83-29597

COMPUTER GRAPHICS

Perspectives on the mixing of a row of jets with a confined crossflow [NASA-TM-83457] p 15 N83-30392

COMPUTER PROGRAMS

Software and system level tests of a test flight mercury ion thruster subsystem [AIAA PAPER 82-1912] p 51 A83-12485
Thermoelastohydrodynamic analysis of an oil pumping ring seal p 137 A83-22322
Pseudo-updated constrained solution algorithm for nonlinear heat conduction p 121 A83-32989
Perspectives on the mixing of a row of jets with a confined crossflow [AIAA PAPER 83-1200] p 122 A83-36276
Automatic algebraic coordinate generation p 189 A83-36793
The development of a generalized advanced propeller analysis system [AIAA PAPER 83-2466] p 26 A83-49581
A computer program for the calculation of the flow field including boundary layer effects for mixed-compression inlets at angle of attack [NASA-CR-168002] p 10 N83-11066
Experimental program for the evaluation of turbofan/turboshaft c conversion technology [NASA-TM-82988] p 27 N83-11130
A software system for emission spectrometry [NASA-TM-83001] p 70 N83-12181
Large displacements and stability analysis of nonlinear propeller structures p 159 N83-12460
Design of a multistage depressed collector for the F-16 radar dual mode transmitter tube [NASA-TM-82982] p 114 N83-14399
Feasibility of water injection into the turbine coolant to permit gas turbine contingency power for helicopter application [NASA-TM-83043] p 31 N83-15307
Development of a multiple-parameter nonlinear perturbation procedure for transonic turbomachinery flows: Preliminary application to design/optimization problems [NASA-CR-3657] p 2 N83-17453
User's manual for three-dimensional analysis of propeller flow fields [NASA-CR-167959] p 12 N83-18671
Free yaw performance of the Mod-0 large horizontal axis 100 kW wind turbine p 175 N83-19235
Predicted and experimental performance of large-bore high-speed ball and roller bearings p 145 N83-20131
Computer program to minimize prediction error in models from experiments with 16 hypercube points and 0 to 6 center points [NASA-TM-82995] p 192 N83-21872
Design analysis of a self-acting spiral-groove ring seal for counter-rotating shafts [NASA-TP-2142] p 36 N83-25712
User's manual for Axisymmetric Diffuser Duct (ADD) code. Volume 1: General ADD code description [NASA-CR-165598-VOL-1] p 211 N83-26757
User's manual for Axisymmetric Diffuser Duct (ADD) code. Volume 3: ADD code coordinate generator [NASA-CR-165598-VOL-3] p 211 N83-26759
Test results and description of a 1-kW free-piston Stirling engine with a dashpot load [NASA-TM-83407] p 182 N83-27346
Capabilities, limitations, and use of BC SAT-R2 conference software [NASA-TM-83383] p 107 N83-29493
Perspectives on the mixing of a row of jets with a confined crossflow [NASA-TM-83457] p 15 N83-30392
Aerothermal modeling program, phase 1 [NASA-CR-168202] p 131 N83-30959
Propeller performance and weight predictions appended to the Navy/NASA engine program [NASA-TM-83458] p 41 N83-32810

COMPUTER SYSTEMS PERFORMANCE

Optical systolic array processor using residue arithmetic p 189 A83-46834

COMPUTER TECHNIQUES

Present technology of rolling-element bearings p 144 N83-20121
A study of dynamic energy equations for Stirling cycle analysis [NASA-CR-168152] p 181 N83-25043

COMPUTERIZED SIMULATION

An analytical evaluation of the icing properties of several low and medium speed airfoils [AIAA PAPER 83-0109] p 3 A83-16525
Computer simulations of optimum boost and buck-boost converters p 111 A83-19032
Numerical simulation of a disk-shaped electron accelerating electrostatic probe p 133 A83-22336
A basic code for the prediction of transient three-dimensional turbulent flowfields p 121 A83-27412
Control design and performance analysis of a 6 MW wind turbine-generator p 165 A83-29897
Numerical simulation of airfoil ice accretion [AIAA PAPER 83-0112] p 16 A83-36042
Importance of inlet boundary conditions for numerical simulation of combustor flows [AIAA PAPER 83-1263] p 23 A83-36314
Numerical simulation of the flow and fuel-air mixing in an axisymmetric piston-cylinder arrangement [NASA-TM-83011] p 126 N83-12358
A 4-cylinder Stirling engine computer program with dynamic energy equations [NASA-TM-83053] p 130 N83-26017
Comparison of road load simulator test results with track tests on electric vehicle propulsion system [NASA-TM-83393] p 184 N83-29811
Propeller performance and weight predictions appended to the Navy/NASA engine program [NASA-TM-83458] p 41 N83-32810
An analytical investigation of NO sub x control techniques for methanol fueled spark ignition engines [NASA-CR-172847] p 151 N83-33168

CONCENTRATION (COMPOSITION)

Microdistribution of oxygen in silicon and its effects on electronic properties p 172 N83-15825
Spectrophotometric analysis of aqueous mixtures of some chromium (III) complexes [NASA-CR-172999] p 74 N83-32872

CONCENTRATORS

Design rules for a 100X maximum efficiency GaAs concentrator solar cell for space applications [NASA-CR-170005] p 177 N83-20362

CONDUCTIVE HEAT TRANSFER

Boundary integral equation method calculations of surface regression effects in flame spreading p 67 A83-13488
Pseudo-updated constrained solution algorithm for nonlinear heat conduction p 121 A83-32989
Design and development of multi-kW power electronic transformers --- for long duration space applications [NASA-CR-168082] p 116 N83-29596

CONES

Some experiments on Yaw stability of wind turbines with various coning angles [NASA-CR-168108] p 177 N83-22740

CONFERENCES

COSAM (Conservation Of Strategic Aerospace Materials) program overview [NASA-TM-83006] p 78 N83-11282
Space Photovoltaic Research and Technology 1982: High Efficiency, Radiation Damage, and Blanket Technology [NASA-CP-2256] p 171 N83-15806
Large Horizontal-Axis Wind Turbines [NASA-CP-2230] p 175 N83-19231
Advanced Power Transmission Technology [NASA-CP-2210] p 144 N83-20119
Aviation Gasolines and Future Alternatives [NASA-CP-2267] p 100 N83-22442
Combustion Fundamentals Research [NASA-CP-2268] p 38 N83-29208
Nonlinear Constitutive Relations for High Temperature Applications [NASA-CP-2271] p 161 N83-34351

CONICAL FLOW

Performance of a tandem-rotor/tandem-stator conical-flow compressor designed for a pressure ratio of 3 [NASA-TP-2034] p 9 N83-11058

CONSERVATION

COSAM program overview p 78 N83-11283

CONSTANTS

Kinetics of copper ion absorption by cross-linked calcium polyacrylate membranes [NASA-TM-83052] p 61 N83-25786

CONSTITUTIVE EQUATIONS

Nonlinear structural and life analyses of a combustor liner p 155 A83-12764
Requirements of constitutive models for two nickel-base superalloys p 74 A83-21071
An uncoupled viscoplastic constitutive model for metals at elevated temperature [AIAA 83-1016] p 156 A83-29798
Materials constitutive models for nonlinear analysis of thermally cycled structures [NASA-TP-2055] p 158 N83-12449

CONTACT RESISTANCE

Infrared emission spectrophotometric study of the changes produced by TIN coating of metal surfaces in an operating EHD contact [NASA-TM-82989] p 92 N83-15466

CONTAMINANTS

Stochastic differential equations and turbulent dispersion [NASA-RP-1103] p 129 N83-22546
Experimental design of an interlaboratory study for trace metal analysis of liquid fluids --- for aerospace vehicles [NASA-TP-2148] p 73 N83-24575

CONTINGENCY
Feasibility of water injection into the turbine coolant to permit gas turbine contingency power for helicopter application
[NASA-TM-83043] p 31 N83-15307
CONTINUITY (MATHEMATICS)
High level continuity for coordinate generation with precise controls p 190 A83-29632
CONTOURS
Microscopic contour changes of tribological surfaces by chemical and mechanical action
[ASLE PREPRINT 82-LC-3B-3] p 136 A83-13237
A turbulence model for three dimensional turbulent shear flows over curved rotating bodies
[AIAA PAPER 83-0559] p 120 A83-16787
Analytical and experimental investigation of stator endwall contouring in a small axial-flow turbine. 1: Stator performance
[NASA-TP-2023] p 26 N83-11125
CONTRAROTATING PROPELLERS
Technology and benefits of aircraft counter rotation propellers
[NASA-TM-82983] p 27 N83-11129
CONTROL EQUIPMENT
A novel feedforward compensation canceling input filter-regulator interaction p 112 A83-33133
Components for digitally controlled aircraft engines
[NASA-CR-165296] p 28 N83-12089
CONTROL STABILITY
Investigations of stability and dynamic performances of switching regulators employing current-injected control p 110 A83-11002
Control design and performance analysis of a 6 MW wind turbine-generator p 165 A83-29897
CONTROL THEORY
Rotordynamic Instability Problems in High-Performance Turbomachinery
[NASA-CP-2250] p 142 N83-15629
NASA propulsion controls research
[NASA-TM-83343] p 36 N83-25711
CONTROL VALVES
Air modulation apparatus — cooling gas turbine engines
[NASA-CASE-LEW-13524-1] p 131 N83-30957
Control means for a gas turbine engine
[NASA-CASE-LEW-14586-1] p 40 N83-31603
CONTROLLERS
Controller scheduling - A possible algebraic viewpoint p 190 A83-37093
A lightweight electronically commutated dc motor for electric passenger vehicles
[NASA-CR-165601] p 113 N83-10348
Improved transistorized AC motor controller for battery powered urban electric passenger vehicles
[NASA-CR-167978] p 113 N83-10349
Improved SCR ac motor controller for battery powered urban electric vehicles
[NASA-CR-167919] p 209 N83-16257
New propulsion components for electric vehicles
[NASA-TM-83404] p 116 N83-25982
CONVECTIVE FLOW
Noise generation by a finite span swept airfoil
[AIAA PAPER 83-0768] p 195 A83-28023
A numerical study of the steady scalar convective diffusion equation for small viscosity
[NASA-CR-172231] p 16 N83-35909
CONVECTIVE HEAT TRANSFER
Finite analytic numerical solution of axisymmetric Navier-Stokes and energy equations
[ASME PAPER 82-HT-42] p 118 A83-12795
Measurement of thermoacoustic convection heat transfer phenomenon
[AIAA PAPER 83-1422] p 121 A83-32701
A mixing-length model for the prediction of convex curvature effects on turbulent boundary layers — for turbine blade convective heat transfer prediction
[ASME PAPER 83-GT-80] p 125 A83-47933
The finite analytic method, volume 5
[NASA-CR-170188] p 191 N83-23089
CONVERGENCE
Formal convergence characteristics of elliptically constrained incremental Newton-Raphson algorithms p 190 A83-10273
Convergence acceleration of viscous flow computations
[NASA-TM-83039] p 190 N83-12930
Fast Euler solver for steady, 1-dimensional flows
[NASA-CR-3689] p 14 N83-27960
Convergence and stability properties of minimal polynomial and reduced rank extrapolation algorithms
[NASA-TM-83443] p 191 N83-31390
CONVERGENT NOZZLES
JT15D 1/2-scale nozzle jet noise experiment and comparison with prediction
[NASA-TM-83370] p 201 N83-27793
COOLANTS
Film-cooling effectiveness with developing coolant flow through straight and curved tubular passages
[NASA-TP-2062] p 126 N83-12360
Aerodynamic effect of a honeycomb rotor tip shroud on a 50.8-centimeter-tip-diameter core turbine
[NASA-TP-2112] p 32 N83-17547
COOLING
Feasibility of water injection into the turbine coolant to permit gas turbine contingency power for helicopter application
[NASA-TM-83043] p 31 N83-15307
The JT8D and JT9D engine component improvement: Performance improvement program
[NASA-CR-167965] p 32 N83-17543
Steam cooled rich-burn combustor liner
[NASA-CASE-LEW-13609-1] p 72 N83-17628
Energy efficient engine sector combustor rig test program
[NASA-CR-167913] p 33 N83-19753
Burner rig study of variables involved in hole plugging of air cooled turbine engine vanes
[NASA-TM-83308] p 83 N83-19887
JT9D thermal barrier coated vanes
[NASA-CR-167964] p 37 N83-27993
Preliminary tests of an advanced high-temperature combustion system
[NASA-TP-2203] p 41 N83-33893
COOLING SYSTEMS
Analysis of coolant entrance boundary shape of porous region to control cooling along exit boundary p 124 A83-43361
COORDINATE TRANSFORMATIONS
Coordinate generation with precise controls over mesh properties p 190 A83-29631
High level continuity for coordinate generation with precise controls p 190 A83-29632
Automatic algebraic coordinate generation p 189 A83-38793
Solution of viscous internal flows on curvilinear grids generated by the Schwarz-Christoffel transformation p 122 A83-38796
COORDINATES
Input generator for Denton 3-dimensional turbomachine-blade-row analysis code
[NASA-TM-23324] p 13 N83-26817
Analytical calculation of a single jet in cross-flow and comparison with experiment p 38 N83-29219
COPOLYMERIZATION
Chemical approach for controlling nadamide cure temperature and rate
[NASA-CASE-LEW-13770-1] p 91 N83-13258
Chemical approach for controlling nadamide cure temperature and rate
[NASA-CASE-LEW-13770-2] p 96 N83-30651
COPOLYMERS
Polyvinyl alcohol membranes as alkaline battery separators
[NASA-TM-82961] p 70 N83-10135
Preparation, characterization, physical testing and performance of fluorocarbon membranes and separators
[NASA-CR-167880] p 73 N83-26936
COPPER
The initial stages of cavitation damage and erosion on copper and brass tested in a rotating disk device p 75 A83-27421
Industrial ion source technology
[NASA-CR-159677] p 102 N83-12259
Initial stages of cavitation damage and erosion on copper and brass tested in a rotating disk device
[NASA-TM-82993] p 81 N83-13231
The orthogonal in-situ machining of single and polycrystalline aluminum and copper, volume 2
[NASA-CR-169528] p 81 N83-13233
Microstructural analysis of solar cell welds p 172 N83-15833
COPPER ALLOYS
Cavitation erosion of copper, brass, aluminum and titanium alloys in mineral oil
[NASA-TM-83402] p 148 N83-24856
COPPER CHLORIDES
Metallic conductivity and air stability in copper chloride intercalated carbon fibers p 111 A83-16095
CORIOLIS EFFECT
Aerodynamic stiffness of an unbound eccentric whirling centrifugal impeller with an infinite number of blades p 142 N83-15650
CORRELATION COEFFICIENTS
Regression analysis of traction characteristics of traction fluids
[NASA-TP-2154] p 148 N83-24862
CORROSION
Combustion system processes leading to corrosive deposits p 69 A83-42246
Friction and wear of iron and nickel in sodium hydroxide solutions p 77 A83-46922
Friction and wear of iron and nickel in sodium hydroxide solutions
[NASA-TM-82935] p 77 N83-10171
Tribology p 140 N83-12167
Reactions of NaCl with gaseous SO3, SO2, and O2
[NASA-TM-83423] p 86 N83-29358
Reaction of cobalt in SO2 atmospheric at elevated temperatures
[NASA-TM-83485] p 88 N83-35104
CORROSION PREVENTION
Heat pipes containing alkali metal working fluid
[NASA-CASE-LEW-12253-1] p 203 N83-19596
Evaluation of fuel additives for reduction of material incompatibilities in methanol-gasoline blends
[NASA-CR-168061] p 86 N83-29359
CORROSION RESISTANCE
Review of factors that influence fretting wear p 137 A83-17259
Advanced ceramic coating development for industrial/utility gas turbine applications
[NASA-CR-165619] p 92 N83-15467
Corrosion of simulated bearing components of three bearing steels in the presence of chloride-contaminated lubricant
[NASA-TM-82955] p 143 N83-20115
Effect of carbide distribution on rolling-element fatigue life of AMS 5749
[NASA-TP-2189] p 151 N83-33186
The effects of metals and inhibitors on thermal oxidative degradation reactions of unbranched perfluoroalkylethers
[NASA-TM-83464] p 97 N83-34049
Covering solid, film cooled surfaces with a duplex thermal barrier coating
[NASA-CASE-LEW-13450-1] p 103 N83-35177
CORROSION TESTS
Effect of the amount of Na2SO4 on the high temperature corrosion of Udimet-700
[NASA-TM-83459] p 87 N83-34016
CORRUGATED PLATES
Stability analysis of Centaur-in-Shuttle composite corrugated adapters
[AIAA 83-1003] p 49 A83-29791
COSMIC RAYS
Environmentally induced discharges on satellites p 105 N83-14365
COST ANALYSIS
Conceptual design and cost analysis of hydraulic output unit for 15 kW free-piston Stirling engine
[NASA-CR-165543] p 167 N83-10561
Preliminary assessment of the tradeoffs between the electric motor and the transmission in electric vehicles
[NASA-CR-168199] p 117 N83-30915
COST EFFECTIVENESS
A summary of EHV propulsion technology — Electric and Hybrid Vehicle p 209 A83-31087
COST ESTIMATES
Future satellite systems - Market demand assessment p 104 A83-19762
Mod-2 wind turbine project assessment and cluster test plans p 176 N83-19262
COUNTER ROTATION
Design analysis of a self-acting spiral-groove ring seal for counter-rotating shafts — o ring seals
[AIAA PAPER 83-1134] p 137 A83-36239
Technology and benefits of aircraft counter rotation propellers
[NASA-TM-82983] p 27 N83-11129
Design analysis of a self-acting spiral-groove ring seal for counter-rotating shafts — o ring seals
[NASA-TM-83346] p 35 N83-23306
COUPLING
Effects of structural coupling on mistuned cascade flutter and response
[NASA-TM-83049] p 159 N83-15672
COUPLING CIRCUITS
Spacecraft IF switch matrix for wideband service applications in 30/20 GHz communications satellite systems: Proof-of-concept model, executive summary
[NASA-CR-168175] p 107 N83-29492
COVERINGS
Tip cap for a rotor blade
[NASA-CASE-LEW-13654-1] p 30 N83-14129
CRACK GEOMETRY
Growth and stability of interacting surface flaws of arbitrary shape p 155 A83-15060
CRACK INITIATION
Requirements of constitutive models for two nickel-base superalloys p 74 A83-21071
Turbine blade nonlinear structural and life analysis p 21 A83-29024
A brittle to ductile transition in NiAl of a critical grain size p 75 A83-29726
Fatigue crack initiation and propagation in several nickel-base superalloys at 650 C p 76 A83-41199

CRACK PROPAGATION
Moving cracks in layered composites p 155 A83-12048
Growth and stability of interacting surface flaws of arbitrary shape p 155 A83-15060
The effect of microstructure on the fatigue behavior of Ni base superalloys p 75 A83-36166
Dynamic fields near a crack tip growing in an elastic-perfectly-plastic solid p 157 A83-38528
Fatigue crack initiation and propagation in several nickel-base superalloys at 650 C p 76 A83-41199
A total life prediction model for stress concentration sites
[NASA-CR-170290] p 160 N83-23629
Crack layer morphology and toughness characterization in steels
[NASA-CR-168154] p 160 N83-27256
Solution of elastic and elasto-plastic problems by the method of lines
[NASA-CR-168125] p 85 N83-28208
CRACK TIPS
Dynamic fields near a crack tip growing in an elastic-perfectly-plastic solid p 157 A83-38528
CRACKING (FRACTURING)
Stress intensity and displacement coefficients for radially cracked ring segments subject to three-point bending
[NASA-TM-83059] p 160 N83-24874
CRACKS
Rotordynamic Instability Problems in High-Performance Turbomachinery
[NASA-CP-2250] p 142 N83-15629
Method of fabricating an abradable gas path seal
[NASA-CASE-LEW-13269-2] p 93 N83-17714
Analysis of an externally radially cracked ring segment subject to three-point radial loading
[NASA-TM-83482] p 163 N83-35413
CRASHES
Assessment of crash fire hazard of LH sub 2 fueled aircraft
[NASA-CR-165525] p 16 N83-11095
CREEP ANALYSIS
Strainrange partitioning: A total strain range version
[NASA-TM-83023] p 81 N83-14246
Creep of plasma sprayed zirconia
[NASA-CR-167868] p 96 N83-29393
CREEP PROPERTIES
The effect of annealing on the creep of plasma sprayed ceramics
[NASA-TM-83396] p 130 N83-24799
Relation of cyclic loading pattern to microstructural fracture in creep fatigue
[NASA-TM-83473] p 161 N83-34349
Constrained self-adaptive solutions procedures for structure subject to high temperature elastic-plastic creep effects p 162 N83-34370
Stress and fracture analyses under elastic-plastic creep conditions: Some basic developments and computational approaches p 162 N83-34371
SSME main combustion chamber life prediction
[NASA-CR-168215] p 60 N83-36101
CREEP RUPTURE STRENGTH
Effects on stress rupture life and tensile strength of tin additions to Inconel 718 p 79 N83-11299
Orientation dependence of the stress rupture properties of Nickel-base superalloy single crystals
[NASA-CR-165394] p 206 N83-13009
Creep-rupture behavior of 6 candidate stirling engine iron-base superalloys in high pressure hydrogen. Volume 1: Air creep-rupture behavior
[NASA-CR-168071] p 83 N83-22389
CREEP STRENGTH
SiC or B4C-B/low strategic element content composite p 80 N83-11308
CREEP TESTS
Creep of plasma-sprayed-ZrO2 thermal-barrier coatings p 89 A83-22273
Gamma prime shape changes during creep of a nickel-base superalloy p 77 A83-47855
CRITICAL FLOW
Studies of flows through N-sequential orifices
[NASA-TM-83313] p 129 N83-19020
CROSS FLOW
Perspectives on the mixing of a row of jets with a confined crossflow
[AIAA PAPER 83-1200] p 122 A83-36276
Effects of free stream turbulence intensity and integral length scale on heat transfer from a circular cylinder in crossflow p 123 A83-42711
Spanwise mass transfer variations on a cylinder in 'nominally' uniform crossflow p 124 A83-43019
Heat transfer characteristics for jet array impingement with initial crossflow
[ASME PAPER 83-GT-28] p 7 A83-47891
Dilution Jet Mixing Program, phase 1
[NASA-CR-168031] p 128 N83-15590
Jet array impingement flow distributions and heat transfer characteristics. Effects of initial crossflow and nonuniform array geometry --- gas turbine engine component cooling
[NASA-CR-3630] p 128 N83-15592
Analytical calculation of a single jet in cross-flow and comparison with experiment p 38 N83-29219
Perspectives on the mixing of a row of jets with a confined crossflow
[NASA-TM-83457] p 15 N83-30392
Experiments in dilution jet mixing
[NASA-TM-83434] p 15 N83-30393
Stagnation region gas film cooling: Effects of dimensionless coolant temperature
[NASA-CR-168197] p 132 N83-30960
CROSSLINKING
Polyvinyl alcohol cross-linked with two aldehydes
[NASA-CASE-LEW-13504-1] p 71 N83-13188
Development and evaluation of polyvinyl-alcohol blend polymer films as battery separators
[NASA-TM-82981] p 71 N83-15372
Preparation, characterization, physical testing and performance of fluorocarbon membranes and separators
[NASA-CR-167880] p 73 N83-26936
Low temperature cross linking polyimides
[NASA-CASE-LEW-12676-2] p 96 N83-29392
Use of high L.E.T. radiation to improve adhesion of metals to polytetrafluoroethylene
[NASA-TM-83413] p 96 N83-30660
Ion exchange selectivity for cross-linked polyacrylic acid
[NASA-TM-83427] p 97 N83-35142
CRUISING FLIGHT
A preliminary comparison between the SR-6 propeller noise in flight and in a wind tunnel
[NASA-TM-83341] p 201 N83-24287
CRYOGENIC FLUID STORAGE
Long term storage of cryogens in space p 102 A83-11487
Cryogenic fluid management experiment trunnion fatigue verification
[AIAA PAPER 83-0911] p 49 A83-32782
CRYOGENIC FLUIDS
Acoustic velocities of two-phase mixtures of cryogenic fluids p 124 A83-43012
CRYOGENIC ROCKET PROPELLANTS
Vapor flow into a capillary propellant-acquisition device
[AIAA PAPER 83-1380] p 55 A83-36371
Modeling of space vehicle propellant mixing --- cryogenic propellants
[NASA-TP-2107] p 100 N83-16545
High speed cryogenic self-acting, shaft seals for liquid rocket turbopumps
[NASA-CR-168194] p 151 N83-32070
CRYOGENICS
Development of tough, strong, iron-base alloy for cryogenic applications p 44 N83-18763
A refrigerated dynamic seal
[NASA-TM-83378] p 130 N83-24798
Study of LH2-fueled topping cycle engine for aircraft propulsion
[NASA-TM-83466] p 41 N83-34942
CRYSTAL DISLOCATIONS
Liquid encapsulated Czochralski growth of low dislocation GaAs p 204 A83-13784
High purity, low dislocation GaAs single crystals
[NASA-CR-168098] p 206 N83-19622
CRYSTAL GROWTH
Production of large-area single-crystal wafers of cubic SiC for semiconductor devices p 205 A83-22767
Microdistribution of oxygen in silicon and its effects on electronic properties p 172 N83-15825
Radiation damage and annealing in large area n+/p/p+ GaAs shallow homojunction solar cells p 172 N83-15826
High purity, low dislocation GaAs single crystals
[NASA-CR-168098] p 206 N83-19622
CRYSTAL LATTICES
Dipole-field sums and Lorentz factors for orthorhombic lattices, and implications for polarizable molecules p 204 A83-17226
Piezoelectricity and pyroelectricity in polyvinylidene fluoride - Influence of the lattice structure p 205 A83-29531
CRYSTAL STRUCTURE
Morphological and frictional behavior of sputtered MoS2 films p 88 A83-12652
Piezoelectricity and pyroelectricity in polyvinylidene fluoride - Influence of the lattice structure p 205 A83-29531
CRYSTAL SURFACES
Diamond /111/ studied by electron energy loss spectroscopy in the characteristic loss region p 68 A83-25675
XPS, AES and friction studies of single-crystal silicon carbide p 89 A83-36973
CRYSTALLIZATION
Mechanisms of devitrification of grain boundary glassy phases in Si3N4 materials
[NASA-CR-169670] p 71 N83-14177
Sliding induced crystallization of metallic glass
[NASA-TP-2140] p 83 N83-21110
CUMULATIVE DAMAGE
Morphology of ductile metals eroded by a jet of spherical particles impinging at normal incidence p 75 A83-32624
CURING
Synthesis and characterization of bisimide amines and bisimide amine-cured epoxy resins p 88 A83-11488
Bisimide amine cured epoxy /IME/ resins and composites. II - Ten-degree off-axis tensile and shear properties of Celion 6000/IME composites p 62 A83-23608
Dynamic mechanical characterization of cure of a polyimide-graphite fiber composite (PMR 15/Celion 6000) p 62 A83-31793
Lower-curing-temperature PMR polyimides p 89 A83-40923
Lower-curing-temperature PMR polyimides
[NASA-TM-82958] p 63 N83-10118
Chemical approach for controlling nadamide cure temperature and rate
[NASA-CASE-LEW-13770-1] p 91 N83-13258
CURRENT DENSITY
Deep discharge reconditioning and shorted storage of batteries --- nickel cadmium batteries
[NASA-CR-167953] p 166 N83-10502
CURRENT REGULATORS
An improved switching converter model
[NASA-CR-169669] p 114 N83-14398
CUTTERS
Geometrical analysis of circular-cut spiral bevel gears
[NASA-CR-168226] p 151 N83-33167
CYCLES
Cyclic oxidation of superalloys p 76 A83-42234
Expected cycle life versus depth of discharge relationships of well behaved single cells and cell strings
[NASA-TM-82957] p 167 N83-10558
Evaluation program for secondary spacecraft cells. Cycle life test
[NASA-CR-172679] p 162 N83-27351
CYCLIC LOADS
Requirements of constitutive models for two nickel-base superalloys p 74 A83-21071
Low cycle fatigue behavior of aluminum/stainless steel composites
[AIAA 83-0806] p 62 A83-29886
Hygrothermomechanical evaluation of transverse filament tape epoxy/polyester fiberglass composites
[NASA-TM-83044] p 65 N83-15362
Experimental verification of the Neuber relation at room and elevated temperatures --- to predict stress-strain behavior in notched specimens of hastelloy x
[NASA-CR-167957] p 159 N83-19121
Development of a simplified analytical method for representing material cyclic response
[NASA-CR-168100] p 160 N83-21390
Relation of cyclic loading pattern to microstructural fracture in creep fatigue
[NASA-TM-83473] p 161 N83-34349
Simplified method for nonlinear structural analysis
[NASA-TP-2208] p 163 N83-34372
SSME main combustion chamber life prediction
[NASA-CR-168215] p 60 N83-36101
CYCLOTRON RESONANCE DEVICES
Gyrotron transmitting tube
[NASA-CASE-LEW-13429-1] p 117 N83-31912
CYLINDRICAL BODIES
NASA LeRC/Akron University Graduate Cooperative Fellowship Program and Graduate Student Researchers Program
[NASA-CR-167943] p 208 N83-10970
Turbine endwall single cylinder program
[NASA-CR-170008] p 44 N83-19761
CYLINDRICAL CHAMBERS
Vortex motion in axisymmetric piston-cylinder configurations
[NASA-TM-85404] p 133 N83-35318
CYLINDRICAL SHELLS
Vibrations of cantilevered circular cylindrical shells Shallow versus deep shell theory p 157 A83-36958
Comparison of predicted and experimental external heat transfer around a film cooled cylinder in crossflow
[NASA-TM-83017] p 127 N83-13392
CZOCHRALSKI METHOD
Liquid encapsulated Czochralski growth of low dislocation GaAs p 204 A83-13784
Residual double acceptors in bulk GaAs p 205 A83-19989

EL2 distributions in doped and undoped liquid encapsulated Czochralski GaAs — deep donor concentration p 205 A83-22756
Advances in large-diameter liquid encapsulated Czochralski GaAs p 171 N83-15819
Microdistribution of oxygen in silicon and its effects on electronic properties p 172 N83-15825
High purity, low dislocation GaAs single crystals [NASA-CR-168098] p 206 N83-19622
Growth and characterization of Czochralski-grown n and p-type GaAs for space solar cell substrates [NASA-CR-168099] p 207 N83-27877

D

DAMAGE ASSESSMENT
Spherical micro-glass particle impingement studies of thermoplastic materials at normal incidence [NASA-TM-83410] p 94 N83-25883
DAMPERS
Design of dry-friction dampers for turbine blades p 22 A83-35883
DAMPERS (VALVES)
Multiple plate hydrostatic viscous damper [NASA-CASE-LEW-13445-2] p 143 N83-17883
DATA ACQUISITION
High speed computerized data acquisition of photovoltaic V-I characteristics [NASA-TM-82967] p 114 N83-14397
Free-jet acoustic investigation of high-radius-ratio coannular plug nozzles. Comprehensive data report, volume 2 [NASA-CR-168066-VOL-2] p 199 N83-18409
Investigation of continuously traversing microphone system for mode measurement [NASA-CR-168040] p 199 N83-19575
DATA COMPRESSION
A new architecture for adaptive transform compression of NTSC composite video signal p 103 A83-19732
DATA MANAGEMENT
Particle-sampling statistics in laser anemometers Sample-and-hold systems and saturable systems p 134 A83-48120
DATA PROCESSING
Development of electrical test procedures for qualification of spacecraft against EID. Volume 1: The CAN test and other relevant data [NASA-CR-165590] p 49 N83-12136
Investigation of continuously traversing microphone system for mode measurement [NASA-CR-168040] p 199 N83-19575
DATA PROCESSING EQUIPMENT
Frequency-multiplexed and pipelined iterative optical systolic array processors p 188 A83-18588
DATA TRANSMISSION
Advances in Serial MSK modems p 111 A83-19789
Satellite provided fixed communication services: A forecast of potential domestic demand through the year 2000. Volume 1: Executive summary [NASA-CR-168145] p 108 N83-34113
Satellite fixed communications service: A forecast of potential domestic demand through the year 2000. Volume 3: Appendices [NASA-CR-168147] p 108 N83-34115
Satellite provided customer premises services: A forecast of potential domestic demand through the year 2000. Volume: Executive summary [NASA-CR-168142] p 109 N83-34116
Satellite provided customer premise services: A forecast of potential domestic demand through the year 2000. Volume 3: Appendices [NASA-CR-168144] p 109 N83-34118
Advanced digital modulation: Communication techniques and monolithic GaAs technology [NASA-CR-174452] p 109 N83-36299
DECODERS
A low-power, high-throughput maximum-likelihood convolutional decoder chip for NASA's 30/20 GHz program p 111 A83-19754
DECOMPOSITION
LU and Cholesky decomposition on an optical systolic array processor p 189 A83-43629
Refinement and application of acoustic impulse technique to study nozzle transmission characteristics [NASA-CR-3656] p 199 N83-20708
DEFLECTION
Experimental results of a deflected thrust V/STOL nozzle research program [AIAA PAPER 83-0170] p 6 A83-42100
Experimental results of a deflected thrust V/STOL nozzle research program [NASA-TM-83069] p 12 N83-25657
DEFORMATION
Finite element analysis of steadily moving contact fields p 158 A83-49437
PMR-15 polyimide modifications for improved prepreg tack [NASA-TM-82951] p 64 N83-12175
Stress and fracture analyses under elastic-plastic creep conditions: Some basic developments and computational approaches p 162 N83-34371
DEGRADATION
Radiation damage in front and back illuminated high resistivity silicon solar cells [NASA-TM-82965] p 206 N83-10962
Use of high pressure liquid chromatography in the study of liquid lubricant oxidation [NASA-TM-83033] p 92 N83-14270
Analysis of a MIL-L-27502 lubricant from a gas-turbine engine test by size-exclusion chromatography [NASA-TP-2063] p 93 N83-16528
DEICERS
NASA Lewis Research Center's program on icing research [AIAA PAPER 83-0204] p 1 A83-16582
NASA Lewis Research Center's Program on Icing Research [NASA-TM-83031] p 16 N83-14078
DEICING
A method of predicting flow rates required to achieve anti-icing performance with a porous leading edge ice protection system [NASA-CR-169996] p 17 N83-19738
Numerical simulation of an electrothermal deicer pad [NASA-CR-168097] p 17 N83-23281
Piezoelectric deicing device [NASA-CASE-LEW-13773-1] p 18 N83-29197
DEMODULATION
Modulation techniques [NASA-CR-169460] p 105 N83-10329
DENSIFICATION
Sintering, properties and fabrication of Si3N4 + Y2O3 based ceramics p 90 A83-48303
DENSITOMETERS
High accuracy fuel flowmeter, phase 1 [NASA-CR-167893] p 134 N83-21314
DEOXYGENATION
Effect of deoxygenation and prestressing on hydrocarbon fuel thermal stability [NASA-TM-83406] p 102 N83-35160
DEPOSITION
Correlation and prediction of thermophoretic and inertial effects on particle deposition from non-isothermal turbulent boundary layers p 121 A83-27481
Combustion system processes leading to corrosive deposits p 69 A83-42246
Plasma deposition and surface modification techniques for wear resistance [NASA-TM-82972] p 90 N83-10194
Studies of the mechanisms of turbine fuel instability [NASA-CR-167963] p 100 N83-18924
Burner rig study of variables involved in hole plugging of air cooled turbine engine vanes [NASA-TM-83308] p 83 N83-19887
DEPOSITS
Deposit formation in hydrocarbon rocket fuels: Executive summary [NASA-CR-165492] p 102 N83-35159
Effect of deoxygenation and prestressing on hydrocarbon fuel thermal stability [NASA-TM-83456] p 102 N83-35160
DESIGN ANALYSIS
End region effects upon the performance of a magnetohydrodynamic channel p 203 A83-10665
MHD channel performance for potential early commercial MHD power plants p 204 A83-23134
Design flexibility of redox flow systems — for energy storage applications p 164 A83-27177
Tip clearance flow in a compressor rotor passage at design and off-design conditions p 4 A83-35855
A comprehensive method for preliminary design optimization of axial gas turbine stages. II - Code verification [AIAA PAPER 83-1403] p 24 A83-36393
Conceptual design and cost analysis of hydraulic output unit for 15 kW free-piston Stirling engine [NASA-CR-165543] p 167 N83-10561
Automotive Stirling Engine Mod 1 Design Review, volume 2 [NASA-CR-167936] p 209 N83-10991
Magnetohydrodynamics (MHD) Engineering Test Facility (ETF) 200 MWe power plant. Conceptual Design Engineering Report (CDER) supplement. Magnet system special investigations [NASA-CR-165509] p 141 N83-14494
Operating experience with the 200 kW MOD-0A wind turbine generators p 174 N83-15916
Design study of a high power rotary transformer [NASA-CR-168012] p 115 N83-16630
Development of a multiple-parameter nonlinear perturbation procedure for transonic turbomachinery flows: Preliminary application to design/optimization problems [NASA-CR-3657] p 2 N83-17453
Large Horizontal-Axis Wind Turbines [NASA-CP-2230] p 175 N83-19231
The response of a 38m horizontal axis teetered rotor to yaw p 175 N83-19232
Fixed pitch rotor performance of large horizontal axis wind turbines p 175 N83-19233
Stall induced instability of a teetered rotor p 175 N83-19234
Free yaw performance of the Mod-0 large horizontal axis 100 kW wind turbine p 175 N83-19235
Experience and assessment of the DOE/NASA Mod-1 2000 kW wind turbine generator at Boone, North Carolina p 176 N83-19257
Mod-2 wind turbine project assessment and cluster test plans p 176 N83-19262
High speed spherical roller-bearing analysis and comparison with experimental performance p 145 N83-20133
Traction calculations and design data for two traction fluids p 145 N83-20136
The optimal design of standard gearsets p 146 N83-20145
New test techniques and analytical procedures for understanding the behavior of advanced propellers [NASA-TM-83360] p 2 N83-22092
Preliminary design of flight hardware for two-phase fluid research [NASA-CR-168072] p 46 N83-25766
Small gas turbine combustor primary zone study [NASA-CR-168122] p 149 N83-28448
Application of advanced reliability methods to local strain fatigue analysis [NASA-CR-168198] p 161 N83-29734
Scaled centrifugal compressor, collector and running gear program [NASA-CR-168167] p 40 N83-30432
Nonlinear Constitutive Relations for High Temperature Applications [NASA-CP-2271] p 161 N83-34351
DETERIORATION
A method of predicting the performance deterioration of a compressor cascade due to sand erosion [AIAA PAPER 83-0178] p 18 A83-16572
Summary report for CF6 jet engine diagnostics program [NASA-CR-165582] p 32 N83-17539
DEVELOPING NATIONS
Market assessment of photovoltaic power systems for agricultural applications worldwide [NASA-CR-165541] p 168 N83-13585
DEW
Water vapor measurement system in global atmospheric sampling program, appendix [NASA-TP-2051] p 187 N83-13643
DEW POINT
Comparison of modern icing cloud instruments [NASA-CR-166008] p 19 N83-18720
DIAMINES
Polyimides formulated from a partially fluorinated diamine for aerospace tribological applications [NASA-TM-83339] p 94 N83-22423
DIAMONDS
Diamond /111/ studied by electron energy loss spectroscopy in the characteristic loss region p 68 A83-25675
Growth of diamondlike films for power applications p 174 N83-15880
Diamondlike flake composites — for use in aerospace structures and components [NASA-CASE-LEW-13837-1] p 67 N83-28095
DIATOMIC MOLECULES
Diatomic molecules and metallic adhesion, cohesion, and chemisorption - A single binding-energy relation p 69 A83-30921
DIBUTYL COMPOUNDS
Effect of oxygen concentration in ZDP containing oils on surface composition and wear [NASA-TM-83000] p 84 N83-24636
DIELECTRIC PROPERTIES
Thermal dielectric breakdown with cylindrical electrodes p 112 A83-38216
High frequency, high power capacitor development [NASA-CR-168035] p 116 N83-27127
DIELECTRICS
Ellipsometric study of silicon nitride on gallium arsenide p 204 A83-11812
Effects of gaps on long range surface plasmon polaritons p 204 A83-46271
Mass analysis of neutral particles and ions released during electrical breakdowns on spacecraft surfaces [NASA-CR-170299] p 50 N83-23347

DIES
The thermal fatigue resistance of H-13 Die Steel for aluminum die casting dies
[NASA-TM-83331] p 87 N83-35103
DIESEL ENGINES
Wind turbine generator interaction with diesel generators on an isolated power system p 165 A83-44673
Further industrial tests of ceramic thermal barrier coatings
[NASA-TP-2057] p 26 N83-10045
Performance and emissions characteristics of aqueous alcohol fumes in a DI diesel engine
[NASA-CR-167917] p 99 N83-12250
Fumigation of alcohol in a light duty automotive diesel engine
[NASA-CR-167915] p 99 N83-13272
Ignition and combustion: Low compression ratio, high output diesel
[NASA-CR-169742] p 31 N83-15309
Analysis of the economics of photovoltaic-diesel-battery energy systems for remote applications
[NASA-TM-83377] p 179 N83-23709
Characterization of a high-pressure diesel fuel injection system as a control technology option to improve engine performance and reduce exhaust emissions
[NASA-TM-83329] p 210 N83-24431
DIESEL FUELS
Catalytic combustion with steam injection
[ASME PAPER 82-JPGC-GT-23] p 164 A83-25271
Measured effect of wind generation on the fuel consumption of an isolated diesel power system p 165 A83-36410
Catalytic combustion with steam injection
[NASA-TM-82923] p 170 N83-15805
Experimental study of the thermal stability of hydrocarbon fuels
[NASA-CR-168027] p 100 N83-17728
Studies of the mechanisms of turbine fuel instability
[NASA-CR-167963] p 100 N83-18924
DIFFERENTIAL EQUATIONS
Stochastic differential equations and turbulent dispersion
[NASA-RP-1103] p 129 N83-22546
The finite analytic method, volume 3
[NASA-CR-170186] p 191 N83-23087
The finite analytic method, volume 5
[NASA-CR-170188] p 191 N83-23089
Time-independent anisotropic plastic behavior by mechanical subelement models p 162 N83-34369
Theoretical investigation of the force and dynamically coupled torsional-axial-lateral dynamic response of eared rotors
[NASA-CR-173013] p 191 N83-34656
DIFFERENTIAL GEOMETRY
Geometrical analysis of circular-cut spiral bevel gears
[NASA-CR-168226] p 151 N83-33167
DIFFUSERS
Effects of interstage diffuser flow distortion on the performance of a 15.41-centimeter tip diameter axial power turbine
[AIAA PAPER 83-1179] p 23 A83-36263
User's manual for Axisymmetric Diffuser Duct (ADD) code. Volume 1: General ADD code description
[NASA-CR-165598-VOL-1] p 211 N83-26757
DIFFUSION
Turbine engine materials durability research p 29 N83-12163
Analytical calculation of a single jet in crossflow and comparison with experiment
[NASA-TM-83027] p 29 N83-14127
Diffusion length measurements in solar cells: An analysis and comparison of techniques p 171 N83-15812
Diffused P+-N solar cells in bulk GaAs p 171 N83-15818
Developments toward an 18% efficient silicon solar cell
[NASA-CR-168141] p 181 N83-25112
A numerical study of the steady scalar convective diffusion equation for small viscosity
[NASA-CR-172231] p 16 N83-35999
DIFFUSION COEFFICIENT
Search for selective ion diffusion through membranes
[NASA-TM-83426] p 97 N83-34048
DIFFUSION FLAMES
Numerical solution of the problem of flame propagation by the use of the random element method
[AIAA PAPER 83-0600] p 69 A83-36062
Experimental study of the thermal-acoustic efficiency in a long turbulent diffusion-flame burner
[NASA-CR-3725] p 202 N83-33683
DIFFUSION WELDING
Metal honeycomb to porous wireform substrate diffusion bond evaluation p 153 A83-39020
DIFFUSIVITY
A new diffusion-inhibited oxidation-resistant coating for superalloys p 74 A83-10299
Determination of hydrogen permeability in uncoated and coated superalloys
[NASA-CR-165209] p 80 N83-12215
DIGITAL INTEGRATORS
VLSI technology and applications
[NASA-CR-174451] p 118 N83-36358
DIGITAL SIMULATION
Digital system for structural dynamics simulation
[NASA-CR-168019] p 43 N83-14139
DIGITAL SYSTEMS
Components for digitally controlled aircraft engines
[NASA-CR-165296] p 28 N83-12089
Design of a high-speed digital processing element for parallel simulation
[NASA-TM-83373] p 117 N83-29597
DIGITAL TECHNIQUES
Modulation techniques
[NASA-CR-169460] p 105 N83-10329
Army/NASA small turboshaft engine digital controls research program
[NASA-TM-82979] p 27 N83-11128
DIGITAL TO ANALOG CONVERTERS
GaAs integrated digital-to-analogue convertor for control of power dual-gate FETs p 112 A83-36479
DILUTION
Dilution Jet Mixing Program, phase 1
[NASA-CR-168031] p 128 N83-15590
DIMENSIONAL ANALYSIS
Modeling of space vehicle propellant mixing — cryogenic propellants
[NASA-TP-2107] p 100 N83-16545
DIMENSIONS
Length to diameter ratio and row number effects in short pin fin heat transfer
[NASA-TM-83005] p 127 N83-14431
DIMERS
Oxidation and formation of deposit precursors in hydrocarbon fuels
[NASA-CR-168121] p 101 N83-23465
DIRECT CURRENT
A lightweight electronically commutated dc motor for electric passenger vehicles
[NASA-CR-165601] p 113 N83-10348
Losses in chopper-controlled DC series motors
[NASA-CR-167845] p 114 N83-13359
Improved SCR ac motor controller for battery powered urban electric vehicles
[NASA-CR-167919] p 209 N83-16257
Advanced axial field D.C. motor development for electric passenger vehicle
[NASA-CR-167985] p 117 N83-30914
DIRECTIONAL SOLIDIFICATION (CRYSTALS)
Effect of swaging on the 1000 C compressive slow plastic flow characteristics of the directionally solidified eutectic alloy gamma/gamma prime-alpha p 77 A83-44340
DISKS (SHAPES)
Effect of sliding speed and contact stress on tribological properties of ultra-high-molecular-weight polyethylene
[NASA-TP-2059] p 91 N83-14269
DISPERSING
Stochastic differential equations and turbulent dispersion
[NASA-RP-1103] p 129 N83-22546
DISPERSION
Progress toward determining the potential of ODS alloys for gas turbine applications
[NASA-TM-83332] p 83 N83-22387
DISPERSIONS
The effect of stress on ultrasonic pulses in fiber reinforced composites
[NASA-CR-3724] p 154 N83-33180
DISPLACEMENT
Large displacements and stability analysis of nonlinear propeller structures p 159 N83-12460
Measurements of self-excited rotor-blade vibrations using optical dispacements
[NASA-TM-82953] p 159 N83-14523
Analysis of an externally radially cracked ring segment subject to three-point radial loading
[NASA-TM-83482] p 163 N83-35413
DISPLACEMENT MEASUREMENT
Stress intensity and displacement coefficients for radially cracked ring segments subject to three-point bending
[NASA-TM-83059] p 160 N83-24874
DISTILLATION
Tests of blending and correlation of distillate fuel properties p 98 A83-11050
DISTORTION
A survey of inlet/engine distortion compatibility
[AIAA PAPER 83-1166] p 6 A83-45509
Dynamic distortion in a short s-shaped subsonic diffuser with flow separation — Lewis 8 by 6 foot Supersonic Wind Tunnel
[AIAA PAPER 83-1412] p 25 A83-45515
Dynamic distortion in a short s-shaped subsonic diffuser with flow separation — Lewis 8 by 6 foot Supersonic Wind Tunnel
[NASA-TM-83412] p 36 N83-26838
A survey of inlet/engine distortion compatibility
[NASA-TM-83421] p 37 N83-27991
DISTRIBUTED PROCESSING
Digital system for structural dynamics simulation
[NASA-CR-168019] p 43 N83-14139
Parallel, Asynchronous Executive (PAX): System concepts, facilities, and architecture
[NASA-TP-2179] p 189 N83-28921
DISTRIBUTION (PROPERTY)
Thermionic energy converters
[NASA-CASE-LEW-12443-1] p 184 N83-32175
DISTRIBUTION FUNCTIONS
Theoretical results for starved elliptical contacts
[NASA-TM-81697] p 150 N83-29710
DOMESTIC SATELLITE COMMUNICATIONS SYSTEMS
Advanced communications satellite systems p 47 A83-49855
DONOR MATERIALS
EL2 distributions in doped and undoped liquid encapsulated Czochralski GaAs — deep donor concentration p 205 A83-22756
DOPED CRYSTALS
EL2 distributions in doped and undoped liquid encapsulated Czochralski GaAs — deep donor concentration p 205 A83-22756
DOPES
Effects of processing and dopant on radiation damage removal in silicon solar cells p 170 N83-14708
DOWNLINKING
Onboard processing for a 30/20 GHz communications satellite p 47 A83-41391
DROP SIZE
Influence of multidroplet size distribution on icing collection efficiency
[AIAA PAPER 83-0110] p 187 A83-16526
Droplet size effects on NO/x/ formation in a one-dimensional monodisperse spray combustion system
[ASME PAPER 82-JPGC-GT-10] p 68 A83-25268
Experimental comparison of icing cloud instruments
[AIAA PAPER 83-0026] p 16 A83-42099
Comparison of modern icing cloud instruments
[NASA-CR-168008] p 19 N83-18720
The structure of particle-laden jets and nonevaporating sprays
[NASA-CR-168059] p 34 N83-20948
Experimental comparison of icing cloud instruments
[NASA-TM-83340] p 17 N83-24487
DROPS (LIQUIDS)
An analytical evaluation of the icing properties of several low and medium speed airfoils
[AIAA PAPER 83-0109] p 3 A83-16525
Aerodynamic-wave break-up of liquid sheets in swirling airflows and combustor modules
[AIAA PAPER 83-1204] p 124 A83-45511
Analytical modeling of operating characteristics of premixing-prevaporizing fuel-air mixing passages. Volume 1: Analysis and results
[NASA-CR-167990-VOL-1] p 126 N83-12353
Analytical modeling of operating characteristics of premixing-prevaporizing fuel-air mixing passages. Volume 2: User's manual
[NASA-CR-167990-VOL-2] p 126 N83-12354
Aerodynamic-wave break-up of liquid sheets in swirling airflows and combustor modules
[NASA-TM-83353] p 130 N83-23545
Structure of evaporating and combusting sprays: Measurements and predictions p 38 N83-29211
Fuel spray diagnostics p 38 N83-29212
DRY FRICTION
Morphological and frictional behavior of sputtered MoS2 films p 88 A83-12652
Effects of friction dampers on aerodynamically unstable rotor stages
[AIAA PAPER 83-0848] p 22 A83-32791
Design of dry-friction dampers for turbine blades p 22 A83-35883
The dryout region in frictionally heated sliding contacts p 124 A83-42762
DUCTED FANS
Sound propagation in segmented exhaust ducts - Theoretical predictions and comparison with measurements
[AIAA PAPER 83-0734] p 194 A83-28016
Investigation of continuously traversing microphone system for mode measurement
[NASA-CR-168040] p 199 N83-19575

DUCTED FLOW
Development of secondary flow and vorticity in curved ducts, cascades, and rotors, including effects of viscosity and rotation p 119 A83-16141
Multi-grid solution of Neumann pressure problem for viscous flows using primitive variables
[AIAA PAPER 83-0557] p 120 A83-16786
Mode propagation in nonuniform circular ducts with potential flow p 122 A83-36082
Measurements of compressible secondary flow in a circular S-duct
[AIAA PAPER 83-1739] p 4 A83-37218
Study of asymptotic incompressible flow in curved ducts using a multi-grid technique p 123 A83-42532
Statistical characteristics of velocity, concentration, mass transport, and momentum transport for coaxial jet mixing in a confined duct
[ASME PAPER 83-GT-39] p 125 A83-47899
Three-dimensional flow measurements in a vaneless radial turbine scroll
[NASA-CR-167994] p 9 N83-11065
User's manual for Axisymmetric Diffuser Duct (ADD) code. Volume 2: Detailed ADD code description
[NASA-CR-165598-VOL-2] p 211 N83-26758
DUCTS
Cross spectra between temperature and pressure in a constant area duct downstream of a combustor
[AIAA PAPER 83-0762] p 196 A83-33487
Composite engine duct fabrication p 1 A83-39941
Analysis of combustion spectra containing organ pipe tone by cepstral techniques
[NASA-TM-83034] p 198 N83-16153
Cross spectra between temperature and pressure in a constant area duct downstream of a combustor
[NASA-TM-83351] p 200 N83-23116
Effects of interstage diffuser flow distortion on the performance of a 15.41-centimeter tip diameter axial power turbine
[NASA-TM-83359] p 35 N83-24505
User's manual for Axisymmetric Diffuser Duct (ADD) code. Volume 1: General ADD code description
[NASA-CR-165598-VOL-1] p 211 N83-26757
Experiments in dilution jet mixing
[NASA-TM-83434] p 15 N83-30393
DURABILITY
Turbine engine materials durability research p 29 N83-12163
DYNAMIC CHARACTERISTICS
Investigations of stability and dynamic performances of switching regulators employing current-injected control p 110 A83-11002
Finite-length solutions for rotodynamic coefficients of turbulent annular seals
[ASME PAPER 82-LUB-42] p 136 A83-13521
Dynamic mechanical characterization of cure of a polyimide-graphite fiber composite (PMR 15/Celion 6000) p 62 A83-31793
Dynamic mechanical properties of n-phenylnadimide modified PMR polyimide composites
[NASA-TM-83051] p 65 N83-15363
Rotordynamic Instability Problems in High-Performance Turbomachinery
[NASA-CP-2250] p 142 N83-15629
Literature search of publications concerning the prediction of dynamic inlet flow distortion and related topics
[NASA-CR-3673] p 33 N83-18729
Development of methodology for horizontal axis wind turbine dynamic analysis
[NASA-CR-168110] p 178 N83-22747
DYNAMIC LOADS
Compliance and stress sensitivity of spur gear teeth p 146 N83-20142
A method for static and dynamic load analysis of standard and modified spur gears p 146 N83-20143
Dynamic tooth loads and stressing for high contact ratio spur gears p 147 N83-20148
Labyrinth seal forces on a whirling rotor
[NASA-CR-168016] p 34 N83-22198
Vapor cavitation in dynamically loaded journal bearings
[NASA-TM-83366] p 160 N83-24875
DYNAMIC MODELS
A 4-cylinder Stirling engine computer program with dynamic energy equations
[NASA-TM-83053] p 130 N83-26017
Analytical calculation of a single jet in cross-flow and comparison with experiment p 38 N83-29219
DYNAMIC RESPONSE
Solution to the backward-Kolmogorov equation for a nonstationary oscillation problem p 192 A83-15697
Flutter and forced response of mistuned rotors using standing wave analysis
[AIAA 83-0845] p 156 A83-29823
The transfer function method for gear system dynamics applied to conventional and minimum excitation gearing designs
[NASA-CR-3626] p 139 N83-11495
Theoretical investigation of the force and dynamically coupled torsional-axial-lateral dynamic response of eared rotors
[NASA-CR-173013] p 191 N83-34656
DYNAMIC STABILITY
A refrigerated dynamic seal
[NASA-TM-83378] p 130 N83-24798
Dynamic effects of internal spur gear drives
[NASA-CR-3692] p 149 N83-28452
DYNAMIC STRUCTURAL ANALYSIS
The coupled aeroelastic response of turbomachinery blading to aerodynamic excitations
[AIAA 83-0644] p 156 A83-29822
Structural dynamics studies of rotating bladed-disk assemblies coupled with flexible shaft motions
[AIAA PAPER 83-0919] p 22 A83-32787
Blade loss transient dynamic analysis of turbomachinery p 25 A83-40864
Vibrations of blades with variable thickness and curvature by shell theory
[ASME PAPER 83-GT-152] p 158 A83-47978
Finite element analysis of steadily moving contact fields p 158 A83-49437
Digital system for structural dynamics simulation
[NASA-CR-168019] p 43 N83-14139
DYNAMOMETERS
Automotive Stirling engine development program
[NASA-CR-167907] p 209 N83-15176

E

EARTH ORBITS
Optimal sun-alignment techniques of large solar arrays in electric propulsion spacecraft
[AIAA PAPER 82-1898] p 48 A83-12475
Test results of a ten cell bipolar nickel-hydrogen battery
[NASA-TM-83384] p 181 N83-26253
Large space systems auxiliary propulsion requirements p 46 N83-26864
EARTH TERMINALS
Method for terminal position determination in Earth terminal-to-satellite burst acquisition and synchronization
[NASA-CASE-LEW-13893-1] p 107 N83-30832
ECONOMIC ANALYSIS
Satellite-aided land mobile communications system implementation considerations p 104 A83-41417
ECONOMIC FACTORS
Customer premises services market demand assessment 1980 - 2000: Volume 2
[NASA-CR-168151] p 108 N83-31926
EFFICIENCY
Comparison of spur gear efficiency prediction methods p 146 N83-20141
Small transport aircraft technology propeller study
[NASA-CR-168045] p 14 N83-29178
Preliminary assessment of the tradeoffs between the electric motor and the transmission in electric vehicles
[NASA-CR-168199] p 117 N83-30915
Propeller performance and weight predictions appended to the Navy/NASA engine program
[NASA-TM-83458] p 41 N83-32810
Analysis of the reflective multibandgap solar cell concept
[NASA-CR-168186] p 185 N83-34454
EJECTORS
Ejector nozzle test results at simulated flight conditions for an advanced supersonic transport propulsion system
[AIAA PAPER 83-1287] p 23 A83-36323
Conceptual design, evaluation and research identification for Remote Augmented Propulsive Lift Systems (RALS) with ejectors for VTOL aircraft
[NASA-CR-167906] p 29 N83-13103
Model aerodynamic test results for a refined actuated inlet ejector nozzle at simulated takeoff and cruise conditions
[NASA-CR-168051] p 13 N83-26816
ELASTIC BODIES
Composites with periodic microstructure p 62 A83-12734
ELASTIC DEFORMATION
Simplified method for nonlinear structural analysis
[NASA-TP-2208] p 163 N83-34372
ELASTIC MEDIA
Propagation of sound in highly porous open-cell elastic foams p 195 A83-28848
Surface acoustic admittance of highly porous open-cell, elastic foams p 195 A83-28849
ELASTIC PROPERTIES
Solution of elastic and elasto-plastic problems by the method of lines
[NASA-CR-168125] p 85 N83-28208
Constrained self-adaptive solutions procedures for structure subject to high temperature elastic-plastic creep effects p 162 N83-34370
ELASTIC WAVES
Measurement of thermoacoustic convection heat transfer phenomenon
[AIAA PAPER 83-1422] p 121 A83-32701
Phenomenological and mechanics aspects of nondestructive evaluation and characterization by sound and ultrasound of material and fracture properties
[NASA-CR-3623] p 153 N83-11506
The transmission or scattering of elastic waves by an inhomogeneity of simple geometry: A comparison of theories
[NASA-CR-3659] p 153 N83-16773
ELASTODYNAMICS
The determination of the elastodynamic fields of an ellipsoidal inhomogeneity
[ASME PAPER 83-APM-19] p 157 A83-37388
ELASTOHYDRODYNAMICS
Infrared emission spectrophotometric study of the changes produced by TiN coating of metal surfaces in an operating EHD contact
[ASLE PREPRINT 82-LC-3C-3] p 135 A83-13229
Thermoelastohydrodynamic analysis of an oil pumping ring seal p 137 A83-22322
The influence of surface dents and grooves on traction in sliding EHD point contacts p 138 A83-37823
Surface temperatures and glassy state investigations in tribology, part 5
[NASA-CR-3632] p 91 N83-11328
Elastohydrodynamic lubrication theory
[NASA-TM-81695] p 140 N83-12432
Theoretical results for fully flooded, elliptical hydrodynamic contacts
[NASA-TM-81696] p 140 N83-13458
Infrared emission spectrophotometric study of the changes produced by TiN coating of metal surfaces in an operating EHD contact
[NASA-TM-82989] p 92 N83-15466
Elastohydrodynamic lubrication of elliptical contacts p 141 N83-15514
A detailed treatment of two-dimensional, starved lubrication in the vicinity of two counter-rotating cylinders p 141 N83-15520
Geometry and starvation effects in hydrodynamic lubrication p 141 N83-15522
Elastohydrodynamic lubrication of rectangular contacts
[NASA-TP-2111] p 143 N83-16759
Assessment of lubricated contacts: Mechanisms of scuffing and scoring
[NASA-TM-83074] p 144 N83-20118
Lubrication background
[NASA-TM-81692] p 147 N83-20159
Regression analysis of traction characteristics of traction fluids
[NASA-TP-2154] p 148 N83-24862
Elastohydrodynamic contacts. Effects of dents and grooves on traction and local film thickness
[NASA-TP-2175] p 150 N83-28453
Non-Newtonian fluid model incorporated into elastohydrodynamic lubrication of rectangular contacts
[NASA-TM-83318] p 150 N83-28454
Theoretical results for starved elliptical contacts
[NASA-TM-81697] p 150 N83-29710
Experimental investigations of elastohydrodynamic lubrication
[NASA-TM-81698] p 150 N83-29711
Elastohydrodynamics of elliptical contacts for materials of low elastic modulus
[NASA-TM-81699] p 151 N83-29712
Applications of film thickness equations
[NASA-TM-81701] p 151 N83-29713
Thermal elastohydrodynamic lubrication of line contacts
[NASA-TM-83424] p 152 N83-34326
ELASTOMERS
Power turbine dynamics - An evaluation of a shear-mounted elastomeric damper
[ASME PAPER 83-GT-228] p 139 A83-48025
ELASTOPLASTICITY
On the solution of elastic-plastic static and dynamic postbuckling collapse of general structure p 155 A83-12746
Dynamic fields near a crack tip growing in an elastic-perfectly-plastic solid p 157 A83-38528
Three-dimensional elastoplastic stress analysis of unidirectional boron/aluminum composites
[NASA-CR-169796] p 65 N83-16394
Solution of elastic and elasto-plastic problems by the method of lines
[NASA-CR-168125] p 85 N83-28208

ELECTRIC ARCS
Effects of arc current on the life in burner-rig thermal cycling of plasma-sprayed ZrO2-O3 p 89 A83-22270
ELECTRIC AUTOMOBILES
Tests of an alternating current propulsion subsystem for electric vehicles on a road load simulator
[NASA-TM-83036] p 178 N83-22749
Preliminary assessment of the tradeoffs between the electric motor and the transmission in electric vehicles
[NASA-CR-168199] p 117 N83-30915
ELECTRIC BATTERIES
Expected cycle life vs. depth of discharge relationships of well-behaved single cells and cell strings
p 165 A83-32627
Expected cycle life versus depth of discharge relationships of well behaved single cells and cell strings
[NASA-TM-82957] p 167 N83-10558
Improved SCR ac motor controller for battery powered urban electric vehicles
[NASA-CR-167919] p 209 N83-16257
The electrochemical fluorination of polymeric materials for high energy density aqueous and non-aqueous battery and fuel cell separators
[NASA-CR-167961] p 72 N83-21056
Analysis of the economics of photovoltaic-diesel-battery energy systems for remote applications
[NASA-TM-83377] p 179 N83-23709
Cycle life test and failure model of nickel-hydrogen cells
[NASA-TM-83375] p 180 N83-25038
NASA Redox Project status summary
[NASA-TM-83401] p 183 N83-29810
Photovoltaic stand-alone modular systems, phase 2
[NASA-CR-168230] p 186 N83-35497
Moderate temperature rechargeable sodium batteries
[NASA-CR-168220] p 118 N83-36359
ELECTRIC CHARGE
Deep discharge reconditioning and shorted storage of batteries — nickel cadmium batteries
[NASA-CR-167953] p 166 N83-10502
ELECTRIC CHOPPERS
Results of chopper-controlled discharge life cycling studies on lead-acid batteries p 164 A83-27183
Losses in chopper-controlled DC series motors
[NASA-CR-167845] p 114 N83-13359
ELECTRIC CONTACTS
The effect of Ta2O5 on the interaction between silicon and its contact metallization
[NASA-TM-82948] p 166 N83-10554
Solar cell having improved back surface reflector
[NASA-CASE-LEW-13620-1] p 168 N83-13579
ELECTRIC CURRENT
High speed computerized data acquisition of photovoltaic V-1 characteristics
[NASA-TM-82967] p 114 N83-14397
ELECTRIC DIPOLES
Dipole-field sums and Lorentz factors for orthorhombic lattices, and implications for polarizable molecules
p 204 A83-17226
ELECTRIC DISCHARGES
Expected cycle life vs. depth of discharge relationships of well-behaved single cells and cell strings
p 165 A83-32627
Expected cycle life versus depth of discharge relationships of well behaved single cells and cell strings
[NASA-TM-82957] p 167 N83-10558
Environmentally induced discharges on satellites
p 105 N83-14365
ELECTRIC ENERGY STORAGE
Parametric study of minimum reactor mass in energy-storage dc-to-dc converters p 110 A83-11011
Electromagnetic studies of redox systems for energy storage
[NASA-CR-169593] p 169 N83-14667
Single cell performance studies on the Fe/Cr Redox Energy Storage System using mixed reactant solutions at elevated temperature
[NASA-TM-83385] p 180 N83-25042
Evaluation program for secondary spacecraft cells. Cycle life test
[NASA-CR-172679] p 182 N83-27351
Evaluation program for secondary spacecraft cells. Cycle life test
[NASA-CR-172680] p 183 N83-27352
Analysis of the visible spectra of concentrated chromic chloride solutions
[NASA-CR-172996] p 74 N83-32870
ELECTRIC FILTERS
A novel input filter compensation scheme for switching regulators p 111 A83-11494
A novel feedforward compensation canceling input filter-regulator interaction p 112 A83-33133
ELECTRIC GENERATORS
Wind turbine generator interaction with diesel generators on an isolated power system p 165 A83-44673
Advanced electrical power system technology for the all electric aircraft
[NASA-TM-83390] p 115 N83-24764
Control of large wind turbine generators connected to utility networks
[NASA-CR-168200] p 185 N83-34451
ELECTRIC HYBRID VEHICLES
A summary of EHV propulsion technology — Electric and Hybrid Vehicle p 209 A83-31087
ELECTRIC MOTOR VEHICLES
Transistorized PWM inverter-induction motor drive system p 110 A83-11488
A lightweight electronically commutated dc motor for electric passenger vehicles
[NASA-CR-165601] p 113 N83-10348
Improved transistorized AC motor controller for battery powered urban electric passenger vehicles
[NASA-CR-167978] p 113 N83-10349
Testing of the permanent magnet material Mn-Al-C for potential use in propulsion motors for electric vehicles
[NASA-CR-169481] p 114 N83-12329
Losses in chopper-controlled DC series motors
[NASA-CR-167845] p 114 N83-13359
Improved SCR ac motor controller for battery powered urban electric vehicles
[NASA-CR-167919] p 209 N83-16257
Advanced AC permanent magnet axial flux disc motor for electric passenger vehicle
[NASA-CR-167975] p 115 N83-16628
Tests of an alternating current propulsion subsystem for electric vehicles on a road load simulator
[NASA-TM-83036] p 178 N83-22749
New propulsion components for electric vehicles
[NASA-TM-83404] p 116 N83-25982
Advanced axial field D.C. motor development for electric passenger vehicle
[NASA-CR-167985] p 117 N83-30914
Advanced single permanent magnet axipolar ironless stator ac motor for electric passenger vehicles
[NASA-CR-167974] p 212 N83-32687
Steady-state and dynamic evaluation of the electric propulsion system test bed vehicle on a road load simulator
[NASA-TM-83445] p 186 N83-35496
ELECTRIC MOTORS
Advanced AC permanent magnet axial flux disc motor for electric passenger vehicle
[NASA-CR-167975] p 115 N83-16628
New propulsion components for electric vehicles
[NASA-TM-83404] p 116 N83-25982
Preliminary assessment of the tradeoffs between the electric motor and the transmission in electric vehicles
[NASA-CR-168199] p 117 N83-30915
Advanced single permanent magnet axipolar ironless stator ac motor for electric passenger vehicles
[NASA-CR-167974] p 212 N83-32687
ELECTRIC POTENTIAL
Potentials on large spacecraft in LEO
p 49 A83-17489
Expected cycle life versus depth of discharge relationships of well behaved single cells and cell strings
[NASA-TM-82957] p 167 N83-10558
High speed computerized data acquisition of photovoltaic V-1 characteristics
[NASA-TM-82967] p 114 N83-14397
Deep impurity trapping concepts for power semiconductor devices p 206 N83-15877
Numerical simulation of a conducting disk partially covered by an insulator interacting with a plasma
p 50 N83-18805
Analytical investigation of critical MHD phenomena
[NASA-CR-168079] p 175 N83-19228
Design considerations for large space electric power systems
[NASA-TM-83064] p 58 N83-24552
A mathematical model for the doubly fed wound rotor generator
[NASA-TM-83454] p 117 N83-34192
The role of potential barrier formation in spacecraft charging
[NASA-TM-83500] p 50 N83-35005
Test methods and results of the 10-cell bipolar Ni-H2 battery p 117 N83-35261
ELECTRIC POWER
Mod-2 wind turbine system development. Volume 2: Detailed report
[NASA-CR-168007] p 185 N83-33343
ELECTRIC POWER PLANTS
Methods of reducing energy consumption of the oxidant supply system for MHD/steam power plants
[AIAA PAPER 83-0468] p 203 A83-16735
MHD channel performance for potential early commercial MHD power plants p 204 A83-23134
Measured effect of wind generation on the fuel consumption of an isolated diesel power system
p 165 A83-36410
Develop and test fuel cell powered on-site integrated total energy system
[NASA-CR-168020] p 173 N83-15839
Task 4 completion report for 40 Kilowatt grid connected modification contract
[NASA-CR-167950] p 208 N83-30297
ELECTRIC POWER SUPPLIES
Modular photovoltaic stand-alone systems: Phase 1
[NASA-CR-168075] p 185 N83-33320
ELECTRIC POWER TRANSMISSION
Design study of a high power rotary transformer
[NASA-CR-168012] p 115 N83-16630
Design considerations for large space electric power systems
[NASA-TM-83064] p 58 N83-24552
ELECTRIC PROPULSION
Advances in series resonant inverter technology and its effect on spacecraft employing electric propulsion
[AIAA PAPER 82-1881] p 51 A83-12466
Operational summary of an electric propulsion long term test facility
[AIAA PAPER 82-1903] p 44 A83-12478
Electric rail gun projectile acceleration to high velocity
[AIAA PAPER 82-1939] p 52 A83-12501
Free radical propulsion concept p 53 A83-13141
Electric propulsion research and technology in the United States
[AIAA PAPER 82-1867] p 53 A83-16925
A summary of EHV propulsion technology — Electric and Hybrid Vehicle p 209 A83-31087
Characterization of advanced electric propulsion systems p 55 A83-33744
Analysis and design of ion thrusters for large space systems
[NASA-CR-165160] p 57 N83-14159
Design, fabrication and testing of porous tungsten vaporizers for mercury ion thrusters
[NASA-TM-83063] p 58 N83-22318
Electric thruster research
[NASA-CR-168134] p 59 N83-32843
ELECTRIC REACTORS
Parametric study of minimum reactor mass in energy-storage dc-to-dc converters p 110 A83-11011
ELECTRIC ROCKET ENGINES
Electric thruster research
[NASA-CR-168134] p 59 N83-32843
ELECTRIC SPARKS
High-voltage spark atomic emission detector for gas chromatography p 67 A83-13108
ELECTRIC SWITCHES
Solar array switching power management
p 54 A83-27132
ELECTRICAL FAULTS
Thermal dielectric breakdown with cylindrical electrodes p 112 A83-38216
Mass analysis of neutral particles and ions released during electrical breakdowns on spacecraft surfaces
[NASA-CR-170298] p 50 N83-23347
ELECTRICAL MEASUREMENT
Diffusion length measurements in solar cells: An analysis and comparison of techniques
p 171 N83-15812
ELECTRICAL PROPERTIES
Microdistribution of oxygen in silicon and its effects on electronic properties p 172 N83-15825
Design and development of multi-kW power electronic transformers — for long duration space applications
[NASA-CR-168082] p 116 N83-29596
ELECTRICAL RESISTANCE
Determination of optimum sunlight concentration level in space for 3-5 cascade solar cells p 171 N83-15814
ELECTRICAL RESISTIVITY
Some properties of r.f.-sputtered hafnium nitride coatings p 88 A83-12653
Metallic conductivity and air stability in copper chloride intercalated carbon fibers p 111 A83-16095
Radiation damage in front and back illuminated high resistivity silicon solar cells
[NASA-TM-82965] p 206 N83-10962
Piezoelectric composite materials
[NASA-CASE-LEW-12582-1] p 207 N83-34796
ELECTRO-OPTICS
Electro-optical processor for optimal control
p 133 A83-23596
Fiberoptics technology and its application to propulsion control systems
[NASA-TM-83009] p 18 N83-15302
ELECTROCATALYSTS
Zirconium carbide as an electrocatalyst for the chromous-chromic redox couple
[NASA-CASE-LEW-13246-1] p 182 N83-27344
ELECTROCHEMICAL CELLS
Experimental study of electrochemical fluorination of trichloroethylene p 68 A83-15870
Pore size engineering applied to starved electrochemical cells and batteries p 164 A83-27201

Pore size engineering applied to starved electrochemical cells and batteries
[NASA-TM-82893] p 70 N83-10134
Expected cycle life versus depth of discharge relationships of well behaved single cells and cell strings
[NASA-TM-82957] p 167 N83-10558
Evaluation program for secondary spacecraft cells. Cycle life test
[NASA-CR-172679] p 182 N83-27351
Evaluation program for secondary spacecraft cells. Cycle life test
[NASA-CR-172680] p 183 N83-27352
Preliminary results of the comparison of the electrochemical behavior of a thioether and biphenyl
[NASA-TM-83450] p 87 N83-34015

ELECTROCHEMISTRY
Electromagnetic studies of redox systems for energy storage
[NASA-CR-169593] p 169 N83-14667
The electrochemical fluorination of polymeric materials for high energy density aqueous and non-aqueous battery and fuel cell separators
[NASA-CR-167961] p 72 N83-21056
Preparation, characterization, physical testing and performance of fluorocarbon membranes and separators
[NASA-CR-167880] p 73 N83-26936
NASA Redox Project status summary
[NASA-TM-83401] p 183 N83-29810

ELECTRODES
Modern multistage depressed collectors - A review p 112 A83-24025
Thermal dielectric breakdown with cylindrical electrodes p 112 A83-38216
Electrolyte management in porous battery components. Static measurements
[NASA-TM-83073] p 72 N83-18862
Analytical investigation of critical MHD phenomena
[NASA-CR-168079] p 175 N83-19228
Optimization and fabrication of porous carbon electrodes for Fe/Cr redox flow cells
[NASA-CR-167921] p 179 N83-23708
NASA redox storage system development project
[NASA-TM-83087] p 181 N83-26252
Thermionic energy converters
[NASA-CASE-LEW-12443-1] p 184 N83-32175
Analysis of the visible spectra of concentrated chromic chloride solutions
[NASA-CR-172998] p 74 N83-32870
The chemical behavior of acidified chromium (3) solutions
[NASA-CR-172997] p 74 N83-32871

ELECTROLYTES
Pore size engineering applied to starved electrochemical cells and batteries p 164 A83-27201
Pore size engineering applied to starved electrochemical cells and batteries
[NASA-TM-82893] p 70 N83-10134
Electrolyte management in porous battery components. Static measurements
[NASA-TM-83073] p 72 N83-18862
A class of nonideal solutions. 2: Application to experimental data
[NASA-TP-1930] p 208 N83-23188
Polyvinyl alcohol battery separator containing inert filler
[NASA-CASE-LEW-13556-2] p 183 N83-29805

ELECTROMAGNETIC ACCELERATION
Gain-enhanced free-electron laser with an electromagnetic pump field p 135 A83-31133

ELECTROMAGNETIC FIELDS
A new strategy for efficient solar energy conversion: Parallel-processing with surface plasmons
[NASA-TM-82867] p 59 N83-28071

ELECTROMAGNETIC INTERFERENCE
Experimental results for the interference between FM television signals p 103 A83-19686
Adjacent channel interference degradation with minimum shift keyed modulation p 103 A83-19698

ELECTROMAGNETIC MEASUREMENT
Near-field measurement facility plans at Lewis Research Center p 46 N83-26897

ELECTROMAGNETIC PROPULSION
Rail accelerator research at Lewis Research Center
[AIAA PAPER 82-1938] p 53 A83-22075
Rail accelerator research at Lewis Research Center
[NASA-TM-83015] p 56 N83-12143
The LeRC rail accelerators: Test designs and diagnostic techniques
[NASA-TM-83496] p 60 N83-35053

ELECTROMAGNETIC RADIATION
Inelastic tunnel diodes
[NASA-CASE-LEW-13833-1] p 116 N83-25983

ELECTROMAGNETIC SURFACE WAVES
Surface-polaritonlike waves guided by thin, lossy metal films p 192 A83-37947
Long-range surface plasmons in electrode structures p 202 A83-40733

ELECTROMAGNETIC WAVE TRANSMISSION
Gyrotron transmitting tube
[NASA-CASE-LEW-13429-1] p 117 N83-31952

ELECTROMECHANICAL DEVICES
Piezoelectric composite materials
[NASA-CASE-LEW-12582-1] p 207 N83-34796

ELECTRON ACCELERATION
Numerical simulation of a disk-shaped electron accelerating electrostatic probe p 133 A83-22336
Gain-enhanced free-electron laser with an electromagnetic pump field p 135 A83-31133

ELECTRON BEAMS
Design of a multistage depressed collector for the F-16 radar dual mode transmitter tube
[NASA-TM-82982] p 114 N83-14399
A linearized traveling wave amplifier with hard limiter characteristics
[NASA-CASE-LEW-13981-1] p 116 N83-25984

ELECTRON BOMBARDMENT
Mechanical bonding of metal method
[NASA-CASE-LEW-12941-1] p 77 N83-10170
Electric thruster research
[NASA-CR-168134] p 59 N83-32843

ELECTRON CYCLOTRON HEATING
High frequency plasma generators for ion thrusters
[NASA-CR-167957] p 59 N83-28072

ELECTRON DIFFUSION
Minority carrier diffusion length measurements - A review and comparison of techniques p 205 A83-28448
Electric thruster research
[NASA-CR-168134] p 59 N83-32843

ELECTRON DISTRIBUTION
Continued development of a detailed model of arc discharge dynamics
[NASA-CR-167977] p 206 N83-16234

ELECTRON EMISSION
Numerical simulation of a conducting disk partially covered by an insulator interacting with a plasma p 50 N83-18805

ELECTRON ENERGY
Diamond /111/ studied by electron energy loss spectroscopy in the characteristic loss region p 68 A83-25675

ELECTRON GUNS
Development program on a Spindt cold-cathode electron gun
[NASA-CR-168055] p 115 N83-18997
Spindt cold cathode electron gun development program
[NASA-CR-168212] p 202 N83-35787

ELECTRON IRRADIATION
Kinetics of copper ion absorption by cross-linked calcium polyacrylate membranes
[NASA-TM-83052] p 61 N83-25786
Use of high L.E.T. radiation to improve adhesion of metals to polytetrafluoroethylene
[NASA-TM-83413] p 96 N83-30660

ELECTRON MICROSCOPY
Friction and wear of some ferrous-base metallic glasses
[NASA-TM-83067] p 82 N83-19886

ELECTRON PHOTON CASCADES
Determination of optimum sunlight concentration level in space for 3-5 cascade solar cells p 170 N83-14732

ELECTRON SOURCES
Development program on a Spindt cold-cathode electron gun
[NASA-CR-168055] p 115 N83-18997

ELECTRON SPECTROSCOPY
Diamond /111/ studied by electron energy loss spectroscopy in the characteristic loss region p 68 A83-25675
Application of modern surface analytical tools in the investigation of surface deterioration processes
[NASA-TM-83452] p 152 N83-34327

ELECTRON TRAJECTORIES
Modern multistage depressed collectors - A review p 112 A83-24025

ELECTRON TUBES
Ion sputter textured graphite --- anode collector plates in electron tube devices
[NASA-CASE-LEW-12919-1] p 63 N83-10117
Gyrotron transmitting tube
[NASA-CASE-LEW-13429-1] p 117 N83-31952

ELECTRON TUNNELING
A new strategy for efficient solar energy conversion: Parallel-processing with surface plasmons
[NASA-TM-82867] p 59 N83-28071

ELECTRONIC CONTROL
Flight evaluation of modifications to a digital electronic engine control system in an F-15 airplane
[AIAA PAPER 83-0537] p 20 A83-19593
Components for digitally controlled aircraft engines
[NASA-CR-165296] p 28 N83-12089
Deep impurity trapping concepts for power semiconductor devices p 206 N83-15877
Characterization of a high-pressure diesel fuel injection system as a control technology option to improve engine performance and reduce exhaust emissions
[NASA-TM-83329] p 210 N83-24431

ELECTRONIC COUNTERMEASURES
Experimental verification of the multistage depressed collector design procedure for a high-perveance, helix-type, traveling-wave tube --- in communications satellites
[NASA-TP-2162] p 116 N83-25985

ELECTRONIC EQUIPMENT
Simplification of power electronics for ion thruster neutralizers
[AIAA PAPER 82-1880] p 53 A83-21099
Simplification of power electronics for ion thruster neutralizers
[NASA-TM-83004] p 56 N83-12141
Development of a rotary instrumentation system, phase 2
[NASA-CR-168013] p 47 N83-18835
Design and development of multi-kW power electronic transformers --- for long duration space applications
[NASA-CR-168082] p 116 N83-29596

ELECTRONS
Development of electrical test procedures for qualification of spacecraft against EID. Volume 1: The CAN test and other relevant data
[NASA-CR-165590] p 49 N83-12136

ELECTROPLATING
Method of forming oxide coatings --- for solar collector heating panels
[NASA-CASE-LEW-13132-1] p 96 N83-29388

ELECTROSTATIC CHARGE
Observations of charging dynamics --- of spacecraft p 49 A83-37591

ELECTROSTATIC ENGINES
Simplified power processing for ion-thruster subsystems p 56 A83-39271

ELECTROSTATIC PROBES
Numerical simulation of a disk-shaped electron accelerating electrostatic probe p 133 A83-22336

ELECTROSTATICS
Numerical simulation of a conducting disk partially covered by an insulator interacting with a plasma p 50 N83-18805

ELECTROTHERMAL ENGINES
Electrothermal thruster diagnostics. Volume 1: Executive summary
[NASA-CR-168174-VOL-1] p 60 N83-33942
Electrothermal thruster diagnostics. Volume 2: Technical
[NASA-CR-168174-VOL-2] p 60 N83-33943

ELLIPSES
Theoretical results for starved elliptical contacts
[NASA-TM-81697] p 150 N83-29710

ELLIPSOIDS
Volume integrals of ellipsoids associated with the inhomogeneous Helmholtz equation p 192 A83-29528
The determination of the elastodynamic fields of an ellipsoidal inhomogeneity
[ASME PAPER 83-APM-19] p 157 A83-37383

ELLIPSOMETERS
Ellipsometric study of silicon nitride on gallium arsenide p 204 A83-11812
An enhanced sensitivity null ellipsometry technique for studying films on substrates - Application to silicon nitride on gallium arsenide p 206 A83-37618

ELLIPTIC FUNCTIONS
Formal convergence characteristics of elliptically constrained incremental Newton-Raphson algorithms p 190 A83-10273

ELLIPTICITY
Theoretical results for fully flooded, elliptical hydrodynamic contacts
[NASA-TM-81696] p 140 N83-13458
Film thickness for different regimes of fluid-film lubrication --- elliptical contacts
[NASA-TM-81700] p 149 N83-28449
Elastohydrodynamics of elliptical contacts for materials of low elastic modulus
[NASA-TM-81699] p 151 N83-29712

ELONGATION
Spherical micro-glass particle impingement studies of thermoplastic materials at normal incidence
[NASA-TM-83410] p 94 N83-25883

EMISSION
Energy efficient engine sector combustor rig test program
[NASA-CR-167913] p 33 N83-19753

EMISSION SPECTRA
A software system for emission spectrometry
[NASA-TM-83001] p 70 N83-12181

ENCAPSULATING
EL2 distributions in doped and undoped liquid encapsulated Czochralski GaAs --- deep donor concentration p 205 A83-22756
High purity, low dislocation GaAs single crystals
[NASA-CR-168098] p 206 N83-19622
ENERGETIC PARTICLES
Space Shuttle Orbiter charging p 49 A83-20415
ENERGY BANDS
A new strategy for efficient solar energy conversion - Parallel-processing with surface plasmons p 164 A83-27140
A new strategy for efficient solar energy conversion: Parallel-processing with surface plasmons
[NASA-TM-82867] p 59 N83-28071
ENERGY CONSERVATION
Energy efficient high-pressure turbine leakage technology report
[NASA-CR-165202] p 30 N83-15304
Energy efficient engine. Core engine bearings, drives and configuration: Detailed design report
[NASA-CR-165376] p 39 N83-30430
ENERGY CONSUMPTION
Methods of reducing energy consumption of the oxidant supply system for MHD/steam power plants
[AIAA PAPER 83-0468] p 203 A83-16735
Methods of reducing energy consumption of the oxidant supply system for MHD/steam power plants
[NASA-TM-83025] p 168 N83-13589
Energy and precious fuels requirements of fuel alcohol production. Volume 2, appendices A and B: Ethanol from grain
[NASA-CR-168091] p 183 N83-28582
Advanced single permanent magnet axipolar ironless stator ac motor for electric passenger vehicles
[NASA-CR-167974] p 212 N83-32087
ENERGY CONVERSION
The application of free-electron lasers to the transmission of energy in space p 135 A83-31141
Cell module and fuel conditioner development
[NASA-CR-165462-A] p 166 N83-12524
The phototron: A light to RF energy conversion device p 173 N83-15866
The MOD-OA 200 kilowatt wind turbine generator design and analysis report
[NASA-CR-165127] p 174 N83-16859
Design and evaluation of low-cost stainless steel fiberglass foam blades for large wind driven generating systems
[NASA-CR-165491] p 174 N83-19226
Study of solar array switching power management technology for space power system
[NASA-CR-167890] p 179 N83-22756
Single cell performance studies on the Fe/Cr Redox Energy Storage System using mixed reactant solutions at elevated temperature
[NASA-TM-83385] p 180 N83-25042
ENERGY CONVERSION EFFICIENCY
Advances in series resonant inverter technology and its effect on spacecraft employing electric propulsion
[AIAA PAPER 82-1881] p 51 A83-12465
Planar multijunction high voltage solar cell chip p 163 A83-13923
MHD channel performance for potential early commercial MHD power plants p 204 A83-23134
Radiative energy receiver for high performance energy conversion cycles p 164 A83-27138
Single and multijunction space solar cells grown by organometallic vapor phase epitaxy /OM-VPE/ p 164 A83-27260
Limitations on solar cell open-circuit voltage and efficiency p 165 A83-37790
GaAs solar cells for concentrator systems in space p 171 N83-15820
Performance and load data from Mod-0A and Mod-1 wind turbine generators p 176 N83-19255
Thermionic energy converters
[NASA-CASE-LEW-12443-1] p 184 N83-32175
ENERGY DISSIPATION
Diamond /111/ studied by electron energy loss spectroscopy in the characteristic loss region p 68 A83-25675
Advances in core loss calculations for magnetic materials
[NASA-TM-82947] p 113 N83-11446
SAFE II: Large systems space plasma evaluation experiment p 46 N83-26903
Incidence loss for fan turbine rotor blade in two-dimensional cascade
[NASA-TP-2188] p 39 N83-30431
ENERGY DISTRIBUTION
Measurements of energy distribution and thrust for microwave plasma coupling of electrical energy to hydrogen for propulsion
[AIAA PAPER 82-1951] p 52 A83-12508
Design of a multistage depressed collector for the F-16 radar dual mode transmitter tube
[NASA-TM-82982] p 114 N83-14399
ENERGY GAPS (SOLID STATE)
Diamond /111/ studied by electron energy loss spectroscopy in the characteristic loss region p 68 A83-25675
ENERGY POLICY
Large Horizontal-Axis Wind Turbines
[NASA-CP-2230] p 175 N83-19231
The response of a 38m horizontal axis teetered rotor to yaw p 175 N83-19232
Fixed pitch rotor performance of large horizontal axis wind turbines p 175 N83-19233
Stall induced instability of a teetered rotor p 175 N83-19234
Free yaw performance of the Mod-0 large horizontal axis 100 kW wind turbine p 175 N83-19235
Fuel supply and distribution. Fixed base operation p 101 N83-22449
ENERGY REQUIREMENTS
Propulsion and fluid management - Station keeping will eat energy on a new scale p 54 A83-24360
ENERGY SOURCES
Mod-2 wind turbine system development. Volume 2: Detailed report
[NASA-CR-168007] p 185 N83-33343
ENERGY STORAGE
Design flexibility of redox flow systems --- for energy storage applications p 164 A83-27177
Alkaline regenerative fuel cell energy storage system for manned orbital satellites p 54 A83-27206
The NASA Redox Storage System Development project, 1980
[NASA-TM-82940] p 169 N83-14683
Assessment of alternative power sources for mobile mining machinery
[NASA-TM-82695] p 169 N83-14691
Research and technology, Lewis Research Center
[NASA-TM-83038] p 208 N83-15169
Study to establish cost predictions for the production of Redox chemicals
[NASA-CR-167882] p 176 N83-20359
Cycle life test and failure model of nickel-hydrogen cells
[NASA-TM-83375] p 180 N83-25030
Space power tubes - very much alive
[NASA-TM-83425] p 107 N83-28295
Evaluation of the use of on-board spacecraft energy storage for electric propulsion missions
[NASA-CR-168209] p 59 N83-32842
The chemical behavior of acidified chromium (3) solutions
[NASA-CR-172997] p 74 N83-32871
Nickel-hydrogen component development
[NASA-TM-83487] p 186 N83-35498
ENERGY TECHNOLOGY
Research and technology, Lewis Research Center
[NASA-TM-83038] p 208 N83-15169
Energy efficient face seal
[NASA-CR-165591] p 142 N83-15659
ENERGY TRANSFER
Measurements of energy distribution and thrust for microwave plasma coupling of electrical energy to hydrogen for propulsion
[AIAA PAPER 82-1951] p 52 A83-12508
Solar energy conversion using surface plasmons for broadband energy transport p 171 N83-15815
ENGINE AIRFRAME INTEGRATION
Fluid Dynamics Panel Symposium on Aerodynamics of Power Plant Installation
[AGARD-AR-173] p 27 N83-11138
ENGINE CONTROL
Fiberoptics technology and its application to propulsion control systems
[AIAA PAPER 83-0534] p 18 A83-16772
Flight evaluation of modifications to a digital electronic engine control system in an F-15 airplane
[AIAA PAPER 83-0537] p 20 A83-19593
Nonlinear multivariable design by total synthesis --- of gas turbine engine control systems p 24 A83-37092
Automotive Stirling Engine Mod 1 Design Review, volume 2
[NASA-CR-167936] p 209 N83-10991
Army/NASA small turboshaft engine digital controls research program
[NASA-TM-82979] p 27 N83-11128
Computer program for a four-cylinder-Stirling-engine controls simulation
[NASA-TM-82774] p 126 N83-12359
Status of fiberoptics technology for propulsion control systems
[NASA-TM-82907] p 32 N83-17537
Alternatives for jet engine control
[NASA-CR-170100] p 33 N83-20945
Control means for a gas turbine engine
[NASA-CASE-LEW-14586-1] p 40 N83-31603
ENGINE COOLANTS
Small gas turbine combustor study - Combustor liner evaluation
[AIAA PAPER 83-0337] p 20 A83-16663
Small gas turbine combustor study: Combustor liner evaluation
[NASA-TM-83028] p 33 N83-18725
Three-dimensional turbulent-mixing-length modeling for discrete-hole coolant injection into a crossflow
[NASA-TP-2200] p 132 N83-34232
ENGINE DESIGN
Multifuel evaluation of rich/quench/lean combustor p 67 A83-11492
Composite fan exit guide vanes for high bypass ratio gas turbine engines p 19 A83-13159
Extended performance 8-cm mercury ion thruster
[AIAA PAPER 82-1913] p 53 A83-21078
Control design for a wind turbine-generator using output feedback p 164 A83-24721
NASA clean catalytic combustor program
[ASME PAPER 82-JPGC-GT-11] p 68 A83-25269
Computation techniques and computer programs to analyze Stirling cycle engines using characteristic dynamic energy equations p 207 A83-27272
Improved Stirling engine performance using jet impingement p 137 A83-27288
The influence of inlet design on the aeroacoustic performance of a JT15D turbofan engine as measured in the NASA-Ames 40 x 80 foot wind tunnel
[AIAA PAPER 83-0681] p 21 A83-28006
Zero-length inlets for subsonic V/STOL aircraft p 4 A83-29012
The aerodynamic design and performance of the General Electric/NASA EEE fan --- Energy Efficient Engine
[AIAA PAPER 83-1160] p 23 A83-36252
Benefits and costs of low thrust propulsion systems
[AIAA PAPER 83-1248] p 49 A83-36306
Application of 3D aerodynamic/combustion model to combustor primary zone study
[AIAA PAPER 83-1265] p 23 A83-36316
Advanced LOX/H2 engine technologies for future OTVs
[AIAA PAPER 83-1312] p 55 A83-36333
Inlet design for high-speed propfans
[SAE PAPER 821359] p 5 A83-37957
Development and operating characteristics of an advanced two-stage combustor p 24 A83-38022
Status report - DARPA/NASA convertible turbofan/turboshaft engine program
[ASME PAPER 83-GT-196] p 25 A83-48000
Design concepts for low cost composite engine frames
[AIAA PAPER 83-2445] p 25 A83-48331
A conceptual study of the potential for automotive-derived and free-piston Stirling engines in 30- to 400-kilowatt stationary power applications
[NASA-CR-165274] p 167 N83-10568
Advanced Gas Turbine (AGT) powertrain system
[NASA-CR-165346] p 139 N83-11497
Advanced Gas Turbine (AGT) powertrain system development program --- automobile engines
[NASA-CR-169475] p 27 N83-12088
Components for digitally controlled aircraft engines
[NASA-CR-165296] p 28 N83-12089
Rotorcraft convertible engines for the 1980s
[NASA-TM-83008] p 28 N83-12091
Advanced Gas Turbine (AGT) powertrain system development for automotive applications
[NASA-CR-165178] p 140 N83-12431
Advanced Gas Turbine (AGT) powertrain system development for automotive applications
[NASA-CR-165329] p 209 N83-13038
Extended performance 8-cm mercury ion thruster
[NASA-TM-83029] p 57 N83-14157
Analysis and design of ion thruster for large space systems
[NASA-CR-165140] p 57 N83-14158
Automotive Stirling engine development program
[NASA-CR-168060] p 209 N83-15177
Energy efficient engine: Fan test hardware detailed design report
[NASA-CR-165148] p 31 N83-16341
The CF6 engine performance improvement
[NASA-CR-165612] p 31 N83-16342
Study of advanced rotary combustion engines for commuter aircraft
[NASA-CR-165399] p 32 N83-17545
The 8-CM ion thruster characterization --- mercury ion engine
[NASA-CR-167887] p 57 N83-17586
Stirling engine application study
[NASA-CR-168087] p 210 N83-22029

An overview of general aviation propulsion research programs at NASA Lewis Research Center
p 35 N83-22456
Design of hydraulic output Stirling engine
[NASA-CR-167976] p 177 N83-22739
Analytical fuel property effects, small combustors, phase 1
[NASA-CR-168138] p 101 N83-23464
Opportunities for research in aerothermodynamics
[NASA-TM-83348] p 35 N83-24506
Automotive Stirling engine development program
[NASA-CR-165263] p 211 N83-26762
Advanced Gas Turbine (AGT) powertrain system development for automotive applications
[NASA-CR-168104] p 211 N83-26763
Multi-fuel rotary engine for general aviation aircraft
[NASA-TM-83429] p 38 N83-29235
Stirling engine design manual, 2nd edition
[NASA-CR-168068] p 212 N83-30328
Energy efficient engine low-pressure compressor component test hardware detailed design report
[NASA-CR-165354] p 39 N83-30427
Energy efficient engine. Core engine bearings, drives and configuration: Detailed design report
[NASA-CR-165376] p 39 N83-30430
Current and future technology in radial and axial gas turbines
[NASA-TM-83414] p 41 N83-32811
Multi-fuel rotary engine for general aviation aircraft
[NASA-TM-85428] p 43 N83-36031

ENGINE FAILURE
Ferrographic and spectrometer oil analysis from a failed gas turbine engine
[NASA-TM-82956] p 140 N83-12433
Sensor failure and multivariable control for airbreathing propulsion systems
[NASA-CR-159791] p 1 N83-16279

ENGINE INLETS
An iterative method for predicting turbofan inlet acoustics p 192 A83-13135
Fiber optics for aircraft engine/inlet control
p 20 A83-22494
Effect of variable guide vanes on the performance of a high-bypass turbofan engine p 20 A83-24028
A theoretical investigation of the sound radiation fields associated with a Bellmouth inlet
[AIAA PAPER 83-0710] p 193 A83-25926
Optimization of acoustic liners by the hybrid finite element-integral approach
[AIAA PAPER 83-0670] p 194 A83-26917
The influence of inlet design on the aeroacoustic performance of a JT15D turbofan engine as measured in the NASA-Ames 40 x 80 foot wind tunnel
[AIAA PAPER 83-0681] p 21 A83-28006
Zero-length inlets for subsonic V/STOL aircraft
p 4 A83-29012
Inlet design for high-speed propfans
[SAE PAPER 821359] p 5 A83-37957
Dynamic distortion in a short s-shaped subsonic diffuser with flow separation --- Lewis 8 by 6 foot Supersonic Wind Tunnel
[AIAA PAPER 83-1412] p 25 A83-45515
Inlet-fan flow field computation
[ASME PAPER 83-GT-41] p 7 A83-47901
Three-dimensional flow measurements in a turbine scroll
[ASME PAPER 83-GT-128] p 8 A83-47957
Wind tunnel tests of a zero length, slotted-lip engine air inlet for a fixed nacelle V/STOL aircraft
[NASA-TM-82939] p 9 N83-10019
Fluid Dynamics Panel Symposium on Aerodynamics of Power Plant Installation
[AGARD-AR-173] p 27 N83-11138
Prediction of sound radiation from different practical jet engine inlets
[NASA-CR-169533] p 197 N83-13936
Dynamic distortion in a short s-shaped subsonic diffuser with flow separation --- Lewis 8 by 6 foot Supersonic Wind Tunnel
[NASA-TM-83412] p 36 N83-26838
Preliminary tests of an advanced high-temperature combustion system
[NASA-TP-2203] p 41 N83-33893
Numerical solutions of Navier-Stokes equations for compressible turbulent two/three dimensional flows in terminal shock region of an inlet/diffuser
[NASA-CR-3723] p 132 N83-34230
Vortex motion in axisymmetric piston-cylinder configurations
[NASA-TM-85404] p 133 N83-35318

ENGINE MONITORING INSTRUMENTS
Design of a microprocessor-based Control, Interface and Monitoring (CIM unit for turbine engine controls research
[NASA-TM-83433] p 2 N83-34885

ENGINE NOISE
Tests of a thermal acoustic shield with a supersonic jet p 192 A83-10183
Rotor wake characteristics relevant to rotor-stator interaction noise generation p 19 A83-10184
Generation of desired signals from acoustic drivers --- for aircraft engine internal noise propagation experiment
p 19 A83-15068
Wind tunnel measurements of blade/vane ratio and spacing effects on fan noise p 192 A83-15317
Pressure transfer function of a JT15D nozzle due to acoustic and convected entropy fluctuations
p 193 A83-16319
Transient difference solutions of the inhomogeneous wave equation - Simulation of the Green's function
[AIAA PAPER 83-0667] p 193 A83-25904
A theoretical investigation of the sound radiation fields associated with a Bellmouth inlet
[AIAA PAPER 83-0710] p 193 A83-25926
Tone generation by rotor-downstream strut interaction
[AIAA PAPER 83-0767] p 21 A83-25957
Comparison of measured and predicted flight effects on high-bypass coaxial jet exhaust noise
[AIAA PAPER 83-0749] p 194 A83-26450
Sound propagation in segmented exhaust ducts - Theoretical predictions and comparison with measurements
[AIAA PAPER 83-0734] p 194 A83-28016
Application of 3-signal coherence to core noise transmission
[AIAA PAPER 83-0759] p 194 A83-28021
Acoustic modal analysis of a full-scale annular combustor
[AIAA PAPER 83-0760] p 196 A83-33486
Cross spectra between temperature and pressure in a constant area duct downstream of a combustor
[AIAA PAPER 83-0762] p 196 A83-33487
Experiments on high bypass internal mixer nozzle jet noise
[NASA-TM-83020] p 198 N83-16152
Tone generation by rotor-downstream strut interaction
[NASA-TM-83330] p 33 N83-19754
Acoustic modal analysis of a full-scale annular combustor
[NASA-TM-83334] p 200 N83-21896
Application of 3-signal coherence to core noise transmission
[NASA-TM-83333] p 200 N83-23114
Cross spectra between temperature and pressure in a constant area duct downstream of a combustor
[NASA-TM-83351] p 200 N83-23116
A compact inflow control device for simulating flight fan noise
[NASA-TM-83349] p 201 N83-26643

ENGINE PARTS
Composite engine duct fabrication p 1 A83-39941
Component qualification and initial build of the AGT 100 advanced automotive gas turbine
[ASME PAPER 83-GT-225] p 138 A83-48023
Progress in net shape fabrication of alpha SiC turbine components
[ASME PAPER 83-GT-238] p 139 A83-48030
Advanced Gas Turbine (AGT) powertrain system development program --- automobile engines
[NASA-CR-168475] p 27 N83-12088
Cast Fe-base cylinder/regenerator housing alloy
[NASA-CR-168474] p 80 N83-12214
Advanced Gas Turbine (AGT) powertrain system development for automotive applications
[NASA-CR-167983] p 210 N83-17424
The JT9D Jet Engine Diagnostics Program
[NASA-CR-167966] p 212 N83-17544
Energy efficient engine component development and integration program
[NASA-CR-170089] p 34 N83-22204
Cavitation pitting and erosion of Al 6061-T6 in mineral oil and water
[NASA-TM-83345] p 148 N83-23606
Test results and description of a 1-kW free-piston Stirling engine with a dashpot load
[NASA-TM-83407] p 182 N83-27346
Energy efficient engine low-pressure compressor component test hardware detailed design report
[NASA-CR-165354] p 39 N83-30427
Energy efficient engine high-pressure turbine single crystal vane and blade fabrication technology report
[NASA-CR-165400] p 39 N83-30429

ENGINE TESTING LABORATORIES
Operational summary of an electric propulsion long term test facility
[AIAA PAPER 82-1903] p 44 A83-12478

ENGINE TESTS
Status of the J-series 30-cm mercury ion thruster
[AIAA PAPER 82-1904] p 51 A83-12479
A direct-measurement technique for estimating discharge-chamber lifetime --- for ion thrusters
[AIAA PAPER 82-1908] p 51 A83-12483
Inert gas test of two 12-cm magnetostatic thrusters
[AIAA PAPER 82-1925] p 51 A83-12494
Plasma characteristics of a 17 cm diameter line-cusp ion thruster
[AIAA PAPER 82-1926] p 52 A83-12495
The aerodynamic design and performance of the General Electric/NASA EEE fan --- Energy Efficient Engine
[AIAA PAPER 83-1160] p 23 A83-36252
Development and operating characteristics of an advanced two-stage combustor p 24 A83-38022
JT9D performance deterioration results from a simulated aerodynamic load test p 25 A83-41040
A survey of inlet/engine distortion compatibility
[AIAA PAPER 83-1166] p 6 A83-45509
Combustion characteristics of hydrogen, Carbon monoxide based gaseous fuels
[NASA-TM-82998] p 167 N83-10560
Cold-air performance of compressor-drive turbine of Department of Energy upgraded automobile gas turbine engine. 2: Stage performance
[NASA-TM-82818] p 9 N83-11063
QCSEE under-the-wing engine-wing-flap aerodynamic profile characteristics
[NASA-TM-82890] p 28 N83-12092
Uniform engine testing program. Phase 1: NASA Lewis Research Center participation
[NASA-TM-82978] p 29 N83-14126
Powder metallurgy Rene 95 rotating turbine engine parts, volume 2
[NASA-CR-165141] p 82 N83-15412
Analysis of strain gage reliability in F-100 jet engine testing at NASA Lewis Research Center
[NASA-TM-83325] p 134 N83-24829
Testing and performance characteristics of a 1-kW free piston Stirling engine
[NASA-TM-82999] p 180 N83-25036
Automotive Stirling Engine Development Program
[NASA-CR-168074] p 212 N83-27925
A survey of inlet/engine distortion compatibility
[NASA-TM-83421] p 37 N83-27991
Effects of wind on turbofan engines in outdoor static test stands
[NASA-TM-83493] p 42 N83-34945
Ceramic applications in turbine engines
[NASA-CR-165494] p 212 N83-37028

ENGINEERING MANAGEMENT
Bibliography of Lewis Research Center technical publications announced in 1982
[NASA-TM-83335] p 208 N83-29124

ENGINES
A conceptual study of the potential for automotive-derived and free-piston Stirling engines in 30- to 400-kilowatt stationary power applications
[NASA-CR-165274] p 167 N83-10568
Assessment of alternative power sources for mobile mining machinery
[NASA-TM-82695] p 169 N83-14691

ENTHALPY
A class of nonideal solutions. 1: Definition and properties
[NASA-TP-1929] p 208 N83-23189
Activation parameters of flow through battery separators
[NASA-TM-83371] p 73 N83-30550

ENTROPY
Pressure transfer function of a JT15D nozzle due to acoustic and convected entropy fluctuations
p 193 A83-16319
Fast Euler solver for steady, 1-dimensional flows
[NASA-CR-3689] p 14 N83-27960
Activation parameters of flow through battery separators
[NASA-TM-83371] p 73 N83-30550

ENVIRONMENTAL TESTS
Environmental effects on graphite fiber reinforced PMR-15 polyimide p 63 A83-33115
The effect of microstructure on the fatigue behavior of Ni base superalloys p 75 A83-36166
A study of the surface deterioration due to erosion --- of gas turbine blades
[ASME PAPER 83-GT-213] p 9 A83-48014

EPOXY COMPOUNDS
Imide modified epoxy matrix resins
[NASA-CR-167942] p 93 N83-18909

EPOXY MATRIX COMPOSITES
Bisimide amine cured epoxy /IME/ resins and composites. II - Ten-degree off-axis tensile and shear properties of Celion 6000/IME composites
p 62 A83-23608
Cryogenic fluid management experiment trunnion fatigue verification
[AIAA PAPER 83-0911] p 49 A83-32782

Synthesis and characterization of bisimide amines and bisimide amine-cured epoxy resins p 90 A83-40924
A study of the stress wave factor technique for the characterization of composite materials
[NASA-CR-3670] p 153 N83-27248

EPOXY RESINS
Synthesis and characterization of bisimide amines and bisimide amine-cured epoxy resins p 88 A83-11486
Bisimide amine cured epoxy /IME/ resins and composites. II - Ten-degree off-axis tensile and shear properties of Celion 6000/IME composites p 62 A83-23608
Dynamics and mechanism of cavitation erosion on perspex and epoxy resin tested in a rotating disk device p 89 A83-27422
Synthesis and characterization of bisimide amines and bisimide amine-cured epoxy resins p 90 A83-40924
Cavitation erosion characteristics of poly(methyl methacrylate) in a rotating disk device p 90 A83-41851
Dynamics and mechanism of cavitation erosion on perspex and epoxy resins tested in a rotating disk device
[NASA-TM-82962] p 91 N83-11329
Construction of low-cost, Mod-OA wood composite wind turbine blades
[NASA-TM-83046] p 174 N83-16857
Fabrication of low-cost Mod-OA wood composite wind turbine blades
[NASA-TM-83323] p 182 N83-27347

EQUATIONS OF MOTION
A similarity analysis of the droplet trajectory equation p 118 A83-13133
Environmental solid particle effects on compressor cascade performance
[NASA-CR-168018] p 11 N83-16285

EQUILIBRIUM METHODS
A new formulation of hybrid/mixed finite element p 155 A83-12739
A search for equilibrium states
[NASA-TM-82896] p 207 N83-20606

EQUIPMENT SPECIFICATIONS
Component qualification and initial build of the AGT 100 advanced automotive gas turbine
[ASME PAPER 83-GT-225] p 138 A83-48023
Advanced Gas Turbine (AGT) powertrain system development program — automobile engines
[NASA-CR-169475] p 27 N83-12088
Advanced 30/20 GHz multiple-beam antennas for communications satellites
[NASA-TM-82952] p 50 N83-13154

EQUIVALENT CIRCUITS
Equivalent-circuit consideration of dual-gate MESFETs at high frequency p 113 A83-44970

EROSION
A direct-measurement technique for estimating discharge-chamber lifetime — for ion thrusters
[AIAA PAPER 82-1906] p 51 A83-12483
A method of predicting the performance deterioration of a compressor cascade due to sand erosion
[AIAA PAPER 83-0178] p 19 A83-16572
The initial stages of cavitation damage and erosion on copper and brass tested in a rotating disk device p 75 - A83-27421
Dynamics and mechanism of cavitation erosion on perspex and epoxy resin tested in a rotating disk device p 89 A83-27422
Solid particle dynamic behavior through twisted blade rows p 3 A83-27478
Morphology of ductile metals eroded by a jet of spherical particles impinging at normal incidence p 75 A83-32624
Cavitation erosion characteristics of poly(methyl methacrylate) in a rotating disk device p 90 A83-41851
A study of the surface deterioration due to erosion — of gas turbine blades
[ASME PAPER 83-GT-213] p 9 A83-48014
- Dynamics and mechanism of cavitation erosion on perspex and epoxy resins tested in a rotating disk device
[NASA-TM-82962] p 91 N83-11329
Initial stages of cavitation damage and erosion on copper and brass tested in a rotating disk device
[NASA-TM-82993] p 81 N83-13231
Universal approach to analysis of cavitation and liquid-impingement erosion data
[NASA-TP-2061] p 82 N83-15413
Compressor cascade performance deterioration caused by sand ingestion
[NASA-CR-168067] p 11 N83-16286
A comprehensive analysis of cavitation and liquid impingement erosion data
[NASA-TM-83352] p 84 N83-24634
Time effect of erosion by solid particle impingement on ductile materials
[NASA-TM-83369] p 84 N83-24637
Morphology of an aluminum alloy eroded by a jet of angular particles impinging at normal incidence
[NASA-TP-2139] p 85 N83-24641
Endurance test of a 30-CM-diameter engineering model ion thruster. Task 12: Investigation of thin-film erosion monitors for ion thrusters
[NASA-CR-168132] p 58 N83-25779
Solid particle impingement erosion characteristics of cylindrical surfaces, pre-existing holes and slits
[NASA-TM-83322] p 85 N83-25853
Spherical micro-glass particle impingement studies of thermoplastic materials at normal incidence
[NASA-TM-83410] p 94 N83-25883
Time dependence of solid-particle impingement erosion of an aluminum alloy
[NASA-TP-2169] p 86 N83-32908
Cavitation pitting and erosion of aluminum 6061-T6 in mineral oil water
[NASA-TP-2146] p 152 N83-35400

ERROR CORRECTING CODES
A low-power, high-throughput maximum-likelihood convolutional decoder chip for NASA's 30/20 GHz program p 111 A83-19754

ERRORS
Computer program to minimize prediction error in models from experiments with 16 hypercube points and 0 to 6 center points
[NASA-TM-82995] p 192 N83-21872

ESTERS
Analysis of a MIL-L-27502 lubricant from a gas-turbine engine test by size-exclusion chromatography
[NASA-TP-2063] p 93 N83-16528

ETCHING
Industrial ion source technology
[NASA-CR-159877] p 102 N83-12259
Spindt cold cathode electron gun development program
[NASA-CR-168212] p 202 N83-35787

ETHYL ALCOHOL
Performance and emissions characteristics of aqueous alcohol fumes in a DI diesel engine
[NASA-CR-167917] p 99 N83-12250
Energy and precious fuels requirements of fuel alcohol production, volume 1
[NASA-CR-168090] p 183 N83-28581
Energy and precious fuels requirements of fuel alcohol production. Volume 2, appendices A and B: Ethanol from grain
[NASA-CR-168091] p 183 N83-28582

EULER EQUATIONS OF MOTION
A finite element formulation for steady transonic Euler equations p 3 A83-22129
Efficient solution of the Euler and Navier-Stokes equations with a vectorized multiple-grid algorithm
[AIAA PAPER 83-1893] p 5 A83-39359
A fast Euler solver for steady flows
[AIAA PAPER 83-1940] p 123 A83-39389
Multiple-gridding of the Euler equations with an implicit scheme
[AIAA PAPER 83-1945] p 5 A83-39392
User's manual for three-dimensional analysis of propeller flow fields
[NASA-CR-167959] p 12 N83-18671
Efficient solution of the Euler and Navier-Stokes equations with a vectorized multiple-grid algorithm
[NASA-TM-83376] p 2 N83-24467
Fast Euler solver for steady, 1-dimensional flows
[NASA-CR-3689] p 14 N83-27960
Flux-based acceleration of the Euler equations
[NASA-TM-83453] p 191 N83-30113
Comparison of two- and three-dimensional flow computations with laser anemometer measurements in a transonic compressor rotor
[NASA-TP-1931] p 15 N83-32774
Stress and fracture analyses under elastic-plastic creep conditions: Some basic developments and computational approaches p 162 N83-34371

EUTECTIC ALLOYS
Effect of aging on the 1000 C compressive slow plastic flow characteristics of the directionally solidified eutectic alloy gamma/gamma prime-alpha p 77 A83-44340

EUTECTIC COMPOSITES
High-temperature composites - Status and future directions p 63 A83-40129
SiC or B4C-B/low strategic element content composite p 80 N83-11308

EVALUATION
Evaluation of solar cell welds by scanning acoustic microscopy p 172 N83-15834
The effects of Ni, Mo, Ti and Si on the mechanical properties of Cr free Mn steel (Fe-25Mn-5Al-2C)
[NASA-TM-83355] p 85 N83-24638

EVAPORATION
The structure of evaporating and combusting sprays: Measurements and predictions
[NASA-CR-170312] p 130 N83-24795
Friction and hardness of gold films deposited by ion plating and evaporation
[NASA-TP-2207] p 87 N83-34019

EXCITATION
The 'whistler-nozzle' phenomenon p 125 A83-49472
The whistler nozzle phenomenon
[NASA-CR-170015] p 199 N83-20706

EXHAUST EMISSION
Development and operating characteristics of an advanced two-stage combustor p 24 A83-38022
Evaluation of advanced combustion concepts for dry NO sub x suppression with coal-derived, gaseous fuels
[NASA-TM-82965] p 166 N83-10557
Multifuel evaluation of rich/quench/lean combustor
[NASA-TM-82966] p 167 N83-10559
Performance and emissions characteristics of aqueous alcohol fumes in a DI diesel engine
[NASA-CR-167917] p 99 N83-12250
Investigation of a low NOx full-scale annular combustor
[NASA-CR-165518] p 29 N83-13104
Effect of flameholder pressure drop on emissions and performance of premixed-prevaporized combustors
[NASA-TP-2131] p 35 N83-23309
Characterization of a high-pressure diesel fuel injection system as a control technology option to improve engine performance and reduce exhaust emissions
[NASA-TM-83329] p 210 N83-24431
Multi-fuel rotary engine for general aviation aircraft
[NASA-TM-83429] p 38 N83-29235
Broad specification fuels technology program, phase 1
[NASA-CR-168180] p 74 N83-30551

EXHAUST FLOW SIMULATION
Scale model performance test investigation of mixed flow exhaust systems for an energy efficient engine /E3/ propulsion system
[AIAA PAPER 83-0541] p 20 A83-16776

EXHAUST GASES
Combustion of coal gas fuels in a staged combustor
[NASA-TM-82967] p 166 N83-10556
Fumigation of alcohol in a light duty automotive diesel engine
[NASA-CR-167915] p 99 N83-13272
Fuel quality/processing study. Volume 4: On site processing studies
[NASA-CR-165326-VOL-4] p 179 N83-22755
An analytical investigation of NO sub x control techniques for methanol fueled spark ignition engines
[NASA-CR-172647] p 151 N83-33168

EXHAUST NOZZLES
Pressure transfer function of a JT15D nozzle due to acoustic and convected entropy fluctuations p 193 A83-16319
Three-dimensional compressible viscous analysis of mixer nozzles
[AIAA PAPER 83-1401] p 4 A83-36391
Conceptual design, evaluation and research identification for Remote Augmented Propulsive Lift Systems (RALS) with ejectors for VTOL aircraft
[NASA-CR-167906] p 29 N83-13103
Thrust performance of a variable-geometry, divergent exhaust nozzle on a turbojet engine at altitude
[NASA-TP-2171] p 36 N83-26839

EXHAUST SYSTEMS
Scale model performance test investigation of mixed flow exhaust systems for an energy efficient engine /E3/ propulsion system
[AIAA PAPER 83-0541] p 20 A83-16776
Sound propagation in segmented exhaust ducts - Theoretical predictions and comparison with measurements
[AIAA PAPER 83-0734] p 194 A83-28016
Acoustical modal analysis of the pressure field in the tailpipe of a turbofan engine
[NASA-TM-83387] p 201 N83-25489

EXISTENCE THEOREMS
Formal convergence characteristics of elliptically constrained incremental Newton-Raphson algorithms p 190 A83-10273

EXPERIMENT DESIGN
Aviation energy and the future of the recreational use of sport and general aviation aircraft p 100 N83-22444

EXTENSOMETERS
An extensometer for axial strain measurement at high temperature p 134 A83-48604

EXTRAPOLATION
Convergence and stability properties of minimal polynomial and reduced rank extrapolation algorithms
[NASA-TM-83443] p 191 N83-31390

EXTREMELY HIGH FREQUENCIES
High-performance K-band GaAs power field-effect transistors prepared by molecular beam epitaxy p 112 A83-33646
Concept for advanced satellite communications and required technologies
[NASA-TM-82984] p 47 N83-11210
Customer premise service study for 30/20 GHz satellite system
[NASA-CR-167986] p 105 N83-17769
Planning assistance for the 30/20 GHz program, volume 2
[NASA-CR-165484-VOL-2] p 108 N83-33011
Planning assistance for the 30/20 GHz program, volume 3
[NASA-CR-165484] p 108 N83-33012
EYRING THEORY
Activation parameters of flow through battery separators
[NASA-TM-83371] p 73 N83-30550

F

F-15 AIRCRAFT
Flight evaluation of modifications to a digital electronic engine control system in an F-15 airplane
[AIAA PAPER 83-0537] p 20 A83-19593
FABRICATION
Development of a microwave 20 x 20 switch matrix for 30/20 GHz SS-TDMA application p 110 A83-11484
Use of column V alkyls in organometallic vapor phase epitaxy (OMVPE) p 70 A83-46608
Progress in net shape fabrication of alpha SiC turbine components
[ASME PAPER 83-GT-238] p 139 A83-48030
Design and fabrication of composite blades for the Mod-1 wind turbine generator
[NASA-CR-167967] p 168 N83-11579
Design and evaluation of low cost blades for large wind driven generating systems p 175 N83-19244
Design, fabrication and testing of porous tungsten vaporizers for mercury ion thrusters
[NASA-TM-83063] p 58 N83-22318
Advanced Gas Turbine (AGT) powertrain system development for automotive applications
[NASA-CR-168104] p 211 N83-26763
JT90 thermal barrier coated vanes
[NASA-CR-167964] p 37 N83-27993
Advanced inorganic separators for alkaline batteries and method of making the same
[NASA-CASE-LEW-13171-2] p 184 N83-32176
FACE CENTERED CUBIC LATTICES
Effect of swaging on the 1000 C compressive slow plastic flow characteristics of the directionally solidified eutectic alloy gamma/gamma prime-alpha p 77 A83-44340
Gamma prime shape changes during creep of a nickel-base superalloy p 77 A83-47855
FACTORIAL DESIGN
Computer program to minimize prediction error in models from experiments with 16 hypercube points and 0 to 6 center points
[NASA-TM-82995] p 192 N83-21872
FAILURE ANALYSIS
Tribology p 140 N83-12167
Ferrographic and spectrometer oil analysis from a failed gas turbine engine
[NASA-TM-82956] p 140 N83-12433
Advanced ceramic coating development for industrial/utility gas turbine applications
[NASA-CR-165619] p 92 N83-15467
Sensor failure and multivariable control for airbreathing propulsion systems
[NASA-CR-159791] p 1 N83-16279
A refrigerated dynamic seal
[NASA-TM-83378] p 130 N83-24798
Cycle life test and failure model of nickel-hydrogen cells
[NASA-TM-83375] p 180 N83-25038
Rotor fragment protection program: Statistics on aircraft gas turbine engine rotor failures that occurred in US commercial aviation during 1979
[NASA-CR-168163] p 38 N83-29234
Application of advanced reliability methods to local strain fatigue analysis
[NASA-CR-168198] p 161 N83-29734
Sensor failure detection for jet engines
[NASA-CR-168190] p 154 N83-33182
Effect of the amount of Na2SO4 on the high temperature corrosion of Udimet-700
[NASA-TM-83459] p 87 N83-34016
FAN BLADES
Zero-length inlets for subsonic V/STOL aircraft p 4 A83-29012
Structural tailoring of engine blades (STAEBL)
[AIAA 83-0828] p 22 A83-29737
Blade loss transient dynamic analysis of turbomachinery p 25 A83-40864
Aerodynamic performance of a fan stage utilizing variable inlet guide vanes (VIGV's) for thrust modulation — subsonic V/STOL aircraft
[AIAA PAPER 83-1162] p 6 A83-45508
Wind tunnel tests of a zero length, slotted-lip engine air inlet for a fixed nacelle V/STOL aircraft
[NASA-TM-82939] p 9 N83-10019
Recent results about fan noise: Its generation, radiation and suppression
[NASA-TM-83002] p 197 N83-13939
Energy efficient engine: Fan test hardware detailed design report
[NASA-CR-165148] p 31 N83-16341
Aircraft turbofan noise
[NASA-TM-83317] p 198 N83-18405
Aerodynamic performance of a fan stage utilizing Variable Inlet Guide Vanes (VIGVs) for thrust modulation — subsonic V/STOL aircraft
[NASA-TM-83438] p 13 N83-27957
Incidence loss for fan turbine rotor blade in two-dimensional cascade
[NASA-TP-2188] p 39 N83-30431
FAR FIELDS
Farfield inflight measurements of high-speed turboprop noise
[AIAA PAPER 83-0745] p 21 A83-25947
Computer program to predict noise of general aviation aircraft: User's guide
[NASA-CR-168050] p 198 N83-17242
Aircraft turbofan noise
[NASA-TM-83317] p 198 N83-18405
Near-field measurement facility plans at Lewis Research Center p 46 N83-26897
FATIGUE (MATERIALS)
Large-bore tapered-roller bearing performance and endurance to 2.4 million DN p 145 N83-20134
A total life prediction model for stress concentration sites
[NASA-CR-170290] p 160 N83-23629
Spherical micro-glass particle impingement studies of thermoplastic materials at normal incidence
[NASA-TM-83410] p 94 N83-25883
Vibration in planetary gear systems with unequal planet stiffnesses
[NASA-TM-83428] p 150 N83-29709
Evaluation of inelastic constitutive models for nonlinear structural analysis p 162 N83-34357
FATIGUE LIFE
Turbine blade nonlinear structural and life analysis p 21 A83-29024
Rolling-element fatigue life with traction fluids and automatic transmission fluid in a high-speed rolling-contact rig
[NASA-TP-2050] p 140 N83-13457
Strainrange partitioning: A total strain range version
[NASA-TM-83023] p 81 N83-14246
Rolling-element fatigue life of AMS 5900 balls
[NASA-TP-2080] p 142 N83-16758
Bearing fatigue investigation 3
[NASA-CR-168029] p 143 N83-17880
Present technology of rolling-element bearings p 144 N83-20121
An update on the life analysis of spur gears p 146 N83-20144
Evaluation of high-contact-ratio spur gears with profile modification p 147 N83-20150
Effect of carbide distribution on rolling-element fatigue life of AMS 5749
[NASA-TP-2189] p 151 N83-33166
The thermal fatigue resistance of H-13 Die Steel for aluminum die casting dies
[NASA-TM-83331] p 87 N83-35103
FATIGUE TESTS
Operational summary of an electric propulsion long term test facility
[AIAA PAPER 82-1903] p 44 A83-12478
Low cycle fatigue behavior of aluminum/stainless steel composites
[AIAA 83-0806] p 62 A83-29886
Cryogenic fluid management experiment trunnion fatigue verification
[AIAA PAPER 83-0911] p 49 A83-32782
Fatigue crack initiation and propagation in several nickel-base superalloys at 650 C p 76 A83-41199
Rolling-element fatigue life of AMS 5900 balls
[NASA-TP-2080] p 142 N83-16758
Structural fatigue test results for large wind turbine blade sections p 159 N83-19246
Fatigue testing of low-cost fiberglass composite wind turbine blade materials
[NASA-CR-165566] p 177 N83-22746
Compression and compression fatigue testing of composite laminates
[NASA-CR-168023] p 66 N83-26928
Statistical summaries of fatigue data for design purposes
[NASA-CR-3697] p 161 N83-29731
FEASIBILITY ANALYSIS
A conceptual study of the potential for automotive-derived and free-piston Stirling engines in 30- to 400-kilowatt stationary power applications
[NASA-CR-165274] p 167 N83-10568
Feasibility of water injection into the turbine coolant to permit gas turbine contingency power for helicopter application
[NASA-TM-83043] p 31 N83-15307
Large rotorcraft transmission technology development program
[NASA-CR-168120] p 18 N83-22188
JT90 thermal barrier coated vanes
[NASA-CR-167964] p 37 N83-27993
FEEDBACK CONTROL
Investigations of stability and dynamic performances of switching regulators employing current-injected control p 110 A83-11002
Transistorized PWM inverter-induction motor drive system p 110 A83-11488
Control design for a wind turbine-generator using output feedback p 164 A83-24721
Control design and performance analysis of a 6 MW wind turbine-generator p 165 A83-29097
Nonlinear multivariable design by total synthesis — of gas turbine engine control systems p 24 A83-37092
Alternatives for jet engine control
[NASA-CR-170233] p 35 N83-23305
FEEDFORWARD CONTROL
A novel input filter compensation scheme for switching regulators p 111 A83-11494
A novel feedforward compensation canceling input filter-regulator interaction p 112 A83-33133
FERRITES
X-ray photoelectron spectroscopy and friction studies of nickel-zinc and manganese-zinc ferrites in contact with metals
[NASA-TP-2163] p 84 N83-23419
FERROELECTRICITY
Piezoelectric and pyroelectric coefficients for ferroelectric crystals with polarizable molecules p 205 A83-17227
FERROGRAPHY
Ferrographic and spectrometer oil analysis from a failed gas turbine engine
[NASA-TM-82956] p 140 N83-12433
FERROUS METALS
Friction and wear of some ferrous-base metallic glasses
[NASA-TM-83067] p 82 N83-19886
FIBER COMPOSITES
Alumina fiber strength improvement
[NASA-CR-167999] p 63 N83-11247
Method and apparatus for gripping uniaxial fibrous composite materials — holding specimens for mechanical property testing
[NASA-CASE-LEW-13758-1] p 64 N83-12176
Research priorities for advanced fibrous composites
[NASA-CR-165414] p 65 N83-18853
Research priorities and history of advanced composite compression testing
[NASA-CR-165415] p 66 N83-18854
Simplified composite micromechanics equations for hygral, thermal and mechanical properties
[NASA-TM-83320] p 66 N83-19817
Hybridized polymer matrix composites
[NASA-CR-165341] p 66 N83-22326
Geometrically nonlinear analysis of layered composite plates and shells
[NASA-CR-168182] p 161 N83-33219
FIBER OPTICS
Fiberoptics technology and its application to propulsion control systems
[AIAA PAPER 83-0534] p 18 A83-16772
Fiber optics for aircraft engine/inlet control p 20 A83-22494
Fiberoptics technology and its application to propulsion control systems
[NASA-TM-83009] p 18 N83-15302
Status of fiberoptics technology for propulsion control systems
[NASA-TM-82907] p 32 N83-17537
FIBER REINFORCED COMPOSITES
Fatigue behavior of SiC reinforced Ti/6Al-4V/ at 650 C p 62 A83-12414
Environmental effects on graphite fiber reinforced PMR-15 polyimide p 63 A83-33115
High-temperature composites - Status and future directions p 63 A83-40129
Acousto-ultrasonic characterization of fiber reinforced composites p 63 N83-11231
PMR polyimide composites for aerospace applications
[NASA-TM-83047] p 65 N83-15364

The 371 deg C(700 deg F) properties of celion 6000/n-phenylnadimide modified PMR polyimide composites
[NASA-TM-83050] p 65 N83-15365
Low temperature cross linking polyimides
[NASA-CASE-LEW-12876-2] p 96 N83-29392
The effect of stress on ultrasonic pulses in fiber reinforced composites
[NASA-CR-3724] p 154 N83-33189

FIELD EFFECT TRANSISTORS
A 1 watt GaAs power amplifier for the NASA 30/20 GHz communication system p 111 A83-11489
High-performance K-band GaAs power field-effect transistors prepared by molecular beam epitaxy p 112 A83-33846
GaAs integrated digital-to-analogue convertor for control of power dual-gate FETs p 112 A83-36479
Equivalent-circuit consideration of dual-gate MESFETs at high frequency p 113 A83-44970

FIELD EMISSION
Development program on a Spindt cold-cathode electron gun
[NASA-CR-168055] p 115 N83-18997

FIGHTER AIRCRAFT
Supersonic STOVL research aircraft
[SAE PAPER 821375] p 17 A83-37965

FILLERS
Polyvinyl alcohol battery separator containing inert filler
[NASA-CASE-LEW-13556-2] p 183 N83-29805

FILM COOLING
Film-cooling effectiveness with developing coolant flow through straight and curved tubular passages
[NASA-TP-2062] p 126 N83-12360
Comparison of predicted and experimental external heat transfer around a film cooled cylinder in crossflow
[NASA-TM-83017] p 127 N83-13392
Curved film cooling admission tube
[NASA-CASE-LEW-13174-1] p 131 N83-27144
Stagnation region gas film cooling: Effects of dimensionless coolant temperature
[NASA-CR-168197] p 132 N83-30960
Three-dimensional turbulent-mixing-length modeling for discrete-hole coolant injection into a crossflow
[NASA-TP-2200] p 132 N83-34232
Covering solid, film cooled surfaces with a duplex thermal barrier coating
[NASA-CASE-LEW-13450-1] p 103 N83-35177

FILM THICKNESS
Film thickness measurement for spiral groove and Rayleigh step lift pad self-acting face seals
[NASA-TP-2058] p 26 N83-11126
Theoretical results for fully flooded, elliptical hydrodynamic contacts
[NASA-TM-81696] p 140 N83-13458
Geometry and starvation effects in hydrodynamic lubrication p 141 N83-15522
The XPS depth profiling and tribological characterization of ion-plated gold on various metals
[NASA-TM-83350] p 83 N83-23417
Optimum parallel step-sector bearing lubricated with an incompressible fluid
[NASA-TM-83356] p 148 N83-24855
Preparation, characterization, physical testing and performance of fluorocarbon membranes and separators
[NASA-CR-167880] p 73 N83-26936
Film thickness for different regimes of fluid-film lubrication — elliptical contacts
[NASA-TM-81700] p 149 N83-28449
Elastohydrodynamic contacts. Effects of dents and grooves on traction and local film thickness
[NASA-TP-2175] p 150 N83-28453
Theoretical results for starved elliptical contacts
[NASA-TM-81697] p 150 N83-29710
Applications of film thickness equations
[NASA-TM-81701] p 151 N83-29713
Thermal elastohydrodynamic lubrication of line contacts
[NASA-TM-83424] p 152 N83-34326

FILTRATION
Activation parameters of flow through battery separators
[NASA-TM-83371] p 73 N83-30550

FINITE DIFFERENCE THEORY
Acoustics in variable area duct - Finite element and finite difference comparisons to experiment p 193 A83-19609
Transient difference solutions of the inhomogeneous wave equation - Simulation of the Green's function
[AIAA PAPER 83-0667] p 193 A83-25904
Finite difference solutions to shocked acoustic waves
[AIAA PAPER 83-0671] p 193 A83-25907
A basic code for the prediction of transient three-dimensional turbulent flowfields p 121 A83-27412
Analytical calculation of a single jet in crossflow and comparison with experiment
[NASA-TM-83027] p 29 N83-14127
Transient difference solutions of the inhomogeneous wave equation: Simulation of the Green's function
[NASA-TM-83336] p 200 N83-21897

FINITE ELEMENT METHOD
A new formulation of hybrid/mixed finite element p 155 A83-12739
Nonlinear structural and life analyses of a combustor liner p 155 A83-12764
An iterative method for predicting turbofan inlet acoustics p 192 A83-13135
Alternative ways for formulation of hybrid stress elements p 155 A83-14710
Growth and stability of interacting surface flaws of arbitrary shape p 155 A83-15060
Acoustics in variable area duct - Finite element and finite difference comparisons to experiment p 193 A83-19809
A finite element formulation for steady transonic Euler equations p 3 A83-22129
Optimization of acoustic liners by the hybrid finite element-integral approach
[AIAA PAPER 83-0670] p 194 A83-26917
Geometrically nonlinear analysis of layered composite shells p 156 A83-27431
Numerical solution of the problem of flame propagation by the use of the random element method
[AIAA PAPER 83-0600] p 69 A83-36062
Finite element analysis of steadily moving contact fields p 158 A83-49437
Utilizing numerical techniques in turbofan inlet acoustic suppressor design
[NASA-TM-82994] p 196 N83-10885
Large displacements and stability analysis of nonlinear propeller structures p 159 N83-12460
Stability analysis of flexible wind turbine blades using finite element method
[NASA-CR-168107] p 177 N83-21508
Development of methodology for horizontal axis wind turbine dynamic analysis
[NASA-CR-168110] p 178 N83-22747
Geometrically nonlinear analysis of layered composite plates and shells
[NASA-CR-168182] p 161 N83-33219
Stress and fracture analyses under elastic-plastic creep conditions: Some basic developments and computational approaches p 162 N83-34371
The structural response of a rail accelerator
[NASA-TM-83491] p 163 N83-35412

FINITE VOLUME METHOD
An experience in mesh generation for three-dimensional calculation of potential flow around a rotating propeller p 5 A83-38798
Finite volume calculation of three-dimensional potential flow around a propeller p 7 A83-45577

FINS
Length to diameter ratio and row number effects in short pin fin heat transfer
[NASA-TM-83005] p 127 N83-14431

FIRE DAMAGE
Assessment of crash fire hazard of LH sub 2 fueled aircraft
[NASA-CR-165525] p 16 N83-11095

FIXED POINTS (MATHEMATICS)
Evaluation of a high performance, fixed-ratio, traction drive p 145 N83-20135

FIXED WINGS
Rotorcraft convertible engine study
[NASA-CR-168161] p 37 N83-27996

FLAKES
Diamondlike flake composites — for use in aerospace structures and components
[NASA-CASE-LEW-13837-1] p 67 N83-28095

FLAME HOLDERS
Effect of flameholder pressure drop on emissions and performance of premixed-prevaporized combustors
[NASA-TP-2131] p 35 N83-23309
Fuel vaporization effects p 101 N83-29214

FLAME PROPAGATION
Boundary integral equation method calculations of surface regression effects in flame spreading p 67 A83-13488
Aerodynamic features of turbulent flames
[AIAA PAPER 83-0470] p 119 A83-16737
Numerical solution of the problem of flame propagation by the use of the random element method
[AIAA PAPER 83-0600] p 69 A83-36062
Correlating downward flame spread rates for thick fuel beds p 69 A83-37045
Turbulent flame propagation and combustion in spark ignition engines p 70 A83-48156
Laser fluorescence studies of the chemical interactions of sodium species with sulfur bearing fuels
[NASA-CR-169861] p 71 N83-17625
Flame radiation measurements p 73 N83-29228
Modeling Interface Motion Of Combustion (MINOC). A computer code for two-dimensional, unsteady turbulent combustion
[NASA-TP-2132] p 40 N83-32806

FLAME RETARDANTS
Hybridized polymer matrix composites
[NASA-CR-165341] p 66 N83-22326

FLAMES
The detailed chemistry and thermodynamics of sodium in oxygen-rich flames
[NASA-CR-169848] p 72 N83-17626
Effects of percentage of blockage and flameholder downstream counterbores on lean combustion limits of premixed, prevaporized propane-air mixture
[NASA-TP-2227] p 41 N83-34941

FLASHBACK
High-pressure flame visualization of autoignition and flashback phenomena with liquid-fuel spray
[NASA-TM-83501] p 42 N83-34948

FLEXIBILITY
Structural dynamics studies of rotating bladed-disk assemblies coupled with flexible shaft motions
[AIAA PAPER 83-0919] p 22 A83-32787

FLIGHT HAZARDS
'Scaling' analysis of the ice accretion process on aircraft surfaces
[ASME PAPER 82-WA/HT-39] p 16 A83-25693
NASA Lewis Research Center's Program on Icing Research
[NASA-TM-83031] p 16 N83-14078

FLIGHT PLANS
Airline flight planning: The weather connection p 17 N83-17461

FLIGHT SIMULATION
Ejector nozzle test results at simulated flight conditions for an advanced supersonic transport propulsion system
[AIAA PAPER 83-1287] p 23 A83-36323
JT9D performance deterioration results from a simulated aerodynamic load test p 25 A83-41040
Tone-excited jet: Theory and experiments
[NASA-CR-3533] p 197 N83-12968
Tone generation by rotor-downstream strut interaction
[NASA-TM-83330] p 33 N83-19754
A compact inflow control device for simulating flight fan noise
[NASA-TM-83349] p 201 N83-26643

FLIGHT TESTS
Software and system level tests of a test flight mercury ion thruster subsystem
[AIAA PAPER 82-1912] p 51 A83-12485
Flight evaluation of modifications to a digital electronic engine control system in an F-15 airplane
[AIAA PAPER 83-0537] p 20 A83-19593
NASA Lewis Research Center's Program on Icing Research
[NASA-TM-83031] p 16 N83-14078
Measured performance of a tip-controlled, teetered rotor with an NACA 64 sub 3-618 tip airfoil
[NASA-TM-82870] p 169 N83-14689
Supersonic fan engines for military aircraft
[NASA-TM-83499] p 42 N83-34947

FLOQUET THEOREM
Some analysis methods for rotating systems with periodic coefficients p 157 A83-32987

FLOW CHARACTERISTICS
Predictions of the structure of turbulent, particle-laden, round jets
[AIAA PAPER 83-0066] p 119 A83-16498
New trends in combustion research for gas turbine engines p 22 A83-35806
Heat transfer and flow characteristics of jets impinging on a concave hemispherical plate p 123 A83-42743
Analysis of spiral-groove face seals for liquid oxygen
[ASLE PREPRINT 83-AM-4B-2] p 138 A83-43339
Heat transfer characteristics for jet array impingement with initial crossflow
[ASME PAPER 83-GT-28] p 7 A83-47891
Advanced technologies for turbomachinery systems: An overview
[NASA-TM-82949] p 28 N83-12090
New trends in combustion research for gas turbine engines
[NASA-TM-83338] p 34 N83-20947
The trend of future gas turbine technology
[NASA-TM-83505] p 2 N83-34886

FLOW DISTORTION
Axial-compressor flow distortion with water ingestion
[AIAA PAPER 83-0004] p 19 A83-16456
Three-dimensional stability of vortex arrays p 120 A83-19022
Rapid distortion of small-scale turbulence by an axisymmetric contraction p 120 A83-22381
A theory of rotating stall of multistage axial compressors. I - Small disturbances
[ASME PAPER 83-GT-44] p 7 A83-47904

A theory of rotating stall of multistage axial compressors. II - Finite disturbances
[ASME PAPER 83-GT-45] p 8 A83-47905
Literature search of publications concerning the prediction of dynamic inlet flow distortion and related topics
[NASA-CR-3673] p 33 N83-18729
FLOW DISTRIBUTION
Measurements and predictions for nonevaporating sprays in a quiescent environment
[AIAA PAPER 83-0151] p 119 A83-16558
Confined swirling flow predictions
[AIAA PAPER 83-0316] p 119 A83-16646
Aerodynamic features of turbulent flames
[AIAA PAPER 83-0470] p 119 A83-16737
An analytical and experimental comparison of the flow field of an advanced swept turboprop
[AIAA PAPER 83-0189] p 3 A83-21080
Mean flowfields in axisymmetric combustor geometries with swirl p 120 A83-24668
A basic code for the prediction of transient three-dimensional turbulent flowfields p 121 A83-27412
Incidence angle effects on convected gust airfoil noise
[AIAA PAPER 83-0765] p 195 A83-28022
Investigation of the tip clearance flow inside and at the exit of a compressor rotor passage. II - Turbulence properties p 4 A83-28643
Prediction of high speed propeller flow fields using a three-dimensional Euler analysis
[AIAA PAPER 83-0188] p 4 A83-29535
Tip clearance flow in a compressor rotor passage at design and off-design conditions p 4 A83-35855
Analytical and experimental study of flow through an axial turbine stage with a nonuniform inlet radial temperature profile
[AIAA PAPER 83-1175] p 6 A83-45510
Inlet-fan flow field computation
[ASME PAPER 83-GT-41] p 7 A83-47901
A computer program for the calculation of the flow field including boundary layer effects for mixed-compression inlets at angle of attack
[NASA-CR-168002] p 10 N83-11066
Analytical and experimental investigation of stator endwall contouring in a small axial-flow turbine. 1: Stator performance
[NASA-TP-2023] p 26 N83-11125
An analytical and experimental comparison of the flow field of an advanced swept turboprop
[NASA-TM-83037] p 1 N83-14061
Rotor redesign for a highly loaded 1800 ft/sec tip speed fan. 3: Laser Doppler velocimeter report
[NASA-CR-167954] p 30 N83-14128
Jet array impingement flow distributions and heat transfer characteristics. Effects of initial crossflow and nonuniform array geometry — gas turbine engine component cooling
[NASA-CR-3630] p 128 N83-15592
User's manual for three-dimensional analysis of propeller flow fields
[NASA-CR-167959] p 12 N83-18671
Prediction of high speed propeller flow fields using a three-dimensional Euler analysis
[NASA-TM-83065] p 12 N83-19710
Turbine endwall single cylinder program
[NASA-CR-170008] p 44 N83-19761
End-wall boundary layer measurements in a two-stage fan
[NASA-TM-83409] p 12 N83-24470
User's manual for Axisymmetric Diffuser Duct (ADD) code. Volume 1: General ADD code description
[NASA-CR-165598-VOL-1] p 211 N83-26757
Analytical and experimental study of flow through an axial turbine stage with a nonuniform inlet radial temperature profile
[NASA-TM-83431] p 14 N83-27958
Small gas turbine combustor primary zone study
[NASA-CR-168122] p 149 N83-28448
Axial compressor middle stage secondary flow study
[NASA-CR-3701] p 14 N83-29174
Small gas turbine combustor primary zone study p 38 N83-29221
Subsonic-transonic stall flutter study
[NASA-CR-165256] p 43 N83-30435
Axial vane-type swirler performance characteristics
[NASA-CR-172995] p 40 N83-32808
Turbulence measurements in a complex flowfield using a crossed hot-wire
[NASA-CR-173080] p 132 N83-35316
FLOW EQUATIONS
A finite element formulation for steady transonic Euler equations p 3 A83-22129
A two-equation turbulence model for two-phase flows p 121 A83-30109
Efficient solution of the Euler and Navier-Stokes equations with a vectorized multiple-grid algorithm
[AIAA PAPER 83-1893] p 5 A83-39359
Multiple-grid convergence acceleration of viscous and inviscid flow computations
[NASA-TM-83361] p 190 N83-21847
The finite analytic method, volume 4
[NASA-CR-170187] p 191 N83-23088
The finite analytic method, volume 5
[NASA-CR-170188] p 191 N83-23089
Efficient solution of the Euler and Navier-Stokes equations with a vectorized multiple-grid algorithm
[NASA-TM-83376] p 2 N83-24467
FLOW GEOMETRY
Three-dimensional stability of vortex arrays p 120 A83-19022
Mean flowfields in axisymmetric combustor geometries with swirl p 120 A83-24668
Study of asymptotic incompressible flow in curved ducts using a multi-grid technique p 123 A83-42532
Mean-flow measurements of the flow field diffusing bend
[NASA-CR-3634] p 10 N83-14066
FLOW MEASUREMENT
Modified gauge for time-resolved skin-friction measurements p 133 A83-14172
Measurements and predictions for nonevaporating sprays in a quiescent environment
[AIAA PAPER 83-0151] p 119 A83-16558
Computed and measured turbulence in axisymmetric reciprocating engines p 21 A83-24669
Single-wire swirl flow turbulence measurements
[AIAA PAPER 83-1202] p 122 A83-36278
NASA low-speed centrifugal compressor for fundamental research
[AIAA PAPER 83-1351] p 43 A83-36353
Measurements of compressible secondary flow in a circular S-duct
[AIAA PAPER 83-1739] p 4 A83-37218
An experimental study of heat induced surface-tension driven flow p 44 A83-43269
Experimental study of the boundary layer on a turbomachinery rotor blade p 7 A83-47022
Statistical characteristics of velocity, concentration, mass transport, and momentum transport for coaxial jet mixing in a confined duct
[ASME PAPER 83-GT-39] p 125 A83-47899
Studies of flows through N-sequential orifices
[ASME PAPER 83-FE-22] p 125 A83-48378
Three-dimensional flow measurements in a vaneless radial turbine scroll
[NASA-CR-167994] p 9 N83-11065
Mean-flow measurements of the flow field diffusing bend
[NASA-CR-3634] p 10 N83-14066
End-wall boundary layer measurements in a two-stage fan
[NASA-TM-83409] p 12 N83-24470
The structure of evaporating and combusting sprays: Measurements and predictions
[NASA-CR-170312] p 130 N83-24795
Subsonic-transonic stall flutter study
[NASA-CR-165256] p 43 N83-30435
The NASA High Accuracy Fuel Flowmeter (HAFF) development program
[NASA-TM-83484] p 19 N83-33883
FLOW REGULATORS
Air modulation apparatus — cooling gas turbine engines
[NASA-CASE-LEW-13524-1] p 131 N83-30957
FLOW STABILITY
Noise and flow structure of a tone-excited jet p 192 A83-13136
Three-dimensional stability of vortex arrays p 120 A83-19022
Vortices, stability, and turbulence p 125 A83-46718
FLOW THEORY
The evolution of Tollmien-Schlichting waves near a leading edge p 120 A83-24410
Evaluation of a stochastic model of particle dispersion in a turbulent round jet p 121 A83-28104
A theory of rotating stall of multistage axial compressors. III - Limit cycles
[ASME PAPER 83-GT-46] p 8 A83-47906
FLOW VELOCITY
Five-hole pitot probe time-mean velocity measurements in confined swirling flows
[AIAA PAPER 83-0315] p 119 A83-16645
Confined swirling flow predictions
[AIAA PAPER 83-0316] p 119 A83-16646
Laser anemometer using a Fabry-Perot interferometer for measuring mean velocity and turbulence intensity along the optical axis in turbomachinery p 133 A83-28834
The velocity perturbations above the orifice of an acoustically excited cavity in grazing flow p 195 A83-29235
Correlating downward flame spread rates for thick fuel beds p 69 A83-37045
Experiments on flow through one to four inlets of the orifice and Borda type p 124 A83-43235
Experimental study of the boundary layer on a turbomachinery rotor blade p 7 A83-47022
Three-dimensional flow measurements in a turbine scroll
[ASME PAPER 83-GT-128] p 8 A83-47957
Turbulence measurements in a swirling confined jet flowfield using a triple hot-wire probe
[NASA-CR-169668] p 127 N83-14434
Into mesh lubrication of spur gears with arbitrary offset oil jet. 1: For jet velocity less than or equal to gear velocity
[NASA-TM-83040] p 143 N83-19092
Into mesh lubrication of spur gears with arbitrary offset oil jet. 2: For jet velocities equal to or greater than gear velocity
[NASA-TM-83041] p 143 N83-19093
A method of predicting flow rates required to achieve anti-icing performance with a porous leading edge ice protection system
[NASA-CR-169996] p 17 N83-19738
Study of lubricant jet flow phenomena in spur gears: Out of mesh condition p 147 N83-20146
The structure of evaporating and combusting sprays: Measurements and predictions
[NASA-CR-170176] p 129 N83-22550
Air modulation apparatus — cooling gas turbine engines
[NASA-CASE-LEW-13524-1] p 131 N83-30957
A method of predicting flow rates required to achieve anti-icing performance with a porous leading edge ice protection system
[NASA-CR-168213] p 17 N83-32782
A comparison of flow rates and pressure profiles for N-sequential inlets and three related seal configurations
[NASA-TM-83442] p 132 N83-33103
FLOW VISUALIZATION
Experimental evaluation of shockless supercritical airfoils in cascade
[AIAA PAPER 83-0003] p 2 A83-16455
A new surface-streamline flow-visualization technique p 133 A83-19016
Turbulence effect on crossflow around a circular cylinder at subcritical Reynolds numbers
[NASA-CR-3622] p 127 N83-13387
Comparison of visualized turbine endwall secondary flows and measured heat transfer patterns
[NASA-TM-83016] p 128 N83-14435
FLOWMETERS
High accuracy fuel flowmeter, phase 1
[NASA-CR-167893] p 134 N83-21314
FLUENCE
Radiation damage p 172 N83-15837
FLUID DYNAMICS
NASA LeRC/Akron University Graduate Cooperative Fellowship Program and Graduate Student Researchers Program
[NASA-CR-167943] p 208 N83-10970
Environmental solid particle effects on compressor cascade performance
[NASA-CR-168018] p 11 N83-16285
Compressor cascade performance deterioration caused by sand ingestion
[NASA-CR-168067] p 11 N83-16286
Modeling of space vehicle propellant mixing — cryogenic propellants
[NASA-TP-2107] p 100 N83-16545
Structure of evaporating and combusting sprays: Measurements and predictions p 38 N83-29211
Aerothermal modeling program, phase 1
[NASA-CR-168202] p 131 N83-30959
FLUID FILMS
An experimental investigation of the vaporous/gaseous cavity characteristics of an eccentric journal bearing
[ASLE PREPRINT 82-LC-3A-1] p 136 A83-13230
Investigation of the effects of initial fluid film profile on pumping ring operation
[ASME PAPER 82-LUB-35] p 136 A83-13516
Analysis of spiral-groove face seals for liquid oxygen
[ASLE PREPRINT 83-AM-4B-2] p 138 A83-43339
Experimental investigation of the vaporous/gaseous cavity characteristics of an eccentric journal bearing
[NASA-TM-82996] p 128 N83-17833
Surface roughness effects in hydrodynamic lubrication: The flow factor method
[NASA-TM-83024] p 129 N83-19016
Lubrication background
[NASA-TM-81692] p 147 N83-20159
Film thickness for different regimes of fluid-film lubrication — elliptical contacts
[NASA-TM-81700] p 149 N83-28449

FLUID FLOW
A semi-direct solver for compressible 3-dimensional rotational flow
[NASA-TM-83314] p 15 N83-34908
FLUID INJECTION
Experiments in dilution jet mixing
[AIAA PAPER 83-1201] p 122 A83-36277
FLUID MANAGEMENT
Long term storage of cryogens in space p 102 A83-11487
Cryogenic fluid management experiment trunnion fatigue verification
[AIAA PAPER 83-0911] p 49 A83-32782
FLUID MECHANICS
Numerical simulation of the flow and fuel-air mixing in an axisymmetric piston-cylinder arrangement
[NASA-TM-83011] p 126 N83-12358
Preliminary design of flight hardware for two-phase fluid research
[NASA-CR-168072] p 46 N83-25766
Fuel spray diagnostics p 38 N83-29212
Comparison of two- and three-dimensional flow computations with laser anemometer measurements in a transonic compressor rotor
[NASA-TP-1931] p 15 N83-32774
FLUID PRESSURE
Multi-grid solution of Neumann pressure problem for viscous flows using primitive variables
[AIAA PAPER 83-0557] p 120 A83-16786
Experiments on flow through one to four inlets of the orifice and Borda type p 124 A83-43235
FLUID-SOLID INTERACTIONS
Effect of particle presence on the incompressible inviscid flow through a two dimensional compressor cascade p 6 A83-42562
FLUIDICS
Propulsion and fluid management - Station keeping will eat energy on a new scale p 54 A83-24360
FLUIDIZED BED PROCESSORS
IGCC performance comparison for variations in gasifier type and gas turbine firing temperature
[NASA-TM-83310] p 180 N83-25037
FLUORESCENCE
Laser-induced fluorescence technique for velocity field measurements in subsonic gas flows p 133 A83-45962
The detailed chemistry and thermodynamics of sodium in oxygen-rich flames
[NASA-CR-169848] p 72 N83-17626
FLUORINATION
Experimental study of electrochemical fluorination of trichloroethylene p 68 A83-15870
The electrochemical fluorination of polymeric materials for high energy density aqueous and non-aqueous battery and fuel cell separators
[NASA-CR-167961] p 72 N83-21056
FLUOROCARBONS
Preparation, characterization, physical testing and performance of flurocarbon membranes and separators
[NASA-CR-169756] p 71 N83-16418
Preparation, characterization, physical testing and performance of fluorocarbon membranes and separators
[NASA-CR-167880] p 73 N83-26936
FLUOROHYDROCARBONS
Experimental study of electrochemical fluorination of trichloroethylene p 68 A83-15870
FLUTTER
Friction damping of flutter in gas turbine engine airfoils p 20 A83-24038
Effects of friction dampers on aerodynamically unstable rotor stages
[AIAA PAPER 83-0848] p 22 A83-32791
Bending-torsion flutter of a highly swept advanced turboprop
[NASA-TM-82975] p 158 N83-11514
Measurements of self-excited rotor-blade vibrations using optical dispacements
[NASA-TM-82953] p 159 N83-14523
FLUTTER ANALYSIS
Flutter and forced response of mistuned rotors using standing wave analysis
[AIAA 83-0845] p 156 A83-29823
Flutter analysis of advanced turbopropellers
[AIAA 83-0846] p 157 A83-29824
FLUX DENSITY
Test methods and results of the 10-cell bipolar Ni-H2 battery p 117 N83-35261
Nickel-hydrogen component development
[NASA-TM-83487] p 163 N83-35498
FOCUSING
Experimental verification of the multistage depressed collector design procedure for a high-perveance, helix-type, traveling-wave tube — in communications satellites
[NASA-TP-2162] p 116 N83-25985
Gyrotron transmitting tube
[NASA-CASE-LEW-13429-1] p 117 N83-31952
FORCED VIBRATION
Flutter and forced response of mistuned rotors using standing wave analysis
[AIAA 83-0845] p 156 A83-29823
Some analysis methods for rotating systems with periodic coefficients p 157 A83-32987
Design of dry-friction dampers for turbine blades p 22 A83-35883
Analysis of an axial compressor blade vibration based on wave reflection theory
[ASME PAPER 83-GT-151] p 25 A83-47970
FORECASTING
Satellite provided customer premise services: A forecast of potential domestic demand through the year 2000. Volume 2: Technical report
[NASA-CR-168143] p 109 N83-34117
FORESTS
Energy and precious fuels requirements of fuel alcohol production. Volume 3, appendices C to F: Methanol from cellulose
[NASA-CR-168092] p 183 N83-28583
FORMALDEHYDE
Shock tube measurements of growth constants in the branched chain formaldehyde-carbon monoxide-oxygen system
[NASA-TM-82954] p 71 N83-12182
FORMULAS (MATHEMATICS)
Film thickness for different regimes of fluid-film lubrication — elliptical contacts
[NASA-TM-81700] p 149 N83-28449
FORWARD SCATTERING
Particle sizing by measurement of forward-scattered light at two angles
[NASA-TP-2156] p 36 N83-24509
FOSSIL FUELS
Fuel quality-processing study. Volume 1: Overview and results
[NASA-CR-165326-VOL-1] p 178 N83-22750
Fuel quality-processing study. Volume 2: Literature survey
[NASA-CR-165326-VOL-2] p 178 N83-22751
FOULING
Correlation and prediction of thermophoretic and inertial effects on particle deposition from non-isothermal turbulent boundary layers p 121 A83-27481
Combustion system processes leading to corrosive deposits p 69 A83-42246
FOURIER ANALYSIS
Determination of physical and chemical states of lubricants in concentrated contacts, part 3
[NASA-CR-3658] p 92 N83-16527
FRACTURE MECHANICS
Mechanics aspects of NDE by sound and ultrasound p 152 A83-25571
Dynamic fields near a crack tip growing in an elastic-perfectly-plastic solid p 157 A83-38528
Phenomenological and mechanics aspects of nondestructive evaluation and characterization by sound and ultrasound of material and fracture properties
[NASA-CR-3623] p 153 N83-11506
Analogy between fluid cavitation and fracture mechanics
[NASA-TM-83071] p 129 N83-22542
Nonlinear Constitutive Relations for High Temperature Applications
[NASA-CP-2271] p 161 N83-34351
FRACTURE STRENGTH
Interrelation of material microstructure, ultrasonic factors, and fracture toughness of a two-phase titanium alloy p 75 A83-23922
Fundamental aspects in quantitative ultrasonic determination of fracture toughness: The scattering of a single ellipsoidal inhomogeneity
[NASA-CR-3625] p 153 N83-11507
Development of tough, strong, iron-base alloy for cryogenic applications p 44 N83-18763
Specimen size and geometry effects on fracture toughness of Al2O3 measured with short rod and short bar chevron-notch specimens
[NASA-TM-83319] p 94 N83-19902
Present technology of rolling-element bearings p 144 N83-20121
Ultrasonic ranking of toughness of tungsten carbide
[NASA-TM-83358] p 153 N83-23620
The thermal fatigue resistance of H-13 Die Steel for aluminum die casting dies
[NASA-TM-83331] p 87 N83-35103
FRACTURING
Relation of cyclic loading pattern to microstructural fracture in creep fatigue
[NASA-TM-83473] p 161 N83-34349
FRAMES
Design concepts for low cost composite engine frames
[AIAA PAPER 83-2445] p 25 A83-46331
FREE CONVECTION
Measurement of thermoacoustic convection heat transfer phenomenon
[AIAA PAPER 83-1422] p 121 A83-32701
FREE ELECTRON LASERS
Gain-enhanced free-electron laser with an electromagnetic pump field p 135 A83-31133
The application of free-electron lasers to the transmission of energy in space p 135 A83-31141
FREE FLOW
Effects of free stream turbulence intensity and integral length scale on heat transfer from a circular cylinder in crossflow p 123 A83-42711
Generation of Tollmien-Schlichting waves by free-stream disturbances at low Mach numbers
[NASA-TM-83026] p 130 N83-23544
FREE JETS
Comparison of measured and predicted flight effects on high-bypass coaxial jet exhaust noise
[AIAA PAPER 83-0749] p 194 A83-26450
Free-jet acoustic investigation of high-radius-ratio coannular plug nozzles. Comprehensive data report, volume 1
[NASA-CR-168088-VOL-1] p 198 N83-18408
FREE RADICALS
Free radical propulsion concept p 53 A83-13141
Shock tube measurements of growth constants in the branched chain formaldehyde-carbon monoxide-oxygen system
[NASA-TM-82954] p 71 N83-12182
FREE VIBRATION
Vibrations of cantilevered circular cylindrical shells Shallow versus deep shell theory p 157 A83-36958
On the three-dimensional vibrations of the cantilevered rectangular parallelepiped p 157 A83-37729
Vibrations of cantilevered doubly-curved shallow shells p 157 A83-39557
Vibrations of blades with variable thickness and curvature by shell theory
[ASME PAPER 83-GT-152] p 158 A83-47978
FREQUENCY ASSIGNMENT
Future satellite systems - Market demand assessment p 104 A83-19762
Engineering calculations for communications systems planning
[NASA-CR-170182] p 106 N83-22494
FREQUENCY DIVISION MULTIPLE ACCESS
Satellite switched FDMA advanced communication technology satellite program
[NASA-CR-168034] p 105 N83-15543
A comparison of Frequency Domain Multiple Access (FDMA) and Time Domain Multiple Access (TDMA) approaches to satellite service for low data rate Earth stations
[NASA-TM-83430] p 109 N83-34120
FREQUENCY DIVISION MULTIPLEXING
Optical systolic array processor using residue arithmetic p 189 A83-46834
FREQUENCY MODULATION
Four-dimensional modulation and coding: An alternate to frequency-reuse
[NASA-CR-174453] p 110 N83-36300
FREQUENCY RESPONSE
Tubes in space - Very much alive p 112 A83-28160
FREQUENCY REUSE
Concept for advanced satellite communications and required technologies
[NASA-TM-82984] p 47 N83-11210
Four-dimensional modulation and coding: An alternate to frequency-reuse
[NASA-CR-174453] p 110 N83-36300
FREQUENCY SHIFT KEYING
Advances in Serial MSK modems p 111 A83-19789
FRETTING
Review of factors that influence fretting wear p 137 A83-17259
FRICTION
Correlation of tensile and shear strengths of metals with their friction properties
[ASLE PREPRINT 82-LC-UB-1] p 74 A83-13226
Friction damping of flutter in gas turbine engine airfoils p 20 A83-24038
Friction and wear of iron and nickel in sodium hydroxide solutions p 77 A83-48922
Friction and wear of iron and nickel in sodium hydroxide solutions
[NASA-TM-82935] p 77 N83-10171
Plasma deposition and surface modification techniques for wear resistance
[NASA-TM-82972] p 90 N83-10194

Tribological properties of amorphous alloys and the role of surfaces in abrasive wear of materials
[NASA-TM-82973] p 140 N83-11498
Tribology p 140 N83-12167
Polyimides: Tribological properties and their use as lubricants
[NASA-TM-82959] p 91 N83-13257
Surface chemistry, friction and wear of Ni-Zn and Mn-Zn ferrites in contact with metals
[NASA-TM-83068] p 93 N83-19901
Assessment of lubricated contacts: Mechanisms of scuffing and scoring
[NASA-TM-83074] p 144 N83-20118
X-ray photoelectron spectroscopy and friction studies of nickel-zinc and manganese-zinc ferrites in contact with metals
[NASA-TP-2163] p 84 N83-23419
Friction, wear, transfer and wear surface morphology of ultra-high-molecular-weight polyethylene
[NASA-TM-83364] p 94 N83-25882
Tribological measurements on a Charnley-type artificial hip joint
[NASA-TM-83440] p 97 N83-32943

FRICTION MEASUREMENT
Modified gauge for time-resolved skin-friction measurements p 133 A83-14172

FRICTION REDUCTION
Effects of friction dampers on aerodynamically unstable rotor stages
[AIAA PAPER 83-0848] p 22 A83-32791
A commentary on solid lubricants and wear resistant solids for use in extreme environments
[NASA-TM-83042] p 92 N83-15468

FROST
Water vapor measurement system in global atmospheric sampling program, appendix
[NASA-TP-2051] p 187 N83-13643

FUEL CELL POWER PLANTS
Task 4 completion report for 40 Kilowatt grid connected modification contract
[NASA-CR-167950] p 208 N83-30297

FUEL CELLS
Pore size engineering applied to starved electrochemical cells and batteries p 164 A83-27201
Pore size engineering applied to starved electrochemical cells and batteries
[NASA-TM-82993] p 70 N83-10134
The electrochemical fluorination of polymeric materials for high energy density aqueous and non-aqueous battery and fuel cell separators
[NASA-CR-167961] p 72 N83-21056
Pore size engineering applied to the design of separators for nickel-hydrogen cells and batteries
[NASA-TM-83386] p 73 N83-24571

FUEL COMBUSTION
Tests of blending and correlation of distillate fuel properties p 98 A83-11050
Multifuel evaluation of rich/quench/lean combustor p 67 A83-11492
NOx results from two combustors tested on medium BTU coal gas p 186 A83-11493
Boundary integral equation method calculations of surface regression effects in flame spreading p 67 A83-13488
Droplet size effects on NO/x/ formation in a one-dimensional monodisperse spray combustion system
[ASME PAPER 82-JPGC-GT-10] p 68 A83-25268
Catalytic combustion with steam injection
[ASME PAPER 82-JPGC-GT-23] p 164 A83-25271
New trends in combustion research for gas turbine engines p 22 A83-35806
Application of 3D aerodynamic/combustion model to combustor primary zone study
[AIAA PAPER 83-1265] p 23 A83-30316
Combustion of coal gas fuels in a staged combustor
[NASA-TM-82987] p 166 N83-10556
Evaluation of advanced combustion concepts for dry NO sub x suppression with coal-derived, gaseous fuels
[NASA-TM-82985] p 166 N83-10557
Multifuel evaluation of rich/quench/lean combustor
[NASA-TM-82986] p 167 N83-10559
Catalytic combustion with steam injection
[NASA-TM-82923] p 170 N83-15805
Analysis of combustion spectra containing organ pipe tone by cepstral techniques
[NASA-TM-83034] p 198 N83-16153
Critical research and advanced technology (CRT) support project
[NASA-TM-83019] p 176 N83-20361
New trends in combustion research for gas turbine engines
[NASA-TM-83338] p 34 N83-20947
Structure of evaporating and combusting sprays: Measurements and predictions p 38 N83-29211
Fuel spray diagnostics p 38 N83-29212
Fuel vaporization effects p 101 N83-29214
The NASA broad-specification fuels combustion technology program: An assessment of phase 1 test results
[NASA-TM-83447] p 39 N83-29236
Broad specification fuels technology program, phase 1
[NASA-CR-168180] p 74 N83-30551

FUEL CONSUMPTION
Measured effect of wind generation on the fuel consumption of an isolated diesel power system p 165 A83-36410
Energy efficient engine. Flight propulsion system preliminary analysis and design
[NASA-CR-159859] p 28 N83-12094
Implementation of R & QA practices in Research and Development programs
[NASA-TM-82997] p 210 N83-19651
Farfield inflight measurement of high-speed turboprop noise
[NASA-TM-83327] p 199 N83-21895
Industry's assessment of the number of airplanes in the general aviation fleet along with their hours flown and fuel consumption data powered by what type of engines, when and for what reasons, through the year 2000 p 101 N83-22445
DOE/NASA Automotive Stirling Engine Project overview '83
[NASA-TM-83405] p 212 N83-27924
Automotive Stirling Engine Development Program
[NASA-CR-168074] p 212 N83-27925
Nacelle Aerodynamic and Inertial Loads (NAIL) project
[NASA-CR-168712] p 18 N83-30402
The NASA High Accuracy Fuel Flowmeter (HAFF) development program
[NASA-TM-83484] p 19 N83-33883

FUEL FLOW
Vapor flow into a capillary propellant-acquisition device
[AIAA PAPER 83-1380] p 55 A83-36371
High accuracy fuel flowmeter, phase 1
[NASA-CR-167893] p 134 N83-21314
User's manual for Axisymmetric Diffuser Duct (ADD) code. Volume 3: ADD code coordinate generator
[NASA-CR-165598-VOL-3] p 211 N83-26759
The NASA High Accuracy Fuel Flowmeter (HAFF) development program
[NASA-TM-83484] p 19 N83-33883

FUEL INJECTION
Catalytic combustion with steam injection
[ASME PAPER 82-JPGC-GT-23] p 164 A83-25271
Aerodynamic-wave break-up of liquid sheets in swirling airflows and combustor modules
[AIAA PAPER 83-1204] p 124 A83-45511
Analytical modeling of operating characteristics of premixing-prevaporizing fuel-air mixing passages. Volume 1: Analysis and results
[NASA-CR-167990-VOL-1] p 126 N83-12353
Analytical modeling of operating characteristics of premixing-prevaporizing fuel-air mixing passages. Volume 2: User's manual
[NASA-CR-167990-VOL-2] p 126 N83-12354
Catalytic combustion with steam injection
[NASA-TM-82923] p 170 N83-15805
Aerodynamic-wave break-up of liquid sheets in swirling airflows and combustor modules
[NASA-TM-83353] p 130 N83-23545
Characterization of a high-pressure diesel fuel injection system as a control technology option to improve engine performance and reduce exhaust emissions
[NASA-TM-83329] p 210 N83-24431
Autoignition in a premixing-prevaporizing fuel duct using 3 different fuel injection systems at inlet air temperatures to 1250 K
[NASA-TM-82938] p 181 N83-26251
Effects of percentage of blockage and flameholder downstream counterbores on lean combustion limits of premixed, prevaporized propane-air mixture
[NASA-TP-2227] p 41 N83-34941

FUEL PRODUCTION
Fuel quality-processing study. Volume 1: Overview and results
[NASA-CR-165326-VOL-1] p 178 N83-22750
Fuel quality-processing study. Volume 2: Literature survey
[NASA-CR-165326-VOL-2] p 178 N83-22751
Fuel quality/processing study. Volume 3: Fuel upgrading studies
[NASA-CR-165326-VOL-3] p 178 N83-22754

FUEL SPRAYS
Measurements and predictions for nonevaporating sprays in a quiescent environment
[AIAA PAPER 83-0151] p 119 A83-16558
Droplet size effects on NO/x/ formation in a one-dimensional monodisperse spray combustion system
[ASME PAPER 82-JPGC-GT-10] p 68 A83-25268
Detailed fuel spray analysis techniques
[NASA-TM-83476] p 42 N83-34943

FUEL SYSTEMS
Automotive Stirling Engine Mod 1 Design Review, volume 2
[NASA-CR-167936] p 209 N83-10991
Aviation Gasolines and Future Alternatives
[NASA-CP-2267] p 100 N83-22442
Fuel supply and distribution. Fixed base operation p 101 N83-22449
The NASA broad-specification fuels combustion technology program: An assessment of phase 1 test results
[NASA-TM-83447] p 39 N83-29236
LOX/hydrocarbon fuel carbon formation and mixing data analysis
[NASA-CR-168066] p 101 N83-31886
The trend of future gas turbine technology
[NASA-TM-83505] p 2 N83-34886
Study of LH2-fueled topping cycle engine for aircraft propulsion
[NASA-TM-83466] p 41 N83-34942
Apparatus for improving the fuel efficiency of a gas turbine engine
[NASA-CASE-LEW-13142-1] p 43 N83-36029

FUEL TESTS
Tests of blending and correlation of distillate fuel properties p 98 A83-11050
A carbon-13 and proton nuclear magnetic resonance study of some experimental referee broadened-specification /ERBS/ turbine fuels p 98 A83-11482

FUEL-AIR RATIO
Numerical simulation of the flow and fuel-air mixing in an axisymmetric piston-cylinder arrangement
[NASA-TM-83011] p 126 N83-12358
Fuel spray diagnostics p 38 N83-29212
Fuel vaporization effects p 101 N83-29214

FUELS
Combustion characteristics of hydrogen, Carbon monoxide based gaseous fuels
[NASA-TM-82998] p 167 N83-10560

FUMIGATION
Fumigation of alcohol in a light duty automotive diesel engine
[NASA-CR-167915] p 99 N83-13272

FUNCTIONS (MATHEMATICS)
A class of nonideal solutions. 2: Application to experimental data
[NASA-TP-1930] p 208 N83-23188

FUSELAGES
Small transport aircraft technology propeller study
[NASA-CR-168045] p 14 N83-29178

G

GALLIUM ARSENIDES
A 1 watt GaAs power amplifier for the NASA 30/20 GHz communication system p 111 A83-11489
Ellipsometric study of silicon nitride on gallium arsenide p 204 A83-11812
Liquid encapsulated Czochralski growth of low dislocation GaAs p 204 A83-13784
Residual double acceptors in bulk GaAs p 205 A83-19989
EL2 distributions in doped and undoped liquid encapsulated Czochralski GaAs — deep donor concentration p 205 A83-22756
High-performance K-band GaAs power field-effect transistors prepared by molecular beam epitaxy p 112 A83-33846
GaAs integrated digital-to-analogue convertor for control of power dual-gate FETs p 112 A83-36479
An enhanced sensitivity null ellipsometry technique for studying films on substrates - Application to silicon nitride on gallium arsenide p 206 A83-37618
A two-stage monolithic buffer amplifier for 20 GHz satellite communication p 112 A83-39272
Diffused P+-N solar cells in bulk GaAs p 171 N83-15818
Advances in large-diameter liquid encapsulated Czochralski GaAs p 171 N83-15819
GaAs solar cells for concentrator systems in space p 171 N83-15820
The effect of different solar simulators on the measurement of short-circuit current temperature coefficients p 172 N83-15821
Radiation damage and annealing in large area n+/p/p+ GaAs shallow homojunction solar cells p 172 N83-15826
Radiation damage p 172 N83-15837
High purity, low dislocation GaAs single crystals
[NASA-CR-168098] p 206 N83-19622

Design rules for a 100X maximum efficiency GaAs concentrator solar cell for space applications
[NASA-CR-170005] p 177 N83-20362
Growth and characterization of Czochralski-grown n and p-type GaAs for space solar cell substrates
[NASA-CR-168099] p 207 N83-27877
Advanced digital modulation: Communication techniques and monolithic GaAs technology
[NASA-CR-174452] p 109 N83-36299
VLSI technology and applications
[NASA-CR-174451] p 118 N83-36358

GAS BEARINGS

Film thickness measurement for spiral groove and Rayleigh step lift pad self-acting face seals
[NASA-TP-2058] p 26 N83-11126
Design analysis of a self-acting spiral-groove ring seal for counter-rotating shafts
[NASA-TP-2142] p 36 N83-25712

GAS CHROMATOGRAPHY

High-voltage spark atomic emission detector for gas chromatography p 67 A83-13108

GAS COMPOSITION

Burner rig study of variables involved in hole plugging of air cooled turbine engine vanes
[NASA-TM-83308] p 83 N83-19887

GAS DENSITY

The thermal conductivity of oxygen
p 207 A83-12094

GAS DISCHARGES

A direct-measurement technique for estimating discharge-chamber lifetime --- for ion thrusters
[AIAA PAPER 82-1908] p 51 A83-12483

GAS DISSOCIATION

Free radical propulsion concept p 53 A83-13141

GAS DYNAMICS

Predictions of the structure of turbulent, particle-laden, round jets
[AIAA PAPER 83-0066] p 119 A83-16498
A new surface-streamline flow-visualization technique
p 133 A83-19016
Radiative energy receiver for high performance energy conversion cycles p 164 A83-27138

GAS FLOW

Measurements of energy distribution and thrust for microwave plasma coupling of electrical energy to hydrogen for propulsion
[AIAA PAPER 82-1951] p 52 A83-12508
High-speed motion picture camera experiments of cavitation in dynamically loaded journal bearings
[ASME PAPER 82-LUB-18] p 136 A83-13509
Transient flow analysis of the AEDC/HPDE MHD generator
[AIAA PAPER 83-0395] p 203 A83-16691
Vapor flow into a capillary propellant-acquisition device
[AIAA PAPER 83-1380] p 55 A83-36371
High-speed motion picture camera experiments of cavitation in dynamically loaded journal bearings
[ASME PAPER 82-LUB-18] p 138 A83-39944
Laser-induced fluorescence technique for velocity field measurements in subsonic gas flows
p 133 A83-45962
Covering solid, film cooled surfaces with a duplex thermal barrier coating
[NASA-CASE-LEW-13450-1] p 103 N83-35177

GAS MIXTURES

Ignition of confined gaseous mixtures by hot surfaces and hot wires
[AIAA PAPER 83-0240] p 68 A83-16606

GAS PRESSURE

The thermal conductivity of oxygen
p 207 A83-12094
Numerical simulation of the flow and fuel-air mixing in an axisymmetric piston-cylinder arrangement
[NASA-TM-83011] p 126 N83-12358

GAS TURBINE ENGINES

Multifuel evaluation of rich/quench/lean combustor
p 67 A83-11492
Composite fan exit guide vanes for high bypass ratio gas turbine engines p 19 A83-13159
Small gas turbine combustor study - Combustor liner evaluation
[AIAA PAPER 83-0337] p 20 A83-16663
Effect of broad properties fuel on injector performance in a reverse flow combustor
[AIAA PAPER 83-0154] p 20 A83-21079
Friction damping of flutter in gas turbine engine airfoils
p 20 A83-24038
NASA clean catalytic combustor program
[ASME PAPER 82-JPGC-GT-11] p 68 A83-25269
Catalyst durability evaluation for advanced gas turbine engines
[ASME PAPER 82-JPGC-GT-21] p 137 A83-25270
Structural tailoring of engine blades (STAEBL)
[AIAA 83-0828] p 22 A83-29737
Effects of friction dampers on aerodynamically unstable rotor stages
[AIAA PAPER 83-0848] p 22 A83-32791
New trends in combustion research for gas turbine engines p 22 A83-35806
Advanced propfan engine characteristics and technology needs
[AIAA PAPER 83-1155] p 23 A83-36250
Effects of interstage diffuser flow distortion on the performance of a 15.41-centimeter tip diameter axial power turbine
[AIAA PAPER 83-1179] p 23 A83-36263
Experiments in dilution jet mixing
[AIAA PAPER 83-1201] p 122 A83-36277
Importance of inlet boundary conditions for numerical simulation of combustor flows
[AIAA PAPER 83-1263] p 23 A83-36314
The performance of an annular vane swirler --- to aid in modeling gas turbine combustor flowfields and swirling confined flow turbulence
[AIAA PAPER 83-1326] p 24 A83-36340
A comprehensive method for preliminary design optimization of axial gas turbine stages. II - Code verification
[AIAA PAPER 83-1403] p 24 A83-36393
Nonlinear multivariable design by total synthesis --- of gas turbine engine control systems p 24 A83-37092
Solution of viscous internal flows on curvilinear grids generated by the Schwarz-Christoffel transformation
p 122 A83-38796
Composite engine duct fabrication p 1 A83-39941
The feasibility of water injection into the turbine coolant to permit gas turbine contingency power for helicopter application
[ASME PAPER 83-GT-66] p 24 A83-39993
Blade loss transient dynamic analysis of turbomachinery p 25 A83-40864
Measurements of heat transfer distribution over the surfaces of highly loaded turbine nozzle guide vanes
[ASME PAPER 83-GT-53] p 8 A83-47910
Three-dimensional flow measurements in a turbine scroll
[ASME PAPER 83-GT-128] p 8 A83-47957
Component qualification and detail build of the AGT 100 advanced automotive gas turbine
[ASME PAPER 83-GT-225] p 138 A83-48023
Progress in net shape fabrication of alpha SiC turbine components
[ASME PAPER 83-GT-238] p 139 A83-48030
Development of advanced high-temperature heat flux sensors
[NASA-CR-165618] p 26 N83-10044
Multifuel evaluation of rich/quench/lean combustor
[NASA-TM-82986] p 167 N83-10559
Performance of a tandem-rotor/tandem-stator conical-flow compressor designed for a pressure ratio of 3
[NASA-TP-2034] p 9 N83-11058
Cold-air performance of compressor-drive turbine of Department of Energy upgraded automobile gas turbine engine. 2: Stage performance
[NASA-TM-82818] p 9 N83-11063
Advanced Gas Turbine (AGT) powertrain system
[NASA-CR-165346] p 139 N83-11497
Advanced Gas Turbine (AGT) powertrain system development program --- automobile engines
[NASA-CR-169475] p 27 N83-12088
Conservation of strategic metals p 80 N83-12154
Advanced Gas Turbine (AGT) powertrain system development for automotive applications
[NASA-CR-165178] p 140 N83-12431
Ferrographic and spectrometer oil analysis from a failed gas turbine engine
[NASA-TM-82956] p 140 N83-12433
Advanced Gas Turbine (AGT) powertrain system development for automotive applications
[NASA-CR-135329] p 209 N83-13038
Effect of broad properties fuel on injector performance in a reverse flow combustor
[NASA-TM-83013] p 29 N83-13101
Tip cap for a rotor blade
[NASA-CASE-LEW-13654-1] p 30 N83-14129
Energy efficient high-pressure turbine leakage technology report
[NASA-CR-165202] p 30 N83-15304
JT9D ceramic outer air seal system refinement program, phase 2
[NASA-CR-167962] p 30 N83-15305
Advanced Gas Turbine (AGT) power-train system development
[NASA-CR-167875] p 142 N83-15627
A method to estimate weight and dimensions of small aircraft propulsion gas turbine engines: User's guide
[NASA-CR-168049] p 31 N83-16343
Analysis of a MIL-L-27502 lubricant from a gas-turbine engine test by size-exclusion chromatography
[NASA-TP-2063] p 93 N83-16528
Advanced Gas Turbine (AGT) powertrain system development for automotive applications
[NASA-CR-167983] p 210 N83-17424
Experimental study of the thermal stability of hydrocarbon fuels
[NASA-CR-168027] p 100 N83-17728
Bearing fatigue investigation 3
[NASA-CR-168029] p 143 N83-17880
Small gas turbine combustor study: Combustor liner evaluation
[NASA-TM-83028] p 33 N83-18725
Development of a rotary instrumentation system, phase 2
[NASA-CR-168013] p 47 N83-18835
Energy efficient engine sector combustor rig test program
[NASA-CR-167913] p 33 N83-19753
Support and power plant documentation for the gas turbine powered bus demonstration program
[NASA-CR-165527] p 210 N83-20829
New trends in combustion research for gas turbine engines
[NASA-TM-83338] p 34 N83-20947
Analytical fuel property effects, small combustors, phase 1
[NASA-CR-168138] p 101 N83-23464
Opportunities for research in aerothermodynamics
[NASA-TM-83348] p 35 N83-24506
Particle sizing by measurement of forward-scattered light at two angles
[NASA-TP-2156] p 36 N83-24509
Advanced Gas Turbine (AGT) powertrain system development for automotive applications
[NASA-CR-168104] p 211 N83-26763
Demonstration and evaluation of gas turbine transit buses
[NASA-CR-165528] p 212 N83-27926
A variable-geometry combustor used to study primary and secondary zone stoichiometry
[NASA-TM-83372] p 37 N83-27995
Rotorcraft convertible engine study
[NASA-CR-168161] p 37 N83-27996
Wear particle analysis using the ferrograph
[NASA-TM-83422] p 96 N83-28243
Fuel vaporization effects p 101 N83-29214
Dilution zone mixing p 131 N83-29216
Rotor fragment protection program: Statistics on aircraft gas turbine engine rotor failures that occurred in US commercial aviation during 1979
[NASA-CR-168163] p 38 N83-29234
Reactions of NaCl with gaseous SO3, SO2, and O2
[NASA-TM-83423] p 86 N83-29358
Experiments in dilution jet mixing
[NASA-TM-83434] p 15 N83-30393
Evaluation of ceramics for stator applications: Gas turbine engines interim report. Stator fabrication and evaluation
[NASA-CR-168140] p 96 N83-30662
Air modulation apparatus --- cooling gas turbine engines
[NASA-CASE-LEW-13524-1] p 131 N83-30957
Stagnation region gas film cooling: Effects of dimensionless coolant temperature
[NASA-CR-168197] p 132 N83-30960
Control means for a gas turbine engine
[NASA-CASE-LEW-14586-1] p 40 N83-31603
Silicon-slurry/aluminide coating --- protecting gas turbine engine vanes and blades
[NASA-CASE-LEW-13343] p 86 N83-31795
Advanced Gas Turbine (AGT) powertrain system development for automotive applications
[NASA-CR-167901] p 212 N83-33800
Evaluation of inelastic constitutive models for nonlinear structural analysis p 162 N83-34357
Simplified method for nonlinear structural analysis
[NASA-TP-2208] p 163 N83-34372
Apparatus for improving the fuel efficiency of a gas turbine engine
[NASA-CASE-LEW-13142-1] p 43 N83-36029

GAS TURBINES

Use of fiber-like materials to augment cycle life of thick, thermoprotective-seal coatings --- for gas turbine engine components p 89 A83-22271
Correlation and prediction of thermophoretic and inertial effects on particle deposition from non-isothermal turbulent boundary layers p 121 A83-27481
Statistical characteristics of velocity, concentration, mass transport, and momentum transport for coaxial jet mixing in a confined duct
[ASME PAPER 83-GT-39] p 125 A83-47899
Combustion characteristics of hydrogen. Carbon monoxide based gaseous fuels
[NASA-TM-82998] p 167 N83-10560

Comparison of predicted and experimental external heat transfer around a film cooled cylinder in crossflow
[NASA-TM-83017] p 127 N83-13392
Advanced ceramic coating development for industrial/utility gas turbine applications
[NASA-CR-165619] p 92 N83-15467
Predicted and experimental performance of large-bore high-speed ball and roller bearings p 145 N83-20131
Evaluation of a high performance, fixed-ratio, traction drive p 145 N83-20135
Critical research and advanced technology (CRT) support project
[NASA-TM-83019] p 176 N83-20361
Progress toward determining the potential of ODS alloys for gas turbine applications
[NASA-TM-83332] p 83 N83-22387
Fuel quality-processing study. Volume 1: Overview and results
[NASA-CR-165326-VOL-1] p 175 N83-22750
Fuel quality-processing study. Volume 2: Literature survey
[NASA-CR-165326-VOL-2] p 178 N83-22751
Fuel quality/processing study. Volume 3: Fuel upgrading studies
[NASA-CR-165326-VOL-3] p 178 N83-22754
Fuel quality/processing study. Volume 4: On site processing studies
[NASA-CR-165326-VOL-4] p 179 N83-22755
IGCC performance comparison for variations in gasifier type and gas turbine firing temperature
[NASA-TM-83310] p 180 N83-25037
Testing of felt-ceramic materials for combustor applications
[NASA-CR-168103] p 36 N83-26837
Thermal-barrier coatings for utility gas turbines
[NASA-TM-83349] p 95 N83-27022
Analytical and experimental evaluation of the heat transfer distribution over the surfaces of turbine vanes
[NASA-CR-168015] p 131 N83-28376
Residual stress in plasma sprayed ceramic turbine tip and gas path seal specimens
[NASA-TM-83418] p 131 N83-28380
Small gas turbine combustor primary zone study
[NASA-CR-168122] p 149 N83-28448
Combustion Fundamentals Research
[NASA-CP-2268] p 38 N83-29208
Small gas turbine combustor primary zone study
p 38 N83-29221
Current and future technology in radial and axial gas turbines
[NASA-TM-83414] p 41 N83-32811
Summary of synfuel characterization and combustion studies
[NASA-TM-83066] p 185 N83-34453
The trend of future gas turbine technology
[NASA-TM-83505] p 2 N83-34886
Turbulence measurements in a complex plowfield using a crossed hot-wire
[NASA-CR-173080] p 132 N83-35316

GAS VALVES
Air modulation apparatus — cooling gas turbine engines
[NASA-CASE-LEW-13524-1] p 131 N83-30957

GAS-METAL INTERACTIONS
Direct contact droplet heat exchangers for thermal management in space p 120 A83-27137
Cyclic oxidation of superalloys p 76 A83-42234
Diffusion processes in Al2O3 scales - Void growth, grain growth and scale growth p 76 A83-42238
The oxidation behavior of a model molybdenum-tungsten-containing alloy in air alone and in air with low levels of NaCl(g) p 76 A83-42241
Determination of hydrogen permeability in uncoated and coated superalloys
[NASA-CR-165209] p 80 N83-12215
Reaction of cobalt in SO2 atmospheric at elevated temperatures
[NASA-TM-83485] p 88 N83-35104

GASEOUS DIFFUSION
Diffusion processes in Al2O3 scales - Void growth, grain growth, and scale growth p 76 A83-42238

GASEOUS FUELS
Combustion characteristics of hydrogen-carbon monoxide based gaseous fuels p 67 A83-11491

GASIFICATION
Advanced Gas Turbine (AGT) power-train system development
[NASA-CR-167875] p 142 N83-15627

GASOLINE
Aviation Gasolines and Future Alternatives
[NASA-CP-2267] p 100 N83-22442
Evaluation of fuel additives for reduction of material incompatibilities in methanol-gasoline blends
[NASA-CR-168061] p 86 N83-29359

GATES (CIRCUITS)
Equivalent-circuit consideration of dual-gate MESFETs at high frequency p 113 A83-44970
Requirements for a mobile communications satellite system. Volume 2: Technical report
[NASA-CR-168129] p 107 N83-23498

GEAR TEETH
Design of an advanced 500-HP helicopter transmission p 21 A83-24834
Experimental and analytical determination of gear tooth temperatures with oil jet lubrication p 142 N83-15530
Compliance and stress sensitivity of spur gear teeth p 146 N83-20142
A method for static and dynamic load analysis of standard and modified spur gears p 146 N83-20143
Gear lubrication and cooling experiment and analysis p 147 N83-20147
Dynamic tooth loads and stressing for high contact ratio spur gears p 147 N83-20148
Large rotorcraft transmission technology development program
[NASA-CR-168120] p 18 N83-22188

GEARS
Life and reliability models for helicopter transmissions
[NASA-TM-82976] p 139 N83-10425
The transfer function method for gear system dynamics applied to conventional and minimum excitation gearing designs
[NASA-CR-3626] p 139 N83-11495
Into mesh lubrication of spur gears with arbitrary offset oil jet. 1: For jet velocity less than or equal to gear velocity
[NASA-TM-83040] p 143 N83-19092
Into mesh lubrication of spur gears with arbitrary offset oil jet. 2: For jet velocities equal to or greater than great velocity
[NASA-TM-83041] p 143 N83-19093
A historical perspective of traction drives and related technology p 144 N83-20123
An overview of advancements in helicopter transmission design p 144 N83-20124
Design of an advanced 500-hp helicopter transmission p 144 N83-20125
Design study of Self-Alining Bearingless Planetary (SABP) gear p 145 N83-20127
Hybrid geared traction transmissions p 145 N83-20128
A basis for the analysis of surface geometry of spiral bevel gears p 146 N83-20138
Spiral-bevel geometry and gear train precision p 146 N83-20139
Comparison of spur gear efficiency prediction methods p 146 N83-20141
An update on the life analysis of spur gears p 146 N83-20144
The optimal design of standard gearsets p 146 N83-20145
Study of lubricant jet flow phenomena in spur gears: Out of mesh condition p 147 N83-20146
Evaluation of high-contact-ratio spur gears with profile modification p 147 N83-20150
Large rotorcraft transmission technology development program
[NASA-CR-168120] p 18 N83-22188
Dynamic effects of internal spur gear drives
[NASA-CR-3692] p 149 N83-28452
Vibration in planetary gear systems with unequal planet stiffnesses
[NASA-TM-83428] p 150 N83-29709
Geometrical analysis of circular-cut spiral bevel gears
[NASA-CR-168226] p 151 N83-33167

GENERAL AVIATION AIRCRAFT
Computer program to predict noise of general aviation aircraft: User's guide
[NASA-CR-168050] p 198 N83-17242
Industry's assessment of the number of airplanes in the general aviation fleet along with their hours flown and fuel consumption data powered by what type of engines, when and for what reasons, through the year 2000 p 101 N83-22445
General Aviation Turbine Engine (GATE) overview p 35 N83-22457
Multi-fuel rotary engine for general aviation aircraft
[NASA-TM-83429] p 38 N83-29235

GEOMETRICAL ACOUSTICS
Phenomenological and mechanics aspects of nondestructive evaluation and characterization by sound and ultrasound of material and fracture properties
[NASA-CR-3623] p 153 N83-11506
Fundamental aspects in quantitative ultrasonic determination of fracture toughness: The scattering of a single ellipsoidal inhomogeneity
[NASA-CR-3625] p 153 N83-11507

GEOMETRY
Rolling-element bearings
[NASA-RP-1105] p 149 N83-27214
A comparison of flow rates and pressure profiles for N-sequential inlets and three related seal configurations
[NASA-TM-83442] p 132 N83-33103

GEOSYNCHRONOUS ORBITS
Large space systems auxiliary propulsion requirements p 46 N83-26864
The role of potential barrier formation in spacecraft charging
[NASA-TM-83500] p 50 N83-35005

GETTERS
Developments toward an 18% efficient silicon solar cell
[NASA-CR-168141] p 181 N83-25112

GIBBS FREE ENERGY
A class of nonideal solutions. 2: Application to experimental data
[NASA-TP-1930] p 208 N83-23188

GLASS
Time effect of erosion by solid particle impingement on ductile materials
[NASA-TM-83369] p 84 N83-24637
Spherical micro-glass particle impingement studies of thermoplastic materials at normal incidence
[NASA-TM-83410] p 94 N83-25883
A study of the stress wave factor technique for the characterization of composite materials
[NASA-CR-3670] p 153 N83-27248
Time dependence of solid-particle impingement erosion of an aluminum alloy
[NASA-TP-2169] p 86 N83-32908

GLASS FIBER REINFORCED PLASTICS
Design and fabrication of composite blades for the Mod-1 wind turbine generator
[NASA-CR-167987] p 168 N83-11579

GLASS FIBERS
Hygrothermomechanical evaluation of transverse filament tape epoxy/polyester fiberglass composites
[NASA-TM-83044] p 65 N83-15362
Design and evaluation of low-cost stainless steel fiberglass foam blades for large wind driven generating systems
[NASA-CR-165491] p 174 N83-19226
Hybridized polymer matrix composites
[NASA-CR-165341] p 66 N83-22326
Fatigue testing of low-cost fiberglass composite wind turbine blade materials
[NASA-CR-165566] p 177 N83-22746
Structural qualification testing and operational loading on a fiberglass rotor blade for the Mod-0A wind turbine
[NASA-TM-83309] p 179 N83-23710

GLAZES
Performance of laser-glazed zirconia thermal barrier coatings in cyclic oxidation and corrosion burner rig tests p 88 A83-10300

GLOBAL AIR SAMPLING PROGRAM
Cloud encounter statistics in the 28.5-43.5 KFT altitude region from four years of GASP observations p 188 A83-38733
Water vapor measurement system in global atmospheric sampling program, appendix
[NASA-TP-2051] p 187 N83-13643
Aircraft measurements of trace gases and particles near the tropopause
[NASA-CR-3691] p 188 N83-27542

GLYCEROLS
Effect of hydrogen bonding on the vibrational dephasing time in glycerol p 61 A83-21054

GOLD
Tribological properties and X-ray photoelectron spectroscopy studies of ion-plated gold on nickel and iron p 74 A83-12650
Friction and hardness of gold films deposited by ion plating and evaporation
[NASA-TP-2207] p 87 N83-34019

GOLD COATINGS
The XPS depth profiling and tribological characterization of ion-plated gold on various metals
[NASA-TM-83350] p 83 N83-23417

GRAIN BOUNDARIES
A brittle to ductile transition in NiAl of a critical grain size p 75 A83-29726
Mechanisms of devitrification of grain boundary glassy phases in Si3N4 materials
[NASA-CR-169670] p 71 N83-14177
Micromechanically based constitutive relations for polycrystalline solids p 162 N83-34359

GRAINS (FOOD)
Energy and precious fuels requirements of fuel alcohol production, volume 1
[NASA-CR-168090] p 183 N83-28581
Energy and precious fuels requirements of fuel alcohol production. Volume 2, appendices A and B: Ethanol from grain
[NASA-CR-168091] p 183 N83-28582

GRAPHITE
Environmental effects on graphite fiber reinforced PMR-15 polyimide p 63 A83-33115
Processing of fused silicide coatings for carbon-based materials
[NASA-TM-83362] p 95 N83-27019
GRAPHITE-EPOXY COMPOSITES
Stability analysis of Centaur-in-Shuttle composite corrugated adapters
[AIAA 83-1003] p 49 A83-29791
Wave propagation in a graphite/epoxy laminate p 158 A83-44050
Dynamic responses of graphite/epoxy laminated beam to impact of elastic spheres
[NASA-CR-165461] p 64 N83-13173
High strain rate properties of undirectional composites, part 1
[NASA-CR-167969] p 64 N83-13178
High strain rate properties of off-axis composite laminates, part 2
[NASA-CR-167970] p 64 N83-13179
High strain properties of angle-ply composite laminate, part 3
[NASA-CR-167971] p 64 N83-13180
Wave propagation in graphite/epoxy laminates due to impact
[NASA-CR-168057] p 66 N83-22325
Hybridized polymer matrix composites
[NASA-CR-165341] p 66 N83-22326
Compression and compression fatigue testing of composite laminates
[NASA-CR-168023] p 66 N83-26928
The effect of stress on ultrasonic pulses in fiber reinforced composites
[NASA-CR-3724] p 154 N83-33180
GRAPHITE-POLYIMIDE COMPOSITES
Dynamic mechanical characterization of cure of a polyimide-graphite fiber composite (PMR 15/Celion 6000) p 62 A83-31793
Composite engine duct fabrication p 1 A83-39941
Lower-curing-temperature PMR polyimides p 89 A83-40923
Lower-curing-temperature PMR polyimides
[NASA-TM-82958] p 63 N83-10118
PMR-15 polyimide modifications for improved prepreg tack
[NASA-TM-82951] p 64 N83-12175
The 371 deg C(700 deg F) properties of celion 6000/n-phenylnadimide modified PMR polyimide composites
[NASA-TM-83050] p 65 N83-15365
GRAVITATIONAL EFFECTS
Measurement of thermoacoustic convection heat transfer phenomenon
[AIAA PAPER 83-1422] p 121 A83-32701
GREAT LAKES (NORTH AMERICA)
Aircraft sampling of the sulfate layer near the tropopause following the eruption of Mount St. Helens p 187 N83-11556
GREEN'S FUNCTIONS
Transient difference solutions of the inhomogeneous wave equation - Simulation of the Green's function
[AIAA PAPER 83-0667] p 193 A83-25904
Transient difference solutions of the inhomogeneous wave equation: Simulation of the Green's function
[NASA-TM-83336] p 200 N83-21897
GRIDS
Analytical calculation of a single jet in crossflow and comparison with experiment
[NASA-TM-83027] p 29 N83-14127
Analytical calculation of a single jet in cross-flow and comparison with experiment p 38 N83-29219
GRINDING (MATERIAL REMOVAL)
Investigation of wear phenomena by microscopy
[NASA-TM-82934] p 81 N83-14245
GROOVES
Design analysis of a self-acting spiral-groove ring seal for counter-rotating shafts --- o ring seals
[AIAA PAPER 83-1134] p 137 A83-36239
The influence of surface dents and grooves on traction in sliding EHD point contacts p 138 A83-37823
Design analysis of a self-acting spiral-groove ring seal for counter-rotating shafts --- o ring seals
[NASA-TM-83346] p 35 N83-23306
Design analysis of a self-acting spiral-groove ring seal for counter-rotating shafts
[NASA-TP-2142] p 36 N83-25712
Elastohydrodynamic contacts. Effects of dents and grooves on traction and local film thickness
[NASA-TP-2175] p 150 N83-28453
GROUND SPEED
Temperature distribution in an aircraft tire at low ground speeds
[NASA-TP-2195] p 161 N83-33217
GROUND SUPPORT EQUIPMENT
Implementation of R & QA practices in Research and Development programs
[NASA-TM-82997] p 210 N83-19651
GROUND TESTS
Uniform engine testing program. Phase 1: NASA Lewis Research Center participation
[NASA-TM-82978] p 29 N83-14126
GROWTH
Shock tube measurements of growth constants in the branched chain formaldehyde-carbon monoxide-oxygen system
[NASA-TM-82954] p 71 N83-12182
GUIDE VANES
Composite fan exit guide vanes for high bypass ratio gas turbine engines p 19 A83-13159
Effect of variable guide vanes on the performance of a high-bypass turbofan engine p 20 A83-24028
The performance of an annular vane swirler --- to aid in modeling gas turbine combustor flowfields and swirling confined flow turbulence
[AIAA PAPER 83-1326] p 24 A83-36340
Aerodynamic performance of a fan stage utilizing variable inlet guide vanes (VIGV's) for thrust modulation --- subsonic V/STOL aircraft
[AIAA PAPER 83-1162] p 6 A83-45508
Measurements of heat transfer distribution over the surfaces of highly loaded turbine nozzle guide vanes
[ASME PAPER 83-GT-53] p 8 A83-47910
Wall boundary layer development near the tip region of an IGV of an axial flow compressor
[ASME PAPER 83-GT-171] p 8 A83-47972
Aerodynamic performance of a fan stage utilizing Variable Inlet Guide Vanes (VIGVs) for thrust modulation --- subsonic V/STOL aircraft
[NASA-TM-83438] p 13 N83-27957
GUMS (SUBSTANCES)
Oxidation and formation of deposit precursors in hydrocarbon fuels
[NASA-CR-168121] p 101 N83-23465
GUN LAUNCHERS
Electric rail gun projectile acceleration to high velocity
[AIAA PAPER 82-1939] p 52 A83-12501
GUST LOADS
Incidence angle effects on convected gust airfoil noise
[AIAA PAPER 83-0765] p 195 A83-28022
Noise generation by a finite span swept airfoil
[AIAA PAPER 83-0768] p 195 A83-28023

H

HAFNIUM ALLOYS
RF sputtered silicon and hafnium nitrides: Properties and adhesion to 440C stainless steel
[NASA-TM-83400] p 95 N83-27020
HAFNIUM COMPOUNDS
Some properties of r.f.-sputtered hafnium nitride coatings p 88 A83-12653
HALF SPACES
Ignition of a combustible half space p 68 A83-22738
HALL EFFECT
Residual double acceptors in bulk GaAs p 205 A83-19989
HARDENERS
Synthesis and characterization of bisimide amines and bisimide amine-cured epoxy resins p 88 A83-11486
HARDENING (MATERIALS)
Nitriding of titanium and titanium: 8 percent aluminum, 1 percent molybdenum, 1 percent vanadium alloy with an ion-beam source
[NASA-TP-2149] p 85 N83-24640
HARDNESS
Friction and hardness of gold films deposited by ion plating and evaporation
[NASA-TP-2207] p 87 N83-34019
HASTELLOY (TRADEMARK)
Experimental verification of the Neuber relation at room and elevated temperatures --- to predict stress-strain behavior in notched specimens of hastelloy x
[NASA-CR-167967] p 159 N83-19121
Development of a simplified analytical method for representing material cyclic response
[NASA-CR-168100] p 160 N83-21390
Experimental verification of the number relation at room and elevated temperatures p 162 N83-34355
HEAT EXCHANGERS
Direct contact droplet heat exchangers for thermal management in space p 120 A83-27137
A refrigerated dynamic seal
[NASA-TM-83378] p 130 N83-24798
Develop and test fuel cell powered on-site integrated total energy systems. Phase 3: Full-scale power plant development
[NASA-CR-168021] p 182 N83-27345
Use of cooling air heat exchangers as replacements for hot section strategic materials
[NASA-TM-83494] p 42 N83-34946
HEAT FLUX
Development of advanced high-temperature heat flux sensors
[NASA-CR-165618] p 26 N83-10044
Experimental feasibility study of a thermoelectric heat flux gage
[NASA-TM-83048] p 134 N83-15602
HEAT OF SOLUTION
A class of nonideal solutions. 1: Definition and properties
[NASA-TP-1929] p 208 N83-23189
HEAT PIPES
Thermionic technology infrastructure for space power p 54 A83-27298
Heat pipes containing alkali metal working fluid
[NASA-CASE-LEW-12253-1] p 203 N83-19596
High thermal power density heat transfer apparatus providing electrical isolation at high temperature using heat pipes
[NASA-CASE-LEW-12950-2] p 183 N83-29804
HEAT PUMPS
Magnetic heat pumping
[NASA-CASE-LEW-12508-3] p 131 N83-29625
HEAT RESISTANT ALLOYS
A new diffusion-inhibited oxidation-resistant coating for superalloys p 74 A83-10299
Requirements of constitutive models for two nickel-base superalloys p 74 A83-21071
Metallurgical instabilities during the high temperature low cycle fatigue of nickel-base superalloys p 75 A83-22019
The effect of microstructure on the fatigue behavior of Ni base superalloys p 75 A83-36166
High-temperature composites - Status and future directions p 63 A83-40129
Fatigue crack initiation and propagation in several nickel-base superalloys at 650 C p 76 A83-41199
Cyclic oxidation of superalloys p 76 A83-42234
Low temperature hot corrosion p 76 A83-42252
Improved performance thermal barrier coatings p 90 A83-42261
Gamma prime shape changes during creep of a nickel-base superalloy p 77 A83-47855
COSAM (Conservation Of Strategic Aerospace Materials) program overview
[NASA-TM-83006] p 78 N83-11282
Superalloy composition modeling p 78 N83-11284
Role of cobalt in nickel base superalloys p 78 N83-11286
Low-cobalt single crystal Rene 150 p 78 N83-11288
Creep-fatigue of low cobalt superalloys p 79 N83-11290
Dual alloy interface stability p 79 N83-11297
Intermetallics as alternative materials p 80 N83-11300
Microstructural behavior of interfaces in hot isostatically pressed, dual alloy combinations
[NASA-TM-82698] p 80 N83-11309
Determination of hydrogen permeability in uncoated and coated superalloys
[NASA-CR-165209] p 80 N83-12215
Orientation dependence of the stress rupture properties of Nickel-base superalloy single crystals
[NASA-CR-165394] p 206 N83-13009
Evaluation of dopants in hydrogen to reduce hydrogen permeation in candidate Stirling engine heater head tube alloys at 760 deg and 820 deg
[NASA-TM-82920] p 81 N83-13232
Mechanism of hot corrosion of IN-738
[NASA-CR-169706] p 81 N83-15411
Coating with overlay metallic-cermet alloy systems
[NASA-CASE-LEW-13639-2] p 82 N83-17683
Creep-rupture behavior of 6 candidate stirling engine iron-base superalloys in high pressure hydrogen. Volume 1: Air creep-rupture behavior
[NASA-CR-168071] p 83 N83-22389
The effects of Ni, Mo, Ti and Si on the mechanical properties of Cr free Mn steel (Fe-25Mn-5Al-2C)
[NASA-TM-83355] p 85 N83-24638
Constitutive relationships for anisotropic high-temperature alloys
[NASA-TM-83437] p 160 N83-28493
Considerations of technology transfer barriers in the modification of strategic superalloys for aircraft turbine engines
[NASA-TM-83395] p 86 N83-29360
Improved thermal barrier coating system
[NASA-CASE-LEW-13324-2] p 86 N83-34014
Relation of cyclic loading pattern to microstructural fracture in creep fatigue
[NASA-TM-83473] p 161 N83-34349

Determination of hydrogen permeability in commercial and modified superalloys
[NASA-CR-168195] p 87 N83-35101
Understanding the roles of the strategic element cobalt in nickel base superalloys
[NASA-TM-83475] p 87 N83-35102

HEAT SHIELDING
Tests of a thermal acoustic shield with a supersonic jet p 192 A83-10183

HEAT SINKS
A refrigerated dynamic seal
[NASA-TM-83378] p 130 N83-24798

HEAT SOURCES
Assessment of alternative power sources for mobile mining machinery
[NASA-TM-82685] p 169 N83-14691

HEAT TRANSFER
Ignition of a combustible half space p 68 A83-22738
Improved Stirling engine performance using jet impingement p 137 A83-27288
Comparison of laser anemometer measurements and theory in an annular turbine cascade with experimental accuracy determined by parameter estimation p 4 A83-28833
Finite analytic numerical solution of heat transfer and flow past a square channel cavity p 123 A83-42703
Effects of free stream turbulence intensity and integral length scale on heat transfer from a circular cylinder in crossflow p 123 A83-42711
Convex curvature effects on the heated turbulent boundary layer p 123 A83-42733
The dryout region in frictionally heated sliding contacts p 124 A83-42762
Analysis of coolant entrance boundary shape of porous region to control cooling along exit boundary p 124 A83-43361
Comparison of predicted and experimental external heat transfer around a film cooled cylinder in crossflow
[NASA-TM-83017] p 127 N83-13392
Length to diameter ratio and row number effects in short pin fin heat transfer
[NASA-TM-83005] p 127 N83-14431
Comparison of visualized turbine endwall secondary flows and measured heat transfer patterns
[NASA-TM-83016] p 128 N83-14435
Jet array impingement flow distributions and heat transfer characteristics. Effects of initial crossflow and nonuniform array geometry --- gas turbine engine component cooling
[NASA-CR-3630] p 128 N83-15592
Finite element formulation for transient heat treat problems
[NASA-TM-83070] p 129 N83-17834
Heat pipes containing alkali metal working fluid
[NASA-CASE-LEW-12253-1] p 203 N83-19596
Thermomechanical loading of multilayered cylindrical geometries in thermal cycling from 300 to 1300 K
[NASA-TM-83312] p 129 N83-20029
Analogy between fluid cavitation and fracture mechanics
[NASA-TM-83071] p 129 N83-22542
Numerical simulation of an electrothermal deicer pad
[NASA-CR-168097] p 17 N83-23281
Analytical fuel property effects, small combustors, phase 1
[NASA-CR-168138] p 101 N83-23464
Preliminary design of flight hardware for two-phase fluid research
[NASA-CR-168072] p 46 N83-25766
NASA interdisciplinary collaboration in tribology. A review of oxidational wear
[NASA-CR-3686] p 95 N83-27021
Analytical and experimental evaluation of the heat transfer distribution over the surfaces of turbine vanes
[NASA-CR-168015] p 131 N83-28376
Residual stress in plasma sprayed ceramic turbine tip and gas path seal specimens
[NASA-TM-83418] p 131 N83-28380
High thermal power density heat transfer apparatus providing electrical isolation at high temperature using heat pipes
[NASA-CASE-LEW-12950-2] p 183 N83-29804

HEAT TRANSFER COEFFICIENTS
Heat transfer and flow characteristics of jets impinging on a concave hemispherical plate p 123 A83-42743
Heat transfer characteristics for jet array impingement with initial crossflow
[ASME PAPER 83-GT-28] p 7 A83-47891
Gear lubrication and cooling experiment and analysis p 147 N83-20147

HEAT TRANSMISSION
Heat transparent high intensity high efficiency solar cell
[NASA-CASE-LEW-12892-1] p 170 N83-14692

HEAT TREATMENT
Finite element formulation for transient heat treat problems
[NASA-TM-83070] p 129 N83-17834

HELICOPTER DESIGN
Design of an advanced 500-HP helicopter transmission p 21 A83-24834

HELICOPTER ENGINES
The feasibility of water injection into the turbine coolant to permit gas turbine contingency power for helicopter application
[ASME PAPER 83-GT-66] p 24 A83-39993
Status report DARPA/NASA convertible turbofan/turboshaft engine program
[ASME PAPER 83-GT-186] p 25 A83-48000
Rotorcraft convertible engines for the 1980s
[NASA-TM-83008] p 28 N83-12091
NASA transmission research and its probable effects on helicopter transmission design
[NASA-TM-83389] p 148 N83-24858

HELICOPTERS
Life and reliability models for helicopter transmissions
[NASA-TM-82976] p 139 N83-10425
Army/NASA small turboshaft engine digital controls research program
[NASA-TM-82979] p 27 N83-11128
Feasibility of water injection into the turbine coolant to permit gas turbine contingency power for helicopter application
[NASA-TM-83043] p 31 N83-15307
NASA helicopter transmission system technology program p 144 N83-20120
An overview of advancements in helicopter transmission design p 144 N83-20124
Design of an advanced 500-hp helicopter transmission p 144 N83-20125
Large rotorcraft transmission technology development program
[NASA-CR-168120] p 18 N83-22188

HELMHOLTZ EQUATIONS
A theoretical investigation of the sound radiation fields associated with a Bellmouth inlet
[AIAA PAPER 83-0710] p 193 A83-25926
Volume integrals of ellipsoids associated with the inhomogeneous Helmholtz equation p 192 A83-29526

HELMHOLTZ RESONATORS
The velocity perturbations above the orifice of an acoustically excited cavity in grazing flow p 195 A83-29235

HIGH FREQUENCIES
Inelastic tunnel diodes
[NASA-CASE-LEW-13833-1] p 116 N83-25983
High frequency, high power capacitor development
[NASA-CR-168035] p 116 N83-27127

HIGH PRESSURE
Use of high pressure liquid chromatography in the study of liquid lubricant oxidation
[NASA-TM-83033] p 92 N83-14270
Creep-rupture behavior of 6 candidate stirling engine iron-base superalloys in high pressure hydrogen. Volume 1: Air creep-rupture behavior
[NASA-CR-168071] p 83 N83-22389
High-pressure liquid chromatography: A brief introduction and its application in analyzing the degradation of a C-ether (Thio-ether) liquid lubricant
[NASA-TM-83474] p 98 N83-35144

HIGH SPEED
Farfield inflight measurements of high-speed turboprop noise
[AIAA PAPER 83-0745] p 21 A83-25947
Bearing fatigue investigation 3
[NASA-CR-168029] p 143 N83-17880
Predicted and experimental performance of large-bore high-speed ball and roller bearings p 145 N83-20131
High speed spherical roller-bearing analysis and comparison with experimental performance p 145 N83-20133
Large-bore tapered-roller bearing performance and endurance to 2.4 million DN p 145 N83-20134
Farfield inflight measurement of high-speed turboprop noise
[NASA-TM-83327] p 199 N83-21895
Design of a high-speed digital processing element for parallel simulation
[NASA-TM-83373] p 117 N83-29597

HIGH TEMPERATURE
Performance of laser-glazed zirconia thermal barrier coatings in cyclic oxidation and corrosion burner rig tests p 88 A83-10300
Turbine engine materials durability research p 29 N83-12163
Use of high pressure liquid chromatography in the study of liquid lubricant oxidation
[NASA-TM-83033] p 92 N83-14270
Correlation of compressive stress with spalling of plasma sprayed ceramic materials
[NASA-TM-83406] p 95 N83-27016
Experimental verification of the number relation at room and elevated temperatures p 162 N83-34355

HIGH TEMPERATURE ENVIRONMENTS
A commentary on solid lubricants and wear resistant solids for use in extreme environments
[NASA-TM-83042] p 92 N83-15468
Bearing fatigue investigation 3
[NASA-CR-168029] p 143 N83-17880

HIGH TEMPERATURE GASES
Curved film cooling admission tube
[NASA-CASE-LEW-13174-1] p 131 N83-27144

HIGH TEMPERATURE LUBRICANTS
A commentary on solid lubricants and wear resistant solids for use in extreme environments
[NASA-TM-83042] p 92 N83-15468
Analysis of a MIL-L-27502 lubricant from a gas-turbine engine test by size-exclusion chromatography
[NASA-TP-2063] p 93 N83-16528

HIGH TEMPERATURE RESEARCH
Reaction of cobalt in SO2 atmospheric at elevated temperatures
[NASA-TM-83485] p 88 N83-35104

HIGH TEMPERATURE TESTS
Influence of thermomechanical processing on elevated temperature slow plastic flow properties of B2 aluminide Fe-39.8at.% Al p 75 A83-22017
Metallurgical instabilities during the high temperature low cycle fatigue of nickel-base superalloys p 75 A83-22019
Interfacial layers in high-temperature-oxidized NiCrAl p 77 A83-44619
An extensometer for axial strain measurement at high temperature p 134 A83-48604
Analysis, design, fabrication and testing of an optical tip clearance sensor --- turbocompressor blade tips
[NASA-CR-165265] p 23 N83-11127

HIGH VOLTAGES
Planar multijunction high voltage solar cell chip p 163 A83-13923
Space Shuttle Orbiter charging p 49 A83-20415
High-frequency high-voltage high-power DC-to-DC converters p 115 N83-21028
SAFE II: Large systems space plasma evaluation experiment p 46 N83-26903
High voltage v-groove solar cell
[NASA-CASE-LEW-13401-2] p 185 N83-32177

HOLDERS
Method and apparatus for gripping uniaxial fibrous composite materials --- holding specimens for mechanical property testing
[NASA-CASE-LEW-13758-1] p 64 N83-12176

HOLE DISTRIBUTION (MECHANICS)
Solid particle impingement erosion characteristics of cylindrical surfaces, pre-existing holes and slits
[NASA-TM-83322] p 85 N83-25853

HOLES (ELECTRON DEFICIENCIES)
Current collection from the space plasma through defects in high voltage solar array insulation
[NASA-CR-168148] p 204 N83-31474

HONEYCOMB STRUCTURES
Metal honeycomb to porous wireform substrate diffusion bond evaluation p 153 A83-39620

HORIZONTAL ORIENTATION
A review of resonance response in large, horizontal-axis wind turbines p 163 A83-13696
Simplified aeroelastic modeling of horizontal axis wind turbines
[NASA-CR-168109] p 177 N83-21509
Some experiments on Yaw stability of wind turbines with various coning angles
[NASA-CR-168108] p 177 N83-22740
Development of methodology for horizontal axis wind turbine dynamic analysis
[NASA-CR-168110] p 178 N83-22747
Results of free yaw tests of the Mod-O 100 kilowatt wind turbine
[NASA-TM-83432] p 184 N83-29813
DOE large horizontal axis wind turbine development at NASA Lewis Research Center
[NASA-TM-83444] p 184 N83-31107

HOT CORROSION
Correlation and prediction of thermophoretic and inertial effects on particle deposition from non-isothermal turbulent boundary layers p 121 A83-27481
Cyclic oxidation of superalloys p 76 A83-42234
The oxidation behavior of a model molybdenum/tungsten-containing alloy in air alone and in air with trace levels of NaCl(g) p 76 A83-42241
Low temperature hot corrosion p 76 A83-42252
Improved performance thermal barrier coatings p 90 A83-42261
Interfacial layers in high-temperature-oxidized NiCrAl p 77 A83-44619

Hot corrosion of low cobalt alloys p 79 N83-11292
Mechanism of hot corrosion of IN-738
[NASA-CR-169706] p 81 N83-15411
Critical research and advanced technology (CRT) support project
[NASA-TM-83019] p 176 N83-20361

HOT PRESSING
Microstructural behavior of interfaces in hot isostatically pressed, dual alloy combinations
[NASA-TM-82698] p 80 N83-11309

HOT-WIRE ANEMOMETERS
Single-wire swirl flow turbulence measurements
[AIAA PAPER 83-1202] p 122 A83-36278
Turbulence measurements in a complex plowfield using a crossed hot-wire
[NASA-CR-173080] p 132 N83-35316

HOT-WIRE FLOWMETERS
Turbulence measurements in a swirling confined jet flowfield using a triple hot-wire probe
[NASA-CR-169668] p 127 N83-14434
Turbulence spectra in the noise source regions of the flow around complex surfaces
[NASA-TM-83392] p 202 N83-30168

HOUSINGS
Cast Fe-base cylinder/regenerator housing alloy
[NASA-CR-168474] p 80 N83-12214

HUBS
Quasi-three-dimensional turbomachinery flow calculations on multiple hub-to-shroud stream surfaces
[AIAA PAPER 83-1820] p 5 A83-38652
End wall flows in rotors and stators of a single stage compressor
[NASA-CR-169800] p 128 N83-16678

HUMIDITY
Effect of humidity on jet engine axial-flow compressor performance p 22 A83-35856

HYBRID PROPULSION
The design and technology development for A 150 mlb resistojet for H2 or NH3
[AIAA PAPER 82-1949] p 52 A83-12506
A summary of EHV propulsion technology --- Electric and Hybrid Vehicle p 209 A83-31087

HYDRAULIC EQUIPMENT
Conceptual design and cost analysis of hydraulic output unit for 15 kW free-piston Stirling engine
[NASA-CR-165543] p 167 N83-10561
A conceptual study of the potential for automotive-derived and free-piston Stirling engines in 30- to 400-kilowatt stationary power applications
[NASA-CR-165274] p 167 N83-10568
Design of hydraulic output Stirling engine
[NASA-CR-167976] p 177 N83-22739
Characterization of a high-pressure diesel fuel injection system as a control technology option to improve engine performance and reduce exhaust emissions
[NASA-TM-83329] p 210 N83-24431
Free-piston Stirling hydraulic engine and drive system for automobiles
[NASA-TM-82992] p 211 N83-25625
Mod-2 wind turbine system development. Volume 1: Executive summary
[NASA-CR-168006] p 184 N83-29812

HYDROCARBON COMBUSTION
Soot formation in pyrolysis of acetylene, allene and 1,3-butadiene p 69 A83-39274

HYDROCARBON FUELS
A carbon-13 and proton nuclear magnetic resonance study of some experimental referee broadened-specification /ERBS/ turbine fuels p 98 A83-11482
Droplet size effects on NO/x/ formation in a one-dimensional monodisperse spray combustion system
[ASME PAPER 82-JPGC-GT-10] p 68 A83-25268
Recent trends in aviation turbine fuel properties
[NASA-TP-2056] p 99 N83-11340
High performance liquid chromatographic hydrocarbon group-type analyses of mid-distillates employing fuel-derived fractions as standards
[NASA-TM-83072] p 100 N83-19920
Oxidation and formation of deposit precursors in hydrocarbon fuels
[NASA-CR-168121] p 101 N83-23465
LOX/hydrocarbon fuel carbon formation and mixing data analysis
[NASA-CR-168066] p 101 N83-31886
Deposit formation in hydrocarbon rocket fuels: Executive summary
[NASA-CR-165492] p 102 N83-35159
Effect of deoxygenation and prestressing on hydrocarbon fuel thermal stability
[NASA-TM-83456] p 102 N83-35160

HYDRODYNAMICS
Surface roughness effects in hydrodynamic lubrication: The flow factor method
[NASA-TM-83024] p 129 N83-19016
Lubrication background
[NASA-TM-81692] p 147 N83-20159
Combustion Fundamentals Research
[NASA-CP-2268] p 38 N83-29208
Activation parameters of flow through battery separators
[NASA-TM-83371] p 73 N83-30550

HYDROGEN
Thermodynamics of silicon nitridation - Effect of hydrogen
[ACS PAPER 33-B-80P] p 88 A83-18052
Combustion characteristics of hydrogen. Carbon monoxide based gaseous fuels
[NASA-TM-82998] p 167 N83-10560
Assessment of crash fire hazard of LH sub 2 fueled aircraft
[NASA-CR-165525] p 16 N83-11095
Determination of hydrogen permeability in uncoated and coated superalloys
[NASA-CR-165209] p 80 N83-12215
Evaluation of dopants in hydrogen to reduce hydrogen permeation in candidate Stirling engine heater head tube alloys at 760 deg and 820 deg
[NASA-TM-82920] p 81 N83-13232
Electrothermal thruster diagnostics. Volume 2: Technical
[NASA-CR-168174-VOL-2] p 60 N83-33943
Determination of hydrogen permeability in commercial and modified superalloys
[NASA-CR-168195] p 87 N83-35101

HYDROGEN ATOMS
Microwave plasma generation of hydrogen atoms for rocket propulsion p 53 A83-13090

HYDROGEN BONDS
Effect of hydrogen bonding on the vibrational dephasing time in glycerol p 61 A83-21054

HYDROGEN FUELS
Combustion characteristics of hydrogen-carbon monoxide based gaseous fuels p 67 A83-11491
Measurements of energy distribution and thrust for microwave plasma coupling of electrical energy to hydrogen for propulsion
[AIAA PAPER 82-1951] p 52 A83-12508

HYDROGEN OXYGEN ENGINES
Advanced LOX/H2 engine technologies for future OTVs
[AIAA PAPER 83-1312] p 55 A83-36333

HYDROGEN PRODUCTION
Applications of ion beam technology
[NASA-CR-169797] p 82 N83-16493

HYDROGEN RECOMBINATIONS
Microwave plasma generation of hydrogen atoms for rocket propulsion p 53 A83-13090
Development of improved hydrogen recombination in sealed nickel-cadmium aerospace cells p 54 A83-27198
Deep discharge reconditioning and shorted storage of batteries --- nickel cadmium batteries
[NASA-CR-167953] p 166 N83-10502

HYDROSTATICS
Multiple plate hydrostatic viscous damper
[NASA-CASE-LEW-13445-2] p 143 N83-17883
Hybrid hydrostatic/ball bearings in high-speed turbomachinery
[NASA-CR-168124] p 149 N83-27213

HYGROSCOPICITY
Imide modified epoxy matrix resins
[NASA-CR-167942] p 93 N83-18909

HYPERBOLAS
A study of dynamic energy equations for Stirling cycle analysis
[NASA-CR-168152] p 181 N83-25043

HYPERVELOCITY LAUNCHERS
Electric rail gun projectile acceleration to high velocity
[AIAA PAPER 82-1939] p 52 A83-12501

HYPERVELOCITY PROJECTILES
Electric rail gun projectile acceleration to high velocity
[AIAA PAPER 82-1939] p 52 A83-12501

I

ICE FORMATION
A similarity analysis of the droplet trajectory equation p 118 A83-13133
An analytical evaluation of the icing properties of several low and medium speed airfoils
[AIAA PAPER 83-0109] p 3 A83-16525
NASA Lewis Research Center's program on icing research
[AIAA PAPER 83-0204] p 1 A83-16582
'Scaling' analysis of the ice accretion process on aircraft surfaces
[ASME PAPER 82-WA/HT-39] p 16 A83-25693
Numerical simulation of airfoil ice accretion
[AIAA PAPER 83-0112] p 16 A83-36042
Experimental comparison of icing cloud instruments
[AIAA PAPER 83-0026] p 16 A83-42099
NASA Lewis Research Center's Program on Icing Research
[NASA-TM-83031] p 16 N83-14078
Development and test of a Microwave Ice Accretion Measurement Instrument (MIAMI)
[NASA-CR-3598] p 18 N83-14123
Wind tunnel evaluation of air-foil performance using simulated ice shapes
[NASA-CR-167960] p 11 N83-15265
A method of predicting flow rates required to achieve anti-icing performance with a porous leading edge ice protection system
[NASA-CR-169996] p 17 N83-19738
Experimental comparison of icing cloud instruments
[NASA-TM-83340] p 17 N83-24487

ICE PREVENTION
NASA Lewis Research Center's program on icing research
[AIAA PAPER 83-0204] p 1 A83-16582
NASA Lewis Research Center's Program on Icing Research
[NASA-TM-83031] p 16 N83-14078
A method of predicting flow rates required to achieve anti-icing performance with a porous leading edge ice protection system
[NASA-CR-168213] p 17 N83-32782

IGNITION
Ignition of confined gaseous mixtures by hot surfaces and hot wires
[AIAA PAPER 83-0240] p 68 A83-16606
Ignition of a combustible half space p 68 A83-22738
Implementation of R & QA practices in Research and Development programs
[NASA-TM-82997] p 210 N83-19651
Autoignition in a premixing-prevaporizing fuel duct using 3 different fuel injection systems at inlet air temperatures to 1250 K
[NASA-TM-82938] p 181 N83-26251
Preliminary tests of an advanced high-temperature combustion system
[NASA-TP-2203] p 41 N83-33893

IMAGE PROCESSING
Satellite provided fixed communication services: A forecast of potential domestic demand through the year 2000. Volume 1: Executive summary
[NASA-CR-168145] p 108 N83-34113

IMPACT
Dynamic responses of graphite/epoxy laminated beam to impact of elastic spheres
[NASA-CR-165461] p 64 N83-13173

IMPACT DAMAGE
A study of the surface deterioration due to erosion --- of gas turbine blades
[ASME PAPER 83-GT-213] p 9 A83-48014
Wave propagation in graphite/epoxy laminates due to impact
[NASA-CR-168057] p 66 N83-22325
Solid spherical glass particle impingement studies of plastic materials
[NASA-TP-2161] p 94 N83-24695

IMPACT LOADS
Wave propagation in a graphite/epoxy laminate p 158 A83-44050

IMPACT TESTS
Morphology of ductile metals eroded by a jet of spherical particles impinging at normal incidence p 75 A83-32624

IMPEDANCE MEASUREMENT
Surface acoustic admittance of highly porous open-cell, elastic foams p 195 A83-28849

IMPELLERS
Aerodynamic stiffness of an unbound eccentric whirling centrifugal impeller with an infinite number of blades p 142 N83-15650

IMPINGEMENT
An analytical evaluation of the icing properties of several low and medium speed airfoils
[AIAA PAPER 83-0109] p 3 A83-16525
Universal approach to analysis of cavitation and liquid-impingement erosion data
[NASA-TP-2061] p 82 N83-15413
Into mesh lubrication of spur gears with arbitrary offset oil jet. 1: For jet velocity less than or equal to gear velocity
[NASA-TM-83039] p 143 N83-19092
Into mesh lubrication of spur gears with arbitrary offset oil jet. 2: For jet velocities equal to or greater than great velocity
[NASA-TM-83041] p 143 N83-19093
A comprehensive analysis of cavitation and liquid impingement erosion data
[NASA-TM-83352] p 84 N83-24634

Solid spherical glass particle impingement studies of plastic materials
[NASA-TP-2161] p 94 N83-24695
Solid particle impingement erosion characteristics of cylindrical surfaces, pre-existing holes and slits
[NASA-TM-83322] p 85 N83-25853

IMPULSES
Refinement and application of acoustic impulse technique to study nozzle transmission characteristics
[NASA-CR-3656] p 199 N83-20708

IMPURITIES
Deep impurity trapping concepts for power semiconductor devices p 206 N83-15877

IN-FLIGHT MONITORING
Farfield inflight measurements of high-speed turboprop noise
[AIAA PAPER 83-0745] p 21 A83-25947

INCIDENCE
Incidence loss for fan turbine rotor blade in two-dimensional cascade
[NASA-TP-2188] p 39 N83-30431
The effect of incidence angle on the overall three-dimensional aerodynamic performance of a classical annular airfoil cascade
[NASA-CR-168127] p 15 N83-34911

INCLUSIONS
Composites with periodic microstructure p 62 A83-12734

INCOMPRESSIBLE FLOW
Study of asymptotic incompressible flow in curved ducts using a multi-grid technique p 123 A83-42532
Effect of particle presence on the incompressible inviscid flow through a two dimensional compressor cascade p 6 A83-42562

INCOMPRESSIBLE FLUIDS
Optimum parallel step-sector bearing lubricated with an incompressible fluid
[NASA-TM-83356] p 148 N83-21855

INCONEL (TRADEMARK)
Effects on stress rupture life and tensile strength of tin additions to Inconel 718 p 79 N83-11299
Benchmark notch test for life prediction
[NASA-CR-165571] p 158 N83-12451

INDUCTION MOTORS
Transistorized PWM inverter-induction motor drive system p 110 A83-11488
Improved transistorized AC motor controller for battery powered urban electric passenger vehicles
[NASA-CR-167978] p 113 N83-10349

INDUSTRIAL ENERGY
The worldwide market for photovoltaics in the rural sector
[NASA-TM-83035] p 173 N83-15840

INELASTIC STRESS
Some inelastic effects of thermal cycling on ZrO2-Y2O3 materials p 89 A83-22272
Materials constitutive models for nonlinear analysis of thermally cycled structures
[NASA-TP-2055] p 158 N83-12449
Strainrange partitioning: A total strain range version
[NASA-TM-83023] p 81 N83-14246
Development of a simplified analytical method for representing material cyclic response
[NASA-CR-168100] p 160 N83-21390

INERTIA
Polyvinyl alcohol battery separator containing inert filler
[NASA-CASE-LEW-13556-2] p 183 N83-29805
Nacelle Aerodynamic and Inertial Loads (NAIL) project
[NASA-CR-168712] p 18 N83-30402

INFRARED ABSORPTION
Residual double acceptors in bulk GaAs p 205 A83-19989

INFRARED ASTRONOMY SATELLITE
Infrared Astronomical Satellite (IRAS) launch
[NASA-TM-85190] p 45 N83-15330

INFRARED DETECTORS
Determination of physical and chemical states of lubricants in concentrated contacts, part 3
[NASA-CR-3658] p 92 N83-16527

INFRARED LASERS
Gain-enhanced free-electron laser with an electromagnetic pump field p 135 A83-31133

INFRARED RADIATION
Direct conversion of infrared radiant energy for space power applications p 173 N83-15865
Atmospheric radiation model for water surfaces
[NASA-CR-167873] p 187 N83-21677

INFRARED SPECTRA
Infrared emission spectrophotometric study of the changes produced by TiN coating of metal surfaces in an operating EHD contact
[ASLE PREPRINT 82-LC-3C-3] p 135 A83-13229

INHIBITORS
The effects of metals and inhibitors on thermal oxidative degradation reactions of unbranched perfluoroalkylethers
[NASA-TM-83464] p 97 N83-34049

INHOMOGENEITY
Fundamental aspects in quantitative ultrasonic determination of fracture toughness: The scattering of a single ellipsoidal inhomogeneity
[NASA-CR-3625] p 153 N83-11507
The transmission or scattering of elastic waves by an inhomogeneity of simple geometry: A comparison of theories
[NASA-CR-3659] p 153 N83-16773

INJECTION MOLDING
Injection molding ceramics to high green densities p 137 A83-33515

INJECTORS
Effect of broad properties fuel on injector performance in a reverse flow combustor
[AIAA PAPER 83-0154] p 20 A83-21079
Effect of broad properties fuel on injector performance in a reverse flow combustor
[NASA-TM-83013] p 29 N83-13101

INKS
Multicolor printing plate joining
[NASA-CASE-LEW-13598-1] p 102 N83-17745

INLET FLOW
Confined swirling flow predictions
[AIAA PAPER 83-0316] p 119 A83-16646
Effects of interstage diffuser flow distortion on the performance of a 15.41-centimeter tip diameter axial power turbine
[AIAA PAPER 83-1179] p 23 A83-36263
Importance of inlet boundary conditions for numerical simulation of combustor flows
[AIAA PAPER 83-1263] p 23 A83-36314
Experimental evaluation of inlet turbulence, wall boundary layer, surface finish, and fillet radius on small axial turbine state performance
[SAE PAPER 821475] p 24 A83-38001
Numerical solution of the Navier-Stokes equations for compressible turbulent two/three dimensional flows in the terminal shock region of an inlet/diffuser
[AIAA PAPER 83-1892] p 5 A83-39358
Experiments on flow through one to four inlets of the orifice and Borda type p 124 A83-43235
Aerodynamic performance of a fan stage utilizing variable inlet guide vanes (VIGV's) for thrust modulation --- subsonic V/STOL aircraft
[AIAA PAPER 83-1162] p 6 A83-45508
Dynamic distortion in a short s-shaped subsonic diffuser with flow separation --- Lewis 8 by 6 foot Supersonic Wind Tunnel
[AIAA PAPER 83-1412] p 25 A83-45515
Low speed performance of a supersonic axisymmetric mixed compression inlet with auxiliary inlets
[AIAA PAPER 83-1414] p 7 A83-45516
Three-dimensional flow measurements in a turbine scroll
[ASME PAPER 83-GT-128] p 8 A83-47957
Mean-flow measurements of the flow field diffusing bend
[NASA-CR-3634] p 10 N83-14066
Experimental evaluation of shockless supercritical airfoils in cascade
[NASA-TM-83045] p 11 N83-15268
Effect of steady-state pressure distortion on inlet flow to a high-bypass-ratio turbofan engine
[NASA-TM-82964] p 30 N83-15306
Validation of a three-dimensional viscous analysis of axisymmetric supersonic inlet flow fields
[NASA-TM-83058] p 32 N83-17538
Literature search of publications concerning the prediction of dynamic inlet flow distortion and related topics
[NASA-CR-3673] p 33 N83-18729
Effects of interstage diffuser flow distortion on the performance of a 15.41-centimeter tip diameter axial power turbine
[NASA-TM-83359] p 35 N83-24505
Dynamic distortion in a short s-shaped subsonic diffuser with flow separation --- Lewis 8 by 6 foot Supersonic Wind Tunnel
[NASA-TM-83412] p 36 N83-26838
Aerodynamic performance of a fan stage utilizing Variable Inlet Guide Vanes (VIGVs) for thrust modulation --- subsonic V/STOL aircraft
[NASA-TM-83438] p 13 N83-27957
Low speed performance of a supersonic axisymmetric mixed compression inlet with auxiliary inlets --- Lewis 9x15-ft anechoic wind tunnel tests
[NASA-TM-83435] p 37 N83-27992

INLET NOZZLES
Three-dimensional flow measurements in a turbine scroll
[ASME PAPER 83-GT-128] p 8 A83-47957
Model aerodynamic test results for a refined actuated inlet ejector nozzle at simulated takeoff and cruise conditions
[NASA-CR-168051] p 13 N83-26816

INLET PRESSURE
Literature search of publications concerning the prediction of dynamic inlet flow distortion and related topics
[NASA-CR-3673] p 33 N83-18729
A comparison of flow rates and pressure profiles for N-sequential inlets and three related seal configurations
[NASA-TM-83442] p 132 N83-33103

INLET TEMPERATURE
Analytical and experimental study of flow through an axial turbine stage with a nonuniform inlet radial temperature profile
[AIAA PAPER 83-1175] p 6 A83-45510
Cold-air performance of compressor-drive turbine of Department of Energy upgraded automobile gas turbine engine. 2: Stage performance
[NASA-TM-82818] p 9 N83-11063
Experimental and analytical determination of gear tooth temperatures with oil jet lubrication p 142 N83-15530
Analytical and experimental study of flow through an axial turbine stage with a nonuniform inlet radial temperature profile
[NASA-TM-83431] p 14 N83-27958

INORGANIC SULFIDES
Thermodynamics of the potassium-sulfur-oxygen and related systems
[NASA-CR-168155] p 61 N83-28077

INPUT
A novel feedforward compensation canceling input filter-regulator interaction p 112 A83-33133
Input generator for Denton 3-dimensional turbomachine-blade-row analysis code
[NASA-TM-23324] p 13 N83-26817

INSTRUCTION SETS (COMPUTERS)
Design of a high-speed digital processing element for parallel simulation
[NASA-TM-83373] p 117 N83-29597

INTAKE SYSTEMS
Experiments on flow through one to four inlets of the orifice and Borda type p 124 A83-43235
A survey of inlet/engine distortion compatibility
[AIAA PAPER 83-1166] p 6 A83-45509
Wall boundary layer development near the tip region of an IGV of an axial flow compressor
[ASME PAPER 83-GT-171] p 8 A83-47972
Utilizing numerical techniques in turbofan inlet acoustic suppressor design
[NASA-TM-82994] p 196 N83-10885
Calculation of compressible flow in and about three-dimensional inlets with and without auxiliary inlets by a higher-order panel method
[NASA-CR-168009] p 10 N83-12047
A survey of inlet/engine distortion compatibility
[NASA-TM-83421] p 37 N83-27991
A comparison of flow rates and pressure profiles for N-sequential inlets and three related seal configurations
[NASA-TM-83442] p 132 N83-33103

INTEGRAL EQUATIONS
Volume integrals of ellipsoids associated with the inhomogeneous Helmholtz equation p 192 A83-29528

INTEGRATED CIRCUITS
GaAs integrated digital-to-analogue convertor for control of power dual-gate FETs p 112 A83-36479
Application of MMIC modules in future multiple beam satellite antenna systems
[NASA-TM-83344] p 48 N83-22313
Phased array-fed antenna configuration study: Technology assessment
[NASA-CR-168078] p 106 N83-22495
Phased array-fed antenna configuration study
[NASA-CR-168077] p 107 N83-27086
Advanced digital modulation: Communication techniques and monolithic GaAs technology
[NASA-CR-174452] p 109 N83-36299

INTEGRATED ENERGY SYSTEMS
Develop and test fuel cell powered on-site integrated total energy system
[NASA-CR-168020] p 173 N83-15839

INTERCALATION
Metallic conductivity and air stability in copper chloride intercalated carbon fibers p 111 A83-16095

INTERFACES
Interfacial layers in high-temperature-oxidized NiCrAl p 77 A83-44619

INTERFACIAL ENERGY
Molecular-orbital model for metal-sapphire interfacial strength p 67 A83-10612

INTERFACIAL TENSION
An experimental study of heat induced surface-tension driven flow p 44 A83-43269
INTERFEROMETERS
Large-aperture interferometer using local reference beam
[NASA-TP-2060] p 203 N83-13979
INTERMEDIATE FREQUENCIES
Spacecraft in switch matrix for wide band service applicatons in 30/20 GHz communications satellite systems
[NASA-CR-168089] p 46 N83-34998
INTERMETALLICS
Influence of thermomechanical processing on elevated temperature slow plastic flow properties of B2 aluminide Fe-39.8at.% Al p 75 A83-22017
A brittle to ductile transition in NiAl of a critical grain size p 75 A83-29726
Intermetallics as alternative materials p 80 N83-11300
Improved nickel base coating alloy --- oxidation resistant coatings
[NASA-CASE-LEW-13834-1] p 85 N83-24639
INTERNAL COMBUSTION ENGINES
Numerical simulation of the flow and fuel-air mixing in an axisymmetric piston-cylinder arrangement
[NASA-TM-83011] p 126 N83-12358
INVISCID FLOW
A viscous-inviscid interactive procedure for rotational flow in cascades of two-dimensional airfoils of arbitrary shape
[AIAA PAPER 83-0256] p 3 A83-16614
Three-dimensional stability of vortex arrays p 120 A83-19022
A semi-direct solver for compressible three-dimensional rotational flow
[AIAA PAPER 83-1909] p 122 A83-39367
A fast Euler solver for steady flows
[AIAA PAPER 83-1940] p 123 A83-39389
Effect of particle presence on the incompressible inviscid flow through a two dimensional compressor cascade p 6 A83-42562
Three dimensional flow computations in a turbine scroll
[NASA-CR-166003] p 10 N83-12045
Multiple-grid convergence acceleration of viscous and inviscid flow computations
[NASA-TM-83361] p 190 N83-21847
User's manual for Axisymmetric Diffuser Duct (ADD) code. Volume 1: General ADD code description
[NASA-CR-165598-VOL-1] p 211 N83-26757
Semidirect computations for transonic flow
[NASA-TM-83451] p 15 N83-34909
ION BEAMS
Industrial ion source technology
[NASA-CR-159877] p 102 N83-12259
Applications of ion beam technology
[NASA-CR-169797] p 82 N83-16493
Nitriding of titanium and titanium: 8 percent aluminum, 1 percent molybdenum, 1 percent vanadium alloy with an ion-beam source
[NASA-TP-2149] p 85 N83-24640
High frequency plasma generators for ion thrusters
[NASA-CR-167957] p 59 N83-28072
ION ENGINES
On-orbit propulsion requirements and performance assessment of ion propulsion subsystems for future GEO large satellite missions
[AIAA PAPER 82-1872] p 48 A83-12460
Advances in series resonant inverter technology and its effect on spacecraft employing electric propulsion
[AIAA PAPER 82-1881] p 51 A83-12466
A direct-measurement technique for estimating discharge-chamber lifetime --- for ion thrusters
[AIAA PAPER 82-1908] p 51 A83-12483
Inert gas test of two 12-cm magnetostatic thrusters
[AIAA PAPER 82-1925] p 51 A83-12494
Plasma characteristics of a 17 cm diameter line-cusp ion thruster
[AIAA PAPER 82-1926] p 52 A83-12495
Development of a large inert gas ion thruster
[AIAA PAPER 82-1927] p 52 A83-12496
Extended-performance 8-cm ion thruster operation
[AIAA PAPER 82-1955] p 53 A83-12512
Ion flow experiments in a multipole discharge chamber
[AIAA PAPER 82-1930] p 203 A83-14398
Simplification of power electronics for ion thruster neutralizers
[AIAA PAPER 82-1880] p 53 A83-21099
Parallel plate radiofrequency ion thruster
[AIAA PAPER 82-1937] p 53 A83-21900
Operation of the J-series thruster using inert gas
[AIAA PAPER 82-1929] p 54 A83-26625
Characterization of advanced electric propulsion systems p 55 A83-33744
Simplified power processing for ion-thruster subsystems
[AIAA PAPER 83-1394] p 55 A83-36384
Simplified power processing for ion-thruster subsystems p 56 A83-39271
Simplification of power electronics for ion thruster neutralizers
[NASA-TM-83004] p 56 N83-12141
Parallel plate radiofrequency ion thruster
[NASA-TM-83014] p 56 N83-12142
Analysis and design of ion thruster for large space systems
[NASA-CR-165140] p 57 N83-14158
Operation of the J-series thruster using inert gas
[NASA-TM-82977] p 57 N83-17587
Ring-cusp ion thruster with shell anode
[NASA-CASE-LEW-13881-1] p 202 N83-21903
ION EXCHANGE MEMBRANE ELECTROLYTES
Activation parameters of flow through battery separators
[NASA-TM-83371] p 73 N83-30550
ION EXCHANGING
Kinetics of copper ion absorption by cross-linked calcium polyacrylate membranes
[NASA-TM-83052] p 61 N83-25786
Ion exchange selectivity for cross-linked polyacrylic acid
[NASA-TM-83427] p 97 N83-35142
ION EXTRACTION
Analysis and design of ion thrusters for large space systems
[NASA-CR-165160] p 57 N83-14159
ION IMPLANTATION
Tribological characteristics of nitrogen (N+) implanted iron p 75 A83-37824
ION MOTION
Ion flow experiments in a multipole discharge chamber
[AIAA PAPER 82-1930] p 203 A83-14398
ION PLATING
Tribological properties and X-ray photoelectron spectroscopy studies of ion-plated gold on nickel and iron p 74 A83-12650
Plasma deposition and surface modification techniques for wear resistance
[NASA-TM-82972] p 90 N83-10194
Vacuum sputtered and ion-plated coatings for wear and corrosion protection
[NASA-TM-83007] p 99 N83-13273
Frictional and morphological characteristics of ion plated soft, metallic films
[NASA-TM-81723] p 83 N83-22390
The XPS depth profiling and tribological characterization of ion-plated gold on various metals
[NASA-TM-83350] p 83 N83-23417
Friction and hardness of gold films deposited by ion plating and evaporation
[NASA-TP-2207] p 87 N83-34019
ION PROPULSION
On-orbit propulsion requirements and performance assessment of ion propulsion subsystems for future GEO large satellite missions
[AIAA PAPER 82-1872] p 48 A83-12460
Advanced-technology 30-cm-diameter mercury ion thruster
[AIAA PAPER 82-1910] p 51 A83-12484
Qualification test results of IAPS 8 cm ion thrusters
[AIAA PAPER 82-1954] p 52 A83-12511
Improved ion containment using a ring-cusp ion thruster
[AIAA PAPER 82-1928] p 53 A83-21100
Simplified power processing for ion-thruster subsystems
[AIAA PAPER 83-1394] p 55 A83-36384
Improved ion containment using a ring-cusp ion thruster
[NASA-TM-82990] p 56 N83-13164
Endurance test of a 30-CM-diameter engineering model ion thruster. Task 12: Investigation of thin-film erosion monitors for ion thrusters
[NASA-CR-168132] p 58 N83-25779
Simplified power processing for ion-thruster subsystems p 60 N83-35018
ION SOURCES
Performance characteristics of a microwave plasma disk ion source --- time varying electric propulsion concept
[AIAA PAPER 82-1935] p 55 A83-27350
Industrial ion source technology
[NASA-CR-159877] p 102 N83-12259
IONIC DIFFUSION
Search for selective ion diffusion through membranes
[NASA-TM-83426] p 97 N83-34048
IONS
Mass analysis of neutral particles and ions released during electrical breakdowns on spacecraft surfaces
[NASA-CR-170299] p 50 N83-23347
IRON
Tribological characteristics of nitrogen (N+) implanted iron p 75 A83-37824
Friction and wear of iron and nickel in sodium hydroxide solutions p 77 A83-48922
Friction and wear of iron and nickel in sodium hydroxide solutions
[NASA-TM-82935] p 77 N83-10171
Electromagnetic studies of redox systems for energy storage
[NASA-CR-169593] p 169 N83-14667
IRON ALLOYS
Dual alloy interface stability p 79 N83-11297
Intermetallics as alternative materials p 80 N83-11300
Development of Fe-Mn-Al-X-C alloys p 80 N83-11307
SiC or B4C-B/low strategic element content composite p 80 N83-11308
Cast Fe-base cylinder/regenerator housing alloy
[NASA-CR-169474] p 80 N83-12214
Development of tough, strong, iron-base alloy for cryogenic applications p 44 N83-18763
Creep-rupture behavior of 6 candidate stirling engine iron-base superalloys in high pressure hydrogen. Volume 1: Air creep-rupture behavior
[NASA-CR-168071] p 83 N83-22389
IRON CHLORIDES
Study to establish cost predictions for the production of Redox chemicals
[NASA-CR-167882] p 176 N83-20359
An electrochemical rebalance cell for Redox systems
[NASA-TM-83363] p 73 N83-29326
ISOLATION
High thermal power density heat transfer apparatus providing electrical isolation at high temperature using heat pipes
[NASA-CASE-LEW-12950-2] p 183 N83-29804
ISOPARAMETRIC FINITE ELEMENTS
A new formulation of hybrid/mixed finite element p 155 A83-12739
Three-dimensional finite-element analysis of layered composite plates p 156 A83-27432
ISOTHERMAL PROCESSES
Elastohydrodynamic lubrication of rectangular contacts
[NASA-TP-2111] p 143 N83-16759
Stirling engine design manual, 2nd edition
[NASA-CR-168088] p 212 N83-30328
ISOTROPIC MEDIA
Ultrasonic attenuation of a void-containing medium for very long wavelengths
[NASA-CR-3693] p 154 N83-28466
ITERATION
Numerical simulation of an electrothermal deicer pad
[NASA-CR-168097] p 17 N83-23281
ITERATIVE SOLUTION
Triangular system solutions on an optical systolic processor p 169 A83-36752

J

JET AIRCRAFT NOISE
Tone generation by rotor-downstream strut interaction
[AIAA PAPER 83-0767] p 21 A83-25957
Coaxial supersonic jet-flows, shock structure and related problems with noise-suppression assessment and prediction
[AIAA PAPER 83-0707] p 194 A83-28011
Tone-excited jet: Theory and experiments
[NASA-CR-3538] p 197 N83-12968
Experiments on high bypass internal mixer nozzle jet noise
[NASA-TM-83020] p 198 N83-16152
Comparison of measured and predicted flight effects on high-bypass coaxial jet exhaust noise
[NASA-TM-83347] p 200 N83-23115
A compact inflow control device for simulating flight fan noise
[NASA-TM-83349] p 201 N83-26643
JT15D 1/2-scale nozzle jet noise experiment and comparison with prediction
[NASA-TM-83370] p 201 N83-27793
JET ENGINE FUELS
A carbon-13 and proton nuclear magnetic resonance study of some experimental referee broadened-specification /ERBS/ turbine fuels p 98 A83-11482
Recent trends in aviation turbine fuel properties
[NASA-TP-2056] p 99 N83-11340
Evaluation of ultraviolet spectrophotometry for simultaneous analysis of alkylbenzenes, alkylnaphthalenes, alkylanthracenes/phenanthrenes and total aromatics in mid-distillate fuels
[NASA-TM-83032] p 99 N83-15483

Experimental and analytical determination of gear tooth temperatures with oil jet lubrication p 142 N83-15530
Fuels research studies at NASA Lewis
[NASA-TM-83003] p 100 N83-19921
Analytical fuel property effects, small combustors, phase 1
[NASA-CR-168138] p 101 N83-23464

JET ENGINES
Effect of humidity on jet engine axial-flow compressor performance p 22 A83-35856
Prediction of sound radiation from different practical jet engine inlets
[NASA-CR-169533] p 197 N83-13936
The JT9D Jet Engine Diagnostics Program
[NASA-CR-167966] p 32 N83-17544
BASIC Data Manipulation And Display System (BDMADS)
[NASA-TM-83328] p 189 N83-19496
Tone generation by rotor-downstream strut interaction
[NASA-TM-83330] p 33 N83-19754
Alternatives for jet engine control
[NASA-CR-170100] p 33 N83-20945
Alternatives for jet engine control
[NASA-CR-170233] p 35 N83-23305
Analysis of strain gage reliability in F-100 jet engine testing at NASA Lewis Research Center
[NASA-TM-83325] p 134 N83-24829
Sensor failure detection for jet engines
[NASA-CR-168190] p 154 N83-33182

JET EXHAUST
Conventional profile coaxial jet noise prediction p 193 A83-22128
Comparison of measured and predicted flight effects on high-bypass coaxial jet exhaust noise
[NASA-TM-83347] p 200 N83-23115

JET FLOW
Noise and flow structure of a tone-excited jet p 192 A83-13136
Tone-excited jet: Theory and experiments
[NASA-CR-3538] p 197 N83-12968
Analytical calculation of a single jet in crossflow and comparison with experiment
[NASA-TM-83027] p 29 N83-14127
Jet array impingement flow distributions and heat transfer characteristics. Effects of initial crossflow and nonuniform array geometry --- gas turbine engine component cooling
[NASA-CR-3630] p 128 N83-15592
Into mesh lubrication of spur gears with arbitrary offset oil jet. 1: For jet velocity less than or equal to gear velocity
[NASA-TM-83040] p 143 N83-19092
Into mesh lubrication of spur gears with arbitrary offset oil jet. 2: For jet velocities equal to or greater than great velocity
[NASA-TM-83041] p 143 N83-19093
Study of lubricant jet flow phenomena in spur gears: Out of mesh condition p 147 N83-20146
Analytical calculation of a single jet in cross-flow and comparison with experiment p 38 N83-29219
Axial vane-type swirler performance characteristics
[NASA-CR-172995] p 40 N83-32808
Numerical analysis of turbulent coaxial flow with internal heat generation
[NASA-CR-172633] p 132 N83-33105

JET IMPINGEMENT
Improved Stirling engine performance using jet impingement p 137 A83-27288
Heat transfer and flow characteristics of jets impinging on a concave hemispherical plate p 123 A83-42743
Heat transfer characteristics for jet array impingement with initial crossflow
[ASME PAPER 83-GT-28] p 7 A83-47891
Experimental and analytical determination of gear tooth temperatures with oil jet lubrication p 142 N83-15530
Jet array impingement flow distributions and heat transfer characteristics. Effects of initial crossflow and nonuniform array geometry --- gas turbine engine component cooling
[NASA-CR-3630] p 128 N83-15592
Gear lubrication and cooling experiment and analysis p 147 N83-20147
Morphology of an aluminum alloy eroded by a jet of angular particles impinging at normal incidence
[NASA-TP-2139] p 85 N83-24641
Spherical micro-glass particle impingement studies of thermoplastic materials at normal incidence
[NASA-TM-83410] p 94 N83-25883
Time dependence of solid-particle impingement erosion of an aluminum alloy
[NASA-TP-2169] p 86 N83-32908

JET LIFT
Conceptual design, evaluation and research identification for Remote Augmented Propulsive Lift Systems (RALS) with ejectors for VTOL aircraft
[NASA-CR-167906] p 29 N83-13103

JET MIXING FLOW
On the shock cell structure and noise of supersonic jets
[AIAA PAPER 83-0703] p 193 A83-25923
Perspectives on the mixing of a row of jets with a confined crossflow
[AIAA PAPER 83-1200] p 122 A83-36276
Experiments in dilution jet mixing
[AIAA PAPER 83-1201] p 122 A83-36277
Statistical characteristics of velocity, concentration, mass transport, and momentum transport for coaxial jet mixing in a confined duct
[ASME PAPER 83-GT-39] p 125 A83-47899
Dilution Jet Mixing Program, phase 1
[NASA-CR-168031] p 128 N83-15590
Modeling of space vehicle propellant mixing --- cryogenic propellants
[NASA-TP-2107] p 100 N83-16545
Dilution zone mixing p 131 N83-29216
Perspectives on the mixing of a row of jets with a confined crossflow
[NASA-TM-83457] p 15 N83-30392
Experiments in dilution jet mixing
[NASA-TM-83434] p 15 N83-30393

JET VANES
Energy efficient engine high-pressure turbine single crystal vane and blade fabrication technology report
[NASA-CR-165400] p 39 N83-30429

JOINING
Evaluation of electrode shape and nondestructive evaluation method for welded solar cell interconnects
[NASA-TM-82966] p 166 N83-10555

JOINTS (ANATOMY)
Tribological measurements on a Charnley-type artificial hip joint
[NASA-TM-83440] p 97 N83-32943

JOURNAL BEARINGS
An experimental investigation of the vaporous/gaseous cavity characteristics of an eccentric journal bearing
[ASLE PREPRINT 82-LC-3A-1] p 136 A83-13230
High-speed motion picture camera experiments of cavitation in dynamically loaded journal bearings
[ASME PAPER 82-LUB-18] p 136 A83-13509
High-speed motion picture camera experiments of cavitation in dynamically loaded journal bearings
[ASME PAPER 82-LUB-18] p 138 A83-39944
Experimental investigation of the vaporous/gaseous cavity characteristics of an eccentric journal bearing
[NASA-TM-82996] p 128 N83-17833
Classification of journal surfaces using surface topography parameters and software methods to compensate for stylus geometry
[NASA-CR-168153] p 148 N83-24857
Vapor cavitation in dynamically loaded journal bearings
[NASA-TM-83366] p 160 N83-24875

K

KALMAN FILTERS
Sensor failure detection for jet engines
[NASA-CR-168190] p 154 N83-33182

KINEMATIC EQUATIONS
Spiral-bevel geometry and gear train precision p 146 N83-20139

KINEMATICS
The optimal design of standard gearsets p 146 N83-20145
Pivoting and slip in an angular contact bearing
[NASA-TM-83408] p 148 N83-26079
Rolling-element bearings
[NASA-RP-1105] p 149 N83-27214
Time-independent anisotropic plastic behavior by mechanical subelement models p 162 N83-34369

KINETIC ENERGY
Analytical and experimental investigation of stator endwall contouring in a small axial-flow turbine. 1: Stator performance
[NASA-TP-2023] p 26 N83-11125
Design of a multistage depressed collector for the F-16 radar dual mode transmitter tube
[NASA-TM-82982] p 114 N83-14399

KLYSTRONS
Modern multistage depressed collectors - A review p 112 A83-24025
Multi-stage Depressed Collectors (MDC) for efficiency improvements of UHF broadcast klystrons
[NASA-TM-82970] p 105 N83-10322

KOLMOGOROFF THEORY
Solution to the backward-Kolmogorov equation for a nonstationary oscillation problem p 192 A83-15697

L

LABYRINTH SEALS
Labyrinth seal forces on a whirling rotor
[NASA-CR-168016] p 34 N83-22198
Comparative evaluation of three shaft seals proposed for high performance turbomachinery
[NASA-TM-83021] p 152 N83-34325

LADDERS
Dielectric based submillimeter backward wave oscillator circuit
[NASA-CASE-LEW-13736-1] p 115 N83-17802

LAGRANGE MULTIPLIERS
Nonlinear program based optimization of boost and buck-boost converter designs p 110 A83-11016

LAGUERRE FUNCTIONS
Geometrically nonlinear analysis of layered composite plates and shells
[NASA-CR-168182] p 161 N83-33219

LAMINAR BOUNDARY LAYER
The evolution of Tollmien-Schlichting waves near a leading edge. II - Numerical determination of amplitudes p 122 A83-35346

LAMINAR FLOW
Finite analytic numerical solution of axisymmetric Navier-Stokes and energy equations
[ASME PAPER 82-HT-42] p 119 A83-12795
Modified gauge for time-resolved skin-friction measurements p 133 A83-14172
Aerodynamic features of turbulent flames
[AIAA PAPER 83-0470] p 119 A83-16737
Numerical solution of the problem of flame propagation by the use of the random element method
[AIAA PAPER 83-0600] p 69 A83-36062
Vortices, stability, and turbulence p 125 A83-46718
Numerical simulation of the flow and fuel-air mixing in an axisymmetric piston-cylinder arrangement
[NASA-TM-83011] p 126 N83-12358

LAMINATES
Moving cracks in layered composites p 155 A83-12048
Geometrically nonlinear analysis of layered composite shells p 156 A83-27431
Three-dimensional finite-element analysis of layered composite plates p 156 A83-27432
Wave propagation in a graphite/epoxy laminate p 158 A83-44050
Dynamic responses of graphite/epoxy laminated beam to impact of elastic spheres
[NASA-CR-165461] p 64 N83-13173
High strain rate properties of off-axis composite laminates, part 2
[NASA-CR-167970] p 64 N83-13179
High strain properties of angle-ply composite laminate, part 3
[NASA-CR-167971] p 64 N83-13180
Research priorities and history of advanced composite compression testing
[NASA-CR-165415] p 66 N83-18854
Wave propagation in graphite/epoxy laminates due to impact
[NASA-CR-168057] p 66 N83-22325
Design and evaluation of low-cost laminated wood composite blades for intermediate size wind turbines: Blade design, fabrication concept, and cost analysis
[NASA-CR-165463] p 179 N83-23704
A study of the stress wave factor technique for the characterization of composite materials
[NASA-CR-3670] p 153 N83-27248
Fabrication of low-cost Mod-0A wood composite wind turbine blades
[NASA-TM-83323] p 182 N83-27347
Piezoelectric composite materials
[NASA-CASE-LEW-12582-1] p 207 N83-34796

LAND MOBILE SATELLITE SERVICE
Satellite-aided land mobile communications system implementation considerations p 104 A83-41417

LAPLACE EQUATION
The finite analytic method, volume 3
[NASA-CR-170186] p 191 N83-23087

LARGE SPACE STRUCTURES
On-orbit propulsion requirements and performance assessment of ion propulsion subsystems for future GEO large satellite missions
[AIAA PAPER 82-1872] p 48 A83-12460
Benefits and costs of low thrust propulsion systems
[AIAA PAPER 83-1248] p 49 A83-36306
Auxiliary propulsion requirements for large space systems
[AIAA PAPER 83-1217] p 56 A83-45512
Analysis and design of ion thruster for large space systems
[NASA-CR-165140] p 57 N83-14158
Analysis and design of ion thrusters for large space systems
[NASA-CR-165160] p 57 N83-14159

Study for analysis of benefit versus cost of low thrust propulsion system
[NASA-CR-168011] p 57 N83-21002
Requirements for a mobile communications satellite system. Volume 3: Large space structures measurements study
[NASA-CR-168105] p 45 N83-22255
Requirements for a mobile communications satellite system. Volume 1: Executive summary
[NASA-CR-168128] p 106 N83-23497
Requirements for a mobile communications satellite system. Volume 2: Technical report
[NASA-CR-168129] p 107 N83-23498
Large space systems auxiliary propulsion requirements p 46 N83-26864
Auxiliary propulsion requirements for large space systems
[NASA-TM-83388] p 58 N83-26922

LASER ANEMOMETERS
Laser anemometer using a Fabry-Perot interferometer for measuring mean velocity and turbulence intensity along the optical axis in turbomachinery p 133 A83-28834
Particle-sampling statistics in laser anemometers Sample-and-hold systems and saturable systems p 134 A83-48120

LASER APPLICATIONS
Performance of laser-glazed zirconia thermal barrier coatings in cyclic oxidation and corrosion burner rig tests p 88 A83-10300
Free-jet acoustic investigation of high-radius-ratio coannular plug nozz Comprehensive data report, volume 2
[NASA-CR-168086-VOL-2] p 199 N83-18409

LASER CAVITIES
The application of free-electron lasers to the transmission of energy in space p 135 A83-31141

LASER DOPPLER VELOCIMETERS
An analytical and experimental comparison of the flow field of an advanced swept turboprop
[AIAA PAPER 83-0189] p 3 A83-21080
Laser-induced fluorescence technique for velocity field measurements in subsonic gas flows p 133 A83-45962
An analytical and experimental comparison of the flow field of an advanced swept turboprop
[NASA-TM-83037] p 1 N83-14061
Rotor redesign for a highly loaded 1800 ft/sec tip speed fan. 3: Laser Doppler velocimeter report
[NASA-CR-167954] p 30 N83-14128

LASER FUSION
Laser surface fusion of plasma sprayed ceramic turbine seals
[NASA-CASE-LEW-13269-1] p 50 N83-20996

LASER INTERFEROMETRY
Extending the laser-specklegram technique to strain analysis of rotating components p 155 A83-12514
Manual for extending the laser specklegram technique to strain analysis of rotating components
[NASA-CR-167932] p 134 N83-15601

LASER MICROSCOPY
Evaluation of solar cell welds by scanning acoustic microscopy p 172 N83-15834

LASER PROPULSION
Radiation energy receiver for laser and solar propulsion systems
[AIAA PAPER 83-1207] p 55 A83-36281

LASER PUMPING
Gain-enhanced free-electron laser with an electromagnetic pump field p 135 A83-31133

LAUNCHERS
Rail accelerator research at Lewis Research Center
[AIAA PAPER 82-1938] p 53 A83-22075
Rail accelerator research at Lewis Research Center
[NASA-TM-83015] p 56 N83-12143

LC CIRCUITS
Transformer induced instability of the series resonant converter p 113 A83-41152

LEAD (METAL)
Joining lead wires to thin platinum alloy films
[NASA-CASE-LEW-13934-1] p 135 N83-35338

LEAD ACID BATTERIES
Results of chopper-controlled discharge life cycling studies on lead-acid batteries p 164 A83-27183

LEADING EDGES
The evolution of Tollmien-Schlichting waves near a leading edge p 120 A83-24410
The evolution of Tollmien-Schlichting waves near a leading edge. II - Numerical determination of amplitudes p 122 A83-35346
Piezoelectric deicing device
[NASA-CASE-LEW-13773-1] p 18 N83-29197
Stagnation region gas film cooling: Effects of dimensionless coolant temperature
[NASA-CR-168197] p 132 N83-30960
A method of predicting flow rates required to achieve anti-icing performance with a porous leading edge ice protection system
[NASA-CR-168213] p 17 N83-32782

LEAKAGE
Assessment of crash fire hazard of LH sub 2 fueled aircraft
[NASA-CR-165525] p 16 N83-11095
Energy efficient high-pressure turbine leakage technology report
[NASA-CR-165202] p 30 N83-15304
Optimum parallel step-sector bearing lubricated with an incompressible fluid
[NASA-TM-83356] p 148 N83-24855
A comparison of flow rates and pressure profiles for N-sequential inlets and three related seal configurations
[NASA-TM-83442] p 132 N83-33103

LEAST SQUARES METHOD
A class of nonideal solutions. 2: Application to experimental data
[NASA-TP-1930] p 208 N83-23188

LENSES
Large-aperture interferometer using local reference beam
[NASA-TP-2060] p 203 N83-13979

LIFE (DURABILITY)
Catalyst durability evaluation for advanced gas turbine engines
[ASME PAPER 82-JPGC-GT-21] p 137 A83-25270
Life and reliability models for helicopter transmissions
[NASA-TM-82976] p 139 N83-10425
Measured and calculated wall temperatures on air-cooled turbine vanes with boundary layer transition
[NASA-TM-83030] p 127 N83-14432
Studies of the mechanisms of turbine fuel instability
[NASA-CR-167963] p 100 N83-18924
Analytical fuel property effects, small combustors, phase 1
[NASA-CR-168138] p 101 N83-23464
Cycle life test and failure model of nickel-hydrogen cells
[NASA-TM-83375] p 180 N83-25038
Endurance test of a 30-CM-diameter engineering model ion thruster. Task 12: Investigation of thin-film erosion monitors for ion thrusters
[NASA-CR-168132] p 58 N83-25779

LIFE CYCLE COSTS
Expected cycle life vs. depth of discharge relationships of well-behaved single cells and cell strings p 165 A83-32627
Market assessment of photovoltaic power systems for agricultural applications worldwide
[NASA-CR-165541] p 168 N83-13585
Advanced single permanent magnet axipolar ironless stator ac motor for electric passenger vehicles
[NASA-CR-167974] p 212 N83-32687

LIFT
Design analysis of a self-acting spiral-groove ring seal for counter-rotating shafts
[NASA-TP-2142] p 36 N83-25712

LIFT AUGMENTATION
Conceptual design, evaluation and research identification for Remote Augmented Propulsive Lift Systems (RALS) with ejectors for VTOL aircraft
[NASA-CR-167906] p 29 N83-13103
V/STOL propulsion control analysis: Phase 2, task 5-9
[NASA-CR-165523] p 40 N83-32804

LIFT FANS
A remote augmentor lift system with a turbine bypass engine p 20 A83-19595
Inlet-fan flow field computation
[ASME PAPER 83-GT-41] p 7 A83-47901
A remote augmentor lift system with a turbine bypass engine
[NASA-TM-82932] p 27 N83-12087

LIFTING BODIES
New test techniques and analytical procedures for understanding the behavior of advanced propellers
[NASA-TM-83360] p 2 N83-22092

LIGHT (VISIBLE RADIATION)
The phototron: A light to RF energy conversion device p 173 N83-15866
Atmospheric radiation model for water surfaces
[NASA-CR-167873] p 187 N83-21677

LIGHT SCATTERING
Particle sizing by measurement of forward-scattered light at two angles
[NASA-TP-2156] p 36 N83-24509

LIGHT SOURCES
A proposed optical pumping system requiring no electric power p 203 N83-15861

LINEAR EQUATIONS
Triangular system solutions on an optical systolic processor p 189 A83-36752

LINEARITY
Sensor failure detection for jet engines
[NASA-CR-168190] p 154 N83-33182

LININGS
Nonlinear structural and life analyses of a combustor liner p 155 A83-12764
Small gas turbine combustor study - Combustor liner evaluation
[AIAA PAPER 83-0337] p 20 A83-16663
Optimization of acoustic liners by the hybrid finite element-integral approach
[AIAA PAPER 83-0670] p 194 A83-26917
Steam cooled rich-burn combustor liner
[NASA-CASE-LEW-13609-1] p 72 N83-17628
Small gas turbine combustor study: Combustor liner evaluation
[NASA-TM-83028] p 33 N83-18725
Experimental verification of the Neuber relation at room and elevated temperatures --- to predict stress-strain behavior in notched specimens of hastelloy x
[NASA-CR-167967] p 159 N83-19121
Energy efficient engine sector combustor rig test program
[NASA-CR-167913] p 33 N83-19753
Fully plasma-sprayed compliant backed ceramic turbine seal
[NASA-CASE-LEW-13268-3] p 149 N83-28450

LIQUID BEARINGS
The performance and application of high speed long life LH2 hybrid bearings for reusable rocket engine turbomachinery
[NASA-TM-83417] p 58 N83-26923

LIQUID CHROMATOGRAPHY
Use of high pressure liquid chromatography in the study of liquid lubricant oxidation
[NASA-TM-83033] p 92 N83-14270
High performance liquid chromatographic hydrocarbon group-type analyses of mid-distillates employing fuel-derived fractions as standards
[NASA-TM-83072] p 100 N83-19920
High-pressure liquid chromatography: A brief introduction and its application in analyzing the degradation of a C-ether (Thio-ether) liquid lubricant
[NASA-TM-83474] p 98 N83-35144

LIQUID FUELS
A carbon-13 and proton nuclear magnetic resonance study of some experimental referee broadened-specification /ERBS/ turbine fuels p 98 A83-11482
Analytical modeling of operating characteristics of premixing-prevaporizing fuel-air mixing passages. Volume 1: Analysis and results
[NASA-CR-167990-VOL-1] p 126 N83-12353
Analytical modeling of operating characteristics of premixing-prevaporizing fuel-air mixing passages. Volume 2: User's manual
[NASA-CR-167990-VOL-2] p 126 N83-12354
Fuel quality-processing study. Volume 1: Overview and results
[NASA-CR-165326-VOL-1] p 178 N83-22750
Fuel quality-processing study. Volume 2: Literature survey
[NASA-CR-165326-VOL-2] p 178 N83-22751
Experimental design of an interlaboratory study for trace metal analysis of liquid fluids --- for aerospace vehicles
[NASA-TP-2148] p 73 N83-24575
Automotive Stirling Engine Development Program
[NASA-CR-168074] p 212 N83-27925
High-pressure flame visualization of autoignition and flashback phenomena with liquid-fuel spray
[NASA-TM-83501] p 42 N83-34948

LIQUID HYDROGEN
Cryogenic fluid management experiment trunnion fatigue verification
[AIAA PAPER 83-0911] p 49 A83-32782
The performance and application of high speed long life LH2 hybrid bearings for reusable rocket engine turbomachinery
[AIAA PAPER 83-1389] p 138 A83-36379
The performance and application of high speed long life LH2 hybrid bearings for reusable rocket engine turbomachinery
[NASA-TM-83417] p 58 N83-26923

LIQUID INJECTION
Aerodynamic-wave break-up of liquid sheets in swirling airflows and combustor modules
[AIAA PAPER 83-1204] p 124 A83-45511
Aerodynamic-wave break-up of liquid sheets in swirling airflows and combustor modules
[NASA-TM-83353] p 130 N83-23545

LIQUID METALS
Direct contact droplet heat exchangers for thermal management in space p 120 A83-27137

LIQUID NEON
NASA Lewis Research Center combustion MHD experiment p 173 N83-15847

LIQUID OXYGEN
Analysis of spiral-groove face seals for liquid oxygen [ASLE PREPRINT 83-AM-4B-2] p 138 A83-43339
LOX/hydrocarbon fuel carbon formation and mixing data analysis [NASA-CR-168066] p 101 N83-31886
LIQUID PHASE EPITAXY
Liquid encapsulated Czochralski growth of low dislocation GaAs p 204 A83-13784
LIQUIDS
A comprehensive analysis of cavitation and liquid impingement erosion data [NASA-TM-83352] p 84 N83-24634
LITERATURE
Literature search of publications concerning the prediction of dynamic inlet flow distortion and related topics [NASA-CR-3673] p 33 N83-18729
LOAD DISTRIBUTION (FORCES)
Rolling-element bearings [NASA-RP-1105] p 149 N83-27214
LOAD TESTS
Steady-state and dynamic evaluation of the electric propulsion system test bed vehicle on a road load simulator [NASA-TM-83445] p 186 N83-35496
LOADING MOMENTS
Energy efficient face seal [NASA-CR-165591] p 142 N83-15659
LOADS (FORCES)
Moving cracks in layered composites p 155 A83-12048
Lubrication of 35-millimeter-bore ball bearings of several designs at speeds to 2.5 million DN p 141 N83-15512
Experimental and analytical determination of gear tooth temperatures with oil jet lubrication p 142 N83-15530
Thermomechanical loading of multilayered cylindrical geometries in thermal cycling from 300 to 1300 K [NASA-TM-83312] p 129 N83-20029
Lubrication of 35-millimeter-bore ball bearings of several designs to 2.5 million DN p 145 N83-20132
Advantage of resonant power conversion in aerospace applications [NASA-TM-83399] p 37 N83-27994
Comparison of road load simulator test results with track tests on electric vehicle propulsion system [NASA-TM-83393] p 184 N83-29811
Time-independent anisotropic plastic behavior by mechanical subelement models p 162 N83-34369
LONG DURATION SPACE FLIGHT
Design and development of multi-kW power electronic transformers --- for long duration space applications [NASA-CR-168082] p 116 N83-29596
LONG TERM EFFECTS
Long term storage of cryogens in space p 102 A83-11487
Advanced ceramic coating development for industrial/utility gas turbine applications [NASA-CR-165619] p 92 N83-15467
A total life prediction model for stress concentration sites [NASA-CR-170290] p 160 N83-23629
A comprehensive analysis of cavitation and liquid impingement erosion data [NASA-TM-83352] p 84 N83-24634
LORENTZ TRANSFORMATIONS
Dipole-field sums and Lorentz factors for orthorhombic lattices, and implications for polarizable molecules p 204 A83-17226
LOW COST
Large area low-cost space solar cell development p 170 N83-14699
LOW SPEED
NASA low-speed centrifugal compressor for fundamental research [AIAA PAPER 83-1351] p 43 A83-36353
Low speed performance of a supersonic axisymmetric mixed compression inlet with auxiliary inlets [AIAA PAPER 83-1414] p 7 A83-45516
Low speed performance of a supersonic axisymmetric mixed compression inlet with auxiliary inlets --- Lewis 9x15-ft anechoic wind tunnel tests [NASA-TM-83435] p 37 N83-27992
Temperature distribution in an aircraft tire at low ground speeds [NASA-TP-2195] p 161 N83-33217
LOW SPEED WIND TUNNELS
A new surface-streamline flow-visualization technique p 133 A83-19016
LOW TEMPERATURE
Low temperature hot corrosion p 76 A83-42252
LOW THRUST
Benefits and costs of low thrust propulsion systems [AIAA PAPER 83-1248] p 49 A83-36306
LOW THRUST PROPULSION
Simplified power processing for ion-thruster subsystems p 56 A83-39271
LUBRICANT TESTS
Lubricant effects on efficiency of a helicopter transmission p 141 N83-15523
LUBRICANTS
Morphological and frictional behavior of sputtered MoS2 films p 88 A83-12652
Surface temperatures and glassy state investigations in tribology, part 5 [NASA-CR-3632] p 91 N83-11328
Rolling-element fatigue life with traction fluids and automatic transmission fluid in a high-speed rolling-contact rig [NASA-TP-2050] p 140 N83-13457
Use of high pressure liquid chromatography in the study of liquid lubricant oxidation [NASA-TM-83033] p 92 N83-14270
Infrared emission spectrophotometric study of the changes produced by TiN coating of metal surfaces in an operating EHD contact [NASA-TM-82989] p 92 N83-15466
A detailed treatment of two-dimensional, starved lubrication in the vicinity of two counter-rotating cylinders p 141 N83-15520
Geometry and starvation effects in hydrodynamic lubrication p 141 N83-15522
Lubricant effects on efficiency of a helicopter transmission p 141 N83-15523
Determination of physical and chemical states of lubricants in concentrated contacts, part 3 [NASA-CR-3658] p 92 N83-16527
Mechanism of lubrication by tricresylphosphate (TCP) [NASA-TP-2053] p 72 N83-18863
Corrosion of simulated bearing components of three bearing steels in the presence of chloride-contaminated lubricant [NASA-TM-82955] p 143 N83-20115
Traction behavior of two traction lubricants [NASA-TM-83311] p 144 N83-20116
Study of lubricant jet flow phenomena in spur gears: Out of mesh condition p 147 N83-20146
Effect of oxygen concentration in ZDP containing oils on surface composition and wear [NASA-TM-83000] p 84 N83-24636
Regression analysis of traction characteristics of traction fluids [NASA-TP-2154] p 148 N83-24862
The adsorption and thermal decomposition of tricresylphosphate (TCP) on iron and gold [NASA-TM-83441] p 62 N83-29311
LUBRICATING OILS
On the mechanism of lubrication by tricresylphosphate /TCP/ - The coefficient of friction as a function of temperature for TCP on M-50 steel [ASLE PREPRINT 82-LC-4C-1] p 135 A83-13228
An experimental investigation of the vaporous/gaseous cavity characteristics of an eccentric journal bearing [ASLE PREPRINT 82-LC-3A-1] p 136 A83-13230
Ferrographic and spectrometer oil analysis from a failed gas turbine engine [NASA-TM-82956] p 140 N83-12433
Experimental and analytical determination of gear tooth temperatures with oil jet lubrication p 142 N83-15530
Energy efficient face seal [NASA-CR-165591] p 142 N83-15659
Experimental investigation of the vaporous/gaseous cavity characteristics of an eccentric journal bearing [NASA-TM-82996] p 128 N83-17833
Into mesh lubrication of spur gears with arbitrary offset oil jet. 1: For jet velocity less than or equal to gear velocity [NASA-TM-83040] p 143 N83-19092
Into mesh lubrication of spur gears with arbitrary offset oil jet. 2: For jet velocities equal to or greater than gear velocity [NASA-TM-83041] p 143 N83-19093
A review of liquid lubricant thermal/oxidative degradation [NASA-TM-83465] p 98 N83-35143
LUBRICATION
Tribological properties of amorphous alloys and the role of surfaces in abrasive wear of materials [NASA-TM-82973] p 140 N83-11498
Tribology p 140 N83-12167
Elastohydrodynamic lubrication theory [NASA-TM-81695] p 140 N83-12432
Theoretical results for fully flooded, elliptical hydrodynamic contacts [NASA-TM-81696] p 140 N83-13458
Elastohydrodynamic lubrication of elliptical contacts p 141 N83-15514
A detailed treatment of two-dimensional, starved lubrication in the vicinity of two counter-rotating cylinders p 141 N83-15520
Geometry and starvation effects in hydrodynamic lubrication p 141 N83-15522
Lubricant effects on efficiency of a helicopter transmission p 141 N83-15523
Elastohydrodynamic lubrication of rectangular contacts [NASA-TP-2111] p 143 N83-18759
Surface roughness effects in hydrodynamic lubrication: The flow factor method [NASA-TM-83024] p 129 N83-19016
Optimum parallel step-sector bearing lubricated with an incompressible fluid [NASA-TM-83356] p 148 N83-24855
Film thickness for different regimes of fluid-film lubrication --- elliptical contacts [NASA-TM-81700] p 149 N83-28449
Non-Newtonian fluid model incorporated into elastohydrodynamic lubrication of rectangular contacts [NASA-TM-83318] p 150 N83-28454
Experimental investigations of elastohydrodynamic lubrication [NASA-TM-81698] p 150 N83-29711
Applications of film thickness equations [NASA-TM-81701] p 151 N83-29713
LUBRICATION SYSTEMS
Lubrication of 35-millimeter-bore ball bearings of several designs at speeds to 2.5 million DN p 141 N83-15512
Assessment of lubricated contacts: Mechanisms of scuffing and scoring [NASA-TM-83074] p 144 N83-20118
Lubrication of 35-millimeter-bore ball bearings of several designs to 2.5 million DN p 145 N83-20132
Large-bore tapered-roller bearing performance and endurance to 2.4 million DN p 145 N83-20134
Sizing criterial for traction drives p 146 N83-20137
Spiral-bevel geometry and gear train precision p 146 N83-20139
The trend of future gas turbine technology [NASA-TM-83505] p 2 N83-34886

M

MACH NUMBER
Generation of Tollmien-Schlichting waves by free-stream disturbances at low Mach numbers [NASA-TM-83026] p 130 N83-23544
Comparison of two- and three-dimensional flow computations with laser anemometer measurements in a transonic compressor rotor [NASA-TP-1931] p 15 N83-32774
MACHINING
The orthogonal in-situ machining of single and polycrystalline aluminum and copper, volume 2 [NASA-CR-169528] p 81 N83-13233
MAGNESIUM ALLOYS
Testing of the permanent magnet material Mn-Al-C for potential use in propulsion motors for electric vehicles [NASA-CR-169481] p 114 N83-12329
MAGNETIC CORES
Advances in core loss calculations for magnetic materials [NASA-TM-82947] p 113 N83-11446
Design study of a high power rotary transformer [NASA-CR-168012] p 115 N83-16630
MAGNETIC FIELD CONFIGURATIONS
Improved ion containment using a ring-cusp ion thruster [AIAA PAPER 82-1928] p 53 A83-21100
Improved ion containment using a ring-cusp ion thruster [NASA-TM-82990] p 56 N83-13164
Ring-cusp ion thruster with shell anode [NASA-CASE-LEW-13881-1] p 202 N83-21903
MAGNETIC FIELDS
Parallel plate radiofrequency ion thruster [AIAA PAPER 82-1937] p 53 A83-21900
Parallel plate radiofrequency ion thruster [NASA-TM-83014] p 56 N83-12142
MAGNETIC PROPERTIES
Advances in core loss calculations for magnetic materials [NASA-TM-82947] p 113 N83-11446
New propulsion components for electric vehicles [NASA-TM-83404] p 116 N83-25982
MAGNETIC PUMPING
Magnetic heat pumping [NASA-CASE-LEW-12508-3] p 131 N83-29625
MAGNETOHYDRODYNAMIC FLOW
MHD channel performance for potential early commercial MHD power plants p 204 A83-23134
MAGNETOHYDRODYNAMIC GENERATORS
End region effects upon the performance of a magnetohydrodynamic channel p 203 A83-10665
Transient flow analysis of the AEDC/HPDE MHD generator [AIAA PAPER 83-0395] p 203 A83-16691

Methods of reducing energy consumption of the oxidant supply system for MHD/steam power plants
[AIAA PAPER 83-0468] p 203 A83-16735
MHD channel performance for potential early commercial MHD power plants p 204 A83-23134
Vaporization thermodynamics of K2S and K2SO3
[NASA-CR-168080] p 61 N83-19812
Parametric analysis of closed cycle magnetohydrodynamic (MHD) power plants
[NASA-CR-165472] p 178 N83-22748
Parametric study of potential early commercial MHD power plants. Task 3: Parameter variation of plant size
[NASA-CR-165445] p 182 N83-26259

MAGNETOHYDRODYNAMICS
Characterization of advanced electric propulsion systems p 55 A83-33744
Methods of reducing energy consumption of the oxidant supply system for MHD/steam power plants
[NASA-TM-83025] p 168 N83-13589
Magnetohydrodynamics (MHD) Engineering Test Facility (ETF) 200 MWe power plant. Conceptual Design Engineering Report (CDER) supplement. Magnet system special investigations
[NASA-CR-165509] p 141 N83-14494
NASA Lewis Research Center combustion MHD experiment p 173 N83-15847
Analytical investigation of critical MHD phenomena
[NASA-CR-168079] p 175 N83-19228

MAGNETOSTRICTION
The initial stages of cavitation damage and erosion on copper and brass tested in a rotating disk device p 75 A83-27421
Initial stages of cavitation damage and erosion on copper and brass tested in a rotating disk device
[NASA-TM-82993] p 81 N83-13231

MANGANESE
Surface chemistry, friction and wear of Ni-Zn and Mn-Zn ferrites in contact with metals
[NASA-TM-83068] p 93 N83-19901
X-ray photoelectron spectroscopy and friction studies of nickel-zinc and manganese-zinc ferrites in contact with metals
[NASA-TP-2163] p 84 N83-23419
The effects of Ni, Mo, Ti and Si on the mechanical properties of Cr free Mn steel (Fe-25Mn-5Al-2C)
[NASA-TM-83355] p 85 N83-24638

MANUFACTURING
High frequency, high power capacitor development
[NASA-CR-168035] p 116 N83-27127

MARKET RESEARCH
Future satellite systems - Market demand assessment p 104 A83-19762
Market assessment of photovoltaic power systems for agricultural applications worldwide
[NASA-CR-165541] p 168 N83-13585
Customer premise service study for 30/20 GHz satellite system
[NASA-CR-167986] p 105 N83-17769
Customer premises services market demand assessment 1980 - 2000. Volume 1: Executive summary
[NASA-CR-168150] p 108 N83-31925
Customer premises services market demand assessment 1980 - 2000: Volume 2
[NASA-CR-168151] p 108 N83-31926

MARKETING
The worldwide market for photovoltaics in the rural sector
[NASA-TM-83035] p 173 N83-15840

MARKOV PROCESSES
Solution to the backward-Kolmogorov equation for a nonstationary oscillation problem p 192 A83-15697

MASS DRIVERS (PAYLOAD DELIVERY)
Characterization of advanced electric propulsion systems p 55 A83-33744

MASS FLOW
Studies of flows through N-sequential orifices
[NASA-TM-83313] p 129 N83-19020
Burner rig study of variables involved in hole plugging of air cooled turbine engine vanes
[NASA-TM-83308] p 83 N83-19887

MASS FLOW RATE
Studies of flows through N-sequential orifices
[ASME PAPER 83-FE-22] p 125 A83-48678
High accuracy fuel flowmeter, phase 1
[NASA-CR-167893] p 134 N83-21314

MASS SPECTRA
Mass analysis of neutral particles and ions released during electrical breakdowns on spacecraft surfaces
[NASA-CR-170299] p 50 N83-23347

MASS TRANSFER
Spanwise mass transfer variations on a cylinder in 'nominally' uniform crossflow p 124 A83-43019

MATCHED FILTERS
Advances in Serial MSK modems p 111 A83-19789

MATERIALS
Development of a simplified analytical method for representing material cyclic response
[NASA-CR-168100] p 160 N83-21390

MATHEMATICAL MODELS
Small particle transport across turbulent nonisothermal boundary layers p 118 A83-10650
An improved switching converter model using discrete and average techniques p 111 A83-11495
Numerical simulation of airfoil ice accretion
[AIAA PAPER 83-0112] p 16 A83-36042
Benefits and costs of low thrust propulsion systems
[AIAA PAPER 83-1248] p 49 A83-36306
Application of 3D aerodynamic/combustion model to combustor primary zone study
[AIAA PAPER 83-1265] p 23 A83-36316
Implicit marching solution of compressible viscous subsonic flow in planar and axisymmetric ducts
[NASA-TM-82876] p 125 N83-10389
Life and reliability models for helicopter transmissions
[NASA-TM-82976] p 139 N83-10425
Elastohydrodynamic lubrication theory
[NASA-TM-81595] p 140 N83-12432
Turbofan noise generation. Volume 1: Analysis
[NASA-CR-167951] p 198 N83-15041
Numerical simulation of a conducting disk partially covered by an insulator interacting with a plasma p 50 N83-18805
Investigation of continuously traversing microphone system for mode measurement
[NASA-CR-168040] p 199 N83-19575
The structure of particle-laden jets and nonevaporating sprays
[NASA-CR-168059] p 34 N83-20948
Stochastic differential equations and turbulent dispersion
[NASA-RP-1103] p 129 N83-22546
The structure of evaporating and combusting sprays: Measurements and predictions
[NASA-CR-170176] p 129 N83-22550
Numerical simulation of an electrothermal deicer pad
[NASA-CR-168097] p 17 N83-23281
The structure of evaporating and combusting sprays: Measurements and predictions
[NASA-CR-170312] p 130 N83-24795
Turbulence spectra in the noise source regions of the flow around complex surfaces
[NASA-TM-83392] p 202 N83-30168
A mathematical model for the doubly fed wound rotor generator
[NASA-TM-83454] p 117 N83-34192
Evaluation of inelastic constitutive models for nonlinear structural analysis p 162 N83-34357

MATRICES (CIRCUITS)
Spacecraft IF switch matrix for wideband service applications in 30/20 GHz communications satellite systems: Proof-of-concept model, executive summary
[NASA-CR-168175] p 107 N83-29492

MATRICES (MATHEMATICS)
Triangular system solutions on an optical systolic processor p 189 A83-36752
LU and Cholesky decomposition on an optical systolic array processor p 189 A83-43629
Time-independent anisotropic plastic behavior by mechanical subelement models p 162 N83-34369

MATRIX MATERIALS
On composites with periodic structure p 154 A83-10283
Resin selection criteria for tough composite structures
[AIAA 83-0801] p 89 A83-29734
Polymer matrix composites research at NASA Lewis Research Center p 91 N83-12151
Research on ultra-high-temperature materials, monolithic ceramics, ceramic matrix composites and carbon/carbon composites p 64 N83-12161
High strain properties of angle-ply composite laminate, part 3
[NASA-CR-167971] p 64 N83-13180

MATRIX METHODS
Micromechanically based constitutive relations for polycrystalline solids p 162 N83-34359

MAXIMUM LIKELIHOOD ESTIMATES
A low-power, high-throughput maximum-likelihood convolutional decoder chip for NASA's 30/20 GHz program p 111 A83-19754

MAXIMUM USABLE FREQUENCY
30/20 GHz experimental communications satellite system p 103 A83-19688

MEAN
Laser anemometer using a Fabry-Perot interferometer for measuring mean velocity and turbulence intensity along the optical axis in turbomachinery p 133 A83-28834

MEASURE AND INTEGRATION
Volume integrals of ellipsoids associated with the inhomogeneous Helmholtz equation p 192 A83-29528

MEASURING INSTRUMENTS
Modified gauge for time-resolved skin-friction measurements p 133 A83-14172
Development and test of a Microwave Ice Accretion Measurement Instrument (MIAMI)
[NASA-CR-3598] p 18 N83-14123
Interpretation of 2-probe turbulence measurements in an axisymmetric contraction
[NASA-CR-169832] p 11 N83-17502

MECHANICAL DEVICES
Method and apparatus for gripping unlaxial fibrous composite materials --- holding specimens for mechanical property testing
[NASA-CASE-LEW-13758-1] p 64 N83-12176

MECHANICAL DRIVES
Advanced AC permanent magnet axial flux disc motor for electric passenger vehicle
[NASA-CR-167975] p 115 N83-16628
Traction behavior of two traction lubricants
[NASA-TM-83311] p 144 N83-20116
A historical perspective of traction drives and related technology p 144 N83-20123
Evaluation of a high performance, fixed-ratio, traction drive p 145 N83-20135
Traction calculations and design data for two traction fluids p 145 N83-20136
Sizing criterial for traction drives p 146 N83-20137
A basis for the analysis of surface geometry of spiral bevel gears p 146 N83-20138
Spiral-bevel geometry and gear train precision p 146 N83-20139
Advances in traction drive technology
[NASA-TM-83397] p 150 N83-28455
Energy efficient engine. Core engine bearings, drives and configuration: Detailed design report
[NASA-CR-165376] p 39 N83-30430
Geometrical analysis of circular-cut spiral bevel gears
[NASA-CR-168226] p 151 N83-33167

MECHANICAL MEASUREMENT
Requirements for a mobile communications satellite system. Volume 3: Large space structures measurements study
[NASA-CR-168105] p 45 N83-22255

MECHANICAL PROPERTIES
Dynamic mechanical characterization of cure of a polyimide-graphite fiber composite (PMR 15/Celion 6000) p 62 A83-31793
Synthesis and characterization of bisimide amines and bisimide amine-cured epoxy resins p 90 A83-40924
Sintering, properties and fabrication of Si3N4 + Y2O3 based ceramics p 90 A83-48303
Influence of cobalt, tantalum, and tungsten on the microstructure and mechanical properties of superalloy single crystals p 79 N83-11293
Rotordynamic Instability Problems in High-Performance Turbomachinery
[NASA-CP-2250] p 142 N83-15629
Design and evaluation of low cost blades for large wind driven generating systems p 175 N83-19244
Simplified composite micromechanics equations for hygral, thermal and mechanical properties
[NASA-TM-83320] p 66 N83-19817
The effects of Ni, Mo, Ti and Si on the mechanical properties of Cr free Mn steel (Fe-25Mn-5Al-2C)
[NASA-TM-83355] p 85 N83-24638
A study of the stress wave factor technique for the characterization of composite materials
[NASA-CR-3670] p 153 N83-27248
Residual stress in plasma sprayed ceramic turbine tip and gas path seal specimens
[NASA-TM-83418] p 131 N83-28380
Micromechanically based constitutive relations for polycrystalline solids p 162 N83-34359

MEDICAL EQUIPMENT
Ion beam sputter-etched ventricular catheter for hydrocephalus shunt
[NASA-CASE-LEW-13107-1] p 188 N83-21785

MELTING POINTS
Evaluation of methods for rapid determination of freezing point of aviation fuels
[NASA-CR-167981] p 98 N83-10207

MELTS (CRYSTAL GROWTH)
EL2 distributions in doped and undoped liquid encapsulated Czochralski GaAs --- deep donor concentration p 205 A83-22756

MEMBRANE STRUCTURES
NASA redox storage system development project
[NASA-TM-83087] p 181 N83-26252
Preparation, characterization, physical testing and performance of fluorocarbon membranes and separators
[NASA-CR-167880] p 73 N83-26936

MEMBRANES
Preparation, characterization, physical testing and performance of flurocarbon membranes and separators
[NASA-CR-169756] p 71 N83-16418

Applications of ion beam technology
[NASA-CR-169797] p 82 N83-16493
Search for selective ion diffusion through membranes
[NASA-TM-83426] p 97 N83-34048

MERCURY ION ENGINES
Status of the J-series 30-cm mercury ion thruster
[AIAA PAPER 82-1904] p 51 A83-12479
Advanced-technology 30-cm-diameter mercury ion thruster
[AIAA PAPER 82-1910] p 51 A83-12484
Software and system level tests of a test flight mercury ion thruster subsystem
[AIAA PAPER 82-1912] p 51 A83-12485
Qualification test results of IAPS 8 cm ion thrusters
[AIAA PAPER 82-1954] p 52 A83-12511
Extended performance 8-cm mercury ion thruster
[AIAA PAPER 82-1913] p 53 A83-21078
Extended performance 8-cm mercury ion thruster
[NASA-TM-83029] p 57 N83-14157
The 8-CM ion thruster characterization --- mercury ion engine
[NASA-CR-167887] p 57 N83-17586

MESH
Coordinate generation with precise controls over mesh properties p 190 A83-29631
Into mesh lubrication of spur gears with arbitrary offset oil jet. 1: For jet velocity less than or equal to gear velocity
[NASA-TM-83040] p 143 N83-19092
Into mesh lubrication of spur gears with arbitrary offset oil jet. 2: For jet velocities equal to or greater than great velocity
[NASA-TM-83041] p 143 N83-19093
The optimal design of standard gearsets p 146 N83-20145

METAL BONDING
Molecular-orbital model for metal-sapphire interfacial strength p 67 A83-10612
Further industrial tests of ceramic thermal barrier coatings
[NASA-TP-2057] p 26 N83-10045
Thermal barrier coating system having improved adhesion
[NASA-CASE-LEW-1335901] p 97 N83-31855
Improved thermal barrier coating system
[NASA-CASE-LEW-13324-2] p 86 N83-34014

METAL COATINGS
A new diffusion-inhibited oxidation-resistant coating for superalloys p 74 A83-10299
Improved uniformity of multiphase ceramic-metal plasma-sprayed coats p 61 A83-22269
Improved nickel base coating alloy --- oxidation resistant coatings
[NASA-CASE-LEW-13834-1] p 85 N83-24639

METAL CRYSTALS
Gamma prime shape changes during creep of a nickel-base superalloy p 77 A83-47855
The orthogonal in-situ machining of single and polycrystalline aluminum and copper, volume 2
[NASA-CR-169528] p 81 N83-13233

METAL FATIGUE
Fatigue behavior of SiC reinforced Ti/6Al-4V/ at 650 C p 62 A83-12414
Metallurgical instabilities during the high temperature low cycle fatigue of nickel-base superalloys p 75 A83-22019
The effect of microstructure on the fatigue behavior of Ni base superalloys p 75 A83-36166
Strainrange partitioning: A total strain range version
[NASA-TM-83023] p 81 N83-14246
Statistical summaries of fatigue data for design purposes
[NASA-CR-3697] p 161 N83-29731
Relation of cyclic loading pattern to microstructural fracture in creep fatigue
[NASA-TM-83473] p 161 N83-34349
The thermal fatigue resistance of H-13 Die Steel for aluminum die casting dies
[NASA-TM-83331] p 87 N83-35103

METAL FIBERS
Low cycle fatigue behavior of aluminum/stainless steel composites
[AIAA 83-0806] p 62 A83-29886
Alumina fiber strength improvement
[NASA-CR-167999] p 63 N83-11247

METAL FILMS
Tribological properties and X-ray photoelectron spectroscopy studies of ion-plated gold on nickel and iron p 74 A83-12650
Surface-polaritonlike waves guided by thin, lossy metal films p 192 A83-37947
Long range surface plasmons in birefringent media p 202 A83-42206
Frictional and morphological characteristics of ion plated soft, metallic films
[NASA-TM-81723] p 83 N83-22390
Friction and hardness of gold films deposited by ion plating and evaporation
[NASA-TP-2207] p 87 N83-34019

METAL FOILS
Metal honeycomb to porous wireform substrate diffusion bond evaluation p 153 A83-39620

METAL JOINTS
Mechanical bonding of metal method
[NASA-CASE-LEW-12941-1] p 77 N83-10170

METAL MATRIX COMPOSITES
Fatigue behavior of SiC reinforced Ti/6Al-4V/ at 650 C p 62 A83-12414
Low cycle fatigue behavior of aluminum/stainless steel composites
[AIAA 83-0806] p 62 A83-29886
High-temperature composites - Status and future directions p 63 A83-40129
Three-dimensional elastoplastic stress analysis of unidirectional boron/aluminum composites
[NASA-CR-169796] p 65 N83-16394
Evaluation of low-cost aluminum composites for aircraft engine structural applications
[NASA-TM-83357] p 66 N83-25790

METAL OXIDE SEMICONDUCTORS
High voltage v-groove solar cell
[NASA-CASE-LEW-13401-2] p 185 N83-32177
VLSI technology and applications
[NASA-CR-174451] p 118 N83-36358

METAL OXIDES
Method for depositing an oxide coating
[NASA-CASE-LEW-13131-1] p 165 N83-10494
Method of forming oxide coatings --- for solar collector heating panels
[NASA-CASE-LEW-13132-1] p 96 N83-29388

METAL PLATES
Multicolor printing plate joining
[NASA-CASE-LEW-13598-1] p 102 N83-17745

METAL POWDER
Improved uniformity of multiphase ceramic-metal plasma-sprayed coats p 61 A83-22269

METAL SURFACES
Microscopic contour changes of tribological surfaces by chemical and mechanical action
[ASLE PREPRINT 82-LC-3B-3] p 136 A83-13237
Long-range surface plasmons in electrode structures p 202 A83-40733
An extensometer for axial strain measurement at high temperature p 134 A83-48604
Surface profile changes of scuffed bearing surfaces --- before and after acid treatment
[NASA-TM-83055] p 82 N83-17682
Coating with overlay metallic-cermet alloy systems
[NASA-CASE-LEW-13639-2] p 82 N83-17683
Mechanism of lubrication by tricresylphosphate (TCP)
[NASA-TP-2053] p 72 N83-18863
The XPS depth profiling and tribological characterization of ion-plated gold on various metals
[NASA-TM-83350] p 83 N83-23417
NASA interdisciplinary collaboration in tribology. A review of oxidational wear
[NASA-CR-3686] p 95 N83-27021

METAL-METAL BONDING
Diatomic molecules and metallic adhesion, cohesion, and chemisorption - A single binding-energy relation p 69 A83-30921
Mechanical bonding of metal method
[NASA-CASE-LEW-12941-1] p 77 N83-10170
Joining lead wires to thin platinum alloy films
[NASA-CASE-LEW-13934-1] p 135 N83-35338

METAL-WATER REACTIONS
Low temperature hot corrosion p 76 A83-42252
Cavitation pitting and erosion of aluminum 6061-T6 in mineral oil/water
[NASA-TP-2146] p 152 N83-35400

METALLIC GLASSES
Tribological properties of amorphous alloys and the role of surfaces in abrasive wear of materials
[NASA-TM-82973] p 140 N83-11498
Friction and wear of some ferrous-base metallic glasses
[NASA-TM-83067] p 82 N83-19886
Sliding induced crystallization of metallic glass
[NASA-TP-2140] p 83 N83-21110

METALLIZING
The effect of Ta2O5 on the interaction between silicon and its contact metallization
[NASA-TM-82948] p 166 N83-10554

METALLOGRAPHY
Gamma prime shape changes during creep of a nickel-base superalloy p 77 A83-47855

METALS
Correlation of tensile and shear strengths of metals with their friction properties
[ASLE PREPRINT 82-LC-1B-1] p 74 A83-13226
An uncoupled viscoplastic constitutive model for metals at elevated temperature
[AIAA 83-1016] p 156 A83-29798
Time effect of erosion by solid particle impingement on ductile materials
[NASA-TM-83369] p 84 N83-24637

METEOROLOGICAL SERVICES
Airline flight planning: The weather connection p 17 N83-17461

METHANE
Assessment of crash fire hazard of LH sub 2 fueled aircraft
[NASA-CR-165525] p 16 N83-11095

METHYL ALCOHOLS
Performance and emissions characteristics of aqueous alcohol fumes in a DI diesel engine
[NASA-CR-167917] p 99 N83-12250
Energy and precious fuels requirements of fuel alcohol production. Volume 4: Appendices G and H, methanol from coal
[NASA-CR-168083] p 183 N83-28580
Energy and precious fuels requirements of fuel alcohol production, volume 1
[NASA-CR-168090] p 183 N83-28581
Energy and precious fuels requirements of fuel alcohol production. Volume 3, appendices C to F: Methanol from cellulose
[NASA-CR-168092] p 183 N83-28583
Evaluation of fuel additives for reduction of material imcompatibilities in methanol-gasoline blends
[NASA-CR-168061] p 86 N83-29359
An analytical investigation of NO sub x control techniques for methanol fueled spark ignition engines
[NASA-CR-172847] p 151 N83-33168

MICROANALYSIS
Microstructural analysis of solar cell welds p 172 N83-15833
Evaluation of solar cell welds by scanning acoustic microscopy p 172 N83-15834

MICROCOMPUTERS
BASIC Data Manipulation And Display System (BDMADS)
[NASA-TM-83328] p 189 N83-19496
Design of a high-speed digital processing element for parallel simulation
[NASA-TM-83373] p 117 N83-29597

MICROCRACKS
Method of fabricating an abradable gas path seal
[NASA-CASE-LEW-13269-2] p 93 N83-17714
Laser surface fusion of plasma sprayed ceramic turbine seals
[NASA-CASE-LEW-13269-1] p 50 N83-20996
Relation of cyclic loading pattern to microstructural fracture in creep fatigue
[NASA-TM-83473] p 161 N83-34349

MICROHARDNESS
Microhardness studies on thin carbon films grown on P-type, (100) silicon
[NASA-TM-82980] p 61 N83-13169

MICROPHONES
Investigation of continuously traversing microphone system for mode measurement
[NASA-CR-168040] p 199 N83-19575

MICROPROCESSORS
Design of a microprocessor-based Control, Interface and Monitoring (CIM unit for turbine engine controls research
[NASA-TM-83433] p 2 N83-34885

MICROSCOPY
Investigation of wear phenomena by microscopy
[NASA-TM-82934] p 81 N83-14245

MICROSTRUCTURE
Composites with periodic microstructure p 62 A83-12734
Interrelation of material microstructure, ultrasonic factors, and fracture toughness of a two-phase titanium alloy p 75 A83-23922
The effect of microstructure on the fatigue behavior of Ni base superalloys p 75 A83-36166
Influence of cobalt, tantalum, and tungsten on the microstructure and mechanical properties of superalloy single crystals p 79 N83-11293
Development of Fe-Mn-Al-X-C alloys p 80 N83-11307
Microstructural behavior of interfaces in hot isostatically pressed, dual alloy combinations
[NASA-TM-82698] p 80 N83-11309
Microstructural analysis of solar cell welds p 172 N83-15833
Simplified composite micromechanics equations for hygral, thermal and mechanical properties
[NASA-TM-83320] p 66 N83-19817
Relation of cyclic loading pattern to microstructural fracture in creep fatigue
[NASA-TM-83473] p 161 N83-34349

Tensile and compressive constitutive response of 316 stainless steel at elevated temperatures
p 162 N83-34353

MICROWAVE AMPLIFIERS
A 1 watt GaAs power amplifier for the NASA 30/20 GHz communication system p 111 A83-11489
High-performance K-band GaAs power field-effect transistors prepared by molecular beam epitaxy
p 112 A83-33846

MICROWAVE ANTENNAS
A multiple beam antenna concept for a 30/20 GHz satellite communications system p 103 A83-11485
Advanced 30/20 GHz multiple beam antenna for future communications satellites p 104 A83-41367
Near-field measurement facility plans at Lewis Research Center p 46 N83-26897

MICROWAVE CIRCUITS
A two-stage monolithic buffer amplifier for 20 GHz satellite communication p 112 A83-39272
Image-optimized, frequency-scalable mixers for millimeter-wave applications p 112 A83-39273

MICROWAVE COUPLING
Measurements of energy distribution and thrust for microwave plasma coupling of electrical energy to hydrogen for propulsion
[AIAA PAPER 82-1951] p 52 A83-12508
Performance characteristics of a microwave plasma disk ion source --- time varying electric propulsion concept
[AIAA PAPER 82-1935] p 55 A83-27350

MICROWAVE EQUIPMENT
Advanced 3-V semiconductor technology assessment
[NASA-CR-168101] p 206 N83-21987
Advanced 3-V semiconductor technology assessment --- space communications
[NASA-CR-168102] p 207 N83-21988

MICROWAVE FREQUENCIES
Application of MMIC modules in future multiple beam satellite antenna systems
[NASA-TM-83344] p 48 N83-22313

MICROWAVE SWITCHING
Development of a microwave 20 x 20 switch matrix for 30/20 GHz SS-TDMA application p 110 A83-11484
A high capacity satellite switched TDMA microwave switch matrix p 104 A83-19776
20 x 20 IF switch matrix for SS-TDMA systems
p 113 A83-41369
Spacecraft IF switch matrix for wideband service applications in 30/20 GHz communications satellite systems: Proof-of-concept model, executive summary
[NASA-CR-168175] p 107 N83-29492
Spacecraft in switch matrix for wide band service applicatons in 30/20 GHz communications satellite systems
[NASA-CR-168089] p 46 N83-34998

MICROWAVE TRANSMISSION
A low-power, high-throughput maximum-likelihood convolutional decoder chip for NASA's 30/20 GHz program p 111 A83-19754
Future satellite systems - Market demand assessment
p 104 A83-19762
A high capacity satellite switched TDMA microwave switch matrix p 104 A83-19776
A network control concept for the 30/20 GHz communication system baseband processor
p 47 A83-41389
Onboard processing for a 30/20 GHz communications satellite p 47 A83-41391

MICROWAVE TUBES
Modern multistage depressed collectors - A review
p 112 A83-24025
Development program on a Spindt cold-cathode electron gun
[NASA-CR-168055] p 115 N83-18997

MICROWAVES
Microwave plasma generation of hydrogen atoms for rocket propulsion p 53 A83-13090
Development and test of a Microwave Ice Accretion Measurement Instrument (MIAMI)
[NASA-CR-3598] p 18 N83-14123

MILITARY TECHNOLOGY
Conservation of strategic metals p 80 N83-12154
Space power tubes - very much alive
[NASA-TM-83425] p 107 N83-28295

MILLIMETER WAVES
Design concepts for a high-impedance narrow-band 42 GHz power TWT using a fundamental/forward ladder-based circuit
[NASA-CR-165282] p 114 N83-12330

MINERAL OILS
Cavitation pitting and erosion of Al 6061-T6 in mineral oil and water
[NASA-TM-83345] p 148 N83-23606
Effect of oxygen concentration in ZDP containing oils on surface composition and wear
[NASA-TM-83000] p 84 N83-24636
Cavitation erosion of copper, brass, aluminum and titanium alloys in mineral oil
[NASA-TM-83402] p 148 N83-24856
Cavitation pitting and erosion of aluminum 6061-T6 in mineral oil water
[NASA-TP-2146] p 152 N83-35400

MINES (EXCAVATIONS)
Assessment of alternative power sources for mobile mining machinery
[NASA-TM-82695] p 169 N83-14691
Energy and precious fuels requirements of fuel alcohol production. Volume 4: Appendices G and H, methanol from coal
[NASA-CR-168093] p 183 N83-28580

MINICOMPUTERS
Vibration in planetary gear systems with unequal planet stiffnesses
[NASA-TM-83428] p 150 N83-29709

MINING
Assessment of alternative power sources for mobile mining machinery
[NASA-TM-82695] p 169 N83-14691

MINORITY CARRIERS
Minority carrier diffusion length measurements - A review and comparison of techniques p 205 A83-28448
Diffusion length measurements in solar cells: An analysis and comparison of techniques
p 171 N83-15812

MIS (SEMICONDUCTORS)
Interfacial electrical properties of ion-beam sputter deposited amorphous carbon on silicon
p 205 A83-33920

MISSION PLANNING
Infrared Astronomical Satellite (IRAS) launch
[NASA-TM-85190] p 45 N83-15330

MIXING CIRCUITS
Image-optimized, frequency-scalable mixers for millimeter-wave applications p 112 A83-39273

MIXING LENGTH FLOW THEORY
A mixing-length model for the prediction of convex curvature effects on turbulent boundary layers --- for turbine blade convective heat transfer prediction
[ASME PAPER 83-GT-80] p 125 A83-47933
Three-dimensional turbulent-mixing-length modeling for discrete-hole coolant injection into a crossflow
[NASA-TP-2200] p 132 N83-34232

MIXTURES
Tests of blending and correlation of distillate fuel properties p 98 A83-11050
Effects of percentage of blockage and flameholder downstream counterbores on lean combustion limits of premixed, prevaporized propane-air mixture
[NASA-TP-2227] p 41 N83-34941

MOBILE COMMUNICATION SYSTEMS
Requirements for a mobile communications satellite system. Volume 2: Technical report
[NASA-CR-168129] p 107 N83-23498
Non-urban mobile radio market demand forecast
[NASA-CR-168065] p 107 N83-28297

MOBILITY
Satellite-aided land mobile communications system implementation considerations p 104 A83-41417
Assessment of alternative power sources for mobile mining machinery
[NASA-TM-82695] p 169 N83-14691

MODAL RESPONSE
Acoustic modal analysis of a full-scale annular combustor
[AIAA PAPER 83-0760] p 196 A83-33486
Acoustic modal analysis of a full-scale annular combustor
[NASA-TM-83334] p 200 N83-21896

MODEMS
Advances in Serial MSK modems p 111 A83-19789

MODULATORS
Modulation techniques
[NASA-CR-169460] p 105 N83-10329

MODULES
Photovoltaic stand-alone modular systems, phase 2
[NASA-CR-168230] p 186 N83-35497

MODULUS OF ELASTICITY
On composites with periodic structure
p 154 A83-10283
Composites with periodic microstructure
p 62 A83-12734
Elastohydrodynamic lubrication of elliptical contacts
p 141 N83-15514
Traction behavior of two traction lubricants
[NASA-TM-83311] p 144 N83-20116
Compliance and stress sensitivity of spur gear teeth
p 146 N83-20142
Evaluation of low-cost aluminum composites for aircraft engine structural applications
[NASA-TM-83357] p 66 N83-25790
Spherical micro-glass particle impingement studies of thermoplastic materials at normal incidence
[NASA-TM-83410] p 94 N83-25883
Elastohydrodynamics of elliptical contacts for materials of low elastic modulus
[NASA-TM-81699] p 151 N83-29712

MOISTURE
Compression and compression fatigue testing of composite laminates
[NASA-CR-168023] p 66 N83-26928

MOISTURE CONTENT
Experimental comparison of icing cloud instruments
[AIAA PAPER 83-0026] p 16 A83-42099
Water vapor measurement system in global atmospheric sampling program, appendix
[NASA-TP-2051] p 187 N83-13643
Comparison of modern icing cloud instruments
[NASA-CR-168008] p 19 N83-18720
Experimental comparison of icing cloud instruments
[NASA-TM-83340] p 17 N83-24487

MOISTURE RESISTANCE
Synthesis and characterization of bisimide amines and bisimide amine-cured epoxy resins p 88 A83-11486
Synthesis and characterization of bisimide amines and bisimide amine-cured epoxy resins p 90 A83-40924
Imide modified epoxy matrix resins
[NASA-CR-167942] p 93 N83-18909

MOLECULAR BEAM EPITAXY
High-performance K-band GaAs power field-effect transistors prepared by molecular beam epitaxy
p 112 A83-33846

MOLECULAR CHAINS
Shock tube measurements of growth constants in the branched chain formaldehyde-carbon monoxide-oxygen system
[NASA-TM-82954] p 71 N83-12182

MOLECULAR ORBITALS
Molecular-orbital model for metal-sapphire interfacial strength p 67 A83-10612

MOLECULAR OSCILLATIONS
Effect of hydrogen bonding on the vibrational dephasing time in glycerol p 61 A83-21054

MOLECULAR SPECTROSCOPY
Effect of hydrogen bonding on the vibrational dephasing time in glycerol p 61 A83-21054

MOLECULAR WEIGHT
Effect of sliding speed and contact stress on tribological properties of ultra-high-molecular-weight polyethylene
[NASA-TP-2059] p 91 N83-14269

MOLYBDENUM SULFIDES
Morphological and frictional behavior of sputtered MoS2 films p 88 A83-12652

MOMENTUM
End wall flow characteristics and overall performance of an axial flow compressor stage
[NASA-CR-3671] p 13 N83-26819

MOMENTUM TRANSFER
The finite analytic method, volume 5
[NASA-CR-170188] p 191 N83-23089

MONITORS
The DOE/NASA wind turbine data acquisition system. Part 3: Unattended power performance monitor
[NASA-CR-165540] p 44 N83-24516

MONOMERS
Chemical approach for controlling nadamide cure temperature and rate
[NASA-CASE-LEW-13770-1] p 91 N83-13258
PMR polyimide composites for aerospace applications
[NASA-TM-83047] p 65 N83-15304
Improved high temperature resistant polyimides
[NASA-CASE-LEW-13864-1] p 93 N83-17715

MORPHOLOGY
Morphological and frictional behavior of sputtered MoS2 films p 88 A83-12652
Morphology of ductile metals eroded by a jet of spherical particles impinging at normal incidence
p 75 A83-32624
Frictional and morphological characteristics of ion plated soft, metallic films
[NASA-TM-81723] p 83 N83-22390
Time effect of erosion by solid particle impingement on ductile materials
[NASA-TM-83369] p 84 N83-24637
Morphology of an aluminum alloy eroded by a jet of angular particles impinging at normal incidence
[NASA-TP-2139] p 85 N83-24641

MULTIBEAM ANTENNAS
A multiple beam antenna concept for a 30/20 GHz satellite communications system p 103 A83-11485
Techniques for low sidelobe, high efficiency offset dual reflector antennas p 104 A83-21072
Packet communication system for a multi-beam beam switched satellite repeater p 104 A83-41336
Advanced 30/20 GHz multiple beam antenna for future communications satellites p 104 A83-41367

Concept for advanced satellite communications and required technologies
[NASA-TM-82984] p 47 N83-11210
Advanced 30/20 GHz multiple-beam antennas for communications satellites
[NASA-TM-82952] p 50 N83-13154
Planning assistance for the 30/20 GHz program, volume 2
[NASA-CR-165484-VOL-2] p 108 N83-33011
Planning assistance for the 30/20 GHz program, volume 3
[NASA-CR-165484] p 108 N83-33012

MULTICHANNEL COMMUNICATION
Comparison of channel assignment techniques for hybrid switching p 104 A83-41363

MULTIPLE BEAM INTERVAL SCANNERS
Application of MMIC modules in future multiple beam satellite antenna systems
[NASA-TM-83344] p 48 N83-22313
Requirements for a mobile communications satellite system. Volume 2: Technical report
[NASA-CR-168129] p 107 N83-23498
Phased array-fed antenna configuration study
[NASA-CR-168077] p 107 N83-27086
NASA's Advanced Communications Technology Satellite (ACTS)
[NASA-TM-83416] p 48 N83-35004

MULTIPOLES
Electric thruster research
[NASA-CR-168134] p 59 N83-32843

N

N-TYPE SEMICONDUCTORS
Advances in large-diameter liquid encapsulated Czochralski GaAs p 171 N83-15819

NACELLES
Prediction of high speed propeller flow fields using a three-dimensional Euler analysis
[AIAA PAPER 83-0188] p 4 A83-29535
Wind tunnel tests of a zero length, slotted-lip engine air inlet for a fixed nacelle V/STOL aircraft
[NASA-TM-82939] p 9 N83-10019
Utilizing numerical techniques in turbofan inlet acoustic suppressor design
[NASA-TM-82994] p 196 N83-10885
Prediction of high speed propeller flow fields using a three-dimensional Euler analysis
[NASA-TM-83065] p 12 N83-19710
Nacelle Aerodynamic and Inertial Loads (NAIL) project
[NASA-CR-168712] p 18 N83-30402

NAPHTHALENE
Evaluation of ultraviolet spectrophotometry for simultaneous analysis of alkylbenzenes, alkylnaphthalenes, alkylanthracenes/phenanthrenes and total aromatics in mid-distillate fuels
[NASA-TM-83032] p 99 N83-15483

NASA PROGRAMS
NASA Lewis Research Center's program on icing research
[AIAA PAPER 83-0204] p 1 A83-16582
NASA clean catalytic combustor program
[ASME PAPER 82-JPGC-GT-11] p 68 A83-25269
Concept for advanced satellite communications and required technologies
[NASA-TM-82984] p 47 N83-11210
NASA Lewis Research Center's Program on Icing Research
[NASA-TM-83031] p 16 N83-14078
The NASA Redox Storage System Development project, 1980
[NASA-TM-82940] p 169 N83-14683
NASA helicopter transmission system technology program p 144 N83-20120
An overview of general aviation propulsion research programs at NASA Lewis Research Center p 35 N83-22456

NASTRAN
Large displacements and stability analysis of nonlinear propeller structures p 159 N83-12460

NAVIER-STOKES EQUATION
Finite analytic numerical solution of axisymmetric Navier-Stokes and energy equations
[ASME PAPER 82-HT-42] p 118 A83-12795
Multi-grid solution of Neumann pressure problem for viscous flows using primitive variables
[AIAA PAPER 83-0557] p 120 A83-16786
Numerical solution of the Navier-Stokes equations for compressible turbulent two/three dimensional flows in the terminal shock region of an inlet/diffuser
[AIAA PAPER 83-1892] p 5 A83-39358
Efficient solution of the Euler and Navier-Stokes equations with a vectorized multiple-grid algorithm
[AIAA PAPER 83-1693] p 5 A83-39359
Study of asymptotic incompressible flow in curved ducts using a multi-grid technique p 123 A83-42532
Turbulent solution of the Navier-Stokes equations for an inhomogenous developing shear layer
[NASA-TM-82969] p 126 N83-12357
Convergence acceleration of viscous flow computations
[NASA-TM-83039] p 190 N83-12930
Analytical calculation of a single jet in crossflow and comparison with experiment
[NASA-TM-83027] p 29 N83-14127
The finite analytic method, volume 3
[NASA-CR-170186] p 191 N83-23087
The finite analytic method, volume 4
[NASA-CR-170187] p 191 N83-23088
Efficient solution of the Euler and Navier-Stokes equations with a vectorized multiple-grid algorithm
[NASA-TM-83376] p 2 N83-24467
Applications of the contravariant form of the Navier-Stokes equations
[NASA-TM-83448] p 14 N83-29179

NEAR FIELDS
Computer program to predict noise of general aviation aircraft: User's guide
[NASA-CR-168050] p 198 N83-17242
Near-field measurement facility plans at Lewis Research Center p 46 N83-26897

NEAR INFRARED RADIATION
Long-range surface plasmons in electrode structures p 202 A83-40733

NETWORK ANALYSIS
An improved switching converter model using discrete and average techniques p 111 A83-11495
Image-optimized, frequency-scalable mixers for millimeter-wave applications p 112 A83-39273
Next generation communications satellites: multiple access and network studies
[NASA-CR-167903] p 45 N83-12129

NETWORK CONTROL
A network control concept for the 30/20 GHz communication system baseband processor p 47 A83-41389
Planning assistance for the NASA 30/20 GHz program. Network control architecture study.
[NASA-CR-168058] p 106 N83-21207

NETWORK SYNTHESIS
Nonlinear program based optimization of boost and buck-boost converter designs p 110 A83-11016
Development of a microwave 20 x 20 switch matrix for 30/20 GHz SS-TDMA application p 110 A83-11484
Image-optimized, frequency-scalable mixers for millimeter-wave applications p 112 A83-39273

NEUMANN PROBLEM
Multi-grid solution of Neumann pressure problem for viscous flows using primitive variables
[AIAA PAPER 83-0557] p 120 A83-16786

NEUTRAL PARTICLES
Mass analysis of neutral particles and ions released during electrical breakdowns on spacecraft surfaces
[NASA-CR-170299] p 50 N83-23347

NEUTRALIZERS
Simplification of power electronics for ion thruster neutralizers
[AIAA PAPER 82-1880] p 53 A83-21099
Simplification of power electronics for ion thruster neutralizers
[NASA-TM-83004] p 56 N83-12141

NEWTON-RAPHSON METHOD
Formal convergence characteristics of elliptically constrained incremental Newton-Raphson algorithms p 190 A83-10273
On the solution of elastic-plastic static and dynamic postbuckling collapse of general structure p 155 A83-12746

NEWTONIAN FLUIDS
A detailed treatment of two-dimensional, starved lubrication in the vicinity of two counter-rotating cylinders p 141 N83-15520

NICKEL
Friction and wear of iron and nickel in sodium hydroxide solutions p 77 A83-48922
Friction and wear of iron and nickel in sodium hydroxide solutions
[NASA-TM-82935] p 77 N83-10171
Orientation dependence of the stress rupture properties of Nickel-base superalloy single crystals
[NASA-CR-165394] p 206 N83-13009
Surface chemistry, friction and wear of Ni-Zn and Mn-Zn ferrites in contact with metals
[NASA-TM-83068] p 93 N83-19901
X-ray photoelectron spectroscopy and friction studies of nickel-zinc and manganese-zinc ferrites in contact with metals
[NASA-TP-2163] p 84 N83-23419
Determination of hydrogen permeability in commercial and modified superalloys
[NASA-CR-168195] p 87 N83-35101

NICKEL ALLOYS
O-18 tracer studies of Al2O3 scale formation on NiCrAl alloys p 74 A83-10249
Requirements of constitutive models for two nickel-base superalloys p 74 A83-21071
Metallurgical instabilities during the high temperature low cycle fatigue of nickel-base superalloys p 75 A83-22019
A brittle to ductile transition in NiAl of a critical grain size p 75 A83-29726
The effect of microstructure on the fatigue behavior of Ni base superalloys p 75 A83-36166
Fatigue crack initiation and propagation in several nickel-base superalloys at 650 C p 76 A83-41199
The oxidation behavior of a model molybdenum/tungsten-containing alloy in air alone and in air with trace levels of NaCl(g) p 76 A83-42241
Effect of swaging on the 1000 C compressive slow plastic flow characteristics of the directionally solidified eutectic alloy gamma/gamma prime-alpha p 77 A83-44340
Interfacial layers in high-temperature-oxidized NiCrAl p 77 A83-44619
Gamma prime shape changes during creep of a nickel-base superalloy p 77 A83-47855
COSAM (Conservation Of Strategic Aerospace Materials) program overview
[NASA-TM-83006] p 78 N83-11282
Superalloy composition modeling p 78 N83-11284
Role of cobalt in nickel base superalloys p 78 N83-11286
Low-cobalt single crystal Rene 150 p 78 N83-11288
Creep-fatigue of low cobalt superalloys p 79 N83-11290
Dual alloy interface stability p 79 N83-11297
Intermetallics as alternative materials p 80 N83-11300
Microstructural behavior of interfaces in hot isostatically pressed, dual alloy combinations
[NASA-TM-82698] p 80 N83-11309
Mechanism of hot corrosion of IN-738
[NASA-CR-169706] p 81 N83-15411
Binary nickel alloy phase diagrams compilation and critical evaluation
[NASA-CR-170016] p 82 N83-19885
Improved nickel base coating alloy --- oxidation resistant coatings
[NASA-CASE-LEW-13834-1] p 85 N83-24639
Relation of cyclic loading pattern to microstructural fracture in creep fatigue
[NASA-TM-83473] p 161 N83-34349
Understanding the roles of the strategic element cobalt in nickel base superalloys
[NASA-TM-83475] p 87 N83-35102

NICKEL CADMIUM BATTERIES
Development of improved hydrogen recombination in sealed nickel-cadmium aerospace cells p 54 A83-27198
Deep discharge reconditioning and shorted storage of batteries --- nickel cadmium batteries
[NASA-CR-167953] p 166 N83-10502
Development of a high capacity toroidal Ni/Cd cell
[NASA-CR-169945] p 176 N83-19273

NICKEL HYDROGEN BATTERIES
Pore size engineering applied to starved electrochemical cells and batteries p 164 A83-27201
Design of a 35-kilowatt bipolar nickel-hydrogen battery for low-earth-orbit applications p 54 A83-27205
Pore size engineering applied to starved electrochemical cells and batteries
[NASA-TM-82893] p 70 N83-10134
Electrolyte management in porous battery components. Static measurements
[NASA-TM-83073] p 72 N83-18862
Pore size engineering applied to the design of separators for nickel-hydrogen cells and batteries
[NASA-TM-83386] p 73 N83-24571
Cycle life test and failure model of nickel-hydrogen cells
[NASA-TM-83375] p 180 N83-25038
Test results of a ten cell bipolar nickel-hydrogen battery
[NASA-TM-83384] p 181 N83-26253
Test methods and results of the 10-cell bipolar Ni-H2 battery p 117 N83-35261
Nickel-hydrogen component development
[NASA-TM-83487] p 186 N83-35498

NICKEL OXIDES
Polyvinyl alcohol membranes as alkaline battery separators
[NASA-TM-82961] p 70 N83-10135

NIOBIUM
COSAM (Conservation Of Strategic Aerospace Materials) program overview
[NASA-TM-83006] p 78 N83-11282
COSAM program overview p 78 N83-11283
Conservation of strategic metals p 80 N83-12154
NIOBIUM ALLOYS
Effects on stress rupture life and tensile strength of tin additions to Inconel 718 p 79 N83-11299
NITRATES
Aircraft sampling of the sulfate layer near the tropopause following the eruption of Mount St. Helens p 187 N83-11556
NITRIDES
Some properties of r.f.-sputtered hafnium nitride coatings p 88 A83-12653
NITRIDING
The effect of silicon particle size on the nitriding behaviour of reaction bonded Si3N4 compacts p 90 A83-48261
Tribological and microstructural characteristics of ion-nitrided steels
[NASA-TM-83368] p 84 N83-24635
Nitriding of titanium and titanium: 8 percent aluminum, 1 percent molybdenum, 1 percent vanadium alloy with an ion-beam source
[NASA-TP-2149] p 85 N83-24640
NITROGEN
Studies of flows through N-sequential orifices
[NASA-TM-83313] p 129 N83-19020
Nitriding of titanium and titanium: 8 percent aluminum, 1 percent molybdenum, 1 percent vanadium alloy with an ion-beam source
[NASA-TP-2149] p 85 N83-24640
Electrothermal thruster diagnostics. Volume 2: Technical
[NASA-CR-168174-VOL-2] p 60 N83-33943
NITROGEN OXIDES
NOx results from two combustors tested on medium BTU coal gas p 186 A83-11493
Droplet size effects on NO/x/ formation in a one-dimensional monodisperse spray combustion system
[ASME PAPER 82-JPGC-GT-10] p 68 A83-25268
Evaluation of advanced combustion concepts for dry NO sub x suppression with coal-derived, gaseous fuels
[NASA-TM-82985] p 166 N83-10557
Multifuel evaluation of rich/quench/lean combustor
[NASA-TM-82986] p 167 N83-10559
Investigation of a low NOx full-scale annular combustor
[NASA-CR-165518] p 29 N83-13104
An analytical investigation of NO sub x control techniques for methanol fueled spark ignition engines
[NASA-CR-172847] p 151 N83-33168
NOISE GENERATORS
Rotor wake characteristics relevant to rotor-stator interaction noise generation p 19 A83-10184
Recent results about fan noise: Its generation, radiation and suppression
[NASA-TM-83002] p 197 N83-13939
Turbofan noise generation. Volume 1: Analysis
[NASA-CR-167951] p 198 N83-15041
NOISE MEASUREMENT
An experimental study of supersonic jet shock-associated noise
[AIAA PAPER 83-0708] p 193 A83-25924
Farfield inflight measurements of high-speed turboprop noise
[AIAA PAPER 83-0745] p 21 A83-25947
Noise of the 10-bladed, 40 deg swept SR-6 propeller in a wind tunnel
[NASA-TM-82950] p 196 N83-11840
Correlation of core noise obtained by three signal coherence techniques
[NASA-TM-83012] p 197 N83-12966
Experiments on identification and control of inflow disturbances in contracting streams
[NASA-CR-169831] p 11 N83-17503
Noise of the 10-bladed 60 deg swept SR-5 propeller in a wind tunnel
[NASA-TM-83054] p 200 N83-23112
NOISE PREDICTION
On the shock cell structure and noise of supersonic jets
[AIAA PAPER 83-0703] p 193 A83-25923
NOISE PREDICTION (AIRCRAFT)
Rotor wake characteristics relevant to rotor-stator interaction noise generation p 19 A83-10184
An iterative method for predicting turbofan inlet acoustics p 192 A83-13135
Conventional profile coaxial jet noise prediction p 193 A83-22128
A theoretical investigation of the sound radiation fields associated with a Bellmouth inlet
[AIAA PAPER 83-0710] p 193 A83-25926
Comparison of measured and predicted flight effects on high-bypass coaxial jet exhaust noise
[AIAA PAPER 83-0749] p 194 A83-26450
Coaxial supersonic jet-flows, shock structure and related problems with noise-suppression assessment and prediction
[AIAA PAPER 83-0707] p 194 A83-28011
Application of 3-signal coherence to core noise transmission
[AIAA PAPER 83-0759] p 194 A83-28021
Incidence angle effects on convected gust airfoil noise
[AIAA PAPER 83-0765] p 195 A83-28022
Computer program to predict noise of general aviation aircraft: User's guide
[NASA-CR-168050] p 198 N83-17242
Comparison of measured and predicted flight effects on high-bypass coaxial jet exhaust noise
[NASA-TM-83347] p 200 N83-23115
JT150 1/2-scale nozzle jet noise experiment and comparison with prediction
[NASA-TM-83370] p 201 N83-27793
NOISE PROPAGATION
Generation of desired signals from acoustic drivers --- for aircraft engine internal noise propagation experiment p 19 A83-15068
Application of 3-signal coherence to core noise transmission
[NASA-TM-83333] p 200 N83-23114
NOISE REDUCTION
Tests of a thermal acoustic shield with a supersonic jet p 192 A83-10183
Design of an advanced 500-HP helicopter transmission p 21 A83-24834
Coaxial supersonic jet-flows, shock structure and related problems with noise-suppression assessment and prediction
[AIAA PAPER 83-0707] p 194 A83-28011
Noise generation by a finite span swept airfoil
[AIAA PAPER 83-0768] p 195 A83-28023
Recent results about fan noise: Its generation, radiation and suppression
[NASA-TM-83002] p 197 N83-13939
Experiments on identification and control of inflow disturbances in contracting streams
[NASA CR-169831] p 11 N83-17503
NOISE SPECTRA
Cross spectra between temperature and pressure in a constant area duct downstream of a combustor
[AIAA PAPER 83-0762] p 196 A83-33487
Correlation of core noise obtained by three signal coherence techniques
[NASA-TM-83012] p 197 N83-12966
Analysis of combustion spectra containing organ pipe tone by cepstral techniques
[NASA-TM-83034] p 198 N83-16153
Cross spectra between temperature and pressure in a constant area duct downstream of a combustor
[NASA-TM-83351] p 200 N83-23116
Turbulence spectra in the noise source regions of the flow around complex surfaces
[NASA-TM-83392] p 202 N83-30168
Experimental study of the thermal-acoustic efficiency in a long turbulent diffusion-flame burner
[NASA-CR-3725] p 202 N83-33683
NOISE TEMPERATURE
Cross spectra between temperature and pressure in a constant area duct downstream of a combustor
[AIAA PAPER 83-0762] p 196 A83-33487
Cross spectra between temperature and pressure in a constant area duct downstream of a combustor
[NASA-TM-83351] p 200 N83-23116
NONDESTRUCTIVE TESTS
Comparison of NDE techniques for sintered-SiC components p 152 A83-22265
Mechanics aspects of NDE by sound and ultrasound p 152 A83-25571
The determination of the elastodynamic fields of an ellipsoidal inhomogeneity
[ASME PAPER 83-APM-19] p 157 A83-37388
Phenomenological and mechanics aspects of nondestructive evaluation and characterization by sound and ultrasound of material and fracture properties
[NASA-CR-3623] p 153 N83-11506
Fundamental aspects in quantitative ultrasonic determination of fracture toughness: The scattering of a single ellipsoidal inhomogeneity
[NASA-CR-3625] p 153 N83-11507
Research priorities for advanced fibrous composites
[NASA-CR-165414] p 65 N83-18853
Effects of specimen resonances on acoustic-ultrasonic testing
[NASA-CR-3679] p 153 N83-21373
Ultrasonic ranking of toughness of tungsten carbide
[NASA-TM-83358] p 153 N83-23620
NONISOTHERMAL PROCESSES
Small particle transport across turbulent nonisothermal boundary layers p 118 A83-10650
NONLINEAR EQUATIONS
Pseudo-updated constrained solution algorithm for nonlinear heat conduction p 121 A83-32989
NONLINEAR PROGRAMMING
Nonlinear program based optimization of boost and buck-boost converter designs p 110 A83-11016
Computer simulations of optimum boost and buck-boost converters p 111 A83-19032
NONLINEAR SYSTEMS
Nonlinear structural and life analyses of a combustor liner p 155 A83-12764
Nonlinear multivariable design by total synthesis --- of gas turbine engine control systems p 24 A83-37092
Controller scheduling - A possible algebraic viewpoint p 190 A83-37093
Large displacements and stability analysis of nonlinear propeller structures p 159 N83-12460
NONLINEARITY
Geometrically nonlinear analysis of layered composite plates and shells
[NASA-CR-168182] p 161 N83-33219
A solution procedure for behavior of thick plates on a nonlinear foundation and postbuckling behavior of long plates
[NASA-TP-2174] p 163 N83-34373
NONNEWTONIAN FLUIDS
Non-Newtonian fluid model incorporated into elastohydrodynamic lubrication of rectangular contacts
[NASA-TM-83318] p 150 N83-28454
NONSTABILIZED OSCILLATION
Solution to the backward-Kolmogorov equation for a nonstationary oscillation problem p 192 A83-15687
NONUNIFORMITY
Rainbow Schlieren
[NASA-TP-2166] p 135 N83-33126
NOTCH SENSITIVITY
Experimental verification of the Neuber relation at room and elevated temperatures --- to predict stress-strain behavior in notched specimens of hastelloy x
[NASA-CR-167967] p 159 N83-19121
NOZZLE DESIGN
Development and operating characteristics of an advanced two-stage combustor p 24 A83-38022
The 'whistler-nozzle' phenomenon p 125 A83-49472
The whistler nozzle phenomenon
[NASA-CR-170015] p 199 N83-20706
NOZZLE EFFICIENCY
The 'whistler-nozzle' phenomenon p 125 A83-49472
The whistler nozzle phenomenon
[NASA-CR-170015] p 199 N83-20706
NOZZLE FLOW
An experimental study of supersonic jet shock-associated noise
[AIAA PAPER 83-0708] p 193 A83-25924
Three-dimensional compressible viscous analysis of mixer nozzles
[AIAA PAPER 83-1401] p 4 A83-36391
Three dimensional flow computations in a turbine scroll
[NASA-CR-168003] p 10 N83-12045
NOZZLE GEOMETRY
The 'whistler-nozzle' phenomenon p 125 A83-49472
Experiments on high bypass internal mixer nozzle jet noise
[NASA-TM-83020] p 198 N83-16152
The whistler nozzle phenomenon
[NASA-CR-170015] p 199 N83-20706
Parametric study of flame radiation characteristics of a tubular-can combustor
[NASA-TM-83436] p 39 N83-29237
NOZZLE THRUST COEFFICIENTS
Experimental results of a deflected thrust V/STOL nozzle research program
[AIAA PAPER 83-0170] p 6 A83-42100
Experimental results of a deflected thrust V/STOL nozzle research program
[NASA-TM-83069] p 12 N83-25657
NUCLEAR BINDING ENERGY
Diatomic molecules and metallic adhesion, cohesion, and chemisorption - A single binding-energy relation p 69 A83-30921
NUCLEAR FUEL ELEMENTS
Overview of high-temperature materials for high-energy space power systems p 173 N83-15869
NUCLEAR FUELS
Overview of high-temperature materials for high-energy space power systems p 173 N83-15869

NUCLEAR REACTORS
High thermal power density heat transfer apparatus providing electrical isolation at high temperature using heat pipes
[NASA-CASE-LEW-12950-2] p 183 N83-29304
NUMERICAL ANALYSIS
Finite analytic numerical solution of heat transfer and flow past a square channel cavity p 123 A83-42703
Turbofan noise generation. Volume 1: Analysis
[NASA-CR-167951] p 198 N83-15041
The finite analytic method, volume 3
[NASA-CR-170186] p 191 N83-23087
The finite analytic method, volume 4
[NASA-CR-170187] p 191 N83-23088
The finite analytic method, volume 5
[NASA-CR-170188] p 191 N83-23089
Small gas turbine combustor primary zone study
[NASA-CR-168122] p 149 N83-28448
Flux-based acceleration of the Euler equations
[NASA-TM-83453] p 191 N83-30113
NUMERICAL CONTROL
Coordinate generation with precise controls over mesh properties p 190 A83-29631
High level continuity for coordinate generation with precise controls p 190 A83-29632
Army/NASA small turboshaft engine digital controls research program
[NASA-TM-82979] p 27 N83-11128
NUMERICAL FLOW VISUALIZATION
Numerical studies of the formation and destruction of vortices in a motored four-stroke piston-cylinder configuration
[AIAA PAPER 83-0497] p 136 A83-16749
NUMERICAL INTEGRATION
Fast Euler solver for steady, 1-dimensional flows
[NASA-CR-3689] p 14 N83-27960
NUMERICAL STABILITY
Formal convergence characteristics of elliptically constrained incremental Newton-Raphson algorithms p 190 A83-10273
Pseudo-updated constrained solution algorithm for nonlinear heat conduction p 121 A83-32989
Convergence and stability properties of minimal polynomial and reduced rank extrapolation algorithms
[NASA-TM-83443] p 191 N83-31390

O

O RING SEALS
Finite-length solutions for rotodynamic coefficients of turbulent annular seals
[ASME PAPER 82-LUB-42] p 136 A83-13521
Thermoelastohydrodynamic analysis of an oil pumping ring seal p 137 A83-22322
Design analysis of a self-acting spiral-groove ring seal for counter-rotating shafts --- o ring seals
[AIAA PAPER 83-1134] p 137 A83-36239
Design analysis of a self-acting spiral-groove ring seal for counter-rotating shafts --- o ring seals
[NASA-TM-83346] p 35 N83-23306
OBLIQUE SHOCK WAVES
Numerical solution to the glancing sidewall oblique shock wave/turbulent boundary layer interaction in three-dimension
[AIAA PAPER 83-0136] p 3 A83-16823
Experimental investigation of a two-dimensional shock-turbulent boundary layer interaction with bleed
[AIAA PAPER 83-0135] p 3 A83-19581
Numerical solution to the glancing sidewall oblique shock wave/turbulent boundary layer interaction in three dimension
[NASA-TM-83056] p 34 N83-22199
Experimental investigation of a two-dimensional shock-turbulent boundary layer interaction with bleed
[NASA-TM-83057] p 34 N83-22200
OH-58 HELICOPTER
Lubricant effects on efficiency of a helicopter transmission p 141 N83-15523
ONBOARD DATA PROCESSING
A network control concept for the 30/20 GHz communication system baseband processor p 47 A83-41389
OPEN CIRCUIT VOLTAGE
Planar multijunction high voltage solar cell chip p 163 A83-13923
Limitations on solar cell open-circuit voltage and efficiency p 165 A83-37790
OPERATING TEMPERATURE
Solar cell having improved back surface reflector
[NASA-CASE-LEW-13620-1] p 168 N83-13579
Experimental study of the thermal stability of hydrocarbon fuels
[NASA-CR-168027] p 100 N83-17726
OPTICAL DATA PROCESSING
Frequency-multiplexed and pipelined iterative optical systolic array processors p 188 A83-18588
Electro-optical processor for optimal control p 133 A83-23596
Triangular system solutions on an optical systolic processor p 189 A83-36752
LU and Cholesky decomposition on an optical systolic array processor p 189 A83-43629
Optical systolic array processor using residue arithmetic p 189 A83-46834
OPTICAL EQUIPMENT
Precision optical angular position marker system for rotating machinery
[NASA-TM-83062] p 144 N83-20117
OPTICAL MEASURING INSTRUMENTS
Fiber optics for aircraft engine/inlet control p 20 A83-22494
Analysis, design, fabrication and testing of an optical tip clearance sensor --- turbocompressor blade tips
[NASA-CR-165265] p 26 N83-11127
OPTICAL PROPERTIES
Measurements of self-excited rotor-blade vibrations using optical dispacements
[NASA-TM-82953] p 159 N83-14523
OPTICAL PUMPING
A proposed optical pumping system requiring no electric power p 203 N83-15861
OPTIMAL CONTROL
Electro-optical processor for optimal control p 133 A83-23596
Control design for a wind turbine-generator using output feedback p 164 A83-24721
OPTIMIZATION
Optimization of acoustic liners by the hybrid finite element-integral approach
[AIAA PAPER 83-0670] p 194 A83-26917
Structural tailoring of engine blades (STAEBL)
[AIAA 83-0828] p 22 A83-29737
Computer program to minimize prediction error in models from experiments with 16 hypercube points and 0 to 6 center points
[NASA-TM-82995] p 192 N83-21872
Optimization and fabrication of porous carbon electrodes for Fe/Cr redox flow cells
[NASA-CR-167931] p 179 N83-23708
ORBIT SPECTRUM UTILIZATION
Engineering calculations for communications systems planning
[NASA-CR-170182] p 106 N83-22494
ORBIT TRANSFER VEHICLES
Advanced LOX/H2 engine technologies for future OTVs
[AIAA PAPER 83-1312] p 55 A83-36333
Advanced propulsion concepts for orbital transfer vehicles
[AIAA PAPER 83-1243] p 56 A83-45513
Advanced propulsion concepts for orbital transfer vehicles
[NASA-TM-83419] p 59 N83-26924
Advanced LOX/H sub 2 engine technologies for future OTVs p 60 N83-35013
ORBITAL SPACE STATIONS
Propulsion and fluid management - Station keeping will eat energy on a new scale p 54 A83-24360
ORGANIC PHOSPHORUS COMPOUNDS
On the mechanism of lubrication by tricresylphosphate /TCP/ - The coefficient of friction as a function of temperature for TCP on M-50 steel
[ASLE PREPRINT 82-LC-4C-1] p 135 A83-13228
ORGANOMETALLIC COMPOUNDS
Single and multijunction space solar cells grown by organometallic vapor phase epitaxy /OM-VPE/ p 164 A83-27260
Use of column V alkyls in organometallic vapor phase epitaxy (OMVPE) p 70 A83-46608
Progress toward cascade cells made by OM-VPE --- organometallic vapor phase epitaxy p 171 N83-15813
ORIFICE FLOW
Studies of flows through N-sequential orifices
[ASME PAPER 83-FE-22] p 125 A83-48678
Experiments in dilution jet mixing
[NASA-TM-83434] p 15 N83-30393
ORIFICES
Experiments on flow through one to four inlets of the orifice and Borda type p 124 A83-43235
Studies of flows through N-sequential orifices
[NASA-TM-83313] p 129 N83-19020
Experiments in dilution jet mixing
[NASA-TM-83434] p 15 N83-30393
ORTHOGONALITY
The orthogonal in-situ machining of single and polycrystalline aluminum and copper, volume 2
[NASA-CR-169528] p 81 N83-13233
OSCILLATING FLOW
The velocity perturbations above the orifice of an acoustically excited cavity in grazing flow p 195 A83-29235
OSCILLATORS
Dielectric based submillimeter backward wave oscillator circuit
[NASA-CASE-LEW-13736-1] p 115 N83-17802
OXIDATION
Oxidation of low cobalt alloys p 79 N83-11291
Turbine engine materials durability research p 29 N83-12163
Shock tube measurements of growth constants in the branched chain formaldehyde-carbon monoxide-oxygen system
[NASA-TM-82954] p 71 N83-12182
Methods of reducing energy consumption of the oxidant supply system for MHD/steam power plants
[NASA-TM-83025] p 168 N83-13589
Use of high pressure liquid chromatography in the study of liquid lubricant oxidation
[NASA-TM-83033] p 92 N83-14270
Mechanism of hot corrosion of IN-738
[NASA-CR-169706] p 81 N83-15471
Plasma-sprayed self-lubricating coatings
[NASA-CR-3680] p 94 N83-22422
Oxidation and formation of deposit precursors in hydrocarbon fuels
[NASA-CR-168121] p 101 N83-23957
Kinetics of copper ion absorption by cross-linked polyacrylate membranes
[NASA-TM-83052] p 61 N83-25854
NASA interdisciplinary collaboration in tribology. A review of oxidational wear
[NASA-CR-3686] p 95 N83-27021
The chemical behavior of acidified chromium (3) solutions
[NASA-CR-172997] p 74 N83-32871
Effect of the amount of Na2SO4 on the high temperature corrosion of Udimet-700
[NASA-TM-83459] p 87 N83-34016
OXIDATION RESISTANCE
A new diffusion-inhibited oxidation-resistant coating for superalloys p 74 A83-10299
Effect of Y2O3 and Al2O3 on the oxidation resistance of Si3N4 p 86 A83-22258
Cyclic oxidation of superalloys p 75 A83-42234
The oxidation behavior of a model molybdenum/tungsten-containing alloy in air alone and in air with trace levels of NaCl(g) p 76 A83-42241
Improved nickel base coating alloy --- oxidation resistant coatings
[NASA-CASE-LEW-13834-1] p 85 N83-24639
Processing of fused silicide coatings for carbon-based materials
[NASA-TM-83362] p 95 N83-27019
Improved thermal barrier coating system
[NASA-CASE-LEW-13324-2] p 86 N83-34014
OXIDE FILMS
Interfacial layers in high-temperature-oxidized NiCrAl p 77 A83-44619
NASA interdisciplinary collaboration in tribology. A review of oxidational wear
[NASA-CR-3686] p 95 N83-27021
Method of forming oxide coatings --- for solar collector heating panels
[NASA-CASE-LEW-13132-1] p 96 N83-29388
OXIDES
Research into the use of pyrolytic oxides and polymers for the fabrication of thin film high energy capacitors
[NASA-CR-173012] p 97 N83-34045
OXYGEN
The thermal conductivity of oxygen p 207 A83-12094
Shock tube measurements of growth constants in the branched chain formaldehyde-carbon monoxide-oxygen system
[NASA-TM-82954] p 71 N83-12182
Microdistribution of oxygen in silicon and its effects on electronic properties p 172 N83-15825
The detailed chemistry and thermodynamics of sodium in oxygen-rich flames
[NASA-CR-169848] p 72 N83-17626
Effect of oxygen concentration in ZDP containing oils on surface composition and wear
[NASA-TM-83000] p 84 N83-24636
Transport properties of oxygen
[NASA-RP-1102] p 130 N83-24800
OXYGEN SUPPLY EQUIPMENT
Methods of reducing energy consumption of the oxidant supply system for MHD/steam power plants
[AIAA PAPER 83-0468] p 203 A83-16735
OXYGEN 18
O-18 tracer studies of Al2O3 scale formation on NiCrAl alloys p 74 A83-10249

OZONE
Aircraft measurements of trace gases and particles near the tropopause
[NASA-CR-3691] p 188 N83-27542

P

P-I-N JUNCTIONS
High voltage v-groove solar cell
[NASA-CASE-LEW-13401-2] p 185 N83-32177
P-N JUNCTIONS
Diffused P+-N solar cells in bulk GaAs
p 171 N83-15818
P-TYPE SEMICONDUCTORS
Advances in large-diameter liquid encapsulated Czochralski GaAs p 171 N83-15819
PACKET SWITCHING
Packet communication system for a multi-beam beam switched satellite repeater p 104 A83-41336
Comparison of channel assignment techniques for hybrid switching p 104 A83-41363
20 x 20 IF switch matrix for SS-TDMA systems
p 113 A83-41369
A network control concept for the 30/20 GHz communication system baseband processor
p 47 A83-41389
PACKING DENSITY
Injection molding ceramics to high green densities
p 137 A83-33515
PANEL METHOD (FLUID DYNAMICS)
A rapid blade-to-blade solution for use in turbomachinery design
[NASA-TM-83010] p 10 N83-13077
PANELS
Method of forming oxide coatings --- for solar collector heating panels
[NASA-CASE-LEW-13132-1] p 96 N83-29388
PARABOLOID MIRRORS
Large-aperture interferometer using local reference beam
[NASA-TP-2060] p 203 N83-13979
PARALLEL FLOW
Optimum parallel step-sector bearing lubricated with an incompressible fluid
[NASA-TM-83356] p 148 N83-24855
PARALLEL PROCESSING (COMPUTERS)
LU and Cholesky decomposition on an optical systolic array processor p 189 A83-43629
Optical systolic array processor using residue arithmetic p 189 A83-46834
Parallel, Asynchronous Executive (PAX): System concepts, facilities, and architecture
[NASA-TP-2179] p 189 N83-28921
Design of a high-speed digital processing element for parallel simulation
[NASA-TM-83373] p 117 N83-29597
PARALLELEPIPEDS
On the three-dimensional vibrations of the cantilevered rectangular parallelepiped p 157 A83-37729
PARAMETER IDENTIFICATION
Continued development of a detailed model of arc discharge dynamics
[NASA-CR-167977] p 206 N83-16234
Parametric study of potential early commercial MHD power plants. Task 3: Parameter variation of plant size
[NASA-CR-165445] p 182 N83-26259
Experimental investigations of elastohydrodynamic lubrication
[NASA-TM-81698] p 150 N83-29711
PARAMETERIZATION
Parametric study of minimum reactor mass in energy-storage dc-to-dc converters p 110 A83-11011
Controller scheduling - A possible algebraic viewpoint
p 190 A83-37093
PARTIAL DIFFERENTIAL EQUATIONS
The finite analytic method, volume 4
[NASA-CR-170187] p 191 N83-23088
PARTICLE ACCELERATORS
Rail accelerator research at Lewis Research Center
[AIAA PAPER 82-1938] p 53 A83-22075
Rail accelerator research at Lewis Research Center
[NASA-TM-83015] p 56 N83-12143
PARTICLE DENSITY (CONCENTRATION)
Aircraft sampling of the sulfate layer near the tropopause following the eruption of Mount St. Helens
p 187 N83-11556
PARTICLE DIFFUSION
Evaluation of a stochastic model of particle dispersion in a turbulent round jet p 121 A83-28104
PARTICLE LADEN JETS
A study of the surface deterioration due to erosion --- of gas turbine blades
[ASME PAPER 83-GT-213] p 9 A83-48014
Morphology of an aluminum alloy eroded by a jet of angular particles impinging at normal incidence
[NASA-TP-2139] p 85 N83-24641
The structure of evaporating and combusting sprays: Measurements and predictions
[NASA-CR-170312] p 130 N83-24795
PARTICLE MOTION
Small particle transport across turbulent nonisothermal boundary layers p 118 A83-10650
Predictions of the structure of turbulent, particle-laden, round jets
[AIAA PAPER 83-0066] p 119 A83-16498
Correlation and prediction of thermophoretic and inertial effects on particle deposition from non-isothermal turbulent boundary layers p 121 A83-27481
PARTICLE SIZE DISTRIBUTION
Small particle transport across turbulent nonisothermal boundary layers p 118 A83-10650
Influence of multidroplet size distribution on icing collection efficiency
[AIAA PAPER 83-0110] p 187 A83-16526
The effect of silicon particle size on the nitriding behaviour of reaction bonded Si3N4 compacts
p 90 A83-48261
Particle sizing by measurement of forward-scattered light at two angles
[NASA-TP-2156] p 36 N83-24509
Aircraft measurements of trace gases and particles near the tropopause
[NASA-CR-3691] p 188 N83-27542
Fuel spray diagnostics p 38 N83-29212
PARTICLE TRAJECTORIES
A similarity analysis of the droplet trajectory equation
p 118 A83-13133
Solid particle dynamic behavior through twisted blade rows p 3 A83-27478
Aircraft sampling of the sulfate layer near the tropopause following the eruption of Mount St. Helens
p 187 N83-11556
PARTICLES
Wear particle analysis using the ferrograph
[NASA-TM-83422] p 96 N83-28243
PARTICULATE SAMPLING
Particle-sampling statistics in laser anemometers Sample-and-hold systems and saturable systems
p 134 A83-48120
PASSAGEWAYS
Film-cooling effectiveness with developing coolant flow through straight and curved tubular passages
[NASA-TP-2062] p 126 N83-12360
PASSENGER AIRCRAFT
Study of advanced rotary combustion engines for commuter aircraft
[NASA-CR-165399] p 32 N83-17545
PATENT APPLICATIONS
Chemical approach for controlling nadamide cure temperature and rate
[NASA-CASE-LEW-13770-1] p 91 N83-13258
PATENTS
Method for depositing an oxide coating
[NASA-CASE-LEW-13131-1] p 165 N83-10494
PAYLOADS
Rail accelerator research at Lewis Research Center
[AIAA PAPER 82-1938] p 53 A83-22075
Rail accelerator research at Lewis Research Center
[NASA-TM-83015] p 56 N83-12143
PENETRATION
Study of lubricant jet flow phenomena in spur gears: Out of mesh condition p 147 N83-20146
PENS
Classification of journal surfaces using surface topography parameters and software methods to compensate for stylus geometry
[NASA-CR-168153] p 148 N83-24857
PERFLUORO COMPOUNDS
The effects of metals and inhibitors on thermal oxidative degradation reactions of unbranched perfluoroalkylethers
[NASA-TM-83464] p 97 N83-34049
PERFORATED SHELLS
Comparison of predicted and experimental external heat transfer around a film cooled cylinder in crossflow
[NASA-TM-83017] p 127 N83-13392
Solid particle impingement erosion characteristics of cylindrical surfaces with pre-existing holes and slits
[NASA-TM-83322] p 85 N83-25853
PERFORMANCE
Performance and load data from Mod-0A and Mod-1 wind turbine generators p 176 N83-19255
PERFORMANCE PREDICTION
An improved switching converter model using discrete and average techniques p 111 A83-11495
A method of predicting the performance deterioration of a compressor cascade due to sand erosion
[AIAA PAPER 83-0178] p 19 A83-16572
Natural frequency of rotating beams using non-rotating modes p 156 A83-18383
Advances in high-speed rolling-element bearings --- for aircraft engine and transmission application
p 137 A83-22319
Thermoelastohydrodynamic analysis of an oil pumping ring seal p 137 A83-22322
Modern multistage depressed collectors - A review
p 112 A83-24025
Performance characteristics of a microwave plasma disk ion source --- time varying electric propulsion concept
[AIAA PAPER 82-1935] p 55 A83-27350
The performance of an annular vane swirler --- to aid in modeling gas turbine combustor flowfields and swirling confined flow turbulence
[AIAA PAPER 83-1326] p 24 A83-36340
A comprehensive method for preliminary design optimization of axial gas turbine stages. II - Code verification
[AIAA PAPER 83-1403] p 24 A83-36393
Analysis of spiral-groove face seals for liquid oxygen
[ASLE PREPRINT 83-AM-4B-2] p 138 A83-43339
A theory of rotating stall of multistage axial compressors. I - Small disturbances
[ASME PAPER 83-GT-44] p 7 A83-47904
The development of a generalized advanced propeller analysis system
[AIAA PAPER 83-2466] p 26 A83-49581
The WISGSK: A computer code for the prediction of a multistage axial compressor performance with water ingestion
[NASA-CR-3624] p 28 N83-12093
Measured and calculated wall temperatures on air-cooled turbine vanes with boundary layer transition
[NASA-TM-83030] p 127 N83-14432
Analytical investigation of critical MHD phenomena
[NASA-CR-168079] p 175 N83-19228
Traction behavior of two traction lubricants
[NASA-TM-83311] p 144 N83-20116
Experimental verification of the number relation at room and elevated temperatures p 162 N83-34355
PERFORMANCE TESTS
Status of the J-series 30-cm mercury ion thruster
[AIAA PAPER 82-1904] p 51 A83-12479
Inert gas test of two 12-cm magnetostatic thrusters
[AIAA PAPER 82-1925] p 51 A83-12494
Results of chopper-controlled discharge life cycling studies on lead-acid batteries p 164 A83-27183
Tubes in space - Very much alive p 112 A83-28160
Power turbine dynamics - An evaluation of a shear-mounted elastomeric damper
[ASME PAPER 83-GT-228] p 139 A83-48025
Lubricant effects on efficiency of a helicopter transmission p 141 N83-15523
Fixed pitch rotor performance of large horizontal axis wind turbines p 175 N83-19233
Stall induced instability of a teetered rotor
p 175 N83-19234
Free yaw performance of the Mod-0 large horizontal axis 100 kW wind turbine p 175 N83-19235
Tests of an alternating current propulsion subsystem for electric vehicles on a road load simulator
[NASA-TM-83036] p 178 N83-22749
Single cell performance studies on the Fe/Cr Redox Energy Storage System using mixed reactant solutions at elevated temperature
[NASA-TM-83385] p 180 N83-25042
Testing of felt-ceramic materials for combustor applications
[NASA-CR-168103] p 36 N83-26837
Near-field measurement facility plans at Lewis Research Center p 46 N83-26897
PERIODIC FUNCTIONS
Some analysis methods for rotating systems with periodic coefficients p 157 A83-32987
PERIODIC VARIATIONS
Composites with periodic microstructure
p 62 A83-12734
PERMEABILITY
Determination of hydrogen permeability in uncoated and coated superalloys
[NASA-CR-165209] p 80 N83-12215
Evaluation of dopants in hydrogen to reduce hydrogen permeation in candidate Stirling engine heater head tube alloys at 760 deg and 820 deg
[NASA-TM-82920] p 81 N83-13232
Determination of hydrogen permeability in commercial and modified superalloys
[NASA-CR-168195] p 87 N83-35101
PERSPEX (TRADEMARK)
Dynamics and mechanism of cavitation erosion on perspex and epoxy resin tested in a rotating disk device
p 89 A83-27422
Cavitation erosion characteristics of poly(methyl methacrylate) in a rotating disk device
p 90 A83-41851

Dynamics and mechanism of cavitation erosion on perspex and epoxy resins tested in a rotating disk device
[NASA-TM-82962] p 91 N83-11329

PERTURBATION THEORY
Development of a multiple-parameter nonlinear perturbation procedure for transonic turbomachinery flows: Preliminary application to design/optimization problems
[NASA-CR-3657] p 2 N83-17453

PERVEANCE
Experimental verification of the multistage depressed collector design procedure for a high-perveance, helix-type, traveling-wave tube --- in communications satellites
[NASA-TP-2162] p 116 N83-25985

PHASE DIAGRAMS
Superalloy composition modeling p 78 N83-11284
Binary nickel alloy phase diagrams compilation and critical evaluation
[NASA-CR-170016] p 82 N83-19885

PHASE MODULATION
An improved algorithm for evaluating trellis phase codes
[NASA-CR-169354] p 105 N83-16600

PHASE SHIFT
Phased array-fed antenna configuration study: Technology assessment
[NASA-CR-168078] p 106 N83-22495

PHASE SHIFT KEYING
Advances in Serial MSK modems p 111 A83-19789
Onboard processing for a 30/20 GHz communications satellite p 47 A83-41391
Modulation techniques
[NASA-CR-169460] p 105 N83-10329

PHASE TRANSFORMATIONS
Kinetics of copper ion absorption by cross-linked calcium polyacrylate membranes
[NASA-TM-83052] p 61 N83-25786

PHASED ARRAYS
Auxiliary propulsion requirements for large space systems
[AIAA PAPER 83-1217] p 56 A83-45512
Auxiliary propulsion requirements for large space systems
[NASA-TM-83388] p 58 N83-26922
Phased array-fed antenna configuration study
[NASA-CR-168077] p 107 N83-27086

PHOSPHATES
On the mechanism of lubrication by tricresylphosphate /TCP/ - The coefficient of friction as a function of temperature for TCP on M-50 steel
[ASLE PREPRINT 82-LC-4C-1] p 135 A83-13228
Mechanism of lubrication by tricresylphosphate (TCP)
[NASA-TP-2053] p 72 N83-18863
The adsorption and thermal decomposition of tricresylphosphate (TCP) on iron and gold
[NASA-TM-83441] p 62 N83-29311

PHOSPHORIC ACID FUEL CELLS
Cell module and fuel conditioner development
[NASA-CR-165462-A] p 168 N83-12524
Develop and test fuel cell powered on-site integrated total energy system
[NASA-CR-168020] p 173 N83-15839
Develop and test fuel cell powered on-site integrated total energy systems. Phase 3: Full-scale power plant development
[NASA-CR-168021] p 182 N83-27345

PHOTOACOUSTIC SPECTROSCOPY
Comparison of NDE techniques for sintered-SiC components p 152 A83-22265

PHOTOELASTIC ANALYSIS
Extending the laser-specklegram technique to strain analysis of rotating components p 155 A83-12514

PHOTOELECTRIC GENERATORS
DOE and AID stand-alone photovoltaic activities
[NASA-TM-83374] p 180 N83-25041
Solar energy converter using surface plasma waves
[NASA-CASE-LEW-13827-1] p 181 N83-26258

PHOTOELECTRON SPECTROSCOPY
Application of modern surface analytical tools in the investigation of surface deterioration processes
[NASA-TM-83452] p 152 N83-34327

PHOTOLUMINESCENCE
Residual double acceptors in bulk GaAs p 205 A83-19989

PHOTOMICROGRAPHY
Sliding induced crystallization of metallic glass
[NASA-TP-2140] p 83 N83-21110

PHOTOTHERMAL CONVERSION
Analysis of the reflective multibandgap solar cell concept
[NASA-CR-168186] p 185 N83-34454

PHOTOVOLTAGES
Minority carrier diffusion length measurements - A review and comparison of techniques p 205 A83-28448

PHOTOVOLTAIC CELLS
Performance degradation and cleaning of photovoltaic arrays p 164 A83-27236
High speed computerized data acquisition of photovoltaic V-I characteristics
[NASA-TM-82867] p 114 N83-14397
Heat transparent high intensity high efficiency solar cell
[NASA-CASE-LEW-12892-1] p 170 N83-14692
Space Photovoltaic Research and Technology 1982: High Efficiency, Radiation Damage, and Blanket Technology
[NASA-CP-2256] p 171 N83-15806
The worldwide market for photovoltaics in the rural sector
[NASA-TM-83035] p 173 N83-15840
Array structure design handbook for stand alone photovoltaic applications
[NASA-TM-82629] p 160 N83-23631
Analysis of the economics of photovoltaic-diesel-battery energy systems for remote applications
[NASA-TM-83377] p 179 N83-23709
Modular photovoltaic stand-alone systems: Phase 1
[NASA-CR-168075] p 185 N83-33320
Practical aspects of photovoltaic technology, applications, and cost
[NASA-CR-168025] p 185 N83-34450
Photovoltaic stand-alone modular systems, phase 2
[NASA-CR-168230] p 186 N83-35497

PHOTOVOLTAIC CONVERSION
Market assessment of photovoltaic power systems for agricultural applications worldwide
[NASA-CR-165541] p 168 N83-13585
Development of a high capacity toroidal Ni/Cd cell
[NASA-CR-169945] p 176 N83-19273

PHOTOVOLTAIC EFFECT
Evaluation of electrode shape and nondestructive evaluation method for welded solar cell interconnects
[NASA-TM-82966] p 166 N83-10555
DOE and AID stand-alone photovoltaic activities
[NASA-TM-83374] p 180 N83-25041
Practical aspects of photovoltaic technology, applications, and cost
[NASA-CR-168025] p 185 N83-34450
Analysis of the reflective multibandgap solar cell concept
[NASA-CR-168186] p 185 N83-34454

PHYSICAL CHEMISTRY
A class of nonideal solutions. 1: Definition and properties
[NASA-TP-1929] p 208 N83-23189

PIEZOELECTRIC CRYSTALS
Piezoelectric and pyroelectric coefficients for ferroelectric crystals with polarizable molecules p 205 A83-17227
Piezoelectricity and pyroelectricity in polyvinylidene fluoride - Influence of the lattice structure p 205 A83-29531

PIEZOELECTRIC TRANSDUCERS
Piezoelectric deicing device
[NASA-CASE-LEW-13773-1] p 18 N83-29197

PIEZOELECTRICITY
Piezoelectric composite materials
[NASA-CASE-LEW-12582-1] p 207 N83-34796

PINS
Length to diameter ratio and row number effects in short pin fin heat transfer
[NASA-TM-83005] p 127 N83-14431

PIPE FLOW
Finite analytic numerical solution of axisymmetric Navier-Stokes and energy equations
[ASME PAPER 82-HT-42] p 118 A83-12795

PIPELINING (COMPUTERS)
Frequency-multiplexed and pipelined iterative optical systolic array processors p 188 A83-18588

PIPES (TUBES)
Acoustical modal analysis of the pressure field in the tailpipe of a turbofan engine
[NASA-TM-83387] p 201 N83-25499

PISTON ENGINES
Numerical studies of the formation and destruction of vortices in a motored four-stroke piston-cylinder configuration
[AIAA PAPER 83-0497] p 136 A83-16749
Computed and measured turbulence in axisymmetric reciprocating engines p 21 A83-24669
Computation techniques and computer programs to analyze Stirling cycle engines using characteristic dynamic energy equations p 207 A83-27272
Turbulent flame propagation and combustion in spark ignition engines p 70 A83-48156
A conceptual study of the potential for automotive-derived and free-piston Stirling engines in 30- to 400-kilowatt stationary power applications
[NASA-CR-165274] p 167 N83-10568
Testing and performance characteristics of a 1-kW free piston Stirling engine
[NASA-TM-82999] p 180 N83-25036
Free-piston Stirling hydraulic engine and drive system for automobiles
[NASA-TM-82992] p 211 N83-25625
Vortex motion in axisymmetric piston-cylinder configurations
[NASA-TM-85404] p 133 N83-35318

PISTONS
Cast Fe-base cylinder/regenerator housing alloy
[NASA-CR-169474] p 80 N83-12214
Numerical simulation of the flow and fuel-air mixing in an axisymmetric piston-cylinder arrangement
[NASA-TM-83011] p 126 N83-12358
Design of hydraulic output Stirling engine
[NASA-CR-167976] p 177 N83-22739
Test results and description of a 1-kW free-piston Stirling engine with a dashpot load
[NASA-TM-83407] p 182 N83-27346

PITCH (INCLINATION)
Study of lubricant jet flow phenomena in spur gears: Out of mesh condition p 147 N83-20146
Mod-2 wind turbine system development. Volume 1: Executive summary
[NASA-CR-168006] p 184 N83-29812

PITOT TUBES
Five-hole pitot probe time-mean velocity measurements in confined swirling flows
[AIAA PAPER 83-0315] p 119 A83-16645

PITTING
Evaluation of high-contact-ratio spur gears with profile modification p 147 N83-20150
Cavitation pitting and erosion of aluminum 6061-T6 in mineral oil water
[NASA-TP-2146] p 152 N83-35400

PIVOTS
Pivoting and slip in an angular contact bearing
[NASA-TM-83408] p 148 N83-26079

PLANE STRAIN
Time-independent anisotropic plastic behavior by mechanical subelement models p 162 N83-34369

PLANETARY ORBITS
Vibration in planetary gear systems with unequal planet stiffnesses
[NASA-TM-83428] p 150 N83-29709

PLASMA CURRENTS
End region effects upon the performance of a magnetohydrodynamic channel p 203 A83-10665
Ion flow experiments in a multipole discharge chamber
[AIAA PAPER 82-1930] p 203 A83-14398

PLASMA DIAGNOSTICS
Plasma characteristics of a 17 cm diameter line-cusp ion thruster
[AIAA PAPER 82-1926] p 52 A83-12495
Numerical simulation of a disk-shaped electron accelerating electrostatic probe p 133 A83-22336
SAFE II: Large systems space plasma evaluation experiment p 46 N83-26903

PLASMA DYNAMICS
Ion flow experiments in a multipole discharge chamber
[AIAA PAPER 82-1930] p 203 A83-14398

PLASMA ENGINES
Plasma characteristics of a 17 cm diameter line-cusp ion thruster
[AIAA PAPER 82-1926] p 52 A83-12495
Inert gas thruster technology p 53 A83-20423

PLASMA GENERATORS
Microwave plasma generation of hydrogen atoms for rocket propulsion p 53 A83-13090
Ring-cusp ion thruster with shell anode
[NASA-CASE-LEW-13881-1] p 202 N83-21903
High frequency plasma generators for ion thrusters
[NASA-CR-167957] p 59 N83-28072

PLASMA INTERACTIONS
Observations of charging dynamics --- of spacecraft p 49 A83-37591
Design considerations for large space electric power systems
[NASA-TM-83064] p 58 N83-24552
SAFE II: Large systems space plasma evaluation experiment p 46 N83-26903

PLASMA PHYSICS
Current collection from the space plasma through defects in high voltage solar array insulation
[NASA-CR-168148] p 204 N83-31474

PLASMA POWER SOURCES
Parallel plate radiofrequency ion thruster
[AIAA PAPER 82-1937] p 53 A83-21900
Parallel plate radiofrequency ion thruster
[NASA-TM-83014] p 56 N83-12142

PLASMA PROPULSION
Plasma characteristics of a 17 cm diameter line-cusp ion thruster
[AIAA PAPER 82-1926] p 52 A83-12495

Measurements of energy distribution and thrust for microwave plasma coupling of electrical energy to hydrogen for propulsion
[AIAA PAPER 82-1951] p 52 A83-12508
Extended-performance 8-cm ion thruster operation
[AIAA PAPER 82-1955] p 53 A83-12512
Microwave plasma generation of hydrogen atoms for rocket propulsion p 53 A83-13090

PLASMA SHEATHS
Numerical simulation of a disk-shaped electron accelerating electrostatic probe p 133 A83-22336

PLASMA SPRAYING
Improved uniformity of multiphase ceramic-metal plasma-sprayed coats p 61 A83-22269
Effects of arc current on the life in burner-rig thermal cycling of plasma-sprayed ZrO2-O3 p 89 A83-22270
Use of fiber-like materials to augment cycle life of thick, thermoprotective-seal coatings --- for gas turbine engine components p 89 A83-22271
Creep of plasma-sprayed-ZrO2 thermal-barrier coatings p 89 A83-22273
Further industrial tests of ceramic thermal barrier coatings
[NASA-TP-2057] p 26 N83-10045
Plasma-sprayed self-lubricating coatings
[NASA-CR-3680] p 94 N83-22422
The effect of annealing on the creep of plasma sprayed ceramics
[NASA-TM-83396] p 130 N83-24799
Correlation of compressive stress with spalling of plasma sprayed ceramic materials
[NASA-TM-83406] p 95 N83-27016
JT9D thermal barrier coated vanes
[NASA-CR-167964] p 37 N83-27993
Residual stress in plasma sprayed ceramic turbine tip and gas path seal specimens
[NASA-TM-83418] p 131 N83-28380
Fully plasma-sprayed compliant backed ceramic turbine seal
[NASA-CASE-LEW-13268-3] p 149 N83-28450
Creep of plasma sprayed zirconia
[NASA-CR-167868] p 96 N83-29393

PLASMONS
A new strategy for efficient solar energy conversion - Parallel-processing with surface plasmons p 164 A83-27140
Surface-polaritonlike waves guided by thin, lossy metal films p 192 A83-37947
Long-range surface plasmons in electrode structures p 202 A83-40733
Long range surface plasmons in birefringent media p 202 A83-42206
Effects of gaps on long range surface plasmon polaritons p 204 A83-46271
Solar energy conversion using surface plasmons for broadband energy transport p 171 N83-15815
Inelastic tunnel diodes
[NASA-CASE-LEW-13633-1] p 116 N83-25983
A new strategy for efficient solar energy conversion: Parallel-processing with surface plasmons
[NASA-TM-82867] p 59 N83-28071

PLASTIC DEFORMATION
Plastic deformation and wear process at a surface during unlubricated sliding p 138 A83-37822
Mechanical bonding of metal method
[NASA-CASE-LEW-12941-1] p 77 N83-10170
Plastic deformation at surface during unlubricated sliding
[NASA-TP-2036] p 139 N83-11496

PLASTIC FLOW
Influence of thermomechanical processing on elevated temperature slow plastic flow properties of B2 aluminide Fe-39.8at.% Al p 75 A83-22017
Effect of swaging on the 1000 C compressive slow plastic flow characteristics of the directionally solidified eutectic alloy gamma/gamma prime-alpha p 77 A83-44340
The effect of annealing on the creep of plasma sprayed ceramics
[NASA-TM-83396] p 130 N83-24799

PLASTIC PROPERTIES
Constrained self-adaptive solutions procedures for structure subject to high temperature elastic-plastic creep effects p 162 N83-34370

PLATE THEORY
Alternative ways for formulation of hybrid stress elements p 155 A83-14710

PLATES (STRUCTURAL MEMBERS)
Heat transfer and flow characteristics of jets impinging on a concave hemispherical plate p 123 A83-42743
A solution procedure for behavior of thick plates on a nonlinear foundation and postbuckling behavior of long plates
[NASA-TP-2174] p 163 N83-34373

PLATING
Method for depositing an oxide coating
[NASA-CASE-LEW-13131-1] p 165 N83-10494
Vacuum sputtered and ion-plated coatings for wear and corrosion protection
[NASA-TM-83007] p 99 N83-13273

PLATINUM ALLOYS
Joining lead wires to thin platinum alloy films
[NASA-CASE-LEW-13934-1] p 135 N83-35338

PLUG NOZZLES
Free-jet acoustic investigation of high-radius-ratio coannular plug nozzles. Comprehensive data report, volume 1
[NASA-CR-168086-VOL-1] p 198 N83-18408

PLUGGING
Burner rig study of variables involved in hole plugging of air cooled turbine engine vanes
[NASA-TM-83308] p 83 N83-19887

PNEUMATIC EQUIPMENT
Apparatus for improving the fuel efficiency of a gas turbine engine
[NASA-CASE-LEW-13142-1] p 43 N83-36029

POINTING CONTROL SYSTEMS
Optimal sun-alignment techniques of large solar arrays in electric propulsion spacecraft
[AIAA PAPER 82-1898] p 48 A83-12475

POLLUTION CONTROL
Multifuel evaluation of rich/quench/lean combustor p 67 A83-11492
An analytical investigation of NO sub x control techniques for methanol fueled spark ignition engines
[NASA-CR-172847] p 151 N83-33168

POLLUTION MONITORING
Water vapor measurement system in global atmospheric sampling program, appendix
[NASA-TP-2051] p 187 N83-13643

POLYCARBONATES
Solid spherical glass particle impingement studies of plastic materials
[NASA-TP-2161] p 94 N83-24695

POLYCHLORINATED BIPHENYLS
Preliminary results of the comparison of the electrochemical behavior of a thioether and biphenyl
[NASA-TM-83450] p 87 N83-34015

POLYCRYSTALS
The initial stages of cavitation damage and erosion on copper and brass tested in a rotating disk device p 75 A83-27421
Initial stages of cavitation damage and erosion on copper and brass tested in a rotating disk device
[NASA-TM-82993] p 81 N83-13231
The orthogonal in-situ machining of single and polycrystalline aluminum and copper, volume 2
[NASA-CR-169528] p 81 N83-13233
Micromechanically based constitutive relations for polycrystalline solids p 162 N83-34359

POLYESTER RESINS
Hygrothermomechanical evaluation of transverse filament tape epoxy/polyester fiberglass composites
[NASA-TM-83044] p 65 N83-15362

POLYETHYLENES
Effect of sliding speed and contact stress on tribological properties of ultra-high-molecular-weight polyethylene
[NASA-TP-2059] p 91 N83-14269
Friction, wear, transfer and wear surface morphology of ultra-high-molecular-weight polyethylene
[NASA-TM-83364] p 94 N83-25882

POLYIMIDE RESINS
Environmental effects on graphite fiber reinforced PMR-15 polyimide p 63 A83-33115
Lower-curing-temperature PMR polyimides p 89 A83-40923
Lower-curing-temperature PMR polyimides
[NASA-TM-82958] p 63 N83-10118
Polymer matrix composites research at NASA Lewis Research Center p 91 N83-12151
PMR-15 polyimide modifications for improved prepreg tack
[NASA-TM-82951] p 64 N83-12175
Polyimides: Tribological properties and their use as lubricants
[NASA-TM-82959] p 91 N83-13257
Chemical approach for controlling nadamide cure temperature and rate
[NASA-CASE-LEW-13770-1] p 91 N83-13258
Dynamic mechanical properties of n-phenylnadimide modified PMR polyimide composites
[NASA-TM-83051] p 65 N83-15363
Improved high temperature resistant polyimides
[NASA-CASE-LEW-13864-1] p 93 N83-17715
Low temperature cross linking polyimides
[NASA-CASE-LEW-12876-2] p 96 N83-29392
Chemical approach for controlling nadamide cure temperature and rate
[NASA-CASE-LEW-13770-2] p 96 N83-30651

POLYIMIDES
PMR polyimides - Review and update --- Polymerization of Monomer Reactants p 62 A83-20447
Fundamental aspects of polyimide dry film and composite lubrication: A review
[NASA-TM-82968] p 92 N83-14271
PMR polyimide composites for aerospace applications
[NASA-TM-83047] p 65 N83-15364
Polyimides formulated from a partially fluorinated diamine for aerospace tribological applications
[NASA-TM-83339] p 94 N83-22423

POLYMER CHEMISTRY
A vortex venturi for reverting antimisting fuel properties
[ASME PAPER 83-GT-137] p 25 A83-47964
Polymer matrix composites research at NASA Lewis Research Center p 91 N83-12151

POLYMER MATRIX COMPOSITES
PMR polyimides - Review and update --- Polymerization of Monomer Reactants p 62 A83-20447

POLYMERIC FILMS
Cross-linked polyvinyl alcohol films as alkaline battery separators p 68 A83-20576
Fundamental aspects of polyimide dry film and composite lubrication: A review
[NASA-TM-82968] p 92 N83-14271
Development and evaluation of polyvinyl-alcohol blend polymer films as battery separators
[NASA-TM-82981] p 71 N83-15372

POLYMERIZATION
PMR polyimides - Review and update --- Polymerization of Monomer Reactants p 62 A83-20447
PMR polyimide composites for aerospace applications
[NASA-TM-83047] p 65 N83-15364
Use of high L.E.T. radiation to improve adhesion of metals to polytetrafluoroethylene
[NASA-TM-83413] p 96 N83-30660
Research into the use of pyrolytic oxides and polymers for the fabrication of thin film high energy capacitors
[NASA-CR-173012] p 97 N83-34045

POLYMERS
The electrochemical fluorination of polymeric materials for high energy density aqueous and non-aqueous battery and fuel cell separators
[NASA-CR-167961] p 72 N83-21056

POLYMETHYL METHACRYLATE
Boundary integral equation method calculations of surface regression effects in flame spreading p 67 A83-13488
Solid spherical glass particle impingement studies of plastic materials
[NASA-TP-2161] p 94 N83-24695

POLYPROPYLENE
Evaluation of production version of the NASA improved inorganic-organic separator
[NASA-TM-83018] p 174 N83-18022

POLYTETRAFLUOROETHYLENE
Solid spherical glass particle impingement studies of plastic materials
[NASA-TP-2161] p 94 N83-24695
Use of high L.E.T. radiation to improve adhesion of metals to polytetrafluoroethylene
[NASA-TM-83413] p 96 N83-30660

POLYURETHANE FOAM
Propagation of sound in highly porous open-cell elastic foams p 195 A83-28848
Surface acoustic admittance of highly porous open-cell, elastic foams p 195 A83-28849

POLYVINYL ALCOHOL
Cross-linked polyvinyl alcohol films as alkaline battery separators p 68 A83-20576
Polyvinyl alcohol cross-linked with two aldehydes
[NASA-CASE-LEW-13504-1] p 71 N83-13188
Development and evaluation of polyvinyl-alcohol blend polymer films as battery separators
[NASA-TM-82981] p 71 N83-15372
Polyvinyl alcohol battery separator containing inert filler
[NASA-CASE-LEW-13556-2] p 183 N83-29805

POLYVINYL FLUORIDE
Piezoelectricity and pyroelectricity in polyvinylidene fluoride - Influence of the lattice structure p 205 A83-29531

POROSITY
Pore size engineering applied to starved electrochemical cells and batteries p 164 A83-27201
Pore size engineering applied to starved electrochemical cells and batteries
[NASA-TM-82893] p 70 N83-10134
Electrolyte management in porous battery components. Static measurements
[NASA-TM-83073] p 72 N83-18862
Search for selective ion diffusion through membranes
[NASA-TM-83426] p 97 N83-34048

POROUS BOUNDARY LAYER CONTROL
Analysis of coolant entrance boundary shape of porous region to control cooling along exit boundary p 124 A83-43361

POROUS MATERIALS
Propagation of sound in highly porous open-cell elastic foams p 195 A83-28848
Surface acoustic admittance of highly porous open-cell, elastic foams p 195 A83-28849
High-intensity sound in air saturated fibrous bulk porous materials
[NASA-CR-167979] p 197 N83-12967
Advanced inorganic separators for alkaline batteries and method of making the same
[NASA-CASE-LEW-13171-2] p 184 N83-32176
A method of predicting flow rates required to achieve anti-icing performance with a porous leading edge ice protection system
[NASA-CR-168213] p 17 N83-32782

POROUS WALLS
Determination of boundary shape of cooled porous region p 118 A83-13487

PORTABLE EQUIPMENT
Evaluation of methods for rapid determination of freezing point of aviation fuels
[NASA-CR-167981] p 98 N83-10207
Assessment of alternative power sources for mobile mining machinery
[NASA-TM-82695] p 169 N83-14691
Computer simulator for a mobile telephone system
[NASA-CR-170181] p 106 N83-22493

POSITIONING
Method for terminal position determination in Earth terminal-to-satellite burst acquisition and synchronization
[NASA-CASE-LEW-13893-1] p 107 N83-30832

POTASSIUM COMPOUNDS
Vaporization thermodynamics of K2S and K2SO3
[NASA-CR-168080] p 61 N83-19812
Thermodynamics of the potassium-sulfur-oxygen and related systems
[NASA-CR-168155] p 61 N83-28077

POTASSIUM HYDROXIDES
Activation parameters of flow through battery separators
[NASA-TM-83371] p 73 N83-30550

POTENTIAL FLOW
Mode propagation in nonuniform circular ducts with potential flow p 122 A83-36082
An experience in mesh generation for three-dimensional calculation of potential flow around a rotating propeller p 5 A83-38798
Finite volume calculation of three-dimensional potential flow around a propeller p 7 A83-45577
Wind tunnel tests of a zero length, slotted-lip engine air inlet for a fixed nacelle V/STOL aircraft
[NASA-TM-82939] p 9 N83-10019

POWDER (PARTICLES)
The effect of silicon particle size on the nitriding behaviour of reaction bonded Si3N4 compacts p 90 A83-48261

POWDER METALLURGY
Dual alloy interface stability p 79 N83-11297
Microstructural behavior of interfaces in hot isostatically pressed, dual alloy combinations
[NASA-TM-82698] p 80 N83-11309
Powder metallurgy Rene 95 rotating turbine engine parts, volume 2
[NASA-CR-165141] p 82 N83-15412

POWER AMPLIFIERS
A 1 watt GaAs power amplifier for the NASA 30/20 GHz communication system p 111 A83-11489
A two-stage monolithic buffer amplifier for 20 GHz satellite communication p 112 A83-39272
Phased array-fed antenna configuration study: Technology assessment
[NASA-CR-168078] p 106 N83-22495

POWER CONDITIONING
Computer simulations of optimum boost and buck-boost converters p 111 A83-19032
Solar array switching power management p 54 A83-27132
Development of improved hydrogen recombination in sealed nickel-cadmium aerospace cells p 54 A83-27198
Simplified power processing for ion-thruster subsystems
[AIAA PAPER 83-1394] p 55 A83-36384
Simplified power processing for ion-thruster subsystems p 56 A83-39271
High-frequency high-voltage high-power DC-to-DC converters p 115 N83-21028
Task 4 completion report for 40 Kilowatt grid connected modification contract
[NASA-CR-167950] p 208 N83-30297
Simplified power processing for ion-thruster subsystems p 60 N83-35018

POWER CONVERTERS
Transformer induced instability of the series resonant converter p 113 A83-41152

POWER EFFICIENCY
Optimal sun-alignment techniques of large solar arrays in electric propulsion spacecraft
[AIAA PAPER 82-1898] p 48 A83-12475
Improved Stirling engine performance using jet impingement p 137 A83-27288
Performance characteristics of a microwave plasma disk ion source --- time varying electric propulsion concept
[AIAA PAPER 82-1935] p 55 A83-27350
Tubes in space - Very much alive p 112 A83-28160
The aerodynamic design and performance of the General Electric/NASA EEE fan --- Energy Efficient Engine
[AIAA PAPER 83-1160] p 23 A83-36252
The feasibility of water injection into the turbine coolant to permit gas turbine contingency power for helicopter application
[ASME PAPER 83-GT-66] p 24 A83-39993
Wind turbine generator interaction with diesel generators on an isolated power system p 165 A83-44673
On the cause of the flat-spot phenomenon observed in silicon solar cells at low temperatures and low intensities p 170 N83-14705
Determination of optimum sunlight concentration level in space for 3-5 cascade solar cells p 170 N83-14732
Study of solar array switching power management technology for space power system
[NASA-CR-167890] p 179 N83-22756
Advantage of resonant power conversion in aerospace applications
[NASA-TM-83399] p 37 N83-27994

POWER FACTOR CONTROLLERS
Kilovolt dc solid state remote power controller development
[NASA-CR-168041] p 115 N83-21236

POWER GAIN
Gain-enhanced free-electron laser with an electromagnetic pump field p 135 A83-31133
GaAs integrated digital-to-analogue convertor for control of power dual-gate FETs p 112 A83-36479

POWER PLANTS
Methods of reducing energy consumption of the oxidant supply system for MHD/steam power plants
[NASA-TM-83025] p 168 N83-13589

POWER SUPPLIES
Assessment of alternative power sources for mobile mining machinery
[NASA-TM-82695] p 169 N83-14691
Advantage of resonant power conversion in aerospace applications
[NASA-TM-83399] p 37 N83-27994
Control of large wind turbine generators connected to utility networks
[NASA-CR-168200] p 185 N83-34451

POWER SUPPLY CIRCUITS
Solar array switching power management p 54 A83-27132
Design study of a high power rotary transformer
[NASA-CR-168012] p 115 N83-16630

POWERED LIFT AIRCRAFT
QCSEE under-the-wing engine-wing-flap aerodynamic profile characteristics
[NASA-TM-82890] p 28 N83-12092

PRECIPITATION HARDENING
Development of Fe-Mn-Al-X-C alloys p 80 N83-11307

PREDICTION ANALYSIS TECHNIQUES
Predictions of the structure of turbulent, particle-laden, round jets
[AIAA PAPER 83-0066] p 119 A83-16498
Turbine blade nonlinear structural and life analysis p 21 A83-29024
A two-equation turbulence model for two-phase flows p 121 A83-30109
Blade loss transient dynamic analysis of turbomachinery p 25 A83-40864
A survey of inlet/engine distortion compatibility
[AIAA PAPER 83-1166] p 6 A83-45509
A survey of inlet/engine distortion compatibility
[NASA-TM-83421] p 37 N83-27991
A method of predicting flow rates required to achieve anti-icing performance with a porous leading edge ice protection system
[NASA-CR-168213] p 17 N83-32782

PRELAUNCH SUMMARIES
Infrared Astronomical Satellite (IRAS) launch
[NASA-TM-85190] p 45 N83-15330

PREMIXED FLAMES
Numerical solution of the problem of flame propagation by the use of the random element method
[AIAA PAPER 83-0600] p 69 A83-36062
Effect of flameholder pressure drop on emissions and performance of premixed-prevaporized combustors
[NASA-TP-2131] p 35 N83-23309

PREMIXING
Analytical modeling of operating characteristics of premixing-prevaporizing fuel-air mixing passages. Volume 1: Analysis and results
[NASA-CR-167990-VOL-1] p 126 N83-12353
Analytical modeling of operating characteristics of premixing-prevaporizing fuel-air mixing passages. Volume 2: User's manual
[NASA-CR-167990-VOL-2] p 126 N83-12354
Fumigation of alcohol in a light duty automotive diesel engine
[NASA-CR-167915] p 99 N83-13272
Autoignition in a premixing-prevaporizing fuel duct using 3 different fuel injection systems at inlet air temperatures to 1250 K
[NASA-TM-82938] p 181 N83-26251
Combustion Fundamentals Research
[NASA-CP-2268] p 38 N83-29208

PREPREGS
PMR-15 polyimide modifications for improved prepreg tack
[NASA-TM-82951] p 64 N83-12175

PRESSURE
A comprehensive analysis of cavitation and liquid impingement erosion data
[NASA-TM-83352] p 84 N83-24634

PRESSURE DISTRIBUTION
Studies of flows through N-sequential orifices
[NASA-TM-83313] p 129 N83-19020
Labyrinth seal forces on a whirling rotor
[NASA-CR-168016] p 34 N83-22198
Acoustical modal analysis of the pressure field in the tailpipe of a turbofan engine
[NASA-TM-83387] p 201 N83-25499
Nacelle Aerodynamic and Inertial Loads (NAIL) project
[NASA-CR-168712] p 18 N83-30402

PRESSURE MEASUREMENT
An experimental investigation of the vaporous/gaseous cavity characteristics of an eccentric journal bearing
[ASLE PREPRINT 82-LC-3A-1] p 136 A83-13230
Studies of flows through N-sequential orifices
[ASME PAPER 83-FE-22] p 125 A83-48678
Analysis of combustion spectra containing organ pipe tone by cepstral techniques
[NASA-TM-83034] p 198 N83-16153
Experimental investigation of the vaporous/gaseous cavity characteristics of an eccentric journal bearing
[NASA-TM-82996] p 128 N83-17833

PRESSURE RATIO
Experimental results of a deflected thrust V/STOL nozzle research program
[AIAA PAPER 83-0170] p 6 A83-42100
Performance of a tandem-rotor/tandem-stator conical-flow compressor designed for a pressure ratio of 3
[NASA-TP-2034] p 9 N83-11058
Experimental results of a deflected thrust V/STOL nozzle research program
[NASA-TM-83069] p 12 N83-25657

PRESSURE REDUCTION
Experimental investigation of a two-dimensional shock-turbulent boundary layer interaction with bleed
[AIAA PAPER 83-0135] p 3 A83-19581
Experimental investigation of a two-dimensional shock-turbulent boundary layer interaction with bleed
[NASA-TM-83057] p 34 N83-22200
Effect of flameholder pressure drop on emissions and performance of premixed-prevaporized combustors
[NASA-TP-2131] p 35 N83-23309

PRESSURE REGULATORS
Ion beam sputter-etched ventricular catheter for hydrocephalus shunt
[NASA-CASE-LEW-13107-1] p 188 N83-21785

PRESSURE SENSORS
Farfield inflight measurement of high-speed turboprop noise
[NASA-TM-83327] p 199 N83-21895

PRESSURE VESSELS
Cycle life test and failure model of nickel-hydrogen cells
[NASA-TM-83375] p 180 N83-25038

PRESTRESSING
Effect of deoxygenation and prestressing on hydrocarbon fuel thermal stability
[NASA-TM-83456] p 102 N83-35160

PREVAPORIZATION
Effect of flameholder pressure drop on emissions and performance of premixed-prevaporized combustors
[NASA-TP-2131] p 35 N83-23309
Autoignition in a premixing-prevaporizing fuel duct using 3 different fuel injection systems at inlet air temperatures to 1250 K
[NASA-TM-82938] p 181 N83-26251

PRINTED CIRCUITS
Screen printed interdigitated back contact solar cell
[NASA-CASE-LEW-13414-1] p 177 N83-20374

PRINTING
Multicolor printing plate joining
[NASA-CASE-LEW-13598-1] p 102 N83-17745
PRIORITIES
Research priorities for advanced fibrous composites
[NASA-CR-165414] p 65 N83-18853
PROBLEM SOLVING
Efficient solution of the Euler and Navier-Stokes equations with a vectorized multiple-grid algorithm
[AIAA PAPER 83-1893] p 5 A83-39359
Convergence acceleration of viscous flow computations
[NASA-TM-83039] p 190 N83-12930
Multiple-grid convergence acceleration of viscous and inviscid flow computations
[NASA-TM-83361] p 190 N83-21847
The finite analytic method, volume 3
[NASA-CR-170186] p 191 N83-23087
The finite analytic method, volume 4
[NASA-CR-170187] p 191 N83-23088
The finite analytic method, volume 5
[NASA-CR-170188] p 191 N83-23089
Efficient solution of the Euler and Navier-Stokes equations with a vectorized multiple-grid algorithm
[NASA-TM-83376] p 2 N83-24467
Convergence and stability properties of minimal polynomial and reduced rank extrapolation algorithms
[NASA-TM-83443] p 191 N83-31390
PROCEEDINGS
Large Horizontal-Axis Wind Turbines
[NASA-CP-2230] p 175 N83-19231
PROCESS CONTROL (INDUSTRY)
Process and quality verification controls for solid propellant manufacturing p 98 A83-39270
PRODUCT DEVELOPMENT
Development of controlled diffusion airfoils for multistage compressor application
[ASME PAPER 83-GT-211] p 9 A83-48012
Large area low-cost space solar cell development p 170 N83-14699
Advanced Gas Turbine (AGT) power-train system development
[NASA-CR-167875] p 142 N83-15627
Scanning beam antenna conceptual design for 20/30 GHz satellite systems p 46 N83-26889
Scaled centrifugal compressor, collector and running gear program
[NASA-CR-168167] p 40 N83-30432
Modular photovoltaic stand-alone systems: Phase 1
[NASA-CR-168075] p 185 N83-33320
PRODUCTION COSTS
Study to establish cost predictions for the production of Redox chemicals
[NASA-CR-167882] p 176 N83-20359
PRODUCTION ENGINEERING
Solar cell having improved back surface reflector
[NASA-CASE-LEW-13620-1] p 168 N83-13579
The Rene 150 directionally solidified superalloy turbine blades, volume 1
[NASA-CR-167992] p 39 N83-20946
PROFILOMETERS
Time effect of erosion by solid particle impingement on ductile materials
[NASA-TM-83369] p 84 N83-24637
Application of modern surface analytical tools in the investigation of surface deterioration processes
[NASA-TM-83452] p 152 N83-34327
PROGRAM VERIFICATION (COMPUTERS)
Software and system level tests of a test flight mercury ion thruster subsystem
[AIAA PAPER 82-1912] p 51 A83-12485
NASA low-speed centrifugal compressor for fundamental research
[AIAA PAPER 83-1351] p 43 A83-36353
PROJECTILES
The LeRC rail accelerators: Test designs and diagnostic techniques
[NASA-TM-83496] p 60 N83-35053
PROP-FAN TECHNOLOGY
Advanced propfan engine characteristics and technology needs
[AIAA PAPER 83-1155] p 23 A83-36250
Inlet design for high-speed propfans
[SAE PAPER 821359] p 5 A83-37957
Technology and benefits of aircraft counter rotation propellers
[NASA-TM-82983] p 27 N83-11129
User's manual for three-dimensional analysis of propeller flow fields
[NASA-CR-167959] p 12 N83-18671
PROPAGATION MODES
Acoustic modal analysis of a full-scale annular combustor
[AIAA PAPER 83-0760] p 196 A83-33486
Mode propagation in nonuniform circular ducts with potential flow p 122 A83-36082
Dynamic fields near a crack tip growing in an elastic-perfectly-plastic solid p 157 A83-38528
Long-range surface plasmons in electrode structures p 202 A83-40733
Acoustic modal analysis of a full-scale annular combustor
[NASA-TM-83334] p 200 N83-21896
PROPAGATION VELOCITY
Moving cracks in layered composites p 155 A83-12048
PROPANE
Effects of percentage of blockage and flameholder downstream counterbores on lean combustion limits of premixed, prevaporized propane-air mixture
[NASA-TP-2227] p 41 N83-34941
PROPELLANT STORAGE
Vapor flow into a capillary propellant-acquisition device
[AIAA PAPER 83-1380] p 55 A83-36371
PROPELLANT TESTS
Process and quality verification controls for solid propellant manufacturing p 98 A83-39270
PROPELLER BLADES
Tensile buckling of advanced turboprops
[AIAA PAPER 82-0776] p 154 A83-10900
Flutter analysis of advanced turbopropellers
[AIAA 83-0846] p 157 A83-29824
An experience in mesh generation for three-dimensional calculation of potential flow around a rotating propeller p 5 A83-38798
Bending-torsion flutter of a highly swept advanced turboprop
[NASA-TM-82975] p 158 N83-11514
Noise of the 10-bladed, 40 deg swept SR-6 propeller in a wind tunnel
[NASA-TM-82950] p 196 N83-11840
Farfield inflight measurement of high-speed turboprop noise
[NASA-TM-83327] p 199 N83-21895
A preliminary comparison between the SR-6 propeller noise in flight and in a wind tunnel
[NASA-TM-83341] p 201 N83-24287
PROPELLER EFFICIENCY
The development of a generalized advanced propeller analysis system
[AIAA PAPER 83-2466] p 26 A83-49581
PROPELLERS
An analytical and experimental comparison of the flow field of an advanced swept turboprop
[AIAA PAPER 83-0189] p 3 A83-21080
Prediction of high speed propeller flow fields using a three-dimensional Euler analysis
[AIAA PAPER 83-0188] p 4 A83-29535
Finite volume calculation of three-dimensional potential flow around a propeller p 7 A83-45577
Noise of the 10-bladed, 40 deg swept SR-6 propeller in a wind tunnel
[NASA-TM-82950] p 196 N83-11840
Large displacements and stability analysis of nonlinear propeller structures p 159 N83-12460
An analytical and experimental comparison of the flow field of an advanced swept turboprop
[NASA-TM-83037] p 1 N83-14061
Prediction of high speed propeller flow fields using a three-dimensional Euler analysis
[NASA-TM-83065] p 12 N83-19710
New test techniques and analytical procedures for understanding the behavior of advanced propellers
[NASA-TM-83360] p 2 N83-22092
Noise of the 10-bladed 60 deg swept SR-5 propeller in a wind tunnel
[NASA-TM-83054] p 200 N83-23112
Small transport aircraft technology propeller study
[NASA-CR-168045] p 14 N83-29178
Propeller performance and weight predictions appended to the Navy/NASA engine program
[NASA-TM-83458] p 41 N83-32810
PROPULSION
QCSEE under-the-wing engine-wing-flap aerodynamic profile characteristics
[NASA-TM-82890] p 28 N83-12092
The structural response of a rail accelerator
[NASA-TM-83491] p 163 N83-35412
PROPULSION SYSTEM CONFIGURATIONS
The design and technology development for A 150 mlb resistojet for H2 or NH3
[AIAA PAPER 82-1949] p 52 A83-12506
Advanced propfan engine characteristics and technology needs
[AIAA PAPER 83-1155] p 23 A83-36250
Advanced propulsion concepts for orbital transfer vehicles
[AIAA PAPER 83-1243] p 56 A83-45513
Analysis, design, fabrication and testing of an optical tip clearance sensor --- turbocompressor blade tips
[NASA-CR-165265] p 26 N83-11127
Research and technology, Lewis Research Center
[NASA-TM-83036] p 208 N83-15169
Fuels research studies at NASA Lewis
[NASA-TM-83003] p 100 N83-19921
Support and power plant documentation for the gas turbine powered bus demonstration program
[NASA-CR-165527] p 210 N83-20829
Energy efficient engine component development and integration program
[NASA-CR-170089] p 34 N83-22204
Advanced hybrid vehicle propulsion system study
[NASA-CR-159773] p 211 N83-24432
NASA propulsion controls research
[NASA-TM-83343] p 36 N83-25711
Large space systems auxiliary propulsion requirements p 46 N83-26864
Advanced propulsion concepts for orbital transfer vehicles
[NASA-TM-83419] p 59 N83-26924
Nacelle Aerodynamic and Inertial Loads (NAIL) project
[NASA-CR-168712] p 18 N83-30402
V/STOL propulsion control analysis: Phase 2, task 5-9
[NASA-CR-165523] p 40 N83-32804
Rotorcraft convertible engine study
[NASA-CR-168241] p 42 N83-34944
PROPULSION SYSTEM PERFORMANCE
On-orbit propulsion requirements and performance assessment of ion propulsion subsystems for future GEO large satellite missions
[AIAA PAPER 82-1872] p 48 A83-12460
Status of the J-series 30-cm mercury ion thruster
[AIAA PAPER 82-1904] p 51 A83-12479
Development of a large inert gas ion thruster
[AIAA PAPER 82-1927] p 52 A83-12496
Electric rail gun projectile acceleration to high velocity
[AIAA PAPER 82-1939] p 52 A83-12501
Qualification test results of IAPS 8 cm ion thrusters
[AIAA PAPER 82-1954] p 52 A83-12511
Extended-performance 8-cm ion thruster operation
[AIAA PAPER 82-1955] p 53 A83-12512
Fiberoptics technology and its application to propulsion control systems
[AIAA PAPER 83-0534] p 18 A83-16772
Scale model performance test investigation of mixed flow exhaust systems for an energy efficient engine /E3/ propulsion system
[AIAA PAPER 83-0541] p 20 A83-16776
Inert gas thruster technology p 53 A83-20423
Effect of variable guide vanes on the performance of a high-bypass turbofan engine p 20 A83-24028
Propulsion and fluid management - Station keeping will eat energy on a new scale p 54 A83-24360
A summary of EHV propulsion technology --- Electric and Hybrid Vehicle p 209 A83-31087
Characterization of advanced electric propulsion systems p 55 A83-33744
Ejector nozzle test results at simulated flight conditions for an advanced supersonic transport propulsion system
[AIAA PAPER 83-1287] p 23 A83-36323
Advanced LOX/H2 engine technologies for future OTVs
[AIAA PAPER 83-1312] p 55 A83-36333
Simplified power processing for ion-thruster subsystems
[AIAA PAPER 83-1394] p 55 A83-36384
JT9D performance deterioration results from a simulated aerodynamic load test p 25 A83-41040
Analysis, design, fabrication and testing of an optical tip clearance sensor --- turbocompressor blade tips
[NASA-CR-165265] p 26 N83-11127
Energy efficient engine. Flight propulsion system preliminary analysis and design
[NASA-CR-159859] p 28 N83-12094
Fiberoptics technology and its application to propulsion control systems
[NASA-TM-83009] p 18 N83-15302
Implementation of R & QA practices in Research and Development programs
[NASA-TM-82997] p 210 N83-19651
Fuels research studies at NASA Lewis
[NASA-TM-83003] p 100 N83-19921
Advanced hybrid vehicle propulsion system study
[NASA-CR-159773] p 211 N83-24432
Electrothermal thruster diagnostics. Volume 1: Executive summary
[NASA-CR-168174-VOL-1] p 60 N83-33942
Electrothermal thruster diagnostics. Volume 2: Technical
[NASA-CR-168174-VOL-2] p 60 N83-33943
PROPULSIVE EFFICIENCY
Inert gas test of two 12-cm magnetostatic thrusters
[AIAA PAPER 82-1925] p 51 A83-12494
Extended performance 8-cm mercury ion thruster
[AIAA PAPER 82-1913] p 53 A83-21078

Improved ion containment using a ring-cusp ion thruster
[AIAA PAPER 82-1928] p 53 A83-21100
Improved ion containment using a ring-cusp ion thruster
[NASA-TM-82990] p 56 N83-13164
Extended performance 8-cm mercury ion thruster
[NASA-TM-83029] p 57 N83-14157
Energy efficient engine component development and integration program
[NASA-CR-170089] p 34 N83-22204
Tests of an alternating current propulsion subsystem for electric vehicles on a road load simulator
[NASA-TM-83036] p 178 N83-22749

PROSTHETIC DEVICES
Tribological measurements on a Charnley-type artificial hip joint
[NASA-TM-83440] p 97 N83-32943

PROTECTIVE COATINGS
Sputtered silicon nitride coatings for wear protection p 88 A83-12651
Some properties of r.f.-sputtered hafnium nitride coatings p 88 A83-12653
Coating with overlay metallic-cermet alloy systems
[NASA-CASE-LEW-13639-2] p 82 N83-17683
Improved nickel base coating alloy --- oxidation resistant coatings
[NASA-CASE-LEW-13834-1] p 85 N83-24639
Processing of fused silicide coatings for carbon-based materials
[NASA-TM-83362] p 95 N83-27019
Curved film cooling admission tube
[NASA-CASE-LEW-13174-1] p 131 N83-27144
Silicon-slurry/aluminide coating --- protecting gas turbine engine vanes and blades
[NASA-CASE-LEW-13343] p 86 N83-31795
Covering solid, film cooled surfaces with a duplex thermal barrier coating
[NASA-CASE-LEW-13450-1] p 103 N83-35177

PROTON MAGNETIC RESONANCE
A carbon-13 and proton nuclear magnetic resonance study of some experimental referee broadened-specification /ERBS/ turbine fuels p 98 A83-11482

PULSE COMMUNICATION
Modulation techniques
[NASA-CR-169460] p 105 N83-10329

PULSE DURATION MODULATION
Transistorized PWM inverter-induction motor drive system p 110 A83-11488

PUMP SEALS
Investigation of the effects of initial fluid film profile on pumping ring operation
[ASME PAPER 82-LUB-35] p 136 A83-13516
Thermoelastohydrodynamic analysis of an oil pumping ring seal p 137 A83-22322
High speed cryogenic self-acting, shaft seals for liquid rocket turbopumps
[NASA-CR-168194] p 151 N83-32070
Comparative evaluation of three shaft seals proposed for high performance turbomachinery
[NASA-TM-83021] p 152 N83-34325

PUMPS
DOE and AID stand-alone photovoltaic activities
[NASA-TM-83374] p 180 N83-25041

PURITY
High purity, low dislocation GaAs single crystals
[NASA-CR-168098] p 206 N83-19622

PYROELECTRICITY
Piezoelectric and pyroelectric coefficients for ferroelectric crystals with polarizable molecules p 205 A83-17227
Piezoelectricity and pyroelectricity in polyvinylidene fluoride - Influence of the lattice structure p 205 A83-29531

PYROLYSIS
Soot formation in pyrolysis of acetylene, allene and 1,3-butadiene p 69 A83-39274

PYROLYTIC GRAPHITE
Ion sputter textured graphite --- anode collector plates in electron tube devices
[NASA-CASE-LEW-12919-1] p 63 N83-10117

PYROLYTIC MATERIALS
Research into the use of pyrolytic oxides and polymers for the fabrication of thin film high energy capacitors
[NASA-CR-173012] p 97 N83-34045

Q

QUALITY CONTROL
Process and quality verification controls for solid propellant manufacturing p 98 A83-39270

QUANTITATIVE ANALYSIS
O-18 tracer studies of Al2O3 scale formation on NiCrAl alloys p 74 A83-10249

QUANTUM EFFICIENCY
Use of column V alkyls in organometallic vapor phase epitaxy (OMVPE) p 70 A83-46608

QUIET ENGINE PROGRAM
Alternatives for jet engine control
[NASA-CR-170100] p 33 N83-20945

R

RADAR TRANSMISSION
Design of a multistage depressed collector for the F-16 radar dual mode transmitter tube
[NASA-TM-82982] p 114 N83-14399

RADIAL DISTRIBUTION
EL2 distributions in doped and undoped liquid encapsulated Czochralski GaAs --- deep donor concentration p 205 A83-22756
Analytical and experimental study of flow through an axial turbine stage with a nonuniform inlet radial temperature profile
[AIAA PAPER 83-1175] p 6 A83-45510
Analytical and experimental study of flow through an axial turbine stage with a nonuniform inlet radial temperature profile
[NASA-TM-83431] p 14 N83-27958
Analysis of an externally radially cracked ring segment subject to three-point radial loading
[NASA-TM-83482] p 163 N83-35413

RADIAL FLOW
Three-dimensional flow measurements in a turbine scroll
[ASME PAPER 83-GT-128] p 8 A83-47957
Computer code for off-design performance analysis of radial-inflow turbines with rotor blade sweep
[NASA-TP-2199] p 40 N83-32807
Current and future technology in radial and axial gas turbines
[NASA-TM-83414] p 41 N83-32811

RADIANCE
Atmospheric radiation model for water surfaces
[NASA-CR-167873] p 187 N83-21677

RADIANT FLUX DENSITY
Flame radiation measurements p 73 N83-29228

RADIANT HEATING
Radiation energy receiver for laser and solar propulsion systems
[AIAA PAPER 83-1207] p 55 A83-36281

RADIATION DAMAGE
Radiation damage in front and back illuminated high resistivity silicon solar cells
[NASA-TM-82965] p 206 N83-10962
Effects of processing and dopant on radiation damage removal in silicon solar cells p 170 N83-14708
Radiation damage and annealing in large area n+/p/p+ GaAs shallow homojunction solar cells p 172 N83-15826
Radiation damage p 172 N83-15837
Use of high L.E.T. radiation to improve adhesion of metals to polytetrafluoroethylene
[NASA-TM-83413] p 96 N83-30660

RADIATION DISTRIBUTION
A theoretical investigation of the sound radiation fields associated with a Bellmouth inlet
[AIAA PAPER 83-0710] p 193 A83-25926
Prediction of sound radiation from different practical jet engine inlets
[NASA-CR-169533] p 197 N83-13936

RADIATION MEASUREMENT
Solar cell measurements p 181 N83-25109

RADIATIVE TRANSFER
Atmospheric radiation model for water surfaces
[NASA-CR-167873] p 187 N83-21677

RADIO COMMUNICATION
Satellite-aided land mobile communications system implementation considerations p 104 A83-41417
Non-urban mobile radio market demand forecast
[NASA-CR-168065] p 107 N83-28297
Mobile radio alternative systems study, executive summary
[NASA-CR-168207] p 109 N83-34119

RADIO FREQUENCIES
Advanced communications satellite systems p 47 A83-49855
NASA's Advanced Communications Technology Satellite (ACTS)
[NASA-TM-83416] p 48 N83-35004

RADIO FREQUENCY DISCHARGE
Performance characteristics of a microwave plasma disk ion source --- time varying electric propulsion concept
[AIAA PAPER 82-1935] p 55 A83-27350

RADIO FREQUENCY HEATING
Gyrotron transmitting tube
[NASA-CASE-LEW-13429-1] p 117 N83-31952

RADIO FREQUENCY INTERFERENCE
Engineering calculations for communications systems planning
[NASA-CR-170182] p 106 N83-22494

RADIO SPECTRA
Requirements for a mobile communications satellite system. Volume 2: Technical report
[NASA-CR-168129] p 107 N83-23498

RADIO TRANSMISSION
Mobile radio alternative systems study, executive summary
[NASA-CR-168207] p 109 N83-34119

RADIO WAVES
The phototron: A light to RF energy conversion device p 173 N83-15866

RADIOTELEPHONES
Non-urban mobile radio market demand forecast
[NASA-CR-168065] p 107 N83-28297

RAILGUN ACCELERATORS
Electric rail gun projectile acceleration to high velocity
[AIAA PAPER 82-1939] p 52 A83-12501
Characterization of advanced electric propulsion systems p 55 A83-33744
The LeRC rail accelerators: Test designs and diagnostic techniques
[NASA-TM-83496] p 60 N83-35053
The structural response of a rail accelerator
[NASA-TM-83491] p 163 N83-35412

RAINBOWS
Rainbow Schlieren
[NASA-TP-2166] p 135 N83-33126

RANDOM VARIABLES
Application of advanced reliability methods to local strain fatigue analysis
[NASA-CR-168198] p 161 N83-29734

RANDOM VIBRATION
Solution to the backward-Kolmogorov equation for a nonstationary oscillation problem p 192 A83-15697

RANDOM WALK
Numerical solution of the problem of flame propagation by the use of the random element method
[AIAA PAPER 83-0600] p 69 A83-36062

RANKINE CYCLE
Power generation from nuclear reactors in aerospace applications
[NASA-TM-83342] p 59 N83-30516

RARE GASES
Inert gas test of two 12-cm magnetostatic thrusters
[AIAA PAPER 82-1925] p 51 A83-12494
Development of a large inert gas ion thruster
[AIAA PAPER 82-1927] p 52 A83-12496
Inert gas thruster technology p 53 A83-20423
Operation of the J-series thruster using inert gas
[AIAA PAPER 82-1929] p 54 A83-26625
Operation of the J-series thruster using inert gas
[NASA-TM-82977] p 57 N83-17587

RATES (PER TIME)
A comprehensive analysis of cavitation and liquid impingement erosion data
[NASA-TM-83352] p 84 N83-24634
Kinetics of copper ion absorption by cross-linked calcium polyacrylate membranes
[NASA-TM-83052] p 61 N83-25786

RATIOS
Evaluation of a high performance, fixed-ratio, traction drive p 145 N83-20135

RAYLEIGH SCATTERING
High speed cryogenic self-acting, shaft seals for liquid rocket turbopumps
[NASA-CR-168194] p 151 N83-32070

REACTION BONDING
Injection molding ceramics to high green densities p 137 A83-33515
The effect of silicon particle size on the nitriding behaviour of reaction bonded Si3N4 compacts p 90 A83-48261
Sintering of reaction bonded silicon nitride p 90 A83-48270

REACTION KINETICS
Experimental study of electrochemical fluorination of trichloroethylene p 60 A83-15870
Mechanism of hot corrosion of IN-738
[NASA-CR-169706] p 81 N83-15411
Laser fluorescence studies of the chemical interactions of sodium species with sulfur bearing fuels
[NASA-CR-169861] p 71 N83-17625
Oxidation and formation of deposit precursors in hydrocarbon fuels
[NASA-CR-168121] p 101 N83-23465
Kinetics of copper ion absorption by cross-linked calcium polyacrylate membranes
[NASA-TM-83052] p 61 N83-25786
Combustion Fundamentals Research
[NASA-CP-2268] p 38 N83-29208

Nonlinear Constitutive Relations for High Temperature Applications
[NASA-CP-2271] p 161 N83-34351
Reaction of cobalt in SO2 atmospheric at elevated temperatures
[NASA-TM-83485] p 88 N83-35104
A review of liquid lubricant thermal/oxidative degradation
[NASA-TM-83465] p 98 N83-35143

REACTION PRODUCTS
Thermodynamics of the potassium-sulfur-oxygen and related systems
[NASA-CR-168155] p 61 N83-28077

REACTIVITY
Surface profile changes of scuffed bearing surfaces --- before and after acid treatment
[NASA-TM-83055] p 82 N83-17682

REACTOR DESIGN
Thermionic technology infrastructure for space power p 54 A83-27298

REAL GASES
Transient flow analysis of the AEDC/HPDE MHD generator
[AIAA PAPER 83-0395] p 203 A83-16691

REAL TIME OPERATION
Design of a high-speed digital processing element for parallel simulation
[NASA-TM-83373] p 117 N83-29597

RECIRCULATIVE FLUID FLOW
Turbulence measurements in a swirling confined jet flowfield using a triple hot-wire probe
[NASA-CR-169668] p 127 N83-14434

RECOMBINATION REACTIONS
Free radical propulsion concept p 53 A83-13141

RECTANGLES
Elastohydrodynamic lubrication of rectangular contacts
[NASA-TP-2111] p 143 N83-16759

RECTANGULAR PLANFORMS
Vibrations of cantilevered circular cylindrical shells Shallow versus deep shell theory p 157 A83-36958

REDOX CELLS
Design flexibility of redox flow systems --- for energy storage applications p 164 A83-27177
Electromagnetic studies of redox systems for energy storage
[NASA-CR-169593] p 169 N83-14667
The NASA Redox Storage System Development project, 1980
[NASA-TM-82940] p 169 N83-14683
Study to establish cost predictions for the production of Redox chemicals
[NASA-CR-167882] p 176 N83-20359
Optimization and fabrication of porous carbon electrodes for Fe/Cr redox flow cells
[NASA-CR-167921] p 179 N83-23708
Single cell performance studies on the Fe/Cr Redox Energy Storage System using mixed reactant solutions at elevated temperature
[NASA-TM-83385] p 180 N83-25042
NASA redox storage system development project
[NASA-TM-83087] p 181 N83-26252
Zirconium carbide as an electrocatalyst for the chromous-chromic redox couple
[NASA-CASE-LEW-13246-1] p 182 N83-27344
An electrochemical rebalance cell for Redox systems
[NASA-TM-83363] p 73 N83-29326
NASA Redox Project status summary
[NASA-TM-83401] p 183 N83-29810
Analysis of the visible spectra of concentrated chromic chloride solutions
[NASA-CR-172998] p 74 N83-32870
Spectrophotometric analysis of aqueous mixtures of some chromium (III) complexes
[NASA-CR-172999] p 74 N83-32872

REDUCED GRAVITY
An experimental study of heat induced surface-tension driven flow p 44 A83-43269

REFERENCE SYSTEMS
Solar cell measurements p 181 N83-25109

REFINING
Fuel quality/processing study. Volume 3: Fuel upgrading studies
[NASA-CR-165326-VOL-3] p 178 N83-22754

REFLECTORS
Solar cell having improved back surface reflector
[NASA-CASE-LEW-13620-1] p 168 N83-13579
Phased array-fed antenna configuration study: Technology assessment
[NASA-CR-168078] p 106 N83-22495
Phased array-fed antenna configuration study
[NASA-CR-168077] p 107 N83-27086

REFRACTIVITY
Some properties of r.f.-sputtered hafnium nitride coatings p 88 A83-12653
Rainbow Schlieren
[NASA-TP-2166] p 135 N83-33126

REFRACTORY COATINGS
Plasma deposition and surface modification techniques for wear resistance
[NASA-TM-82972] p 90 N83-10194

REFRACTORY MATERIALS
Research on ultra-high-temperature materials, monolithic ceramics, ceramic matrix composites and carbon/carbon composites p 64 N83-12161
PMR polyimide composites for aerospace applications
[NASA-TM-83047] p 65 N83-15364
Overview of high-temperature materials for high-energy space power systems p 173 N83-15869

REFRIGERATING
A refrigerated dynamic seal
[NASA-TM-83378] p 130 N83-24798
Magnetic heat pumping
[NASA-CASE-LEW-12508-3] p 131 N83-29625

REFRIGERATORS
DOE and AID stand-alone photovoltaic activities
[NASA-TM-83374] p 180 N83-25041

REGENERATIVE FUEL CELLS
Alkaline regenerative fuel cell energy storage system for manned orbital satellites p 54 A83-27206
Study to establish cost predictions for the production of Redox chemicals
[NASA-CR-167882] p 176 N83-20359

REGENERATORS
Magnetic heat pumping
[NASA-CASE-LEW-12508-3] p 131 N83-29625
Advanced Gas Turbine (AGT) powertrain system development for automotive applications
[NASA-CR-167901] p 212 N83-33800

REGRESSION ANALYSIS
Computer program to minimize prediction error in models from experiments with 16 hypercube points and 0 to 6 center points
[NASA-TM-82995] p 192 N83-21872
Regression analysis of traction characteristics of traction fluids
[NASA-TP-2154] p 148 N83-24862

REGRESSION COEFFICIENTS
Traction behavior of two traction lubricants
[NASA-TM-83311] p 144 N83-20116

REINFORCED PLATES
Three-dimensional finite-element analysis of layered composite plates p 156 A83-27432

REINFORCED SHELLS
Geometrically nonlinear analysis of layered composite shells p 156 A83-27431

REISSNER THEORY
A new formulation of hybrid/mixed finite element p 155 A83-12739
Alternative ways for formulation of hybrid stress elements p 155 A83-14710

RELIABILITY
Research priorities for advanced fibrous composites
[NASA-CR-165414] p 65 N83-18853

RELIABILITY ANALYSIS
Life and reliability models for helicopter transmissions
[NASA-TM-82976] p 139 N83-10425
Design, fabrication and testing of porous tungsten vaporizers for mercury ion thrusters
[NASA-TM-83063] p 58 N83-22318
Analysis of strain gage reliability in F-100 jet engine testing at NASA Lewis Research Center
[NASA-TM-83325] p 134 N83-24829
Statistical summaries of fatigue data for design purposes
[NASA-CR-3697] p 161 N83-29731
Application of advanced reliability methods to local strain fatigue analysis
[NASA-CR-168198] p 161 N83-29734

RELIABILITY ENGINEERING
Demonstration and evaluation of gas turbine transit buses
[NASA-CR-165528] p 212 N83-27926

RELIEF VALVES
Ion beam sputter-etched ventricular catheter for hydrocephalus shunt
[NASA-CASE-LEW-13107-1] p 188 N83-21785

REMOTE CONTROL
Kilovolt dc solid state remote power controller development
[NASA-CR-168041] p 115 N83-21236

RENE 95
Powder metallurgy Rene 95 rotating turbine engine parts, volume 2
[NASA-CR-165141] p 82 N83-15412

REPEATERS
Packet communication system for a multi-beam beam switched satellite repeater p 104 A83-41336

REQUIREMENTS
Requirements for a mobile communications satellite system. Volume 1: Executive summary
[NASA-CR-168128] p 106 N83-23497

RESEARCH AIRCRAFT
Supersonic STOVL research aircraft
[SAE PAPER 821375] p 17 A83-37965

RESEARCH AND DEVELOPMENT
Development of a large inert gas ion thruster
[AIAA PAPER 82-1927] p 52 A83-12496
Electric propulsion research and technology in the United States
[AIAA PAPER 82-1867] p 53 A83-16925
The NASA Lewis large wind turbine program p 174 N83-15911
NASA transmission research and its probable effects on helicopter transmission design
[NASA-TM-83389] p 148 N83-24858
Considerations of technology transfer barriers in the modification of strategic superalloys for aircraft turbine engines
[NASA-TM-83395] p 86 N83-29360

RESEARCH MANAGEMENT
Bibliography of Lewis Research Center technical publications announced in 1982
[NASA-TM-83335] p 208 N83-29124

RESIN MATRIX COMPOSITES
Resin selection criteria for tough composite structures
[AIAA 83-0801] p 89 A83-29734
Improved high temperature resistant polyimides
[NASA-CASE-LEW-13864-1] p 93 N83-17715
Imide modified epoxy matrix resins
[NASA-CR-167942] p 93 N83-18909

RESINS
Resin selection criteria for tough composite structures
[AIAA 83-0801] p 89 A83-29734
Polyvinyl alcohol cross-linked with two aldehydes
[NASA-CASE-LEW-13504-1] p 71 N83-13188

RESISTOJET ENGINES
The design and technology development for A 150 mlb resistojet for H2 or NH3
[AIAA PAPER 82-1949] p 52 A83-12506

RESONANCE
A review of resonance response in large, horizontal-axis wind turbines p 163 A83-13696
Transformer induced instability of the series resonant converter p 113 A83-41152
Effects of specimen resonances on acoustic-ultrasonic testing
[NASA-CR-3679] p 153 N83-21373

RESONANT FREQUENCIES
A review of resonance response in large, horizontal-axis wind turbines p 163 A83-13696
Natural frequency of rotating beams using non-rotating modes p 156 A83-18383

RESONANT VIBRATION
Variable force, eddy-current or magnetic damper
[NASA-CASE-LEW-13717-1] p 159 N83-20284

RESOURCE ALLOCATION
Comparison of channel assignment techniques for hybrid switching p 104 A83-41363

REUSABLE ROCKET ENGINES
The performance and application of high speed long life LH2 hybrid bearings for reusable rocket engine turbomachinery
[AIAA PAPER 83-1389] p 138 A83-36379

REVERSED FLOW
Effect of broad properties fuel on injector performance in a reverse flow combustor
[AIAA PAPER 83-0154] p 20 A83-21079
Application of 3D aerodynamic/combustion model to combustor primary zone study
[AIAA PAPER 83-1265] p 23 A83-36316
Effect of broad properties fuel on injector performance in a reverse flow combustor
[NASA-TM-83013] p 29 N83-13101

REYNOLDS EQUATION
Surface roughness effects in hydrodynamic lubrication: The flow factor method
[NASA-TM-83024] p 129 N83-19016

REYNOLDS NUMBER
Turbulence effect on crossflow around a circular cylinder at subcritical Reynolds numbers
[NASA-CR-3622] p 127 N83-13387
Effect of steady-state pressure distortion on inlet flow to a high-bypass-ratio turbofan engine
[NASA-TM-82964] p 30 N83-15306
Geometry and starvation effects in hydrodynamic lubrication p 141 N83-15522

REYNOLDS STRESS
A turbulence model for three dimensional turbulent shear flows over curved rotating bodies
[AIAA PAPER 83-0559] p 120 A83-16787
Implicit marching solution of compressible viscous subsonic flow in planar and axisymmetric ducts
[NASA-TM-82976] p 125 N83-10389

RHEOLOGY
Traction calculations and design data for two traction fluids p 145 N83-20136

RIBS (SUPPORTS)
Auxiliary propulsion requirements for large space systems
[AIAA PAPER 83-1217] p 56 A83-45512
Auxiliary propulsion requirements for large space systems
[NASA-TM-83388] p 58 N83-26922
RING STRUCTURES
Investigation of the effects of initial fluid film profile on pumping ring operation
[ASME PAPER 82-LUB-35] p 136 A83-13516
Stress intensity and displacement coefficients for radially cracked ring segments subject to three-point bending
[NASA-TM-83059] p 160 N83-24874
Analysis of an externally radially cracked ring segment subject to three-point radial loading
[NASA-TM-83482] p 163 N83-35413
RITZ AVERAGING METHOD
Vibrations of cantilevered doubly-curved shallow shells p 157 A83-39557
ROADS
Comparison of road load simulator test results with track tests on electric vehicle propulsion system
[NASA-TM-83393] p 184 N83-29811
ROCKET ENGINE DESIGN
Status of the J-series 30-cm mercury ion thruster
[AIAA PAPER 82-1904] p 51 A83-12479
Advanced-technology 30-cm-diameter mercury ion thruster
[AIAA PAPER 82-1910] p 51 A83-12484
Development of a large inert gas ion thruster
[AIAA PAPER 82-1927] p 52 A83-12496
Qualification test results of IAPS 8 cm ion thrusters
[AIAA PAPER 82-1954] p 52 A83-12511
Extended-performance 8-cm ion thruster operation
[AIAA PAPER 82-1955] p 53 A83-12512
Inert gas thruster technology p 53 A83-20423
Simplified power processing for ion-thruster subsystems p 56 A83-39271
ROCKET ENGINES
Microwave plasma generation of hydrogen atoms for rocket propulsion p 53 A83-13090
Study for analysis of benefit versus cost of low thrust propulsion system
[NASA-CR-168011] p 57 N83-21002
Evaluation of the use of on-board spacecraft energy storage for electric propulsion missions
[NASA-CR-168209] p 59 N83-32842
ROCKET PROPELLANTS
Radiation energy receiver for laser and solar propulsion systems
[AIAA PAPER 83-1207] p 55 A83-36281
Deposit formation in hydrocarbon rocket fuels: Executive summary
[NASA-CR-165492] p 102 N83-35159
RODS
Specimen size and geometry effects on fracture toughness of Al2O3 measured with short rod and short bar chevron-notch specimens
[NASA-TM-83319] p 94 N83-19902
ROLLER BEARINGS
Advances in high-speed rolling-element bearings --- for aircraft engine and transmission application p 137 A83-22319
Design of an advanced 500-HP helicopter transmission p 21 A83-24834
Bearing fatigue investigation 3
[NASA-CR-168029] p 143 N83-17880
Advanced Power Transmission Technology
[NASA-CP-2210] p 144 N83-20119
Present technology of rolling-element bearings p 144 N83-20121
Predicted and experimental performance of large-bore high-speed ball and roller bearings p 145 N83-20131
High speed spherical roller-bearing analysis and comparison with experimental performance p 145 N83-20133
Large-bore tapered-roller bearing performance and endurance to 2.4 million DN p 145 N83-20134
Sizing criterial for traction drives p 146 N83-20137
Rolling-element bearings
[NASA-RP-1105] p 149 N83-27214
Energy efficient engine. Core engine bearings, drives and configuration: Detailed design report
[NASA-CR-165376] p 39 N83-30430
Effect of carbide distribution on rolling-element fatigue life of AMS 5749
[NASA-TP-2189] p 151 N83-33166
ROLLING CONTACT LOADS
Finite element analysis of steadily moving contact fields p 158 A83-49437
Rolling-element fatigue life with traction fluids and automatic transmission fluid in a high-speed rolling-contact rig
[NASA-TP-2050] p 140 N83-13457
ROOM TEMPERATURE
Friction and wear of iron and nickel in sodium hydroxide solutions p 77 A83-48922
Friction and wear of iron and nickel in sodium hydroxide solutions
[NASA-TM-82935] p 77 N83-10171
ROTARY STABILITY
Some analysis methods for rotating systems with periodic coefficients p 157 A83-32987
Labyrinth seal forces on a whirling rotor
[NASA-CR-168016] p 34 N83-22198
ROTARY WING AIRCRAFT
Experimental program for the evaluation of turbofan/turboshaft c conversion technology
[NASA-TM-82988] p 27 N83-11130
Rotorcraft convertible engines for the 1980s
[NASA-TM-83008] p 28 N83-12091
Large rotorcraft transmission technology development program
[NASA-CR-168120] p 18 N83-22188
Rotorcraft convertible engine study
[NASA-CR-168161] p 37 N83-27996
Rotorcraft convertible engine study
[NASA-CR-168241] p 42 N83-34944
ROTARY WINGS
Rotorcraft convertible engine study
[NASA-CR-168241] p 42 N83-34944
ROTATING BODIES
Extending the laser-specklegram technique to strain analysis of rotating components p 155 A83-12514
A turbulence model for three dimensional turbulent shear flows over curved rotating bodies
[AIAA PAPER 83-0559] p 120 A83-16787
Natural frequency of rotating beams using non-rotating modes p 156 A83-18383
Manual for extending the laser specklegram technique to strain analysis of rotating components
[NASA-CR-167932] p 134 N83-15601
Design study of a high power rotary transformer
[NASA-CR-168012] p 115 N83-16630
Vibration in planetary gear systems with unequal planet stiffnesses
[NASA-TM-83428] p 150 N83-29709
ROTATING CYLINDERS
Computer program for a four-cylinder-Stirling-engine controls simulation
[NASA-TM-82774] p 126 N83-12359
A detailed treatment of two-dimensional, starved lubrication in the vicinity of two counter-rotating cylinders p 141 N83-15520
ROTATING DISKS
The initial stages of cavitation damage and erosion on copper and brass tested in a rotating disk device p 75 A83-27421
Dynamics and mechanism of cavitation erosion on perspex and epoxy resin tested in a rotating disk device p 89 A83-27422
Structural dynamics studies of rotating bladed-disk assemblies coupled with flexible shaft motions
[AIAA PAPER 83-0919] p 22 A83-32787
Cavitation erosion characteristics of poly(methyl methacrylate) in a rotating disk device p 90 A83-41851
Dynamics and mechanism of cavitation erosion on perspex and epoxy resins tested in a rotating disk device
[NASA-TM-82952] p 91 N83-11329
Initial stages of cavitation damage and erosion on copper and brass tested in a rotating disk device
[NASA-TM-82993] p 81 N83-13231
Powder metallurgy Rene 95 rotating turbine engine parts, volume 2
[NASA-CR-165141] p 82 N83-15412
A comprehensive analysis of cavitation and liquid impingement erosion data
[NASA-TM-83352] p 84 N83-24634
ROTATING FLUIDS
A viscous-inviscid interactive procedure for rotational flow in cascades of two-dimensional airfoils of arbitrary shape
[AIAA PAPER 83-0256] p 3 A83-16614
ROTATING GENERATORS
A mathematical model for the doubly fed wound rotor generator
[NASA-TM-83454] p 117 N83-34192
ROTATING SHAFTS
An experimental investigation of the vaporous/gaseous cavity characteristics of an eccentric journal bearing
[ASLE PREPRINT 82-LC-3A-1] p 136 A83-13230
Experimental investigation of the vaporous/gaseous cavity characteristics of an eccentric journal bearing
[NASA-TM-82996] p 128 N83-17833
Multiple plate hydrostatic viscous damper
[NASA-CASE-LEW-13445-2] p 143 N83-17883
Development of a rotary instrumentation system, phase 2
[NASA-CR-168013] p 47 N83-18835
Variable force, eddy-current or magnetic damper
[NASA-CASE-LEW-13717-1] p 159 N83-20284
ROTATING STALLS
A theory of rotating stall of multistage axial compressors. I - Small disturbances
[ASME PAPER 83-GT-44] p 7 A83-47904
A theory of rotating stall of multistage axial compressors. II - Finite disturbances
[ASME PAPER 83-GT-45] p 8 A83-47905
A theory of rotating stall of multistage axial compressors. III - Limit cycles
[ASME PAPER 83-GT-46] p 8 A83-47906
ROTATION
Sizing criterial for traction drives p 146 N83-20137
ROTOR AERODYNAMICS
Rotor wake characteristics relevant to rotor-stator interaction noise generation p 19 A83-10184
Development of secondary flow and vorticity in curved ducts, cascades, and rotors, including effects of viscosity and rotation p 119 A83-16141
Blade loading and rotation effects on compressor rotor wake near end walls p 3 A83-22138
Flutter and forced response of mistuned rotors using standing wave analysis
[AIAA 83-0845] p 156 A83-29823
Cold-air performance of compressor-drive turbine of Department of Energy upgraded automobile gas turbine engine. 2: Stage performance
[NASA-TM-82818] p 9 N83-11063
Incidence loss for fan turbine rotor blade in two-dimensional cascade
[NASA-TP-2188] p 39 N83-30431
T55 power turbine rotor multiplane-multispeed balancing study
[NASA-CR-167891] p 41 N83-33894
ROTOR BLADES
Investigation of the tip clearance flow inside and at the exit of a compressor rotor passage. II - Turbulence properties p 4 A83-28843
Tip clearance flow in a compressor rotor passage at design and off-design conditions p 4 A83-35855
ROTOR BLADES (TURBOMACHINERY)
Wind tunnel measurements of blade/vane ratio and spacing effects on fan noise p 192 A83-15317
Blade loading and rotation effects on compressor rotor wake near end walls p 3 A83-22138
Experimental study of the boundary layer on a turbomachinery rotor blade p 7 A83-47022
Measurements of self-excited rotor-blade vibrations using optical dispacements
[NASA-TM-82953] p 159 N83-14523
Advanced Gas Turbine (AGT) power-train system development
[NASA-CR-167875] p 142 N83-15627
Three dimensional flow field inside compressor rotor, including blade boundary layers
[NASA-CR-169788] p 128 N83-16679
Multiple plate hydrostatic viscous damper
[NASA-CASE-LEW-13445-2] p 143 N83-17883
Large Horizontal-Axis Wind Turbines
[NASA-CP-2230] p 175 N83-19231
The response of a 38m horizontal axis teetered rotor to yaw p 175 N83-19232
Fixed pitch rotor performance of large horizontal axis wind turbines p 175 N83-19233
Stall induced instability of a teetered rotor p 175 N83-19234
Free yaw performance of the Mod-0 large horizontal axis 100 kW wind turbine p 175 N83-19235
Structural fatigue test results for large wind turbine blade [illegible] p 159 N83-19246
Structural qualification testing and operational loading on a fiberglass rotor blade for the Mod-OA wind turbine
[NASA-TM-83309] p 179 N83-23710
End wall flow characteristics and overall performance of an axial flow compressor stage
[NASA-CR-3671] p 13 N83-26819
Residual stress in plasma sprayed ceramic turbine tip and gas path seal specimens
[NASA-TM-83418] p 131 N83-28380
Computer code for off-design performance analysis of radial-inflow turbines with rotor blade sweep
[NASA-TP-2199] p 40 N83-32807
ROTOR BODY INTERACTIONS
Tone generation by rotor-downstream strut interaction
[AIAA PAPER 83-0767] p 21 A83-25957
ROTOR SPEED
Blade loading and rotation effects on compressor rotor wake near end walls p 3 A83-22138
ROTORS
Finite-length solutions for rotodynamic coefficients of turbulent annular seals
[ASME PAPER 82-LUB-42] p 136 A83-13521

Performance of a tandem-rotor/tandem-stator conical-flow compressor designed for a pressure ratio of 3
[NASA-TP-2034] p 9 N83-11058
Rotor redesign for a highly loaded 1800 ft/sec tip speed fan. 3: Laser Doppler velocimeter report
[NASA-CR-167954] p 30 N83-14128
The effect of yaw on horizontal axis wind turbine loading and performance
[NASA-TM-82778] p 169 N83-14688
Measured performance of a tip-controlled, teetered rotor with an NACA 64 sub 3-618 tip airfoil
[NASA-TM-82870] p 169 N83-14689
Rotordynamic Instability Problems in High-Performance Turbomachinery
[NASA-CP-2250] p 142 N83-15629
Aerodynamic effect of a honeycomb rotor tip shroud on a 50.8-centimeter-tip-diameter core turbine
[NASA-TP-2112] p 32 N83-17547
Labyrinth seal forces on a whirling rotor
[NASA-CR-168016] p 34 N83-22198
Rotor fragment protection program: Statistics on aircraft gas turbine engine rotor failures that occurred in US commercial aviation during 1979
[NASA-CR-168163] p 38 N83-29234
Theoretical investigation of the force and dynamically coupled torsional-axial-lateral dynamic response of eared rotors
[NASA-CR-173013] p 191 N83-34656

RURAL AREAS
The worldwide market for photovoltaics in the rural sector
[NASA-TM-83035] p 173 N83-15840
Non-urban mobile radio market demand forecast
[NASA-CR-168065] p 107 N83-28297

S

S GLASS
High strain rate properties of undirectional composites, part 1
[NASA-CR-167969] p 64 N83-13178
High strain rate properties of off-axis composite laminates, part 2
[NASA-CR-167970] p 64 N83-13179

S-N DIAGRAMS
Statistical summaries of fatigue data for design purposes
[NASA-CR-3697] p 161 N83-29731

SAFETY
Assessment of crash fire hazard of LH sub 2 fueled aircraft
[NASA-CR-165525] p 16 N83-11095

SANDS
A method of predicting the performance deterioration of a compressor cascade due to sand erosion
[AIAA PAPER 83-0178] p 19 A83-16572
Compressor cascade performance deterioration caused by sand ingestion
[NASA-CR-168067] p 11 N83-16286

SAPPHIRE
Molecular-orbital model for metal-sapphire interfacial strength p 67 A83-10612

SATELLITE ANTENNAS
A multiple beam antenna concept for a 30/20 GHz satellite communications system p 103 A83-11485
Packet communication system for a multi-beam beam switched satellite repeater p 104 A83-41336
Advanced 30/20 GHz multiple beam antenna for future communications satellites p 104 A83-41367
Advanced 30/20 GHz multiple-beam antennas for communications satellites
[NASA-TM-82952] p 50 N83-13154

SATELLITE DRAG
Optimal sun-alignment techniques of large solar arrays in electric propulsion spacecraft
[AIAA PAPER 82-1898] p 48 A83-12475

SATELLITE LIFETIME
Space power tubes - very much alive
[NASA-TM-83425] p 107 N83-28295

SATELLITE NETWORKS
A high capacity satellite switched TDMA microwave switch matrix p 104 A83-19776
Auxiliary propulsion requirements for large space systems
[AIAA PAPER 83-1217] p 56 A83-45512
Advanced communications satellite systems p 47 A83-49855
Customer premise service study for 30/20 GHz satellite system
[NASA-CR-167986] p 105 N83-17769
A study of 60 Gigahertz intersatellite link applications
[NASA-TM-83337] p 47 N83-20994
Engineering calculations for communications systems planning
[NASA-CR-170182] p 106 N83-22494
Requirements for a mobile communications satellite system. Volume 1: Executive summary
[NASA-CR-168128] p 106 N83-23497
Auxiliary propulsion requirements for large space systems
[NASA-TM-83388] p 58 N83-26922

SATELLITE POWER TRANSMISSION (TO EARTH)
Large area low-cost space solar cell development p 170 N83-14699

SATELLITE SOLAR ENERGY CONVERSION
Radiative energy receiver for high performance energy conversion cycles p 164 A83-27138

SATELLITE TELEVISION
Experimental results for the interference between FM television signals p 103 A83-19686
A new architecture for adaptive transform compression of NTSC composite video signal p 103 A83-19732

SATELLITE TRANSMISSION
Satellite-aided land mobile communications system implementation considerations p 104 A83-41417
Satellite switched FDMA advanced communication technology satellite program
[NASA-CR-168034] p 105 N83-15543
A study of 60 Gigahertz intersatellite link applications
[NASA-TM-83337] p 47 N83-20994
Planning assistance for the 30/20 GHz program, volume 1
[NASA-CR-165484-VOL-1] p 108 N83-33010

SATELLITE-BORNE INSTRUMENTS
Observations of charging dynamics --- of spacecraft p 49 A83-37591

SCALE (CORROSION)
O-18 tracer studies of Al2O3 scale formation on NiCrAl alloys p 74 A83-10249
Diffusion processes in Al2O3 scales - Void growth, grain growth, and scale growth p 76 A83-42238
The oxidation behavior of a model molybdenum/tungsten-containing alloy in air alone and in air with trace levels of NaCl(g) p 76 A83-42241

SCALE EFFECT
Experimental evaluation of inlet turbulence, wall boundary layer, surface finish, and fillet radius on small axial turbine state performance
[SAE PAPER 821475] p 24 A83-38001

SCALE MODELS
Scale model performance test investigation of mixed flow exhaust systems for an energy efficient engine /E3/ propulsion system
[AIAA PAPER 83-0541] p 20 A83-16776

SCALING LAWS
'Scaling' analysis of the ice accretion process on aircraft surfaces
[ASME PAPER 82-WA/HT-39] p 16 A83-25693

SCATHA SATELLITE
Development of electrical test procedures for qualification of spacecraft against EID. Volume 1: The CAN test and other relevant data
[NASA-CR-165590] p 49 N83-12136
Development of electrical test procedures for qualification of spacecraft against EID. Volume 2: Review and specification of test procedures
[NASA-CR-165590] p 50 N83-12137

SCHLIEREN PHOTOGRAPHY
Experimental evaluation of shockless supercritical airfoils in cascade
[NASA-TM-83045] p 11 N83-15268
Rainbow Schlieren
[NASA-TP-2166] p 135 N83-33126

SCHWARZ-CHRISTOFFEL TRANSFORMATION
Solution of viscous internal flows on curvilinear grids generated by the Schwarz-Christoffel transformation p 122 A83-38796

SCORING
Assessment of lubricated contacts: Mechanisms of scuffing and scoring
[NASA-TM-83074] p 144 N83-20118

SEA LEVEL
Energy efficient engine sector combustor rig test program
[NASA-CR-167913] p 33 N83-19753

SEALING
The JT8D and JT9D engine component improvement: Performance improvement program
[NASA-CR-167965] p 32 N83-17543
Method of fabricating an abradable gas path seal
[NASA-CASE-LEW-13269-2] p 93 N83-17714
A refrigerated dynamic seal
[NASA-TM-83378] p 130 N83-24798

SEALS (STOPPERS)
Analysis of spiral-groove face seals for liquid oxygen
[ASLE PREPRINT 83-AM-4B-2] p 138 A83-43339
Film thickness measurement for spiral groove and Rayleigh step lift pad self-acting face seals
[NASA-TP-2058] p 26 N83-11126
Energy efficient high-pressure turbine leakage technology report
[NASA-CR-165202] p 30 N83-15304
JT90 ceramic outer air seal system refinement program, phase 2
[NASA-CR-167962] p 30 N83-15305
Advanced Gas Turbine (AGT) power-train system development
[NASA-CR-167875] p 142 N83-15627
Energy efficient face seal
[NASA-CR-165591] p 142 N83-15659
Design analysis of a self-acting spiral-groove ring seal for counter-rotating shafts
[NASA-TP-2142] p 36 N83-25712
Correlation of compressive stress with spalling of plasma sprayed ceramic materials
[NASA-TM-83406] p 95 N83-27016
Fully plasma-sprayed compliant backed ceramic turbine seal
[NASA-CASE-LEW-13268-3] p 149 N83-28450
High speed cryogenic self-acting, shaft seals for liquid rocket turbopumps
[NASA-CR-168194] p 151 N83-32070
A comparison of flow rates and pressure profiles for N-sequential inlets and three related seal configurations
[NASA-TM-83442] p 132 N83-33103
The trend of future gas turbine technology
[NASA-TM-83505] p 2 N83-34886

SEARCH PROFILES
A search for equilibrium states
[NASA-TM-82898] p 207 N83-20808

SECONDARY FLOW
Development of secondary flow and vorticity in curved ducts, cascades, and rotors, including effects of viscosity and rotation p 119 A83-16141
Measurements of compressible secondary flow in a circular S-duct
[AIAA PAPER 83-1739] p 4 A83-37218
Mean-flow measurements of the flow field diffusing bend
[NASA-CR-3634] p 10 N83-14066
Comparison of visualized turbine endwall secondary flows and measured heat transfer patterns
[NASA-TM-83016] p 123 N83-14435
Axial compressor middle stage secondary flow study
[NASA-CR-3701] p 14 N83-29174

SELECTION
Resin selection criteria for tough composite structures
[AIAA 83-0801] p 89 A83-29734

SELF ALIGNMENT
Design study of Self-Alining Bearingless Planetary (SABP) gear p 145 N83-20127

SELF INDUCED VIBRATION
The coupled aeroelastic response of turbomachinery blading to aerodynamic excitations
[AIAA 83-0844] p 156 A83-29822

SELF LUBRICATING MATERIALS
Improved uniformity of multiphase ceramic-metal plasma-sprayed coats p 61 A83-22269

SELF LUBRICATION
A commentary on solid lubricants and wear resistant solids for use in extreme environments
[NASA-TM-83042] p 92 N83-15468
Plasma-sprayed self-lubricating coatings
[NASA-CR-3680] p 94 N83-22422

SEMICONDUCTING FILMS
An enhanced sensitivity null ellipsometry technique for studying films on substrates - Application to silicon nitride on gallium arsenide p 206 A83-37618
Use of column V alkyls in organometallic vapor phase epitaxy (OMVPE) p 70 A83-46608

SEMICONDUCTOR DEVICES
Production of large-area single-crystal wafers of cubic SiC for semiconductor devices p 205 A83-22767
Minority carrier diffusion length measurements - A review and comparison of techniques p 205 A83-28448
Experimental feasibility study of a thermoelectric heat flux gage
[NASA-TM-83048] p 134 N83-15602
Deep impurity trapping concepts for power semiconductor devices p 206 N83-15877
Screen printed interdigitated back contact solar cell
[NASA-CASE-LEW-13414-1] p 177 N83-20374
Advanced 3-V semiconductor technology assessment
[NASA-CR-168101] p 206 N83-21987
Advanced 3-V semiconductor technology assessment --- space communications
[NASA-CR-168102] p 207 N83-21988
Inelastic tunnel diodes
[NASA-CASE-LEW-13833-1] p 116 N83-25983

SEMICONDUCTOR JUNCTIONS
Single and multijunction space solar cells grown by organometallic vapor phase epitaxy /OM-VPE/ p 164 A83-27260

SENSORS
Sensor failure detection for jet engines [NASA-CR-168190] p 154 N83-33182

SEPARATED FLOW
Dynamic distortion in a short s-shaped subsonic diffuser with flow separation --- Lewis 8 by 6 foot Supersonic Wind Tunnel [AIAA PAPER 83-1412] p 25 A83-45515
Dynamic distortion in a short s-shaped subsonic diffuser with flow separation --- Lewis 8 by 6 foot Supersonic Wind Tunnel [NASA-TM-83412] p 36 N83-26838

SEPARATORS
Cross-linked polyvinyl alcohol films as alkaline battery separators p 68 A83-20576
Polyvinyl alcohol membranes as alkaline battery separators [NASA-TM-82961] p 70 N83-10135
Development and evaluation of polyvinyl-alcohol blend polymer films as battery separators [NASA-TM-82981] p 71 N83-15372
Preparation, characterization, physical testing and performance of flurocarbon membranes and separators [NASA-CR-169756] p 71 N83-16418
Evaluation of production version of the NASA improved inorganic-organic separator [NASA-TM-83018] p 174 N83-18022
Electrolyte management in porous battery components. Static measurements [NASA-TM-83073] p 72 N83-18862
The electrochemical fluorination of polymeric materials for high energy density aqueous and non-aqueous battery and fuel cell separators [NASA-CR-167961] p 72 N83-21056
Preparation, characterization, physical testing and performance of fluorocarbon membranes and separators [NASA-CR-167880] p 73 N83-26936
Rolling-element bearings [NASA-RP-1105] p 149 N83-27214
Polyvinyl alcohol battery separator containing inert filler [NASA-CASE-LEW-13556-2] p 183 N83-29805
Advanced inorganic separators for alkaline batteries and method of making the same [NASA-CASE-LEW-13171-2] p 184 N83-32176

SERVICE LIFE
A direct-measurement technique for estimating discharge-chamber lifetime --- for ion thrusters [AIAA PAPER 82-1908] p 51 A83-12483
Effects of arc current on the life in burner-rig thermal cycling of plasma-sprayed ZrO2-O3 p 89 A83-22270
Results of chopper-controlled discharge life cycling studies on lead-acid batteries p 164 A83-27183
Development of improved hydrogen recombination in sealed nickel-cadmium aerospace cells p 54 A83-27198
Expected cycle life vs. depth of discharge relationships of well-behaved single cells and cell strings p 165 A83-32627
The performance and application of high speed long life LH2 hybrid bearings for reusable rocket engine turbomachinery [AIAA PAPER 83-1389] p 138 A83-36379
Materials constitutive models for nonlinear analysis of thermally cycled structures [NASA-TP-2055] p 158 N83-12449
Benchmark notch test for life prediction [NASA-CR-165571] p 158 N83-12451
The 371 deg C(700 deg F) properties of celion 6000/n-phenylnadimide modified PMR polyimide composites [NASA-TM-83050] p 65 N83-15365
Classification of journal surfaces using surface topography parameters and software methods to compensate for stylus geometry [NASA-CR-168153] p 148 N83-24857
Nickel-hydrogen component development [NASA-TM-83487] p 186 N83-35498
SSME main combustion chamber life prediction [NASA-CR-168215] p 60 N83-36101

SERVOCONTROL
Automotive Stirling Engine Mod 1 Design Review, volume 2 [NASA-CR-167936] p 209 N83-10991

SHAFTS (MACHINE ELEMENTS)
Investigation of the effects of initial fluid film profile on pumping ring operation [ASME PAPER 82-LUB-35] p 136 A83-13516
Cryogenic fluid management experiment trunnion fatigue verification [AIAA PAPER 83-0911] p 49 A83-32782
Powder metallurgy Rene 95 rotating turbine engine parts, volume 2 [NASA-CR-165141] p 82 N83-15412
Development of methodology for horizontal axis wind turbine dynamic analysis [NASA-CR-168110] p 178 N83-22747
Classification of journal surfaces using surface topography parameters and software methods to compensate for stylus geometry [NASA-CR-168153] p 148 N83-24857
High speed cryogenic self-acting, shaft seals for liquid rocket turbopumps [NASA-CR-168194] p 151 N83-32070

SHALE OIL
High performance liquid chromatographic hydrocarbon group-type analyses of mid-distillates employing fuel-derived fractions as standards [NASA-TM-83072] p 100 N83-19920

SHALLOW SHELLS
Vibrations of cantilevered doubly-curved shallow shells p 157 A83-39557

SHEAR FLOW
A turbulence model for three dimensional turbulent shear flows over curved rotating bodies [AIAA PAPER 83-0559] p 120 A83-16787
Unsteady turbulent shear flow in shock tube discontinuities p 124 A83-46445
Turbulent solution of the Navier-Stokes equations for an inhomogenous developing shear layer [NASA-TM-82969] p 126 N83-12357

SHEAR LAYERS
Turbulent solution of the Navier-Stokes equations for an inhomogenous developing shear layer [NASA-TM-82969] p 126 N83-12357
Excited waves in shear layers [DFVLR-FB-82-23] p 106 N83-21218

SHEAR PROPERTIES
Bisimide amine cured epoxy /IME/ resins and composites. II - Ten-degree off-axis tensile and shear properties of Celion 6000/IME composites p 62 A83-23608
Dynamic mechanical properties of n-phenylnadimide modified PMR polyimide composites [NASA-TM-83051] p 65 N83-15363
The 371 deg C(700 deg F) properties of celion 6000/n-phenylnadimide modified PMR polyimide composites [NASA-TM-83050] p 65 N83-15365

SHEAR STRENGTH
Correlation of tensile and shear strengths of metals with their friction properties [ASLE PREPRINT 82-LC-UB-1] p 74 A83-13226

SHEAR STRESS
Traction behavior of two traction lubricants [NASA-TM-83311] p 144 N83-20116
Correlation of compressive stress with spalling of plasma sprayed ceramic materials [NASA-TM-83406] p 95 N83-27016

SHELL THEORY
Geometrically nonlinear analysis of layered composite shells p 156 A83-27431
Vibrations of cantilevered circular cylindrical shells Shallow versus deep shell theory p 157 A83-36958
Vibrations of blades with variable thickness and curvature by shell theory [ASME PAPER 83-GT-152] p 158 A83-47978

SHELLS (STRUCTURAL FORMS)
Ring-cusp ion thruster with shell anode [NASA-CASE-LEW-13881-1] p 202 N83-21903

SHOCK DISCONTINUITY
Unsteady turbulent shear flow in shock tube discontinuities p 124 A83-46445

SHOCK RESISTANCE
Method of fabricating an abradable gas path seal [NASA-CASE-LEW-13269-2] p 93 N83-17714
Laser surface fusion of plasma sprayed ceramic turbine seals [NASA-CASE-LEW-13269-1] p 50 N83-20996

SHOCK TUBES
Unsteady turbulent shear flow in shock tube discontinuities p 124 A83-46445

SHOCK WAVE INTERACTION
Numerical solution to the glancing sidewall oblique shock wave/turbulent boundary layer interaction in three-dimension [AIAA PAPER 83-0136] p 3 A83-16823
Experimental investigation of a two-dimensional shock-turbulent boundary layer interaction with bleed [AIAA PAPER 83-0135] p 3 A83-19581
Numerical solution to the glancing sidewall oblique shock wave/turbulent boundary layer interaction in three dimension [NASA-TM-83056] p 34 N83-22199
Experimental investigation of a two-dimensional shock-turbulent boundary layer interaction with bleed [NASA-TM-83057] p 34 N83-22200

SHOCK WAVE PROPAGATION
Dynamic responses of graphite/epoxy laminated beam to impact of elastic spheres [NASA-CR-165461] p 64 N83-13173

SHOCK WAVES
Finite difference solutions to shocked acoustic waves [AIAA PAPER 83-0671] p 193 A83-25907
On the shock cell structure and noise of supersonic jets [AIAA PAPER 83-0703] p 193 A83-25923
An experimental study of supersonic jet shock-associated noise [AIAA PAPER 83-0708] p 193 A83-25924
Coaxial supersonic jet-flows, shock structure and related problems with noise-suppression assessment and prediction [AIAA PAPER 83-0707] p 194 A83-28011
Numerical solution of the Navier-Stokes equations for compressible turbulent two/three dimensional flows in the terminal shock region of an inlet/diffuser [AIAA PAPER 83-1892] p 5 A83-39358
A computer program for the calculation of the flow field including boundary layer effects for mixed-compression inlets at angle of attack [NASA-CR-168002] p 10 N83-11066
Numerical solutions of Navier-Stokes equations for compressible turbulent two/three dimensional flows in terminal shock region of an inlet/diffuser [NASA-CR-3723] p 132 N83-34230

SHORT CIRCUITS
The effect of different solar simulators on the measurement of short-circuit current temperature coefficients p 172 N83-15821

SHRINKAGE
Imide modified epoxy matrix resins [NASA-CR-167942] p 93 N83-18909

SHROUDED TURBINES
Quasi-three-dimensional turbomachinery flow calculations on multiple hub-to-shroud stream surfaces [AIAA PAPER 83-1820] p 5 A83-38652
Aerodynamic effect of a honeycomb rotor tip shroud on a 50.8-centimeter-tip-diameter core turbine [NASA-TP-2112] p 32 N83-17547
Laser surface fusion of plasma sprayed ceramic turbine seals [NASA-CASE-LEW-13269-1] p 50 N83-20996

SHROUDS
CF6 jet engine diagnostics program. High pressure turbine roundness/clearance investigation [NASA-CR-165581] p 29 N83-13100
Method of fabricating an abradable gas path seal [NASA-CASE-LEW-13269-2] p 93 N83-17714

SIDELOBE REDUCTION
Techniques for low sidelobe, high efficiency offset dual reflector antennas p 104 A83-21072

SIGNAL ENCODING
A new architecture for adaptive transform compression of NTSC composite video signal p 103 A83-19732
An improved algorithm for evaluating trellis phase codes [NASA-CR-169354] p 105 N83-16600

SIGNAL GENERATORS
Generation of desired signals from acoustic drivers --- for aircraft engine internal noise propagation experiment p 19 A83-15068

SIGNAL PROCESSING
An improved algorithm for evaluating trellis phase codes [NASA-CR-169354] p 105 N83-16600
Refinement and application of acoustic impulse technique to study nozzle transmission characteristics [NASA-CR-3656] p 199 N83-20708

SIGNAL TO NOISE RATIOS
Adjacent channel interference degradation with minimum shift keyed modulation p 103 A83-19698

SIGNAL TRANSMISSION
Four-dimensional modulation and coding: An alternate to frequency-reuse [NASA-CR-174453] p 110 N83-36300

SILICIDES
Processing of fused silicide coatings for carbon-based materials [NASA-TM-83362] p 95 N83-27019

SILICON
The effect of Ta2O5 on the interaction between silicon and its contact metallization [NASA-TM-82948] p 166 N83-10554
Radiation damage in front and back illuminated high resistivity silicon solar cells [NASA-TM-82965] p 206 N83-10962
Industrial ion source technology [NASA-CR-159877] p 102 N83-12259
Large area low-cost space solar cell development p 170 N83-14699
Effects of processing and dopant on radiation damage removal in silicon solar cells p 170 N83-14708

Radiation damage p 172 N83-15837
Deep impurity trapping concepts for power semiconductor devices p 206 N83-15877
Developments toward an 18% efficient silicon solar cell
[NASA-CR-168141] p 181 N83-25112
SILICON CARBIDES
Fatigue behavior of SiC reinforced Ti/6Al-4V/ at 650 C p 62 A83-12414
Comparison of NDE techniques for sintered-SiC components p 152 A83-22265
Production of large-area single-crystal wafers of cubic SiC for semiconductor devices p 205 A83-22767
Tribological properties of sintered polycrystalline and single-crystal silicon carbide p 89 A83-29397
XPS, AES and friction studies of single-crystal silicon carbide p 89 A83-36973
Progress in net shape fabrication of alpha SiC turbine components
[ASME PAPER 83-GT-238] p 139 A83-48030
SILICON COMPOUNDS
Silicon-slurry/aluminide coating --- protecting gas turbine engine vanes and blades
[NASA-CASE-LEW-13343] p 86 N83-31795
SILICON CONTROLLED RECTIFIERS
A lightweight electronically commutated dc motor for electric passenger vehicles
[NASA-CR-165601] p 113 N83-10348
SILICON FILMS
Sputtered silicon nitride coatings for wear protection p 88 A83-12651
SILICON JUNCTIONS
Planar multijunction high voltage solar cell chip p 163 A83-13923
Interfacial electrical properties of ion-beam sputter deposited amorphous carbon on silicon p 205 A83-33920
SILICON NITRIDES
Ellipsometric study of silicon nitride on gallium arsenide p 204 A83-11812
Sputtered silicon nitride coatings for wear protection p 88 A83-12651
Thermodynamics of silicon nitridation - Effect of hydrogen
[ACS PAPER 33-B-80P] p 88 A83-18052
Effect of Y2O3 and Al2O3 on the oxidation resistance of Si3N4 p 88 A83-22258
Injection molding ceramics to high green densities p 137 A83-33515
An enhanced sensitivity null ellipsometry technique for studying films on substrates - Application to silicon nitride on gallium arsenide p 206 A83-37618
The effect of silicon particle size on the nitriding behaviour of reaction bonded Si3N4 compacts p 90 A83-48261
Sintering of reaction bonded silicon nitride p 90 A83-48270
Sintering, properties and fabrication of Si3N4 + Y2O3 based ceramics p 90 A83-48303
Mechanisms of devitrification of grain boundary glassy phases in Si3N4 materials
[NASA-CR-169670] p 71 N83-14177
RF sputtered silicon and hafnium nitrides: Properties and adhesion to 440C stainless steel
[NASA-TM-83400] p 95 N83-27020
SILVER
Microstructural analysis of solar cell welds p 172 N83-15833
SILVER ZINC BATTERIES
Polyvinyl alcohol membranes as alkaline battery separators
[NASA-TM-82961] p 70 N83-10135
SILVICULTURE
Energy and precious fuels requirements of fuel alcohol production. Volume 3, appendices C to F: Methanol from cellulose
[NASA-CR-168092] p 183 N83-28583
SIMULATORS
Digital system for structural dynamics simulation
[NASA-CR-168019] p 43 N83-14139
SIMULTANEOUS EQUATIONS
Triangular system solutions on an optical systolic processor p 189 A83-36752
SINE WAVES
High-intensity sound in air saturated fibrous bulk porous materials
[NASA-CR-167979] p 197 N83-12967
SINGLE CRYSTALS
Dipole-field sums and Lorentz factors for orthorhombic lattices, and implications for polarizable molecules p 204 A83-17226
Piezoelectric and pyroelectric coefficients for ferroelectric crystals with polarizable molecules p 205 A83-17227
Production of large-area single-crystal wafers of cubic SiC for semiconductor devices p 205 A83-22767
Influence of cobalt, tantalum, and tungsten on the microstructure and mechanical properties of superalloy single crystals p 79 N83-11293
Orientation dependence of the stress rupture properties of Nickel-base superalloy single crystals
[NASA-CR-165394] p 206 N83-13009
The orthogonal in-situ machining of single and polycrystalline aluminum and copper, volume 2
[NASA-CR-169528] p 81 N83-13233
Energy efficient engine high-pressure turbine single crystal vane and blade fabrication technology report
[NASA-CR-165400] p 39 N83-30429
SINTERING
Tribological properties of sintered polycrystalline and single-crystal silicon carbide p 89 A83-29397
Sintering of reaction bonded silicon nitride p 90 A83-48270
Sintering, properties and fabrication of Si3N4 + Y2O3 based ceramics p 90 A83-48303
SITE SELECTION
Large Horizontal-Axis Wind Turbines
[NASA-CP-2230] p 175 N83-19231
SIZE (DIMENSIONS)
A method to estimate weight and dimensions of small aircraft propulsion gas turbine engines: User's guide
[NASA-CR-168049] p 31 N83-16343
Parametric study of potential early commercial MHD power plants. Task 3: Parameter variation of plant size
[NASA-CR-165445] p 182 N83-26259
SIZE DISTRIBUTION
Pore size engineering applied to starved electrochemical cells and batteries p 164 A83-27201
Pore size engineering applied to starved electrochemical cells and batteries
[NASA-TM-82893] p 70 N83-10134
Comparison of modern icing cloud instruments
[NASA-CR-168008] p 19 N83-18720
Pore size engineering applied to the design of separators for nickel-hydrogen cells and batteries
[NASA-TM-83386] p 73 N83-24571
SKIN FRICTION
Modified gauge for time-resolved skin-friction measurements p 133 A83-14172
SLIDING
Plastic deformation at surface during unlubricated sliding
[NASA-TP-2036] p 139 N83-11496
Regression analysis of traction characteristics of traction fluids
[NASA-TP-2154] p 148 N83-24862
Pivoting and slip in an angular contact bearing
[NASA-TM-83408] p 148 N83-26079
SLIDING FRICTION
Infrared emission spectrophotometric study of the changes produced by TiN coating of metal surfaces in an operating EHD contact
[ASLE PREPRINT 82-LC-3C-3] p 135 A83-13229
Tribological properties of sintered polycrystalline and single-crystal silicon carbide p 89 A83-29397
XPS, AES and friction studies of single-crystal silicon carbide p 89 A83-36973
Plastic deformation and wear process at a surface during unlubricated sliding p 138 A83-37822
The influence of surface dents and grooves on traction in sliding EHD point contacts p 138 A83-37823
Tribological characteristics of nitrogen (N+) implanted iron p 75 A83-37824
The dryout region in frictionally heated sliding contacts p 124 A83-42762
Effect of sliding speed and contact stress on tribological properties of ultra-high-molecular-weight polyethylene
[NASA-TP-2059] p 91 N83-14269
Elastohydrodynamic lubrication of rectangular contacts
[NASA-TP-2111] p 143 N83-16759
Friction and wear of some ferrous-base metallic glasses
[NASA-TM-83067] p 82 N83-19886
Sliding induced crystallization of metallic glass
[NASA-TP-2140] p 83 N83-21110
Polyimides formulated from a partially fluorinated diamine for aerospace tribological applications
[NASA-TM-83339] p 94 N83-22423
X-ray photoelectron spectroscopy and friction studies of nickel-zinc and manganese-zinc ferrites in contact with metals
[NASA-TP-2163] p 84 N83-23419
Elastohydrodynamic contacts. Effects of dents and grooves on traction and local film thickness
[NASA-TP-2175] p 150 N83-28453
Friction and hardness of gold films deposited by ion plating and evaporation
[NASA-TP-2207] p 87 N83-34019
SLOTS
Wind tunnel tests of a zero length, slotted-lip engine air inlet for a fixed nacelle V/STOL aircraft
[NASA-TM-82939] p 9 N83-10019
SLURRIES
Processing of fused silicide coatings for carbon-based materials
[NASA-TM-83362] p 95 N83-27019
Silicon-slurry/aluminide coating --- protecting gas turbine engine vanes and blades
[NASA-CASE-LEW-13343] p 86 N83-31795
SMALL PERTURBATION FLOW
Finite-length solutions for rotodynamic coefficients of turbulent annular seals
[ASME PAPER 82-LUB-42] p 136 A83-13521
Rapid distortion of small-scale turbulence by an axisymmetric contraction p 120 A83-22381
A theory of rotating stall of multistage axial compressors. II - Finite disturbances
[ASME PAPER 83-GT-45] p 8 A83-47905
SMOOTHING
High level continuity for coordinate generation with precise controls p 190 A83-29632
SODIUM
Laser fluorescence studies of the chemical interactions of sodium species with sulfur bearing fuels
[NASA-CR-169861] p 71 N83-17625
The detailed chemistry and thermodynamics of sodium in oxygen-rich flames
[NASA-CR-169848] p 72 N83-17626
SODIUM CHLORIDES
Reactions of NaCl with gaseous SO3, SO2, and O2
[NASA-TM-83423] p 86 N83-29358
SODIUM SULFATES
Combustion system processes leading to corrosive deposits p 69 A83-42246
Reactions of NaCl with gaseous SO3, SO2, and O2
[NASA-TM-83423] p 86 N83-29358
Effect of the amount of Na2SO4 on the high temperature corrosion of Udimet-700
[NASA-TM-83459] p 87 N83-34016
SOLAR ARRAYS
Optimal sun-alignment techniques of large solar arrays in electric propulsion spacecraft
[AIAA PAPER 82-1898] p 48 A83-12475
Solar array switching power management p 54 A83-27132
Performance degradation and cleaning of photovoltaic arrays p 164 A83-27236
Large area low-cost space solar cell development p 170 N83-14699
Evaluation of solar cell welds by scanning acoustic microscopy p 172 N83-15834
Study of solar array switching power management technology for space power system
[NASA-CR-167890] p 179 N83-22756
Array structure design handbook for stand alone photovoltaic applications
[NASA-TM-82629] p 160 N83-23631
Design considerations for large space electric power systems
[NASA-TM-83064] p 58 N83-24552
SAFE II: Large systems space plasma evaluation experiment p 46 N83-26903
Modular photovoltaic stand-alone systems: Phase 1
[NASA-CR-168075] p 185 N83-33320
Analysis of the reflective multibandgap solar cell concept
[NASA-CR-168186] p 185 N83-34454
SOLAR CELLS
Liquid encapsulated Czochralski growth of low dislocation GaAs p 204 A83-13784
Planar multijunction high voltage solar cell chip p 163 A83-13923
Single and multijunction space solar cells grown by organometallic vapor phase epitaxy /OM-VPE/ p 164 A83-27260
Minority carrier diffusion length measurements - A review and comparison of techniques p 205 A83-28448
Limitations on solar cell open-circuit voltage and efficiency p 165 A83-37790
The effect of Ta2O5 on the interaction between silicon and its contact metallization
[NASA-TM-82948] p 166 N83-10554
Evaluation of electrode shape and nondestructive evaluation method for welded solar cell interconnects
[NASA-TM-82966] p 166 N83-10555
Radiation damage in front and back illuminated high resistivity silicon solar cells
[NASA-TM-82965] p 206 N83-10962
Solar cell having improved back surface reflector
[NASA-CASE-LEW-13620-1] p 168 N83-13579
Heat transparent high intensity high efficiency solar cell
[NASA-CASE-LEW-12892-1] p 170 N83-14692
Large area low-cost space solar cell development p 170 N83-14699
On the cause of the flat-spot phenomenon observed in silicon solar cells at low temperatures and low intensities p 170 N83-14705

Effects of processing and dopant on radiation damage removal in silicon solar cells p 170 N83-14708
Determination of optimum sunlight concentration level in space for 3-5 cascade solar cells p 170 N83-14732
Diffusion length measurements in solar cells: An analysis and comparison of techniques p 171 N83-15812
Progress toward cascade cells made by OM-VPE --- organometallic vapor phase epitaxy p 171 N83-15813
Determination of optimum sunlight concentration level in space for 3-5 cascade solar cells p 171 N83-15814
Diffused P+-N solar cells in bulk GaAs p 171 N83-15818
GaAs solar cells for concentrator systems in space p 171 N83-15820
The effect of different solar simulators on the measurement of short-circuit current temperature coefficients p 172 N83-15821
Microdistribution of oxygen in silicon and its effects on electronic properties p 172 N83-15825
Radiation damage and annealing in large area n+/p/p+ GaAs shallow homojunction solar cells p 172 N83-15826
Microstructural analysis of solar cell welds p 172 N83-15833
Evaluation of solar cell welds by scanning acoustic microscopy p 172 N83-15834
Radiation damage p 172 N83-15837
Design rules for a 100X maximum efficiency GaAs concentrator solar cell for space applications [NASA-CR-170005] p 177 N83-20362
Screen printed interdigitated back contact solar cell [NASA-CASE-LEW-13414-1] p 177 N83-20374
Solar cell measurements p 181 N83-25109
Developments toward an 18% efficient silicon solar cell [NASA-CR-168141] p 181 N83-25112
Solar energy converter using surface plasma waves [NASA-CASE-LEW-13827-1] p 181 N83-26258
Growth and characterization of Czochralski-grown n and p-type GaAs for space solar cell substrates [NASA-CR-168099] p 207 N83-27877
High voltage v-groove solar cell [NASA-CASE-LEW-13401-2] p 185 N83-32177
Practical aspects of photovoltaic technology, applications, and cost [NASA-CR-168025] p 185 N83-34450
Analysis of the reflective multibandgap solar cell concept [NASA-CR-168186] p 185 N83-34454

SOLAR COLLECTORS
Radiative energy receiver for high performance energy conversion cycles p 164 A83-27138
GaAs solar cells for concentrator systems in space p 171 N83-15820
Method of forming oxide coatings --- for solar collector heating panels [NASA-CASE-LEW-13132-1] p 96 N83-29388
Current collection from the space plasma through defects in high voltage solar array insulation [NASA-CR-168148] p 204 N83-31474

SOLAR ELECTRIC PROPULSION
Optimal sun-alignment techniques of large solar arrays in electric propulsion spacecraft [AIAA PAPER 82-1898] p 48 A83-12475
Status of the J-series 30-cm mercury ion thruster [AIAA PAPER 82-1904] p 51 A83-12479
Evaluation of the use of on-board spacecraft energy storage for electric propulsion missions [NASA-CR-168209] p 59 N83-32842

SOLAR ENERGY
Study of solar array switching power management technology for space power system [NASA-CR-167890] p 179 N83-22756
Practical aspects of photovoltaic technology, applications, and cost [NASA-CR-168025] p 185 N83-34450

SOLAR ENERGY ABSORBERS
Radiative energy receiver for high performance energy conversion cycles p 164 A83-27138

SOLAR ENERGY CONVERSION
A new strategy for efficient solar energy conversion - Parallel-processing with surface plasmons p 164 A83-27140
Solar energy conversion using surface plasmons for broadband energy transport p 171 N83-15815
DOE and AID stand-alone photovoltaic activities [NASA-TM-83374] p 180 N83-25041
Solar energy converter using surface plasma waves [NASA-CASE-LEW-13827-1] p 181 N83-26258
A new strategy for efficient solar energy conversion: Parallel-processing with surface plasmons [NASA-TM-82867] p 59 N83-28071

SOLAR GENERATORS
Practical aspects of photovoltaic technology, applications, and cost [NASA-CR-168025] p 185 N83-34450

SOLAR POWER SATELLITES
Direct conversion of infrared radiant energy for space power applications p 173 N83-15865

SOLAR PROPULSION
Radiation energy receiver for laser and solar propulsion systems [AIAA PAPER 83-1207] p 55 A83-36281

SOLAR RADIATION
Solar cell measurements p 181 N83-25109

SOLAR SPECTRA
A new strategy for efficient solar energy conversion: Parallel-processing with surface plasmons [NASA-TM-82867] p 59 N83-28071

SOLDERING
Microstructural analysis of solar cell welds p 172 N83-15833
Multicolor printing plate joining [NASA-CASE-LEW-13598-1] p 102 N83-17745

SOLID ELECTRODES
Long-range surface plasmons in electrode structures p 202 A83-40733

SOLID LUBRICANTS
Polyimides: Tribological properties and their use as lubricants [NASA-TM-82959] p 91 N83-13257
Fundamental aspects of polyimide dry film and composite lubrication: A review [NASA-TM-82968] p 92 N83-14271
A commentary on solid lubricants and wear resistant solids for use in extreme environments [NASA-TM-83042] p 92 N83-15468

SOLID PROPELLANTS
Process and quality verification controls for solid propellant manufacturing p 98 A83-39270

SOLID STATE DEVICES
Tubes in space - Very much alive p 112 A83-28160
Kilovolt dc solid state remote power controller development [NASA-CR-168041] p 115 N83-21236
Space power tubes - very much alive [NASA-TM-83425] p 107 N83-28295

SOLID SURFACES
Ignition of a combustible half space p 68 A83-22738
Application of modern surface analytical tools in the investigation of surface deterioration processes [NASA-TM-83452] p 152 N83-34327

SOLID-SOLID INTERFACES
Molecular-orbital model for metal-sapphire interfacial strength p 67 A83-10612
XPS, AES and friction studies of single-crystal silicon carbide p 89 A83-36973
Microstructural behavior of interfaces in hot isostatically pressed, dual alloy combinations [NASA-TM-82698] p 80 N83-11309

SOLIDIFICATION
Constitutive relationships for anisotropic high-temperature alloys [NASA-TM-83437] p 160 N83-28493

SOLIDS
Analogy between fluid cavitation and fracture mechanics [NASA-TM-83071] p 129 N83-22542
Micromechanically based constitutive relations for polycrystalline solids p 162 N83-34359

SOLIDS FLOW
Environmental solid particle effects on compressor cascade performance [NASA-CR-168018] p 11 N83-16285
Compressor cascade performance deterioration caused by sand ingestion [NASA-CR-168067] p 11 N83-16286

SOLUBILITY
Determination of hydrogen permeability in uncoated and coated superalloys [NASA-CR-165209] p 80 N83-12215

SOLUTIONS
A class of nonideal solutions. 2: Application to experimental data [NASA-TP-1930] p 208 N83-23188
A class of nonideal solutions. 1: Definition and properties [NASA-TP-1929] p 208 N83-23189

SOLVENT REFINED COAL
Literature survey of properties of synfuels derived from coal [NASA-TM-82739] p 99 N83-10208

SOLVENTS
Evaluation of production version of the NASA improved inorganic-organic separator [NASA-TM-83018] p 174 N83-18022

SOOT
Soot formation in pyrolysis of acetylene, allene and 1,3-butadiene p 68 A83-39274
Fumigation of alcohol in a light duty automotive diesel engine [NASA-CR-167915] p 99 N83-13272

SOUND FIELDS
An iterative method for predicting turbofan inlet acoustics p 192 A83-13135
A theoretical investigation of the sound radiation fields associated with a Bellmouth inlet [AIAA PAPER 83-0710] p 193 A83-25926
Acoustical modal analysis of the pressure field in the tailpipe of a turbofan engine [NASA-TM-83387] p 201 N83-25499

SOUND INTENSITY
Sound radiation from annular ducts/nozzles using modal decomposition of in-duct acoustic power [AIAA PAPER 83-0714] p 194 A83-25929
High-intensity sound in air saturated fibrous bulk porous materials [NASA-CR-167979] p 197 N83-12967

SOUND PRESSURE
Cross spectra between temperature and pressure in a constant area duct downstream of a combustor [AIAA PAPER 83-0762] p 196 A83-33487
Noise of the 10-bladed, 40 deg swept SR-6 propeller in a wind tunnel [NASA-TM-82950] p 196 N83-11840
Analysis of combustion spectra containing organ pipe tone by cepstral techniques [NASA-TM-83034] p 198 N83-16153
Cross spectra between temperature and pressure in a constant area duct downstream of a combustor [NASA-TM-83351] p 200 N83-23116

SOUND PROPAGATION
An iterative method for predicting turbofan inlet acoustics p 192 A83-13135
Pressure transfer function of a JT15D nozzle due to acoustic and convected entropy fluctuations p 193 A83-16319
Acoustics in variable area duct - Finite element and finite difference comparisons to experiment p 193 A83-19809
Sound propagation in segmented exhaust ducts - Theoretical predictions and comparison with measurements [AIAA PAPER 83-0734] p 194 A83-28016
Effect of flow on the acoustic performance of extended reaction lined ducts [AIAA PAPER 83-0778] p 195 A83-28024
Propagation of sound in highly porous open-cell elastic foams p 195 A83-28848
Turbofan noise generation. Volume 1: Analysis [NASA-CR-167951] p 198 N83-15041
Analysis of combustion spectra containing organ pipe tone by cepstral techniques [NASA-TM-83034] p 198 N83-16153

SOUND TRANSMISSION
Application of 3-signal coherence to core noise transmission [AIAA PAPER 83-0759] p 194 A83-28021

SOUND WAVES
Mechanics aspects of NDE by sound and ultrasound p 152 A83-25571
Sound diffraction at wall impedance discontinuities in a circular cylinder - Investigated using Wiener-Hopf technique [AIAA PAPER 83-0730] p 195 A83-33485
Prediction of sound radiation from different practical jet engine inlets [NASA-CR-169533] p 197 N83-13936
Sound diffraction at wall impedance discontinuities in a circular cylinder, investigated using Wiener-Hopf technique [NASA-TM-83365] p 201 N83-23117

SPACE COMMUNICATION
Space tubes: A major challenge [NASA-TM-82971] p 113 N83-11447
Design concepts for a high-impedance narrow-band 42 GHz power TWT using a fundamental/forward ladder-based circuit [NASA-CR-165282] p 114 N83-12330
Advanced 3-V semiconductor technology assessment [NASA-CR-168101] p 206 N83-21987
Advanced 3-V semiconductor technology assessment --- space communications [NASA-CR-168102] p 207 N83-21988
Space power tubes - very much alive [NASA-TM-83425] p 107 N83-28295

SPACE PLASMAS
Numerical simulation of a conducting disk partially covered by an insulator interacting with a plasma p 50 N83-18805
SAFE II: Large systems space plasma evaluation experiment p 46 N83-26900

Current collection from the space plasma through defects in high voltage solar array insulation
[NASA-CR-168148] p 204 N83-31474

SPACE PLATFORMS
Auxiliary propulsion requirements for large space systems
[AIAA PAPER 83-1217] p 56 A83-45512
Space Photovoltaic Research and Technology 1982: High Efficiency, Radiation Damage, and Blanket Technology
[NASA-CP-2256] p 171 N83-15806
Auxiliary propulsion requirements for large space systems
[NASA-TM-83388] p 58 N83-26922

SPACE POWER REACTORS
Thermionic technology infrastructure for space power p 54 A83-27298

SPACE PROCESSING
An experimental study of heat induced surface-tension driven flow p 44 A83-43269

SPACE SHUTTLE MAIN ENGINE
SSME main combustion chamber life prediction
[NASA-CR-168215] p 60 N83-36101

SPACE SHUTTLE ORBITERS
Space Shuttle Orbiter charging p 49 A83-20415
Preliminary design of flight hardware for two-phase fluid research
[NASA-CR-168072] p 46 N83-25766

SPACE SHUTTLES
Stability analysis of Centaur-in-Shuttle composite corrugated adapters
[AIAA 83-1003] p 49 A83-29791
Role of simulation and emulation in the development of Shuttle-Centaur (STS-Centaur)
[NASA-TM-83326] p 45 N83-29292

SPACE STATIONS
Application of a space station to communications satellites
[AAS PAPER 83-197] p 45 A83-43773

SPACE STORAGE
Long term storage of cryogens in space p 102 A83-11487

SPACE TRANSPORTATION SYSTEM
Cryogenic fluid management experiment trunnion fatigue verification
[AIAA PAPER 83-0911] p 49 A83-32782
Application of a space station to communications satellites
[AAS PAPER 83-197] p 45 A83-43773
Role of simulation and emulation in the development of Shuttle-Centaur (STS-Centaur)
[NASA-TM-83326] p 45 N83-29292
Advanced LOX/H sub 2 engine technologies for future OTVs p 60 N83-35013

SPACECRAFT
High frequency, high power capacitor development
[NASA-CR-168035] p 116 N83-27127

SPACECRAFT ANTENNAS
Phased array-fed antenna configuration study: Technology assessment
[NASA-CR-168078] p 106 N83-22495
Scanning beam antenna conceptual design for 20/30 GHz satellite systems p 46 N83-26889

SPACECRAFT CHARGING
Potentials on large spacecraft in LEO p 49 A83-17489
Space Shuttle Orbiter charging p 49 A83-20415
Observations of charging dynamics --- of spacecraft p 49 A83-37591
Development of electrical test procedures for qualification of spacecraft against EID. Volume 1: The CAN test and other relevant data
[NASA-CR-165590] p 49 N83-12136
Development of electrical test procedures for qualification of spacecraft against EID. Volume 2: Review and specification of test procedures
[NASA-CR-165590] p 50 N83-12137
Environmentally induced discharges on satellites p 105 N83-14365
Mass analysis of neutral particles and ions released during electrical breakdowns on spacecraft surfaces
[NASA-CR-170299] p 50 N83-23347
The role of potential barrier formation in spacecraft charging
[NASA-TM-83500] p 50 N83-35005

SPACECRAFT COMMUNICATION
Adjacent channel interference degradation with minimum shift keyed modulation p 103 A83-19698
A two-stage monolithic buffer amplifier for 20 GHz satellite communication p 112 A83-39272
Application of a space station to communications satellites
[AAS PAPER 83-197] p 45 A83-43773
Modulation techniques
[NASA-CR-169460] p 105 N83-10329
Concept for advanced satellite communications and required technologies
[NASA-TM-82984] p 47 N83-11210
Capabilities, limitations, and use of BC SAT-R2 conference software
[NASA-TM-83383] p 107 N83-29493
Customer premises services market demand assessment 1980 - 2000. Volume 1: Executive summary
[NASA-CR-168150] p 108 N83-31925
NASA's Advanced Communications Technology Satellite (ACTS)
[NASA-TM-83416] p 48 N83-35004

SPACECRAFT CONSTRUCTION MATERIALS
Overview of high-temperature materials for high-energy space power systems p 173 N83-15869
Research priorities for advanced fibrous composites
[NASA-CR-165414] p 65 N83-18853
Diamondlike flake composites --- for use in aerospace structures and components
[NASA-CASE-LEW-13837-1] p 67 N83-28095

SPACECRAFT ELECTRONIC EQUIPMENT
High-frequency high-voltage high-power DC-to-DC converters p 115 N83-21028

SPACECRAFT LAUNCHING
Infrared Astronomical Satellite (IRAS) launch
[NASA-TM-85190] p 45 N83-15330
Study for analysis of benefit versus cost of low thrust propulsion system
[NASA-CR-168011] p 57 N83-21002

SPACECRAFT POWER SUPPLIES
Solar array switching power management p 54 A83-27132
Radiative energy receiver for high performance energy conversion cycles p 164 A83-27138
Design of a 35-kilowatt bipolar nickel-hydrogen battery for low-earth-orbit applications p 54 A83-27205
Alkaline regenerative fuel cell energy storage system for manned orbital satellites p 54 A83-27206
Single and multijunction space solar cells grown by organometallic vapor phase epitaxy /OM-VPE/ p 164 A83-27260
Simplified power processing for ion-thruster subsystems
[AIAA PAPER 83-1394] p 55 A83-36384
Space Photovoltaic Research and Technology 1982: High Efficiency, Radiation Damage, and Blanket Technology
[NASA-CP-2256] p 171 N83-15806
A proposed optical pumping system requiring no electric power p 203 N83-15861
Direct conversion of infrared radiant energy for space power applications p 173 N83-15865
Overview of high-temperature materials for high-energy space power systems p 173 N83-15869
Growth of diamondlike films for power applications p 174 N83-15880
Design study of a high power rotary transformer
[NASA-CR-168012] p 115 N83-16630
Development of a high capacity toroidal Ni/Cd cell
[NASA-CR-169945] p 176 N83-19273
Design considerations for large space electric power systems
[NASA-TM-83064] p 58 N83-24552
Evaluation program for secondary spacecraft cells. Cycle life test
[NASA-CR-172679] p 182 N83-27351
Evaluation program for secondary spacecraft cells. Cycle life test
[NASA-CR-172680] p 183 N83-27352
Test methods and results of the 10-cell bipolar Ni-H2 battery p 117 N83-35261
Nickel-hydrogen component development
[NASA-TM-83487] p 186 N83-35498

SPACECRAFT PROPULSION
On-orbit propulsion requirements and performance assessment of ion propulsion subsystems for future GEO large satellite missions
[AIAA PAPER 82-1872] p 48 A83-12460
Advances in series resonant inverter technology and its effect on spacecraft employing electric propulsion
[AIAA PAPER 82-1881] p 51 A83-12466
The design and technology development for A 150 mlb resistojet for H2 or NH3
[AIAA PAPER 82-1949] p 52 A83-12506
Extended-performance 8-cm ion thruster operation
[AIAA PAPER 82-1955] p 53 A83-12512
Free radical propulsion concept p 53 A83-13141
Electric propulsion research and technology in the United States
[AIAA PAPER 82-1867] p 53 A83-16925
Inert gas thruster technology p 53 A83-20423
Propulsion and fluid management - Station keeping will eat energy on a new scale p 54 A83-24360
Operation of the J-series thruster using inert gas
[AIAA PAPER 82-1929] p 54 A83-26625
Radiation energy receiver for laser and solar propulsion systems
[AIAA PAPER 83-1207] p 55 A83-36281
Benefits and costs of low thrust propulsion systems
[AIAA PAPER 83-1246] p 49 A83-36306
Advanced LOX/H2 engine technologies for future OTVs
[AIAA PAPER 83-1312] p 55 A83-36333
The performance and application of high speed long life LH2 hybrid bearings for reusable rocket engine turbomachinery
[AIAA PAPER 83-1389] p 138 A83-36379
Simplified power processing for ion-thruster subsystems
[AIAA PAPER 83-1394] p 55 A83-36384
Advanced propulsion concepts for orbital transfer vehicles
[AIAA PAPER 83-1243] p 56 A83-45513
Modeling of space vehicle propellant mixing --- cryogenic propellants
[NASA-TP-2107] p 100 N83-16545
Operation of the J-series thruster using inert gas
[NASA-TM-82977] p 57 N83-17587
Study for analysis of benefit versus cost of low thrust propulsion system
[NASA-CR-168011] p 57 N83-21002
The performance and application of high speed long life LH2 hybrid bearings for reusable rocket engine turbomachinery
[NASA-TM-83417] p 58 N83-26923
Advanced propulsion concepts for orbital transfer vehicles
[NASA-TM-83419] p 59 N83-26924
Advanced LOX/H sub 2 engine technologies for future OTVs p 60 N83-35013

SPACECRAFT RADIATORS
Advances in series resonant inverter technology and its effect on spacecraft employing electric propulsion
[AIAA PAPER 82-1881] p 51 A83-12466
The design and technology development for A 150 mlb resistojet for H2 or NH3
[AIAA PAPER 82-1949] p 52 A83-12506
Direct contact droplet heat exchangers for thermal management in space p 120 A83-27137

SPALLING
The effect of annealing on the creep of plasma sprayed ceramics
[NASA-TM-83396] p 130 N83-24799

SPANWISE BLOWING
Spanwise mass transfer variations on a cylinder in 'nominally' uniform crossflow p 124 A83-43019

SPARK IGNITION
Computed and measured turbulence in axisymmetric reciprocating engines p 21 A83-24669
Turbulent flame propagation and combustion in spark ignition engines p 70 A83-48156
Ignition and combustion: Low compression ratio, high output diesel
[NASA-CR-169742] p 31 N83-15309
Free-piston Stirling hydraulic engine and drive system for automobiles
[NASA-TM-82992] p 211 N83-25625

SPECIFICATIONS
Mod-2 wind turbine project assessment and cluster test plans p 176 N83-19262

SPECIMEN GEOMETRY
On composites with periodic structure p 154 A83-10283

SPECKLE PATTERNS
Extending the laser-specklegram technique to strain analysis of rotating components p 155 A83-12514
Manual for extending the laser specklegram technique to strain analysis of rotating components
[NASA-CR-167932] p 134 N83-15601

SPECTROGRAPHS
A software system for emission spectrometry
[NASA-TM-83001] p 70 N83-12181

SPECTROMETERS
A software system for emission spectrometry
[NASA-TM-83001] p 70 N83-12181

SPECTROPHOTOMETRY
Infrared emission spectrophotometric study of the changes produced by TiN coating of metal surfaces in an operating EHD contact
[ASLE PREPRINT 82-LC-3C-3] p 135 A83-13229
Determination of physical and chemical states of lubricants in concentrated contacts, part 3
[NASA-CR-3658] p 92 N83-16527

SPECTROSCOPIC ANALYSIS
High-voltage spark atomic emission detector for gas chromatography p 67 A83-13108
X-ray photoelectron spectroscopy and friction studies of nickel-zinc and manganese-zinc ferrites in contact with metals
[NASA-TP-2163] p 84 N83-23419

SPECTRUM ANALYSIS
Ferrographic and spectrometer oil analysis from a failed gas turbine engine
[NASA-TM-82956] p 140 N83-12433
Coherent conversion of the sunlight spectrum
[NASA-CR-170185] p 179 N83-25026
SPHERICAL COORDINATES
Solution of viscous internal flows on curvilinear grids generated by the Schwarz-Christoffel transformation p 122 A83-36796
SPHERICAL SHELLS
High speed spherical roller-bearing analysis and comparison with experimental performance p 145 N83-20133
SPINEL
Oxidation of low cobalt alloys p 79 N83-11291
SPIRAL WRAPPING
A basis for the analysis of surface geometry of spiral bevel gears p 146 N83-20138
Spiral-bevel geometry and gear train precision p 146 N83-20139
Geometrical analysis of circular-cut spiral bevel gears
[NASA-CR-168226] p 151 N83-33167
SPIRALS (CONCENTRATORS)
Three-dimensional flow measurements in a vaneless radial turbine scroll
[NASA-CR-167994] p 9 N83-11065
SPRAY CHARACTERISTICS
The structure of evaporating and combusting sprays: Measurements and predictions
[NASA-CR-170176] p 129 N83-22550
High-pressure flame visualization of autoignition and flashback phenomena with liquid-fuel spray
[NASA-TM-83501] p 42 N83-34948
SPRAY NOZZLES
Structure of evaporating and combusting sprays: Measurements and predictions p 38 N83-29211
SPRAYED COATINGS
Sputtered silicon nitride coatings for wear protection p 88 A83-12651
Improved uniformity of multiphase ceramic-metal plasma-sprayed coats p 61 A83-22269
Creep of plasma-sprayed-ZrO2 thermal-barrier coatings p 89 A83-22273
Advanced ceramic coating development for industrial/utility gas turbine applications
[NASA-CR-165619] p 92 N83-15467
Plasma-sprayed self-lubricating coatings
[NASA-CR-3680] p 94 N83-22422
Creep of plasma sprayed zirconia
[NASA-CR-167868] p 96 N83-29393
Thermal barrier coating system having improved adhesion
[NASA-CASE-LEW-13359-1] p 97 N83-31855
SPRAYERS
The structure of particle-laden jets and nonevaporating sprays
[NASA-CR-168059] p 34 N83-20948
The structure of evaporating and combusting sprays: Measurements and predictions
[NASA-CR-170176] p 129 N83-22550
Particle sizing by measurement of forward-scattered light at two angles
[NASA-TP-2156] p 36 N83-24509
The structure of evaporating and combusting sprays: Measurements and predictions
[NASA-CR-170312] p 130 N83-24795
SPRAYING
Fuel spray diagnostics p 38 N83-29212
SPUTTERING
A direct-measurement technique for estimating discharge-chamber lifetime --- for ion thrusters
[AIAA PAPER 82-1908] p 51 A83-12483
Sputtered silicon nitride coatings for wear protection p 88 A83-12651
Morphological and frictional behavior of sputtered MoS2 films p 88 A83-12652
Some properties of r.f.-sputtered hafnium nitride coatings p 88 A83-12653
Interfacial electrical properties of ion-beam sputter deposited amorphous carbon on silicon p 205 A83-33920
Ion sputter textured graphite --- anode collector plates in electron tube devices
[NASA-CASE-LEW-12919-1] p 63 N83-10117
Mechanical bonding of metal method
[NASA-CASE-LEW-12941-1] p 77 N83-10170
Plasma deposition and surface modification techniques for wear resistance
[NASA-TM-82972] p 90 N83-10194
Microhardness studies on thin carbon films grown on P-type, (100) silicon
[NASA-TM-82980] p 61 N83-13169
Vacuum sputtered and ion-plated coatings for wear and corrosion protection
[NASA-TM-83007] p 99 N83-13273
Applications of ion beam technology
[NASA-CR-169797] p 82 N83-16493
Endurance test of a 30-CM-diameter engineering model ion thruster. Task 12: Investigation of thin-film erosion monitors for ion thrusters
[NASA-CR-168132] p 58 N83-25779
RF sputtered silicon and hafnium nitrides: Properties and adhesion to 440C stainless steel
[NASA-TM-83400] p 95 N83-27020
STABILITY
Rotordynamic Instability Problems in High-Performance Turbomachinery
[NASA-CP-2250] p 142 N83-15629
Stability analysis of flexible wind turbine blades using finite element method
[NASA-CR-168107] p 177 N83-21508
Requirements for a mobile communications satellite system. Volume 3: Large space structures measurements study
[NASA-CR-168105] p 45 N83-22255
Research on aviation fuel instability
[NASA-TM-83420] p 101 N83-28255
Constrained self-adaptive solutions procedures for structure subject to high temperature elastic-plastic creep effects p 162 N83-34370
STABILITY TESTS
Studies of the mechanisms of turbine fuel instability
[NASA-CR-167963] p 100 N83-18924
STACKS
Cell module and fuel conditioner development
[NASA-CR-165462-A] p 168 N83-12524
STAGNATION FLOW
Turbulence effect on crossflow around a circular cylinder at subcritical Reynolds numbers
[NASA-CR-3622] p 127 N83-13387
STAGNATION POINT
Stagnation region gas film cooling: Effects of dimensionless coolant temperature
[NASA-CR-168197] p 132 N83-30960
STAGNATION PRESSURE
A comparison of flow rates and pressure profiles for N-sequential inlets and three related seal configurations
[NASA-TM-83442] p 132 N83-33103
STAINLESS STEELS
Sputtered silicon nitride coatings for wear protection p 88 A83-12651
Low cycle fatigue behavior of aluminum/stainless steel composites
[AIAA 83-0806] p 62 A83-29886
Plastic deformation and wear process at a surface during unlubricated sliding p 138 A83-37822
Plastic deformation at surface during unlubricated sliding
[NASA-TP-2036] p 139 N83-11496
Effect of sliding speed and contact stress on tribological properties of ultra-high-molecular-weight polyethylene
[NASA-TP-2059] p 91 N83-14269
Rolling-element fatigue life of AMS 5900 balls
[NASA-TP-2080] p 142 N83-16758
Tribological and microstructural characteristics of ion-nitrided steels
[NASA-TM-83368] p 84 N83-24635
RF sputtered silicon and hafnium nitrides: Properties and adhesion to 440C stainless steel
[NASA-TM-83400] p 95 N83-27020
Relation of cyclic loading pattern to microstructural fracture in creep fatigue
[NASA-TM-83473] p 161 N83-34349
Tensile and compressive constitutive response of 316 stainless steel at elevated temperatures p 162 N83-34353
STANDARDS
Research priorities and history of advanced composite compression testing
[NASA-CR-165415] p 66 N83-18854
Solar cell measurements p 181 N83-25109
STANDING WAVES
Flutter and forced response of mistuned rotors using standing wave analysis
[AIAA 83-0845] p 156 A83-29823
STATIC INVERTERS
Transistorized PWM inverter-induction motor drive system p 110 A83-11488
STATIC LOADS
Hygrothermomechanical evaluation of transverse filament tape epoxy/polyester fiberglass composites
[NASA-TM-83044] p 65 N83-15362
A method for static and dynamic load analysis of standard and modified spur gears p 146 N83-20143
Design procedures for fiber composite structural components: Rods, columns and beam columns
[NASA-TM-83321] p 66 N83-24559
Rolling-element bearings
[NASA-RP-1105] p 149 N83-27214
STATIC PRESSURE
Effect of steady-state pressure distortion on inlet flow to a high-bypass-ratio turbofan engine
[NASA-TM-82964] p 30 N83-15306
STATIC STABILITY
Dynamic effects of internal spur gear drives
[NASA-CR-3692] p 149 N83-28452
STATIONKEEPING
Propulsion and fluid management - Station keeping will eat energy on a new scale p 54 A83-24360
STATISTICAL ANALYSIS
Cloud encounter statistics in the 28.5-43.5 KFT altitude region from four years of GASP observations p 188 A83-36733
Particle-sampling statistics in laser anemometers Sample-and-hold systems and saturable systems p 134 A83-48120
Statistical summaries of fatigue data for design purposes
[NASA-CR-3697] p 161 N83-29731
STATORS
Experimental evaluation of inlet turbulence, wall boundary layer, surface finish, and fillet radius on small axial turbine state performance
[SAE PAPER 821475] p 24 A83-38001
Performance of a tandem-rotor/tandem-stator conical-flow compressor designed for a pressure ratio of 3
[NASA-TP-2034] p 9 N83-11058
Analytical and experimental investigation of stator endwall contouring in a small axial-flow turbine. 1: Stator performance
[NASA-TP-2023] p 26 N83-11125
End wall flows in rotors and stators of a single stage compressor
[NASA-CR-169800] p 128 N83-16678
Evaluation of ceramics for stator applications: Gas turbine engines interim report. Stator fabrication and evaluation
[NASA-CR-168140] p 96 N83-30662
STEADY FLOW
A finite element formulation for steady transonic Euler equations p 3 A83-22129
A fast Euler solver for steady flows
[AIAA PAPER 83-1940] p 123 A83-39389
Critical review of the trailing edge condition in steady and unsteady flow. Blade flutter in compressors and fans: Numerical simulation of the aerodynamic loading
[NASA-CR-169705] p 10 N83-15264
Fast Euler solver for steady, 1-dimensional flows
[NASA-CR-3689] p 14 N83-27960
STEADY STATE
Effect of steady-state pressure distortion on inlet flow to a high-bypass-ratio turbofan engine
[NASA-TM-82964] p 30 N83-15306
STEAM
Catalytic combustion with steam injection
[ASME PAPER 82-JPGC-GT-23] p 164 A83-25271
Catalytic combustion with steam injection
[NASA-TM-82923] p 170 N83-15805
Steam cooled rich-burn combustor liner
[NASA-CASE-LEW-13609-1] p 72 N83-17028
STEAM TURBINES
Analysis of potential benefits of integrated-gasifier combined cycles for a utility system
[NASA-TP-2172] p 186 N83-36549
STEELS
Corrosion of simulated bearing components of three bearing steels in the presence of chloride-contaminated lubricant
[NASA-TM-82955] p 143 N83-20115
The effects of Ni, Mo, Ti and Si on the mechanical properties of Cr free Mn steel (Fe-25Mn-5Al-2C)
[NASA-TM-83355] p 85 N83-24638
Crack layer morphology and toughness characterization in steels
[NASA-CR-168154] p 160 N83-27256
The thermal fatigue resistance of H-13 Die Steel for aluminum die casting dies
[NASA-TM-83331] p 87 N83-35103
STIFFNESS
Aerodynamic stiffness of an unbound eccentric whirling centrifugal impeller with an infinite number of blades p 142 N83-15650
Dynamic tooth loads and stressing for high contact ratio spur gears p 147 N83-20148
Vibration in planetary gear systems with unequal planet stiffnesses
[NASA-TM-83428] p 150 N83-29709
STIFFNESS MATRIX
Alternative ways for formulation of hybrid stress elements p 155 A83-14710
STIRLING CYCLE
Computation techniques and computer programs to analyze Stirling cycle engines using characteristic dynamic energy equations p 207 A83-27272

Improved Stirling engine performance using jet impingement p 137 A83-27288
Conceptual design and cost analysis of hydraulic output unit for 15 kW free-piston Stirling engine
[NASA-CR-165543] p 167 N83-10561
A conceptual study of the potential for automotive-derived and free-piston Stirling engines in 30- to 400-kilowatt stationary power applications
[NASA-CR-165274] p 167 N83-10568
Automotive Stirling Engine Mod 1 Design Review, volume 2
[NASA-CR-167936] p 209 N83-10991
Cast Fe-base cylinder/regenerator housing alloy
[NASA-CR-169474] p 80 N83-12214
Computer program for a four-cylinder-Stirling-engine controls simulation
[NASA-TM-82774] p 126 N83-12359
Evaluation of dopants in hydrogen to reduce hydrogen permeation in candidate Stirling engine heater head tube alloys at 760 deg and 820 deg
[NASA-TM-82920] p 81 N83-13232
Automotive Stirling engine development program
[NASA-CR-167907] p 209 N83-15176
Automotive Stirling engine development program
[NASA-CR-168060] p 209 N83-15177
Computer program for Stirling engine performance calculations
[NASA-TM-82960] p 210 N83-17423
Stirling engine application study
[NASA-CR-168087] p 210 N83-22029
Creep-rupture behavior of 6 candidate stirling engine iron-base superalloys in high pressure hydrogen. Volume 1: Air creep-rupture behavior
[NASA-CR-168071] p 83 N83-22389
Design of hydraulic output Stirling engine
[NASA-CR-167976] p 177 N83-22739
Testing and performance characteristics of a 1-kW free piston Stirling engine
[NASA-TM-82999] p 180 N83-25036
A study of dynamic energy equations for Stirling cycle analysis
[NASA-CR-168152] p 181 N83-25043
Free-piston Stirling hydraulic engine and drive system for automobiles
[NASA-TM-82992] p 211 N83-25625
A 4-cylinder Stirling engine computer program with dynamic energy equations
[NASA-TM-83053] p 130 N83-26017
Automotive Stirling engine development program
[NASA-CR-165263] p 211 N83-26762
Test results and description of a 1-kW free-piston Stirling engine with a dashpot load
[NASA-TM-83407] p 182 N83-27346
DOE/NASA Automotive Stirling Engine Project overview '83
[NASA-TM-83405] p 212 N83-27924
Automotive Stirling Engine Development Program
[NASA-CR-168074] p 212 N83-27925
Stirling engine design manual, 2nd edition
[NASA-CR-168088] p 212 N83-30328

STOCHASTIC PROCESSES
Evaluation of a stochastic model of particle dispersion in a turbulent round jet p 121 A83-28104
Stochastic differential equations and turbulent dispersion
[NASA-RP-1103] p 129 N83-22546
Structure of evaporating and combusting sprays: Measurements and predictions p 38 N83-29211

STOICHIOMETRY
A variable-geometry combustor used to study primary and secondary zone stoichiometry
[NASA-TM-83372] p 37 N83-27995
Preliminary tests of an advanced high-temperature combustion system
[NASA-TP-2203] p 41 N83-33893

STORAGE RINGS (PARTICLE ACCELERATORS)
Improved ion containment using a ring-cusp ion thruster
[AIAA PAPER 82-1928] p 53 A83-21100
Improved ion containment using a ring-cusp ion thruster
[NASA-TM-82990] p 56 N83-13164

STORAGE STABILITY
Studies of the mechanisms of turbine fuel instability
[NASA-CR-167963] p 100 N83-18624

STRAIN GAGES
An extensometer for axial strain measurement at high temperature p 134 A83-48604
Analysis of strain gage reliability in F-100 jet engine testing at NASA Lewis Research Center
[NASA-TM-83325] p 134 N83-24829

STRAIN RATE
Intermetallics as alternative materials p 80 N83-11300
High strain rate properties of undirectional composites, part 1
[NASA-CR-167969] p 64 N83-13178
High strain properties of angle-ply composite laminate, part 3
[NASA-CR-167971] p 64 N83-13180

STREAMLINING
A new surface-streamline flow-visualization technique p 133 A83-19016

STREAMS
Experiments on identification and control of inflow disturbances in contracting streams
[NASA-CR-169831] p 11 N83-17503

STRESS ANALYSIS
Moving cracks in layered composites p 155 A83-12048
A new formulation of hybrid/mixed finite element p 155 A83-12739
On the solution of elastic-plastic static and dynamic postbuckling collapse of general structure p 155 A83-12746
Alternative ways for formulation of hybrid stress elements p 155 A83-14710
Natural frequency of rotating beams using non-rotating modes p 156 A83-18383
Turbine blade nonlinear structural and life analysis p 21 A83-29024
An uncoupled viscoplastic constitutive model for metals at elevated temperature
[AIAA 83-1016] p 156 A83-29798
Benchmark notch test for life prediction
[NASA-CR-165571] p 158 N83-12451
Manual for extending the laser specklegram technique to strain analysis of rotating components
[NASA-CR-167932] p 134 N83-15601
Three-dimensional elastoplastic stress analysis of unidirectional boron/aluminum composites
[NASA-CR-169796] p 65 N83-16394
Compliance and stress sensitivity of spur gear teeth p 146 N83-20142
Dynamic tooth loads and stressing for high contact ratio spur gears p 147 N83-20148
Correlation of compressive stress with spalling of plasma sprayed ceramic materials
[NASA-TM-83406] p 95 N83-27016

STRESS CONCENTRATION
A total life prediction model for stress concentration sites
[NASA-CR-170290] p 160 N83-23629

STRESS FUNCTIONS
Three-dimensional elastoplastic stress analysis of unidirectional boron/aluminum composites
[NASA-CR-169796] p 65 N83-16394

STRESS INTENSITY FACTORS
Moving cracks in layered composites p 155 A83-12048
Stress intensity and displacement coefficients for radially cracked ring segments subject to three-point bending
[NASA-TM-83059] p 160 N83-24874
Analysis of an externally radially cracked ring segment subject to three-point radial loading
[NASA-TM-83482] p 163 N83-35413

STRESS MEASUREMENT
Extending the laser-specklegram technique to strain analysis of rotating components p 155 A83-12514
Manual for extending the laser specklegram technique to strain analysis of rotating components
[NASA-CR-167932] p 134 N83-15601
Development of a rotary instrumentation system, phase 2
[NASA-CR-168013] p 47 N83-18835

STRESS RELIEVING
Steam cooled rich-burn combustor liner
[NASA-CASE-LEW-13606-1] p 72 N83-17628

STRESS WAVES
Wave propagation in a graphite/epoxy laminate p 158 A83-44050
Acousto-ultrasonic characterization of fiber reinforced composites p 63 N83-11231
A study of the stress wave factor technique for the characterization of composite materials
[NASA-CR-3670] p 153 N83-27248
The effect of stress on ultrasonic pulses in fiber reinforced composites
[NASA-CR-3724] p 154 N83-33180

STRESS-STRAIN RELATIONSHIPS
Experimental verification of the Neuber relation at room and elevated temperatures --- to predict stress-strain behavior in notched specimens of hastelloy x
[NASA-CR-167967] p 159 N83-19121
Development of a simplified analytical method for representing material cyclic response
[NASA-CR-168100] p 160 N83-21390
Experimental verification of the number relation at room and elevated temperatures p 162 N83-34355
Evaluation of inelastic constitutive models for nonlinear structural analysis p 162 N83-34357
Simplified method for nonlinear structural analysis
[NASA-TP-2208] p 163 N83-34372

STRESS-STRAIN-TIME RELATIONS
Creep-rupture behavior of 6 candidate stirling engine iron-base superalloys in high pressure hydrogen. Volume 1: Air creep-rupture behavior
[NASA-CR-168071] p 83 N83-22389

STRUCTURAL ANALYSIS
On composites with periodic structure p 154 A83-10283
On the solution of elastic-plastic static and dynamic postbuckling collapse of general structure p 155 A83-12746
The determination of the elastodynamic fields of an ellipsoidal inhomogeneity
[ASME PAPER 83-APM-19] p 157 A83-37388
NASA LeRC/Akron University Graduate Cooperative Fellowship Program and Graduate Student Researchers Program
[NASA-CR-167943] p 208 N83-10970
Materials constitutive models for nonlinear analysis of thermally cycled structures
[NASA-TP-2055] p 158 N83-12449
Effects of structural coupling on mistuned cascade flutter and response
[NASA-TM-83049] p 159 N83-15672
Design and evaluation of low cost blades for large wind driven generating systems p 175 N83-19244
Structural fatigue test results for large wind turbine blade sections p 159 N83-19246
Evaluation of inelastic constitutive models for nonlinear structural analysis p 162 N83-34357
Constrained self-adaptive solutions procedures for structure subject to high temperature elastic-plastic creep effects p 162 N83-34370
Simplified method for nonlinear structural analysis
[NASA-TP-2208] p 163 N83-34372
The structural response of a rail accelerator
[NASA-TM-83491] p 163 N83-35412

STRUCTURAL DESIGN
Structural tailoring of engine blades (STAEBL)
[AIAA 83-0828] p 22 A83-29737
Parametric analysis of closed cycle magnetohydrodynamic (MHD) power plants
[NASA-CR-165472] p 178 N83-22748
Parametric study of potential early commercial MHD power plants. Task 3: Parameter variation of plant size
[NASA-CR-165445] p 182 N83-26259
Statistical summaries of fatigue data for design purposes
[NASA-CR-3697] p 161 N83-29731

STRUCTURAL DESIGN CRITERIA
Design and fabrication of composite blades for the Mod-1 wind turbine generator
[NASA-CR-167987] p 168 N83-11579
Array structure design handbook for stand alone photovoltaic applications
[NASA-TM-82629] p 160 N83-23631
Design procedures for fiber composite structural components: Rods, columns and beam columns
[NASA-TM-83321] p 66 N83-24559
Nonlinear Constitutive Relations for High Temperature Applications
[NASA-CP-2271] p 161 N83-34351

STRUCTURAL ENGINEERING
Research and technology, Lewis Research Center
[NASA-TM-83038] p 208 N83-15169

STRUCTURAL FAILURE
On the solution of elastic-plastic static and dynamic postbuckling collapse of general structure p 155 A83-12746
Turbine blade nonlinear structural and life analysis p 21 A83-29024
Application of advanced reliability methods to local strain fatigue analysis
[NASA-CR-168198] p 161 N83-29734

STRUCTURAL STABILITY
Growth and stability of interacting surface flaws of arbitrary shape p 155 A83-15060
Stability analysis of Centaur-in-Shuttle composite corrugated adapters
[AIAA 83-1003] p 49 A83-29791
Large displacements and stability analysis of nonlinear propeller structures p 159 N83-12460

STRUCTURAL STRAIN
A solution procedure for behavior of thick plates on a nonlinear foundation and postbuckling behavior of long plates
[NASA-TP-2174] p 163 N83-34373

STRUCTURAL VIBRATION
Vibrations of cantilevered doubly-curved shallow shells p 157 A83-39557

Analysis of an axial compressor blade vibration based on wave reflection theory
[ASME PAPER 83-GT-151] p 25 A83-47970
Vibrations of blades with variable thickness and curvature by shell theory
[ASME PAPER 83-GT-152] p 158 A83-47978

STRUCTURAL WEIGHT
A method to estimate weight and dimensions of small aircraft propulsion gas turbine engines: User's guide
[NASA-CR-168049] p 31 N83-16343
Advanced electrical power system technology for the all electric aircraft
[NASA-TM-83390] p 115 N83-24764

SUBROUTINES
User's manual for Axisymmetric Diffuser Duct (ADD) code. Volume 2: Detailed ADD code description
[NASA-CR-165598-VOL-2] p 211 N83-26758

SUBSONIC AIRCRAFT
Zero-length inlets for subsonic V/STOL aircraft
p 4 A83-29012
The development of a generalized advanced propeller analysis system
[AIAA PAPER 83-2466] p 26 A83-49581

SUBSONIC FLOW
Laser-induced fluorescence technique for velocity field measurements in subsonic gas flows
p 133 A83-45962
Implicit marching solution of compressible viscous subsonic flow in planar and axisymmetric ducts
[NASA-TM-82876] p 125 N83-10389

SUBSONIC FLUTTER
Subsonic-transonic stall flutter study
[NASA-CR-165256] p 43 N83-30435

SUBSONIC SPEED
Model aerodynamic test results for a refined actuated inlet ejector nozzle at simulated takeoff and cruise conditions
[NASA-CR-168051] p 13 N83-26816

SUBSTRATES
Method for depositing an oxide coating
[NASA-CASE-LEW-13131-1] p 165 N83-10494
Coating with overlay metallic-cermet alloy systems
[NASA-CASE-LEW-13639-2] p 82 N83-17683
Screen printed interdigitated back contact solar cell
[NASA-CASE-LEW-13414-1] p 177 N83-20374
Correlation of compressive stress with spalling of plasma sprayed ceramic materials
[NASA-TM-83406] p 95 N83-27016
Method of forming oxide coatings --- for solar collector heating panels
[NASA-CASE-LEW-13132-1] p 96 N83-29388
Improved thermal barrier coating system
[NASA-CASE-LEW-13324-2] p 86 N83-34014

SULFATES
Aircraft sampling of the sulfate layer near the tropopause following the eruption of Mount St. Helens
p 187 N83-11556

SULFIDES
Vaporization thermodynamics of K2S and K2SO3
[NASA-CR-168080] p 61 N83-19812
Moderate temperature rechargeable sodium batteries
[NASA-CR-168220] p 118 N83-36359

SULFITES
Vaporization thermodynamics of K2S and K2SO3
[NASA-CR-168080] p 61 N83-19812
Thermodynamics of the potassium-sulfur-oxygen and related systems
[NASA-CR-168155] p 61 N83-28077

SULFUR
Laser fluorescence studies of the chemical interactions of sodium species with sulfur bearing fuels
[NASA-CR-169861] p 71 N83-17625

SUNLIGHT
Determination of optimum sunlight concentration level in space for 3-5 cascade solar cells p 170 N83-14732
Determination of optimum sunlight concentration level in space for 3-5 cascade solar cells p 171 N83-15814
Coherent conversion of the sunlight spectrum
[NASA-CR-170185] p 179 N83-25026

SUPERCONDUCTING MAGNETS
Magnetohydrodynamics (MHD) Engineering Test Facility (ETF) 200 MWe power plant. Conceptual Design Engineering Report (CDER) supplement. Magnet system special investigations
[NASA-CR-165509] p 141 N83-14494

SUPERCRITICAL FLOW
Design of supercritical cascades with high solidity
p 6 A83-43446
Experimental evaluation of shockless supercritical airfoils in cascade
[NASA-TM-83045] p 11 N83-15268

SUPERCRITICAL WINGS
Experimental evaluation of shockless supercritical airfoils in cascade
[AIAA PAPER 83-0003] p 2 A83-16455

SUPERHIGH FREQUENCIES
Equivalent-circuit consideration of dual-gate MESFETs at high frequency p 113 A83-44970
Engineering calculations for communications systems planning
[NASA-CR-170182] p 106 N83-22494

SUPERSONIC AIRCRAFT
Supersonic STOVL research aircraft
[SAE PAPER 821375] p 17 A83-37965

SUPERSONIC COMBUSTION
Investigation of a low NOx full-scale annular combustor
[NASA-CR-165518] p 29 N83-13104

SUPERSONIC DIFFUSERS
Dynamic distortion in a short s-shaped subsonic diffuser with flow separation --- Lewis 8 by 6 foot Supersonic Wind Tunnel
[AIAA PAPER 83-1412] p 25 A83-45515
Dynamic distortion in a short s-shaped subsonic diffuser with flow separation --- Lewis 8 by 6 foot Supersonic Wind Tunnel
[NASA-TM-83412] p 36 N83-26838

SUPERSONIC FLOW
An experimental investigation of internal area ruling for transonic and supersonic channel flow
[NASA-CR-169638] p 10 N83-14068
Validation of a three-dimensional viscous analysis of axisymmetric supersonic inlet flow fields
[NASA-TM-83058] p 32 N83-17538

SUPERSONIC INLETS
Low speed performance of a supersonic axisymmetric mixed compression inlet with auxiliary inlets
[AIAA PAPER 83-1414] p 7 A83-45516
Low flight speed acoustic results for a supersonic inlet with auxiliary inlet doors
[AIAA PAPER 83-1415] p 196 A83-45517
A computer program for the calculation of the flow field including boundary layer effects for mixed-compression inlets at angle of attack
[NASA-CR-168002] p 10 N83-11063
Low flight speed acoustic results for a supersonic inlet with auxiliary inlet doors
[NASA-TM-83411] p 201 N83-27794
Low speed performance of a supersonic axisymmetric mixed compression inlet with auxiliary inlets --- Lewis 9x15-ft anechoic wind tunnel tests
[NASA-TM-83435] p 37 N83-27992

SUPERSONIC JET FLOW
Tests of a thermal acoustic shield with a supersonic jet p 192 A83-10183
On the shock cell structure and noise of supersonic jets
[AIAA PAPER 83-0703] p 193 A83-25923
An experimental study of supersonic jet shock-associated noise
[AIAA PAPER 83-0708] p 193 A83-25924
Coaxial supersonic jet-flows, shock structure and related problems with noise-suppression assessment and prediction
[AIAA PAPER 83-0707] p 194 A83-28011
User's manual for Axisymmetric Diffuser Duct (ADD) code. Volume 1: General ADD code description
[NASA-CR-165598-VOL-1] p 211 N83-26757

SUPERSONIC SPEEDS
Noise of the 10-bladed, 40 deg swept SR-6 propeller in a wind tunnel
[NASA-TM-82950] p 196 N83-11840
Model aerodynamic test results for a refined actuated inlet ejector nozzle at simulated takeoff and cruise conditions
[NASA-CR-168051] p 13 N83-26816

SUPERSONIC TRANSPORTS
Ejector nozzle test results at simulated flight conditions for an advanced supersonic transport propulsion system
[AIAA PAPER 83-1287] p 23 A83-36323

SUPPRESSORS
Utilizing numerical techniques in turbofan inlet acoustic suppressor design
[NASA-TM-82994] p 196 N83-10885

SURFACE ACOUSTIC WAVE DEVICES
Surface acoustic admittance of highly porous open-cell, elastic foams p 195 A83-28849

SURFACE COOLING
Determination of boundary shape of cooled porous region p 118 A83-13487

SURFACE DEFECTS
Growth and stability of interacting surface flaws of arbitrary shape p 155 A83-15060
Elastohydrodynamic contacts. Effects of dents and grooves on traction and local film thickness
[NASA-TP-2175] p 150 N83-28453

SURFACE FINISHING
Laser surface fusion of plasma sprayed ceramic turbine seals
[NASA-CASE-LEW-13269-1] p 50 N83-20996

SURFACE GEOMETRY
Investigation of the effects of initial fluid film profile on pumping ring operation
[ASME PAPER 82-LUB-35] p 136 A83-13516
Convex curvature effects on the heated turbulent boundary layer p 123 A83-42733
A basis for the analysis of surface geometry of spiral bevel gears p 146 N83-20138

SURFACE PROPERTIES
Mechanical bonding of metal method
[NASA-CASE-LEW-12941-1] p 77 N83-10170
Surface chemistry, friction and wear of Ni-Zn and Mn-Zn ferrites in contact with metals
[NASA-TM-83068] p 93 N83-19901
Atmospheric radiation model for water surfaces
[NASA-CR-167873] p 187 N83-21677
Time effect of erosion by solid particle impingement on ductile materials
[NASA-TM-83369] p 84 N83-24637
Application of modern surface analytical tools in the investigation of surface deterioration processes
[NASA-TM-83452] p 152 N83-34327

SURFACE REACTIONS
Microscopic contour changes of tribological surfaces by chemical and mechanical action
[ASLE PREPRINT 82-LC-3B-3] p 136 A83-13237
Boundary integral equation method calculations of surface regression effects in flame spreading
p 67 A83-13488
Ignition of a combustible half space
p 68 A83-22735
XPS, AES and friction studies of single-crystal silicon carbide p 89 A83-36973

SURFACE ROUGHNESS
The influence of surface dents and grooves on traction in sliding EHD point contacts p 138 A83-37823
Ion sputter textured graphite --- anode collector plates in electron tube devices
[NASA-CASE-LEW-12919-1] p 63 N83-10117
Compressor cascade performance deterioration caused by sand ingestion
[NASA-CR-168067] p 11 N83-16286
Surface profile changes of scuffed bearing surfaces --- before and after acid treatment
[NASA-TM-83055] p 82 N83-17682
Lubrication background
[NASA-TM-81692] p 147 N83-20159
The effect of annealing on the creep of plasma sprayed ceramics
[NASA-TM-83396] p 130 N83-24799
Classification of journal surfaces using surface topography parameters and software methods to compensate for stylus geometry
[NASA-CR-168153] p 148 N83-24857
Current collection from the space plasma through defects in high voltage solar array insulation
[NASA-CR-168148] p 204 N83-31474

SURFACE ROUGHNESS EFFECTS
Surface roughness effects in hydrodynamic lubrication: The flow factor method
[NASA-TM-83024] p 129 N83-19016

SURFACE TEMPERATURE
XPS, AES and friction studies of single-crystal silicon carbide p 89 A83-36973
Surface temperatures and glassy state investigations in tribology, part 5
[NASA-CR-3632] p 91 N83-11328
Experimental and analytical determination of gear tooth temperatures with oil jet lubrication p 142 N83-15530
Gear lubrication and cooling experiment and analysis
p 147 N83-20147
Curved film cooling admission tube
[NASA-CASE-LEW-13174-1] p 131 N83-27144
Current collection from the space plasma through defects in high voltage solar array insulation
[NASA-CR-168148] p 204 N83-31474

SURFACE WATER
Atmospheric radiation model for water surfaces
[NASA-CR-167873] p 187 N83-21677

SWAGING
Effect of swaging on the 1000 C compressive slow plastic flow characteristics of the directionally solidified eutectic alloy gamma/gamma prime-alpha p 77 A83-44340
Development of a high capacity toroidal Ni/Cd cell
[NASA-CR-169945] p 176 N83-19273

SWEAT COOLING
Small gas turbine combustor study - Combustor liner evaluation
[AIAA PAPER 83-0337] p 20 A83-16663
Small gas turbine combustor study: Combustor liner evaluation
[NASA-TM-83028] p 33 N83-18725

SWEPT WINGS
Noise generation by a finite span swept airfoil
[AIAA PAPER 83-0768] p 195 A83-28023

SWIRLING
Five-hole pitot probe time-mean velocity measurements in confined swirling flows
[AIAA PAPER 83-0315] p 119 A83-16645
Confined swirling flow predictions
[AIAA PAPER 83-0316] p 119 A83-16646
Mean flowfields in axisymmetric combustor geometries with swirl p 120 A83-24668
Prediction of high speed propeller flow fields using a three-dimensional Euler analysis
[AIAA PAPER 83-0188] p 4 A83-29535
Single-wire swirl flow turbulence measurements
[AIAA PAPER 83-1202] p 122 A83-36278
The performance of an annular vane swirler --- to aid in modeling gas turbine combustor flowfields and swirling confined flow turbulence
[AIAA PAPER 83-1326] p 24 A83-36340
Prediction of high speed propeller flow fields using a three-dimensional Euler analysis
[NASA-TM-83065] p 12 N83-19710
Axial vane-type swirler performance characteristics
[NASA-CR-172995] p 40 N83-32808
SWITCHING
Satellite switched FDMA advanced communication technology satellite program
[NASA-CR-168034] p 105 N83-15543
SWITCHING CIRCUITS
Investigations of stability and dynamic performances of switching regulators employing current-injected control p 110 A83-11002
Development of a microwave 20 x 20 switch matrix for 30/20 GHz SS-TDMA application p 110 A83-11484
A novel input filter compensation scheme for switching regulators p 111 A83-11494
An improved switching converter model using discrete and average techniques p 111 A83-11495
Solar array switching power management p 54 A83-27132
Comparison of channel assignment techniques for hybrid switching p 104 A83-41363
An improved switching converter model
[NASA-CR-169669] p 114 N83-14398
Study of solar array switching power management technology for space power system
[NASA-CR-167890] p 179 N83-22756
Spacecraft IF switch matrix for wideband service applications in 30/20 GHz communications satellite systems: Proof-of-concept model, executive summary
[NASA-CR-168175] p 107 N83-29492
SYNCHRONOUS SATELLITES
On-orbit propulsion requirements and performance assessment of ion propulsion subsystems for future GEO large satellite missions
[AIAA PAPER 82-1872] p 48 A83-12460
SYNTHESIS (CHEMISTRY)
Synthesis and characterization of bisimide amines and bisimide amine-cured epoxy resins p 88 A83-11486
Synthesis and characterization of bisimide amines and bisimide amine-cured epoxy resins p 90 A83-40924
Polyvinyl alcohol cross-linked with two aldehydes
[NASA-CASE-LEW-13504-1] p 71 N83-13188
SYNTHETIC FUELS
Literature survey of properties of synfuels derived from coal
[NASA-TM-82739] p 99 N83-10208
Summary of synfuel characterization and combustion studies
[NASA-TM-83066] p 185 N83-34453
SYSTEM EFFECTIVENESS
The DOE/NASA wind turbine data acquisition system. Part 3: Unattended power performance monitor
[NASA-CR-165540] p 44 N83-24516
SYSTEMS ENGINEERING
30/20 GHz experimental communications satellite system p 103 A83-19688
Control design for a wind turbine-generator using output feedback p 164 A83-24721
NASA low-speed centrifugal compressor for fundamental research
[AIAA PAPER 83-1351] p 43 A83-36353
Controller scheduling - A possible algebraic viewpoint p 190 A83-37093
Power turbine dynamics - An evaluation of a shear-mounted elastomeric damper
[ASME PAPER 83-GT-228] p 139 A83-48025
Digital system for structural dynamics simulation
[NASA-CR-168019] p 43 N83-14139
Magnetohydrodynamics (MHD) Engineering Test Facility (ETF) 200 MWe power plant. Conceptual Design Engineering Report (CDER) supplement. Magnet system special investigations
[NASA-CR-165509] p 141 N83-14494
Pore size engineering applied to the design of separators for nickel-hydrogen cells and batteries
[NASA-TM-83386] p 73 N83-24571
Advanced Gas Turbine (AGT) powertrain system development for automotive applications
[NASA-CR-174104] p 211 N83-26763
SYSTEMS INTEGRATION
Comparison of channel assignment techniques for hybrid switching p 104 A83-41363
Role of simulation and emulation in the development of Shuttle-Centaur (STS-Centaur)
[NASA-TM-83326] p 45 N83-29292
SYSTEMS SIMULATION
Digital system for structural dynamics simulation
[NASA-CR-168019] p 43 N83-14139
Role of simulation and emulation in the development of Shuttle-Centaur (STS-Centaur)
[NASA-TM-83326] p 45 N83-29292
SYSTEMS STABILITY
Transformer induced instability of the series resonant converter p 113 A83-41152

T

TACKINESS
PMR-15 polyimide modifications for improved prepreg tack
[NASA-TM-82951] p 64 N83-12175
TAKEOFF
Model aerodynamic test results for a refined actuated inlet ejector nozzle at simulated takeoff and cruise conditions
[NASA-CR-168051] p 13 N83-26816
TANTALUM
COSAM (Conservation Of Strategic Aerospace Materials) program overview
[NASA-TM-83006] p 78 N83-11282
COSAM program overview p 78 N83-11283
Conservation of strategic metals p 80 N83-12154
TANTALUM ALLOYS
Influence of cobalt, tantalum, and tungsten on the microstructure and mechanical properties of superalloy single crystals p 79 N83-11293
Relation of cyclic loading pattern to microstructural fracture in creep fatigue
[NASA-TM-83473] p 161 N83-34349
TANTALUM OXIDES
The effect of Ta2O5 on the interaction between silicon and its contact metallization
[NASA-TM-82948] p 166 N83-10554
TAPERING
Vibrations of blades with variable thickness and curvature by shell theory
[ASME PAPER 83-GT-152] p 158 A83-47978
Large-bore tapered-roller bearing performance and endurance to 2.4 million DN p 145 N83-20134
TAXIING
Temperature distribution in an aircraft tire at low ground speeds
[NASA-TP-2195] p 161 N83-33217
TECHNOLOGICAL FORECASTING
Future satellite systems - Market demand assessment p 104 A83-19762
Advanced LOX/H2 engine technologies for future OTVs
[AIAA PAPER 83-1312] p 55 A83-36333
Satellite provided fixed communications services: A forecast of potential domestic demand through the year 2000: Volume 2: Main test
[NASA-CR-168146] p 108 N83-34114
TECHNOLOGY ASSESSMENT
Electric propulsion research and technology in the United States
[AIAA PAPER 82-1867] p 53 A83-16925
30/20 GHz experimental communications satellite system p 103 A83-19688
Inert gas thruster technology p 53 A83-20423
PMR polyimides - Review and update --- Polymerization of Monomer Reactants p 62 A83-20447
Thermionic technology infrastructure for space power p 54 A83-27298
Tubes in space - Very much alive p 112 A83-28160
A summary of EHV propulsion technology --- Electric and Hybrid Vehicle p 209 A83-31087
Advanced propfan engine characteristics and technology needs
[AIAA PAPER 83-1155] p 23 A83-36250
Preliminary assessment of the tradeoffs between the electric motor and the transmission in electric vehicles
[NASA-CR-168199] p 117 N83-30915
Current and future technology in radial and axial gas turbines
[NASA-TM-83414] p 41 N83-32811
Spindt cold cathode electron gun development program
[NASA-CR-168212] p 202 N83-35787
TECHNOLOGY TRANSFER
The NASA Redox Storage System Development project, 1980
[NASA-TM-82940] p 169 N83-14683
TECHNOLOGY UTILIZATION
Stirling engine application study
[NASA-CR-168087] p 210 N83-22029
TEETERING
The effect of yaw on horizontal axis wind turbine loading and performance
[NASA-TM-82778] p 169 N83-14688
The response of a 38m horizontal axis teetered rotor to yaw p 175 N83-19232
Stall induced instability of a teetered rotor p 175 N83-19234
TELECOMMUNICATION
A 1 watt GaAs power amplifier for the NASA 30/20 GHz communication system p 111 A83-11489
30/20 GHz experimental communications satellite system p 103 A83-19688
Requirements for a mobile communications satellite system. Volume 1: Executive summary
[NASA-CR-168128] p 106 N83-23497
Method for terminal position determination in Earth terminal-to-satellite burst acquisition and synchronization
[NASA-CASE-LEW-13893-1] p 107 N83-30832
Customer premises services market demand assessment 1980 - 2000. Volume 1: Executive summary
[NASA-CR-168150] p 108 N83-31925
Customer premises services market demand assessment 1980 - 2000: Volume 2
[NASA-CR-168151] p 108 N83-31926
Satellite provided fixed communication services: A forecast of potential domestic demand through the year 2000. Volume 1: Executive summary
[NASA-CR-168145] p 108 N83-34113
Satellite provided fixed communications services: A forecast of potential domestic demand through the year 2000: Volume 2: Main test
[NASA-CR-168146] p 108 N83-34114
Satellite fixed communications service: A forecast of potential domestic demand through the year 2000. Volume 2: Appendices
[NASA-CR-168147] p 108 N83-34115
Satellite provided customer premise services: A forecast of potential domestic demand through the year 2000. Volume 2: Technical report
[NASA-CR-168143] p 109 N83-34117
Mobile radio alternative systems study, executive summary
[NASA-CR-168207] p 109 N83-34119
TELEMETRY
Development of a rotary instrumentation system, phase 2
[NASA-CR-168013] p 47 N83-18835
TELEPHONES
Computer simulator for a mobile telephone system
[NASA-CR-170181] p 106 N83-22493
TELEVISION RECEPTION
Experimental results for the interference between FM television signals p 103 A83-19686
TELEVISION TRANSMISSION
Experimental results for the interference between FM television signals p 103 A83-19686
Multi-stage Depressed Collectors (MDC) for efficiency improvements of UHF broadcast klystrons
[NASA-TM-82970] p 105 N83-10322
TEMPERATURE
Lower-curing-temperature PMR polyimides p 89 A83-40923
Lower-curing-temperature PMR polyimides
[NASA-TM-82958] p 63 N83-10118
Comparison of modern icing cloud instruments
[NASA-CR-168008] p 19 N83-18720
TEMPERATURE CONTROL
Direct contact droplet heat exchangers for thermal management in space p 120 A83-27137
Analysis of coolant entrance boundary shape of porous region to control cooling along exit boundary p 124 A83-43361
Magnetic heat pumping
[NASA-CASE-LEW-12508-3] p 131 N83-29625
TEMPERATURE DEPENDENCE
Metallic conductivity and air stability in copper chloride intercalated carbon fibers p 111 A83-16095
Dynamic mechanical properties of n-phenylnadimide modified PMR polyimide composites
[NASA-TM-83051] p 65 N83-15363
TEMPERATURE DISTRIBUTION
Determination of boundary shape of cooled porous region p 118 A83-13487
Analytical and experimental evaluation of the heat transfer distribution over the surfaces of turbine vanes
[NASA-CR-168015] p 131 N83-28376

Perspectives on the mixing of a row of jets with a confined crossflow
[NASA-TM-83457] p 15 N83-30392
Numerical analysis of turbulent coaxial flow with internal heat generation
[NASA-CR-172633] p 132 N83-33105
Temperature distribution in an aircraft tire at low ground speeds
[NASA-TP-2195] p 161 N83-33217

TEMPERATURE EFFECTS
Small particle transport across turbulent nonisothermal boundary layers p 118 A83-10650
An uncoupled viscoplastic constitutive model for metals at elevated temperature
[AIAA 83-1016] p 156 A83-29798
An experimental study of heat induced surface-tension driven flow p 44 A83-43269
Development of tough, strong, iron-base alloy for cryogenic applications p 44 N83-18763
Design procedures for fiber composite structural components: Rods, columns and beam columns
[NASA-TM-83321] p 66 N83-24559
Low temperature cross linking polyimides
[NASA-CASE-LEW-12876-2] p 96 N83-29392
Spectrophotometric analysis of aqueous mixtures of some chromium (III) complexes
[NASA-CR-172999] p 74 N83-32872
Three-dimensional turbulent-mixing-length modeling for discrete-hole coolant injection into a crossflow
[NASA-TP-2200] p 132 N83-34232
Thermal elastohydrodynamic lubrication of line contacts
[NASA-TM-83424] p 152 N83-34326

TEMPERATURE GRADIENTS
Use of fiber-like materials to augment cycle life of thick, thermoprotective-seal coatings --- for gas turbine engine components p 89 A83-22271

TEMPERATURE MEASUREMENT
The thermal conductivity of oxygen p 207 A83-12094
An experimental investigation of the vaporous/gaseous cavity characteristics of an eccentric journal bearing
[ASLE PREPRINT 82-LC-3A-1] p 136 A83-13230
Measurement of thermoacoustic convection heat transfer phenomenon
[AIAA PAPER 83-1422] p 121 A83-32701
Measured and calculated wall temperatures on air-cooled turbine vanes with boundary layer transition
[NASA-TM-83030] p 127 N83-14432
Infrared emission spectrophotometric study of the changes produced by TiN coating of metal surfaces in an operating EHD contact
[NASA-TM-82989] p 92 N83-13466
Experimental investigation of the vaporous/gaseous cavity characteristics of an eccentric journal bearing
[NASA-TM-82996] p 128 N83-17833
Development of a rotary instrumentation system, phase 2
[NASA-CR-168013] p 47 N83-18835
Mechanism of lubrication by tricresylphosphate (TCP)
[NASA-TP-2053] p 72 N83-18863

TEMPERATURE MEASURING INSTRUMENTS
Evaluation of methods for rapid determination of freezing point of aviation fuels
[NASA-CR-167981] p 98 N83-10207
Experimental feasibility study of a thermoelectric heat flux gage
[NASA-TM-83048] p 134 N83-15602

TEMPERATURE PROBES
Development of advanced high-temperature heat flux sensors
[NASA-CR-165618] p 26 N83-10044

TEMPERATURE PROFILES
Perspectives on the mixing of a row of jets with a confined crossflow
[AIAA PAPER 83-1200] p 122 A83-36276
Analytical and experimental study of flow through an axial turbine stage with a nonuniform inlet radial temperature profile
[AIAA PAPER 83-1175] p 6 A83-45510
Analytical and experimental study of flow through an axial turbine stage with a nonuniform inlet radial temperature profile
[NASA-TM-83431] p 14 N83-27958

TENSILE CREEP
Tensile and compressive constitutive response of 316 stainless steel at elevated temperatures p 162 N83-34353

TENSILE PROPERTIES
Bisimide amine cured epoxy /IME/ resins and composites. II - Ten-degree off-axis tensile and shear properties of Celion 6000/IME composites p 52 A83-23608

TENSILE STRENGTH
Correlation of tensile and shear strengths of metals with their friction properties
[ASLE PREPRINT 82-LC-UB-1] p 74 A83-13226
A brittle to ductile transition in NiAl of a critical grain size p 75 A83-29726
Effects on stress rupture life and tensile strength of tin additions to Inconel 718 p 79 N83-11299
Development of Fe-Mn-Al-X-C alloys p 80 N83-11307
SiC or B4C-B/low strategic element content composite p 80 N83-11308
Design procedures for fiber composite structural components: Rods, columns and beam columns
[NASA-TM-83321] p 66 N83-24559
Evaluation of low-cost aluminum composites for aircraft engine structural applications
[NASA-TM-83357] p 66 N83-25790

TENSILE STRESS
Tensile buckling of advanced turboprops
[AIAA PAPER 82-0776] p 154 A83-10900
Benchmark notch test for life prediction
[NASA-CR-165571] p 158 N83-12451
The effect of stress on ultrasonic pulses in fiber reinforced composites
[NASA-CR-3724] p 154 N83-33180

TENSILE TESTS
Method and apparatus for gripping uniaxial fibrous composite materials --- holding specimens for mechanical property testing
[NASA-CASE-LEW-13758-1] p 64 N83-12176

TENSORS
Alternatives for jet engine control
[NASA-CR-170100] p 33 N83-20945
Alternatives for jet engine control
[NASA-CR-170233] p 35 N83-23305

TERRESTRIAL RADIATION
Direct conversion of infrared radiant energy for space power applications p 173 N83-15365

TEST FACILITIES
End region effects upon the performance of a magnetohydrodynamic channel p 203 A83-10665
NASA low-speed centrifugal compressor for fundamental research
[AIAA PAPER 83-1351] p 43 A83-36353
Development of electrical test procedures for qualification of spacecraft against EID. Volume 2: Review and specification of test procedures
[NASA-CR-165590] p 50 N83-12137
Magnetohydrodynamics (MHD) Engineering Test Facility (ETF) 200 MWe power plant. Conceptual Design Engineering Report (CDER) supplement. Magnet system special investigations
[NASA-CR-165509] p 141 N83-14494
NASA low-speed centrifugal compressor for fundamental research
[NASA-TM-83398] p 13 N83-25662
A compact inflow control device for simulating flight fan noise
[NASA-TM-83349] p 201 N83-26643
Test results and description of a 1-kW free-piston Stirling engine with a dashpot load
[NASA-TM-83407] p 182 N83-27346
Scaled centrifugal compressor, collector and running gear program
[NASA-CR-168167] p 40 N83-30432

TEST VEHICLES
Steady-state and dynamic evaluation of the electric propulsion system test bed vehicle on a road load simulator
[NASA-TM-83445] p 186 N83-35496

TEXTURES
Ion sputter textured graphite --- anode collector plates in electron tube devices
[NASA-CASE-LEW-12919-1] p 63 N83-10117
Industrial ion source technology
[NASA-CR-159877] p 102 N83-12259

TF-34 ENGINE
Status report - DARPA/NASA convertible turbofan/turboshaft engine program
[ASME PAPER 83-GT-196] p 25 A83-48000

THERMAL BOUNDARY LAYER
Determination of boundary shape of cooled porous region p 118 A83-13487

THERMAL CONDUCTIVITY
The thermal conductivity of oxygen p 207 A83-12094
Pseudo-updated constrained solution algorithm for nonlinear heat conduction p 121 A83-32989
Growth of diamondlike films for power applications p 174 N83-15880
Transport properties of oxygen
[NASA-RP-1102] p 130 N83-24800
Theoretical results for starved elliptical contacts
[NASA-TM-81697] p 150 N83-29710

THERMAL CONTROL COATINGS
Performance of laser-glazed zirconia thermal barrier coatings in cyclic oxidation and corrosion burner rig tests p 88 A83-10300
Improved uniformity of multiphase ceramic-metal plasma-sprayed coats p 61 A83-22269
Effects of arc current on the life in burner-rig thermal cycling of plasma-sprayed ZrO2-O3 p 89 A83-22270
Improved performance thermal barrier coatings p 90 A83-42261
Further industrial tests of ceramic thermal barrier coatings
[NASA-TP-2057] p 26 N83-10045
Turbine engine materials durability research p 29 N83-12163
Creep of plasma sprayed zirconia
[NASA-CR-167868] p 96 N83-29393
Improved thermal barrier coating system
[NASA-CASE-LEW-13324-2] p 86 N83-34014

THERMAL CYCLING TESTS
Metallurgical instabilities during the high temperature low cycle fatigue of nickel-base superalloys p 75 A83-22019
Effects of arc current on the life in burner-rig thermal cycling of plasma-sprayed ZrO2-O3 p 89 A83-22270
Use of fiber-like materials to augment cycle life of thick, thermoprotective-seal coatings --- for gas turbine engine components p 89 A83-22271
Some inelastic effects of thermal cycling on ZrO2-Y2O3 materials p 89 A83-22272
An uncoupled viscoplastic constitutive model for metals at elevated temperature
[AIAA 83-1016] p 156 A83-29798
Thermomechanical loading of multilayered cylindrical geometries in thermal cycling from 300 to 1300 K
[NASA-TM-83312] p 129 N83-20029
Testing of felt-ceramic materials for combustor applications
[NASA-CR-168[illegible]] p 36 N83-26837
Evaluation of ceramics for stator applications: Gas turbine engines interim report. Stator fabrication and evaluation
[NASA-CR-168140] p 96 N83-30662

THERMAL DECOMPOSITION
The adsorption and thermal decomposition of tricresylphosphate (TCP) on iron and gold
[NASA-TM-83441] p 62 N83-29311

THERMAL DEGRADATION
Research on aviation fuel instability
[NASA-TM-83420] p 101 N83-28255
The effects of metals and inhibitors on thermal oxidative degradation reactions of unbranched perfluoroalkylethers
[NASA-TM-83464] p 97 N83-34049
A review of liquid lubricant thermal/oxidative degradation
[NASA-TM-83465] p 98 N83-35143
High-pressure liquid chromatography: A brief introduction and its application in analyzing the degradation of a C-ether (Thio-ether) liquid lubricant
[NASA-TM-83474] p 98 N83-35144

THERMAL DIFFUSIVITY
Transport properties of oxygen
[NASA-RP-1102] p 130 N83-24800

THERMAL ENERGY
Apparatus for improving the fuel efficiency of a gas turbine engine
[NASA-CASE-LEW-13142-1] p 43 N83-36029

THERMAL EXPANSION
The effect of annealing on the creep of plasma sprayed ceramics
[NASA-TM-83396] p 130 N83-24799

THERMAL FATIGUE
Metallurgical instabilities during the high temperature low cycle fatigue of nickel-base superalloys p 75 A83-22019
Thermal fatigue resistance of cobalt-modified UDIMET 700 p 78 N83-11289
The thermal fatigue resistance of H-13 Die Steel for aluminum die casting dies
[NASA-TM-83331] p 87 N83-35103

THERMAL INSULATION
Thermal-barrier coatings for utility gas turbines
[NASA-TM-85349] p 95 N83-27022

THERMAL PROTECTION
Use of fiber-like materials to augment cycle life of thick, thermoprotective-seal coatings --- for gas turbine engine components p 89 A83-22271
Creep of plasma-sprayed-ZrO2 thermal-barrier coatings p 89 A83-22273
Silicon-slurry/aluminide coating --- protecting gas turbine engine vanes and blades
[NASA-CASE-LEW-13343] p 86 N83-31795
Thermal barrier coating system having improved adhesion
[NASA-CASE-LEW-1335901] p 97 N83-31855

Covering solid, film cooled surfaces with a duplex thermal barrier coating
[NASA-CASE-LEW-13450-1] p 103 N83-35177
THERMAL RESISTANCE
Development of Fe-Mn-Al-X-C alloys p 80 N83-11307
SiC or B4C-B/low strategic element content composite p 80 N83-11308
Design and development of multi-kW power electronic transformers --- for long duration space applications
[NASA-CR-168082] p 116 N83-29596
THERMAL SHOCK
Method of fabricating an abradable gas path seal
[NASA-CASE-LEW-13269-2] p 93 N83-17714
Laser surface fusion of plasma sprayed ceramic turbine seals
[NASA-CASE-LEW-13269-1] p 50 N83-20996
THERMAL STABILITY
Improved high temperature resistant polyimides
[NASA-CASE-LEW-13864-1] p 93 N83-17715
Experimental study of the thermal stability of hydrocarbon fuels
[NASA-CR-168027] p 100 N83-17728
Studies of the mechanisms of turbine fuel instability
[NASA-CR-167963] p 100 N83-18924
Low temperature cross linking polyimides
[NASA-CASE-LEW-12876-2] p 96 N83-29392
High-pressure liquid chromatography: A brief introduction and its application in analyzing the degradation of a C-ether (Thio-ether) liquid lubricant
[NASA-TM-83474] p 98 N83-35144
Effect of deoxygenation and prestressing on hydrocarbon fuel thermal stability
[NASA-TM-83456] p 102 N83-35160
THERMAL STRESSES
DOE and AID stand-alone photovoltaic activities
[NASA-TM-83374] p 180 N83-25041
THERMIONIC CONVERTERS
Thermionic technology infrastructure for space power p 54 A83-27298
High thermal power density heat transfer apparatus providing electrical isolation at high temperature using heat pipes
[NASA-CASE-LEW-12950-2] p 183 N83-29804
Thermionic energy converters
[NASA-CASE-LEW-12443-1] p 184 N83-32175
THERMOCHEMICAL PROPERTIES
Literature survey of properties of synfuels derived from coal
[NASA-TM-82739] p 99 N83-10208
THERMOCHEMISTRY
Thermodynamics of the potassium-sulfur-oxygen and related systems
[NASA-CR-168155] p 61 N83-28077
THERMOCOUPLES
Development of advanced high-temperature heat flux sensors
[NASA-CR-165618] p 26 N83-10044
Joining lead wires to thin platinum alloy films
[NASA-CASE-LEW-13934-1] p 135 N83-35338
THERMODYNAMIC EFFICIENCY
End region effects upon the performance of a magnetohydrodynamic channel p 203 A83-10665
Performance and emissions characteristics of aqueous alcohol fumes in a DI diesel engine
[NASA-CR-167917] p 99 N83-12250
Experimental study of the thermal-acoustic efficiency in a long turbulent diffusion-flame burner
[NASA-CR-170003] p 72 N83-19824
THERMODYNAMIC EQUILIBRIUM
Thermodynamics of silicon nitridation - Effect of hydrogen
[ACS PAPER 33-B-80P] p 88 A83-18052
Structure of evaporating and combusting sprays: Measurements and predictions p 38 N83-29211
THERMODYNAMIC PROPERTIES
Computer program for Stirling engine performance calculations
[NASA-TM-82960] p 210 N83-17423
Vaporization thermodynamics of K2S and K2SO3
[NASA-CR-168080] p 61 N83-19812
Simplified composite micromechanics equations for hygral, thermal and mechanical properties
[NASA-TM-83320] p 66 N83-19817
Plasma-sprayed self-lubricating coatings
[NASA-CR-3680] p 94 N83-22422
A class of nonideal solutions. 2: Application to experimental data
[NASA-TP-1930] p 208 N83-23188
THERMODYNAMICS
Hygrothermomechanical evaluation of transverse filament tape epoxy/polyester fiberglass composites
[NASA-TM-83044] p 65 N83-15362
The detailed chemistry and thermodynamics of sodium in oxygen-rich flames
[NASA-CR-169848] p 72 N83-17626
Energy efficient engine sector combustor rig test program
[NASA-CR-167913] p 33 N83-19753
Thermomechanical loading of multilayered cylindrical geometries in thermal cycling from 300 to 1300 K
[NASA-TM-83312] p 129 N83-20029
A search for equilibrium states
[NASA-TM-82898] p 207 N83-20808
Design, fabrication and testing of porous tungsten vaporizers for mercury ion thrusters
[NASA-TM-83063] p 58 N83-22318
A class of nonideal solutions. 1: Definition and properties
[NASA-TP-1929] p 208 N83-23189
A 4-cylinder Stirling engine computer program with dynamic energy equations
[NASA-TM-83053] p 130 N83-26017
THERMOELASTICITY
Thermoelastohydrodynamic analysis of an oil pumping ring seal p 137 A83-22322
THERMOELECTRIC POWER GENERATION
Power generation from nuclear reactors in aerospace applications
[NASA-TM-83342] p 59 N83-30516
THERMOELECTRICITY
Experimental feasibility study of a thermoelectric heat flux gage
[NASA-TM-83048] p 134 N83-15602
THERMOGRAVIMETRY
Preparation, characterization, physical testing and performance of fluorocarbon membranes and separators
[NASA-CR-167880] p 73 N83-26936
THERMOMECHANICAL TREATMENT
Influence of thermomechanical processing on elevated temperature slow plastic flow properties of B2 aluminide Fe-39.8at.% Al p 75 A83-22017
Finite element formulation for transient heat treat problems
[NASA-TM-83070] p 129 N83-17834
Simplified method for nonlinear structural analysis
[NASA-TP-2208] p 163 N83-34372
THERMOPLASTIC RESINS
Advanced inorganic separators for alkaline batteries and method of making the same
[NASA-CASE-LEW-13171-2] p 184 N83-32176
THERMOPLASTICITY
Nonlinear structural and life analyses of a combustor liner p 155 A83-12764
Spherical micro-glass particle impingement studies of thermoplastic materials at normal incidence
[NASA-TM-83410] p 94 N83-25883
THERMOSETTING RESINS
Dynamic mechanical characterization of cure of a polyimide-graphite fiber composite (PMR 15/Celion 6000) p 62 A83-31793
THICKNESS
Further industrial tests of ceramic thermal barrier coatings
[NASA-TP-2057] p 26 N83-10045
THIN FILMS
Ellipsometric study of silicon nitride on gallium arsenide p 204 A83-11812
Morphological and frictional behavior of sputtered MoS2 films p 88 A83-12652
Interfacial electrical properties of ion-beam sputter deposited amorphous carbon on silicon p 205 A83-33920
Surface-polaritonlike waves guided by thin, lossy metal films p 192 A83-37947
Long range surface plasmons in birefringent media p 202 A83-42206
The dryout region in frictionally heated sliding contacts p 124 A83-42762
Microhardness studies on thin carbon films grown on P-type, (100) silicon
[NASA-TM-82980] p 61 N83-13169
Determination of physical and chemical states of lubricants in concentrated contacts, part 3
[NASA-CR-3658] p 92 N83-16527
Development program on a Spindt cold-cathode electron gun
[NASA-CR-168055] p 115 N83-18997
Frictional and morphological characteristics of ion plated soft, metallic films
[NASA-TM-81723] p 83 N83-22390
Endurance test of a 30-CM-diameter engineering model ion thruster. Task 12: Investigation of thin-film erosion monitors for ion thrusters
[NASA-CR-168132] p 58 N83-25779
Research into the use of pyrolytic oxides and polymers for the fabrication of thin film high energy capacitors
[NASA-CR-173012] p 97 N83-34045
THIOLS
Preliminary results of the comparison of the electrochemical behavior of a thioether and biphenyl
[NASA-TM-83450] p 87 N83-34015
THREE DIMENSIONAL FLOW
A turbulence model for three dimensional turbulent shear flows over curved rotating bodies
[AIAA PAPER 83-0559] p 120 A83-16787
Numerical solution to the glancing sidewall oblique shock wave/turbulent boundary layer interaction in three-dimension
[AIAA PAPER 83-0136] p 3 A83-16823
Three-dimensional stability of vortex arrays p 120 A83-19022
A basic code for the prediction of transient three-dimensional turbulent flowfields p 121 A83-27412
Three-dimensional compressible viscous analysis of mixer nozzles
[AIAA PAPER 83-1401] p 4 A83-36391
Quasi-three-dimensional turbomachinery flow calculations on multiple hub-to-shroud stream surfaces
[AIAA PAPER 83-1820] p 5 A83-38652
An experience in mesh generation for three-dimensional calculation of potential flow around a rotating propeller p 5 A83-38798
A semi-direct solver for compressible three-dimensional rotational flow
[AIAA PAPER 83-1909] p 122 A83-39367
Finite volume calculation of three-dimensional potential flow around a propeller p 7 A83-45577
Three-dimensional flow measurements in a turbine scroll
[ASME PAPER 83-GT-128] p 8 A83-47957
Three-dimensional flow measurements in a vaneless radial turbine scroll
[NASA-CR-167994] p 9 N83-11065
A computer program for the calculation of the flow field including boundary layer effects for mixed-compression inlets at angle of attack
[NASA-CR-168002] p 10 N83-11066
Three dimensional flow computations in a turbine scroll
[NASA-CR-168003] p 10 N83-12045
Calculation of compressible flow in and about three-dimensional inlets with and without auxiliary inlets by a higher-order panel method
[NASA-CR-168009] p 10 N83-12047
Three dimensional flow field inside compressor rotor, including blade boundary layers
[NASA-CR-169788] p 128 N83-16679
Validation of a three-dimensional viscous analysis of axisymmetric supersonic inlet flow fields
[NASA-TM-83058] p 32 N83-17538
Numerical solution to the glancing sidewall oblique shock wave/turbulent boundary layer interaction in three dimension
[NASA-TM-83056] p 34 N83-22199
Applications of the contravariant form of the Navier-Stokes equations
[NASA-TM-83448] p 14 N83-29179
Analytical calculation of a single jet in cross-flow and comparison with experiment p 38 N83-29219
Numerical solutions of Navier-Stokes equations for compressible turbulent two/three dimensional flows in terminal shock region of an inlet/diffuser
[NASA-CR-3723] p 132 N83-34230
Three-dimensional turbulent-mixing-length modeling for discrete-hole coolant injection into a crossflow
[NASA-TP-2200] p 132 N83-34232
A semi-direct solver for compressible 3-dimensional rotational flow
[NASA-TM-83314] p 15 N83-34908
THRUST
Aerodynamic performance of a fan stage utilizing variable inlet guide vanes (VIGV's) for thrust modulation --- subsonic V/STOL aircraft
[AIAA PAPER 83-1162] p 6 A83-45508
Aerodynamic performance of a fan stage utilizing Variable Inlet Guide Vanes (VIGVs) for thrust modulation --- subsonic V/STOL aircraft
[NASA-TM-83438] p 13 N83-27957
THRUST AUGMENTATION
Extended performance 8-cm mercury ion thruster
[AIAA PAPER 82-1913] p 53 A83-21078
The feasibility of water injection into the turbine coolant to permit gas turbine contingency power for helicopter application
[ASME PAPER 83-GT-66] p 24 A83-39993
Extended performance 8-cm mercury ion thruster
[NASA-TM-83029] p 57 N83-14157
THRUST BEARINGS
Optimum parallel step-sector bearing lubricated with an incompressible fluid
[NASA-TM-83356] p 148 N83-24855
THRUST CHAMBERS
Advanced LOX/H sub 2 engine technologies for future OTVs p 60 N83-35013

THRUST LOADS
Power turbine dynamics - An evaluation of a shear-mounted elastomeric damper
[ASME PAPER 83-GT-228] p 139 A83-48025
THRUST PROGRAMMING
Large space systems auxiliary propulsion requirements p 46 N83-26864
THRUST REVERSAL
Thrust performance of a variable-geometry, divergent exhaust nozzle on a turbojet engine at altitude
[NASA-TP-2171] p 36 N83-26839
THRUST VECTOR CONTROL
Thrust performance of a variable-geometry, divergent exhaust nozzle on a turbojet engine at altitude
[NASA-TP-2171] p 36 N83-26839
TIME DIVISION MULTIPLE ACCESS
Development of a microwave 20 x 20 switch matrix for 30/20 GHz SS-TDMA application p 110 A83-11484
A high capacity satellite switched TDMA microwave switch matrix p 104 A83-19776
20 x 20 IF switch matrix for SS-TDMA systems p 113 A83-41369
A network control concept for the 30/20 GHz communication system baseband processor p 47 A83-41389
Onboard processing for a 30/20 GHz communications satellite p 47 A83-41391
Next generation communications satellites: multiple access and network studies
[NASA-CR-167903] p 45 N83-12129
Planning assistance for the NASA 30/20 GHz program. Network control architecture study.
[NASA-CR-168058] p 106 N83-21207
Method for terminal position determination in Earth terminal-to-satellite burst acquisition and synchronization
[NASA-CASE-LEW-13893-1] p 107 N83-30832
A comparison of Frequency Domain Multiple Access (FDMA) and Time Domain Multiple Access (TDMA) approaches to satellite service for low data rate Earth stations
[NASA-TM-83430] p 109 N83-34120
Spacecraft in switch matrix for wide band service applicatons in 30/20 GHz communications satellite systems
[NASA-CR-168089] p 46 N83-34998
TIME DIVISION MULTIPLEXING
Comparison of channel assignment techniques for hybrid switching p 104 A83-41363
TIN ALLOYS
Effects on stress rupture life and tensile strength of tin additions to Inconel 718 p 79 N83-11299
TIP SPEED
An experience in mesh generation for three-dimensional calculation of potential flow around a rotating propeller p 5 A83-38798
TIRES
Applications of ion beam technology
[NASA-CR-169797] p 82 N83-16493
TITANIUM ALLOYS
Fatigue behavior of SiC reinforced Ti/6Al-4V/ at 650 C p 62 A83-12414
Interrelation of material microstructure, ultrasonic factors, and fracture toughness of a two-phase titanium alloy p 75 A83-23922
Cavitation erosion of copper, brass, aluminum and titanium alloys in mineral oil
[NASA-TM-83402] p 148 N83-24856
TITANIUM NITRIDES
Infrared emission spectrophotometric study of the changes produced by TiN coating of metal surfaces in an operating EHD contact
[ASLE PREPRINT 82-LC-3C-3] p 135 A83-13229
Infrared emission spectrophotometric study of the changes produced by TiN coating of metal surfaces in an operating EHD contact
[NASA-TM-82989] p 92 N83-15466
Nitriding of titanium and titanium: 8 percent aluminum, 1 percent molybdenum, 1 percent vanadium alloy with an ion-beam source
[NASA-TP-2149] p 85 N83-24640
TOLERANCES (MECHANICS)
Analysis, design, fabrication and testing of an optical tip clearance sensor --- turbocompressor blade tips
[NASA-CR-165265] p 26 N83-11127
TOLLMIEN-SCHLICHTING WAVES
The evolution of Tollmien-Schlichting waves near a leading edge p 120 A83-24410
The evolution of Tollmien-Schlichting waves near a leading edge. II - Numerical determination of amplitudes p 122 A83-35346
Generation of Tollmien-Schlichting waves by free-stream disturbances at low Mach numbers
[NASA-TM-83026] p 130 N83-23544
TOPOGRAPHY
Lubrication background
[NASA-TM-81692] p 147 N83-20159
TOPOLOGY
An improved algorithm for evaluating trellis phase codes
[NASA-CR-169354] p 105 N83-16600
TOROIDS
Development of a high capacity toroidal Ni/Cd cell
[NASA-CR-169945] p 176 N83-19273
TORQUE
Film thickness measurement for spiral groove and Rayleigh step lift pad self-acting face seals
[NASA-TP-2058] p 26 N83-11126
Experimental program for the evaluation of turbofan/turboshaft c conversion technology
[NASA-TM-82988] p 27 N83-11130
Energy efficient face seal
[NASA-CR-165591] p 142 N83-15659
TORQUE CONVERTERS
Advantage of resonant power conversion in aerospace applications
[NASA-TM-83399] p 37 N83-27994
TOUGHNESS
Resin selection criteria for tough composite structures
[AIAA 83-0801] p 89 A83-29734
Imide modified epoxy matrix resins
[NASA-CR-167942] p 93 N83-18909
Crack layer morphology and toughness characterization in steels
[NASA-CR-168154] p 160 N83-27256
TRACE ELEMENTS
Experimental design of an interlaboratory study for trace metal analysis of liquid fluids --- for aerospace vehicles
[NASA-TP-2148] p 73 N83-24575
TRACTION
The influence of surface dents and grooves on traction in sliding EHD point contacts p 138 A83-37823
Surface temperatures and glassy state investigations in tribology, part 5
[NASA-CR-3632] p 91 N83-11328
Rolling-element fatigue life with traction fluids and automatic transmission fluid in a high-speed rolling-contact rig
[NASA-TP-2050] p 140 N83-13457
Infrared emission spectrophotometric study of the changes produced by TiN coating of metal surfaces in an operating EHD contact
[NASA-TM-82989] p 92 N83-15466
Traction behavior of two traction lubricants
[NASA-TM-83311] p 144 N83-20116
Advanced Power Transmission Technology
[NASA-CP-2210] p 144 N83-20119
A historical perspective of traction drives and related technology p 144 N83-20123
Hybrid geared traction transmissions p 145 N83-20128
Evaluation of a high performance, fixed-ratio, traction drive p 145 N83-20135
Traction calculations and design data for two traction fluids p 145 N83-20136
Sizing criterial for traction drives p 146 N83-20137
Regression analysis of traction characteristics of traction fluids
[NASA-TP-2154] p 148 N83-24862
Elastohydrodynamic contacts. Effects of dents and grooves on traction and local film thickness
[NASA-TP-2175] p 150 N83-28453
Advances in traction drive technology
[NASA-TM-83397] p 150 N83-28455
TRAILING EDGES
Experimental evaluation of shockless supercritical airfoils in cascade
[AIAA PAPER 83-0003] p 2 A83-16455
Critical review of the trailing edge condition in steady and unsteady flow. Blade flutter in compressors and fans: Numerical simulation of the aerodynamic loading
[NASA-CR-169705] p 10 N83-15264
TRAJECTORY ANALYSIS
A similarity analysis of the droplet trajectory equation p 118 A83-13133
TRANSDUCERS
Precision optical angular position marker system for rotating machinery
[NASA-TM-83062] p 144 N83-20117
TRANSFER FUNCTIONS
Pressure transfer function of a JT15D nozzle due to acoustic and convected entropy fluctuations p 193 A83-16319
The transfer function method for gear system dynamics applied to conventional and minimum excitation gearing designs
[NASA-CR-3626] p 139 N83-11495
TRANSFER ORBITS
Benefits and costs of low thrust propulsion systems
[AIAA PAPER 83-1248] p 49 A83-36306
Study for analysis of benefit versus cost of low thrust propulsion system
[NASA-CR-168011] p 57 N83-21002
TRANSFORMERS
Transformer induced instability of the series resonant converter p 113 A83-41152
Design study of a high power rotary transformer
[NASA-CR-168012] p 115 N83-16630
Design and development of multi-kW power electronic transformers --- for long duration space applications
[NASA-CR-168082] p 116 N83-29596
TRANSIENT HEATING
Finite element formulation for transient heat treat problems
[NASA-TM-83070] p 129 N83-17834
TRANSIENT LOADS
Solution to the backward-Kolmogorov equation for a nonstationary oscillation problem p 192 A83-15697
TRANSIENT PRESSURES
Transient difference solutions of the inhomogeneous wave equation - Simulation of the Green's function
[AIAA PAPER 83-0667] p 193 A83-25904
TRANSIENT RESPONSE
Transient flow analysis of the AEDC/HPDE MHD generator
[AIAA PAPER 83-0395] p 203 A83-16691
Blade loss transient dynamic analysis of turbomachinery p 25 A83-40864
Geometrically nonlinear analysis of layered composite plates and shells
[NASA-CR-168182] p 161 N83-33219
TRANSISTOR CIRCUITS
Transistorized PWM inverter-induction motor drive system p 110 A83-11488
TRANSISTORS
Improved transistorized AC motor controller for battery powered urban electric passenger vehicles
[NASA-CR-167978] p 113 N83-10349
TRANSITION FLOW
Vortices, stability, and turbulence p 125 A83-46718
TRANSITION TEMPERATURE
The 371 deg C(700 deg F) properties of celion 6000/n-phenylnadimide modified PMR polyimide composites
[NASA-TM-83050] p 65 N83-15365
TRANSMISSION
Large rotorcraft transmission technology development program
[NASA-CR-168120] p 18 N83-22188
TRANSMISSION EFFICIENCY
Advances in Serial MSK modems p 111 A83-19789
Multi-stage Depressed Collectors (MDC) for efficiency improvements of UHF broadcast klystrons
[NASA-TM-82970] p 105 N83-10322
TRANSMISSION FLUIDS
Rolling-element fatigue life with traction fluids and automatic transmission fluid in a high-speed rolling-contact rig
[NASA-TP-2050] p 140 N83-13457
TRANSMISSIONS (MACHINE ELEMENTS)
Advances in high-speed rolling-element bearings --- for aircraft engine and transmission application p 137 A83-22319
Design of an advanced 500-HP helicopter transmission p 21 A83-24834
Life and reliability models for helicopter transmissions
[NASA-TM-82976] p 139 N83-10425
The transfer function method for gear system dynamics applied to conventional and minimum excitation gearing designs
[NASA-CR-3626] p 139 N83-11495
Lubricant effects on efficiency of a helicopter transmission p 141 N83-15523
Advanced Power Transmission Technology
[NASA-CP-2210] p 144 N83-20119
NASA helicopter transmission system technology program p 144 N83-20120
An overview of advancements in helicopter transmission design p 144 N83-20124
Design of an advanced 500-hp helicopter transmission p 144 N83-20125
Hybrid geared traction transmissions p 145 N83-20128
NASA transmission research and its probable effects on helicopter transmission design
[NASA-TM-83389] p 148 N83-24858
Free-piston Stirling hydraulic engine and drive system for automobiles
[NASA-TM-82992] p 211 N83-25625
New propulsion components for electric vehicles
[NASA-TM-83404] p 116 N83-25982
Advances in traction drive technology
[NASA-TM-83397] p 150 N83-28455
Advanced Gas Turbine (AGT) powertrain system development for automotive applications
[NASA-CR-167901] p 212 N83-33800
TRANSMITTANCE
The application of free-electron lasers to the transmission of energy in space p 135 A83-31141

TRANSONIC FLIGHT
Model aerodynamic test results for a refined actuated inlet ejector nozzle at simulated takeoff and cruise conditions
[NASA-CR-168051] p 13 N83-26816
TRANSONIC FLOW
Experimental evaluation of shockless supercritical airfoils in cascade
[AIAA PAPER 83-0003] p 2 A83-16455
A finite element formulation for steady transonic Euler equations p 3 A83-22129
Multiple-gridding of the Euler equations with an implicit scheme
[AIAA PAPER 83-1945] p 5 A83-39392
An experimental investigation of internal area ruling for transonic and supersonic channel flow
[NASA-CR-169638] p 10 N83-14068
Development of a multiple-parameter nonlinear perturbation procedure for transonic turbomachinery flows: Preliminary application to design/optimization problems
[NASA-CR-3657] p 2 N83-17453
Fast Euler solver for steady, 1-dimensional flows
[NASA-CR-3689] p 14 N83-27960
Subsonic-transonic stall flutter study
[NASA-CR-165256] p 43 N83-30435
Semidirect computations for transonic flow
[NASA-TM-83451] p 15 N83-34909
TRANSONIC FLUTTER
Subsonic-transonic stall flutter study
[NASA-CR-165256] p 43 N83-30435
TRANSPONDERS
Advanced 3-V semiconductor technology assessment --- space communications
[NASA-CR-168102] p 207 N83-21988
Space power tubes - very much alive
[NASA-TM-83425] p 107 N83-28295
TRANSPORT AIRCRAFT
Assessment of crash fire hazard of LH sub 2 fueled aircraft
[NASA-CR-165525] p 16 N83-11095
Technology and benefits of aircraft counter rotation propellers
[NASA-TM-82983] p 27 N83-11129
Fluid Dynamics Panel Symposium on Aerodynamics of Power Plant Installation
[AGARD-AR-173] p 27 N83-11138
QCSEE under-the-wing engine-wing-flap aerodynamic profile characteristics
[NASA-TM-82890] p 28 N83-12092
Energy efficient engine. Flight propulsion system preliminary analysis and design
[NASA-CR-159659] p 28 N83-12094
Small transport aircraft technology propeller study
[NASA-CR-168045] p 14 N83-29178
TRAVELING WAVE AMPLIFIERS
A linearized traveling wave amplifier with hard limiter characteristics
[NASA-CASE-LEW-13981-1] p 116 N83-25984
TRAVELING WAVE TUBES
Modern multistage depressed collectors - A review p 112 A83-24025
Tubes in space - Very much alive p 112 A83-28160
Space tubes: A major challenge
[NASA-TM-82971] p 113 N83-11447
Design concepts for a high-impedance narrow-band 42 GHz power TWT using a fundamental/forward ladder-based circuit
[NASA-CR-165282] p 114 N83-12330
Design of a multistage depressed collector for the F-16 radar dual mode transmitter tube
[NASA-TM-82982] p 114 N83-14399
A linearized traveling wave amplifier with hard limiter characteristics
[NASA-CASE-LEW-13981-1] p 116 N83-25984
Experimental verification of the multistage depressed collector design procedure for a high-perveance, helix-type, traveling-wave tube --- in communications satellites
[NASA-TP-2162] p 116 N83-25985
Space power tubes - very much alive
[NASA-TM-83425] p 107 N83-28295
TRAVELING WAVES
Bending-torsion flutter of a highly swept advanced turboprop
[NASA-TM-82975] p 158 N83-11514
TRIBOLOGY
Tribological properties and X-ray photoelectron spectroscopy studies of ion-plated gold on nickel and iron p 74 A83-12650
Correlation of tensile and shear strengths of metals with their friction properties
[ASLE PREPRINT 82-LC-UB-1] p 74 A83-13226
Microscopic contour changes of tribological surfaces by chemical and mechanical action
[ASLE PREPRINT 82-LC-3B-3] p 136 A83-13237
Tribological properties of sintered polycrystalline and single-crystal silicon carbide p 89 A83-29397
Tribological characteristics of nitrogen (N+) implanted iron p 75 A83-37824
Surface temperatures and glassy state investigations in tribology, part 5
[NASA-CR-3632] p 91 N83-11328
Tribological properties of amorphous alloys and the role of surfaces in abrasive wear of materials
[NASA-TM-82973] p 140 N83-11498
Tribology p 140 N83-12167
Elastohydrodynamic lubrication theory
[NASA-TM-81695] p 140 N83-12432
Polyimides: Tribological properties and their use as lubricants
[NASA-TM-82959] p 91 N83-13257
Effect of sliding speed and contact stress on tribological properties of ultra-high-molecular-weight polyethylene
[NASA-TP-2059] p 91 N83-14269
Fundamental aspects of polyimide dry film and composite lubrication: A review
[NASA-TM-82968] p 92 N83-14271
Lubrication background
[NASA-TM-81692] p 147 N83-20159
Frictional and morphological characteristics of ion plated soft, metallic films
[NASA-TM-81723] p 83 N83-22390
Polyimides formulated from a partially fluorinated diamine for aerospace tribological applications
[NASA-TM-83339] p 94 N83-22423
The XPS depth profiling and tribological characterization of ion-plated gold on various metals
[NASA-TM-83350] p 83 N83-23417
NASA interdisciplinary collaboration in tribology. A review of oxidational wear
[NASA-CR-3686] p 95 N83-27021
Tribological measurements on a Charnley-type artificial hip joint
[NASA-TM-83440] p 97 N83-32943
Thermal elastohydrodynamic lubrication of line contacts
[NASA-TM-83424] p 152 N83-34326
TROPICAL METEOROLOGY
Cloud encounter statistics in the 28.5-43.5 KFT altitude region from four years of GASP observations p 188 A83-38733
TROPOPAUSE
Aircraft sampling of the sulfate layer near the tropopause following the eruption of Mount St. Helens p 187 N83-11556
Aircraft measurements of trace gases and particles near the tropopause
[NASA-CR-3691] p 188 N83-27542
TUNGSTEN
Design, fabrication and testing of porous tungsten vaporizers for mercury ion thrusters
[NASA-TM-83063] p 58 N83-22318
TUNGSTEN ALLOYS
Influence of cobalt, tantalum, and tungsten on the microstructure and mechanical properties of superalloy single crystals p 79 N83-11293
TUNGSTEN CARBIDES
Energy efficient face seal
[NASA-CR-165591] p 142 N83-15659
Ultrasonic ranking of toughness of tungsten carbide
[NASA-TM-83358] p 153 N83-23620
TUNING
Effects of structural coupling on mistuned cascade flutter and response
[NASA-TM-83049] p 159 N83-15672
TUNNEL DIODES
Inelastic tunnel diodes
[NASA-CASE-LEW-13833-1] p 116 N83-25983
TURBINE BLADES
Requirements of constitutive models for two nickel-base superalloys p 74 A83-21071
Friction damping of flutter in gas turbine engine airfoils p 20 A83-24038
Comparison of laser anemometer measurements and theory in an annular turbine cascade with experimental accuracy determined by parameter estimation p 4 A83-28833
Turbine blade nonlinear structural and life analysis p 21 A83-29024
Structural dynamics studies of rotating bladed-disk assemblies coupled with flexible shaft motions
[AIAA PAPER 83-0919] p 22 A83-32987
Some analysis methods for rotating systems with periodic coefficients p 157 A83-32987
Design of dry-friction dampers for turbine blades p 22 A83-35883
Effects of interstage diffuser flow distortion on the performance of a 15.41-centimeter tip diameter axial power turbine
[AIAA PAPER 83-1179] p 23 A83-36263
Heat transfer characteristics for jet array impingement with initial crossflow
[ASME PAPER 83-GT-28] p 7 A83-47891
A mixing-length model for the prediction of convex curvature effects on turbulent boundary layers --- for turbine blade convective heat transfer prediction
[ASME PAPER 83-GT-80] p 125 A83-47933
A study of the surface deterioration due to erosion --- of gas turbine blades
[ASME PAPER 83-GT-213] p 9 A83-48014
NASA LeRC/Akron University Graduate Cooperative Fellowship Program and Graduate Student Researchers Program
[NASA-CR-167943] p 208 N83-10970
Design and fabrication of composite blades for the Mod-1 wind turbine generator
[NASA-CR-167987] p 168 N83-11579
Film-cooling effectiveness with developing coolant flow through straight and curved tubular passages
[NASA-TP-2062] p 126 N83-12360
CF6 jet engine diagnostics program. High pressure turbine roundness/clearance investigation
[NASA-CR-165581] p 29 N83-13100
Tip cap for a rotor blade
[NASA-CASE-LEW-13654-1] p 30 N83-14129
Measured and calculated wall temperatures on air-cooled turbine vanes with boundary layer transition
[NASA-TM-83030] p 127 N83-14432
Feasibility of water injection into the turbine coolant to permit gas turbine contingency power for helicopter application
[NASA-TM-83043] p 31 N83-15307
Materials for advanced turbine engines. Volume 1: Advanced blade tip seal system
[NASA-CR-167851-VOL-1] p 31 N83-15308
Hygrothermomechanical evaluation of transverse filament tape epoxy/polyester fiberglass composites
[NASA-TM-83044] p 65 N83-15362
Aerodynamic stiffness of an unbound eccentric whirling centrifugal impeller with an infinite number of blades p 142 N83-15650
Effects of structural coupling on mistuned cascade flutter and response
[NASA-TM-83049] p 159 N83-15672
The NASA Lewis large wind turbine program p 174 N83-15911
Operating experience with the 200 kW MOD-OA wind turbine generators p 174 N83-15916
Construction of low-cost, Mod-OA wood composite wind turbine blades
[NASA-TM-83046] p 174 N83-16857
Design and evaluation of low-cost stainless steel fiberglass foam blades for large wind driven generating systems
[NASA-CR-165491] p 174 N83-19226
Design and evaluation of low cost blades for large wind driven generating systems p 175 N83-19244
Structural fatigue test results for large wind turbine blade sections p 159 N83-19246
The Rene 150 directionally solidified superalloy turbine blades, volume 1
[NASA-CR-167992] p 33 N83-20946
Stability analysis of flexible wind turbine blades using finite element method
[NASA-CR-168107] p 177 N83-21508
Progress toward determining the potential of ODS alloys for gas turbine applications
[NASA-TM-83332] p 83 N83-22387
Design and evaluation of low-cost laminated wood composite blades for intermediate size wind turbines: Blade design, fabrication concept, and cost analysis
[NASA-CR-165463] p 179 N83-23704
Thermal-barrier coatings for utility gas turbines
[NASA-TM-85349] p 95 N83-27022
Fabrication of low-cost Mod-OA wood composite wind turbine blades
[NASA-TM-83323] p 182 N83-27347
Energy efficient engine high-pressure turbine single crystal vane and blade fabrication technology report
[NASA-CR-165400] p 39 N83-30429
TURBINE ENGINES
Combustion system processes leading to corrosive deposits p 69 A83-42246
Recent trends in aviation turbine fuel properties
[NASA-TP-2056] p 99 N83-11340
Energy efficient engine. Flight propulsion system preliminary analysis and design
[NASA-CR-159859] p 28 N83-12094
Turbine engine materials durability research p 29 N83-12163
Feasibility of water injection into the turbine coolant to permit gas turbine contingency power for helicopter application
[NASA-TM-83043] p 31 N83-15307

Powder metallurgy Rene 95 rotating turbine engine parts, volume 2
[NASA-CR-165141] p 82 N83-15412
The Rene 150 directionally solidified superalloy turbine blades, volume 1
[NASA-CR-167992] p 33 N83-20946
Energy efficient engine component development and integration program
[NASA-CR-170089] p 34 N83-22204
General Aviation Turbine Engine (GATE) overview p 35 N83-22457
Considerations of technology transfer barriers in the modification of strategic superalloys for aircraft turbine engines
[NASA-TM-83395] p 86 N83-29360
T55 power turbine rotor multiplane-multispeed balancing study
[NASA-CR-167891] p 41 N83-33894
Design of a microprocessor-based Control, Interface and Monitoring (CIM unit for turbine engine controls research
[NASA-TM-83433] p 2 N83-34885
Ceramic applications in turbine engines
[NASA-CR-165494] p 212 N83-37028

TURBINE EXHAUST NOZZLES
The CF6 engine performance improvement
[NASA-CR-165612] p 31 N83-16342

TURBINE PUMPS
High speed cryogenic self-acting, shaft seals for liquid rocket turbopumps
[NASA-CR-168194] p 151 N83-32070
Comparative evaluation of three shaft seals proposed for high performance turbomachinery
[NASA-TM-83021] p 152 N83-34325

TURBINE WHEELS
Effects of friction dampers on aerodynamically unstable rotor stages
[AIAA PAPER 83-0848] p 22 A83-32791
A comprehensive method for preliminary design optimization of axial gas turbine stages. II - Code verification
[AIAA PAPER 83-1403] p 24 A83-36393
Power turbine dynamics - An evaluation of a shear-mounted elastomeric damper
[ASME PAPER 83-GT-228] p 139 A83-48025

TURBINES
Three-dimensional flow measurements in a vaneless radial turbine scroll
[NASA-CR-167994] p 9 N83-11065
Hot corrosion of low cobalt alloys p 79 N83-11292
Three dimensional flow computations in a turbine scroll
[NASA-CR-168003] p 10 N83-12045
Advanced technologies for turbomachinery systems: An overview
[NASA-TM-82949] p 28 N83-12090
Fully plasma-sprayed compliant backed ceramic turbine seal
[NASA-CASE-LEW-13268-3] p 149 N83-28450
Computer code for off-design performance analysis of radial-inflow turbines with rotor blade sweep
[NASA-TP-2199] p 40 N83-32807

TURBOCOMPRESSORS
Axial-compressor flow distortion with water ingestion
[AIAA PAPER 83-0004] p 19 A83-16456
Effect of humidity on jet engine axial-flow compressor performance p 22 A83-35856
A theory of rotating stall of multistage axial compressors. I - Small disturbances
[ASME PAPER 83-GT-44] p 7 A83-47904
A theory of rotating stall of multistage axial compressors. II - Finite disturbances
[ASME PAPER 83-GT-45] p 8 A83-47905
A theory of rotating stall of multistage axial compressors. III - Limit cycles
[ASME PAPER 83-GT-46] p 8 A83-47906
Effect of particle presence on the incompressible inviscid flow through a two dimensional compressor cascade
[ASME PAPER 83-GT-95] p 8 A83-47941
Analysis of an axial compressor blade vibration based on wave reflection theory
[ASME PAPER 83-GT-151] p 25 A83-47970
Wall boundary layer development near the tip region of an IGV of an axial flow compressor
[ASME PAPER 83-GT-171] p 8 A83-47972
Development of controlled diffusion airfoils for multistage compressor application
[ASME PAPER 83-GT-211] p 9 A83-48012
The WISGSK: A computer code for the prediction of a multistage axial compressor performance with water ingestion
[NASA-CR-3624] p 28 N83-12093
Study of advanced rotary combustion engines for commuter aircraft
[NASA-CR-165399] p 32 N83-17545
End wall flow characteristics and overall performance of an axial flow compressor stage
[NASA-CR-3671] p 13 N83-26819
Axial compressor middle stage secondary flow study
[NASA-CR-3701] p 14 N83-29174

TURBOFAN ENGINES
Rotor wake characteristics relevant to rotor-stator interaction noise generation p 19 A83-10184
An iterative method for predicting turbofan inlet acoustics p 192 A83-13135
Composite fan exit guide vanes for high bypass ratio gas turbine engines p 19 A83-13159
Wind tunnel measurements of blade/vane ratio and spacing effects on fan noise p 192 A83-15317
Scale model performance test investigation of mixed flow exhaust systems for an energy efficient engine /E3/ propulsion system
[AIAA PAPER 83-0541] p 20 A83-16776
A remote augmentor lift system with a turbine bypass engine p 20 A83-19595
Electro-optical processor for optimal control p 133 A83-23596
Effect of variable guide vanes on the performance of a high-bypass turbofan engine p 20 A83-24028
Transient difference solutions of the inhomogeneous wave equation - Simulation of the Green's function
[AIAA PAPER 83-0667] p 193 A83-25904
Tone generation by rotor-downstream strut interaction
[AIAA PAPER 83-0767] p 21 A83-25957
Optimization of acoustic liners by the hybrid finite element-integral approach
[AIAA PAPER 83-0670] p 194 A83-26917
The influence of inlet design on the aeroacoustic performance of a JT15D turbofan engine as measured in the NASA-Ames 40 x 80 foot wind tunnel
[AIAA PAPER 83-0681] p 21 A83-28006
Sound propagation in segmented exhaust ducts - Theoretical predictions and comparison with measurements
[AIAA PAPER 83-0734] p 194 A83-28016
Application of 3-signal coherence to core noise transmission
[AIAA PAPER 83-0759] p 194 A83-28021
Structural dynamics studies of rotating bladed-disk assemblies coupled with flexible shaft motions
[AIAA PAPER 83-0919] p 22 A83-32787
Acoustic modal analysis of a full-scale annular combustor
[AIAA PAPER 83-0760] p 196 A83-33486
The aerodynamic design and performance of the General Electric/NASA EEE fan --- Energy Efficient Engine
[AIAA PAPER 83-1160] p 23 A83-36252
JT9D performance deterioration results from a simulated aerodynamic load test p 25 A83-41040
Status report - DARPA/NASA convertible turbofan/turboshaft engine program
[ASME PAPER 83-GT-196] p 25 A83-48000
Utilizing numerical techniques in turbofan inlet acoustic suppressor design
[NASA-TM-82994] p 196 N83-10885
Experimental program for the evaluation of turbofan/turboshaft c conversion technology
[NASA-TM-82988] p 27 N83-11130
A remote augmentor lift system with a turbine bypass engine
[NASA-TM-82932] p 27 N83-12087
Correlation of core noise obtained by three signal coherence techniques
[NASA-TM-83012] p 197 N83-12966
CF6 jet engine diagnostics program. High pressure turbine roundness/clearance investigation
[NASA-CR-165581] p 29 N83-13100
Effect of steady-state pressure distortion on inlet flow to a high-bypass-ratio turbofan engine
[NASA-TM-82964] p 30 N83-15306
Experiments on high bypass internal mixer nozzle jet noise
[NASA-TM-83020] p 198 N83-16152
Sensor failure and multivariable control for airbreathing propulsion systems
[NASA-CR-159791] p 1 N83-16279
Energy efficient engine: Fan test hardware detailed design report
[NASA-CR-165148] p 31 N83-16341
The CF6 engine performance improvement
[NASA-CR-165612] p 31 N83-16342
Turbofan blade stresses induced by the flow distortion of a VTOL inlet at high angles of attack
[NASA-TM-82963] p 12 N83-17509
Summary report for CF6 jet engine diagnostics program
[NASA-CR-165582] p 32 N83-17539
Aircraft turbofan noise
[NASA-TM-83317] p 198 N83-18405
Acoustic modal analysis of a full-scale annular combustor
[NASA-TM-83334] p 200 N83-21896
Application of 3-signal coherence to core noise transmission
[NASA-TM-83333] p 200 N83-23114
Acoustical modal analysis of the pressure field in the tailpipe of a turbofan engine
[NASA-TM-83387] p 201 N83-25499
Design analysis of a self-acting spiral-groove ring seal for counter-rotating shafts
[NASA-TP-2142] p 36 N83-25712
A compact inflow control device for simulating flight fan noise
[NASA-TM-83349] p 201 N83-26643
Incidence loss for fan turbine rotor blade in two-dimensional cascade
[NASA-TP-2188] p 39 N83-30431
Effects of wind on turbofan engines in outdoor static test stands
[NASA-TM-83493] p 42 N83-34945
Use of cooling air heat exchangers as replacements for hot section strategic materials
[NASA-TM-83494] p 42 N83-34946
Supersonic fan engines for military aircraft
[NASA-TM-83499] p 42 N83-34947

TURBOFANS
Recent results about fan noise: Its generation, radiation and suppression
[NASA-TM-83002] p 197 N83-13939
Rotor redesign for a highly loaded 1800 ft/sec tip speed fan. 3: Laser Doppler velocimeter report
[NASA-CR-167954] p 30 N83-14128
Turbofan noise generation. Volume 1: Analysis
[NASA-CR-167951] p 198 N83-15041
Rotorcraft convertible engine study
[NASA-CR-168241] p 42 N83-34944

TURBOGENERATORS
Study of advanced rotary combustion engines for commuter aircraft
[NASA-CR-165399] p 32 N83-17545

TURBOJET ENGINE CONTROL
Electro-optical processor for optimal control p 133 A83-23596

TURBOJET ENGINES
Uniform engine testing program. Phase 1: NASA Lewis Research Center participation
[NASA-TM-82978] p 29 N83-14126
Thrust performance of a variable-geometry, divergent exhaust nozzle on a turbojet engine at altitude
[NASA-TP-2171] p 36 N83-26839

TURBOMACHINE BLADES
The coupled aeroelastic response of turbomachinery blading to aerodynamic excitations
[AIAA 83-0844] p 156 A83-29822
Quasi-three-dimensional turbomachinery flow calculations on multiple hub-to-shroud stream surfaces
[AIAA PAPER 83-1820] p 5 A83-38652
Design of supercritical cascades with high solidity p 6 A83-43446
Vibrations of blades with variable thickness and curvature by shell theory
[ASME PAPER 83-GT-152] p 158 A83-47978
Critical review of the trailing edge condition in steady and unsteady flow. Blade flutter in compressors and fans: Numerical simulation of the aerodynamic loading
[NASA-CR-169705] p 10 N83-15264
Turbofan blade stresses induced by the flow distortion of a VTOL inlet at high angles of attack
[NASA-TM-82963] p 12 N83-17509
Input generator for Denton 3-dimensional turbomachine-blade-row analysis code
[NASA-TM-23324] p 13 N83-26817

TURBOMACHINERY
Solid particle dynamic behavior through twisted blade rows p 3 A83-27478
The performance and application of high speed long life LH2 hybrid bearings for reusable rocket engine turbomachinery
[AIAA PAPER 83-1389] p 138 A83-36379
Quasi-three-dimensional turbomachinery flow calculations on multiple hub-to-shroud stream surfaces
[AIAA PAPER 83-1820] p 5 A83-38652
Advanced technologies for turbomachinery systems: An overview
[NASA-TM-82949] p 28 N83-12090
A rapid blade-to-blade solution for use in turbomachinery design
[NASA-TM-83010] p 10 N83-13077
Rotordynamic Instability Problems in High-Performance Turbomachinery
[NASA-CP-2250] p 142 N83-15629
Development of a multiple-parameter nonlinear perturbation procedure for transonic turbomachinery flows: Preliminary application to design/optimization problems
[NASA-CR-3657] p 2 N83-17453

Aerodynamic effect of a honeycomb rotor tip shroud on a 50.8-centimeter-tip-diameter core turbine
[NASA-TP-2112] p 32 N83-17547
Method of fabricating an abradable gas path seal
[NASA-CASE-LEW-13269-2] p 93 N83-17714
Precision optical angular position marker system for rotating machinery
[NASA-TM-83062] p 144 N83-20117
Predicted and experimental performance of large-bore high-speed ball and roller bearings p 145 N83-20131
Lubrication of 35-millimeter-bore ball bearings of several designs to 2.5 million DN p 145 N83-20132
Evaluation of a high performance, fixed-ratio, traction drive p 145 N83-20135
Hybrid hydrostatic/ball bearings in high-speed turbomachinery
[NASA-CR-168124] p 149 N83-27213
Applications of the contravariant form of the Navier-Stokes equations
[NASA-TM-83448] p 14 N83-29179
Comparison of two- and three-dimensional flow computations with laser anemometer measurements in a transonic compressor rotor
[NASA-TP-1931] p 15 N83-32774

TURBOPROP AIRCRAFT
Bending-torsion flutter of a highly swept advanced turboprop
[NASA-TM-82975] p 158 N83-11514
Farfield inflight measurement of high-speed turboprop noise
[NASA-TM-83327] p 199 N83-21895

TURBOPROP ENGINES
An analytical and experimental comparison of the flow field of an advanced swept turboprop
[AIAA PAPER 83-0189] p 3 A83-21080
Flutter analysis of advanced turbopropellers
[AIAA 83-0846] p 157 A83-29824
Technology and benefits of aircraft counter rotation propellers
[NASA-TM-82983] p 27 N83-11129
An analytical and experimental comparison of the flow field of an advanced swept turboprop
[NASA-TM-83037] p 1 N83-14061
A preliminary comparison between the SR-6 propeller noise in flight and in a wind tunnel
[NASA-TM-83341] p 201 N83-24287
Propeller performance and weight predictions appended to the Navy/NASA engine program
[NASA-TM-83458] p 41 N83-32810

TURBOSHAFTS
Structural dynamics studies of rotating bladed-disk assemblies coupled with flexible shaft motions
[AIAA PAPER 83-0919] p 22 A83-32787
Status report - DARPA/NASA convertible turbofan/turboshaft engine program
[ASME PAPER 83-GT-196] p 25 A83-48000
Army/NASA small turboshaft engine digital controls research program
[NASA-TM-82979] p 27 N83-11128
Rotorcraft convertible engine study
[NASA-CR-168241] p 42 N83-34944

TURBULENCE
Laser anemometer using a Fabry-Perot interferometer for measuring mean velocity and turbulence intensity along the optical axis in turbomachinery p 133 A83-28834
Turbulent solution of the Navier-Stokes equations for an inhomogenous developing shear layer
[NASA-TM-82969] p 126 N83-12357
Tone-excited jet: Theory and experiments
[NASA-CR-3538] p 197 N83-12968
Turbulence measurements in a swirling confined jet flowfield using a triple hot-wire probe
[NASA-CR-169668] p 127 N83-14434
Interpretation of 2-probe turbulence measurements in an axisymmetric contraction
[NASA-CR-169832] p 11 N83-17502
Three-dimensional turbulent-mixing-length modeling for discrete-hole coolant injection into a crossflow
[NASA-TP-2200] p 132 N83-34232

TURBULENCE EFFECTS
Effects of free stream turbulence intensity and integral length scale on heat transfer from a circular cylinder in crossflow p 123 A83-42711

TURBULENT BOUNDARY LAYER
Small particle transport across turbulent nonisothermal boundary layers p 118 A83-10650
Numerical solution to the glancing sidewall oblique shock wave/turbulent boundary layer interaction in three-dimension
[AIAA PAPER 83-0136] p 3 A83-16823
Experimental investigation of a two-dimensional shock-turbulent boundary layer interaction with bleed
[AIAA PAPER 83-0135] p 3 A83-19581
Correlation and prediction of thermophoretic and inertial effects on particle deposition from non-isothermal turbulent boundary layers p 121 A83-27481
Convex curvature effects on the heated turbulent boundary layer p 123 A83-42733
Experimental study of the boundary layer on a turbomachinery rotor blade p 7 A83-47022
A mixing-length model for the prediction of convex curvature effects on turbulent boundary layers --- for turbine blade convective heat transfer prediction
[ASME PAPER 83-GT-80] p 125 A83-47933
Turbulence effect on crossflow around a circular cylinder at subcritical Reynolds numbers
[NASA-CR-3622] p 127 N83-13387
Numerical solution to the glancing sidewall oblique shock wave/turbulent boundary layer interaction in three dimension
[NASA-TM-83056] p 34 N83-22199
Experimental investigation of a two-dimensional shock-turbulent boundary layer interaction with bleed
[NASA-TM-83057] p 34 N83-22200

TURBULENT DIFFUSION
Effects of free stream turbulence intensity and integral length scale on heat transfer from a circular cylinder in crossflow p 123 A83-42711
Experimental study of the thermal-acoustic efficiency in a long turbulent diffusion-flame burner
[NASA-CR-170003] p 72 N83-19824
Stochastic differential equations and turbulent dispersion
[NASA-RP-1103] p 129 N83-22546

TURBULENT FLOW
Noise and flow structure of a tone-excited jet p 192 A83-13136
Finite-length solutions for rotodynamic coefficients of turbulent annular seals
[ASME PAPER 82-LUB-42] p 136 A83-13521
Modified gauge for time-resolved skin-friction measurements p 133 A83-14172
Aerodynamic features of turbulent flames
[AIAA PAPER 83-0470] p 119 A83-16737
Numerical studies of the formation and destruction of vortices in a motored four-stroke piston-cylinder configuration
[AIAA PAPER 83-0497] p 136 A83-16749
A turbulence model for three dimensional turbulent shear flows over curved rotating bodies
[AIAA PAPER 83-0559] p 120 A83-16787
Rapid distortion of small-scale turbulence by an axisymmetric contraction p 120 A83-22381
Computed and measured turbulence in axisymmetric reciprocating engines p 21 A83-24669
A basic code for the prediction of transient three-dimensional turbulent flowfields p 121 A83-27412
Investigation of the tip clearance flow inside and at the exit of a compressor rotor passage. II - Turbulence properties p 4 A83-28843
A two-equation turbulence model for two-phase flows p 121 A83-30109
Single-wire swirl flow turbulence measurements
[AIAA PAPER 83-1202] p 122 A83-36278
Prediction of an axisymmetric combusting flow
[AIAA PAPER 83-1264] p 69 A83-36315
Experimental evaluation of inlet turbulence, wall boundary layer, surface finish, and fillet radius on small axial turbine state performance
[SAE PAPER 821475] p 24 A83-38001
Numerical solution of the Navier-Stokes equations for compressible turbulent two/three dimensional flows in the terminal shock region of an inlet/diffuser
[AIAA PAPER 83-1892] p 5 A83-39358
Spanwise mass transfer variations on a cylinder in 'nominally' uniform crossflow p 124 A83-43019
Unsteady turbulent shear flow in shock tube discontinuities p 124 A83-46445
Vortices, stability, and turbulence p 125 A83-46718
Turbulent flame propagation and combustion in spark ignition engines p 70 A83-48156
Implicit marching solution of compressible viscous subsonic flow in planar and axisymmetric ducts
[NASA-TM-82876] p 125 N83-10389
Turbulence effect on crossflow around a circular cylinder at subcritical Reynolds numbers
[NASA-CR-3622] p 127 N83-13387
Mean-flow measurements of the flow field diffusing bend
[NASA-CR-3634] p 10 N83-14066
User's manual for Axisymmetric Diffuser Duct (ADD) code. Volume 2: Detailed ADD code description
[NASA-CR-165598-VOL-2] p 211 N83-26758
Structure of evaporating and combusting sprays: Measurements and predictions p 38 N83-29211
Turbulence spectra in the noise source regions of the flow around complex surfaces
[NASA-TM-83392] p 202 N83-30168
Modeling Interface Motion Of Combustion (MINOC). A computer code for two-dimensional, unsteady turbulent combustion
[NASA-TP-2132] p 40 N83-32806
Numerical analysis of turbulent coaxial flow with internal heat generation
[NASA-CR-172633] p 132 N83-33105
Numerical solutions of Navier-Stokes equations for compressible turbulent two/three dimensional flows in terminal shock region of an inlet/diffuser
[NASA-CR-3723] p 132 N83-34230
Turbulence measurements in a complex flowfield using a crossed hot-wire
[NASA-CR-173080] p 132 N83-35316

TURBULENT JETS
Predictions of the structure of turbulent, particle-laden, round jets
[AIAA PAPER 83-0066] p 119 A83-16498
Evaluation of a stochastic model of particle dispersion in a turbulent round jet p 121 A83-28104
Turbulence measurements in a swirling confined jet flowfield using a triple hot-wire probe
[NASA-CR-169668] p 127 N83-14434
The structure of particle-laden jets and nonevaporating sprays
[NASA-CR-168059] p 34 N83-20948

TURBULENT MIXING
Analytical calculation of a single jet in crossflow and comparison with experiment
[NASA-TM-83027] p 29 N83-14127

TURBULENT WAKES
Rotor wake characteristics relevant to rotor-stator interaction noise generation p 19 A83-10184
Blade loading and rotation effects on compressor rotor wake near end walls p 3 A83-22138

TWO DIMENSIONAL BOUNDARY LAYER
Experimental investigation of a two-dimensional shock-turbulent boundary layer interaction with bleed
[AIAA PAPER 83-0135] p 3 A83-19581
Experimental investigation of a two-dimensional shock-turbulent boundary layer interaction with bleed
[NASA-TM-83057] p 34 N83-22200

TWO DIMENSIONAL FLOW
A fast Euler solver for steady flows
[AIAA PAPER 83-1940] p 123 A83-39389
Effect of particle presence on the incompressible inviscid flow through a two dimensional compressor cascade p 6 A83-42562
Effect of particle presence on the incompressible inviscid flow through a two dimensional compressor cascade
[ASME PAPER 83-GT-95] p 8 A83-47941
Analytical and experimental evaluation of the heat transfer distribution over the surfaces of turbine vanes
[NASA-CR-168015] p 131 N83-28376
Flux-based acceleration of the Euler equations
[NASA-TM-83453] p 191 N83-30113
Incidence loss for fan turbine rotor blade in two-dimensional cascade
[NASA-TP-2188] p 39 N83-30431
Modeling Interface Motion Of Combustion (MINOC). A computer code for two-dimensional, unsteady turbulent combustion
[NASA-TP-2132] p 40 N83-32806
Numerical solutions of Navier-Stokes equations for compressible turbulent two/three dimensional flows in terminal shock region of an inlet/diffuser
[NASA-CR-3723] p 132 N83-34230

TWO DIMENSIONAL JETS
Dilution Jet Mixing Program, phase 1
[NASA-CR-168031] p 128 N83-15590

TWO PHASE FLOW
Predictions of the structure of turbulent, particle-laden, round jets
[AIAA PAPER 83-0066] p 119 A83-16498
A two-equation turbulence model for two-phase flows p 121 A83-30109
The dryout region in frictionally heated sliding contacts p 124 A83-42762
Acoustic velocities of two-phase mixtures of cryogenic fluids p 124 A83-43012
Effect of particle presence on the incompressible inviscid flow through a two dimensional compressor cascade
[ASME PAPER 83-GT-95] p 8 A83-47941
The structure of particle-laden jets and nonevaporating sprays
[NASA-CR-168059] p 34 N83-20948
Analogy between fluid cavitation and fracture mechanics
[NASA-TM-83071] p 129 N83-22542
Preliminary design of flight hardware for two-phase fluid research
[NASA-CR-168072] p 46 N83-25766

TWO REFLECTOR ANTENNAS
Techniques for low sidelobe, high efficiency offset dual reflector antennas p 104 A83-21072

Scanning beam antenna conceptual design for 20/30 GHz satellite systems p 46 N83-26689

U

UDIMET ALLOYS
Effect of reduced cobalt contents on hot isostatically pressed powder metallurgy U-700 alloys p 78 N83-11287
Thermal fatigue resistance of cobalt-modified UDIMET 700 p 78 N83-11289
Effect of the amount of Na2SO4 on the high temperature corrosion of Udimet-700 [NASA-TM-83459] p 87 N83-34016
ULTRAHIGH FREQUENCIES
Multi-stage Depressed Collectors (MDC) for efficiency improvements of UHF broadcast klystrons [NASA-TM-82970] p 105 N83-10322
ULTRASONIC FLAW DETECTION
Comparison of NDE techniques for sintered-SiC components p 152 A83-22265
Mechanics aspects of NDE by sound and ultrasound p 152 A83-25571
Fundamental aspects in quantitative ultrasonic determination of fracture toughness: The scattering of a single ellipsoidal inhomogeneity [NASA-CR-3625] p 153 N83-11507
ULTRASONIC RADIATION
Ultrasonic attenuation of a void-containing medium for very long wavelengths [NASA-CR-3693] p 154 N83-28466
ULTRASONIC TESTS
Interrelation of material microstructure, ultrasonic factors, and fracture toughness of a two-phase titanium alloy p 75 A83-23922
Phenomenological and mechanics aspects of nondestructive evaluation and characterization by sound and ultrasound of material and fracture properties [NASA-CR-3623] p 153 N83-11506
Ultrasonic ranking of toughness of tungsten carbide [NASA-TM-83358] p 153 N83-23620
ULTRASONIC WAVE TRANSDUCERS
Acousto-ultrasonic characterization of fiber reinforced composites p 63 N83-11231
Effects of specimen resonances on acoustic-ultrasonic testing [NASA-CR-3679] p 153 N83-21373
ULTRASONICS
Effects of specimen resonances on acoustic-ultrasonic testing [NASA-CR-3679] p 153 N83-21373
UNIQUENESS THEOREM
Formal convergence characteristics of elliptically constrained incremental Newton-Raphson algorithms p 190 A83-10273
UNSTEADY FLOW
Transient flow analysis of the AEDC/HPDE MHD generator [AIAA PAPER 83-0395] p 203 A83-16691
Unsteady turbulent shear flow in shock tube discontinuities p 124 A83-46445
Critical review of the trailing edge condition in steady and unsteady flow. Blade flutter in compressors and fans: Numerical simulation of the aerodynamic loading [NASA-CR-169705] p 10 N83-15264
Aircraft turbofan noise [NASA-TM-83317] p 198 N83-18405
UPGRADING
Fuel quality/processing study. Volume 3: Fuel upgrading studies [NASA-CR-165326-VOL-3] p 178 N83-22754
Fuel quality/processing study. Volume 4: On site processing studies [NASA-CR-165326-VOL-4] p 179 N83-22755
UPLINKING
Onboard processing for a 30/20 GHz communications satellite p 47 A83-41391
URBAN TRANSPORTATION
Improved transistorized AC motor controller for battery powered urban electric passenger vehicles [NASA-CR-167978] p 113 N83-10349
Support and power plant documentation for the gas turbine powered bus demonstration program [NASA-CR-165527] p 210 N83-20829
Demonstration and evaluation of gas turbine transit buses [NASA-CR-165528] p 212 N83-27926
USER MANUALS (COMPUTER PROGRAMS)
User's manual for Axisymmetric Diffuser Duct (ADD) code. Volume 2: Detailed ADD code description [NASA-CR-165598-VOL-2] p 211 N83-26758
User's manual for Axisymmetric Diffuser Duct (ADD) code. Volume 3: ADD code coordinate generator [NASA-CR-165598-VOL-3] p 211 N83-26759
Input generator for Denton 3-dimensional turbomachine-blade-row analysis code [NASA-TM-23324] p 13 N83-26817
UTILITIES
Operating experience with the 200 kW MOD-0A wind turbine generators p 174 N83-15916
Mod-2 wind turbine project assessment and cluster test plans p 176 N83-19262

V

V GROOVES
High voltage v-groove solar cell [NASA-CASE-LEW-13401-2] p 185 N83-32177
V/STOL AIRCRAFT
Effect of variable guide vanes on the performance of a high-bypass turbofan engine p 20 A83-24028
Zero-length inlets for subsonic V/STOL aircraft p 4 A83-29012
Supersonic STOVL research aircraft [SAE PAPER 821375] p 17 A83-37965
Aerodynamic performance of a fan stage utilizing variable inlet guide vanes (VIGV's) for thrust modulation --- subsonic V/STOL aircraft [AIAA PAPER 83-1162] p 6 A83-45508
Inlet-fan flow field computation [ASME PAPER 83-GT-41] p 7 A83-47901
Wind tunnel tests of a zero length, slotted-lip engine air inlet for a fixed nacelle V/STOL aircraft [NASA-TM-82939] p 9 N83-10019
Aerodynamic performance of a fan stage utilizing Variable Inlet Guide Vanes (VIGVs) for thrust modulation --- subsonic V/STOL aircraft [NASA-TM-83438] p 13 N83-27957
V/STOL propulsion control analysis: Phase 2, task 5-9 [NASA-CR-165523] p 40 N83-32804
VACUUM DEPOSITION
Microhardness studies on thin carbon films grown on P-type, (100) silicon [NASA-TM-82980] p 61 N83-13169
VACUUM TUBE OSCILLATORS
The phototron: A light to RF energy conversion device p 173 N83-15866
VANES
NASA LeRC/Akron University Graduate Cooperative Fellowship Program and Graduate Student Researchers Program [NASA-CR-167943] p 208 N83-10970
Measured and calculated wall temperatures on air-cooled turbine vanes with boundary layer transition [NASA-TM-83030] p 127 N83-14432
Analytical and experimental evaluation of the heat transfer distribution over the surfaces of turbine vanes [NASA-CR-168015] p 131 N83-28376
Stagnation region gas film cooling: Effects of dimensionless coolant temperature [NASA-CR-168197] p 132 N83-30960
VAPOR DEPOSITION
Production of large-area single-crystal wafers of cubic SiC for semiconductor devices p 205 A83-22767
VAPOR PHASE EPITAXY
Single and multijunction space solar cells grown by organometallic vapor phase epitaxy /OM-VPE/ p 164 A83-27260
Use of column V alkyls in organometallic vapor phase epitaxy (OMVPE) p 70 A83-46608
Progress toward cascade cells made by OM-VPE --- organometallic vapor phase epitaxy p 171 N83-15813
Radiation damage and annealing in large area n+/p/p+ GaAs shallow homojunction solar cells p 172 N83-15826
VAPOR PHASES
Analytical modeling of operating characteristics of premixing-prevaporizing fuel-air mixing passages. Volume 1: Analysis and results [NASA-CR-167990-VOL-1] p 126 N83-12353
Analytical modeling of operating characteristics of premixing-prevaporizing fuel-air mixing passages. Volume 2: User's manual [NASA-CR-167990-VOL-2] p 126 N83-12354
VAPORIZERS
Design, fabrication and testing of porous tungsten vaporizers for mercury ion thrusters [NASA-TM-83063] p 58 N83-22318
VAPORIZING
Vaporization thermodynamics of K2S and K2SO3 [NASA-CR-168080] p 61 N83-19812
Fuel vaporization effects p 101 N83-29214
LOX/hydrocarbon fuel carbon formation and mixing data analysis [NASA-CR-168066] p 101 N83-31886
VAPORS
High-speed motion picture camera experiments of cavitation in dynamically loaded journal bearings [ASME PAPER 82-LUB-18] p 136 A83-13509
High-speed motion picture camera experiments of cavitation in dynamically loaded journal bearings [ASME PAPER 82-LUB-18] p 138 A83-39944
VARIABLE GEOMETRY STRUCTURES
Acoustics in variable area duct - Finite element and finite difference comparisons to experiment p 193 A83-19809
VARIATIONAL PRINCIPLES
Alternative ways for formulation of hybrid stress elements p 155 A83-14710
VECTORS (MATHEMATICS)
Convergence and stability properties of minimal polynomial and reduced rank extrapolation algorithms [NASA-TM-83443] p 191 N83-31390
VELOCITY DISTRIBUTION
Confined swirling flow predictions [AIAA PAPER 83-0316] p 119 A83-16646
The performance of an annular vane swirler --- to aid in modeling gas turbine combustor flowfields and swirling confined flow turbulence [AIAA PAPER 83-1326] p 24 A83-36340
Laser-induced fluorescence technique for velocity field measurements in subsonic gas flows p 133 A83-45962
Applications of the contravariant form of the Navier-Stokes equations [NASA-TM-83448] p 14 N83-29179
Fuel spray diagnostics p 38 N83-29212
Numerical analysis of turbulent coaxial flow with internal heat generation [NASA-CR-172633] p 132 N83-33105
VELOCITY MEASUREMENT
Five-hole pitot probe time-mean velocity measurements in confined swirling flows [AIAA PAPER 83-0315] p 119 A83-16645
Comparison of laser anemometer measurements and theory in an annular turbine cascade with experimental accuracy determined by parameter estimation p 4 A83-28833
Laser anemometer using a Fabry-Perot interferometer for measuring mean velocity and turbulence intensity along the optical axis in turbomachinery p 133 A83-28834
Laser-induced fluorescence technique for velocity field measurements in subsonic gas flows p 133 A83-45962
Free-jet acoustic investigation of high-radius-ratio coannular plug nozzles. Comprehensive data report, volume 2 [NASA-CR-168086-VOL-2] p 199 N83-18409
The LeRC rail accelerators: Test designs and diagnostic techniques [NASA-TM-83496] p 60 N83-35053
VENTURI TUBES
A vortex venturi for reverting antimisting fuel properties [ASME PAPER 83-GT-137] p 25 A83-47964
VERTICAL TAKEOFF AIRCRAFT
A remote augmentor lift system with a turbine bypass engine p 20 A83-19595
A remote augmentor lift system with a turbine bypass engine [NASA-TM-82932] p 27 N83-12087
Conceptual design, evaluation and research identification for Remote Augmented Propulsive Lift Systems (RALS) with ejectors for VTOL aircraft [NASA-CR-167906] p 29 N83-13103
VIBRATION
The transfer function method for gear system dynamics applied to conventional and minimum excitation gearing designs [NASA-CR-3626] p 139 N83-11495
Bending-torsion flutter of a highly swept advanced turboprop [NASA-TM-82975] p 156 N83-11514
VIBRATION DAMPING
Friction damping of flutter in gas turbine engine airfoils p 20 A83-24038
Design of dry-friction dampers for turbine blades p 22 A83-35883
Variable force, eddy-current or magnetic damper [NASA-CASE-LEW-13717-1] p 159 N83-20284
VIBRATION ISOLATORS
Power turbine dynamics - An evaluation of a shear-mounted elastomeric damper [ASME PAPER 83-GT-228] p 139 A83-48025
VIBRATION MODE
On the three-dimensional vibrations of the cantilevered rectangular parallelepiped p 157 A83-37729
VIBRATION TESTS
Measurements of self-excited rotor-blade vibrations using optical dispacements [NASA-TM-82953] p 159 N83-14523

Rotordynamic Instability Problems in High-Performance Turbomachinery
[NASA-CP-2250] p 142 N83-15629
VIBRATIONAL SPECTRA
Effect of hydrogen bonding on the vibrational dephasing time in glycerol p 61 A83-21054
VIBRATIONAL STRESS
Turbofan blade stresses induced by the flow distortion of a VTOL inlet at high angles of attack
[NASA-TM-82963] p 12 N83-17509
VIDEO COMMUNICATION
A new architecture for adaptive transform compression of NTSC composite video signal p 103 A83-19732
Satellite switched FDMA advanced communication technology satellite program
[NASA-CR-168034] p 105 N83-15543
Satellite provided customer premises services: A forecast of potential domestic demand through the year 2000. Volume: Executive summary
[NASA-CR-168142] p 109 N83-34116
Satellite provided customer premise services: A forecast of potential domestic demand through the year 2000. Volume 2: Technical report
[NASA-CR-168143] p 109 N83-34117
VIDEO DATA
A new architecture for adaptive transform compression of NTSC composite video signal p 103 A83-19732
Satellite fixed communications service: A forecast of potential domestic demand through the year 2000. Volume 3: Appendices
[NASA-CR-168147] p 108 N83-34115
Satellite provided customer premise services: A forecast of potential domestic demand through the year 2000. Volume 3: Appendices
[NASA-CR-168144] p 109 N83-34118
VISCOELASTICITY
A detailed treatment of two-dimensional, starved lubrication in the vicinity of two counter-rotating cylinders p 141 N83-15520
VISCOMETERS
High accuracy fuel flowmeter, phase 1
[NASA-CR-167893] p 134 N83-21314
VISCOMETRY
Surface temperatures and glassy state investigations in tribology, part 5
[NASA-CR-3632] p 91 N83-11328
VISCOPLASTICITY
An uncoupled viscoplastic constitutive model for metals at elevated temperature
[AIAA 83-1016] p 156 A83-29798
Constitutive relationships for anisotropic high-temperature alloys
[NASA-TM-83437] p 160 N83-28493
VISCOSITY
A detailed treatment of two-dimensional, starved lubrication in the vicinity of two counter-rotating cylinders p 141 N83-15520
Geometry and starvation effects in hydrodynamic lubrication p 141 N83-15522
Lubricant effects on efficiency of a helicopter transmission p 141 N83-15523
A refrigerated dynamic seal
[NASA-TM-83378] p 130 N83-24798
Transport properties of oxygen
[NASA-RP-1102] p 130 N83-24800
A numerical study of the steady scalar convective diffusion equation for small viscosity
[NASA-CR-172231] p 16 N83-35999
VISCOUS FLOW
A viscous-inviscid interactive procedure for rotational flow in cascades of two-dimensional airfoils of arbitrary shape
[AIAA PAPER 83-0256] p 3 A83-16614
Multi-grid solution of Neumann pressure problem for viscous flows using primitive variables
[AIAA PAPER 83-0557] p 120 A83-16786
Three-dimensional compressible viscous analysis of mixer nozzles
[AIAA PAPER 83-1401] p 4 A83-36391
Solution of viscous internal flows on curvilinear grids generated by the Schwarz-Christoffel transformation p 122 A83-38796
Implicit marching solution of compressible viscous subsonic flow in planar and axisymmetric ducts
[NASA-TM-82876] p 125 N83-10389
Convergence acceleration of viscous flow computations
[NASA-TM-83039] p 190 N83-12930
Validation of a three-dimensional viscous analysis of axisymmetric supersonic inlet flow fields
[NASA-TM-83058] p 32 N83-17538
Multiple-grid convergence acceleration of viscous and inviscid flow computations
[NASA-TM-83361] p 190 N83-21847
End-wall boundary layer measurements in a two-stage fan
[NASA-TM-83409] p 12 N83-24470
Micromechanically based constitutive relations for polycrystalline solids p 162 N83-34359
VISCOUS FLUIDS
Vortices, stability, and turbulence p 125 A83-46718
VITON
Power turbine dynamics - An evaluation of a shear-mounted elastomeric damper
[ASME PAPER 83-GT-228] p 139 A83-48025
VOICE COMMUNICATION
Satellite switched FDMA advanced communication technology satellite program
[NASA-CR-168034] p 105 N83-15543
Satellite provided fixed communication services: A forecast of potential domestic demand through the year 2000. Volume 1: Executive summary
[NASA-CR-168145] p 108 N83-34113
Satellite fixed communications service: A forecast of potential domestic demand through the year 2000. Volume 3: Appendices
[NASA-CR-168147] p 108 N83-34115
Satellite provided customer premises services: A forecast of potential domestic demand through the year 2000. Volume: Executive summary
[NASA-CR-168142] p 109 N83-34116
Satellite provided customer premise services: A forecast of potential domestic demand through the year 2000. Volume 2: Technical report
[NASA-CR-168143] p 109 N83-34117
Satellite provided customer premise services: A forecast of potential domestic demand through the year 2000. Volume 3: Appendices
[NASA-CR-168144] p 109 N83-34118
VOIDS
Diffusion processes in Al2O3 scales - Void growth, grain growth, and scale growth p 76 A83-42238
Ultrasonic attenuation of a void-containing medium for very long wavelengths
[NASA-CR-3693] p 154 N83-28466
VOLCANOES
Aircraft sampling of the sulfate layer near the tropopause following the eruption of Mount St. Helens p 187 N83-11556
VOLT-AMPERE CHARACTERISTICS
End region effects upon the performance of a magnetohydrodynamic channel p 203 A83-10665
Numerical simulation of a disk-shaped electron accelerating electrostatic probe p 133 A83-22336
Performance characteristics of a microwave plasma disk ion source --- time varying electric propulsion concept
[AIAA PAPER 82-1935] p 55 A83-27350
A mathematical model for the doubly fed wound rotor generator
[NASA-TM-83454] p 117 N83-34192
VOLTAGE CONVERTERS (DC TO DC)
Investigations of stability and dynamic performances of switching regulators employing current-injected control p 110 A83-11002
Parametric study of minimum reactor mass in energy-storage dc-to-dc converters p 110 A83-11011
Nonlinear program based optimization of boost and buck-boost converter designs p 110 A83-11016
A novel input filter compensation scheme for switching regulators p 111 A83-11494
An improved switching converter model using discrete and average techniques p 111 A83-11495
Computer simulations of optimum boost and buck-boost converters p 111 A83-19032
Advances in core loss calculations for magnetic materials
[NASA-TM-82947] p 113 N83-11446
An improved switching converter model
[NASA-CR-169669] p 114 N83-14398
High-frequency high-voltage high-power DC-to-DC converters p 115 N83-21028
VOLTAGE REGULATORS
Investigations of stability and dynamic performances of switching regulators employing current-injected control p 110 A83-11002
Nonlinear program based optimization of boost and buck-boost converter designs p 110 A83-11016
A novel input filter compensation scheme for switching regulators p 111 A83-11494
An improved switching converter model using discrete and average techniques p 111 A83-11495
Control design and performance analysis of a 6 MW wind turbine-generator p 165 A83-29897
VOLUME
Time dependence of solid-particle impingement erosion of an aluminum alloy
[NASA-TP-2169] p 86 N83-32908
VORTEX BREAKDOWN
Numerical studies of the formation and destruction of vortices in a motored four-stroke piston-cylinder configuration
[AIAA PAPER 83-0497] p 136 A83-16749
VORTICES
Three-dimensional stability of vortex arrays p 120 A83-19022
A semi-direct solver for compressible three-dimensional rotational flow
[AIAA PAPER 83-1909] p 122 A83-39367
Vortices, stability, and turbulence p 125 A83-46718
A vortex venturi for reverting antimisting fuel properties
[ASME PAPER 83-GT-137] p 25 A83-47964
Modeling Interface Motion Of Combustion (MINOC). A computer code for two-dimensional, unsteady turbulent combustion
[NASA-TP-2132] p 40 N83-32806
A semi-direct solver for compressible 3-dimensional rotational flow
[NASA-TM-83314] p 15 N83-34908
Vortex motion in axisymmetric piston-cylinder configurations
[NASA-TM-85404] p 133 N83-35318
VORTICITY
Experiments on identification and control of inflow disturbances in contracting streams
[NASA-CR-169831] p 11 N83-17503
VORTICITY EQUATIONS
Development of secondary flow and vorticity in curved ducts, cascades, and rotors, including effects of viscosity and rotation p 119 A83-16141

W

WAFERS
High voltage v-groove solar cell
[NASA-CASE-LEW-13401-2] p 185 N83-32177
WALL FLOW
Blade loading and rotation effects on compressor rotor wake near end walls p 3 A83-22138
Wall boundary layer development near the tip region of an IGV of an axial flow compressor
[ASME PAPER 83-GT-171] p 8 A83-47972
End wall flows in rotors and stators of a single stage compressor
[NASA-CR-169800] p 128 N83-16678
WALL TEMPERATURE
Film-cooling effectiveness with developing coolant flow through straight and curved tubular passages
[NASA-TP-2062] p 126 N83-12360
Measured and calculated wall temperatures on air-cooled turbine vanes with boundary layer transition
[NASA-TM-83030] p 127 N83-14432
Curved film cooling admission tube
[NASA-CASE-LEW-13174-1] p 131 N83-27144
WALLS
Analytical and experimental investigation of stator endwall contouring in a small axial-flow turbine. 1: Stator performance
[NASA-TP-2023] p 26 N83-11125
WANKEL ENGINES
Multi-fuel rotary engine for general aviation aircraft
[NASA-TM-85428] p 43 N83-36031
WASHINGTON
Aircraft sampling of the sulfate layer near the tropopause following the eruption of Mount St. Helens p 187 N83-11556
WASTE ENERGY UTILIZATION
Apparatus for improving the fuel efficiency of a gas turbine engine
[NASA-CASE-LEW-13142-1] p 43 N83-36029
WATER
Evaluation of production version of the NASA improved inorganic-organic separator
[NASA-TM-83018] p 174 N83-18022
Cavitation pitting and erosion of Al 6061-T6 in mineral oil and water
[NASA-TM-83345] p 148 N83-23606
WATER INJECTION
The feasibility of water injection into the turbine coolant to permit gas turbine contingency power for helicopter application
[ASME PAPER 83-GT-66] p 24 A83-39993
WATER VAPOR
Axial-compressor flow distortion with water ingestion
[AIAA PAPER 83-0004] p 19 A83-16456
Water vapor measurement system in global atmospheric sampling program, appendix
[NASA-TP-2051] p 187 N83-13643
WAVE ATTENUATION
The effect of stress on ultrasonic pulses in fiber reinforced composites
[NASA-CR-3724] p 154 N83-33180

WAVE DIFFRACTION
Sound diffraction at wall impedance discontinuities in a circular cylinder - Investigated using Wiener-Hopf technique
[AIAA PAPER 83-0730] p 195 A83-33485
Sound diffraction at wall impedance discontinuities in a circular cylinder, investigated using Wiener-Hopf technique
[NASA-TM-83365] p 201 N83-23117
WAVE DISPERSION
Long range surface plasmons in birefringent media p 202 A83-42206
WAVE EQUATIONS
Transient difference solutions of the inhomogeneous wave equation - Simulation of the Green's function
[AIAA PAPER 83-0667] p 193 A83-25904
Transient difference solutions of the inhomogeneous wave equation: Simulation of the Green's function
[NASA-TM-83336] p 200 N83-21897
WAVE GENERATION
The evolution of Tollmien-Schlichting waves near a leading edge. II - Numerical determination of amplitudes p 122 A83-35346
Generation of Tollmien-Schlichting waves by free-stream disturbances at low Mach numbers
[NASA-TM-83026] p 130 N83-23544
WAVE PROPAGATION
Mode propagation in nonuniform circular ducts with potential flow p 122 A83-36082
Surface-polaritonlike waves guided by thin, lossy metal films p 192 A83-37947
Long-range surface plasmons in electrode structures p 202 A83-40733
Wave propagation in a graphite/epoxy laminate p 158 A83-44050
Transient difference solutions of the inhomogeneous wave equation: Simulation of the Green's function
[NASA-TM-83336] p 200 N83-21897
Wave propagation in graphite/epoxy laminates due to impact
[NASA-CR-168057] p 66 N83-22325
WAVE REFLECTION
Analysis of an axial compressor blade vibration based on wave reflection theory
[ASME PAPER 83-GT-151] p 25 A83-47970
WAVE SCATTERING
The transmission or scattering of elastic waves by an inhomogeneity of simple geometry: A comparison of theories
[NASA-CR-3659] p 153 N83-16773
WAVEGUIDES
Effects of gaps on long range surface plasmon polaritons p 204 A83-46271
WEAR
Review of factors that influence fretting wear p 137 A83-17259
Plastic deformation and wear process at a surface during unlubricated sliding p 138 A83-37822
Tribological characteristics of nitrogen (N+) implanted iron p 75 A83-37824
The dryout region in frictionally heated sliding contacts p 124 A83-42762
Friction and wear of iron and nickel in sodium hydroxide solutions p 77 A83-48922
Friction and wear of iron and nickel in sodium hydroxide solutions
[NASA-TM-82935] p 77 N83-10171
Plasma deposition and surface modification techniques for wear resistance
[NASA-TM-82972] p 90 N83-10194
Plastic deformation at surface during unlubricated sliding
[NASA-TP-2036] p 139 N83-11496
Tribological properties of amorphous alloys and the role of surfaces in abrasive wear of materials
[NASA-TM-82973] p 140 N83-11498
Tribology p 140 N83-12167
Polyimides: Tribological properties and their use as lubricants
[NASA-TM-82959] p 91 N83-13257
Investigation of wear phenomena by microscopy
[NASA-TM-82954] p 81 N83-14245
Effect of sliding speed and contact stress on tribological properties of ultra-high-molecular-weight polyethylene
[NASA-TP-2059] p 91 N83-14269
Friction and wear of some ferrous-base metallic glasses
[NASA-TM-83067] p 82 N83-19886
Assessment of lubricated contacts: Mechanisms of scuffing and scoring
[NASA-TM-83074] p 144 N83-20118
Tribological and microstructural characteristics of ion-nitrided steels
[NASA-TM-83368] p 84 N83-24635
Effect of oxygen concentration in ZDP containing oils on surface composition and wear
[NASA-TM-83000] p 84 N83-24636
Morphology of an aluminum alloy eroded by a jet of angular particles impinging at normal incidence
[NASA-TP-2139] p 85 N83-24641
Friction, wear, transfer and wear surface morphology of ultra-high-molecular-weight polyethylene
[NASA-TM-83364] p 94 N83-25882
NASA interdisciplinary collaboration in tribology. A review of oxidational wear
[NASA-CR-3686] p 95 N83-27021
The adsorption and thermal decomposition of tricresylphosphate (TCP) on iron and gold
[NASA-TM-83441] p 62 N83-29311
Tribological measurements on a Charnley-type artificial hip joint
[NASA-TM-83440] p 97 N83-32943
WEAR INHIBITORS
On the mechanism of lubrication by tricresylphosphate /TCP/ - The coefficient of friction as a function of temperature for TCP on M-50 steel
[ASLE PREPRINT 82-LC-4C-1] p 135 A83-13228
Nitriding of titanium and titanium- 8 percent aluminum, 1 percent molybdenum, 1 percent vanadium alloy with an ion-beam source
[NASA-TP-2149] p 85 N83-24640
WEAR TESTS
Sputtered silicon nitride coatings for wear protection p 83 A83-12651
A study of the surface deterioration due to erosion --- of gas turbine blades
[ASME PAPER 83-GT-213] p 9 A83-48014
Sliding induced crystallization of metallic glass
[NASA-TP-2140] p 83 N83-21110
Polyimides formulated from a partially fluorinated diamine for aerospace tribological applications
[NASA-TM-83339] p 94 N83-22423
WEIGHT REDUCTION
Computer simulations of optimum boost and buck-boost converters p 111 A83-19032
The 371 deg C(700 deg F) properties of celion 6000/n-phenylnadimide modified PMR polyimide composites
[NASA-TM-83050] p 65 N83-15365
Advanced electrical power system technology for the all electric aircraft
[NASA-TM-83390] p 115 N83-24764
WELDED JOINTS
Microstructural analysis of solar cell welds p 172 N83-15833
Evaluation of solar cell welds by scanning acoustic microscopy p 172 N83-15834
WELDING
Evaluation of electrode shape and nondestructive evaluation method for welded solar cell interconnects
[NASA-TM-82966] p 166 N83-10555
Microstructural analysis of solar cell welds p 172 N83-15833
Evaluation of solar cell welds by scanning acoustic microscopy p 172 N83-15834
Joining lead wires to thin platinum alloy films
[NASA-CASE-LEW-13934-1] p 135 N83-35338
WETTABILITY
Pore size engineering applied to the design of separators for nickel-hydrogen cells and batteries
[NASA-TM-83386] p 73 N83-24571
WHISKER COMPOSITES
High-temperature composites - Status and future directions p 63 A83-40129
WHISTLERS
The 'whistler-nozzle' phenomenon p 125 A83-49472
The whistler nozzle phenomenon
[NASA-CR-170015] p 199 N83-20706
WIDEBAND COMMUNICATION
Spacecraft in switch matrix for wide band service applicatons in 30/20 GHz communications satellite systems
[NASA-CR-168089] p 46 N83-34998
WIND (METEOROLOGY)
Large Horizontal-Axis Wind Turbines
[NASA-CP-2230] p 175 N83-19231
WIND EFFECTS
Effects of wind on turbofan engines in outdoor static test stands
[NASA-TM-83493] p 42 N83-34945
WIND TUNNEL TESTS
Wind tunnel measurements of blade/vane ratio and spacing effects on fan noise p 192 A83-15317
A new surface-streamline flow-visualization technique p 133 A83-19016
Comparison of measured and predicted flight effects on high-bypass coaxial jet exhaust noise
[AIAA PAPER 83-0749] p 194 A83-26450
The influence of inlet design on the aeroacoustic performance of a JT15D turbofan engine as measured in the NASA-Ames 40 x 80 foot wind tunnel
[AIAA PAPER 83-0681] p 21 A83-28006
Zero-length inlets for subsonic V/STOL aircraft p 4 A83-29012
Ejector nozzle test results at simulated flight conditions for an advanced supersonic transport propulsion system
[AIAA PAPER 83-1287] p 23 A83-36323
Aerodynamic performance of a fan stage utilizing variable inlet guide vanes (VIGV's) for thrust modulation --- subsonic V/STOL aircraft
[AIAA PAPER 83-1162] p 6 A83-45508
Low speed performance of a supersonic axisymmetric mixed compression inlet with auxiliary inlets
[AIAA PAPER 83-1414] p 7 A83-45516
Low flight speed acoustic results for a supersonic inlet with auxiliary inlet doors
[AIAA PAPER 83-1415] p 196 A83-45517
Wind tunnel tests of a zero length, slotted-lip engine air inlet for a fixed nacelle V/STOL aircraft
[NASA-TM-82939] p 9 N83-10019
Bending-torsion flutter of a highly swept advanced turboprop
[NASA-TM-82975] p 158 N83-11514
Wind tunnel evaluation of air-foil performance using simulated ice shapes
[NASA-CR-167960] p 11 N83-15265
Turbine endwall single cylinder program
[NASA-CR-170008] p 44 N83-19761
Noise of the 10-bladed 60 deg swept SR-5 propeller in a wind tunnel
[NASA-TM-83054] p 200 N83-23112
Low flight speed acoustic results for a supersonic inlet with auxiliary inlet doors
[NASA-TM-83411] p 201 N83-27794
Aerodynamic performance of a fan stage utilizing Variable Inlet Guide Vanes (VIGVs) for thrust modulation --- subsonic V/STOL aircraft
[NASA-TM-83438] p 13 N83-27957
Low speed performance of a supersonic axisymmetric mixed compression inlet with auxiliary inlets --- Lewis 9x15-ft anechoic wind tunnel tests
[NASA-TM-83435] p 37 N83-27992
WIND TURBINES
A review of resonance response in large, horizontal-axis wind turbines p 163 A83-13696
Control design for a wind turbine-generator using output feedback p 164 A83-24721
Control design and performance analysis of a 6 MW wind turbine-generator p 165 A83-29897
Measured effect of wind generation on the fuel consumption of an isolated diesel power system p 165 A83-36410
Wind turbine generator interaction with diesel generators on an isolated power system p 165 A83-44673
Design and fabrication of composite blades for the Mod-1 wind turbine generator
[NASA-CR-167987] p 168 N83-11579
The effect of yaw on horizontal axis wind turbine loading and performance
[NASA-TM-82778] p 169 N83-14688
Measured performance of a tip-controlled, teetered rotor with an NACA 64 sub 3-618 tip airfoil
[NASA-TM-82870] p 169 N83-14689
DOE/NASA Lewis large wind turbine program
[NASA-TM-82991] p 169 N83-14690
Hygrothermomechanical evaluation of transverse filament tape epoxy/polyester fiberglass composites
[NASA-TM-83044] p 65 N83-15362
The NASA Lewis large wind turbine program p 174 N83-15911
Operating experience with the 200 kW MOD-OA wind turbine generators p 174 N83-15916
Construction of low-cost, Mod-OA wood composite wind turbine blades
[NASA-TM-83046] p 174 N83-16857
The MOD-OA 200 kilowatt wind turbine generator design and analysis report
[NASA-CR-165127] p 174 N83-16859
Design and evaluation of low-cost stainless steel fiberglass foam blades for large wind driven generating systems
[NASA-CR-165491] p 174 N83-19226
Large Horizontal-Axis Wind Turbines
[NASA-CP-2230] p 175 N83-19231
The response of a 38m horizontal axis teetered rotor to yaw p 175 N83-19232
Fixed pitch rotor performance of large horizontal axis wind turbines p 175 N83-19233
Stall induced instability of a teetered rotor p 175 N83-19234
Free yaw performance of the Mod-0 large horizontal axis 100 kW wind turbine p 175 N83-19235
Design and evaluation of low cost blades for large wind driven generating systems p 175 N83-19244

Structural fatigue test results for large wind turbine blade sections p 159 N83-19246
Performance and load data from Mod-0A and Mod-1 wind turbine generators p 176 N83-19255
Operating experience with four 200 kW Mod-0A wind turbine generators p 176 N83-19256
Experience and assessment of the DOE/NASA Mod-1 2000 kW wind turbine generator at Boone, North Carolina p 176 N83-19257
Mod-2 wind turbine project assessment and cluster test plans p 176 N83-19262
Stability analysis of flexible wind turbine blades using finite element method
[NASA-CR-168107] p 177 N83-21508
Simplified aeroelastic modeling of horizontal axis wind turbines
[NASA-CR-168109] p 177 N83-21509
Some experiments on Yaw stability of wind turbines with various coning angles
[NASA-CR-168108] p 177 N83-22740
Fatigue testing of low-cost fiberglass composite wind turbine blade materials
[NASA-CR-165566] p 177 N83-22746
Development of methodology for horizontal axis wind turbine dynamic analysis
[NASA-CR-168110] p 178 N83-22747
Design and evaluation of low-cost laminated wood composite blades for intermediate size wind turbines: Blade design, fabrication concept, and cost analysis
[NASA-CR-165463] p 179 N83-23704
Structural qualification testing and operational loading on a fiberglass rotor blade for the Mod-OA wind turbine
[NASA-TM-83309] p 179 N83-23710
The DOE/NASA wind turbine data acquisition system. Part 3: Unattended power performance monitor
[NASA-CR-165540] p 44 N83-24516
Mod-2 wind turbine system development. Volume 1: Executive summary
[NASA-CR-168006] p 184 N83-29812
Results of free yaw tests of the Mod-O 100 kilowatt wind turbine
[NASA-TM-83432] p 184 N83-29813
DOE large horizontal axis wind turbine development at NASA Lewis Research Center
[NASA-TM-83444] p 184 N83-31107
Mod-2 wind turbine system development. Volume 2: Detailed report
[NASA-CR-168007] p 185 N83-33343
Control of large wind turbine generators connected to utility networks
[NASA-CR-168200] p 185 N83-34451

WINDPOWER UTILIZATION
DOE/NASA Lewis large wind turbine program
[NASA-TM-82991] p 169 N83-14690
The MOD-OA 200 kilowatt wind turbine generator design and analysis report
[NASA-CR-165127] p 174 N83-16859
Mod-2 wind turbine project assessment and cluster test plans p 176 N83-19262
Mod-2 wind turbine system development. Volume 2: Detailed report
[NASA-CR-168007] p 185 N83-33343

WINDPOWERED GENERATORS
Control design for a wind turbine-generator using output feedback p 164 A83-24721
Control design and performance analysis of a 6 MW wind turbine-generator p 165 A83-29897
Measured effect of wind generation on the fuel consumption of an isolated diesel power system p 165 A83-36410
The MOD-OA 200 kilowatt wind turbine generator design and analysis report
[NASA-CR-165127] p 174 N83-16859
Design and evaluation of low-cost stainless steel fiberglass foam blades for large wind driven generating systems
[NASA-CR-165491] p 174 N83-19226
Large Horizontal-Axis Wind Turbines
[NASA-CP-2230] p 175 N83-19231
The response of a 38m horizontal axis teetered rotor to yaw p 175 N83-19232
Fixed pitch rotor performance of large horizontal axis wind turbines p 175 N83-19233
Stall induced instability of a teetered rotor p 175 N83-19234
Free yaw performance of the Mod-0 large horizontal axis 100 kW wind turbine p 175 N83-19235
Performance and load data from Mod-0A and Mod-1 wind turbine generators p 176 N83-19255
Operating experience with four 200 kW Mod-0A wind turbine generators p 176 N83-19256
Experience and assessment of the DOE/NASA Mod-1 2000 kW wind turbine generator at Boone, North Carolina p 176 N83-19257
Control of large wind turbine generators connected to utility networks
[NASA-CR-168200] p 185 N83-34451

WING FLAPS
QCSEE under-the-wing engine-wing-flap aerodynamic profile characteristics
[NASA-TM-82890] p 28 N83-12092

WING LOADING
Incidence angle effects on convected gust airfoil noise
[AIAA PAPER 83-0765] p 195 A83-28022
QCSEE under-the-wing engine-wing-flap aerodynamic profile characteristics
[NASA-TM-82890] p 28 N83-12092

WINGS
Wind tunnel evaluation of air-foil performance using simulated ice shapes
[NASA-CR-167960] p 11 N83-15265
Piezoelectric deicing device
[NASA-CASE-LEW-13773-1] p 18 N83-29197

WIRE
Joining lead wires to thin platinum alloy films
[NASA-CASE-LEW-13934-1] p 135 N83-35338

WIRE CLOTH
Metal honeycomb to porous wireform substrate diffusion bond evaluation p 153 A83-39620

WOOD
Design and evaluation of low-cost laminated wood composite blades for intermediate size wind turbines: Blade design, fabrication concept, and cost analysis
[NASA-CR-165463] p 179 N83-23704

WORKING FLUIDS
Heat pipes containing alkali metal working fluid
[NASA-CASE-LEW-12253-1] p 203 N83-19596

X

X RAY INSPECTION
Comparison of NDE techniques for sintered-SiC components p 152 A83-22265

X RAY SPECTROSCOPY
Investigation of wear phenomena by microscopy
[NASA-TM-82934] p 81 N83-14245
Application of modern surface analytical tools in the investigation of surface deterioration processes
[NASA-TM-83452] p 152 N83-34327

XENON
Analysis and design of ion thrusters for large space systems
[NASA-CR-165160] p 57 N83-14159

Y

YAW
The effect of yaw on horizontal axis wind turbine loading and performance
[NASA-TM-82778] p 169 N83-14688
The response of a 38m horizontal axis teetered rotor to yaw p 175 N83-19232
Free yaw performance of the Mod-0 large horizontal axis 100 kW wind turbine p 175 N83-19235
Results of free yaw tests of the Mod-O 100 kilowatt wind turbine
[NASA-TM-83432] p 184 N83-29813

YAWING MOMENTS
Some experiments on Yaw stability of wind turbines with various coning angles
[NASA-CR-168108] p 177 N83-22740
Development of methodology for horizontal axis wind turbine dynamic analysis
[NASA-CR-168110] p 178 N83-22747

YIELD STRENGTH
Development of tough, strong, iron-base alloy for cryogenic applications p 44 N83-18763
Evaluation of low-cost aluminum composites for aircraft engine structural applications
[NASA-TM-83357] p 66 N83-25790
Time-independent anisotropic plastic behavior by mechanical subelement models p 162 N83-34369

YTTRIUM OXIDES
Effect of Y2O3 and Al2O3 on the oxidation resistance of Si3N4 p 88 A83-22258
Some inelastic effects of thermal cycling on ZrO2-Y2O3 materials p 89 A83-22272
Sintering, properties and fabrication of Si3N4 + Y2O3 based ceramics p 90 A83-46203

Z

ZINC
Surface chemistry, friction and wear of Ni-Zn and Mn-Zn ferrites in contact with metals
[NASA-TM-83068] p 93 N83-19901
X-ray photoelectron spectroscopy and friction studies of nickel-zinc and manganese-zinc ferrites in contact with metals
[NASA-TP-2163] p 84 N83-23419

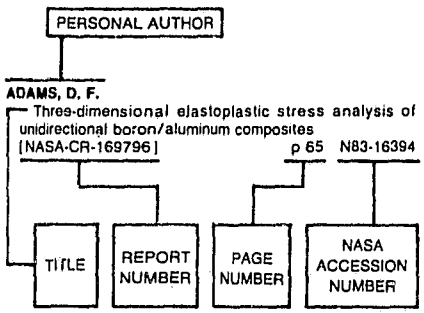
ZINC COMPOUNDS
Effect of oxygen concentration in ZDP containing oils on surface composition and wear
[NASA-TM-83000] p 84 N83-24636

ZIRCONIUM
Improved nickel base coating alloy --- oxidation resistant coatings
[NASA-CASE-LEW-13834-1] p 85 N83-24639

ZIRCONIUM CARBIDES
Zirconium carbide as an electrocatalyst for the chromous-chromic redox couple
[NASA-CASE-LEW-13246-1] p 182 N83-27344

ZIRCONIUM OXIDES
Performance of laser-glazed zirconia thermal barrier coatings in cyclic oxidation and corrosion burner rig tests p 88 A83-10300
Some inelastic effects of thermal cycling on ZrO2-Y2O3 materials p 89 A83-22272
Creep of plasma-sprayed-ZrO2 thermal-barrier coatings p 89 A83-22273
Creep of plasma sprayed zirconia
[NASA-CR-167868] p 96 N83-29393

Typical Personal Author Index Listing



Listings in this index are arranged alphabetically by personal author. The title of the document provides the user with a brief description of the subject matter. The report number helps to indicate the type of document listed (e.g., NASA report, translation, NASA contractor report). The page and accession numbers are located beneath and to the right of the title. Under any one author's name the accession numbers are arranged in sequence with the AIAA accession numbers appearing first.

A

ABBEY, K. M.
Pore size engineering applied to starved electrochemical cells and batteries p 164 A83-27201
Pore size engineering applied to starved electrochemical cells and batteries
[NASA-TM-82893] p 70 N83-10134
Electrolyte management in porous battery components. Static measurements
[NASA-TM-83073] p 72 N83-18862
Pore size engineering applied to the design of separators for nickel-hydrogen cells and batteries
[NASA-TM-83386] p 73 N83-24571

ABDELNOUR, Z. A.
Testing of the permanent magnet material Mn-Al-C for potential use in propulsion motors for electric vehicles
[NASA-CR-169481] p 114 N83-12329

ABOU-ARAB, T. W.
A two-equation turbulence model for two-phase flows p 121 A83-30109

ABRAHAM, K. M.
Moderate temperature rechargeable sodium batteries
[NASA-CR-168220] p 118 N83-36359

ABUJELALA, M. T.
Confined swirling flow predictions
[AIAA PAPER 83-0316] p 119 A83-16646

ACEVEDO, J. C.
An electrochemical rebalance cell for Redox systems
[NASA-TM-83363] p 73 N83-29326

ADAM, P. W.
NASA low-speed centrifugal compressor for fundamental research
[AIAA PAPER 83-1351] p 43 A83-36353
NASA low-speed centrifugal compressor for fundamental research
[NASA-TM-83398] p 13 N83-25662

ADAMCZYK, J. J.
A semi-direct solver for compressible three-dimensional rotational flow
[AIAA PAPER 83-1909] p 122 A83-39367
A semi-direct solver for compressible 3-dimensional rotational flow
[NASA-TM-83314] p 15 N83-34908
Semidirect computations for transonic flow
[NASA-TM-83451] p 15 N83-34909

ADAMS, D. F.
Three-dimensional elastoplastic stress analysis of unidirectional boron/aluminum composites
[NASA-CR-169796] p 65 N83-16394

ADAMS, E. W.
A mixing-length model for the prediction of convex curvature effects on turbulent boundary layers
[ASME PAPER 83-GT-80] p 125 A83-47933

ADAMS, J. W.
Creep of plasma-sprayed-ZrO2 thermal-barrier coatings p 89 A83-22273
Creep of plasma sprayed zirconia
[NASA-CR-167868] p 96 N83-29393

ADAMS, K.
Experimental comparison of icing cloud instruments
[AIAA PAPER 83-0026] p 16 A83-42099
Experimental comparison of icing cloud instruments
[NASA-TM-83340] p 17 N83-24487

ADLER, A.
Development of a rotary instrumentation system, phase 2
[NASA-CR-168013] p 47 N83-18835

AHUJA, K. K.
Noise and flow structure of a tone-excited jet p 192 A83-13136
Generation of desired signals from acoustic drivers p 19 A83-15068
Tone-excited jet: Theory and experiments
[NASA-CR-3538] p 197 N83-12968

AIELLO, R. A.
Tensile buckling of advanced turboprops
[AIAA PAPER 82-0776] p 154 A83-10900
Large displacements and stability analysis of nonlinear propeller structures p 159 N83-12460

AJAGU, C. O.
Modified gauge for time-resolved skin-friction measurements p 133 A83-14172

AKAY, H. U.
A finite element formulation for steady transonic Euler equations p 3 A83-22129

AKHTER, M. M.
Sensor failure detection for jet engines
[NASA-CR-168190] p 154 N83-33182

AKIN, L. S.
Experimental and analytical determination of gear tooth temperatures with oil jet lubrication p 142 N83-15530
Into mesh lubrication of spur gears with arbitrary offset oil jet. 1: For jet velocity less than or equal to gear velocity
[NASA-TM-83040] p 143 N83-19092
Into mesh lubrication of spur gears with arbitrary offset oil jet. 2: For jet velocities equal to or greater than great velocity
[NASA-TM-83041] p 143 N83-19093
Study of lubricant jet flow phenomena in spur gears: Out of mesh condition p 147 N83-20146
Gear lubrication and cooling experiment and analysis p 147 N83-20147

AKLE, W.
Requirements for a mobile communications satellite system. Volume 3: Large space structures measurements study
[NASA-CR-168105] p 45 N83-22255

AL-KINANI, G.
Planning assistance for the 30/20 GHz program, volume 1
[NASA-CR-165484-VOL-1] p 108 N83-33010
Planning assistance for the 30/20 GHz program, volume 2
[NASA-CR-165484-VOL-2] p 108 N83-33011
Planning assistance for the 30/20 GHz program, volume 3
[NASA-CR-165484] p 108 N83-33012
Satellite provided fixed communication services: A forecast of potential domestic demand through the year 2000. Volume 1: Executive summary
[NASA-CR-168145] p 108 N83-34113
Satellite provided customer premises services: A forecast of potential domestic demand through the year 2000. Volume: Executive summary
[NASA-CR-168142] p 109 N83-34116
Satellite provided customer premise services: A forecast of potential domestic demand through the year 2000 Volume 3: Appendices
[NASA-CR-168144] p 109 N83-34118

ALAM, J.
Solution of elastic and elasto-plastic problems by the method of lines
[NASA-CR-168125] p 85 N83-28208

ALBRIGHT, A. E.
A method of predicting flow rates required to achieve anti-icing performance with a porous leading edge ice protection system
[NASA-CR-168213] p 17 N83-32782

ALFANO, R. R.
Effect of hydrogen bonding on the vibrational dephasing time in glycerol p 61 A83-21054

ALLAIRE, P. E.
Aerodynamic stiffness of an unbound eccentric whirling centrifugal impeller with an infinite number of blades p 142 N83-15650

ALLEN, J.
Advanced ceramic coating development for industrial/utility gas turbine applications
[NASA-CR-165619] p 92 N83-15467

ALSTON, W. B.
PMR polyimides - Review and update p 62 A83-20447

ALTENKIRCH, R. A.
Boundary integral equation method calculations of surface regression effects in flame spreading p 67 A83-13488
Correlating downward flame spread rates for thick fuel beds p 69 A83-37045

ALTEROVITZ, S. A.
Ellipsometric study of silicon nitride on gallium arsenide p 204 A83-11812
An enhanced sensitivity null ellipsometry technique for studying films on substrates - Application to silicon nitride on gallium arsenide p 206 A83-37318

AMERO, R.
Fuel quality-processing study. Volume 2: Literature survey
[NASA-CR-165326-VOL-2] p 178 N83-22751

AMMANN, P. R.
Study to establish cost predictions for the production of Redox chemicals
[NASA-CR-167882] p 176 N83-20359

ANCONA, W.
Design of dry-friction dampers for turbine blades p 22 A83-35883

ANDERSEN, T. S.
The MOD-0A 200 kilowatt wind turbine generator design and analysis report
[NASA-CR-165127] p 174 N83-16859

ANDERSON, B. H.
Numerical solution to the glancing sidewall oblique shock wave/turbulent boundary layer interaction in three-dimension
[AIAA PAPER 83-0136] p 3 A83-16823
Validation of a three-dimensional viscous analysis of axisymmetric supersonic inlet flow fields
[NASA-TM-83058] p 32 N83-17538
Numerical solution to the glancing sidewall oblique shock wave/turbulent boundary layer interaction in three dimension
[NASA-TM-83056] p 34 N83-22199

ANDERSON, D. N.
Catalytic combustion with steam injection
[ASME PAPER 82-JPGC-GT-23] p 164 A83-25271
Catalytic combustion with steam injection
[NASA-TM-82923] p 170 N83-15805
Critical research and advanced technology (CRT) support project
[NASA-TM-83019] p 176 N83-20361

ANDERSON, L. M.
A new strategy for efficient solar energy conversion - Parallel-processing with surface plasmons p 164 A83-27140
Solar energy conversion using surface plasmons for broadband energy transport p 171 N83-15815
Inelastic tunnel diodes
[NASA-CASE-LEW-13833-1] p 116 N83-25983

Solar energy converter using surface plasma waves
[NASA-CASE-LEW-13827-1] p 181 N83-26258
A new strategy for efficient solar energy conversion: Parallel-processing with surface plasmons
[NASA-TM-82867] p 59 N83-28071

ANDERSON, N. E.
Evaluation of a high performance, fixed-ratio, traction drive p 145 N83-20135
Comparison of spur gear efficiency prediction methods p 146 N83-20141
Advances in traction drive technology
[NASA-TM-83397] p 150 N83-28455

ANDERSON, O. L.
Solution of viscous internal flows on curvilinear grids generated by the Schwarz-Christoffel transformation p 122 A83-38796
Analytical modeling of operating characteristics of premixing-prevaporizing fuel-air mixing passages. Volume 1: Analysis and results
[NASA-CR-167990-VOL-1] p 126 N83-12353
Analytical modeling of operating characteristics of premixing-prevaporizing fuel-air mixing passages. Volume 2: User's manual
[NASA-CR-167990-VOL-2] p 126 N83-12354
User's manual for Axisymmetric Diffuser Duct (ADD) code. Volume 1: General ADD code description
[NASA-CR-165598-VOL-1] p 211 N83-26757
User's manual for Axisymmetric Diffuser Duct (ADD) code. Volume 2: Detailed ADD code description
[NASA-CR-165598-VOL-2] p 211 N83-26758
User's manual for Axisymmetric Diffuser Duct (ADD) code. Volume 3: ADD code coordinate generator
[NASA-CR-165598-VOL-3] p 211 N83-26759

ANDERSON, R. D.
Advanced propfan engine characteristics and technology needs
[AIAA PAPER 83-1155] p 23 A83-36250

ANDERSON, R. E.
Mobile radio alternative systems study, executive summary
[NASA-CR-168207] p 109 N83-34119

ANDERSON, W. J.
Rolling-element bearings
[NASA-RP-1105] p 149 N83-27214

ANDERSSON, C. A.
Advanced ceramic coating development for industrial/utility gas turbine applications
[NASA-CR-165619] p 92 N83-15467

ANTOINE, A. C.
Fuels research studies at NASA Lewis
[NASA-TM-83003] p 100 N83-19921

ANTOLOVICH, S. D.
Metallurgical instabilities during the high temperature low cycle fatigue of nickel-base superalloys p 75 A83-22019
The effect of microstructure on the fatigue behavior of Ni base superalloys p 75 A83-36166

ANTONELLI, M.
Automotive Stirling engine development program
[NASA-CR-167907] p 209 N83-15176
Automotive Stirling engine development program
[NASA-CR-168060] p 209 N83-15177
Automotive Stirling Engine Development Program
[NASA-CR-168074] p 212 N83-27925

ANZIC, G.
A study of 60 Gigahertz intersatellite link applications
[NASA-TM-83337] p 47 N83-20994

APPLE, S. A.
Support and power plant documentation for the gas turbine powered bus demonstration program
[NASA-CR-165527] p 210 N83-20829

ARECHAGA, T.
Formal convergence characteristics of elliptically constrained incremental Newton-Raphson algorithms p 190 A83-10273

ARGENBRIGHT, L. A.
An analytical investigation of NO sub x control techniques for methanol fueled spark ignition engines
[NASA-CR-172847] p 151 N83-33168

ARNDT, R. A.
Limitations on solar cell open-circuit voltage and efficiency p 165 A83-37790

ARNON, N.
Evaluation of ceramics for stator applications: Gas turbine engines interim report. Stator fabrication and evaluation
[NASA-CR-168140] p 96 N83-30662

ARON, P. R.
Sputtered silicon nitride coatings for wear protection p 88 A83-12651
Some properties of r.f.-sputtered hafnium nitride coatings p 88 A83-12653
RF sputtered silicon and hafnium nitrides: Properties and adhesion to 440C stainless steel
[NASA-TM-83400] p 95 N83-27020

ARP, V.
The dryout region in frictionally heated sliding contacts p 124 A83-42762

ASMUSSEN, J.
Measurements of energy distribution and thrust for microwave plasma coupling of electrical energy to hydrogen for propulsion
[AIAA PAPER 82-1951] p 52 A83-12508
Microwave plasma generation of hydrogen atoms for rocket propulsion p 53 A83-13090
Performance characteristics of a microwave plasma disk ion source
[AIAA PAPER 82-1935] p 55 A83-27350

ASTLEY, R. J.
Acoustics in variable area duct - Finite element and finite difference comparisons to experiment p 193 A83-19809

ATENCIO, A.
The influence of inlet design on the aeroacoustic performance of a JT15D turbofan engine as measured in the NASA-Ames 40 x 80 foot wind tunnel
[AIAA PAPER 83-0681] p 21 A83-28006

ATKINSON, W. H.
Development of advanced high-temperature heat flux sensors
[NASA-CR-165618] p 26 N83-10044

ATLURI, S. N.
Stress and fracture analyses under elastic-plastic creep conditions: Some basic developments and computational approaches p 162 N83-34371

ATWOOD, S.
Satellite switched FDMA advanced communication technology satellite program
[NASA-CR-168034] p 105 N83-15543

AUGUST, R.
Dynamic effects of internal spur gear drives
[NASA-CR-3692] p 149 N83-28452
Vibration in planetary gear systems with unequal planet stiffnesses
[NASA-TM-83428] p 150 N83-29709

AUPING, J. V.
A software system for emission spectrometry
[NASA-TM-83001] p 70 N83-12181

AVERY, J. W.
Development of a high capacity toroidal Ni/Cd cell
[NASA-CR-169945] p 176 N83-19273

AYDELOTT, J. C.
Modeling of space vehicle propellant mixing
[NASA-TP-2107] p 100 N83-16545

B

BAAKLINI, G. Y.
The effect of stress on ultrasonic pulses in fiber reinforced composites
[NASA-CR-3724] p 154 N83-33180

BABER, B. B.
Evaluation of high-contact-ratio spur gears with profile modification p 147 N83-20150

BACH, L. J.
Blade loss transient dynamic analysis of turbomachinery p 25 A83-40864

BACK, G.
Energy and precious fuels requirements of fuel alcohol production. Volume 4: Appendices G and H, methanol from coal
[NASA-CR-168093] p 183 N83-28580
Energy and precious fuels requirements of fuel alcohol production. Volume 3, appendices C to F: Methanol from cellulose
[NASA-CR-168092] p 183 N83-28583

BAEZ, A. N.
Army/NASA small turboshaft engine digital controls research program
[NASA-TM-82979] p 27 N83-11128

BAILEY, W. J.
Cryogenic fluid management experiment trunnion fatigue verification
[AIAA PAPER 83-0911] p 49 A83-32782

BAIR, S.
Surface temperatures and glassy state investigations in tribology, part 5
[NASA-CR-3632] p 91 N83-11328

BAKER, C. E.
Research on aviation fuel instability
[NASA-TM-83420] p 101 N83-28255
High-pressure flame visualization of autoignition and flashback phenomena with liquid-fuel spray
[NASA-TM-83501] p 42 N83-34948

BALAN, C.
A method of predicting the performance deterioration of a compressor cascade due to sand erosion
[AIAA PAPER 83-0178] p 19 A83-16572
Effect of particle presence on the incompressible inviscid flow through a two dimensional compressor cascade p 6 A83-42562
Effect of particle presence on the incompressible inviscid flow through a two dimensional compressor cascade
[ASME PAPER 83-GT-95] p 8 A83-47941
A study of the surface deterioration due to erosion
[ASME PAPER 83-GT-213] p 9 A83-48014
Environmental solid particle effects on compressor cascade performance
[NASA-CR-168018] p 11 N83-16285
Compressor cascade performance deterioration caused by sand ingestion
[NASA-CR-168067] p 11 N83-16286

BALDERRAMA, E.
20 x 20 IF switch matrix for SS-TDMA systems p 113 A83-41369

BALDWIN, D. H.
The NASA Lewis large wind turbine program p 174 N83-15911

BALL, C. L.
End-wall boundary layer measurements in a two-stage fan
[NASA-TM-83409] p 12 N83-24470

BALL, D. E.
Phased array-fed antenna configuration study: Technology assessment
[NASA-CR-168078] p 106 N83-22495
Phased array-fed antenna configuration study
[NASA-CR-168077] p 107 N83-27086

BALOMBIN, J. R.
Rotor wake characteristics relevant to rotor-stator interaction noise generation p 19 A83-10184
Farfield inflight measurements of high-speed turboprop noise
[AIAA PAPER 83-0745] p 21 A83-25947
Tone generation by rotor-downstream strut interaction
[AIAA PAPER 83-0767] p 21 A83-25957
Tone generation by rotor-downstream strut interaction
[NASA-TM-83330] p 33 N83-19754
Farfield inflight measurement of high-speed turboprop noise
[NASA-TM-83327] p 199 N83-21895

BAMBERGER, E. N.
Bearing fatigue investigation 3
[NASA-CR-168029] p 143 N83-17880
Corrosion of simulated bearing components of three bearing steels in the presence of chloride-contaminated lubricant
[NASA-TM-82955] p 143 N83-20115
Effect of carbide distribution on rolling-element fatigue life of AMS 5749
[NASA-TP-2189] p 151 N83-33166

BANKAITIS, H.
Implementation of R & QA practices in Research and Development programs
[NASA-TM-82997] p 210 N83-19651

BANKS, B.
Interfacial electrical properties of ion-beam sputter deposited amorphous carbon on silicon p 205 A83-33920

BANKS, B. A.
Mechanical bonding of metal method
[NASA-CASE-LEW-12941-1] p 77 N83-10170
Growth of diamondlike films for power applications p 174 N83-15880
Ion beam sputter etched ventricular catheter for hydrocephalus shunt
[NASA-CASE-LEW-13107-2] p 188 N83-20539
Ion beam sputter-etched ventricular catheter for hydrocephalus shunt
[NASA-CASE-LEW-13107-1] p 188 N83-21785
Diamondlike flake composites
[NASA-CASE-LEW-13837-1] p 67 N83-28095
Piezoelectric deicing device
[NASA-CASE-LEW-13773-1] p 18 N83-29197

BARAONA, C. R.
Evaluation of electrode shape and nondestructive evaluation method for welded solar cell interconnects
[NASA-TM-82966] p 166 N83-10555
Microstructural analysis of solar cell welds p 172 N83-15833
Evaluation of solar cell welds by scanning acoustic microscopy p 172 N83-15834
Screen printed interdigitated back contact solar cell
[NASA-CASE-LEW-13414-1] p 177 N83-20374

BARBEE, J. G.
Evaluation of fuel additives for reduction of material incompatibilities in methanol-gasoline blends
[NASA-CR-168061] p 86 N83-29359

BARBER, J. P.
Electric rail gun projectile acceleration to high velocity
[AIAA PAPER 82-1939] p 52 A83-12501

BAREFOOT, J.
Superalloy composition modeling p 78 N83-11284

C-4

Role of cobalt in nickel base superalloys p 78 N83-11286

BARKER, D. R.
A brittle to ductile transition in NiAl of a critical grain size p 75 A83-29726

BARNETT, A. N.
Design rules for a 100X maximum efficiency GaAs concentrator solar cell for space applications [NASA-CR-170005] p 177 N83-20362

BARONA, C. R.
Large area low-cost space solar cell development p 170 N83-14699

BARRANGER, J. P.
Precision optical angular position marker system for rotating machinery [NASA-TM-83062] p 144 N83-20117

BARRETT, C. A.
Cyclic oxidation of superalloys p 76 A83-42234
Oxidation of low cobalt alloys p 79 N83-11291
Improved nickel base coating alloy [NASA-CASE-LEW-13834-1] p 85 N83-24639

BARROWS, R. R.
Characterization of a high-pressure diesel fuel injection system as a control technology option to improve engine performance and reduce exhaust emissions [NASA-TM-83329] p 210 N83-24431

BARTON, C. K.
Computer program to predict noise of general aviation aircraft: User's guide [NASA-CR-168050] p 198 N83-17242

BARTON, R. S.
Control design and performance analysis of a 6 MW wind turbine-generator p 165 A83-29897
Experience and assessment of the DOE/NASA Mod-1 2000 kW wind turbine generator at Boone, North Carolina p 176 N83-19257

BATESOLE, W. R.
Design and fabrication of composite blades for the Mod-1 wind turbine generator [NASA-CR-167987] p 168 N83-11579

BATTLES, R. A.
Design of an advanced 500-hp helicopter transmission p 144 N83-20125

BAUER, D. P.
Electric rail gun projectile acceleration to high velocity [AIAA PAPER 82-1939] p 52 A83-12501

BAUMANN, K. J.
Research priorities for advanced fibrous composites [NASA-CR-165414] p 65 N83-18853
Research priorities and history of advanced composite compression testing [NASA-CR-165415] p 66 N83-18854

BAUMBICK, R. J.
Fiberoptics technology and its application to propulsion control systems [AIAA PAPER 83-0534] p 18 A83-16772
Fiber optics for aircraft engine/inlet control p 20 A83-22494
Fiberoptics technology and its application to propulsion control systems [NASA-TM-83009] p 18 N83-15302
Status of fiberoptics technology for propulsion control systems [NASA-TM-82907] p 32 N83-17537

BAUMEISTE, K. J.
Transient difference solutions of the inhomogeneous wave equation: Simulation of the Green's function [NASA-TM-83336] p 200 N83-21897

BAUMEISTER, K. J.
Acoustics in variable area duct - Finite element and finite difference comparisons to experiment p 193 A83-19809
Transient difference solutions of the inhomogeneous wave equation - Simulation of the Green's function [AIAA PAPER 83-0667] p 193 A83-25904
Utilizing numerical techniques in turbofan inlet acoustic suppressor design [NASA-TM-82994] p 196 N83-10885

BEATTIE, E. C.
Sensor failure detection for jet engines [NASA-CR-168190] p 154 N83-33182

BEATTIE, J. R.
A direct-measurement technique for estimating discharge-chamber lifetime [AIAA PAPER 82-1908] p 51 A83-12483
Advanced-technology 30-cm-diameter mercury ion thruster [AIAA PAPER 82-1910] p 51 A83-12484
Endurance test of a 30-CM-diameter engineering model ion thruster. Task 12: Investigation of thin-film erosion monitors for ion thrusters [NASA-CR-168132] p 58 N83-25779

BEAUCHAMP, E. D.
Advanced single permanent magnet axipolar ironless stator ac motor for electric passenger vehicles [NASA-CR-167974] p 212 N83-32687

BECHERT, D. W.
Excited waves in shear layers [DFVLR-FB-82-23] p 106 N83-21218

BECHTEL, R. T.
Operational summary of an electric propulsion long term test facility [AIAA PAPER 82-1903] p 44 A83-12478
Status of the J-series 30-cm mercury ion thruster [AIAA PAPER 82-1904] p 51 A83-12479

BECK, W. E.
Zero-length inlets for subsonic V/STOL aircraft p 4 A83-29012

BECK, W. E., JR.
Wind tunnel tests of a zero length, slotted-lip engine air inlet for a fixed nacelle V/STOL aircraft [NASA-TM-82939] p 9 N83-10019

BEEBE, K. W.
Evaluation of advanced combustion concepts for dry NO sub x suppression with coal-derived, gaseous fuels [NASA-TM-82985] p 166 N83-10557

BEERS, B. L.
Thermal dielectric breakdown with cylindrical electrodes p 112 A83-38216
Continued development of a detailed model of arc discharge dynamics [NASA-CR-167977] p 206 N83-16234

BEHBEHANI, K.
Sensor failure and multivariable control for airbreathing propulsion systems [NASA-CR-159791] p 1 N83-16279

BEITLER, R. S.
Control means for a gas turbine engine [NASA-CASE-LEW-14586-1] p 40 N83-31603

BELLIN, A. I.
Status report - DARPA/NASA convertible turbofan/turboshaft engine program [ASME PAPER 83-GT-196] p 25 A83-48000

BENNET, J. E.
Vaporization thermodynamics of K2S and K2SO3 [NASA-CR-168080] p 61 N83-19812

BENNETT, G. W.
Control means for a gas turbine engine [NASA-CASE-LEW-14586-1] p 40 N83-31603

BENNETT, J. C.
Statistical characteristics of velocity, concentration, mass transport, and momentum transport for coaxial jet mixing in a confined duct [ASME PAPER 83-GT-39] p 125 A83-47899

BENNETT, L. C.
Fatigue testing of low-cost fiberglass composite wind turbine blade materials [NASA-CR-165566] p 177 N83-22746

BENSON, T. J.
Numerical solution to the glancing sidewall oblique shock wave/turbulent boundary layer interaction in three-dimension [AIAA PAPER 83-0136] p 3 A83-16823
Validation of a three-dimensional viscous analysis of axisymmetric supersonic inlet flow fields [NASA-TM-83058] p 32 N83-17538
Numerical solution to the glancing sidewall oblique shock wave/turbulent boundary layer interaction in three dimension [NASA-TM-83056] p 34 N83-22199

BEREMAND, D. G.
Free-piston Stirling hydraulic engine and drive system for automobiles [NASA-TM-82992] p 211 N83-25625
DOE/NASA Automotive Stirling Engine Project overview '83 [NASA-TM-83405] p 212 N83-27924

BERENFELD, A.
Experiments in dilution jet mixing [AIAA PAPER 83-1201] p 122 A83-36277
Dilution Jet Mixing Program, phase 1 [NASA-CR-168031] p 128 N83-15590
Experiments in dilution jet mixing [NASA-TM-83434] p 15 N83-30393

BERETTA, G. P.
Turbulent flame propagation and combustion in spark ignition engines p 70 A83-48156

BERG, R.
Parametric analysis of closed cycle magnetohydrodynamic (MHD) power plants [NASA-CR-165472] p 178 N83-22748

BERGSTEN, D. E.
The effect of incidence angle on the overall three-dimensional aerodynamic performance of a classical annular airfoil cascade [NASA-CR-168127] p 15 N83-34911

BERKOWITZ, M.
Development of a microwave 20 x 20 switch matrix for 30/20 GHz SS-TDMA application p 110 A83-11484
A high capacity satellite switched TDMA microwave switch matrix p 104 A83-19776
Study of advanced rotary combustion engines for commuter aircraft [NASA-CR-165399] p 32 N83-17545

BERNARD, S.
Aircraft measurements of trace gases and particles near the tropopause [NASA-CR-3691] p 188 N83-27542

BESSENDORF, M.
Crack layer morphology and toughness characterization in steels [NASA-CR-168154] p 160 N83-27256

BHAGAT, R. B.
Low cycle fatigue behavior of aluminum/stainless steel composites [AIAA 83-0806] p 62 A83-29886

BHAT, M. K.
Measurements of compressible secondary flow in a circular S-duct [AIAA PAPER 83-1739] p 4 A83-37218

BHATT, R. T.
Fatigue behavior of SiC reinforced Ti/6Al-4V/ at 650 C p 62 A83-12414

BHATTACHARYYA, S.
Determination of hydrogen permeability in uncoated and coated superalloys [NASA-CR-165209] p 80 N83-12215
Creep-rupture behavior of 6 candidate stirling engine iron-base superalloys in high pressure hydrogen. Volume 1: Air creep-rupture behavior [NASA-CR-168071] p 83 N83-22389
Determination of hydrogen permeability in commercial and modified superalloys [NASA-CR-168195] p 87 N83-35101

BHUSHAN, C.
Satellite provided fixed communication services: A forecast of potential domestic demand through the year 2000. Volume 1: Executive summary [NASA-CR-168145] p 108 N83-34113
Satellite provided fixed communications services: A forecast of potential domestic demand through the year 2000: Volume 2: Main test [NASA-CR-168146] p 108 N83-34114
Satellite fixed communications service: A forecast of potential domestic demand through the year 2000. Volume 3: Appendices [NASA-CR-168147] p 108 N83-34115
Satellite provided customer premises services: A forecast of potential domestic demand through the year 2000. Volume: Executive summary [NASA-CR-168142] p 109 N83-34116

BHUTIANI, P. K.
Free-jet acoustic investigation of high-radius-ratio coannular plug nozzles. Comprehensive data report, volume 2 [NASA-CR-168086-VOL-2] p 199 N83-18409

BIFANO, W. J.
COE and AID stand-alone photovoltaic activities [NASA-TM-83374] p 180 N83-25041

BILL, R. C.
Review of factors that influence fretting wear p 137 A83-17259
Some inelastic effects of thermal cycling on ZrO2-Y2O3 materials p 89 A83-22272
Method of fabricating an abradable gas path seal [NASA-CASE-LEW-13269-2] p 93 N83-17714
Laser surface fusion of plasma sprayed ceramic turbine seals [NASA-CASE-LEW-13269-1] p 50 N83-20996
Fully plasma-sprayed compliant backed ceramic turbine seal [NASA-CASE-LEW-13268-3] p 149 N83-28450
Thermal barrier coating system having improved adhesion [NASA-CASE-LEW-1335901] p 97 N83-31855

BILL, R. C., JR.
Creep of plasma-sprayed-ZrO2 thermal-barrier coatings p 89 A83-22273

BIRCHENOUGH, A. G.
Operating experience with the 200 kW MOD-0A wind turbine generators p 174 N83-15916
Operating experience with four 200 kW Mod-0A wind turbine generators p 176 N83-19256

BITTKER, D. A.
Research on aviation fuel instability [NASA-TM-83420] p 101 N83-28255
Effect of deoxygenation and prestressing on hydrocarbon fuel thermal stability [NASA-TM-83456] p 102 N83-35160

BIZON, P. T.
Thermal fatigue resistance of cobalt-modified UDIMET 700 p 78 N83-11289

BLACK, B. M.
Small transport aircraft technology propeller study [NASA-CR-168045] p 14 N83-29178

BLACK, G.
Blade loss transient dynamic analysis of turbomachinery p 25 A83-40864
BLACKMORE, W. L.
Three-dimensional compressible viscous analysis of mixer nozzles
[AIAA PAPER 83-1401] p 4 A83-36391
BLANTON, J. C.
Evaluation of catalytic combustion of actual coal-derived gas
[NASA-CR-167842] p 168 N83-13588
BLECHERMAN, S. S.
Composite fan exit guide vanes for high bypass ratio gas turbine engines p 19 A83-13159
BLESIADNY, T.
Uniform engine testing program. Phase 1: NASA Lewis Research Center participation
[NASA-TM-82978] p 29 N83-14126
BLOKHRA, R. L.
Activation parameters of flow through battery separators
[NASA-TM-83371] p 73 N83-30550
BLOOMER, H. E.
QCSEE under-the-wing engine-wing-flap aerodynamic profile characteristics
[NASA-TM-82890] p 28 N83-12092
BOARDSEN, S. A.
Plasma characteristics of a 17 cm diameter line-cusp ion thruster
[AIAA PAPER 82-1926] p 52 A83-12495
BOBER, L. J.
An analytical and experimental comparison of the flow field of an advanced swept turboprop
[AIAA PAPER 83-0189] p 3 A83-21080
Prediction of high speed propeller flow fields using a three-dimensional Euler analysis
[AIAA PAPER 83-0188] p 4 A83-29535
An analytical and experimental comparison of the flow field of an advanced swept turboprop
[NASA-TM-83037] p 1 N83-14061
Prediction of high speed propeller flow fields using a three-dimensional Euler analysis
[NASA-TM-83065] p 12 N83-19710
New test techniques and analytical procedures for understanding the behavior of advanced propellers
[NASA-TM-83560] p 2 N83-22092
BOBULA, G. A.
Effect of variable guide vanes on the performance of a high-bypass turbofan engine p 20 A83-24028
Effect of steady-state pressure distortion on inlet flow to a high-bypass-ratio turbofan engine
[NASA-TM-82964] p 30 N83-15306
BODENSCHATZ, C. A.
The MOD-OA 200 kilowatt wind turbine generator design and analysis report
[NASA-CR-165127] p 174 N83-16859
BOLDMAN, D. R.
Experimental evaluation of shockless supercritical airfoils in cascade
[AIAA PAPER 83-0003] p 2 A83-16455
Experimental evaluation of shockless supercritical airfoils in cascade
[NASA-TM-83045] p 11 N83-15268
Turbulence spectra in the noise source regions of the flow around complex surfaces
[NASA-TM-83392] p 202 N83-30168
BONNELYCKE, B.
Planning assistance for the NASA 30/20 GHz program. Network control architecture study.
[NASA-CR-168058] p 106 N83-21207
BONNICE, M. A.
Stagnation region gas film cooling: Effects of dimensionless coolant temperature
[NASA-CR-168197] p 132 N83-30983
BORDEN, P. G.
Single and multijunction space solar cells grown by organometallic vapor phase epitaxy /OM-VPE/ p 164 A83-27260
Progress toward cascade cells made by OM-VPE p 171 N83-15813
BORNSTEIN, N. S.
The oxidation behavior of a model molybdenum/tungsten-containing alloy in air alone and in air with trace levels of NaCl(g) p 76 A83-42241
BORREGO, J. M.
Diffused P+-N solar cells in bulk GaAs p 171 N83-15818
BOSE, S. K.
Packet communication system for a multi-beam beam switched satellite repeater p 104 A83-41336
BOSQUE, M. A.
Fuel spray diagnostics p 38 N83-29212
Fuel vaporization effects p 101 N83-29214
Detailed fuel spray analysis techniques
[NASA-TM-83476] p 42 N83-34943
BOWDEN, J. N.
Tests of blending and correlation of distillate fuel properties p 98 A83-11050
BOWDITCH, D. N.
A survey of inlet/engine distortion compatibility
[AIAA PAPER 83-1166] p 6 A83-45509
A survey of inlet/engine distortion compatibility
[NASA-TM-83421] p 37 N83-27991
BOWLES, E. B.
Vapor flow into a capillary propellant-acquisition device
[AIAA PAPER 83-1380] p 55 A83-36371
BOWYER, J.
Satellite provided fixed communication services: A forecast of potential domestic demand through the year 2000. Volume 1: Executive summary
[NASA-CR-168145] p 108 N83-34113
Satellite provided fixed communications services: A forecast of potential domestic demand through the year 2000: Volume 2: Main test
[NASA-CR-168146] p 108 N83-34114
Satellite fixed communications service: A forecast of potential domestic demand through the year 2000. Volume 3: Appendices
[NASA-CR-168147] p 108 N83-34115
Satellite provided customer premises services: A forecast of potential domestic demand through the year 2000. Volume: Executive summary
[NASA-CR-168142] p 109 N83-34116
Satellite provided customer premise services: A forecast of potential domestic demand through the year 2000. Volume 3: Appendices
[NASA-CR-168144] p 109 N83-34118
BOYLE, M. T.
A new surface-streamline flow-visualization technique p 133 A83-19016
BRABBS, T. A.
Shock tube measurements of growth constants in the branched chain formaldehyde-carbon monoxide-oxygen system
[NASA-TM-82954] p 71 N83-12182
BRACCO, F. V.
Computed and measured turbulence in axisymmetric reciprocating engines p 21 A83-24669
BRADDOCK, C. E.
Design of an advanced 500-HP helicopter transmission p 21 A83-24834
Design of an advanced 500-hp helicopter transmission p 144 N83-20125
BRADLEY, E.
Technology and benefits of aircraft counter rotation propellers
[NASA-TM-82983] p 27 N83-11129
BRADY, F. J.
A mathematical model for the doubly fed wound rotor generator
[NASA-TM-83454] p 117 N83-34192
BRAGG, M. B.
A similarity analysis of the droplet trajectory equation p 118 A83-13133
An analytical evaluation of the icing properties of several low and medium speed airfoils
[AIAA PAPER 83-0109] p 3 A83-16525
Wind tunnel evaluation of air-foil performance using simulated ice shapes
[NASA-CR-167960] p 11 N83-15265
BRAINARD, W. A.
The worldwide market for photovoltaics in the rural sector
[NASA-TM-83035] p 173 N83-15840
Analysis of the economics of photovoltaic-diesel-battery energy systems for remote applications
[NASA-TM-83377] p 179 N83-23709
Effect of oxygen concentration in ZDP containing oils on surface composition and wear
[NASA-TM-83000] p 84 N83-24636
BRAITHWAITE, W.
Uniform engine testing program. Phase 1: NASA Lewis Research Center participation
[NASA-TM-82978] p 29 N83-14126
BRANAGAN, L. A.
Aerodynamic stiffness of an unbound eccentric whirling centrifugal impeller with an infinite number of blades p 142 N83-15650
BRANDHORST, H. W., JR.
Radiation damage in front and back illuminated high resistivity silicon solar cells
[NASA-TM-82965] p 206 N83-10962
On the cause of the flat-spot phenomenon observed in silicon solar cells at low temperatures and low intensities p 170 N83-14705
Effects of processing and dopant on radiation damage removal in silicon solar cells p 170 N83-14708
BRATTON, R. J.
Advanced ceramic coating development for industrial/utility gas turbine applications
[NASA-CR-165619] p 92 N83-15467
BRAUN, J.
The dryout region in frictionally heated sliding contacts p 124 A83-42762
BRAUN, M. J.
An experimental investigation of the vaporous/gaseous cavity characteristics of an eccentric journal bearing
[ASLE PREPRINT 82-LC-3A-1] p 136 A83-13230
Experimental investigation of the vaporous/gaseous cavity characteristics of an eccentric journal bearing
[NASA-TM-82996] p 128 N83-17833
Thermomechanical loading of multilayered cylindrical geometries in thermal cycling from 300 to 1300 K
[NASA-TM-83312] p 129 N83-20029
Analogy between fluid cavitation and fracture mechanics
[NASA-TM-83071] p 129 N83-22542
BRESNAHAN, D. L.
Ejector nozzle test results at simulated flight conditions for an advanced supersonic transport propulsion system
[AIAA PAPER 83-1287] p 23 A83-36323
BREWE, D.
Geometry and starvation effects in hydrodynamic lubrication p 141 N83-15522
BREWER, G. D.
Assessment of crash fire hazard of LH sub 2 fueled aircraft
[NASA-CR-165525] p 16 N83-11095
BRIEHL, D.
Application of 3D aerodynamic/combustion model to combustor primary zone study
[AIAA PAPER 83-1265] p 23 A83-36316
A variable-geometry combustor used to study primary and secondary zone stoichiometry
[NASA-TM-83372] p 37 N83-27995
BRIGHAM, B. A.
Length to diameter ratio and row number effects in short pin fin heat transfer
[NASA-TM-83005] p 127 N83-14431
BRINKER, D. J.
Radiation damage and annealing in large area n+/p/p+ GaAs shallow homojunction solar cells p 172 N83-15826
BRITT, E. J.
Improved Stirling engine performance using jet impingement p 137 A83-27288
BRITTON, D. L.
Electrolyte management in porous battery components. Static measurements
[NASA-TM-83073] p 72 N83-18862
Pore size engineering applied to the design of separators for nickel-hydrogen cells and batteries
[NASA-TM-83386] p 73 N83-24571
BROCKETT, W. D.
Experimental evaluation of inlet turbulence, wall boundary layer, surface finish, and fillet radius on small axial turbine state performance
[SAE PAPER 821475] p 24 A83-38001
BRODER, J. D.
On the cause of the flat-spot phenomenon observed in silicon solar cells at low temperatures and low intensities p 170 N83-14705
BROKAW, R. S.
Shock tube measurements of growth constants in the branched chain formaldehyde-carbon monoxide-oxygen system
[NASA-TM-82954] p 71 N83-12182
BROMAN, C. L.
Energy efficient engine. Core engine bearings, drives and configuration: Detailed design report
[NASA-CR-165376] p 39 N83-30430
BRONSTEIN, L. M.
A multiple beam antenna concept for a 30/20 GHz satellite communications system p 103 A83-11485
BROOKS, A.
Status report DARPA/NASA convertible turbofan/turboshaft engine program
[ASME PAPER 83-GT-196] p 25 A83-48000
BROUKHIYAN, E. M. H.
Fumigation of alcohol in a light duty automotive diesel engine
[NASA-CR-167915] p 99 N83-13272
BROWN, G. V.
Magnetic heat pumping
[NASA-CASE-LEW-12508-3] p 131 N83-29625
BROWN, K. W.
Structural tailoring of engine blades (STAEBL)
[AIAA 83-0828] p 22 A83-29737
BROWN, W. H.
Refinement and application of acoustic impulse technique to study nozzle transmission characteristics
[NASA-CR-3656] p 199 N83-20708

BROWNING, L. H.
An analytical investigation of NO sub x control techniques for methanol fueled spark ignition engines [NASA-CR-172847] p 151 N83-33168
BROWNING, R.
Interfacial layers in high-temperature-oxidized NiCrAl p 77 A83-44619
BRUCKNER, A. P.
Direct contact droplet heat exchangers for thermal management in space p 120 A83-27137
BRUGGINK, P.
Fuel quality/processing study. Volume 3: Fuel upgrading studies [NASA-CR-165326-VOL-3] p 178 N83-22754
BRUSHAN, C.
Satellite provided customer premise services: A forecast of potential domestic demand through the year 2000. Volume 3: Appendices [NASA-CR-168144] p 109 N83-34118
BU-ABBUD, G. H.
Ellipsometric study of silicon nitride on gallium arsenide p 204 A83-11812
An enhanced sensitivity null ellipsometry technique for studying films on substrates - Application to silicon nitride on gallium arsenide p 206 A83-37618
BUCHELE, D. R.
Particle sizing by measurement of forward-scattered light at two angles [NASA-TP-2156] p 36 N83-24509
BUCKLEY, D. H.
Tribological properties and X-ray photoelectron spectroscopy studies of ion-plated gold on nickel and iron p 74 A83-12650
Correlation of tensile and shear strengths of metals with their friction properties [ASLE PREPRINT 82-LC-UB-1] p 74 A83-13226
Tribological properties of sintered polycrystalline and single-crystal silicon carbide p 89 A83-29397
Morphology of ductile metals eroded by a jet of spherical particles impinging at normal incidence p 75 A83-32624
XPS, AES and friction studies of single-crystal silicon carbide p 89 A83-36973
Plastic deformation and wear process at a surface during unlubricated sliding p 138 A83-37822
Friction and wear of iron and nickel in sodium hydroxide solutions p 77 A83-48922
Friction and wear of iron and nickel in sodium hydroxide solutions [NASA-TM-82935] p 77 N83-10171
Plastic deformation at surface during unlubricated sliding [NASA-TP-2036] p 139 N83-11496
Tribological properties of amorphous alloys and the role of surfaces in abrasive wear of materials [NASA-TM-82973] p 140 N83-11498
Tribology p 140 N83-12167
Investigation of wear phenomena by microscopy [NASA-TM-82934] p 81 N83-14245
Friction and wear of some ferrous-base metallic glasses [NASA-TM-83067] p 82 N83-19886
Surface chemistry, friction and wear of Ni-Zn and Mn-Zn ferrites in contact with metals [NASA-TM-83068] p 93 N83-19901
Sliding induced crystallization of metallic glass [NASA-TP-2140] p 83 N83-21110
The XPS depth profiling and tribological characterization of ion-plated gold on various metals [NASA-TM-83350] p 83 N83-23417
X-ray photoelectron spectroscopy and friction studies of nickel-zinc and manganese-zinc ferrites in contact with metals [NASA-TP-2163] p 84 N83-23419
Cavitation pitting and erosion of Al 6061-T6 in mineral oil and water [NASA-TM-83345] p 148 N83-23606
Time effect of erosion by solid particle impingement on ductile materials [NASA-TM-83369] p 84 N83-24637
Morphology of an aluminum alloy eroded by a jet of angular particles impinging at normal incidence [NASA-TP-2139] p 85 N83-24641
Solid spherical glass particle impingement studies of plastic materials [NASA-TP-2161] p 94 N83-24695
Cavitation erosion of copper, brass, aluminum and titanium alloys in mineral oil [NASA-TM-83402] p 148 N83-24856
Solid particle impingement erosion characteristics of cylindrical surfaces, pre-existing holes and slits [NASA-TM-83322] p 85 N83-25853
Spherical micro-glass particle impingement studies of thermoplastic materials at normal incidence [NASA-TM-83410] p 94 N83-25883
Time dependence of solid-particle impingement erosion of an aluminum alloy [NASA-TP-2169] p 86 N83-32908
Friction and hardness of gold films deposited by ion plating and evaporation [NASA-TP-2207] p 87 N83-34019
Application of modern surface analytical tools in the investigation of surface deterioration processes [NASA-TM-83452] p 152 N83-34327
Cavitation pitting and erosion of aluminum 6061-T6 in mineral oil water [NASA-TP-2146] p 152 N33-35400
BUGGELE, A. E.
Experimental evaluation of shockless supercritical airfoils in cascade [AIAA PAPER 83-0003] p 2 A83-16455
NASA low-speed centrifugal compressor for fundamental research [AIAA PAPER 83-1351] p 43 A83-36353
Experimental evaluation of shockless supercritical airfoils in cascade [NASA-TM-83045] p 11 N83-15268
NASA low-speed centrifugal compressor for fundamental research [NASA-TM-83398] p 13 N83-25662
BUNCH, W. D.
Analysis of the visible spectra of concentrated chromic chloride solutions [NASA-CR-172998] p 74 N83-32870
BUNDAS, D.
Some experiments on Yaw stability of wind turbines with various coning angles [NASA-CR-168108] p 177 N83-22740
BUNDAS, D. J.
Flutter and forced response of mistuned rotors using standing wave analysis [AIAA 83-0845] p 156 A83-29823
BURCH, J.
A 1 watt GaAs power amplifier for the NASA 30/20 GHz communication system p 111 A83-11489
BURCHAM, F. W., JR.
Flight evaluation of modifications to a digital electronic engine control system in an F-15 airplane [AIAA PAPER 83-0537] p 20 A83-19593
BURCHAM, R. E.
High speed cryogenic self-acting, shaft seals for liquid rocket turbopumps [NASA-CR-168194] p 151 N83-32070
BURIAN, L. C.
Fuel supply and distribution. Fixed base operation p 101 N83-22449
BURKARDT, L.
Uniform engine testing program. Phase 1: NASA Lewis Research Center participation [NASA-TM-82978] p 29 N83-14126
BURKARDT, L. A.
Effect of variable guide vanes on the performance of a high-bypass turbofan engine p 20 A83-24028
BURKE, J. J.
Surface-polaritonlike waves guided by thin, lossy metal films p 192 A83-37947
Long-range surface plasmons in electrode structures p 202 A83-40733
Effects of gaps on long range surface plasmon polaritons p 204 A83-46271
BURRIN, R. H.
Noise and flow structure of a tone-excited jet p 192 A83-13136
Tone-excited jet: Theory and experiments [NASA-CR-3538] p 197 N83-12968
BURSTADT, P. L.
Experimental results of a deflected thrust V/STOL nozzle research program [AIAA PAPER 83-0170] p 6 A83-42100
Experimental results of a deflected thrust V/STOL nozzle research program [NASA-TM-83069] p 12 N83-25657
BUSNAINA, A. A.
A basic code for the prediction of transient three-dimensional turbulent flowfields p 121 A83-27412
BUTTRILL, S. E., JR.
Oxidation and formation of deposit precursors in hydrocarbon fuels [NASA-CR-168121] p 101 N83-23465
BUZEK, B.
Frictional and morphological characteristics of ion plated soft, metallic films [NASA-TM-81723] p 83 N83-22390
BYRD, J. A.
Ceramic applications in turbine engines [NASA-CR-165494] p 212 N83-37028

C

CABRAAL, A.
Market assessment of photovoltaic power systems for agricultural applications worldwide [NASA-CR-165541] p 168 N83-13585
CAIRELLI, J. E.
Assessment of alternative power sources for mobile mining machinery [NASA-TM-82695] p 169 N83-14691
CALKIN, C. L.
High-voltage spark atomic emission detector for gas chromatography p 67 A83-13108
CALLANDER, S. M.
Comparison of modern icing cloud instruments [NASA-CR-168008] p 19 N83-18720
CAMPBELL, J.
Development of a microwave 20 x 20 switch matrix for 30/20 GHz SS-TDMA application p 110 A83-11484
CARL, D. E.
NOx results from two combustors tested on medium BTU coal gas p 186 A83-11493
CARLOTTO, M.
Electro-optical processor for optimal control p 133 A83-23596
CARPENTER, R. T.
Plasma characteristics of a 17 cm diameter line-cusp ion thruster [AIAA PAPER 82-1926] p 52 A83-12495
CARRUTH, M. R., JR.
SAFE II: Large systems space plasma evaluation experiment p 46 N83-26903
CARTER, R. A.
Investigations of stability and dynamic performances of switching regulators employing current-injected control p 110 A83-11002
CASASENT, D.
Frequency-multiplexed and pipelined iterative optical systolic array processors p 188 A83-18588
Electro-optical processor for optimal control p 133 A83-23596
Triangular system solutions on an optical systolic processor p 189 A83-36752
LU and Cholesky decomposition on an optical systolic array processor p 189 A83-43629
Optical systolic array processor using residue arithmetic p 189 A83-46834
CASSINELLI, J. E.
Solar array switching power management p 54 A83-27132
Study of solar array switching power management technology for space power system [NASA-CR-167890] p 179 N83-22756
CASTRUCCIO, P. A.
Non-urban mobile radio market demand forecast [NASA-CR-168065] p 107 N83-28297
CATALDO, R.
Test methods and results of the 10-cell bipolar Ni-H2 battery p 117 N83-35261
CATALDO, R. L.
Design of a 35-kilowatt bipolar nickel-hydrogen battery for low-earth-orbit applications p 54 A83-27205
Test results of a ten cell bipolar nickel-hydrogen battery [NASA-TM-83384] p 181 N83-26253
CATELLA, G. C.
Gain-enhanced free-electron laser with an electromagnetic pump field p 135 A83-31133
The application of free-electron lasers to the transmission of energy in space p 135 A83-31141
CERNANSKY, N. P.
Droplet size effects on NO/x/ formation in a one-dimensional monodisperse spray combustion system [ASME PAPER 82-JPGC-GT-10] p 68 A83-25268
CHAI, A. T.
Solar cell having improved back surface reflector [NASA-CASE-LEW-13620-1] p 168 N83-13579
Screen printed interdigitated back contact solar cell [NASA-CASE-LEW-13414-1] p 177 N83-20374
High voltage v-groove solar cell [NASA-CASE-LEW-13401-2] p 185 N83-32177
CHAKY, R. C.
Numerical simulation of a conducting disk partially covered by an insulator interacting with a plasma p 50 N83-18805
CHAMBERLIN, R.
Scale model performance test investigation of mixed flow exhaust systems for an energy efficient engine /E3/ propulsion system [AIAA PAPER 83-0541] p 20 A83-16776
CHAMIS, C. C.
Tensile buckling of advanced turboprops [AIAA PAPER 82-0776] p 154 A83-10900
Resin selection criteria for tough composite structures [AIAA 83-0801] p 89 A83-29734

Structural tailoring of engine blades (STAEBL)
[AIAA 83-0828] p 22 A83-29737
Design concepts for low cost composite engine frames
[AIAA PAPER 83-2445] p 25 A83-48331
Large displacements and stability analysis of nonlinear propeller structures p 159 N83-12460
Hygrothermomechanical evaluation of transverse filament tape epoxy/polyester fiberglass composites
[NASA-TM-83044] p 65 N83-15362
Simplified composite micromechanics equations for hygral, thermal and mechanical properties
[NASA-TM-83320] p 66 N83-19817
Design procedures for fiber composite structural components: Rods, columns and beam columns
[NASA-TM-83321] p 66 N83-24559

CHAN, A.
High accuracy fuel flowmeter, phase 1
[NASA-CR-167893] p 134 N83-21314

CHANG, G. C.
Performance degradation and cleaning of photovoltaic arrays p 164 A83-27236

CHANG, H.-P.
Influence of multidroplet size distribution on icing collection efficiency
[AIAA PAPER 83-0110] p 187 A83-16526

CHANG, L. K.
An analytical and experimental comparison of the flow field of an advanced swept turboprop
[NASA-TM-83037] p 1 N83-14061

CHANG, L.-K.
An analytical and experimental comparison of the flow field of an advanced swept turboprop
[AIAA PAPER 83-0189] p 3 A83-21080

CHANG, S. C.
A semi-direct solver for compressible 3-dimensional rotational flow
[NASA-TM-83314] p 15 N83-34908

CHANG, S.-C.
A semi-direct solver for compressible three-dimensional rotational flow
[AIAA PAPER 83-1909] p 122 A83-39367

CHAO, W. C.
Geometrically nonlinear analysis of layered composite shells p 156 A83-27431
Geometrically nonlinear analysis of layered composite plates and shells
[NASA-CR-168182] p 161 N83-33219

CHAPMAN, R.
Measurements of energy distribution and thrust for microwave plasma coupling of electrical energy to hydrogen for propulsion
[AIAA PAPER 82-1951] p 52 A83-12508
Microwave plasma generation of hydrogen atoms for rocket propulsion p 53 A83-13090

CHARLESTON, J. A.
Nickel-hydrogen component development
[NASA-TM-83487] p 186 N83-35498

CHARWAT, A. F.
The velocity perturbations above the orifice of an acoustically excited cavity in grazing flow
p 195 A83-29235

CHAUSSEE, D. S.
Prediction of high speed propeller flow fields using a three-dimensional Euler analysis
[AIAA PAPER 83-0188] p 4 A83-29535
User's manual for three-dimensional analysis of propeller flow fields
[NASA-CR-167959] p 12 N83-18671
Prediction of high speed propeller flow fields, using a three-dimensional Euler analysis
[NASA-TM-83065] p 12 N83-19710

CHEN, C. C.
Advanced 30/20 GHz multiple beam antenna for future communications satellites p 104 A83-41367

CHEN, C. J.
The finite analytic method, volume 3
[NASA-CR-170186] p 191 N83-23087
The finite analytic method, volume 4
[NASA-CR-170187] p 191 N83-23088
The finite analytic method, volume 5
[NASA-CR-170188] p 191 N83-23089

CHEN, C. S.
Aircraft measurements of trace gases and particles near the tropopause
[NASA-CR-3691] p 188 N83-27542

CHEN, C.-J.
Finite analytic numerical solution of axisymmetric Navier-Stokes and energy equations
[ASME PAPER 82-HT-42] p 118 A83-12795
Finite analytic numerical solution of heat transfer and flow past a square channel cavity p 123 A83-42703

CHEN, D.-P.
A new formulation of hybrid/mixed finite element
p 155 A83-12739
Alternative ways for formulation of hybrid stress elements p 155 A83-14710

CHEN, E. P.
Moving cracks in layered composites
p 155 A83-12048

CHEN, H. C.
The finite analytic method, volume 4
[NASA-CR-170187] p 191 N83-23088

CHEN, H. S.
A conceptual study of the potential for automotive-derived and free-piston Stirling engines in 30- to 400-kilowatt stationary power applications
[NASA-CR-165274] p 167 N83-10568

CHEN, L.-D.
Predictions of the structure of turbulent, particle-laden, round jets
[AIAA PAPER 83-0066] p 119 A83-16498
Evaluation of a stochastic model of particle dispersion in a turbulent round jet p 121 A83-28104

CHEN, R. T.
Liquid encapsulated Czochralski growth of low dislocation GaAs p 204 A83-13784
EL2 distributions in doped and undoped liquid encapsulated Czochralski GaAs p 205 A83-22756
Advances in large-diameter liquid encapsulated Czochralski GaAs p 171 N83-15819
High purity, low dislocation GaAs single crystals
[NASA-CR-168098] p 206 N83-19622
Growth and characterization of Czochralski-grown n and p-type GaAs for space solar cell substrates
[NASA-CR-168099] p 207 N83-27877

CHEN, S.-C.
Rapid distortion of small-scale turbulence by an axisymmetric contraction p 120 A83-22381

CHEN, Y. S.
Literature search of publications concerning the prediction of dynamic inlet flow distortion and related topics
[NASA-CR-3673] p 33 N83-18729

CHENG, W. S.
The finite analytic method, volume 5
[NASA-CR-170188] p 191 N83-23089

CHIANG, K. T.
Low temperature hot corrosion p 76 A83-42252

CHIANG, N.
20 x 20 IF switch matrix for SS-TDMA systems
p 113 A83-41369

CHIAPPETTA, L. M.
Analytical modeling of operating characteristics of premixing-prevaporizing fuel-air mixing passages. Volume 1: Analysis and results
[NASA-CR-167990-VOL-1] p 126 N83-12353
Analytical modeling of operating characteristics of premixing-prevaporizing fuel-air mixing passages. Volume 2: User's manual
[NASA-CR-167990-VOL-2] p 126 N83-12354

CHIEN, C. H.
Extending the laser-specklegram technique to strain analysis of rotating components p 155 A83-12514

CHIEN, L. C.
Manual for extending the laser specklegram technique to strain analysis of rotating components
[NASA-CR-167932] p 134 N83-15601

CHILDS, D. W.
Finite-length solutions for rotodynamic coefficients of turbulent annular seals
[ASME PAPER 82-LUB-42] p 136 A83-13521

CHIMA, R. V.
Efficient solution of the Euler and Navier-Stokes equations with a vectorized multiple-grid algorithm
[AIAA PAPER 83-1893] p 5 A83-39359
Efficient solution of the Euler and Navier-Stokes equations with a vectorized multiple-grid algorithm
[NASA-TM-83376] p 2 N83-24467
Comparison of two- and three-dimensional flow computations with laser anemometer measurements in a transonic compressor rotor
[NASA-TP-1931] p 15 N83-32774

CHIN, B.
High accuracy fuel flowmeter, phase 1
[NASA-CR-167893] p 134 N83-21314

CHITWOOD, J. S.
A study of 60 Gigahertz intersatellite link applications
[NASA-TM-83337] p 47 N83-20994

CHO, Y. C.
Mode propagation in nonuniform circular ducts with potential flow p 122 A83-36082
Sound diffraction at wall impedance discontinuities in a circular cylinder, investigated using Wiener-Hopf technique
[NASA-TM-83365] p 201 N83-23117

CHO, Y.-C.
Sound diffraction at wall impedance discontinuities in a circular cylinder - investigated using Wiener-Hopf technique
[AIAA PAPER 83-0730] p 195 A83-33485

CHOO, Y. K.
Analysis of potential benefits of integrated-gasifier combined cycles for a utility system
[NASA-TP-2172] p 186 N83-36549

CHUDNOVSKY, A.
Crack layer morphology and toughness characterization in steels
[NASA-CR-168154] p 160 N83-27256

CHUNG, B. T.
Thermomechanical loading of multilayered cylindrical geometries in thermal cycling from 300 to 1300 K
[NASA-TM-83312] p 129 N83-20029

CHUNG, Y.
Ellipsometric study of silicon nitride on gallium arsenide p 204 A83-11812
Interfacial electrical properties of ion-beam sputter deposited amorphous carbon on silicon
p 205 A83-33920

CICON, D. E.
Investigation of continuously traversing microphone system for mode measurement
[NASA-CR-168040] p 199 N83-19575

CIMA, R.
Assessment of crash fire hazard of LH sub 2 fueled aircraft
[NASA-CR-165525] p 16 N83-11095

CIONI, J. L.
Large area low-cost space solar cell development
p 170 N83-14699

CIVINSKAS, K. C.
Effects of interstage diffuser flow distortion on the performance of a 15.41-centimeter tip diameter axial power turbine
[AIAA PAPER 83-1179] p 23 A83-36263
Effects of interstage diffuser flow distortion on the performance of a 15.41-centimeter tip diameter axial power turbine
[NASA-TM-83359] p 35 N83-24505

CLAING, R. G.
Joining lead wires to thin platinum alloy films
[NASA-CASE-LEW-13934-1] p 135 N83-35338

CLAUS, R. W.
Analytical calculation of a single jet in cross-flow and comparison with experiment p 38 N83-29219
Flame radiation measurements p 73 N83-29228
Parametric study of flame radiation characteristics of a tubular-can combustor
[NASA-TM-83436] p 39 N83-29237

CLAUSS, R. W.
Analytical calculation of a single jet in crossflow and comparison with experiment
[NASA-TM-83027] p 29 N83-14127

COBAN, E.
20 x 20 IF switch matrix for SS-TDMA systems
p 113 A83-41369
Spacecraft IF switch matrix for wideband service applications in 30/20 GHz communications satellite systems: Proof-of-concept model, executive summary
[NASA-CR-168175] p 107 N83-29492

COCHRAN, T.
Electric propulsion research and technology in the United States
[AIAA PAPER 82-1867] p 53 A83-16925

COE, H. H.
Predicted and experimental performance of large-bore high-speed ball and roller bearings p 145 N83-20131

COFFINBERRY, G. A.
Apparatus for improving the fuel efficiency of a gas turbine engine
[NASA-CASE-LEW-13142-1] p 43 N83-35029

COHEN, J. D.
Analytical fuel property effects, small combustors, phase 1
[NASA-CR-168138] p 101 N83-23464

COHEN, P. H.
The orthogonal in-situ machining of single and polycrystalline aluminum and copper, volume 2
[NASA-CR-169528] p 81 N83-13233

COHEN, S. M.
Research on aviation fuel instability
[NASA-TM-83420] p 101 N83-28255

COLKET, M. B.
Experimental study of the thermal stability of hydrocarbon fuels
[NASA-CR-168027] p 100 N83-17728

COLLETT, C.
Qualification test results of IAPS 8 cm ion thrusters
[AIAA PAPER 82-1954] p 52 A83-12511

COLLINS, J. L.
Experience and assessment of the DOE/NASA Mod-1 2000 kW wind turbine generator at Boone, North Carolina p 176 N83-19257

COLLOM, R. R.
Thrust performance of a variable-geometry, divergent exhaust nozzle on a turbojet engine at altitude
[NASA-TP-2171] p 36 N83-26839

COLTRIN, R. E.
A survey of inlet/engine distortion compatibility
[AIAA PAPER 83-1166] p 6 A83-45509
A survey of inlet/engine distortion compatibility
[NASA-TM-83421] p 37 N83-27991
CONNOLLY, D. J.
A study of 60 Gigahertz intersatellite link applications
[NASA-TM-83337] p 47 N83-20994
COOK, R. T.
SSME main combustion chamber life prediction
[NASA-CR-168215] p 60 N83-36101
COOK, T. S.
Requirements of constitutive models for two nickel-base superalloys p 74 A83-21071
COOKE, D. L.
Potentials on large spacecraft in LEO
p 49 A83-17489
COOPER, A. R.
O-18 tracer studies of Al2O3 scale formation on NiCrAl alloys p 74 A83-10249
COOPER, C. B., III
Use of column V alkyls in organometallic vapor phase epitaxy (OMVPE) p 70 A83-46608
COOPER, J.
Non-urban mobile radio market demand forecast
[NASA-CR-168065] p 107 N83-28297
COOPER, L. P.
Advanced propulsion concepts for orbital transfer vehicles
[AIAA PAPER 83-1243] p 56 A83-45513
Advanced propulsion concepts for orbital transfer vehicles
[NASA-TM-83419] p 59 N83-26924
CORNELL, R. W.
Compliance and stress sensitivity of spur gear teeth
p 146 N83-20142
Dynamic tooth loads and stressing for high contact ratio spur gears p 147 N83-20148
CORREA, S. M.
Prediction of an axisymmetric combusting flow
[AIAA PAPER 83-1264] p 69 A83-36315
CORRIGAN, R. D.
The effect of yaw on horizontal axis wind turbine loading and performance
[NASA-TM-82778] p 169 N83-14688
Measured performance of a tip-controlled, teetered rotor with an NACA 64 sub 3-618 tip airfoil
[NASA-TM-82870] p 169 N83-14689
Fixed pitch rotor performance of large horizontal axis wind turbines p 175 N83-19233
Stall induced instability of a teetered rotor
p 175 N83-19234
Free yaw performance of the Mod-0 large horizontal axis 100 kW wind turbine p 175 N83-19235
Results of free yaw tests of the Mod-O 100 kilowatt wind turbine
[NASA-TM-83432] p 184 N83-29813
CORSMEIER, R. J.
Air modulation apparatus
[NASA-CASE-LEW-13524-1] p 131 N83-30957
CORY, B. J.
Development of a microwave 20 x 20 switch matrix for 30/20 GHz SS-TDMA application p 110 A83-11484
A high capacity satellite switched TDMA microwave switch matrix p 104 A83-19776
Spacecraft in switch matrix for wide band service applicatons in 30/20 GHz communications satellite systems
[NASA-CR-168089] p 46 N83-34998
COTTS, D. B.
Oxidation and formation of deposit precursors in hydrocarbon fuels
[NASA-CR-168121] p 101 N83-23465
COY, J. J.
Life and reliability models for helicopter transmissions
[NASA-TM-82975] p 139 N83-10425
Lubricant effects on efficiency of a helicopter transmission p 141 N83-15523
Sizing criterial for traction drives p 146 N83-20137
A basis for the analysis of surface geometry of spiral bevel gears p 146 N83-20138
Spiral-bevel geometry and gear train precision
p 146 N83-20139
An update on the life analysis of spur gears
p 146 N83-20144
The optimal design of standard gearsets
p 146 N83-20145
NASA transmission research and its probable effects on helicopter transmission design
[NASA-TM-83389] p 148 N83-24858
CRAWFORD, D.
The development of a generalized advanced propeller analysis system
[AIAA PAPER 83-2466] p 26 A83-49581
CRAWFORD, J. J.
A low-power, high-throughput maximum-likelihood convolutional decoder chip for NASA's 30/20 GHz program p 111 A83-19754
CROMWELL, N.
Mobile radio alternative systems study, executive summary
[NASA-CR-168207] p 109 N83-34119
CRONENWORTH, J.
An uncoupled viscoplastic constitutive model for metals at elevated temperature
[AIAA 83-1016] p 156 A83-29798
CROSSWELL, W. F.
Scanning beam antenna conceptual design for 20/30 GHz satellite systems p 46 N83-26889
Phased array-fed antenna configuration study
[NASA-CR-168077] p 107 N83-27086
CROSWELL, W. F.
Phased array-fed antenna configuration study: Technology assessment
[NASA-CR-168078] p 106 N83-22495
CROUCH, S. R.
High-voltage spark atomic emission detector for gas chromatography p 67 A83-13108
CUBBISON, R. W.
Low speed performance of a supersonic axisymmetric mixed compression inlet with auxiliary inlets
[AIAA PAPER 83-1414] p 7 A83-45516
Low speed performance of a supersonic axisymmetric mixed compression inlet with auxiliary inlets
[NASA-TM-83435] p 37 N83-27992
CUELLAR, J. P., JR.
Evaluation of fuel additives for reduction of material imcompatibilities in methanol-gasoline blends
[NASA-CR-168061] p 86 N83-29359
CULL, R. C.
Performance degradation and cleaning of photovoltaic arrays p 164 A83-27236
High speed computerized data acquisition of photovoltaic V-I characteristics
[NASA-TM-82967] p 114 N83-14397
CUNNINGHAM, D.
Stirling engine application study
[NASA-CR-168087] p 210 N83-22029
CUNNINGHAM, R.
Power turbine dynamics - An evaluation of a shear-mounted elastomeric damper
[ASME PAPER 83-GT-228] p 139 A83-48025
CUNNINGHAM, R. E.
Variable force, eddy-current or magnetic damper
[NASA-CASE-LEW-13717-1] p 159 N83-20284
CURREN, A. N.
Ion sputter textured graphite
[NASA-CASE-LEW-12919-1] p 63 N83-10117
CURTIS, H. B.
Determination of optimum sunlight concentration level in space for 3-5 cascade solar cells p 170 N83-14732
Determination of optimum sunlight concentration level in space for 3-5 cascade solar cells p 171 N83-15814
The effect of different solar simulators on the measurement of short-circuit current temperature coefficients p 172 N83-15821
Solar cell measurements p 181 N83-25109
CUSANO, C.
The influence of surface dents and grooves on traction in sliding EHD point contacts p 138 A83-37823
Elastohydrodynamic contacts. Effects of dents and grooves on traction and local film thickness
[NASA-TP-2175] p 150 N83-28453
CUTRONE, M.
Fuel quality-processing study. Volume 2: Literature survey
[NASA-CR-165326-VOL-2] p 178 N83-22751
Fuel quality/processing study. Volume 4: On site processing studies
[NASA-CR-165326-VOL-4] p 179 N83-22755
CWYNAR, D. S.
Design of a high-speed digital processing element for parallel simulation
[NASA-TM-83373] p 117 N83-29597
CYBYK, B. Z.
Rail accelerator research at Lewis Research Center
[AIAA PAPER 82-1938] p 53 A83-22075
Rail accelerator research at Lewis Research Center
[NASA-TM-83015] p 56 N83-12143

D

DAILEY, C. L.
Optimal sun-alignment techniques of large solar arrays in electric propulsion spacecraft
[AIAA PAPER 82-1898] p 48 A83-12475
DALLING, D. K.
A carbon-13 and proton nuclear magnetic resonance study of some experimental referee broadened-specification /ERBS/ turbine fuels
p 98 A83-11482
DANIEL, I. M.
High strain rate properties of undirectional composites, part 1
[NASA-CR-167969] p 64 N83-13178
High strain rate properties of off-axis composite laminates, part 2
[NASA-CR-167970] p 64 N83-13179
High strain properties of angle-ply composite laminate, part 3
[NASA-CR-167971] p 64 N83-13180
DANIEL, S. R.
Studies of the mechanisms of turbine fuel instability
[NASA-CR-167963] p 100 N83-18924
DANIELE, C. J.
A 4-cylinder Stirling engine computer program with dynamic energy equations
[NASA-TM-83053] p 130 N83-26017
DANIELS, C. J.
Computer program for a four-cylinder-Stirling-engine controls simulation
[NASA-TM-82774] p 126 N83-12359
DANIELS, S. W.
Plasma characteristics of a 17 cm diameter line-cusp ion thruster
[AIAA PAPER 82-1926] p 52 A83-12495
DAVID, J. W.
Theoretical investigation of the force and dynamically coupled torsional-axial-lateral dynamic response of eared rotors
[NASA-CR-173013] p 191 N83-34656
DAVIS, R. E.
Cloud encounter statistics in the 28.5-43.5 KFT altitude region from four years of GASP observations
p 188 A83-38733
DAVIS, R. T.
Solution of viscous internal flows on curvilinear grids generated by the Schwarz-Christoffel transformation
p 122 A83-38796
DAWICKE, D. S.
A total life prediction model for stress concentration sites
[NASA-CR-170290] p 160 N83-23629
DAYTON, J. A., JR.
Design of a multistage depressed collector for the F-16 radar dual mode transmitter tube
[NASA-TM-82982] p 114 N83-14399
Experimental verification of the multistage depressed collector design procedure for a high-perveance, helix-type, traveling-wave tube
[NASA-TP-2162] p 116 N83-25985
DEADMORE, D. L.
Burner rig study of variables involved in hole plugging of air cooled turbine engine vanes
[NASA-TM-83308] p 83 N83-19887
Silicon-slurry/aluminide coating
[NASA-CASE-LEW-13343] p 86 N83-31795
DEBOER, G. J.
The Rene 150 directionally solidified superalloy turbine blades, volume 1
[NASA-CR-167992] p 33 N83-20946
DEESPOSTI, R. S.
On-orbit propulsion requirements and performance assessment of ion propulsion subsystems for future GEO large satellite missions
[AIAA PAPER 82-1872] p 48 A83-12460
DEISSLER, R. G.
Turbulent solution of the Navier-Stokes equations for an inhomogenous developing shear layer
[NASA-TM-82969] p 126 N83-12357
DELAAT, J. C.
Design of a microprocessor-based Control, Interface and Monitoring (CIM unit for turbine engine controls research
[NASA-TM-83433] p 2 N83-34885
DELASANTA, D.
Market assessment of photovoltaic power systems for agricultural applications worldwide
[NASA-CR-165541] p 168 N83-13585
DELOMBARD, R.
High speed computerized data acquisition of photovoltaic V-1 characteristics
[NASA-TM-82967] p 114 N83-14397
DELUCIA, R. A.
Rotor fragment protection program: Statistics on aircraft gas turbine engine rotor failures that occurred in US commercial aviation during 1979
[NASA-CR-168163] p 38 N83-29234
DELVIGS, P.
PMR polyimides - Review and update
p 62 A83-20447
Lower-curing-temperature PMR polyimides
p 89 A83-40923

Lower-curing-temperature PMR polyimides
[NASA-TM-82958] p 63 N83-10118
Low temperature cross linking polyimides
[NASA-CASE-LEW-12876-2] p 96 N83-29392
DERIKART, T. A.
Automotive Stirling engine development program
[NASA-CR-165263] p 211 N83-26762
DETWILER, A.
Aircraft measurements of trace gases and particles near the tropopause
[NASA-CR-3691] p 188 N83-27542
DEVRIES, W. R.
Classification of journal surfaces using surface topography parameters and software methods to compensate for stylus geometry
[NASA-CR-168153] p 148 N83-24857
DEZELICK, R. A.
Characterization of a high-pressure diesel fuel injection system as a control technology option to improve engine performance and reduce exhaust emissions
[NASA-TM-83329] p 210 N83-24431
DI RUSSO, EL
Design analysis of a self-acting spiral-groove ring seal for counter-rotating shafts
[AIAA PAPER 83-1134] p 137 A83-36239
DIDELOT, R. C.
Array structure design handbook for stand alone photovoltaic applications
[NASA-TM-82629] p 160 N83-23631
DIEDRICH, J. H.
Turbofan blade stresses induced by the flow distortion of a VTOL inlet at high angles of attack
[NASA-TM-82963] p 12 N83-17509
DINEEN, J.
A conceptual study of the potential for automotive-derived and free-piston Stirling engines in 30- to 400-kilowatt stationary power applications
[NASA-CR-165274] p 167 N83-10568
DIRUSSO, E.
Film thickness measurement for spiral groove and Rayleigh step lift pad self-acting face seals
[NASA-TP-2058] p 26 N83-11126
Design analysis of a self-acting spiral-groove ring seal for counter-rotating shafts
[NASA-TM-83346] p 35 N83-23306
Design analysis of a self-acting spiral-groove ring seal for counter-rotating shafts
[NASA-TP-2142] p 36 N83-25712
DITTMAR, J. H.
Noise of the 10-bladed, 40 deg swept SR-6 propeller in a wind tunnel
[NASA-TM-82950] p 196 N83-11840
Noise of the 10-bladed 60 deg swept SR-5 propeller in a wind tunnel
[NASA-TM-83054] p 200 N83-23112
A preliminary comparison between the SR-6 propeller noise in flight and in a wind tunnel
[NASA-TM-83341] p 201 N83-24287
DIVERGILIO, W. F.
High frequency plasma generators for ion thrusters
[NASA-CR-167957] p 59 N83-28072
DODDS, W. J.
NASA clean catalytic combustor program
[ASME PAPER 82-JPGC-GT-11] p 68 A83-25269
DODGE, F. T.
Vapor flow into a capillary propellant-acquisition device
[AIAA PAPER 83-1380] p 55 A83-36371
DOERING, H.
Fuel quality/processing study. Volume 4: On site processing studies
[NASA-CR-165326-VOL-4] p 179 N83-22755
DOMAS, P. A.
Benchmark notch test for life prediction
[NASA-CR-165571] p 158 N83-12451
DONOVAN, L. F.
A class of nonideal solutions. 2: Application to experimental data
[NASA-TP-1930] p 208 N83-23188
DORSINVILLE, R.
Effect of hydrogen bonding on the vibrational dephasing time in glycerol p 61 A83-21054
DOSANJH, D. S.
Coaxial supersonic jet-flows, shock structure and related problems with noise-suppression assessment and prediction
[AIAA PAPER 83-0707] p 194 A83-28011
DOWELL, E. H.
Design of dry-friction dampers for turbine blades p 22 A83-35893
DOWSON, D.
Elastohydrodynamic lubrication theory
[NASA-TM-81695] p 140 N83-12432
Theoretical results for fully flooded, elliptical hydrodynamic contacts
[NASA-TM-81696] p 140 N83-13458
Lubrication background
[NASA-TM-81692] p 147 N83-20159
Film thickness for different regimes of fluid-film lubrication
[NASA-TM-81700] p 149 N83-28449
Theoretical results for starved elliptical contacts
[NASA-TM-81697] p 150 N83-29710
Experimental investigations of elastohydrodynamic lubrication
[NASA-TM-81698] p 150 N83-29711
Elastohydrodynamics of elliptical contacts for materials of low elastic modulus
[NASA-TM-81699] p 151 N83-29712
Applications of film thickness equations
[NASA-TM-81701] p 151 N83-29713
DRESHFIELD, R. L.
Effects on stress rupture life and tensile strength of tin additions to Inconel 718 p 79 N83-11299
Progress toward determining the potential of ODS alloys for gas turbine applications
[NASA-TM-83332] p 83 N83-22387
Understanding the roles of the strategic element cobalt in nickel base superalloys
[NASA-TM-83475] p 87 N83-35102
DRING, R. P.
Axial compressor middle stage secondary flow study
[NASA-CR-3701] p 14 N83-29174
DUBIEL, D. J.
Energy efficient engine sector combustor rig test program
[NASA-CR-167913] p 33 N83-19753
DUDZINSKI, T. J.
Water vapor measurement system in global atmospheric sampling program, appendix
[NASA-TP-2051] p 187 N83-13643
DUERR, R. A.
Effect of flameholder pressure drop on emissions and performance of premixed-prevaporized combustors
[NASA-TP-2131] p 35 N83-23309
DUGUNDJI, J.
Flutter and forced response of mistuned rotors using standing wave analysis
[AIAA 83-0845] p 156 A83-29823
Some analysis methods for rotating systems with periodic coefficients p 157 A83-32987
Some experiments on Yaw stability of wind turbines with various coning angles
[NASA-CR-168108] p 177 N83-22740
Development of methodology for horizontal axis wind turbine dynamic analysis
[NASA-CR-168110] p 178 N83-22747
DUKE, J. C., JR.
A study of the stress wave factor technique for the characterization of composite materials
[NASA-CR-3670] p 153 N83-27248
DULGEROFF, C. R.
Status of the J-series 30-cm mercury ion thruster
[AIAA PAPER 82-1904] p 51 A83-12479
Extended-performance 8-cm ion thruster operation
[AIAA PAPER 82-1955] p 53 A83-12512
DUMITRU, E. T.
Preparation, characterization, physical testing and performance of flurocarbon membranes and separators
[NASA-CR-169756] p 71 N83-16418
Preparation, characterization, physical testing and performance of fluorocarbon membranes and separators
[NASA-CR-167880] p 73 N83-26936
DURBIN, P. A.
Stochastic differential equations and turbulent dispersion
[NASA-RP-1103] p 129 N83-22546
DURGAPRASAD, M. B.
Soot formation in pyrolysis of acetylene, allene and 1,3-butadiene p 69 A83-39274
DUSTIN, M. O.
Comparison of road load simulator test results with track tests on electric vehicle propulsion system
[NASA-TM-83393] p 184 N83-29811
Steady-state and dynamic evaluation of the electric propulsion system test bed vehicle on a road load simulator
[NASA-TM-83445] p 186 N83-35496
DUTTA, S.
Effect of Y2O3 and Al2O3 on the oxidation resistance of Si3N4 p 88 A83-22258
DYBA, G.
High speed spherical roller-bearing analysis and comparison with experimental performance p 145 N83-20133
DYSON, A.
Assessment of lubricated contacts: Mechanisms of scuffing and scoring
[NASA-TM-83074] p 144 N83-20118

E

EARLE, R. V.
Rotorcraft convertible engine study
[NASA-CR-168161] p 37 N83-27996
EARLEY, J. W.
Stability analysis of Centaur-in-Shuttle composite corrugated adapters
[AIAA 83-1003] p 49 A83-29791
EBERHARDT, R. N.
Long term storage of cryogens in space p 102 A83-11487
EBERT, L. J.
Gamma prime shape changes during creep of a nickel-base superalloy p 77 A83-47855
Influence of cobalt, tantalum, and tungsten on the microstructure and mechanical properties of superalloy single crystals p 79 N83-11293
ECER, A.
A finite element formulation for steady transonic Euler equations p 3 A83-22129
ECHOLDS, E. F.
A lightweight electronically commutated dc motor for electric passenger vehicles
[NASA-CR-165601] p 113 N83-10348
ECKERLE, W. A.
Turbine endwall single cylinder program
[NASA-CR-170008] p 44 N83-19761
EDWARDS, D. E.
Solution of viscous internal flows on curvilinear grids generated by the Schwarz-Christoffel transformation p 122 A83-38796
Analytical modeling of operating characteristics of premixing-prevaporizing fuel-air mixing passages. Volume 1: Analysis and results
[NASA-CR-167990-VOL-1] p 126 N83-12353
Analytical modeling of operating characteristics of premixing-prevaporizing fuel-air mixing passages. Volume 2: User's manual
[NASA-CR-167990-VOL-2] p 126 N83-12354
User's manual for Axisymmetric Diffuser Duct (ADD) code. Volume 1: General ADD code description
[NASA-CR-165598-VOL-1] p 211 N83-26757
User's manual for Axisymmetric Diffuser Duct (ADD) code. Volume 2: Detailed ADD code description
[NASA-CR-165598-VOL-2] p 211 N83-26758
User's manual for Axisymmetric Diffuser Duct (ADD) code. Volume 3: ADD code coordinate generator
[NASA-CR-165598-VOL-3] p 211 N83-26759
EDWARDS, J. G.
Thermodynamics of the potassium-sulfur-oxygen and related systems
[NASA-CR-168155] p 61 N83-28077
EDWARDS, R. V.
Particle-sampling statistics in laser anemometers Sample-and-hold systems and saturable systems p 134 A83-48120
EGGERS, A. G.
The MOD-0A 200 kilowatt wind turbine generator design and analysis report
[NASA-CR-165127] p 174 N83-16859
EGGERT, W. S.
Design and evaluation of low-cost stainless steel fiberglass foam blades for large wind driven generating systems
[NASA-CR-165491] p 174 N83-19226
Design and evaluation of low cost blades for large wind driven generating systems p 175 N83-19244
EHLERS, R. C.
A variable-geometry combustor used to study primary and secondary zone stoichiometry
[NASA-TM-83372] p 37 N83-27995
EHRESMAN, C. M.
Effect of humidity on jet engine axial-flow compressor performance p 22 A83-35856
EICHHORN, R.
Boundary integral equation method calculations of surface regression effects in flame spreading p 67 A83-13488
Correlating downward flame spread rates for thick fuel beds p 69 A83-37045
EISEMAN, P. R.
Coordinate generation with precise controls over mesh properties p 190 A83-29631
High level continuity for coordinate generation with precise controls p 190 A83-29632
Automatic algebraic coordinate generation p 189 A83-38793
EISENBERG, J. D.
Rotorcraft convertible engines for the 1980s
[NASA-TM-83008] p 28 N83-12091
EKAMBARAM, C.
A new architecture for adaptive transform compression of NTSC composite video signal p 103 A83-19732

EKSTEDT, E. E.
NASA clean catalytic combustor program
[ASME PAPER 82-JPGC-GT-11] p 68 A83-25269
ELCHURI, V.
Flutter analysis of advanced turbopropellers
[AIAA 83-0846] p 157 A83-29824
ELGHOBASHI, S. E.
A two-equation turbulence model for two-phase flows
p 121 A83-30109
ELLIOTT, J. E.
Moderate temperature rechargeable sodium batteries
[NASA-CR-168220] p 118 N83-36359
ELLIOTT, J. P.
Development of a multiple-parameter nonlinear perturbation procedure for transonic turbomachinery flows: Preliminary application to design/optimization problems
[NASA-CR-3657] p 2 N83-17453
ELLIOTT, K. R.
Residual double acceptors in bulk GaAs
p 205 A83-19989
ELLIS, D. R.
Multi-fuel rotary engine for general aviation aircraft
[NASA-TM-83429] p 38 N83-29235
Multi-fuel rotary engine for general aviation aircraft
[NASA-TM-85428] p 43 N83-36031
ENGLISH, R. E.
Power generation from nuclear reactors in aerospace applications
[NASA-TM-83342] p 59 N83-30516
ENGLUND, D. R.
Water vapor measurement system in global atmospheric sampling program, appendix
[NASA-TP-2051] p 187 N83-13643
ENOCH, J.
Numerical simulation of a disk-shaped electron accelerating electrostatic probe p 133 A83-22336
Numerical simulation of a conducting disk partially covered by an insulator interacting with a plasma
p 50 N83-18805
ENVIA, E.
Noise generation by a finite span swept airfoil
[AIAA PAPER 83-0768] p 195 A83-28023
ERNST, W.
Automotive Stirling engine development program
[NASA-CR-167907] p 209 N83-15176
Automotive Stirling engine development program
[NASA-CR-168060] p 209 N83-15177
Automotive Stirling Engine Development Program
[NASA-CR-168074] p 212 N83-27925
ERWIN, J.
Tests of blending and correlation of distillate fuel properties p 98 A83-11050
ETSION, I.
Energy efficient face seal
[NASA-CR-165591] p 142 N83-15659
EVANS, D. G.
Assessment of alternative power sources for mobile mining machinery
[NASA-TM-82695] p 169 N83-14691
EVANS, J. C., JR.
Planar multijunction high voltage solar cell chip
p 163 A83-13923
Heat transparent high intensity high efficiency solar cell
[NASA-CASE-LEW-12892-1] p 170 N83-14692
High voltage v-groove solar cell
[NASA-CASE-LEW-13401-2] p 185 N83-32177
EVERSMAN, W.
Acoustics in variable area duct - Finite element and finite difference comparisons to experiment
p 193 A83-19809
Finite difference solutions to shocked acoustic waves
[AIAA PAPER 83-0671] p 193 A83-25907
EWASHINKA, J. G.
Results of chopper-controlled discharge life cycling studies on lead-acid batteries p 164 A83-27183

F

FADDOUL, J. R.
Structural fatigue test results for large wind turbine blade sections p 159 N83-19246
FAETH, F. M.
The structure of evaporating and comousting sprays: Measurements and predictions
[NASA-CR-170312] p 130 N83-24795
FAETH, G. M.
Predictions of the structure of turbulent, particle-laden, round jets
[AIAA PAPER 83-0066] p 119 A83-16498
Measurements and predictions for nonevaporating sprays in a quiescent environment
[AIAA PAPER 83-0151] p 119 A83-16558
Evaluation of a stochastic model of particle dispersion in a turbulent round jet p 121 A83-28104
The structure of particle-laden jets and nonevaporating sprays
[NASA-CR-168059] p 34 N83-20948
The structure of evaporating and combusting sprays: Measurements and predictions
[NASA-CR-170176] p 129 N83-22550
Structure of evaporating and combusting sprays: Measurements and predictions p 38 N83-29211
FAIRBANKS, N. P.
Materials for advanced turbine engines. Volume 1: Advanced blade tip seal system
[NASA-CR-167851-VOL-1] p 31 N83-15308
FALCONER, P.
Aircraft measurements of trace gases and particles near the tropopause
[NASA-CR-3691] p 188 N83-27542
FAN, J. C. C.
Radiation damage and annealing in large area n+/p/p+ GaAs shallow homojunction solar cells
p 172 N83-15826
FANG, J.
LOX/hydrocarbon fuel carbon formation and mixing data analysis
[NASA-CR-168066] p 101 N83-31886
FARRELL, C. A., JR.
Inlet-fan flow field computation
[ASME PAPER 83-GT-41] p 7 A83-47901
FASCHING, W. A.
CF6 jet engine diagnostics program. High pressure turbine roundness/clearance investigation
[NASA-CR-165581] p 29 N83-13100
The CF6 engine performance improvement
[NASA-CR-165612] p 31 N83-16342
Summary report for CF6 jet engine diagnostics program
[NASA-CR-165582] p 32 N83-17539
FAUT, O. D.
On the mechanism of lubrication by tricresylphosphate /TCP/ - The coefficient of friction as a function of temperature for TCP on M-50 steel
[ASLE PREPRINT 82-LC-4C-1] p 135 A83-13228
Mechanism of lubrication by tricresylphosphate (TCP)
[NASA-TP-2053] p 72 N83-18863
The adsorption and thermal decomposition of tricresylphosphate (TCP) on iron and gold
[NASA-TM-83441] p 62 N83-29311
FEAR, J. S.
The NASA broad-specification fuels combustion technology program: An assessment of phase 1 test results
[NASA-TM-83447] p 39 N83-29236
FEILER, C. E.
Recent results about fan noise: Its generation, radiation and suppression
[NASA-TM-83002] p 197 N83-13939
FEIMAN, V.
Development of a high capacity toroidal Ni/Cd cell
[NASA-CR-169945] p 176 N83-19273
FERET, J. M.
Cell module and fuel conditioner development
[NASA-CR-165462-A] p 168 N83-12524
FERNANDEZ DE LA MORA, J.
Small particle transport across turbulent nonisothermal boundary layers p 118 A83-10650
Correlation and prediction of thermophoretic and inertial effects on particle deposition from non-isothermal turbulent boundary layers p 121 A83-27481
FERNANDEZ, M. A. B.
Effects of percentage of blockage and flameholder downstream counterbores on lean combustion limits of premixed, prevaporized propane-air mixture
[NASA-TP-2227] p 41 N83-34941
FERNANDEZ, P. A.
Stability analysis of Centaur-in-Shuttle composite corrugated adapters
[AIAA 83-1003] p 49 A83-29791
FERRANTE, J.
Diatomic molecules and metallic adhesion, cohesion, and chemisorption - A single binding-energy relation
p 69 A83-30921
Tribological characteristics of nitrogen (N+) implanted iron p 75 A83-37824
Effect of oxygen concentration in ZDP containing oils on surface composition and wear
[NASA-TM-83000] p 84 N83-24636
FERTIS, D. G.
NASA LeRC/Akron University Graduate Cooperative Fellowship Program and Graduate Student Researchers Program
[NASA-CR-167943] p 208 N83-10970
FESTER, D. A.
Long term storage of cryogens in space
p 102 A83-11487
Cryogenic fluid management experiment trunnion fatigue verification
[AIAA PAPER 83-0911] p 49 A83-32782
FIELDER, W. L.
Reactions of NaCl with gaseous SO3, SO2, and O2
[NASA-TM-83423] p 86 N83-29358
FILPUS, J.
Measurements of energy distribution and thrust for microwave plasma coupling of electrical energy to hydrogen for propulsion
[AIAA PAPER 82-1951] p 52 A83-12508
Microwave plasma generation of hydrogen atoms for rocket propulsion p 53 A83-13090
FINK, R. C.
Piezoelectric deicing device
[NASA-CASE-LEW-13773-1] p 18 N83-29197
FINKE, R. C.
Direct conversion of infrared radiant energy for space power applications p 173 N83-15865
Design considerations for large space electric power systems
[NASA-TM-83064] p 58 N83-24552
Advanced electrical power system technology for the all electric aircraft
[NASA-TM-83390] p 115 N83-24764
FIRESTONE, R. F.
Creep of plasma-sprayed-ZrO2 thermal-barrier coatings p 89 A83-22273
Creep of plasma sprayed zirconia
[NASA-CR-167868] p 96 N83-29393
FISCHER, G. K.
Advanced Power Transmission Technology
[NASA-CP-2210] p 144 N83-20119
FISHBACH, L. H.
A remote augmentor lift system with a turbine bypass engine p 20 A83-19595
A remote augmentor lift system with a turbine bypass engine
[NASA-TM-82932] p 27 N83-12087
Study of LH2-fueled topping cycle engine for aircraft propulsion
[NASA-TM-83466] p 41 N83-34942
FISKE, G. H.
Sound propagation in segmented exhaust ducts - Theoretical predictions and comparison with measurements
[AIAA PAPER 83-0734] p 194 A83-28016
FLEETER, S.
The coupled aeroelastic response of turbomachinery blading to aerodynamic excitations
[AIAA 83-0844] p 156 A83-29822
The effect of incidence angle on the overall three-dimensional aerodynamic performance of a classical annular airfoil cascade
[NASA-CR-168127] p 15 N83-34911
FLOOD, D. J.
Radiation damage and annealing in large area n+/p/p+ GaAs shallow homojunction solar cells
p 172 N83-15826
FLORES, F.
Literature survey of properties of synfuels derived from coal
[NASA-TM-82739] p 99 N83-10208
FLORSCHUETZ, L. W.
Heat transfer characteristics for jet array impingement with initial crossflow
[ASME PAPER 83-GT-28] p 7 A83-47891
Jet array impingement flow distributions and heat transfer characteristics. Effects of initial crossflow and nonuniform array geometry
[NASA-CR-3630] p 128 N83-15592
FOLENTA, D. J.
Design study of Self-Alining Bearingless Planetary (SABP) gear p 145 N83-20127
FOOS, J. S.
Development of a high capacity toroidal Ni/Cd cell
[NASA-CR-169945] p 176 N83-19273
FORESTIERI, A. F.
Evaluation of electrode shape and nondestructive evaluation method for welded solar cell interconnects
[NASA-TM-82966] p 166 N83-10555
On the cause of the flat-spot phenomenon observed in silicon solar cells at low temperatures and low intensities p 170 N83-14705
FORMAN, B. J.
A multiple beam antenna concept for a 30/20 GHz satellite communications system p 103 A83-11485
FORMAN, R.
Ion sputter textured graphite
[NASA-CASE-LEW-12919-1] p 63 N83-10117
FOSNIGHT, V. V.
High frequency plasma generators for ion thrusters
[NASA-CR-167957] p 59 N83-28072
FRANCISCUS, L. C.
A remote augmentor lift system with a turbine bypass engine p 20 A83-19595
A remote augmentor lift system with a turbine bypass engine
[NASA-TM-82932] p 27 N83-12087

Supersonic fan engines for military aircraft
[NASA-TM-83499] p 42 N83-34947
FRANKFORT, M.
Planning assistance for the 30/20 GHz program, volume 1
[NASA-CR-165484-VOL-1] p 108 N83-33010
Planning assistance for the 30/20 GHz program, volume 2
[NASA-CR-165484-VOL-2] p 108 N83-33011
Planning assistance for the 30/20 GHz program, volume 3
[NASA-CR-165484] p 108 N83-33012
FRANKLIN, W. M.
Effect of hydrogen bonding on the vibrational dephasing time in glycerol p 61 A83-21054
FRATER, J. L.
Dynamic effects of internal spur gear drives
[NASA-CR-3692] p 149 N83-28452
Vibration in planetary gear systems with unequal planet stiffnesses
[NASA-TM-83428] p 150 N83-29709
FREEDENBERG, P.
Customer premise service study for 30/20 GHz satellite system
[NASA-CR-167986] p 105 N83-17769
FREEMAN, J. W.
The phototron: A light to RF energy conversion device p 173 N83-15866
FRENCH, K. W.
Sintering, properties and fabrication of Si3N4 + Y2O3 based ceramics p 90 A83-48303
FRENKLACH, M.
Soot formation in pyrolysis of acetylene, allene and 1,3-butadiene p 69 A83-39274
FRENSLEY, W. R.
GaAs integrated digital-to-analogue convertor for control of power dual-gate FETs p 112 A83-36479
FREY, W. E.
Evaluation of electrode shape and nondestructive evaluation method for welded solar cell interconnects
[NASA-TM-82966] p 166 N83-10555
Evaluation of solar cell welds by scanning acoustic microscopy p 172 N83-15834
FRIEDMAN, D. M.
Calculation of compressible flow in and about three-dimensional inlets with and without auxiliary inlets by a higher-order panel method
[NASA-CR-168009] p 10 N83-12047
FRIEDMAN, R.
Recent trends in aviation turbine fuel properties
[NASA-TP-2056] p 99 N83-11340
FRISA, L. E.
Ion flow experiments in a multipole discharge chamber
[AIAA PAPER 82-1930] p 203 A83-14398
FROST, W.
Influence of multidroplet size distribution on icing collection efficiency
[AIAA PAPER 83-0110] p 187 A83-16526
FRYK, E. E.
SSME main combustion chamber life prediction
[NASA-CR-168215] p 60 N83-36101
FU, L. S.
Mechanics aspects of NDE by sound and ultrasound p 152 A83-25571
Volume integrals of ellipsoids associated with the inhomogeneous Helmholtz equation p 192 A83-29528
The determination of the elastodynamic fields of an ellipsoidal inhomogeneity
[ASME PAPER 83-APM-19] p 157 A83-37388
The transmission or scattering of elastic waves by an inhomogeneity of simple geometry: A comparison of theories
[NASA-CR-3659] p 153 N83-16773
FU, L. S. W.
Phenomenological and mechanics aspects of nondestructive evaluation and characterization by sound and ultrasound of material and fracture properties
[NASA-CR-3623] p 153 N83-11506
Fundamental aspects in quantitative ultrasonic determination of fracture toughness: The scattering of a single ellipsoidal inhomogeneity
[NASA-CR-3625] p 153 N83-11507
FUKANO, J. L.
Stability analysis of Centaur-in-Shuttle composite corrugated adapters
[AIAA 83-1003] p 49 A83-29791
FULTON, D. L.
Advanced LOX/H2 engine technologies for future OTVs
[AIAA PAPER 83-1312] p 55 A83-36833
FUNG, S. S.
Microscopic contour changes of tribological surfaces by chemical and mechanical action
[ASLE PREPRINT 82-LC-3B-3] p 136 A83-13237
Surface profile changes of scuffed bearing surfaces
[NASA-TM-83055] p 82 N83-17682
FURIGA, A.
Satellite switched FDMA advanced communication technology satellite program
[NASA-CR-168034] p 105 N83-15543
FURMAN, E. R.
Critical research and advanced technology (CRT) support project
[NASA-TM-83019] p 176 N83-20361
FUSARO, R. L.
Polyimides: Tribological properties and their use as lubricants
[NASA-TM-82959] p 91 N83-13257
Effect of sliding speed and contact stress on tribological properties of ultra-high-molecular-weight polyethylene
[NASA-TP-2059] p 91 N83-14269
Fundamental aspects of polyimide dry film and composite lubrication: A review
[NASA-TM-82968] p 92 N83-14271
Polyimides formulated from a partially fluorinated diamine for aerospace tribological applications
[NASA-TM-83339] p 94 N83-22423
Friction, wear, transfer and wear surface morphology of ultra-high-molecular-weight polyethylene
[NASA-TM-83364] p 94 N83-25862

G

GAFFIN, W. O.
The JT8D and JT9D engine component improvement: Performance improvement program
[NASA-CR-167965] p 32 N83-17543
GAFFNEY, E. F.
Blade loss transient dynamic analysis of turbomachinery p 25 A83-40864
GAHN, R. F.
Single cell performance studies on the Fe/Cr Redox Energy Storage System using mixed reactant solutions at elevated temperature
[NASA-TM-83385] p 180 N83-25042
Zirconium carbide as an electrocatalyst for the chromous-chromic redox couple
[NASA-CASE-LEW-13246-1] p 182 N83-27344
GALLARDO, V.
Blade loss transient dynamic analysis of turbomachinery p 25 A83-40864
GALMES, J. M.
A turbulence model for three dimensional turbulent shear flows over curved rotating bodies
[AIAA PAPER 83-0559] p 120 A83-16787
Three dimensional flow field inside compressor rotor, including blade boundary layers
[NASA-CR-169788] p 128 N83-16679
GAMBLE, R. B.
Customer premises services market demand assessment 1980 - 2000. Volume 1: Executive summary
[NASA-CR-168150] p 108 N83-31925
Customer premises services market demand assessment 1980 - 2000: Volume 2
[NASA-CR-168151] p 108 N83-31926
GANGULY, S.
Next generation communications satellites: multiple access and network studies
[NASA-CR-167903] p 45 N83-12129
GAO, Y. C.
Dynamic fields near a crack tip growing in an elastic-perfectly-plastic solid p 157 A83-38528
GARDNER, W. B.
Energy efficient high-pressure turbine leakage technology report
[NASA-CR-165202] p 30 N83-15304
GARVIN, H. L.
A direct-measurement technique for estimating discharge-chamber lifetime
[AIAA PAPER 82-1908] p 51 A83-12483
GASKILL, D. W.
Atmospheric radiation model for water surfaces
[NASA-CR-167873] p 187 N83-21677
GATOS, H. C.
Microdistribution of oxygen in silicon and its effects on electronic properties p 172 N83-15825
GAUGEON, M.
Design and evaluation of low-cost laminated wood composite blades for intermediate size wind turbines: Blade design, fabrication concept, and cost analysis
[NASA-CR-165463] p 179 N83-23704
GAUGLER, R. E.
Comparison of predicted and experimental external heat transfer around a film cooled cylinder in crossflow
[NASA-TM-83017] p 127 N83-13392
Measured and calculated wall temperatures on air-cooled turbine vanes with boundary layer transition
[NASA-TM-83030] p 127 N83-14432
Comparison of visualized turbine endwall secondary flows and measured heat transfer patterns
[NASA-TM-83016] p 128 N83-14435
GAUNTNER, J. W.
Use of cooling air heat exchangers as replacements for hot section strategic materials
[NASA-TM-83494] p 42 N83-34946
GAY, C. H., JR.
Tip cap for a rotor blade
[NASA-CASE-LEW-13654-1] p 30 N83-14129
GAYDA, J.
Fatigue crack initiation and propagation in several nickel-base superalloys at 650 C p 76 A83-41199
GEDNEY, R. T.
NASA's Advanced Communications Technology Satellite (ACTS)
[NASA-TM-83416] p 48 N83-35004
GEDWILL, M. A.
A new diffusion-inhibited oxidation-resistant coating for superalloys p 74 A83-10299
Coating with overlay metallic-cermet alloy systems
[NASA-CASE-LEW-13639-2] p 82 N83-17683
GELERINTER, E.
Applications of ion beam technology
[NASA-CR-169797] p 82 N83-16493
GHANDHI, S. K.
Diffused P+-N solar cells in bulk GaAs p 171 N83-15818
GHANTOUS, C. A.
Three dimensional flow computations in a turbine scroll
[NASA-CR-168003] p 10 N83-12045
GHIA, K. N.
Multi-grid solution of Neumann pressure problem for viscous flows using primitive variables
[AIAA PAPER 83-0557] p 120 A83-16786
Study of asymptotic incompressible flow in curved ducts using a multi-grid technique p 123 A83-42532
GHIA, U.
Multi-grid solution of Neumann pressure problem for viscous flows using primitive variables
[AIAA PAPER 83-0557] p 120 A83-16786
Study of asymptotic incompressible flow in curved ducts using a multi-grid technique p 123 A83-42532
GHONEIM, A. F.
Modeling Interface Motion Of Combustion (MINOC). A computer code for two-dimensional, unsteady turbulent combustion
[NASA-TP-2132] p 40 N83-32806
GHONIEM, A. F.
Aerodynamic features of turbulent flames
[AIAA PAPER 83-0470] p 119 A83-16737
Numerical solution of the problem of flame propagation by the use of the random element method
[AIAA PAPER 83-0600] p 69 A83-36062
GHOSH, A.
Triangular system solutions on an optical systolic processor p 189 A83-36752
LU and Cholesky decomposition on an optical systolic array processor p 189 A83-43629
GHOSH, M. K.
Thermal elastohydrodynamic lubrication of line contacts
[NASA-TM-83424] p 152 N83-34326
GIAMATI, C. C.
Dynamic distortion in a short s-shaped subsonic diffuser with flow separation
[AIAA PAPER 83-1412] p 25 A83-45515
Dynamic distortion in a short s-shaped subsonic diffuser with flow separation
[NASA-TM-83412] p 36 N83-26838
GIAMEI, A. F.
Energy efficient engine high-pressure turbine single crystal vane and blade fabrication technology report
[NASA-CR-165400] p 39 N83-30429
GIARRATANO, P. J.
The dryout region in frictionally heated sliding contacts p 124 A83-42762
GIBALA, R.
Diffusion processes in Al2O3 scales - Void growth, grain growth, and scale growth p 76 A83-42238
GIBSON, R. K.
Advanced Gas Turbine (AGT) power-train system development
[NASA-CR-167875] p 142 N83-15627
GILES, M. B.
A numerical study of the steady scalar convective diffusion equation for small viscosity
[NASA-CR-172231] p 16 N83-35999
GILL, A.
Nitriding of titanium and titanium: 8 percent aluminum, 1 percent molybdenum, 1 percent vanadium alloy with an ion-beam source
[NASA-TP-2149] p 85 N83-24640

GILL, J. C.
Advanced propfan engine characteristics and technology needs
[AIAA PAPER 83-1155] p 23 A83-36250
Rotorcraft convertible engine study
[NASA-CR-166161] p 37 N83-27996
GITLOW, B.
Alkaline regenerative fuel cell energy storage system for manned orbital satellites p 54 A83-27206
GLADDEN, H. J.
Measurements of heat transfer distribution over the surfaces of highly loaded turbine nozzle guide vanes
[ASME PAPER 83-GT-53] p 8 A83-47910
Measured and calculated wall temperatures on air-cooled turbine vanes with boundary layer transition
[NASA-TM-83030] p 127 N83-14432
GLASER, F. W.
Wind tunnel measurements of blade/vane ratio and spacing effects on fan noise p 192 A83-15317
Low flight speed acoustic results for a supersonic inlet with auxiliary inlet doors
[AIAA PAPER 83-1415] p 196 A83-45517
Low flight speed acoustic results for a supersonic inlet with auxiliary inlet doors
[NASA-TM-83411] p 201 N83-27794
GLASGOW, E. R.
Zero-length inlets for subsonic V/STOL aircraft p 4 A83-29012
Wind tunnel tests of a zero length, slotted-lip engine air inlet for a fixed nacelle V/STOL aircraft
[NASA-TM-82939] p 9 N83-10019
GLASGOW, J. C.
The effect of yaw on horizontal axis wind turbine loading and performance
[NASA-TM-82778] p 169 N83-14688
Measured performance of a tip-controlled, teetered rotor with an NACA 64 sub 3-618 tip airfoil
[NASA-TM-82870] p 169 N83-14689
The response of a 38m horizontal axis teetered rotor to yaw p 175 N83-19232
Stall induced instability of a teetered rotor p 175 N83-19234
Results of free yaw tests of the Mod-O 100 kilowatt wind turbine
[NASA-TM-83432] p 184 N83-29813
GLASGOW, T. K.
A new diffusion-inhibited oxidation-resistant coating for superalloys p 74 A83-10299
Coating with overlay metallic-cermet alloy systems
[NASA-CASE-LEW-13639-2] p 82 N83-17683
GLASS, J.
Advanced LOX/H sub 2 engine technologies for future OTVs p 60 N83-35013
GLASSMAN, A. J.
Input generator for Denton 3-dimensional turbomachine-blade-row analysis code
[NASA-TM-23324] p 13 N83-26817
Computer code for off-design performance analysis of radial-inflow turbines with rotor blade sweep
[NASA-TP-2199] p 40 N83-32807
GLATT, L.
The development of a generalized advanced propeller analysis system
[AIAA PAPER 83-2466] p 26 A83-49581
GLOR, C.
Digital system for structural dynamics simulation
[NASA-CR-168019] p 43 N83-14139
GODSTON, J.
Technology and benefits of aircraft counter rotation propellers
[NASA-TM-82983] p 27 N83-11129
GOEDE, H.
High frequency plasma generators for ion thrusters
[NASA-CR-167957] p 59 N83-28072
GOEL, J.
A 1 watt GaAs power amplifier for the NASA 30/20 GHz communication system p 111 A83-11489
GOLDMAN, L. J.
Comparison of laser anemometer measurements and theory in an annular turbine cascade with experimental accuracy determined by parameter estimation p 4 A83-28833
Laser anemometer using a Fabry-Perot interferometer for measuring mean velocity and turbulence intensity along the optical axis in turbomachinery p 133 A83-28834
GOLDSTEIN, D. N.
Rotorcraft convertible engine study
[NASA-CR-168241] p 42 N83-34944
GOLDSTEIN, M. E.
The evolution of Tollmien-Schlichting waves near a leading edge p 120 A83-24410
The evolution of Tollmien-Schlichting waves near a leading edge. II - Numerical determination of amplitudes p 122 A83-35346
Generation of Tollmien-Schlichting waves by free-stream disturbances at low Mach numbers
[NASA-TM-83026] p 130 N83-23544
GONSALVEZ, D.
Engineering calculations for communications systems planning
[NASA-CR-170182] p 106 N83-22494
GONZALEZ-SANABRIA, O.
Polyvinyl alcohol membranes as alkaline battery separators
[NASA-TM-82961] p 70 N83-10135
GONZALEZ-SANABRIA, O. D.
Cross-linked polyvinyl alcohol films as alkaline battery separators p 68 A83-20576
GOODYKOONTZ, J. H.
Experiments on high bypass internal mixer nozzle jet noise
[NASA-TM-83020] p 198 N83-16152
GOPAL, I.
Next generation communications satellites: multiple access and network studies
[NASA-CR-167903] p 45 N83-12129
GORADIA, C. P.
Radiation damage in front and back illuminated high resistivity silicon solar cells
[NASA-TM-82965] p 206 N83-10962
High voltage v-groove solar cell
[NASA-CASE-LEW-13401-2] p 185 N83-32177
GORDAN, A. L.
Role of simulation and emulation in the development of Shuttle-Centaur (STS-Centaur)
[NASA-TM-83326] p 45 N83-29292
GORDON, L. H.
Mod-2 wind turbine project assessment and cluster test plans p 176 N83-19262
GORLA, R. S. R.
Effects of free stream turbulence intensity and integral length scale on heat transfer from a circular cylinder in crossflow p 123 A83-42711
GOUGEON, M.
Fabrication of low-cost Mod-OA wood composite wind turbine blades
[NASA-TM-83323] p 182 N83-27347
GOVADA, A.
A study of the stress wave factor technique for the characterization of composite materials
[NASA-CR-3670] p 153 N83-27248
GOVINDAN, T. R.
Blade loading and rotation effects on compressor rotor wake near end walls p 3 A83-22138
Experimental study of the boundary layer on a turbomachinery rotor blade p 7 A83-47022
End wall flows in rotors and stators of a single stage compressor
[NASA-CR-169800] p 128 N83-16678
GOYAL, R. K.
Three-dimensional compressible viscous analysis of mixer nozzles
[AIAA PAPER 83-1401] p 4 A83-36391
GRAHAM, R. W.
Film-cooling effectiveness with developing coolant flow through straight and curved tubular passages
[NASA-TP-2062] p 126 N83-12360
Opportunities for research in aerothermodynamics
[NASA-TM-83348] p 35 N83-24506
Curved film cooling admission tube
[NASA-CASE-LEW-13174-1] p 131 N83-27144
GRASSO, F.
Computed and measured turbulence in axisymmetric reciprocating engines p 21 A83-24669
GRAZIANI, R. A.
JT9D thermal barrier coated vanes
[NASA-CR-167964] p 37 N83-27993
GREENBAUER-SENG, L. A.
Experimental design of an interlaboratory study for trace metal analysis of liquid fluids
[NASA-TP-2148] p 73 N83-24575
GREENE, W.
Development and operating characteristics of an advanced two-stage combustor p 24 A83-38022
Energy efficient engine sector combustor rig test program
[NASA-CR-167913] p 33 N83-19753
GREGOREK, G. M.
An analytical evaluation of the icing properties of several low and medium speed airfoils
[AIAA PAPER 83-0109] p 3 A83-16525
Wind tunnel evaluation of air-foil performance using simulated ice shapes
[NASA-CR-167960] p 11 N83-15265
GREGORY, P. E.
Single and multijunction space solar cells grown by organometallic vapor phase epitaxy /OM-VPE/ p 164 A83-27260
GREGORY, W.
High accuracy fuel flowmeter, phase 1
[NASA-CR-167893] p 134 N83-21314
GRIFFIN, J. H.
Friction damping of flutter in gas turbine engine airfoils p 20 A83-24038
Effects of friction dampers on aerodynamically unstable rotor stages
[AIAA PAPER 83-0846] p 22 A83-32791
GRIGGS, E. I.
Acoustic velocities of two-phase mixtures of cryogenic fluids p 124 A83-43012
GRILL, A.
Sputtered silicon nitride coatings for wear protection p 88 A83-12651
Some properties of r.f.-sputtered hafnium nitride coatings p 88 A83-12653
RF sputtered silicon and hafnium nitrides: Properties and adhesion to 440C stainless steel
[NASA-TM-83400] p 95 N83-27020
GRIMES, H. H.
Fatigue behavior of SiC reinforced Ti/6Al-4V/ at 650 C p 62 A83-12414
Research on ultra-high-temperature materials, monolithic ceramics, ceramic matrix composites and carbon/carbon composites p 64 N83-12161
GROENEWEG, J. F.
Aircraft turbofan noise
[NASA-TM-83317] p 198 N83-18405
GROESBECK, D. E.
Conventional profile coaxial jet noise prediction p 193 A83-22128
JT15D 1/2-scale nozzle jet noise experiment and comparison with prediction
[NASA-TM-83370] p 201 N83-27793
GROSS, B.
Stress intensity and displacement coefficients for radially cracked ring segments subject to three-point bending
[NASA-TM-83059] p 160 N83-24874
Analysis of an externally radially cracked ring segment subject to three-point radial loading
[NASA-TM-83482] p 163 N83-35413
GROUMPOS, P. P.
Experimental results for the interference between FM television signals p 103 A83-19686
GRUBER, R. P.
Simplification of power electronics for ion thruster neutralizers
[AIAA PAPER 82-1880] p 53 A83-21099
Simplification of power electronics for ion thruster neutralizers
[NASA-TM-83004] p 56 N83-12141
GUNSALLUS, C. T.
Design and fabrication of composite blades for the Mod-1 wind turbine generator
[NASA-CR-167987] p 168 N83-11579
GUPTA, A. K.
A two-stage monolithic buffer amplifier for 20 GHz satellite communication p 112 A83-39272
GUSTAFSON, T. K.
Coherent conversion of the sunlight spectrum
[NASA-CR-170185] p 179 N83-25026

H

HAAS, J. E.
Experimental evaluation of inlet turbulence, wall boundary layer, surface finish, and fillet radius on small axial turbine state performance
[SAE PAPER 821475] p 24 A83-38001
Cold-air performance of compressor-drive turbine of Department of Energy upgraded automobile gas turbine engine. 2: Stage performance
[NASA-TM-82818] p 9 N83-11063
Analytical and experimental investigation of stator endwall contouring in a small axial-flow turbine. 1: Stator performance
[NASA-TP-2023] p 26 N83-11125
HADFIELD, J. R.
Advanced single permanent magnet axipolar ironless stator ac motor for electric passenger vehicles
[NASA-CR-167974] p 212 N83-32687
HAGEDORN, N. H.
Design flexibility of redox flow systems p 164 A83-27177
Single cell performance studies on the Fe/Cr Redox Energy Storage System using mixed reactant solutions at elevated temperature
[NASA-TM-83385] p 180 N83-25042
NASA Redox Project status summary
[NASA-TM-83401] p 183 N83-29810
HAGER, R. D.
The aerodynamic design and performance of the General Electric/NASA EEE fan
[AIAA PAPER 83-1160] p 23 A83-36252

HAH, C.
Experimental study of the boundary layer on a turbomachinery rotor blade p 7 A83-47022
HAISLER, W. E.
An uncoupled viscoplastic constitutive model for metals at elevated temperature
[AIAA 83-1016] p 156 A83-29798
HALE, P. L.
A method to estimate weight and dimensions of small aircraft propulsion gas turbine engines: User's guide
[NASA-CR-168049] p 31 N83-16343
HALFORD, G. R.
Nonlinear structural and life analyses of a combustor liner p 155 A83-12764
Turbine blade nonlinear structural and life analysis p 21 A83-29024
Creep-fatigue of low cobalt superalloys p 79 N83-11290
Strainrange partitioning: A total strain range version
[NASA-TM-83023] p 81 N83-14246
Relation of cyclic loading pattern to microstructural fracture in creep fatigue
[NASA-TM-83473] p 161 N83-34349
Tensile and compressive constitutive response of 316 stainless steel at elevated temperatures p 162 N83-34353
HALL, D. G.
Surface-polaritonlike waves guided by thin, lossy metal films p 192 A83-37947
HALLE, J. E.
Energy efficient engine low-pressure compressor component test hardware detailed design report
[NASA-CR-165354] p 39 N83-30427
HALLEYY, A.
The DOE/NASA wind turbine data acquisition system. Part 3: Unattended power performance monitor
[NASA-CR-165540] p 44 N83-24516
HALS, F. A.
Parametric study of potential early commercial MHD power plants. Task 3: Parameter variation of plant size
[NASA-CR-165445] p 182 N83-26259
HAMED, A.
Solid particle dynamic behavior through twisted blade rows p 3 A83-27478
Three dimensional flow computations in a turbine scroll
[NASA-CR-168003] p 10 N83-12045
HAMILTON, H. B.
Losses in chopper-controlled DC series motors
[NASA-CR-167845] p 114 N83-13359
HAMLYN, K. M.
Study for analysis of benefit versus cost of low thrust propulsion system
[NASA-CR-168011] p 57 N83-21002
HAMROCK, B. J.
High-speed motion picture camera experiments of cavitation in dynamically loaded journal bearings
[ASME PAPER 82-LUB-18] p 136 A83-13509
High-speed motion picture camera experiments of cavitation in dynamically loaded journal bearings
[ASME PAPER 82-LUB-18] p 138 A83-39944
Elastohydrodynamic lubrication theory
[NASA-TM-81695] p 140 N83-12432
Theoretical results for fully flooded, elliptical hydrodynamic contacts
[NASA-TM-81696] p 140 N83-13458
Elastohydrodynamic lubrication of elliptical contacts p 141 N83-15514
Geometry and starvation effects in hydrodynamic lubrication p 141 N83-15522
Elastohydrodynamic lubrication of rectangular contacts
[NASA-TP-2111] p 143 N83-16759
Lubrication background
[NASA-TM-81692] p 147 N83-20159
Optimum parallel step-sector bearing lubricated with an incompressible fluid
[NASA-TM-83356] p 148 N83-24855
Vapor cavitation in dynamically loaded journal bearings
[NASA-TM-83366] p 160 N83-24875
Rolling-element bearings
[NASA-RP-1105] p 149 N83-27214
Film thickness for different regimes of fluid-film lubrication
[NASA-TM-81700] p 149 N83-28449
Non-Newtonian fluid model incorporated into elastohydrodynamic lubrication of rectangular contacts
[NASA-TM-82018] p 150 N83-28454
Theoretical results for starved elliptical contacts
[NASA-TM-81697] p 150 N83-29710
Experimental investigations of elastohydrodynamic lubrication
[NASA-TM-81698] p 150 N83-29711
Elastohydrodynamics of elliptical contacts for materials of low elastic modulus
[NASA-TM-81699] p 151 N83-29712
Applications of film thickness equations
[NASA-TM-81701] p 151 N83-29713
Thermal elastohydrodynamic lubrication of line contacts
[NASA-TM-83424] p 152 N83-34326
HANCOCK, D. J.
Simplified power processing for ion-thruster subsystems
[AIAA PAPER 83-1394] p 55 A83-36384
Simplified power processing for ion-thruster subsystems p 56 A83-39271
Simplified power processing for ion-thruster subsystems p 60 N83-35018
HANKINS, G. B.
Solution of viscous internal flows on curvilinear grids generated by the Schwarz-Christoffel transformation p 122 A83-36796
HANKINS, G. B., JR.
User's manual for Axisymmetric Diffuser Duct (ADD) code. Volume 1: General ADD code description
[NASA-CR-165598-VOL-1] p 211 N83-26757
User's manual for Axisymmetric Diffuser Duct (ADD) code. Volume 2: Detailed ADD code description
[NASA-CR-165598-VOL-2] p 211 N83-26758
User's manual for Axisymmetric Diffuser Duct (ADD) code. Volume 3: ADD code coordinate generator
[NASA-CR-165598-VOL-3] p 211 N83-26759
HANNUM, N. P.
The performance and application of high speed long life LH2 hybrid bearings for reusable rocket engine turbomachinery
[AIAA PAPER 83-1389] p 138 A83-36379
The performance and application of high speed long life LH2 hybrid bearings for reusable rocket engine turbomachinery
[NASA-TM-83417] p 58 N83-26923
HANSEN, I. G.
Design considerations for large space electric power systems
[NASA-TM-83064] p 58 N83-24552
Advantage of resonant power conversion in aerospace applications
[NASA-TM-83399] p 37 N83-27994
HANSON, M. P.
Environmental effects on graphite fiber reinforced PMR-15 polyimide p 63 A83-33115
HANSON, R. K.
Laser-induced fluorescence technique for velocity field measurements in subsonic gas flows p 133 A83-45962
HARADA, Y.
Improved uniformity of multiphase ceramic-metal plasma-sprayed coats p 61 A83-22269
Plasma-sprayed self-lubricating coatings
[NASA-CR-3680] p 94 N83-22422
HARCAR, A. R.
Customer premise service study for 30/20 GHz satellite system
[NASA-CR-167986] p 105 N83-17769
HARF, F. H.
Effect of reduced cobalt contents on hot isostatically pressed powder metallurgy U-700 alloys p 78 N83-11287
Dual alloy interface stability p 79 N83-11297
Microstructural behavior of interfaces in hot isostatically pressed, dual alloy combinations
[NASA-TM-82698] p 80 N83-11309
HARKNESS, J. D.
Evaluation program for secondary spacecraft cells. Cycle life test
[NASA-CR-172679] p 182 N83-27351
Evaluation program for secondary spacecraft cells. Cycle life test
[NASA-CR-172680] p 183 N83-27352
HARLACHER, B. L.
Development of electrical test procedures for qualification of spacecraft against EID. Volume 1: The CAN test and other relevant data
[NASA-CR-165590] p 49 N83-12136
Development of electrical test procedures for qualification of spacecraft against EID. Volume 2: Review and specification of test procedures
[NASA-CR-165590] p 50 N83-12137
HARRIS, D. H. L.
The effects of metals and inhibitors on thermal oxidative degradation reactions of unbranched perfluoroalkylethers
[NASA-TM-83464] p 97 N83-34049
HART, R. E., JR.
The effect of different solar simulators on the measurement of short-circuit current temperature coefficients p 172 N83-15821
Radiation damage and annealing in large area n+/p/p+ GaAs shallow homojunction solar cells p 172 N83-15826
HARTMAN, G. A.
A total life prediction model for stress concentration sites
[NASA-CR-170290] p 160 N83-23629
HARTMAN, M. J.
The trend of future gas turbine technology
[NASA-TM-83505] p 2 N83-34886
HARTMANN, M. J.
Advanced technologies for turbomachinery systems: An overview
[NASA-TM-82949] p 28 N83-12090
HARVEY, A. C.
Design of hydraulic output Stirling engine
[NASA-CR-167976] p 177 N83-22739
HARVEY, W. B.
Rotor redesign for a highly loaded 1800 ft/sec tip speed fan. 3: Laser Doppler velocimeter report
[NASA-CR-167954] p 30 N83-14128
HARVEY, W. W.
Study to establish cost predictions for the production of Redox chemicals
[NASA-CR-167882] p 176 N83-20359
HASAN, M. A. Z.
The 'whistler-nozzle' phenomenon p 125 A83-49472
The whistler nozzle phenomenon
[NASA-CR-170015] p 199 N83-20706
HAUGLAND, E. J.
A study of 60 Gigahertz intersatellite link applications
[NASA-TM-83337] p 47 N83-20994
HAWKINS, C. E.
Free radical propulsion concept p 53 A83-13141
HAWLEY, M.
Measurements of energy distribution and thrust for microwave plasma coupling of electrical energy to hydrogen for propulsion
[AIAA PAPER 82-1951] p 52 A83-12508
Microwave plasma generation of hydrogen atoms for rocket propulsion p 53 A83-13090
HAY, R. E.
A network control concept for the 30/20 GHz communication system baseband processor p 47 A83-41389
Method for terminal position determination in Earth terminal-to-satellite burst acquisition and synchronization
[NASA-CASE-LEW-13693-1] p 107 N83-30832
HAYES, C. W.
Energy efficient engine high-pressure turbine single crystal vane and blade fabrication technology report
[NASA-CR-165400] p 39 N83-30429
HEAD, V.
Three-dimensional compressible viscous analysis of mixer nozzles
[AIAA PAPER 83-1401] p 4 A83-36391
HEIDELBERG, L. J.
A compact inflow control device for simulating flight fan noise
[NASA-TM-83349] p 201 N83-26643
HEIDENRICH, G. A.
Customer premises services market demand assessment 1980 - 2000. Volume 1: Executive summary
[NASA-CR-168150] p 108 N83-31925
Customer premises services market demand assessment 1980 - 2000: Volume 2
[NASA-CR-168151] p 108 N83-31926
HEIDKAMP, D.
The DOE/NASA wind turbine data acquisition system. Part 3: Unattended power performance monitor
[NASA-CR-165540] p 44 N83-24516
HEISEY, J. B.
Performance and emissions characteristics of aqueous alcohol fumes in a DI diesel engine
[NASA-CR-167917] p 99 N83-12250
HEJAZI, M.
On composites with periodic structure p 154 A83-10283
HELMS, H. E.
Advanced Gas Turbine (AGT) powertrain system
[NASA-CR-165346] p 139 N83-11497
Advanced Gas Turbine (AGT) power-train system development
[NASA-CR-167875] p 142 N83-15627
HEMANN, J. H.
The effect of stress on ultrasonic pulses in fiber reinforced composites
[NASA-CR-3724] p 154 N83-33180
HENCH, L. L.
Effect of Y2O3 and Al2O3 on the oxidation resistance of Si3N4 p 88 A83-22258
Mechanisms of devitrification of grain boundary glassy phases in Si3N4 materials
[NASA-CR-169670] p 71 N83-14177

HENDERSON, W. P.
Fluid Dynamics Panel Symposium on Aerodynamics of Power Plant Installation
[AGARD-AR-173] p 27 N83-11138
HENDRICKS, R. C.
An experimental investigation of the vaporous/gaseous cavity characteristics of an eccentric journal bearing
[ASLE PREPRINT 82-LC-3A-1] p 136 A83-13230
Effects of arc current on the life in burner-rig thermal cycling of plasma-sprayed ZrO2-O3 p 89 A83-22270
Use of fiber-like materials to augment cycle life of thick, thermoprotective-seal coatings p 89 A83-22271
Some inelastic effects of thermal cycling on ZrO2-Y2O3 materials p 89 A83-22272
The dryout region in frictionally heated sliding contacts p 124 A83-42762
Acoustic velocities of two-phase mixtures of cryogenic fluids p 124 A83-43012
Experiments on flow through one to four inlets of the orifice and Borda type p 124 A83-43235
Studies of flows through N-sequential orifices
[ASME PAPER 83-FE-22] p 125 A83-48678
Experimental investigation of the vaporous/gaseous cavity characteristics of an eccentric journal bearing
[NASA-TM-82996] p 128 N83-17833
Finite element formulation for transient heat treat problems
[NASA-TM-83070] p 129 N83-17834
Studies of flows through N-sequential orifices
[NASA-TM-83313] p 129 N83-19020
Thermomechanical loading of multilayered cylindrical geometries in thermal cycling from 300 to 1300 K
[NASA-TM-83312] p 129 N83-20029
Analogy between fluid cavitation and fracture mechanics
[NASA-TM-83071] p 129 N83-22542
A refrigerated dynamic seal
[NASA-TM-83378] p 130 N83-24798
The effect of annealing on the creep of plasma sprayed ceramics
[NASA-TM-83396] p 130 N83-24799
Correlation of compressive stress with spalling of plasma sprayed ceramic materials
[NASA-TM-83406] p 95 N83-27016
Residual stress in plasma sprayed ceramic turbine tip and gas path seal specimens
[NASA-TM-83418] p 131 N83-28380
A comparison of flow rates and pressure profiles for N-sequential inlets and three related seal configurations
[NASA-TM-83442] p 132 N83-33103
Comparative evaluation of three shaft seals proposed for high performance turbomachinery
[NASA-TM-83021] p 152 N83-34325
HENNEKE, E. G., II
A study of the stress wave factor technique for the characterization of composite materials
[NASA-CR-3670] p 153 N83-27248
HENSHAW, J.
Hybridized polymer matrix composites
[NASA-CR-165341] p 66 N83-22326
HERMANN, A. M.
Minority carrier diffusion length measurements - A review and comparison of techniques p 205 A83-28448
Diffusion length measurements in solar cells: An analysis and comparison of techniques p 171 N83-15812
HERSH, A. S.
Effect of flow on the acoustic performance of extended reaction lined ducts
[AIAA PAPER 83-0778] p 195 A83-28024
HERTZBERG, A.
Direct contact droplet heat exchangers for thermal management in space p 120 A83-27137
Radiative energy receiver for high performance energy conversion cycles p 164 A83-27138
Radiation energy receiver for laser and solar propulsion systems
[AIAA PAPER 83-1207] p 55 A83-36281
HESS, J. L.
Calculation of compressible flow in and about three-dimensional inlets with and without auxiliary inlets by a higher-order panel method
[NASA-CR-168009] p 10 N83-12047
HICKEY, J.
Fuel quality/processing study. Volume 4: On site processing studies
[NASA-CR-165326-VOL-4] p 179 N83-22755
HIDDLESTON, H. R.
Gain-enhanced free-electron laser with an electromagnetic pump field p 135 A83-31133
The application of free-electron lasers to the transmission of energy in space p 135 A83-31141
HIGTON, G. H.
Satellite switched FDMA advanced communication technology satellite program
[NASA-CR-168034] p 105 N83-15543
HILL, J. P.
Alternatives for jet engine control
[NASA-CR-170100] p 33 N83-20945
HILL, V. L.
Determination of hydrogen permeability in uncoated and coated superalloys
[NASA-CR-165209] p 80 N83-12215
HILLER, B.
Laser-induced fluorescence technique for velocity field measurements in subsonic gas flows p 133 A83-45862
HINGST, W. R.
Experimental investigation of a two-dimensional shock-turbulent boundary layer interaction with bleed
[AIAA PAPER 83-0135] p 3 A83-19581
HINRICHSEN, E. N.
Control of large wind turbine generators connected to utility networks
[NASA-CR-168200] p 185 N83-34451
HINSON, B. L.
Inlet design for high-speed propfans
[SAE PAPER 821359] p 5 A83-37957
HINST, W. R.
Experimental investigation of a two-dimensional shock-turbulent boundary layer interaction with bleed
[NASA-TM-83057] p 34 N83-22200
HIRSCHKRON, R.
Rotorcraft convertible engine study
[NASA-CR-168241] p 42 N83-34944
HO, K. S.
The finite analytic method, volume 5
[NASA-CR-170188] p 191 N83-23089
HO, P. T.
20 x 20 IF switch matrix for SS-TDMA systems p 113 A83-41369
Spacecraft IF switch matrix for wideband service applications in 30/20 GHz communications satellite systems: Proof-of-concept model, executive summary
[NASA-CR-168175] p 107 N83-29492
HOBART, H. F.
The NASA High Accuracy Fuel Flowmeter (HAFF) development program
[NASA-TM-83484] p 19 N83-33883
HOBBS, D. E.
Development of controlled diffusion airfoils for multistage compressor application
[ASME PAPER 83-GT-211] p 9 A83-48012
Rotor redesign for a highly loaded 1800 ft/sec tip speed fan. 3: Laser Doppler velocimeter report
[NASA-CR-167954] p 30 N83-14128
HODGE, P. E.
Critical research and advanced technology (CRT) support project
[NASA-TM-83019] p 176 N83-20361
HOFER, K. E.
Fatigue testing of low-cost fiberglass composite wind turbine blade materials
[NASA-CR-165566] p 177 N83-22746
HOFFMAN, J. D.
Implicit marching solution of compressible viscous subsonic flow in planar and axisymmetric ducts
[NASA-TM-82876] p 125 N83-10389
A computer program for the calculation of the flow field including boundary layer effects for mixed-compression inlets at angle of attack
[NASA-CR-168002] p 10 N83-11066
HOFFMAN, P. S.
High frequency, high power capacitor development
[NASA-CR-168035] p 116 N83-27127
HOFLE, M. M.
Correlation of compressive stress with spalling of plasma sprayed ceramic materials
[NASA-TM-83406] p 95 N83-27016
HOGAN, A.
Aircraft measurements of trace gases and particles near the tropopause
[NASA-CR-3691] p 188 N83-27542
HOLANDA, R.
Analysis of strain gage reliability in F-100 jet engine testing at NASA Lewis Research Center
[NASA-TM-83325] p 134 N83-24829
HOLDEMAN, J. D.
Perspectives on the mixing of a row of jets with a confined crossflow
[AIAA PAPER 83-1200] p 122 A83-36276
Experiments in dilution jet mixing
[AIAA PAPER 83-1201] p 122 A83-36277
Cloud encounter statistics in the 28.5-43.5 KFT altitude region from four years of GASP observations p 188 A83-38733
Dilution zone mixing p 131 N83-29216
Perspectives on the mixing of a row of jets with a confined crossflow
[NASA-TM-83457] p 15 N83-30392
Experiments in dilution jet mixing
[NASA-TM-83434] p 15 N83-30393
HOLLECK, G. L.
Development of a high capacity toroidal Ni/Cd cell
[NASA-CR-169945] p 176 N83-19273
HOLM, R. G.
The influence of inlet design on the aeroacoustic performance of a JT15D turbofan engine as measured in the NASA-Ames 40 x 80 foot wind tunnel
[AIAA PAPER 83-0681] p 21 A83-28006
HOLMES, D. E.
Liquid encapsulated Czochralski growth of low dislocation GaAs p 204 A83-13784
EL2 distributions in doped and undoped liquid encapsulated Czochralski GaAs p 205 A83-22756
Advances in large-diameter liquid encapsulated Czochralski GaAs p 171 N83-15819
High purity, low dislocation GaAs single crystals
[NASA-CR-168098] p 206 N83-19622
HOLMS, A. G.
Computer program to minimize prediction error in models from experiments with 16 hypercube points and 0 to 6 center points
[NASA-TM-82995] p 192 N83-21872
HOMYAK, L.
A compact inflow control device for simulating flight fan noise
[NASA-TM-83349] p 201 N83-26643
HONTAS, J.
Binary nickel alloy phase diagrams compilation and critical evaluation
[NASA-CR-170016] p 82 N83-19885
HOPPIN, G., III
Progress toward determining the potential of ODS alloys for gas turbine applications
[NASA-TM-83332] p 83 N83-22387
HORNE, C.
The influence of inlet design on the aeroacoustic performance of a JT15D turbofan engine as measured in the NASA-Ames 40 x 80 foot wind tunnel
[AIAA PAPER 83-0681] p 21 A83-28006
HOROWITZ, S. J.
An iterative method for predicting turbofan inlet acoustics p 192 A83-13135
Optimization of acoustic liners by the hybrid finite element-integral approach
[AIAA PAPER 83-0670] p 194 A83-26917
HORSTEIN, M.
Requirements for a mobile communications satellite system. Volume 2: Technical report
[NASA-CR-168129] p 107 N83-23498
HOWARD, W. D.
CF6 jet engine diagnostics program. High pressure turbine roundness/clearance investigation
[NASA-CR-165581] p 29 N83-13100
HOWES, W. L.
Large-aperture interferometer using local reference beam
[NASA-TP-2060] p 203 N83-13979
Rainbow Schlieren
[NASA-TP-2166] p 135 N83-33126
HOYNIAK, D.
The coupled aeroelastic response of turbomachinery blading to aerodynamic excitations
[AIAA 83-0844] p 156 A83-29822
HRYCAK, P.
Heat transfer and flow characteristics of jets impinging on a concave hemispherical plate p 123 A83-42743
HSU, L. C.
Polyvinyl alcohol cross-linked with two aldehydes
[NASA-CASE-LEW-13504-1] p 71 N83-13188
Polyvinyl alcohol battery separator containing inert filler
[NASA-CASE-LEW-13556-2] p 183 N83-29805
HUDSON, W. R.
Electric propulsion research and technology in the United States
[AIAA PAPER 82-1867] p 53 A83-16925
HUFFMAN, F.
Thermionic technology infrastructure for space power p 54 A83-27298
HUGHES, P. S.
The MOD-OA 200 kilowatt wind turbine generator design and analysis report
[NASA-CR-165127] p 174 N83-16859
HULL, D. R.
Interrelation of material microstructure, ultrasonic factors, and fracture toughness of a two-phase titanium alloy p 75 A83-23922
Metal honeycomb to porous wireform substrate diffusion bond evaluation p 153 A83-39620
Ultrasonic ranking of toughness of tungsten carbide
[NASA-TM-83358] p 153 N83-23620
HULTGREN, L. S.
Rapid distortion of small-scale turbulence by an axisymmetric contraction p 120 A83-22381

HUMBERT, M. C.
Comparison of modern icing cloud instruments
[NASA-CR-168008] p 19 N83-18720
HUMENIK, F. M.
Fuel spray diagnostics p 38 N83-29212
Flame radiation measurements p 73 N83-29228
Parametric study of flame radiation characteristics of a tubular-can combustor
[NASA-TM-83436] p 39 N83-29237
Detailed fuel spray analysis techniques
[NASA-TM-83476] p 42 N83-34943
HUNT, L. E.
Materials constitutive models for nonlinear analysis of thermally cycled structures
[NASA-TP-2055] p 158 N83-12449
HURWITZ, F. I.
Dynamic mechanical characterization of cure of a polyimide-graphite fiber composite (PMR 15/Celion 6000) p 62 A83-31793
Method and apparatus for gripping uniaxial fibrous composite materials
[NASA-CASE-LEW-13758-1] p 64 N83-12176
HUSSAIN, A. K. M. F.
The 'whistler-nozzle' phenomenon
p 125 A83-49472
The whistler nozzle phenomenon
[NASA-CR-170015] p 199 N83-20706
HUSTON, R. L.
A basis for the analysis of surface geometry of spiral bevel gears p 146 N83-20138
Geometrical analysis of circular-cut spiral bevel gears
[NASA-CR-168226] p 151 N83-33167
HUSTVEDT, D. C.
Preliminary design of flight hardware for two-phase fluid research
[NASA-CR-168072] p 46 N83-25766
HYLTON, L. D.
Measurements of heat transfer distribution over the surfaces of highly loaded turbine nozzle guide vanes
[ASME PAPER 83-GT-53] p 8 A83-47910
Analytical and experimental evaluation of the heat transfer distribution over the surfaces of turbine vanes
[NASA-CR-168015] p 131 N83-28376
HYNES, A. J.
The detailed chemistry and thermodynamics of sodium in oxygen-rich flames
[NASA-CR-169848] p 72 N83-17626

I

INGARD, K. U.
Mode propagation in nonuniform circular ducts with potential flow p 122 A83-36082
INGEBO, R.
Aerodynamic-wave break-up of liquid sheets in swirling airflows and combustor modules
[AIAA PAPER 83-1204] p 124 A83-45511
Aerodynamic-wave break-up of liquid sheets in swirling airflows and combustor modules
[NASA-TM-83353] p 130 N83-23545
INGLEHART, L. J.
Comparison of NDE techniques for sintered-SiC components p 152 A83-22265
INUKAI, T.
Planning assistance for the NASA 30/20 GHz program. Network control architecture study.
[NASA-CR-168058] p 106 N83-21207
ISODA, Y.
Jet array impingement flow distributions and heat transfer characteristics. Effects of initial crossflow and nonuniform array geometry
[NASA-CR-3630] p 128 N83-15592
IVES, S. T.
Continued development of a detailed model of arc discharge dynamics
[NASA-CR-167977] p 206 N83-16234
IWAKUMA, T.
On composites with periodic structure
p 154 A83-10283
Composites with periodic microstructure
p 62 A83-12734
Micromechanically based constitutive relations for polycrystalline solids p 162 N83-34359

J

JACKSON, B.
Electrothermal thruster diagnostics. Volume 1: Executive summary
[NASA-CR-168174-VOL-1] p 60 N83-33942
Electrothermal thruster diagnostics. Volume 2: Technical
[NASA-CR-168174-VOL-2] p 60 N83-33943
JACKSON, J.
Frequency-multiplexed and pipelined iterative optical systolic array processors p 188 A83-18588
Optical systolic array processor using residue arithmetic p 189 A83-46834
JACKSON, J. A.
On the shock cell structure and noise of supersonic jets
[AIAA PAPER 83-0703] p 193 A83-25923
JACKSON, T. W.
Single-wire swirl flow turbulence measurements
[AIAA PAPER 83-1202] p 122 A83-36278
JACOBS, R. E.
Preliminary tests of an advanced high-temperature combustion system
[NASA-TP-2203] p 41 N83-33893
JACOBSON, B. O.
High-speed motion picture camera experiments of cavitation in dynamically loaded journal bearings
[ASME PAPER 82-LUB-18] p 136 A83-13509
High-speed motion picture camera experiments of cavitation in dynamically loaded journal bearings
[ASME PAPER 82-LUB-18] p 138 A83-39944
Elastohydrodynamic lubrication of rectangular contacts
[NASA-TP-2111] p 143 N83-16759
Vapor cavitation in dynamically loaded journal bearings
[NASA-TM-83366] p 160 N83-24875
Non-Newtonian fluid model incorporated into elastohydrodynamic lubrication of rectangular contacts
[NASA-TM-83318] p 150 N83-28454
JACOBSON, N. S.
Reaction of cobalt in SO2 atmospheric at elevated temperatures
[NASA-TM-83485] p 88 N83-35104
JACOBSON, T. P.
Improved uniformity of multiphase ceramic-metal plasma-sprayed coats p 61 A83-22269
JAHNSEN, L. J.
Comparison of modern icing cloud instruments
[NASA-CR-168008] p 19 N83-18720
JALAN, V.
Optimization and fabrication of porous carbon electrodes for Fe/Cr redox flow cells
[NASA-CR-167921] p 179 N83-23708
JAMES, E. L.
Operational summary of an electric propulsion long term test facility
[AIAA PAPER 82-1903] p 44 A83-12478
Analysis and design of ion thrusters for large space systems
[NASA-CR-165160] p 57 N83-14159
JAN, Y.
Satellite switched FDMA advanced communication technology satellite program
[NASA-CR-168034] p 105 N83-15543
JANARDAN, B. A.
Free-jet acoustic investigation of high-radius-ratio coannular plug nozzles. Comprehensive data report, volume 1
[NASA-CR-168086-VOL-1] p 198 N83-18408
JANETZKE, D. C.
Performance and load data from Mod-0A and Mod-1 wind turbine generators p 176 N83-19255
JANJUA, S. I.
Turbulence measurements in a swirling confined jet flowfield using a triple hot-wire probe
[NASA-CR-169668] p 127 N83-14434
JANOVICZ, M. A.
Ceramic applications in turbine engines
[NASA-CR-165494] p 212 N83-37028
JARRETT, R.
Superalloy composition modeling p 78 N83-11284
Role of cobalt in nickel base superalloys
p 78 N83-11286
JASPERSON, W. H.
Cloud encounter statistics in the 28.5-43.5 KFT altitude region from four years of GASP observations
p 188 A83-38733
Flight summaries and temperature climatology at airliner cruise altitudes from GASP (Global Atmospheric Sampling Program) data
[NASA-CR-168106] p 188 N83-24048
JAVID, S. H.
Control design for a wind turbine-generator using output feedback p 164 A83-24721
Control design and performance analysis of a 6 MW wind turbine-generator p 165 A83-29897
JAYARAMAN, N.
Metallurgical instabilities during the high temperature low cycle fatigue of nickel-base superalloys
p 75 A83-22019
The effect of microstructure on the fatigue behavior of Ni base superalloys p 75 A83-36166
JENKINS, D.
Energy and precious fuels requirements of fuel alcohol production, volume 1
[NASA-CR-168090] p 183 N83-28581
JENKINS, R. M.
A comprehensive method for preliminary design optimization of axial gas turbine stages. II - Code verification
[AIAA PAPER 83-1403] p 24 A83-36393
JENSEN, A. S.
Particle-sampling statistics in laser anemometers Sample-and-hold systems and saturable systems
p 134 A83-48120
JERACKI, R. J
Noise of the 10-bladed, 40 deg swept SR-6 propeller in a wind tunnel
[NASA-TM-82950] p 196 N83-11840
Noise of the 10-bladed 60 deg swept SR-5 propeller in a wind tunnel
[NASA-TM-83054] p 200 N83-23112
JEROSZKO, R. A.
Broad specification fuels technology program, phase 1
[NASA-CR-168180] p 74 N83-30551
JOHNS, A. L.
Experimental results of a deflected thrust V/STOL nozzle research program
[AIAA PAPER 83-0170] p 6 A83-42100
Experimental results of a deflected thrust V/STOL nozzle research program
[NASA-TM-83069] p 12 N83-25657
JOHNSON, B. V.
Statistical characteristics of velocity, concentration, mass transport, and momentum transport for coaxial jet mixing in a confined duct
[ASME PAPER 83-GT-39] p 125 A83-47899
JOHNSON, D. C.
Improved Stirling engine performance using jet impingement p 137 A83-27288
JOHNSON, G. K.
Develop and test fuel cell powered on-site integrated total energy system
[NASA-CR-168020] p 173 N83-15839
JOHNSON, G. M.
Efficient solution of the Euler and Navier-Stokes equations with a vectorized multiple-grid algorithm
[AIAA PAPER 83-1893] p 5 A83-39359
Convergence acceleration of viscous flow computations
[NASA-TM-83039] p 190 N83-12930
Multiple-grid convergence acceleration of viscous and inviscid flow computations
[NASA-TM-83361] p 190 N83-21847
Efficient solution of the Euler and Navier-Stokes equations with a vectorized multiple-grid algorithm
[NASA-TM-83376] p 2 N83-24467
Flux-based acceleration of the Euler equations
[NASA-TM-83453] p 191 N83-30113
JOHNSON, J. A., III
Unsteady turbulent shear flow in shock tube discontinuities p 124 A83-46445
JOHNSON, K. H.
Molecular-orbital model for metal-sapphire interfacial strength p 67 A83-10612
JOHNSON, R. A.
Component qualification and initial build of the AGT 100 advanced automotive gas turbine
[ASME PAPER 83-GT-225] p 138 A83-48023
Advanced Gas Turbine (AGT) power-train system development
[NASA-CR-167875] p 142 N83-15627
JOHNSON, S. H.
Critical review of the trailing edge condition in steady and unsteady flow. Blade flutter in compressors and fans: Numerical simulation of the aerodynamic loading
[NASA-CR-169705] p 10 N83-15264
JOHNSON, W.
Effects on stress rupture life and tensile strength of tin additions to Inconel 718 p 79 N83-11299
JOHNSTON, J. P.
A mixing-length model for the prediction of convex curvature effects on turbulent boundary layers
[ASME PAPER 83-GT-80] p 125 A83-47933
JOHNSTON, R. P.
Energy efficient engine. Flight propulsion system preliminary analysis and design
[NASA-CR-159859] p 28 N83-12094
JOHNSTON, W.
A viscous-inviscid interactive procedure for rotational flow in cascades of two-dimensional airfoils of arbitrary shape
[AIAA PAPER 83-0256] p 3 A83-16614
JONES, C.
Study of advanced rotary combustion engines for commuter aircraft
[NASA-CR-165399] p 32 N83-17545

Multi-fuel rotary engine for general aviation aircraft
[NASA-TM-83429] p 38 N83-29235
Multi-fuel rotary engine for general aviation aircraft
[NASA-TM-85428] p 43 N83-36031
JONES, G. E., JR.
Fuel quality-processing study. Volume 1: Overview and results
[NASA-CR-165326-VOL-1] p 178 N83-22750
Fuel quality-processing study. Volume 2: Literature survey
[NASA-CR-165326-VOL-2] p 178 N83-22751
Fuel quality/processing study. Volume 3: Fuel upgrading studies
[NASA-CR-165326-VOL-3] p 178 N83-22754
Fuel quality/processing study, Volume 4: On site processing studies
[NASA-CR-165326-VOL-4] p 179 N83-22755
JONES, H. F.
Analysis of spiral-groove face seals for liquid oxygen
[ASLE PREPRINT 83-AM-4B-2] p 138 A83-43339
JONES, W. H.
Parallel, Asynchronous Executive (PAX): System concepts, facilities, and architecture
[NASA-TP-2179] p 189 N83-28921
JONES, W. J.
Advanced axial field D.C. motor development for electric passenger vehicle
[NASA-CR-167985] p 117 N83-30914
JONES, W. R.
Preliminary results of the comparison of the electrochemical behavior of a thioether and biphenyl
[NASA-TM-83450] p 87 N83-34015
JONES, W. R., JR.
Infrared emission spectrophotometric study of the changes produced by TiN coating of metal surfaces in an operating EHD contact
[ASLE PREPRINT 82-LC-3C-3] p 135 A83-13229
Tribological characteristics of nitrogen (N+) implanted iron p 75 A83-37824
Ferrographic and spectrometer oil analysis from a failed gas turbine engine
[NASA-TM-82956] p 140 N83-12433
Infrared emission spectrophotometric study of the changes produced by TiN coating of metal surfaces in an operating EHD contact
[NASA-TM-82989] p 92 N83-15466
Analysis of a MIL-L-27502 lubricant from a gas-turbine engine test by size-exclusion chromatography
[NASA-TP-2063] p 93 N83-16528
Surface profile changes of scuffed bearing surfaces
[NASA-TM-83055] p 82 N83-17682
Wear particle analysis using the ferrograph
[NASA-TM-83422] p 96 N83-28243
Tribological measurements on a Charnley-type artificial hip joint
[NASA-TM-83440] p 97 N83-32943
The effects of metals and inhibitors on thermal oxidative degradation reactions of unbranched perfluoroalkylethers
[NASA-TM-83464] p 97 N83-34049
A review of liquid lubricant thermal/oxidative degradation
[NASA-TM-83465] p 98 N83-35143
JOSHI, M. C.
Sound propagation in segmented exhaust ducts - Theoretical predictions and comparison with measurements
[AIAA PAPER 83-0734] p 194 A83-28016
JOSLYN, H. D.
Axial compressor middle stage secondary flow study
[NASA-CR-3701] p 14 N83-29174
JOU, W.-H.
An experience in mesh generation for three-dimensional calculation of potential flow around a rotating propeller p 5 A83-36798
Finite volume calculation of three-dimensional potential flow around a propeller p 7 A83-45577
JUDGE, R. J. R.
Development of electrical test procedures for qualification of spacecraft against EID. Volume 1: The CAN test and other relevant data
[NASA-CR-165590] p 49 N83-12136
JUHASZ, A. J.
Methods of reducing energy consumption of the oxidant supply system for MHD/steam power plants
[AIAA PAPER 83-0468] p 203 A83-16735
Methods of reducing energy consumption of the oxidant supply system for MHD/steam power plants
[NASA-TM-83025] p 168 N83-13589

K

KAHN, E. B.
Effects of specimen resonances on acoustic-ultrasonic testing
[NASA-CR-3679] p 153 N83-21373
KAMATH, G. S.
GaAs solar cells for concentrator systems in space p 171 N83-15820
KAMI, S.
Status of the J-series 30-cm mercury ion thruster
[AIAA PAPER 82-1904] p 51 A83-12479
Advanced-technology 30-cm-diameter mercury ion thruster
[AIAA PAPER 82-1910] p 51 A83-12484
Analysis and design of ion thruster for large space systems
[NASA-CR-165140] p 57 N83-14158
Design, fabrication and testing of porous tungsten vaporizers for mercury ion thrusters
[NASA-TM-83063] p 58 N83-22318
KAMOTANI, Y.
An experimental study of heat induced surface-tension driven flow p 44 A83-43269
KAMOULAKOS, A.
Stability analysis of flexible wind turbine blades using finite element method
[NASA-CR-168107] p 177 N83-21508
KANG, D.
A new formulation of hybrid/mixed finite element p 155 A83-12739
KAPOOR, V. J.
Planar multijunction high voltage solar cell chip p 163 A83-13923
KARCHMER, A.
The influence of inlet design on the aeroacoustic performance of a JT15D turbofan engine as measured in the NASA-Ames 40 x 80 foot wind tunnel
[AIAA PAPER 83-0681] p 21 A83-28006
KARCHMER, A. M.
Acoustic modal analysis of a full-scale annular combustor
[AIAA PAPER 83-0760] p 196 A83-33486
Acoustic modal analysis of a full-scale annular combustor
[NASA-TM-83334] p 200 N83-21896
Acoustical modal analysis of the pressure field in the tailpipe of a turbofan engine
[NASA-TM-83387] p 201 N83-25499
KARP, A.
Design concepts for a high-impedance narrow-band 42 GHz power TWT using a fundamental/forward ladder-based circuit
[NASA-CR-165282] p 114 N83-12330
KASPER, H. J.
Cryogenic fluid management experiment trunnion fatigue verification
[AIAA PAPER 83-0911] p 49 A83-32782
KASUBA, R.
A method for static and dynamic load analysis of standard and modified spur gears p 146 N83-20143
Dynamic effects of internal spur gear drives
[NASA-CR-3692] p 149 N83-28452
KATSANIS, T.
Applications of the contravariant form of the Navier-Stokes equations
[NASA-TM-83448] p 14 N83-29179
KATZ, I.
Potentials on large spacecraft in LEO p 49 A83-17489
Space Shuttle Orbiter charging p 49 A83-20415
KAUFELD, J.
Advanced Gas Turbine (AGT) powertrain system
[NASA-CR-165346] p 139 N83-11497
KAUFMAN, A.
Nonlinear structural and life analyses of a combustor liner p 155 A83-12764
Turbine blade nonlinear structural and life analysis p 21 A83-29024
Materials constitutive models for nonlinear analysis of thermally cycled structures
[NASA-TP-2055] p 158 N83-12449
Develop and test fuel cell powered on-site integrated total energy system
[NASA-CR-168020] p 173 N83-15839
Evaluation of inelastic constitutive models for nonlinear structural analysis p 162 N83-34357
Simplified method for nonlinear structural analysis
[NASA-TP-2208] p 163 N83-34372
KAUFMAN, H. R.
Ion flow experiments in a multipole discharge chamber
[AIAA PAPER 82-1930] p 203 A83-14398
Inert gas thruster technology p 53 A83-20423
Industrial ion source technology
[NASA-CR-159877] p 102 N83-12259
Electric thruster research
[NASA-CR-168134] p 59 N83-32843
KAUSHAL, D.
Planning assistance for the 30/20 GHz program, volume 1
[NASA-CR-165484-VOL-1] p 108 N83-33010
Planning assistance for the 30/20 GHz program, volume 2
[NASA-CR-165484-VOL-2] p 108 N83-33011
Planning assistance for the 30/20 GHz program, volume 3
[NASA-CR-165484] p 108 N83-33012
Satellite provided fixed communication services: A forecast of potential domestic demand through the year 2000. Volume 1: Executive summary
[NASA-CR-168145] p 108 N83-34113
Satellite provided customer premises services: A forecast of potential domestic demand through the year 2000. Volume: Executive summary
[NASA-CR-168142] p 109 N83-34116
Satellite provided customer premise services: A forecast of potential domestic demand through the year 2000. Volume 3: Appendices
[NASA-CR-168144] p 109 N83-34118
KAZA, K. R. V.
Bending-torsion flutter of a highly swept advanced turboprop
[NASA-TM-82975] p 158 N83-11514
Effects of structural coupling on mistuned cascade flutter and response
[NASA-TM-83049] p 159 N83-15672
KECK, J. C.
Turbulent flame propagation and combustion in spark ignition engines p 70 A83-48156
KEITH, T. G., JR.
Investigation of the effects of initial fluid film profile on pumping ring operation
[ASME PAPER 82-LUB-35] p 136 A83-13516
Thermoelastohydrodynamic analysis of an oil pumping ring seal p 137 A83-22322
KELKAR, S. S.
A novel input filter compensation scheme for switching regulators p 111 A83-11494
A novel feedforward compensation canceling input filter-regulator interaction p 112 A83-33133
KELLER, L. E.
Infrared emission spectrophotometric study of the changes produced by TiN coating of metal surfaces in an operating EHD contact
[ASLE PREPRINT 82-LC-3C-3] p 135 A83-13229
Infrared emission spectrophotometric study of the changes produced by TiN coating of metal surfaces in an operating EHD contact
[NASA-TM-82989] p 92 N83-15466
Determination of physical and chemical states of lubricants in concentrated contacts, part 3
[NASA-CR-3658] p 92 N83-16527
KENDALL, B. R. F.
Mass analysis of neutral particles and ions released during electrical breakdowns on spacecraft surfaces
[NASA-CR-170299] p 50 N83-23347
KENEHAN, J. G.
Scaled centrifugal compressor, collector and running gear program
[NASA-CR-168167] p 40 N83-30432
KERBER, R.
Measurements of energy distribution and thrust for microwave plasma coupling of electrical energy to hydrogen for propulsion
[AIAA PAPER 82-1951] p 52 A83-12508
Microwave plasma generation of hydrogen atoms for rocket propulsion p 53 A83-13090
KERSCHEN, E. J.
Incidence angle effects on convected gust airfoil noise
[AIAA PAPER 83-0765] p 195 A83-28022
Noise generation by a finite span swept airfoil
[AIAA PAPER 83-0768] p 195 A83-28023
KERSLAKE, W. R.
Rail accelerator research at Lewis Research Center
[AIAA PAPER 82-1938] p 53 A83-22075
Rail accelerator research at Lewis Research Center
[NASA-TM-83015] p 56 N83-12143
The LeRC rail accelerators: Test designs and diagnostic techniques
[NASA-TM-83496] p 60 N83-35053
KESHOCK, E. G.
'Scaling' analysis of the ice accretion process on aircraft surfaces
[ASME PAPER 82-WA/HT-39] p 16 A83-25693
KHADER, N.
Natural frequency of rotating beams using non-rotating modes p 156 A83-18383
Structural dynamics studies of rotating bladed-disk assemblies coupled with flexible shaft motions
[AIAA PAPER 83-0919] p 22 A83-32787

KHALIGHI, B.
The finite analytic method, volume 3
[NASA-CR-170186] p 191 N83-23087
KHAN, A. A.
Minority carrier diffusion length measurements - A review and comparison of techniques p 205 A83-28448
Interfacial electrical properties of ion-beam sputter deposited amorphous carbon on silicon p 205 A83-33920
Diffusion length measurements in solar cells: An analysis and comparison of techniques p 171 N83-15812
KIDWELL, G. H., JR.
Supersonic STOVL research aircraft
[SAE PAPER 821375] p 17 A83-37965
KIELB, R. E.
Bending-torsion flutter of a highly swept advanced turboprop
[NASA-TM-82975] p 158 N83-11514
Effects of structural coupling on mistuned cascade flutter and response
[NASA-TM-83049] p 159 N83-15672
KIM, B.
GaAs integrated digital-to-analogue convertor for control of power dual-gate FETs p 112 A83-36479
Equivalent-circuit consideration of dual-gate MESFETs at high frequency p 113 A83-44970
KIM, W. S.
Evaluation of ultraviolet spectrophotometry for simultaneous analysis of alkylbenzenes, alkylnaphthalenes, alkylanthracenes/phenanthrenes and total aromatics in mid-distillate fuels
[NASA-TM-83032] p 99 N83-15483
KIMBLE, K. R.
Influence of multidroplet size distribution on icing collection efficiency
[AIAA PAPER 83-0110] p 187 A83-16526
KINDLIMANN, L.
Cast Fe-base cylinder/regenerator housing alloy
[NASA-CR-169474] p 80 N83-12214
KING, R. J.
Transformer induced instability of the series resonant converter p 113 A83-41152
KINGLER, T. A.
Alternatives for jet engine control
[NASA-CR-170100] p 33 N83-20945
KINGSBURY, E.
Pivoting and slip in an angular contact bearing
[NASA-TM-83408] p 148 N83-26079
KINGSLEY, J. D.
Analysis, design, fabrication and testing of an optical tip clearance sensor
[NASA-CR-165265] p 26 N83-11127
KIRALY, L. J.
Piezoelectric composite materials
[NASA-CASE-LEW-12582-1] p 207 N83-34796
KIRKPATRICK, C. G.
Liquid encapsulated Czochralski growth of low dislocation GaAs p 204 A83-13784
Advances in large-diameter liquid encapsulated Czochralski GaAs p 171 N83-15819
High purity, low dislocation GaAs single crystals
[NASA-CR-168098] p 206 N83-19622
KISNER, L. S.
Computer program to predict noise of general aviation aircraft: User's guide
[NASA-CR-168050] p 198 N83-17242
KLANN, J. L.
Assessment of alternative power sources for mobile mining machinery
[NASA-TM-82695] p 169 N83-14691
KLECKNER, R. J.
High speed spherical roller-bearing analysis and comparison with experimental performance p 145 N83-20133
KLIMA, S. J.
Evaluation of electrode shape and nondestructive evaluation method for welded solar cell interconnects
[NASA-TM-82966] p 166 N83-10555
Evaluation of solar cell welds by scanning acoustic microscopy p 172 N83-15834
KLIMAN, G. B.
Advanced AC permanent magnet axial flux disc motor for electric passenger vehicle
[NASA-CR-167975] p 115 N83-16628
KLINE, A.
Satellite switched FDMA advanced communication technology satellite program
[NASA-CR-168034] p 105 N83-15543
KLINE, J. F.
Incidence loss for fan turbine rotor blade in two-dimensional cascade
[NASA-TP-2188] p 39 N83-30431
KNAPP, W. D.
Performance degradation and cleaning of photovoltaic arrays p 164 A83-27236
KNECHTLI, R. C.
GaAs solar cells for concentrator systems in space p 171 N83-15820
KNIP, G.
Technology and benefits of aircraft counter rotation propellers
[NASA-TM-82983] p 27 N83-11129
KNORR, R. J.
Life and reliability models for helicopter transmissions
[NASA-TM-82976] p 139 N83-10425
KNOTT, P. R.
Free-jet acoustic investigation of high-radius-ratio coannular plug nozzles. Comprehensive data report, volume 1
[NASA-CR-168086-VOL-1] p 198 N83-18408
Free-jet acoustic investigation of high-radius-ratio coannular plug nozzles. Comprehensive data report, volume 2
[NASA-CR-168086-VOL-2] p 199 N83-18409
KNUTSON, W. K.
Evaluation of fuel additives for reduction of material imcompatibilities in methanol-gasoline blends
[NASA-CR-168061] p 86 N83-29359
KOCUR, J. A.
Aerodynamic stiffness of an unbound eccentric whirling centrifugal impeller with an infinite number of blades p 142 N83-15650
KOEPLIN, S. M.
High-voltage spark atomic emission detector for gas chromatography p 67 A83-13108
KOFFEL, W. K.
Tip cap for a rotor blade
[NASA-CASE-LEW-13654-1] p 30 N83-14129
KOFSKEY, M. G.
Effects of interstage diffuser flow distortion on the performance of a 15.41-centimeter tip diameter axial power turbine
[AIAA PAPER 83-1179] p 23 A83-36263
Effects of interstage diffuser flow distortion on the performance of a 15.41-centimeter tip diameter axial power turbine
[NASA-TM-83359] p 35 N83-24505
KOHL, F. J.
Combustion system processes leading to corrosive deposits p 69 A83-42246
Reactions of NaCl with gaseous SO3, SO2, and O2
[NASA-TM-83423] p 86 N83-29358
Effect of the amount of Na2SO4 on the high temperature corrosion of Udimet-700
[NASA-TM-83459] p [illegible] N83-34016
KOHLMAN, D. L.
A method of predicting flow rates required to achieve anti-icing performance with a porous leading edge ice protection system
[NASA-CR-169996] p 17 N83-19738
A method of predicting flow rates required to achieve anti-icing performance with a porous leading edge ice protection system
[NASA-CR-168213] p 17 N83-32782
KOLECKI, J. C.
Microhardness studies on thin carbon films grown on P-type, (100) silicon
[NASA-TM-82980] p 61 N83-13169
KONARSKI, M.
Conceptual design, evaluation and research identification for Remote Augmented Propulsive Lift Systems (RALS) with ejectors for VTOL aircraft
[NASA-CR-167906] p 29 N83-13103
KORDES, R.
Advanced Gas Turbine (AGT) powertrain system
[NASA-CR-165346] p 139 N83-11497
KOSMAHL, H.
Space tubes: A major challenge
[NASA-TM-82971] p 113 N83-11447
KOSMAHL, H. G.
Modern multistage depressed collectors - A review p 112 A83-24025
Tubes in space - Very much alive p 112 A83-28160
Multi-stage Depressed Collectors (MDC) for efficiency improvements of UHF broadcast klystrons
[NASA-TM-82970] p 105 N83-10322
Dielectric based submillimeter backward wave oscillator circuit
[NASA-CASE-LEW-13736-1] p 115 N83-17802
A study of 60 Gigahertz intersatellite link applications
[NASA-TM-83337] p 47 N83-20994
A linearized traveling wave amplifier with hard limiter characteristics
[NASA-CASE-LEW-13961-1] p 116 N83-25984
Experimental verification of the multistage depressed collector design procedure for a high-perveance, helix-type, traveling-wave tube
[NASA-TP-2162] p 116 N83-25985
Space power tubes - very much alive
[NASA-TM-83425] p 107 N83-28295
Gyrotron transmitting tube
[NASA-CASE-LEW-13429-1] p 117 N83-31952
KOSMATKA, J.
The development of a generalized advanced propeller analysis system
[AIAA PAPER 83-2466] p 26 A83-49581
KOT, R. C.
Advanced digital modulation: Communication techniques and monolithic GaAs technology
[NASA-CR-174452] p 109 N83-36299
KOZAK, A. A.
Experimental evaluation of inlet turbulence, wall boundary layer, surface finish, and fillet radius on small axial turbine state performance
[SAE PAPER 821475] p 24 A83-38001
KRAFT, R. E.
Sound propagation in segmented exhaust ducts - Theoretical predictions and comparison with measurements
[AIAA PAPER 83-0734] p 194 A83-28016
KRAIMECHE, B.
Comparison of channel assignment techniques for hybrid switching p 104 A83-41363
Next generation communications satellites: multiple access and network studies
[NASA-CR-167903] p 45 N83-12129
KRATOCHVIL, D.
Satellite provided fixed communication services: A forecast of potential domestic demand through the year 2000. Volume 1: Executive summary
[NASA-CR-168145] p 108 N83-34113
Satellite provided fixed communications services: A forecast of potential domestic demand through the year 2000: Volume 2: Main test
[NASA-CR-168146] p 108 N83-34114
Satellite fixed communications service: A forecast of potential domestic demand through the year 2000. Volume 3: Appendices
[NASA-CR-168147] p 108 N83-34115
Satellite provided customer premises services: A forecast of potential domestic demand through the year 2000. Volume: Executive summary
[NASA-CR-168142] p 109 N83-34116
Satellite provided customer premise services: A forecast of potential domestic demand through the year 2000. Volume 3: Appendices
[NASA-CR-168144] p 109 N83-34118
KRATZER, R. H.
The effects of metals and inhibitors on thermal oxidative degradation reactions of unbranched perfluoroalkylethers
[NASA-TM-83464] p 97 N83-34049
KRAUTER, A. I.
Digital system for structural dynamics simulation
[NASA-CR-168019] p 43 N83-14139
KREBSCHULL, K.
Aircraft measurements of trace gases and particles near the tropopause
[NASA-CR-3691] p 188 N83-27542
KREJSA, E. A.
Pressure transfer function of a JT15D nozzle due to acoustic and convected entropy fluctuations p 193 A83-16319
Application of 3-signal coherence to core noise transmission
[AIAA PAPER 83-0759] p 194 A83-28021
Cross spectra between temperature and pressure in a constant area duct downstream of a combustor
[AIAA PAPER 83-0762] p 196 A83-33487
Correlation of core noise obtained by three signal coherence techniques
[NASA-TM-83012] p 197 N83-12966
Application of 3-signal coherence to core noise transmission
[NASA-TM-83333] p 200 N83-23114
Cross spectra between temperature and pressure in a constant area duct downstream of a combustor
[NASA-TM-83351] p 200 N83-23116
Acoustical modal analysis of the pressure field in the tailpipe of a turbofan engine
[NASA-TM-83387] p 201 N83-25499
KROEGER, E.
Design, fabrication and testing of porous tungsten vaporizers for mercury ion thrusters
[NASA-TM-83063] p 58 N83-22318
KUBASCO, A. J.
Combustion characteristics of hydrogen-carbon monoxide based gaseous fuels p 67 A83-11491
Combustion characteristics of hydrogen, Carbon monoxide based gaseous fuels
[NASA-TM-82998] p 167 N83-10560
KUCHAR, A. P.
Scale model performance test investigation of mixed flow exhaust systems for an energy efficient engine /E3/ propulsion system
[AIAA PAPER 83-0541] p 20 A83-16776

KUNTZ, H. L., II
High-intensity sound in air saturated fibrous bulk porous materials
[NASA-CR-167979] p 197 N83-12967
KURKOV, A. P.
Measurements of self-excited rotor-blade vibrations using optical dispacements
[NASA-TM-82953] p 159 N83-14523
KUTLER, P.
Prediction of high speed propeller flow fields using a three-dimensional Euler analysis
[AIAA PAPER 83-0188] p 4 A83-29535
User's manual for three-dimensional analysis of propeller flow fields
[NASA-CR-167959] p 12 N83-18671
Prediction of high speed propeller flow fields using a three-dimensional Euler analysis
[NASA-TM-83065] p 12 N83-19710
KWATRA, S. C.
A new architecture for adaptive transform compression of NTSC composite video signal p 103 A83-19732

L

LAFLEN, J. H.
Requirements of constitutive models for two nickel-base superalloys p 74 A83-21071
Turbine blade nonlinear structural and life analysis p 21 A83-29024
LAGACE, L. J.
Digital system for structural dynamics simulation
[NASA-CR-168019] p 43 N83-14139
LAGOW, R. J.
Preparation, characterization, physical testing and performance of flurocarbon membranes and separators
[NASA-CR-169756] p 71 N83-16418
Preparation, characterization, physical testing and performance of fluorocarbon membranes and separators
[NASA-CR-167880] p 73 N83-26936
LAGOWSKI, J.
Microdistribution of oxygen in silicon and its effects on electronic properties p 172 N83-15825
LAKSHMANA RAO, N. S.
The initial stages of cavitation damage and erosion on copper and brass tested in a rotating disk device p 75 A83-27421
Dynamics and mechanism of cavitation erosion on perspex and epoxy resin tested in a rotating disk device p 89 A83-27422
LAKSHMINARAYANA, B.
Development of secondary flow and vorticity in curved ducts, cascades, and rotors, including effects of viscosity and rotation p 119 A83-16141
A turbulence model for three dimensional turbulent shear flows over curved rotating bodies
[AIAA PAPER 83-0559] p 120 A83-16787
Blade loading and rotation effects on compressor rotor wake near end walls p 3 A83-22138
Investigation of the tip clearance flow inside and at the exit of a compressor rotor passage. II - Turbulence properties p 4 A83-28843
Tip clearance flow in a compressor rotor passage at design and off-design conditions p 4 A83-35855
Experimental study of the boundary layer on a turbomachinery rotor blade p 7 A83-47022
Wall boundary layer development near the tip region of an IGV of an axial flow compressor
[ASME PAPER 83-GT-171] p 8 A83-47972
End wall flows in rotors and stators of a single stage compressor
[NASA-CR-169800] p 128 N83-16678
Three dimensional flow field inside compressor rotor, including blade boundary layers
[NASA-CR-169788] p 128 N83-16679
End wall flow characteristics and overall performance of an axial flow compressor stage
[NASA-CR-3671] p 13 N83-26819
LAMBERT, R. F.
Propagation of sound in highly porous open-cell elastic foams p 195 A83-28848
Surface acoustic admittance of highly porous open-cell, elastic foams p 195 A83-28849
LAMPE, R. F.
The MOD-OA 200 kilowatt wind turbine generator design and analysis report
[NASA-CR-165127] p 174 N83-16859
LAN, B.
Oxidation and formation of deposit precursors in hydrocarbon fuels
[NASA-CR-168121] p 101 N83-23465
LANGER, D.
Ellipsometric study of silicon nitride on gallium arsenide p 204 A83-11812
LANGSTON, L. S.
A new surface-streamline flow-visualization technique p 133 A83-19016
Turbine endwall single cylinder program
[NASA-CR-170008] p 44 N83-19761
LAPRAD, R. F.
Sensor failure detection for jet engines
[NASA-CR-168190] p 154 N83-33182
LARK, R. F.
Construction of low-cost, Mod-OA wood composite wind turbine blades
[NASA-TM-83046] p 174 N83-16857
Fabrication of low-cost Mod-OA wood composite wind turbine blades
[NASA-TM-83323] p 182 N83-27347
LARK, R. L.
Hygrothermomechanical evaluation of transverse filament tape epoxy/polyester fiberglass composites
[NASA-TM-83044] p 65 N83-15362
LARSON, F.
Cast Fe-base cylinder/regenerator housing alloy
[NASA-CR-169474] p 80 N83-12214
LARSON, L. A.
Interfacial layers in high-temperature-oxidized NiCrAl p 77 A83-44619
LARSON, V. H.
Computation techniques and computer programs to analyze Stirling cycle engines using characteristic dynamic energy equations p 207 A83-27272
A study of dynamic energy equations for Stirling cycle analysis
[NASA-CR-168152] p 181 N83-25043
LARUE, J. C.
Modified gauge for time-resolved skin-friction measurements p 133 A83-14172
LARUE, R. A.
Single and multijunction space solar cells grown by organometallic vapor phase epitaxy /OM-VPE/ p 164 A83-27260
Progress toward cascade cells made by OM-VPE p 171 N83-15813
LASAGNA, P. L.
A preliminary comparison between the SR-6 propeller noise in flight and in a wind tunnel
[NASA-TM-83341] p 201 N83-24287
LATOS, T. S.
Improved SCR ac motor controller for battery powered urban electric vehicles
[NASA-CR-167919] p 209 N83-16257
LAU, S. K.
Advanced ceramic coating development for industrial/utility gas turbine applications
[NASA-CR-165619] p 92 N83-15467
LAUER, J. L.
Infrared emission spectrophotometric study of the changes produced by TiN coating of metal surfaces in an operating EHD contact
[ASLE PREPRINT 82-LC-3C-3] p 135 A83-13229
Microscopic contour changes of tribological surfaces by chemical and mechanical action
[ASLE PREPRINT 82-LC-3B-3] p 136 A83-13237
Infrared emission spectrophotometric study of the changes produced by TiN coating of metal surfaces in an operating EHD contact
[NASA-TM-82989] p 92 N83-15466
Determination of physical and chemical states of lubricants in concentrated contacts, part 3
[NASA-CR-3658] p 92 N83-16527
Surface profile changes of scuffed bearing surfaces
[NASA-TM-83055] p 82 N83-17682
LAUVER, R. W.
Chemical approach for controlling nadamide cure temperature and rate
[NASA-CASE-LEW-13770-1] p 91 N83-13258
Chemical approach for controlling nadamide cure temperature and rate
[NASA-CASE-LEW-13770-2] p 96 N83-30651
LAWLER, D.
Comparison of NDE techniques for sintered-SiC components p 152 A83-22265
LAWRENCE, M. F.
Energy and precious fuels requirements of fuel alcohol production, volume 1
[NASA-CR-168090] p 183 N83-28581
LECREN, R. T.
Combustion characteristics of hydrogen-carbon monoxide based gaseous fuels p 67 A83-11491
Combustion characteristics of hydrogen. Carbon monoxide based gaseous fuels
[NASA-TM-82998] p 167 N83-10560
LECUYER, M. R.
Stagnation region gas film cooling: Effects of dimensionless coolant temperature
[NASA-CR-168197] p 132 N83-30960
LEE, A. H.
Experiments on identification and control of inflow disturbances in contracting streams
[NASA-CR-169831] p 11 N83-17503
LEE, D.
Rotor redesign for a highly loaded 1800 ft/sec tip speed fan. 3: Laser Doppler velocimeter report
[NASA-CR-167954] p 30 N83-14128
LEE, F. C.
Investigations of stability and dynamic performances of switching regulators employing current-injected control p 110 A83-11002
Nonlinear program based optimization of boost and buck-boost converter designs p 110 A83-11016
A novel input filter compensation scheme for switching regulators p 111 A83-11494
An improved switching converter model using discrete and average techniques p 111 A83-11495
A novel feedforward compensation canceling input filter-regulator interaction p 112 A83-33133
LEE, J. K.
Vibrations of cantilevered circular cylindrical shells Shallow versus deep shell theory p 157 A83-36958
Vibrations of cantilevered doubly-curved shallow shells p 157 A83-39557
Vibrations of blades with variable thickness and curvature by shell theory
[ASME PAPER 83-GT-152] p 158 A83-47978
LEE, K.
Design of hydraulic output Stirling engine
[NASA-CR-167976] p 177 N83-22739
LEE, S. S.
Effects of specimen resonances on acoustic-ultrasonic testing
[NASA-CR-3679] p 153 N83-21373
Ultrasonic attenuation of a void-containing medium for very long wavelengths
[NASA-CR-3693] p 154 N33-28466
LEE, S. Y.
Advanced ceramic coating development for industrial/utility gas turbine applications
[NASA-CR-165619] p 92 N83-15467
LEE, Y. M.
Transient flow analysis of the AEDC/HPDE MHD generator
[AIAA PAPER 83-0395] p 203 A83-16691
LEGG, J.
20 x 20 IF switch matrix for SS-TDMA systems p 113 A83-41369
LEISSA, A.
On the three-dimensional vibrations of the cantilevered rectangular parallelepiped p 157 A83-37729
LEISSA, A. W.
Vibrations of cantilevered circular cylindrical shells Shallow versus deep shell theory p 157 A83-36958
Vibrations of cantilevered doubly-curved shallow shells p 157 A83-39557
Vibrations of blades with variable thickness and curvature by shell theory
[ASME PAPER 83-GT-152] p 158 A83-47978
LEMASCON, A.
A study of the stress wave factor technique for the characterization of composite materials
[NASA-CR-3670] p 153 N83-27248
LENAHAN, D. T.
Air modulation apparatus
[NASA-CASE-LEW-13524-1] p 131 N83-30957
LEPICOVSKY, J.
Noise and flow structure of a tone-excited jet p 192 A83-13136
Tone-excited jet: Theory and experiments
[NASA-CR-3538] p 197 N83-12968
LEROY, B. E.
Satellite-aided land mobile communications system implementation considerations p 104 A83-41417
LESTER, H. L.
Mobile radio alternative systems study, executive summary
[NASA-CR-168207] p 109 N83-34119
LESTZ, S. S.
Performance and emissions characteristics of aqueous alcohol fumes in a DI diesel engine
[NASA-CR-167917] p 99 N83-12250
Fumigation of alcohol in a light duty automotive diesel engine
[NASA-CR-167915] p 99 N83-13272
LEVI, E.
Preliminary assessment of the tradeoffs between the electric motor and the transmission in electric vehicles
[NASA-CR-168199] p 117 N83-30915
LEVINE, S. R.
A new diffusion-inhibited oxidation-resistant coating for superalloys p 74 A83-10299
Improved performance thermal barrier coatings p 90 A83-42261

Further industrial tests of ceramic thermal barrier coatings
[NASA-TP-2057] p 26 N83-10045
Turbine engine materials durability research p 29 N83-12163
Coating with overlay metallic-cermet alloy systems
[NASA-CASE-LEW-13639-2] p 82 N83-17683
Thermal-barrier coatings for utility gas turbines
[NASA-TM-83549] p 95 N83-27022

LEVIS, C. A.
Engineering calculations for communications systems planning
[NASA-CR-170182] p 106 N83-22494

LEZBERG, E. A.
Aircraft sampling of the sulfate layer near the tropopause following the eruption of Mount St. Helens p 187 N83-11556

LI, C. J.
Classification of journal surfaces using surface topography parameters and software methods to compensate for stylus geometry
[NASA-CR-168153] p 148 N83-24857

LIBBY, P. A.
Modified gauge for time-resolved skin-friction measurements p 133 A83-14172

LIEBERT, C. H.
Further industrial tests of ceramic thermal barrier coatings
[NASA-TP-2057] p 26 N83-10045
Measured and calculated wall temperatures on air-cooled turbine vanes with boundary layer transition
[NASA-TM-83030] p 127 N83-14432
Covering solid, film cooled surfaces with a duplex thermal barrier coating
[NASA-CASE-LEW-13450-1] p 103 N83-35177

LIEBLEIN, S.
Design and evaluation of low-cost laminated wood composite blades for intermediate size wind turbines: Blade design, fabrication concept, and cost analysis
[NASA-CR-165463] p 179 N83-23704

LIERZER, J. R.
Atmospheric radiation model for water surfaces
[NASA-CR-167873] p 187 N83-21677

LILLEY, D. G.
Five-hole pitot probe time-mean velocity measurements in confined swirling flows
[AIAA PAPER 83-0315] p 119 A83-16645
Confined swirling flow predictions
[AIAA PAPER 83-0316] p 119 A83-16646
Mean flowfields in axisymmetric combustor geometries with swirl p 120 A83-24668
A basic code for the prediction of transient three-dimensional turbulent flowfields p 121 A83-27412
Single-wire swirl flow turbulence measurements
[AIAA PAPER 83-1202] p 122 A83-36278
The performance of an annular vane swirler
[AIAA PAPER 83-1326] p 24 A83-36340

LIN, A.
Numerical analysis of turbulent coaxial flow with internal heat generation
[NASA-CR-172633] p 132 N83-33105

LIN, I.
Unsteady turbulent shear flow in shock tube discontinuities p 124 A83-46445

LING, J. S.
Single cell performance studies on the Fe/Cr Redox Energy Storage System using mixed reactant solutions at elevated temperature
[NASA-TM-83385] p 180 N83-25042

LINSCOTT, B. S.
DOE large horizontal axis wind turbine development at NASA Lewis Research Center
[NASA-TM-83444] p 184 N83-31107

LIPNER, M. H.
The MOD-0A 200 kilowatt wind turbine generator design and analysis report
[NASA-CR-165127] p 174 N83-16859

LITTLE, B. H., JR.
Inlet design for high-speed propfans
[SAE PAPER 821359] p 5 A83-37957

LITVIN, F. L.
Spiral-bevel geometry and gear train precision p 146 N83-20139

LIU, C. C.
Experimental study of electrochemical fluorination of trichloroethylene p 68 A83-15870
The electrochemical fluorination of polymeric materials for high energy density aqueous and non-aqueous battery and fuel cell separators
[NASA-CR-167961] p 72 N83-21056

LIU, D.
Ellipsometric study of silicon nitride on gallium arsenide p 204 A83-11812

LIU, D. C.
An enhanced sensitivity null ellipsometry technique for studying films on substrates - Application to silicon nitride on gallium arsenide p 206 A83-37618

LIU, N. S.
Numerical solutions of Navier-Stokes equations for compressible turbulent two/three dimensional flows in terminal shock region of an inlet/diffuser
[NASA-CR-3723] p 132 N83-34230

LIU, N.-S.
Numerical solution of the Navier-Stokes equations for compressible turbulent two/three dimensional flows in the terminal shock region of an inlet/diffuser
[AIAA PAPER 83-1892] p 5 A83-39358

LIVER, P.
Measurements of compressible secondary flow in a circular S-duct
[AIAA PAPER 83-1739] p 4 A83-37218

LOEFFLER, I. J.
Farfield inflight measurements of high-speed turboprop noise
[AIAA PAPER 83-0745] p 21 A83-25947
Farfield inflight measurement of high-speed turboprop noise
[NASA-TM-83327] p 199 N83-21895

LOEWENTHAL, S. H.
Rolling-element fatigue life with traction fluids and automatic transmission fluid in a high-speed rolling-contact rig
[NASA-TP-2050] p 140 N83-13457
Traction behavior of two traction lubricants
[NASA-TM-83311] p 144 N83-20116
A historical perspective of traction drives and related technology p 144 N83-20123
Evaluation of a high performance, fixed-ratio, traction drive p 145 N83-20135
Sizing criterial for traction drives p 146 N83-20137
Comparison of spur gear efficiency prediction methods p 146 N83-20141
Regression analysis of traction characteristics of traction fluids
[NASA-TP-2154] p 148 N83-24862
Advances in traction drive technology
[NASA-TM-83397] p 150 N83-28455

LOEWY, R. G.
Natural frequency of rotating beams using non-rotating modes p 156 A83-18383
Structural dynamics studies of rotating bladed-disk assemblies coupled with flexible shaft motions
[AIAA PAPER 83-0919] p 22 A83-32787

LOGAN, W. R.
Improved uniformity of multiphase ceramic-metal plasma-sprayed coats p 61 A83-22269
Creep of plasma-sprayed-ZrO2 thermal-barrier coatings p 89 A83-22273
Plasma-sprayed self-lubricating coatings
[NASA-CR-3680] p 94 N83-22422
Creep of plasma sprayed zirconia
[NASA-CR-167868] p 96 N83-29393

LOHMANN, R. P.
Broad specification fuels technology program, phase 1
[NASA-CR-168180] p 74 N83-30551

LOO, R. Y.
GaAs solar cells for concentrator systems in space p 171 N83-15820

LOPEZ, I.
Experimental feasibility study of a thermoelectric heat flux gage
[NASA-TM-83048] p 134 N83-15602

LORENZO, C. F.
Computer program for a four-cylinder-Stirling-engine controls simulation
[NASA-TM-82774] p 126 N83-12359
A 4-cylinder Stirling engine computer program with dynamic energy equations
[NASA-TM-83053] p 130 N83-26017

LORETH, M.
Study to establish cost predictions for the production of Redox chemicals
[NASA-CR-167882] p 176 N83-20359

LOW, C. A., JR.
Software and system level tests of a test flight mercury ion thruster subsystem
[AIAA PAPER 82-1912] p 51 A83-12485

LOWELL, C. E.
Cyclic oxidation of superalloys p 76 A83-42234
Burner rig study of variables involved in hole plugging of air cooled turbine engine vanes
[NASA-TM-83308] p 83 N83-19887
Critical research and advanced technology (CRT) support project
[NASA-TM-83019] p 176 N83-20361
Improved nickel base coating alloy
[NASA-CASE-LEW-13834-1] p 85 N83-24639

LOWRY, S.
An experimental study of heat induced surface-tension driven flow p 44 A83-43269

LUBOMSKI, J. F.
Bending-torsion flutter of a highly swept advanced turboprop
[NASA-TM-82975] p 158 N83-11514

LUCAS, J. G.
Low flight speed acoustic results for a supersonic inlet with auxiliary inlet doors
[AIAA PAPER 83-1415] p 196 A83-45517
Low flight speed acoustic results for a supersonic inlet with auxiliary inlet doors
[NASA-TM-83411] p 201 N83-27794

LUCAS, L. J.
Experimental verification of the Neuber relation at room and elevated temperatures
[NASA-CR-167967] p 159 N83-19121
Experimental verification of the number relation at room and elevated temperatures p 162 N83-34355

LUDEMA, K. C.
Classification of journal surfaces using surface topography parameters and software methods to compensate for stylus geometry
[NASA-CR-168153] p 148 N83-24857

LUDOWISE, M. J.
Single and multijunction space solar cells grown by organometallic vapor phase epitaxy /OM-VPE/ p 164 A83-27260
Use of column V alkyls in organometallic vapor phase epitaxy (OMVPE) p 70 A83-46608
Progress toward cascade cells made by OM-VPE p 171 N83-15813

LUDWIG, L. P.
Multiple plate hydrostatic viscous damper
[NASA-CASE-LEW-13445-2] p 143 N83-17883

LYON, C. A.
Computer program to predict noise of general aviation aircraft: User's guide
[NASA-CR-168050] p 198 N83-17242

LYON, T. F.
NASA clean catalytic combustor program
[ASME PAPER 82-JPGC-GT-11] p 68 A83-25269

LYONS, V. J.
Effect of flameholder pressure drop on emissions and performance of premixed-prevaporized combustors
[NASA-TP-2131] p 35 N83-23309

M

MACARTHUR, C. D.
Numerical simulation of airfoil ice accretion
[AIAA PAPER 83-0112] p 16 A83-36042

MACHLES, G. W.
Auxiliary propulsion requirements for large space systems
[AIAA PAPER 83-1217] p 56 A83-45512
Auxiliary propulsion requirements for large space systems
[NASA-TM-83388] p 58 N83-26922

MACK, J. C.
Large rotorcraft transmission technology development program
[NASA-CR-168120] p 18 N83-22188

MACKALL, K. G.
A preliminary comparison between the SR-6 propeller noise in flight and in a wind tunnel
[NASA-TM-83341] p 201 N83-24287

MACKAY, R. A.
Orientation dependence of the stress rupture properties of Nickel-base superalloy single crystals
[NASA-CR-165394] p 206 N83-13009

MAGENHEIM, B.
Development and test of a Microwave Ice Accretion Measurement Instrument (MIAMI)
[NASA-CR-3598] p 18 N83-14123

MAGLIOZZI, B.
Small transport aircraft technology propeller study
[NASA-CR-168045] p 14 N83-29178

MAHAN, J. R.
Experimental study of the thermal-acoustic efficiency in a long turbulent diffusion-flame burner
[NASA-CR-170003] p 72 N83-19824
Experimental study of the thermal-acoustic efficiency in a long turbulent diffusion-flame burner
[NASA-CR-3725] p 202 N83-33683

MAHISHI, J. M.
Three-dimensional elastoplastic stress analysis of unidirectional boron/aluminum composites
[NASA-CR-169796] p 65 N83-16394

MAJJIGI, R. K.
Free-jet acoustic investigation of high-radius-ratio coannular plug nozzles. Comprehensive data report, volume 1
[NASA-CR-168086-VOL-1] p 198 N83-18408

MALOY, J. E.
Benefits and costs of low thrust propulsion systems
[AIAA PAPER 83-1248] p 49 A83-36306
Auxiliary propulsion requirements for large space systems
[AIAA PAPER 83-1217] p 56 A83-45512
Large space systems auxiliary propulsion requirements
p 46 N83-26864
Auxiliary propulsion requirements for large space systems
[NASA-TM-83388] p 58 N83-26922
MANCINI, J. H.
An overview of advancements in helicopter transmission design p 144 N83-20124
MANDELL, M. J.
Potentials on large spacecraft in LEO
p 49 A83-17489
MANGELS, J. A.
Injection molding ceramics to high green densities
p 137 A83-33515
The effect of silicon particle size on the nitriding behaviour of reaction bonded Si3N4 compacts
p 90 A83-48261
Sintering of reaction bonded silicon nitride
p 90 A83-48270
MANGIAROTTY, R. A.
Tests of a thermal acoustic shield with a supersonic jet p 192 A83-10183
MANSON, S. S.
Relation of cyclic loading pattern to microstructural fracture in creep fatigue
[NASA-TM-83473] p 161 N83-34349
Tensile and compressive constitutive response of 316 stainless steel at elevated temperatures
p 162 N83-34353
MANTENIEKS, M. A.
Extended performance 8-cm mercury ion thruster
[AIAA PAPER 82-1913] p 53 A83-21078
Extended performance 8-cm mercury ion thruster
[NASA-TM-83029] p 57 N83-14157
MANTENIEKS, M. E.
On-orbit propulsion requirements and performance assessment of ion propulsion subsystems for future GEO large satellite missions
[AIAA PAPER 82-1872] p 48 A83-12460
MANZO, M. A.
Cross-linked polyvinyl alcohol films as alkaline battery separators p 68 A83-20576
Polyvinyl alcohol membranes as alkaline battery separators
[NASA-TM-82961] p 70 N83-10135
Polyvinyl alcohol cross-linked with two aldehydes
[NASA-CASE-LEW-13504-1] p 71 N83-13188
Development and evaluation of polyvinyl-alcohol blend polymer films as battery separators
[NASA-TM-82981] p 71 N83-15372
Polyvinyl alcohol battery separator containing inert filler
[NASA-CASE-LEW-13556-2] p 183 N83-29805
MAO, B. Y.
Microdistribution of oxygen in silicon and its effects on electronic properties p 172 N83-15825
MAR, H. M.
Rotorcraft convertible engine study
[NASA-CR-168161] p 37 N83-27996
MARANO, J. J.
Numerical simulation of an electrothermal deicer pad
[NASA-CR-168097] p 17 N83-23281
MAREK, C. J.
Modeling Interface Motion Of Combustion (MINOC). A computer code for two-dimensional, unsteady turbulent combustion
[NASA-TP-2132] p 40 N83-32806
High-pressure flame visualization of autoignition and flashback phenomena with liquid-fuel spray
[NASA-TM-83501] p 42 N83-34948
MARGULIS, R.
Energy and precious fuels requirements of fuel alcohol production. Volume 3, appendices C to F: Methanol from cellulose
[NASA-CR-168092] p 183 N83-28583
MARION-MOULIN, C.
Interpretation of 2-probe turbulence measurements in an axisymmetric contraction
[NASA-CR-169832] p 11 N83-17502
MARK, W. D.
The transfer function method for gear system dynamics applied to conventional and minimum excitation gearing designs
[NASA-CR-3626] p 139 N83-11495
Turbofan noise generation. Volume 1: Analysis
[NASA-CR-167951] p 198 N83-15041
MARKHAM, R.
Planning assistance for the 30/20 GHz program, volume 1
[NASA-CR-165484-VOL-1] p 108 N83-33010
Planning assistance for the 30/20 GHz program, volume 2
[NASA-CR-165484-VOL-2] p 108 N83-33011
Planning assistance for the 30/20 GHz program, volume 3
[NASA-CR-165484] p 108 N83-33012
MARPLE, D. T. F.
Analysis, design, fabrication and testing of an optical tip clearance sensor
[NASA-CR-165265] p 26 N83-11127
MARSHALL, N. A.
Modular photovoltaic stand-alone systems: Phase 1
[NASA-CR-168075] p 185 N83-33320
Photovoltaic stand-alone modular systems, phase 2
[NASA-CR-168230] p 186 N83-35497
MARTENEY, P. J.
Experimental study of the thermal stability of hydrocarbon fuels
[NASA-CR-168027] p 100 N83-17728
MARTIN, C. H.
Engineering calculations for communications systems planning
[NASA-CR-170182] p 106 N83-22494
MARTIN, J. F.
Experimental verification of the number relation at room and elevated temperatures p 162 N83-34355
MARTIN, M. R.
T55 power turbine rotor multiplane-multispeed balancing study
[NASA-CR-167891] p 41 N83-33894
MARTIN, R. E.
Alkaline regenerative fuel cell energy storage system for manned orbital satellites p 54 A83-27206
MARTINEZ, A.
Advanced LOX/H2 engine technologies for future OTVs
[AIAA PAPER 83-1312] p 55 A83-36333
Advanced LOX/H sub 2 engine technologies for future OTVs p 60 N83-35013
MARTINI, W. R.
Stirling engine design manual, 2nd edition
[NASA-CR-168088] p 212 N83-30328
MARZIALE, M.
Spanwise mass transfer variations on a cylinder in 'nominally' uniform crossflow p 124 A83-43019
MATHEWS, D.
Development of electrical test procedures for qualification of spacecraft against EID. Volume 2: Review and specification of test procedures
[NASA-CR-165590] p 50 N83-12137
MATHEWS, D. C.
Investigation of continuously traversing microphone system for mode measurement
[NASA-CR-168040] p 199 N83-19575
MATHIPRAKASAM, B.
Evaluation of methods for rapid determination of freezing point of aviation fuels
[NASA-CR-167981] p 98 N83-10207
MATSUO, K.
Next generation communications satellites: multiple access and network studies
[NASA-CR-167903] p 45 N83-12129
MATULA, R. A.
Soot formation in pyrolysis of acetylene, allene and 1,3-butadiene p 69 A83-39274
MATWEY, M. D.
Inlet-fan flow field computation
[ASME PAPER 83-GT-41] p 7 A83-47901
MAY, C. E.
Kinetics of copper ion absorption by cross-linked calcium polyacrylate membranes
[NASA-TM-83052] p 61 N83-25786
Search for selective ion diffusion through membranes
[NASA-TM-83426] p 97 N83-34048
Ion exchange selectivity for cross-linked polyacrylic acid
[NASA-TM-83427] p 97 N83-35142
MAYER, C.
High accuracy fuel flowmeter, phase 1
[NASA-CR-167893] p 134 N83-21314
MAYLE, R. E.
Spanwise mass transfer variations on a cylinder in 'nominally' uniform crossflow p 124 A83-43019
MAYO, F. R.
Oxidation and formation of deposit precursors in hydrocarbon fuels
[NASA-CR-168121] p 101 N83-23465
MAZARIS, G. A.
Screen printed interdigitated back contact solar cell
[NASA-CASE-LEW-13414-1] p 177 N83-20374
MCAFEE, R. S., JR.
Coaxial supersonic jet-flows, shock structure and related problems with noise-suppression assessment and prediction
[AIAA PAPER 83-0707] p 194 A83-28011
MCARDLE, J. G.
Experimental program for the evaluation of turbofan/turboshaft c conversion technology
[NASA-TM-82988] p 27 N83-11130
A compact inflow control device for simulating flight fan noise
[NASA-TM-83349] p 201 N83-26643
Effects of wind on turbofan engines in outdoor static test stands
[NASA-TM-83493] p 42 N83-34945
MCCALLISTER, R. D.
A low-power, high-throughput maximum-likelihood convolutional decoder chip for NASA's 30/20 GHz program p 111 A83-19754
MCCARTY, J. L.
Temperature distribution in an aircraft tire at low ground speeds
[NASA-TP-2195] p 161 N83-33217
MCCORMICK, T. J.
Electric rail gun projectile acceleration to high velocity
[AIAA PAPER 82-1939] p 52 A83-12501
MCDANIEL, J. C.
Laser-induced fluorescence technique for velocity field measurements in subsonic gas flows
p 133 A83-45962
MCDANIELS, D. L.
Evaluation of low-cost aluminum composites for aircraft engine structural applications
[NASA-TM-83357] p 66 N83-25790
MCDONALD, G.
Effects of arc current on the life in burner-rig thermal cycling of plasma-sprayed ZrO2-O3 p 89 A83-22270
Use of fiber-like materials to augment cycle life of thick, thermoprotective-seal coatings p 89 A83-22271
Some inelastic effects of thermal cycling on ZrO2-Y2O3 materials p 89 A83-22272
Thermomechanical loading of multilayered cylindrical geometries in thermal cycling from 300 to 1300 K
[NASA-TM-83312] p 129 N83-20029
The effect of annealing on the creep of plasma sprayed ceramics
[NASA-TM-83396] p 130 N83-24799
Correlation of compressive stress with spalling of plasma sprayed ceramic materials
[NASA-TM-83406] p 95 N83-27016
Residual stress in plasma sprayed ceramic turbine tip and gas path seal specimens
[NASA-TM-83418] p 131 N83-28380
MCDONALD, G. E.
Method for depositing an oxide coating
[NASA-CASE-LEW-13131-1] p 165 N83-10494
Method of forming oxide coatings
[NASA-CASE-LEW-13132-1] p 96 N83-29388
MCDONALD, H.
Numerical solution of the Navier-Stokes equations for compressible turbulent two/three dimensional flows in the terminal shock region of an inlet/diffuser
[AIAA PAPER 83-1892] p 5 A83-39358
Numerical solutions of Navier-Stokes equations for compressible turbulent two/three dimensional flows in terminal shock region of an inlet/diffuser
[NASA-CR-3723] p 132 N83-34230
MCFADDEN, J. J.
Characterization of a high-pressure diesel fuel injection system as a control technology option to improve engine performance and reduce exhaust emissions
[NASA-TM-83329] p 210 N83-24431
MCFARLAND, E. R.
A rapid blade-to-blade solution for use in turbomachinery design
[NASA-TM-83010] p 10 N83-13077
MCKILLOP, B. E.
Turbulence measurements in a complex plowfield using a crossed hot-wire
[NASA-CR-173080] p 132 N83-35316
MCKNIGHT, R. L.
Turbine blade nonlinear structural and life analysis
p 21 A83-29024
MCLALLIN, K. L.
Effects of interstage diffuser flow distortion on the performance of a 15.41-centimeter tip diameter axial power turbine
[AIAA PAPER 83-1179] p 23 A83-36263
Effects of interstage diffuser flow distortion on the performance of a 15.41-centimeter tip diameter axial power turbine
[NASA-TM-83359] p 35 N83-24505
MCLAUGHLIN, D. K.
Mean flowfields in axisymmetric combustor geometries with swirl p 120 A83-24668
Turbulence measurements in a swirling confined jet flowfield using a triple hot-wire probe
[NASA-CR-169668] p 127 N83-14434

MCMANUS, K. R.
Importance of inlet boundary conditions for numerical simulation of combustor flows
[AIAA PAPER 83-1263] p 23 A83-36314
MCMILLAN, O. J.
Mean-flow measurements of the flow field diffusing bend
[NASA-CR-3634] p 10 N83-14066
MCVEY, J. B.
Combustion of coal gas fuels in a staged combustor
[NASA-TM-82987] p 166 N83-10556
Analytical modeling of operating characteristics of premixing-prevaporizing fuel-air mixing passages, Volume 1: Analysis and results
[NASA-CR-167990-VOL-1] p 126 N83-12353
Analytical modeling of operating characteristics of premixing-prevaporizing fuel-air mixing passages, Volume 2: User's manual
[NASA-CR-167990-VOL-2] p 126 N83-12354
MEADOR, J. B.
Components for digitally controlled aircraft engines
[NASA-CR-165296] p 28 N83-12089
MEADOWS, H. E.
Next generation communications satellites: multiple access and network studies
[NASA-CR-167903] p 45 N83-12129
MEDROW, R. A.
A detailed treatment of two-dimensional, starved lubrication in the vicinity of two counter-rotating cylinders p 141 N83-15520
MEGARGLE, R. G.
A software system for emission spectrometry
[NASA-TM-83001] p 70 N83-12181
MEHMED, O.
Bending-torsion flutter of a highly swept advanced turboprop
[NASA-TM-82975] p 158 N83-11514
MEHTA, S.
Effects of processing and dopant on radiation damage removal in silicon solar cells p 170 N83-14708
MEIER, G. H.
Low temperature hot corrosion p 76 A83-42252
Mechanism of hot corrosion of IN-738
[NASA-CR-169706] p 81 N83-15411
MEISSINGER, H. F.
Optimal sun-alignment techniques of large solar arrays in electric propulsion spacecraft
[AIAA PAPER 82-1898] p 48 A83-12475
MEITNER, P. L.
Computer code for off-design performance analysis of radial-inflow turbines with rotor blade sweep
[NASA-TP-2199] p 40 N83-32807
MENDELSON, A.
Solution of elastic and elasto-plastic problems by the method of lines
[NASA-CR-168125] p 85 N83-28208
MENG, P. R.
Multi-fuel rotary engine for general aviation aircraft
[NASA-TM-83429] p 38 N83-29235
Multi-fuel rotary engine for general aviation aircraft
[NASA-TM-85428] p 43 N83-36031
MERRILL, O.
Thermionic technology infrastructure for space power p 54 A83-27298
METZGER, D. E.
Heat transfer characteristics for jet array impingement with initial crossflow
[ASME PAPER 82-GT-28] p 7 A83-47891
Jet array impingement flow distributions and heat transfer characteristics. Effects of initial crossflow and nonuniform array geometry
[NASA-CR-3630] p 128 N83-15592
MEULENBERG, A., JR.
Limitations on solar cell open-circuit voltage and efficiency p 165 A83-37790
Developments toward an 18% efficient silicon solar cell
[NASA-CR-168141] p 181 N83-25112
MEYER, W. L.
A theoretical investigation of the sound radiation fields associated with a Bellmouth inlet
[AIAA PAPER 83-0710] p 193 A83-25926
Prediction of sound radiation from different practical jet engine inlets
[NASA-CR-169533] p 197 N83-13936
MEYERS, G. J.
Nonlinear structural and life analyses of a combustor liner p 155 A83-12764
MIAO, D.
Free-piston Stirling hydraulic engine and drive system for automobiles
[NASA-TM-82992] p 211 N83-25625
MICHAEL, C. J.
Energy efficient engine low-pressure compressor component test hardware detailed design report
[NASA-CR-165354] p 39 N83-30427
MIHELC, M. S.
Measurements of heat transfer distribution over the surfaces of highly loaded turbine nozzle guide vanes
[ASME PAPER 83-GT-53] p 8 A83-47910
Analytical and experimental evaluation of the heat transfer distribution over the surfaces of turbine vanes
[NASA-CR-168015] p 131 N83-28376
MILDRUM, H. F.
Testing of the permanent magnet material Mn-Al-C for potential use in propulsion motors for electric vehicles
[NASA-CR-169481] p 114 N83-12329
MILES, G.
Application of 3D aerodynamic/combustion model to combustor primary zone study
[AIAA PAPER 83-1265] p 23 A83-36316
MILES, G. A.
Small gas turbine combustor primary zone study
[NASA-CR-168122] p 149 N83-28448
MILES, J. H.
Pressure transfer function of a JT15D nozzle due to acoustic and convected entropy fluctuations p 193 A83-16319
Cross spectra between temperature and pressure in a constant area duct downstream of a combustor
[AIAA PAPER 83-0762] p 196 A83-33487
Analysis of combustion spectra containing organ pipe tone by cepstral techniques
[NASA-TM-83034] p 198 N83-16153
Cross spectra between temperature and pressure in a constant area duct downstream of a combustor
[NASA-TM-83351] p 200 N83-23116
MILLER, D. R.
The effect of yaw on horizontal axis wind turbine loading and performance
[NASA-TM-82778] p 169 N83-14688
MILLER, E. F.
Capabilities, limitations, and use of BC SAT-R2 conference software
[NASA-TM-83383] p 107 N83-29493
MILLER, R. A.
Improved performance thermal barrier coatings p 90 A83-42261
Thermal-barrier coatings for utility gas turbines
[NASA-TM-85349] p 95 N83-27022
MILLER, T. J.
Research on ultra-high-temperature materials, monolithic ceramics, ceramic matrix composites and carbon/carbon composites p 64 N83-12161
MILNER, E. J.
Design of a high-speed digital processing element for parallel simulation
[NASA-TM-83373] p 117 N83-29597
MILTON, R. T.
Customer premise service study for 30/20 GHz satellite system
[NASA-CR-167986] p 105 N83-17769
MINER, R. V.
Fatigue crack initiation and propagation in several nickel-base superalloys at 650 C p 76 A83-41199
MISENCIK, J. A.
Evaluation of dopants in hydrogen to reduce hydrogen permeation in candidate Stirling engine heater head tube alloys at 760 deg and 820 deg
[NASA-TM-82920] p 81 N83-13232
MISKOLCZY, G.
Thermionic technology infrastructure for space power p 54 A83-27298
MISRA, A. K.
Effect of the amount of Na2SO4 on the high temperature corrosion of Udimet-700
[NASA-TM-83459] p 87 N83-34016
MISSIMER, J. R.
'Scaling' analysis of the ice accretion process on aircraft surfaces
[ASME PAPER 82-WA/HT-39] p 16 A83-25693
MITCHELL, A. M.
Lubricant effects on efficiency of a helicopter transmission p 141 N83-15523
MITCHELL, J. A.
Computer program to predict noise of general aviation aircraft: User's guide
[NASA-CR-168050] p 198 N83-17242
MITCHELL, J. T.
Kilovolt dc solid state remote power controller development
[NASA-CR-168041] p 115 N83-21236
MITCHELL, L. D.
Theoretical investigation of the force and dynamically coupled torsional-axial-lateral dynamic response of eared rotors
[NASA-CR-173013] p 191 N83-34656
MIYOSHI, K.
Tribological properties and X-ray photoelectron spectroscopy studies of ion-plated gold on nickel and iron p 74 A83-12650
Correlation of tensile and shear strengths of metals with their friction properties
[ASLE PREPRINT 82-LC-UB-1] p 74 A83-13226
Tribological properties of sintered polycrystalline and single-crystal silicon carbide p 89 A83-29397
XPS, AES and friction studies of single-crystal silicon carbide p 89 A83-36973
Friction and wear of iron and nickel in sodium hydroxide solutions p 77 A83-48922
Friction and wear of iron and nickel in sodium hydroxide solutions
[NASA-TM-82935] p 77 N83-10171
Tribological properties of amorphous alloys and the role of surfaces in abrasive wear of materials
[NASA-TM-82973] p 140 N83-11498
Friction and wear of some ferrous-base metallic glasses
[NASA-TM-83067] p 82 N83-19886
Surface chemistry, friction and wear of Ni-Zn and Mn-Zn ferrites in contact with metals
[NASA-TM-83068] p 93 N83-19901
Sliding induced crystallization of metallic glass
[NASA-TP-2140] p 83 N83-21110
The XPS depth profiling and tribological characterization of ion-plated gold on various metals
[NASA-TM-83350] p 83 N83-23417
X-ray photoelectron spectroscopy and friction studies of nickel-zinc and manganese-zinc ferrites in contact with metals
[NASA-TP-2163] p 84 N83-23419
Friction and hardness of gold films deposited by ion plating and evaporation
[NASA-TP-2207] p 87 N83-34019
MOFFAT, R. J.
Convex curvature effects on the heated turbulent boundary layer p 123 A83-42733
MOFFITT, T. P.
Aerodynamic effect of a honeycomb rotor tip shroud on a 50.8-centimeter-tip-diameter core turbine
[NASA-TP-2112] p 32 N83-17547
Incidence loss for fan turbine rotor blade in two-dimensional cascade
[NASA-TP-2188] p 39 N83-30431
MONGIA, H. C.
Dilution Jet Mixing Program, phase 1
[NASA-CR-168031] p 128 N83-15590
MOORE, A. S.
Effects of wind on turbofan engines in outdoor static test stands
[NASA-TM-83493] p 42 N83-34945
MOORE, F. K.
A theory of rotating stall of multistage axial compressors. I - Small disturbances
[ASME PAPER 83-GT-44] p 7 A83-47904
A theory of rotating stall of multistage axial compressors. II - Finite disturbances
[ASME PAPER 83-GT-45] p 8 A83-47905
A theory of rotating stall of multistage axial compressors. III - Limit cycles
[ASME PAPER 83-GT-46] p 8 A83-47906
MOORE, T. J.
Evaluation of electrode shape and nondestructive evaluation method for welded solar cell interconnects
[NASA-TM-82966] p 166 N83-10555
Microstructural analysis of solar cell welds p 172 N83-15833
MOORHEAD, P. E.
Metal honeycomb to porous wireform substrate diffusion bond evaluation p 153 A83-39620
MORALES, W.
Use of high pressure liquid chromatography in the study of liquid lubricant oxidation
[NASA-TM-83033] p 92 N83-14270
Analysis of a MIL-L-27502 lubricant from a gas-turbine engine test by size-exclusion chromatography
[NASA-TP-2063] p 93 N83-16528
Preliminary results of the comparison of the electrochemical behavior of a thioether and biphenyl
[NASA-TM-83450] p 87 N83-34015
MORENO, V.
Nonlinear structural and life analyses of a combustor liner p 155 A83-12764
Development of a simplified analytical method for representing material cyclic response
[NASA-CR-168100] p 160 N83-21390
MORETTI, G.
A fast Euler solver for steady flows
[AIAA PAPER 83-1940] p 123 A83-39389
Fast Euler solver for steady, 1-dimensional flows
[NASA-CR-3689] p 14 N83-27960
MORIN, T.
Measurements of energy distribution and thrust for microwave plasma coupling of electrical energy to hydrogen for propulsion
[AIAA PAPER 82-1951] p 52 A83-12508

Microwave plasma generation of hydrogen atoms for rocket propulsion p 53 A83-13090
MORRIS, J. F.
Heat pipes containing alkali metal working fluid [NASA-CASE-LEW-12253-1] p 203 N83-19596
High thermal power density heat transfer apparatus providing electrical isolation at high temperature using heat pipes [NASA-CASE-LEW-12950-2] p 183 N83-29804
Thermionic energy converters [NASA-CASE-LEW-12443-1] p 184 N83-32175
MORRIS, P. J.
Tone-excited jet: Theory and experiments [NASA-CR-3538] p 197 N83-12963
MORRISEAU, B.
Optimization and fabrication of porous carbon electrodes for Fe/Cr redox flow cells [NASA-CR-167921] p 179 N83-23708
MOTOIE, K.
An extensometer for axial strain measurement at high temperature p 134 A83-48604
MOTSINGER, R. E.
Sound propagation in segmented exhaust ducts - Theoretical predictions and comparison with measurements [AIAA PAPER 83-0734] p 194 A83-28016
MULARZ, E. J.
New trends in combustion research for gas turbine engines p 22 A83-35806
New trends in combustion research for gas turbine engines [NASA-TM-83338] p 34 N83-20947
Detailed fuel spray analysis techniques [NASA-TM-83476] p 42 N83-34943
MULLEN, R. L.
Finite element formulation for transient heat treat problems [NASA-TM-83070] p 129 N83-17834
Thermomechanical loading of multilayered cylindrical geometries in thermal cycling from 300 to 1300 K [NASA-TM-83312] p 129 N83-20029
Analogy between fluid cavitation and fracture mechanics [NASA-TM-83071] p 129 N83-22542
The effect of annealing on the creep of plasma sprayed ceramics [NASA-TM-83396] p 130 N83-24799
Correlation of compressive stress with spalling of plasma sprayed ceramic materials [NASA-TM-83406] p 95 N83-27016
Residual stress in plasma sprayed ceramic turbine tip and gas path seal specimens [NASA-TM-83418] p 131 N83-28380
MULLIGAN, M. G.
An improved algorithm for evaluating trellis phase codes [NASA-CR-169354] p 105 N83-16600
MUNSON, K. E.
Advanced ceramic coating development for industrial/utility gas turbine applications [NASA-CR-165619] p 92 N83-15467
MUNZ, D. G.
Specimen size and geometry effects on fracture toughness of Al2O3 measured with short rod and short bar chevron-notch specimens [NASA-TM-83319] p 94 N83-19902
MURA, T.
Volume integrals of ellipsoids associated with the inhomogeneous Helmholtz equation p 192 A83-28528
The determination of the elastodynamic fields of an ellipsoidal inhomogeneity [ASME PAPER 83-APM-19] p 157 A83-37388
MURAKAMI, Y.
Growth and stability of interacting surface flaws of arbitrary shape p 155 A83-15060
MURALIDHARAN, U.
Tensile and compressive constitutive response of 316 stainless steel at elevated temperatures p 162 N83-34353
MURDOCH, A.
Control design for a wind turbine-generator using output feedback p 164 A83-24721
Control design and performance analysis of a 6 MW wind turbine-generator p 165 A83-29897
MURTHY, B.
Fuel quality-processing study. Volume 2: Literature survey [NASA-CR-165326-VOL-2] p 178 N83-22751
MURTHY, K. N. S.
End wall flows in rotors and stators of a single stage compressor [NASA-CR-169800] p 128 N83-16678
MURTHY, R.
Parametric analysis of closed cycle magnetohydrodynamic (MHD) power plants [NASA-CR-165472] p 178 N83-22748
MURTHY, S. N. B.
Axial-compressor flow distortion with water ingestion [AIAA PAPER 83-0004] p 19 A83-16456
Effect of humidity on jet engine axial-flow compressor performance p 22 A83-35856
The WISGSK: A computer code for the prediction of a multistage axial compressor performance with water ingestion [NASA-CR-3624] p 28 N83-12093
MYERS, D.
Study of advanced rotary combustion engines for commuter aircraft [NASA-CR-165399] p 32 N83-17545
MYERS, L. P.
Flight evaluation of modifications to a digital electronic engine control system in an F-15 airplane [AIAA PAPER 83-0537] p 20 A83-19593
MYERS, M. R.
Incidence angle effects on convected gust airfoil noise [AIAA PAPER 83-0765] p 195 A83-28022
MYHRE, R. W.
Advanced 30/20 GHz multiple beam antenna for future communications satellites p 104 A83-41367
Advanced 30/20 GHz multiple-beam antennas for communications satellites [NASA-TM-82952] p 50 N83-13154

N

NAFF, G. J.
Modular photovoltaic stand-alone systems: Phase 1 [NASA-CR-168075] p 185 N83-33520
Photovoltaic stand-alone modular systems, phase 2 [NASA-CR-168230] p 186 N83-35497
NAGEL, R. T.
An experimental study of supersonic jet shock-associated noise [AIAA PAPER 83-0708] p 193 A83-25924
NAGIB, H. M.
Interpretation of 2-probe turbulence measurements in an axisymmetric contraction [NASA-CR-169832] p 11 N83-17502
Experiments on identification and control of inflow disturbances in contracting streams [NASA-CR-169831] p 11 N83-17503
NAGY, A.
Evaluation of high-contact-ratio spur gears with profile modification p 147 N83-20150
NAHM, A. H.
Rolling-element fatigue life with traction fluids and automatic transmission fluid in a high-speed rolling-contact rig [NASA-TP-2050] p 140 N83-13457
Bearing fatigue investigation 3 [NASA-CR-168029] p 143 N83-17880
Corrosion of simulated bearing components of three bearing steels in the presence of chloride-contaminated lubricant [NASA-TM-82955] p 143 N83-20115
NAINIGER, J. J.
Critical research and advanced technology (CRT) support project [NASA-TM-83019] p 176 N83-20361
IGCC performance comparison for variations in gasifier type and gas turbine firing temperature [NASA-TM-83310] p 180 N83-25037
NAKAMURA, H. H.
Improved uniformity of multiphase ceramic-metal plasma-sprayed coats p 61 A83-22269
Plasma-sprayed self-lubricating coatings [NASA-CR-3680] p 94 N83-22422
NAKANISHI, S.
Measurements of energy distribution and thrust for microwave plasma coupling of electrical energy to hydrogen for propulsion [AIAA PAPER 82-1951] p 52 A83-12508
Free radical propulsion concept p 53 A83-13141
Parallel plate radiofrequency ion thruster [AIAA PAPER 82-1937] p 53 A83-21900
Performance characteristics of a microwave plasma disk ion source [AIAA PAPER 82-1935] p 55 A83-27350
Parallel plate radiofrequency ion thruster [NASA-TM-83014] p 56 N83-12142
NASTROM, G. D.
Cloud encounter statistics in the 28.5-43.5 KFT altitude region from four years of GASP observations p 188 A83-38733
Flight summaries and temperature climatology at airliner cruise altitudes from GASP (Global Atmospheric Sampling Program) data [NASA-CR-168106] p 188 N83-24048
NASVYTIS, A. L.
Hybrid geared traction transmissions p 145 N83-20128
NATHAL, M. V.
Gamma prime shape changes during creep of a nickel-base superalloy p 77 A83-47855
Influence of cobalt, tantalum, and tungsten on the microstructure and mechanical properties of superalloy single crystals p 79 N83-11293
NAUKA, K.
Microdistribution of oxygen in silicon and its effects on electronic properties p 172 N83-15825
NAUM, R. G.
Progress in net shape fabrication of alpha SiC turbine components [ASME PAPER 83-GT-238] p 139 A83-48030
NEALY, D. A.
Measurements of heat transfer distribution over the surfaces of highly loaded turbine nozzle guide vanes [ASME PAPER 83-GT-53] p 6 A83-47910
Analytical and experimental evaluation of the heat transfer distribution over the surfaces of turbine vanes [NASA-CR-168015] p 131 N83-28376
NEELY, G. M.
Flame radiation measurements p 73 N83-29220
Parametric study of flame radiation characteristics of a tubular-can combustor [NASA-TM-83436] p 39 N83-29237
NEIL, J. T.
Sintering, properties and fabrication of Si3N4 + Y2O3 based ceramics p 90 A83-48303
NELSON, D. C.
Alumina fiber strength improvement [NASA-CR-167999] p 63 N83-11247
NELSON, D. P.
Ejector nozzle test results at simulated flight conditions for an advanced supersonic transport propulsion system [AIAA PAPER 83-1287] p 23 A83-36323
Model aerodynamic test results for a refined actuated inlet ejector nozzle at simulated takeoff and cruise conditions [NASA-CR-168051] p 13 N83-26816
NEMAT-NASSER, S.
On composites with periodic structure p 154 A83-10283
Composites with periodic microstructure p 62 A83-12734
Growth and stability of interacting surface flaws of arbitrary shape p 155 A83-15060
Dynamic fields near a crack tip growing in an elastic-perfectly-plastic solid p 157 A83-38528
Micromechanically based constitutive relations for polycrystalline solids p 162 N83-34359
NEMETH, N.
Effects of free stream turbulence intensity and integral length scale on heat transfer from a circular cylinder in crossflow p 123 A83-42711
NEUMAN, C.
Frequency-multiplexed and pipelined iterative optical systolic array processors p 168 A83-18588
Electro-optical processor for optimal control p 133 A83-23596
NEUMANN, H.
The development of a generalized advanced propeller analysis system [AIAA PAPER 83-2466] p 26 A83-49581
NEUMANN, H. E.
An analytical and experimental comparison of the flow field of an advanced swept turboprop [AIAA PAPER 83-0189] p 3 A83-21080
Dynamic distortion in a short s-shaped subsonic diffuser with flow separation [AIAA PAPER 83-1412] p 25 A83-45515
An analytical and experimental comparison of the flow field of an advanced swept turboprop [NASA-TM-83037] p 1 N83-14061
New test techniques and analytical procedures for understanding the behavior of advanced propellers [NASA-TM-83360] p 2 N83-22092
Dynamic distortion in a short s-shaped subsonic diffuser with flow separation [NASA-TM-83412] p 36 N83-26838
NEUSTADTER, H.
The DOE/NASA wind turbine data acquisition system. Part 3: Unattended power performance monitor [NASA-CR-165540] p 44 N83-24516
NEVIN, J. H.
Research into the use of pyrolytic oxides and polymers for the fabrication of thin film high energy capacitors [NASA-CR-173012] p 97 N83-34045
NEWELL, J. F.
SSME main combustion chamber life prediction [NASA-CR-168215] p 60 N83-36101
NIELSON, C. E.
The performance and application of high speed long life LH2 hybrid bearings for reusable rocket engine turbomachinery [AIAA PAPER 83-1389] p 138 A83-36379

The performance and application of high speed long life LH2 hybrid bearings for reusable rocket engine turbomachinery
[NASA-TM-83417] p 58 N83-26923
Hybrid hydrostatic/ball bearings in high-speed turbomachinery
[NASA-CR-168124] p 149 N83-27213
NIGHTINGALE, N.
Automotive Stirling engine development program
[NASA-CR-168060] p 209 N83-15177
Automotive Stirling Engine Development Program
[NASA-CR-168074] p 212 N83-27925
NIGRO, D. N.
Support and power plant documentation for the gas turbine powered bus demonstration program
[NASA-CR-165527] p 210 N83-20829
NISHINO, S.
Production of large-area single-crystal wafers of cubic SiC for semiconductor devices p 205 A83-22767
NIZAMI, A. A.
Droplet size effects on NO/x/ formation in a one-dimensional monodisperse spray combustion system
[ASME PAPER 82-JPGC-GT-10] p 68 A83-25268
NOLFI, J.
Market assessment of photovoltaic power systems for agricultural applications worldwide
[NASA-CR-165541] p 168 N83-13585
NONNAST, J. H.
Numerical simulation of a disk-shaped electron accelerating electrostatic probe p 133 A83-22336
Numerical simulation of a conducting disk partially covered by an insulator interacting with a plasma p 50 N83-18805
NORGREN, C. T.
Small gas turbine combustor study - Combustor liner evaluation
[AIAA PAPER 83-0337] p 20 A83-16663
Effect of broad properties fuel on injector performance in a reverse flow combustor
[AIAA PAPER 83-0154] p 20 A83-21079
Effect of broad properties fuel on injector performance in a reverse flow combustor
[NASA-TM-83013] p 29 N83-13101
Small gas turbine combustor study: Combustor liner evaluation
[NASA-TM-83028] p 33 N83-18725
NOTARDONATO, J.
Multifuel evaluation of rich/quench/lean combustor p 67 A83-11492
NOTARDONATO, J. J.
Combustion characteristics of hydrogen-carbon monoxide based gaseous fuels p 67 A83-11491
NOx results from two combustors tested on medium BTU coal gas p 186 A83-11493
Evaluation of advanced combustion concepts for dry NO sub x suppression with coal-derived, gaseous fuels
[NASA-TM-82985] p 166 N83-10557
Multifuel evaluation of rich/quench/lean combustor
[NASA-TM-82986] p 167 N83-10559
Combustion characteristics of hydrogen. Carbon monoxide based gaseous fuels
[NASA-TM-82998] p 167 N83-10560
NOVICK, A. S.
Multifuel evaluation of rich/quench/lean combustor p 67 A83-11492
Advanced propfan engine characteristics and technology needs
[AIAA PAPER 83-1155] p 23 A83-36250
Multifuel evaluation of rich/quench/lean combustor
[NASA-TM-82986] p 167 N83-10559
NOWOGRODZKI, M.
Advanced 3-V semiconductor technology assessment
[NASA-CR-168101] p 206 N83-21987
Advanced 3-V semiconductor technology assessment
[NASA-CR-168102] p 207 N83-21988
NUSSLE, R. C.
Free-piston Stirling hydraulic engine and drive system for automobiles
[NASA-TM-82992] p 211 N83-25625
NYLAND, T. W.
Operating experience with the 200 kW MOD-OA wind turbine generators p 174 N83-15916
Operating experience with four 200 kW Mod-0A wind turbine generators p 176 N83-19256

O

OBASIH, K.
Finite analytic numerical solution of heat transfer and flow past a square channel cavity p 123 A83-42703
OCKMAN, N.
Effect of hydrogen bonding on the vibrational dephasing time in glycerol p 61 A83-21054
ODWYER, J. J.
Thermal dielectric breakdown with cylindrical electrodes p 112 A83-38216
OHTA, H. H.
A multiple beam antenna concept for a 30/20 GHz satellite communications system p 103 A83-11485
OKEEFE, J. V.
Tests of a thermal acoustic shield with a supersonic jet p 192 A83-10183
OLDRIEVE, R. E.
Relation of cyclic loading pattern to microstructural fracture in creep fatigue
[NASA-TM-83473] p 161 N83-34349
OLIVER, J. D., JR.
Advanced digital modulation: Communication techniques and monolithic GaAs technology
[NASA-CR-174452] p 109 N83-36299
OLMSTEAD, W. E.
Ignition of a combustible half space p 68 A83-22738
OLSEN, R. C.
Observations of charging dynamics p 49 A83-37591
OLSEN, W.
Experimental comparison of icing cloud instruments
[AIAA PAPER 83-0026] p 16 A83-42099
Experimental comparison of icing cloud instruments
[NASA-TM-83340] p 17 N83-24487
OLSEN, W. A.
Turbulence spectra in the noise source regions of the flow around complex surfaces
[NASA-TM-83392] p 202 N83-30168
OLSEN, W. A., JR.
NASA Lewis Research Center's program on icing research
[AIAA PAPER 83-0204] p 1 A83-16582
NASA Lewis Research Center's Program on Icing Research
[NASA-TM-83031] p 16 N83-14078
OLSON, R.
The DOE/NASA wind turbine data acquisition system. Part 3: Unattended power performance monitor
[NASA-CR-165540] p 44 N83-24516
OLSSON, W. J.
The JT9D Jet Engine Diagnostics Program
[NASA-CR-167966] p 32 N83-17544
OONK, R. L.
Preliminary design of flight hardware for two-phase fluid research
[NASA-CR-168072] p 46 N83-25766
OPPENHEIM, A. K.
Aerodynamic features of turbulent flames
[AIAA PAPER 83-0470] p 119 A83-16737
Numerical solution of the problem of flame propagation by the use of the random element method
[AIAA PAPER 83-0600] p 69 A83-36062
Modeling Interface Motion Of Combustion (MINOC). A computer code for two-dimensional, unsteady turbulent combustion
[NASA-TP-2132] p 40 N83-32806
ORANSKY, G.
A 1 watt GaAs power amplifier for the NASA 30/20 GHz communication system p 111 A83-11489
OSHIMA, H.
Metallic conductivity and air stability in copper chloride intercalated carbon fibers p 111 A83-16095
OSTRACH, S.
An experimental study of heat induced surface-tension driven flow p 44 A83-43269
OSULLIVAN, P.
A 1 watt GaAs power amplifier for the NASA 30/20 GHz communication system p 111 A83-11489
OSWALD, F. B.
Vibration in planetary gear systems with unequal planet stiffnesses
[NASA-TM-83428] p 150 N83-29709
OTTERSON, D. A.
Aircraft sampling of the sulfate layer near the tropopause following the eruption of Mount St. Helens p 187 N83-11556
High performance liquid chromatographic hydrocarbon group-type analyses of mid-distillates employing fuel-derived fractions as standards
[NASA-TM-83072] p 100 N83-19920
OWCZAREK, J. A.
Analysis of an axial compressor blade vibration based on wave reflection theory
[ASME PAPER 83-GT-151] p 25 A83-47970
OWEN, A. K.
Performance of a tandem-rotor/tandem-stator conical-flow compressor designed for a pressure ratio of 3
[NASA-TP-2034] p 9 N83-11058
OWEN, H. A.
High-frequency high-voltage high-power DC-to-DC converters p 115 N83-21028
OWEN, H. A., JR.
Parametric study of minimum reactor mass in energy-storage dc-to-dc converters p 110 A83-11011
OWENS, W.
Parametric analysis of closed cycle magnetohydrodynamic (MHD) power plants
[NASA-CR-165472] p 178 N83-22748

P

PACIOREK, K. J. L.
The effects of metals and inhibitors on thermal oxidative degradation reactions of unbranched perfluoroalkylethers
[NASA-TM-83464] p 97 N83-34049
PADOVAN, J.
Formal convergence characteristics of elliptically constrained incremental Newton-Raphson algorithms p 190 A83-10273
On the solution of elastic-plastic static and dynamic postbuckling collapse of general structure p 155 A83-12746
Pseudo-updated constrained solution algorithm for nonlinear heat conduction p 121 A83-32989
Finite element analysis of steadily moving contact fields p 158 A83-49437
Thermomechanical loading of multilayered cylindrical geometries in thermal cycling from 300 to 1300 K
[NASA-TM-83312] p 129 N83-20029
Constrained self-adaptive solutions procedures for structure subject to high temperature elastic-plastic creep effects p 162 N83-34370
PAGE, R. J.
The design and technology development for A 150 mlb resistojet for H2 or NH3
[AIAA PAPER 82-1949] p 52 A83-12506
PALMER, F. M.
Evaluation of the use of on-board spacecraft energy storage for electric propulsion missions
[NASA-CR-168209] p 59 N83-32842
PANDYA, A.
Investigation of the tip clearance flow inside and at the exit of a compressor rotor passage. II - Turbulence properties p 4 A83-28843
Tip clearance flow in a compressor rotor passage at design and off-design conditions p 4 A83-35855
PAPATHAKOS, L. C.
Aircraft sampling of the sulfate layer near the tropopause following the eruption of Mount St. Helens p 187 N83-11556
PAPATHANSIOU, A. G.
An experimental study of supersonic jet shock-associated noise
[AIAA PAPER 83-0708] p 193 A83-25924
PAPELL, S. S.
Film-cooling effectiveness with developing coolant flow through straight and curved tubular passages
[NASA-TP-2062] p 126 N83-12360
Curved film cooling admission tube
[NASA-CASE-LEW-13174-1] p 131 N83-27144
Three-dimensional turbulent-mixing-length modeling for discrete-hole coolant injection into a crossflow
[NASA-TP-2200] p 132 N83-34232
PARANG, M.
Measurement of thermoacoustic convection heat transfer phenomenon
[AIAA PAPER 83-1422] p 121 A83-32701
PARKER, R. J.
Rolling-element fatigue life with traction fluids and automatic transmission fluid in a high-speed rolling-contact rig
[NASA-TP-2050] p 140 N83-13457
Rolling-element fatigue life of AMS 5900 balls
[NASA-TP-2080] p 142 N83-16758
Corrosion of simulated bearing components of three bearing steels in the presence of chloride-contaminated lubricant
[NASA-TM-82955] p 143 N83-20115
Present technology of rolling-element bearings p 144 N83-20121
Large-bore tapered-roller bearing performance and endurance to 2.4 million DN p 145 N83-20134
Effect of carbide distribution on rolling-element fatigue life of AMS 5749
[NASA-TP-2189] p 151 N83-33166
PARKS, D. E.
Space Shuttle Orbiter charging p 49 A83-20415
PARMLEY, R.
Assessment of crash fire hazard of LH sub 2 fueled aircraft
[NASA-CR-165525] p 16 N83-11095
PATER, R. H.
Dynamic mechanical properties of n-phenylnadimide modified PMR polyimide composites
[NASA-TM-83051] p 65 N83-15363

The 371 deg C(700 deg F) properties of celion 6000/n-phenylnadimide modified PMR polyimide composites
[NASA-TM-83050] p 65 N83-15365
Improved high temperature resistant polyimides
[NASA-CASE-LEW-13864-1] p 93 N83-17715
PATTEN, J.
Parametric analysis of closed cycle magnetohydrodynamic (MHD) power plants
[NASA-CR-165472] p 178 N83-22748
PATTERSON, D. J.
Aviation Gasolines and Future Alternatives
[NASA-CP-2267] p 100 N83-22442
PAWLIK, E.
Electric propulsion research and technology in the United States
[AIAA PAPER 82-1867] p 53 A83-16925
PEAK, S. C.
Transistorized PWM inverter-induction motor drive system p 110 A83-11488
Improved transistorized AC motor controller for battery powered urban electric passenger vehicles
[NASA-CR-167978] p 113 N83-10349
PECZKOWSKI, J. L.
Nonlinear multivariable design by total synthesis p 24 A83-37092
PELOSE, J.
Spacecraft IF switch matrix for wideband service applications in 30/20 GHz communications satellite systems: Proof-of-concept model, executive summary
[NASA-CR-168175] p 107 N83-29492
PELOSE, J. R.
20 x 20 IF switch matrix for SS-TDMA systems p 113 A83-41369
PEPPER, R. T.
Alumina fiber strength improvement
[NASA-CR-167999] p 63 N83-11247
PEPPER, S. V.
Molecular-orbital model for metal-sapphire interfacial strength p 67 A83-10612
Diamond /111/ studied by electron energy loss spectroscopy in the characteristic loss region p 68 A83-25675
Use of high L.E.T. radiation to improve adhesion of metals to polytetrafluoroethylene
[NASA-TM-83413] p 96 N83-30660
PESSAGNO, S. L.
Catalyst durability evaluation for advanced gas turbine engines
[ASME PAPER 82-JPGC-GT-21] p 137 A83-25270
PETERMAN, W.
Determination of hydrogen permeability in commercial and modified superalloys
[NASA-CR-168195] p 87 N83-35101
PETERSEN, W. C.
A two-stage monolithic buffer amplifier for 20 GHz satellite communication p 112 A83-39272
PETERSON, D. F.
Image-optimized, frequency-scalable mixers for millimeter-wave applications p 112 A83-39273
PETRASEK, D. W.
SiC or B4C-B/low strategic element content composite p 80 N83-11308
PETRASH, D. A.
Propulsion and fluid management - Station keeping will eat energy on a new scale p 54 A83-24360
PETTIT, F. S.
Low temperature hot corrosion p 76 A83-42252
PFANNER, H. G.
The response of a 38m horizontal axis teetered rotor to yaw p 175 N83-19232
PHILIPP, W. H.
Kinetics of copper ion absorption by cross-linked calcium polyacrylate membranes
[NASA-TM-83052] p 61 N83-25786
Search for selective ion diffusion through membranes
[NASA-TM-83426] p 97 N83-34048
Ion exchange selectivity for cross-linked polyacrylic acid
[NASA-TM-83427] p 97 N83-35142
PHILLIPS, B. R.
A proposed optical pumping system requiring no electric power p 203 N83-15661
PIAN, T. H. H.
A new formulation of hybrid/mixed finite element p 155 A83-12739
Alternative ways for formulation of hybrid stress elements p 155 A83-14710
Time-independent anisotropic plastic behavior by mechanical subelement models p 162 N83-34369
PICKUP, N.
Tests of a thermal acoustic shield with a supersonic jet p 192 A83-10183
PILLER, S.
Automotive Stirling engine development program
[NASA-CR-167907] p 209 N83-15176
PINE, V. W.
Continued development of a detailed model of arc discharge dynamics
[NASA-CR-167977] p 206 N83-16234
PINTZ, A.
Dynamic effects of internal spur gear drives
[NASA-CR-3692] p 149 N83-28452
PITTS, L.
Moderate temperature rechargeable sodium batteries
[NASA-CR-168220] p 118 N83-33359
PLENCNER, R. M.
Propeller performance and weight predictions appended to the Navy/NASA engine program
[NASA-TM-83458] p 41 N83-32810
PLUNKETT, A. B.
Transistorized PWM inverter-induction motor drive system p 110 A83-11488
POBEREZNY, P.
Aviation energy and the future of the recreational use of sport and general aviation aircraft p 100 N83-22444
POESCHEL, R. L.
Analysis and design of ion thruster for large space systems
[NASA-CR-165140] p 57 N83-14158
Evaluation of the use of on-board spacecraft energy storage for electric propulsion missions
[NASA-CR-168209] p 59 N83-32842
POLISENA, C.
Experimental study of electrochemical fluorination of trichloroethylene p 68 A83-15870
POOR, R. H.
Experience and assessment of the DOE/NASA Mod-1 2000 kW wind turbine generator at Boone, North Carolina p 176 N83-19257
POPPA, H.
Interfacial layers in high-temperature-oxidized NiCrAl p 77 A83-44619
POPPEL, G. L.
Analysis, design, fabrication and testing of an optical tip clearance sensor
[NASA-CR-165265] p 26 N83-11127
PORTER, T. R.
Compression and compression fatigue testing of composite laminates
[NASA-CR-168023] p 66 N83-26928
POUAGARE, M.
Development of secondary flow and vorticity in curved ducts, cascades, and rotors, including effects of viscosity and rotation p 119 A83-16141
Three dimensional flow field inside compressor rotor, including blade boundary layers
[NASA-CR-169788] p 128 N83-16679
POVINELLI, L.
Three-dimensional compressible viscous analysis of mixer nozzles
[AIAA PAPER 83-1401] p 4 A83-36391
POWELL, J. A.
Production of large-area single-crystal wafers of cubic SiC for semiconductor devices p 205 A83-22767
POWER, J. L.
Qualification test results of IAPS 8 cm ion thrusters
[AIAA PAPER 82-1954] p 52 A83-12511
PRATT, R.
Aircraft measurements of trace gases and particles near the tropopause
[NASA-CR-3691] p 188 N83-27542
PRATT, R. D.
Composite engine duct fabrication p 1 A83-39941
PRATT, T. K.
Structural tailoring of engine blades (STAEBL)
[AIAA 83-0828] p 22 A83-29737
PRZYBYSZEWSKI, J. S.
Joining lead wires to thin platinum alloy films
[NASA-CASE-LEW-13934-1] p 135 N83-35338
PUGMIRE, R. J.
A carbon-13 and proton nuclear magnetic resonance study of some experimental referee broadened-specification /ERBS/ turbine fuels p 98 A83-11482
PURVIS, C. K.
Dipole-field sums and Lorentz factors for orthorhombic lattices, and implications for polarizable molecules p 204 A83-17226
Piezoelectric and pyroelectric coefficients for ferroelectric crystals with polarizable molecules p 205 A83-17227
Piezoelectricity and pyroelectricity in polyvinylidene fluoride - Influence of the lattice structure p 205 A83-29531
Observations of charging dynamics p 49 A83-37591
SAFE II: Large systems space plasma evaluation experiment p 46 N83-26903
The role of potential barrier formation in spacecraft charging
[NASA-TM-83500] p 50 N83-35005
PUTCHA, N. S.
Three-dimensional finite-element analysis of layered composite plates p 156 A83-27432

Q

QUACKENBUSH, C. L.
Sintering, properties and fabrication of Si3N4 + Y2O3 based ceramics p 90 A83-48303
QUINN, T. F. J.
NASA interdisciplinary collaboration in tribology. A review of oxidational wear
[NASA-CR-3686] p 95 N83-27021

R

RACKLEY, R. A.
Advanced Gas Turbine (AGT) powertrain system development program
[NASA-CR-169475] p 27 N83-12088
RADDLEBAUGH, S. M.
Effect of broad properties fuel on injector performance in a reverse flow combustor
[NASA-TM-83013] p 29 N83-13101
RADWAN, S. F.
Critical review of the trailing edge condition in steady and unsteady flow. Blade flutter in compressors and fans: Numerical simulation of the aerodynamic loading
[NASA-CR-169705] p 10 N83-15264
RAGSDELL, K. M.
Quasi-three-dimensional turbomachinery flow calculations on multiple hub-to-shroud stream surfaces
[AIAA PAPER 83-1820] p 5 A83-38652
RAHMAN, S.
Nonlinear program based optimization of boost and buck-boost converter designs p 110 A83-11016
Computer simulations of optimum boost and buck-boost converters p 111 A83-19032
RAMAIAH, R.
Unsteady turbulent shear flow in shock tube discontinuities p 124 A83-46445
RAMAKRISHNAN, R.
Generation of desired signals from acoustic drivers p 19 A83-15068
Refinement and application of acoustic impulse technique to study nozzle transmission characteristics
[NASA-CR-3656] p 199 N83-20708
RAMAMURTI, R.
Multi-grid solution of Neumann pressure problem for viscous flows using primitive variables
[AIAA PAPER 83-0557] p 120 A83-16786
RAMINS, P.
Experimental verification of the multistage depressed collector design procedure for a high-perveance, helix-type, traveling-wave tube
[NASA-TP-2162] p 116 N83-25985
RAMLER, J. R.
Application of a space station to communications satellites
[AAS PAPER 83-197] p 45 A83-43773
Concept for advanced satellite communications and required technologies
[NASA-TM-82984] p 47 N83-11210
RAMOS, J. I.
Ignition of confined gaseous mixtures by hot surfaces and hot wires
[AIAA PAPER 83-0240] p 68 A83-16606
Numerical studies of the formation and destruction of vortices in a motored four-stroke piston-cylinder configuration
[AIAA PAPER 83-0497] p 136 A83-16749
RAMSEY, W. D.
Inert gas test of two 12-cm magnetostatic thrusters
[AIAA PAPER 82-1925] p 51 A83-12494
RANSON, W. F.
Extending the laser-specklegram technique to strain analysis of rotating components p 155 A83-12514
RAO, B. C. S.
Cavitation erosion characteristics of poly(methyl methacrylate) in a rotating disk device p 90 A83-41851
Dynamics and mechanism of cavitation erosion on perspex and epoxy resins tested in a rotating disk device
[NASA-TM-82962] p 81 N83-11329
Initial stages of cavitation damage and erosion on copper and brass tested in a rotating disk device
[NASA-TM-82993] p 81 N83-13231
Cavitation pitting and erosion of Al 6061-T6 in mineral oil and water
[NASA-TM-83345] p 148 N83-23606

Cavitation erosion of copper, brass, aluminum and titanium alloys in mineral oil
[NASA-TM-83402] p 148 N83-24856
Cavitation pitting and erosion of aluminum 6061-T6 in mineral oil water
[NASA-TP-2146] p 152 N83-35400

RAO, N. S. L.
Cavitation erosion characteristics of poly(methyl methacrylate) in a rotating disk device
p 90 A83-41851
Dynamics and mechanism of cavitation erosion on perspex and epoxy resins tested in a rotating disk device
[NASA-TM-82962] p 91 N83-11329
Initial stages of cavitation damage and erosion on copper and brass tested in a rotating disk device
[NASA-TM-82993] p 81 N83-13231

RAO, P. V.
Dynamics and mechanism of cavitation erosion on perspex and epoxy resins tested in a rotating disk device
[NASA-TM-82962] p 91 N83-11329
Initial stages of cavitation damage and erosion on copper and brass tested in a rotating disk device
[NASA-TM-82993] p 81 N83-13231
Universal approach to analysis of cavitation and liquid-impingement erosion data
[NASA-TP-2061] p 82 N83-15413
A comprehensive analysis of cavitation and liquid impingement erosion data
[NASA-TM-83352] p 84 N83-24634
Time effect of erosion by solid particle impingement on ductile materials
[NASA-TM-83369] p 84 N83-24637
Morphology of an aluminum alloy eroded by a jet of angular particles impinging at normal incidence
[NASA-TP-2139] p 85 N83-24641
Solid spherical glass particle impingement studies of plastic materials
[NASA-TP-2161] p 94 N83-24695
Solid particle impingement erosion characteristics of cylindrical surfaces, pre-existing holes and slits
[NASA-TM-83322] p 85 N83-25853
Spherical micro-glass particle impingement studies of thermoplastic materials at normal incidence
[NASA-TM-83410] p 94 N83-25883

RASHIDI, M.
Turbulent flame propagation and combustion in spark ignition engines p 70 A83-48156

RATAJCZAK, A. F.
DOE and AID stand-alone photovoltaic activities
[NASA-TM-83374] p 180 N83-25041

RAULT, D.
Radiative energy receiver for high performance energy conversion cycles p 164 A83-27138

RAULT, D. F. G.
Radiation energy receiver for laser and solar propulsion systems
[AIAA PAPER 83-1207] p 55 A83-36281

RAUSCH, M.
Satellite switched FDMA advanced communication technology satellite program
[NASA-CR-168034] p 105 N83-15543

RAWLIN, V. K.
Operation of the J-series thruster using inert gas
[AIAA PAPER 82-1929] p 54 A83-26625
Operation of the J-series thruster using inert gas
[NASA-TM-82977] p 57 N83-17587
Ring-cusp ion thruster with shell anode
[NASA-CASE-LEW-13881-1] p 202 N83-21903

RAY, P. K.
Characterization of advanced electric propulsion systems p 55 A83-33744

REA, E. C., JR.
Laser-induced fluorescence technique for velocity field measurements in subsonic gas flows
p 133 A83-45962

REAGAN, P.
Thermionic technology infrastructure for space power
p 54 A83-27298

REDDEN, T. K.
Powder metallurgy Rene 95 rotating turbine engine parts, volume 2
[NASA-CR-165141] p 82 N83-15412

REDDY, J. N.
Geometrically nonlinear analysis of layered composite shells p 156 A83-27431
Three-dimensional finite-element analysis of layered composite plates p 156 A83-27432
Geometrically nonlinear analysis of layered composite plates and shells
[NASA-CR-168182] p 161 N83-33219

REDDY, K. P. R.
O-18 tracer studies of Al2O3 scale formation on NiCrAl alloys p 74 A83-10249

REDDY, T. S.
Energy and precious fuels requirements of fuel alcohol production. Volume 4: Appendices G and H, methanol from coal
[NASA-CR-168093] p 183 N83-28580
Energy and precious fuels requirements of fuel alcohol production. Volume 2, appendices A and B: Ethanol from grain
[NASA-CR-168091] p 183 N83-28582
Energy and precious fuels requirements of fuel alcohol production. Volume 3, appendices C to F: Methanol from cellulose
[NASA-CR-168092] p 183 N83-28583

REED, K. W.
Stress and fracture analyses under elastic-plastic creep conditions: Some basic developments and computational approaches p 162 N83-34371

REID, L.
End-wall boundary layer measurements in a two-stage fan
[NASA-TM-83409] p 12 N83-24470

REID, M. A.
Zirconium carbide as an electrocatalyst for the chromous-chromic redox couple
[NASA-CASE-LEW-13246-1] p 182 N83-27344

REINER, P. S.
Future satellite systems - Market demand assessment
p 104 A83-19762

REINMANN, J. J.
NASA Lewis Research Center's program on icing research
[AIAA PAPER 83-0204] p 1 A83-16582
NASA Lewis Research Center's Program on Icing Research
[NASA-TM-83031] p 16 N83-14078

REISENFELD, S.
Onboard processing for a 30/20 GHz communications satellite p 47 A83-41391

RENGSTORFF, G. P.
Friction and wear of iron and nickel in sodium hydroxide solutions p 77 A83-48922

RENGSTORFF, G. W. P.
Friction and wear of iron and nickel in sodium hydroxide solutions
[NASA-TM-82935] p 77 N83-10171

RENZ, D. D.
Design considerations for large space electric power systems
[NASA-TM-83064] p 58 N83-24552

REYNOLDS, B.
Blade loading and rotation effects on compressor rotor wake near end walls p 3 A83-22138

REZAYAT, M.
Boundary integral equation method calculations of surface regression effects in flame spreading
p 67 A83-13488

RHODE, D. L.
Mean flowfields in axisymmetric combustor geometries with swirl p 120 A83-24668

RICE, E. J.
Aircraft turbofan noise
[NASA-TM-83317] p 198 N83-18405

RICHARDS, C. R.
Advanced digital modulation: Communication techniques and monolithic GaAs technology
[NASA-CR-174452] p 109 N83-36299

RICHEY, A.
Automotive Stirling engine development program
[NASA-CR-167907] p 209 N83-15176
Automotive Stirling engine development program
[NASA-CR-168060] p 209 N83-15177
Automotive Stirling Engine Development Program
[NASA-CR-168074] p 212 N83-27925

RIDDLEBAUGH, S. M.
Small gas turbine combustor study - Combustor liner evaluation
[AIAA PAPER 83-0337] p 20 A83-16663
Effect of broad properties fuel on injector performance in a reverse flow combustor
[AIAA PAPER 83-0154] p 20 A83-21079
Small gas turbine combustor study: Combustor liner evaluation
[NASA-TM-83028] p 33 N83-18725

RIEKE, K. L.
Advanced ceramic coating development for industrial/utility gas turbine applications
[NASA-CR-165619] p 92 N83-15467

RIEKER, L. L.
Polyvinyl alcohol cross-linked with two aldehydes
[NASA-CASE-LEW-13504-1] p 71 N83-13188

RITTERMAN, P. F.
Development of improved hydrogen recombination in sealed nickel-cadmium aerospace cells
p 54 A83-27198
Deep discharge reconditioning and shorted storage of batteries
[NASA-CR-167953] p 166 N83-10502

RIZVI, A. R.
Correlating downward flame spread rates for thick fuel beds p 69 A83-37045

RIZVI, G.
An experimental investigation of internal area ruling for transonic and supersonic channel flow
[NASA-CR-169638] p 10 N83-14068

RIZZO, F. J.
Boundary integral equation method calculations of surface regression effects in flame spreading
p 67 A83-13488

ROBACK, R.
Deposit formation in hydrocarbon rocket fuels: Executive summary
[NASA-CR-165492] p 102 N83-35159

ROBERTS, W. B.
An experimental investigation of internal area ruling for transonic and supersonic channel flow
[NASA-CR-169638] p 10 N83-14068

ROBERTS, W. K.
Aircraft sampling of the sulfate layer near the tropopause following the eruption of Mount St. Helens
p 187 N83-11556

ROBERTSON, R. I.
Benefits and costs of low thrust propulsion systems
[AIAA PAPER 83-1248] p 49 A83-36306
Study for analysis of benefit versus cost of low thrust propulsion system
[NASA-CR-168011] p 57 N83-21002

ROBINSON, A. C.
Three-dimensional stability of vortex arrays
p 120 A83-19022

ROBINSON, D. N.
Constitutive relationships for anisotropic high-temperature alloys
[NASA-TM-83437] p 160 N83-28493

ROBINSON, M. A.
Quasi-three-dimensional turbomachinery flow calculations on multiple hub-to-shroud stream surfaces
[AIAA PAPER 83-1820] p 5 A83-36652

ROBINSON, R. S.
Ion flow experiments in a multipole discharge chamber
[AIAA PAPER 82-1930] p 203 A83-14398
Inert gas thruster technology p 53 A83-20423
Industrial ion source technology
[NASA-CR-159877] p 102 N83-12259
Electric thruster research
[NASA-CR-168134] p 59 N83-32843

ROBSON, R. R.
Advances in series resonant inverter technology and its effect on spacecraft employing electric propulsion
[AIAA PAPER 82-1881] p 51 A83-12406
Software and system level tests of a test flight mercury ion thruster subsystem
[AIAA PAPER 82-1912] p 51 A83-12485

ROCK, S. M.
Sensor failure detection for jet engines
[NASA-CR-168190] p 154 N83-33182

ROCKS, J. K.
Development and test of a Microwave Ice Accretion Measurement Instrument (MIAMI)
[NASA-CR-3598] p 18 N83-14123

ROCKWELL, D. O.
Critical review of the trailing edge condition in steady and unsteady flow. Blade flutter in compressors and fans: Numerical simulation of the aerodynamic loading
[NASA-CR-169705] p 10 N83-15264

RODER, H. M.
The thermal conductivity of oxygen
p 207 A83-12094
Transport properties of oxygen
[NASA-RP-1102] p 130 N83-24800

RODRIGUEZ, C. F.
Evaluation of fuel additives for reduction of material imcompatibilities in methanol-gasoline blends
[NASA-CR-168061] p 86 N83-29359

ROELKE, R. J.
Cold-air performance of compressor-drive turbine of Department of Energy upgraded automobile gas turbine engine. 2: Stage performance
[NASA-TM-82818] p 9 N83-11063

ROFFE, G.
Testing of felt-ceramic materials for combustor applications
[NASA-CR-168103] p 36 N83-26837

ROGERS, A.
Supersonic STOVL research aircraft
[SAE PAPER 821375] p 17 A83-37965

ROGERS, C. J.
Process and quality verification controls for solid propellant manufacturing p 98 A83-39270

ROHLIK, H. E.
Current and future technology in radial and axial gas turbines
[NASA-TM-83414] p 41 N83-32811
ROHN, D. A.
Traction behavior of two traction lubricants
[NASA-TM-83311] p 144 N83-20116
Evaluation of a high performance, fixed-ratio, traction drive p 145 N83-20135
Sizing criterial for traction drives p 146 N83-20137
Regression analysis of traction characteristics of traction fluids
[NASA-TP-2154] p 148 N83-24862
Advances in traction drive technology
[NASA-TM-83397] p 150 N83-28455
ROHRBACH, C.
Small transport aircraft technology propeller study
[NASA-CR-166045] p 14 N83-29178
ROMAN, R. F.
Ring-cusp ion thruster with shell anode
[NASA-CASE-LEW-13881-1] p 202 N83-21903
ROOT, J.
Performance characteristics of a microwave plasma disk ion source
[AIAA PAPER 82-1935] p 55 A83-27350
ROSE, J. H.
Diatomic molecules and metallic adhesion, cohesion, and chemisorption - A single binding-energy relation p 69 A83-30921
ROSE, L.
High accuracy fuel flowmeter, phase 1
[NASA-CR-167893] p 134 N83-21314
ROSE, L. J.
Benefits and costs of low thrust propulsion systems
[AIAA PAPER 83-1248] p 49 A83-36306
Study for analysis of benefit versus cost of low thrust propulsion system
[NASA-CR-168011] p 57 N83-21002
ROSE, M. E.
A numerical study of the steady scalar convective diffusion equation for small viscosity
[NASA-CR-172231] p 16 N83-35999
ROSEN, J.
Market assessment of photovoltaic power systems for agricultural applications worldwide
[NASA-CR-165541] p 168 N83-13585
ROSENBLUM, L.
Practical aspects of photovoltaic technology, applications, and cost
[NASA-CR-168025] p 185 N83-34450
ROSFJORD, T. J.
Combustion of coal gas fuels in a staged combustor
[NASA-TM-82987] p 166 N83-10556
ROSNER, D. E.
Small particle transport across turbulent nonisothermal boundary layers p 118 A83-10650
Correlation and prediction of thermophoretic and inertial effects on particle deposition from non-isothermal turbulent boundary layers p 121 A83-27481
Combustion system processes leading to corrosive deposits p 69 A83-42246
ROSS, D. P.
Customer premise service study for 30/20 GHz satellite system
[NASA-CR-167986] p 105 N83-17769
RUPICH, M. W.
Moderate temperature rechargeable sodium-batteries
[NASA-CR-168220] p 118 N83-36359
RUSSELL, L. M.
Comparison of visualized turbine endwall secondary flows and measured heat transfer patterns
[NASA-TM-83016] p 128 N83-14435
RYAN, C. R.
Advances in Serial MSK modems p 111 A83-19789

S

SABLA, P. E.
NASA clean catalytic combustor program
[ASME PAPER 82-JPGC-GT-11] p 68 A83-25269
SABOURIN, D. J.
A network control concept for the 30/20 GHz communication system baseband processor p 47 A83-41389
Method for terminal position determination in Earth terminal-to-satellite burst acquisition and synchronization
[NASA-CASE-LEW-13893-1] p 107 N83-30832
SADEH, W. Z.
Turbulence effect on crossflow around a circular cylinder at subcritical Reynolds numbers
[NASA-CR-3622] p 127 N83-13387
SAFFMAN, P. G.
Three-dimensional stability of vortex arrays p 120 A83-19022
Vortices, stability, and turbulence p 125 A83-46718
SAHARON, D. B.
Turbulence effect on crossflow around a circular cylinder at subcritical Reynolds numbers
[NASA-CR-3622] p 127 N83-13387
SAIN, M.
Controller scheduling - A possible algebraic viewpoint p 190 A83-37093
SAIN, M. K.
Nonlinear multivariable design by total synthesis p 24 A83-37092
Alternatives for jet engine control
[NASA-CR-170100] p 33 N83-20945
Alternatives for jet engine control
[NASA-CR-170233] p 35 N83-23305
SAKANE, M.
An extensometer for axial strain measurement at high temperature p 134 A83-48604
SALAH-EDDINE, A.
Measurement of thermoacoustic convection heat transfer phenomenon
[AIAA PAPER 83-1422] p 121 A83-32701
SALIKUDDIN, M.
Generation of desired signals from acoustic drivers p 19 A83-15068
Sound radiation from annular ducts/nozzles using modal decomposition of in-duct acoustic power
[AIAA PAPER 83-0714] p 194 A83-25929
Refinement and application of acoustic impulse technique to study nozzle transmission characteristics
[NASA-CR-3656] p 199 N83-20708
SALKELD, R. W.
Energy efficient engine high-pressure turbine single crystal vane and blade fabrication technology report
[NASA-CR-165400] p 39 N83-30429
SALTSMAN, J. F.
Strainrange partitioning: A total strain range version
[NASA-TM-83023] p 81 N83-14246
SALVINO, J. T.
Rotor fragment protection program: Statistics on aircraft gas turbine engine rotor failures that occurred in US commercial aviation during 1979
[NASA-CR-168163] p 38 N83-29234
SALZMAN, J. A.
Concept for advanced satellite communications and required technologies
[NASA-TM-82984] p 47 N83-11210
SAMANICH, N. E.
QCSEE under-the-wing engine-wing-flap aerodynamic profile characteristics
[NASA-TM-82890] p 28 N83-12092
SANCHEZ, J.
Superalloy composition modeling p 78 N83-11284
Role of cobalt in nickel base superalloys p 78 N83-11286
SANDER, G. F.
The performance of an annular vane swirler
[AIAA PAPER 83-1326] p 24 A83-36340
Axial vane-type swirler performance characteristics
[NASA-CR-172995] p 40 N83-32808
SANZ, J.
The evolution of Tollmien-Schlichting waves near a leading edge. II - Numerical determination of amplitudes p 122 A83-35346
SANZ, J. M.
Design of supercritical cascades with high solidity p 6 A83-43446
Improved design of subcritical and supercritical cascades using complex characteristics and boundary layer correction
[NASA-CR-168166] p 12 N83-24474
SAPORTA, L.
Customer premises services market demand assessment 1980 - 2000. Volume 1: Executive summary
[NASA-CR-168150] p 108 N83-31925
Customer premises services market demand assessment 1980 - 2000: Volume 2
[NASA-CR-168151] p 108 N83-31926
SARV, H.
Droplet size effects on NO/x/ formation in a one-dimensional monodisperse spray combustion system
[ASME PAPER 82-JPGC-GT-10] p 66 A83-25268
SAUNDERS, A. L.
Operating experience with the 200 kW MOD-OA wind turbine generators p 174 N83-15916
Operating experience with four 200 kW Mod-0A wind turbine generators p 176 N83-19256
SAUNDERS, N. T.
Overview of high-temperature materials for high-energy space power systems p 173 N83-15869
SAUNIER, P.
High-performance K-band GaAs power field-effect transistors prepared by molecular beam epitaxy p 112 A83-33846
GaAs integrated digital-to-analogue convertor for control of power dual-gate FETs p 112 A83-36479
SAVAGE, M.
Life and reliability models for helicopter transmissions
[NASA-TM-82976] p 139 N83-10425
The optimal design of standard gearsets p 146 N83-20145
SAVINELL, R. F.
Experimental study of electrochemical fluorination of trichloroethylene p 68 A83-15870
SCHERSON, D.
Electromagnetic studies of redox systems for energy storage
[NASA-CR-169593] p 169 N83-14667
SCHEUERMANN, C. M.
Low-cobalt single crystal Rene 150 p 78 N83-11288
SCHIAVONE, A.
Development of a microwave 20 x 20 switch matrix for 30/20 GHz SS-TDMA application p 110 A83-11484
SCHILLING, D. L.
Modulation techniques
[NASA-CR-169460] p 105 N83-10329
Computer simulator for a mobile telephone system
[NASA-CR-170181] p 106 N83-22493
VLSI technology and applications
[NASA-CR-174451] p 118 N83-36358
SCHMIDT, J.
An extensometer for axial strain measurement at high temperature p 134 A83-48604
SCHMIDT, J. F.
End-wall boundary layer measurements in a two-stage fan
[NASA-TM-83409] p 12 N83-24470
SCHOCK, H. J.
Numerical studies of the formation and destruction of vortices in a motored four-stroke piston-cylinder configuration
[AIAA PAPER 83-0497] p 136 A83-16749
SCHOEN, D.
Customer premise service study for 30/20 GHz satellite system
[NASA-CR-167986] p 105 N83-17769
SCHOENHALS, R. J.
Acoustic velocities of two-phase mixtures of cryogenic fluids p 124 A83-43012
SCHOFIELD, K.
Laser fluorescence studies of the chemical interactions of sodium species with sulfur bearing fuels
[NASA-CR-169861] p 71 N83-17625
The detailed chemistry and thermodynamics of sodium in oxygen-rich flames
[NASA-CR-169848] p 72 N83-17626
SCHORNHORST, J. R.
The MOD-OA 200 kilowatt wind turbine generator design and analysis report
[NASA-CR-165127] p 174 N83-16859
SCHREIBER, J.
Testing and performance characteristics of a 1-kW free piston Stirling engine
[NASA-TM-82999] p 180 N83-25036
Test results and description of a 1-kW free-piston Stirling engine with a dashpot load
[NASA-TM-83407] p 192 N83-27346
SCHULLER, F. T.
Lubrication of 35-millimeter-bore ball bearings of several designs at speeds to 2.5 million DN p 141 N83-15512
Lubrication of 35-millimeter-bore ball bearings of several designs to 2.5 million DN p 145 N83-20132
SCHULSON, E. M.
A brittle to ductile transition in NiAl of a critical grain size p 75 A83-29726
SCHULTZ, D. F.
Combustion of coal gas fuels in a staged combustor
[NASA-TM-82987] p 166 N83-10556
Steam cooled rich-burn combustor liner
[NASA-CASE-LEW-13609-1] p 72 N83-17628
Critical research and advanced technology (CRT) support project
[NASA-TM-83019] p 176 N83-20361
A variable-geometry combustor used to study primary and secondary zone stoichiometry
[NASA-TM-83372] p 37 N83-27995
Summary of synfuel characterization and combustion studies
[NASA-TM-83066] p 185 N83-34453
SCHUMANN, L. F.
Performance of a tandem-rotor/tandem-stator conical-flow compressor designed for a pressure ratio of 3
[NASA-TP-2034] p 9 N83-11058
SCHUON, S. R.
Development of Fe-Mn-Al-X-C alloys p 80 N83-11307

The effects of Ni, Mo, Ti and Si on the mechanical properties of Cr free Mn steel (Fe-25Mn-5Al-2C)
[NASA-TM-83355] p 85 N83-24636
SCHWAB, J.
NOx results from two combustors tested on medium BTU coal gas p 186 A83-11493
SCHWAB, J. R.
Analytical and experimental study of flow through an axial turbine stage with a nonuniform inlet radial temperature profile
[AIAA PAPER 83-1175] p 6 A83-45510
Analytical and experimental study of flow through an axial turbine stage with a nonuniform inlet radial temperature profile
[NASA-TM-83431] p 14 N83-27958
SCHWARTZ, H. J.
A summary of EHV propulsion technology p 209 A83-31087
SCHWARTZ, M.
Comparison of channel assignment techniques for hybrid switching p 104 A83-41363
Next generation communications satellites: multiple access and network studies
[NASA-CR-167903] p 45 N83-12129
SCHWARZ, R.
Advanced hybrid vehicle propulsion system study
[NASA-CR-159773] p 211 N83-24432
SCHWEIKHHARD, W. G.
Literature search of publications concerning the prediction of dynamic inlet flow distortion and related topics
[NASA-CR-3673] p 33 N83-18729
SCOLA, D. A.
Synthesis and characterization of bisimide amines and bisimide amine-cured epoxy resins p 88 A83-11486
Bisimide amine cured epoxy /IME/ resins and composites. II - Ten-degree off-axis tensile and shear properties of Celion 6000/IME composites p 62 A83-23608
Synthesis and characterization of bisimide amines and bisimide amine-cured epoxy resins p 90 A83-40924
Imide modified epoxy matrix resins
[NASA-CR-167942] p 93 N83-18909
SCOTT, G. W.
Measured effect of wind generation on the fuel consumption of an isolated diesel power system p 165 A83-36410
Wind turbine generator interaction with diesel generators on an isolated power system p 165 A83-44673
SEASHOLTZ, R. G.
Comparison of laser anemometer measurements and theory in an annular turbine cascade with experimental accuracy determined by parameter estimation p 4 A83-28833
Laser anemometer using a Fabry-Perot interferometer for measuring mean velocity and turbulence intensity along the optical axis in turbomachinery p 133 A83-28834
SECUNDE, R. R.
New propulsion components for electric vehicles
[NASA-TM-83404] p 116 N83-25982
SEDERQUIST, R. A.
Combustion of coal gas fuels in a staged combustor
[NASA-TM-82987] p 166 N83-10556
SEDY, J.
Energy efficient face seal
[NASA-CR-165591] p 142 N83-15659
SEGALL, S. B.
Gain-enhanced free-electron laser with an electromagnetic pump field p 135 A83-31133
The application of free-electron lasers to the transmission of energy in space p 135 A83-31141
SEHNAL, J.
Energy efficient face seal
[NASA-CR-165591] p 142 N83-15659
SEIDEL, B. S.
Inlet-fan flow field computation
[ASME PAPER 83-GT-41] p 7 A83-47901
SELLERS, F. J.
Control means for a gas turbine engine
[NASA-CASE-LEW-14586-1] p 40 N83-31603
SELLERS, J. F.
Army/NASA small turboshaft engine digital controls research program
[NASA-TM-82979] p 27 N83-11128
SENG, G. T.
Evaluation of ultraviolet spectrophotometry for simultaneous analysis of alkylbenzenes, alkylnaphthalenes, alkylanthracenes/phenanthrenes and total aromatics in mid-distillate fuels
[NASA-TM-83032] p 99 N83-15483
High performance liquid chromatographic hydrocarbon group-type analyses of mid-distillates employing fuel-derived fractions as standards
[NASA-TM-83072] p 100 N83-19920
Research on aviation fuel instability
[NASA-TM-83420] p 101 N83-28255
SENTY, P.
Propeller performance and weight predictions appended to the Navy/NASA engine program
[NASA-TM-83458] p 41 N83-32810
SERAFINI, J. S.
An analytical and experimental comparison of the flow field of an advanced swept turboprop
[AIAA PAPER 83-0189] p 3 A83-21080
An analytical and experimental comparison of the flow field of an advanced swept turboprop
[NASA-TM-83037] p 1 N83-14061
SERAFINI, T. T.
PMR polyimides - Review and update p 62 A83-20447
Environmental effects on graphite fiber reinforced PMR-15 polyimide p 63 A83-33115
Polymer matrix composites research at NASA Lewis Research Center p 91 N83-12151
PMR polyimide composites for aerospace applications
[NASA-TM-83047] p 65 N83-15364
Low temperature cross linking polyimides
[NASA-CASE-LEW-12876-2] p 96 N83-29392
SHALTENS, R. K.
Measured effect of wind generation on the fuel consumption of an isolated diesel power system p 165 A83-36410
Wind turbine generator interaction with diesel generators on an isolated power system p 165 A83-44673
Operating experience with the 200 kW MOD-0A wind turbine generators p 174 N83-15916
Operating experience with four 200 kW Mod-0A wind turbine generators p 176 N83-19256
Experience and assessment of the DOE/NASA Mod-1 2000 kW wind turbine generator at Boone, North Carolina p 176 N83-19257
SHAMROTH, S. J.
Numerical solution of the Navier-Stokes equations for compressible turbulent two/three dimensional flows in the terminal shock region of an inlet/diffuser
[AIAA PAPER 83-1892] p 5 A83-39358
Numerical solutions of Navier-Stokes equations for compressible turbulent two/three dimensional flows in terminal shock region of an inlet/diffuser
[NASA-CR-3723] p 132 N83-34230
SHANNON, J. L., JR.
Specimen size and geometry effects on fracture toughness of Al2O3 measured with short rod and short bar chevron-notch specimens
[NASA-TM-83319] p 94 N83-19902
Analysis of an externally radially cracked ring segment subject to three-point radial loading
[NASA-TM-83482] p 163 N83-35413
SHAPIRO, W.
Analysis of spiral-groove face seals for liquid oxygen
[ASLE PREPRINT 83-AM-4B-2] p 138 A83-43339
SHARP, R. G.
Near-field measurement facility plans at Lewis Research Center p 46 N83-26897
SHARPE, W. N.
Benchmark notch test for life prediction
[NASA-CR-165571] p 158 N83-12451
SHAW, L. M.
Rotor wake characteristics relevant to rotor-stator interaction noise generation p 19 A83-10184
Experimental evaluation of shockless supercritical airfoils in cascade
[AIAA PAPER 83-0003] p 2 A83-16455
Experimental evaluation of shockless supercritical airfoils in cascade
[NASA-TM-83045] p 11 N83-15268
SHAW, N. J.
Thermodynamics of silicon nitridation - Effect of hydrogen
[ACS PAPER 33-B-80P] p 88 A83-18052
SHAW, R. J.
Influence of multidroplet size distribution on icing collection efficiency
[AIAA PAPER 83-0110] p 187 A83-16526
NASA Lewis Research Center's program on icing research
[AIAA PAPER 83-0204] p 1 A83-16582
NASA Lewis Research Center's Program on Icing Research
[NASA-TM-83031] p 16 N83-14078
Turbofan blade stresses induced by the flow distortion of a VTOL inlet at high angles of attack
[NASA-TM-82963] p 12 N83-17509
SHEFFLER, K.
Progress toward determining the potential of ODS alloys for gas turbine applications
[NASA-TM-83332] p 83 N83-22387
SHEFFLER, K. D.
JT9D thermal barrier coated vanes
[NASA-CR-167964] p 37 N83-27993
SHEIBLEY, D.
Evaluation of production version of the NASA improved inorganic-organic separator
[NASA-TM-83018] p 174 N83-18022
SHEIBLEY, D. W.
Cross-linked polyvinyl alcohol films as alkaline battery separators p 68 A83-20576
Alkaline regenerative fuel cell energy storage system for manned orbital satellites p 54 A83-27206
Polyvinyl alcohol membranes as alkaline battery separators
[NASA-TM-82961] p 70 N83-10135
Polyvinyl alcohol cross-linked with two aldehydes
[NASA-CASE-LEW-13504-1] p 71 N83-13188
Polyvinyl alcohol battery separator containing inert filler
[NASA-CASE-LEW-13556-2] p 183 N83-29805
Advanced inorganic separators for alkaline batteries and method of making the same
[NASA-CASE-LEW-13171-2] p 184 N83-32176
SHEIKHOLESLAMI, M. Z.
The finite analytic method, volume 3
[NASA-CR-170186] p 191 N83-23087
SHERLOCK, T. P.
NOx results from two combustors tested on medium BTU coal gas p 186 A83-11493
SHESKIN, T. J.
Performance degradation and cleaning of photovoltaic arrays p 164 A83-27236
SHEU, Y. C.
The transmission or scattering of elastic waves by an inhomogeneity of simple geometry: A comparison of theories
[NASA-CR-3659] p 153 N83-16773
SHIEH, D.
Development of a microwave 20 x 20 switch matrix for 30/20 GHz SS-TDMA application p 110 A83-11484
SHIEMBOB, L. T.
JT9D ceramic outer air seal system refinement program, phase 2
[NASA-CR-167962] p 30 N83-15305
SHIH, H. D.
High-performance K-band GaAs power field-effect transistors prepared by molecular beam epitaxy p 112 A83-33846
SHIH, T. I. P.
Numerical simulation of the flow and fuel-air mixing in an axisymmetric piston-cylinder arrangement
[NASA-TM-83011] p 126 N83-12358
Vortex motion in axisymmetric piston-cylinder configurations
[NASA-TM-85404] p 133 N83-35318
SHIN, C. T.
Study of asymptotic incompressible flow in curved ducts using a multi-grid technique p 123 A83-42532
SHIPERS, L. R.
A detailed treatment of two-dimensional, starved lubrication in the vicinity of two counter-rotating cylinders p 141 N83-15520
SHISLER, R. A.
Evaluation of catalytic combustion of actual coal-derived gas
[NASA-CR-167842] p 168 N83-13588
SHORTT, D. J.
An improved switching converter model using discrete and average techniques p 111 A83-11495
An improved switching converter model
[NASA-CR-169669] p 114 N83-14398
SHUEN, J. S.
The structure of particle-laden jets and nonevaporating sprays
[NASA-CR-168059] p 34 N83-20948
The structure of evaporating and combusting sprays: Measurements and predictions
[NASA-CR-170176] p 129 N83-22550
The structure of evaporating and combusting sprays: Measurements and predictions
[NASA-CR-170312] p 130 N83-24795
Structure of evaporating and combusting sprays: Measurements and predictions p 38 N83-29211
SHUEN, J.-S.
Predictions of the structure of turbulent, particle-laden, round jets
[AIAA PAPER 83-0066] p 119 A83-16498
Measurements and predictions for nonevaporating sprays in a quiescent environment
[AIAA PAPER 83-0151] p 119 A83-16558
Evaluation of a stochastic model of particle dispersion in a turbulent round jet p 121 A83-28104
SHUTIANI, P. K.
Free-jet acoustic investigation of high-radius-ratio coannular plug nozzles. Comprehensive data report, volume 1
[NASA-CR-168086-VOL-1] p 198 N83-18408

SIDI, A.
Convergence and stability properties of minimal polynomial and reduced rank extrapolation algorithms
[NASA-TM-83443] p 191 N83-31390
SIDIK, S. M.
Results of chopper-controlled discharge life cycling studies on lead-acid batteries p 164 A83-27183
SIEGEL, R.
Determination of boundary shape of cooled porous region p 118 A83-13487
Analysis of coolant entrance boundary shape of porous region to control cooling along exit boundary p 124 A83-43361
SIGMAN, R. K.
An iterative method for predicting turbofan inlet acoustics p 192 A83-13135
Optimization of acoustic liners by the hybrid finite element-integral approach
[AIAA PAPER 83-0670] p 194 A83-26917
SIGNER, H. R.
Lubrication of 35-millimeter-bore ball bearings of several designs at speeds to 2.5 million DN p 141 N83-15512
Bearing fatigue investigation 3
[NASA-CR-168029] p 143 N83-17860
SIGNORELLI, R. A.
High-temperature composites - Status and future directions p 63 A83-40129
Evaluation of low-cost aluminum composites for aircraft engine structural applications
[NASA-TM-83357] p 66 N83-25790
SIH, G. C.
Moving cracks in layered composites p 155 A83-12048
SIMETKOSKY, M.
Automotive Stirling engine development program
[NASA-CR-167907] p 209 N83-15176
Automotive Stirling engine development program
[NASA-CR-168060] p 209 N83-15177
Automotive Stirling Engine Development Program
[NASA-CR-168074] p 212 N83-27925
SIMON, A. L.
NASA LeRC/Akron University Graduate Cooperative Fellowship Program and Graduate Student Researchers Program
[NASA-CR-167943] p 208 N83-10970
SIMON, T. W.
Convex curvature effects on the heated turbulent boundary layer p 123 A83-42733
SIMONS, S.
The phototron: A light to RF energy conversion device p 173 N83-15866
SINGH, K.
The finite analytic method, volume 3
[NASA-CR-170186] p 191 N83-23087
SINHA, A.
Friction damping of flutter in gas turbine engine airfoils p 20 A83-24038
Effects of friction dampers on aerodynamically unstable rotor stages
[AIAA PAPER 83-0848] p 22 A83-32791
SINKO, G. C.
JT9D thermal barrier coated vanes
[NASA-CR-167964] p 37 N83-27993
SINNETT, C.
Fuel quality/processing study. Volume 3: Fuel upgrading studies
[NASA-CR-165326-VOL-3] p 178 N83-22754
SIPERKO, C.
Planning assistance for the 30/20 GHz program, volume 1
[NASA-CR-165484-VOL-1] p 108 N83-33010
Planning assistance for the 30/20 GHz program, volume 2
[NASA-CR-165484-VOL-2] p 108 N83-33011
Planning assistance for the 30/20 GHz program, volume 3
[NASA-CR-165484] p 108 N83-33012
SIROCKY, P. J.
Measured performance of a tip-controlled, teetered rotor with an NACA 64 sub 3-618 tip airfoil
[NASA-TM-82870] p 169 N83-14689
SITARAM, N.
Wall boundary layer development near the tip region of an IGV of an axial flow compressor
[ASME PAPER 83-GT-171] p 8 A83-47972
End wall flow characteristics and overall performance of an axial flow compressor stage
[NASA-CR-3671] p 13 N83-26819
SIVO, J. N.
30/20 GHz experimental communications satellite system p 103 A83-19688
Advanced communications satellite systems p 47 A83-49855
SKIDMORE, W.
Development of a rotary instrumentation system, phase 2
[NASA-CR-168013] p 47 N83-18835
SLABY, J. G.
Free-piston Stirling hydraulic engine and drive system for automobiles
[NASA-TM-82992] p 211 N83-25625
SLEEPER, H. A.
Four-dimensional modulation and coding: An alternate to frequency-reuse
[NASA-CR-174453] p 110 N83-36300
SLETTEN, C. J.
Techniques for low sidelobe, high efficiency offset dual reflector antennas p 104 A83-21072
SLINEY, H. E.
Improved uniformity of multiphase ceramic-metal plasma-sprayed coats p 61 A83-22269
A commentary on solid lubricants and wear resistant solids for use in extreme environments
[NASA-TM-83042] p 92 N83-15468
SMEGGIL, J. G.
The oxidation behavior of a model molybdenum/tungsten-containing alloy in air alone and in air with trace levels of NaCl(g) p 76 A83-42241
SMETANA, J.
Application of MMIC modules in future multiple beam satellite antenna systems
[NASA-TM-83344] p 48 N83-22313
Scanning beam antenna conceptual design for 20/30 GHz satellite systems p 46 N83-26889
SMIALEK, J.
Interfacial layers in high-temperature-oxidized NiCrAl p 77 A83-44619
SMIALEK, J. L.
O-18 tracer studies of Al2O3 scale formation on NiCrAl alloys p 74 A83-10249
Cyclic oxidation of superalloys p 76 A83-42234
Diffusion processes in Al2O3 scales - Void growth, grain growth, and scale growth p 76 A83-42238
Processing of fused silicide coatings for carbon-based materials
[NASA-TM-83362] p 95 N83-27019
SMITH, C. E.
Rotorcraft convertible engine study
[NASA-CR-168241] p 42 N83-34944
SMITH, G.
Automotive Stirling Engine Development Program
[NASA-CR-168074] p 212 N83-27925
SMITH, G. C. C.
Flutter analysis of advanced turbopropellers
[AIAA 83-0846] p 157 A83-29824
SMITH, G. E.
Numerical simulation of the flow and fuel-air mixing in an axisymmetric piston-cylinder arrangement
[NASA-TM-83011] p 126 N83-12358
Vortex motion in axisymmetric piston-cylinder configurations
[NASA-TM-85404] p 133 N83-35318
SMITH, G. T.
Resin selection criteria for tough composite structures
[AIAA 83-0801] p 89 A83-29734
SMITH, J. M.
End region effects upon the performance of a magnetohydrodynamic channel p 203 A83-10625
NASA Lewis Research Center combustion MHD experiment p 173 N83-15847
Preliminary tests of an advanced high-temperature combustion system
[NASA-TP-2203] p 41 N83-33893
SMITH, J. R.
Diatomic molecules and metallic adhesion, cohesion, and chemisorption - A single binding-energy relation p 69 A83-30921
SMITH, J. T.
Sintering, properties and fabrication of Si3N4 + Y2O3 based ceramics p 90 A83-48303
SMITH, L. D.
Solar array switching power management p 54 A83-27132
SMITH, P. J.
Investigation of the effects of initial fluid film profile on pumping ring operation
[ASME PAPER 82-LUB-35] p 136 A83-13516
Thermoelastohydrodynamic analysis of an oil pumping ring seal p 137 A83-22322
SMITH, T. J.
Industry's assessment of the number of airplanes in the general aviation fleet along with their hours flown and fuel consumption data powered by what type of engines, when and for what reasons, through the year 2000 p 101 N83-22445
SMITH, W. W.
Auxiliary propulsion requirements for large space systems
[AIAA PAPER 83-1217] p 56 A83-45512
Large space systems auxiliary propulsion requirements p 46 N83-26864
Auxiliary propulsion requirements for large space systems
[NASA-TM-83388] p 58 N83-26922
SMITHRICK, J. J.
Design of a 35-kilowatt bipolar nickel-hydrogen battery for low-earth-orbit applications p 54 A83-27205
Cycle life test and failure model of nickel-hydrogen cells
[NASA-TM-83375] p 160 N83-25038
SMYTHE, M. E.
The effects of metals and inhibitors on thermal oxidative degradation reactions of unbranched perfluoroalkylethers
[NASA-TM-83464] p 97 N83-34049
SNELLENBERGER, R.
Microwave plasma generation of hydrogen atoms for rocket propulsion p 53 A83-13090
SNOW, G. C.
Catalyst durability evaluation for advanced gas turbine engines
[ASME PAPER 82-JPGC-GT-21] p 137 A83-25270
SNYDER, A.
Determination of boundary shape of cooled porous region p 118 A83-13487
Analysis of coolant entrance boundary shape of porous region to control cooling along exit boundary p 124 A83-43361
SOCKOL, P.
A viscous-inviscid interactive procedure for rotational flow in cascades of two-dimensional airfoils of arbitrary shape
[AIAA PAPER 83-0256] p 3 A83-16614
SOCKOL, P. M.
The evolution of Tollmien-Schlichting waves near a leading edge. II - Numerical determination of amplitudes p 122 A83-35346
SOEDER, J. F.
Design of a microprocessor-based Control, Interface and Monitoring (CIM unit for turbine engine controls research
[NASA-TM-83433] p 2 N83-34885
SOEDER, R. H.
Effect of variable guide vanes on the performance of a high-bypass turbofan engine p 20 A83-24028
Effect of steady-state pressure distortion on inlet flow to a high-bypass-ratio turbofan engine
[NASA-TM-82954] p 30 N83-15306
SOFRIN, T. G.
Investigation of continuously traversing microphone system for mode measurement
[NASA-CR-168040] p 199 N83-19575
SOKOLOWSKI, D. E.
Development and operating characteristics of an advanced two-stage combustor p 24 A83-38022
SOLOMON, A. S. P.
Measurements and predictions for nonevaporating sprays in a quiescent environment
[AIAA PAPER 83-0151] p 119 A83-16558
The structure of particle-laden jets and nonevaporating sprays
[NASA-CR-168059] p 34 N83-20948
The structure of evaporating and combusting sprays: Measurements and predictions
[NASA-CR-170176] p 129 N83-22550
The structure of evaporating and combusting sprays: Measurements and predictions
[NASA-CR-170312] p 130 N83-24795
Structure of evaporating and combusting sprays: Measurements and predictions p 38 N83-29211
SOLOMOS, G. P.
Solution to the backward-Kolmogorov equation for a nonstationary oscillation problem p 192 A83-15697
SORBELLO, R.
Scanning beam antenna conceptual design for 20/30 GHz satellite systems p 46 N83-26889
SOSOKA, D. J.
Numerical studies of the formation and destruction of vortices in a motored four-stroke piston-cylinder configuration
[AIAA PAPER 83-0497] p 136 A83-16749
SOUKUP, R. J.
Diffusion length measurements in solar cells: An analysis and comparison of techniques p 171 N83-15812
SOVEY, J. S.
Improved ion containment using a ring-cusp ion thruster
[AIAA PAPER 82-1928] p 53 A83-21100
Ion sputter textured graphite
[NASA-CASE-LEW-12919-1] p 63 N83-10117
Improved ion containment using a ring-cusp ion thruster
[NASA-TM-82990] p 56 N83-13164
Ring-cusp ion thruster with shell anode
[NASA-CASE-LEW-13881-1] p 202 N83-21903

Thermal barrier coating system having improved adhesion
[NASA-CASE-LEW-1335901] p 97 N83-31855

SPADACCINI, L. J.
Deposit formation in hydrocarbon rocket fuels: Executive summary
[NASA-CR-165492] p 102 N83-35159

SPALVINS, T.
Tribological properties and X-ray photoelectron spectroscopy studies of ion-plated gold on nickel and iron p 74 A83-12650
Morphological and frictional behavior of sputtered MoS2 films p 88 A83-12652
Plasma deposition and surface modification techniques for wear resistance
[NASA-TM-82972] p 90 N83-10194
Vacuum sputtered and ion-plated coatings for wear and corrosion protection
[NASA-TM-83007] p 99 N83-13273
Frictional and morphological characteristics of ion plated soft, metallic films
[NASA-TM-81723] p 83 N83-22390
The XPS depth profiling and tribological characterization of ion-plated gold on various metals
[NASA-TM-83350] p 83 N83-23417
Tribological and microstructural characteristics of ion-nitrided steels
[NASA-TM-83368] p 84 N83-24635
Friction and hardness of gold films deposited by ion plating and evaporation
[NASA-TP-2207] p 87 N83-34019

SPANOS, P.-T. D.
Solution to the backward-Kolmogorov equation for a nonstationary oscillation problem p 192 A83-15697

SPERA, D. A.
Performance and load data from Mod-0A and Mod-1 wind turbine generators p 176 N83-19255

SPIELBERG, N.
Applications of ion beam technology
[NASA-CR-169797] p 82 N83-16493

SPIER, E. E.
Stability analysis of Centaur-in-Shuttle composite corrugated adapters
[AIAA 83-1003] p 49 A83-29791

SPINDT, C. A.
Development program on a Spindt cold-cathode electron gun
[NASA-CR-168055] p 115 N83-18997
Spindt cold cathode electron gun development program
[NASA-CR-168212] p 202 N83-35787

SPREITER, J. R.
Development of a multiple-parameter nonlinear perturbation procedure for transonic turbomachinery flows: Preliminary application to design/optimization problems
[NASA-CR-3657] p 2 N83-17453

SPRINGER, G. S.
Numerical simulation of the flow and fuel-air mixing in an axisymmetric piston-cylinder arrangement
[NASA-TM-83011] p 126 N83-12358
Vortex motion in axisymmetric piston-cylinder configurations
[NASA-TM-85404] p 133 N83-35318

SRAWLEY, J. E.
Stress intensity and displacement coefficients for radially cracked ring segments subject to three-point bending
[NASA-TM-83059] p 160 N83-24874

SRAWLWY, J. E.
Analysis of an externally radially cracked ring segment subject to three-point radial loading
[NASA-TM-83482] p 163 N83-35413

SRINIVASAN, M.
Comparison of NDE techniques for sintered-SiC components p 152 A83-22265
Tribological properties of sintered polycrystalline and single-crystal silicon carbide p 89 A83-29397

SRINIVASAN, R.
Experiments in dilution jet mixing
[AIAA PAPER 83-1201] p 122 A83-36277
Dilution Jet Mixing Program, phase 1
[NASA-CR-168031] p 128 N83-15590
Experiments in dilution jet mixing
[NASA-TM-83434] p 15 N83-30393

ST.JOHN, G. A.
Oxidation and formation of deposit precursors in hydrocarbon fuels
[NASA-CR-168121] p 101 N83-23465

ST.JOHN, K.
Energy and precious fuels requirements of fuel alcohol production. Volume 3, appendices C to F: Methanol from cellulose
[NASA-CR-168092] p 183 N83-28583

STABE, R. G.
Analytical and experimental study of flow through an axial turbine stage with a nonuniform inlet radial temperature profile
[AIAA PAPER 83-1175] p 6 A83-45510
Analytical and experimental study of flow through an axial turbine stage with a nonuniform inlet radial temperature profile
[NASA-TM-83431] p 14 N83-27958
Incidence loss for fan turbine rotor blade in two-dimensional cascade
[NASA-TP-2188] p 39 N83-30431

STAHARA, S. S.
Development of a multiple-parameter nonlinear perturbation procedure for transonic turbomachinery flows: Preliminary application to design/optimization problems
[NASA-CR-3657] p 2 N83-17453

STAKOLICH, E. G.
JT9D performance deterioration results from a simulated aerodynamic load test p 25 A83-41040

STALLONE, M. J.
Blade loss transient dynamic analysis of turbomachinery p 25 A83-40864

STALNAKER, D. K.
An electrochemical rebalance cell for Redox systems
[NASA-TM-83363] p 73 N83-29326

STANKUNAS, T. N.
Composite fan exit guide vanes for high bypass ratio gas turbine engines p 19 A83-13159

STARDTER, H.
Subsonic-transonic stall flutter study
[NASA-CR-165256] p 43 N83-30435

STEARNS, C. A.
Combustion system processes leading to corrosive deposits p 69 A83-42246
Hot corrosion of low cobalt alloys p 79 N83-11292
Turbine engine materials durability research p 29 N83-12163
Reactions of NaCl with gaseous SO3, SO2, and O2
[NASA-TM-83423] p 86 N83-29358

STECKRA, S.
Improved thermal barrier coating system
[NASA-CASE-LEW-13324-2] p 86 N83-34014

STECURA, S.
Improved performance thermal barrier coatings p 90 A83-42261

STEFKO, G. L.
Noise of the 10-bladed, 40 deg swept SR-6 propeller in a wind tunnel
[NASA-TM-82950] p 196 N83-11840
New test techniques and analytical procedures for understanding the behavior of advanced propellers
[NASA-TM-83360] p 2 N83-22092
Noise of the 10-bladed 60 deg swept SR-5 propeller in a wind tunnel
[NASA-TM-83054] p 200 N83-23112

STEGEMAN, G. I.
Surface-polaritonlike waves guided by thin, lossy metal films p 192 A83-37947
Long-range surface plasmons in electrode structures p 202 A83-40733
Long range surface plasmons in birefringent media p 202 A83-42206
Effects of gaps on long range surface plasmon polaritons p 204 A83-46271

STEIN, M.
A solution procedure for behavior of thick plates on a nonlinear foundation and postbuckling behavior of long plates
[NASA-TP-2174] p 163 N83-34373

STEIN, P. A.
A solution procedure for behavior of thick plates on a nonlinear foundation and postbuckling behavior of long plates
[NASA-TP-2174] p 163 N83-34373

STEINBERG, M.
Laser fluorescence studies of the chemical interactions of sodium species with sulfur bearing fuels
[NASA-CR-169861] p 71 N83-17625
The detailed chemistry and thermodynamics of sodium in oxygen-rich flames
[NASA-CR-169848] p 72 N83-17626

STEINBERG, R.
Airline flight planning: The weather connection p 17 N83-17461

STEINBRECHER, D. H.
Image-optimized, frequency-scalable mixers for millimeter-wave applications p 112 A83-39273

STEINER, G.
Development of a large inert gas ion thruster
[AIAA PAPER 82-1927] p 52 A83-12496

STEINNAGEL, K.
Satellite provided fixed communication services: A forecast of potential domestic demand through the year 2000. Volume 1: Executive summary
[NASA-CR-168145] p 108 N83-34113
Satellite provided customer premises services: A forecast of potential domestic demand through the year 2000. Volume: Executive summary
[NASA-CR-168142] p 109 N83-34116
Satellite provided customer premise services: A forecast of potential domestic demand through the year 2000. Volume 3: Appendices
[NASA-CR-168144] p 109 N83-34118

STENGER, F. J.
Tests of an alternating current propulsion subsystem for electric vehicles on a road load simulator
[NASA-TM-83036] p 178 N83-22749

STEPHENS, J. R.
COSAM program overview p 78 N83-11283
Conservation of strategic metals p 80 N83-12154
Development of tough, strong, iron-base alloy for cryogenic applications p 44 N83-18763
Considerations of technology transfer barriers in the modification of strategic superalloys for aircraft turbine engines
[NASA-TM-83395] p 86 N83-29360
Understanding the roles of the strategic element cobalt in nickel base superalloys
[NASA-TM-83475] p 87 N83-35102

STEPKA, F. S.
Comparison of predicted and experimental external heat transfer around a film cooled cylinder in crossflow
[NASA-TM-83017] p 127 N83-13392

STERMAN, A. P.
Tip cap for a rotor blade
[NASA-CASE-LEW-13654-1] p 30 N83-14129
Air modulation apparatus
[NASA-CASE-LEW-13524-1] p 131 N83-30957

STERN, T. E.
Next generation communications satellites: multiple access and network studies
[NASA-CR-167903] p 45 N83-12129

STERN, T. G.
Analysis of the reflective multibandgap solar cell concept
[NASA-CR-168186] p 185 N83-34454

STETZ, T. T.
Experiments on flow through one to four inlets of the orifice and Borda type p 124 A83-43235
Studies of flows through N-sequential orifices
[ASME PAPER 83-FE-22] p 125 A83-48678

STEVENS, G.
Spectrophotometric analysis of aqueous mixtures of some chromium (III) complexes
[NASA-CR-172999] p 74 N83-32872
A comparison of Frequency Domain Multiple Access (FDMA) and Time Domain Multiple Access (TDMA) approaches to satellite service for low data rate Earth stations
[NASA-TM-83430] p 109 N83-34120

STEVENS, N. J.
Environmentally induced discharges on satellites p 105 N83-14365
Design considerations for large space electric power systems
[NASA-TM-83064] p 58 N83-24552
SAFE II: Large systems space plasma evaluation experiment p 46 N83-26903

STEWART, C. S.
Transient flow analysis of the AEDC/HPDE MHD generator
[AIAA PAPER 83-0395] p 203 A83-16691

STEWART, R. G.
Support and power plant documentation for the gas turbine powered bus demonstration program
[NASA-CR-165527] p 210 N83-20829

STILLER, P. H.
Measured effect of wind generation on the fuel consumption of an isolated diesel power system p 165 A83-36410

STILLWELL, R. P.
Current collection from the space plasma through defects in high voltage solar array insulation
[NASA-CR-168148] p 204 N83-31474

STINCHCOMB, W. W.
A study of the stress wave factor technique for the characterization of composite materials
[NASA-CR-3670] p 153 N83-27248

STOCHL, R. J.
IGCC performance comparison for variations in gasifier type and gas turbine firing temperature
[NASA-TM-83310] p 180 N83-25037

STONE, J. R.
Conventional profile coaxial jet noise prediction p 193 A83-22128
Comparison of measured and predicted flight effects on high-bypass coaxial jet exhaust noise
[AIAA PAPER 83-0749] p 194 A83-26450
Comparison of measured and predicted flight effects on high-bypass coaxial jet exhaust noise
[NASA-TM-83347] p 200 N83-23115

STONER, W. A.
The design and technology development for A 150 mlb resistojet for H2 or NH3
[AIAA PAPER 82-1949] p 52 A83-12506
STONESIFER, R. B.
Stress and fracture analyses under elastic-plastic creep conditions: Some basic developments and computational approaches p 162 N83-34371
STORACE, A. F.
Blade loss transient dynamic analysis of turbomachinery p 25 A83-40864
STORM, R. S.
Progress in net shape fabrication of alpha SiC turbine components
[ASME PAPER 83-GT-238] p 139 A83-48030
STOTLER, C. L.
Composite engine duct fabrication p 1 A83-39941
STRACK, W. C.
Technology and benefits of aircraft counter rotation propellers
[NASA-TM-82983] p 27 N83-11129
General Aviation Turbine Engine (GATE) overview p 35 N83-22457
STRAIGHT, D. M.
Thrust performance of a variable-geometry, divergent exhaust nozzle on a turbojet engine at altitude
[NASA-TP-2171] p 36 N83-26839
STRANGE, R. R.
Development of advanced high-temperature heat flux sensors
[NASA-CR-165618] p 26 N83-10044
STRAZISAR, A. J.
Comparison of two- and three-dimensional flow computations with laser anemometer measurements in a transonic compressor rotor
[NASA-TP-1931] p 15 N83-32774
STRICKLAND, S.
Planning assistance for the NASA 30/20 GHz program. Network control architecture study.
[NASA-CR-168058] p 106 N83-21207
STRICKLIN, R.
Summary report for CF6 jet engine diagnostics program
[NASA-CR-165582] p 32 N83-17539
STRNAT, K. J.
Testing of the permanent magnet material Mn-Al-C for potential use in propulsion motors for electric vehicles
[NASA-CR-169481] p 114 N83-12329
STROMBERG, W. J.
JT9D performance deterioration results from a simulated aerodynamic load test p 25 A83-41040
STUART, T. A.
Transformer induced instability of the series resonant converter p 113 A83-41152
STUBBS, R. M.
Multiple-gridding of the Euler equations with an implicit scheme
[AIAA PAPER 83-1945] p 5 A83-39392
STUMPF, R.
Dynamic distortion in a short s-shaped subsonic diffuser with flow separation
[AIAA PAPER 83-1412] p 25 A83-45515
Dynamic distortion in a short s-shaped subsonic diffuser with flow separation
[NASA-TM-83412] p 36 N83-26838
STURGESS, G. J.
Importance of inlet boundary conditions for numerical simulation of combustor flows
[AIAA PAPER 83-1263] p 23 A83-36314
Aerothermal modeling program, phase 1
[NASA-CR-168202] p 131 N83-30959
STURMAN, J. C.
The LeRC rail accelerators: Test designs and diagnostic techniques
[NASA-TM-83496] p 60 N83-35053
SU, C. C.
Heat transfer characteristics for jet array impingement with initial crossflow
[ASME PAPER 83-GT-28] p 7 A83-47891
Jet array impingement flow distributions and heat transfer characteristics. Effects of initial crossflow and nonuniform array geometry
[NASA-CR-3630] p 128 N83-15592
SULLIVAN, R. E.
Application of 3D aerodynamic/combustion model to combustor primary zone study
[AIAA PAPER 83-1265] p 23 A83-36316
Small gas turbine combustor primary zone study
[NASA-CR-168122] p 149 N83-28448
Small gas turbine combustor primary zone study p 38 N83-29221
SULLIVAN, T. J.
The aerodynamic design and performance of the General Electric/NASA EEE fan
[AIAA PAPER 83-1160] p 23 A83-36252
Energy efficient engine: Fan test hardware detailed design report
[NASA-CR-165148] p 31 N83-16341
SULLIVAN, T. L.
A review of resonance response in large, horizontal-axis wind turbines p 163 A83-13696
Structural fatigue test results for large wind turbine blade sections p 159 N83-19246
Structural qualification testing and operational loading on a fiberglass rotor blade for the Mod-OA wind turbine
[NASA-TM-83309] p 179 N83-23710
SUN, C. T.
Wave propagation in a graphite/epoxy laminate p 158 A83-44050
Dynamic responses of graphite/epoxy laminated beam to impact of elastic spheres
[NASA-CR-165461] p 64 N83-13173
Wave propagation in graphite/epoxy laminates due to impact
[NASA-CR-168057] p 66 N83-22325
SUNDBERG, G. R.
Deep impurity trapping concepts for power semiconductor devices p 206 N83-15877
Advanced electrical power system technology for the all electric aircraft
[NASA-TM-83390] p 115 N83-24764
SUNDT, C. V.
Energy efficient engine sector combustor rig test program
[NASA-CR-167913] p 33 N83-19753
SUTHERLAND, M. V.
Conceptual design, evaluation and research identification for Remote Augmented Propulsive Lift Systems (RALS) with ejectors for VTOL aircraft
[NASA-CR-167906] p 29 N83-13103
SUTTON, R.
Application of 3D aerodynamic/combustion model to combustor primary zone study
[AIAA PAPER 83-1265] p 23 A83-36316
SUTTON, R. D.
Small gas turbine combustor primary zone study p 38 N83-29221
SWALLOM, D. W.
MHD channel performance for potential early commercial MHD power plants p 204 A83-23134
SWARTZ, C. K.
Radiation damage in front and back illuminated high resistivity silicon solar cells
[NASA-TM-82965] p 206 N83-10962
Effects of processing and dopant on radiation damage removal in silicon solar cells p 170 N83-14708
Radiation damage and annealing in large area n+/p/p+ GaAs shallow homojunction solar cells p 172 N83-15826
SWEDLOW, J. L.
Research priorities for advanced fibrous composites
[NASA-CR-165414] p 65 N83-18853
SWETTE, L.
Optimization and fabrication of porous carbon electrodes for Fe/Cr redox flow cells
[NASA-CR-167921] p 179 N83-23708
SWIGART, R.
The development of a generalized advanced propeller analysis system
[AIAA PAPER 83-2466] p 26 A83-49581
SWINSON, W. F.
Extending the laser-specklegram technique to strain analysis of rotating components p 155 A83-12514
Manual for extending the laser specklegram technique to strain analysis of rotating components
[NASA-CR-167932] p 134 N83-15601
SWISSHELM, J. M.
Semidirect computations for transonic flow
[NASA-TM-83451] p 15 N83-34909
SYAMALA RAO, B. C.
The initial stages of cavitation damage and erosion on copper and brass tested in a rotating disk device p 75 A83-27421
Dynamics and mechanism of cavitation erosion on perspex and epoxy resin tested in a rotating disk device p 89 A83-27422
SYED, A. A.
Sound propagation in segmented exhaust ducts - Theoretical predictions and comparison with measurements
[AIAA PAPER 83-0734] p 194 A83-28016
SYED, S. A.
Importance of inlet boundary conditions for numerical simulation of combustor flows
[AIAA PAPER 83-1263] p 23 A83-36314
SYMONDS, R. A.
Evaluation of advanced combustion concepts for dry NO sub x suppression with coal-derived, gaseous fuels
[NASA-TM-82985] p 166 N83-10557
SZANISZLO, A. J.
NASA clean catalytic combustor program
[ASME PAPER 82-JPGC-GT-11] p 68 A83-25269
SZETELA, E. J.
A vortex venturi for reverting antimisting fuel properties
[ASME PAPER 83-GT-137] p 25 A83-47964
Deposit formation in hydrocarbon rocket fuels: Executive summary
[NASA-CR-165492] p 102 N83-35159
SZUCH, J. R.
BASIC Data Manipulation And Display System (BDMADS)
[NASA-TM-83328] p 189 N83-19496

T

TABAKOFF, W.
A method of predicting the performance deterioration of a compressor cascade due to sand erosion
[AIAA PAPER 83-0178] p 19 A83-16572
Effect of particle presence on the incompressible inviscid flow through a two dimensional compressor cascade p 6 A83-42562
Effect of particle presence on the incompressible inviscid flow through a two dimensional compressor cascade
[ASME PAPER 83-GT-95] p 8 A83-47941
Three-dimensional flow measurements in a turbine scroll
[ASME PAPER 83-GT-128] p 8 A83-47957
A study of the surface deterioration due to erosion
[ASME PAPER 83-GT-213] p 9 A83-48014
Three-dimensional flow measurements in a vaneless radial turbine scroll
[NASA-CR-167994] p 9 N83-11065
Environmental solid particle effects on compressor cascade performance
[NASA-CR-168018] p 11 N83-16285
Compressor cascade performance deterioration caused by sand ingestion
[NASA-CR-168067] p 11 N83-16286
TABRIZI, A. H.
'Scaling' analysis of the ice accretion process on aircraft surfaces
[ASME PAPER 82-WA/HT-39] p 16 A83-25693
TACINA, R. R.
Catalytic combustion with steam injection
[ASME PAPER 82-JPGC-GT-23] p 164 A83-25271
Catalytic combustion with steam injection
[NASA-TM-82923] p 170 N83-15805
Autoignition in a premixing-prevaporizing fuel duct using 3 different fuel injection systems at inlet air temperatures to 1250 K
[NASA-TM-82938] p 181 N83-26251
TAKEUCHI, D.
Experimental comparison of icing cloud instruments
[AIAA PAPER 83-0026] p 16 A83-42099
TAKEUCHI, D. M.
Comparison of modern icing cloud instruments
[NASA-CR-168008] p 19 N83-18720
Experimental comparison of icing cloud instruments
[NASA-TM-83340] p 17 N83-24487
TAKI, S.
Soot formation in pyrolysis of acetylene, allene and 1,3-butadiene p 69 A83-39274
TAM, C. K. W.
On the shock cell structure and noise of supersonic jets
[AIAA PAPER 83-0703] p 193 A83-25923
Tone-excited jet: Theory and experiments
[NASA-CR-3538] p 197 N83-12968
TAN-ATICHAT, J.
Interpretation of 2-probe turbulence measurements in an axisymmetric contraction
[NASA-CR-169832] p 11 N83-17502
Experiments on identification and control of inflow disturbances in contracting streams
[NASA-CR-169831] p 11 N83-17503
TAN, T. M.
Wave propagation in a graphite/epoxy laminate p 158 A83-44050
Wave propagation in graphite/epoxy laminates due to impact
[NASA-CR-168057] p 66 N83-22325
TANJI, F. T.
Experimental investigation of a two-dimensional shock-turbulent boundary layer interaction with bleed
[AIAA PAPER 83-0135] p 3 A83-19581
Experimental investigation of a two-dimensional shock-turbulent boundary layer interaction with bleed
[NASA-TM-83057] p 34 N83-22200
TANNA, H. K.
Refinement and application of acoustic impulse technique to study nozzle transmission characteristics
[NASA-CR-3656] p 199 N83-20708

TANNER, J. A.
Temperature distribution in an aircraft tire at low ground speeds
[NASA-TP-2195] p 161 N83-33217
TANRIKUT, S.
Development and operating characteristics of an advanced two-stage combustor p 24 A83-38022
Energy efficient engine sector combustor rig test program
[NASA-CR-167913] p 33 N83-19753
TAYLOR, P. L.
Dipole-field sums and Lorentz factors for orthorhombic lattices, and implications for polarizable molecules p 204 A83-17228
Piezoelectric and pyroelectric coefficients for ferroelectric crystals with polarizable molecules p 205 A83-17227
Piezoelectricity and pyroelectricity in polyvinylidene fluoride - Influence of the lattice structure p 205 A83-29531
TAYLOR, R. C.
Phased array-fed antenna configuration study: Technology assessment
[NASA-CR-168078] p 106 N83-22495
Phased array-fed antenna configuration study
[NASA-CR-168077] p 107 N83-27086
TEAGAN, W. P.
Stirling engine application study
[NASA-CR-168087] p 210 N83-22029
TERDAN, F. F.
The LeRC rail accelerators: Test designs and diagnostic techniques
[NASA-TM-83496] p 60 N83-35053
TEREN, F.
NASA propulsion controls research
[NASA-TM-83343] p 36 N83-25711
TERMAN, D. K.
The chemical behavior of acidified chromium (3) solutions
[NASA-CR-172997] p 74 N83-32871
TEVAARWERK, J. L.
Traction calculations and design data for two traction fluids p 145 N83-20136
TEVELDE, J.
A vortex venturi for reverting antimisting fuel properties
[ASME PAPER 83-GT-137] p 25 A83-47964
TEW, R. C., JR.
Computer program for Stirling engine performance calculations
[NASA-TM-82960] p 210 N83-17423
THALLER, L. H.
Design flexibility of redox flow systems p 164 A83-27177
Pore size engineering applied to starved electrochemical cells and batteries p 164 A83-27201
Expected cycle life vs. depth of discharge relationships of well-behaved single cells and cell strings p 165 A83-32627
Pore size engineering applied to starved electrochemical cells and batteries
[NASA-TM-82893] p 70 N83-10134
Expected cycle life versus depth of discharge relationships of well behaved single cells and cell strings
[NASA-TM-82957] p 167 N83-10558
THEOBALD, M. A.
Turbofan noise generation. Volume 1: Analysis
[NASA-CR-167951] p 198 N83-15041
THIEME, L. G.
Improved Stirling engine performance using jet impingement p 137 A83-27288
THOMAS, G.
Design and evaluation of low-cost laminated wood composite blades for intermediate size wind turbines: Blade design, fabrication concept, and cost analysis
[NASA-CR-165463] p 179 N83-23704
Fabrication of low-cost Mod-0A wood composite wind turbine blades
[NASA-TM-83323] p 182 N83-27347
THOMAS, R. L.
Comparison of NDE techniques for sintered-SiC components p 152 A83-22265
DOE/NASA Lewis large wind turbine program
[NASA-TM-82991] p 169 N83-14690
The NASA Lewis large wind turbine program p 174 N83-15911
THOMPSON, H. D.
Quasi-three-dimensional turbomachinery flow calculations on multiple hub-to-shroud stream surfaces
[AIAA PAPER 83-1820] p 5 A83-38652
THRASHER, S. R.
Ceramic applications in turbine engines
[NASA-CR-165494] p 212 N83-37028
THRESHER, R. W.
Large Horizontal-Axis Wind Turbines
[NASA-CP-2230] p 175 N83-19231
TIEN, J.
Superalloy composition modeling p 78 N83-11284
Role of cobalt in nickel base superalloys p 78 N83-11286
TIEN, J. K.
Considerations of technology transfer barriers in the modification of strategic superalloys for aircraft turbine engines
[NASA-TM-83395] p 86 N83-29360
TOMAZIC, W. A.
Assessment of alternative power sources for mobile mining machinery
[NASA-TM-82695] p 169 N83-14691
TOSCANO, W. M.
Design of hydraulic output Stirling engine
[NASA-CR-167976] p 177 N83-22739
TOTH, J. M., JR.
Cryogenic fluid management experiment trunnion fatigue verification
[AIAA PAPER 83-0911] p 49 A83-32782
TOVICHAKCHAIKUL, S.
On the solution of elastic-plastic static and dynamic postbuckling collapse of general structure p 155 A83-12746
Pseudo-updated constrained solution algorithm for nonlinear heat conduction p 121 A83-32989
Finite element analysis of steadily moving contact fields p 158 A83-49437
Constrained self-adaptive solutions procedures for structure subject to high temperature elastic-plastic creep effects p 162 N83-34370
TOWNE, C. E.
Implicit marching solution of compressible viscous subsonic flow in planar and axisymmetric ducts
[NASA-TM-82876] p 125 N83-10389
TOWNSEND, D. P.
Experimental and analytical determination of gear tooth temperatures with oil jet lubrication p 142 N83-15530
Into mesh lubrication of spur gears with arbitrary offset oil jet. 1: For jet velocity less than or equal to gear velocity
[NASA-TM-83040] p 143 N83-19092
Into mesh lubrication of spur gears with arbitrary offset oil jet. 2: For jet velocities equal to or greater than great velocity
[NASA-TM-83041] p 143 N83-19093
An update on the life analysis of spur gears p 146 N83-20144
The optimal design of standard gearsets p 146 N83-20145
Study of lubricant jet flow phenomena in spur gears: Out of mesh condition p 147 N83-20146
Gear lubrication and cooling experiment and analysis p 147 N83-20147
Evaluation of high-contact-ratio spur gears with profile modification p 147 N83-20150
NASA transmission research and its probable effects on helicopter transmission design
[NASA-TM-83389] p 148 N83-24858
TREFNY, C. J.
Low speed performance of a supersonic axisymmetric mixed compression inlet with auxiliary inlets
[AIAA PAPER 83-1414] p 7 A83-45516
Low speed performance of a supersonic axisymmetric mixed compression inlet with auxiliary inlets
[NASA-TM-83435] p 37 N83-27992
TRELA, W.
Evaluation of ceramics for stator applications: Gas turbine engines interim report. Stator fabrication and evaluation
[NASA-CR-168140] p 96 N83-30662
TRINER, J. E.
Advances in core loss calculations for magnetic materials
[NASA-TM-82947] p 113 N83-11446
Design considerations for large space electric power systems
[NASA-TM-83064] p 58 N83-24552
TRIPP, J. H.
Surface roughness effects in hydrodynamic lubrication: The flow factor method
[NASA-TM-83024] p 129 N83-19016
TROCK, D. C.
Inert gas thruster technology p 53 A83-20423
TROEGER, R. E.
Tip cap for a rotor blade
[NASA-CASE-LEW-13654-1] p 30 N83-14129
TROTH, D. L.
Multifuel evaluation of rich/quench/lean combustor p 67 A83-11492
Multifuel evaluation of rich/quench/lean combustor
[NASA-TM-82986] p 167 N83-10559
TROUT, A. M.
Preliminary tests of an advanced high-temperature combustion system
[NASA-TP-2203] p 41 N83-33893
TRUMP, G. E.
Operational summary of an electric propulsion long term test facility
[AIAA PAPER 82-1903] p 44 A83-12478
TSENG, H. H.
Jet array impingement flow distributions and heat transfer characteristics. Effects of initial crossflow and nonuniform array geometry
[NASA-CR-3630] p 128 N83-15592
TSUCHIYA, T.
Axial-compressor flow distortion with water ingestion
[AIAA PAPER 83-0004] p 19 A83-16456
Effect of humidity on jet engine axial-flow compressor performance p 22 A83-35856
The WISGSK: A computer code for the prediction of a multistage axial compressor performance with water ingestion
[NASA-CR-3624] p 28 N83-12093
TULEY, E. N.
Tip cap for a rotor blade
[NASA-CASE-LEW-13654-1] p 30 N83-14129
TURHOLLOW, A., JR.
Energy and precious fuels requirements of fuel alcohol production. Volume 2, appendices A and B: Ethanol from grain
[NASA-CR-168091] p 190 N83-28582
TURNER, E. R.
Analytical and experimental evaluation of the heat transfer distribution over the surfaces of turbine vanes
[NASA-CR-168015] p 131 N83-28376
TURNER, J. L.
Extending the laser-specklegram technique to strain analysis of rotating components p 155 A83-12514
Manual for extending the laser specklegram technique to strain analysis of rotating components
[NASA-CR-167932] p 134 N83-15601
TURNER, R. E.
Atmospheric radiation model for water surfaces
[NASA-CR-167873] p 187 N83-21677
TURNEY, G. E.
Supersonic STOVL research aircraft
[SAE PAPER 821375] p 17 A83-37965
Study of LH2-fueled topping cycle engine for aircraft propulsion
[NASA-TM-83466] p 41 N83-34942

U

ULMER, R.
Market assessment of photovoltaic power systems for agricultural applications worldwide
[NASA-CR-165541] p 168 N83-13585

V

VADYAK, J.
A computer program for the calculation of the flow field including boundary layer effects for mixed-compression inlets at angle of attack
[NASA-CR-168002] p 10 N83-11066
VAIDYANATHAN, P. N.
Effect of Y2O3 and Al2O3 on the oxidation resistance of Si3N4 p 88 A83-22258
VAKILI, A.
Measurements of compressible secondary flow in a circular S-duct
[AIAA PAPER 83-1739] p 4 A83-37218
VALCO, G. J.
Planar multijunction high voltage solar cell chip p 163 A83-13923
VALGORA, M.
Solar array switching power management p 54 A83-27132
VALGORA, M. E.
Optimal sun-alignment techniques of large solar arrays in electric propulsion spacecraft
[AIAA PAPER 82-1898] p 48 A83-12475
VAN FOSSEN, G. J.
The feasibility of water injection into the turbine coolant to permit gas turbine contingency power for helicopter application
[ASME PAPER 83-GT-66] p 24 A83-39993
VANFOSSEN, G. J.
Length to diameter ratio and row number effects in short pin fin heat transfer
[NASA-TM-83005] p 127 N83-14431
Feasibility of water injection into the turbine coolant to permit gas turbine contingency power for helicopter application
[NASA-TM-83043] p 31 N83-15307
Experimental feasibility study of a thermoelectric heat flux gage
[NASA-TM-83048] p 134 N83-15602

VANNUCCI, R. D.
PMR-15 polyimide modifications for improved prepreg tack
[NASA-TM-82951] p 64 N83-12175
VANRINTEL, H. L.
An experimental investigation of internal area ruling for transonic and supersonic channel flow
[NASA-CR-169638] p 10 N83-14068
VARY, A.
Interrelation of material microstructure, ultrasonic factors, and fracture toughness of a two-phase titanium alloy p 75 A83-23922
Metal honeycomb to porous wireform substrate diffusion bond evaluation p 153 A83-39620
Acousto-ultrasonic characterization of fiber reinforced composites p 63 N83-11231
Ultrasonic ranking of toughness of tungsten carbide
[NASA-TM-83358] p 153 N83-23620
VATSKY, A.
A conceptual study of the potential for automotive-derived and free-piston Stirling engines in 30- to 400-kilowatt stationary power applications
[NASA-CR-165274] p 167 N83-10568
VEERABHADRA RAO, P.
The initial stages of cavitation damage and erosion on copper and brass tested in a rotating disk device p 75 A83-27421
Dynamics and mechanism of cavitation erosion on perspex and epoxy resin tested in a rotating disk device p 89 A83-27422
Morphology of ductile metals eroded by a jet of spherical particles impinging at normal incidence p 75 A83-32624
Cavitation erosion characteristics of poly(methyl methacrylate) in a rotating disk device p 90 A83-41851
VEERABHADRARAO, P.
Time dependence of solid-particle impingement erosion of an aluminum alloy
[NASA-TP-2169] p 86 N83-32908
VENKAT, R. S.
Testing of felt-ceramic materials for combustor applications
[NASA-CR-168103] p 36 N83-26837
VENTRES, C. S.
Turbofan noise generation. Volume 1: Analysis
[NASA-CR-167951] p 198 N83-15041
VERMES, G.
NOx results from two combustors tested on medium BTU coal gas p 186 A83-11493
VERNON, G. D.
Experimental results for the interference between FM television signals p 103 A83-19686
VERSAW, E. F.
Assessment of crash fire hazard of LH sub 2 fueled aircraft
[NASA-CR-165525] p 16 N83-11095
VESELY, E. J., JR.
Determination of hydrogen permeability in uncoated and coated superalloys
[NASA-CR-165209] p 80 N83-12215
VITERNA, L. A.
Fixed pitch rotor performance of large horizontal axis wind turbines p 175 N83-19233
Free yaw performance of the Mod-0 large horizontal axis 100 kW wind turbine p 175 N83-19235
VITTAL, B. V. R.
Three-dimensional flow measurements in a turbine scroll
[ASME PAPER 83-GT-128] p 8 A83-47957
Three-dimensional flow measurements in a vaneless radial turbine scroll
[NASA-CR-167994] p 9 N83-11065
VOGT, J. H.
Task 4 completion report for 40 Kilowatt grid connected modification contract
[NASA-CR-167950] p 208 N83-30297
VOGT, P. G.
Free-jet acoustic investigation of high-radius-ratio coannular plug nozzles. Comprehensive data report, volume 1
[NASA-CR-168086-VOL-1] p 198 N83-18408
Free-jet acoustic investigation of high-radius-ratio coannular plug nozzles. Comprehensive data report, volume 2
[NASA-CR-168086-VOL-2] p 199 N83-18409
VONDRA, R. J.
Electric propulsion research and technology in the United States
[AIAA PAPER 82-1867] p 53 A83-16925
VONGLAHN, U.
Correlation of core noise obtained by three signal coherence techniques
[NASA-TM-83012] p 197 N83-12966
VRANOS, A.
Experimental study of the thermal stability of hydrocarbon fuels
[NASA-CR-168027] p 100 N83-17728

W

WAGNER, J. H.
Axial compressor middle stage secondary flow study
[NASA-CR-3701] p 14 N83-29174
WALKER, B.
Effect of flow on the acoustic performance of extended reaction lined ducts
[AIAA PAPER 83-0778] p 195 A83-28024
WALKER, B. E.
The velocity perturbations above the orifice of an acoustically excited cavity in grazing flow p 195 A83-29235
WALKINGTON, N. J.
Finite difference solutions to shocked acoustic waves
[AIAA PAPER 83-0671] p 193 A83-25907
WALL, M.
Planning assistance for the 30/20 GHz program, volume 1
[NASA-CR-165484-VOL-1] p 108 N83-33010
Planning assistance for the 30/20 GHz program, volume 2
[NASA-CR-165484-VOL-2] p 108 N83-33011
Planning assistance for the 30/20 GHz program, volume 3
[NASA-CR-165484] p 108 N83-33012
WALLA, P. S.
A lightweight electronically commutated dc motor for electric passenger vehicles
[NASA-CR-165601] p 113 N83-10348
WALLIS, R.
Development of a microwave 20 x 20 switch matrix for 30/20 GHz SS-TDMA application p 110 A83-11484
WALOWIT, J.
Analysis of spiral-groove face seals for liquid oxygen
[ASLE PREPRINT 83-AM-4B-2] p 138 A83-43339
WALTHER, E. G.
Assessment of crash fire hazard of LH sub 2 fueled aircraft
[NASA-CR-165525] p 16 N83-11095
WALTON, J.
Power turbine dynamics - An evaluation of a shear-mounted elastomeric damper
[ASME PAPER 83-GT-228] p 139 A83-48025
WANG, A. J.
Vibrations of cantilevered circular cylindrical shells Shallow versus deep shell theory p 157 A83-36958
Vibrations of cantilevered doubly-curved shallow shells p 157 A83-39557
Vibrations of blades with variable thickness and curvature by shell theory
[ASME PAPER 83-GT-152] p 158 A83-47978
WANG, C. R.
Film-cooling effectiveness with developing coolant flow through straight and curved tubular passages
[NASA-TP-2062] p 126 N83-12360
Three-dimensional turbulent-mixing-length modeling for discrete-hole coolant injection into a crossflow
[NASA-TP-2200] p 132 N83-34232
WANG, C. W.
Engineering calculations for communications systems planning
[NASA-CR-170182] p 106 N83-22494
WANG, S. Y.
End region effects upon the performance of a magnetohydrodynamic channel p 203 A83-10665
The LeRC rail accelerators: Test designs and diagnostic techniques
[NASA-TM-83496] p 60 N83-35053
The structural response of a rail accelerator
[NASA-TM-83491] p 163 N83-35412
WANG, T.
Dynamic responses of graphite/epoxy laminated beam to impact of elastic spheres
[NASA-CR-165461] p 64 N83-13173
WARD, M.
Benchmark notch test for life prediction
[NASA-CR-165571] p 158 N83-12451
WASSERBAUER, C. A.
Cross spectra between temperature and pressure in a constant area duct downstream of a combustor
[AIAA PAPER 83-0762] p 196 A83-33487
Analysis of combustion spectra containing organ pipe tone by cepstral techniques
[NASA-TM-83034] p 198 N83-16153
Cross spectra between temperature and pressure in a constant area duct downstream of a combustor
[NASA-TM-83351] p 200 N83-23116
JT15D 1/2-scale nozzle jet noise experiment and comparison with prediction
[NASA-TM-83370] p 201 N83-27793
WASSERBAUER, J. F.
Low speed performance of a supersonic axisymmetric mixed compression inlet with auxiliary inlets
[AIAA PAPER 83-1414] p 7 A83-45516
Low speed performance of a supersonic axisymmetric mixed compression inlet with auxiliary inlets
[NASA-TM-83435] p 37 N83-27992
WATERS, W. J.
Multicolor printing plate joining
[NASA-CASE-LEW-13598-1] p 102 N83-17745
WATSON, G. K.
Microstructural analysis of solar cell welds p 172 N83-15833
WEAR, J. D.
Preliminary tests of an advanced high-temperature combustion system
[NASA-TP-2203] p 41 N83-33893
WEATHERS, J.
Manual for extending the laser speckle gram technique to strain analysis of rotating components
[NASA-CR-167932] p 134 N83-15601
WEDEVEN, L. D.
The influence of surface dents and grooves on traction in sliding EHD point contacts p 138 A83-37823
Assessment of lubricated contacts: Mechanisms of scuffing and scoring
[NASA-TM-83074] p 144 N83-20118
Elastohydrodynamic contacts. Effects of dents and grooves on traction and local film thickness
[NASA-TP-2175] p 150 N83-28453
WEINBERG, I.
Radiation damage in front and back illuminated high resistivity silicon solar cells
[NASA-TM-82965] p 206 N83-10962
Effects of processing and dopant on radiation damage removal in silicon solar cells p 170 N83-14708
Radiation damage p 172 N83-15837
WEINBERGER, S. M.
Design study of a high power rotary transformer
[NASA-CR-168012] p 115 N83-16630
WEINBLATT, H.
Energy and precious fuels requirements of fuel alcohol production. Volume 4: Appendices G and H, methanol from coal
[NASA-CR-168093] p 183 N83-28580
Energy and precious fuels requirements of fuel alcohol production, volume 1
[NASA-CR-168090] p 183 N83-28581
Energy and precious fuels requirements of fuel alcohol production. Volume 2, appendices A and B: Ethanol from grain
[NASA-CR-168091] p 183 N83-28582
WEINGOLD, H. D.
Development of controlled diffusion airfoils for multistage compressor application
[ASME PAPER 83-GT-211] p 9 A83-48012
WEINSTEIN, H.
Numerical analysis of turbulent coaxial flow with internal heat generation
[NASA-CR-172633] p 132 N83-33105
WEISBRICH, A. L.
Technology and benefits of aircraft counter rotation propellers
[NASA-TM-82983] p 27 N83-11129
WEIZER, V. G.
The effect of Ta2O5 on the interaction between silicon and its contact metallization
[NASA-TM-82948] p 166 N83-10554
On the cause of the flat-spot phenomenon observed in silicon solar cells at low temperatures and low intensities p 170 N83-14705
WELSH, J. P.
Design and development of multi-kW power electronic transformers
[NASA-CR-168082] p 116 N83-29596
WENDELL, J. H.
Some analysis methods for rotating systems with periodic coefficients p 157 A83-32987
Simplified aeroelastic modeling of horizontal axis wind turbines
[NASA-CR-168109] p 177 N83-21509
WENZEL, L. M.
Experimental program for the evaluation of turbofan/turboshaft c conversion technology
[NASA-TM-82988] p 27 N83-11130
WESSEL, F. J.
On-orbit propulsion requirements and performance assessment of ion propulsion subsystems for future GEO large satellite missions
[AIAA PAPER 82-1872] p 48 A83-12460
Extended-performance 8-cm ion thruster operation
[AIAA PAPER 82-1955] p 53 A83-12512

Simplified power processing for ion-thruster subsystems
[AIAA PAPER 83-1394] p 55 A83-36384
Simplified power processing for ion-thruster subsystems p 56 A83-39271
The 8-CM ion thruster characterization
[NASA-CR-167887] p 57 N83-17586
Simplified power processing for ion-thruster subsystems p 60 N83-35018
WESTERKAMP, E. J.
The response of a 38m horizontal axis teetered rotor to yaw p 175 N83-19232
WESTERVELT, W. W.
Dynamic tooth loads and stressing for high contact ratio spur gears p 147 N83-20148
WHEELER, D. R.
On the mechanism of lubrication by tricresylphosphate /TCP/ - The coefficient of friction as a function of temperature for TCP on M-50 steel
[ASLE PREPRINT 82-LC-4C-1] p 135 A83-13228
Mechanism of lubrication by tricresylphosphate (TCP)
[NASA-TP-2053] p 72 N83-18863
The adsorption and thermal decomposition of tricresylphosphate (TCP) on iron and gold
[NASA-TM-83441] p 62 N83-29311
Use of high L.E.T. radiation to improve adhesion of metals to polytetrafluoroethylene
[NASA-TM-83413] p 96 N83-30660
WHITE, C. W.
High frequency, high power capacitor development
[NASA-CR-168035] p 116 N83-27127
WHITE, D. J.
Combustion characteristics of hydrogen-carbon monoxide based gaseous fuels p 67 A83-11491
Combustion characteristics of hydrogen. Carbon monoxide based gaseous fuels
[NASA-TM-82998] p 167 N83-10560
WHITE, G.
Hybrid geared traction transmissions p 145 N83-20128
WHITE, J. W.
Acoustics in variable area duct - Finite element and finite difference comparisons to experiment p 193 A83-19809
WHITE, M. A.
Conceptual design and cost analysis of hydraulic output unit for 15 kW free-piston Stirling engine
[NASA-CR-165543] p 167 N83-10561
WHITNEY, W. J.
Analytical and experimental study of flow through an axial turbine stage with a nonuniform inlet radial temperature profile
[AIAA PAPER 83-1175] p 6 A83-45510
Aerodynamic effect of a honeycomb rotor tip shroud on a 50.8-centimeter-tip-diameter core turbine
[NASA-TP-2112] p 32 N83-17547
Analytical and experimental study of flow through an axial turbine stage with a nonuniform inlet radial temperature profile
[NASA-TM-83431] p 14 N83-27958
WHITTENBERGER, J. D.
Influence of thermomechanical processing on elevated temperature slow plastic flow properties of B2 aluminide Fe-39.8at.% Al p 75 A83-22017
Effect of swaging on the 1000 C compressive slow plastic flow characteristics of the directionally solidified eutectic alloy gamma/gamma prime-alpha p 77 A83-44340
Intermetallics as alternative materials p 80 N83-11300
Method and apparatus for gripping uniaxial fibrous composite materials
[NASA-CASE-LEW-13758-1] p 64 N83-12176
WICKENHEISER, T. J.
Propeller performance and weight predictions appended to the Navy/NASA engine program
[NASA-TM-83458] p 41 N83-32810
WILBERS, L. G.
Powder metallurgy Rene 95 rotating turbine engine parts, volume 2
[NASA-CR-165141] p 82 N83-15412
WILKENFELD, J. M.
Development of electrical test procedures for qualification of spacecraft against EID. Volume 1: The CAN test and other relevant data
[NASA-CR-165590] p 49 N83-12136
Development of electrical test procedures for qualification of spacecraft against EID. Volume 2: Review and specification of test procedures
[NASA-CR-165590] p 50 N83-12137
WILL, H. A.
Production of large-area single-crystal wafers of cubic SiC for semiconductor devices p 205 A83-22767
WILLIAMS, J. H., JR.
Effects of specimen resonances on acoustic-ultrasonic testing
[NASA-CR-3679] p 153 N83-21373
Ultrasonic attenuation of a void-containing medium for very long wavelengths
[NASA-CR-3693] p 154 N83-28466
WILLIAMS, J. R.
Small gas turbine combustor primary zone study
[NASA-CR-168122] p 149 N83-28448
WILLIAMS, K. F.
Rotor redesign for a highly loaded 1800 ft/sec tip speed fan. 3: Laser Doppler velocimeter report
[NASA-CR-167954] p 30 N83-14128
WILLIAMS, M. C.
Rotor redesign for a highly loaded 1800 ft/sec tip speed fan. 3: Laser Doppler velocimeter report
[NASA-CR-167954] p 30 N83-14128
WILLIAMS, R. C.
Turbofan blade stresses induced by the flow distortion of a VTOL inlet at high angles of attack
[NASA-TM-82963] p 12 N83-17509
WILLIAMS, R. M.
Injection molding ceramics to high green densities p 137 A83-33515
WILLIAMSON, W. S.
Extended-performance 8-cm ion thruster operation
[AIAA PAPER 82-1955] p 53 A83-12512
The 8-CM ion thruster characterization
[NASA-CR-167887] p 57 N83-17586
WILLIS, E. A.
An overview of general aviation propulsion research programs at NASA Lewis Research Center p 35 N83-22456
WILLIS, W. S.
Conceptual design, evaluation and research identification for Remote Augmented Propulsive Lift Systems (RALS) with ejectors for VTOL aircraft
[NASA-CR-167906] p 29 N83-13103
WILREKER, V. F.
Wind turbine generator interaction with diesel generators on an isolated power system p 165 A83-44673
WILSON, A. J.
Composite engine duct fabrication p 1 A83-39941
WILSON, D. R.
Transient flow analysis of the AEDC/HPDE MHD generator
[AIAA PAPER 83-0395] p 203 A83-16691
WILSON, P. M.
High-frequency high-voltage high-power DC-to-DC converters p 115 N83-21028
WILSON, S. B., III
Supersonic STOVL research aircraft
[SAE PAPER 821375] p 17 A83-37965
WILSON, S. G.
An improved algorithm for evaluating trellis phase codes
[NASA-CR-169354] p 105 N83-16600
Advanced digital modulation: Communication techniques and monolithic GaAs technology
[NASA-CR-174452] p 109 N83-36299
Four-dimensional modulation and coding: An alternate to frequency-reuse
[NASA-CR-174453] p 110 N83-36300
WILSON, T. G.
Parametric study of minimum reactor mass in energy-storage dc-to-dc converters p 110 A83-11011
High-frequency high-voltage high-power DC-to-DC converters p 115 N83-21028
WINER, W. O.
Surface temperatures and glassy state investigations in tribology, part 5
[NASA-CR-3632] p 91 N83-11328
WINKELMAN, J. R.
Control design for a wind turbine-generator using output feedback p 164 A83-24721
Control design and performance analysis of a 6 MW wind turbine-generator p 165 A83-29897
WINTER, E. R. F.
Acoustic velocities of two-phase mixtures of cryogenic fluids p 124 A83-43012
WINTERS, W.
Aircraft measurements of trace gases and particles near the tropopause
[NASA-CR-3691] p 188 N83-27542
WINTUCKY, E. G.
Ion sputter textured graphite
[NASA-CASE-LEW-12919-1] p 63 N83-10117
WIRSCHING, P. H.
Statistical summaries of fatigue data for design purposes
[NASA-CR-3697] p 161 N83-29731
Application of advanced reliability methods to local strain fatigue analysis
[NASA-CR-168198] p 161 N83-29734
WIRTH, G.
Effect of swaging on the 1000 C compressive slow plastic flow characteristics of the directionally solidified eutectic alloy gamma/gamma prime-alpha p 77 A83-44340
WISANDER, D. W.
Method of fabricating an abradable gas path seal
[NASA-CASE-LEW-13269-2] p 93 N83-17714
Laser surface fusion of plasma sprayed ceramic turbine seals
[NASA-CASE-LEW-13269-1] p 50 N83-20996
Fully plasma-sprayed compliant backed ceramic turbine seal
[NASA-CASE-LEW-13268-3] p 149 N83-28450
WISNIEWSKI, J. H.
20 x 20 IF switch matrix for SS-TDMA systems p 113 A83-41369
WITTLIN, G.
Assessment of crash fire hazard of LH sub 2 fueled aircraft
[NASA-CR-165525] p 16 N83-11095
WITTWER, D. M.
Experiments on identification and control of inflow disturbances in contracting streams
[NASA-CR-169831] p 11 N83-17503
WOJNAR, M. K.
Digital system for structural dynamics simulation
[NASA-CR-168019] p 43 N83-14139
WONG, E.
The development of a generalized advanced propeller analysis system
[AIAA PAPER 83-2466] p 26 A83-49581
WONG, R. C.
Parametric study of minimum reactor mass in energy-storage dc-to-dc converters p 110 A83-11011
WOOD, B.
Three-dimensional flow measurements in a turbine scroll
[ASME PAPER 83-GT-128] p 8 A83-47957
Three-dimensional flow measurements in a vaneless radial turbine scroll
[NASA-CR-167994] p 9 N83-11065
WOOD, J. R.
NASA low-speed centrifugal compressor for fundamental research
[AIAA PAPER 83-1351] p 43 A83-36353
Performance of a tandem-rotor/tandem-stator conical-flow compressor designed for a pressure ratio of 3
[NASA-TP-2034] p 9 N83-11058
NASA low-speed centrifugal compressor for fundamental research
[NASA-TM-83398] p 13 N83-25662
Input generator for Denton 3-dimensional turbomachine-blade-row analysis code
[NASA-TM-23324] p 13 N83-26817
WOOD, K.
Satellite switched FDMA advanced communication technology satellite program
[NASA-CR-168034] p 105 N83-15543
WOODWARD, R. P.
Wind tunnel measurements of blade/vane ratio and spacing effects on fan noise p 192 A83-15317
Tone generation by rotor-downstream strut interaction
[AIAA PAPER 83-0767] p 21 A83-25957
Low flight speed acoustic results for a supersonic inlet with auxiliary inlet doors
[AIAA PAPER 83-1415] p 196 A83-45517
Tone generation by rotor-downstream strut interaction
[NASA-TM-83330] p 33 N83-19754
Low flight speed acoustic results for a supersonic inlet with auxiliary inlet doors
[NASA-TM-83411] p 201 N83-27794
WOOLLAM, J. A.
Ellipsometric study of silicon nitride on gallium arsenide p 204 A83-11812
Metallic conductivity and air stability in copper chloride intercalated carbon fibers p 111 A83-16095
Minority carrier diffusion length measurements - A review and comparison of techniques p 205 A83-28448
Interfacial electrical properties of ion-beam sputter deposited amorphous carbon on silicon p 205 A83-33920
An enhanced sensitivity null ellipsometry technique for studying films on substrates - Application to silicon nitride on gallium arsenide p 206 A83-37618
Diffusion length measurements in solar cells: An analysis and comparison of techniques p 171 N83-15812
WOOLLETT, R. R.
Zero-length inlets for subsonic V/STOL aircraft p 4 A83-29012
Aerodynamic performance of a fan stage utilizing variable inlet guide vanes (VIGV's) for thrust modulation
[AIAA PAPER 83-1162] p 6 A83-45508
Wind tunnel tests of a zero length, slotted-lip engine air inlet for a fixed nacelle V/STOL aircraft
[NASA-TM-82939] p 9 N83-10019
Aerodynamic performance of a fan stage utilizing Variable Inlet Guide Vanes (VIGVs) for thrust modulation
[NASA-TM-83438] p 13 N83-27957

WORRELL, W. L.
Reaction of cobalt in SO2 atmospheric at elevated temperatures
[NASA-TM-83485] p 88 N83-35104
WRIGHT, D. V.
Labyrinth seal forces on a whirling rotor
[NASA-CR-168016] p 34 N83-22198
WU, C. D.
Electromagnetic studies of redox systems for energy storage
[NASA-CR-169593] p 169 N83-14667
WU, J. M.
Measurements of compressible secondary flow in a circular S-duct
[AIAA PAPER 83-1739] p 4 A83-37218
WU, T. T.
Application of advanced reliability methods to local strain fatigue analysis
[NASA-CR-168198] p 161 N83-29734
WUERTZ, K. L.
Advanced single permanent magnet axipolar ironless stator ac motor for electric passenger vehicles
[NASA-CR-167974] p 212 N83-32687

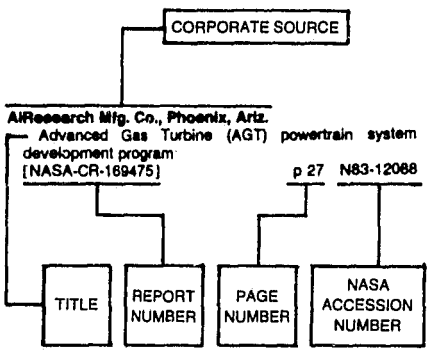
Y

YAMAMOTO, T.
Plastic deformation and wear process at a surface during unlubricated sliding p 138 A83-37822
Plastic deformation at surface during unlubricated sliding
[NASA-TP-2036] p 139 N83-11456
YANG, C. Y.
Zirconium carbide as an electrocatalyst for the chromous-chromic redox couple
[NASA-CASE-LEW-13246-1] p 182 N83-27344
YANG, J.
EL2 distributions in doped and undoped liquid encapsulated Czochralski GaAs p 205 A83-22756
YAU, J. F.
Benchmark notch test for life prediction
[NASA-CR-165571] p 158 N83-12451
YAVROUIAN, A.
Metallic conductivity and air stability in copper chloride intercalated carbon fibers p 111 A83-16095
YEAGER, E.
Electromagnetic studies of redox systems for energy storage
[NASA-CR-169593] p 169 N83-14667
YOON, H. K.
Five-hole pitot probe time-mean velocity measurements in confined swirling flows
[AIAA PAPER 83-0315] p 119 A83-16645
YOON, Y.-H.
Finite analytic numerical solution of axisymmetric Navier-Stokes and energy equations
[ASME PAPER 82-HT-42] p 118 A83-12795
YORK, R. E.
Analytical and experimental evaluation of the heat transfer distribution over the surfaces of turbine vanes
[NASA-CR-168015] p 131 N83-28376
YOUNG, E.
Application of 3D aerodynamic/combustion model to combustor primary zone study
[AIAA PAPER 83-1265] p 23 A83-36316
YOUNG, E. R.
Small gas turbine combustor primary zone study
[NASA-CR-168122] p 149 N83-28448
YOUNG, L. E.
SAFE II: Large systems space plasma evaluation experiment p 46 N83-26903
YOUNG, S. G.
Morphology of ductile metals eroded by a jet of spherical particles impinging at normal incidence p 75 A83-32624
Universal approach to analysis of cavitation and liquid-impingement erosion data
[NASA-TP-2061] p 82 N83-15413
A comprehensive analysis of cavitation and liquid impingement erosion data
[NASA-TM-83352] p 84 N83-24634
Morphology of an aluminum alloy eroded by a jet of angular particles impinging at normal incidence
[NASA-TP-2139] p 85 N83-24641
Solid spherical glass particle impingement studies of plastic materials
[NASA-TP-2161] p 94 N83-24695
Silicon-slurry/aluminide coating
[NASA-CASE-LEW-13343] p 86 N83-31795
YUAN, S.
A 1 watt GaAs power amplifier for the NASA 30/20 GHz communication system p 111 A83-11489
YUECE, H.
Ultrasonic attenuation of a void-containing medium for very long wavelengths
[NASA-CR-3693] p 154 N83-28466
YUHAS, D.
Comparison of NDE techniques for sintered-SiC components p 152 A83-22265
YURKOVICH, S.
Controller scheduling - A possible algebraic viewpoint p 190 A83-37093
Alternatives for jet engine control
[NASA-CR-170100] p 33 N83-20945

Z

ZAFRAN, S.
Electrothermal thruster diagnostics. Volume 1: Executive summary
[NASA-CR-168174-VOL-1] p 60 N83-33942
Electrothermal thruster diagnostics. Volume 2: Technical
[NASA-CR-168174-VOL-2] p 60 N83-33943
ZAGULI, R. J.
Wind tunnel evaluation of air-foil performance using simulated ice shapes
[NASA-CR-167960] p 11 N83-15265
ZANA, L. M.
The LeRC rail accelerators: Test designs and diagnostic techniques
[NASA-TM-83496] p 60 N83-35053
ZAPLATYNSKY, I.
Performance of laser-glazed zirconia thermal barrier coatings in cyclic oxidation and corrosion burner rig tests p 88 A83-10300
ZARETSKY, E. V.
Advances in high-speed rolling-element bearings p 137 A83-22319
NASA helicopter transmission system technology program p 144 N83-20120
An update on the life analysis of spur gears p 146 N83-20144
NASA transmission research and its probable effects on helicopter transmission design
[NASA-TM-83389] p 148 N83-24858
ZAVESKY, R.
Design, fabrication and testing of porous tungsten vaporizers for mercury ion thrusters
[NASA-TM-83063] p 58 N83-22318
ZEID, I.
Finite element analysis of steadily moving contact fields p 158 A83-49437
ZEISLOFT, H.
Aviation energy and the future of the recreational use of sport and general aviation aircraft p 100 N83-22444
ZEISSER, M. H.
Energy efficient engine sector combustor rig test program
[NASA-CR-167913] p 33 N83-19753
ZELAHY, J. W.
Materials for advanced turbine engines. Volume 1: Advanced blade tip seal system
[NASA-CR-167851-VOL-1] p 31 N83-15308
ZELEZNIK, F. J.
Thermodynamics of silicon nitridation - Effect of hydrogen
[ACS PAPER 33-B-80P] p 88 A83-18052
A search for equilibrium states
[NASA-TM-82898] p 207 N83-20808
A class of nonideal solutions. 2: Application to experimental data
[NASA-TP-1930] p 208 N83-23188
A class of nonideal solutions. 1: Definition and properties
[NASA-TP-1929] p 208 N83-23189
ZELLER, J. R.
Flight evaluation of modifications to a digital electronic engine control system in an F-15 airplane
[AIAA PAPER 83-0537] p 20 A83-19593
ZHANG, Q. F.
The structure of particle-laden jets and nonevaporating sprays
[NASA-CR-168059] p 34 N83-20948
ZHANG, Q.-F.
Measurements and predictions for nonevaporating sprays in a quiescent environment
[AIAA PAPER 83-0151] p 119 A83-16558
ZHANG, Z.-D.
On the three-dimensional vibrations of the cantilevered rectangular parallelepiped p 157 A83-37729
ZIEGLER, C.
Computer simulator for a mobile telephone system
[NASA-CR-170181] p 106 N83-22493
ZIEMER, R. E.
Adjacent channel interference degradation with minimum shift keyed modulation p 103 A83-19698
ZINN, B. T.
An iterative method for predicting turbofan inlet acoustics p 192 A83-13135
A theoretical investigation of the sound radiation fields associated with a Bellmouth inlet
[AIAA PAPER 83-0710] p 193 A83-25926
Optimization of acoustic liners by the hybrid finite element-integral approach
[AIAA PAPER 83-0670] p 194 A83-26917
Prediction of sound radiation from different practical jet engine inlets
[NASA-CR-169533] p 197 N83-13936
ZOBENS, A.
Energy efficient face seal
[NASA-CR-165591] p 142 N83-15659
ZOLA, C. L.
Conventional profile coaxial jet noise prediction p 193 A83-22128
ZORZI, E. S.
Power turbine dynamics - An evaluation of a shear-mounted elastomeric damper
[ASME PAPER 83-GT-228] p 139 A83-48025
ZUECK, M.
Design and evaluation of low-cost laminated wood composite blades for intermediate size wind turbines: Blade design, fabrication concept, and cost analysis
[NASA-CR-165463] p 179 N83-23704
ZUTECK, M.
Fabrication of low-cost Mod-OA wood composite wind turbine blades
[NASA-TM-83323] p 182 N83-27347

Typical Corporate Source Index Listing



Listings in this index are arranged alphabetically by corporate source. The title of the document is used to provide a brief description of the subject matter. The page number and the accession number are included in each entry to assist the user in locating the abstract in the abstract section. If applicable, a report number is also included as an aid in identifying the document.

A

Acurex Corp., Mountain View, Calif.
Catalyst durability evaluation for advanced gas turbine engines
[ASME PAPER 82-JPGC-GT-21] p 137 A83-25270
Development of a rotary instrumentation system, phase 2
[NASA-CR-168013] p 47 N83-18835

Advisory Group for Aerospace Research and Development, Neuilly-Sur-Seine (France).
Fluid Dynamics Panel Symposium on Aerodynamics of Power Plant Installation
[AGARD-AR-173] p 27 N83-11138

Aerojet Liquid Rocket Co., Sacramento, Calif.
LOX/hydrocarbon fuel carbon formation and mixing data analysis
[NASA-CR-168066] p 101 N83-31886

Aerojet Tactical Systems, Sacramento, Calif.
Process and quality verification controls for solid propellant manufacturing p 98 A83-39270

Air Force Avionics Lab., Wright-Patterson AFB, Ohio.
Ellipsometric study of silicon nitride on gallium arsenide p 204 A83-11812

Air Force Flight Test Center, Edwards AFB, Calif.
Experimental comparison of icing cloud instruments
[AIAA PAPER 83-0026] p 16 A83-42099

Air Force Rocket Propulsion Lab., Edwards AFB, Calif.
Electric propulsion research and technology in the United States
[AIAA PAPER 82-1867] p 53 A83-16925

AiResearch Mfg. Co., Phoenix, Ariz.
Advanced Gas Turbine (AGT) powertrain system development program
[NASA-CR-169475] p 27 N83-12088

AiResearch Mfg. Co., Torrance, Calif.
A lightweight electronically commutated dc motor for electric passenger vehicles
[NASA-CR-165601] p 113 N83-10348
Advanced single permanent magnet axipolar ironless stator ac motor for electric passenger vehicles
[NASA-CR-167974] p 212 N83-32687

Akron Univ., Ohio.
Formal convergence characteristics of elliptically constrained incremental Newton-Raphson algorithms p 190 A83-10273
On the solution of elastic-plastic static and dynamic postbuckling collapse of general structure p 155 A83-12746
An experimental investigation of the vaporous/gaseous cavity characteristics of an eccentric journal bearing
[ASLE PREPRINT 82-LC-3A-1] p 136 A83-13230
Experimental study of electrochemical fluorination of trichloroethylene p 68 A83-15870
Pseudo-updated constrained solution algorithm for nonlinear heat conduction p 121 A83-32989
The dryout region in frictionally heated sliding contacts p 124 A83-42762
Finite element analysis of steadily moving contact fields p 158 A83-49437
NASA LeRC/Akron University Graduate Cooperative Fellowship Program and Graduate Student Researchers Program
[NASA-CR-167943] p 208 N83-10970
Constrained self-adaptive solutions procedures for structure subject to high temperature elastic-plastic creep effects p 162 N83-34370

Alabama Univ., Huntsville.
Observations of charging dynamics p 49 A83-37591

American Society of Metals, Metals Park, Ohio.
Binary nickel alloy phase diagrams compilation and critical evaluation
[NASA-CR-170016] p 82 N83-19885

American Telephone and Telegraph Co., New York.
Customer premises services market demand assessment 1980 - 2000. Volume 1: Executive summary
[NASA-CR-168150] p 108 N83-31925

Ames Lab., Iowa.
Diatomic molecules and metallic adhesion, cohesion, and chemisorption - A single binding-energy relation p 69 A83-30921

Arizona State Univ., Tempe.
Heat transfer characteristics for jet array impingement with initial crossflow
[ASME PAPER 83-GT-28] p 7 A83-47891
Jet array impingement flow distributions and heat transfer characteristics. Effects of initial crossflow and nonuniform array geometry
[NASA-CR-3630] p 128 N83-15592

Arizona Univ., Tucson.
Incidence angle effects on convected gust airfoil noise
[AIAA PAPER 83-0765] p 195 A83-28022
Noise generation by a finite span swept airfoil
[AIAA PAPER 83-0768] p 195 A83-28023
Surface-polaritonlike waves guided by thin, lossy metal films p 192 A83-37947
Quasi-three-dimensional turbomachinery flow calculations on multiple hub-to-shroud stream surfaces
[AIAA PAPER 83-1820] p 5 A83-38652
Long-range surface plasmons in electrode structures p 202 A83-40733
Long range surface plasmons in birefringent media p 202 A83-42206
Effects of gaps on long range surface plasmon polaritons p 204 A83-46271
Statistical summaries of fatigue data for design purposes
[NASA-CR-3697] p 161 N83-29731
Application of advanced reliability methods to local strain fatigue analysis
[NASA-CR-168198] p 161 N83-29734

Arkansas State Univ., State University.
Vaporization thermodynamics of K2S and K2SO3
[NASA-CR-168080] p 61 N83-19812

Army Aviation Research and Development Command, Cleveland, Ohio.
PMR polyimides - Review and update p 62 A83-20447
Life and reliability models for helicopter transmissions
[NASA-TM-82976] p 139 N83-10425
Cold-air performance of compressor-drive turbine of Department of Energy upgraded automobile gas turbine engine. 2: Stage performance
[NASA-TM-82818] p 9 N83-11063
Effect of steady-state pressure distortion on inlet flow to a high-bypass-ratio turbofan engine
[NASA-TM-82964] p 30 N83-15306
Experimental feasibility study of a thermoelectric heat flux gage
[NASA-TM-83048] p 134 N83-15602
New trends in combustion research for gas turbine engines
[NASA-TM-83338] p 34 N83-20947
Advances in traction drive technology
[NASA-TM-83397] p 150 N83-28455

Army Electronics Research and Development Command, Fort Belvoir, Va.
High purity, low dislocation GaAs single crystals
[NASA-CR-168098] p 206 N83-19622

Army Propulsion Lab., Cleveland, Ohio.
Fatigue behavior of SiC reinforced Ti/6Al-4V/ at 650 C p 62 A83-12414
Effect of variable guide vanes on the performance of a high-bypass turbofan engine p 20 A83-24028
New trends in combustion research for gas turbine engines p 22 A83-35806
Effects of interstage diffuser flow distortion on the performance of a 15.41-centimeter tip diameter axial power turbine
[AIAA PAPER 83-1179] p 23 A83-36263

Army Research and Technology Labs., Cleveland, Ohio.
Detailed fuel spray analysis techniques
[NASA-TM-83476] p 42 N83-34943

Auburn Univ., Ala.
Extending the laser-speckiegram technique to strain analysis of rotating components p 155 A83-12514
Manual for extending the laser specklegram technique to strain analysis of rotating components
[NASA-CR-167932] p 134 N83-15601

Avco Corp., Lowell, Mass.
Hybridized polymer matrix composites
[NASA-CR-165341] p 66 N83-22326

Avco-Everett Research Lab., Mass.
MHD channel performance for potential early commercial MHD power plants p 204 A83-23134
Parametric study of potential early commercial MHD power plants. Task 3: Parameter variation of plant size
[NASA-CR-165445] p 182 N83-26259

Avco Lycoming Div., Stratford, Conn.
Experimental evaluation of inlet turbulence, wall boundary layer, surface finish, and fillet radius on small axial turbine state performance
[SAE PAPER 821475] p 24 A83-38001

B

Battelle Columbus Labs., Ohio.
Energy and precious fuels requirements of fuel alcohol production, volume 1
[NASA-CR-168090] p 183 N83-28581
Energy and precious fuels requirements of fuel alcohol production. Volume 3, appendices C to F: Methanol from cellulose
[NASA-CR-168092] p 183 N83-28583

Beech Aircraft Corp., Boulder, Colo.
Preliminary design of flight hardware for two-phase fluid research
[NASA-CR-168072] p 46 N83-25766

Beers Associates, Inc., Reston, Va.
Thermal dielectric breakdown with cylindrical electrodes p 112 A83-38216
Continued development of a detailed model of arc discharge dynamics
[NASA-CR-167977] p 206 N83-16234

Bell Helicopter Co., Fort Worth, Tex.
Design of an advanced 500-hp helicopter transmission p 144 N83-20125

Bendix Corp., South Bend, Ind.
Nonlinear multivariable design by total synthesis p 24 A83-37092
Boeing Aerospace Co., Seattle, Wash.
Auxiliary propulsion requirements for large space systems
[AIAA PAPER 83-1217] p 56 A83-45512
Boeing Co., Seattle, Wash.
Tests of a thermal acoustic shield with a supersonic jet p 192 A83-10183
Boeing Commercial Airplane Co., Seattle, Wash.
Nacelle Aerodynamic and Inertial Loads (NAIL) project
[NASA-CR-168712] p 18 N83-30402
Boeing Engineering and Construction Co., Seattle, Wash.
Mod-2 wind turbine system development. Volume 1: Executive summary
[NASA-CR-168006] p 184 N83-29812
Mod-2 wind turbine system development. Volume 2: Detailed report
[NASA-CR-168007] p 185 N83-33343
Boeing Military Airplane Development, Seattle, Wash.
Compression and compression fatigue testing of composite laminates
[NASA-CR-168023] p 66 N83-26928
Boeing Vertol Co., Philadelphia, Pa.
Large rotorcraft transmission technology development program
[NASA-CR-168120] p 18 N83-22188
Bolt, Beranek, and Newman, Inc., Cambridge, Mass.
The transfer function method for gear system dynamics applied to conventional and minimum excitation gearing designs
[NASA-CR-3626] p 139 N83-11495
Turbofan noise generation. Volume 1: Analysis
[NASA-CR-167951] p 198 N83-15041
Booz-Allen and Hamilton, Inc., Bethesda, Md.
Demonstration and evaluation of gas turbine transit buses
[NASA-CR-165528] p 212 N83-27926
Budd Co., Fort Washington, Pa.
Design and evaluation of low-cost stainless steel fiberglass foam blades for large wind driven generating systems
[NASA-CR-165491] p 174 N83-19226
Budd Co., Philadelphia, Pa.
Design and evaluation of low cost blades for large wind driven generating systems p 175 N83-19244

C

California Inst. of Tech., Pasadena.
Three-dimensional stability of vortex arrays p 120 A83-19022
Vortices, stability, and turbulence p 125 A83-46718
California Univ., Berkeley.
Aerodynamic features of turbulent flames
[AIAA PAPER 83-0470] p 119 A83-16737
Numerical solution of the problem of flame propagation by the use of the random element method
[AIAA PAPER 83-0600] p 69 A83-36062
Coherent conversion of the sunlight spectrum
[NASA-CR-170185] p 179 N83-25026
California Univ., Irvine.
Modified gauge for time-resolved skin-friction measurements p 133 A83-14172
A two-equation turbulence model for two-phase flows p 121 A83-30109
California Univ., La Jolla.
Modified gauge for time-resolved skin-friction measurements p 133 A83-14172
California Univ., Los Angeles.
The velocity perturbations above the orifice of an acoustically excited cavity in grazing flow p 195 A83-29235
California Univ., Santa Barbara.
Diatomic molecules and metallic adhesion, cohesion, and chemisorption - A single binding-energy relation p 69 A83-30921
Laser fluorescence studies of the chemical interactions of sodium species with sulfur bearing fuels
[NASA-CR-169861] p 71 N83-17625
The detailed chemistry and thermodynamics of sodium in oxygen-rich flames
[NASA-CR-169848] p 72 N83-17626
Carborundum Co., Niagara Falls, N. Y.
Comparison of NDE techniques for sintered-SiC components p 152 A83-22265
Tribological properties of sintered polycrystalline and single-crystal silicon carbide p 89 A83-29397
Carnegie-Mellon Univ., Pittsburgh, Pa.
Ignition of confined gaseous mixtures by hot surfaces and hot wires
[AIAA PAPER 83-0240] p 68 A83-16606
Numerical studies of the formation and destruction of vortices in a motored four-stroke piston-cylinder configuration
[AIAA PAPER 83-0497] p 136 A83-16749
Frequency-multiplexed and pipelined iterative optical systolic array processors p 188 A83-18588
Electro-optical processor for optimal control p 133 A83-23596
Friction damping of flutter in gas turbine engine airfoils p 20 A83-24038
Effects of friction dampers on aerodynamically unstable rotor stages
[AIAA PAPER 83-0848] p 22 A83-32791
Triangular system solutions on an optical systolic processor p 189 A83-36752
LU and Cholesky decomposition on an optical systolic array processor p 189 A83-43629
Optical systolic array processor using residue arithmetic p 189 A83-46834
Research priorities for advanced fibrous composites
[NASA-CR-165414] p 65 N83-18853
Research priorities and history of advanced composite compression testing
[NASA-CR-165415] p 66 N83-18854
Case Western Reserve Univ., Cleveland, Ohio.
O-18 tracer studies of Al2O3 scale formation on NiCrAl alloys p 74 A83-10249
Planar multijunction high voltage solar cell chip p 163 A83-13923
Experimental study of electrochemical fluorination of trichloroethylene p 68 A83-15870
Dipole-field sums and Lorentz factors for orthorhombic lattices, and implications for polarizable molecules p 204 A83-17226
Piezoelectric and pyroelectric coefficients for ferroelectric crystals with polarizable molecules p 205 A83-17227
Piezoelectricity and pyroelectricity in polyvinylidene fluoride - Influence of the lattice structure p 205 A83-29531
Diffusion processes in Al2O3 scales - Void growth, grain growth, and scale growth p 76 A83-42238
An experimental study of heat induced surface-tension driven flow p 44 A83-43269
Particle-sampling statistics in laser anemometers Sample-and-hold systems and saturable systems p 134 A83-48120
Orientation dependence of the stress rupture properties of Nickel-base superalloy single crystals
[NASA-CR-165394] p 206 N83-13009
Electromagnetic studies of redox systems for energy storage
[NASA-CR-169593] p 169 N83-14667
The electrochemical fluorination of polymeric materials for high energy density aqueous and non-aqueous battery and fuel cell separators
[NASA-CR-167961] p 72 N83-21056
Crack layer morphology and toughness characterization in steels
[NASA-CR-168154] p 160 N83-27256
Solution of elastic and elasto-plastic problems by the method of lines
[NASA-CR-168125] p 85 N83-28208
Tensile and compressive constitutive response of 316 stainless steel at elevated temperatures p 162 N83-34353
Charles River Associates, Inc., Boston, Mass.
Study to establish cost predictions for the production of Redox chemicals
[NASA-CR-167882] p 176 N83-20359
Cincinnati Univ., Ohio.
A method of predicting the performance deterioration of a compressor cascade due to sand erosion
[AIAA PAPER 83-0178] p 19 A83-16572
Multi-grid solution of Neumann pressure problem for viscous flows using primitive variables
[AIAA PAPER 83-0557] p 120 A83-16786
Metallurgical instabilities during the high temperature low cycle fatigue of nickel-base superalloys p 75 A83-22019
Solid particle dynamic behavior through twisted blade rows p 3 A83-27478
The effect of microstructure on the fatigue behavior of Ni base superalloys p 75 A83-36166
Solution of viscous internal flows on curvilinear grids generated by the Schwarz-Christoffel transformation p 122 A83-38796
Study of asymptotic incompressible flow in curved ducts using a multi-grid technique p 123 A83-42532
Effect of particle presence on the incompressible inviscid flow through a two dimensional compressor cascade p 6 A83-42562
Effect of particle presence on the incompressible inviscid flow through a two dimensional compressor cascade
[ASME PAPER 83-GT-95] p 8 A83-47941
Three-dimensional flow measurements in a turbine scroll
[ASME PAPER 83-GT-128] p 8 A83-47957
A study of the surface deterioration due to erosion
[ASME PAPER 83-GT-213] p 9 A83-48014
Three-dimensional flow measurements in a vaneless radial turbine scroll
[NASA-CR-167994] p 9 N83-11065
Three dimensional flow computations in a turbine scroll
[NASA-CR-168003] p 10 N83-12045
Environmental solid particle effects on compressor cascade performance
[NASA-CR-168018] p 11 N83-16285
Compressor cascade performance deterioration caused by sand ingestion
[NASA-CR-168067] p 11 N83-16286
A basis for the analysis of surface geometry of spiral bevel gears p 146 N83-20138
Geometrical analysis of circular-cut spiral bevel gears
[NASA-CR-168226] p 151 N83-33167
Research into the use of pyrolytic oxides and polymers for the fabrication of thin film high energy capacitors
[NASA-CR-173012] p 97 N83-34045
City Coll. of the City Univ. of New York.
Effect of hydrogen bonding on the vibrational dephasing time in glycerol p 61 A83-21054
Modulation techniques
[NASA-CR-169460] p 105 N83-10329
Computer simulator for a mobile telephone system
[NASA-CR-170181] p 106 N83-22493
Numerical analysis of turbulent coaxial flow with internal heat generation
[NASA-CR-172633] p 132 N83-33105
VLSI technology and applications
[NASA-CR-174451] p 118 N83-36358
Cleveland State Univ., Ohio.
Experimental results for the interference between FM television signals p 103 A83-19686
Performance degradation and cleaning of photovoltaic arrays p 164 A83-27236
Computation techniques and computer programs to analyze Stirling cycle engines using characteristic dynamic energy equations p 207 A83-27272
Effects of free stream turbulence intensity and integral length scale on heat transfer from a circular cylinder in crossflow p 123 A83-42711
A method for static and dynamic load analysis of standard and modified spur gears p 146 N83-20143
A study of dynamic energy equations for Stirling cycle analysis
[NASA-CR-168152] p 181 N83-25043
Dynamic effects of internal spur gear drives
[NASA-CR-3692] p 149 N83-28452
Vibration in planetary gear systems with unequal planet stiffnesses
[NASA-TM-83428] p 150 N83-29709
The effect of stress on ultrasonic pulses in fiber reinforced composites
[NASA-CR-3724] p 154 N83-33180
Colorado School of Mines, Golden.
Studies of the mechanisms of turbine fuel instability
[NASA-CR-167963] p 100 N83-18924
Colorado State Univ., Fort Collins.
Ion flow experiments in a multipole discharge chamber
[AIAA PAPER 82-1930] p 203 A83-14398
Inert gas thruster technology p 53 A83-20423
Industrial ion source technology
[NASA-CR-159877] p 102 N83-12259
Turbulence effect on crossflow around a circular cylinder at subcritical Reynolds numbers
[NASA-CR-3622] p 127 N83-13387
Current collection from the space plasma through defects in high voltage solar array insulation
[NASA-CR-168148] p 204 N83-31474
Electric thruster research
[NASA-CR-168134] p 59 N83-32843
Columbia Univ., New York.
Coordinate generation with precise controls over mesh properties p 190 A83-29631
High level continuity for coordinate generation with precise controls p 190 A83-29632
Automatic algebraic coordinate generation p 189 A83-38793
Comparison of channel assignment techniques for hybrid switching p 104 A83-41363
Superalloy composition modeling p 78 N83-11284
Role of cobalt in nickel base superalloys p 78 N83-11286
Next generation communications satellites: multiple access and network studies
[NASA-CR-167903] p 45 N83-12129
Communications Satellite Corp., Clarksburg, Md.
Limitations on solar cell open-circuit voltage and efficiency p 165 A83-37790

Planning assistance for the NASA 30/20 GHz program. Network control architecture study.
[NASA-CR-168058] p 106 N83-21207
Developments toward an 18% efficient silicon solar cell
[NASA-CR-168141] p 181 N83-25112

Connecticut Univ., Storrs.
A new surface-streamline flow-visualization technique p 133 A83-19016
Statistical characteristics of velocity, concentration, mass transport, and momentum transport for coaxial jet mixing in a confined duct
[ASME PAPER 83-GT-39] p 125 A83-47899
Turbine endwall single cylinder program
[NASA-CR-170008] p 44 N83-19761

Control Data Corp., Minneapolis, Minn.
Cloud encounter statistics in the 28.5-43.5 KFT altitude region from four years of GASP observations p 188 A83-38733
Flight summaries and temperature climatology at airliner cruise altitudes from GASP (Global Atmospheric Sampling Program) data
[NASA-CR-168106] p 188 N83-24048

Cornell Univ., Ithaca, N.Y.
A theory of rotating stall of multistage axial compressors. I - Small disturbances
[ASME PAPER 83-GT-44] p 7 A83-47904
A theory of rotating stall of multistage axial compressors. II - Finite disturbances
[ASME PAPER 83-GT-45] p 8 A83-47905
A theory of rotating stall of multistage axial compressors. III - Limit cycles
[ASME PAPER 83-GT-46] p 8 A83-47906

Crane Packing Co., Morton Grove, Ill.
Energy efficient face seal
[NASA-CR-165591] p 142 N83-15659

Curtiss-Wright Corp., Wood-Ridge, N.J.
Study of advanced rotary combustion engines for commuter aircraft
[NASA-CR-165399] p 32 N83-17545

D

Dartmouth Coll., Hanover, N.H.
A brittle to ductile transition in NiAl of a critical grain size p 75 A83-29726

Dayton Univ., Ohio.
Numerical simulation of airfoil ice accretion
[AIAA PAPER 83-0112] p 16 A83-36042
Testing of the permanent magnet material Mn-Al-C for potential use in propulsion motors for electric vehicles
[NASA-CR-169481] p 114 N83-12329

Delaware Univ., Newark.
Inlet-fan flow field computation
[ASME PAPER 83-GT-41] p 7 A83-47901
Design rules for a 100X maximum efficiency GaAs concentrator solar cell for space applications
[NASA-CR-170005] p 177 N83-20362

Department of Energy, Washington, D. C.
Advanced Gas Turbine (AGT) powertrain system development for automotive applications
[NASA-CR-167901] p 212 N83-33800

Detroit Diesel Allison, Indianapolis, Ind.
Application of 3D aerodynamic/combustion model to combustor primary zone study
[AIAA PAPER 83-1265] p 23 A83-36316
Component qualification and initial build of the AGT 100 advanced automotive gas turbine
[ASME PAPER 83-GT-225] p 138 A83-48023
Advanced Gas Turbine (AGT) powertrain system
[NASA-CR-165346] p 139 N83-11497
Components for digitally controlled aircraft engines
[NASA-CR-165296] p 28 N83-12089
Advanced Gas Turbine (AGT) powertrain system development for automotive applications
[NASA-CR-165178] p 140 N83-12431
Advanced Gas Turbine (AGT) power-train system development
[NASA-CR-167875] p 142 N83-15627
Support and power plant documentation for the gas turbine powered bus demonstration program
[NASA-CR-165527] p 210 N83-20829
Rotorcraft convertible engine study
[NASA-CR-168161] p 37 N83-27996
Analytical and experimental evaluation of the heat transfer distribution over the surfaces of turbine vanes
[NASA-CR-168015] p 131 N83-28376
Small gas turbine combustor primary zone study p 38 N83-29221

Deutsche Forschungs- und Versuchsanstalt fuer Luft- und Raumfahrt, Berlin (West Germany).
Excited waves in shear layers
[DFVLR-FB-82-23] p 106 N83-21218

Deutsche Forschungs- und Versuchsanstalt fuer Luft- und Raumfahrt, Cologne (West Germany).
Effect of swaging on the 1000 C compressive slow plastic flow characteristics of the directionally solidified eutectic alloy gamma/gamma prime-alpha p 77 A83-44340

Donovan, Hamester and Rattien, Inc., Washington, D. C.
Market assessment of photovoltaic power systems for agricultural applications worldwide
[NASA-CR-165541] p 168 N83-13585

Douglas Aircraft Co., Inc., Long Beach, Calif.
Sound propagation in segmented exhaust ducts - Theoretical predictions and comparison with measurements
[AIAA PAPER 83-0734] p 194 A83-28016
Calculation of compressible flow in and about three-dimensional inlets with and without auxiliary inlets by a higher-order panel method
[NASA-CR-168009] p 10 N83-12047

Drexel Univ., Philadelphia, Pa.
Droplet size effects on NO/x/ formation in a one-dimensional monodisperse spray combustion system
[ASME PAPER 82-JPGC-GT-10] p 68 A83-25268

Duke Univ., Durham, N. C.
Parametric study of minimum reactor mass in energy-storage dc-to-dc converters p 110 A83-11011
High-frequency high-voltage high-power DC-to-DC converters p 115 N83-21028

Dynamics Technology, Inc., Torrance, Calif.
Mean flowfields in axisymmetric combustor geometries with swirl p 120 A83-24668
Turbulence measurements in a swirling confined jet flowfield using a triple hot-wire probe
[NASA-CR-169668] p 127 N83-14434

E

Ecosystems International, Inc., Gambrills, Md.
Non-urban mobile radio market demand forecast
[NASA-CR-168065] p 107 N83-28297

EIC, Inc., Newton, Mass.
Development of a high capacity toroidal Ni/Cd cell
[NASA-CR-169945] p 176 N83-19273
Moderate temperature rechargeable sodium batteries
[NASA-CR-168220] p 118 N83-36359

Engelhard Industries, Inc., Edison, N.J.
Develop and test fuel cell powered on-site integrated total energy system
[NASA-CR-168020] p 173 N83-15839
Develop and test fuel cell powered on-site integrated total energy systems. Phase 3: Full-scale power plant development
[NASA-CR-168021] p 182 N83-27345

Environmental Systems Corp., Knoxville, Tenn.
'Scaling' analysis of the ice accretion process on aircraft surfaces
[ASME PAPER 82-WA/HT-39] p 16 A83-25693

F

Fairchild Weston Systems, Inc., Sarasota, Fla.
The DOE/NASA wind turbine data acquisition system. Part 3: Unattended power performance monitor
[NASA-CR-165540] p 44 N83-24516

Faucett (Jack) Associates, Inc., Chevy Chase, Md.
Energy and precious fuels requirements of fuel alcohol production. Volume 4: Appendices G and H, methanol from coal
[NASA-CR-168093] p 183 N83-28580
Energy and precious fuels requirements of fuel alcohol production, volume 1
[NASA-CR-168090] p 183 N83-28581
Energy and precious fuels requirements of fuel alcohol production. Volume 2, appendices A and B: Ethanol from grain
[NASA-CR-168091] p 183 N83-28582
Energy and precious fuels requirements of fuel alcohol production. Volume 3, appendices C to F: Methanol from cellulose
[NASA-CR-168092] p 183 N83-28583

Fiber Materials, Inc., Biddeford, Maine.
Alumina fiber strength improvement
[NASA-CR-167999] p 63 N83-11247

Florida State Univ., Tallahassee.
On the shock cell structure and noise of supersonic jets
[AIAA PAPER 83-0703] p 193 A83-25923

Florida Univ., Gainesville.
Effect of Y2O3 and Al2O3 on the oxidation resistance of Si3N4 p 88 A83-22258
Mechanisms of devitrification of grain boundary glassy phases in Si3N4 materials
[NASA-CR-169670] p 71 N83-14177

Vortex motion in axisymmetric piston-cylinder configurations
[NASA-TM-85404] p 133 N83-35318

Flow Research, Inc., Kent, Wash.
An experience in mesh generation for three-dimensional calculation of potential flow around a rotating propeller p 5 A83-38798
Finite volume calculation of three-dimensional potential flow around a propeller p 7 A83-45577
Conceptual design and cost analysis of hydraulic output unit for 15 kW free-piston Stirling engine
[NASA-CR-165543] p 167 N83-10561

Flow Simulations, Inc., Sunnyville, Calif.
User's manual for three-dimensional analysis of propeller flow fields
[NASA-CR-167959] p 12 N83-18671

Ford Aerospace and Communications Corp., Palo Alto, Calif.
20 x 20 IF switch matrix for SS-TDMA systems p 113 A83-41369
Spacecraft IF switch matrix for wideband service applications in 30/20 GHz communications satellite systems: Proof-of-concept model, executive summary
[NASA-CR-168175] p 107 N83-29492

Ford Motor Co., Dearborn, Mich.
Injection molding ceramics to high green densities p 137 A83-33515
The effect of silicon particle size on the nitriding behaviour of reaction bonded Si3N4 compacts p 90 A83-48261
Sintering of reaction bonded silicon nitride p 90 A83-48270
Evaluation of ceramics for stator applications: Gas turbine engines interim report. Stator fabrication and evaluation
[NASA-CR-168140] p 96 N83-30662

Foster-Miller Associates, Inc., Waltham, Mass.
Design of hydraulic output Stirling engine
[NASA-CR-167976] p 177 N83-22739

Fukui Univ. (Japan).
Soot formation in pyrolysis of acetylene, allene and 1,3-butadiene p 69 A83-39274

FWG Associates, Inc., Tullahoma, Tenn.
Influence of multidroplet size distribution on icing collection efficiency
[AIAA PAPER 83-0110] p 187 A83-16526

G

Garrett Turbine Engine Co., Phoenix, Ariz.
Experiments in dilution jet mixing
[AIAA PAPER 83-1201] p 122 A83-36277
Three-dimensional compressible viscous analysis of mixer nozzles
[AIAA PAPER 83-1401] p 4 A83-36391
Advanced Gas Turbine (AGT) powertrain system development for automotive applications
[NASA-CR-165329] p 209 N83-13038
Dilution Jet Mixing Program, phase 1
[NASA-CR-168031] p 128 N83-15590
A method to estimate weight and dimensions of small aircraft propulsion gas turbine engines: User's guide
[NASA-CR-168049] p 31 N83-16343
Computer program to predict noise of general aviation aircraft: User's guide
[NASA-CR-168050] p 198 N83-17242
Advanced Gas Turbine (AGT) powertrain system development for automotive applications
[NASA-CR-167983] p 210 N83-17424
Advanced Gas Turbine (AGT) powertrain system development for automotive applications
[NASA-CR-168104] p 211 N83-26763
Scaled centrifugal compressor, collector and running gear program
[NASA-CR-168167] p 40 N83-30432
Advanced Gas Turbine (AGT) powertrain system development for automotive applications
[NASA-CR-167901] p 212 N83-33800

Gaugeon Bros., Inc., Bay City, Mich.
Design and evaluation of low-cost laminated wood composite blades for intermediate size wind turbines: Blade design, fabrication concept, and cost analysis
[NASA-CR-165463] p 179 N83-23704

General Applied Science Labs., Inc., Westbury, N. Y.
Testing of felt-ceramic materials for combustor applications
[NASA-CR-168103] p 36 N83-26837

General Dynamics/Convair, San Diego, Calif.
Stability analysis of Centaur-in-Shuttle composite corrugated adapters
[AIAA 83-1003] p 49 A83-29791

General Dynamics Corp., St. Louis, Mo.
Analysis of the reflective multibandgap solar cell concept
[NASA-CR-168186] p 185 N83-34454

General Dynamics/Fort Worth, Tex.
Transient flow analysis of the AEDC/HPDE MHD generator
[AIAA PAPER 83-0395] p 203 A83-16691
General Electric Co., Cincinnati, Ohio.
Scale model performance test investigation of mixed flow exhaust systems for an energy efficient engine /E3/ propulsion system
[AIAA PAPER 83-0541] p 20 A83-16776
Requirements of constitutive models for two nickel-base superalloys p 74 A83-21071
NASA clean catalytic combustor program
[ASME PAPER 82-JPGC-GT-11] p 68 A83-25269
The influence of inlet design on the aeroacoustic performance of a JT15D turbofan engine as measured in the NASA-Ames 40 x 80 foot wind tunnel
[AIAA PAPER 83-0681] p 21 A83-28006
Turbine blade nonlinear structural and life analysis p 21 A83-29024
The aerodynamic design and performance of the General Electric/NASA EEE fan
[AIAA PAPER 83-1160] p 23 A83-36252
Composite engine duct fabrication p 1 A83-39941
Blade loss transient dynamic analysis of turbomachinery p 25 A83-40864
Analysis, design, fabrication and testing of an optical tip clearance sensor
[NASA-CR-165265] p 26 N83-11127
Benchmark notch test for life prediction
[NASA-CR-165571] p 158 N83-12451
CF6 jet engine diagnostics program. High pressure turbine roundness/clearance investigation
[NASA-CR-165581] p 29 N83-13100
Conceptual design, evaluation and research identification for Remote Augmented Propulsive Lift Systems (RALS) with ejectors for VTOL aircraft
[NASA-CR-167906] p 29 N83-13103
Tip cap for a rotor blade
[NASA-CASE-LEW-13654-1] p 30 N83-14129
Materials for advanced turbine engines. Volume 1: Advanced blade tip seal system
[NASA-CR-167851-VOL-1] p 31 N83-15308
Powder metallurgy Rene 95 rotating turbine engine parts, volume 2
[NASA-CR-165141] p 82 N83-15412
Energy efficient engine: Fan test hardware detailed design report
[NASA-CR-165148] p 31 N83-16341
The CF6 engine performance improvement
[NASA-CR-165612] p 31 N83-16342
Bearing fatigue investigation 3
[NASA-CR-168029] p 143 N83-17880
Free-jet acoustic investigation of high-radius-ratio coannular plug nozzles. Comprehensive data report, volume I
[NASA-CR-168086-VOL-1] p 198 N83-18408
Free-jet acoustic investigation of high-radius-ratio coannular plug nozzles. Comprehensive data report, volume 2
[NASA-CR-168086-VOL-2] p 199 N83-18409
The Rene 150 directionally solidified superalloy turbine blades, volume 1
[NASA-CR-167992] p 33 N83-20946
Energy efficient engine component development and integration program
[NASA-CR-170089] p 34 N83-22204
Energy efficient engine. Core engine bearings, drives and configuration: Detailed design report
[NASA-CR-165376] p 39 N83-30430
Control means for a gas turbine engine
[NASA-CASE-LEW-14586-1] p 40 N83-31603
Apparatus for improving the fuel efficiency of a gas turbine engine
[NASA-CASE-LEW-13142-1] p 43 N83-36029
General Electric Co., Evendale, Ohio.
Sound propagation in segmented exhaust ducts - Theoretical predictions and comparison with measurements
[AIAA PAPER 83-0734] p 194 A83-28016
Energy efficient engine. Flight propulsion system preliminary analysis and design
[NASA-CR-159859] p 28 N83-12094
Summary report for CF6 jet engine diagnostics program
[NASA-CR-165582] p 32 N83-17539
V/STOL propulsion control analysis: Phase 2, task 5-9
[NASA-CR-165523] p 40 N83-32604
General Electric Co., Lynn, Mass.
Status report - DARPA/NASA convertible turbofan/turboshaft engine program
[ASME PAPER 83-GT-196] p 25 A83-48000
Analytical fuel property effects, small combustors, phase 1
[NASA-CR-168138] p 101 N83-23464
Rotorcraft convertible engine study
[NASA-CR-168241] p 42 N83-34944
General Electric Co., Philadelphia, Pa.
Development of a microwave 20 x 20 switch matrix for 30/20 GHz SS-TDMA application p 110 A83-11484
A high capacity satellite switched TDMA microwave switch matrix p 104 A83-19776
Control design and performance analysis of a 6 MW wind turbine-generator p 165 A83-29897
Design study of a high power rotary transformer
[NASA-CR-168012] p 115 N83-16630
Customer premise service study for 30/20 GHz satellite system
[NASA-CR-167986] p 105 N83-17769
Experience and assessment of the DOE/NASA Mod-1 2000 kW wind turbine generator at Boone, North Carolina p 176 N83-19257
Spacecraft in switch matrix for wide band service applicatons in 30/20 GHz communications satellite systems
[NASA-CR-168089] p 46 N83-34998
General Electric Co., Schenectady, N. Y.
Transistorized PWM inverter-induction motor drive system p 110 A83-11488
Control design for a wind turbine-generator using output feedback p 164 A83-24721
Sound propagation in segmented exhaust ducts - Theoretical predictions and comparison with measurements
[AIAA PAPER 83-0734] p 194 A83-28016
Control design and performance analysis of a 6 MW wind turbine-generator p 165 A83-29897
Prediction of an axisymmetric combusting flow
[AIAA PAPER 83-1264] p 69 A83-36315
Packet communication system for a multi-beam beam switched satellite repeater p 104 A83-41336
Improved transistorized AC motor controller for battery powered urban electric passenger vehicles
[NASA-CR-167978] p 113 N83-10349
Evaluation of catalytic combustion of actual coal-derived gas
[NASA-CR-167842] p 168 N83-13588
Advanced AC permanent magnet axial flux disc motor for electric passenger vehicle
[NASA-CR-167975] p 115 N83-16628
Mobile radio alternative systems study, executive summary
[NASA-CR-168207] p 109 N83-34119
General Electric Co., Wilmington, Mass.
High accuracy fuel flowmeter, phase 1
[NASA-CR-167893] p 134 N83-21314
General Motors Corp., Indianapolis, Ind.
Multifuel evaluation of rich/quench/lean combustor p 67 A83-11492
Advanced propfan engine characteristics and technology needs
[AIAA PAPER 83-1155] p 23 A83-36250
Measurements of heat transfer distribution over the surfaces of highly loaded turbine nozzle guide vanes
[ASME PAPER 83-GT-53] p 8 A83-47910
Small gas turbine combustor primary zone study
[NASA-CR-168122] p 149 N83-28448
Ceramic applications in turbine engines
[NASA-CR-165494] p 212 N83-37028
General Motors Research Labs., Warren, Mich.
Diatomic molecules and metallic adhesion, cohesion, and chemisorption - A single binding-energy relation p 69 A83-30921
Georgia Inst. of Tech., Atlanta.
An iterative method for predicting turbofan inlet acoustics p 192 A83-13135
A viscous-inviscid interactive procedure for rotational flow in cascades of two-dimensional airfoils of arbitrary shape
[AIAA PAPER 83-0256] p 3 A83-16614
A theoretical investigation of the sound radiation fields associated with a Bellmouth inlet
[AIAA PAPER 83-0710] p 193 A83-25926
Optimization of acoustic liners by the hybrid finite element-integral approach
[AIAA PAPER 83-0670] p 194 A83-26917
Surface temperatures and glassy state investigations in tribology, part 5
[NASA-CR-3632] p 91 N83-11328
Prediction of sound radiation from different practical jet engine inlets
[NASA-CR-169533] p 197 N83-13936
NASA interdisciplinary collaboration in tribology. A review of oxidational wear
[NASA-CR-3686] p 95 N83-27021
Stress and fracture analyses under elastic-plastic creep conditions: Some basic developments and computational approaches p 162 N83-34371
Gilbert (Glen A.) and Associates, Inc., Reading, Pa.
Parametric analysis of closed cycle magnetohydrodynamic (MHD) power plants
[NASA-CR-165472] p 178 N83-22748
Giner, Inc., Waltham, Mass.
Optimization and fabrication of porous carbon electrodes for Fe/Cr redox flow cells
[NASA-CR-167921] p 179 N83-23708
GMAF, Inc., Freeport, N.Y.
A fast Euler solver for steady flows
[AIAA PAPER 83-1940] p 123 A83-39389
Fast Euler solver for steady, 1-dimensional flows
[NASA-CR-3689] p 14 N83-27960
Gould, Inc., Rolling Meadows, Ill.
Improved SCR ac motor controller for battery powered urban electric vehicles
[NASA-CR-167918] p 209 N83-16257
GTE Labs., Inc., Waltham, Mass.
Sintering, properties and fabrication of Si3N4 + Y2O3 based ceramics p 90 A83-48303
Gulf Research and Development Co., Pittsburgh, Pa.
Fuel quality-processing study. Volume 1: Overview and results
[NASA-CR-165326-VOL-1] p 178 N83-22750
Fuel quality-processing study. Volume 2: Literature survey
[NASA-CR-165326-VOL-2] p 178 N83-22751
Fuel quality/processing study. Volume 3: Fuel upgrading studies
[NASA-CR-165326-VOL-3] p 178 N83-22754
Fuel quality/processing study. Volume 4: On site processing studies
[NASA-CR-165326-VOL-4] p 179 N83-22755

H

Hamilton Standard, Windsor Locks, Conn.
Small transport aircraft technology propeller study
[NASA-CR-168045] p 14 N83-29178
Hamilton Standard Div., United Aircraft Corp., Windsor Locks, Conn.
Compliance and stress sensitivity of spur gear teeth p 146 N83-20142
Dynamic tooth loads and stressing for high contact ratio spur gears p 147 N83-20148
Harris Corp., Melbourne, Fla.
Phased array-fed antenna configuration study: Technology assessment
[NASA-CR-168078] p 106 N83-22495
Phased array-fed antenna configuration study
[NASA-CR-168077] p 107 N83-27086
Hersh Acoustical Engineering, Chatsworth, Calif.
Effect of flow on the acoustic performance of extended reaction lined ducts
[AIAA PAPER 83-0778] p 195 A83-28024
Houston Univ., Tex.
The 'whistler-nozzle' phenomenon p 125 A83-49472
The whistler nozzle phenomenon
[NASA-CR-170015] p 199 N83-20706
Hughes Aircraft Co., Culver City, Calif.
Onboard processing for a 30/20 GHz communications satellite p 47 A83-41391
Hughes Aircraft Co., El Segundo, Calif.
A multiple beam antenna concept for a 30/20 GHz satellite communications system p 103 A83-11485
Hughes Aircraft Co., Long Beach, Calif.
Modular photovoltaic stand-alone systems: Phase 1
[NASA-CR-168075] p 185 N83-33320
Photovoltaic stand-alone modular systems, phase 2
[NASA-CR-168230] p 186 N83-35497
Hughes Research Labs., Malibu, Calif.
On-orbit propulsion requirements and performance assessment of ion propulsion subsystems for future GEO large satellite missions
[AIAA PAPER 82-1872] p 48 A83-12460
Advances in series resonant inverter technology and its effect on spacecraft employing electric propulsion
[AIAA PAPER 82-1881] p 51 A83-12466
Status of the J-series 30-cm mercury ion thruster
[AIAA PAPER 82-1904] p 51 A83-12479
A direct-measurement technique for estimating discharge-chamber lifetime
[AIAA PAPER 82-1908] p 51 A83-12483
Advanced-technology 30-cm-diameter mercury ion thruster
[AIAA PAPER 82-1910] p 51 A83-12484
Software and system level tests of a test flight mercury ion thruster subsystem
[AIAA PAPER 82-1912] p 51 A83-12485
Qualification test results of IAPS 8 cm ion thrusters
[AIAA PAPER 82-1954] p 52 A83-12511
Extended-performance 8-cm ion thruster operation
[AIAA PAPER 82-1955] p 53 A83-12512

Simplified power processing for ion-thruster subsystems
[AIAA PAPER 83-1394] p 55 A83-36384
Simplified power processing for ion-thruster subsystems p 56 A83-39271
Analysis and design of ion thruster for large space systems
[NASA-CR-165140] p 57 N83-14158
GaAs solar cells for concentrator systems in space p 171 N83-15820
The 8-CM ion thruster characterization
[NASA-CR-167887] p 57 N83-17586
Endurance test of a 30-CM-diameter engineering model ion thruster. Task 12: Investigation of thin-film erosion monitors for ion thrusters
[NASA-CR-168132] p 58 N83-25779
Evaluation of the use of on-board spacecraft energy storage for electric propulsion missions
[NASA-CR-168209] p 59 N83-32842
Simplified power processing for ion-thruster subsystems p 60 N83-35018

I

IAP Research, Inc., Dayton, Ohio.
Electric rail gun projectile acceleration to high velocity
[AIAA PAPER 82-1939] p 52 A83-12501
Ideal Research, Inc., Rockville, Md.
Development and test of a Microwave Ice Accretion Measurement Instrument (MIAMI)
[NASA-CR-3598] p 18 N83-14123
IIT Research Inst., Chicago, Ill.
Improved uniformity of multiphase ceramic-metal plasma-sprayed coats p 61 A83-22269
Creep of plasma-sprayed-ZrO2 thermal-barrier coatings p 89 A83-22273
Determination of hydrogen permeability in uncoated and coated superalloys
[NASA-CR-165209] p 80 N83-12215
High strain rate properties of undirectional composites, part 1
[NASA-CR-167969] p 64 N83-13178
High strain rate properties of off-axis composite laminates, part 2
[NASA-CR-167970] p 64 N83-13179
High strain properties of angle-ply composite laminate, part 3
[NASA-CR-167971] p 64 N83-13180
Creep-rupture behavior of 6 candidate stirling engine iron-base superalloys in high pressure hydrogen. Volume 1: Air creep-rupture behavior
[NASA-CR-168071] p 83 N83-22389
Plasma-sprayed self-lubricating coatings
[NASA-CR-3680] p 94 N83-22422
Fatigue testing of low-cost fiberglass composite wind turbine blade materials
[NASA-CR-165566] p 177 N83-22746
Creep of plasma sprayed zirconia
[NASA-CR-167868] p 96 N83-29393
Determination of hydrogen permeability in commercial and modified superalloys
[NASA-CR-168195] p 87 N83-35101
Illinois Inst. of Tech., Chicago.
Rapid distortion of small-scale turbulence by an axisymmetric contraction p 120 A83-22381
Interpretation of 2-probe turbulence measurements in an axisymmetric contraction
[NASA-CR-169832] p 11 N83-17502
Experiments on identification and control of inflow disturbances in contracting streams
[NASA-CR-169831] p 11 N83-17503
Illinois Univ., Urbana.
Extending the laser-specklegram technique to strain analysis of rotating components p 155 A83-12514
The influence of surface dents and grooves on traction in sliding EHD point contacts p 138 A83-37823
Indian Inst. of Science, Bangalore.
The initial stages of cavitation damage and erosion on copper and brass tested in a rotating disk device p 75 A83-27421
Dynamics and mechanism of cavitation erosion on perspex and epoxy resin tested in a rotating disk device p 89 A83-27422
Cavitation erosion characteristics of poly(methyl methacrylate) in a rotating disk device p 90 A83-41851
Indian Inst. of Tech., Bombay.
Low cycle fatigue behavior of aluminum/stainless steel composites
[AIAA 83-0806] p 62 A83-29886
International Telephone and Telegraph Corp., Secaucus, N.J.
Customer premises services market demand assessment 1980 - 2000: Volume 2
[NASA-CR-168151] p 108 N83-31926
Iowa Univ., Iowa City.
Plasma characteristics of a 17 cm diameter line-cusp ion thruster
[AIAA PAPER 82-1926] p 52 A83-12495
Finite analytic numerical solution of axisymmetric Navier-Stokes and energy equations
[ASME PAPER 82-HT-42] p 118 A83-12795
Finite analytic numerical solution of heat transfer and flow past a square channel cavity p 123 A83-42703
The finite analytic method, volume 3
[NASA-CR-170186] p 191 N83-23087
The finite analytic method, volume 4
[NASA-CR-170187] p 191 N83-23088
The finite analytic method, volume 5
[NASA-CR-170188] p 191 N83-23089
IRT Corp., San Diego, Calif.
Development of electrical test procedures for qualification of spacecraft against EID. Volume 1: The CAN test and other relevant data
[NASA-CR-165590] p 49 N83-12136
Development of electrical test procedures for qualification of spacecraft against EID. Volume 2: Review and specification of test procedures
[NASA-CR-165590] p 50 N83-12137

J

Jet Propulsion Lab., California Inst. of Tech., Pasadena.
Metallic conductivity and air stability in copper chloride intercalated carbon fibers p 111 A83-16095
Electric propulsion research and technology in the United States
[AIAA PAPER 82-1867] p 53 A83-16925
Joint Center for Graduate Study, Richland, Wash.
Conceptual design and cost analysis of hydraulic output unit for 15 kW free-piston Stirling engine
[NASA-CR-165543] p 167 N83-10561

K

Kaman Aerospace Corp., Bloomfield, Conn.
Design and fabrication of composite blades for the Mod-1 wind turbine generator
[NASA-CR-167987] p 168 N83-11579
Kansas Univ., Lawrence.
Numerical simulation of a disk-shaped electron accelerating electrostatic probe p 133 A83-22336
Literature search of publications concerning the prediction of dynamic inlet flow distortion and related topics
[NASA-CR-3673] p 33 N83-18729
Kansas Univ. Center for Research, Inc., Lawrence.
A method of predicting flow rates required to achieve anti-icing performance with a porous leading edge ice protection system
[NASA-CR-169996] p 17 N83-19738
A method of predicting flow rates required to achieve anti-icing performance with a porous leading edge ice protection system
[NASA-CR-168213] p 17 N83-32782
Kent State Univ., Ohio.
Applications of ion beam technology
[NASA-CR-169797] p 82 N83-16493
Kentucky Univ., Lexington.
Boundary integral equation method calculations of surface regression effects in flame spreading p 67 A83-13488
Correlating downward flame spread rates for thick fuel beds p 69 A83-37045
KMS Fusion, Inc., Ann Arbor, Mich.
Gain-enhanced free-electron laser with an electromagnetic pump field p 135 A83-31133
The application of free-electron lasers to the transmission of energy in space p 135 A83-31141

L

Lehigh Univ., Bethlehem, Pa.
Moving cracks in layered composites p 155 A83-12048
Analysis of an axial compressor blade vibration based on wave reflection theory
[ASME PAPER 83-GT-151] p 25 A83-47970
Critical review of the trailing edge condition in steady and unsteady flow. Blade flutter in compressors and fans: Numerical simulation of the aerodynamic loading
[NASA-CR-169705] p 10 N83-15264
Levi (Enrico), Inc., Forest Hills, N.Y.
Preliminary assessment of the tradeoffs between the electric motor and the transmission in electric vehicles
[NASA-CR-168199] p 117 N83-30915
Lincoln Lab., Mass. Inst. of Tech., Lexington.
Microdistribution of oxygen in silicon and its effects on electronic properties p 172 N83-15825
Little (Arthur D.), Inc., Cambridge, Mass.
Stirling engine application study
[NASA-CR-168087] p 210 N83-22029
Lockheed-California Co., Burbank.
Zero-length inlets for subsonic V/STOL aircraft p 4 A83-29012
Assessment of crash fire hazard of LH sub 2 fueled aircraft
[NASA-CR-165525] p 16 N83-11095
Lockheed-Georgia Co., Marietta.
Generation of desired signals from acoustic drivers p 19 A83-15068
Sound radiation from annular ducts/nozzles using modal decomposition of in-duct acoustic power
[AIAA PAPER 83-0714] p 194 A83-25929
Inlet design for high-speed propfans
[SAE PAPER 821359] p 5 A83-37957
Tone-excited jet: Theory and experiments
[NASA-CR-3538] p 197 N83-12968
Refinement and application of acoustic impulse technique to study nozzle transmission characteristics
[NASA-CR-3656] p 199 N83-20708
Lockheed Missiles and Space Co., Palo Alto, Calif.
Noise and flow structure of a tone-excited jet p 192 A83-13136
Louisiana State Univ., Baton Rouge.
Soot formation in pyrolysis of acetylene, allene and 1,3-butadiene p 69 A83-39274
Benchmark notch test for life prediction
[NASA-CR-165571] p 158 N83-12451

M

Martin Marietta Aerospace, Denver, Colo.
Long term storage of cryogens in space p 102 A83-11487
Cryogenic fluid management experiment trunnion fatigue verification
[AIAA PAPER 83-0911] p 49 A83-32782
Benefits and costs of low thrust propulsion systems
[AIAA PAPER 83-1248] p 49 A83-36306
Study for analysis of benefit versus cost of low thrust propulsion system
[NASA-CR-168011] p 57 N83-21002
Martini Engineering, Richland, Wash.
Stirling engine design manual, 2nd edition
[NASA-CR-168088] p 212 N83-30328
Massachusetts Inst. of Tech., Cambridge.
Molecular-orbital model for metal-sapphire interfacial strength p 67 A83-10612
A new formulation of hybrid/mixed finite element p 155 A83-12739
Alternative ways for formulation of hybrid stress elements p 155 A83-14710
Flutter and forced response of mistuned rotors using standing wave analysis
[AIAA 83-0845] p 156 A83-29823
Some analysis methods for rotating systems with periodic coefficients p 157 A83-32987
Mode propagation in nonuniform circular ducts with potential flow p 122 A83-36082
Turbulent flame propagation and combustion in spark ignition engines p 70 A83-48156
Magnetohydrodynamics (MHD) Engineering Test Facility (ETF) 200 MWe power plant. Conceptual Design Engineering Report (CDER) supplement. Magnet system special investigations
[NASA-CR-165509] p 141 N83-14494
Effects of specimen resonances on acoustic-ultrasonic testing
[NASA-CR-3679] p 153 N83-21373
Stability analysis of flexible wind turbine blades using finite element method
[NASA-CR-168107] p 177 N83-21508
Simplified aeroelastic modeling of horizontal axis wind turbines
[NASA-CR-168109] p 177 N83-21509
Some experiments on Yaw stability of wind turbines with various coning angles
[NASA-CR-168108] p 177 N83-22740
Development of methodology for horizontal axis wind turbine dynamic analysis
[NASA-CR-168110] p 178 N83-22747
Ultrasonic attenuation of a void-containing medium for very long wavelengths
[NASA-CR-3693] p 154 N83-28466
Time-independent anisotropic plastic behavior by mechanical subelement models p 162 N83-34369
Maxwell Labs., Inc., San Diego, Calif.
High frequency, high power capacitor development
[NASA-CR-168035] p 116 N83-27127

Mechanical Technology, Inc., Latham, N. Y.
Analysis of spiral-groove face seals for liquid oxygen
[ASLE PREPRINT 83-AM-4B-2] p 138 A83-43339
Power turbine dynamics - An evaluation of a shear-mounted elastomeric damper
[ASME PAPER 83-GT-228] p 139 A83-48025
A conceptual study of the potential for automotive-derived and free-piston Stirling engines in 30- to 400-kilowatt stationary power applications
[NASA-CR-165274] p 167 N83-10568
Automotive Stirling Engine Mod 1 Design Review, volume 2
[NASA-CR-167936] p 209 N83-10991
Automotive Stirling engine development program
[NASA-CR-167907] p 209 N83-15176
Automotive Stirling engine development program
[NASA-CR-168060] p 209 N83-15177
Automotive Stirling engine development program
[NASA-CR-165263] p 211 N83-26762
Automotive Stirling Engine Development Program
[NASA-CR-168074] p 212 N83-27925
T55 power turbine rotor multiplane-multispeed balancing study
[NASA-CR-167891] p 41 N83-33894
Meteorology Research, Inc., Altadena, Calif.
Experimental comparison of icing cloud instruments
[AIAA PAPER 83-0026] p 16 A83-42099
Comparison of modern icing cloud instruments
[NASA-CR-168008] p 19 N83-18720
Michigan State Univ., East Lansing.
Measurements of energy distribution and thrust for microwave plasma coupling of electrical energy to hydrogen for propulsion
[AIAA PAPER 82-1951] p 52 A83-12508
Microwave plasma generation of hydrogen atoms for rocket propulsion p 53 A83-13090
High-voltage spark atomic emission detector for gas chromatography p 67 A83-13108
Performance characteristics of a microwave plasma disk ion source
[AIAA PAPER 82-1935] p 55 A83-27350
Experimental verification of the Neuber relation at room and elevated temperatures
[NASA-CR-167967] p 159 N83-19121
Experimental verification of the number relation at room and elevated temperatures p 162 N83-34355
Michigan Univ., Ann Arbor.
Image-optimized, frequency-scalable mixers for millimeter-wave applications p 112 A83-39273
Ignition and combustion: Low compression ratio, high output diesel
[NASA-CR-169742] p 31 N83-15309
Classification of journal surfaces using surface topography parameters and software methods to compensate for stylus geometry
[NASA-CR-168153] p 148 N83-24857
Practical aspects of photovoltaic technology, applications, and cost
[NASA-CR-168025] p 185 N83-34450
Vortex motion in axisymmetric piston-cylinder configurations
[NASA-TM-85404] p 133 N83-35318
Midwest Research Inst., Kansas City, Mo.
Evaluation of methods for rapid determination of freezing point of aviation fuels
[NASA-CR-167981] p 98 N83-10207
Minnesota Univ., Minneapolis.
Propagation of sound in highly porous open-cell elastic foams p 195 A83-28848
Surface acoustic admittance of highly porous open-cell, elastic foams p 195 A83-28849
Convex curvature effects on the heated turbulent boundary layer p 123 A83-42733
Missouri Univ., Rolla.
Adjacent channel interference degradation with minimum shift keyed modulation p 103 A83-19698
Acoustics in variable area duct - Finite element and finite difference comparisons to experiment p 193 A83-19809
Finite difference solutions to shocked acoustic waves
[AIAA PAPER 83-0671] p 193 A83-25907
A detailed treatment of two-dimensional, starved lubrication in the vicinity of two counter-rotating cylinders p 141 N83-15520
Motorola, Inc., Scottsdale, Ariz.
A low-power, high-throughput maximum-likelihood convolutional decoder chip for NASA's 30/20 GHz program p 111 A83-19754
Advances in Serial MSK modems p 111 A83-19789
A network control concept for the 30/20 GHz communication system baseband processor p 47 A83-41389
Satellite switched FDMA advanced communication technology satellite program
[NASA-CR-168034] p 105 N83-15543

N

National Aeronautics and Space Administration, Washington, D. C.
Electric propulsion research and technology in the United States
[AIAA PAPER 82-1867] p 53 A83-16925
Gamma prime shape changes during creep of a nickel-base superalloy p 77 A83-47855
National Aeronautics and Space Administration. Ames Research Center, Moffett Field, Calif.
The influence of inlet design on the aeroacoustic performance of a JT15D turbofan engine as measured in the NASA-Ames 40 x 80 foot wind tunnel
[AIAA PAPER 83-0681] p 21 A83-28006
Prediction of high speed propeller flow fields using a three-dimensional Euler analysis
[AIAA PAPER 83-0188] p 4 A83-29535
Supersonic STOVL research aircraft
[SAE PAPER 821375] p 17 A83-37965
Interfacial layers in high-temperature-oxidized NiCrAl p 77 A83-44619
National Aeronautics and Space Administration. Flight Research Center, Edwards, Calif.
Flight evaluation of modifications to a digital electronic engine control system in an F-15 airplane
[AIAA PAPER 83-0537] p 20 A83-19593
National Aeronautics and Space Administration. Langley Research Center, Hampton, Va.
Cloud encounter statistics in the 28.5-43.5 KFT altitude region from four years of GASP observations p 188 A83-38733
Modeling Interface Motion Of Combustion (MINOC). A computer code for two-dimensional, unsteady turbulent combustion
[NASA-TP-2132] p 40 N83-32806
A numerical study of the steady scalar convective diffusion equation for small viscosity
[NASA-CR-172231] p 16 N83-35999
National Aeronautics and Space Administration. Marshall Space Flight Center, Huntsville, Ala.
Operational summary of an electric propulsion long term test facility
[AIAA PAPER 82-1903] p 44 A83-12478
Status of the J-series 30-cm mercury ion thruster
[AIAA PAPER 82-1904] p 51 A83-12479
SAFE II: Large systems space plasma evaluation experiment p 46 N83-26903
National Bureau of Standards, Boulder, Colo.
The thermal conductivity of oxygen p 207 A83-12094
The dryout region in frictionally heated sliding contacts p 124 A83-42762
Transport properties of oxygen
[NASA-RP-1102] p 130 N83-24800
Naval Air Propulsion Test Center, Trenton, N.J.
Rotor fragment protection program: Statistics on aircraft gas turbine engine rotor failures that occurred in US commercial aviation during 1979
[NASA-CR-168163] p 38 N83-29234
Naval Weapons Support Center, Crane, Ind.
Evaluation program for secondary spacecraft cells. Cycle life test
[NASA-CR-172679] p 182 N83-27351
Evaluation program for secondary spacecraft cells. Cycle life test
[NASA-CR-172680] p 183 N83-27352
Nebraska Univ., Lincoln.
Ellipsometric study of silicon nitride on gallium arsenide p 204 A83-11812
Metallic conductivity and air stability in copper chloride intercalated carbon fibers p 111 A83-16095
Minority carrier diffusion length measurements - A review and comparison of techniques p 205 A83-28448
Interfacial electrical properties of ion-beam sputter deposited amorphous carbon on silicon p 205 A83-33920
An enhanced sensitivity null ellipsometry technique for studying films on substrates - Application to silicon nitride on gallium arsenide p 206 A83-37618
Diffusion length measurements in solar cells: An analysis and comparison of techniques p 171 N83-15812
Negev Univ., Beersheva (Israel).
Sputtered silicon nitride coatings for wear protection p 88 A83-12651
Some properties of r.f.-sputtered hafnium nitride coatings p 88 A83-12653
Nielsen Engineering and Research Co., Palo Alto, Calif.
Mean-flow measurements of the flow field diffusing bend
[NASA-CR-3634] p 10 N83-14066
Nielsen Engineering and Research, Inc., Mountain View, Calif.
Development of a multiple-parameter nonlinear perturbation procedure for transonic turbomachinery flows: Preliminary application to design/optimization problems
[NASA-CR-3657] p 2 N83-17453
New Jersey Inst. of Tech., Newark.
Heat transfer and flow characteristics of jets impinging on a concave hemispherical plate p 123 A83-42743
North Carolina State Univ., Raleigh.
An experimental study of supersonic jet shock-associated noise
[AIAA PAPER 83-0708] p 193 A83-25924
Northwestern Univ., Evanston, Ill.
On composites with periodic structure p 154 A83-10283
Composites with periodic microstructure p 62 A83-12734
Growth and stability of interacting surface flaws of arbitrary shape p 155 A83-15060
Ignition of a combustible half space p 68 A83-22738
Volume integrals of ellipsoids associated with the inhomogeneous Helmholtz equation p 192 A83-29528
The determination of the elastodynamic fields of an ellipsoidal inhomogeneity
[ASME PAPER 83-APM-19] p 157 A83-37388
Dynamic fields near a crack tip growing in an elastic-perfectly-plastic solid p 157 A83-38528
An extensometer for axial strain measurement at high temperature p 134 A83-48604
Micromechanically based constitutive relations for polycrystalline solids p 162 N83-34359
Notre Dame Univ., Ind.
Nonlinear multivariable design by total synthesis p 24 A83-37092
Controller scheduling - A possible algebraic viewpoint p 190 A83-37093
Alternatives for jet engine control
[NASA-CR-170100] p 33 N83-20945
Alternatives for jet engine control
[NASA-CR-170233] p 35 N83-23305

O

Ohio State Univ., Columbus.
A similarity analysis of the droplet trajectory equation p 118 A83-13133
An analytical evaluation of the icing properties of several low and medium speed airfoils
[AIAA PAPER 83-0109] p 3 A83-16525
Mechanics aspects of NDE by sound and ultrasound p 152 A83-25571
Volume integrals of ellipsoids associated with the inhomogeneous Helmholtz equation p 192 A83-29528
Vibrations of cantilevered circular cylindrical shells Shallow versus deep shell theory p 157 A83-36958
The determination of the elastodynamic fields of an ellipsoidal inhomogeneity
[ASME PAPER 83-APM-19] p 157 A83-37388
On the three-dimensional vibrations of the cantilevered rectangular parallelepiped p 157 A83-37729
Vibrations of cantilevered doubly-curved shallow shells p 157 A83-39557
Vibrations of blades with variable thickness and curvature by shell theory
[ASME PAPER 83-GT-152] p 158 A83-47978
Phenomenological and mechanics aspects of nondestructive evaluation and characterization by sound and ultrasound of material and fracture properties
[NASA-CR-3623] p 153 N83-11506
Fundamental aspects in quantitative ultrasonic determination of fracture toughness: The scattering of a single ellipsoidal inhomogeneity
[NASA-CR-3625] p 153 N83-11507
The orthogonal in-situ machining of single and polycrystalline aluminum and copper, volume 2
[NASA-CR-169528] p 81 N83-13233
Wind tunnel evaluation of ice-foil performance using simulated ice shapes
[NASA-CR-167960] p 11 N83-15265
The transmission or scattering of elastic waves by an inhomogeneity of simple geometry: A comparison of theories
[NASA-CR-3659] p 153 N83-16773
Engineering calculations for communications systems planning
[NASA-CR-170182] p 106 N83-22494
Oklahoma State Univ., Stillwater.
Five-hole pitot probe time-mean velocity measurements in confined swirling flows
[AIAA PAPER 83-0315] p 119 A83-16645
Confined swirling flow predictions
[AIAA PAPER 83-0316] p 119 A83-16646
Mean flowfields in axisymmetric combustor geometries with swirl p 120 A83-24668
A basic code for the prediction of transient

three-dimensional turbulent flowfields
p 121 A83-27412
Single-wire swirl flow turbulence measurements
[AIAA PAPER 83-1202] p 122 A83-36278
The performance of an annular vane swirler
[AIAA PAPER 83-1326] p 24 A83-36340
Turbulence measurements in a swirling confined jet flowfield using a triple hot-wire probe
[NASA-CR-169668] p 127 N83-14434
Axial vane-type swirler performance characteristics
[NASA-CR-172995] p 40 N83-32808
Turbulence measurements in a complex flowfield using a crossed hot-wire
[NASA-CR-173080] p 132 N83-35316

P

Page (R. J.) Co., Santa Ana, Calif.
The design and technology development for A 150 mlb resistojet for H2 or NH3
[AIAA PAPER 82-1949] p 52 A83-12506
Pennsylvania State Univ., University Park.
Development of secondary flow and vorticity in curved ducts, cascades, and rotors, including effects of viscosity and rotation p 119 A83-16141
Predictions of the structure of turbulent, particle-laden, round jets
[AIAA PAPER 83-0066] p 119 A83-16498
Measurements and predictions for nonevaporating sprays in a quiescent environment
[AIAA PAPER 83-0151] p 119 A83-16558
A turbulence model for three dimensional turbulent shear flows over curved rotating bodies
[AIAA PAPER 83-0559] p 120 A83-16787
Blade loading and rotation effects on compressor rotor wake near end walls p 3 A83-22138
Evaluation of a stochastic model of particle dispersion in a turbulent round jet p 121 A83-28104
Investigation of the tip clearance flow inside and at the exit of a compressor rotor passage, II - Turbulence properties p 4 A83-28843
Tip clearance flow in a compressor rotor passage at design and off-design conditions p 4 A83-35855
Experimental study of the boundary layer on a turbomachinery rotor blade p 7 A83-47022
Wall boundary layer development near the tip region of an IGV of an axial flow compressor
[ASME PAPER 83-GT-171] p 8 A83-47972
Performance and emissions characteristics of aqueous alcohol fumes in a DI diesel engine
[NASA-CR-167917] p 99 N83-12250
Fumigation of alcohol in a light duty automotive diesel engine
[NASA-CR-167915] p 99 N83-13272
End wall flows in rotors and stators of a single stage compressor
[NASA-CR-169800] p 128 N83-16678
Three dimensional flow field inside compressor rotor, including blade boundary layers
[NASA-CR-169788] p 128 N83-16679
The structure of particle-laden jets and nonevaporating sprays
[NASA-CR-168059] p 34 N83-20948
The structure of evaporating and combusting sprays: Measurements and predictions
[NASA-CR-170176] p 129 N83-22550
Mass analysis of neutral particles and ions released during electrical breakdowns on spacecraft surfaces
[NASA-CR-170299] p 50 N83-23347
The structure of evaporating and combusting sprays: Measurements and predictions
[NASA-CR-170312] p 130 N83-24795
End wall flow characteristics and overall performance of an axial flow compressor stage
[NASA-CR-3671] p 13 N83-26819
Structure of evaporating and combusting sprays: Measurements and predictions p 38 N83-29211
Pittsburgh Univ., Pa.
Low temperature hot corrosion p 76 A83-42252
Losses in chopper-controlled DC series motors
[NASA-CR-167845] p 114 N83-13359
Mechanism of hot corrosion of IN-738
[NASA-CR-169706] p 81 N83-15411
Power Technologies, Inc., Schenectady, N. Y.
Control of large wind turbine generators connected to utility networks
[NASA-CR-168200] p 185 N83-34451
Pratt and Whitney Aircraft Group, East Hartford, Conn.
Nonlinear structural and life analyses of a combustor liner p 155 A83-12764
Structural tailoring of engine blades (STAEBL)
[AIAA 83-0828] p 22 A83-29737
Ejector nozzle test results at simulated flight conditions for an advanced supersonic transport propulsion system
[AIAA PAPER 83-1287] p 23 A83-36323
Development and operating characteristics of an advanced two-stage combustor p 24 A83-38022
Development of advanced high-temperature heat flux sensors
[NASA-CR-165618] p 26 N83-10044
Energy efficient high-pressure turbine leakage technology report
[NASA-CR-165202] p 30 N83-15304
JT90 ceramic outer air seal system refinement program, phase 2
[NASA-CR-167962] p 30 N83-15305
The JT8D and JT9D engine component improvement: Performance improvement program
[NASA-CR-167965] p 32 N83-17543
The JT9D Jet Engine Diagnostics Program
[NASA-CR-167966] p 32 N83-17544
Investigation of continuously traversing microphone system for mode measurement
[NASA-CR-168040] p 199 N83-19575
Energy efficient engine sector combustor rig test program
[NASA-CR-167913] p 33 N83-19753
Development of a simplified analytical method for representing material cyclic response
[NASA-CR-168100] p 160 N83-21390
Model aerodynamic test results for a refined actuated inlet ejector nozzle at simulated takeoff and cruise conditions
[NASA-CR-168051] p 13 N83-26816
JT90 thermal barrier coated vanes
[NASA-CR-167964] p 37 N83-27993
Energy efficient engine high-pressure turbine single crystal vane and blade fabrication technology report
[NASA-CR-165400] p 39 N83-30429
Subsonic-transonic stall flutter study
[NASA-CR-165256] p 43 N83-30435
Broad specification fuels technology program, phase 1
[NASA-CR-168180] p 74 N83-30551
Aerothermal modeling program, phase 1
[NASA-CR-168202] p 131 N83-30959
Sensor failure detection for jet engines
[NASA-CR-168190] p 154 N83-33182
Pratt and Whitney Aircraft Group, Middletown, Conn.
Composite fan exit guide vanes for high bypass ratio gas turbine engines p 19 A83-13159
Princeton Univ., N. J.
Computed and measured turbulence in axisymmetric reciprocating engines p 21 A83-24669
Design of dry-friction dampers for turbine blades p 22 A83-35883
Purdue Univ., Lafayette, Ind.
Axial-compressor flow distortion with water ingestion
[AIAA PAPER 83-0004] p 19 A83-16456
An analytical and experimental comparison of the flow field of an advanced swept turboprop
[AIAA PAPER 83-0189] p 3 A83-21080
Effect of humidity on jet engine axial-flow compressor performance p 22 A83-35856
Quasi-three-dimensional turbomachinery flow calculations on multiple hub-to-shroud stream surfaces
[AIAA PAPER 83-1820] p 5 A83-38652
Acoustic velocities of two-phase mixtures of cryogenic fluids p 124 A83-43012
Wave propagation in a graphite/epoxy laminate p 158 A83-44050
A computer program for the calculation of the flow field including boundary layer effects for mixed-compression inlets at angle of attack
[NASA-CR-168002] p 10 N83-11066
The WISGSK: A computer code for the prediction of a multistage axial compressor performance with water ingestion
[NASA-CR-3624] p 28 N83-12093
Dynamic responses of graphite/epoxy laminated beam to impact of elastic spheres
[NASA-CR-165461] p 64 N83-13173
Wave propagation in graphite/epoxy laminates due to impact
[NASA-CR-168057] p 66 N83-22325
Stagnation region gas film cooling: Effects of dimensionless coolant temperature
[NASA-CR-168197] p 132 N83-30960
The effect of incidence angle on the overall three-dimensional aerodynamic performance of a classical annular airfoil cascade
[NASA-CR-168127] p 15 N83-34911
Purdue Univ. School of Science at Indianapolis, Ind.
A finite element formulation for steady transonic Euler equations p 3 A83-22129

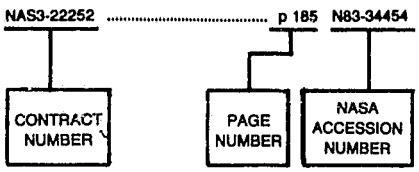
R

Radio Corp. of America, Indianapolis, Ind.
Experimental results for the interference between FM television signals p 103 A83-19686
Rasor Associates, Inc., Sunnyvale, Calif.
Improved Stirling engine performance using jet impingement p 137 A83-27288
RCA Labs., Princeton, N. J.
Advanced 3-V semiconductor technology assessment
[NASA-CR-168101] p 206 N83-21987
Advanced 3-V semiconductor technology assessment
[NASA-CR-168102] p 207 N83-21988
Rensselaer Polytechnic Inst., Troy, N. Y.
Infrared emission spectrophotometric study of the changes produced by TiN coating of metal surfaces in an operating EHD contact
[ASLE PREPRINT 82-LC-3C-3] p 135 A83-13229
Microscopic contour changes of tribological surfaces by chemical and mechanical action
[ASLE PREPRINT 82-LC-3B-3] p 136 A83-13237
Natural frequency of rotating beams using non-rotating modes p 156 A83-18383
Structural dynamics studies of rotating bladed-disk assemblies coupled with flexible shaft motions
[AIAA PAPER 83-0919] p 22 A83-32787
Spanwise mass transfer variations on a cylinder in 'nominally' uniform crossflow p 124 A83-43019
Infrared emission spectrophotometric study of the changes produced by TiN coating of metal surfaces in an operating EHD contact
[NASA-TM-82989] p 92 N83-15466
Diffused P+-N solar cells in bulk GaAs p 171 N83-15818
Determination of physical and chemical states of lubricants in concentrated contacts, part 3
[NASA-CR-3658] p 92 N83-16527
Rice Univ., Houston, Tex.
The phototron: A light to RF energy conversion device p 173 N83-15866
Riso National Lab., Roskilde (Denmark).
Particle-sampling statistics in laser anemometers Sample-and-hold systems and saturable systems p 134 A83-48120
Rochester Univ., N. Y.
Surface-polaritonlike waves guided by thin, lossy metal films p 192 A83-37947
Rocketdyne, Canoga Park, Calif.
Hybrid hydrostatic/ball bearings in high-speed turbomachinery
[NASA-CR-168124] p 149 N83-27213
Advanced LOX/H sub 2 engine technologies for future OTVs p 60 N83-35013
SSME main combustion chamber life prediction
[NASA-CR-168215] p 60 N83-36101
Rockwell International Corp., Canoga Park, Calif.
Advanced LOX/H2 engine technologies for future OTVs
[AIAA PAPER 83-1312] p 55 A83-36333
The performance and application of high speed long life LH2 hybrid bearings for reusable rocket engine turbomachinery
[AIAA PAPER 83-1389] p 138 A83-36379
High speed cryogenic self-acting, shaft seals for liquid rocket turbopumps
[NASA-CR-168194] p 151 N83-32070
Rockwell International Corp., Thousand Oaks, Calif.
Liquid encapsulated Czochralski growth of low dislocation GaAs p 204 A83-13784
Residual double acceptors in bulk GaAs p 205 A83-19989
EL2 distributions in doped and undoped liquid encapsulated Czochralski GaAs p 205 A83-22756
A two-stage monolithic buffer amplifier for 20 GHz satellite communication p 112 A83-39272
Advances in large-diameter liquid encapsulated Czochralski GaAs p 171 N83-15819
High purity, low dislocation GaAs single crystals
[NASA-CR-168098] p 206 N83-19622
Growth and characterization of Czochralski-grown n and p-type GaAs for space solar cell substrates
[NASA-CR-168099] p 207 N83-27877
Rutgers Univ., New Brunswick, N. J.
Unsteady turbulent shear flow in shock tube discontinuities p 124 A83-46445

S

San Jose State Univ., Calif.
An experimental investigation of internal area ruling for transonic and supersonic channel flow
[NASA-CR-169638] p 10 N83-14068

Typical Contract Number Index Listing



Listings in this index are arranged alphanumerically by contract number. Under each contract number, the accession numbers denoting documents that have been produced as a result of research done under that contract are arranged in ascending order with the AIAA accession numbers appearing first. The accession number denotes the number by which the citation is identified in the abstract section. Preceding the accession number is the page number on which the citation may be found.

AF-AFOSR-005-81 ..... p 82 N83-17682
AF-AFOSR-3473-78 ..... p 92 N83-15466
AF-AFOSR-78-3473 ..... p 135 A83-13229
AF-AFOSR-79-0091D ..... p 189 A83-43629
AF-AFOSR-79-0091 ..... p 188 A83-18588
AF-AFOSR-80-0065 ..... p 75 A83-22019
p 75 A83-36166
AF-AFOSR-80-0160 ..... p 120 A83-16786
p 123 A83-42532
AF-AFOSR-81-0005 ..... p 136 A83-13237
DA PROJ. 1L1-62209-AH-76 ..... p 34 N83-22198
p 149 N83-28448
p 14 N83-29174
DAAG29-78-G-0064 ..... p 204 A83-17226
p 205 A83-17227
DAAG29-79-C-0168 ..... p 154 A83-10283
DAAG29-79-C-0204 ..... p 135 A83-13229
DAAG29-81-K-0090 ..... p 192 A83-29528
DAAG29-82-K-0018 ..... p 192 A83-37947
DAAG29-82-K-0029 ..... p 19 A83-16572
p 6 A83-42562
p 8 A83-47941
DAAJ02-76-C-0044 ..... p 144 N83-20124
DE-AC01-79ET-13547 ..... p 76 A83-42252
DE-AC02-76ET-11291 ..... p 54 A83-27298
DE-AC02-78ER-04650 ..... p 68 A83-22738
DE-AC02-79ER-10515A000 ..... p 123 A83-42703
DE-AC02-79ER-10515 ..... p 118 A83-12795
DE-AC02-81CS-90215 ..... p 54 A83-27298
DE-AC03-79SF-10610 ..... p 70 A83-46608
DE-AC04-81AL-16338 ..... p 21 A83-24669
DE-AI01-71ET-13111 ..... p 176 N83-22754
DE-AI01-76ET-2030 ..... p 168 N83-11579
DE-AI01-76ET-20320 ..... p 169 N83-14689
p 169 N83-14690
p 174 N83-16857
p 177 N83-21508
p 177 N83-21509
p 177 N83-22740
p 178 N83-22747
p 179 N83-23704
p 179 N83-23710
p 184 N83-29813
p 117 N83-34192
p 185 N83-34451
DE-AI01-76ET-20370 ..... p 174 N83-16859
DE-AI01-77CS-51040 ..... p 23 A83-36263
p 209 N83-10991
p 126 N83-12359
p 81 N83-13232
p 210 N83-17423
p 210 N83-19651
p 210 N83-22029
p 83 N83-22389
p 35 N83-24505
p 130 N83-26017
p 181 N83-26251
p 211 N83-26757
p 211 N83-26758
p 211 N83-26759
p 212 N83-27924
p 212 N83-30328
DE-AI01-77CS-51044 ..... p 119 N83-10348
p 113 N83-10349
p 114 N83-13359
p 209 N83-16257
p 115 N83-16628
p 178 N83-22749
p 211 N83-24432
p 116 N83-25982
p 184 N83-29811
p 117 N83-30914
p 117 N83-30915
p 212 N83-32687
p 186 N83-35496
DE-AI01-77ET-10350 ..... p 90 A83-42261
p 99 N83-10208
p 168 N83-13588
p 176 N83-20361
DE-AI01-77ET-10769 ..... p 168 N83-13589
p 141 N83-14494
p 175 N83-19228
p 61 N83-19812
p 178 N83-22748
DE-AI01-77ET-13111 ..... p 90 A83-42261
p 166 N83-10556
p 166 N83-10557
p 167 N83-10559
p 167 N83-10560
p 92 N83-15467
p 179 N83-22755
p 185 N83-34453
DE-AI01-77ET-710769 ..... p 182 N83-26259
DE-AI01-79ET-20320 ..... p 174 N83-19226
p 177 N83-22746
p 182 N83-27347
DE-AI01-79ET-20485 ..... p 168 N83-13585
p 114 N83-14397
p 173 N83-15840
p 160 N83-23631
p 179 N83-23709
p 180 N83-25041
p 185 N83-33320
p 186 N83-35497
DE-AI01-80CS-50194 ..... p 210 N83-24431
p 148 N83-24857
DE-AI01-80ET-17088 ..... p 168 N83-12524
p 173 N83-15839
p 182 N83-27345
DE-AI01-81CS-50006 ..... p 99 N83-12250
p 99 N83-13272
p 183 N83-28580
p 183 N83-28581
p 183 N83-28582
p 183 N83-28583
p 86 N83-29359
DE-AI01-82ET-20305 ..... p 184 N83-29812
p 185 N83-33343
DE-AI04-80AL-12726 ..... p 169 N83-14683
p 176 N83-20359
p 179 N83-23708
p 180 N83-25042
p 181 N83-26252
p 73 N83-28326
p 183 N83-29810
DE-AI05-82OR-1055 ..... p 182 N83-27346
DE-AI07-76ET-20320 ..... p 169 N83-14688
DE-AI21-80ET-17088 ..... p 208 N83-30297
DE-AJ01-77ET-13111 ..... p 178 N83-22750
p 178 N83-22751
DE-AM03-76SF-00034 ..... p 72 N83-17626
DE-A101-77CS-51040 ..... p 80 N83-12215
p 87 N83-35101
DE-FG22-80PC-30247 ..... p 69 A83-39274
DE-FG22-80PC-30303 ..... p 121 A83-30109
DEN3-0019 ..... p 96 N83-30662
DEN3-101 ..... p 179 N83-23704
DEN3-110 ..... p 92 N83-15467
DEN3-129 ..... p 174 N83-19226
p 175 N83-19244
DEN3-131 ..... p 168 N83-11579
DEN3-136 ..... p 178 N83-22748
DEN3-142 ..... p 212 N83-27926
DEN3-145 ..... p 67 A83-11491
DEN3-149 ..... p 166 N83-10556
DEN3-153 ..... p 164 A83-24721
p 165 A83-29897
DEN3-161 ..... p 168 N83-12524
DEN3-163 ..... p 174 N83-16859
DEN3-167 ..... p 152 A83-22265
p 139 A83-48030
p 90 A83-48270
p 27 N83-12088
p 209 N83-13038
p 210 N83-17424
p 211 N83-26763
p 212 N83-33800
DEN3-168 ..... p 152 A83-22265
p 138 A83-48023
p 139 A83-48030
p 139 N83-11497
p 140 N83-12431
p 142 N83-15627
DEN3-175 ..... p 178 N83-22750
p 178 N83-22751
p 178 N83-22754
p 179 N83-22755
DEN3-177 ..... p 137 A83-27288
DEN3-17 ..... p 139 A83-48030
p 90 A83-48303
p 212 N83-37028
DEN3-180 ..... p 168 N83-13585
DEN3-182 ..... p 177 N83-22746
DEN3-187 ..... p 210 N83-20829
DEN3-189 ..... p 114 N83-12329
DEN3-198 ..... p 179 N83-23708
DEN3-202 ..... p 175 N83-19228
DEN3-207 ..... p 185 N83-33320
p 186 N83-35497
DEN3-20 ..... p 137 A83-33515
p 90 A83-48261
DEN3-210 ..... p 208 N83-30297
DEN3-212 ..... p 167 N83-10561
DEN3-217 ..... p 63 N83-22389
DEN3-234 ..... p 80 N83-12214
DEN3-235 ..... p 122 A83-38796
p 211 N83-26757
p 211 N83-26758
p 211 N83-26759
DEN3-241 ..... p 173 N83-15839
p 182 N83-27345
DEN3-251 ..... p 176 N83-20359
DEN3-252 ..... p 185 N83-34451
DEN3-254 ..... p 210 N83-22029
DEN3-275 ..... p 165 A83-36410
p 165 A83-44673
DEN3-287 ..... p 86 N83-29359
DEN3-292 ..... p 183 N83-28580
p 183 N83-28581
p 183 N83-28582
p 183 N83-28583
DEN3-2 ..... p 184 N83-29812
p 185 N83-33343
DEN3-32 ..... p 209 N83-10991
p 209 N83-15176
p 209 N83-15177
p 211 N83-26762
p 212 N83-27925
DEN3-35 ..... p 145 N83-20136
DEN3-51 ..... p 204 A83-23134
p 182 N83-26259
DEN3-59 ..... p 110 A83-11488
p 113 N83-10349
DEN3-60 ..... p 209 N83-16257
DEN3-64 ..... p 113 N83-10348
DEN3-6 ..... p 80 N83-12215
p 87 N83-35101

NSG-3198 ..... p 197 N83-12967
NSG-3210 ..... p 153 N83-21373
p 154 N83-28466
NSG-3212 ..... p 119 A83-16141
p 4 A83-28843
p 4 A83-35855
p 128 N83-16678
NSG-3214 ..... p 76 A83-42252
p 81 N83-15411
NSG-3217 ..... p 65 N83-16394
NSG-3218 ..... p 19 A83-16572
p 3 A83-27478
p 6 A83-42562
p 8 A83-47941
p 9 A83-48014
p 11 N83-16285
p 11 N83-16286
NSG-3219 ..... p 133 A83-14172
NSG-3220 ..... p 120 A83-22381
p 11 N83-17502
p 11 N83-17503
NSG-3236 ..... p 195 A83-29235
NSG-3238 ..... p 133 A83-19016
p 44 N83-19761
NSG-3239 ..... p 191 N83-34656
NSG-3245 ..... p 70 A83-48156
NSG-3246 ..... p 206 N83-13009
NSG-3249 ..... p 61 N83-19812
NSG-3250 ..... p 61 N83-28077
NSG-3251 ..... p 85 N83-28208
NSG-3254 ..... p 88 A83-22258
p 71 N83-14177
NSG-3255 ..... p 203 A83-16691
NSG-3256 ..... p 71 N83-17625
p 72 N83-17626
NSG-3257 ..... p 207 A83-27272
p 181 N83-25043
NSG-3260 ..... p 3 A83-16614
NSG-3262 ..... p 124 A83-43019
NSG-3263 ..... p 75 A83-22019
p 75 A83-36166
NSG-3266 ..... p 120 A83-16787
p 7 A83-47022
p 128 N83-16679
NSG-3267 ..... p 120 A83-16786
p 123 A83-42532
NSG-3269 ..... p 152 A83-25571
p 192 A83-29528
p 157 A83-37388
p 153 N83-11506
p 153 N83-11507
p 153 N83-16773
NSG-3270 ..... p 7 A83-47901
NSG-3274 ..... p 111 A83-11495
p 114 N83-14398
NSG-3280 ..... p 124 A83-46445
NSG-3281 ..... p 113 A83-41152
NSG-3285 ..... p 15 N83-34911
NSG-3290 ..... p 133 A83-22336
p 50 N83-18805
NSG-3294 ..... p 3 A83-22129
NSG-3295 ..... p 24 A83-36393
NSG-3299 ..... p 53 A83-13090
NSG-3301 ..... p 50 N83-23347
NSG-3303 ..... p 157 A83-32987
p 177 N83-21508
p 177 N83-21509
p 177 N83-22740
p 178 N83-22747
NSG-3305 ..... p 118 A83-12795
p 123 A83-42703
p 191 N83-23087
p 191 N83-23088
p 191 N83-23089
NSG-3308 ..... p 70 N83-12181
NSG-330 ..... p 77 A83-47855
NSG-3311 ..... p 10 N83-11066
N00014-78-C-0590 ..... p 3 A83-27478
N00014-78-C-0647 ..... p 156 A83-27431
p 156 A83-27432
N00014-80-C-0196 ..... p 68 A83-22738
N00014-80-C-0614 ..... p 135 A83-31133
N00019-77-C-0546 ..... p 9 A83-48012
N00019-82-C-0077 ..... p 1 A83-39941
SRI PROJ. 2590 ..... p 115 N83-18997
SRI PROJ. 4032 ..... p 202 N83-35787
W-7405-ENG-48 ..... p 119 A83-16737
p 69 A83-36062
W-7405-ENG-82 ..... p 69 A83-30921
XP-9-8081-1 ..... p 164 A83-27260
p 70 A83-46608
500-53-1B ..... p 150 N83-28454
505-04-22 ..... p 32 N83-17547
505-15-83 ..... p 13 N83-26819
505-31-0A ..... p 2 N83-17453
p 14 N83-29179
505-31-0A ..... p 15 N83-34909
505-31-01 ..... p 14 N83-27960
p 15 N83-34908
505-31-02 ..... p 34 N83-22199
505-31-0 ..... p 190 N83-12930
p 2 N83-24467
p 13 N83-26817
p 191 N83-30113
505-31-32 ..... p 197 N83-12966
p 11 N83-15269
p 198 N83-16152
p 198 N83-16153
p 198 N83-18405
p 198 N83-18408
p 199 N83-19575
p 33 N83-19754
p 200 N83-21896
p 200 N83-23114
p 200 N83-23115
p 200 N83-23116
p 201 N83-23117
p 201 N83-24287
p 12 N83-24470
p 13 N83-25662
505-31-42 ..... p 71 N83-12182
p 127 N83-13392
p 29 N83-14127
p 127 N83-14431
p 128 N83-14435
p 31 N83-15307
p 134 N83-15602
p 100 N83-17728
p 100 N83-19920
p 100 N83-19921
p 34 N83-20947
p 34 N83-20948
p 101 N83-23465
p 35 N83-24506
p 14 N83-27958
p 101 N83-28255
p 183 N83-28580
p 183 N83-28581
p 183 N83-28582
p 39 N83-29237
p 86 N83-29359
p 132 N83-34232
p 41 N83-34941
p 42 N83-34943
p 102 N83-35160
505-31-54 ..... p 134 N83-21314
p 19 N83-33883
505-31 ..... p 190 N83-21847
505-32-02 ..... p 196 N83-10885
p 197 N83-12968
p 199 N83-20708
p 200 N83-21897
p 129 N83-22546
p 202 N83-33683
505-32-1B ..... p 144 N83-20118
p 150 N83-28453
505-32-12 ..... p 125 N83-10389
p 10 N83-11066
p 12 N83-18671
p 33 N83-18729
505-32-2A ..... p 9 N83-11058
p 28 N83-12093
p 10 N83-14066
505-32-2B ..... p 26 N83-10045
p 26 N83-11125
p 126 N83-12360
505-32-32 ..... p 98 N83-10207
p 99 N83-10208
p 33 N83-18725
p 100 N83-18924
p 207 N83-20808
p 35 N83-23309
p 40 N83-32806
p 41 N83-33893
p 42 N83-34948
505-32-33 ..... p 14 N83-29174
505-32-4A ..... p 28 N83-12090
505-32-40 ..... p 92 N83-14271
505-32-42 ..... p 139 N83-10425
p 26 N83-11126
p 140 N83-12432
p 140 N83-12433
p 91 N83-13257
p 140 N83-13458
p 91 N83-14269
p 92 N83-15466
p 142 N83-15629
p 93 N83-16528
p 142 N83-16758
p 143 N83-16759
p 82 N83-17682
p 128 N83-17833
p 72 N83-18863
p 129 N83-19016
p 144 N83-20116
p 147 N83-20159
p 94 N83-24695
p 36 N83-25712
p 95 N83-27021
p 149 N83-27214
p 96 N83-28243
p 149 N83-28449
p 150 N83-29710
p 150 N83-29711
p 151 N83-29712
p 151 N83-29713
p 97 N83-32943
p 151 N83-33166
p 97 N83-34049
p 152 N83-34325
p 98 N83-35143
505-32-4 ..... p 81 N83-14245
505-32-52 ..... p 126 N83-12357
p 10 N83-13077
p 66 N83-19817
p 12 N83-24474
p 130 N83-24798
p 15 N83-32774
505-32-6A ..... p 29 N83-14126
p 159 N83-14523
p 30 N83-15306
p 42 N83-34945
505-32-6B ..... p 27 N83-11128
p 32 N83-17537
p 189 N83-19496
505-32-72 ..... p 99 N83-11340
p 208 N83-23188
p 208 N83-23189
505-32-82 ..... p 26 N83-10044
p 187 N83-13643
p 203 N83-13979
p 47 N83-18835
p 36 N83-24509
p 135 N83-33126
505-33-1A ..... p 70 N83-12181
p 83 N83-19887
p 83 N83-22387
p 61 N83-25786
p 86 N83-29358
p 87 N83-34016
p 88 N83-35104
505-33-1B ..... p 160 N83-24875
p 87 N83-34015
p 152 N83-34326
p 98 N83-35144
505-33-113 ..... p 92 N83-15468
p 94 N83-22423
505-33-12 ..... p 78 N83-11282
p 80 N83-11309
p 192 N83-21872
p 73 N83-24575
p 95 N83-27019
505-33-22 ..... p 158 N83-12449
p 158 N83-12451
p 159 N83-19121
p 94 N83-19902
p 153 N83-21373
p 160 N83-27256
p 85 N83-28208
p 161 N83-29734
p 161 N83-34349
p 163 N83-34372
p 87 N83-35103
505-33-32 ..... p 63 N83-10118
p 64 N83-12175
p 65 N83-15363
p 65 N83-15364
p 65 N83-15365
p 160 N83-24874
p 66 N83-25790
505-33-33-06 ..... p 163 N83-34373
505-33-42 ..... p 159 N83-15672
505-33-52 ..... p 65 N83-15362
p 129 N83-17834
p 129 N83-20029
p 129 N83-22542
p 35 N83-23306
p 130 N83-24799
p 131 N83-28380
p 160 N83-28493
p 132 N83-33103
505-33-72 ..... p 161 N83-29731
505-34-02 ..... p 2 N83-34885
505-36-12 ..... p 127 N83-13387
p 130 N83-23544
505-36-22 ..... p 161 N83-33219
505-40-02 ..... p 32 N83-17538
p 34 N83-22200

PAGE D-3 INTENTIONALLY BLANK

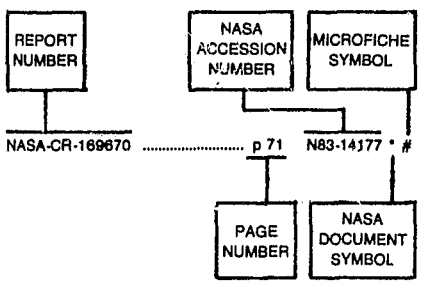
PRECEDING PAGE BLANK NOT FILMED

D-2 + D-3

	p 36	N83-26838
	p 37	N83-27991
505-40-22	p 127	N83-14432
	p 130	N83-23545
	p 188	N83-24048
	p 37	N83-27995
	p 39	N83-29236
	p 39	N83-30431
505-40-32	p 1	N83-14061
	p 2	N83-22092
	p 14	N83-29178
505-40-42	p 143	N83-19092
	p 143	N83-20115
	p 148	N83-24858
	p 151	N83-33167
505-40-5A	p 144	N83-20117
	p 134	N83-24829
505-40-5B	p 18	N83-15302
	p 36	N83-25711
	p 117	N83-29597
505-40-6A	p 189	N83-28921
505-40-6B	p 32	N83-17545
	p 38	N83-29235
505-40-6C	p 41	N83-34942
505-40-62C	p 41	N83-32810
	p 42	N83-34946
505-40-62	p 100	N83-22442
505-40-82	p 42	N83-34947
505-41-32	p 126	N83-12358
505-42-42	p 150	N83-28455
505-43-02	p 9	N83-10019
	p 12	N83-17509
	p 12	N83-25657
	p 13	N83-27957
505-43-22	p 36	N83-26839
505-43-92	p 27	N83-12087
505-44-12	p 18	N83-14123
	p 11	N83-15265
505-45-01A	p 17	N83-32782
505-45-02	p 16	N83-14078
	p 17	N83-24487
	p 202	N83-30168
505-45-12	p 19	N83-18720
505-45-23-01	p 161	N83-33217
505-53-1B	p 84	N83-24634
505-55-52	p 73	N83-24571
	p 186	N83-35498
506-13-1B	p 152	N83-34327
506-23-52	p 113	N83-11446
506-31-32	p 201	N83-25499
506-33-12	p 139	N83-11496
506-52-42	p 100	N83-16545
	p 57	N83-21002
	p 58	N83-26923
506-52-62	p 153	N83-11506
	p 153	N83-16773
506-53-1A	p 153	N83-23620
506-53-1B	p 77	N83-10171
	p 140	N83-11498
	p 89	N83-13273
	p 92	N83-14270
	p 82	N83-19886
	p 93	N83-19901
	p 83	N83-23417
	p 84	N83-24636
	p 84	N83-24637
	p 148	N83-24855
	p 148	N83-24855
	p 85	N83-25853
	p 94	N83-25883
	p 96	N83-30660
	p 86	N83-32908
	p 87	N83-34019
	p 152	N83-35400
506-53-113	p 81	N83-13231
506-53-12B	p 83	N83-21110
	p 85	N83-24640
506-53-12	p 90	N83-10194
	p 91	N83-11328
	p 91	N83-11329
	p 140	N83-13457
	p 82	N83-15413
	p 92	N83-16527
	p 83	N83-22390
	p 85	N83-24641
	p 148	N83-26079
506-53-13	p 148	N83-23606
	p 84	N83-24635
	p 62	N83-29311
506-54-22	p 113	N83-11447
506-55-22	p 56	N83-12141
	p 56	N83-12142
	p 56	N83-13164
	p 57	N83-17587
	p 72	N83-21056
	p 59	N83-32842
	p 60	N83-35053
	p 163	N83-35412
506-55-32	p 56	N83-12143
506-55-42	p 166	N83-10554
	p 166	N83-10555
	p 206	N83-10962
	p 171	N83-15806
	p 59	N83-28071
506-55-52	p 70	N83-10134
	p 70	N83-10135
	p 167	N83-10558
	p 71	N83-15372
	p 174	N83-18022
	p 72	N83-18862
	p 180	N83-25038
	p 181	N83-26253
	p 118	N83-36359
506-55-62	p 59	N83-30516
506-55-72	p 61	N83-13169
	p 58	N83-24552
	p 50	N83-35005
506-58-22	p 105	N83-10322
	p 48	N83-22315
506-60-42	p 58	N83-26922
	p 59	N83-26924
506-61-42	p 114	N83-14399
	p 116	N83-25985
530-05-12	p 27	N83-11129
532-06-12	p 28	N83-12091
	p 28	N83-12092
	p 37	N83-27996
	p 149	N83-28448
533-04-1A	p 15	N83-30392
	p 15	N83-30393
533-04-1B	p 85	N83-24638
	p 97	N83-34048
	p 87	N83-35102
	p 97	N83-35142
534-02-22	p 37	N83-27994
534-03-13	p 93	N83-18909
535-02-12	p 158	N83-11514
535-03-12	p 196	N83-11840
	p 12	N83-19710
	p 199	N83-21895
	p 200	N83-23112
	p 2	N83-34886
535-04-12	p 32	N83-17543
	p 32	N83-17544
535-05-12	p 40	N83-32807
	p 41	N83-32811
542-05-12	p 58	N83-22318
56-5212	p 102	N83-35159
605-60-26	p 108	N83-34113
643-10-01	p 107	N83-29493
643-10-02	p 45	N83-22255
	p 106	N83-23497
	p 107	N83-23498
650-20-16	p 109	N83-34120
650-6-20	p 50	N83-13154
650-60-26	p 47	N83-11210
	p 108	N83-31925
	p 108	N83-31926
	p 108	N83-34114
	p 108	N83-34115
	p 109	N83-34116
	p 109	N83-34117
	p 109	N83-34118
	p 48	N83-35004
776-16-02	p 180	N83-25036
776-31-41	p 117	N83-34192
776-33-41	p 169	N83-14689
	p 169	N83-14690
	p 174	N83-16857
	p 177	N83-21508
	p 178	N83-22747
	p 179	N83-23704
	p 179	N83-23710
	p 184	N83-31107
	p 185	N83-34451
776-36-06	p 178	N83-22749
776-52-41	p 114	N83-14397
	p 173	N83-15840
	p 160	N83-23631
	p 179	N83-23709
776-54-01	p 180	N83-25041
776-72-41	p 169	N83-14683
	p 176	N83-20359
	p 179	N83-23708
	p 180	N83-25042
	p 181	N83-26252
	p 73	N83-29326
	p 183	N83-29810
	p 74	N83-32870
	p 74	N83-32871
778-11-05	p 168	N83-13589
	p 141	N83-14494
	p 175	N83-19229
	p 61	N83-19812
778-11-06	p 168	N83-13583
	p 176	N83-20361
	p 185	N83-34453
778-14-10	p 166	N83-10557
	p 167	N83-10559
	p 167	N83-10560
	p 180	N83-25037
	p 186	N83-36549
778-16-12	p 182	N83-27346
778-18-12	p 169	N83-14691
778-32-01	p 140	N83-12431
	p 210	N83-19651
	p 181	N83-26251
	p 211	N83-26757
	p 211	N83-26758
	p 211	N83-26759
778-34-22	p 210	N83-24431
778-35-03	p 209	N83-10991
	p 126	N83-12359
	p 81	N83-13232
	p 210	N83-17423
	p 181	N83-25043
778-36-06	p 113	N83-10349
	p 114	N83-13359
	p 209	N83-16257
	p 211	N83-24432
	p 116	N83-25982
	p 184	N83-29811
	p 117	N83-30915
	p 186	N83-35496
778-38-12	p 99	N83-12250
778-45-12	p 170	N83-15805
778-46-22	p 167	N83-10568
	p 177	N83-22739
	p 211	N83-25625
779-34-12	p 148	N83-24857
917-60-00	p 45	N83-29292

REPORT NUMBER INDEX

Typical Report Number Index Listing



Listings in this index are arranged alphanumerically by report number. The page number indicates the page on which the citation is located. The accession number denotes the number by which the citation is identified. An asterisk (*) indicates that the item is a NASA report. A pound sign (#) indicates that the item is available on microfiche.

AAS PAPER 83-197 ..... p 45 A83-43773 * #

ACC-80-17602 ..... p 80 N83-12214 * #

ACS PAPER 33-B-80P ..... p 88 A83-18052 * #

ACUREX-TR-82-02/AD ..... p 47 N83-18835 * #

AD-A119357 ..... p 27 N83-11138 #
AD-A130069 ..... p 36 N83-26837 * #
AD-A130463 ..... p 38 N83-29234 * #

AESD-TME-3051 ..... p 174 N83-16859 * #

AGARD-AR-173 ..... p 27 N83-11138 #

AHS-RWP-16 ..... p 139 N83-10425 * #
AHS-RWP-19 ..... p 27 N83-11130 * #
AHS-RWP-7 ..... p 27 N83-11128 * #

AIAA PAPER 82-0776 ..... p 154 A83-10900 * #
AIAA PAPER 82-1867 ..... p 53 A83-16925 * #
AIAA PAPER 82-1872 ..... p 48 A83-12460 * #
AIAA PAPER 82-1880 ..... p 53 A83-21099 * #
AIAA PAPER 82-1881 ..... p 51 A83-12466 * #
AIAA PAPER 82-1898 ..... p 48 A83-12475 * #
AIAA PAPER 82-1903 ..... p 44 A83-12478 * #
AIAA PAPER 82-1904 ..... p 51 A83-12479 * #
AIAA PAPER 82-1908 ..... p 51 A83-12483 * #
AIAA PAPER 82-1910 ..... p 51 A83-12484 * #
AIAA PAPER 82-1912 ..... p 51 A83-12485 * #
AIAA PAPER 82-1913 ..... p 53 A83-21078 * #
AIAA PAPER 82-1925 ..... p 51 A83-12494 * #
AIAA PAPER 82-1926 ..... p 52 A83-12495 * #
AIAA PAPER 82-1927 ..... p 52 A83-12496 * #
AIAA PAPER 82-1928 ..... p 53 A83-21100 * #
AIAA PAPER 82-1929 ..... p 54 A83-26625 * #
AIAA PAPER 82-1930 ..... p 203 A83-14398 * #
AIAA PAPER 82-1935 ..... p 55 A83-27350 * #
AIAA PAPER 82-1937 ..... p 53 A83-21900 * #
AIAA PAPER 82-1938 ..... p 53 A83-22075 * #
AIAA PAPER 82-1939 ..... p 52 A83-12501 * #
AIAA PAPER 82-1949 ..... p 52 A83-12506 * #
AIAA PAPER 82-1951 ..... p 52 A83-12508 * #
AIAA PAPER 82-1954 ..... p 52 A83-12511 * #
AIAA PAPER 82-1955 ..... p 53 A83-12512 * #
AIAA PAPER 83-0003 ..... p 2 A83-16455 * #
AIAA PAPER 83-0004 ..... p 19 A83-13456 * #
AIAA PAPER 83-0026 ..... p 16 A83-42099 * #
AIAA PAPER 83-0066 ..... p 119 A83-16498 * #
AIAA PAPER 83-0109 ..... p 3 A83-16525 * #
AIAA PAPER 83-0110 ..... p 187 A83-16526 * #
AIAA PAPER 83-0112 ..... p 16 A83-36042 * #
AIAA PAPER 83-0135 ..... p 3 A83-19581 * #
AIAA PAPER 83-0136 ..... p 3 A83-16823 * #

AIAA PAPER 83-0151 ..... p 119 A83-16558 * #
AIAA PAPER 83-0154 ..... p 20 A83-21079 * #
AIAA PAPER 83-0170 ..... p 6 A83-42100 * #
AIAA PAPER 83-0178 ..... p 19 A83-16572 * #
AIAA PAPER 83-0188 ..... p 4 A83-29535 * #
AIAA PAPER 83-0189 ..... p 3 A83-21080 * #
AIAA PAPER 83-0204 ..... p 1 A83-16582 * #
AIAA PAPER 83-0240 ..... p 68 A83-16606 * #
AIAA PAPER 83-0256 ..... p 3 A83-16614 * #
AIAA PAPER 83-0315 ..... p 119 A83-16645 * #
AIAA PAPER 83-0316 ..... p 119 A83-16646 * #
AIAA PAPER 83-0337 ..... p 20 A83-16663 * #
AIAA PAPER 83-0395 ..... p 203 A83-16691 * #
AIAA PAPER 83-0468 ..... p 203 A83-16735 * #
AIAA PAPER 83-0470 ..... p 119 A83-16737 * #
AIAA PAPER 83-0497 ..... p 136 A83-16749 * #
AIAA PAPER 83-0534 ..... p 18 A83-16772 * #
AIAA PAPER 83-0537 ..... p 20 A83-19593 * #
AIAA PAPER 83-0541 ..... p 20 A83-16776 * #
AIAA PAPER 83-0557 ..... p 120 A83-16786 * #
AIAA PAPER 83-0559 ..... p 120 A83-16787 * #
AIAA PAPER 83-0600 ..... p 69 A83-36062 * #
AIAA PAPER 83-0667 ..... p 193 A83-25904 * #
AIAA PAPER 83-0670 ..... p 194 A83-26917 * #
AIAA PAPER 83-0671 ..... p 193 A83-25907 * #
AIAA PAPER 83-0681 ..... p 21 A83-28006 * #
AIAA PAPER 83-0703 ..... p 193 A83-25923 * #
AIAA PAPER 83-0707 ..... p 194 A83-28011 * #
AIAA PAPER 83-0708 ..... p 193 A83-25924 * #
AIAA PAPER 83-0710 ..... p 193 A83-25926 * #
AIAA PAPER 83-0714 ..... p 194 A83-25929 * #
AIAA PAPER 83-0730 ..... p 195 A83-33485 * #
AIAA PAPER 83-0734 ..... p 194 A83-28016 * #
AIAA PAPER 83-0745 ..... p 21 A83-25947 * #
AIAA PAPER 83-0749 ..... p 194 A83-26450 * #
AIAA PAPER 83-0759 ..... p 194 A83-28021 * #
AIAA PAPER 83-0760 ..... p 196 A83-33486 * #
AIAA PAPER 83-0762 ..... p 196 A83-33487 * #
AIAA PAPER 83-0765 ..... p 195 A83-28022 * #
AIAA PAPER 83-0767 ..... p 21 A83-25957 * #
AIAA PAPER 83-0768 ..... p 195 A83-28023 * #
AIAA PAPER 83-0778 ..... p 195 A83-28024 * #
AIAA PAPER 83-0848 ..... p 22 A83-32791 * #
AIAA PAPER 83-0911 ..... p 49 A83-32782 * #
AIAA PAPER 83-0919 ..... p 22 A83-32787 * #
AIAA PAPER 83-1134 ..... p 137 A83-36239 * #
AIAA PAPER 83-1155 ..... p 23 A83-36250 * #
AIAA PAPER 83-1160 ..... p 23 A83-36252 * #
AIAA PAPER 83-1162 ..... p 6 A83-45508 * #
AIAA PAPER 83-1166 ..... p 6 A83-45509 * #
AIAA PAPER 83-1175 ..... p 6 A83-45510 * #
AIAA PAPER 83-1178 ..... p 23 A83-36263 * #
AIAA PAPER 83-1200 ..... p 122 A83-36276 * #
AIAA PAPER 83-1201 ..... p 122 A83-36277 * #
AIAA PAPER 83-1202 ..... p 122 A83-36278 * #
AIAA PAPER 83-1204 ..... p 124 A83-45511 * #
AIAA PAPER 83-1207 ..... p 55 A83-36281 * #
AIAA PAPER 83-1217 ..... p 56 A83-45512 * #
AIAA PAPER 83-1243 ..... p 56 A83-45513 * #
AIAA PAPER 83-1248 ..... p 49 A83-36306 * #
AIAA PAPER 83-1263 ..... p 23 A83-36314 * #
AIAA PAPER 83-1264 ..... p 69 A83-36315 * #
AIAA PAPER 83-1265 ..... p 23 A83-36316 * #
AIAA PAPER 83-1287 ..... p 23 A83-36323 * #
AIAA PAPER 83-1312 ..... p 55 A83-36333 * #
AIAA PAPER 83-1326 ..... p 24 A83-36340 * #
AIAA PAPER 83-1351 ..... p 43 A83-36353 * #
AIAA PAPER 83-1380 ..... p 55 A83-36371 * #
AIAA PAPER 83-1389 ..... p 138 A83-36379 * #
AIAA PAPER 83-1394 ..... p 55 A83-36384 * #
AIAA PAPER 83-1401 ..... p 4 A83-36391 * #
AIAA PAPER 83-1403 ..... p 24 A83-36393 * #
AIAA PAPER 83-1412 ..... p 25 A83-45515 * #
AIAA PAPER 83-1414 ..... p 7 A83-45516 * #
AIAA PAPER 83-1415 ..... p 196 A83-45517 * #
AIAA PAPER 83-1422 ..... p 121 A83-32701 * #
AIAA PAPER 83-1739 ..... p 4 A83-37218 * #
AIAA PAPER 83-1820 ..... p 5 A83-38652 * #
AIAA PAPER 83-1892 ..... p 5 A83-39358 * #
AIAA PAPER 83-1893 ..... p 5 A83-39359 * #
AIAA PAPER 83-1909 ..... p 122 A83-39367 * #
AIAA PAPER 83-1940 ..... p 123 A83-39389 * #
AIAA PAPER 83-1945 ..... p 5 A83-39392 * #

AIAA PAPER 83-2445 ..... p 25 A83-46331 * #
AIAA PAPER 83-2466 ..... p 26 A83-49581 * #

AIAA 83-0801 ..... p 89 A83-29734 * #
AIAA 83-0806 ..... p 62 A83-29886 * #
AIAA 83-0828 ..... p 22 A83-29737 * #
AIAA 83-0844 ..... p 156 A83-29822 * #
AIAA 83-0845 ..... p 156 A83-29823 * #
AIAA 83-0846 ..... p 157 A83-29824 * #
AIAA 83-1003 ..... p 49 A83-29791 * #
AIAA 83-1016 ..... p 156 A83-29798 * #

AIAA-PAPER-82-1929 ..... p 57 N83-17587 * #

AIAA-82-1880 ..... p 56 N83-12141 * #
AIAA-82-1913 ..... p 57 N83-14157 * #
AIAA-82-1938 ..... p 56 N83-12143 * #
AIAA-83-0026 ..... p 17 N83-24467 * #
AIAA-83-0135 ..... p 34 N83-22200 * #
AIAA-83-0136 ..... p 34 N83-22199 * #
AIAA-83-0154 ..... p 29 N83-13101 * #
AIAA-83-0188 ..... p 12 N83-19710 * #
AIAA-83-0189 ..... p 1 N83-14061 * #
AIAA-83-0204 ..... p 16 N83-14078 * #
AIAA-83-0337 ..... p 33 N83-18725 * #
AIAA-83-0680 ..... p 201 N83-26643 * #
AIAA-83-0730 ..... p 201 N83-23117 * #
AIAA-83-0749 ..... p 200 N83-23115 * #
AIAA-83-0759 ..... p 200 N83-23114 * #
AIAA-83-0760 ..... p 200 N83-21896 * #
AIAA-83-0762 ..... p 200 N83-23116 * #
AIAA-83-1175 ..... p 14 N83-27958 * #
AIAA-83-1179 ..... p 35 N83-24505 * #
AIAA-83-1200 ..... p 15 N83-30392 * #
AIAA-83-1201 ..... p 15 N83-30393 * #
AIAA-83-1217 ..... p 58 N83-26922 * #
AIAA-83-1340 ..... p 38 N83-29235 * #
AIAA-83-1389 ..... p 58 N83-26923 * #
AIAA-83-9745 ..... p 199 N83-21895 * #

AIRESEARCH-82-19211 ..... p 212 N83-32687 * #

AMC-31-3480(11) ..... p 27 N83-12088 * #
AMC-81-18266 ..... p 113 N83-10348 * #

AR-18 ..... p 182 N83-27351 * #
AR-19 ..... p 182 N83-27352 * #

ARL-TR-82-54 ..... p 197 N83-12967 * #

ASLE PREPRINT 82-LC-UB-1 ..... p 74 A83-13226 * #
ASLE PREPRINT 82-LC-3A-1 ..... p 136 A83-13230 * #
ASLE PREPRINT 82-LC-3B-3 ..... p 136 A83-13237 * #
ASLE PREPRINT 82-LC-3C-3 ..... p 135 A83-13229 * #
ASLE PREPRINT 82-LC-4C-1 ..... p 135 A83-13228 * #
ASLE PREPRINT 83-AM-4B-2 ..... p 138 A83-43339 * #

ASME PAPER 82-HT-42 ..... p 118 A83-12795 * #
ASME PAPER 82-JPGC-GT-10 ..... p 68 A83-25268 * #
ASME PAPER 82-JPGC-GT-11 ..... p 68 A83-25269 * #
ASME PAPER 82-JPGC-GT-21 ..... p 137 A83-25270 * #
ASME PAPER 82-JPGC-GT-23 ..... p 164 A83-25271 * #
ASME PAPER 82-LUB-18 ..... p 136 A83-13509 * #
ASME PAPER 82-LUB-18 ..... p 136 A83-39944 * #
ASME PAPER 82-LUB-35 ..... p 136 A83-13516 * #
ASME PAPER 82-LUB-42 ..... p 136 A83-13521 * #
ASME PAPER 82-WA/HT-39 ..... p 16 A83-25693 * #
ASME PAPER 83-APM-19 ..... p 157 A83-37388 * #
ASME PAPER 83-FE-22 ..... p 125 A83-48678 * #
ASME PAPER 83-GT-128 ..... p 8 A83-47957 * #
ASME PAPER 83-GT-137 ..... p 25 A83-47964 * #
ASME PAPER 83-GT-151 ..... p 25 A83-47970 * #
ASME PAPER 83-GT-152 ..... p 158 A83-47978 * #
ASME PAPER 83-GT-171 ..... p 8 A83-47972 * #
ASME PAPER 83-GT-196 ..... p 25 A83-48000 * #
ASME PAPER 83-GT-211 ..... p 9 A83-48012 * #
ASME PAPER 83-GT-213 ..... p 9 A83-48014 * #
ASME PAPER 83-GT-225 ..... p 138 A83-48023 * #
ASME PAPER 83-GT-228 ..... p 139 A83-48025 * #
ASME PAPER 83-GT-238 ..... p 139 A83-48030 * #
ASME PAPER 83-GT-28 ..... p 7 A83-47891 * #
ASME PAPER 83-GT-39 ..... p 125 A83-47899 * #
ASME PAPER 83-GT-41 ..... p 7 A83-47901 * #

ASME PAPER 83-GT-44 ..... p 7 A83-47904 * #
ASME PAPER 83-GT-45 ..... p 8 A83-47905 * #
ASME PAPER 83-GT-46 ..... p 8 A83-47906 * #
ASME PAPER 83-GT-53 ..... p 8 A83-47910 * #
ASME PAPER 83-GT-66 ..... p 24 A83-39993 * #
ASME PAPER 83-GT-80 ..... p 125 A83-47933 * #
ASME PAPER 83-GT-95 ..... p 8 A83-47941 * #

AVRADCOM-TR-81-C-27 ..... p 30 N83-15306 * #
AVRADCOM-TR-81-C-5 ..... p 9 N83-11058 * #
AVRADCOM-TR-82-C-14 ..... p 27 N83-11128 * #
AVRADCOM-TR-82-C-15 ..... p 139 N83-10425 * #
AVRADCOM-TR-82-C-16 ..... p 144 N83-20119 * #
AVRADCOM-TR-82-C-17 ..... p 134 N83-15602 * #
AVRADCOM-TR-82-C-1 ..... p 9 N83-11063 * #
AVRADCOM-TR-82-C-4 ..... p 26 N83-11125 * #
AVRADCOM-TR-83-C-1 ..... p 34 N83-20947 * #
AVRADCOM-TR-83-C-2 ..... p 35 N83-24505 * #
AVRADCOM-TR-83-C-3 ..... p 148 N83-24858 * #
AVRADCOM-TR-83-C-4 ..... p 40 N83-32807 * #
AVRADCOM-TR-83-C-5 ..... p 150 N83-28455 * #
AVRADCOM-TR-83-C-7 ..... p 42 N83-34943 * #

BAC-ER-15049 ..... p 46 N83-25766 * #

BATT-92880 ..... p 18 N83-14123 * #

BBN-4712 ..... p 139 N83-11495 * #

BEERS-1-82-16-23 ..... p 206 N83-16234 * #

CAES-590-81 ..... p 99 N83-12250 * #
CAES-600-81 ..... p 99 N83-13272 * #

CER-81-82-WZS-DBS51 ..... p 127 N83-13387 * #

CML-82-4 ..... p 64 N83-13173 * #
CML-82-5 ..... p 66 N83-22325 * #

CONF-810752 ..... p 175 N83-19231 * #

CW-WR-81-022F ..... p 32 N83-17545 * #

DDA-EDR-10327 ..... p 140 N83-12431 * #
DDA-EDR-10672 ..... p 212 N83-37028 * #
DDA-EDR-10885 ..... p 210 N83-20829 * #
DDA-EDR-10977 ..... p 142 N83-15627 * #
DDA-EDR-10978 ..... p 37 N83-27996 * #
DDA-EDR-11170 ..... p 149 N83-28448 * #

DE83-900154 ..... p 95 N83-27022 * #

DFVLR-FB-82-23 ..... p 106 N83-21218 * #

DOE/NASA-0032-15 ..... p 209 N83-15176 * #
DOE/NASA-0032-15 ..... p 209 N83-15177 * #

DOE/NASA/DEN-175-1-VOL-1 .... p 178 N83-22750 * #
DOE/NASA/DEN-175-1-VOL-2 .... p 178 N83-22751 * #
DOE/NASA/DEN-175-1-VOL-3 .... p 178 N83-22754 * #
DOE/NASA/DEN-175-1-VOL-4 .... p 179 N83-22755 * #

DOE/NASA/0002-1 ..... p 184 N83-29812 * #
DOE/NASA/0002-2 ..... p 185 N83-33343 * #
DOE/NASA/0006-1 ..... p 80 N83-12215 * #
DOE/NASA/0006-2 ..... p 87 N83-35101 * #
DOE/NASA/0011-1 ..... p 148 N83-24857 * #
DOE/NASA/0017-3 ..... p 212 N83-37028 * #
DOE/NASA/0019-83/1 ..... p 96 N83-30662 * #
DOE/NASA/0032-17-VOL-2 ..... p 209 N83-10991 * #
DOE/NASA/0032-81/11 ..... p 211 N83-26762 * #
DOE/NASA/0051-3 ..... p 182 N83-26259 * #
DOE/NASA/0059-82/1 ..... p 113 N83-10349 * #
DOE/NASA/0060-82/1 ..... p 209 N83-16257 * #
DOE/NASA/0075-82/1 ..... p 117 N83-30914 * #
DOE/NASA/0076-82/1 ..... p 115 N83-16628 * #
DOE/NASA/0077-81/1 ..... p 212 N83-32687 * #
DOE/NASA/0091-1 ..... p 99 N83-13272 * #
DOE/NASA/0091-2 ..... p 99 N83-12250 * #
DOE/NASA/0093-1 ..... p 211 N83-24432 * #
DOE/NASA/0100-1 ..... p 141 N83-14494 * #
DOE/NASA/0101-1 ..... p 179 N83-23704 * #
DOE/NASA/0129-1 ..... p 174 N83-19226 * #
DOE/NASA/0131-1 ..... p 168 N83-11579 * #
DOE/NASA/0136-1 ..... p 178 N83-22748 * #
DOE/NASA/0142-83/1 ..... p 212 N83-27926 * #
DOE/NASA/0161-9A ..... p 168 N83-12524 * #
DOE/NASA/0163-1 ..... p 174 N83-16859 * #
DOE/NASA/0167-81/2 ..... p 209 N83-13038 * #
DOE/NASA/0167-81/3 ..... p 212 N83-33800 * #
DOE/NASA/0167-82/4 ..... p 210 N83-17424 * #
DOE/NASA/0168-80/1 ..... p 140 N83-12431 * #
DOE/NASA/0168-82/4 ..... p 142 N83-15627 * #
DOE/NASA/0180-6 ..... p 168 N83-13585 * #
DOE/NASA/0182-1 ..... p 177 N83-22746 * #
DOE/NASA/0187-82/1 ..... p 210 N83-20829 * #

DOE/NASA/0198-1 ..... p 179 N83-23708 * #
DOE/NASA/0202-1 ..... p 175 N83-19228 * #
DOE/NASA/0207-1 ..... p 165 N83-33320 * #
DOE/NASA/0212-1 ..... p 167 N83-10561 * #
DOE/NASA/0219-1 ..... p 208 N83-30297 * #
DOE/NASA/0235-2-VOL-1 ..... p 211 N83-26757 * #
DOE/NASA/0235-2-VOL-2 ..... p 211 N83-26758 * #
DOE/NASA/0235-2-VOL-3 ..... p 211 N83-26759 * #
DOE/NASA/0241-6 ..... p 182 N83-27345 * #
DOE/NASA/0251-1 ..... p 176 N83-20359 * #
DOE/NASA/0252-1 ..... p 185 N83-34451 * #
DOE/NASA/0254-1 ..... p 210 N83-22029 * #
DOE/NASA/0287-1 ..... p 86 N83-29359 * #
DOE/NASA/0292-1 ..... p 183 N83-28580 * #
DOE/NASA/0292-1 ..... p 183 N83-28581 * #
DOE/NASA/0292-1 ..... p 183 N83-28582 * #
DOE/NASA/0292-1 ..... p 183 N83-28583 * #
DOE/NASA/1005-1 ..... p 182 N83-27346 * #
DOE/NASA/1011-36 ..... p 9 N83-11063 * #
DOE/NASA/10350-30 ..... p 99 N83-10208 * #
DOE/NASA/10350-35 ..... p 176 N83-20361 * #
DOE/NASA/10769-28 ..... p 168 N83-13589 * #
DOE/NASA/12726-18 ..... p 169 N83-14663 * #
DOE/NASA/12726-19 ..... p 181 N83-26252 * #
DOE/NASA/12726-20 ..... p 73 N83-29326 * #
DOE/NASA/12726-21 ..... p 180 N83-25042 * #
DOE/NASA/12726-22 ..... p 183 N83-29810 * #
DOE/NASA/13111-10 ..... p 167 N83-10559 * #
DOE/NASA/13111-11 ..... p 166 N83-10557 * #
DOE/NASA/13111-12 ..... p 166 N83-10556 * #
DOE/NASA/13111-13 ..... p 167 N83-10560 * #
DOE/NASA/13111-15 ..... p 185 N83-34453 * #
DOE/NASA/1981-1 ..... p 117 N83-30915 * #
DOE/NASA/20320-35 ..... p 169 N83-14688 * #
DOE/NASA/20320-40 ..... p 169 N83-14689 * #
DOE/NASA/20320-42 ..... p 169 N83-14690 * #
DOE/NASA/20320-43 ..... p 174 N83-16857 * #
DOE/NASA/20320-45 ..... p 182 N83-27347 * #
DOE/NASA/20320-46 ..... p 184 N83-29813 * #
DOE/NASA/20320-47 ..... p 184 N83-31107 * #
DOE/NASA/20320-48 ..... p 117 N83-34192 * #
DOE/NASA/20485-12 ..... p 114 N83-14397 * #
DOE/NASA/20485-13 ..... p 173 N83-15840 * #
DOE/NASA/20485-14 ..... p 179 N83-23709 * #
DOE/NASA/20485-15 ..... p 180 N83-25041 * #
DOE/NASA/20485-2 ..... p 160 N83-23631 * #
DOE/NASA/2818-1 ..... p 168 N83-13588 * #
DOE/NASA/3163-1 ..... p 114 N83-13359 * #
DOE/NASA/3194-1 ..... p 212 N83-30328 * #
DOE/NASA/3249-1 ..... p 61 N83-19812 * #
DOE/NASA/3303-1 ..... p 177 N83-22740 * #
DOE/NASA/3303-2 ..... p 177 N83-21508 * #
DOE/NASA/3303-3 ..... p 177 N83-21509 * #
DOE/NASA/3303-4 ..... p 178 N83-22747 * #
DOE/NASA/50194-37 ..... p 210 N83-24431 * #
DOE/NASA/51040-37 ..... p 126 N83-12359 * #
DOE/NASA/51040-41 ..... p 61 N83-13232 * #
DOE/NASA/51040-42 ..... p 210 N83-17423 * #
DOE/NASA/51040-42 ..... p 210 N83-19651 * #
DOE/NASA/51040-45 ..... p 181 N83-26251 * #
DOE/NASA/51040-46 ..... p 35 N83-24505 * #
DOE/NASA/51040-48 ..... p 212 N83-27924 * #
DOE/NASA/51044-29 ..... p 178 N83-22749 * #
DOE/NASA/51044-30 ..... p 184 N83-29811 * #
DOE/NASA/51044-31 ..... p 116 N83-25982 * #
DOE/NASA/51044-32 ..... p 186 N83-35496 * #
DOE/NASA/52040-44 ..... p 130 N83-26017 * #

DT-8178-02 ..... p 127 N83-14434 * #

D180-27619-1 ..... p 66 N83-26928 * #
D210-11944-1 ..... p 18 N83-22188 * #

E-020 ..... p 208 N83-23188 * #
E-021 ..... p 208 N83-23189 * #
E-1007 ..... p 15 N83-32774 * #
E-1008-1 ..... p 117 N83-34192 * #
E-1036 ..... p 139 N83-11496 * #
E-1052 ..... p 99 N83-10208 * #
E-1060 ..... p 91 N83-14269 * #
E-1075 ..... p 93 N83-16528 * #
E-1087 ..... p 82 N83-15413 * #
E-1091 ..... p 140 N83-13457 * #
E-1103 ..... p 126 N83-12359 * #
E-1108 ..... p 169 N83-14688 * #
E-1122 ..... p 94 N83-24695 * #
E-1125 ..... p 158 N83-12449 * #
E-1127 ..... p 99 N83-11340 * #
E-1153 ..... p 203 N83-13979 * #
E-1166 ..... p 85 N83-24641 * #
E-1167 ..... p 187 N83-13643 * #
E-1169 ..... p 26 N83-11126 * #
E-1173 ..... p 135 N83-33126 * #
E-1179 ..... p 36 N83-24509 * #
E-1180 ..... p 26 N83-11125 * #
E-1184 ..... p 26 N83-10045 * #

E-1190 ..... p 142 N83-16758 * #
E-1206 ..... p 126 N83-12360 * #
E-1227 ..... p 85 N83-24640 * #
E-1239 ..... p 81 N83-14245 * #
E-1240 ..... p 169 N83-14689 * #
E-1243 ..... p 151 N83-33166 * #
E-1244 ..... p 72 N83-18863 * #
E-1251 ..... p 125 N83-10389 * #
E-1253 ..... p 35 N83-23306 * #
E-1253 ..... p 36 N83-25712 * #
E-1260 ..... p 100 N83-22442 * #
E-1261 ..... p 32 N83-17547 * #
E-1267 ..... p 140 N83-12433 * #
E-1268 ..... p 28 N83-12092 * #
E-1271 ..... p 70 N83-10134 * #
E-1275 ..... p 100 N83-16545 * #
E-1277 ..... p 143 N83-16759 * #
E-1278 ..... p 63 N83-21110 * #
E-1281 ..... p 207 N83-20808 * #
E-1287 ..... p 142 N83-15629 * #
E-1291 ..... p 32 N83-17537 * #
E-1300 ..... p 148 N83-24862 * #
E-1302 ..... p 28 N83-12090 * #
E-1303 ..... p 171 N83-15806 * #
E-1311 ..... p 73 N83-24575 * #
E-1315 ..... p 170 N83-15805 * #
E-1317 ..... p 92 N83-14271 * #
E-1330 ..... p 27 N83-12087 * #
E-1333 ..... p 150 N83-28453 * #
E-1334 ..... p 181 N83-26251 * #
E-1338 ..... p 9 N83-10019 * #
E-1339 ..... p 126 N83-12357 * #
E-1340 ..... p 169 N83-14683 * #
E-1348 ..... p 130 N83-26017 * #
E-1349 ..... p 84 N83-23419 * #
E-1353 ..... p 113 N83-11446 * #
E-1354 ..... p 166 N83-10554 * #
E-1357 ..... p 196 N83-11840 * #
E-1358 ..... p 35 N83-23309 * #
E-1359 ..... p 140 N83-11498 * #
E-1361 ..... p 64 N83-12175 * #
E-1362 ..... p 116 N83-25985 * #
E-1365 ..... p 50 N83-13154 * #
E-1368 ..... p 159 N83-14523 * #
E-1370 ..... p 143 N83-20115 * #
E-1371 ..... p 71 N83-12182 * #
E-1372 ..... p 167 N83-10558 * #
E-1375 ..... p 63 N83-10118 * #
E-1376 ..... p 91 N83-13257 * #
E-1376 ..... p 13 N83-27957 * #
E-1377 ..... p 210 N83-17423 * #
E-1378 ..... p 70 N83-10135 * #
E-1379 ..... p 91 N83-11329 * #
E-1380 ..... p 12 N83-17509 * #
E-1381 ..... p 86 N83-32908 * #
E-1382 ..... p 78 N83-11282 * #
E-1383 ..... p 30 N83-15306 * #
E-1384 ..... p 206 N83-10962 * #
E-1386 ..... p 166 N83-10555 * #
E-1387 ..... p 114 N83-14397 * #
E-1388 ..... p 84 N83-24634 * #
E-1389 ..... p 143 N83-19092 * #
E-1390 ..... p 143 N83-19093 * #
E-1391 ..... p 105 N83-10322 * #
E-1394 ..... p 153 N83-16773 * #
E-1395 ..... p 2 N83-17453 * #
E-1396 ..... p 150 N83-28454 * #
E-1397 ..... p 113 N83-11447 * #
E-1398 ..... p 92 N83-15466 * #
E-1399 ..... p 90 N83-10194 * #
E-1401 ..... p 160 N83-24875 * #
E-1402 ..... p 82 N83-17682 * #
E-1404 ..... p 158 N83-11514 * #
E-1405 ..... p 139 N83-10425 * #
E-1406 ..... p 57 N83-17587 * #
E-1407 ..... p 29 N83-14126 * #
E-1408 ..... p 27 N83-11128 * #
E-1409 ..... p 92 N83-14270 * #
E-1410 ..... p 61 N83-13169 * #
E-1411 ..... p 99 N83-13273 * #
E-1412 ..... p 71 N83-15372 * #
E-1413 ..... p 114 N83-14399 * #
E-1414 ..... p 27 N83-11129 * #
E-1415 ..... p 47 N83-11210 * #
E-1417 ..... p 166 N83-10557 * #
E-1418 ..... p 167 N83-10559 * #
E-1419 ..... p 166 N83-10556 * #
E-1420 ..... p 27 N83-11130 * #
E-1421 ..... p 211 N83-25625 * #
E-1422 ..... p 56 N83-13164 * #
E-1423 ..... p 169 N83-14690 * #
E-1424 ..... p 81 N83-13231 * #
E-1425 ..... p 129 N83-22546 * #
E-1427 ..... p 196 N83-10885 * #
E-1428 ..... p 192 N83-21872 * #
E-1429 ..... p 128 N83-17833 * #

E-1430 ..... p 210 N83-19651 * #
E-1432 ..... p 56 N83-12142 * #
E-1434 ..... p 167 N83-10560 * #
E-1435 ..... p 180 N83-25036 * #
E-1436 ..... p 84 N83-24636 * #
E-1437 ..... p 70 N83-12181 * #
E-1438 ..... p 197 N83-13939 * #
E-1439 ..... p 100 N83-19921 * #
E-1440 ..... p 149 N83-27214 * #
E-1441 ..... p 56 N83-12141 * #
E-1442 ..... p 127 N83-14431 * #
E-1443 ..... p 28 N83-12091 * #
E-1444 ..... p 18 N83-15302 * #
E-1445 ..... p 10 N83-13077 * #
E-1446 ..... p 126 N83-12358 * #
E-1447 ..... p 197 N83-12966 * #
E-1448 ..... p 29 N83-13101 * #
E-1449 ..... p 56 N83-12143 * #
E-1450 ..... p 128 N83-14435 * #
E-1451 ..... p 36 N83-26839 * #
E-1452 ..... p 127 N83-13392 * #
E-1453 ..... p 174 N83-18022 * #
E-1455 ..... p 176 N83-20361 * #
E-1456 ..... p 198 N83-16152 * #
E-1457 ..... p 152 N83-34325 * #
E-1459 ..... p 81 N83-14246 * #
E-1460 ..... p 129 N83-19016 * #
E-1461 ..... p 168 N83-13589 * #
E-1462 ..... p 29 N83-14127 * #
E-1463 ..... p 33 N83-18725 * #
E-1464 ..... p 57 N83-14157 * #
E-1465 ..... p 186 N83-36549 * #
E-1466 ..... p 127 N83-14432 * #
E-1467 ..... p 47 N83-20994 * #
E-1469 ..... p 16 N83-14078 * #
E-1470 ..... p 99 N83-15483 * #
E-1472 ..... p 198 N83-16153 * #
E-1473 ..... p 173 N83-15840 * #
E-1478 ..... p 144 N83-20118 * #
E-1479 ..... p 178 N83-22749 * #
E-1480 ..... p 130 N83-23544 * #
E-1481 ..... p 1 N83-14061 * #
E-1484 ..... p 190 N83-12930 * #
E-1486 ..... p 92 N83-15468 * #
E-1490 ..... p 31 N83-15307 * #
E-1491 ..... p 65 N83-15362 * #
E-1492 ..... p 11 N83-15268 * #
E-1493 ..... p 174 N83-16857 * #
E-1494 ..... p 65 N83-15364 * #
E-1497 ..... p 132 N83-34232 * #
E-1498 ..... p 134 N83-15602 * #
E-1500 ..... p 159 N83-15672 * #
E-1501 ..... p 97 N83-32943 * #
E-1502 ..... p 82 N83-19886 * #
E-1503 ..... p 93 N83-19901 * #
E-1504 ..... p 65 N83-15365 * #
E-1505 ..... p 65 N83-15363 * #
E-1506 ..... p 61 N83-25786 * #
E-1507 ..... p 144 N83-20116 * #
E-1508 ..... p 200 N83-23112 * #
E-1510 ..... p 198 N83-18405 * #
E-1516 ..... p 148 N83-23606 * #
E-1516 ..... p 152 N83-35400 * #
E-1518 ..... p 129 N83-20029 * #
E-1519 ..... p 129 N83-22542 * #
E-1520 ..... p 129 N83-17834 * #
E-1521 ..... p 34 N83-22199 * #
E-1522 ..... p 34 N83-22200 * #
E-1523 ..... p 32 N83-17538 * #
E-1524 ..... p 160 N83-24874 * #
E-1525 ..... p 38 N83-29208 * #
E-1526 ..... p 85 N83-25853 * #
E-1528 ..... p 87 N83-34019 * #
E-1533 ..... p 144 N83-20117 * #
E-1534 ..... p 58 N83-22318 * #
E-1535 ..... p 58 N83-24552 * #
E-1537 ..... p 185 N83-34453 * #
E-1539 ..... p 12 N83-25657 * #
E-1541 ..... p 161 N83-34351 * #
E-1544 ..... p 100 N83-19920 * #
E-1545 ..... p 72 N83-18862 * #
E-1546 ..... p 181 N83-26252 * #
E-1547 ..... p 83 N83-19887 * #
E-1548 ..... p 179 N83-23710 * #
E-1549 ..... p 180 N83-25037 * #
E-1554 ..... p 129 N83-19020 * #
E-1555 ..... p 87 N83-34015 * #
E-1556 ..... p 15 N83-34908 * #
E-1558 ..... p 36 N83-25711 * #
E-1559-5 ..... p 98 N83-35143 * #
E-1560 ..... p 94 N83-19902 * #
E-1561 ..... p 66 N83-19817 * #
E-1562 ..... p 66 N83-24559 * #
E-1563 ..... p 12 N83-19710 * #
E-1564 ..... p 182 N83-27347 * #
E-1565 ..... p 13 N83-26817 * #
E-1568 ..... p 45 N83-29292 * #
E-1569 ..... p 40 N83-32806 * #
E-1570 ..... p 148 N83-26079 * #
E-1573 ..... p 95 N83-27021 * #
E-1574 ..... p 199 N83-21895 * #
E-1575 ..... p 189 N83-19496 * #
E-1577 ..... p 33 N83-19754 * #
E-1578 ..... p 87 N83-35103 * #
E-1579 ..... p 83 N83-22387 * #
E-1580 ..... p 200 N83-23114 * #
E-1581 ..... p 200 N83-21896 * #
E-1582 ..... p 83 N83-23417 * #
E-1584 ..... p 189 N83-28921 * #
E-1585 ..... p 208 N83-29124 * #
E-1586 ..... p 200 N83-21897 * #
E-1587 ..... p 39 N83-30431 * #
E-1588 ..... p 41 N83-34941 * #
E-1590 ..... p 34 N83-20947 * #
E-1591 ..... p 94 N83-25883 * #
E-1592 ..... p 84 N83-24637 * #
E-1593 ..... p 94 N83-22423 * #
E-1595 ..... p 17 N83-24487 * #
E-1596 ..... p 201 N83-24287 * #
E-1597 ..... p 59 N83-30516 * #
E-1598 ..... p 48 N83-22313 * #
E-1601 ..... p 148 N83-24858 * #
E-1604 ..... p 200 N83-23115 * #
E-1605 ..... p 35 N83-24506 * #
E-1606 ..... p 201 N83-26643 * #
E-1608 ..... p 200 N83-23116 * #
E-1609 ..... p 84 N83-24635 * #
E-1610 ..... p 130 N83-23545 * #
E-1612 ..... p 85 N83-24638 * #
E-1614 ..... p 148 N83-24856 * #
E-1616 ..... p 148 N83-24855 * #
E-1617 ..... p 152 N83-34326 * #
E-1618 ..... p 66 N83-25790 * #
E-1619 ..... p 153 N83-23620 * #
E-1621 ..... p 35 N83-24505 * #
E-1622 ..... p 2 N83-22092 * #
E-1623 ..... p 190 N83-21847 * #
E-1624 ..... p 95 N83-27019 * #
E-1628 ..... p 73 N83-29326 * #
E-1629 ..... p 94 N83-25882 * #
E-1631 ..... p 201 N83-23117 * #
E-1633 ..... p 41 N83-33893 * #
E-1636 ..... p 201 N83-27793 * #
E-1637 ..... p 73 N83-30550 * #
E-1640 ..... p 37 N83-27995 * #
E-1641 ..... p 117 N83-29597 * #
E-1642 ..... p 180 N83-25041 * #
E-1643 ..... p 180 N83-25038 * #
E-1644 ..... p 2 N83-24467 * #
E-1645 ..... p 179 N83-23709 * #
E-1646 ..... p 163 N83-34372 * #
E-1648 ..... p 96 N83-28243 * #
E-1649 ..... p 130 N83-24798 * #
E-1656 ..... p 107 N83-29493 * #
E-1657 ..... p 181 N83-26253 * #
E-1659 ..... p 191 N83-31390 * #
E-1662 ..... p 180 N83-25042 * #
E-1663 ..... p 73 N83-24571 * #
E-1665 ..... p 201 N83-25499 * #
E-1666 ..... p 58 N83-26922 * #
E-1667 ..... p 115 N83-24764 * #
E-1669 ..... p 202 N83-30168 * #
E-1672 ..... p 86 N83-29360 * #
E-1673 ..... p 130 N83-24799 * #
E-1674 ..... p 150 N83-28455 * #
E-1675 ..... p 13 N83-25662 * #
E-1676 ..... p 37 N83-27994 * #
E-1677 ..... p 95 N83-27020 * #
E-1679 ..... p 183 N83-29810 * #
E-1682 ..... p 116 N83-25982 * #
E-1683 ..... p 212 N83-27924 * #
E-1684 ..... p 95 N83-27016 * #
E-1688 ..... p 182 N83-27346 * #
E-1692 ..... p 12 N83-24470 * #
E-1694 ..... p 201 N83-27794 * #
E-1695 ..... p 36 N83-26838 * #
E-1701 ..... p 96 N83-30660 * #
E-1702 ..... p 41 N83-32811 * #
E-1704 ..... p 48 N83-35004 * #
E-1706 ..... p 131 N83-28380 * #
E-1707 ..... p 58 N83-26923 * #
E-1709 ..... p 59 N83-26924 * #
E-170 ..... p 184 N83-29811 * #
E-1710 ..... p 101 N83-28255 * #
E-1711 ..... p 37 N83-27991 * #
E-1712 ..... p 86 N83-29358 * #
E-1714 ..... p 107 N83-28295 * #
E-1715 ..... p 97 N83-34048 * #
E-1716 ..... p 150 N83-29709 * #
E-1717 ..... p 97 N83-35142 * #
E-1718 ..... p 38 N83-29235 * #
E-1721 ..... p 109 N83-34120 * #
E-1722 ..... p 14 N83-27958 * #
E-1724 ..... p 184 N83-29813 * #
E-1725 ..... p 2 N83-34685 * #
E-1727 ..... p 15 N83-30393 * #
E-1729 ..... p 97 N83-34049 * #
E-1730 ..... p 37 N83-27992 * #
E-1731 ..... p 39 N83-29237 * #
E-1733 ..... p 160 N83-28493 * #
E-1735 ..... p 41 N83-34942 * #
E-1738 ..... p 62 N83-29311 * #
E-1741 ..... p 132 N83-33103 * #
E-1744 ..... p 184 N83-31107 * #
E-1745 ..... p 186 N83-35496 * #
E-1749 ..... p 14 N83-29179 * #
E-1753 ..... p 39 N83-29236 * #
E-1765 ..... p 15 N83-34909 * #
E-1766 ..... p 152 N83-34327 * #
E-1767 ..... p 191 N83-30113 * #
E-1769 ..... p 98 N83-35144 * #
E-1771 ..... p 102 N83-35160 * #
E-1772 ..... p 15 N83-30392 * #
E-1773 ..... p 41 N83-32810 * #
E-1774 ..... p 87 N83-34016 * #
E-1787 ..... p 161 N83-34349 * #
E-1790 ..... p 87 N83-35102 * #
E-1792 ..... p 42 N83-34943 * #
E-1804 ..... p 163 N83-35413 * #
E-1807 ..... p 19 N83-33883 * #
E-1809 ..... p 88 N83-35104 * #
E-1811 ..... p 186 N83-35498 * #
E-1820 ..... p 163 N83-35412 * #
E-1824 ..... p 42 N83-34945 * #
E-1827 ..... p 42 N83-34946 * #
E-1830 ..... p 60 N83-35053 * #
E-1833 ..... p 42 N83-34947 * #
E-1837 ..... p 50 N83-35005 * #
E-1840 ..... p 42 N83-34948 * #
E-1844 ..... p 2 N83-34886 * #
E-209 ..... p 140 N83-12432 * #
E-209 ..... p 140 N83-13458 * #
E-209 ..... p 147 N83-20159 * #
E-209 ..... p 149 N83-28449 * #
E-209 ..... p 150 N83-29710 * #
E-209 ..... p 150 N83-29711 * #
E-209 ..... p 151 N83-29712 * #
E-209 ..... p 151 N83-29713 * #
E-369 ..... p 9 N83-11058 * #
E-638 ..... p 77 N83-10171 * #
E-760 ..... p 83 N83-22390 * #
E-817 ..... p 144 N83-20119 * #
E-882 ..... p 160 N83-23631 * #
E-885-83-01 ..... p 45 N83-15330 * #
E-978 ..... p 169 N83-14691 * #
E-981 ..... p 80 N83-11309 * #

EDR-10578 ..... p 139 N83-11497 * #
EDR-10696 ..... p 28 N83-12089 * #
EDR-11209 ..... p 131 N83-28376 * #

EPRI-AP-2618 ..... p 95 N83-27022 * #

ERC-R-82038 ..... p 128 N83-15592 * #

ESL-713533-2 ..... p 106 N83-22494 * #

FCR-4294 ..... p 208 N83-30297 * #

FM-15 ..... p 199 N83-20706 * #

FSI-60-04 ..... p 12 N83-18671 * #

FWS-7621 ..... p 44 N83-24516 * #

GARRETT-21-4270-1.1 ..... p 31 N83-16343 * #
GARRETT-21-4270-2 ..... p 198 N83-17242 * #
GARRETT-21-4302 ..... p 128 N83-15590 * #
GARRETT-31-3725(3) ..... p 212 N83-33800 * #
GARRETT-31-3725(4) ..... p 210 N83-17424 * #

GDC-SP-83-041 ..... p 185 N83-34454 * #

GE-R82AEB304 ..... p 143 N83-17880 * #

GE-82SDS4222 ..... p 115 N83-16630 * #
GE-83SDS4206 ..... p 105 N83-17769 * #

GR-21-4269 ..... p 40 N83-30432 * #

GR/DC-625RL137-VOL-2 ..... p 178 N83-22751 * #
GR/DC-625RN209-VOL-1 ..... p 178 N83-22750 * #

GRDC-625-RL-153-VOL-3 ..... p 178 N83-22754 * #
GRDC-625-RL-154-VOL-4 ..... p 179 N83-22755 * #

GT-83-001 ..... p 212 N83-27926 * #

GTEC-31-3725(2) ..... p 209 N83-13038 * #
GTEC-31-3725(5) ..... p 211 N83-26763 * #

HAC-E8179 ..... p 186 N83-35497 * #

HAC-F107-500 ..... p 185 N83-33320 * #

HSER-8826 ..... p 14 N83-29178 * #

ICASE-83-57 ..... p 16 N83-35999 * #

IIHR-232-III-VOL-3 ..... p 191 N83-23087 #
IIHR-232-IV-VOL-4 ..... p 191 N83-23088 #
IIHR-232-V-VOL-5 ..... p 191 N83-23089 #

IIT-FHT-R82-3 ..... p 11 N83-17503 * #
IIT-FHT-R83-1 ..... p 11 N83-17502 * #

IITRE-M06004-36 ..... p 80 N83-12215 * #

IITRI-M06004-67 ..... p 87 N83-35101 * #
IITRI-M06051-33 ..... p 94 N83-22422 * #
IITRI-M06061-38 ..... p 83 N83-22389 * #
IITRI-M06066-22 ..... p 177 N83-22746 * #
IITRI-M06071-20 ..... p 96 N83-29393 * #

IRT-8195-018-VOL-1 ..... p 49 N83-12136 * #
IRT-8195-022-1-VOL-2 ..... p 50 N83-12137 * #

ISBN-92-835-1436-2 ..... p 27 N83-11138 #

JACKFAU-82-299-VOL-1 ..... p 183 N83-28581 * #
JACKFAU-82-299-VOL-2 ..... p 183 N83-28582 * #
JACKFAU-82-299-VOL-3 ..... p 183 N83-28583 * #
JACKFAU-82-299-VOL-4 ..... p 183 N83-28580 * #

JO-19128 ..... p 114 N83-12330 * #

KU-FRL-464-5-REV-A ..... p 17 N83-32782 * #
KU-FRL-464-5 ..... p 17 N83-19738 * #

L-15587 ..... p 163 N83-34373 * #
L-15605 ..... p 161 N83-33217 * #

LG82ER0031 ..... p 197 N83-12968 * #
LG82ER0115 ..... p 199 N83-20708 * #

LOG-J13452 ..... p 133 N83-35318 * #

LR-30060 ..... p 16 N83-11095 * #

MCR-82-521 ..... p 57 N83-21002 * #

MDC-J2548 ..... p 10 N83-12047 * #

ME-TSPC-TR-83-02 ..... p 15 N83-34911 * #

MIT-ARSL-TR-197-3 ..... p 177 N83-21508 * #

MIT-ASRL-TR-197-2 ..... p 177 N83-22740 * #
MIT-ASRL-TR-197-4 ..... p 177 N83-21509 * #
MIT-ASRL-TR-197-5 ..... p 178 N83-22747 * #

MLR-1430 ..... p 116 N83-27127 * #

MRDC41054.59FR ..... p 206 N83-19622 * #
MRDC41092.35FR ..... p 207 N83-27877 * #

MRI-7014-G ..... p 98 N83-10207 * #
MRI-82-FR-1862 ..... p 19 N83-18720 * #

MTI-81ASE185QT11 ..... p 211 N83-26762 * #
MTI-82TR38 ..... p 167 N83-10568 * #
MTI-83TR12 ..... p 43 N83-14139 * #
MTI-83TR55 ..... p 41 N83-33894 * #

MTPR-11 ..... p 27 N83-12088 * #

NAPC-PE-80 ..... p 38 N83-29234 * #

NAS 1.15:23324 ..... p 13 N83-26817 * #
NAS 1.15:81692 ..... p 147 N83-20159 * #
NAS 1.15:81695 ..... p 140 N83-12432 * #
NAS 1.15:81696 ..... p 140 N83-13458 * #
NAS 1.15:81697 ..... p 150 N83-29710 * #
NAS 1.15:81698 ..... p 150 N83-29711 * #
NAS 1.15:81699 ..... p 151 N83-29712 * #
NAS 1.15:81700 ..... p 149 N83-28449 * #
NAS 1.15:81701 ..... p 151 N83-29713 * #
NAS 1.15:81723 ..... p 83 N83-22390 * #
NAS 1.15:82629 ..... p 160 N83-23631 * #
NAS 1.15:82695 ..... p 169 N83-14691 * #
NAS 1.15:82698 ..... p 80 N83-11309 * #
NAS 1.15:82739 ..... p 99 N83-10208 * #
NAS 1.15:82774 ..... p 126 N83-12359 * #
NAS 1.15:82778 ..... p 169 N83-14688 * #
NAS 1.15:82818 ..... p 9 N83-11063 * #
NAS 1.15:82867 ..... p 59 N83-28071 * #
NAS 1.15:82870 ..... p 169 N83-14689 * #
NAS 1.15:82876 ..... p 125 N83-10389 * #
NAS 1.15:82890 ..... p 28 N83-12092 * #
NAS 1.15:82893 ..... p 70 N83-10134 * #
NAS 1.15:82898 ..... p 207 N83-20808 * #
NAS 1.15:82907 ..... p 32 N83-17537 * #
NAS 1.15:82920 ..... p 81 N83-13232 * #
NAS 1.15:82923 ..... p 170 N83-15805 * #
NAS 1.15:82932 ..... p 27 N83-12087 * #
NAS 1.15:82934 ..... p 81 N83-14245 * #
NAS 1.15:82935 ..... p 77 N83-10171 * #
NAS 1.15:82938 ..... p 181 N83-26251 * #
NAS 1.15:82939 ..... p 9 N83-10019 * #
NAS 1.15:82940 ..... p 169 N83-14683 * #
NAS 1.15:82947 ..... p 113 N83-11446 * #
NAS 1.15:82948 ..... p 166 N83-10554 * #
NAS 1.15:82949 ..... p 28 N83-12090 * #
NAS 1.15:82950 ..... p 196 N83-11840 * #
NAS 1.15:82951 ..... p 64 N83-12175 * #
NAS 1.15:82952 ..... p 50 N83-13154 * #
NAS 1.15:82953 ..... p 159 N83-14523 * #
NAS 1.15:82954 ..... p 71 N83-12182 * #
NAS 1.15:82955 ..... p 143 N83-20115 * #
NAS 1.15:82956 ..... p 140 N83-12433 * #
NAS 1.15:82957 ..... p 167 N83-10558 * #
NAS 1.15:82958 ..... p 63 N83-10118 * #
NAS 1.15:82959 ..... p 91 N83-13257 * #
NAS 1.15:82960 ..... p 210 N83-17423 * #
NAS 1.15:82961 ..... p 70 N83-10135 * #
NAS 1.15:82962 ..... p 91 N83-11329 * #
NAS 1.15:82963 ..... p 12 N83-17509 * #
NAS 1.15:82964 ..... p 30 N83-15306 * #
NAS 1.15:82965 ..... p 206 N83-10962 * #
NAS 1.15:82966 ..... p 166 N83-10555 * #
NAS 1.15:82967 ..... p 114 N83-14397 * #
NAS 1.15:82968 ..... p 92 N83-14271 * #
NAS 1.15:82969 ..... p 126 N83-12357 * #
NAS 1.15:82970 ..... p 105 N83-10322 * #
NAS 1.15:82971 ..... p 113 N83-11447 * #
NAS 1.15:82972 ..... p 90 N83-10194 * #
NAS 1.15:82973 ..... p 140 N83-11498 * #
NAS 1.15:82975 ..... p 158 N83-11514 * #
NAS 1.15:82976 ..... p 139 N83-10425 * #
NAS 1.15:82977 ..... p 57 N83-17587 * #
NAS 1.15:82978 ..... p 29 N83-14126 * #
NAS 1.15:82979 ..... p 27 N83-11128 * #
NAS 1.15:82980 ..... p 61 N83-13169 * #
NAS 1.15:82981 ..... p 71 N83-15372 * #
NAS 1.15:82982 ..... p 114 N83-14399 * #
NAS 1.15:82983 ..... p 27 N83-11129 * #
NAS 1.15:82984 ..... p 47 N83-11210 * #
NAS 1.15:82985 ..... p 166 N83-10557 * #
NAS 1.15:82986 ..... p 167 N83-10559 * #
NAS 1.15:82987 ..... p 166 N83-10556 * #
NAS 1.15:82988 ..... p 27 N83-11130 * #
NAS 1.15:82989 ..... p 92 N83-15466 * #
NAS 1.15:82990 ..... p 56 N83-13164 * #
NAS 1.15:82991 ..... p 169 N83-14690 * #
NAS 1.15:82992 ..... p 211 N83-25625 * #
NAS 1.15:82993 ..... p 81 N83-13231 * #
NAS 1.15:82994 ..... p 196 N83-10885 * #
NAS 1.15:82995 ..... p 192 N83-21872 * #
NAS 1.15:82996 ..... p 128 N83-17833 * #
NAS 1.15:82997 ..... p 210 N83-19651 * #
NAS 1.15:82998 ..... p 167 N83-10560 * #
NAS 1.15:82999 ..... p 180 N83-25036 * #
NAS 1.15:83000 ..... p 84 N83-24636 * #
NAS 1.15:83001 ..... p 70 N83-12181 * #
NAS 1.15:83002 ..... p 197 N83-13939 * #
NAS 1.15:83003 ..... p 28 N83-12091 * #
NAS 1.15:83003 ..... p 100 N83-19921 * #
NAS 1.15:83004 ..... p 56 N83-12141 * #
NAS 1.15:83005 ..... p 127 N83-14431 * #
NAS 1.15:83006 ..... p 78 N83-11282 * #
NAS 1.15:83007 ..... p 99 N83-13273 * #
NAS 1.15:83009 ..... p 18 N83-15302 * #
NAS 1.15:83010 ..... p 10 N83-13077 * #
NAS 1.15:83011 ..... p 126 N83-12358 * #
NAS 1.15:83012 ..... p 197 N83-12966 * #
NAS 1.15:83013 ..... p 29 N83-13101 * #
NAS 1.15:83014 ..... p 56 N83-12142 * #
NAS 1.15:83015 ..... p 56 N83-12143 * #
NAS 1.15:83016 ..... p 128 N83-14435 * #
NAS 1.15:83017 ..... p 127 N83-13392 * #
NAS 1.15:83018 ..... p 174 N83-18022 * #
NAS 1.15:83019 ..... p 176 N83-20361 * #
NAS 1.15:83020 ..... p 198 N83-16152 * #
NAS 1.15:83021 ..... p 152 N83-34325 * #
NAS 1.15:83023 ..... p 81 N83-14246 * #
NAS 1.15:83024 ..... p 129 N83-19016 * #
NAS 1.15:83025 ..... p 166 N83-13589 * #
NAS 1.15:83026 ..... p 130 N83-23544 * #
NAS 1.15:83027 ..... p 29 N83-14127 * #
NAS 1.15:83028 ..... p 33 N83-18725 * #
NAS 1.15:83029 ..... p 57 N83-14157 * #
NAS 1.15:83030 ..... p 127 N83-14432 * #
NAS 1.15:83031 ..... p 16 N83-14078 * #
NAS 1.15:83032 ..... p 99 N83-15483 * #
NAS 1.15:83033 ..... p 92 N83-14270 * #
NAS 1.15:83034 ..... p 198 N83-16153 * #
NAS 1.15:83035 ..... p 173 N83-15840 * #
NAS 1.15:83036 ..... p 178 N83-22749 * #
NAS 1.15:83037 ..... p 1 N83-14061 * #
NAS 1.15:83038 ..... p 208 N83-15169 * #
NAS 1.15:83039 ..... p 190 N83-12930 * #
NAS 1.15:83040 ..... p 143 N83-19092 * #
NAS 1.15:83041 ..... p 143 N83-19093 * #
NAS 1.15:83042 ..... p 92 N83-15468 * #
NAS 1.15:83043 ..... p 31 N83-15307 * #
NAS 1.15:83044 ..... p 65 N83-15362 * #
NAS 1.15:83045 ..... p 11 N83-15268 * #
NAS 1.15:83046 ..... p 174 N83-16857 * #
NAS 1.15:83047 ..... p 65 N83-15364 * #
NAS 1.15:83048 ..... p 134 N83-15602 * #
NAS 1.15:83049 ..... p 159 N83-15672 * #
NAS 1.15:83050 ..... p 65 N83-15365 * #
NAS 1.15:83051 ..... p 65 N83-15363 * #
NAS 1.15:83052 ..... p 61 N83-25786 * #
NAS 1.15:83053 ..... p 130 N83-26017 * #
NAS 1.15:83054 ..... p 200 N83-23112 * #
NAS 1.15:83055 ..... p 82 N83-17682 * #
NAS 1.15:83056 ..... p 34 N83-22199 * #
NAS 1.15:83057 ..... p 34 N83-22200 * #
NAS 1.15:83058 ..... p 32 N83-17538 * #
NAS 1.15:83059 ..... p 160 N83-24874 * #
NAS 1.15:83062 ..... p 144 N83-20117 * #
NAS 1.15:83063 ..... p 58 N83-22318 * #
NAS 1.15:83064 ..... p 58 N83-24552 * #
NAS 1.15:83065 ..... p 12 N83-19710 * #
NAS 1.15:83066 ..... p 185 N83-34453 * #
NAS 1.15:83067 ..... p 82 N83-19886 * #
NAS 1.15:83068 ..... p 93 N83-19901 * #
NAS 1.15:83069 ..... p 12 N83-25657 * #
NAS 1.15:83070 ..... p 129 N83-17834 * #
NAS 1.15:83071 ..... p 129 N83-22542 * #
NAS 1.15:83072 ..... p 100 N83-19920 * #
NAS 1.15:83073 ..... p 72 N83-18862 * #
NAS 1.15:83074 ..... p 144 N83-20118 * #
NAS 1.15:83087 ..... p 181 N83-26252 * #
NAS 1.15:83308 ..... p 83 N83-19887 * #
NAS 1.15:83309 ..... p 179 N83-23710 * #
NAS 1.15:83310 ..... p 180 N83-25037 * #
NAS 1.15:83311 ..... p 144 N83-20116 * #
NAS 1.15:83312 ..... p 129 N83-20029 * #
NAS 1.15:83313 ..... p 129 N83-19020 * #
NAS 1.15:83314 ..... p 15 N83-34908 * #
NAS 1.15:83317 ..... p 198 N83-18405 * #
NAS 1.15:83318 ..... p 150 N83-28454 * #
NAS 1.15:83319 ..... p 94 N83-19902 * #
NAS 1.15:83320 ..... p 66 N83-19817 * #
NAS 1.15:83321 ..... p 66 N83-24559 * #
NAS 1.15:83322 ..... p 85 N83-25853 * #
NAS 1.15:83323 ..... p 182 N83-27347 * #
NAS 1.15:83325 ..... p 134 N83-24829 * #
NAS 1.15:83326 ..... p 45 N83-29292 * #
NAS 1.15:83327 ..... p 199 N83-21895 * #
NAS 1.15:83328 ..... p 189 N83-19496 * #
NAS 1.15:83329 ..... p 210 N83-24431 * #
NAS 1.15:83330 ..... p 33 N83-19754 * #
NAS 1.15:83331 ..... p 87 N83-35103 * #
NAS 1.15:83332 ..... p 83 N83-22387 * #
NAS 1.15:83333 ..... p 200 N83-23114 * #
NAS 1.15:83334 ..... p 200 N83-21896 * #
NAS 1.15:83335 ..... p 208 N83-29124 * #
NAS 1.15:83336 ..... p 200 N83-21897 * #
NAS 1.15:83337 ..... p 47 N83-20994 * #
NAS 1.15:83338 ..... p 34 N83-20947 * #
NAS 1.15:83339 ..... p 94 N83-22423 * #
NAS 1.15:83340 ..... p 17 N83-24487 * #
NAS 1.15:83341 ..... p 201 N83-24287 * #
NAS 1.15:83342 ..... p 59 N83-30516 * #
NAS 1.15:83343 ..... p 36 N83-25711 * #
NAS 1.15:83344 ..... p 48 N83-22313 * #
NAS 1.15:83345 ..... p 148 N83-23606 * #
NAS 1.15:83346 ..... p 35 N83-23306 * #
NAS 1.15:83347 ..... p 200 N83-23115 * #
NAS 1.15:83348 ..... p 35 N83-24506 * #
NAS 1.15:83349 ..... p 201 N83-26643 * #
NAS 1.15:83350 ..... p 83 N83-23417 * #
NAS 1.15:83351 ..... p 200 N83-23116 * #
NAS 1.15:83352 ..... p 84 N83-24634 * #
NAS 1.15:83353 ..... p 130 N83-23545 * #
NAS 1.15:83355 ..... p 85 N83-24638 * #
NAS 1.15:83356 ..... p 148 N83-24855 * #
NAS 1.15:83357 ..... p 66 N83-25790 * #
NAS 1.15:83358 ..... p 153 N83-23620 * #
NAS 1.15:83359 ..... p 35 N83-24505 * #
NAS 1.15:83360 ..... p 2 N83-22092 * #
NAS 1.15:83361 ..... p 190 N83-21847 * #
NAS 1.15:83362 ..... p 95 N83-27019 * #

NAS 1.15:83363 ..... p 73 N83-29326 * #
NAS 1.15:83364 ..... p 94 N83-25882 * #
NAS 1.15:83365 ..... p 201 N83-23117 * #
NAS 1.15:83366 ..... p 160 N83-24875 * #
NAS 1.15:83368 ..... p 84 N83-24635 * #
NAS 1.15:83369 ..... p 84 N83-24637 * #
NAS 1.15:83370 ..... p 201 N83-27793 * #
NAS 1.15:83371 ..... p 73 N83-30550 * #
NAS 1.15:83372 ..... p 37 N83-27995 * #
NAS 1.15:83373 ..... p 117 N83-29597 * #
NAS 1.15:83374 ..... p 180 N83-25041 * #
NAS 1.15:83375 ..... p 180 N83-25038 * #
NAS 1.15:83376 ..... p 2 N83-24467 * #
NAS 1.15:83377 ..... p 179 N83-23709 * #
NAS 1.15:83378 ..... p 130 N83-24798 * #
NAS 1.15:83383 ..... p 107 N83-29493 * #
NAS 1.15:83384 ..... p 181 N83-26253 * #
NAS 1.15:83385 ..... p 180 N83-25042 * #
NAS 1.15:83386 ..... p 73 N83-24571 * #
NAS 1.15:83387 ..... p 201 N83-25499 * #
NAS 1.15:83388 ..... p 58 N83-26922 * #
NAS 1.15:83389 ..... p 148 N83-24858 * #
NAS 1.15:83390 ..... p 115 N83-24764 * #
NAS 1.15:83392 ..... p 202 N83-30168 * #
NAS 1.15:83393 ..... p 184 N83-29811 * #
NAS 1.15:83395 ..... p 86 N83-29360 * #
NAS 1.15:83396 ..... p 130 N83-24799 * #
NAS 1.15:83397 ..... p 150 N83-28455 * #
NAS 1.15:83398 ..... p 13 N83-25662 * #
NAS 1.15:83399 ..... p 37 N83-27994 * #
NAS 1.15:83400 ..... p 95 N83-27020 * #
NAS 1.15:83401 ..... p 183 N83-29810 * #
NAS 1.15:83402 ..... p 148 N83-24856 * #
NAS 1.15:83404 ..... p 116 N83-25982 * #
NAS 1.15:83405 ..... p 212 N83-27924 * #
NAS 1.15:83406 ..... p 95 N83-27016 * #
NAS 1.15:83407 ..... p 182 N83-27346 * #
NAS 1.15:83408 ..... p 148 N83-26079 * #
NAS 1.15:83409 ..... p 12 N83-24470 * #
NAS 1.15:83410 ..... p 94 N83-25883 * #
NAS 1.15:83411 ..... p 201 N83-27794 * #
NAS 1.15:83412 ..... p 36 N83-26838 * #
NAS 1.15:83413 ..... p 96 N83-30660 * #
NAS 1.15:83414 ..... p 41 N83-32811 * #
NAS 1.15:83416 ..... p 48 N83-35004 * #
NAS 1.15:83417 ..... p 58 N83-26923 * #
NAS 1.15:83418 ..... p 131 N83-28380 * #
NAS 1.15:83419 ..... p 59 N83-26924 * #
NAS 1.15:83420 ..... p 101 N83-28255 * #
NAS 1.15:83421 ..... p 37 N83-27991 * #
NAS 1.15:83422 ..... p 96 N83-28243 * #
NAS 1.15:83423 ..... p 86 N83-29358 * #
NAS 1.15:83424 ..... p 152 N83-34326 * #
NAS 1.15:83425 ..... p 107 N83-28295 * #
NAS 1.15:83426 ..... p 97 N83-34048 * #
NAS 1.15:83427 ..... p 97 N83-35142 * #
NAS 1.15:83428 ..... p 150 N83-29709 * #
NAS 1.15:83429 ..... p 38 N83-29235 * #
NAS 1.15:83430 ..... p 109 N83-34120 * #
NAS 1.15:83431 ..... p 14 N83-27958 * #
NAS 1.15:83432 ..... p 184 N83-29813 * #
NAS 1.15:83433 ..... p 2 N83-34885 * #
NAS 1.15:83434 ..... p 15 N83-30393 * #
NAS 1.15:83435 ..... p 37 N83-27992 * #
NAS 1.15:83436 ..... p 39 N83-29237 * #
NAS 1.15:83437 ..... p 160 N83-28493 * #
NAS 1.15:83438 ..... p 13 N83-27957 * #
NAS 1.15:83440 ..... p 97 N83-32943 * #
NAS 1.15:83441 ..... p 62 N83-29311 * #
NAS 1.15:83442 ..... p 132 N83-33103 * #
NAS 1.15:83443 ..... p 191 N83-31390 * #
NAS 1.15:83444 ..... p 184 N83-31107 * #
NAS 1.15:83445 ..... p 186 N83-35496 * #
NAS 1.15:83447 ..... p 39 N83-29236 * #
NAS 1.15:83448 ..... p 14 N83-29179 * #
NAS 1.15:83450 ..... p 87 N83-34015 * #
NAS 1.15:83451 ..... p 15 N83-34909 * #
NAS 1.15:83452 ..... p 152 N83-34327 * #
NAS 1.15:83453 ..... p 191 N83-30113 * #
NAS 1.15:83454 ..... p 117 N83-34192 * #
NAS 1.15:83456 ..... p 102 N83-35160 * #
NAS 1.15:83457 ..... p 15 N83-30392 * #
NAS 1.15:83458 ..... p 41 N83-32810 * #
NAS 1.15:83459 ..... p 87 N83-34016 * #
NAS 1.15:83464 ..... p 97 N83-34049 * #
NAS 1.15:83465 ..... p 98 N83-35143 * #
NAS 1.15:83466 ..... p 41 N83-34942 * #
NAS 1.15:83473 ..... p 161 N83-34349 * #
NAS 1.15:83474 ..... p 98 N83-35144 * #
NAS 1.15:83475 ..... p 87 N83-35102 * #
NAS 1.15:83478 ..... p 42 N83-34943 * #
NAS 1.15:83482 ..... p 163 N83-35413 * #
NAS 1.15:83484 ..... p 19 N83-33883 * #
NAS 1.15:83485 ..... p 88 N83-35104 * #
NAS 1.15:83487 ..... p 186 N83-35498 * #
NAS 1.15:83491 ..... p 163 N83-35412 * #
NAS 1.15:83493 ..... p 42 N83-34945 * #
NAS 1.15:83494 ..... p 42 N83-34946 * #
NAS 1.15:83496 ..... p 60 N83-35053 * #
NAS 1.15:83499 ..... p 42 N83-34947 * #
NAS 1.15:83500 ..... p 50 N83-35005 * #
NAS 1.15:83501 ..... p 42 N83-34948 * #
NAS 1.15:83505 ..... p 2 N83-34886 * #
NAS 1.15:85190 ..... p 45 N83-15330 * #
NAS 1.15:85349 ..... p 95 N83-27022 * #
NAS 1.15:85404 ..... p 133 N83-35318 * #
NAS 1.15:85428 ..... p 43 N83-36031 * #
NAS 1.26:167901 ..... p 212 N83-33800 * #
NAS 1.26:10186 ..... p 191 N83-23087 * #
NAS 1.26:159773 ..... p 211 N83-24432 * #
NAS 1.26:159791 ..... p 1 N83-16279 * #
NAS 1.26:159859 ..... p 28 N83-12094 * #
NAS 1.26:159877 ..... p 102 N83-12259 * #
NAS 1.26:165127 ..... p 174 N83-16859 * #
NAS 1.26:165140 ..... p 57 N83-14158 * #
NAS 1.26:165141 ..... p 82 N83-15412 * #
NAS 1.26:165148 ..... p 31 N83-16341 * #
NAS 1.26:165160 ..... p 57 N83-14159 * #
NAS 1.26:165178 ..... p 140 N83-12431 * #
NAS 1.26:165202 ..... p 30 N83-15304 * #
NAS 1.26:165209 ..... p 80 N83-12215 * #
NAS 1.26:165256 ..... p 43 N83-30435 * #
NAS 1.26:165263 ..... p 211 N83-26762 * #
NAS 1.26:165265 ..... p 26 N83-11127 * #
NAS 1.26:165274 ..... p 167 N83-10568 * #
NAS 1.26:165282 ..... p 114 N83-12330 * #
NAS 1.26:165296 ..... p 28 N83-12089 * #
NAS 1.26:165326-VOL-1 ..... p 178 N83-22750 * #
NAS 1.26:165326-VOL-2 ..... p 178 N83-22751 * #
NAS 1.26:165326-VOL-3 ..... p 178 N83-22754 * #
NAS 1.26:165326-VOL-4 ..... p 179 N83-22755 * #
NAS 1.26:165329 ..... p 209 N83-13038 * #
NAS 1.26:165341 ..... p 66 N83-22326 * #
NAS 1.26:165346 ..... p 139 N83-11497 * #
NAS 1.26:165354 ..... p 39 N83-30427 * #
NAS 1.26:165376 ..... p 39 N83-30430 * #
NAS 1.26:165394 ..... p 206 N83-13009 * #
NAS 1.26:165399 ..... p 32 N83-17545 * #
NAS 1.26:165400 ..... p 39 N83-30429 * #
NAS 1.26:165414 ..... p 65 N83-18853 * #
NAS 1.26:165415 ..... p 66 N83-18854 * #
NAS 1.26:165445 ..... p 182 N83-26259 * #
NAS 1.26:165461 ..... p 64 N83-13173 * #
NAS 1.26:165462-A ..... p 168 N83-12524 * #
NAS 1.26:165463 ..... p 179 N83-23704 * #
NAS 1.26:165472 ..... p 178 N83-22748 * #
NAS 1.26:165484-VOL-1 ..... p 108 N83-33010 * #
NAS 1.26:165484-VOL-2 ..... p 108 N83-33011 * #
NAS 1.26:165491 ..... p 174 N83-19226 * #
NAS 1.26:165492 ..... p 102 N83-35159 * #
NAS 1.26:165494 ..... p 212 N83-37028 * #
NAS 1.26:165509 ..... p 141 N83-14494 * #
NAS 1.26:165518 ..... p 29 N83-13104 * #
NAS 1.26:165523 ..... p 40 N83-32804 * #
NAS 1.26:165525 ..... p 16 N83-11095 * #
NAS 1.26:165527 ..... p 210 N83-20829 * #
NAS 1.26:165528 ..... p 212 N83-27926 * #
NAS 1.26:165540 ..... p 44 N83-24516 * #
NAS 1.26:165541 ..... p 168 N83-13585 * #
NAS 1.26:165543 ..... p 167 N83-10561 * #
NAS 1.26:165566 ..... p 177 N83-22746 * #
NAS 1.26:165571 ..... p 158 N83-12451 * #
NAS 1.26:165581 ..... p 29 N83-13100 * #
NAS 1.26:165582 ..... p 32 N83-17539 * #
NAS 1.26:165590 ..... p 50 N83-12137 * #
NAS 1.26:165591 ..... p 142 N83-15659 * #
NAS 1.26:165598-VOL-1 ..... p 211 N83-26757 * #
NAS 1.26:165598-VOL-2 ..... p 211 N83-26758 * #
NAS 1.26:165598-VOL-3 ..... p 211 N83-26759 * #
NAS 1.26:165601 ..... p 113 N83-10348 * #
NAS 1.26:165612 ..... p 3 N83-16342 * #
NAS 1.26:165618 ..... p 26 N83-10044 * #
NAS 1.26:165619 ..... p 92 N83-15467 * #
NAS 1.26:165990 ..... p 49 N83-12136 * #
NAS 1.26:167842 ..... p 168 N83-13588 * #
NAS 1.26:167845 ..... p 114 N83-13359 * #
NAS 1.26:167851-VOL-1 ..... p 31 N83-15308 * #
NAS 1.26:167868 ..... p 96 N83-29393 * #
NAS 1.26:167873 ..... p 187 N83-21677 * #
NAS 1.26:167875 ..... p 142 N83-15627 * #
NAS 1.26:167880 ..... p 73 N83-26936 * #
NAS 1.26:167882 ..... p 176 N83-20359 * #
NAS 1.26:167887 ..... p 57 N83-17586 * #
NAS 1.26:167890 ..... p 179 N83-22756 * #
NAS 1.26:167891 ..... p 41 N83-33894 * #
NAS 1.26:167893 ..... p 134 N83-21314 * #
NAS 1.26:167903 ..... p 45 N83-12129 * #
NAS 1.26:167906 ..... p 29 N83-13103 * #
NAS 1.26:167907 ..... p 209 N83-15176 * #
NAS 1.26:167913 ..... p 33 N83-19753 * #
NAS 1.26:167915 ..... p 99 N83-13272 * #
NAS 1.26:167917 ..... p 99 N83-12250 * #
NAS 1.26:167919 ..... p 209 N83-16257 * #
NAS 1.26:167921 ..... p 179 N83-23708 * #
NAS 1.26:167932 ..... p 134 N83-15601 * #
NAS 1.26:167936 ..... p 209 N83-10991 * #
NAS 1.26:167942 ..... p 93 N83-18909 * #
NAS 1.26:167943 ..... p 208 N83-10970 * #
NAS 1.26:167950 ..... p 208 N83-30297 * #
NAS 1.26:167951 ..... p 198 N83-15041 * #
NAS 1.26:167953 ..... p 166 N83-10502 * #
NAS 1.26:167954 ..... p 30 N83-14128 * #
NAS 1.26:167957 ..... p 59 N83-28072 * #
NAS 1.26:167959 ..... p 12 N83-18671 * #
NAS 1.26:167960 ..... p 11 N83-15265 * #
NAS 1.26:167961 ..... p 72 N83-21056 * #
NAS 1.26:167962 ..... p 30 N83-15305 * #
NAS 1.26:167963 ..... p 100 N83-18924 * #
NAS 1.26:167964 ..... p 37 N83-27993 * #
NAS 1.26:167965 ..... p 32 N83-17543 * #
NAS 1.26:167966 ..... p 32 N83-17544 * #
NAS 1.26:167967 ..... p 159 N83-19121 * #
NAS 1.26:167969 ..... p 64 N83-13178 * #
NAS 1.26:167970 ..... p 64 N83-13179 * #
NAS 1.26:167971 ..... p 64 N83-13180 * #
NAS 1.26:167974 ..... p 212 N83-32687 * #
NAS 1.26:167975 ..... p 115 N83-16628 * #
NAS 1.26:167976 ..... p 177 N83-22739 * #
NAS 1.26:167977 ..... p 206 N83-16234 * #
NAS 1.26:167978 ..... p 113 N83-10349 * #
NAS 1.26:167979 ..... p 197 N83-12967 * #
NAS 1.26:167981 ..... p 98 N83-10207 * #
NAS 1.26:167983 ..... p 210 N83-17424 * #
NAS 1.26:167985 ..... p 117 N83-30914 * #
NAS 1.26:167986 ..... p 105 N83-17769 * #
NAS 1.26:167987 ..... p 168 N83-11579 * #
NAS 1.26:167990-VOL-1 ..... p 126 N83-12353 * #
NAS 1.26:167990-VOL-2 ..... p 126 N83-12354 * #
NAS 1.26:167992 ..... p 33 N83-20946 * #
NAS 1.26:167994 ..... p 9 N83-11065 * #
NAS 1.26:167999 ..... p 63 N83-11247 * #
NAS 1.26:168002 ..... p 10 N83-11066 * #
NAS 1.26:168003 ..... p 10 N83-12045 * #
NAS 1.26:168006 ..... p 184 N83-29812 * #
NAS 1.26:168007 ..... p 185 N83-33343 * #
NAS 1.26:168008 ..... p 19 N83-18720 * #
NAS 1.26:168009 ..... p 10 N83-12047 * #
NAS 1.26:168011 ..... p 57 N83-21002 * #
NAS 1.26:168012 ..... p 115 N83-16630 * #
NAS 1.26:168013 ..... p 47 N83-18835 * #
NAS 1.26:168015 ..... p 131 N83-28376 * #
NAS 1.26:168016 ..... p 34 N83-22198 * #
NAS 1.26:168018 ..... p 11 N83-16285 * #
NAS 1.26:168019 ..... p 43 N83-14139 * #
NAS 1.26:168020 ..... p 173 N83-15839 * #
NAS 1.26:168021 ..... p 182 N83-27345 * #
NAS 1.26:168023 ..... p 66 N83-26928 * #
NAS 1.26:168025 ..... p 185 N83-34450 * #
NAS 1.26:168027 ..... p 100 N83-17728 * #
NAS 1.26:168029 ..... p 143 N83-17880 * #
NAS 1.26:168031 ..... p 128 N83-15590 * #
NAS 1.26:168034 ..... p 105 N83-15543 * #
NAS 1.26:168035 ..... p 116 N83-27127 * #
NAS 1.26:168040 ..... p 159 N83-19575 * #
NAS 1.26:168041 ..... p 115 N83-21236 * #
NAS 1.26:168045 ..... p 14 N83-29178 * #
NAS 1.26:168049 ..... p 31 N83-16343 * #
NAS 1.26:168050 ..... p 198 N83-17242 * #
NAS 1.26:168051 ..... p 13 N83-26816 * #
NAS 1.26:168055 ..... p 115 N83-18997 * #
NAS 1.26:168057 ..... p 66 N83-22325 * #
NAS 1.26:168058 ..... p 106 N83-21207 * #
NAS 1.26:168059 ..... p 34 N83-20948 * #
NAS 1.26:168060 ..... p 209 N83-15177 * #
NAS 1.26:168061 ..... p 86 N83-29359 * #
NAS 1.26:168065 ..... p 107 N83-28297 * #
NAS 1.26:168066 ..... p 101 N83-31886 * #
NAS 1.26:168067 ..... p 11 N83-16286 * #
NAS 1.26:168071 ..... p 83 N83-22389 * #
NAS 1.26:168072 ..... p 46 N83-25766 * #
NAS 1.26:168074 ..... p 212 N83-27925 * #
NAS 1.26:168075 ..... p 185 N83-33320 * #
NAS 1.26:168077 ..... p 107 N83-27086 * #
NAS 1.26:168078 ..... p 106 N83-22495 * #
NAS 1.26:168079 ..... p 175 N83-19228 * #
NAS 1.26:168080 ..... p 61 N83-19812 * #
NAS 1.26:168082 ..... p 116 N83-29596 * #
NAS 1.26:168086-VOL-1 ..... p 198 N83-18408 * #
NAS 1.26:168087 ..... p 210 N83-22029 * #
NAS 1.26:168088 ..... p 212 N83-30328 * #
NAS 1.26:168089 ..... p 46 N83-34998 * #
NAS 1.26:168090 ..... p 183 N83-28581 * #
NAS 1.26:168091 ..... p 183 N83-28582 * #
NAS 1.26:168092 ..... p 183 N83-28583 * #
NAS 1.26:168093 ..... p 183 N83-28580 * #
NAS 1.26:168097 ..... p 17 N83-23281 * #
NAS 1.26:168099 ..... p 207 N83-27877 * #
NAS 1.26:16809 ..... p 206 N83-19622 * #

NAS 1.26:168100 ..... p 160 N83-21390 * #
NAS 1.26:168101 ..... p 206 N83-21987 * #
NAS 1.26:168102 ..... p 207 N83-21988 * #
NAS 1.26:168103 ..... p 36 N83-26837 * #
NAS 1.26:168104 ..... p 211 N83-26763 * #
NAS 1.26:168105 ..... p 45 N83-22255 * #
NAS 1.26:168106 ..... p 188 N83-24046 * #
NAS 1.26:168107 ..... p 177 N83-21508 * #
NAS 1.26:168108 ..... p 177 N83-22740 * #
NAS 1.26:168109 ..... p 177 N83-21509 * #
NAS 1.26:168110 ..... p 178 N83-22747 * #
NAS 1.26:168120 ..... p 18 N83-22188 * #
NAS 1.26:168121 ..... p 101 N83-23465 * #
NAS 1.26:168122 ..... p 149 N83-28448 * #
NAS 1.26:168124 ..... p 149 N83-27213 * #
NAS 1.26:168125 ..... p 85 N83-28208 * #
NAS 1.26:168127 ..... p 15 N83-34911 * #
NAS 1.26:168128 ..... p 106 N83-23497 * #
NAS 1.26:168129 ..... p 107 N83-23498 * #
NAS 1.26:168132 ..... p 58 N83-25779 * #
NAS 1.26:168134 ..... p 59 N83-32843 * #
NAS 1.26:168138 ..... p 101 N83-23464 * #
NAS 1.26:168140 ..... p 96 N83-30662 * #
NAS 1.26:168141 ..... p 181 N83-25112 * #
NAS 1.26:168142 ..... p 109 N83-34116 * #
NAS 1.26:168143 ..... p 109 N83-34117 * #
NAS 1.26:168144 ..... p 109 N83-34118 * #
NAS 1.26:168145 ..... p 108 N83-34113 * #
NAS 1.26:168146 ..... p 108 N83-34114 * #
NAS 1.26:168147 ..... p 108 N83-34115 * #
NAS 1.26:168148 ..... p 204 N83-31474 * #
NAS 1.26:168150 ..... p 108 N83-31925 * #
NAS 1.26:168151 ..... p 108 N83-31926 * #
NAS 1.26:168152 ..... p 181 N83-25043 * #
NAS 1.26:168153 ..... p 148 N83-24857 * #
NAS 1.26:168154 ..... p 160 N83-27256 * #
NAS 1.26:168155 ..... p 61 N83-26077 * #
NAS 1.26:168161 ..... p 37 N83-27996 * #
NAS 1.26:168163 ..... p 38 N83-29234 * #
NAS 1.26:168166 ..... p 12 N83-24474 * #
NAS 1.26:168167 ..... p 40 N83-30432 * #
NAS 1.26:168174-VOL-1 ..... p 60 N83-33942 * #
NAS 1.26:168174-VOL-2 ..... p 60 N83-33943 * #
NAS 1.26:168175 ..... p 107 N83-29492 * #
NAS 1.26:168180 ..... p 74 N83-30551 * #
NAS 1.26:168182 ..... p 161 N83-33219 * #
NAS 1.26:168186 ..... p 185 N83-34454 * #
NAS 1.26:168190 ..... p 154 N83-33182 * #
NAS 1.26:168194 ..... p 151 N83-32070 * #
NAS 1.26:168195 ..... p 87 N83-35101 * #
NAS 1.26:168197 ..... p 132 N83-30960 * #
NAS 1.26:168198 ..... p 161 N83-29734 * #
NAS 1.26:168199 ..... p 117 N83-30915 * #
NAS 1.26:168200 ..... p 185 N83-34451 * #
NAS 1.26:168202 ..... p 131 N83-30959 * #
NAS 1.26:168207 ..... p 109 N83-34119 * #
NAS 1.26:168209 ..... p 59 N83-32842 * #
NAS 1.26:168212 ..... p 202 N83-35787 * #
NAS 1.26:168213 ..... p 17 N83-32782 * #
NAS 1.26:168215 ..... p 60 N83-33101 * #
NAS 1.26:168220 ..... p 118 N83-36359 * #
NAS 1.26:168226 ..... p 151 N83-33167 * #
NAS 1.26:168230 ..... p 186 N83-35497 * #
NAS 1.26:168241 ..... p 42 N83-34944 * #
NAS 1.26:168712 ..... p 18 N83-30402 * #
NAS 1.26:169086-VOL-2 ..... p 199 N83-18409 * #
NAS 1.26:169354 ..... p 105 N83-16600 * #
NAS 1.26:169460 ..... p 105 N83-10329 * #
NAS 1.26:169474 ..... p 30 N83-12214 * #
NAS 1.26:169475 ..... p 27 N83-12088 * #
NAS 1.26:169481 ..... p 114 N83-12329 * #
NAS 1.26:169528 ..... p 81 N83-13233 * #
NAS 1.26:169533 ..... p 197 N83-13936 * #
NAS 1.26:169583 ..... p 169 N83-14667 * #
NAS 1.26:169638 ..... p 10 N83-14068 * #
NAS 1.26:169668 ..... p 127 N83-14434 * #
NAS 1.26:169669 ..... p 114 N83-14398 * #
NAS 1.26:169670 ..... p 71 N83-14177 * #
NAS 1.26:169705 ..... p 10 N83-15264 * #
NAS 1.26:169706 ..... p 81 N83-15411 * #
NAS 1.26:169742 ..... p 31 N83-15309 * #
NAS 1.26:169758 ..... p 71 N83-16418 * #
NAS 1.26:169788 ..... p 128 N83-16679 * #
NAS 1.26:169796 ..... p 65 N83-16394 * #
NAS 1.26:169797 ..... p 82 N83-16493 * #
NAS 1.26:169800 ..... p 128 N83-16678 * #
NAS 1.26:169831 ..... p 11 N83-17503 * #
NAS 1.26:169832 ..... p 11 N83-17502 * #
NAS 1.26:169848 ..... p 72 N83-17626 * #
NAS 1.26:169861 ..... p 71 N83-17625 * #
NAS 1.26:169945 ..... p 176 N83-19273 * #
NAS 1.26:169996 ..... p 17 N83-19738 * #
NAS 1.26:170003 ..... p 72 N83-19824 * #
NAS 1.26:170005 ..... p 177 N83-20362 * #
NAS 1.26:170008 ..... p 44 N83-19761 * #
NAS 1.26:170015 ..... p 199 N83-20706 * #
NAS 1.26:170016 ..... p 82 N83-19885 * #
NAS 1.26:170089 ..... p 34 N83-22204 * #
NAS 1.26:170100 ..... p 33 N83-20945 * #
NAS 1.26:170176 ..... p 129 N83-22550 * #
NAS 1.26:170181 ..... p 106 N83-22493 * #
NAS 1.26:170182 ..... p 106 N83-22494 * #
NAS 1.26:170185 ..... p 179 N83-25026 * #
NAS 1.26:170187 ..... p 191 N83-23088 #
NAS 1.26:170188 ..... p 191 N83-23089 #
NAS 1.26:170233 ..... p 35 N83-23305 * #
NAS 1.26:170290 ..... p 160 N83-23629 * #
NAS 1.26:170299 ..... p 50 N83-23347 * #
NAS 1.26:170312 ..... p 130 N83-24795 * #
NAS 1.26:172231 ..... p 16 N83-35999 * #
NAS 1.26:172633 ..... p 132 N83-33105 * #
NAS 1.26:172679 ..... p 182 N83-27351 * #
NAS 1.26:172680 ..... p 183 N83-27352 * #
NAS 1.26:172847 ..... p 151 N83-33168 * #
NAS 1.26:172995 ..... p 40 N83-32808 * #
NAS 1.26:172997 ..... p 74 N83-32871 * #
NAS 1.26:172998 ..... p 74 N83-32870 * #
NAS 1.26:172999 ..... p 74 N83-32872 * #
NAS 1.26:173012 ..... p 97 N83-34045 * #
NAS 1.26:173013 ..... p 191 N83-34656 * #
NAS 1.26:173080 ..... p 132 N83-35316 * #
NAS 1.26:174451 ..... p 118 N83-36358 * #
NAS 1.26:174452 ..... p 109 N83-36299 * #
NAS 1.26:174453 ..... p 110 N83-36300 * #
NAS 1.26:3538 ..... p 197 N83-12968 * #
NAS 1.26:3598 ..... p 18 N83-14123 * #
NAS 1.26:3622 ..... p 127 N83-13387 * #
NAS 1.26:3623 ..... p 153 N83-11506 * #
NAS 1.26:3624 ..... p 28 N83-12093 * #
NAS 1.26:3624 ..... p 10 N83-14066 * #
NAS 1.26:3625 ..... p 153 N83-11507 * #
NAS 1.26:3626 ..... p 139 N83-11495 * #
NAS 1.26:3630 ..... p 128 N83-15592 * #
NAS 1.26:3632 ..... p 91 N83-11328 * #
NAS 1.26:3634 ..... p 10 N83-14066 * #
NAS 1.26:3656 ..... p 199 N83-20708 * #
NAS 1.26:3657 ..... p 2 N83-17453 * #
NAS 1.26:3658 ..... p 92 N83-16527 * #
NAS 1.26:3659 ..... p 153 N83-16773 * #
NAS 1.26:3670 ..... p 153 N83-27248 * #
NAS 1.26:3671 ..... p 13 N83-26819 * #
NAS 1.26:3673 ..... p 33 N83-18729 * #
NAS 1.26:3679 ..... p 153 N83-21373 * #
NAS 1.26:3680 ..... p 94 N83-22422 * #
NAS 1.26:3686 ..... p 95 N83-27021 * #
NAS 1.26:3689 ..... p 14 N83-27960 * #
NAS 1.26:3691 ..... p 188 N83-27542 * #
NAS 1.26:3692 ..... p 149 N83-28452 * #
NAS 1.26:3693 ..... p 154 N83-28466 * #
NAS 1.26:3697 ..... p 161 N83-29731 * #
NAS 1.26:3701 ..... p 14 N83-29174 * #
NAS 1.26:3723 ..... p 132 N83-34230 * #
NAS 1.26:3724 ..... p 154 N83-33180 * #
NAS 1.26:3725 ..... p 202 N83-33683 * #
NAS 1.55:2210 ..... p 144 N83-20119 * #
NAS 1.55:2230 ..... p 175 N83-19231 * #
NAS 1.55:2250 ..... p 142 N83-15629 * #
NAS 1.55:2256 ..... p 171 N83-15806 * #
NAS 1.55:2267 ..... p 100 N83-22442 * #
NAS 1.55:2268 ..... p 38 N83-29208 * #
NAS 1.55:2271 ..... p 161 N83-34351 * #
NAS 1.60:1929 ..... p 208 N83-23189 * #
NAS 1.60:1930 ..... p 208 N83-23188 * #
NAS 1.60:1931 ..... p 15 N83-32774 * #
NAS 1.60:2023 ..... p 26 N83-11125 * #
NAS 1.60:2034 ..... p 9 N83-11058 * #
NAS 1.60:2036 ..... p 139 N83-11496 * #
NAS 1.60:2050 ..... p 140 N83-13457 * #
NAS 1.60:2051 ..... p 187 N83-13643 * #
NAS 1.60:2053 ..... p 72 N83-18863 * #
NAS 1.60:2055 ..... p 158 N83-12449 * #
NAS 1.60:2056 ..... p 99 N83-11340 * #
NAS 1.60:2057 ..... p 26 N83-10045 * #
NAS 1.60:2058 ..... p 26 N83-11126 * #
NAS 1.60:2059 ..... p 91 N83-14269 * #
NAS 1.60:2060 ..... p 203 N83-13979 * #
NAS 1.60:2061 ..... p 82 N83-15413 * #
NAS 1.60:2062 ..... p 126 N83-12360 * #
NAS 1.60:2063 ..... p 93 N83-16528 * #
NAS 1.60:2080 ..... p 142 N83-16758 * #
NAS 1.60:2107 ..... p 100 N83-10548 * #
NAS 1.60:2111 ..... p 143 N83-16759 * #
NAS 1.60:2112 ..... p 32 N83-17547 * #
NAS 1.60:2131 ..... p 35 N83-23309 * #
NAS 1.60:2132 ..... p 40 N83-32808 * #
NAS 1.60:2139 ..... p 85 N83-24641 * #
NAS 1.60:2140 ..... p 83 N83-21110 * #
NAS 1.60:2142 ..... p 36 N83-25712 * #
NAS 1.60:2146 ..... p 152 N83-25400 * #
NAS 1.60:2148 ..... p 73 N83-24575 * #
NAS 1.60:2149 ..... p 85 N83-24640 * #
NAS 1.60:2154 ..... p 148 N83-24862 * #
NAS 1.60:2156 ..... p 36 N83-24509 * #
NAS 1.60:2161 ..... p 94 N83-24695 * #
NAS 1.60:2162 ..... p 116 N83-25985 * #
NAS 1.60:2163 ..... p 84 N83-23416 * #
NAS 1.60:2166 ..... p 135 N83-33126 * #
NAS 1.60:2169 ..... p 86 N83-32908 * #
NAS 1.60:2171 ..... p 36 N83-26839 * #
NAS 1.60:2172 ..... p 186 N83-36549 * #
NAS 1.60:2174 ..... p 163 N83-34373 * #
NAS 1.60:2175 ..... p 150 N83-28453 * #
NAS 1.60:2179 ..... p 189 N83-28921 * #
NAS 1.60:2188 ..... p 39 N83-30431 * #
NAS 1.60:2189 ..... p 151 N83-33166 * #
NAS 1.60:2195 ..... p 161 N83-33217 * #
NAS 1.60:2199 ..... p 40 N83-32807 * #
NAS 1.60:2200 ..... p 132 N83-34232 * #
NAS 1.60:2203 ..... p 41 N83-33893 * #
NAS 1.60:2207 ..... p 87 N83-34019 * #
NAS 1.60:2208 ..... p 163 N83-34372 * #
NAS 1.60:2227 ..... p 41 N83-34941 * #
NAS 1.61:1102 ..... p 130 N83-24600 * #
NAS 1.61:1103 ..... p 129 N83-22546 * #
NAS 1.61:1105 ..... p 149 N83-27214 * #
NAS 126:168124 ..... p 149 N83-27213 * #

NAS,1:28165484-VOL-3 ..... p 108 N83-33012 * #

NAS-E-1 ..... p 141 N83-14494 * #

NASA-CASE-LEW-12253-1 ..... p 203 N83-19596 * #
NASA-CASE-LEW-12443-1 ..... p 184 N83-32175 * #
NASA-CASE-LEW-12508-3 ..... p 131 N83-29625 * #
NASA-CASE-LEW-12582-1 ..... p 207 N83-34796 * #
NASA-CASE-LEW-12876-2 ..... p 96 N83-29392 * #
NASA-CASE-LEW-12892-1 ..... p 170 N83-14692 * #
NASA-CASE-LEW-12919-1 ..... p 63 N83-10117 * #
NASA-CASE-LEW-12941-1 ..... p 77 N83-10170 * #
NASA-CASE-LEW-12950-2 ..... p 183 N83-29804 * #
NASA-CASE-LEW-13107-1 ..... p 188 N83-21785 * #
NASA-CASE-LEW-13107-2 ..... p 188 N83-20539 * #
NASA-CASE-LEW-13131-1 ..... p 165 N83-10494 * #
NASA-CASE-LEW-13132-1 ..... p 96 N83-29388 * #
NASA-CASE-LEW-13142-1 ..... p 43 N83-36029 * #
NASA-CASE-LEW-13171-2 ..... p 184 N83-32176 * #
NASA-CASE-LEW-13174-1 ..... p 131 N83-27144 * #
NASA-CASE-LEW-13245-1 ..... p 182 N83-27344 * #
NASA-CASE-LEW-13268-3 ..... p 149 N83-28450 * #
NASA-CASE-LEW-13269-1 ..... p 50 N83-20996 * #
NASA-CASE-LEW-13269-2 ..... p 93 N83-17714 * #
NASA-CASE-LEW-13324-2 ..... p 86 N83-34014 * #
NASA-CASE-LEW-13343 ..... p 86 N83-31795 * #
NASA-CASE-LEW-1335901 ..... p 97 N83-31855 * #
NASA-CASE-LEW-13401-2 ..... p 185 N83-32177 * #
NASA-CASE-LEW-13414-1 ..... p 177 N83-20374 * #
NASA-CASE-LEW-13429-1 ..... p 117 N83-31952 * #
NASA-CASE-LEW-13445-2 ..... p 143 N83-17883 * #
NASA-CASE-LEW-13450-1 ..... p 103 N83-35177 * #
NASA-CASE-LEW-13504-1 ..... p 71 N83-13188 * #
NASA-CASE-LEW-13524-1 ..... p 131 N83-30957 * #
NASA-CASE-LEW-13556-2 ..... p 183 N83-29805 * #
NASA-CASE-LEW-13598-1 ..... p 102 N83-17745 * #
NASA-CASE-LEW-13609-1 ..... p 72 N83-17628 * #
NASA-CASE-LEW-13620-1 ..... p 168 N83-13579 * #
NASA-CASE-LEW-13639-2 ..... p 82 N83-17683 * #
NASA-CASE-LEW-13654-1 ..... p 30 N83-14129 * #
NASA-CASE-LEW-13717-1 ..... p 159 N83-20284 * #
NASA-CASE-LEW-13736-1 ..... p 115 N83-17802 * #
NASA-CASE-LEW-13758-1 ..... p 64 N83-12176 * #
NASA-CASE-LEW-13770-1 ..... p 91 N83-13258 * #
NASA-CASE-LEW-13770-2 ..... p 96 N83-30651 * #
NASA-CASE-LEW-13773-1 ..... p 18 N83-29197 * #
NASA-CASE-LEW-13827-1 ..... p 181 N83-26258 * #
NASA-CASE-LEW-13833-1 ..... p 116 N83-25983 * #
NASA-CASE-LEW-13834-1 ..... p 85 N83-24639 * #
NASA-CASE-LEW-13837-1 ..... p 67 N83-28095 * #
NASA-CASE-LEW-13864-1 ..... p 93 N83-17715 * #
NASA-CASE-LEW-13881-1 ..... p 202 N83-21903 * #
NASA-CASE-LEW-13893-1 ..... p 107 N83-30832 * #
NASA-CASE-LEW-13934-1 ..... p 135 N83-35338 * #
NASA-CASE-LEW-13981-1 ..... p 116 N83-25984 * #
NASA-CASE-LEW-14586-1 ..... p 40 N83-31603 * #

NASA-CP-2210 ..... p 144 N83-20119 * #
NASA-CP-2230 ..... p 175 N83-19231 * #
NASA-CP-2250 ..... p 142 N83-15629 * #
NASA-CP-2256 ..... p 171 N83-15806 * #
NASA-CP-2267 ..... p 100 N83-22442 * #
NASA-CP-2268 ..... p 38 N83-29208 * #
NASA-CP-2271 ..... p 161 N83-34351 * #

NASA-CR-159773 ..... p 211 N83-24432 * #
NASA-CR-159791 ..... p 1 N83-16279 * #
NASA-CR-159859 ..... p 28 N83-12094 * #
NASA-CR-159877 ..... p 102 N83-12259 * #
NASA-CR-165127 ..... p 174 N83-16859 * #
NASA-CR-165140 ..... p 57 N83-14158 * #

NASA-CR-165141 ..... p 82 N83-15412 * #
NASA-CR-165148 ..... p 31 N83-16341 * #
NASA-CR-165160 ..... p 57 N83-14159 * #
NASA-CR-165178 ..... p 140 N83-12431 * #
NASA-CR-165202 ..... p 30 N83-15304 * #
NASA-CR-165209 ..... p 80 N83-12215 * #
NASA-CR-165256 ..... p 43 N83-30435 * #
NASA-CR-165263 ..... p 211 N83-26762 * #
NASA-CR-165265 ..... p 26 N83-11127 * #
NASA-CR-165274 ..... p 167 N83-10568 * #
NASA-CR-165282 ..... p 114 N83-12330 * #
NASA-CR-165296 ..... p 28 N83-12089 * #
NASA-CR-165326-VOL-1 ..... p 178 N83-22750 * #
NASA-CR-165326-VOL-2 ..... p 178 N83-22751 * #
NASA-CR-165326-VOL-3 ..... p 178 N83-22754 * #
NASA-CR-165326-VOL-4 ..... p 179 N83-22755 * #
NASA-CR-165329 ..... p 209 N83-13038 * #
NASA-CR-165341 ..... p 66 N83-22326 * #
NASA-CR-165346 ..... p 139 N83-11497 * #
NASA-CR-165354 ..... p 39 N83-30427 * #
NASA-CR-165376 ..... p 39 N83-30430 * #
NASA-CR-165394 ..... p 206 N83-13009 * #
NASA-CR-165399 ..... p 32 N83-17545 * #
NASA-CR-165400 ..... p 39 N83-30429 * #
NASA-CR-165414 ..... p 65 N83-18853 * #
NASA-CR-165415 ..... p 66 N83-18854 * #
NASA-CR-165445 ..... p 182 N83-26259 * #
NASA-CR-165461 ..... p 64 N83-13173 * #
NASA-CR-165462-A ..... p 168 N83-12524 * #
NASA-CR-165463 ..... p 179 N83-23704 * #
NASA-CR-165472 ..... p 178 N83-22748 * #
NASA-CR-165484-VOL-1 ..... p 108 N83-33010 * #
NASA-CR-165484-VOL-2 ..... p 108 N83-33011 * #
NASA-CR-165484 ..... p 108 N83-33012 * #
NASA-CR-165491 ..... p 174 N83-19226 * #
NASA-CR-165492 ..... p 102 N83-35159 * #
NASA-CR-165494 ..... p 212 N83-37028 * #
NASA-CR-165509 ..... p 141 N83-14494 * #
NASA-CR-165518 ..... p 29 N83-13104 * #
NASA-CR-165523 ..... p 40 N83-32804 * #
NASA-CR-165525 ..... p 16 N83-11095 * #
NASA-CR-165527 ..... p 210 N83-20829 * #
NASA-CR-165528 ..... p 212 N83-27926 * #
NASA-CR-165540 ..... p 44 N83-24516 * #
NASA-CR-165541 ..... p 168 N83-13585 * #
NASA-CR-165543 ..... p 167 N83-10561 * #
NASA-CR-165566 ..... p 177 N83-22746 * #
NASA-CR-165571 ..... p 158 N83-12451 * #
NASA-CR-165581 ..... p 29 N83-13100 * #
NASA-CR-165582 ..... p 32 N83-17539 * #
NASA-CR-165590 ..... p 49 N83-12136 * #
NASA-CR-165590 ..... p 50 N83-12137 * #
NASA-CR-165591 ..... p 142 N83-15659 * #
NASA-CR-165598-VOL-1 ..... p 211 N83-26757 * #
NASA-CR-165598-VOL-2 ..... p 211 N83-26758 * #
NASA-CR-165598-VOL-3 ..... p 211 N83-26759 * #
NASA-CR-165601 ..... p 113 N83-10348 * #
NASA-CR-165612 ..... p 31 N83-16342 * #
NASA-CR-165618 ..... p 26 N83-10044 * #
NASA-CR-165619 ..... p 92 N83-15467 * #
NASA-CR-165990 ..... p 49 N83-12136 * #
NASA-CR-167842 ..... p 168 N83-13588 * #
NASA-CR-167845 ..... p 114 N83-13359 * #
NASA-CR-167851-VOL-1 ..... p 31 N83-15308 * #
NASA-CR-167868 ..... p 96 N83-29393 * #
NASA-CR-167873 ..... p 187 N83-21677 * #
NASA-CR-167875 ..... p 142 N83-15627 * #
NASA-CR-167880 ..... p 73 N83-26936 * #
NASA-CR-167882 ..... p 176 N83-20359 * #
NASA-CR-167887 ..... p 57 N83-17586 * #
NASA-CR-167890 ..... p 179 N83-22756 * #
NASA-CR-167891 ..... p 41 N83-33894 * #
NASA-CR-167893 ..... p 134 N83-21314 * #
NASA-CR-167901 ..... p 212 N83-33800 * #
NASA-CR-167903 ..... p 45 N83-12129 * #
NASA-CR-167906 ..... p 29 N83-13103 * #
NASA-CR-167907 ..... p 209 N83-15176 * #
NASA-CR-167913 ..... p 33 N83-19753 * #
NASA-CR-167915 ..... p 99 N83-13272 * #
NASA-CR-167917 ..... p 99 N83-12250 * #
NASA-CR-167919 ..... p 209 N83-16257 * #
NASA-CR-167921 ..... p 179 N83-23708 * #
NASA-CR-167932 ..... p 134 N83-15601 * #
NASA-CR-167936 ..... p 209 N83-10991 * #
NASA-CR-167942 ..... p 93 N83-18909 * #
NASA-CR-167943 ..... p 208 N83-10970 * #
NASA-CR-167950 ..... p 208 N83-30297 * #
NASA-CR-167951 ..... p 198 N83-15041 * #
NASA-CR-167953 ..... p 166 N83-10502 * #
NASA-CR-167954 ..... p 30 N83-14128 * #
NASA-CR-167957 ..... p 59 N83-28072 * #
NASA-CR-167959 ..... p 12 N83-18671 * #
NASA-CR-167960 ..... p 11 N83-15265 * #
NASA-CR-167961 ..... p 72 N83-21056 * #
NASA-CR-167962 ..... p 30 N83-15305 * #
NASA-CR-167963 ..... p 100 N83-18924 * #
NASA-CR-167964 ..... p 37 N83-27993 * #
NASA-CR-167965 ..... p 32 N83-17543 * #
NASA-CR-167966 ..... p 32 N83-17544 * #
NASA-CR-167967 ..... p 159 N83-19121 * #
NASA-CR-167969 ..... p 64 N83-13178 * #
NASA-CR-167970 ..... p 64 N83-13179 * #
NASA-CR-167971 ..... p 64 N83-13180 * #
NASA-CR-167974 ..... p 212 N83-32687 * #
NASA-CR-167975 ..... p 115 N83-16628 * #
NASA-CR-167976 ..... p 177 N83-22739 * #
NASA-CR-167977 ..... p 206 N83-16234 * #
NASA-CR-167978 ..... p 113 N83-10349 * #
NASA-CR-167979 ..... p 197 N83-12967 * #
NASA-CR-167981 ..... p 98 N83-10207 * #
NASA-CR-167983 ..... p 210 N83-17424 * #
NASA-CR-167985 ..... p 117 N83-30914 * #
NASA-CR-167986 ..... p 105 N83-17769 * #
NASA-CR-167987 ..... p 168 N83-11579 * #
NASA-CR-167990-VOL-1 ..... p 126 N83-12353 * #
NASA-CR-167990-VOL-2 ..... p 126 N83-12354 * #
NASA-CR-167992 ..... p 33 N83-20946 * #
NASA-CR-167994 ..... p 9 N83-11065 * #
NASA-CR-167999 ..... p 63 N83-11247 * #
NASA-CR-168002 ..... p 10 N83-11066 * #
NASA-CR-168003 ..... p 10 N83-12045 * #
NASA-CR-168006 ..... p 184 N83-29812 * #
NASA-CR-168007 ..... p 185 N83-33343 * #
NASA-CR-168008 ..... p 19 N83-18720 * #
NASA-CR-168009 ..... p 10 N83-12047 * #
NASA-CR-168011 ..... p 57 N83-21002 * #
NASA-CR-168012 ..... p 115 N83-16630 * #
NASA-CR-168013 ..... p 47 N83-18835 * #
NASA-CR-168015 ..... p 131 N83-28376 * #
NASA-CR-168016 ..... p 34 N83-22198 * #
NASA-CR-168018 ..... p 11 N83-16285 * #
NASA-CR-168019 ..... p 43 N83-14139 * #
NASA-CR-168020 ..... p 173 N83-15839 * #
NASA-CR-168021 ..... p 182 N83-27345 * #
NASA-CR-168023 ..... p 66 N83-26928 * #
NASA-CR-168025 ..... p 185 N83-34450 * #
NASA-CR-168027 ..... p 100 N83-17728 * #
NASA-CR-168029 ..... p 143 N83-17880 * #
NASA-CR-168031 ..... p 128 N83-15590 * #
NASA-CR-168034 ..... p 105 N83-15543 * #
NASA-CR-168035 ..... p 116 N83-27127 * #
NASA-CR-168040 ..... p 199 N83-19575 * #
NASA-CR-168041 ..... p 115 N83-21236 * #
NASA-CR-168045 ..... p 14 N83-29178 * #
NASA-CR-168049 ..... p 31 N83-16343 * #
NASA-CR-168050 ..... p 198 N83-17242 * #
NASA-CR-168051 ..... p 13 N83-26816 * #
NASA-CR-168055 ..... p 115 N83-18997 * #
NASA-CR-168057 ..... p 66 N83-22325 * #
NASA-CR-168058 ..... p 106 N83-21207 * #
NASA-CR-168059 ..... p 34 N83-20948 * #
NASA-CR-168060 ..... p 209 N83-15177 * #
NASA-CR-168061 ..... p 86 N83-29359 * #
NASA-CR-168065 ..... p 107 N83-28297 * #
NASA-CR-168066 ..... p 101 N83-31886 * #
NASA-CR-168067 ..... p 11 N83-16286 * #
NASA-CR-168071 ..... p 83 N83-22389 * #
NASA-CR-168072 ..... p 46 N83-25766 * #
NASA-CR-168074 ..... p 212 N83-27925 * #
NASA-CR-168075 ..... p 185 N83-33320 * #
NASA-CR-168077 ..... p 107 N83-27086 * #
NASA-CR-168078 ..... p 106 N83-22495 * #
NASA-CR-168079 ..... p 175 N83-19228 * #
NASA-CR-168080 ..... p 61 N83-19812 * #
NASA-CR-168082 ..... p 116 N83-29596 * #
NASA-CR-168086-VOL-1 ..... p 198 N83-18406 * #
NASA-CR-168086-VOL-2 ..... p 199 N83-18409 * #
NASA-CR-168087 ..... p 210 N83-22029 * #
NASA-CR-168088 ..... p 212 N83-30328 * #
NASA-CR-168089 ..... p 46 N83-34998 * #
NASA-CR-168090 ..... p 183 N83-28581 * #
NASA-CR-168091 ..... p 183 N83-28582 * #
NASA-CR-168092 ..... p 183 N83-28583 * #
NASA-CR-168093 ..... p 183 N83-28580 * #
NASA-CR-168097 ..... p 17 N83-23281 * #
NASA-CR-168098 ..... p 206 N83-19622 * #
NASA-CR-168099 ..... p 207 N83-27877 * #
NASA-CR-168100 ..... p 160 N83-21390 * #
NASA-CR-168101 ..... p 206 N83-21987 * #
NASA-CR-168102 ..... p 207 N83-21988 * #
NASA-CR-168103 ..... p 36 N83-26837 * #
NASA-CR-168104 ..... p 211 N83-26763 * #
NASA-CR-168105 ..... p 45 N83-22255 * #
NASA-CR-168106 ..... p 188 N83-24048 * #
NASA-CR-168107 ..... p 177 N83-21508 * #
NASA-CR-168108 ..... p 177 N83-22740 * #
NASA-CR-168109 ..... p 177 N83-21509 * #
NASA-CR-168110 ..... p 178 N83-22747 * #
NASA-CR-168120 ..... p 18 N83-22188 * #
NASA-CR-168121 ..... p 101 N83-23465 * #
NASA-CR-168122 ..... p 149 N83-28448 * #
NASA-CR-168124 ..... p 149 N83-27213 * #
NASA-CR-168125 ..... p 85 N83-28208 * #
NASA-CR-168127 ..... p 15 N83-34911 * #
NASA-CR-168128 ..... p 106 N83-23497 * #
NASA-CR-168129 ..... p 107 N83-23498 * #
NASA-CR-168132 ..... p 58 N83-25779 * #
NASA-CR-168134 ..... p 59 N83-32843 * #
NASA-CR-168138 ..... p 101 N83-23464 * #
NASA-CR-168140 ..... p 96 N83-30662 * #
NASA-CR-168141 ..... p 181 N83-25112 * #
NASA-CR-168142 ..... p 109 N83-34116 * #
NASA-CR-168143 ..... p 109 N83-34117 * #
NASA-CR-168144 ..... p 109 N83-34118 * #
NASA-CR-168145 ..... p 108 N83-34113 * #
NASA-CR-168146 ..... p 108 N83-34114 * #
NASA-CR-168147 ..... p 108 N83-34115 * #
NASA-CR-168148 ..... p 204 N83-31474 * #
NASA-CR-168150 ..... p 108 N83-31925 * #
NASA-CR-168151 ..... p 108 N83-31926 * #
NASA-CR-168152 ..... p 181 N83-25043 * #
NASA-CR-168153 ..... p 148 N83-24857 * #
NASA-CR-168154 ..... p 160 N83-27256 * #
NASA-CR-168155 ..... p 61 N83-28077 * #
NASA-CR-168161 ..... p 37 N83-27996 * #
NASA-CR-168163 ..... p 38 N83-29234 * #
NASA-CR-168166 ..... p 12 N83-24474 * #
NASA-CR-168167 ..... p 40 N83-30432 * #
NASA-CR-168174-VOL-1 ..... p 60 N83-33942 * #
NASA-CR-168174-VOL-2 ..... p 60 N83-33943 * #
NASA-CR-168175 ..... p 107 N83-29492 * #
NASA-CR-168180 ..... p 74 N83-30551 * #
NASA-CR-168182 ..... p 161 N83-33219 * #
NASA-CR-168186 ..... p 185 N83-34454 * #
NASA-CR-168190 ..... p 154 N83-33182 * #
NASA-CR-168194 ..... p 151 N83-32070 * #
NASA-CR-168195 ..... p 87 N83-35101 * #
NASA-CR-168197 ..... p 132 N83-30960 * #
NASA-CR-168198 ..... p 161 N83-29734 * #
NASA-CR-168199 ..... p 117 N83-30915 * #
NASA-CR-168200 ..... p 185 N83-34451 * #
NASA-CR-168202 ..... p 131 N83-30959 * #
NASA-CR-168207 ..... p 109 N83-34119 * #
NASA-CR-168209 ..... p 59 N83-32842 * #
NASA-CR-168212 ..... p 202 N83-35787 * #
NASA-CR-168213 ..... p 17 N83-32782 * #
NASA-CR-168215 ..... p 60 N83-36101 * #
NASA-CR-168220 ..... p 118 N83-36359 * #
NASA-CR-168226 ..... p 151 N83-33167 * #
NASA-CR-168230 ..... p 186 N83-35497 * #
NASA-CR-168241 ..... p 42 N83-34944 * #
NASA-CR-168712 ..... p 18 N83-30402 * #
NASA-CR-169354 ..... p 105 N83-16600 * #
NASA-CR-169460 ..... p 105 N83-10329 * #
NASA-CR-169474 ..... p 80 N83-12214 * #
NASA-CR-169475 ..... p 27 N83-12088 * #
NASA-CR-169481 ..... p 114 N83-12329 * #
NASA-CR-169528 ..... p 81 N83-13233 * #
NASA-CR-169533 ..... p 197 N83-13936 * #
NASA-CR-169593 ..... p 169 N83-14667 * #
NASA-CR-169638 ..... p 10 N83-14068 * #
NASA-CR-169668 ..... p 127 N83-14434 * #
NASA-CR-169669 ..... p 114 N83-14398 * #
NASA-CR-169670 ..... p 71 N83-14177 * #
NASA-CR-169705 ..... p 10 N83-15264 * #
NASA-CR-169706 ..... p 81 N83-15411 * #
NASA-CR-169742 ..... p 31 N83-15309 * #
NASA-CR-169756 ..... p 71 N83-16418 * #
NASA-CR-169788 ..... p 128 N83-16679 * #
NASA-CR-169796 ..... p 65 N83-16394 * #
NASA-CR-169797 ..... p 82 N83-16493 * #
NASA-CR-169800 ..... p 128 N83-16678 * #
NASA-CR-169831 ..... p 11 N83-17503 * #
NASA-CR-169832 ..... p 11 N83-17502 * #
NASA-CR-169848 ..... p 72 N83-17626 * #
NASA-CR-169861 ..... p 71 N83-17625 * #
NASA-CR-169945 ..... p 176 N83-19273 * #
NASA-CR-169996 ..... p 17 N83-19738 * #
NASA-CR-170003 ..... p 72 N83-19824 * #
NASA-CR-170005 ..... p 177 N83-20362 * #
NASA-CR-170008 ..... p 44 N83-19761 * #
NASA-CR-170015 ..... p 199 N83-20706 * #
NASA-CR-170016 ..... p 82 N83-19885 * #
NASA-CR-170089 ..... p 34 N83-22204 * #
NASA-CR-170100 ..... p 33 N83-20945 * #
NASA-CR-170176 ..... p 129 N83-22550 * #
NASA-CR-170181 ..... p 106 N83-22493 * #
NASA-CR-170182 ..... p 106 N83-22494 * #
NASA-CR-170185 ..... p 179 N83-25026 * #
NASA-CR-170186 ..... p 191 N83-23087 #
NASA-CR-170187 ..... p 191 N83-23088 #
NASA-CR-170188 ..... p 191 N83-23089 #
NASA-CR-170233 ..... p 35 N83-23305 * #
NASA-CR-170290 ..... p 160 N83-23629 * #
NASA-CR-170299 ..... p 50 N83-23347 * #
NASA-CR-170312 ..... p 130 N83-24795 * #
NASA-CR-172231 ..... p 16 N83-35999 * #
NASA-CR-172633 ..... p 132 N83-33105 * #

NASA-CR-172679 ..... p 182 N83-27351 * #
NASA-CR-172680 ..... p 183 N83-27352 * #
NASA-CR-172847 ..... p 151 N83-33168 * #
NASA-CR-172995 ..... p 40 N83-32808 * #
NASA-CR-172997 ..... p 74 N83-32871 * #
NASA-CR-172998 ..... p 74 N83-32870 * #
NASA-CR-172999 ..... p 74 N83-32872 * #
NASA-CR-173012 ..... p 97 N83-34045 * #
NASA-CR-173013 ..... p 191 N83-34656 * #
NASA-CR-173080 ..... p 132 N83-35316 * #
NASA-CR-174451 ..... p 118 N83-36356 * #
NASA-CR-174452 ..... p 109 N83-36299 * #
NASA-CR-174453 ..... p 110 N83-36300 * #
NASA-CR-3538 ..... p 197 N83-12968 * #
NASA-CR-3598 ..... p 18 N83-14123 * #
NASA-CR-3622 ..... p 127 N83-13387 * #
NASA-CR-3623 ..... p 153 N83-11506 * #
NASA-CR-3624 ..... p 28 N83-12093 * #
NASA-CR-3625 ..... p 153 N83-11507 * #
NASA-CR-3626 ..... p 139 N83-11495 * #
NASA-CR-3630 ..... p 128 N83-15592 * #
NASA-CR-3632 ..... p 91 N83-11328 * #
NASA-CR-3634 ..... p 10 N83-14066 * #
NASA-CR-3656 ..... p 199 N83-20708 * #
NASA-CR-3657 ..... p 2 N83-17453 * #
NASA-CR-3658 ..... p 92 N83-16527 * #
NASA-CR-3659 ..... p 153 N83-16773 * #
NASA-CR-3670 ..... p 153 N83-27248 * #
NASA-CR-3671 ..... p 13 N83-26819 * #
NASA-CR-3673 ..... p 33 N83-18729 * #
NASA-CR-3679 ..... p 153 N83-21373 * #
NASA-CR-3680 ..... p 94 N83-22422 * #
NASA-CR-3686 ..... p 95 N83-27021 * #
NASA-CR-3689 ..... p 14 N83-27960 * #
NASA-CR-3691 ..... p 188 N83-27542 * #
NASA-CR-3692 ..... p 149 N83-28452 * #
NASA-CR-3693 ..... p 154 N83-28466 * #
NASA-CR-3697 ..... p 161 N83-29731 * #
NASA-CR-3701 ..... p 14 N83-29174 * #
NASA-CR-3723 ..... p 132 N83-34230 * #
NASA-CR-3724 ..... p 154 N83-33180 * #
NASA-CR-3725 ..... p 202 N83-33683 * #

NASA-RP-1102 ..... p 130 N83-24800 * #
NASA-RP-1103 ..... p 129 N83-22546 * #
NASA-RP-1105 ..... p 149 N83-27214 * #

NASA-TM-23324 ..... p 13 N83-26817 * #
NASA-TM-81692 ..... p 147 N83-20159 * #
NASA-TM-81695 ..... p 140 N83-12432 * #
NASA-TM-81696 ..... p 140 N83-13458 * #
NASA-TM-81697 ..... p 150 N83-29710 * #
NASA-TM-81698 ..... p 150 N83-29711 * #
NASA-TM-81699 ..... p 151 N83-29712 * #
NASA-TM-81700 ..... p 149 N83-28449 * #
NASA-TM-81701 ..... p 151 N83-29713 * #
NASA-TM-81723 ..... p 83 N83-22390 * #
NASA-TM-82629 ..... p 160 N83-23631 * #
NASA-TM-82695 ..... p 169 N83-14691 * #
NASA-TM-82698 ..... p 80 N83-11309 * #
NASA-TM-82739 ..... p 99 N83-10208 * #
NASA-TM-82774 ..... p 126 N83-12359 * #
NASA-TM-82778 ..... p 169 N83-14688 * #
NASA-TM-82818 ..... p 9 N83-11063 * #
NASA-TM-82867 ..... p 59 N83-28071 * #
NASA-TM-82870 ..... p 169 N83-14689 * #
NASA-TM-82876 ..... p 125 N83-10389 * #
NASA-TM-82890 ..... p 28 N83-12092 * #
NASA-TM-82893 ..... p 70 N83-10134 * #
NASA-TM-82898 ..... p 207 N83-20608 * #
NASA-TM-82907 ..... p 32 N83-17537 * #
NASA-TM-82920 ..... p 81 N83-13232 * #
NASA-TM-82923 ..... p 170 N83-15805 * #
NASA-TM-82932 ..... p 27 N83-12087 * #
NASA-TM-82934 ..... p 81 N83-14245 * #
NASA-TM-82935 ..... p 77 N83-10171 * #
NASA-TM-82938 ..... p 181 N83-26251 * #
NASA-TM-82939 ..... p 9 N83-10019 * #
NASA-TM-82940 ..... p 169 N83-14683 * #
NASA-TM-82947 ..... p 113 N83-11446 * #
NASA-TM-82948 ..... p 166 N83-10554 * #
NASA-TM-82949 ..... p 28 N83-12090 * #
NASA-TM-82950 ..... p 196 N83-11840 * #
NASA-TM-82951 ..... p 64 N83-12175 * #
NASA-TM-82952 ..... p 50 N83-13154 * #
NASA-TM-82953 ..... p 159 N83-14523 * #
NASA-TM-82954 ..... p 71 N83-12182 * #
NASA-TM-82955 ..... p 143 N83-20115 * #
NASA-TM-82956 ..... p 140 N83-12433 * #
NASA-TM-82957 ..... p 167 N83-10558 * #
NASA-TM-82958 ..... p 63 N83-10118 * #
NASA-TM-82959 ..... p 91 N83-13257 * #
NASA-TM-82960 ..... p 210 N83-17423 * #
NASA-TM-82961 ..... p 70 N83-10135 * #
NASA-TM-82962 ..... p 91 N83-11329 * #
NASA-TM-82963 ..... p 12 N83-17509 * #
NASA-TM-82964 ..... p 30 N83-15306 * #
NASA-TM-82965 ..... p 206 N83-10962 * #
NASA-TM-82966 ..... p 166 N83-10555 * #
NASA-TM-82967 ..... p 114 N83-14397 * #
NASA-TM-82968 ..... p 92 N83-14271 * #
NASA-TM-82969 ..... p 126 N83-12357 * #
NASA-TM-82970 ..... p 105 N83-10322 * #
NASA-TM-82971 ..... p 113 N83-11447 * #
NASA-TM-82972 ..... p 90 N83-10194 * #
NASA-TM-82973 ..... p 140 N83-11498 * #
NASA-TM-82975 ..... p 158 N83-11514 * #
NASA-TM-82976 ..... p 139 N83-10425 * #
NASA-TM-82977 ..... p 57 N83-17587 * #
NASA-TM-82978 ..... p 29 N83-14126 * #
NASA-TM-82979 ..... p 27 N83-11128 * #
NASA-TM-82980 ..... p 61 N83-13169 * #
NASA-TM-82981 ..... p 71 N83-15372 * #
NASA-TM-82982 ..... p 114 N83-14399 * #
NASA-TM-82983 ..... p 27 N83-11129 * #
NASA-TM-82984 ..... p 47 N83-11210 * #
NASA-TM-82985 ..... p 166 N83-10557 * #
NASA-TM-82986 ..... p 167 N83-10559 * #
NASA-TM-82987 ..... p 166 N83-10556 * #
NASA-TM-82988 ..... p 27 N83-11130 * #
NASA-TM-82989 ..... p 92 N83-15466 * #
NASA-TM-82990 ..... p 56 N83-13164 * #
NASA-TM-82991 ..... p 169 N83-14690 * #
NASA-TM-82992 ..... p 211 N83-25625 * #
NASA-TM-82993 ..... p 81 N83-13231 * #
NASA-TM-82994 ..... p 196 N83-10885 * #
NASA-TM-82995 ..... p 192 N83-21872 * #
NASA-TM-82996 ..... p 128 N83-17833 * #
NASA-TM-82997 ..... p 210 N83-19651 * #
NASA-TM-82998 ..... p 167 N83-10560 * #
NASA-TM-82999 ..... p 180 N83-25036 * #
NASA-TM-83000 ..... p 84 N83-24636 * #
NASA-TM-83001 ..... p 70 N83-12181 * #
NASA-TM-83002 ..... p 197 N83-13939 * #
NASA-TM-83003 ..... p 100 N83-19921 * #
NASA-TM-83004 ..... p 56 N83-12141 * #
NASA-TM-83005 ..... p 127 N83-14431 * #
NASA-TM-83006 ..... p 78 N83-11282 * #
NASA-TM-83007 ..... p 99 N83-13273 * #
NASA-TM-83008 ..... p 28 N83-12091 * #
NASA-TM-83009 ..... p 18 N83-15302 * #
NASA-TM-83010 ..... p 10 N83-13077 * #
NASA-TM-83011 ..... p 126 N83-12358 * #
NASA-TM-83012 ..... p 197 N83-12966 * #
NASA-TM-83013 ..... p 29 N83-13101 * #
NASA-TM-83014 ..... p 56 N83-12142 * #
NASA-TM-83015 ..... p 56 N83-12143 * #
NASA-TM-83016 ..... p 128 N83-14435 * #
NASA-TM-83017 ..... p 127 N83-13392 * #
NASA-TM-83018 ..... p 174 N83-18022 * #
NASA-TM-83019 ..... p 176 N83-20361 * #
NASA-TM-83020 ..... p 198 N83-16152 * #
NASA-TM-83021 ..... p 152 N83-34325 * #
NASA-TM-83023 ..... p 81 N83-14246 * #
NASA-TM-83024 ..... p 129 N83-19016 * #
NASA-TM-83025 ..... p 168 N83-13589 * #
NASA-TM-83026 ..... p 130 N83-23544 * #
NASA-TM-83027 ..... p 29 N83-14127 * #
NASA-TM-83028 ..... p 33 N83-18725 * #
NASA-TM-83029 ..... p 57 N83-14157 * #
NASA-TM-83030 ..... p 127 N83-14432 * #
NASA-TM-83031 ..... p 16 N83-14078 * #
NASA-TM-83032 ..... p 99 N83-15483 * #
NASA-TM-83033 ..... p 92 N83-14270 * #
NASA-TM-83034 ..... p 198 N83-16153 * #
NASA-TM-83035 ..... p 173 N83-15840 * #
NASA-TM-83036 ..... p 178 N83-22749 * #
NASA-TM-83037 ..... p 1 N83-14061 * #
NASA-TM-83038 ..... p 208 N83-15169 * #
NASA-TM-83039 ..... p 190 N83-12930 * #
NASA-TM-83040 ..... p 143 N83-19092 * #
NASA-TM-83041 ..... p 143 N83-19093 * #
NASA-TM-83042 ..... p 92 N83-15468 * #
NASA-TM-83043 ..... p 31 N83-15307 * #
NASA-TM-83044 ..... p 65 N83-15362 * #
NASA-TM-83045 ..... p 11 N83-15268 * #
NASA-TM-83046 ..... p 174 N83-16857 * #
NASA-TM-83047 ..... p 65 N83-15364 * #
NASA-TM-83048 ..... p 134 N83-15602 * #
NASA-TM-83049 ..... p 159 N83-15672 * #
NASA-TM-83050 ..... p 65 N83-15365 * #
NASA-TM-83051 ..... p 65 N83-15363 * #
NASA-TM-83052 ..... p 61 N83-25786 * #
NASA-TM-83053 ..... p 130 N83-26017 * #
NASA-TM-83054 ..... p 200 N83-23112 * #
NASA-TM-83055 ..... p 82 N83-17682 * #
NASA-TM-83056 ..... p 34 N83-22199 * #
NASA-TM-83057 ..... p 34 N83-22200 * #
NASA-TM-83058 ..... p 32 N83-17538 * #
NASA-TM-83059 ..... p 160 N83-24874 * #
NASA-TM-83062 ..... p 144 N83-20117 * #
NASA-TM-83063 ..... p 58 N83-22318 * #
NASA-TM-83064 ..... p 58 N83-24552 * #
NASA-TM-83065 ..... p 12 N83-19710 * #
NASA-TM-83066 ..... p 185 N83-34453 * #
NASA-TM-83067 ..... p 82 N83-19886 * #
NASA-TM-83068 ..... p 93 N83-19901 * #
NASA-TM-83069 ..... p 12 N83-25657 * #
NASA-TM-83070 ..... p 129 N83-17834 * #
NASA-TM-83071 ..... p 129 N83-22542 * #
NASA-TM-83072 ..... p 100 N83-19920 * #
NASA-TM-83073 ..... p 72 N83-18862 * #
NASA-TM-83074 ..... p 144 N83-20118 * #
NASA-TM-83087 ..... p 181 N83-26252 * #
NASA-TM-83308 ..... p 83 N83-19887 * #
NASA-TM-83309 ..... p 179 N83-23710 * #
NASA-TM-83310 ..... p 180 N83-25037 * #
NASA-TM-83311 ..... p 144 N83-20116 * #
NASA-TM-83312 ..... p 129 N83-20029 * #
NASA-TM-83313 ..... p 129 N83-19020 * #
NASA-TM-83314 ..... p 15 N83-34908 * #
NASA-TM-83317 ..... p 198 N83-18405 * #
NASA-TM-83318 ..... p 150 N83-28454 * #
NASA-TM-83319 ..... p 94 N83-19902 * #
NASA-TM-83320 ..... p 66 N83-19817 * #
NASA-TM-83321 ..... p 66 N83-24559 * #
NASA-TM-83322 ..... p 85 N83-25853 * #
NASA-TM-83323 ..... p 182 N83-27347 * #
NASA-TM-83325 ..... p 134 N83-24829 * #
NASA-TM-83326 ..... p 45 N83-29292 * #
NASA-TM-83327 ..... p 199 N83-21895 * #
NASA-TM-83328 ..... p 189 N83-19496 * #
NASA-TM-83329 ..... p 210 N83-24431 * #
NASA-TM-83330 ..... p 33 N83-19754 * #
NASA-TM-83331 ..... p 87 N83-35103 * #
NASA-TM-83332 ..... p 83 N83-22387 * #
NASA-TM-83333 ..... p 200 N83-23114 * #
NASA-TM-83334 ..... p 200 N83-21896 * #
NASA-TM-83335 ..... p 208 N83-29124 * #
NASA-TM-83336 ..... p 200 N83-21897 * #
NASA-TM-83337 ..... p 47 N83-20994 * #
NASA-TM-83338 ..... p 34 N83-20947 * #
NASA-TM-83339 ..... p 94 N83-22423 * #
NASA-TM-83340 ..... p 17 N83-24487 * #
NASA-TM-83341 ..... p 201 N83-24287 * #
NASA-TM-83342 ..... p 59 N83-30516 * #
NASA-TM-83343 ..... p 36 N83-25711 * #
NASA-TM-83344 ..... p 48 N83-22313 * #
NASA-TM-83345 ..... p 148 N83-23606 * #
NASA-TM-83346 ..... p 35 N83-23306 * #
NASA-TM-83347 ..... p 200 N83-23115 * #
NASA-TM-83348 ..... p 35 N83-24506 * #
NASA-TM-83349 ..... p 201 N83-26643 * #
NASA-TM-83350 ..... p 83 N83-23417 * #
NASA-TM-83351 ..... p 200 N83-23116 * #
NASA-TM-83352 ..... p 84 N83-24634 * #
NASA-TM-83353 ..... p 130 N83-23545 * #
NASA-TM-83355 ..... p 85 N83-24638 * #
NASA-TM-83356 ..... p 148 N83-24855 * #
NASA-TM-83357 ..... p 66 N83-25790 * #
NASA-TM-83358 ..... p 153 N83-23620 * #
NASA-TM-83359 ..... p 35 N83-24505 * #
NASA-TM-83360 ..... p 2 N83-22092 * #
NASA-TM-83361 ..... p 190 N83-21847 * #
NASA-TM-83362 ..... p 95 N83-27019 * #
NASA-TM-83363 ..... p 73 N83-29326 * #
NASA-TM-83364 ..... p 94 N83-25882 * #
NASA-TM-83365 ..... p 201 N83-23117 * #
NASA-TM-83366 ..... p 160 N83-24875 * #
NASA-TM-83368 ..... p 84 N83-24635 * #
NASA-TM-83369 ..... p 84 N83-24637 * #
NASA-TM-83370 ..... p 201 N83-27793 * #
NASA-TM-83371 ..... p 73 N83-30550 * #
NASA-TM-83372 ..... p 37 N83-27995 * #
NASA-TM-83373 ..... p 117 N83-29597 * #
NASA-TM-83374 ..... p 180 N83-25041 * #
NASA-TM-83375 ..... p 180 N83-25038 * #
NASA-TM-83376 ..... p 2 N83-24467 * #
NASA-TM-83377 ..... p 179 N83-23709 * #
NASA-TM-83378 ..... p 130 N83-24798 * #
NASA-TM-83383 ..... p 107 N83-29493 * #
NASA-TM-83384 ..... p 181 N83-26253 * #
NASA-TM-83385 ..... p 180 N83-25042 * #
NASA-TM-83386 ..... p 73 N83-24571 * #
NASA-TM-83387 ..... p 201 N83-25499 * #
NASA-TM-83388 ..... p 58 N83-26922 * #
NASA-TM-83389 ..... p 148 N83-24858 * #
NASA-TM-83390 ..... p 115 N83-24764 * #
NASA-TM-83392 ..... p 202 N83-30168 * #
NASA-TM-83393 ..... p 184 N83-29811 * #
NASA-TM-83395 ..... p 86 N83-29360 * #
NASA-TM-83396 ..... p 130 N83-24799 * #
NASA-TM-83397 ..... p 150 N83-28455 * #
NASA-TM-83398 ..... p 13 N83-25662 * #
NASA-TM-83399 ..... p 37 N83-27994 * #
NASA-TM-83400 ..... p 95 N83-27020 * #
NASA-TM-83401 ..... p 183 N83-29810 * #
NASA-TM-83402 ..... p 148 N83-24856 * #

NASA-TM-83404 ..... p 116 N83-25982 * #
NASA-TM-83405 ..... p 212 N83-27924 * #
NASA-TM-83406 ..... p 95 N83-27016 * #
NASA-TM-83407 ..... p 182 N83-27346 * #
NASA-TM-83408 ..... p 148 N83-26079 * #
NASA-TM-83409 ..... p 12 N83-24470 * #
NASA-TM-83410 ..... p 94 N83-25883 * #
NASA-TM-83411 ..... p 201 N83-27794 * #
NASA-TM-83412 ..... p 36 N83-26838 * #
NASA-TM-83413 ..... p 96 N83-30660 * #
NASA-TM-83414 ..... p 41 N83-32811 * #
NASA-TM-83416 ..... p 48 N83-35004 * #
NASA-TM-83417 ..... p 58 N83-26923 * #
NASA-TM-83418 ..... p 131 N83-28380 * #
NASA-TM-83419 ..... p 59 N83-26924 * #
NASA-TM-83420 ..... p 101 N83-28255 * #
NASA-TM-83421 ..... p 37 N83-27991 * #
NASA-TM-83422 ..... p 96 N83-28243 * #
NASA-TM-83423 ..... p 86 N83-29358 * #
NASA-TM-83424 ..... p 152 N83-34326 * #
NASA-TM-83425 ..... p 107 N83-28295 * #
NASA-TM-83426 ..... p 97 N83-34048 * #
NASA-TM-83427 ..... p 97 N83-35142 * #
NASA-TM-83428 ..... p 150 N83-29709 * #
NASA-TM-83429 ..... p 38 N83-29235 * #
NASA-TM-83430 ..... p 109 N83-34120 * #
NASA-TM-83431 ..... p 14 N83-27958 * #
NASA-TM-83432 ..... p 184 N83-29813 * #
NASA-TM-83433 ..... p 2 N83-34885 * #
NASA-TM-83434 ..... p 15 N83-30393 * #
NASA-TM-83435 ..... p 37 N83-27992 * #
NASA-TM-83436 ..... p 39 N83-29237 * #
NASA-TM-83437 ..... p 160 N83-28493 * #
NASA-TM-83438 ..... p 13 N83-27957 * #
NASA-TM-83440 ..... p 97 N83-32943 * #
NASA-TM-83441 ..... p 62 N83-29311 * #
NASA-TM-83442 ..... p 132 N83-33103 * #
NASA-TM-83443 ..... p 191 N83-31390 * #
NASA-TM-83444 ..... p 184 N83-31107 * #
NASA-TM-83445 ..... p 186 N83-35496 * #
NASA-TM-83447 ..... p 39 N83-29236 * #
NASA-TM-83448 ..... p 14 N83-29179 * #
NASA-TM-83450 ..... p 87 N83-34015 * #
NASA-TM-83451 ..... p 15 N83-34909 * #
NASA-TM-83452 ..... p 152 N83-34327 * #
NASA-TM-83453 ..... p 191 N83-30113 * #
NASA-TM-83454 ..... p 117 N83-34192 * #
NASA-TM-83456 ..... p 102 N83-35160 * #
NASA-TM-83457 ..... p 15 N83-30392 * #
NASA-TM-83458 ..... p 41 N83-32810 * #
NASA-TM-83459 ..... p 87 N83-34016 * #
NASA-TM-83464 ..... p 97 N83-34049 * #
NASA-TM-83465 ..... p 98 N83-35143 * #
NASA-TM-83466 ..... p 41 N83-34942 * #
NASA-TM-83473 ..... p 161 N83-34349 * #
NASA-TM-83474 ..... p 98 N83-35144 * #
NASA-TM-83475 ..... p 87 N83-35102 * #
NASA-TM-83476 ..... p 42 N83-34943 * #
NASA-TM-83482 ..... p 163 N83-35413 * #
NASA-TM-83484 ..... p 19 N83-33883 * #
NASA-TM-83485 ..... p 88 N83-35104 * #
NASA-TM-83487 ..... p 186 N83-35498 * #
NASA-TM-83491 ..... p 163 N83-35412 * #
NASA-TM-83493 ..... p 42 N83-34945 * #
NASA-TM-83494 ..... p 42 N83-34946 * #
NASA-TM-83496 ..... p 60 N83-35053 * #
NASA-TM-83499 ..... p 42 N83-34947 * #
NASA-TM-83500 ..... p 50 N83-35005 * #
NASA-TM-83501 ..... p 42 N83-34948 * #
NASA-TM-83505 ..... p 2 N83-34886 * #
NASA-TM-85190 ..... p 45 N83-15330 * #
NASA-TM-85349 ..... p 95 N83-27022 * #
NASA-TM-85404 ..... p 133 N83-35318 * #
NASA-TM-85428 ..... p 43 N83-36031 * #

NASA-TP-1929 ..... p 208 N83-23189 * #
NASA-TP-1930 ..... p 208 N83-23188 * #
NASA-TP-1931 ..... p 15 N83-32774 * #
NASA-TP-2023 ..... p 26 N83-11125 * #
NASA-TP-2034 ..... p 9 N83-11058 * #
NASA-TP-2036 ..... p 139 N83-11496 * #
NASA-TP-2050 ..... p 140 N83-13457 * #
NASA-TP-2051 ..... p 187 N83-13643 * #
NASA-TP-2053 ..... p 72 N83-18863 * #
NASA-TP-2055 ..... p 158 N83-12449 * #
NASA-TP-2056 ..... p 99 N83-11340 * #
NASA-TP-2057 ..... p 26 N83-10045 * #
NASA-TP-2058 ..... p 26 N83-11126 * #
NASA-TP-2059 ..... p 91 N83-14269 * #
NASA-TP-2060 ..... p 203 N83-13979 * #
NASA-TP-2061 ..... p 82 N83-15413 * #
NASA-TP-2062 ..... p 126 N83-12360 * #
NASA-TP-2063 ..... p 93 N83-16528 * #
NASA-TP-2080 ..... p 142 N83-16758 * #
NASA-TP-2107 ..... p 100 N83-16545 * #
NASA-TP-2111 ..... p 143 N83-16759 * #
NASA-TP-2112 ..... p 32 N83-17547 * #
NASA-TP-2131 ..... p 35 N83-23309 * #
NASA-TP-2132 ..... p 40 N83-32806 * #
NASA-TP-2139 ..... p 85 N83-24641 * #
NASA-TP-2140 ..... p 83 N83-21110 * #
NASA-TP-2142 ..... p 36 N83-25712 * #
NASA-TP-2146 ..... p 152 N83-35400 * #
NASA-TP-2148 ..... p 73 N83-24575 * #
NASA-TP-2149 ..... p 85 N83-24640 * #
NASA-TP-2154 ..... p 148 N83-24862 * #
NASA-TP-2156 ..... p 36 N83-24509 * #
NASA-TP-2161 ..... p 94 N83-24695 * #
NASA-TP-2162 ..... p 116 N83-25985 * #
NASA-TP-2163 ..... p 84 N83-23419 * #
NASA-TP-2166 ..... p 135 N83-33126 * #
NASA-TP-2169 ..... p 86 N83-32908 * #
NASA-TP-2171 ..... p 36 N83-26839 * #
NASA-TP-2172 ..... p 186 N83-36549 * #
NASA-TP-2174 ..... p 163 N83-34373 * #
NASA-TP-2175 ..... p 150 N83-28453 * #
NASA-TP-2179 ..... p 189 N83-28921 * #
NASA-TP-2188 ..... p 39 N83-30431 * #
NASA-TP-2190 ..... p 151 N83-33166 * #
NASA-TP-2195 ..... p 161 N83-33217 * #
NASA-TP-2199 ..... p 40 N83-32807 * #
NASA-TP-2200 ..... p 132 N83-34232 * #
NASA-TP-2203 ..... p 41 N83-33893 * #
NASA-TP-2207 ..... p 87 N83-34019 * #
NASA-TP-2208 ..... p 163 N83-34372 * #
NASA-TP-2227 ..... p 41 N83-34941 * #

NASA/DOE/20320-44 ..... p 179 N83-23710 * #

NAUFP-202-1 ..... p 208 N83-10970 * #

NBSIR-82-1672 ..... p 130 N83-24800 * #

NE-1236 ..... p 59 N83-28071 * #

NEAR-TR-271 ..... p 10 N83-14066 * #
NEAR-TR-276 ..... p 2 N83-17453 * #

OSURF-760931/710709 ..... p 81 N83-13233 * #

PJ050 ..... p 105 N83-15543 * #

PSU/TURBO-82-5 ..... p 13 N83-26819 * #
PSU/TURBO-83-1 ..... p 128 N83-16679 * #
PSU/TURBO-83-2 ..... p 128 N83-16678 * #

PWA-5512-96 ..... p 32 N83-17544 * #
PWA-5515-175 ..... p 30 N83-15305 * #
PWA-5515-176 ..... p 37 N83-27993 * #
PWA-5515-177 ..... p 32 N83-17543 * #
PWA-5517-31 ..... p 43 N83-30435 * #
PWA-5523-122 ..... p 30 N83-14128 * #
PWA-5594-106 ..... p 30 N83-15304 * #
PWA-5594-152 ..... p 39 N83-30429 * #
PWA-5594-157 ..... p 39 N83-30427 * #
PWA-5594-180 ..... p 33 N83-19753 * #
PWA-5719-34 ..... p 74 N83-30551 * #
PWA-5723-27 ..... p 26 N83-10044 * #
PWA-5766-29 ..... p 13 N83-26816 * #
PWA-5843-13 ..... p 160 N83-21390 * #
PWA-5846-26 ..... p 199 N83-19575 * #
PWA-5891-18 ..... p 154 N83-33182 * #
PWA-5907-19 ..... p 131 N83-30959 * #

P81-915216-2 ..... p 102 N83-35159 * #

QR-5 ..... p 173 N83-15839 * #
QR-6 ..... p 182 N83-27345 * #
QR-8 ..... p 168 N83-12524 * #

QTNR-1 ..... p 80 N83-12214 * #

R-1309 ..... p 81 N83-13232 * #

RCA-PRRL-82-CR-18 ..... p 206 N83-21987 * #
RCA-PRRL-82-CR-18 ..... p 207 N83-21988 * #

REPT-110-5 ..... p 106 N83-21207 * #
REPT-2 ..... p 169 N83-14667 * #
REPT-4770 ..... p 198 N83-15041 * #
REPT-80ASE142DR1-VOL-2 ..... p 209 N83-10991 * #
REPT-815-008 ..... p 209 N83-16257 * #
REPT-82ASE248SA1 ..... p 209 N83-15176 * #
REPT-82ASE278SA2 ..... p 209 N83-15177 * #
REPT-83-ASE-308-SA-3 ..... p 212 N83-27925 * #
REPT-83-8J22-EVMOT-R1 ..... p 117 N83-30914 * #
REPT-83SRD038 ..... p 109 N83-34119 * #

RF-TECH-104 ..... p 153 N83-16773 * #

RI/RD83-104 ..... p 149 N83-27213 * #
RI/RD83-150 ..... p 60 N83-36101 * #
RI/RD83-163 ..... p 151 N83-32070 * #

RR-1685 ..... p 168 N83-11579 * #

R19-83 ..... p 185 N83-34451 * #
R80AEG396 ..... p 28 N83-12094 * #
R80AEG417 ..... p 31 N83-16341 * #
R80AEG664-VOL-2 ..... p 82 N83-15412 * #
R81AEG212-VOL-1 ..... p 198 N83-18408 * #
R81AEG212-VOL-2 ..... p 199 N83-18409 * #
R81AEG215 ..... p 26 N83-11127 * #
R81AEG307 ..... p 39 N83-30430 * #
R81AEG316 ..... p 34 N83-22204 * #
R81AEG654 ..... p 32 N83-17539 * #
R81AEG759 ..... p 40 N83-32804 * #
R82-915362-40-VOL-1 ..... p 126 N83-12353 * #
R82-915362-40-VOL-2 ..... p 126 N83-12354 * #
R82-915366-13 ..... p 93 N83-18909 * #
R82-955319-20 ..... p 100 N83-17728 * #
R82AEB078 ..... p 101 N83-23464 * #
R82AEB315 ..... p 29 N83-13103 * #
R82AEB340 ..... p 29 N83-13100 * #
R82AEB358 ..... p 158 N83-12451 * #
R82AEB403-VOL-1 ..... p 31 N83-15308 * #
R82AEB540-VOL-1 ..... p 33 N83-20946 * #
R82AE511 ..... p 31 N83-16342 * #
R83AEB047 ..... p 42 N83-34944 * #

SAE PAPER 821359 ..... p 5 A83-37957 * #
SAE PAPER 821375 ..... p 17 A83-37965 * #
SAE PAPER 821475 ..... p 24 A83-38001 * #

SAE-830729 ..... p 2 N83-22092 * #

SAI-82-002-AA ..... p 187 N83-21677 * #

SAPR-2 ..... p 209 N83-13038 * #
SAPR-3 ..... p 212 N83-33800 * #
SAPR-4 ..... p 210 N83-17424 * #
SAPR-5 ..... p 211 N83-26763 * #

SAR-1 ..... p 140 N83-12431 * #
SAR-4 ..... p 142 N83-15627 * #
SAR-6 ..... p 34 N83-22204 * #

SASR-7 ..... p 50 N83-23347 * #

SATR-2 ..... p 160 N83-23629 * #
SATR-3 ..... p 212 N83-27925 * #

SATSR-2 ..... p 139 N83-11497 * #

SERI/CP-635-1273 ..... p 175 N83-19231 * #

SM-79-15A ..... p 65 N83-18853 * #
SM-79-25B ..... p 66 N83-18854 * #

SR-1 ..... p 106 N83-22494 * #

SRD-81-088 ..... p 113 N83-10349 * #
SRD-81-097 ..... p 115 N83-16628 * #
SRD-82-023 ..... p 168 N83-13588 * #

SRI-2115 ..... p 101 N83-23465 * #

SR82-R-4621-36 ..... p 29 N83-13104 * #

STDR-82-15 ..... p 175 N83-19228 * #

SWRI-7080 ..... p 86 N83-29359 * #

TR-1 ..... p 105 N83-10329 * #

TRS-107 ..... p 179 N83-23704 * #

TRW-3724 ..... p 179 N83-22756 * #
TRW-39152-6011-UE-00-VOL-1 ... p 60 N83-33942 * #
TRW-39152-6012-UE-00-VOL-2 ... p 60 N83-33943 * #

TTL-83-1 ..... p 116 N83-29596 * #

UDR-TR-83-57 ..... p 160 N83-23629 * #

US-PATENT-APPL-SN-132364 ..... p 43 N83-36029 * #
US-PATENT-APPL-SN-163122 ..... p 40 N83-31603 * #
US-PATENT-APPL-SN-200634 ..... p 131 N83-27144 * #
US-PATENT-APPL-SN-210632 ..... p 77 N83-10170 * #
US-PATENT-APPL-SN-212949 ..... p 135 N83-35338 * #
US-PATENT-APPL-SN-220212 ..... p 117 N83-31952 * #
US-PATENT-APPL-SN-229233 ..... p 97 N83-31855 * #
US-PATENT-APPL-SN-235797 ..... p 184 N83-32175 * #
US-PATENT-APPL-SN-235868 ..... p 131 N83-29625 * #
US-PATENT-APPL-SN-238257 ..... p 131 N83-30957 * #
US-PATENT-APPL-SN-242795 ..... p 50 N83-20996 * #
US-PATENT-APPL-SN-242796 ..... p 168 N83-13579 * #
US-PATENT-APPL-SN-243682 ..... p 203 N83-19596 * #

US-PATENT-APPL-SN-245571 ..... p 30 N83-14129 * #
US-PATENT-APPL-SN-246772 ..... p 165 N83-10494 * #
US-PATENT-APPL-SN-264378 ..... p 63 N83-10117 * #
US-PATENT-APPL-SN-264380 ..... p 170 N83-14692 * #
US-PATENT-APPL-SN-266255 ..... p 182 N83-27344 * #
US-PATENT-APPL-SN-272152 ..... p 96 N83-29388 * #
US-PATENT-APPL-SN-272234 ..... p 71 N83-13188 * #
US-PATENT-APPL-SN-272407 ..... p 188 N83-21785 * #
US-PATENT-APPL-SN-293418 ..... p 86 N83-31795 * #
US-PATENT-APPL-SN-328760 ..... p 103 N83-35177 * #
US-PATENT-APPL-SN-333537 ..... p 184 N83-32176 * #
US-PATENT-APPL-SN-359388 ..... p 185 N83-32177 * #
US-PATENT-APPL-SN-387622 ..... p 107 N83-30832 * #
US-PATENT-APPL-SN-393583 ..... p 96 N83-29392 * #
US-PATENT-APPL-SN-397281 ..... p 207 N83-34796 * #
US-PATENT-APPL-SN-404809 ..... p 91 N83-13258 * #
US-PATENT-APPL-SN-418139 ..... p 64 N83-12176 * #
US-PATENT-APPL-SN-425203 ..... p 102 N83-17745 * #
US-PATENT-APPL-SN-431448 ..... p 93 N83-17714 * #
US-PATENT-APPL-SN-434084 ..... p 115 N83-17802 * #
US-PATENT-APPL-SN-434087 ..... p 93 N83-17715 * #
US-PATENT-APPL-SN-444124 ..... p 188 N83-20539 * #
US-PATENT-APPL-SN-452465 ..... p 72 N83-17628 * #
US-PATENT-APPL-SN-456460 ..... p 82 N83-17683 * #
US-PATENT-APPL-SN-456929 ..... p 143 N83-17883 * #
US-PATENT-APPL-SN-463440 ..... p 183 N83-29805 * #
US-PATENT-APPL-SN-463456 ..... p 159 N83-20284 * #
US-PATENT-APPL-SN-465364 ..... p 177 N83-20374 * #
US-PATENT-APPL-SN-469867 ..... p 18 N83-29197 * #
US-PATENT-APPL-SN-473498 ..... p 202 N83-21903 * #
US-PATENT-APPL-SN-478131 ..... p 85 N83-24639 * #
US-PATENT-APPL-SN-486470 ..... p 121 N83-26258 * #
US-PATENT-APPL-SN-486471 ..... p 116 N83-25983 * #
US-PATENT-APPL-SN-492522 ..... p 116 N83-25984 * #
US-PATENT-APPL-SN-495381 ..... p 67 N83-28095 * #
US-PATENT-APPL-SN-500045 ..... p 149 N83-28450 * #
US-PATENT-APPL-SN-507626 ..... p 183 N83-29804 * #
US-PATENT-APPL-SN-516217 ..... p 96 N83-30651 * #
US-PATENT-APPL-SN-523297 ..... p 86 N83-34014 * #

US-PATENT-CLASS-136-249 ..... p 185 N83-32177 * #
US-PATENT-CLASS-136-255 ..... p 170 N83-14692 * #
US-PATENT-CLASS-136-256 ..... p 168 N83-13579 * #
US-PATENT-CLASS-136-256 ..... p 170 N83-14692 * #
US-PATENT-CLASS-136-259 ..... p 168 N83-13579 * #
US-PATENT-CLASS-136-259 ..... p 170 N83-14692 * #
US-PATENT-CLASS-165-104.26 .. p 203 N83-19596 * #
US-PATENT-CLASS-165-134R .... p 203 N83-19596 * #
US-PATENT-CLASS-204-192E ..... p 63 N83-10117 * #
US-PATENT-CLASS-204-35N ..... p 96 N83-29388 * #
US-PATENT-CLASS-204-37R ..... p 96 N83-29388 * #
US-PATENT-CLASS-204-56R ..... p 165 N83-10494 * #
US-PATENT-CLASS-204-56R ..... p 96 N83-29388 * #
US-PATENT-CLASS-228-103 ..... p 135 N83-35338 * #
US-PATENT-CLASS-228-193 ..... p 135 N83-35338 * #
US-PATENT-CLASS-228-263.18 .. p 135 N83-35338 * #
US-PATENT-CLASS-264-104 ..... p 71 N83-13188 * #
US-PATENT-CLASS-29-157.3H ... p 203 N83-19596 * #
US-PATENT-CLASS-29-458 ..... p 77 N83-10170 * #
US-PATENT-CLASS-29-521 ..... p 77 N83-10170 * #
US-PATENT-CLASS-29-572 ..... p 168 N83-13579 * #
US-PATENT-CLASS-29-623.5 ..... p 184 N83-32176 * #
US-PATENT-CLASS-310-306 ..... p 184 N83-32175 * #
US-PATENT-CLASS-310-332 ..... p 207 N83-34796 * #
US-PATENT-CLASS-310-800 ..... p 207 N83-34796 * #
US-PATENT-CLASS-313-106 ..... p 63 N83-10117 * #
US-PATENT-CLASS-313-107 ..... p 63 N83-10117 * #
US-PATENT-CLASS-315-3 ..... p 117 N83-31952 * #
US-PATENT-CLASS-315-4 ..... p 117 N83-31952 * #
US-PATENT-CLASS-315-5.35 ..... p 117 N83-31952 * #
US-PATENT-CLASS-315-5.38 ..... p 63 N83-10117 * #
US-PATENT-CLASS-315-5.38 ..... p 117 N83-31952 * #
US-PATENT-CLASS-315-5 ..... p 117 N83-31952 * #
US-PATENT-CLASS-357-30 ..... p 168 N83-13579 * #
US-PATENT-CLASS-357-30 ..... p 185 N83-32177 * #
US-PATENT-CLASS-403-282 ..... p 77 N83-10170 * #
US-PATENT-CLASS-415-115 ..... p 131 N83-27144 * #
US-PATENT-CLASS-415-118 ..... p 135 N83-35338 * #
US-PATENT-CLASS-415-174 ..... p 50 N83-20996 * #
US-PATENT-CLASS-415-175 ..... p 40 N83-31603 * #
US-PATENT-CLASS-415-178 ..... p 40 N83-31603 * #
US-PATENT-CLASS-415-197 ..... p 50 N83-20996 * #
US-PATENT-CLASS-415-1 ..... p 40 N83-31603 * #
US-PATENT-CLASS-415-47 ..... p 40 N83-31603 * #
US-PATENT-CLASS-416-1 ..... p 131 N83-27144 * #
US-PATENT-CLASS-416-97R ..... p 131 N83-27144 * #
US-PATENT-CLASS-427-219.2 .... p 97 N83-31855 * #
US-PATENT-CLASS-427-243 ..... p 103 N83-35177 * #
US-PATENT-CLASS-427-247 ..... p 103 N83-35177 * #
US-PATENT-CLASS-427-318 ..... p 86 N83-31795 * #
US-PATENT-CLASS-427-34 ..... p 97 N83-31855 * #
US-PATENT-CLASS-427-34 ..... p 103 N83-35177 * #
US-PATENT-CLASS-427-405 ..... p 97 N83-31855 * #
US-PATENT-CLASS-427-419.2 .... p 86 N83-31795 * #
US-PATENT-CLASS-427-423 ..... p 97 N83-31855 * #
US-PATENT-CLASS-427-423 ..... p 103 N83-35177 * #
US-PATENT-CLASS-427-88 ..... p 168 N83-13579 * #
US-PATENT-CLASS-427-89 ..... p 168 N83-13579 * #
US-PATENT-CLASS-427-90 ..... p 168 N83-13579 * #
US-PATENT-CLASS-427-91 ..... p 168 N83-13579 * #
US-PATENT-CLASS-428-294 ..... p 207 N83-34796 * #
US-PATENT-CLASS-428-421 ..... p 207 N83-34796 * #
US-PATENT-CLASS-428-422 ..... p 207 N83-34796 * #
US-PATENT-CLASS-428-450 ..... p 86 N83-31795 * #
US-PATENT-CLASS-428-469 ..... p 86 N83-31795 * #
US-PATENT-CLASS-428-623 ..... p 97 N83-31855 * #
US-PATENT-CLASS-428-633 ..... p 97 N83-31855 * #
US-PATENT-CLASS-428-641 ..... p 86 N83-31795 * #
US-PATENT-CLASS-428-650 ..... p 86 N83-31795 * #
US-PATENT-CLASS-428-678 ..... p 97 N83-31855 * #
US-PATENT-CLASS-428-680 ..... p 86 N83-31795 * #
US-PATENT-CLASS-429-105 ..... p 182 N83-27344 * #
US-PATENT-CLASS-429-107 ..... p 182 N83-27344 * #
US-PATENT-CLASS-429-109 ..... p 182 N83-27344 * #
US-PATENT-CLASS-429-144 ..... p 184 N83-32176 * #
US-PATENT-CLASS-429-206 ..... p 71 N83-13188 * #
US-PATENT-CLASS-429-251 ..... p 184 N83-32176 * #
US-PATENT-CLASS-429-253 ..... p 71 N83-13188 * #
US-PATENT-CLASS-429-254 ..... p 184 N83-32176 * #
US-PATENT-CLASS-429-34 ..... p 182 N83-27344 * #
US-PATENT-CLASS-429-40 ..... p 182 N83-27344 * #
US-PATENT-CLASS-525-61 ..... p 71 N83-13188 * #
US-PATENT-CLASS-60-39.07 ..... p 43 N83-36029 * #
US-PATENT-CLASS-604-280 ..... p 188 N83-21785 * #
US-PATENT-CLASS-604-8 ..... p 188 N83-21785 * #
US-PATENT-CLASS-62-3 ..... p 131 N83-29625 * #

US-PATENT-4,335,190 ..... p 97 N83-31855 * #
US-PATENT-4,335,196 ..... p 168 N83-13579 * #
US-PATENT-4,338,061 ..... p 40 N83-31603 * #
US-PATENT-4,349,424 ..... p 63 N83-10117 * #
US-PATENT-4,349,954 ..... p 77 N83-10170 * #
US-PATENT-4,350,574 ..... p 165 N83-10494 * #
US-PATENT-4,357,402 ..... p 71 N83-13188 * #
US-PATENT-4,360,701 ..... p 170 N83-14692 * #
US-PATENT-4,371,596 ..... p 184 N83-32176 * #
US-PATENT-4,372,377 ..... p 203 N83-19596 * #
US-PATENT-4,373,142 ..... p 184 N83-32175 * #
US-PATENT-4,374,183 ..... p 86 N83-31795 * #
US PATENT-4,376,872 ..... p 185 N83-32177 * #
US-PATENT-4,377,169 ..... p 188 N83-21785 * #
US-PATENT-4,377,371 ..... p 50 N83-20996 * #
US-PATENT-4,382,116 ..... p 182 N83-27344 * #
US-PATENT-4,384,823 ..... p 131 N83-27144 * #
US-PATENT-4,392,356 ..... p 131 N83-29625 * #
US-PATENT-4,392,920 ..... p 96 N83-29388 * #
US-PATENT-4,395,656 ..... p 117 N83-31952 * #
US-PATENT-4,400,642 ..... p 207 N83-34796 * #
US-PATENT-4,402,447 ..... p 135 N83-35338 * #
US-PATENT-4,402,992 ..... p 103 N83-35177 * #
US-PATENT-4,404,793 ..... p 43 N83-36029 * #

UTRC81-65-VOL-1 ..... p 211 N83-26757 * #
UTRC81-65-VOL-2 ..... p 211 N83-26758 * #
UTRC81-65-VOL-3 ..... p 211 N83-26759 * #

UVA/528200/EE82/104 ..... p 105 N83-16600 * #
UVA/528200/EE83/107 ..... p 110 N83-36300 * #
UVA/528219/EE84/101 ..... p 109 N83-36299 * #

UWME-DR-201-107-1 ..... p 65 N83-16394 * #

VPI-E-83.10 ..... p 161 N83-33219 * #

WES/DL-82-07E ..... p 115 N83-21236 * #

WQEC/C-82-23 ..... p 182 N83-27351 * #
WQEC/C-83-1 ..... p 183 N83-27352 * #

WSCI-82-45 ..... p 72 N83-17626 * #

WUT-3413-10-VOL-1 ..... p 108 N83-33010 * #
WUT-3413-10-VOL-2 ..... p 108 N83-33011 * #
WUT-3413-10-VOL-3 ..... p 108 N83-33012 * #

XAL-72760-AL ..... p 168 N83-12524 * #

*USGPO: 1984-759-100-535